ONF-800428 — Vol. 3
olume 3 of 3 Volumes

Dr. 1848

253
10/14/80
T.S.

MASTER

The Proceedings of the Sixth International Conference on Fluidized Bed Combustion

Volume III — Technical Sessions

April 9-11, 1980

Atlanta Hilton
Atlanta, Georgia

Published August 1980

6th

U.S. Department of Energy
Assistant Secretary for Fossil Energy
Office of Coal Utilization

DISTRIBUTION OF THIS DOCUMENT IS UNLIMITED

DISCLAIMER

This report was prepared as an account of work sponsored by an agency of the United States Government. Neither the United States Government nor any agency Thereof, nor any of their employees, makes any warranty, express or implied, or assumes any legal liability or responsibility for the accuracy, completeness, or usefulness of any information, apparatus, product, or process disclosed, or represents that its use would not infringe privately owned rights. Reference herein to any specific commercial product, process, or service by trade name, trademark, manufacturer, or otherwise does not necessarily constitute or imply its endorsement, recommendation, or favoring by the United States Government or any agency thereof. The views and opinions of authors expressed herein do not necessarily state or reflect those of the United States Government or any agency thereof.

DISCLAIMER

Portions of this document may be illegible in electronic image products. Images are produced from the best available original document.

Printed in the United States of America

Available from

National Technical Information Service
U.S. Department of Commerce
5285 Port Royal Road
Springfield, VA 22161

NTIS price codes

Printed Copy:	$15.25
Microfiche Copy:	$ 3.50

CONF-800428 — Vol. 3
Volume 3 of 3 Volumes
UC-90e

The Proceedings of the Sixth International Conference on Fluidized Bed Combustion

Volume III — Technical Sessions

April 9-11, 1980

Atlanta Hilton
Atlanta, Georgia

Published August 1980

Sponsored by
U.S. Department of Energy
Electric Power Research Institute
U.S. Environmental Protection Agency
Tennessee Valley Authority

Coordinated by
Courtesy Associates, Inc.

U.S. Department of Energy
Assistant Secretary for Fossil Energy
Office of Coal Utilization
Washington, D.C. 20585

DISCLAIMER

This book was prepared as an account of work sponsored by an agency of the United States Government. Neither the United States Government nor any agency thereof, nor any of their employees, makes any warranty, express or implied, or assumes any legal liability or responsibility for the accuracy, completeness, or usefulness of any information, apparatus, product, or process disclosed, or represents that its use would not infringe privately owned rights. Reference herein to any specific commercial product, process, or service by trade name, trademark, manufacturer, or otherwise, does not necessarily constitute or imply its endorsement, recommendation, or favoring by the United States Government or any agency thereof. The views and opinions of authors expressed herein do not necessarily state or reflect those of the United States Government or any agency thereof.

DISTRIBUTION OF THIS DOCUMENT IS UNLIMITED

NEITHER THE U.S. GOVERNMENT NOR ANY OF ITS EMPLOYEES
MAKES ANY WARRANTY EXPRESS OR IMPLIED OR ASSUMES ANY LEGAL LIABILITY
OR RESPONSIBILITY FOR THE ACCURACY, COMPLETENESS, OR USEFULNESS
OF ANY INFORMATION, APPARATUS, PRODUCT, OR PROCESS DISCLOSED OR
REPRESENTS THAT ITS USE DOES NOT INFRINGE UPON PRIVATELY OWNED RIGHTS.

TABLE OF CONTENTS

	Page
VOLUME III - TECHNICAL SESSIONS	
MODELING	772
A Mathematical Model for Simulation of AFBC Systems: J.W. Wells, R.P. Kirshnan, C.E. Ball, Oak Ridge National Laboratory, Oak Ridge, Tennessee	773
Modeling of Flow Behavior and Finned Tube Performance in the Turbulent Flow Regime: F.W. Staub, M. Kuwata, A.C. Ku, R.T. Wood, General Electric Company, Schenectady, New York	784
A Plume Model for Large Scale Atmospheric Fluidized Bed Combustors: D. Park, O. Levenspiel, T.J. Fitzgerald, Oregon State University, Corvallis, Oregon	791
A Technique to Project the Sulfur Removal Performance of Fluidized-Bed Combustors: R.A. Newby, N.H. Ulerich, D.L. Keairns, Westinghouse R&D Center, Pittsburgh, Pennsylvania	803
Cold Fluidized Bed Modeling: T.J. Fitzgerald, S.D. Crane, Oregon State University, Corvallis, Oregon	815
COMBUSTION AND BED PHENOMENA LOW GRADE FUEL COMBUSTION	821
Operational Application of Fluidized-Bed Furnaces in Burning Low-Calorific and Waste Fuels In Czechoslovakia: P. Knor, P. Novotny, Fuel Research Institute, Prague, CSSR	822
Combustion Characteristics of Anthracite Culm in a Fluidized Bed: A.W. Leon, P.J. Choksey, Dorr-Oliver Incorporated, Stamford, Connecticut	827
Fluidized-Bed Combustion of Israeli Oil Shale: J.S. Mei, J.Y. Shang, R.L. Rice, U. Grimm, J.S. Balow, U.S. Department of Energy, Morgantown, West Virginia, W.J. Ayers, Jr., EG&G, Morgantown, West Virginia; Y. Keren, IMI, Haifa, Israel	834
Combustion of Western Coal in a Fluidized Bed: W.T. Albe, R.L. Rice, J.Y. Shang, U.S. Department of Energy, Morgantown, West Virginia; W.J. Ayers, Jr., EG&G Morgantown, West Virginia; D.G. Turek, Science Applications, Inc., Morgantown, West Virginia	840
Atmospheric Fluidized Bed Combustion Testing of North Dakota Lignite: G. Goblirsch, Grand Forks Energy Technology Center/DOE, North Dakota; R.H. Vander Molen, Keith Wilson, Combustion Power Company, Menlo Park, California; D. Hajicek, Grand Forks Technology Center/DOE, North Dakota	850
Fluidized-Bed Combustion of North Dakota Lignite: R.L. Rice, J.Y. Shang, U.S. Department of Energy, Morgantown, West Virginia; W.J. Ayers, EG&G, Morgantown, West Virginia	863

Page

VOLUME III - Continued

Atmospheric Fluidized Bed Combustion of Municipal Solid Waste: Test Program Results: L.C. Preuit, K.B. Wilson, Combustion Power Company, Inc., Menlo Park, California 872

SORBENT UTILIZATION 884

Status of Research on Agricultural Uses of Fluidized Bed Combustion Residue: O.L. Bennett, W.L. Stout, J.L. Hern, R.L. Reid, U.S. Department of Agriculture in cooperation with the U.S. Department of Energy 885

Research Program to Assess the Impact of the Land Application of Fluidized Bed Combustion Residue on Human Nutrition: W.L. Stout, E. Fashandi, M.K. Head, R.L. Reid, O.L. Bennett, USDA-SEA and West Virginia University, Morgantown, West Virginia 892

Fluidized-Bed Combustion Residue Disposal: Environmental Impact and Utilization: C.C. Sun, C.H. Peterson, Westinghouse R&D Center, Pittsburgh, Pennsylvania 900

Utilization of the By-Products from Fluidized Bed Combustion Systems: L. John Minnick, Research Consultant, Devon, Pennsylvania; Richard H. Miller, Consultant, Devon, Pennsylvania; Richard H. Miller, Valley Forge Laboratories, Inc., Devon, Pennsylvania 913

Laboratory and Field Studies of Pressurized FBC Waste Leachate Generation and Attenuation: T.W. Grimshaw, D.N. Garner, W.F. Holland, Radian Corp., Austin, Texas; D.A. Kirchgessner, EPA Industrial Environmental Research Laboratory, Research Park Triangle Park, North Carolina 925

Use of Fluidized Bed Combustion Spent Sorbent in Energy Forrest Production and Agriculture: D.A.A. Arthursson, K. Valdman, Arthursson-Laboratoriet, Enkoeping, Sweden 939

ENVIRONMENTAL EMISSIONS NO_x AND SO_2 EMISSIONS 941

NO Formation and Reduction in Fluidized Bed Combustion of Coal: J.M. Beer, A.F. Sarofim, Y.Y. Lee, Massachusetts Institute of Technology, Cambridge, Massachusetts 942

NO_x Control through Staged Combustion in Fluidized-Bed Combustion Systems: T.E. Taylor, Foster Wheeler Development Corporation, Livingston, New Jersey 957

Research and Development of NO_x Emission Abatement in a Fluidized Bed Coal Combustor in Japan: M. Horio, Nagoya University, Japan; S. Mori, Nagoya Institute of Technology, Japan; T. Furusawa, University of Tokyo, Japan; S. Tamanuki, Japan Coal Mining Research Center, Tokyo, Japan 968

Page

VOLUME III - Continued

Control of Sulfur Dioxide and Nitrogen Oxide Emissions by Battelle's Multisold Fluidized-Bed Combustion Process: H. Nack, Battelle, Columbus, Ohio; K.T. Liu, Gulf Science & Technology Company; C.J. Lyons, Battelle, Columbus, Ohio 979

Simultaneous NO_x and SO_2 Emission Reduction with Fluidized Bed Combustion: J. Tatebayashi, Y. Okada, S. Ikeda, Kawasaki Heavy Industries, Ltd., Osaka, Japan 986

SORBENT EFFECTIVENESS 996

Sulfur Capturing Effectivity of Limestone and Dolomites in Fluidized Bed Combustion: H. Munzner, B. Bonn, Bergbau-Forschung GmbH, Essen, Federal Republic of Germany 997

Agglomeration Methods of Improving FBC Sorbent Utilization and Combustion: P.G. Dunne, Pope, Evans & Robbins, Inc., Alexandria, Virginia; L.L. Gasner, University of Maryland, College Park, Maryland 1004

Hydration Process for Reactivating Spent Limestone and Dolomite Sorbents for Reuse in Fluidized-Bed Coal Combustion: J.A. Shearer, G.W. Smith, D.S. Moulton, E.B. Smyk, K.M. Myles, W.M. Swift, I. Johnson, Argonne National Laboratory, Argonne, Illinois 1015

Natural Sorbent Attrition Studies Related to Fluidized Bed Coal Combustion: J.F Franceschi, A. Kolar, G. Miller, V. Zakkay, C. Ho, W. Skelley, S. Hakim, New York University, Westbury, New York 1028

An Assessment of Advanced Sulfur Removal System for Electric Utility AFBC: R.A. Newby, D.W. Bachovchin, C.H. Peterson, N.D. Rohatgi, N.H. Ulerich, D.L. Keairns, Westinghouse R&D Center, Pittsburgh, Pennsylvania 1044

Regeneration Portland Cement Sorbents for Fluidized-Bed Combustion of Coal: A.S. Albanese, D. Sethi, M. Steinberg, Brookhaven National Laboratory, Upton, New York 1060

MODELING 1069

An In-Situ Model of Fluidized Bed Coal Combustion: S. Rajan, D. Dey, Southern Illinois University, Carbondale, Illinois 1070

A Radiative Packet Model for Heat Transfer in Fluidised Beds: K.K. Pillai, National Coal Board, Leatherhead, England 1081

The Effects of Devolatization Kinetics on the Injector Region of Fluidized Beds: R.J. Bywater, The Aerospace Corporation, El Segundo, California 1092

Page

VOLUME III - Continued

Ignition and Extinction Characteristics of Atmospheric Fluidized Bed Coal Combustors: J.P. Congalidis, C. Georgakis, Massachusetts Institute of Technology, Cambridge, Massachusetts 1103

A Fluidized Bed Combustor Freeboard Model: C.Y. Wen, L.H. Chen, West Virginia University, Morgantown, West Virginia 1115

Char Combustion in the Freeboard Region: S.E. Tung, T.Z. Chaung, P.K. Sharma, J. Hodges, J.F. Louis, Massachusetts Institute of Technology, Cambridge, Massachusetts 1131

A Mathematical Model for Char Combustion in a Fluidized Bed: S.C. Saxena, A. Relmat, Argonne National Laboratory, Argonne, Illinois 1138

HEAT TRANSFER, INSTRUMENTATION AND CONTROL 1151

Design Relationships for Predicting Heat Transfer to Tube Bundles in Fluidized Bed Combustors: L.R. Glicksman, N.A. Decker, Massachusetts Institute of Technology, Cambridge, Massachusetts 1152

An Investigation of the Influence of Bed Parameters on the Variation of the Local Radiative and Total Heat Transfer Coefficients Around an Embedded Horizontal Tube in a Fluidized Bed Combustor: R. Vadivel, V.N. Vedamurthy, Perarignar Anna University of Technology, Madras, India 1159

High Temperature Heat Transfer Studies in a Tube Filled Bed: L.P. Golan, G.V. LaLonde, S.C. Weiner, Exxon Research and Engineering Company, Florham Park, New Jersey 1173

Automatic Control of the Georgetown Atmospheric Fluidized-Bed Boiler: R.J. Divilio, Pope, Evans and Robbins, Alexandria, Virginia; R.L. Criswell, Foster Wheeler Energy Corporation, Livingston, New Jersey 1186

A Transient Sulfur Capture Model for a Fluidized Bed Combustor: K.J. Daniel, S.D. Finnigan, General Electrical Company, Schenectady, New York 1196

ENVIRONMENTAL EMISSIONS 1235

Update on Emission Measurements from Fluidized-Bed Combustion Facilities: P.F. Fennelly, R.R. Hall, C.W. Young, J.M. Robinson, R.J. Kindya, G. Hunt, GCA Corporation, Bedford, Massachusetts 1236

Control of Particulate Emissions from Fluidized-Bed Combustion: Fabric Filters or Electrostatic Precipitators: D.V. Bubenick, D.C. Lee, R.R. Hall, P.F. Fennelly, GCA Corporation, Bedford, Massachusetts 1245

VOLUME III - Continued

	Page
The Response of Hot-Side Electrostatic Precipitators and Fabric Filters to Fluidized Bed Combustors: N.Z. Shilling, W.J. Morris, Envirotech Corporation, Lebanon, Pennsylvania	1260
Physical, Chemical and Biological Characterization of AFB Coal Combustion Effluents: C.H. Hobbs, A.L. Brooks, R.L. Carpenter, C.R.C Clark, P.B. DeNee, R.L. Hanson, R.F. Henderson, J.O. Hill, G.J. Newton, S.J. Rothenberg, S.H. Weissman, H.C. Yeh, Inhalation Toxicology Research Institute, Albuquerque, New Mexico	1274
Comprehensive Characterization of Emissions from a 6' x 6' Atmospheric Fluidized Bed Combustion System: J.E. Howes, Jr., S.E. Miller, Battelle Columbus Laboratories, Columbus, Ohio; T. Modrak, Babcock and Wilcox Research Center, Alliance, Ohio; C. Aulisio, Electric Power Research Institute, Palo Alto, California.	1284

THIS PAGE

WAS INTENTIONALLY

LEFT BLANK

A MATHEMATICAL MODEL FOR SIMULATION OF AFBC SYSTEMS*

J. W. Wells, R. P. Krishnan, C. E. Ball**

Oak Ridge National Laboratory
Oak Ridge, Tennessee 37830

Oak Ridge National Laboratory (ORNL) at present is providing technical support to the Tennessee Valley Authority (TVA) in their atmospheric fluidized bed combustion (AFBC) demonstration plant program. As a part of this program, ORNL is developing a steady state model which can be used to predict the performance of AFBC systems. This paper describes the progress made to date in the steady state AFBC mathematical modeling activities at ORNL. The objective of the modeling task is to develop a flexible predictive code that can be used to simulate performance of the Tennessee Valley Authority/Electric Power Research Institute (TVA/EPRI) pilot and demonstration plants under various operating conditions. The model will also be used in planning and developing experimental test programs for the 20 MW(e) TVA/EPRI pilot plant presently being designed.

The AFBC system model was originally developed at ORNL to analyze the proposed design of the Department of Energy Component Test and Integration Unit (CTIU) at Morgantown, West Virginia. The design of the CTIU called for multiple heat exchanger equipment arrangements and multiple operating conditions. In order to simulate such a configuration, a flexible system code was developed. This code contains several computer routines to perform the material and energy balances for the steam side and coal side of the AFBC. The major routines used in the system code are:

1. material balance,
2. energy balance,
3. physical and thermodynamic properties,
4. heat transfer coefficients,
5. output, and
6. control routines.

In this code the AFBC main cell is divided into the following sections (see Fig. 1):

1. plenum,
2. bed (dense region),
3. less dense region,
4. freeboard, and
5. freeboard bundle.

These sections represent operations or phenomena which are known to occur on the coal side of a typical AFBC. Each of these sections is further divided into indices. For each index or group of indices, the geometry of the heat transfer surface is read in. Appropriate correlations (depending on the type and location of heat duties) are used to calculate the overall heat transfer coefficients in each segment. The material balance calculations are based on user-supplied data. The results from a typical material balance of a multicell AFBC are shown in Fig. 2.

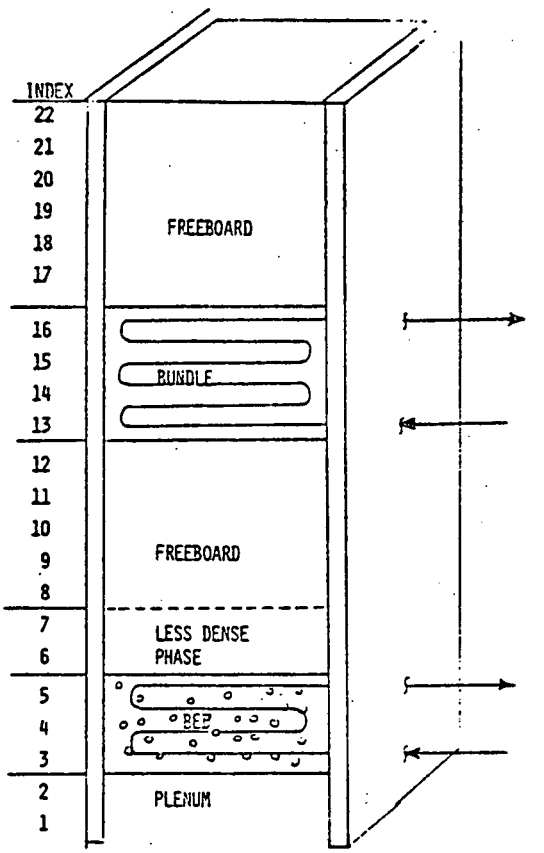

Fig. 1. Schematic showing breakdown of AFBC cell into input indicies.

At present, the overall AFBC system code does not contain predictive subcodes to calculate bubble hydrodynamics, sorbent/coal-ash attrition and elutriation, coal combustion, sorbent utilization and freeboard reactions. These are assumed (user supplied) to complete the material and energy balances of the incoming and outgoing streams in each segment of the AFBC. In the past year, efforts have been initiated to develop the predictive subcodes which will eventually be incorporated

*Research sponsored by Tennessee Valley Authority under Interagency Agreement TV-48296A, Subagreement 5, under Union Carbide Corporation Contract W-7405-eng-26 with the U.S. Department of Energy.

**Employed by Tennessee Valley Authority, Chattanooga, Tennessee 37401.

By acceptance of this article, the publisher or recipient acknowledges the U.S. Government's right to retain a nonexclusive, royalty-free license in and to any copyright covering this article.

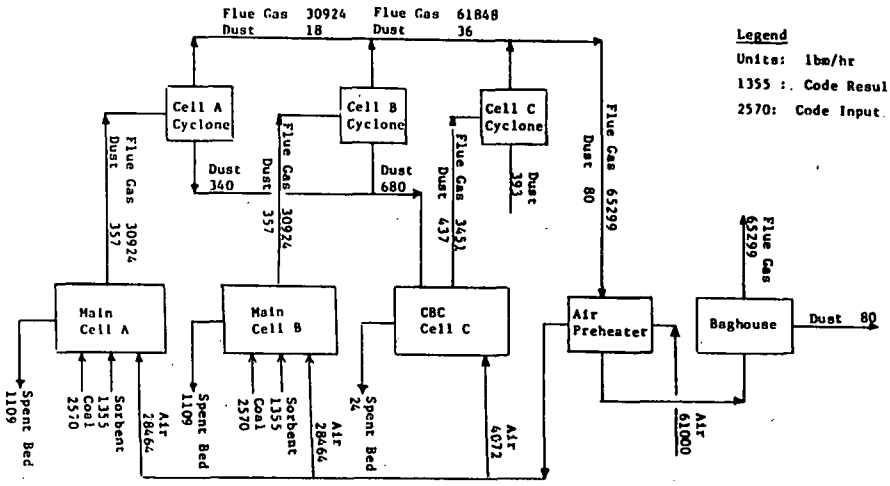

Fig. 2. Typical overall AFBC material balance results.

into the overall system code. Three predictive subcodes developed during calendar year 1979 are:

1. bubble growth,
2. sorbent/coal-ash elutriation and attrition, and
3. coal combustion.

These subcodes are discussed next under the appropriate headings.

Bubble Growth Subcode

Simulation of fluid bed combustors requires the accurate prediction of bubble size and bubble growth in the bed. The mass transfer of gas between the bubble phase and emulsion phase is a strong function of bubble size. The prediciton of bubble size is necessary for the calculation of combustion efficiency (coal utilization) and sulfur capture in fluid bed combustors. The solids mixing and elutriation from the bed are dependent on bubble properties. As a consequence, the size of the bubble is of primary importance in the scale up of fluidized beds [Werther (1978), Botton (1966)]. Many bubble growth correlations have been proposed for small particles and low superficial velocities [Mori and Wen (1975), Cranfield and Geldart (1974), Werther (1978)]. Analysis of these correlations shows that they are valid only for a limited range of operating conditions. They are inadequate for the large particles and high superficial velocities typical of fluidized bed combustion.

The bubble growth subcode developed in this work relates bubble growth to bed expansion. Bubble growth in fluidized beds is caused by the decrease in hydrostatic pressure as the bubble rises, one bubble overtaking another vertically, and one bubble combining with another horizontally. Bed expansion is caused by the formation and coalescence of bubbles and the expansion of the emulsion phase. This implies that the bed expansion is related to the bubble diameter and bubble growth. After a review of the literature, the correlation for bed expansion proposed by Babu et al. (1978) was selected. A comparison of bed expansion results obtained from this correlation with experimental data [Modrak et al. (1978) and Canada et al. (1978)] is shown in Figs. 3 and 4. While the agreement is not consistently good in all cases, the correlation does seem to predict the right trend.

From two-phase theory the average bed bubble voidage is related to bed expansion by

$$\bar{\epsilon}_B = 1 - (L_{mf}/L_f) . \qquad (1)$$

L_f/L_{mf} in this work is given by the bed expansion relation of Babu et al. (1978).

$$L_f/L_{mf} = 1 + \frac{1.9544(U_o - U_{mf})^{0.738} d_p^{1.006} \rho_s^{0.376}}{(U_{mf})^{0.937} \rho_g^{0.126}} . \qquad (2)$$

U_{mf}, which is the minimum fluidization velocity, is calculated from the equation given by Wen and Yu (1966).

$$U_{mf} = \frac{\mu}{d_p \rho_g} \left\{ \left[(33.7)^2 \times \frac{0.0408 d_p^3 \rho_g (\rho_s - \rho_g) g}{\mu^2} \right]^{0.5} - 33.7 \right\} \qquad (3)$$

where d_p is the mean particle diameter given by

$$d_p = \frac{1}{\sum \text{all } i (x_i / d_{pi})} . \qquad (4)$$

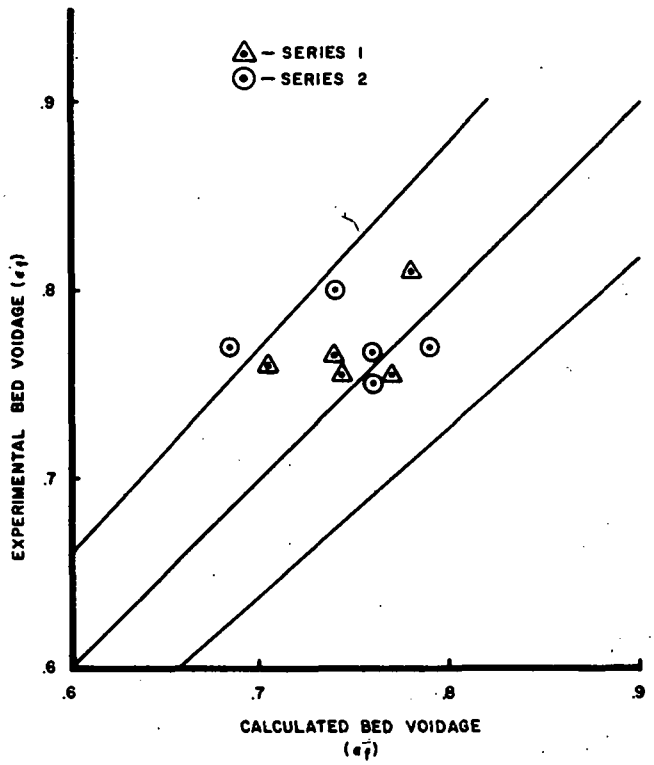

Fig. 3. Comparison of bed expansion data from Modrak et al. (1979) to calculated values from Eq. 2.

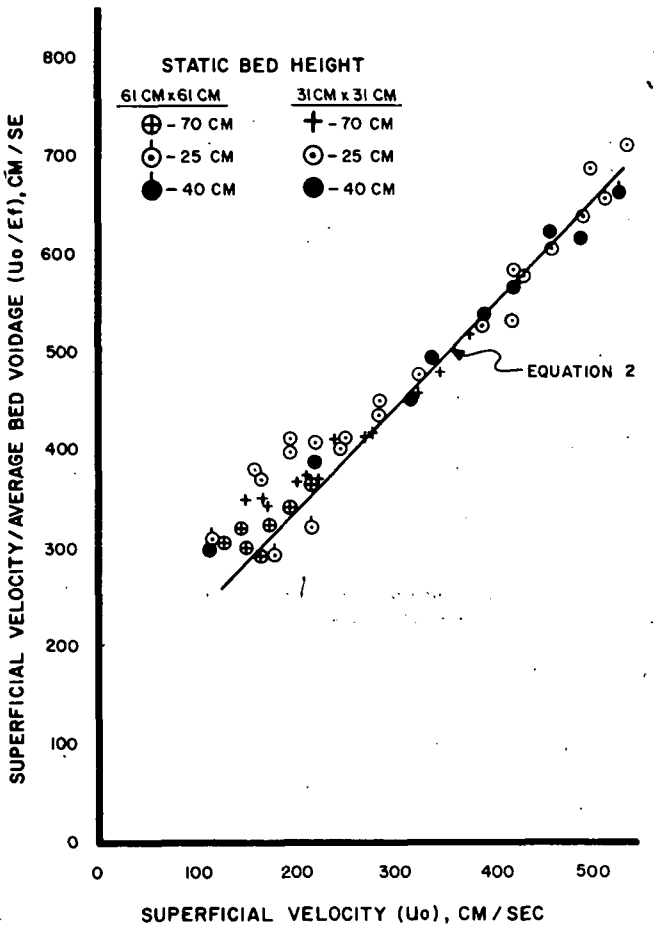

Fig. 4. Comparison of bed expansion data from Canada et al. (1978) for 2600 μparticles to results from Eq. 2.

Average bubble voidage ($\bar{\epsilon}_B$) can also be related to the bubble diameter [Wells and Krishnan (1980)] as,

$$\bar{\epsilon}_B = \frac{1}{L_f} \int_o^{L_f} \frac{V_B''}{\psi\sqrt{g d_B}}\, dZ , \tag{5}$$

ψ is volumetric flux through the bubble phase and is obtained from Eq. 6 [Cranfield and Geldart (1974)].

$$V_B'' = 0.363(U_o - U_{mf})^{1.11} Z^{0.09} . \tag{6}$$

ψ is a constant related to the reactor diameter [Werther (1978)].

$$\psi = \begin{cases} 0.64 & D_t \leq 10 \text{ cm} \\ 0.225\,(D_t)^{0.4} & 10 < D_t \leq 100 \text{ cm} \\ 1.6 & D_t > 100 \text{ cm} \end{cases} \tag{7}$$

The calculation of $\bar{\epsilon}_B$ from Eq. 5 requires a functional relation between bubble size d_B and height h. In this study the Mori and Wen (1975) form was chosen, viz

$$\frac{d_{BM} - d_B}{d_{BM} - d_{BO}} = \exp(-kZ/D_t) , \tag{8}$$

where

$$d_{BM} = 0.431 \left[\frac{A_{xs}\phi(U_o - U_{mf})}{\psi}\right]^{2/5} , \tag{9}$$

$$d_{BO} = 0.347[A_{xs}(U_o - U_{mf})/n_d]^{2/5} . \tag{10}$$

The expression for d_{BM} has been modified in this study for large particle and high superficial velocity systems [Wells and Krishnan (1980)].

Equations 1 and 5 permit calculation of the average bubble voidage in the AFBC by two different approaches with an adjustable parameter k in Eq. 8. The value of k is varied until $\bar{\epsilon}_B$ calculated via Eq. 1 agrees with $\bar{\epsilon}_B$ calculated from Eq. 5.

Fig. 5 shows a comparison between this technique and other correlations for bubble growth under typical AFBC conditions. Although one cannot establish the accuracy of any of these methods without experimental data, a number of parametric studies using the present method does indicate the validity of the approach. The preliminary results [Wells and Krishnan (1980)] also indicate that the method is reasonable, provided one can estimate bed expansion accurately.

Elutriation and Attrition Subcode

In fluidized bed combustion, the major loss in combustion efficiency is due to elutriation of unburned carbon fines in the flue gas. The fine particles may come directly from the feed or be generated in the bed by attrition. It is necessary to recover these fines in order to maintain a high combustion efficiency. Also, the amount of fines and their size distribution should be known in order to properly design the solids removal system. These considerations dictate the need for accurate estimation of the attrition and elutriation rates of the bed material.

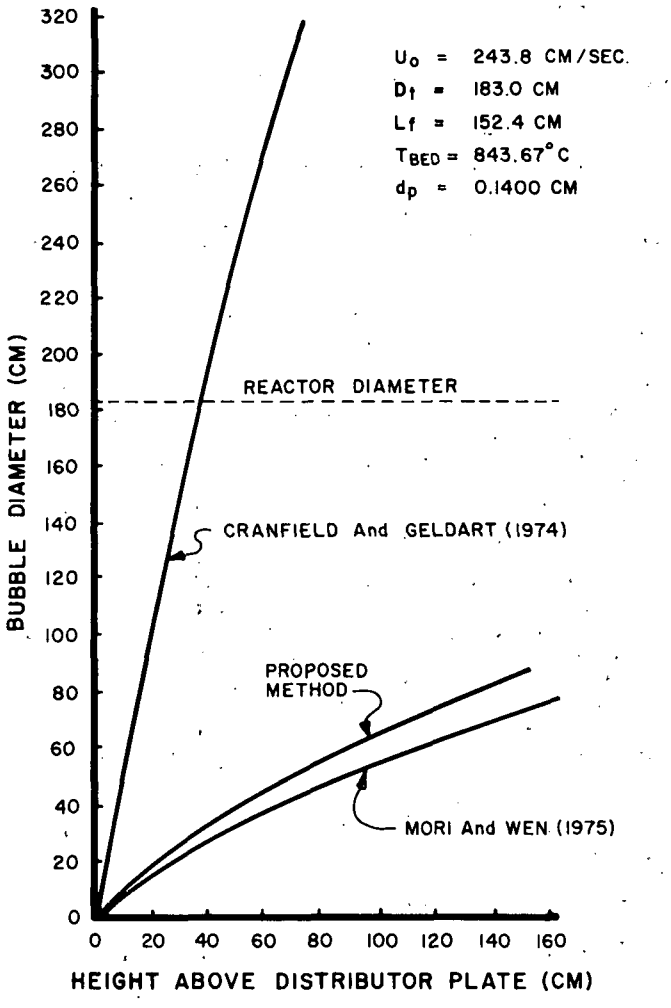

Fig. 5. A comparison of bubble growth relations.

Experimental data on attrition and elutriation rates obtained in both batch and continuous fluidized bed reactors have been correlated by several investigators. These correlations have been reviewed by Geldart et al. (1979). Except for the Merrick and Highley (1974) and Wen and Hashinger (1960) correlations, all others were developed for solids other than coal char, limestone, and coal-ash. Although the Merrick and Highley and Wen and Hashinger correlations are system specific, they can be used to develop a mathematical model for attrition and elutriation.

The limestone/coal-ash attrition and elutriation subcode is based on the following assumptions. First, the system is assumed to be at steady state, i.e., time invariant. Second, the solids in the fluid bed are assumed well mixed. Third, the attrition rate expressions of Merrick and Highley (1974) apply for the limestone and coal-ash particles, i.e.,

$$F_{att} = K_{att}(U_o - U_{mf})W_B \,, \tag{11}$$

$$dr/dt = k_{att}f_{fp}(U_o - U_{mf})r \,. \tag{12}$$

Fourth, the particle entrainment rate constants for limestone and coal-ash are obstained from the Merrick and Highley correlation (1974).

$$K(r) = [A + 130\exp\{-10.4[U_t(r)/U_o]^{0.5} [U_{mf}/(U_o - U_{mf})]^{0.25}\}] \times \frac{\rho_g U_o A_{xs}}{W_B} \tag{13}$$

Fifth, the elutriation and attrition of the limestone and coal-ash are assumed independent of each other. Sixth, the fines produced by attrition of a particle in the bed are assumed to be less than 125μm and are immediately entrained. Finally, the bed expansion is predicted by Eq. 2. The Merrick and Highley expressions were developed from National Coal Board data obtained in a 305 cm × 305 cm AFBC with a 4m freeboard at superficial velocities from 122 to 244 cm/sec. These rate expressions are system specific and do not account for differences in feed system, freeboard configuration, etc. They do, however, account for bed and freeboard hydrodynamics. At present, the work of Merrick and Highley represents the best available correlation for the estimation of attrition and elutriation. The performance of the limestone and coal-ash solids in the fluid bed is determined by the following quantities.

1. Bed mass (W_B).
2. Differential bed size distribution (p_B).
3. Underflow rate (F_1).
4. Differential underflow size distribution (p_1).
5. Elutriated solids flow rate (F_2).
6. Differential elutriated solids size distribution (p_2).
7. Attrition fines flow rate (F_{att}).
8. Differential attrition fines size distribution (p_A).

The information required to find these quantities are the solids and gas physical properties, the feed rates (F_o) and size distribution of the solids in the feed (p_o), the superficial gas velocity, and the dimensions of the bed.

Based on the above assumptions, the following governing equations were developed to determine bed performance. The total mass of limestone and coal-ash solids in the bed is given by

$$W_B = L_{mf}A_{xs}(1 - \epsilon_{mf})\rho_s \,. \tag{14}$$

The bed height at minimum fluidization is determined from Eq. 2. The overall material balance and differential mass balance on particles between sizes r and r + dr are given by Eqs. 15 and 16, respectively.

$$F_1 + F_2 - F_0 = F_{att} = \int_{all\ r} \frac{3W_B p_B(r)\dot{R}(r)dr}{r} \tag{15}$$

$$F_o p_o(r) - F_1 p_1(r) - W_B K(r) p_B(r) - W_B \frac{d[\dot{R}(r)p_B(r)]}{dr} + \frac{3W_B p_B(r)\dot{R}(r)}{r} = 0 \,. \tag{16}$$

From the second assumption,

$$p_B(r) = p_1(r) \,. \tag{17}$$

The differential mass balance can then be written as

$$dp_B(r)/dr = \frac{F_o p_o(r)}{W_B \dot{R}(r)} - \left[\frac{F_1}{W_B \dot{R}(r)} + \frac{K(r)}{\dot{R}(r)} + \frac{1}{\dot{R}(r)}\frac{d\dot{R}(r)}{dr} - \frac{3}{r}\right] p_B(r) \tag{18}$$

and finally by definition of differential particle size distribution

$$\int_{all\ r} p_B(r)dr = 1 \,. \tag{19}$$

In the above equations

$$\dot{R}(r) = \frac{dr}{dt} \,. \tag{20}$$

and is given by Eq. 12. The term K(r) represents the elutriation constant given by Eq. 13. Because of the functional form of Eq. 12, the attrition rate decreases as the radius of the particle decreases. For some radius r (usually less than 500 μm) the attrition rate becomes negligible. At this point Eq. 16 can be simplified as follows.

$$p_B(r) = \frac{F_o p_o(r)}{F_1 + W_B K(r)} \,. \tag{21}$$

Equations 18 through 20 apply to both coal-ash and limestone in the bed. F_1, F_2, W_B, and F_{att} are obtained separately for both coal-ash and sorbent. The total mass flow rates of product streams are the summation of the ash and sorbent.

A typical output obtained from the code is given in Table 1. The comparison of the results with experimental data from the Babcock and Wilcox (B&W)/EPRI 183 cm × 183 cm AFBC unit is shown in Table 2. The model underpredicts the total solids "blown out" of the bed by 23% and underpredicts the total overflow from the bed by 36% (Table 2). The material balance closure is acceptable within ±10% for both coal-ash and limestone. A preliminary calculation of the attrition rate based on the estimate given by Newby et al. (1978), roughly 4% of the bed weight attrited in an hour, yields an attrition rate for the bed of 36.5 g/sec as compared to 15.8 g/sec predicted by the model. These differences are to an extent due to the uncertainty in the rate constants appearing in the attrition-elutriation correlations used in the code.

Figure 6 shows typical calculated size distribution curves. From this figure the effects of attrition and recycle on bed particle size distribution may be seen. When the rate constant for attrition is increased from 2.73×

Table 1. Output from Limestone-Coal-Ash Elutriation and Attrition Code

Definition	Variable Name	Limestone	Coal Ash
Underflow	F_1	66.3 g/sec (526.3 lbm/hr)	5 g/sec (39.4 lbm/hr)
Elutriated solids	F_2	12.5 g/sec (99.2 lbm/hr)	8.7 g/sec (69.0 lbm/hr)
Attrited solids	F_{att}	15.8 g/sec (125.4 lbm/hr)	3.3 g/sec (26.2 lbm/hr)
Bed mass	W_B	3,218,366 g (7095.2 lbm)	214,834 g (473.6 lbm)
Surface mean particle size	d_p	1550 μm (0.061 in.)	1062 μm (0.042 in.)

Table 2. Comparison of Attrition-Elutriation Code Results with B&W's Data

Quantity	B&W	ORNL	% Difference
Total solids "blown out"	52.4 g/sec (415.9 lbm/hr)	40.3 g/sec (319.8 lbm/hr)	23.1
Percent feed limestone-ash solids "blown out"	47.0%	36.3%	—
Bed mass	3.295×10^6 g (7264.1 lbm)	3.433×10^6 g (7568.3 lbm)	4.0
Underflow	52.5 g/sec (417 lbm/hr)	71.3 g/sec (565.87 lbm/hr)	36.0
Total limestone and coal ash feed	111.4 g/sec (884 lbm/hr)	111.4 g/sec (884 lbm/hr)	0
Total sorbent and coal ash leaving bed	105 g/sec (834 lbm/hr)	111.6 g/sec (886 lbm/hr)	6.3
Closure on material balance	−5.7%	0.2%	—

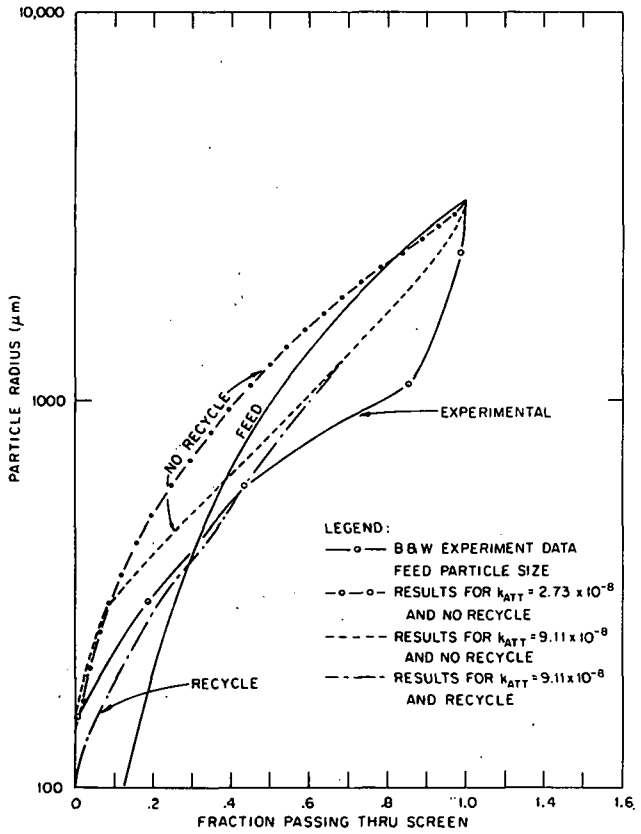

Fig. 6. Effect of the limestone attrition rate constant and recycle on bed particle size distribution.

10^{-8} to 9.11×10^{-8} cm^{-1}, the mean bed particle size is reduced. Also, the recycle of particles larger than 200 μm causes the number of particles in the bed smaller than 1400 μm to increase. The comparison of these results with the B&W/EPRI 183 cm × 183 cm AFBC bed particle size distribution shows that a much higher attrition rate exists in the B&W system.

Analysis of the B&W series 5 and series 6 data seemed to indicate that the attrition is strongly influenced by the feed system design of the AFBC. For example, the series 6 data can be correlated by the following expression.

$$F_{att} = 6.74(d_{pf})^{0.5} U_o \tau^{-1.224} . \quad (22)$$

However, Eq. 22 does not fit the series 5 data (Fig. 7). Between these two series, the feed system was modified by B&W which might have altered the attrition rate in the system. The analysis of the data further revealed that the bed size distribution starts at around 300 μm and above for all the runs and the cylcone catch is always less than 300 μm. This is contrary to data reported in the literature by Merrick and Highley (1974) and Geldart (1979). Based on their estimates, the bed particle size distribution for the B&W operating conditions should be around 600 μm. A possible explanation for the contradiction is the presence of freeboard tube bundles in the B&W/EPRI unit. These cooling bundles act as a baffle and lower the flue gas temperature (1144 to 644° K) resulting in a lower flue gas velocity. As a result, particles larger than 300μm but smaller than 600μm may be trapped in the bed freeboard convective section and attrited down to 300 before they are released to the cyclone. The experimental bed size distribution of the B&W/EPRI system (Fig. 6) has a shape similar to what was observed by Merrick and Highley with fines recycle. Although the B&W data were obtained with no fines recycle, it is possible that freeboard cooling might have resulted in an indirect recycle of the fines to the bed.

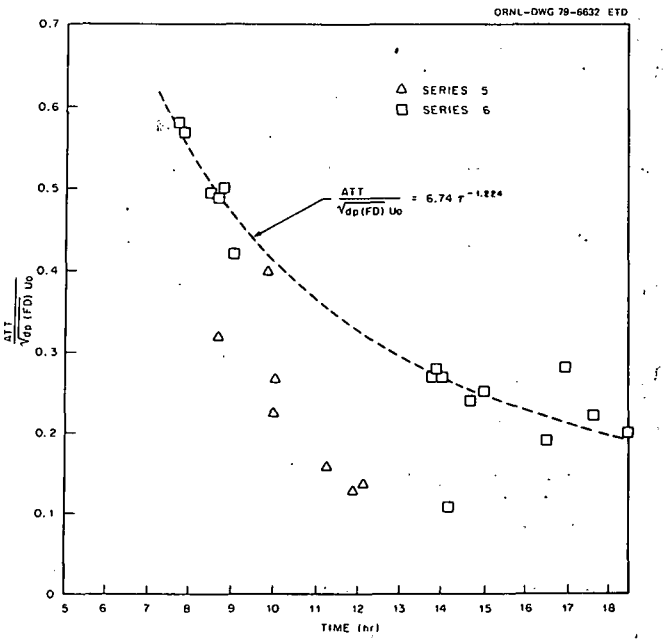

Fig. 7. Effect of feed system changes on attrition rate.

Coal Combustion Subcode

Many parameters (operational and geometric) affect the heat release and coal utilization in an AFBC. The main purpose of a combustion model is to predict the amount of coal consumed in an AFBC at a given set of conditions. The coal utilization rate is affected by bed hydrodynamics, solids mixing, solids attrition and elutriation, and the kinetics of chemical reactions (devolatilization and combustion).

A schematic of the ORNL combustion subcode is shown in Fig. 8. Several assumptions are made in developing the coal combustion subcode. The fluidized bed consists of the emulsion phase and the bubble phase. The solids present in the emulsion phase are assumed to be well mixed (back mix), and the voidage in the emulsion phase is assumed to be

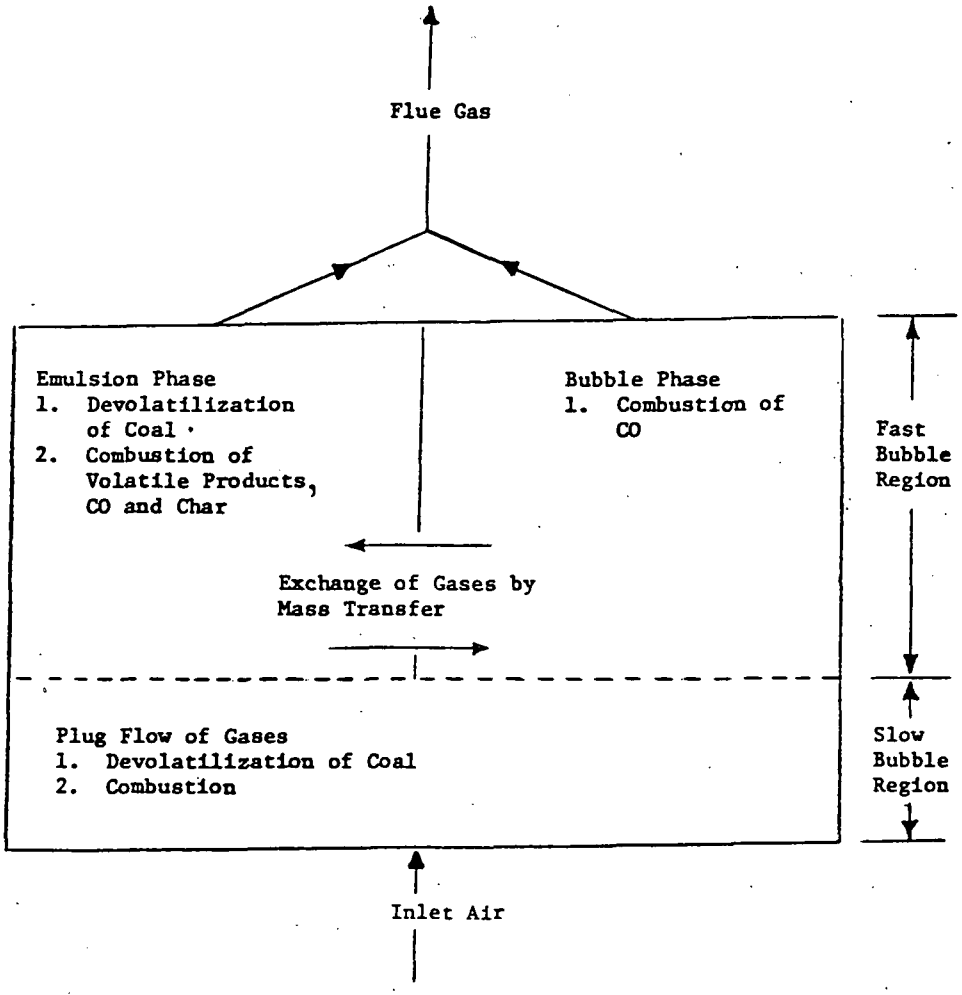

Fig. 8. Schematic of combustion model.

the voidage corresponding to minimum fluidization. The gas is assumed to flow through the emulsion phase in the upward direction in plug flow, with its velocity corresponding to the minimum fluidization velocity. The reactions considered in the emulsion phase are:

1. $C + \frac{1}{2} O_2 \rightarrow CO$
2. $CO + \frac{1}{2} O_2 \rightarrow CO_2$
3. $CO_2 + C \rightarrow 2CO$
4. Devolatilization.

The devolatilization reaction is assumed to occur uniformly throughout the emulsion phase. For the prediction of the amount of carbon in the volatiles released, the pyrolysis models of Suuberg et al. (1977) and Reklaitis et al. (1977) developed for Montana lignite and Illinois No. 6 bituminous coal, respectively, are used. The carbon released during devolatilization is assumed to form carbon monoxide (CO) instantaneously. The carbon monoxide is then consumed by reaction 2. The resulting char is consumed by reactions 1 and 3. Reactions 1 and 3 are heterogeneous gas-solid reactions. Their overall rates, therefore, are dependent on both the chemical reaction rate at the solid surface (intrinsic) and the mass transfer rate of gaseous species to the solid surface. Specifically, it is assumed that oxygen and carbon dioxide are transferred to the surface of the particle where they undergo reactions 1 and 3, respectively. The product carbon monoxide then diffuses back into the interstitial spaces where it is consumed by reaction 2. The intrinsic rate for reaction 1 is based on the bituminous kinetics of Smith (1971). For the Boudard reaction (reaction 3) the estimate given by Caram and Amundson (1977) and modified by Horio et al (1977) is used. The rate expressions for gas species mass transfer to the surface is obtained from Field et al. (1967). The kinetics for the gas phase reaction (reaction 2) is obtained from Horio et al. (1977). These expressions are summarized in Table 3. The particle surface temperature is calculated via a heat balance between the particle and surrounding gas as given by Smith (1971).

In addition to the emulsion phase, the bubble phase is also considered in the subcode. The bubbles are assumed to have a very thin cloud and are devoid of solids. The only reaction occurring in the bubble phase is the combustion of carbon monoxide (reaction 2). The rate constant for this reaction is given in Table 3. The interchange coefficient between the bubble phase and the emulsion phase is estimated from the Davidson model [Davidson and Harrison (1963)] and is given by

$$K_{BE} = [4.5(U_{mf}/d_B)] + [(5.85D^{1/2}g^{1/4})/(d_B^{5/4})] \quad (31)$$

The bubble size and bubble velocity are estimated from the ORNL bubble growth subcode described earlier. The bubble phase is also assumed to contain fast and slow bubbles [Catapovic et al. (1978)]. The elutriation rate constant for char is given by the Wen and Hashinger (1960) expression.

Table 3. Reaction rate expressions

Chemical Reaction Rate Constants (intrinsic)

1. $C + \frac{1}{2} O_2 \rightarrow CO$: $k_1^I = .667\ EXP(-16000/R_G T_p)$ [=] $\frac{\text{gmoles of carbon consumed}}{\text{cm}^2\text{-sec-atm}}$ (23)

2. $CO + \frac{1}{2} O_2 \rightarrow CO_2$: $k_2^I = 1.3 \times 10^{14}\ EXP(-30000/R_G T_G)$ [=] $\frac{\text{cm}^3 \text{ of gas}}{\text{gmoles sec}}$ (24)

3. $CO_2 + C \rightarrow 2CO$: $k_3^I = \frac{4.1 \times 10^{10}}{R_{GG} T_G} EXP(-59200/R_G T_G)$ [=] $\frac{\text{gmoles of carbon consumed}}{\text{cm}^2\text{-sec-atm}}$ (25)

Mass Transfer Reaction Rate Constants

1. $C + \frac{1}{2} O_2 \rightarrow CO$: $k_1^M = \frac{4D}{d_p R_{GG} T_G}$ [=] $\frac{\text{gmoles of carbon consumed}}{\text{cm}^2\text{-sec-atm}}$ (26)

2. $CO + \frac{1}{2} O_2 \rightarrow OC_2$: $K_2^M = 0$

3. $CO_2 + C \rightarrow 2CO$: $k_3^M = \frac{2D}{d_p R_{GG} T_G}$ [=] $\frac{\text{gmoles of carbon consumed}}{\text{cm}^2\text{-sec-atm}}$ (27)

Overall Reaction Rate Constant

1. $C + \frac{1}{2} O_2 \rightarrow CO$: $R_1^T = \frac{1}{(1/k_1^I + 1/k_1^M)} C_{O_2}^{EMUL} R_{GG} T_G$ [=] $\frac{\text{gmoles of carbon consumed}}{\text{cm}^2\text{-sec}}$ (28)

2. $CO + \frac{1}{2} O_2 \rightarrow CO_2$: $R_2^T = k_2^I (C_{H_2O}^{EMUL})^{1/2} (C_{CO}^{EMUL}) (C_{O_2}^{EMUL})^{1/2}$ [=] $\frac{\text{gmoles of carbon monoxide consumed}}{\text{cm}^3 \text{ of gas-sec}}$ (29)

3. $CO_2 + C \rightarrow 2CO$: $R_3^T = \frac{1}{(1/k_3^I + 1/k_3^M)} C_{O_2}^{EMUL} R_{GG} T_G$ [=] $\frac{\text{gmoles of carbon consumed}}{\text{cm}^2\text{-sec}}$ (30)

$$K(r) = \frac{1.7 \times 10^{-5} \rho_B [U_o - U_t(r)] A_{xs}}{W_B} \times \{[U_o - U_t(r)]^2 / 2gr\}^{0.5} Re_t^{0.725} \times [(\rho_s - \rho_g)/\rho_g]^{1.15} [(U_o - U_t(r)/U_t(r)]^{0.1} \quad (32)$$

The validity of some of the above assumptions have not yet been established. The present combustion subcode is structured to allow relatively easy modification as more information becomes available.

The gas and char material balance equations are developed based on the above assumptions. These equations given in Tables 4 & 5 consider the devolatilization and subsequent combustion of the char. Table4 gives the equations for the slow bubble region, while Table 5 gives the equations for the fast bubble region of the bed. The solution of these equations gives the profiles of O_2, CO, and CO_2 in the bed.

The char side material balance is completed by solving the performance equations for the char particles. These equations are given by

$$F_1 + F_2 - F_o = \int_{\text{all r}} \frac{3 W_B p_B(r) \dot{R}(r) dr}{r}, \quad (48)$$

and the differential char mass balance is given by

$$F_o p_o(r) - F_1 p_1(r) - W_B K(r) p_B(r) - W_B \frac{d[\dot{R}(r) p_B(r)]}{dr} + \frac{3 W_B p_B(r) \dot{R}(r)}{r} = 0. \quad (49)$$

Table 4. Slow bubble region differential material balances

O_2 Balance

$$dC_{O_2}^{SB}/dZ = \frac{A_{xs}}{\dot{V}_T} \left[-\frac{1}{2} \sum_i^{\text{all r}} (R_1^T \xi_{plug})_i (1 - \delta) - \frac{1}{2} R_2^T \delta - \Phi_{O_2} \frac{(1 - \bar{\epsilon}_B)}{(1 - \bar{\delta})} (1 - \delta) \right] \quad (33)$$

CO Balance

$$dC_{CO}^{SB}/dZ = \frac{A_{xs}}{\dot{V}_T} \left\{ \left[\sum_i^{\text{all r}} (R_1^T \xi_{plug})_i + 2 \sum_i^{\text{all r}} (R_3^T \xi_{plug})_i \right] (1 - \delta) - R_2^T \delta + \Phi_{CO} \frac{(1 - \bar{\epsilon}_B)}{(1 - \bar{\delta})} (1 - \delta) \right\} \quad (34)$$

CO_2 Balance

$$dC_{CO_2}^{SB}/dZ = \frac{A_{xs}}{\dot{V}_T} \left[R_2^T \delta - \sum_i^{\text{all r}} (R_3^T \xi_{plug})_i (1 - \delta) \right] \quad (35)$$

Table 5. Fast bubble region differential material balances

Emulsion Phase O_2 Balance

$$dC_{O_2}^{EMUL}/dZ = \frac{1}{(1-\epsilon_B)}\left[(1/U_{mf})\,(dF_{O_2}^{EMUL}/dV) - C_{O_2}^{EMUL}\,\frac{d\,(1-\epsilon_B)}{dZ}\right] \tag{36}$$

where

$$dF_{O_2}^{EMUL}/dV = -(1/2)\left[\sum_i^{all\ r}(R_1{}^T\xi_{EMUL})_i + R_2{}^T\epsilon_{mf} + 2\Phi_{O_2}\right](1-\epsilon_B) + K_{BE}(C_{O_2}^{BUB} - C_{O_2}^{EMUL})\epsilon_B \tag{37}$$

Emulsion Phase CO Balance

$$dC_{CO}^{EMUL}/dZ = \frac{1}{1-\epsilon_B}\left[(1/U_{mf})\,(dF_{CO}^{EMUL}/dV) - C_{CO}^{EMUL}\,\frac{d(1-\epsilon_B)}{dZ}\right] \tag{38}$$

where

$$dF_{CO}^{EMUL}/dV = \left[\sum_i^{all\ r}(R_1{}^T\xi_{EMUL})_i + 2\sum_i^{all\ r}(R_3{}^T\xi_{EMUL})_i - R_2{}^T\epsilon_{mf} + \Phi_{CO}\right](1-\epsilon_B) \tag{39}$$

$$+ K_{BE}(C_{CO}^{BUB} - C_{CO}^{EMUL})\,\epsilon_B$$

Emulsion Phase CO_2 Balance

$$dC_{CO_2}^{EMUL}/dZ = \frac{1}{(1-\epsilon_B)}\left[(1/U_{mf})\,(dF_{CO_2}^{EMUL}/dV) - C_{CO_2}^{EMUL}\,\frac{d(1-\epsilon_B)}{dZ}\right] \tag{40}$$

where

$$dF_{CO_2}^{EMUL}/dV = \left[R_2{}^T\epsilon_{mf} - \sum_i^{all\ r}(R_3{}^T\xi_{EMUL})_i\right](1-\epsilon_B) + K_{BE}(C_{CO_2}^{BUB} - C_{CO_2}^{EMUL})\epsilon_B \tag{41}$$

Bubble Phase O_2 Balance

$$dC_{O_2}^{BUB}/dZ = (1/\dot{V}_B'')\left[(dF_{O_2}^{BUB}/dV) - C_{O_2}^{BUB}\,\frac{d\dot{V}_B''}{dZ}\right] \tag{42}$$

where

$$dF_{O_2}^{BUB}/dV = \left[-(1/2)R_2{}^T\epsilon_B - K_{BE}(C_{O_2}^{BUB} - C_{O_2}^{EMUL})\epsilon_B\right] \tag{43}$$

Bubble Phase CO Balance

$$dC_{CO}^{BUB}/dZ = (1/V_B'')\left[(dF_{CO}^{BUB}/dV) - C_{CO}^{BUB}\,(dV_B''/dZ)\right] \tag{44}$$

where

$$dF_{CO}^{BUB}/dV = -R_2{}^T\epsilon_B - K_{BE}(C_{CO}^{BUB} - C_{CO}^{EMUL})\epsilon_B \tag{45}$$

Bubble Phase CO_2 Balance

$$dC_{CO_2}^{BUB}/dZ = (1/\dot{V}_B'')\,(dF_{CO_2}^{BUB}/dV) - C_{CO_2}^{BUB}\,(d\dot{V}_B''/dZ) \tag{46}$$

where

$$dF_{CO_2}^{BUB}/dV = R_2{}^T\epsilon_B - K_{BE}(C_{CO_2}^{BUB} - C_{CO_2}^{EMUL})\epsilon_B \tag{47}$$

From experimental data, the char composition of the underflow (F_1) appears very small (about 0.1%). For this reason, the underflow (F_1) is set to zero, and the differential balance can then be written as

$$dp_B(r)/dr = \frac{F_o p_o(r)}{W_B \dot{R}(r)} - \left[\frac{K(r)}{\dot{R}(r)} + \frac{1}{\dot{R}(r)}\frac{d\dot{R}(r)}{dr} - \frac{3}{r}\right]p_B(r)\,. \tag{50}$$

and finally by definition of differential particle size distribution.

$$\int_{all\ r} p_B(r)dr = 1\,. \tag{51}$$

In the above equations, $\dot{R}(r)$ represents the rate of particle shrinkage due to combustion and is given by

$$\dot{R}(r) = dr/dt = \frac{\overline{R}_T(r)}{\rho_{char}} . \quad (52)$$

$\overline{R}_T(r)$ is the average rate of total char consumed per unit surface area of a particle of radius r and is given by

$$\overline{R}_T(r) = \sum_j^{N_h} [R_1^T(r) + R_3^T(r)]_j / N_h . \quad (53)$$

The output from the combustion subcode is shown in Table 6 and Fig 9. Table 6 gives a preliminary comparison of the results with data from the B&W/EPRI AFBC. As can be seen, the char elutriation rate (F_2) predicted by the code exceeds the measured value by 31%. Three possible reasons may exist for this discrepancy. First, the present subcode does not yet account for the carbon consumed in the freeboard. Second, the freeboard cooling may cause larger char particles to disengage from the flue gas and fall back to the bed. This increases the residence time of the char particle in the bed and results in improved carbon utilization.

Table 6. Comparison of combustion subcode results with B&W data

Quantity	Variable name	ORNL	B&W
Char bed weight	W_B	22745.3 g (50.11 lbm)	NA
Char weight percent in bed	PCB	0.7	NA
Char elutriation rate	F_2	19.2 g/sec (152.4 lbm/hr)	14.6 g/sec (116.1 lbm/hr)
Char underflow rate	F_1	0.0 g/sec	.06 g/sec (.5 lbm/hr)
Combustion efficiency, %	ETC	91.5	93.0

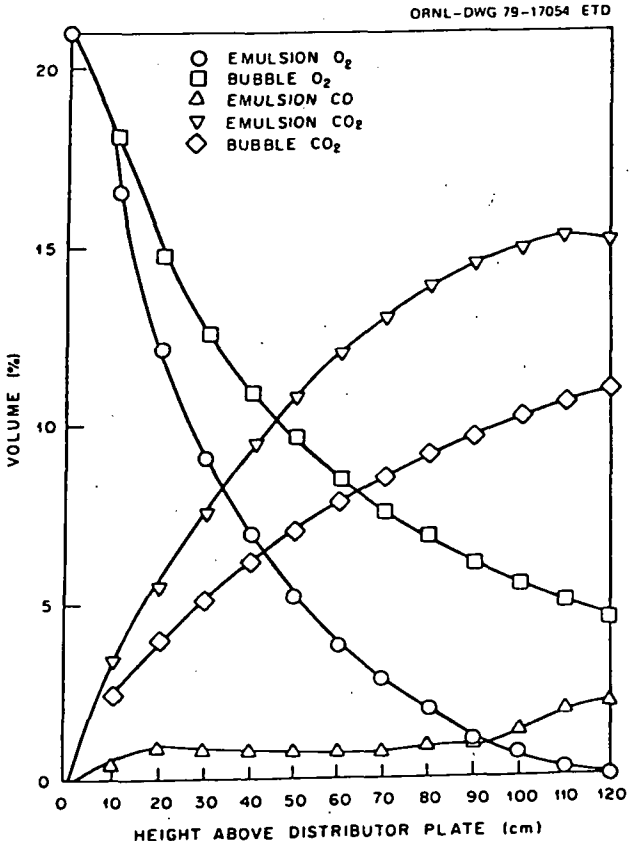

Fig. 9. Calculated gas phase profiles.

Third, the elutriation constant calculated from Wen and Hashinger's correlation may not be accurate. This correlation was developed at conditions different from a typical AFBC. Table 6 also shows that the assumption of no char in the underflow is justified due to the very small underflow rates measured by B&W. As can be seen, the predicted and measured values of the combustion efficiency agree within 1.6%. Figure 9 shows the predicted emulsion and bubble phase concentration profiles for O_2, CO, and CO_2 in the bed. The difference in the emulsion and bubble phase concentrations shown in this figure are due to the nature of the fast bubbles. In fast bubbles, the gas is essentially trapped and is only transferred to or from the emulsion phase by mass transfer. In the slow bubble region the gas is assumed to move in a uniform front (plug flow) with no observable concentration differences between the bubble and emulsion phases. At present very little experimental data are available for comparison with the computational results.

Conclusions

The overall AFBC system model described in this paper is a flexible code which will allow simulation of many different design configurations. At present this model does not incorporate predictive subcodes to calculate bubble hydrodynamics, solids elutriation, coal devolatilization and combustion, sulfur capture, and NO_x reduction. The bubble growth, elutriation and attrition, and coal combustion subcodes as described in this paper, have been developed and are being incorporated into the overall system model. At present efforts are underway to develop the sulfur capture and NO_x reduction subcodes. The model is constantly being tested and refined with operating AFBC data.

References

1. S. P. Babu, B. Shah, A. Talwalkar, AIChE Symposium Series, No. 176, Vol. 74, pp. 176–186, 1978.
2. R. J. Botton, AIChE Symposium Series, No. 101, Vol. 66, pp. 8–18, 1966.
3. G. S. Canada, M. H. McLaughlin, G. W. Staub, AIChE Symposium Series, No. 176, Vol. 74, pp. 14–26, 1978.
4. H. S. Caram, N. R. Amundson, *Ind. Eng. Chem. Fundam.*, Vol. 16, No. 2, pp. 171-181, 1977.
5. N. M. Catipovic, G. N. Jovanovic, T. J. Fitzgerald, *AIChE Journal*, Vol. 24, No. 3, pp. 543-547, 1978.
6. R. R. Cranfield, D. Geldart, *Chemical Engineering Science*, Vol. 29, pp. 935-947, 1974.
7. J. F. Davidson, D. Harrison, *Fluidized Particles*, University Press, Cambridge, 1963.
8. M. A. Field, D. W. Gill, B. B. Morgan, P. G. W. Hawksley, "Combustion of Pulverized Fuel, Part 4, Thermal Decomposition," The British Coal Utilization Research Association, 3(4), pp. 186-218, April 1967.
9. D. Geldart, "Gas Fluidization," Center for Professional Advancement, Somerville, New Jersey, 1977.
10. M. Horio, S. Mori, I. Muchi, *Proceedings of Fifth Pacific Conference on Fluidization*, Washington, D.C., 1977.
11. D. Merrick, J. Highley, "Recent Advances in Air Pollution Control," AIChE Symposium Series, **70**, No. 137, pp. 366-378, 1974.
12. T. M. Modrak, T. A. Morris, W. C. Lapple, C.J. Aulisio, paper presented at AIChE Conference, April 1979.
13. S. Mori, C. Y. Wen, *AIChE Journal*, Vol. 21, No. 1, pp. 109–115, January 1975.
14. R. A. Newby, N. H. Ulerich, E. P. O'Neill, D. F. Ciliberti, D. L. Keairns, "Effect of SO_2 Emission Requirements on Fluidized-Bed Combustion Systems," EPA-600/7-78-163, pp. 148, 1978.

15. G. V. Reklaitis, J. M. Woods, F. Kaylhan, M. Sood, "System Studies of Coal Conversion Processes Using a Reference Simulator," quarterly report prepared under ERDA Contract EX 76-C-001-2275, April 1977.
16. I. W. Smith, *Combustion and Flame,* 17, pp. 303-314, 1971.
17. E. H. Suuberg, W. A. Peters, J. B. Howard, "Product Composition and Kinetics of Lignite Pyrolysis," paper presented at 173rd National Meeting of the American Chemical Society, New Orleans, Louisiana, March 21-25 1977
18. J. W. Wells, R. P. Krishnan, "ORNL Interim Annual Report on TVA AFBC Simulation." In preparation 1980.
19. C. Y. Wen, R. F. Hashinger, *AIChE Journal,* Vol. 6, pp. 220, 1960.
20. J. Werther, *Ger. Chem. Eng.,* Vol. 1, pp. 243-251, 1978.
21. Y. H. Yu, C. Y. Wen, *AIChE Journal,* Vol. 12, pp. 610, 1966.

Nomenclature

A_{xs} = reactor cross sectional area, cm^2

C = molar concentration, $gmole/cm^3$

D = diffusivity, cm^2/sec

D_t = reactor diameter, cm

d_B = diameter of bubble, cm

d_p = particle diameter, cm

d_{pf} = mean feed particle size distribution, cm

F_{att} = attrition fines flow rate, g/sec

F_o = solids feed rate, g/sec

F_1 = underflow rate, g/sec

F_2 = total rate of elutriated solids, g/sec

f_{fp} = fraction of particles in bed less than radius r

g = gravitational acceleration, 980 cm/sec^2

K_{att} = attrition rate constant defined by Eq. 11, cm^{-1}

K_{BE} = gas interchange coefficient defined by Eq. 31, 1/sec

$K(r)$ = elutriation constant of a particle of radius r defined by Eq. 13 or Eq. 32

k = constant in Equation (8)

k_{att} = attrition rate constant defined by Eq. 12, cm^{-1}

k_1 = reaction rate constant for $C + \frac{1}{2} O_2 \rightarrow CO$ (see Table 2), $gmole/(cm^2\text{-sec-atm})$

k_2 = reaction rate constant for $CO + \frac{1}{2} O_2$ CO_2 (see Table 2), $cm^3/(gmole\ sec)$

k_3 = reaction rate constant for $C + CO_2 \rightarrow 2CO$ (see Table 2), $gmole/cm^2\text{-sec-atm}$

L_f = expanded bed height, cm

L_{mf} = bed height at minimum fluidization, cm

N_h = the number of incremental volumes ΔV in bed

n_d = number of holes in distributor plate

$p_B(r)$ = differential particle size distribution of bed, cm^{-1}

$p_o(r)$ = differential feed size distribution, cm^{-1}

$p_1(r)$ = differential underflow size distribution, cm^{-1}

$p_2(r)$ = differential particle size distribution of elutriated solids, cm^{-1}

R_G = universal gas constant, 1.987 cal/gmole °K

R_{GG} = universal gas constant, 82.06 atm $cm^3/gmole$ °K

$\dot{R}(r)$ = rate of change of particle radius due to attrition for particle radius r, cm/sec

$\overline{R_T}(r)$ = the average rate of total carbon consumption per unit surface area of a particle of radius r, $gmole/sec^2\text{-sec}$

R_1^T = overall rate of $C + \frac{1}{2} O_2 \rightarrow CO$ (see Table 3), $gmole/cm^2$ sec

R_2^T = overall rate of $CO + \frac{1}{2} O_2 \rightarrow CO_2$ (see Table 3), $gmole/cm^3\text{-sec}$

R_3^T = overall rate of $CO_2 + C \rightarrow 2CO$ (see Table 3), $gmole/cm^2\text{-sec}$

r = particle radius, cm

T_G = gas temperature, °K

T_p = surface temperature of particle, °K

U_o = superficial velocity, cm/sec

U_{mf} = minimum fluidizing velocity, cm/sec

$U_t(r)$ = terminal velocity corresponding to particle radius r, cm/sec

V_B'' = volumetric flux through the bubble phase, $cm^3/cm^2 \cdot sec$

V_{EMUL} = volume of the emulsion phase, cm^3

W_B = bed weight, g

x = weight fraction, unitless

Z = height above distributor plate, cm

Greek notation

δ = total void fraction (bubble and emulsion) in control volume ΔV, unitless

$\overline{\delta}$ = average total void fraction for bed, unitless

ϵ_B = bubble voidage at bed height h, unitless

$\overline{\epsilon}_B$ = average bed bubble voidage, unitless

ϵ_{mf} = fractional bed voidage at minimum fluidization, unitless

μ_g = gas viscosity, g/cm-sec

ρ_{char} = density of char, g/cm^3

ξ = surface area of char per unit volume, cm^2/cm^3

ρ_g = gas phase density, g/cm^3

ρ_s = solid bed material density, g/cm^3

τ = weight space time (bed weight/limestone flow rate), hr

ψ = constant defined in Equation (7)

ϕ = average amount of component produced or consumed per unit volume of emulsion phase, $gmoles/cm^3$ of emulsion

Subscripts

CO = carbon monoxide component

CO_2 = carbon dioxide component

H_2O = water component

O_2 = oxygen component

plug = plug flow

Superscripts

I = intrinsic

M = mass transfer

BUB = bubble phase

EMUL = emulsion phase

SB = slow bubble

The contents of this paper do not necessarily reflect the views and policies of the Tennessee Valley Authority, nor does mention of trade names, commercial products, or companies constitute endorsement or recommendation for use.

MODELING OF FLOW BEHAVIOR AND FINNED TUBE PERFORMANCE IN THE TURBULENT FLOW REGIME

F.W. Staub, M. Kuwata, A.C. Ku, and R.T. Wood

General Electric Company
Schenectady, New York 12301

Introduction

Cold modeling results related to the design of horizontal finned tube banks to operate in high-velocity turbulent fluidized bed combustors are summarized here together with preliminary data to validate the scaling of turbulent bed behavior from room-temperature to high-temperature conditions.

The high volumetric heat removal rate required by high-velocity turbulent fluidized bed combustion renders desirable the use of extended surface heat exchanger tubing. For this purpose, the feasibility of employing helical finned horizontal tubes in the turbulent bed has been investigated in a cold modeling heat transfer study prior to their use in a fluidized bed combustor.

Preliminary data taken in a 0.6 m x 0.6 m high-temperature, atmospheric pressure fluidized bed are also reported here and compared with the fluidized bed expansion and flow regime behavior predicted by models derived from cold modeling experiments.

Finned Tube Performance

There is reasonable agreement among various authors who report finned tube data in fluidized beds (References 1-5) that certain fin structures provide a significant increase in the thermal duty per unit length of tube over that obtained with bare tubes. However, considerable disagreement exists about the effect of fin spacing on the heat transfer coefficient. For example, a correlation suggested in Reference 2 indicates that a 40 percent reduction in the heat transfer coefficient occurs when the ratio of the particle diameter d_p to the fin spacing s reaches a value of 0.4; whereas in Reference 3 the same reduction in heat transfer is obtained when this ratio reaches a value of 0.09. The present results for large particles (d_p > 0.6 mm) show that much higher values of d_p/s are possible before the heat transfer performance becomes noticeably reduced.

Cold modeling heat transfer data (Reference 6) were obtained for both bare and helically finned, electrically heated, horizontal steel tube banks in a 0.3 m x 0.3 m facility. The bare tube bank had 10 rows of 32 mm o.d. bare tubes in a staggered array that approximated, to within 4 percent, the minimum cross-sectional flow areas between tubes for the 10-row finned tube configurations listed in Table 1. The fins were made of 409 stainless steel. Values of the reduced velocity U_{sg}/U_t (ratio of the superficial gas velocity to the particle terminal velocity) from 0.1 to 0.7 were covered in beds of uniformly sized glass beads (0.65, 2.6 mm) and mixed silica sand sizes (0.93, 1.4, 2.6 mm). Pressures from 0.1 MPa (1 atm) to 1 MPa (10 atm) were tested. Static bed depths ranged from 0.25 m to 0.70 m. In general, the tube-to-tube variation of the heat transfer coefficient was ±15% from the bank average.

Table 1

FINNED TUBE CONFIGURATIONS (10-ROW BANK)

Tube o.d. (mm)	25	25	25
Fin Height (mm)	13	13	6.4
Fin Thickness (mm)	2.7	1.5	1.5
Fin Pitch (fins/m)	98	197	197
Tube Pitch (mm)			
Vertical	57	57	57
Horizontal	102	102	102

The pertinent tube bank average heat transfer data are summarized in Table 2, where the heat transfer coefficient has been based on the total exposed surface area after correction for the fin effectiveness (see Reference 6). The conductance is based on the heat transferred per unit tube length for conditions taken at a reduced velocity of 0.5 and for the 0.65 mm particles.

The bare tube data correlate well with the heat transfer model described in References 6 and 8. In view of this fact, the same model was applied (References 6 and 7)

Table 2

AVERAGE TUBE BANK HEAT TRANSFER PERFORMANCE

Pressure (atm)	Tube Type	Heat Transfer Coefficient $h_{ff}/(W/m^2\ C)$	Overall Conductance (W/m C)
1	Bare	210	21
	Finned (98 fins/m)†	115	36
	Finned (197 fins/m)†	85	44
5	Bare	260	26
	Finned (98 fins/m)†	125	39
10	Bare	310	31
	Finned (98 fins/m)†	180	51

†13-mm high stainless steel fins

to correlate the finned tube bank data taken both in this investigation and in the experiments reported in References 3 and 4 for 10 mm high aluminum fins on 20 mm o.d. tubes having fin spacings from 1.9 mm to 16 mm. The comparison of the correlation with these data is shown in Figure 1. The relationships for the principal quantities in the correlation are given below together with the heat transfer coefficient h_{fu} for the finned bank without particles (gas only):

$$\frac{U_{sd}}{m/s} = 0.41\ (1 - \bar{\alpha})\ \left(\frac{\Delta Z_m}{m}\right)^{0.4} \qquad (1)$$

$$f(d_p) = \begin{cases} \left(\dfrac{0.15}{d_p/mm}\right)^{0.73} & : \quad 0.02 < \dfrac{d_p}{mm} \leq 1.0 \\ 0.25 & : \quad 1.0 \leq \dfrac{d_p}{mm} < 3 \end{cases} \qquad (2)$$

$$\frac{h_{fu}}{W/m^2\ C} = 20 \left(\frac{\rho_g U_{sg}}{kg/m^2\ s}\right)^{0.68} \qquad (3)$$

where the geometrically dictated mixing height ΔZ_m is 0.16 m for the present tube bank spacing. In Equation 3 the coefficient of 20 applies to the 13-mm high finned tubes; forced convection data for the 6.4-mm high finned tubes were correlated by a coefficient of 18. The determination of the bed average void fraction $\bar{\alpha}$ is described later in connection with Equation 4. As can be seen, when normalized to the appropriate limiting performance for gas convection alone, the model developed for bare tube heat transfer continues to hold for the helically finned tube banks investigated. The prediction method is further discussed and compared with data in Reference 6.

As evident in Figure 1, there is no significant reduction in the finned-tube heat transfer coefficient as the ratio of particle size to fin spacing is increased from 0.087 to values as high as 0.73. Thus, in large particle fluidization, increasing the particle size will not necessarily force a finned tube design to lower fin counts from a thermal point of view until the particle size approaches the fin spacing.

The more extensive data presented in Reference 5 for a single horizontal tube support the above finding. For 12.5-mm high fins, there is only a 14 percent reduction in local heat transfer over a particle-diameter-to-fin-spacing ratio of 0.045 to 0.3 for constant particle size. The confusion in the literature on this point is probably due to the fact that some authors have not varied particle size independently of fin spacing to differentiate the performance change that each of these variables causes independently. The data of Reference 5 also imply that, as the fin height is increased, the effect of fin spacing becomes larger and the finned tube to bare tube heat-transfer ratio decreases.

Until more data become available, it appears that the correlation technique outlined above and discussed in Reference 6 will allow the generalized prediction of the performance of helically finned tube banks having about 13 mm-high stainless-steel fins. The heat transfer coefficient will be larger for shorter fins and smaller for longer fins. Since there is a relatively weak dependency of heat transfer on particle size for the mixtures tested, it can be concluded that the heat-transfer performance of a finned tube bank in a bed of mixed particle sizes can be adequately described by employing the mass-surface mean particle diameter in Equation 2.

Bed Flow Regime

The unsteady behavior of the bed pressure drop was shown by cold modeling results in Reference 6 to reflect the change from the observed bubbling or slugging bed behavior to the turbulent flow regime. Near

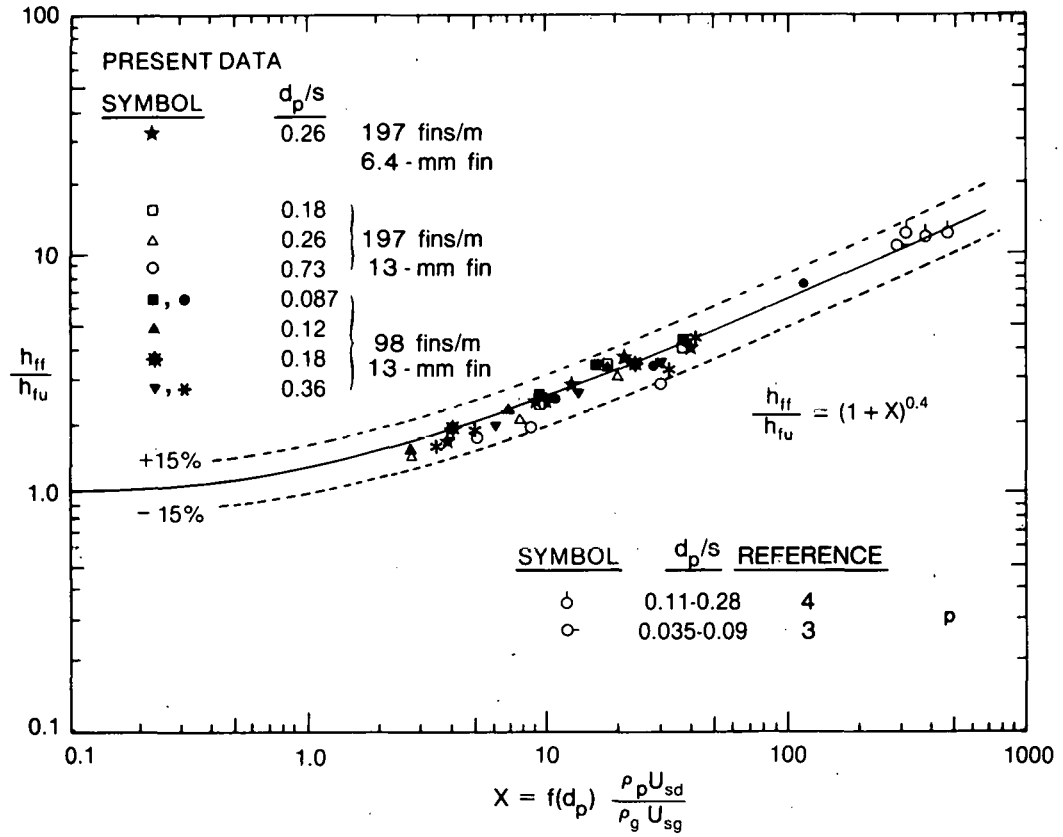

Figure 1. Correlation of Finned Tube Performance Using Flow and Heat Transfer Models – (References 6 and 8) – Effect of Particle Size d_p to Fin Spacing s

the transition point the bed pressure drop fluctuations became less severe and their form changed from generally sinusoidal oscillations to more random fluctuations.

The bed pressure drop ratio measured between 40 C (100 F) and 540 C (1000 F) without a tube bank for 0.93 mm particles is shown in Figure 2, where the ordinate is the peak-to-peak amplitude of the bed pressure drop fluctuation normalized to the average bed pressure drop. As was the case with the cold modeling results obtained in a 0.3 m x 0.3 m bed, the amplitude of the pressure drop fluctuation in the 0.6 m x 0.6 m hot facility exhibited the following trend with increasing gas velocity: the amplitude increased, reached a maximum toward the end of the bubbling-slugging regime, and then decreased in the turbulent regime. The turbulent regime occurred at fluidizing velocities greater than approximately one-half of the particle terminal velocity (U_t) for this particle size. Correspondingly, the sinusoidal character of the fluctuation degenerated to randomness as the turbulent regime was attained. It is apparent from both the amplitude data shown in Figure 2 and the pressure drop oscillograms (not shown) that the same tendencies characterize the behavior of the bed pressure drop in both facilities.

A detailed comparison between the present and previous data reveals that the peak pressure drop ratio of about 1 in the present tests is, over the temperature range from 40 C to 540 C, higher than the maximum of $\pm$ 0.8 which was seen in the 0.3 m x 0.3 m cold facility (without a tube bank). While the sinusoidal nature of the pressure drop fluctuations observed at higher velocities in the larger facility is more persistent than seen before in the smaller facility, this behavior disappeared in subsequent measurements taken in the presence of a ten-row tube bank.

Aside from a somewhat larger amplitude, the pressure drop fluctuations in the 0.6 m x 0.6 m facility were very similar to those measured in the cold 0.3 m x 0.3 m facility, with the 0.93 mm particle data falling between those taken for the 0.65 mm and 2.6 mm particles in the cold facility. As noted below, the bed expansion correlation developed using the cold modeling data (Reference 6) also correlated the expansion data obtained in the 0.6 m x 0.6 m hot facility.

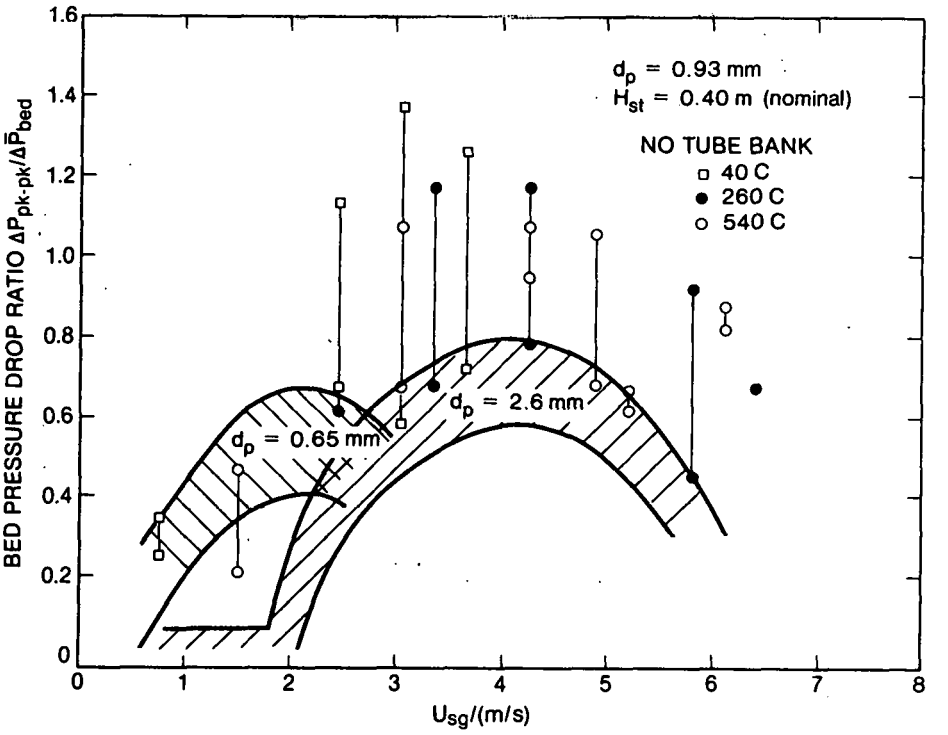

Figure 2. Ratio of Peak-to-Peak Amplitude ΔP_{pk-pk} of Bed Pressure Drop Fluctuation to Average Value of Bed Pressure Drop $\Delta \bar{P}_{bed}$ in 0.6 m x 0.6 m Hot Fluidized Bed Test Facility. Hatched regions show ranges of data reported in Reference 6 for 0.3 m x 0.3 m room-temperature facility.

Bed Expansion and Void Fraction

A key measure of bed performance is the void fraction. In the present tests, this quantity was determined by first visually locating the maximum and minimum expanded bed heights with the aid of the several windows that are installed along the length of the test section. The average of the maximum and minimum heights was then used to compute the average void fraction $\bar{\alpha}$ of the bed. Values of the void fraction determined in this way for a range of fluidizing velocities and at two air temperatures and bed heights are shown plotted in volumetric flux coordinates in Figure 3. These coordinates, which have a semitheoretical basis, were demonstrated to represent the extensive void fraction data gathered during the previous cold modeling studies (References 6 and 7).

In terms of these coordinates, the void fraction correlation described in Reference 6 has the following general form:

$$\frac{U_{sg}}{\bar{\alpha}} = C_o U_{sg} + \bar{V}_{gu} \quad , \qquad (4)$$

where $\bar{\alpha}$ is the bed average void fraction, C_o is a distribution parameter, and $\bar{V}_{gu}$ is the relative or drift velocity. Although flow-regime dependent, C_o can be identified as the slope of data curves for $U_{sg}/\bar{\alpha}$ plotted against values of U_{sg}, whereas the drift velocity $\bar{V}_{gu}$ can be determined as the intercept of these curves with the ordinate. In most cases (see Figure 3), the data curves in each flow regime are straight lines; hence, the drift velocity (as well as the slope C_o) can be represented as a different constant in each regime. Expressions for $\bar{V}_{gu}$ are derivable from known conditions at the end points of the regimes; thus

$$\bar{V}_{gu} = \begin{cases} U_{mf}\left(\frac{1}{\bar{\alpha}_{mf}} - 1\right) & : \text{bubbling-slugging regime} \\ U_t\,(1 - C_o) & : \text{turbulent regime.} \end{cases} \qquad (5)$$

Here the minimum fluidization velocity U_{mf} and the terminal velocity U_t are calculable from well-established correlations which depend on pressure, temperature, and particle properties. The distribution parameter C_o is most strongly dependent on particle size, although not enough different particle sizes have yet been investigated to permit a general correlation for C_o to be advanced at this time.

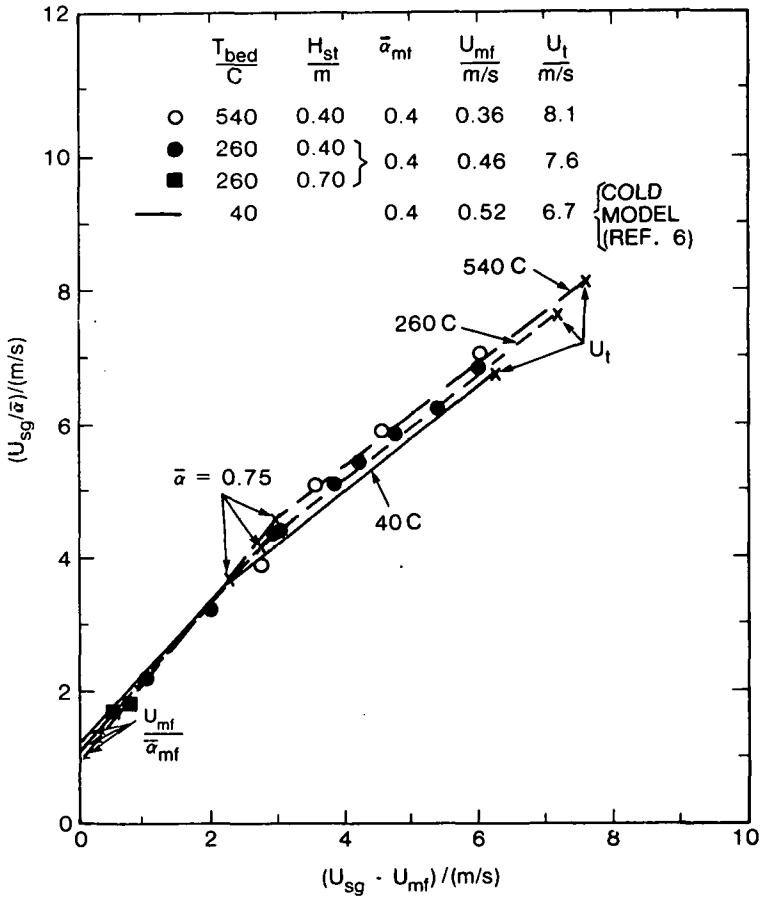

Figure 3. Volumetric Flux Plot of Average Void Fraction of Open Beds of 0.93 mm Particles Fluidized by Preheated Air in the Hot Fluidized Bed Test Facility. (Solid line is correlation obtained in 0.3 m x 0.3 m room-temperature facility, Reference 6.)

It is evident in Figure 3 that the present high-temperature data for void fraction continue to be well correlated by volumetric flux coordinates. At higher velocities, the correlation lines for the high-temperature data have the same slope as the cold modeling results (solid line) and pass through the correct (calculated) terminal velocity end points in the limit of the void fraction approaching one. Therefore, the present results strongly support the applicability of volumetric flux coordinates to high-temperature fluidization.

Referring to Figure 3, we see that the high-temperature data lines, like the room-temperature line, suffer a break in slope to span the range from the minimum fluidization velocity to the terminal velocity. It is known from the cold modeling work that this break occurs at a void fraction of 0.75 and that it signals the onset of the turbulent regime at higher velocities. Therefore, despite the lack of lower velocity data to define transition points, it may be concluded that the high-temperature beds operated in the turbulent flow regime at velocities greater than about 3 m/s (10 ft/s). The point where the void fraction reaches 0.75 has been marked on each curve in Figure 3, and it is seen that this value provides a transition point which is consistent with the data.

The unsteady bed pressure drop behavior and the preliminary bed expansion observed under high-temperature conditions are thus consistent with the data obtained in the cold modeling facility. The same bed expansion (void fraction) correlation and conditions at flow regime transition continue to hold, and this fact increases confidence in the generality of both the correlation technique and the flow regime transition from bubbling-slugging flow to turbulent fluidization conditions in beds of large particles.

Conclusions

Cold modeling results have established the feasibility of employing horizonta banks of finned tubes in fluidized beds o

large particles. No significant reduction in the heat transfer coefficient was measured as the ratio of particle size to fin spacing was increased from 0.087 to values as high as 0.73 for combinations of particle diameters of 0.65, 0.93, 1.4, and 2.6 mm and interfin spacings of 3.6 mm and 7.5 mm.

The flow and heat transfer models developed to predict the performance of bare tube banks in the turbulent flow regime continue to apply to helically finned tubes, provided that the fluidized bed performance (h_{ff}) of the latter is normalized to the corresponding heat transfer performance (h_{fu}) at the same gas velocity in a flow without particles.

High-temperature data for the behavior of unsteady bed pressure drop and bed expansion (void fraction) are consistent with cold modeling results. The same bed expansion correlation developed from cold modeling studies and the conditions at the transition to the turbulent flow regime continue to apply at high temperature.

Gas combustion experiments, to be followed by coal combustion, are presently being conducted to define the opportunities available with high-velocity, turbulent bed combustion.

Acknowledgments

The complementary support of the Electric Power Research Institute (Mr. C. Aulisio, Program Director) and the New York State Energy Research and Development Authority (Mr. T.E. Mullen, Program Director) is gratefully acknowledged.

We also thank Messrs. S.P. Urbaetis, S.J. Brzozowski, G.S. Winters, and K. Hardcastle for their help in constructing and running the experiments.

Nomenclature

C_o	Distribution parameter in void fraction correlation, Equation 4 (slope in volumetric flux coordinates)
d_p	Particle diameter (mass surface mean)
$f(d_p)$	Particle size function defined by Equation 2
h_{ff}	Average finned tube heat transfer coefficient in fluidized bed
h_{fu}	Average finned tube heat transfer coefficient in gas flow without particles
s	Spacing between fins
U_{sd}	Superficial velocity of particle (discontinuous) phase
U_{sg}	Superficial velocity of gas (continuous) phase
U_t	Terminal velocity ($\bar{\alpha} = 1$)
$\bar{V}_{gu}$	Drift velocity defined by Equation 4
$\bar{\alpha}$	Average void fraction of bed
$\overline{\Delta P}_{bed}$	Temporally averaged bed pressure drop
ΔP_{pk-pk}	Peak-to-peak amplitude of bed pressure drop fluctuation
ΔZ_m	Mixing height in bed flow model Equation 1
ρ	Density

Subscripts

g	Gas phase
mf	Minimum fluidization point ($\bar{\alpha} = \alpha_{mf}$)
p	Particle
t	Terminal condition ($\bar{\alpha} = 1$)

References

1. N.J. Gel'perin et al., "Heat Transfer Between a Fluidized Bed and Staggered Bundles of Horizontal Tubes," International Chemical Engineering, Vol. 9, No. 1, 1969, pp. 137-142.

2. W.E. Genetti, R.A. Schmall, and E.S. Grimmett, "The Effect of Tube Orientation on Heat Transfer with Base and Finned Tubes in a Fluidized Bed," AIChE Symposium Series, Vol. 67, No. 116, 1971, pp. 90-96.

3. N.I. Gel'perin et al., "Heat Exchange Between Finned Tubes and a Fluidized Bed of Granular Material," Chemistry and Technology of Fuels and Oils, Vol. 8, 1972, p. 697.

4. J.C. Petrie, W.A. Freeby, and J.A. Buckham, "In-bed Heat Exhcanges," Chemical Engineering Progress, Vol. 64, 1968.

5. H. Natusch and H. Bleuke, "Heat Transfer Along Finned Tubes in Gas Fluidized Bed," Verfahrenstechnik, Vol. 7, 1973, p. 293.

6. F.W. Staub, R.T. Wood (ed.), G.S. Canada, and M.H. McLaughlin, "Two-Phase Flow and Heat Transfer in Fluidized Beds," Final Technical Report for Electric Power Research Institute, Contract No. RP525-1, Report No. SRD-78-103, General Electric Corporate Research and Development, Schenectady, New York, December 1978.

7. R.T. Wood and F.W. Staub, "Finned Tube Heat Transfer and Bare Tube Erosion in Fluidized Beds," Final Report for New York State Energy Research and Development Authority, NYSERDA/GE 30 March 1977 Agreement-Exhibit A1, Report No. SRD-78-129, General Electric Corporate Research and Development, Schenectady, New York, June 1978.

8. F.W. Staub, "Solids Circulation in Turbulent Fluidized Beds and Heat Transfer to Immersed Tube Banks," ASME Journal of Heat Transfer, Vol. 101, No. 3, 1979, pp. 391-396.

A PLUME MODEL FOR LARGE SCALE ATMOSPHERIC FLUIDIZED BED COMBUSTORS

Dalkeun Park, Octave Levenspiel and Thomas J. Fitzgerald

Department of Chemical Engineering
Oregon State University
Corvallis, Oregon 97331

At present, the United States is studying and evaluating the atmospheric fluidized bed combustor (AFBC) as an alternative to the pulverized coal burner. Even a "small" AFBC (250 mw) would be enormous by chemical industry standards, consisting of four or five fluidized beds filled to a depth of about one meter with limestone particles and fluidized with air at two to four meters per second. For good distribution of coal one class of design visualizes coal entering through about a hundred feed points at the bottom of the bed.

A properly designed atmospheric fluidized bed combustor should:

- minimize the loss of unburned coal,
- minimize the release of pollutants: sulfur dioxide, nitrogen oxides and particulates,
- operate with a minimum of excess air, and
- maximize the utilization of limestone for sulfur dioxide retention.

These are competing requirements and, to predict the tradeoffs involved in different AFBC designs, requires the use of some sort of model for the operation. In order to model the AFBC we have to understand many different kinds of physical and chemical processes occurring in the AFBC: flow of gases and solids in the bed, devolatilization of coal, elutriation of unburned char and limestone particles, attrition of solids in the bed, gas-solid reactions and gas-gas reactions within the bed and above the bed. Any general model which tries to incorporate all these factors will be extremely complex. So a judicious choice of simplifications is needed if we are to develop a working model.

There are three main aspects to the operation of the AFBC: the combustion of coal, sulfur retention with limestone and the fluidization itself. Each of these is quite a subject in itself but the problem is complicated because these factors are interrelated. Nevertheless, the first thing we have to investigate is the fluidization in the bed because combustion and sulfur retention are processes occurring in the fluidized bed. The AFBC has unique features not found in other applications of fluidized beds. First, high gas velocities, essential in keeping the size of the bed within reason, requires the use of large particles in the bed. At the same time the immersed tubes in the d restrict the growth of bubbles therein. Thus, e bed is in either the slow bubble regime or in turbulent-churning flow but certainly not in the fast bubble regime for which theories of fluidization were developed and used extensively in the past.

Next, there is so much more limestone than coal in the bed that the physical behavior of the bed is insensitive to the hold-up of coal and is dependent primarily on the limestone and its products. This fact allows us to decouple coal combustion from the fluid dynamics of the bed.

Sulfur retention in the AFBC occurs primarily through the chemical reaction between calcined limestone (CaO) and sulfur dioxide, one of many combustion products of coal. Thus, we have to know how and where in the bed does sulfur dioxide evolve in order to model its reaction with calcined limestone. And as the retention of sulfur dioxide consumes only a minute fraction of the inlet oxygen, we can treat the sulfur retention after dealing with the combustion of coal which dictates the sulfur dioxide formation. In this paper our interest is limited to the combustion of coal; sulfur retention is not treated here.

MODELS IN THE LITERATURE[1-12]

Let us examine the critical assumptions underlying the models in the open literature, listed in Table 1, and see whether they are useful for representing and modeling the large utility scale AFBC's.

Gas Flow in the Bed

As mentioned earlier AFBC's are operated in either the slow bubble regime or in turbulent-churning regime but not in fast bubble regime. But, as Table 1 shows, most model builders have used the two-phase theory developed for fluidized beds in the fast bubble regime with their severe gas bypassing. Thus, these two-phase gas flow models, originally developed for catalytic reactors with their fine particles, are not applicable for coal combustion with their large particles, high gas velocities and small bubbles.

Mixing of Solids

Good solid mixing occurs in fluidized beds and, thus, the assumption of uniform solid concentration in the bed has been widely used. But AFBC's are so large in cross-sectional area that we cannot expect

this and the problem is how many feed points are necessary for relatively uniform solid concentration (see Highley and Merrick[13]). For sulfur retention we do not have serious problems because residence time of limestone is in the order of hour. But combustion of coal is much faster, so we have to compare the time scales involved. For 0.9 m x 0.9 m particles take at least 15 seconds to be well mixed[14] and the time for complete combustion of a char particle in the bed is of the order of minutes, about five minutes for 3000 μm particles and about a minute for 300 μm particles, and for still smaller particles the time is in terms of seconds. Therefore, if feed coal contains a significant amount of very small particles, say 50 μm, the AFBC is far from the perfect mixer for the combustion of coal if it has one feed point per square meter. But one advantage of using AFBC is that it can burn coal of relatively large size, and using of relatively large coal particles saves crushing cost. Thus, for the combustion of char, one feed point per square meter is not that bad. But the problem is complicated because of the volatiles in coal that evolve once the coal enters in the hot bed. If the dispersion of feed coal is much faster than the devolatilization then each coal particle will have its own tiny diffusion flame as long as its volatiles evolve and burn. However, if devolatilization is faster than the dispersion from a coal feed point, the volatiles will combine to form a large plume of unburned gas rising from the entry port. Since this plume can contain as much as 50% of the heating value of the fuel it is not something which we can or should ignore.

Measurements show that the time for devolatilization is less then one second for 200 μm particles[15] and less than ten seconds for 3000 μm particles[10]. Therefore, we can see that one feed point per square meter is not enough if we want to do without the plume while burning coals not much bigger than 3000 μm. Some models simply ignore volatiles and some others assume uniform release of volatiles throughout the bed.

Carbon Utilization

Unburned fuel can leave the AFBC in three ways:

1) with the spent bed material,
2) as unburned gases, CO and others, and
3) as elutriated char particles.

Results of Babcock and Wilcox studies[16] and others show that there is negligible char in the exit solids and that unburned CO and other gases will rapidly burn to near completion above the bed. Thus, the only significant contribution to unburned fuel is the elutriation of fine char particles. Thus, models which ignore the elutriation loss are useless for correlating combustion efficiency with parameters like gas velocity or size of feed coal.

PLUME MODEL

As we discussed so far, none of the models are satisfactory. Here we propose a plume model which accounts for the general features of the AFBC and can explain some phenomena observed.

Assumptions of the Plume Model

The major assumptions of the plume model are as follows:

1. Plug flow of gas: For beds of large particles, high minimum fluidizing velocity (0.5 ~ 3 m/s) and small bubbles, one cannot use any of the two-phase models for gas flow with their cloud-surrounded bubbles. We have, in fact, a slow bubble bed or a churning-turbulent bed for which the best simple representation is straight plug flow.

2. Devolatilization of entering coal particles is instantaneous and occurs at the feed entry ports to give plumes of unburned combustible gases, which rise through the bed at the same velocity as the surrounding gases.

   This assumption represents AFBC in which coal is fed from below by entrained air in discrete entry ports. We show later that other methods of coal feed can be treated as special cases of the entry port analysis and that the entry port analysis, with its plume of rising volatiles, is the most complex situation to treat.

3. Combustion occurs at the boundary between volatiles and the surrounding oxygen-rich gas. This follows diffusion flame kinetics, the whole plume acting very much like a burning gas flame, with oxygen and combustibles moving to the plume boundary with an effective diffusion (or dispersion) coefficient which can be found by experiment.

4. The volatiles in the plume which pass through the bed unburned mix with oxygen-rich gas just above the bed to burn rapidly to completion.

5. The devolatilized solids are well mixed throughout the bed. They burn everywhere in the bed except in the plume. They maintain a constant density, the ash peeling off as it is formed. Hence, reaction of the char follows shrinking particle kinetics and is first order with respect to oxygen.

6. The bed is uniform in temperature.

7. Large char particles shrink as they burn in the bed and, at any bed condition, a distinct size exists above which no elutriation occurs. Below this size, the change of elutriation increases progressively as particles shrink.

Figure 1 sketches the main features of the

bottom-fed coal burning AFBC.

COMBUSTION OF CHAR, VOLATILES AND OXYGEN IN THE BED

As the main form of fuel loss in an AFBC is the elutriation of unburned char particles, we concentrate on the combustion of char particles of elutriable size for the prediction of combustion efficiency. Larger particles must burn and shrink down to this size in the bed no matter what the mechanism or kinetics of their combustor actually may be.

The weight of shrinking char solids in a size interval between R_i and R_{i+1} in bed is given by (see reference 17)[1]

$$W(\bar{R}_i) = \frac{F_0(\bar{R}_i)\Delta R_i - W(\bar{R}_{i+1})R(\bar{R}_{i+1})(\frac{\Delta R_i}{\Delta R_{i+1}})}{\frac{F_1}{W}\Delta R_i - R(\bar{R}_i) + \kappa(\bar{R}_i)\Delta R_i - \frac{3W(\bar{R}_i)}{\bar{R}_i}R(\bar{R}_i)\Delta R_i} \quad (1)$$

the total weight of char in the bed by

$$W = \sum_i W(\bar{R}_i),$$

the carryover of unburned char by

$$F_2 = \sum_i W(\bar{R}_i)\kappa(\bar{R}_i), \quad (2)$$

and the conversion of char in the bed by

$$X_b = 1 - F_2/F_{0,\text{total}} \quad (3)$$

Now put $F_1 = 0$, meaning that no unburned carbon leaves in the overflow solids. Also, notice that all the values are for elutriable particles. Particles that are too big to be elutriated can be incorporated into the largest size fraction with adjusted mass except $F_{0,\text{total}}$ which represents total char feed rate before the adjustment.

Now to calculate F_2, we need the elutriation and shrinkage rate of particles. For $\kappa(\bar{R}_i)$, we use the expression of Colakyan[18], good for any size of solids R_i

$$\kappa(R_i) = \kappa_0(1 - \frac{u_t(R_i)}{u_o})^2 \quad (4)$$

and the shrinking rate

$$R_{(R)} \equiv \frac{dR}{dt}(R) = \frac{-12k\, C^*_{O_2}}{\rho_c\, \xi_c}$$

For the particles of interest, i.e., of elutriable size, we have to account for both the film diffusion and surface reaction. Thus

$$k'' = \frac{1}{\frac{1}{2k_g} + \frac{1}{k_s}},$$

and by adopting the expression of Field[19] we also have

$$k_x = 5.96 \times 10^2\, T_s \exp\left[\frac{1.494 \times 10^6}{RT_s}\right].$$

The particle surface temperature is given by the energy balance

$$h(T_s - T_b) + \varepsilon\sigma(T_s^4 - T_b^4) = -r_c(-\Delta H_r).$$

More than one stable state surface temperature is possible under some circumstances but the chance of realizing the high temperature stable state is very small for the particles of interest (see Appendix). Calculations also show that k" does not vary much with different size of particles and oxygen concentration. Therefore, we can use the simple space average concentration for oxygen without introducing much error. Notice that we assumed first order reaction rate with respect to oxygen.

At this point we must look at the combustion of volatiles in order to know the average oxygen concentration, $C^*_{O_2}$, encountered by the well mixed solids within the bed. Let A denote combustible volatiles and B, oxygen. Then

$$A + \nu B \rightarrow (1 + \nu)[\text{Combustion Products}]$$

Here ν is a stoichiometric coefficient characterizing the composition of volatiles and it is assumed that there is no change in moles by the reaction. Neglecting axial dispersion, we obtain the following equations by mass balances for oxygen and combustible volatiles:

INSIDE THE PLUME

$$\frac{C_A}{z} = \frac{D_A}{u_o r}\frac{\partial}{\partial r}(r\frac{\partial C_A}{\partial r}) \quad (6)$$

I.C. $\quad C_A = C_{A_0}$ for $0 \leq r < L_0$

B.C. $\quad \frac{\partial C_A}{\partial r} = 0$ ar $r = 0$

$\quad C_A = 0$ at $r = L_i(z)$ $\quad$ for all $z > 0$

OUTSIDE THE PLUME

$$\frac{C_B}{\partial z} = \frac{D_B}{u_o r}\frac{\partial}{\partial r}(r\frac{C_B}{\partial r}) - \frac{k}{u_o}C_B \quad (7)$$

I.C. $\quad C_B = C_{B_0}$ for $L_0 < r \leq L_2$

B.C. $\quad C_B = 0$ at $r = L_i(z)$ $\quad$ for all $z > 0$

$\quad \frac{\partial C_B}{\partial r} = 0$ at $r = L_2$

ON THE PLUME SURFACE

$$D_A \frac{\partial C_A}{\partial r}\bigg|_{r = L_1(z)^-} = -\nu D_B \frac{\partial C_B}{\partial r}\bigg|_{r = L_2(z)^+} \quad (8)$$

Here we assume that volatiles evolve from a circular region on the bottom of the bed centered on the coal feed port. The radius of that circle, L_0, is determined by the amount of volatiles that move upward at the same velocity as the fluidizing air. The radius of the plume at any elevation z is set by Equations (6), (7) and (8). Typical concentration profiles are sketched in Figure 2.

We also assume that the gases rise in plug flow with a certain lateral dispersion which is surprisingly small and not too different from that found in a packed bed. We adopt this picture as a result of the experimental studies by Jovanović[20] on the spread of a plume of tracer gas. In essence, he found that the time averaged concentration profiles showed a large amount of lateral dispersion. However, the true instantaneous dispersion of gas out from the axis of the meandering plume was much smaller. And it is this instantaneous coefficient which is to be used in the above equations for D_A and D_B.

We can simplify the problem by assuming that $D_A = D_B$ because small scale eddy diffusion and not molecular diffusion is the main mechanism of the gas dispersion. Applying the classical treatment of Burke and Schumann[21], we treat the concentration of combustible volatiles as a negative oxygen concentration. Oxygen and combustible volatiles have to move to the flame front (surface of the plume) stoichiometrically so that Equation (8) is satisfied. Then C_A that satisfies Equation (6) can be applied to Equation (7) if we put $C_A = -\nu C_B$. Dropping subscripts A and B, we can now combine Equations (6) and (7).

Letting $\hat{C} = \frac{C}{C_o}$, $\hat{z} = \frac{z}{H}$, and $\hat{r} = \frac{r}{L_2}$, we obtain the final equation

$$\frac{\partial \hat{C}}{\partial \hat{z}} = \left(\frac{HD}{u_o L_2^2}\right) \frac{\partial}{\hat{r}\,\partial \hat{r}} - \frac{Hk}{u_o} \hat{C}\, I \quad (9)$$

where

$$I = \begin{cases} 0 & \text{if } \hat{C} \leq 0 \\ 1 & \text{if } \hat{C} > 0 \end{cases}$$

I.C. $$\hat{C} = \begin{cases} -\nu C_{A_0}/C_0 & \text{for } 0 < \hat{r} < S_0 \\ C_{B_0}/C_0 & \text{for } S_0 < \hat{r} \leq 1 \end{cases}$$

where $S_0 = L_0/L_2$

B.C. $$\frac{\partial \hat{C}}{\partial \hat{r}} = 0 \text{ at } \hat{r} = 0 \text{ and } \hat{r} = 1 \text{ for all } \hat{z} > 0$$

In this notation the surface of the plume is where $\hat{C} = 0$ and the new concentration profile is as shown in Figure 3. Equation (9) can be solved to give the mean oxygen concentration in the bed without much difficulty using numerical methods with given initial and boundary conditions.

The value of k in Equation (9) represents the local oxygen disappearance rate constant and is constant throughout the bed since we have assumed mixed flow for solids in the bed. But notice that the value of k is determined by the given bed conditions and feed coal and this value must be found by trial and error.

By solving Equation (9) with an assumed value for k we can obtain

$$X_v = 1 - 2 \int_0^{\hat{L}_1(1)} \hat{C}\, \hat{r}\, d\hat{r} / (S_0^2\, \gamma C_{A_0}/C_0) \quad (10)$$

$$X_{0_2} = 1 - 2 \int_{L_1(1)}^{1} \hat{C}\, \hat{r}\, d\hat{r} / [(1-S_0^2) C_{B_0}/C_0] \quad (11)$$

Then, from an oxygen balance the conversion of char in the bed is

$$X_b = [X_{0_2}(1 + E_x) - X_v(1 - f_2)]/f_2 \quad (12)$$

where E_x is the excess air ration.

This X_b has to be the same as the one from Equation (3). Thus, using Equations (1), (2), (3), (9), (10), (11) and (12), we can find k and conversions by a trial and error procedure.

COMBUSTION ABOVE THE BED

On entering the freeboard region, unburned combustible gases rapidly mix with oxygen giving essentially complete combustion within a short distance above the top of the bed. This results in an abrupt temperature jump. Although much sparser than in the bed, there are many particles moving in all directions in the freeboard. Thus, there is the combustion of particles though its contribution is much smaller than that of in the bed, owing to much smaller char hold-up in the freeboard. But the elutriation rate constant is, by the definition, the measure of the probability of a particle to be elutriated out of the bed against to stay in the bed and in the freeboard. Therefore, using Equation (1), we already lumped the combustion of char in the freeboard, which burst into the freeboard and eventually settle down back to the bed, with the combustion of the particles in the bed. Rigorously speaking, Equation (1) and others have to be modified to account for this but it is not necessary as char combustion in the freeboard has minor effect on the combustion in the bed. The remaining problem is how to treat those elutriating particles. But it is evident that combustion of elutriating particles comes into the picture only when the freeboard is

high enough so that there is region where practically no down coming particle is present. But it is unlikely that any AFBC will have such high freeboard, thus, let us forget about the further combustion of elutriating particles farther up in the freeboard, which at any rate is insignificant.

The overall carbon efficiency is given by

$$X_{ce} = 1 - (1-X_b)f_1 \qquad (13)$$

where f_1 is the ratio of fixed carbon to total carbon in the feed coal.

EFFECTS OF TRANSPORT AIR

So far we assumed that no air enters into the bed with coal through the feed port. But actually air is used as carrier gas for the transport of coal into the bed and its amount can be significant.

Entering the bed coal will release volatiles which will burn as coal particles are dispersed in the transport air. Thus, if the transport air is sufficient in amount to burn all the volatiles, all the volatiles will combust near the feed port and there will be no plume of unburned volatiles. But we expect that, usually, the amount of transport is not sufficient for the complete combustion of volatiles (around 10% of total air in B & W pilot plant operation[16]). In this case, all the oxygen in the transport air will be quickly consumed near the feed port and there will be adjustment in the value of ν while the size of plume increases by the amount of the transport air. Also, we have to modify Equations (10) and (11) accordingly.

$$X_v = 1 - \frac{2[1-f_2-f_3(1+E_x)]}{1-f_2} \int_0^{S_0} \hat{C}\,\hat{r}\,d\hat{r}/(S_0^2\,\gamma\,C_{A_0}/C_0) \qquad (10')$$

$$X_{O_2} = 1 - 2(1-f_3)\int_{S_0}^{1} \hat{C}\,\hat{r}\,d\hat{r}/(1-S_0^2)(C_{B_0}/C_0) \qquad (11')$$

where f_3 is the ratio of transport air to the total air to the bed.

RESULTS OF CALCULATIONS

For the typical coal of properties shown in Table 3 let us first compare the "plume" model with the "plumeless" model. By "plumeless" model we mean the extreme case where the particles of feed coal disperse uniformly throughout the bed before any devolatilization and the release of the volatiles, and their subsequent combustion, is complete before the onset of the char combustion. In the "plumeless" model, the average oxygen concentration in the bed is given as

$$C^*_{O_2} = \frac{C_{B_0}[1-(1-X_b)f_2]}{(1+E_x)\,\ell n[\frac{1+E_x}{(1-X_b)f_2+E_x}]} \qquad (14)$$

where f_2 is the ratio of stoichiometric oxygen for char combustion to that for total coal combustion.

We can now find X_b from Equation (14) together with Equation (1), (2) and (3), although the procedure again involves trial and error. This X_b of the "plumeless" model is always smaller than that of the "plume" model because the complete combustion of volatiles in the plumeless bed results in a lower average oxygen concentration in the bed. Calculations show that the maximum difference in the carbon efficiency is about 5% for the most sensitive coal feed size and that, in most practical cases, the difference is much smaller. This is a useful finding for it now allows us to rapidly estimate char efficiency without needing to solve the plume model, Equation (9). All we need to do is solve the very much simpler Equations (1), (2), (3) and (14).

Figures 4, 5 and 6 show the effect of different superficial gas velocities, excess air and elutriation rate constants on char combustion efficiency in the bed which is fed different sizes of typical coal particles whose properties are given in Table 3. All the calculations in this paper are performed for a bed temperature of 1116 K. These figures all show that char conversion is nearly complete for small feed particles and large feed particles while intermediate size particles have lower conversion.

The reason for this somewhat unexpected behavior is as follows. For very small feed particles, reaction to completion is more likely than elutriation, hence, high combustion efficiency. For intermediate sized particles, elutriation is more likely than reaction, hence, lowered conversion of solids. But for very large feed particles, most of the solids are consumed before the particles get down to elutriable size, hence, high combustion efficiency once again. This prediction shows that there is one critical intermediate size of feed solids which gives minimum char efficiency in the bed.

Figure 7 shows that one parameter, $HD/u_oL_2^2$, determines the conversion of volatiles in the bed. X_v is insensitive to X_b and excess air level which affect the average oxygen concentration in the bed. Notice that for sufficiently large values of $HD/u_oL_2^2$, volatiles burn completely in the bed and the plume closes and disappears within the bed.

The adiabatic temperature jump in the freeboard is shown in Figure 8. The effect of transport air is shown in Figure 9.

DISCUSSION AND CONCLUSION

The plume model is developed here to represent a tube filled AFBC with large particles in which air-entrained coal enter in a number of feed ports from below. It assumes that the volatiles are rapidly released from the coal at the feed entry ports to rise as plumes of combustible vapors.

Graphs have been prepared (Figures 4 & 9) to display the predictions of this model for narrow size cuts of a typical coal feed (Table 2). For a feed of wide size distribution, use these single size charts and properly sum.

Figures 4, 5 and 6 show that the lowest carbon efficiency always comes with an intermediate size of feed coal, not with very large or very small feed sizes. Thus, the coal feed to the AFBC should try to avoid this critical size.

The plume behavior, whether it breaks the surface of the bed, the temperature jump above the bed, concentration variations across the bed, etc., are all governed by one dimensionless group $HD/u_oL_2^2$ which accounts primarily on the spacing of feed ports in the bed. As an example, Figure 7 shows that doubling the distance between feed ports lower the volatiles burned in the bed from 90% to about 50%.

For a given coal feed, the carbon efficiency depends only on superficial gas velocity in the bed, the excess air and elutriation rate constant.

The special case and simplification of this model views the coal as being uniformly distributed all over the bed before the volatiles are released. Here, analysis is very much simpler (Equations (1), (2), (3) and (14) only) not involving plumes and no volatiles leaving the bed. This plumeless model should reasonably represent AFBC using large feed particles, introduced across the top of the bed and then rapidly mixed by large scale convective flow of solids.

The analysis of this paper shows that even in beds with plumes the simpler plumeless model can be used with negligible error to calculate carbon efficiency in the bed. However, for volatile efficiency, temperature jumps, composition variations across the bed, the complete plume model must be used.

Acknowledgement

This study was part of the project sponsored by the Electric Power Research Institute, Babcock and Wilcox Company and the U.S. Department of Energy.

NOMENCLATURE

- C, C_A, C_B – Gas concentration [kg-mol/m^3]
- $C^*_{O_2}$ – Average oxygen concentration in the bed [kg-mol/m^3]
- D, D_A, D_B – Gas dispersion coefficient in the bed [m^{3}gas/m bed]
- E_x – Excess air ratio
- $F_0(\bar{R}_i)$ – Char feed rate of size $\bar{R}_i$ [kg/s]
- F_1 – Char outflow rate [kg/s]
- $F_2(\bar{R}_i)$ – Elutriation rate of char of size $\bar{R}_i$ [kg/s]
- f_1 – Ratio of fixed carbon to total carbon in coal
- f_2 – Ratio of oxygen needed for char combustion to total coal combustion
- f_3 – Ratio of transport air to
- H – Height of the bed [m]
- h – Convective heat transfer coefficient [kJ/m^{2}Ks]
- k – Reaction rate constant for the disappearance of oxygen in the bed [1/m^{3}bed·s]
- k'' – Reaction rate constant for char $\frac{\text{kg-mol carbon}}{\text{kg-mol } O^2/m^3} \quad \frac{1}{m^2 \text{ char surface}\cdot s}$
- k_s – Rate constant for surface reaction [1/m^2 of char surface·s]
- $L_0, L_1(Z)$ – Radius of plume; at the bottom of the bed, at height Z, respectively [m]
- L_2 – Radius of module for one feed coal point [m]
- R – Radius of shrinking coal particle
- $\bar{R}_i$ – Average radius of particles in i^{th} size interval [m]
- r – Radial distance from the coal feed point [m]
- R – Rate of particle shrinkage [m/s]
- S_0 – L_0/L_2
- T_b – Temperature of the bed [K]
- T_s – Surface temperature of a burning char particle [K]
- u_o – Superficial gas velocity in the bed [m/s]
- u_t – Terminal velocity of an elutriating particle [m/s]
- $W(\bar{R}_i)$ – Char weight of i^{th} size interval [kg]
- X_b – Conversion of char in bed
- X_{ce} – Overall carbon efficiency
- X_{O_2} – Conversion of oxygen in bed
- X_v – Conversion of volatiles in bed
- z – Vertical distance in the bed [m]

Greek Letters

- ε – Emissivity of char particles
- ν – Stoichiometry coefficient
- κ_0 – An elutriation constant, [s^{-1}], see Equation (4)
- $\kappa(\bar{R}_i)$ – Elutriation rate constant for particles of size $\bar{R}_i$[s^{-1}]
- ξ_c – Mass fraction of carbon in char
- ρ_c – Density of char [kg/m^3]
- σ – Boltzmann coefficient

REFERENCES

1. Avedesian, M.M. and Davidson, J.F., Trans. Instn. Chem. Engrs., 1973, 51, 121.
2. Campbell, E.K. and Davidson, J.F., Paper A-2, Institute of Fuel Symposium Series No. 1, London, 1975.
3. Gibbs, B.M., Paper A-5, Inst. of Fuel Symposium Series No. 1, London, 1975.
4. Gordon, A.L. and Amundson, N.R., Chem. Eng. Sci., 1976, 31, 1163.
5. Gordon, A.L., Caram, H.S. and Amundson, N.R., Chem. Eng. Sci., 1978, 33, 713.
6. Chen, T.P. and Saxena, S., Fuel, 1977, 56, 401.
7. Horio, M., Mori, S. and Muchi, I., Proc. of 5th Int. FBC Conf., Washington D.C., 1977, Vol. 2, p. 605.
8. Horio, M. and Wen, C.Y., AIChE Symp. Ser., 1978, 74, (176), 101.

9. Rajan, R., Krishnan, R. and Wen, C.Y., AIChE Symp. Ser., 1978, 74, (176), 112.
10. Baron, R.E., Hodges, J.L. and Sarofim, A.F., AIChE Symp. Ser., 1978, 74 (176).
11. Baron, R.E., Beer, J.M., Borghi, G., Hodges, J. L. and Sarofim, A.F., Proc. of 5th Int. FBC Conf., Washington D.C., 1977, Vol. III, p. 406.
12. Fan, L.T., Tojo, K. and Change, C.C., Ind. Eng. Chem. Pro. Des. Dev., 1979, 18, 333.
13. Highley, J. and Merrick, D., AIChE Symp. Ser., 1971, 67 (116), 219.
14. OSU Quarterly Progress Report for January 1, 1979 to March 31, 1979, issued as a supplement for the Babcock and Wilcox Quarterly Report on EFBC prepared for EPRI.
15. Badzioch, S., Britich Coal Tuitlization Research Association Monthly Bulletin, 1961, 25, 285.
16. The Babcock and Wilcox Company, Quarterly Tech. Progress Report for January to March 1979, prepared for EPRI.
17. Levenspiel, O., "Chemical Reactor Omnibook", OSU Book Stores, Inc., Corvallis, OR, 1979.
18. Colakyan, M., M.S. Thesis, Oregon State University, 1979.
19. Field, M.A., Gill, D.W., Morgan, B.B. and Hawksley, P.G.W., "Combustion of Pulverized Coal", BCURA, Letherhead, England, 1967.
20. Jovanović, G., Ph.D. Thesis, Oregon State University, 1979.
21. Burke, S.P. and Schumann, T.E.W., Ind. Eng. Chem., 1928, 20, 998.

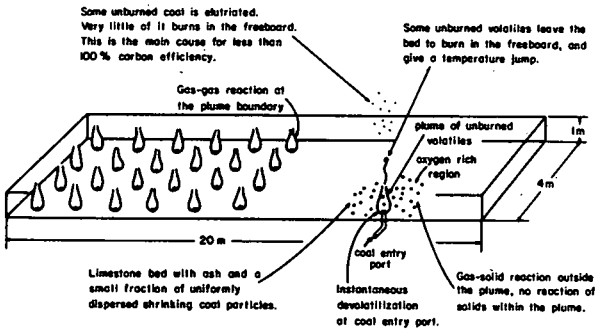

Figure 1. Sketch of the Main Features of Plume Model for the Bottom Coal Feed AFBC.

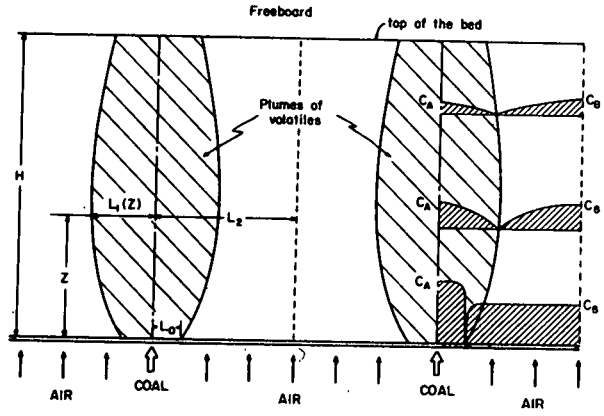

Figure 2. Typical Concentration Profile of Volatiles (A) and Oxygen (B) in the Vicinity of the Plume.

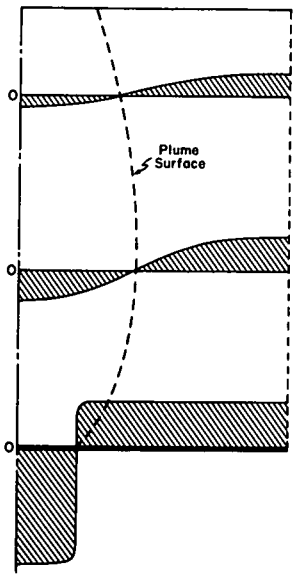

Figure 3. Concentration Profile of Oxygen (+) and Volatiles (-).

TABLE 1. MODELS ON FBC

Model Number and Authors	A	B	C	D	E	F
1. Avedesian & Davidson (1973)	I	a	I	c	I	No
2. Campbell & Davidson (1975)	I	a	I	c	I	No
3. Gibbs (1975)	I	a	I	a	I	Yes
4. Gordon & Amundson (1976)	I	a	I	c	I & III	No
5. Gordon & co-workers (1978)	I	a	I	c	III	No
6. Chen & Saxena (1977)	II	c	I	c	I	Yes
7. Horio & co-workers (1977)	I	a	I	c	II	Yes
8. Horio & Wen (1978) Rajan & co-workers (1978)	III	b	II	a	II	Yes
9. Baron & co-workers (1977)	I & IV	a & d	I	b	II	Yes
Baron & co-workers (1978)	I	a	I	c	I	Yes
10. Fan & co-workers (1979)	I	a	III	c	I	No
11. This work	IV	d	I	d	II	Yes

See Table 2 for description.

TABLE 2. FEATURES OF MODELS IN TABLE 1

A. Model for Fluidized Bed
- I. Two phase bubbling bed model: bubble phase and emulsion phase.
- II. Three phase bubbling bed model: bubble, cloud and emulsion phases.
- III. Compartments in series model: two phases in each compartment.
- IV. Slow bubble regime model: no distinction is made between the bubble phase and the emulsion phase.

B. Gas Flow Pattern in the Bed
- a. Plug flow in the bubble phase, mixed flow in the emulsion phase.
- b. Mixed flow in both phases.
- c. Plug flow in both phases. Gas exchange between two phases is finite.
- d. Plug flow through the bed. No distinction between phases.

C. Movement of Solids in the Bed
- I. Well mixed.
- II. Well mixed in each compartment.
- III. Dispersion of solid is finite. Dispersion coefficient is used for mass balance.

D. Devolatilization of Feed Coal
- a. Instantaneous devolatilization. Volatiles evolve uniformly across the plane representing coal feed point.
- b. Devolatilization is slower than mixing of the feed coal. Volatiles evolve uniformly throughout the bed.
- c. Not considered.
- d. Devolatilization is instantaneous at the feed point.

E. Kinetics of Solid Coal Combustion
- I. Film diffusion controlling.
- II. Both film diffusion and surface reaction influence the rate, but homogenous oxidation of CO to CO_2 is assumed to be very fast.
- III. Rate of CO oxidation is comparable to that of other reactions.

F. Is Elutriation Considered?

TABLE 3. PROPERTIES OF COAL USED FOR CALCULATION

Total Carbon:	73% (moisture free)
Fixed Carbon:	49% (moisture free)
Volatile Matter:	43.7% (moisture free)
Volume of Volatiles:	0.25 m^3/kg of coal
Stoichiometric Air for the Combustion of Coal:	317 mol air/kg coal
f_2:	0.576
γ Calculated Using the Above Values:	2.53
Heating Value of Coal:	31000 kJ/kg coal (dry basis)
Density of Char:	1000 kg/m^3
Maximum (possible) Temperature Rise from Combustion of Volatiles	944.4k

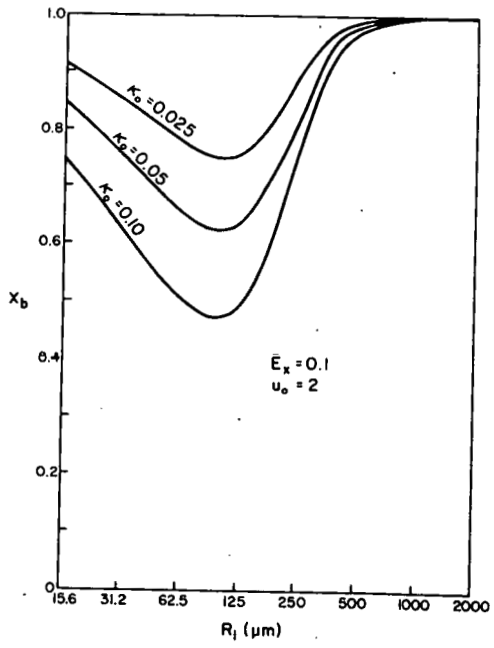

Figure 4. Conversion of Char in the Bed as a Function of Size of Coal Feed and Elutriation Constant.

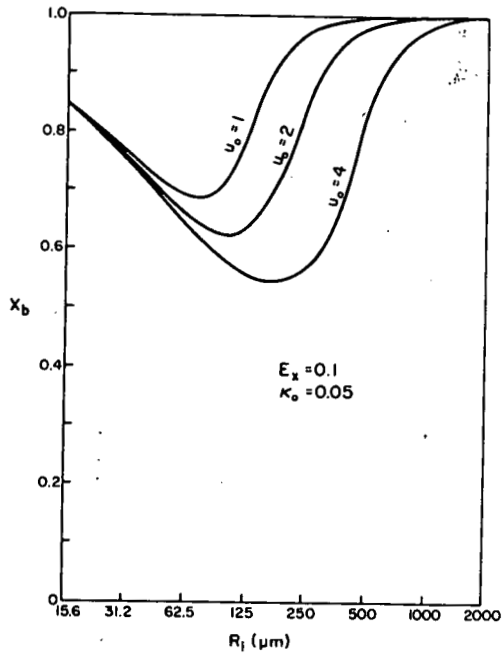

Figure 5. Conversion of Char in the Bed as a Function of Size of Coal Feed and Superficial Gas Velocity in the Bed.

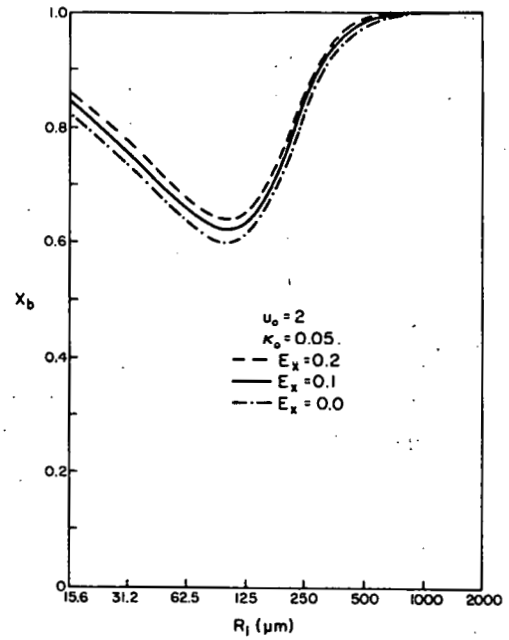

Figure 6. Conversion of Char in the Bed as a Function of Size of Coal Feed and Excess Air.

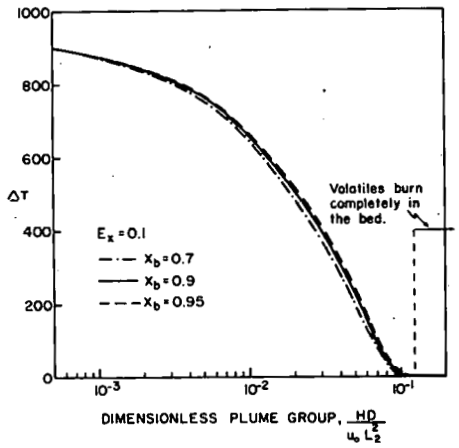

Figure 8. Temperature Jump Above the Bed.

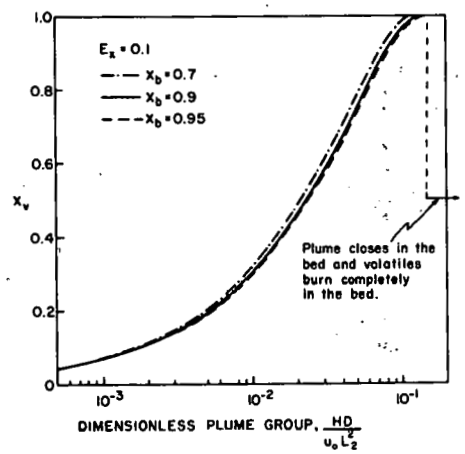

Figure 7. Conversion of Volatiles in the Bed.

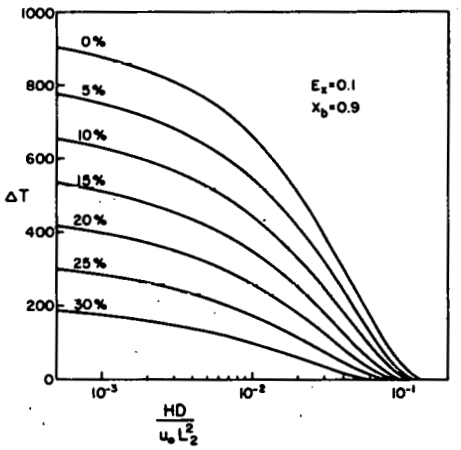

Figure 9. Temperature Jump Above the Bed as a Function of f_3.

APPENDIX

TEMPERATURE OF BURNING COAL CHAR PARTICLES

It is well known that more than one stable temperature is possible for burning coal particles (Field, et al[19]). But the question is at which temperature, if there be more than one, are these burning coal particles in the AFBC.

For the modeling of AFBC's we need a simple but useful representation of this process. As our concern is for char particles of elutriable size, we concentrate on the combustion of small particles, <1mm. In addition, if we assume that only the homogeneous reaction $CO + 1/2O_2 \rightarrow CO_2$ occurs away from the surface of the particle the energy and mass balance is greatly simplified.

In general we have three different regimes of behavior (see Figure A1). Regime A: Only one high temperature steady state. Here, the particle is much hotter than the rest of the bed, the reaction rate constant is very high and consequently the overall combustion rate is controlled by film diffusion. Regime B: Here, we notice three possible char temperatures X, Y and Z. At X the combustion is slow and reaction controlled, at Z the particle is hot, reaction is fast and diffusion controlled. Point Y is unstable and physically unrealizable. If a particle enters Regime B at high temperature, it settles to point X. Regime C: Only one steady state. Here the particle temperature is close to that of the bed, the reaction rate constant is low and the overall combustion rate is slow and chemical reaction controlled.

The regime in which a char particle finds itself depends on the ambient temperature, oxygen concentration, size of particle and the reactivity of the particle. Since a particle shrinks and moves about the bed into widely different oxygen environments (high at bottom of bed, low at the top, zero in the plume), it experiences frequent changes in regime during its lifetime. This can be conveniently displayed as follows.

First, adopting the approach of Field, et al., we evaluate the overall combustion rate of individual particles in a bed at 1116K. This is shown in Figure A2 as a function of oxygen concentration and particle size.

Figure A3 is a more useful representation of these results. It shows that Regime A can only be attained for large particles at high oxygen concentration, while Regime C can be found for the entire range of particle sizes at low oxygen concentrations.

Since coal particles enter the bed cold those smaller than 1mm have no chance of attaining the higher temperature point of Regime B (point Z). However, particles larger than 1mm could well enter Regime A (see point 1 of Figure A3). These remain at high temperature even when they move to point 2. But they are quenched if they move further into Regime C (point 3). In addition, once quenched, they cannot go back to the higher temperature even when they return to Regime B (from point 4 to point 5). A very few particles may be "lucky" enough to stay in Regime B throughout their lifetimes (from point 1 to point 6), but most do not because the lifetime of particles in the bed is longer than their mixing time, and the fraction of bed in Regime C is larger than the fraction in B and A.

Thus, with a bed at 1116K most of the elutriable particles are at the low stable temperature, close to that of the bed.

But the picture is different at higher bed temperature as shown in Figure A4. Here, particles in Regime C (point 1) have a good chance of entering Regime A (point 2) thereby experiencing a temperature jump. They then maintain this high temperature even if they enter Regime B (point 3), as long as they do not return to Regime C. Since the fraction of elutriable solids in Regime A is significant, the chance of having hot elutriable solids is not negligible in this bed.

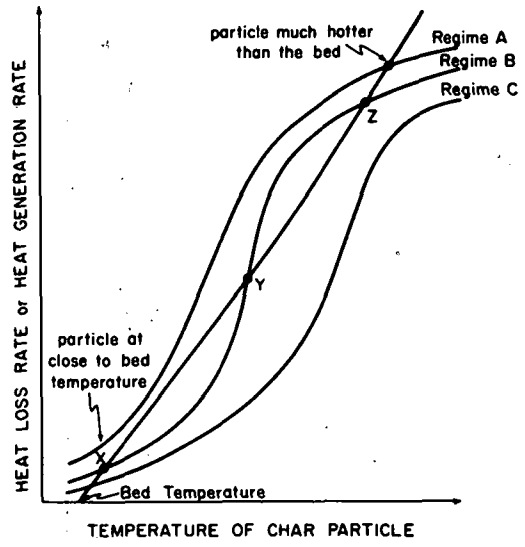

Figure A1. Possible Stable Temperatures in Char Combustion.

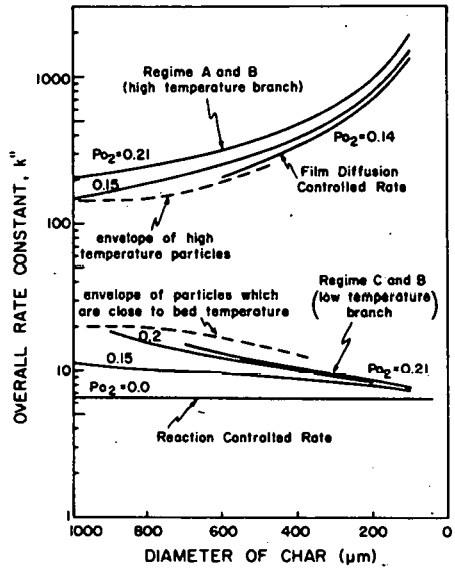

Figure A2. Reaction Rate Constant of Char as a Function of Size of Coal Feed and Oxygen Partial Pressure.

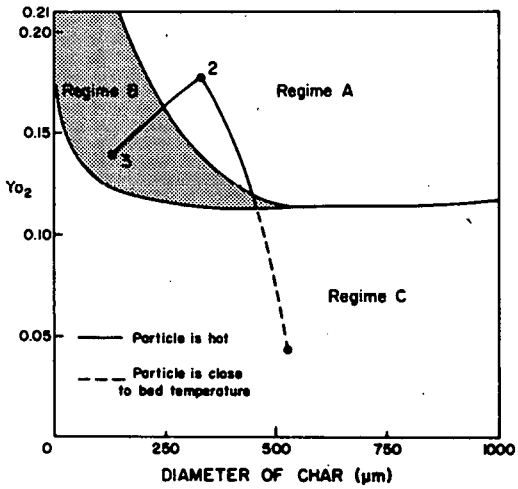

Figure A4. Regimes of Char Combustion at 1228K.

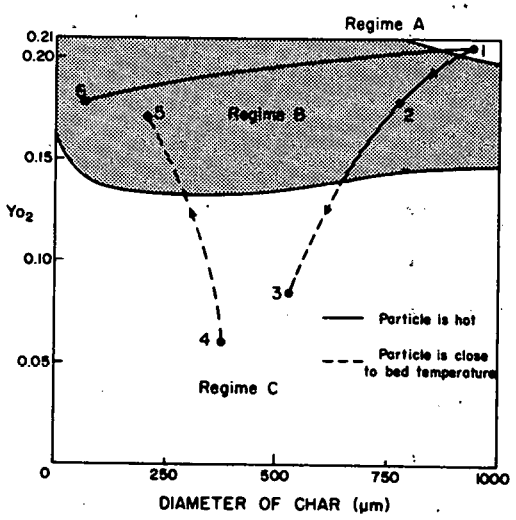

Figure A3. Regimes of Char Combustion at 1116K.

A TECHNIQUE TO PROJECT THE SULFUR REMOVAL PERFORMANCE OF FLUIDIZED-BED COMBUSTORS

R. A. Newby, N. H. Ulerich, D. L. Keairns

Westinghouse R&D Center
Pittsburgh, PA

INTRODUCTION: THE NEED FOR A SULFUR REMOVAL MODEL

A practical model of sulfur removal in fluidized-bed combustors is a desirable tool for several reasons. First of all, it is important that we understand sulfur removal in fluidized-bed combustion because:

- Sulfur removal is a key environmental constraint on the system performance, as is illustrated by the current EPA NSPS for utility boilers in Figure 1.
- Sulfur oxide (SO_x) control directly involves, and greatly affects other plant systems, such as the particulate control system, the solid waste handling and disposal system, potential alkali control systems, and solids feeding or reinjection systems.
- Sulfur removal relates directly to other combustor performance elements, such as corrosion, erosion, deposition, and nitrogen oxide (NO_x) control.
- The plant efficiency and cost of electricity are both very sensitive to the calcium-to-sulfur (Ca/S) ratio, as is illustrated for AFBC and PFBC in Figures 2 and 3.[1]
- Sulfur removal is, itself, very sensitive to the combustor design and operating conditions and to the coal and sorbent properties.
- The understanding of SO_x control is a long-term need since each fluidized-bed combustion plant may be unique in many of its features and with respect to its sorbent and coal properties, and future revisions in SO_2 control standards may occur.

Secondly, this understanding of fluidized-bed combustion sulfur removal cannot be provided solely through the operation of development facilities because of the extremely broad range of parameters characterizing atmospheric-pressure (AFBC) and pressurized fluidized-bed combustion (PFBC) (power cycles, process configurations, combustor designs, combustor operating conditions, and coal and sorbent properties). The operation of pilot equipment

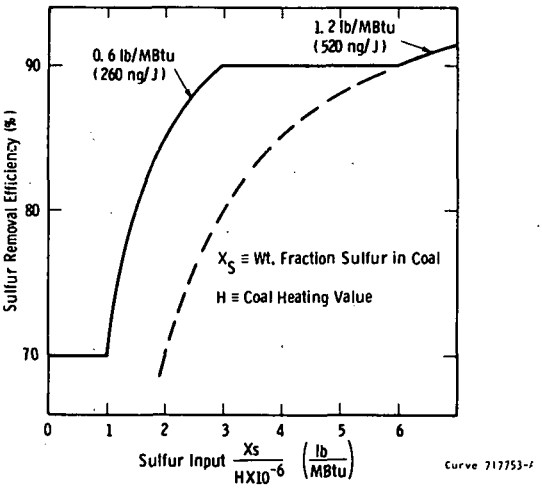

Figure 1 - SO_x NSPS for Coal-Fired Electric Utility Steam Generating Units (>250 MBtu/hr)

over a broad range of parameters is expensive and time consuming, and many parameters are difficult to control independently on a fixed piece of equipment. In addition, the results from development unit operation can lead to significant conclusions only when evaluated with some type of system model.

Finally, a practical sulfur removal model can be applied to:

- Correlate and explain plant data
- Plan experiments
- Design hardware and processes
- Evaluate process performance
- Simulate control dynamics
- Select sorbents
- Identify ways to improve performance.

The potential benefits, thus, go far beyond the satisfaction of academic interests.

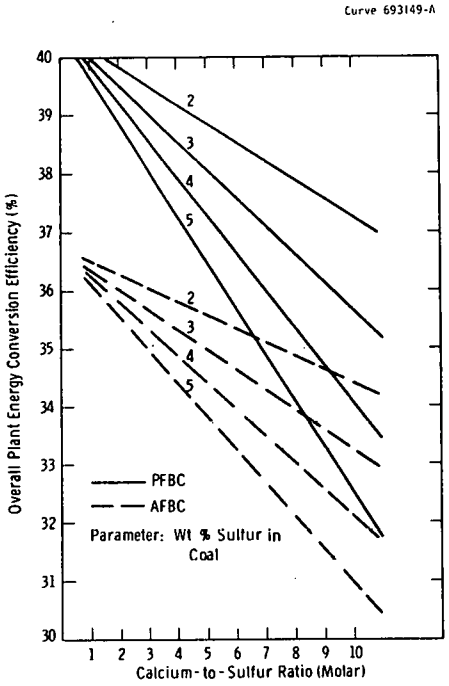

Figure 2 - FBC Power Plant Energy Conversion Efficiency

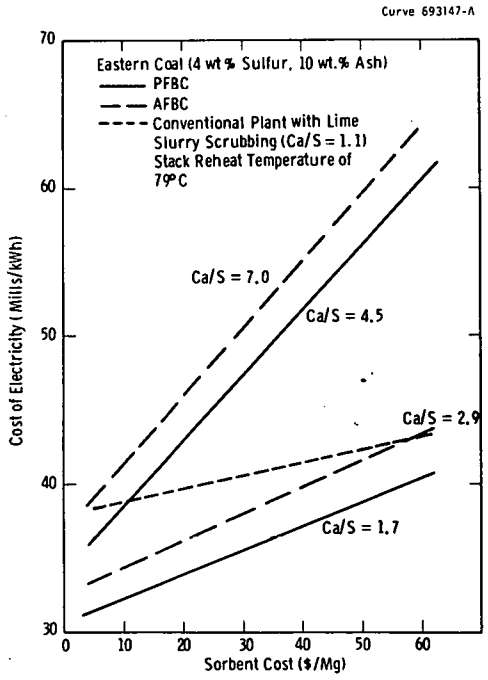

Figure 3 - Comparison between AFBC, PFBC, and FGD for SO_x Emission Requirement of 90% Sulfur Removal

PHENOMENA OF CONCERN AND CURRENT MODELING CAPABILITIES

In order to model fluidized-bed combustor sulfur removal, two general classes of phenomena must be described in a modeling sense: sorbent particle reaction phenomena and fluid-bed phenomena. The need to consider these classes of phenomena is evident from a general material balance on SO_x within a differential volume of a fluid-bed combustor bounded by two horizontal planes separated by a distance ΔX (Figure 4):

$$\frac{\partial}{\partial t}\int_v c\,dv = \int_{A_X} \underline{u}\cdot c\,d\underline{S} - \int_{A_{X+\Delta X}} \underline{u}\cdot c\,d\underline{S} + \int_v g\,dv - \int_v r\,dv \quad . \qquad (1)$$

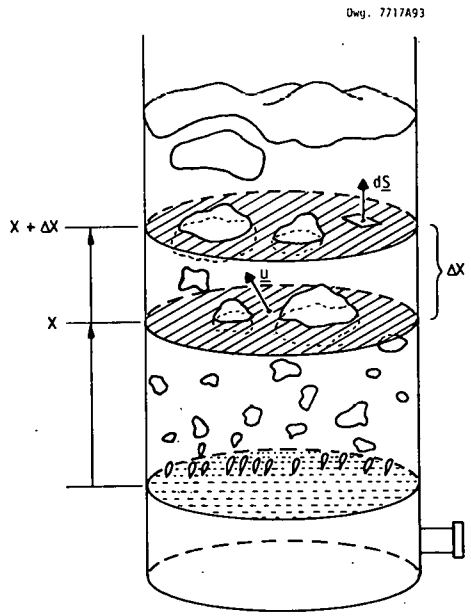

Figure 4 - Material Balance for SO_x

In equation 1, c and $\underline{u}$ are the local, instantaneous values of the SO_x concentration and the gas velocity; g is the local, instantaneous rate of SO_x generation; and r is the local, instantaneous rate of SO_x capture by reaction with the bed sorbent.

For steady-state operation, the time-averaging of equation 1 results in:

$$0 = \int_{A_X} \overline{\underline{u}c}\cdot d\underline{S} - \int_{A_{X+\Delta X}} \overline{\underline{u}c}\cdot d\underline{S} + \int_v \overline{g}\,dv - \int_v \overline{r}\,dv \quad . \qquad (2)$$

where $\overline{uc}$, $\overline{g}$ and $\overline{r}$ are the time-averaged convective, generation and reaction terms. The solution of equation 2 requires descriptions of the dynamics of gas and solids mixing, the SO_x generation rate (directly related to the rate of coal combustion), and the SO_x-sorbent reaction rate. This general equation holds above the bed as well as within the bed.

Sorbent Particle Reaction Phenomena

Figure 5 illustrates conceptually the phenomena occurring as a single, stationary sorbent particle, limestone or dolomite, contacts a hot combustion-product gas containing SO_x. The raw sorbent particle is comprised of individual grains or crystallites which are held together by natural binding agents. The binding agents could consist of many materials, such as calcium and magnesium carbonates, silica, and so on. The grains may also interlock. A wide variety of impurity concentrations typically exist in different sorbent sources (Al_2O_3, Fe_2O_3, SiO_2, Na_2O, K_2O, $MgCO_3$, etc.), and the impurities may reside both in the crystallites and in the binding agent. The porosity of the raw sorbent and the size of the grains also vary widely among sorbent sources. For example, we have measured average grain diameters in limestones and dolomites ranging from 15 to 400 μm, and porosities have been found to range typically between 1 and 10 percent.

The raw sorbent particle initially passes through a heating and calcining stage which generally results in an increase in porosity, pore diameter, and surface area, although interaction with impurities and sintering effects can eventually

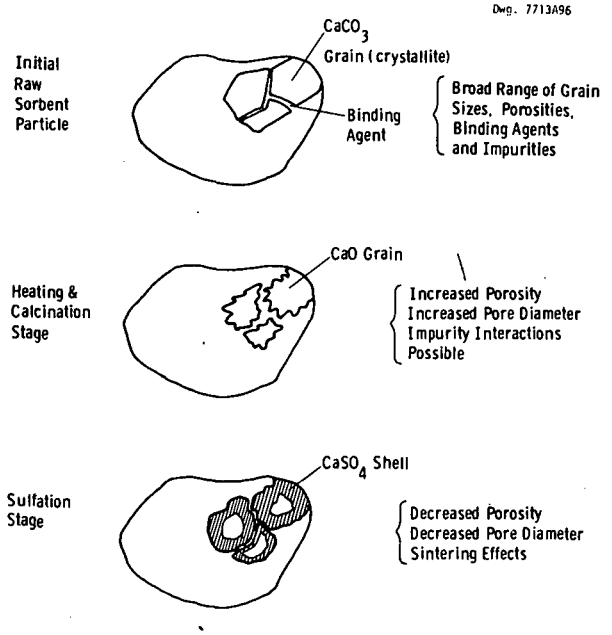

Figure 5 - Sorbent Particle Reaction Phenomena

lead to reductions in these parameters, though on a much longer time-scale than is required for calcination. Following the calcination-heatup stage, the sorbent particle reacts with SO_x, diffusing to the grain surfaces, to form $CaSO_4$. Because of the larger molecular volume of $CaSO_4$ relative to that of CaO and $CaCO_3$, the reaction products promote a decrease in the particle porosity and pore diameter, with an eventual reduction in the reaction rate to a negligible level before complete sulfation has been achieved. Again, sintering may play a part in the reduction in reaction rate.

A great deal of empirical information is available with respect to the nature of the SO_x-sorbent reaction phenomena.[2-6]

In summary form:

- Sorbent reaction behavior varies widely among sorbent sources.
- Sorbent performance is very sensitive to rate of calcination (mainly dependent upon the rate of heating, peak temperature, and CO_2 pressure) and impurity interactions; time-temperature phenomena may be important with some sorbents.
- The sulfation rate is approximately first-order in SO_x concentration, zero-order in O_2 concentration.
- Grain size, porosity, and impurity level of the raw sorbent seem to be the key sorbent characteristics, but these have yet to be correlated with the sorbent performance.
- Sorbent performance trends have been extensively explored and characterized with respect to
  - Particle size
  - Temperature
  - Pressure
  - Calcining conditions
  - Sorbent properties and types
  - SO_x concentration
  - O_2 concentration
  - CO_2 concentration
  - Water vapor
  - Impact of impurities.

While the phenomena of importance have been identified and trends in behavior recorded, our ability to model these phenomena is hindered by the complexity of this gas-solid reaction system so

characterized by transient chemical/physical properties. The current limitations in modeling are:

- Initial particle structure/chemical nature
  - Simple geometric descriptions are possible.
- Calcination step
  - The rate and resulting structure are currently unpredictable.
  - The rate-determining steps have not been resolved.
- Sintering and impurity interactions
  - No models or correlations are available on even relative impacts.
- Overall sulfation reaction
  - Pore diffusion is transient in resistance; simple models have been attempted.[7,8]
  - Basic reaction mechanisms are as yet unresolved.
  - Solid state diffusion is not yet described in these systems.

Overall, a model of the sorbent particle reaction phenomena having the necessary features cannot be currently realized, and we conclude that empirical techniques are necessary.

Fluid-Bed Phenomena

The major aspects of fluid-bed phenomena of concern to fluid-bed sulfur removal are the mixing behavior of the bed particles and the fluidizing gas, particle elutriation, and particle attrition.

The conceptual picture of the sorbent reaction phenomena shown in Figure 5 for a stationary particle is further complicated by sorbent particle attrition. A large number of attrition sources arising from mechanical, thermal and chemical stresses[9] are available in any fluidized-bed combustion system. Figure 6 conceptually depicts the history of a sorbent particle as it undergoes sulfation and attrition in a fluidized-bed combustion system, in contrast to the situation shown in Figure 5. A single particle of sorbent passes through various stages of attrition, generally at a rate decreasing greatly with particle residence time in the bed, in which its initial identity with respect to size and shape may be lost. The impact of elutriation is to segregate the sorbent material into two streams having significantly different properties: the elutriated sorbent material is of a fine size distribution, is relatively young (a few minutes' to an hour's residence in the bed), and has significant residual activity; the bed overflow stream is relatively coarse, old (2-50 hours'

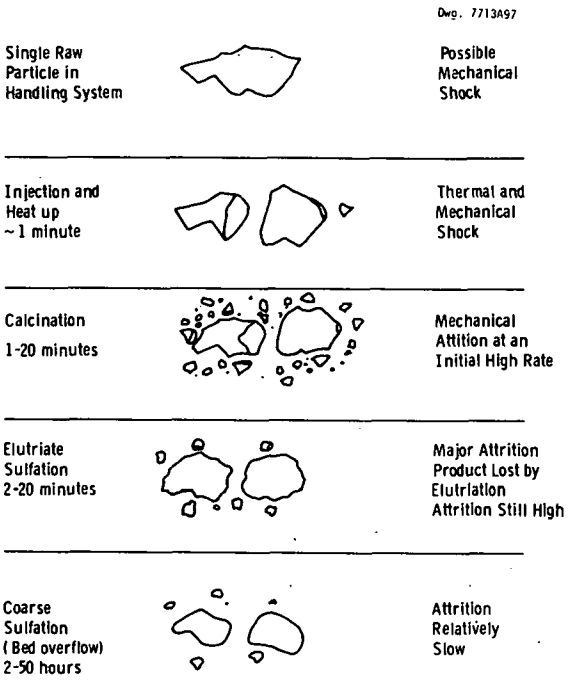

Figure 6 - Bed Dynamics

residence time for operation with high-sulfur coals and up to 500 hours for operation with subbituminous coals), and of low activity.

Researchers have generated models of specific particle attrition mechanisms (thermal shock, bubbling-bed attrition, high-velocity mechanical shock) and have developed fluid-bed sorbent attrition screening tests.[10,11] The attrition behavior of sorbents is known to vary considerably among sorbent sources, as indicated in Figure 7. The attrition rate also has been observed to be sensitive to particle residence time (Figure 8). This behavior has been mathematically described,[9] but, in general, our understanding of attrition remains the greatest limitation to predicting particle size distributions in fluid-bed combustion systems.

The dynamics of gas and particle mixing determine the effectiveness of the contact between the SO_x and the sorbent particles and determines the profile of combustion and SO_x release in the bed. The gas and particle mixing is ultimately related to the nature of voids (bubbles) passing through the bed and is influenced by the presence of heat transfer surface in the bed.

We know empirically that for large particle systems ($\geq$200 μm diameter) at the operating conditions typical of fluidized-bed combustors where "slow bubbles" may be representative and in the presence of internals such as heat transfer surface, plug flow of the gas through the bed is a reasonable assumption to apply for sulfur removal modeling[12,13] (where SO_x is being generated within

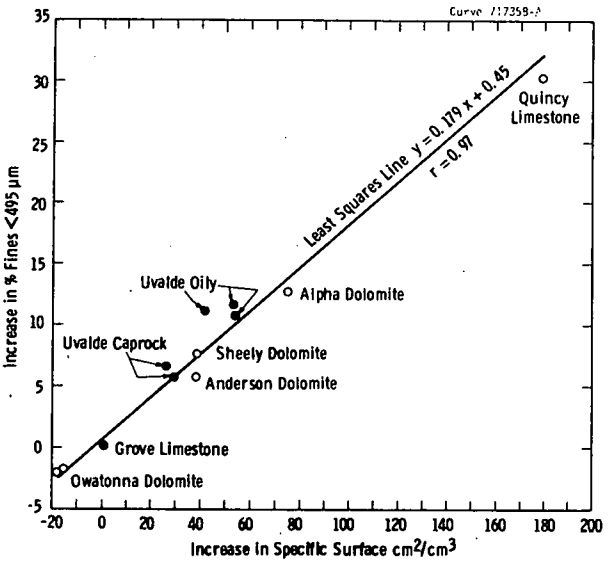

Figure 7 - Comparison of Sorbent Attrition Behavior for Two-Hour Hot Fluidization Test

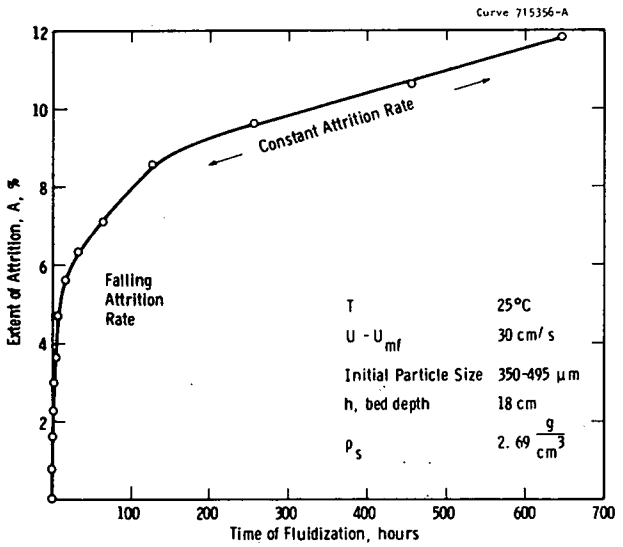

Figure 8 - Change of Extent of Attrition with Time in Bubbling Fluidization

the emulsion phase). The plug flow assumption may be less realistic with respect to coal combustion phenomena. It is also safe to assume perfect mixing of sorbent particles within the bed because the mixing rate of particles is high relative to the sulfation rate and relative to the particle residence time in the bed.[14] Again, the assumption of perfect particle mixing may be less reasonable in the case of char particle combustion.

Sulfur oxide is released in parallel with the combustion of char and volatiles. Both in-bed and above-bed combustion of char particles and volatiles may occur, with a resulting release of SO_x both in the bed and above the bed. Figure 9 illustrates the regions of the fluidized-bed combustor where substantially differing SO_x release and capture rates occur. Generally, the most significant SO_2 release and capture occurs within the dense bed. In the splash region directly above the bed, minor-to-significant release of SO_x can occur through combustion of unburned volatiles and of elutriated char particles. Relatively coarse particles will be propelled into this region and will drop back into the bed, resulting in reflux-type behavior. The time-averaged concentration of particles in the splash region will be sufficiently low that only minor capture of SO_x will occur. Above the splash region a minor amount of SO_x will be released as fine char particles are pneumatically transported, and a negligible amount of SO_x will be captured because of the low sorbent particle concentration and the generally short gas residence time. Because of the randomly fluctuating nature of the bed surface determining its time-average position is difficult and prone to error.

This simple picture of SO_x release can be extended to describe the two extremes of behavior shown in Figure 10. The region of intense combustion in the bed (and resulting intense SO_x release) is such that we may reasonably assume that in AFBC SO_x is released uniformly within the bed (typically about 1 meter deep). In PFBC, with generally deep beds and higher excess air levels, SO_x release will prevail near the base of the bed, and we may assume instantaneous release at the base of the bed. In formulating this picture, we have also assumed in-bed feeding of coal near the base of the bed. Above-bed feeding could modify this description, depending on the size distribution of the coal.

Our ability to model fluidized-bed combustion phenomena is summarized as follows:

- Particle mixing
  - Understanding is primitive, although the mechanisms are known.

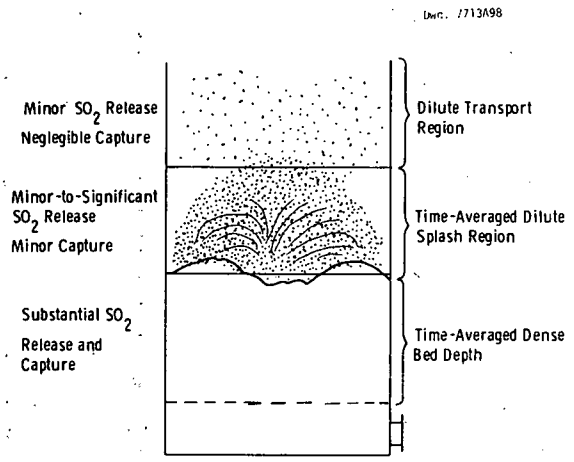

Figure 9 - Bed SO_2 Release and Capture Regions

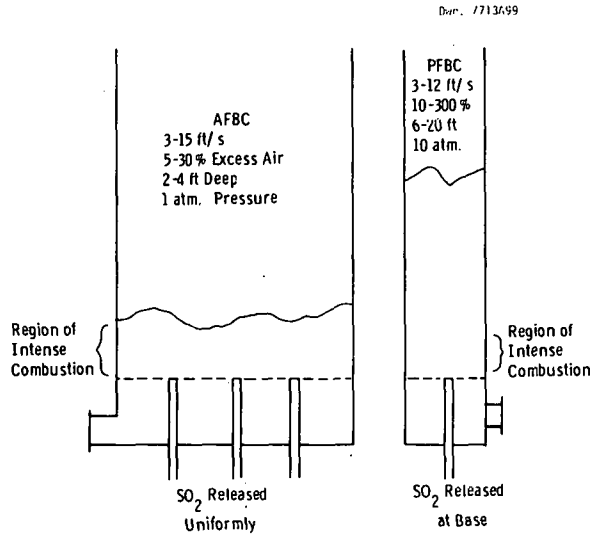

Figure 10 - Mode of SO_x Release

- Empirical models are available (perfect mixing, diffusion, bubble-wake-induced circulation).
- Large-scale mixing or mixing near internals has not been successfully modeled.

- Gas mixing
  - Understanding is limited to single bubbles, in the absence of internals.
  - Empirical models are available for bubble sizes, mass transfer, flow-through of bubbles.
  - Basic two-phase fluid-bed models, while useful, are still controversial and in a state of development
- Particle elutriation
  - Many correlations are available, but do not give consistent results.
  - Understanding is limited and mechanisms are unresolved.
- Particle attrition
  - A multitude of attrition mechanisms have been identified.
  - Some attrition phenomena have been correlated and modeled.
  - No general correlations are available; limited plant data have been evaluated.
  - Relationship to sorbent properties is unresolved.
- Coal combustion
  - Empirical models of devolatilization are available but the data are limited.
  - The basic principles and mechanisms are are understood, and some practical modeling concepts have been proposed.[15]
  - Modeling of combustion of volatiles and char is limited by inadequate knowledge of gas and particle mixing, coal attrition, and elutriation.

ASSESSMENT OF FBC SULFUR REMOVAL MODELING

Overall, the assessment of our ability to model, in detail, the major phenomena of concern to FBC sulfur removal is rather negative. Several system models have been attempted. These may be broken down into four general classes of models. These classes and their characteristics are as follows:

- First-Principle Models (e.g., Systems, Science and Software[16])
  - The first-principle relationships are not all known.
  - The ability to solve the first-principle conservation equations is limited.
- Bubbling Bed Models (e.g., West Virginia Univ.,[17] Univ. Illinois,[18] MIT[19])
  - Structure is based on a variety of bubbling fluid-bed empirical descriptions.
  - A large number of specific assumptions have been applied.
  - A huge number of parameters and empirical coefficients need to be specified.
  - Complex computer solutions are required.
  - The results are difficult to apply for design purposes or for data correlation.
- Empirical Expressions (e.g., B&W[20])
  - Limited physical basis
  - Limited to specific test conditions
- Practical, Semitheoretical Models (e.g., Westinghouse[1,21])
  - Uses empirical, specific kinetic data
  - Based on fundamental framework with assumptions based on experimental observations
  - Can be simple or complex, depending on needs.

WESTINGHOUSE SULFUR REMOVAL MODEL

The point of view applied in developing a practical model of fluidized-bed combustion sulfur removal is based, in part, on the conceptual pictures of the phenomena of concern presented in the previous sections of this paper. A practical model must, above all, be a usable tool and should be developed from a fundamental basis. It should be as detailed as is needed to produce performance predictions that represent trends to within the accuracy of plant data. In determining sulfur removal performance from FBC plant data, we must measure gas and solids compositions and stream flow rates. The determination of the plant sulfur removal efficiency, for example, requires the measurement of at least five parameters, each of which is subject to measurement errors. We estimate that errors of ±3 to 10% in experimentally determined FBC sulfur removal efficiencies and ±10 to 20 percent in the Ca/S ratios are typical of FBC development unit results. Continuous fluctuations in raw material properties (coal and sorbent) and the reporting of non-steady plant data result in further inaccuracy in plant performance data.

The key observation in the formulation of the Westinghouse model is that in most cases the controlling resistance in transporting released SO_x to active sorbent reaction sites resides in the diffusion of SO_x through the sorbent particle pores. Two important consequences result from this observation:

1. Sulfur oxide transport mechanisms within the bed, other than those occurring within the sorbent particle pores, need not be described in great detail.

2. The kinetics of SO_x capture by sorbents may be simulated in small-scale laboratory equipment and these measurements applied to predict fluid-bed combustor performance with an appropriate model for the bed dynamics.

With respect to consequence 2, Westinghouse is operating thermogravimetric balances (such as the pressurized unit pictured in Figure 11) to simulate sorbent behavior and to produce rate curves like those shown in Figure 12.

In returning to the general time-averaged material balance (equation 2), we apply the assumptions and observations described to make the following simplifications:

$$\overline{\underline{u}\ c} \equiv \underline{\overline{u}}\ \overline{c} + u'c' \qquad (3)$$

where u' and c' are the local fluctuations in the time-averaged quantities $\underline{\overline{u}}$ and $\overline{c}$. With high rates of lateral gas mixing between the bubbles and emulsion phase and generally plug flow c' is small across any horizontal plane and

$$\overline{\underline{u}\ c} \approx \underline{\overline{u}}\ \overline{c} \quad . \qquad (4)$$

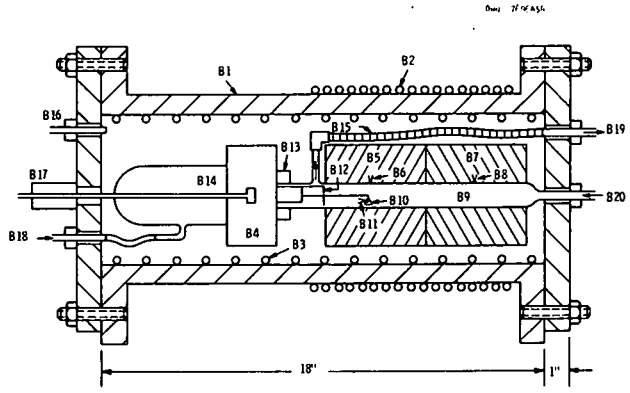

KEY TO FIGURE 11

B1	Stainless Steel Pressure Vessel
B2	External Cooling Coil
B3	Internal Cooling Coil
B4	TG Balance Housing
B5	Reaction Zone Furnace
B6	Reaction Zone Thermocouple
B7	Preheat Zone Furnace
B8	Preheat Zone Thermocouple
B9	Quartz Reaction Tube
B10	Sample Basket
B11	Sample Thermocouple
B12	Baffle Assembly
B13	Reaction Tube Retaining Ring
B14	TG Bell Jar
B15	Flexible Metal Exhaust Hose
B16	Atmospheric-Pressure Vent
B17	TG Balance Electrical Feedthrough
B18	Inert Purge Gas Inlet
B19	Exhaust Gas Outlet
B20	Reaction Gas Inlet

Figure 11 - The Pressurized TG Apparatus

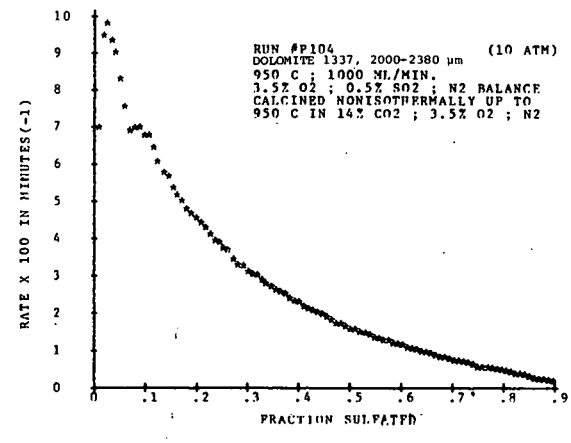

Figure 12 - TG Sulfation Rate Data
Dolomite 1337 at
10 atm Pressure

Relationship 2 becomes

$$U \frac{dC}{dX} = G - R \tag{5}$$

where U is the superficial velocity,

$$U = \frac{\int_A \underline{u} \cdot d\underline{S}}{A} , \tag{6}$$

and

$$C = \overline{c}(X) . \tag{7}$$

The term G is the time-averaged SO_x release rate defined as

$$G \equiv \underset{\Delta X \to 0}{\text{limit}} \frac{\int_v \overline{g} dv}{A \Delta X} , \tag{8}$$

and R is the time-averaged sulfation reaction rate defined as

$$R \equiv \underset{\Delta X \to 0}{\text{limit}} \frac{\int_v \overline{r} dv}{A \Delta X} . \tag{9}$$

Because the sulfation reaction is first order with respect to the SO_x concentration

$$\overline{r} \propto \overline{c} , \tag{10}$$

and it follows from equation 9 that

$$R = \frac{k}{v_p} C(1-\delta)(1-\varepsilon)(1-f_p)(1-f_H), \tag{11}$$

where k is the reaction rate constant per sorbent particle of a sorbent particle having a diameter and sulfation level equal to the mean surface diameter and mean sulfation level of all sorbent particles in the bed, δ is the volumetric bubble fraction in the bed, ε is the emulsion phase voidage, f_I is the volume fraction of inert particle in the bed (char, ash, rocks, etc.), f_H is the volume fraction of the bed occupied by heat transfer surface, and $\overline{v}_p$ is the average sorbent particle volume in the bed.

If we write

$$R \equiv k'C , \tag{12}$$

then

$$U \cdot \frac{dC}{dx} = G - k'C \tag{13}$$

where G is a function of x.

The general solution of equation 13 is

$$C = \exp\left\{-\frac{k'}{U} x\right\}\left[\int_o^x \frac{G}{U} \exp\left\{\frac{k'}{U} x\right\} dx\right] . \tag{14}$$

The sulfur removal efficiency of the bed is defined by

$$E \equiv 1 - \left[\frac{C(x=h)U}{\int_o^h G dx}\right] , \tag{15}$$

where h is the expanded bed depth.

Applying the two extremes in behavior describing the SO_x release term G for AFBC and PFBC (Figure 10) results in the two final forms for the sulfur removal efficiency:

AFBC: SO_x is released uniformly throughout the bed:

$$E = 1 - \frac{U}{k'h}\left[1 - \exp\left\{-k' \frac{h}{U}\right\}\right]; \tag{16}$$

PFBC: SO_x is released at the base of the bed:

$$E = 1 - \exp\left\{-k' \frac{h}{U}\right\} . \tag{17}$$

The ratio h/U may be defined as a gas residence time τ.

The rate constant k (in equation 11) is a function of the fractional sulfation level of the sorbent particles in the bed and, because of the basic premises above, is directly related to the kinetic results taken from the thermogravimetric system by

$$k = \left(\frac{d\alpha}{dt}\right)_{TG} \frac{v_p \rho}{C_{TG}} \tag{18}$$

In equation (18), $(d\alpha/dt)_{TG}$ is the sulfation rate of sorbent particles in the thermogravimetric system at the same sulfation level as in the fluid-bed combustor, with the experiment run under appropriate temperature, pressure, and calcination conditions, using sorbent particles having the same surface-mean diameter as in the combustor and using an SO_2 concentration C_{TG}. The molar density of the sorbent particle (moles of calcium per unit particle volume) is represented by ρ.

The forms of the general expressions 16 and 17 are shown in Figure 13 as a function of $k'\tau$. In addition, a curve representing the case where perfect gas mixing prevails in the bed is included. The curve for perfect gas mixing differs little from the curve for uniform SO_x release in the bed,

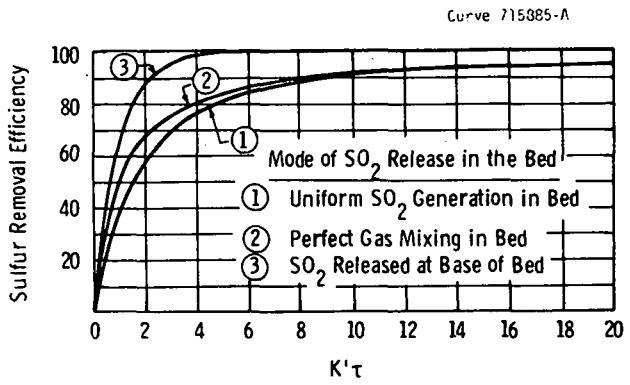

Figure 13 - Alternative Forms of Sulfur Removal Model

and the two modes of mixing would be indistinguishable, based on experimental fluid-bed combustor results. Obviously, release of SO_x at the base of the bed results in more effective sulfur capture.

The sensitivity of the predicted sulfur removal efficiency to the portion of the bed in which the coal sulfur content is substantially released is shown in Figure 14. As the figure shows, release of SO_x substantially in the lower-half of the bed would result in a sulfur removal performance very similar to that obtained with release entirely at the base of the bed. If conditions in the splash region are identical to those in the bed (i.e., same mean particle diameter, same sorbent particle sulfation level, same SO_x release profile), then equations 16 and 17 will include the capture of SO_x in the splash region if the inventory (time-averaged) of sorbent material is included in the bed to give an effective bed depth. In most cases this has a small impact.

The model expressed in relationships 16 and 17 is then applied quite simply, using appropriate TG kinetic data, to predict the sulfur removal efficiency, E, as a function of the fractional sulfation level, α, and the Ca/S ratio:

$$Ca/S = E/\alpha \quad . \qquad (19)$$

The model is also easily extended to include:

- Above bed sulfur capture
- Integration with
  - Elutriation and attrition models (for example, a general particle profile model Westinghouse[22] developed)
  - Combustion models
- Coals having active ashes (lignites, subbituminous coals[21])

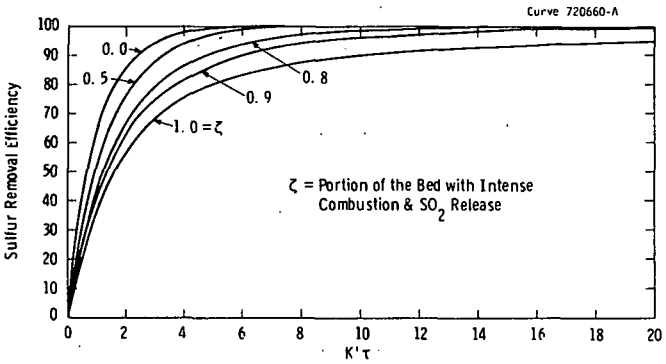

Figure 14 - Impact of SO_x Generation Pattern on Sulfur Removal

- Systems integration (e.g., carbon burnup cell, fines recycles)
- Advanced sulfur removal systems[23] (for example, precalcination, salt exposure, agglomeration, regeneration).

APPLICATIONS OF THE WESTINGHOUSE SULFUR-REMOVAL MODEL

The model whose development is described here has been applied in a variety of EPA, EPRI, and DOE sponsored programs over the past eight years to correlate and review FBC plant data, to design and evaluate FBC hardware and processes, to simulate FBC SO_x control dynamics, for the selection of sorbents, and to identify methods of improving FBC sulfur removal performance. A summary of these activities follows:

- Plant Data Correlation and Review
  - B&W 3' x 3' and 6' x 6' AFBC units[24,25]
  - METC AFBC data (unpublished)
  - PER AFBC data[26]
  - FluiDyne AFBC data (current EPA program)
  - GFETC subbituminous coal AFBC data[26]
  - Exxon PFBC data[27]
  - Leatherhead PFBC data (current EPRI program)
- Hardware and Process Design and Evaluation
  - AFBC electric utility application[1]
  - AFBC industrial boiler application[28]
  - PFBC electric utility application[1,29,30]
  - Advanced sulfur removal systems for AFBC application (regeneration, precalcination, agglomeration)[23,25]
- SO_x Control dynamics simulation
  - AFBC and PFBC application (current EPA program)
- Sorbent Selection
  - Performed in programs with B&W, FluiDyne, Burns & Roe, Leatherhead, Conoco

- Performance Improvement Techniques
  Precalcination[31]
  Selection of sorbent particle size and operating conditions.[1,3,32]

Selected examples of results from these applications of the model are included. Figure 15 is a generalized projection of the sorbent requirements for AFBC as a function of sorbent particle size and sorbent activity class. Three classes of limestones (high, medium, and low reactivity) have been proposed on the basis of an analysis of our TG data bank. The figure displays the kind of variation in performance to be expected with AFBC.

Figures 16 through 19 are model comparisons of B&W AFBC and Exxon PFBC data which have been previously reported.[24,25,27] Since the average particle size of the bed material was not known, projections of the Exxon data in Figures 18 and 19 were made with a range of sorbent particle sizes. In all cases nominal operating conditions were applied to make the projections, while conditions varied from test point to test point. The agreement shown is typical of all comparisons performed and has provided confidence in the validity of this approach. Ongoing programs with EPA and EPRI are being performed to confirm the model in greater detail.

Curve 718911-A

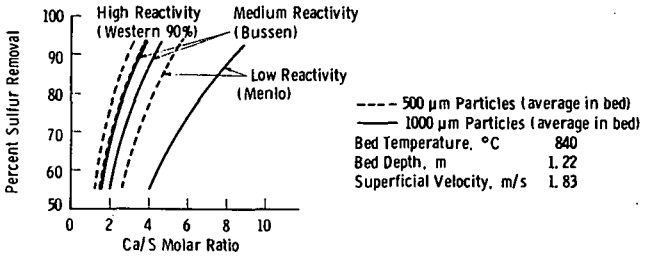

Figure 15 - Effect of Sorbent Activity Category and Particle Size on Ca/S Molar Feed Ratio Requirement

CONCLUSIONS

The major conclusions drawn from this work are:

- A model of sulfur removal in FBC is of key importance to the successful development and application of FBC.
- Currently, the details of the phenomena of concern to FBC sulfur removal cannot be quantitatively modeled; an empirical approach is required.
- A practical model of FBC sulfur removal can be developed based on the observation that the major resistance to the capture of SO_x resides in the pores of the sorbent

Curve 690412-A

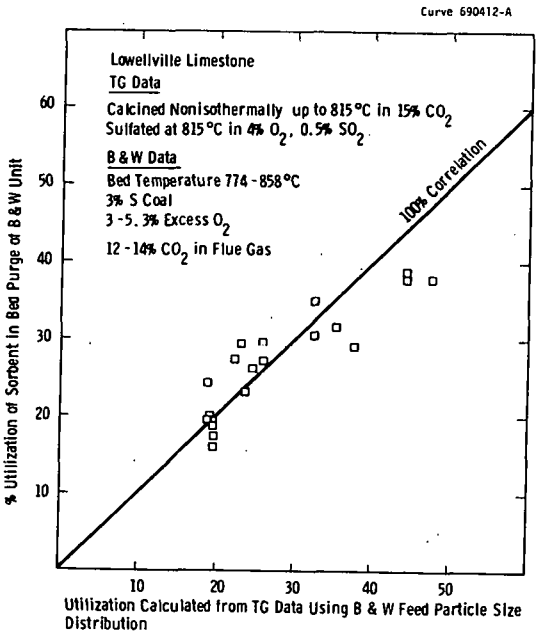

Figure 16 - Comparison of Sorbent Capacity Obtained from Westinghouse TG Data with B&W 3 ft x 3 ft Fluid-Bed Results

Curve 715890-A

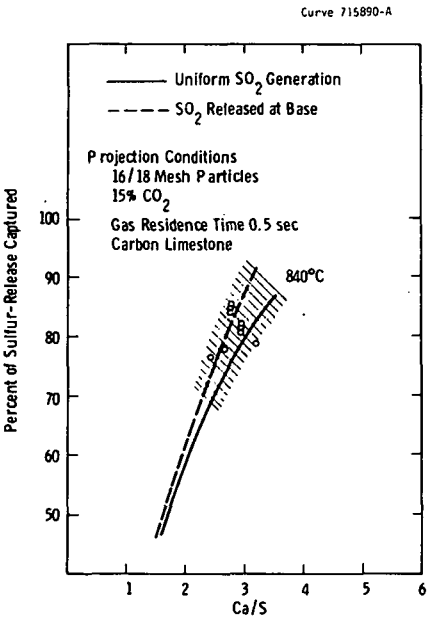

Figure 17 - Comparison of Projections with B&W 6 ft x 6 ft Run Series 2 Data for Nonisothermal TG Data at 840°C (1554°F)

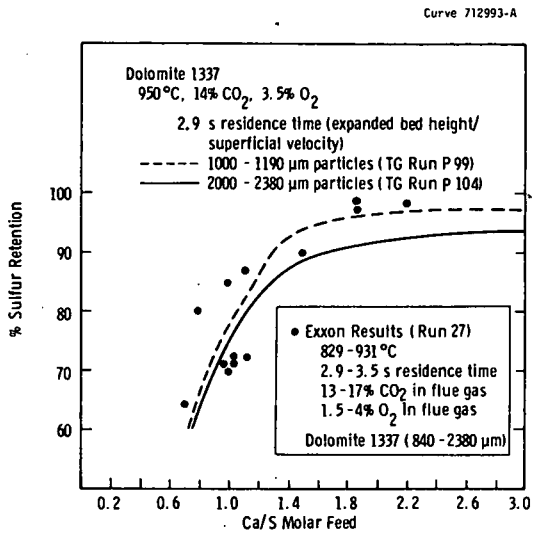

Figure 18 - Sulfur Removal Projected from TG Data and Measured on the Exxon Miniplant

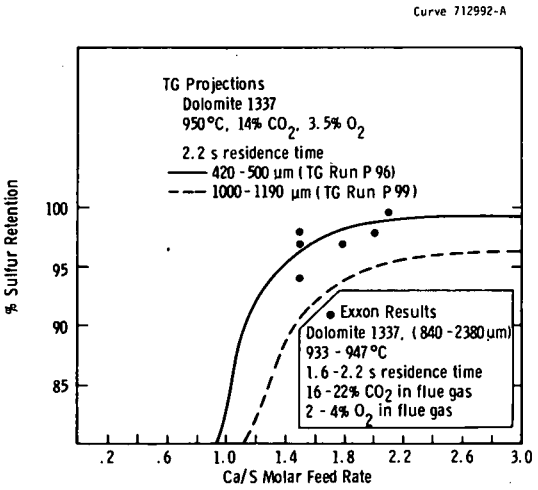

Figure 19 - Comparison of TG Projections for Greater than 90% Sulfur Removal with Exxon Data for Dolomite 1337

particles. Thus, laboratory equipment such as a TG balance can be operated to provide sorbent sulfation kinetic data, and this kinetic data can be combined with an approximate model of the fluid-bed dynamics to generate acceptably accurate predictions of FBC performance.

- The FBC sulfur removal model Westinghouse developed shows acceptable agreement with AFBC and PFBC plant data, accurately predicts performance trends, and is a useful tool for FBC hardware and process design.

REFERENCES

1. Newby, R. A., N. H. Ulerich, E. P. O'Neill, D. F. Ciliberti, and D. L. Keairns, Effect of SO_2 Emission Requirements on Fluidized-Bed Combustion Systems: Preliminary Technical/Economic Assessment, August 1978, EPA-600/7-78-163, NTIS PB 286 977/7ST.

2. O'Neill, E. P., D. L. Keairns, and W. F. Kittle, a Thermogravimetric Study of the Sulfation of Limestone and Dolomite-The Effect of Calcination Conditions. Proceedings of the Annual Meeting of the North American Thermal Analysis Society, Trent University, Peterborough, Ont., June 8-12, 1975; published in Thermochimica Acta, 14: 209-220; 1976.

3. O'Neill, E. P., N. H. Ulerich, D. L. Keairns, R. A. Newby, and D. H. Archer, Optimizing Sorbent Utilization in Once-Through Atmospheric Pressure Fluidized Bed Combustion. Proceedings of the Fluidized Bed Combustion Technology Exchange Workshop, Reston, VA, April 13-15, 1977; NTIS No. CONF-770447-P-1 and CONF 770447-P-2.

4. Ulerich, N. H., E. P. O'Neill, and D. L. Keairns, A Thermogravimetric Study of the Effect of Pore Volume - Pore Size Distribution on the Sulfation of Calcined Limestones. Proceedings of the 7th North American Thermal Analysis Society Conference, St. Louis, MO, September 25-28, 1977.

5. Shearer, J., I. Johnson, and C. Turner, The Effects of $CaCl_2$ on Limestone Sulfation in Fluidized-Bed Coal Combustion, Thermochimica Acta, 35(105); 1980.

6. Johnson, I., J. Shearer, R. Snyder, G. J. Vogel, Factors Limiting Limestone Utilization Efficiency in Fluidized-Bed Combustion. Proceedings of the 13th Intersociety Energy Conversion Engineering Conference, 523; 1978.

7. Hartman, M., R. W. Coughlin, Reaction of Sulfur Dioxide with Limestone and the Influence of Pore Structure, Ind. Eng. Chem., Process Des. Develop., 13(3): 248; 1974.

8. Hartman, M., R. W. Coughlin, Reaction of Sulfur Dioxide with Limestone and Grain Model, AIChE Journal, 22(3): 490; 1976.

9. Vaux, W. G., Attrition of Particles in the Bubbling Zone of a Fluidized Bed, American Power Conference, Chicago, April 1979.

10. Vaux, W. G., A. W. Fellers, Measurement of Attrition Tendency in Fluidization, AIChE 72nd Annual Meeting, San Francisco, CA, 1979.

11. Kono, H., Attrition Rates of Relatively Coarse Solid Particles in Fluidized Beds of Various Types, AIChE 72nd Annual Meeting, San Francisco, CA, 1979.

12. Catipovic, N. M., G. N. Jovanovic, T. J. Fitzgerald, Regimes of Fluidization for Large Particles, AIChE Journal, 24(3): 543; 1978.

13. Glicksman, L., W. Lord, J. Valenzuela, A. Bar-Cohen, R. Hughes, A Model of the Fluid Mechanics in Fluidized Bed Combustors, AIChE 72nd Annual Meeting, San Francisco, CA, 1979.

14. Fitzgerald, T., H. Catipovic, G. Jovanovic, Experimental Measurement of Solids Movement in a Tube-Filled Fluidized Bed, AIChE 70th Annual Meeting, New York, NY, 1977.

15. Park, D., O. Levenspiel, T. J. Fitzgerald, A Model for Large Scale Atmospheric Fluidized Bed Combustors, AIChE 72nd Annual Meeting, San Francisco, CA, 1979.

16. Systems, Science and Software, Computer Modeling of Coal Gasification Reactors, Annual Report, June 1976-June 1977, Fe-1770-32.

17. West Virginia University, Simulation of Fluidized Bed Coal Combustors, February 1979, NASA CR-159529.

18. Chen, T-P, S. C. Saxena, Mathematical Modeling of Coal Combustion in Fluidized Beds with Sulfur Emission Control by Limestone or Dolomite Fuel, 56: 401; 1977.

19. MIT, Modeling of Fluidized Bed Combustion of Coal, Executive Summary, July 1975, HCP/T2295-01.

20. B&W, Conceptual Studies and Preliminary Design of a Fluid Bed Fired Boiler for Service in an Electric Utility, Contract Report to TVA, April 1978.

21. Ulerich, N. H., R. A. Newby, D. L. Keairns, Appendix B of Conceptual Design of a Gulf Coast Lignite-Fired Atmospheric Fluidized-Bed Power Plant, prepared by Burns & Roe, EPRI Report FP-1173.

22. Ciliberti, D. F., A. Y. Ranadive, D. L. Keairns, Particle Profiles in Fluidized Bed Systems, Contract Report to Argonne National Laboratory, January 1979.

23. Newby, R. A., D. M. Bachovchin, C. H. Peterson, N. P. Rohatgi, N. H. Ulerich, D. L. Keairns, An Assessment of Advanced Sulfur Removal Systems for Electric Utility AFBC, 6th International Conference on Fluidized Bed Combustion, Atlanta, GA, April 1980.

24. O'Neill, E. P., N. H. Ulerich, M. A. Alvin, D. L. Keairns, Criteria for the Selection of SO_2 Sorbents for Atmospheric Pressure Fluidized-Bed Combustors, Volume 2, EPRI FP-1307, December 1979.

25. Newby, R. A., et al., Sulfur Removal Systems Assessment, Annual Report for 1979, Submitted to B&W, December 1979.

26. Bradley, W. J., S. Panico, D. L. Keairns, R. A. Newby, N. H. Ulerich, G. M. Goblirsch, W. M. Neher, Effect of Subbituminous Western Coal Ash on AFBC Power Generating Costs, presented at the Houston, TX, AIChE Annual Meeting, April 1979.

27. Ulerich, N. H., R. A. Newby, D. L. Keairns, A Thermogravimetric Study of the Sulfation of Limestone and Dolomite, Thermochimica Acta, 36, 1 (1980).

28. Ahmed, M. M., D. L. Keairns, R. A. Newby, Effect of Potential New Source Performance Standards on the Performance and Cost of Industrial Fluidized-Bed Steam Generators, Submitted to EPA, 1979.

29. Wolfe, R. W., et al., Energy Conversion Alternatives Study (ECAS), Westinghouse Phase I-Final Report, Volume XI-Advanced Steam Systems, Prepared for NASA, February 1976, NASA CR-134941-XI.

30. Ulerich, N. H., R. A. Newby, and D. L. Keairns, Calcium-Based Sorbent Desulfurization in Pressurized Fluidized-Bed Combustion Systems, Submitted by Westinghouse to EPRI, 1980.

31. Ulerich, N. H., E. P. O'Neill, and D. L. Keairns, The Influence of Limestone Calcination on the Utilization of the Sulfur-Sorbent in Atmospheric Pressure Fluid-Bed Combustors, Report to EPRI, August 1977, Project 720-1, EPRI FP-426.

32. Ulerich, N. H., W. G. Vaux, R. A. Newby, D. L. Keairns, Experimental/Engineering Support for EPA's FBC Program: Final Report, Volume I. Sulfur Oxide Control, January 1980, EPA-600/7-80-015a.

COLD FLUIDIZED BED MODELING

Thomas J. Fitzgerald
Stephen D. Crane

Dept. of Chemical Engineering
Oregon State University
Corvallis, OR 97331

Much work has been done recently using cold fluidized bed models to study many of the characteristics of hot fluidized bed combustors.

The advantages of cold fluidized bed modeling are many. Cold models are cheaper to construct and operate, easier to instrument and easier to modify for studying a variety of parameters. However, little work has been done to determine if cold models have the same hydrodynamic properties and other characteristics of hot fluidized bed combustors.

As a first step toward addressing this question experiments were conducted to determine if dimensionless groups can be used to correlate fluidization hydrodynamics. Four dimensionless groups, first described by Scharff, M.F., et al., (1) were chosen for this study. They are:

$\frac{\rho_s}{\rho_g}$ — the ratio of solid density to gas density.

$\frac{d_p}{L}$ — the ratio of particle size to a characteristic bed dimension.

$\frac{U^2}{Lg}$ — the ratio of superficial gas velocity squared to the product of the acceleration of gravity times a characteristic bed dimension.

$\frac{d_p U \rho_g}{\mu_g}$ — the particle Reynolds number: the ratio of the superficial gas velocity times particle size to the kinematic viscosity of the gas.

If one sets all these dimensionless numbers to be identical when comparing two beds, then both beds should have similar fluidization hydrodynamics.

Procedure

To test this theory experiments were conducted using two cold fluidized bed models with identical dimensionless numbers. The experimental conditions were:

	Cork/Air Bed #1	Sand/R12 Freon Bed #2
Bed width inches (cm)	19.0 (48.3)	2.22 (5.64)
Bed thickness inches (cm)	5.0 (12.7)	0.58 (1.47)
Distributor Plate	Glass Spheres	Lead Shot
(a) Diameter inches (cm)	0.5 (1.27)	0.079 (0.20)
(b) Height	9.0 (22.9)	1.05 (2.67)
Bed Media	Cork	Sand
(a) Mean paticle size	2068 μ	240 μ
(b) Density	0.15	2.65
Fluidizing Gas	Air	R12 Freon (Dichlorodifluoromethane)
(a) Bed pressure, psia	≈ 14.7	61.0
(b) Temperature °F (°C)	77° (25°)	77° (25°)

Scaling Factors

$\frac{L_1}{L_2} = 8.558$ where: L_1 = a characteristic bed dimension for the cork/air system

L_2 = a characteristic bed dimension for the sand/Freon system

$\frac{U_1}{U_2} = 2.925$ velocity/time scaling factor

U_1 = the superficial gas velocity for the cork/air system

U_2 = the superficial gas velocity for the sand/Freon system

The L_1/L_2 scaling factor of 8.558 was used to scale all of the physical dimensions parameters (i.e. bed dimensions, mean particle size) of the two beds. The densities were scaled by $(L_1/L_2)^{.666}$.

The ratio of the superficial gas velocities, U_1/U_2, was used to determine if the fluidization hydrodynamics were similar. Pressure measurements were made across both beds at U_{mf} and various multiples of U_{mf} (up to 2.0 U_{mf}) (Figure 2-1). These data were analyzed using a Fast Fourier Transform power spectrum to determine the frequency of the pressure fluctuations. The ratio of the average frequencies should be equal, to the predicted velocity/time scaling factor of 2.92. The ratio of the measured superficial gas velocities at U_{mf} should also be equal to this value.

Movies of both systems were also taken for each experimental condition. The film speed was adjusted to take into consideration the differences in the superficial gas velocities. Since the ratio of the gas velocity of the cork/air system to that of the sand/Freon system is predicted to be 2.92 the movies of the sand/Freon system were taken at 54 frames per second vs. 18 frames per second for the cork/air system. In real time the cork/air system is 2.92 times slower than the sand/Freon system.

Movies and pressure measurements were also taken in a slugging bed configuration using an 8" diameter cylinder for the cork/air system and a 1" diameter cylinder for the sand/Freon system. In addition, movies were made comparing tungsten carbide/water system with an expanded-polystyrene/air system with identical dimensionless number at velocities up to 4 U_{mf}.

Results

Movies taken of the sand/Freon system vs. the cork/air system in two bed configurations (rectangular and cylindrical) and tungsten carbide/water vs. expanded-polystyrene/air in a cylindrical bed configuration at U_{mf} and various multiples of U_{mf} showed similarities in bubble growth and solids flow patterns. In addition, in the slugging beds the slugs appear to be nearly equal in scaled length, they rise to the same scaled height, and they rise at nearly the same scaled velocity. The measured U_{mf} ratio, U_{mf} Cork/U_{mf} Sand in the rectangular beds was within 20% of the predicted values may be a result of the angular shape of the cork particles which, because of their interlocking nature, yield a higher U_{mf}.

The ratios of the average frequency of pressure fluctuations for the cork/air vs. sand/Freon system in the rectangular bed configuration were near the predicted value of 2.92 (see Figures 3-2, 3-3, 3-4, 3-5, 3-6, 3-7, and Table 3-1). These frequencies were not calculated for the slugging bed configurations.

Table 3-1

U_{mf}	1.0	1.2	1.4	1.6	1.8	2.0
Ratio of average frequency of pressure fluctuations	*	*	*	2.8	2.0	2.2

*Pressure fluctuations in the cork/air system were too low to measure.

Conclusions

The results strongly indicate that the four dimensionless groups can be used for scaling cold models. That is, the performance of one cold model can be used, reliably, to predict the performance of an exactly scaled second model even in extreme cases (i.e. tungsten/water vs. expanded-polystyrene/air). It therefore seems likely that the fluidization hydrodynamics of a hot fluidized bed can be modeled in a scaled cold bed using the same dimensionless groups.

References

1. Scharff, M.F., et al., of JAYCOR. Final report to U.S. Department of Energy, Morgantown Energy Research Center, Contract EY-77-C-21-8156, "Project to Provide an Experimental Plan for the Merc 6' x 6' Fluidized Bed Cold Test Model," (1977).

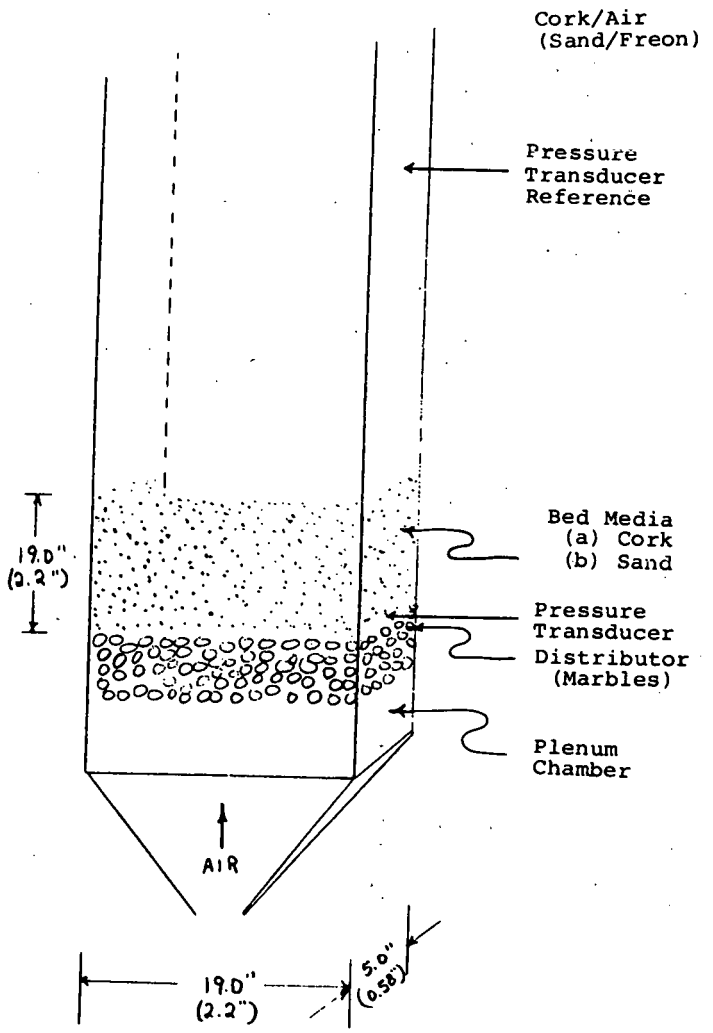

Figure 1. Rectangular Bed Configuration of Cold Scaled Fluidized Bed Model.

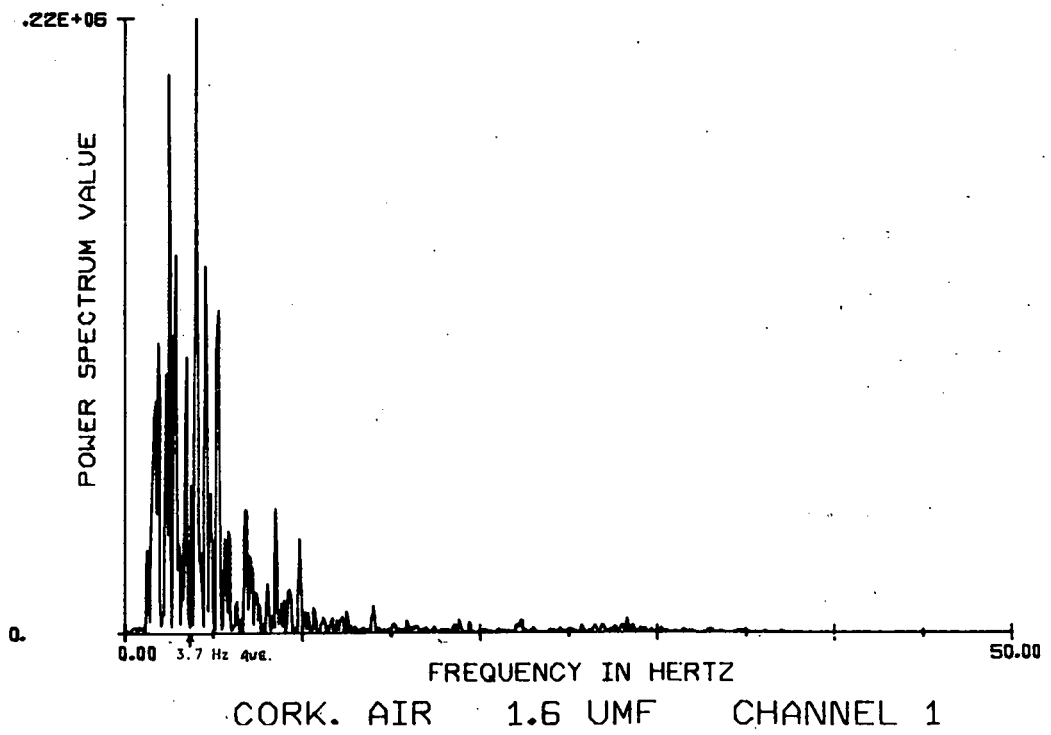

Figure 2. Frequency of Pressure Fluctuations of Cork/Air System at 1.6 U_{mf} with Average Measured Value Indicated.

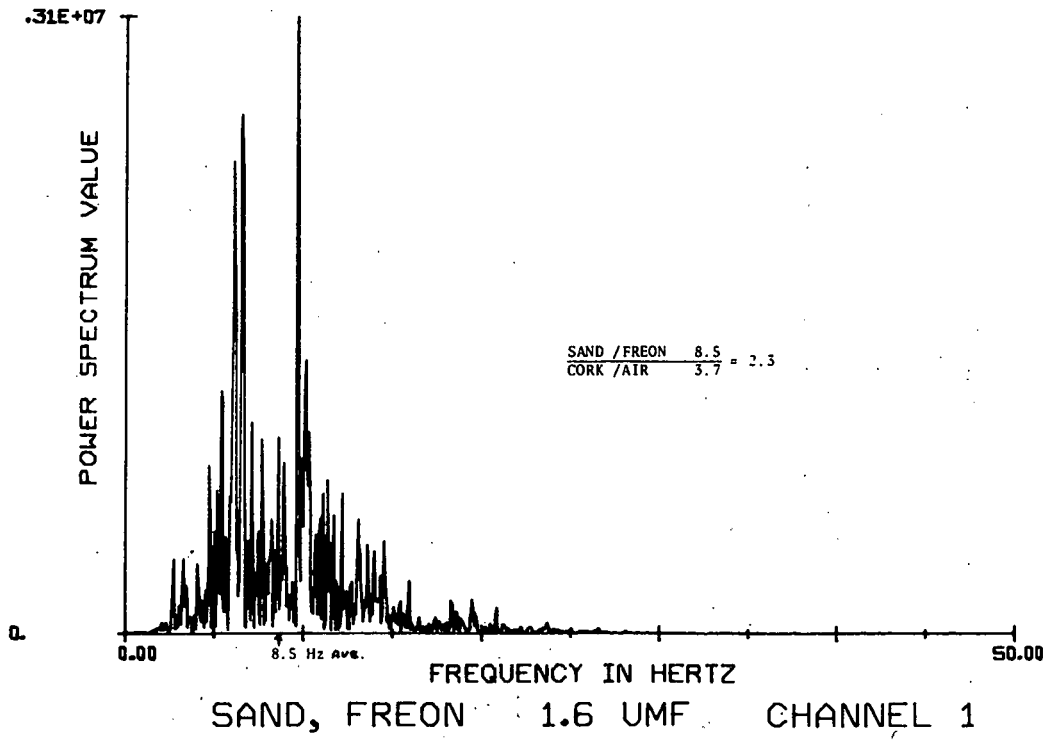

Figure 3. Frequency of Pressure Fluctuations at 1.6 U_{mf} Sand/Freon System with Average Measured Value Indicated. Ratio of Average Frequency is near Predicted Value of 2.9.

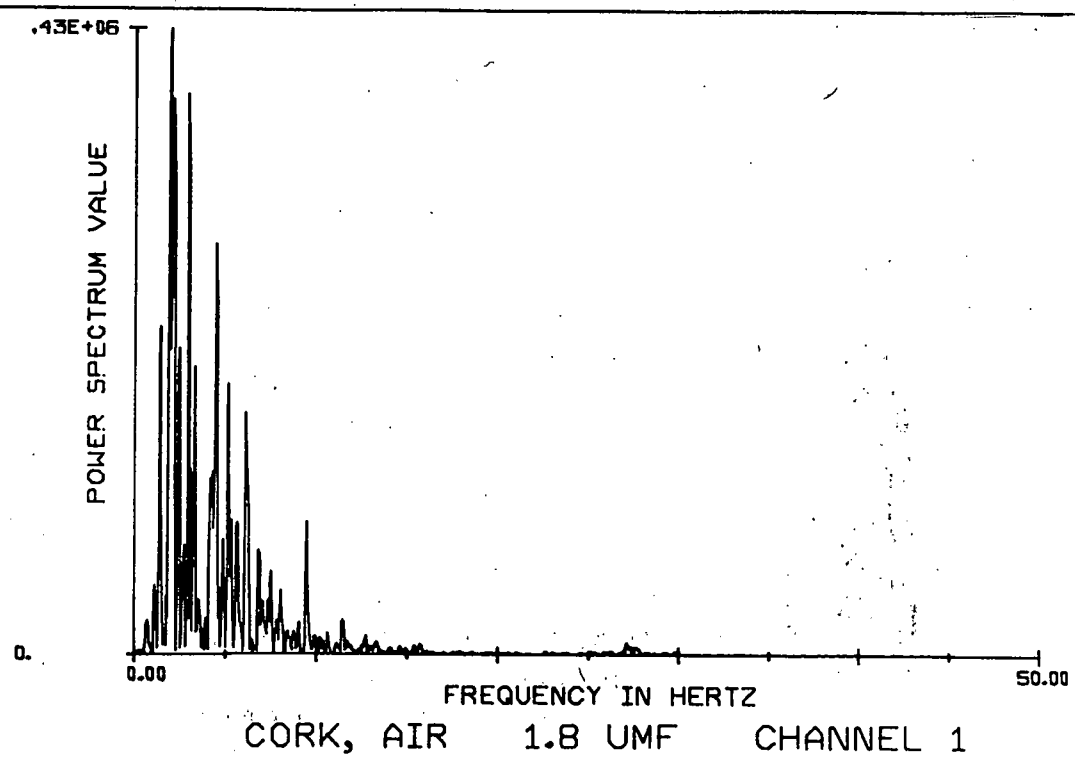

Figure 4. Frequency of Pressure Fluctuations of Cork/Air System at 1.8 U_{mf} with Average Measured Value Indicated.

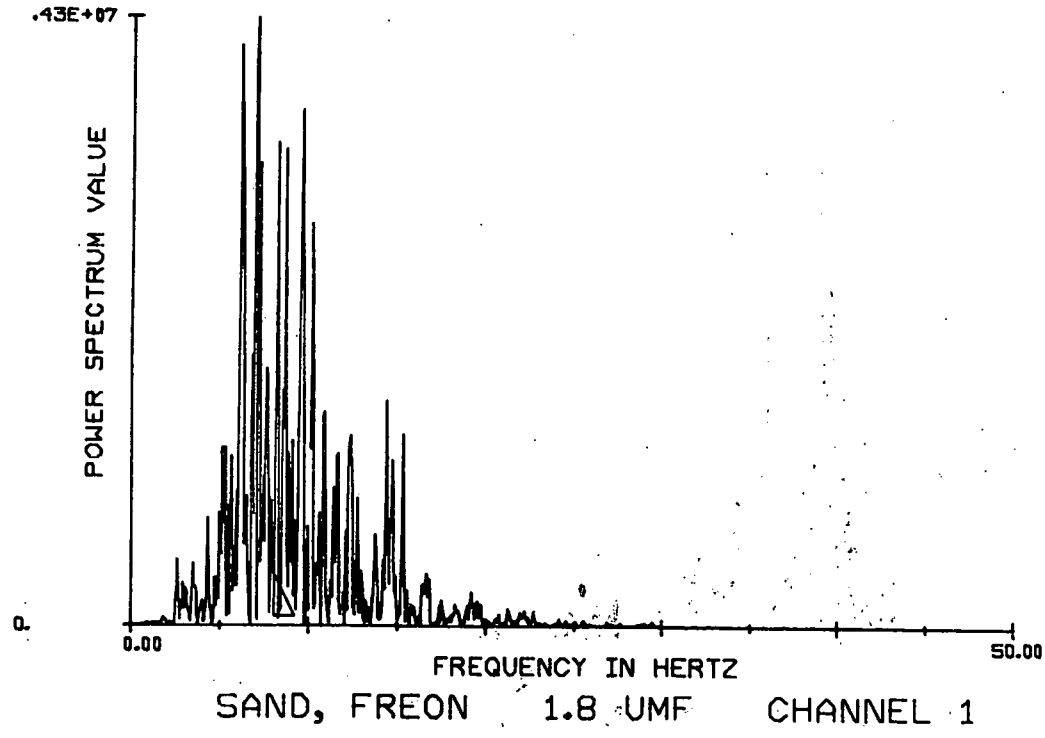

Figure 5. Frequency of Pressure Fluctuations of Sand/Freon System at 1.8 U_{mf} with Average Measured Value Indicated. Ratio of Average Frequency Near Predicted Value of 2.9.

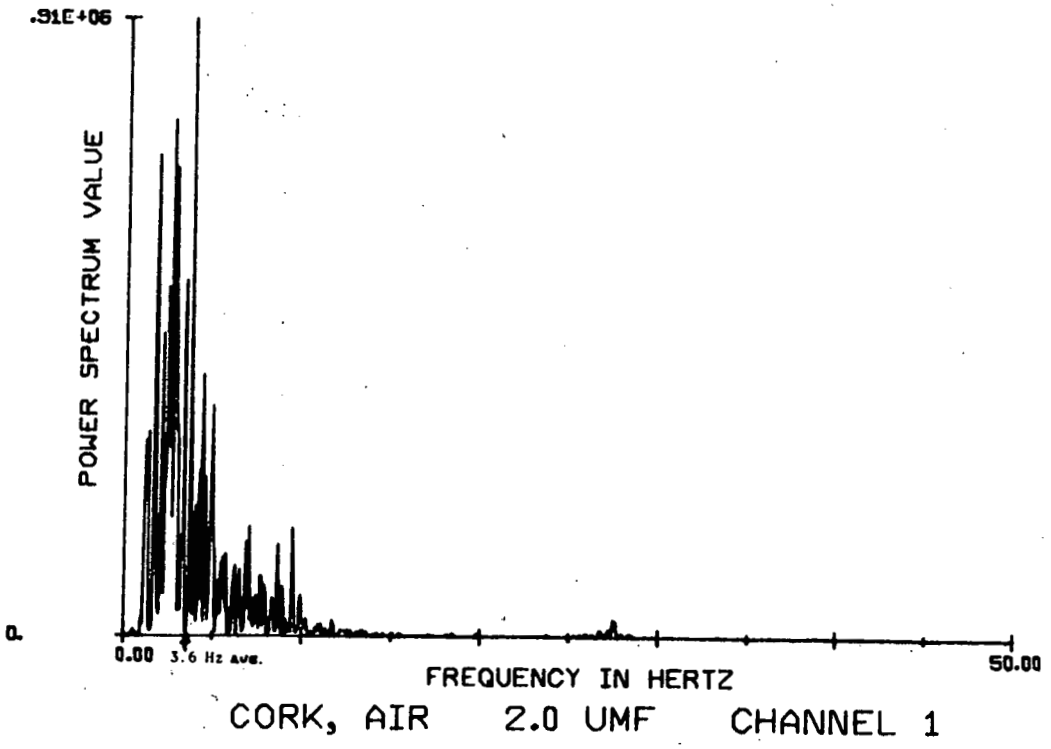

Figure 6. Frequency of Pressure Fluctuations of Cork/Air System at 2.0 U_{mf} with Average Measured Value Indicated.

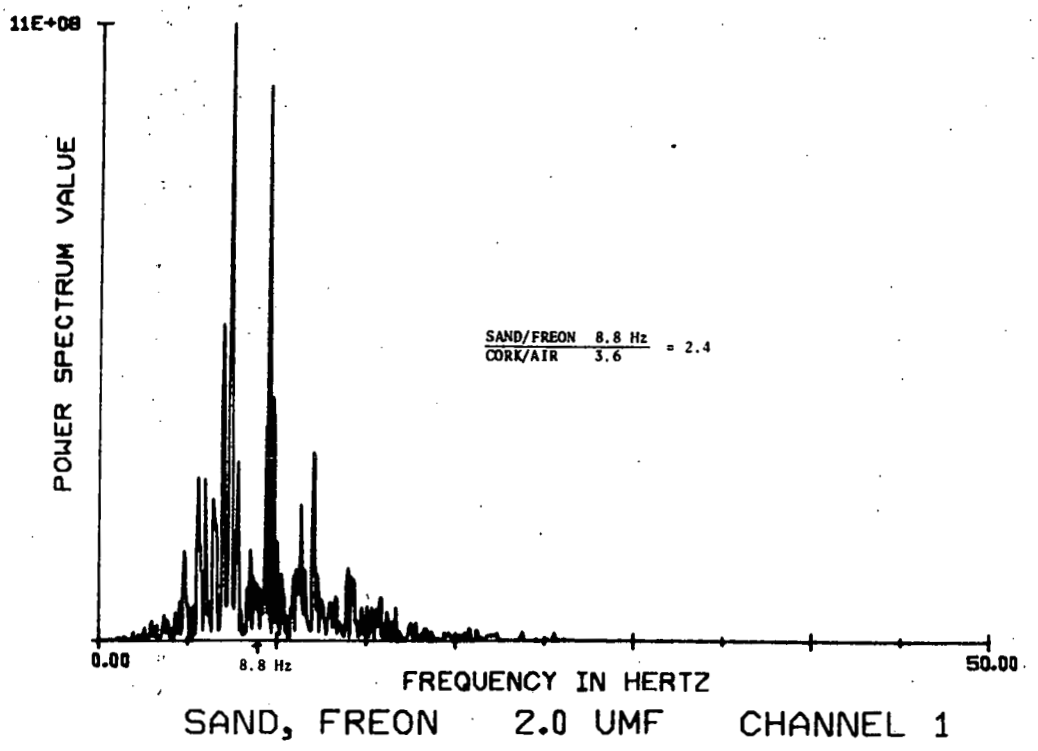

Figure 7. Frequency of Pressure Fluctuations of Sand/Freon System at 2.0 U_{mf} with Average Measured Value Indicated. Ratio of Average Frequency Near Predicted Value of 2.9.

QUESTIONS/ANSWERS/COMMENTS

Question to S. Crane:

Q: (Participant not identified)

Your original idea was to compare a cold system with a hot system. In actuality, you have compared two cold systems.

A: Our original goal was to first see if you could compare *two* cold models using dimensional groups. The next step was to compare a cold bed with a hot bed. Hopefully, in the near future, we will be able to take some data on a hot bed.

COMBUSTION AND BED PHENOMENA

LOW GRADE FUEL COMBUSTION

OPERATIONAL APPLICATION OF FLUIDISED-BED FURNACES IN BURNING LOW-CALORIFIC AND WASTE FUELS IN CZECHOSLOVAKIA

František Knor and Pavel Novotny

Fuel Research Institute,
Prague 9-Běchovice, CSSR

Looking for new energy sources is at present one of the most important world-wide problems. One of the possibilities of widening the fuel and energy sources is the utilization of the thermal energy of coal of waste quality, of combustible liquid wastes and off-gases and of plastic wastes.

In order to exploit these not yet utilized energy sources, the two-stage fluidised-bed combustion technology, which is a universal way of burning all above mentioned wastes, may be advantageously used.

In spite of the fact that a number of research organizations abroad focus their attention on the research, development and commercial mastering of the one-stage fluidised-bed combustion technology, it cannot be used for burning these wastes on the basis of both the theoretical analysis and own long-term operating experience.

Suitability of the two-stage fluidised-bed combustion technology for burning these fuels is given by a very good adaptability of this technology to the immediate quality of fuel burnt.

The thermal balance of the first degree of burning is exclusively given by the amount of oxygen fed to the fluidised-bed and by the heat consumption for heating the fluidisation air and the mass of fuel up to the fluidised-bed temperature. By changing the amount of oxygen fed, ie of fluidisation air, the fluidised-bed furnace adapts to any operating situation and change of the quality and calorific value of the fuel fed. The change in the quality of fuel is then transferred to another combustion space - the next centre of combustion, mostly formed in the combustion chamber of a boiler unit. When using larger boilers and when burning fuels above the limit of the minimum calorific value for the autothermal combustion process, a fluidised-bed furnace may be solved as a hybrid one - with partial heat removal from the fluidised bed.

Contrary to this technology, the one-stage fluidised-bed furnaces due to a considerable heat removal directly from the fluidised bed are dependent on the quality of burnt fuel, since with the decreasing of its calorific value the amount of heat, which may be removed from the fluidised bed without impairing the stability of the combustion process, also abruptly decreases.

In the fluidised bed of a two-stage fluidised-bed furnace the combustion itself does not take place but fuel particles according to the following mechanism are gasified: When entering the bed, oxygen from the fluidisation air reacts with carbon of the fluidised bed particles and causes the increase in their temperature. Due to mixing, these warmer particles are cooled when entering the upper layers of the fluidised bed. Carbon dioxide CO_2 formed is reduced in the upper part of the fluidised bed to carbon monoxide CO. After entering the fludised-bed reactor, fresh fuel particles are very quickly heated, their volatile portion of the combustible matter evaporates in passing into the gas leaving the fluidised bed. Since this gas does not contain any oxygen, this carbonization gas cannot be burnt.

Oxygen inlet to the fluidised bed should be limited to such an amount so that only a part of the combustible matter of fuel may be burnt in order to substitute the required thermal energy for the thermical preparation of fed fuel, for heating the fluidisation air, and for covering heat losses through the fluidised-bed reactor walls by the heat generated.

More than ten years' experience with the operation of the two-stage fluidised-bed furnaces in Czechoslovakia has fully confirmed these findings.

Waste kinds of solid fuels in coal mining in Czechoslovakia are of two types.

As to bituminous coal preparation, concerned are mainly bituminous coal washing rejects whose ash content in dry matter attains as much as 70 to 80 % and whose calorific value ranges from 4.2 to 7.5 MJ/kg^{-1} or froth flotation tailings whose ash content in dry matter attains as much as 70 % and whose moisture content is variable.

When preparing brown coals, wastes represent high-ash fractions of run-of-mine coal with the moisture content W^r = 20 %, ash content in dry matter A^d = as much as 67 % and

calorific value of about 5 MJ/kg^{-1}; in mining this coal, overlaying and underlaying seams, whose ash content in dry matter A^d ranges from 55 to 65 % and calorific value from 5 to 8.5 MJ/kg^{-1}, are considered wastes. At present this coal cannot be burnt alone in stokers and in pulverized-fuel-fired furnaces, it is either discharged to a dump or left in the floor of seam without its exploiting .

In order to burn these fuels in a fluidised bed furnace, these materials should be crushed to particles below 5 to 15 mm and water should be dried off to such an extent to obtain loose duff which can be transported, stored and fed to the furnace.

Fuel of a minimum calorific value 5 MJ/kg^{-1} may be burnt in these furnaces by using a self--supporting combustion process with feeding cold fludisation air without any stabilization. The advantages of using the two-stage fluidised-bed combustion technology are as follows: a wide range of performance control (25 to 100 %), the possibility of a long-term warm shut-down of the furnace, control of solid and gaseous emissions etc. Furnaces of this type are to a considerable extent universal and in case of need they may be converted to burning conventional types of coals for power generation, in particular brown coals without any modification of the furnace.

In Czechoslovakia several furnaces of this type are operational at present and use coal whose quality nearly equals coal rejects in boiler units with an output of 3.3 to 14 t/h of steam, the furnace of a boiler unit with an output of 40 t/h of steam is under construction and the reconstruction of a boiler unit with an output of 110 t/h of steam, equipped with a fluidised-bed furnace, is prepared for design.

The universal character of the fluidised--bed furnaces may also be exploited for burning wastes of plastics crushed to particles whose weight does not exceed the tenfold weight of the fluidised-bed largest particles; they may be burnt in combination with low-calorific types of coals, particularly of those with high-ash content whilst carryover of fine ash particles or of a suitable alkaline additive from the fluidised bed may bond formed chlorine (Cl) ions while burning PVC type mass thus preventing high-temperature corrosion of boiler heating surfaces.

Another possibility is the use of these furnaces for burning liquid wastes, either of the petroleum or of the tar group. These liquid wastes may be brought directly to the fluidised bed of inert mass glowing particles and thus their complete liquidation in exploiting their thermal energy may be ensured. The fluidised-bed furnaces may also be used for the crematory incineration of liquid wastes, deficient in energy content, whereas for the combustion process solid or liquid fuels or other suitable wastes re used.

In the same way various kinds of off-gases may be burnt in the fluidised-bed furnaces of this type .

The design solution of the fluidised-bed furnaces will be dependent particularly on the purpose for which a furnace is intended in the technical practice. The first furnaces using the fluidised-bed technique were calcining kilns for firing iron sulphides, zinc etc, ie technological furnaces used mainly for the production of sulphuric acid and the thermal energy produced was thus a by-product.

Quite another case is when a fluidised bed should serve as a heating installation of a steam or hot water boiler. In this case the overall design solution of a furnace should fully correspond to the purpose for which the boiler is intended. In the first place the reliability of a boiler is concerned. The boiler represents a source of steam or of heating water, its operating use is mostly of a long-term nature. The expression "seasonal use", so common with technological furnaces, is not in use in the field of heat generation. Another important demand is the range of performance control; this demand, in comparison with technological furnaces, is also considerably particular. Thermal energy cannot be stocked , the boiler operation should be modified in a short delay to thermal energy needs and to the same extent the furnace of a boiler should be adapted to this consumption. Further demands on a fluidised-bed furnace of a steam boiler are a wide range of quality of burnt fuel, high efficiency, low operating costs and investments etc. In addition to these demands, the environmental problems, ie control of solid and gaseous emissions, have recently received much attention. This brief survey indicates that the demands on the design solution of a fluidised-bed furnace are relatively high and it cannot be claimed that the fulfilment of all these demands in a single type of the installation can be expected.

The outlook of the fluidised-bed furnaces is at present associated with the renaissance of coal exploitation, again on a world-wide scale. Limited sources of oil and gas and their uneven division into individual production centres together with complicated economic and political conditions of their obtaining support the comeback of a number of power installations to the coal fuel base. In a new evaluation of the fuel and energy sources, the fluidised-bed furnaces of all known types display priority outlooks.

In Czechoslovakia the research works in this respect have been carried out at the Fuel Research Institute at Běchovice since 1958. The objective of research was to make use of favourable conditions of this technology for effective power exploitation of low-rank types of coals or wastes in their preparation. Research works were first carried out in laboratories and then on a pilot-plant scale. The two-stage fluidised-bed

combustion technology was applied, where the first stage was performed by a fluidised-bed reactor which a combustible gas left and glowing carryover particles were burnt in the following separated space by addition of secondary air and an autothermal combustion of a number of high-ash coals both brown and bituminous with a minimum calorific value $Q_i^r = 5400$ kJ kg^{-1} and ash content in dry matter $A^d = 75$ % was attained.

These favourable results may be explained by both the high concentration of the combustible matter in the reaction space of the fluidised bed and the high intensity of heat transfer from the glowing particles of the fluidised bed to those of just fed fuel. The high concentration of the combustible matter in the fluidised bed space is based on simple considerations. The weight of the expanded fluidised bed is approximately equal to 100 kg.m^{-3}. If the carbon content in ash particles equals 1 %, the concentration of the combustible matter is approximately 10 kg.m^{-3}. At the pulverized fuel burner port the concentration of the combustible matter higher than 1 kg.m^{-3} cannot be attained, which is by one order inferior.

When observing the course of burning of coal particles in classical types of furnaces, it has been found that the ash content increases in dependence on the time of burning. If the fuel had this high ash content when entering the furnace, the use of the classical combustion technique would impair the stability of burning. In spite of this fact the combustion process continues. The task in burning high-ash fuels is to ensure such intensive thermal preparation of fuel particles so that they may reach as soon as possible such a state in which are the particles of originally high-grade fuel after a certain time of burning. The research works have also proved a considerably universal character of the technology application to both bituminous and brown coals, as well as a wide range of performance control ranging from 25 to 100 % of nominal output.

This technique is of particular importance to the field of using high-ash fuels even of waste quality which, according to the evaluation carried out up to now, show zero or negative utility values, namely due to the fact that in using classical methods of burning either in stokers or in pulverized-fuel-fired furnaces, the autothermal combustion of these fuels cannot be ensured.

The full-scale application of the two-stage fluidised-bed combustion technology has provided very satisfactory results, particularly when using fine-grain fractions of refractory schistous clay up to the maximum particle size of 6 mm containing a minor fraction of the bituminous-coal combustible matter.

The installation used is presented in Figure 1. To a standard boiler, originally equipped with a stoker, a fluidised-bed reactor has been added to which a waste schistous clay below 6 mm grain size is fed. Combustible gas together with the glowing particles of carryover from the fluidised-bed reactor burns after the addition of secondary air to the combustion chamber of the boiler. The carryover particles separated by gravity fall on a grate where they are completely burnt at the simultaneous action of flame radiation in the combustion chamber.

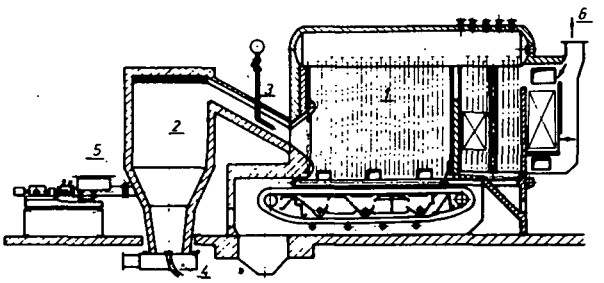

Figure 1

1 - Boiler combustion chamber
2 - Fluidised bed combustor
3 - Secondary air
4 - Air plenum
5 - Fuel feed
6 - Flue gas outlet

When carrying out the guarantee tests of this installation, a waste schistous clay of the following quality was burnt:

Test No.		1	2
Ash content in dry matter A^d	%	63.26	69.12
Calorific value MJ/kg^{-1}		7.44	5.07
ø Steam output t/h		1.9	4.2
Combustion efficiency	%	92.3	82.3
Carbon content in rough fraction of ash	%	1.1	2.3

A relatively low ash content in dry matter with regard to calorific values may be explained by a high value of the ash factor (f = 1.2), which represents the content of ash matter in fuel samples expressed by the values 75.91 % and 82.94 %. In the combustion test No. 2 the steam output of 5 t/h of steam, ie 120 % of the nominal output of a boiler unit, was attained in spite of a relatively low quality of this fuel.

In order to burn coal rejects and liquid wastes in cleaning and disinfection of railway tanks and waggons, four boiler units of the system "Duklafluid" (Figure 2) with a steam output of 14 t/h of steam per boiler have been constructed. By burning liquid wastes an energetically self-supporting closed cycle is reached and the required thermal energy for the cleaning and disinfection process is obtained by burning wastes produced.

The next development stage of these fluidised-bed furnaces is indicated by a principal solution as shown in Figure 3, where the situa-

tion of the fluidised-bed reactor in the lower part of the boiler unit enables an easy solution of a fluidised-bed furnace of a hybrid type, where the first combustion stage - the fluidised-bed reactor - is cooled by a heat-exchanging surface in the border walls in maintaining a two-stage combustion.

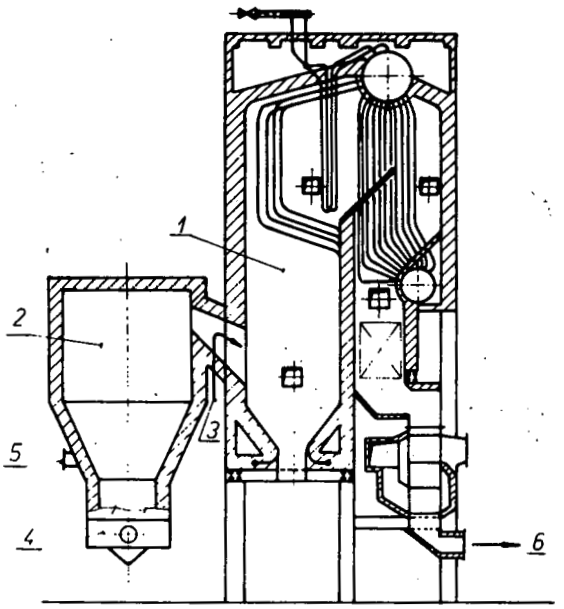

Figure 2

1 - Boiler combustion chamber
2 - Fluidised bed combustor
3 - Secondary air
4 - Air plenum
5 - Fuel feed
6 - Flue gas outlet

This solution permits to reduce the flame temperature in the second stage of combustion and thus slagging of the combustion chamber walls may be effectively limited and more favourable conditions may be created even for increasing the efficiency of flue gas additive desulphurization, as well as another bond of pollutants to an additive added may be increased.

Within the framework of technical assistance rendered to prospective customers abroad, our institute has offered such assistance in the experimental verification of the feasibility in combustion of different types of solid fuels which cannot either be burnt by hitherto known methods or only in pulverized-fuel-fired furnaces of high outputs.

In order to verify on an experimental base minor fuel samples, our institute has built a pilot two-stage fluidised-bed furnace with a thermal performance amounting approximately to 1 MW (Figure 4).

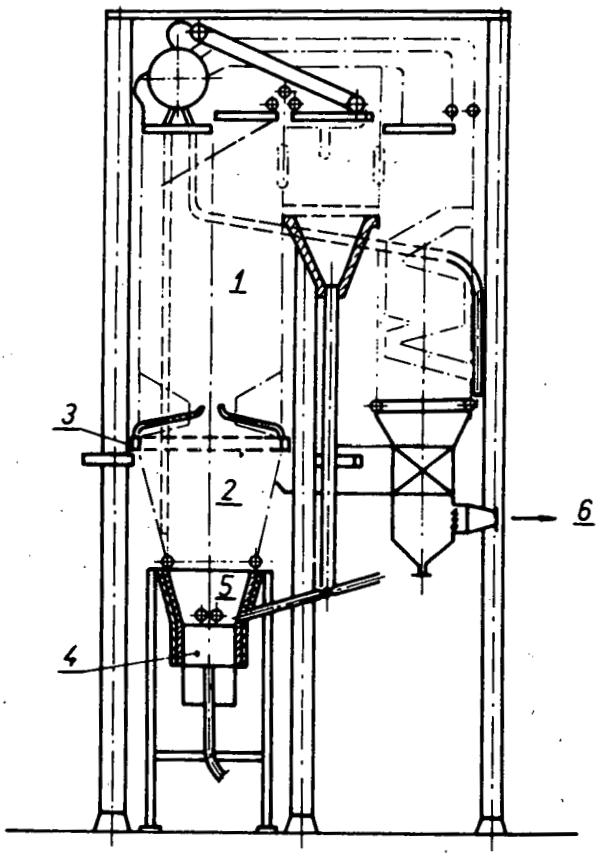

Figure 3

1 - Boiler combustion chamber
2 - Fluidised bed combustor
3 - Secondary air
4 - Air plenum
5 - Fuel feed
6 - Flue gas outlet

In this furnace the feasibility of burning different fuels (waste Albanian petroleum coke, Roumanian lignite, low-rank types of Bulgarian coals) has been verified on an experimental scale.

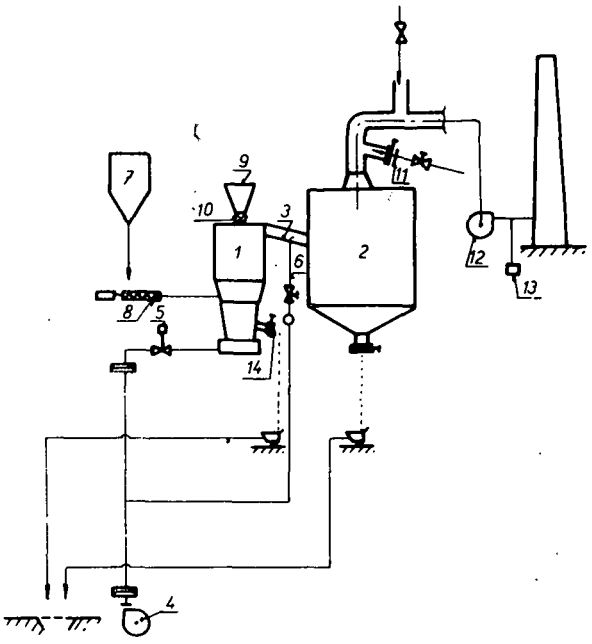

Figure 4

1 - Fluidised bed combustor
2 - After-combustion chamber
3 - Junction socket
4 - Fan
5 - Valve with servodrive
6 - Secondary air nozzles
7 - Fuel bin
8 - Screw feeder
9 - Inert material bin
10 - Bin gate
11 - Water feed
12 - Flue gas fan
13 - Entrained solids sampler

Conclusion

It may be stated that the fluidised-bed combustion technology using the slag-free process in the bed may effectively exploit different types of low-rank coals, not included in the national energy balance, of a minimum calorific value of 5 MJ/kg (1200 kcal/kg), as well as different types of liquid and some solid industrial wastes.

In our national fuel and energy economy, as well as in other countries, the utilization of waste types of coals and of other wastes may represent a new and effective fuel and energy source whose exploiting may help to solve or reduce the shortage of basic classical fuel and energy raw materials.

COMBUSTION CHARACTERISTICS OF ANTHRACITE CULM IN A FLUIDIZED BED

A. M. Leon and P. J. Choksey

Dorr-Oliver Incorporated
Stamford, Connecticut

INTRODUCTION

Anthracite culm is a generic term for any non-salable by-product resulting from production of marketable anthracite coal. It contains appreciable amount of coal and is essentially a low cost, poor quality fuel reserve. About 910 million cubic yards of refuse is found in the northeastern Pennsylvania. The refuse banks are eyesores which not only occupy valuable land, but pollute the air, land, and water of the region as a result of spontaneous combustion and acid runoff.

The burning of anthracite culm in a fluidized bed boiler is considered to be a feasible, cost effective way of utilizing this fuel in an environmentally acceptable manner. The fluidized bed combustor is essentially a furnace which can burn a variety of fuels including culm at low temperatures (1400°-1700°F). The sulfur dioxide release can be controlled within environmentally acceptable levels by use of limestone or dolomite as a sulfur sorbent. The relatively low combustion temperature also keeps the nitrogen oxide level low. The use of boiler tubes in the fluidized bed to extract heat is a very efficient method of steam generation due to the high heat transfer coefficient.

To demonstrate the viability of this technology, an anthracite-culm-fueled fluidized-bed boiler to produce 20,000 lbs/hr of steam has been designed and will be built under the sponsorship of DOE. This boiler will be located at an industrial park of the Shamokin Area Industrial Corporation (SAIC) in Paxinos, PA. The boiler will be fueled by anthracite culm with heating values ranging from 3000 to 5000 Btu/lb. The boiler will supply 150 psig saturated steam to a paper products manufacturer at the industrial park.

OBJECTIVES

The basic purpose of the combustion study was to provide the process data needed to design the boiler system when using the supplied culm and limestone.

Data was needed on:

1. Combustion Efficiency
2. Sorbent Requirements
3. Emissions
4. Heat Transfer

EXPERIMENTAL PROCEDURE

The test work was performed at Dorr-Oliver's research laboratory in a 12 inch fluid bed combustor as shown in Figure 1.

Metered fluidizing air is blown into the bottom of the fluid bed through a removable windbox containing an air distributor. Culm and limestone are fed into the reactor premixed. A screw feeder is used for accurate solid feed metering. The bed product is periodically discharged to maintain a constant bed level as determined by the pressure drop of the bed. Stack gases containing elutriated solids are passed through a cyclone mounted at the top of the reactor and finally to a gas scrubber. The bottom products of the cyclone are then recycled back to the combustor. Periodically samples are withdrawn from this ash recycle system for analysis.

Water cooled heat exchanger tubes were located in the bed and freeboard regions. The bed cooling tubes were made from 1/2 inch carbon steel schedule 40 pipe. The freeboard tubes were made from 1 inch schedule 40 pipe. Water temperatures in and out of the tubes and flow rates were measured to obtain heat transfer data.

The concentration of the flue gas constituents: O_2, CO_2, CO, NO_x and SO_2 were determined by continuous on-line gas analyzers. Chemical analyses of the culm fuel, limestone and ash products were analyzed in Dorr-Oliver's Analytic Chemistry laboratory. The data from this analytic work, from the gas analyses and from flow measurements were used to calculate combustion efficiencies and mass balances.

A low purity limestone from a nearby supplier, Meckley Limestone Company, was

used as the sorbent with Ca/S mole ratios varying from 3.0 to 9.8. Both coarse and fine limestone with mean diameters of 1500 microns and 270 microns respectively were used. The test runs were conducted with culm from a colliery close to the boiler site. The heating values from several samples of the culm were less than 5000 Btu/lb. Generally the culm contained 0.6% Sulfur and more than 60% ash. Chemical analyses of culm and limestone are given in Table 1 and Table 2 respectively.

TESTS

The study was divided into three series of tests. The first series of runs were for screening purposes, to crudely characterize the fuel and to select the proper range of operating conditions for use in later tests.

A second series of tests were run to obtain detailed data on the effects of critical operating parameters. This parametric study was conducted using at least three levels of each of the variables: temperature, fluidization velocity, excess air and bed height while using the coarse limestone at a Ca/S ratio of 3.0. The test matrix was based on a "Computer Optimized Experimental Design", (COED), technique to minimize the number of test conditions required. The variable effects from the parametric study were analyzed statistically using the computer based (COED) analysis program.

The effect of Ca/S ratio on sulfur removal was examined in the final series of runs. These tests were conducted with a finer limestone having an average particle size of 270 microns.

RESULTS AND DISCUSSION

Initial screening tests showed that culm crushed to minus 1/4 inch did not burn well causing poor fluidization, hot spots and clinker formation. For final screening tests the culm was crushed to pass 4 Tyler mesh. This material exhibited much better fluidization as combustion was easily controlled. Though culm burned at 1250°F, good combustion was not achieved until 1400°F was reached. Based on this screening work, the parametric study was conducted using the -4 mesh size culm. Particle size distributions of the culm feed, the two limestones, bed underflow and cyclone catch are shown in Figure 2.

The following ranges of controlled variables were examined in the parametric study:

Bed Temperature	1450° - 1695°F
Excess Air	10 - 60%
Fluidization Velocity	3.5 - 6.8 ft/sec
Bed Depth	3 - 6 ft
Ca/S Mole Ratio	3.0 - 9.8

Combustion Efficiency

Combustion efficiency from a carbon balance was calculated and found to increase with an increase in bed temperature. The effect of bed temperature on combustion efficiency at various excess air levels is shown in Figure 3. The combustion efficiency increases with an increase in the excess air at constant temperature, bed height and fluidization velocity. The combustion efficiency decreased with an increase in bed fluidization velocity. This effect is shown in Figure 4 at 1550°F. Efficiencies of 95% or better were observed during all tests when using ash recycle.

Sulfur Removal

The initial parametric tests were conducted using a Ca/S ratio of 3.0 with the coarser limestone having an average particle size of 1500 microns. The effect of bed temperature on sulfur removal at various levels of excess air and bed depths is shown in Figure 5. Maximum sulfur capture was achieved in the 1530° to 1570°F temperature range as expected. This figure also shows that sulfur capture increases as excess air and bed depth increases. The increase in sulfur capture with excess air can be due to a higher oxygen partial pressure being available for the sulfation reaction. The effect of bed height on sulfur removal is related to the solids and the gas residence time in the bed.

The effect of bed fluidization velocity on sulfur removal is shown in Figure 6 at 1450°F and 1550°F bed temperature. Increasing the bed fluidization velocity (also reducing residence times) results in a decrease in sulfur retention.

Tests were run to reach the targeted ∿90% sulfur capture level using finer limestone ($\overline{Dp}$ = 270 microns) and Ca/S ratios ranging from 3.3 to 9.8. The sulfur removal increases rapidly as the Ca/S ratio is increased from 3.3 to 5.0 as shown in Figure 7. Then it approaches 100% asymptotically as Ca/S ratio is increased from 5.0 to 9.8.

A compromise must be made in selecting the optimum combustion temperature since the mid-1500s °F is good for sulfur capture and higher temperatures are needed

for maximum combustion efficiency. It is estimated that better than 97% combustion efficiency can be obtained at 1550°F and 6 ft/sec velocity. This operating condition is also good for sulfur capture.

NO_x Emission

The emission of oxides of nitrogen were below the 0.7 $lb/10^6$ Btu EPA limit. The amount of NO_x in the flue gas was dependent on excess air and bed temperatures, increasing with increases in the excess air and bed temperature. This is shown in Figure 8.

Heat Transfer Coefficients

Heat transfer coefficients for the bed tubes ranged from 30-73 Btu/hr ft^2 °F. This wide range was achieved by varying the extent of the tube emersed in the bed. The coefficient increases as both fluidization velocity and bed depth increases. The freeboard tube heat transfer coefficients were in the range of 5-20 Btu/hr ft^2 °F. The wide range here was mainly caused by changes in gas velocity. At higher velocities the convective component is higher. The freeboard tube heat transfer coefficient was also affected by temperature as it increased with increase in the freeboard temperature. This effect is due to the radiation component of heat transfer being significant.

CONCLUSIONS

The following conclusions have been reached on the basis of this culm combustion study:

1. Culm combustion efficiencies greater than 95% should be expected when using ash recycle and properly sized feed.
2. Sulfur capture is highly dependent on the particle size of the sorbent feed.
3. Sulfur retentions higher than 90% can be achieved with the Meckley Limestone.
4. Emissions of NO_x are well below existing requirements.
5. Heat transfer coefficients can vary widely depending on the bed depth, fluidization velocity and temperature.

REFERENCES

1. Dorr-Oliver Incorporated, Combustion Studies, Test Period October 1978 - February 1979, U.S. Department of Energy, April 1979.

2. Call, R., Mei, J., and Wilson, J., Fluidized Bed Combustion Test of Low Quality Fuels - ANTHRACITE REFUSE, Morgantown Energy Research Center, May 1977.

TABLE 1

ULTIMATE ANALYSIS – ANTHRACITE CULM

	% DRY BASIS
CARBON	27.02
HYDROGEN	1.42
NITROGEN	0.66
OXYGEN	3.48
SULFUR	0.57
ASH	66.85
HEATING VALUE, HHV	4,198 BTU/LB

TABLE 2

CHEMICAL ANALYSES LIMESTONE

	Limestone (Fine)	Limestone (Coarse)
$CaCO_3$, %	66.34	59.84
$MgCO_3$, %	4.80	7.18
SiO_2, %	15.86	19.05
Al_2O_3, %	2.31	2.82
Fe, %	1.37	1.56
Na, ppm	248	253
K, ppm	242	332

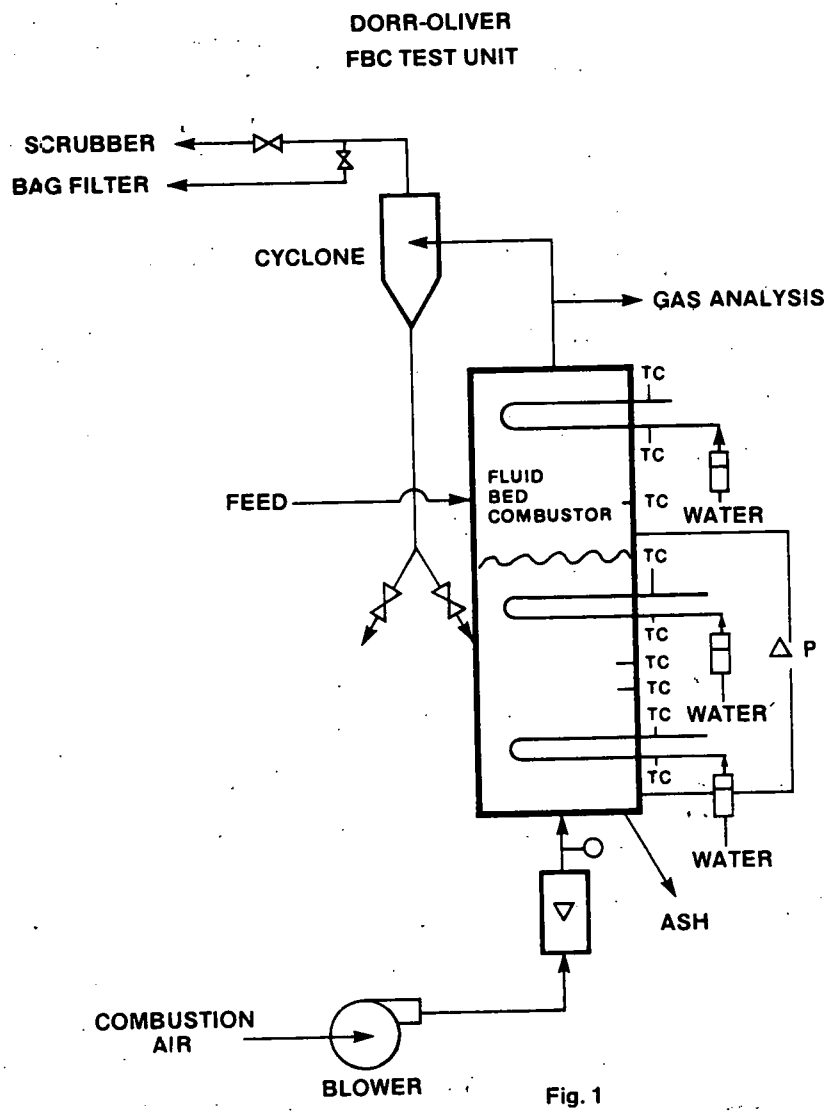

Fig. 1

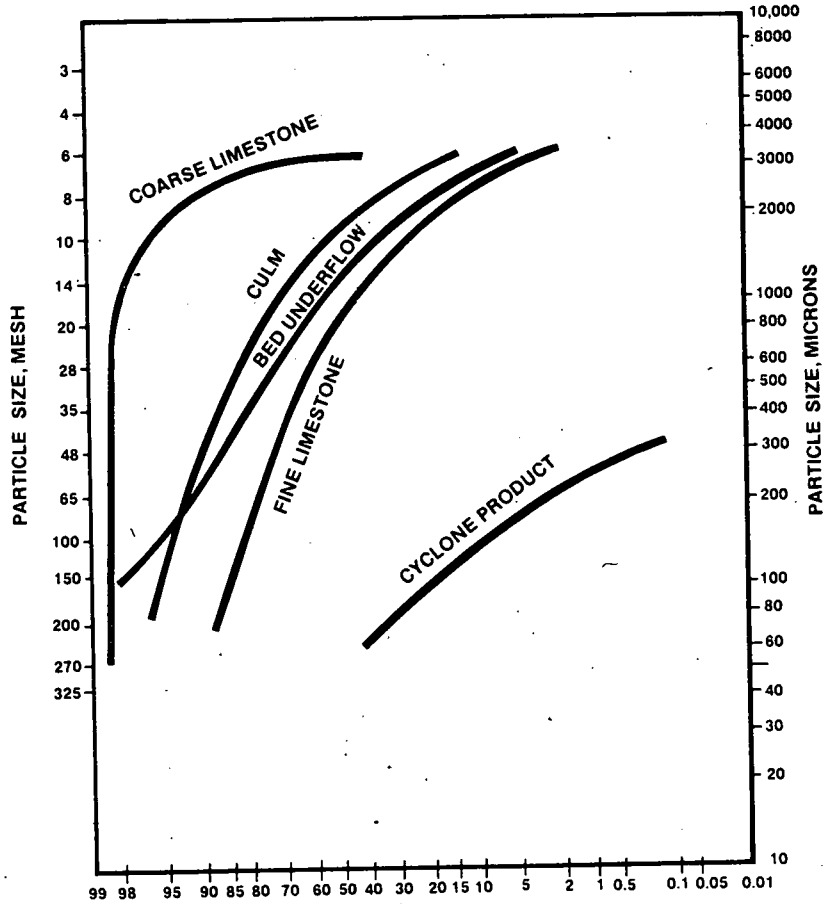

SIZE ANALYSES OF FEED AND PRODUCTS

Fig. 2

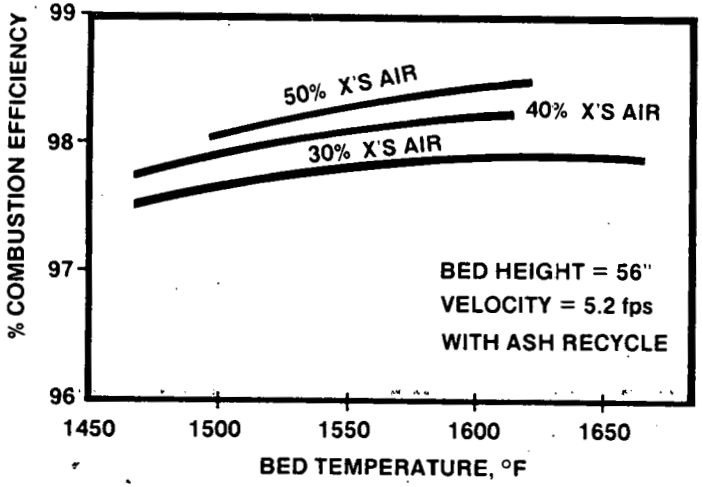

EFFECT OF BED TEMPERATURE ON COMBUSTION EFFICIENCY

Fig. 3

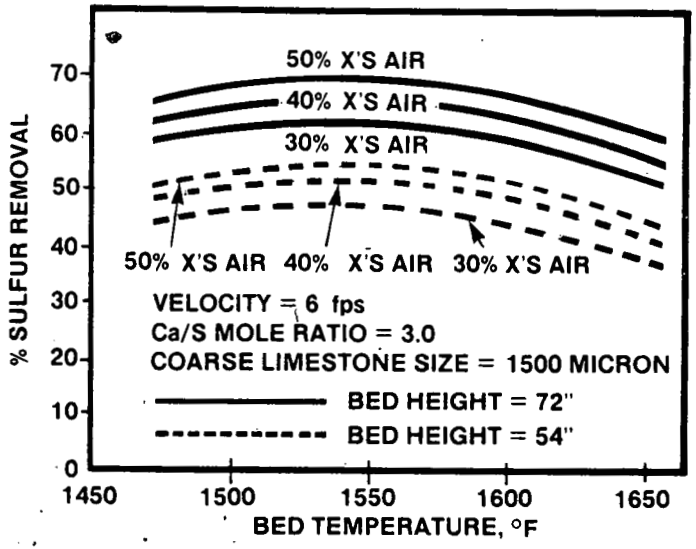

Fig. 5

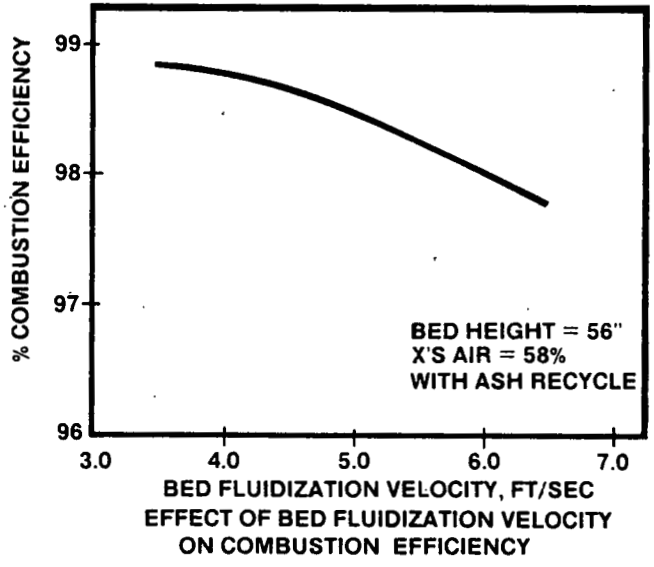

EFFECT OF BED FLUIDIZATION VELOCITY ON COMBUSTION EFFICIENCY

Fig. 4

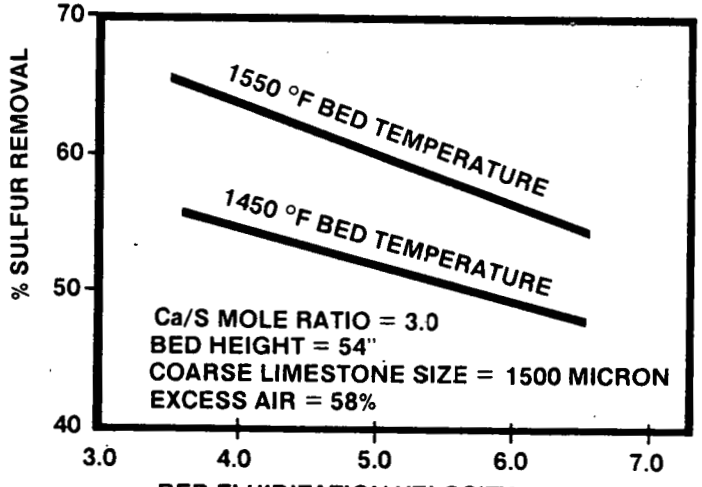

EFFECT OF BED FLUIDIZATION VELOCITY ON SULFUR REMOVAL

Fig. 6

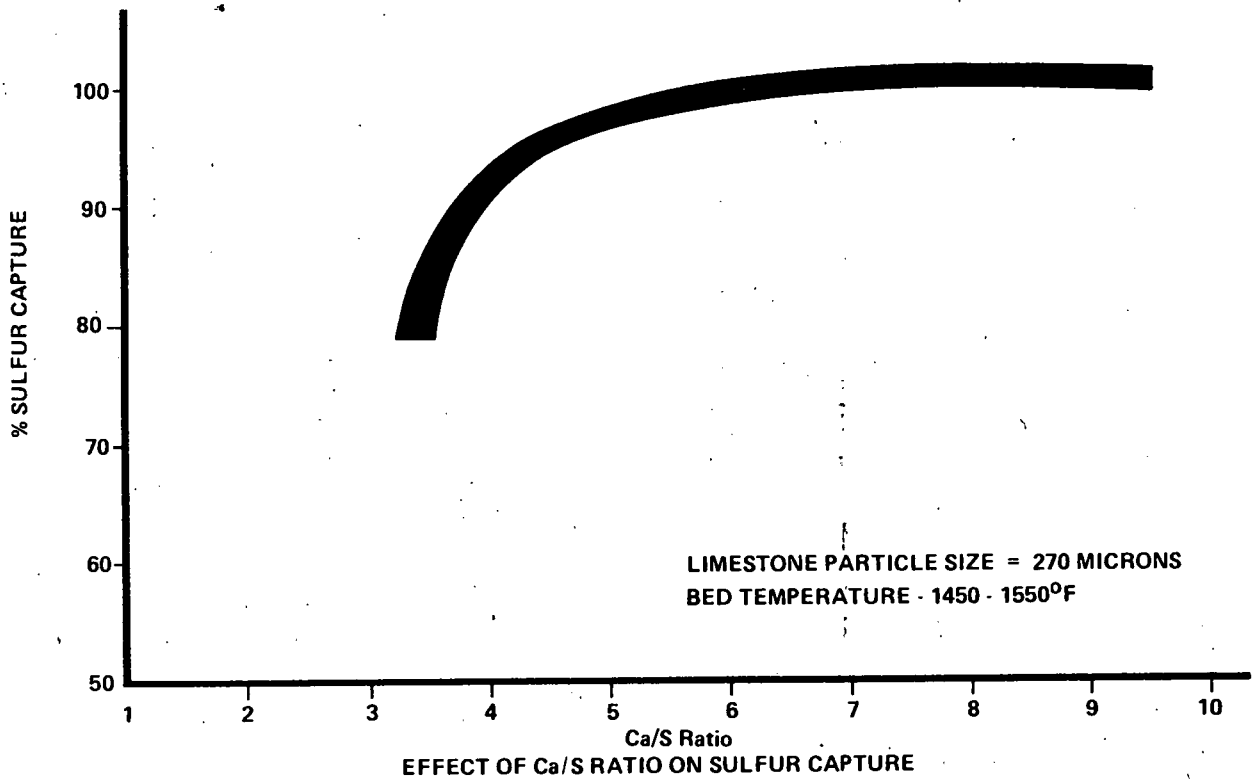

EFFECT OF Ca/S RATIO ON SULFUR CAPTURE

Fig. 7

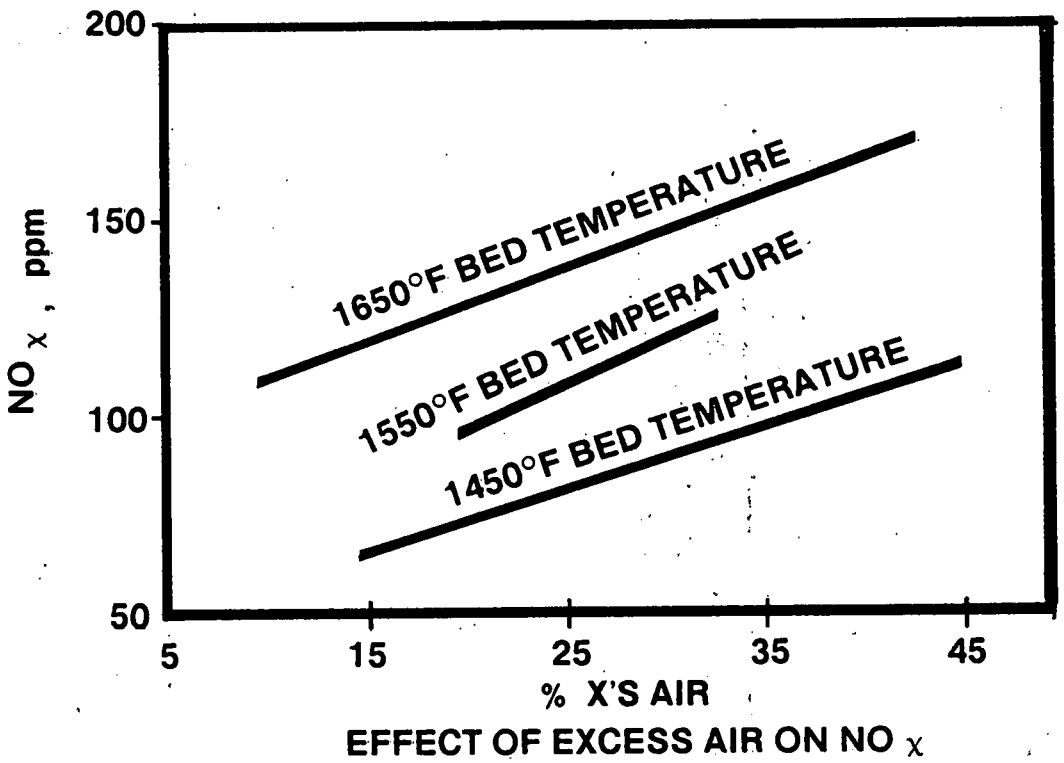

EFFECT OF EXCESS AIR ON NO χ

Fig. 8

FLUIDIZED-BED COMBUSTION OF ISRAELI OIL SHALE

J. S. Mei, J. Y. Shang, R. L. Rice
U. Grimm, and J. S. Halow
"Department of Energy, Morgantown, West Virginia

W. J. Ayers, Jr.
EG&G, Morgantown, West Virginia

Y. Keren, IMI, Haifa, Israel

Introduction

One of the many advantages of the fluidized-bed combustion system over the conventional-type combustion systems is its ability to burn high and/or variable inert content fuels (1). In addition, relatively low temperature combustion may be achieved because of the stable ignition of the injected fuel that can be assured by the high specific heat content of the bed solids which is rapidly transferred to the fuel and the air by a turbulent mixing process (2). In order to take full advantage of these facts, the Morgantown Energy Technology Center of the U.S. Department of Energy began a program a few years ago to examine the application of atmospheric fluidized-bed combustion (AFBC) technology to low-grade fuels which have low heating values and high inert contents. During the past few years, various low-grade fuels such as anthracite culm, lignite and lignite refuse, sub-bituminous coal, peat and oil shale were investigated systematically in our 6-inch diameter laboratory-scale unit as well as in the 18-inch diameter bench-scale fluid-bed combustor to determine their combustion, emissions, and operational characteristics. This paper presents the results of our recent combustion tests of Israeli oil shale in both the 6-inch diameter and the 18-inch diameter fluidized-bed combustors. The combustion tests had four objectives. They were:

- Investigate the feasibility of direct combustion of Israeli oil shale in atmospheric pressure fluidized-bed combustors.
- Ascertain for Israeli oil shale
  - carbon combustion efficiency,
  - extent of carbonate decomposition,
  - heat release, and
  - heat transfer coefficients.
- Determine the combustion and operational characteristics which may be unique to Israeli oil shale.
- Perform the conceptual design of a fluidized-bed combustor for the combustion of Israeli oil shale based on the experimental data.

According to the geological survey of Israel (3), current oil shale reserves are estimated to be 2,200 million tons, which constitute a substantial fuel source. Successful combustion of the oil shale and the recovery of its heating value represents a potential source of energy for the state of Israel.

Geological surveys of oil shale deposits and occurrences in Israel were initiated in the beginning of the century during the British Mandatory times. Five oil shale deposits, which are shown in Figure 1, have been identified. The principal oil shale deposits are found in the Hartuv-Zora area which contains over 900 million tons, or 40 percent of the total identified oil shale deposits. The other deposits can be found in Nabi Muser, Ein Boqeq, Efe, and Oron. The oil shale tested in our combustors came from the Efe deposit which was discovered in 1962 during a survey of phosphorite in that area.

Figure #1 OIL SHALE DEPOSITS AND OCCURRENCES IN ISRAEL

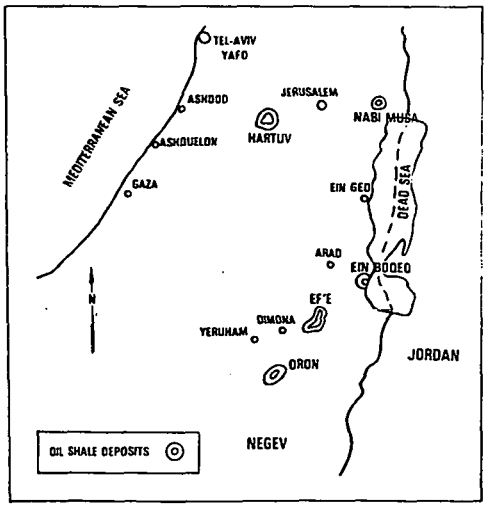

Experimental Facility

The experimental facility of the laboratory-scale and the bench-scale fluidized-bed combustors are shown schematically in Figures 2 and 3, respectively. The laboratory-scale fluidized-bed combustor is a 6-inch diameter, refractory-lined, cylindrical vessel. The bed region is 16 inches high. The expanded freeboard section of 8-inch diameter is 100 inches high. The 6-inch unit has a conical distributor plate which has an open area of 0.59 percent of the distributor area. Oil shale was metered and fed directly into the bed by a screw feeder which was protected by a water jacket. Spent bed material was removed through the overflow tube and the drain pipe at the bottom of the conical distributor. The flue gas was continuously sampled and analyzed after passing through a primary and a secondary cyclone. The 6-inch diameter combustor does not have a fly ash recycling system, nor does it have internal heat exchangers.

The 18-inch bench-scale fluid-bed combustor shown in Figure 3 is basically a refractory-lined cyclindrical combustor having an internal diameter of 18 inches in the bed region and an expanded freeboard section of a 24-inch diameter. The unit also consists of a set of hairpin-type water-cooled bed heat exchanger tubes and a single-pass water-cooled freeboard heat exchanger. Oil shale was metered from a hopper and was fed into a fuel injection chamber by a screw feeder. The oil shale was then entrained into the bed through the base of the conical distributor plate by compressed air. In order to maintain the desired temperatures, oil shale was also fed by the limestone screw feeder directly into the top of the expanded bed. In these tests, the bed was built entirely from oil shale; no additional sorbent or bed material was added to either the 6-inch or the 18-inch combustor. Particulates in the flue gas were removed in the cyclones and bag filters. During the combustion test of Israeli oil shale, particulates or fines removed in the primary cyclone were recycled into the bed for additional carbon burnup. Flue gas leaving the combustor was continuously sampled and analyzed. CO and CO_2 were determined by nondispersive infrared analyzers. A chemiluminesence analyzer was used to determine NO and NO_2 concentrations in the flue gas. SO_2 and total hydrocarbon analyses were made by a flame photometric analyzer and a flame ionization analyzer respectively, and the concentration of O_2 in the flue gas was determined by a paramagnetic analyzer.

Figure #2

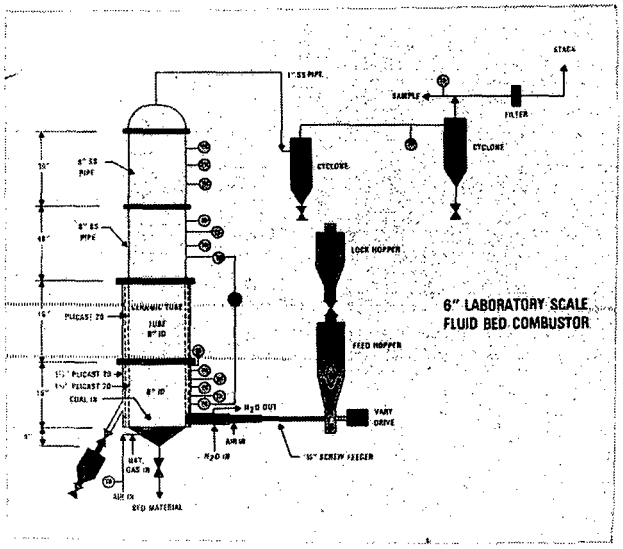

Figure #3

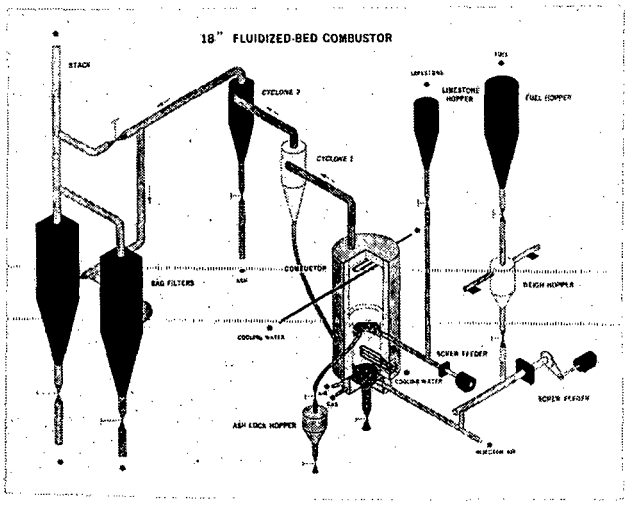

Chemical Analysis of Israeli Oil Shale

The ultimate and ash analysis of the typical oil shales which were tested in both the 6-inch and the 18-inch units are given in Table 1. The Israeli oil shale has a rather high ash content, approximately 55 percent, and a low heating value, below 2000 Btu/lb. The oil shale contains only 9 percent organic carbon. The volatile matter and calcium carbonate content, which are not shown in this table, are 38 percent and 47 percent, respectively. Based on the ash analysis, the Israeli oil shale has an inherent calcium to sulfur molar ratio slightly over 7. Differential thermal analysis of the Israeli oil shale indicated that evolution of volatile matter is completed at a temperature of about 1000°F. Gas chromatographic analysis of the extracted liquid product from the oil shale revealed that the percentage of identifiable straight-chain hydrocarbon was 38 percent. The straight-chain organic compounds contain 10 to 32 carbons and have a boiling range of 345°F (174°C) to 874°F (468°C). The oil shale contains a greater percentage of low boiling point hydrocarbons (26 percent below 391°C).

TABLE 1

CHEMICAL ANALYSIS OF ISRAELI OIL SHALE

ULTIMATE ANALYSIS:

	ISRAELI OIL SHALE FED TO 6'' FBC	ISRAELI OIL SHALE FED TO 18''FBC
MOISTURE,%	7.93	8.15
ASH,%	55.28	56.93
SULFUR,%	2.43	2.35
HYDROGEN,%	1.45	2.05
NITROGEN,%	0.44	0.29
TOTAL CARBON,%	14.69	14.84**
OXYGEN,%	17.78	15.29
CARBONATE AS CO_2,%	20.60	22.36
HEATING VALUE BTU/LB.	1902	1993

* CARBON (CO_2) = 5.62% ORGANIC CARBON = 9.07%
** CARBON (CO_2) = 6.10% ORGANIC CARBON = 8.84%

ASH ANALYSIS:

	ISRAELI OIL SHALE FED TO 6''FBC	ISRAELI OIL SHALE FED TO 18''FBC
SILICON, SiO_2	20.85	23.17
ALUMINUM, Al_2O_3	8.27	9.24
IRON, Fe_2O_3	3.66	4.48
CALCIUM, CaO	55.04	51.85
MAGNESIUM, MgO	0.68	1.17
SODIUM, Na_2O	2.46	0.50
POTASSIUM, K_2O	0.52	0.62
PHOSPHORUS, P_2O_5	0.37	2.42
TITANIUM, TiO_2	———	0.35
SULFUR, SO_3	6.56	5.99

Operating Conditions for Fluidized-Bed Combustion of Israeli Oil Shale

The operating conditions explored to date for the combustion of Israeli oil shale in our 6-inch and 18-inch fluid-bed combustors are given in Table 2. Israeli oil shales with moisture content as high as 18.5 percent were tested in the laboratory-scale combustor with preheated air. Bed temperatures were maintained in the range between 1180° to 1490°F. The lowest operating temperature occurred when burning an Israeli oil shale with 18 percent moisture without using preheated air. The highest bed temperature, 1490°F, was attained when the oil shale contained only 5 percent moisture and was burned in the 6-inch unit with air preheated to 600°F. The operating conditions for the 18-inch fluid-bed combustor were set up based on the results obtained from the combustion tests in the 6-inch laboratory-scale unit.

TABLE 2 OPERATING CONDITIONS FOR FLUIDIZED BED COMBUSTION OF ISRAELI OIL SHALE

CONDITIONS / COMBUSTOR	6-INCH DIAMETER	18-INCH DIAMETER
MOISTURE CONTENT, %	2.0 - 18.5	8.0 - 16.0
FEED SIZE, IN OR MESH	1/8"x 0 & 14 MESH	1/4"x 0
FUEL FEED RATE, LB/HR	18.5 - 52	180 - 300
EXCESS AIR, %	12 - 50	28 - 72
PREHEATED AIR TEMP., °F	70° - 875°	70°
BED TEMPERATURE, °F	1180° - 1490°	1250° - 1400°
BED DEPTH, IN	12	36
SUP. VELOCITY, FT/SEC	2.5 - 6.0	2.8 - 4.5

EXPERIMENTAL RESULTS OF COMBUSTION TESTS OF ISRAELI OIL SHALE

Combustion Efficiency

Carbon combustion efficiency as a function of temperature for the combustion tests of Israeli oil shale in both combustors at various operating conditions is plotted in Figure 4. As can be seen, a 98 percent or better carbon combustion efficiency is attainable in the 6-inch combustor without the recycling of fines. With the recycling of the fines collected from the primary cyclone, carbon combustion efficiency of 96 percent or better can be obtained for the 18-inch diameter bench-scale combustor. The higher combustion efficiency for the 6-inch unit can be attributed to the higher freeboard section which gives a much longer gas residence time to the volatiles for complete combustion in the combustor. This explanation was confirmed by the much lower carbon monoxide and hydrocarbon concentration measurements in the flue gases from the 6-inch laboratory unit. As mentioned earlier, devolatilization of the oil shale was completed at about 1000°F. The combustion of oil shale, therefore, took place in the homogeneous gas phase in the bed and/or in the freeboard and, consequently, led to a high combustion efficiency for the Israeli oil shale.

Figure #4

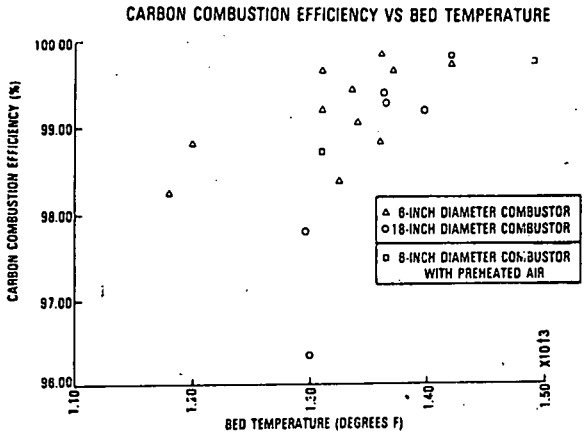

Based on the chemical analysis, a rather high percentage of calcium carbonate (approximately 47 weight percent) was found in the Israeli oil shale. Since the reaction is endothermic, a considerable amount of heat will be consumed as calcium carbonate decomposes. However, the heat losses due to calcination can be minimized by maintaining low bed temperatures. Figure 5 shows the extent of calcium carbonate decomposition as a function of bed temperature. As can be seen, calcium carbonate decomposition ranges from a low of 28 percent at 1180°F to a high of 86 percent at 1490°F. The lower temperature limit is dictated by the bed stability.

Figure #5

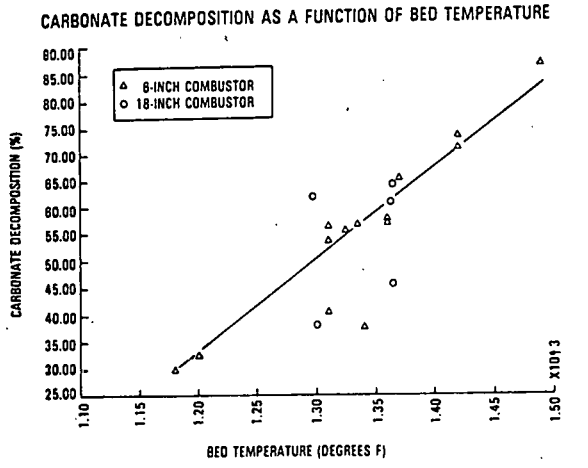

Temperature Distribution

Axial temperature profiles for two typical tests in the 6-inch diameter fluid-bed combustor are plotted in Figure 6. The upper curve is the profile for a rather short gas residence time in the bed (0.2 seconds). The temperature rises along the freeboard until it reaches a maximum, which in this particular test is approximately 50 degrees higher than the bed temperature, then gradually decreases. This suggests that combustion also took place in the freeboard section. The lower curve, however, shows no sign of freeboard combustion when the gas had a longer residence time in the bed. Figure 7 illustrates the temperature profile of a typical test in the 18-inch bench-scale combustor. As can be seen, temperature in the freeboard section remains nearly the same as the bed temperature. Throughout the combustion tests of Israeli oil shale in the 18-inch diameter unit, freeboard combustion was not observed for gas residence times ranging from 0.7 to 1.07 seconds.

Figure #6

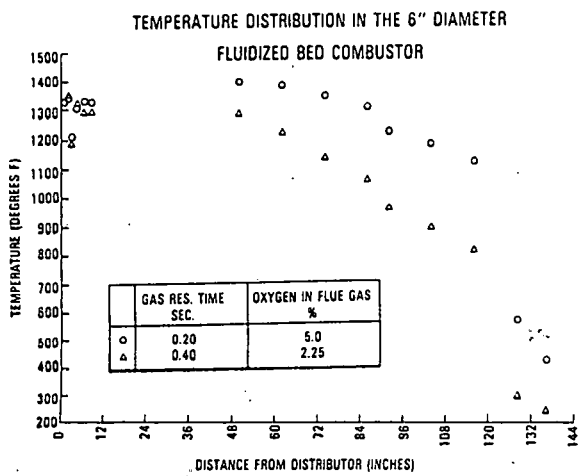

Figure #7

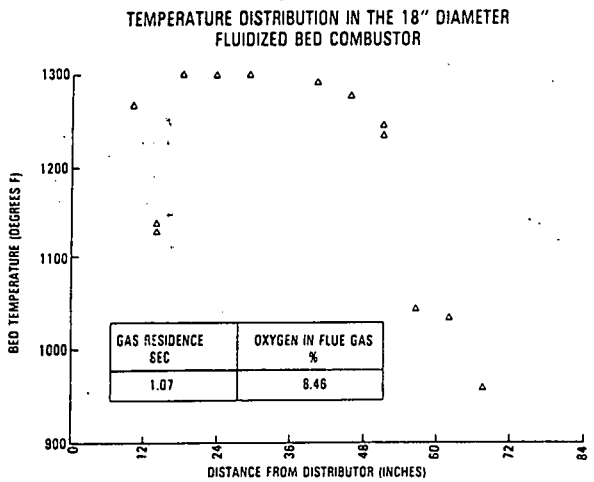

Heat Transfer and Heat Release Rates

Based on the data, overall heat transfer coefficients for the in-bed tubes and for the freeboard heat exchanger tube were found to be 53.4 and 7.5 Btu/ft^2-hr-°F, respectively (Table 3). It was also found that 25 percent of the total heat input into the 18-inch diameter fluid-bed combustor can be extracted through the freeboard heat exchanger where water was used as a cooling medium. Five percent of the total heat input can be recovered through the in-bed tubes where saturated steam at 30 psia and 250°F was used. Table 3 also shows the heat release rates for both the 6-inch laboratory-scale and the 18-inch bench-scale units. For the 6-inch combustor, the heat release rate was found to be 0.44 x 10^6 Btu/ft^2-hr. The heat release rate for the 18-inch unit is 0.30 x 10^6 Btu/ft^2-hr, which is lower than the result obtained from the laboratory combustor. The lower heat release rate in the bench-scale combustor is attributed to its fuel feed capacity which is limited to a maximum of 300 lbs/hr of Israeli oil shale with both feeders.

TABLE 3

HEAT TRANSFER DATA FROM 18-INCH DIAMETER COMBUSTER

OPERATING CONDITIONS				HEAT TRANSFER DATA*	
BED TEMPERATURE °F	SUP. VEL FT/SEC	BED DEPTH IN	OIL SHALE SIZE IN	OVERALL BED TO TUBE BTU/FT^2-HR°F	OVERALL FREEBOARD TO TUBE BTU/FT^2-HR°F
1280	2.8	36	1/4"×0	53.4	7.5

*COOLING MEDIUM: SATURATED STEAM AT 30psia AND 250°F

HEAT EXTRACTED THROUGH IN-BED & FREEBOARD HEAT EXCHANGERS

TOTAL HEAT INPUT 10^6 BTU	TOTAL HEAT EXTRACTED 10^6 BTU	HEAT EXTRACTED IN BED		HEAT EXTRACTED IN FREEBOARD	
		10^6 BTU	PERCENT OF TOTAL HEAT INPUT	10^6 BTU	PERCENT OF TOTAL HEAT INPUT
6.75	2.04	0.34	5.1	1.70	25.30

HEAT RELEASE RATES

HEAT RELEASE RATE FOR 18" FLUIDIZED BED COMBUSTOR=0.32×10^6 BTU/FT^2-HR
HEAT RELEASE RATE FOR 6" FLUIDIZED BED COMBUSTOR=0.44×10^6 BTU/FT^2-HR

Operating Characteristics and Problems

During the combustion tests of the Israeli oil shale the following operating characteristics and problems were observed:

- Israeli oil shale with moisture content over 11 percent tends to be compacted under normal stresses. This leads to bridging in the coal hopper and blockage in the feed nozzle due to the formation of hard scale on the wall.
- Israeli oil shale tends to be broken in response to mild shear stress. In addition, the oil shale crumbles easily as it dries out on exposure to elevated temperatures. It produces considerable amounts of fly ash on combustion.
- High ash, high moisture content, and the large amount of calcium carbonate in ash combined with the low heating value of the Israeli oil shale requires the feeding of large quantities of oil shale in order to maintain the desired bed temperature. The handling of large quantities of oil shale and the subsequent spent bed is one of the specific operating problems that must be considered in designing any commercial unit.
- The spent bed material contains a considerable amount of the heat from the system. Recovery of this heat through a cooler would aid the overall process efficiency.

Conclusions

Based on the combustion test data obtained from both the 6-inch and 18-inch units, several conclusions can be drawn from the present feasibility studies on fluidized-bed combustion of Israeli oil shale:

- Differential thermal analysis indicated that the devolatilization of Israeli oil shale was completed at a temperature of 1076°F (580°C).
- Direct combustion of Israeli oil shale was successfully conducted in the 6-inch and 18-inch fluidized-bed combustors.

- Combustion of Israeli oil shale with a moisture content as high as 18 percent can be sustained without using preheated air.

- Ninety-eight percent or better carbon combustion efficiency is attainable in the 6-inch unit without recycling of fines. With recycling of fines, 96 percent or better carbon combustion efficiency is attainable in the 18-inch unit.

- Carbon combustion in the bed and/or in the freeboard takes place in the homogeneous gas phase.

- Emissions of NO_x and SO_2 from the 18-inch combustor were low (0.4 lb $NO_2/10^6$ Btu, 0.7 lb $SO_2/10^6$ Btu).

- Overall heat transfer coefficients of 53.4 and 7.5 Btu/ft^2-hr-°F are obtained for in-bed and freeboard heat exchange tubes in the 18-inch diameter combustor.

- Over 25 percent of total heat input was extracted from freeboard, and 5 percent was recovered through in-bed tubes.

- Heat release rates of 0.32 x 10^6 and 0.44 x 10^6 Btu/ft^2-hr were attained for the 18-inch diameter combustor and the 6-inch diameter combustor.

Conceptual Design of a Hybrid System for the Combustion of Israeli Oil Shale

Analysis of the experimental data and the observed operating characteristics suggests that a hybrid combustion system would be the best means for the direct combustion of Israeli oil shale. The concept of the hybrid system is illustrated schematically in Figure 8. Devolatilization of the oil shale takes place in the main section of the fluidized-bed reactor which is operated at substoichiometric conditions (90 percent of the stoichiometric air is supplied for partial combustion). The bed temperature is kept below 1300°F so that calcium carbonate decomposition is minimized, thereby reducing the heat loss due to calcination. The subsequent combustion of the volatiles is carried out in the freeboard section using either a pulverized fuel burner if a high temperature flame is required, or a second-stage fluidized-bed combustor where the fluid bed will be maintained at a higher temperature to achieve better combustion efficiency. Heat in the spent bed material is partially recovered through a moving-bed cooler which will preheat the fluidizing air.

REFERENCES

1. Morrison, G. F., Combustion of Low-Grade Coal, International Energy Agency Coal Research, Report Number ICTIS/TROZ, London, UK, 1978.

2. Reh, L., Fluid-Bed Combustion in Processing, Environmental Protection and Energy Supply, Paper presented at the International Fluidized-Bed Combustion Symposium of the American Flame Research Committee, Boston, MA, 1979.

3. Shirav, M. and Ginzburg, D., A Guidebook to the Oil Shale Deposits in Israel, Geological Survey of Israel, Mineral Resources Division, Ministry of Energy and Infrastructure, Prepared for the International Symposium on Oil Shale Chemistry and Technology, Jerusalem, 1978.

Figure 8. - Conceptual Design of Hybrid FBC System

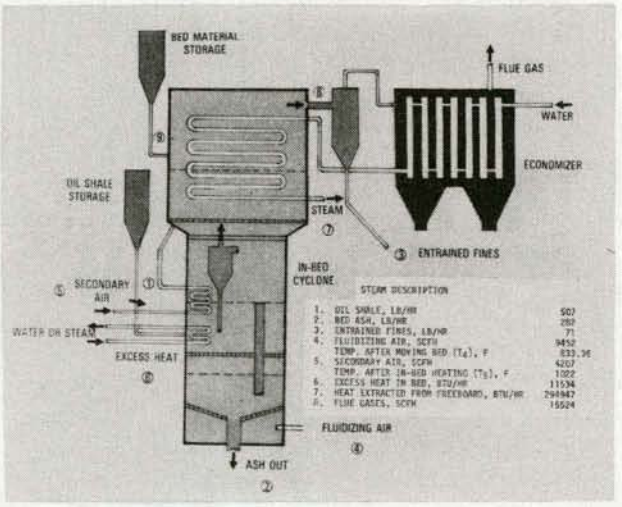

COMBUSTION OF WESTERN COAL IN A FLUIDIZED BED

W. T. Abel, R. L. Rice, and J. Y. Shang
Department of Energy/Morgantown Energy
Technology Center (DOE/METC)
W. J. Ayers, Jr., EG&G, Morgantown, WV
D. G. Turek, Science Applications, Inc.,
Morgantown, WV

Introduction

Western subbituminous coals make up about 25 percent of the nation's coal reserves[1,2]. They are particularly attractive because of their low sulfur content and ease of mining. Much effort is being made to increase their utilization. Fluidized-bed combustion appears to be an effective method of using these coals, since sulfur is retained without need for added water as in the wet cleaning processes. In many western areas where water is scarce, this is an important advantage. In addition, the high alkali content of the coal may allow the sulfur emission limits to be met without added sorbent. As noted by Goblirsch, et al.,[3] of GFETC, the alkali will be a more effective sorbent in fluidized-bed combustion as opposed to pulverized coal combustion because of the lower combustion temperature and the increased contact time between the sulfur dioxide and the alkali in the ash. Their tests with lignite and western subbituminous coals confirm that a significant degree of sulfur capture can be achieved in a fluidized bed without added sorbent and that reinjecting the flyash from the primary cyclone increases the sulfur retention. Their results and other tests with Texas lignite and lignite refuse[2] indicate that sulfur retention is greatest for bed temperatures in the range of 1400-1450°F. For high sulfur bituminous coal burning in a bed containing limestone, the maximum sulfur retention occurs at about 1550°F.

In this present work a subbituminous coal from the Rosebud mine in Montana was burned in an 18-inch diameter fluidized bed, with and without added limestone. The goals included:

- Studying the combustion characteristics in the bench scale, 18-inch fluidized-bed unit.
- Further examining the possibility of meeting sulfur dioxide emission limits without added limestone.
- Identifying any operational problems.

Experimental Facility And Start-Up Procedure

The experimental facility at the Morgantown Energy Technology Center for the fluidized-bed combustion studies is shown schematically in Figure 1. It is basically a refractory-lined, cylindrical combustor having an internal diameter of 18 inches in the 45-inch high bed region with a 27-inch high expanded freeboard section of 24 inches diameter.

The combustor contains a set of hairpin type, water-cooled heat exchanger tubes located in the bed region and a single pass water-cooled heat exchanger in the expanded freeboard. Coal is metered from a hopper and is fed into a fuel injection chamber by a screw feeder. The coal is then injected into the bed near the base of the conical air distributor plate by compressed air. Limestone, when used, is metered from a hopper and fed by a screw feeder directly into the top of the expanded bed. Entrained particulate matter in the flue gas leaving the combustor is removed by two stages of cyclones followed by bag filters. Particulate matter removed by the primary cyclone is reinjected into the bed for additional carbon burnup. Flue gas leaving the combustor is continuously sampled and analyzed. CO and CO_2 are determined by non-dispersive infrared analyzers. A chemiluminescence analyzer is used to determine NO and NO_x. SO_2 and total hydrocarbon analyses are made by a flame photometric analyzer and a flame ionization analyzer, respectively, and O_2 by a paramagnetic analyzer.

Start-up of the unit is accomplished by preheating the lower part of the combustor to 1400°F with premixed natural gas and air. When the desired temperature level is reached, approximately 40 lbs of bed material is added at a slow rate until it is also up to a temperature of about 1400°F. Then fuel feed is started and continued until the desired bed level is attained. The natural gas is then shut off and the fuel combustion is self-sustaining. Desired operating conditions are then established and the unit allowed to stabilize before a data-taking period is started. Further details of the unit may be found in Reference 4.

Fuel and Sorbent

Fuel used in these tests was Rosebud coal, a subbituminous coal from southeastern Montana as shown in Figure 2. The coal was crushed to ¼-inch by 0 size. Chemical analysis of the coal and ash is shown in Table 1. Size analysis of the coal is shown in Table 2.

The sorbent used in the study was Greer Limestone crushed to ½-inch by 0 size. Chemical and size analyses are shown in Table 3.

Figure 1. — 18-INCH DIAMETER FLUIDIZED BED COMBUSTOR AT METC

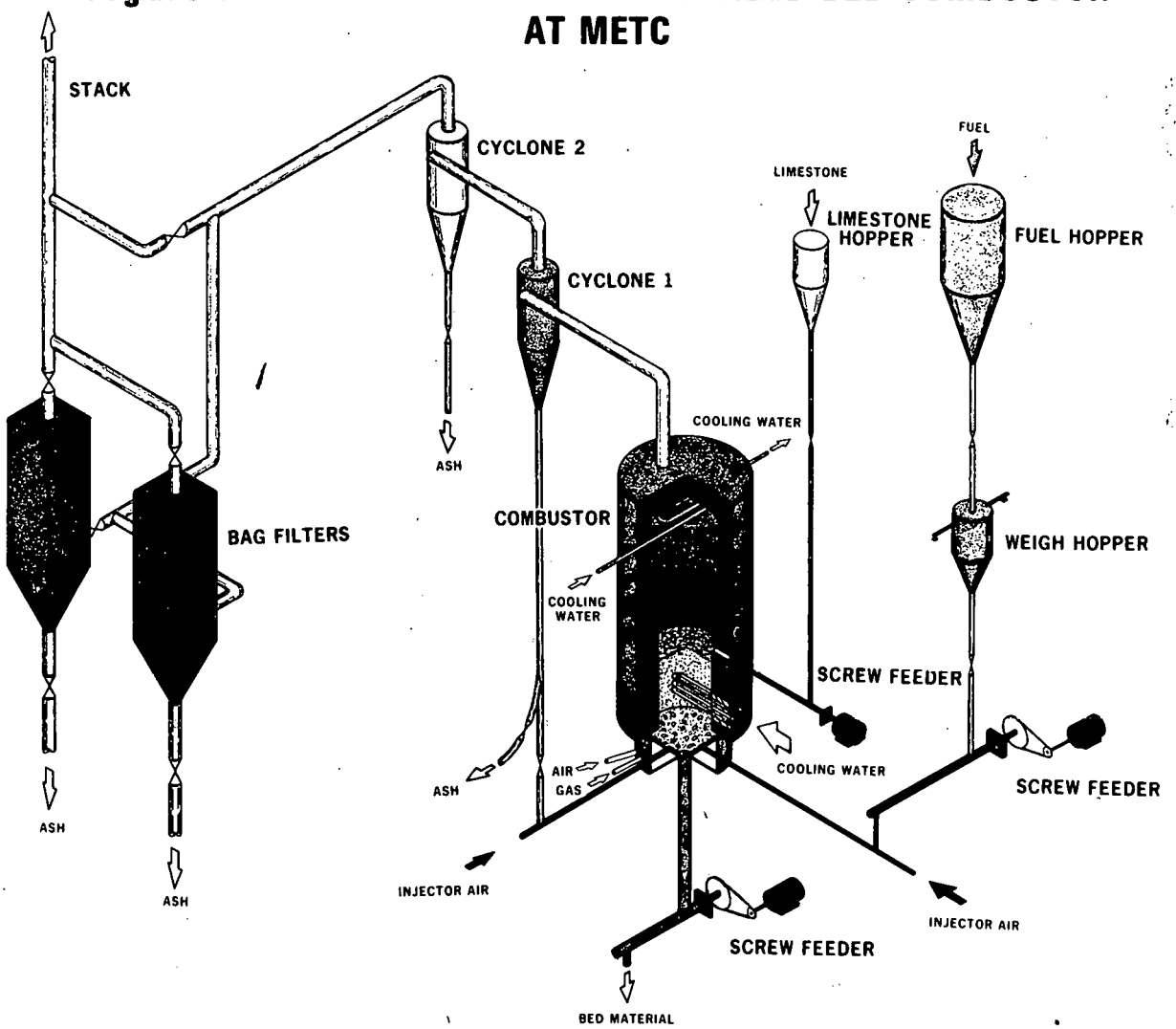

Montana

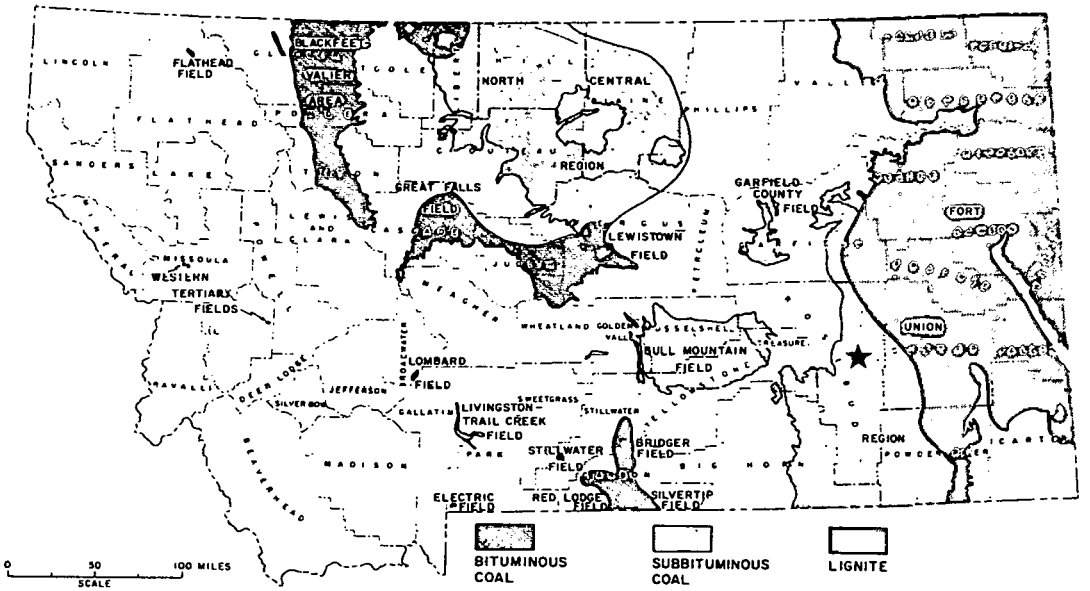

FIG. 2 Index Map of Montana Coal Fields

TABLE 1.

CHEMICAL ANALYSIS OF ROSEBUD COAL AND ASH

Coal		Ash	
Moisture	14.28%	SiO_2	43.70%
Sulfur	.96%	Al_2O_3	18.42%
Ash	11.36%	Fe_2O_3	6.13%
Hydrogen	4.46%	CaO	11.41%
Total Carbon	56.85%	MgO	4.22%
Nitrogen	.73%	Na_2O	1.71%
Oxygen	11.36%	K_2O	.80%
		P_2O_5	.61%
		TiO_2	.79%
		SO_3	9.94%

Heating Value 9,600 Btu/lb.

TABLE 2.

SIZE ANALYSIS OF 1/4-INCH X 0-INCH ROSEBUD COAL

Size Range	Weight Percent
1/4" - 4 mesh (U.S. Sieve No.)	----
4 - 6	4.9
6 - 10	25.7
10 - 16	15.5
16 - 30	25.7
30 - 50	16.1
50 - 100	6.2
100 - 200	3.3
200 - 0	2.6

TABLE 3.

SIZE AND CHEMICAL ANALYSIS OF
1/4-INCH X 0-INCH GREER LIMESTONE

Size Range	Weight Percent
1/4" - 4 mesh (U.S. Sieve No.)	2.28
4 - 8	34.83
8 - 16	30.34
16 - 30	14.61
30 - 50	5.32
50 - 100	4.03
100 - 0	8.59

CHEMICAL COMPOSITION

CaO	44.86%
MgO	2.15%
CO_2	47.37%
Ash	5.62%

Operating Variables

The range of operating conditions for the tests are shown in Table 4. The conditions for each individual run, along with the test results, are shown in Table 5.

The bed temperature was established by adjusting the flow rate of coolant to the in-bed heat exchange tubes while maintaining the desired fuel, limestone, and air rates.

Results And Discussion

Carbon Combustion Efficiency

The carbon combustion efficiency as a function of excess air is shown in Figure 3. Although the scatter is wide, there is a trend toward increased efficiency with increased excess air as expected. There is no obvious pattern for the effect of bed temperature on carbon combustion efficiency. During these tests the bottom product of the primary cyclone was reinjected in the combustor contributing to improved carbon combustion. Carbon combustion efficiency averaged about 94 percent for the runs.

Sulfur Retention and SO_2 Emissions

The percent sulfur retention achieved in these tests as a function of bed temperature and calcium to sulfur (Ca/S) molar ratio is shown in Figure 4. Sulfur retention increased with decreasing temperature at least down to 1450°F. The Rosebud coal has an inherent Ca/S molar ratio of 0.77 and a total alkali to sulfur molar ratio of 1.01. Without added limestone, the sulfur retention varied from nearly 80 percent at 1450°F to about 40 percent at bed temperatures around 1650°F. With added limestone, the sulfur retention at higher temperatures improves markedly, becoming less dependent on the bed temperature as the Ca/S molar ratio increases.

Tests at GFETC[3] and at METC with lignites[2] also show a maximum sulfur retention at about 1450°F. For bituminous coal burning in a bed containing limestone, the maximum sulfur retention occurs at about 1550°F[4].

In analyzing the lignite data from GFETC, Westinghouse Research[5] made the assumption that the complex $CaO\text{-}Al_2O_3\text{-}2SiO_2$ is formed to the extent that alumina or silica are present in the ash and that only the remaining calcium is available for sulfur capture. For the Rosebud coal, if $CaO\text{-}Al_2O_3\text{-}2SiO_2$ formed to complete utilization of the limiting compound (Al_2O_3), nearly all of the calcium would be tied up and unavailable for sulfur capture. As Figure 4 shows, this assumption is not valid in this case. At 1450°F nearly all the calcium in the ash is utilized for sulfur capture. This high utilization of the inherent calcium may be due to the eutectic action of the other alkali compounds in the ash[6,7]. The decrease in sulfur retention with increasing temperature may be partly due to tying up of calcium in the ash as this or some similar compound. However, pore blockage by calcium sulfate formation is the more obvious mechanism.

The effect of Ca/S molar ratio and bed temperature on sulfur dioxide emission is shown in Figure 5. With bed temperatures in the 1450° to 1470°F range,

TABLE 4.

RANGE OF OPERATING CONDITIONS FOR
FLUIDIZED-BED COMBUSTION OF ROSEBUD COAL

Bed Temperature (°F)	1450 to 1670
Superficial Gas Velocity (ft/sec)	2.76 to 4.0
Expanded Bed Height (ft)	2.67 to 3.50
Excess Air (%)	5.27 to 25.10
Fuel Feed Rate (lb/hr)	0 to 7.81
Limestone Feed Rate (lb/hr)	42.79 to 66.69
Calcium to Sulfur Molar Ratio	0.77 to 4.67
Gas Residence Time in Bed (sec)	0.86 to 1.0

TABLE 5.

OPERATING CONDITIONS AND RESULTS; FLUIDIZED-BED COMBUSTION OF ROSEBUD COAL

	Operating Conditions									Heat Transfer, Btu/ft²/°F		
										In-Bed		Over-Bed
Run No.	Coal Rate, lb/hr	Limestone Rate, lb/hr	Air In, scfh	Superficial Velocity, ft/sec	Bed Height, ft	Length of Run, hrs	Bed Temp., °F	Excess Air, Percent	Ca/S Molar Ratio	To Water	To Steam	To Water
RB5-1	50.70	4.76	5385	3.58	3.08	21	1669	14.03	3.27	34	--	10
RB5-5	51.02	4.73	5537	3.37	3.08	12	1544	13.32	3.24	--	--	9
RB5-6	53.37	7.81	5500	3.27	3.08	14	1535	5.52	4.67	--	47	7
RB5-8	52.30	3.62	5341	3.18	3.08	17	1452	9.35	2.62	41	--	13
RB5-9	52.62	4.01	5332	3.19	3.08	12	1459	8.60	2.80	42	--	12
RB5-2	54.63	2.99	5374	3.58	3.08	27	1662	6.15	2.93	--	32	10
RB6-1	42.79	--	4542	3.07	2.67	20	1665	16.07	.77	--	37	11
RB6-2	46.97	3.26	4588	3.09	2.67	14	1658	6.79	2.62	32	41	11
RB6-3	46.42	6.19	4519	3.02	2.67	13	1651	5.96	4.33	30	51	12
RB6-4	43.74	--	4568	2.92	2.67	31	1565	13.31	.77	--	42	3
RB6-5	46.39	4.59	4520	2.91	2.67	13	1568	6.35	3.41	--	57	1
RB6-6	46.74	5.66	4525	2.76	2.67	14	1468	5.27	4.00	50	--	2
RB6-7	45.04	--	4771	2.77	2.67	26	1459	10.20	.77	52	--	3
RB7-5	44.48	1.16	5029	3.04	2.67	34	1466	21.99	1.47	48	35	8
RB4-2	51.91	4.63	6225	4.00	3.50	49	1658	25.09	3.15	--	33	15
RB4-6	53.16	6.21	6149	3.77	3.50	9	1563	20.49	3.89	--	49	14
RB7-4	66.69	2.25	5811	3.56	3.08	15	1585	-10.28	1.67	--	57	11
RB7-3	52.88	3.33	5681	3.57	3.08	12	1565	14.62	2.45	45	45	11
RB7-1	60.21	4.33	6203	4.00	3.50	6	1659	7.77	2.69	--	37	13
RB4-7	55.56	--	6188	3.67	3.50	9	1462	18.16	.77	43	--	11
RB4-8	53.99	--	6197	3.50	3.50	7	1457	10.87	.77	45	--	10

	Combustion Description							Flue Gas Description					
						NO_x Emission, $lb/10^6$ Btu							
Run No.	Combustion Efficiency, Percent	Sulfur Retention, Percent (Gas Data)	Sulfur Retention, Percent (Solids Data)	Calcium Utilization, Percent	SO_2 Emission, $lb/10^6$ Btu	as NO	as NO_2	CO_2, Percent	O_2, Percent	CO, Percent	SO_2, PPM	NO_x, PPM	THC, PPM
RB5-1	93.89	76.35	65.77	23.32	.48	.28	.43	15.34	11.12	.02	236	293	4
RB5-5	95.19	71.80	63.00	22.15	.57	.31	.48	15.72	8.08	.06	285	334	1
RB5-6	96.13	90.15	70.98	19.29	.20	.27	.41	17.86	2.26	.07	110	320	27
RB5-8	96.98	99.66	125.29	38.09	.01	.14	.21	15.58	13.87	.10	3	144	5
RB5-9	95.49	99.48	104.02	35.49	.01	.13	.20	15.89	11.83	.11	5	136	10
RB5-2	90.90	72.32	85.92	24.68	.56	.14	.21	15.62	11.68	.03	294	161	14
RB6-1	94.51	31.74	45.41	41.16	1.38	.09	.14	14.89	11.24	.07	683	91	7
RB6-2	83.69	38.90	73.62	14.84	1.23	.08	.12	15.39	7.42	.09	694	102	2
RB6-3	97.57	90.99	108.63	21.03	.18	.06	.09	18.15	6.08	.12	101	67	0
RB6-4	103.36	77.93	59.50	101.07	.45	.16	.25	17.09	7.09	.06	232	174	0
RB6-5	81.76	72.23	89.08	21.19	.56	.10	.15	15.47	6.60	.08	319	126	0
RB6-6	84.67	91.73	122.83	22.93	.17	.05	.08	15.65	16.00	.09	84	52	0
RB6-7	98.66	63.46	73.78	82.30	.74	.06	.09	15.67	9.73	.13	370	69	0
RB7-5	93.76	98.49	113.46	67.16	.03	.26	.40	14.38	11.05	.03	14	257	0
RB4-2	108.53	28.42	73.76	9.03	1.44	.22	.34	15.08	13.85	.05	610	200	8
RB4-6	99.74	89.69	101.08	23.08	.21	.18	.28	14.48	14.99	.06	90	169	5
RB7-4	84.54	65.28	54.21	39.08	.70	.22	.34	17.45	4.17	.13	449	300	200
RB7-3	96.68	80.98	105.78	33.05	.38	.21	.32	16.72	4.45	.08	201	230	14
RB7-1	91.36	70.09	103.03	26.07	.60	.15	.23	16.37	3.87	.20	333	174	172
RB4-7	93.66	72.00	81.80	93.51	.56	.20	.31	15.23	4.01	.23	292	216	116
RB4-8	109.51	86.95	90.53	112.76	.26	.19	.29	17.00	3.50	.24	130	204	240

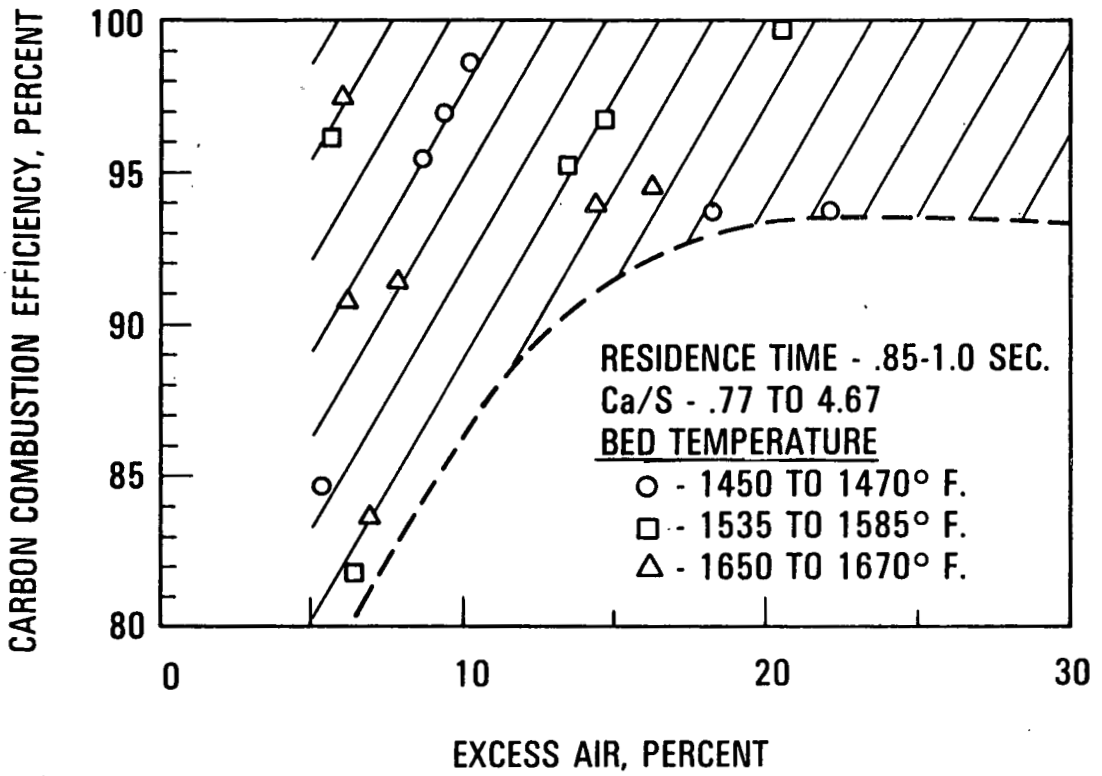

Figure 3. — THE EFFECT OF EXCESS AIR AND BED TEMPERATURE ON CARBON COMBUSTION EFFICIENCY

sulfur dioxide emission was well below the EPA allowable limit of 1.2 lb SO_2/ 10^6 Btu without benefit of added limestone. At higher bed temperatures some limestone addition may be necessary.

Nitrogen Oxide Emission

Figure 6 shows the nitrogen oxide emission as affected by excess air up to 25 percent. Although the scatter of the data is wide, all the points lie below the EPA allowable limit for NO_x (0.6 lbs $NO_2/10^6$ Btu). Attempts to correlate NO_x emission with bed temperature were unsuccessful.

Heat Transfer

Overall heat transfer coefficients to cooling tubes in bed were nearly five times those for the overhead tubes as shown in Table 5. The coefficients should, however, be taken only as approximate values since coolant flow to the in-bed tubes flipped randomly from water to steam during the tests.

Operational Characteristics and Problems

During five of the test periods (RB4-7, RB4-8, RB7-1, RB7-3, RB7-4), it was observed that the 2-inch diameter recycle line from the primary cyclone was plugged up with solids. Other than this, no problems were found in handling, feeding, or burning the Rosebud coal. During tests with a North Dakota lignite, which has a higher alkali content, unusual deposits formed on the heat exchanger tubes and around the distributor jets[8]. No such deposits were noticed with the Rosebud coal.

With all fuels it was occasionally necessary to clean out the exhaust stack beyond the bag filters due to a build up of a cement-like material on the walls. Frequency of cleanout increased with high ash materials.

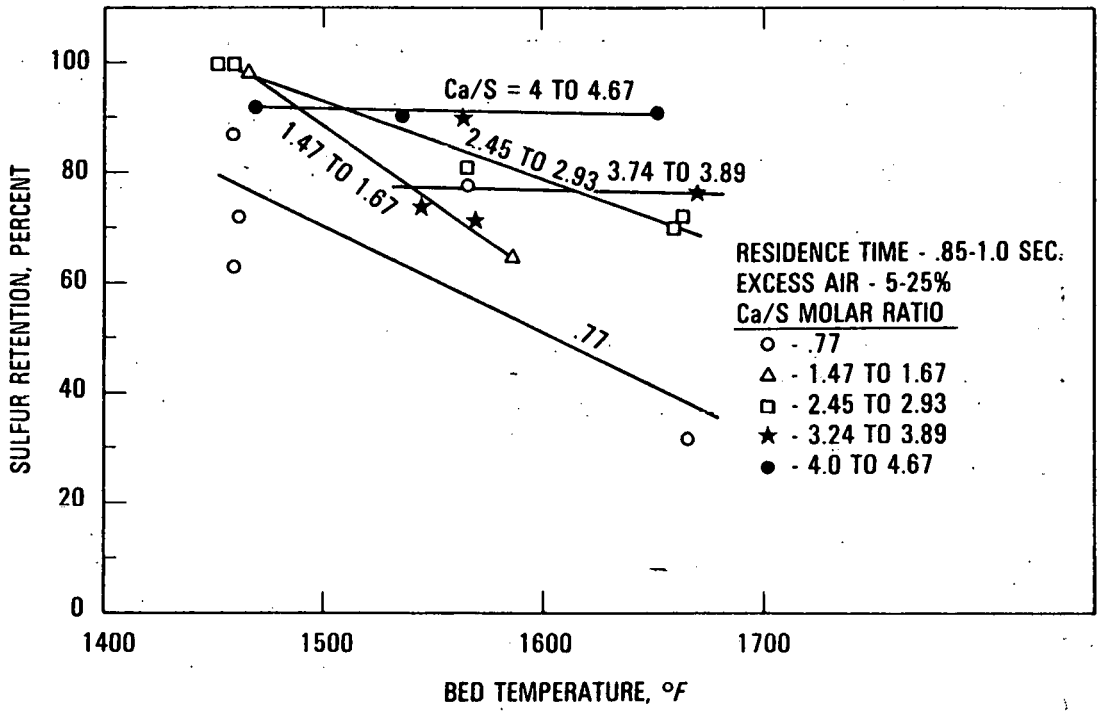

Figure 4. — THE EFFECT OF BED TEMPERATURE AND Ca/S RATIO ON SULFUR RETENTION

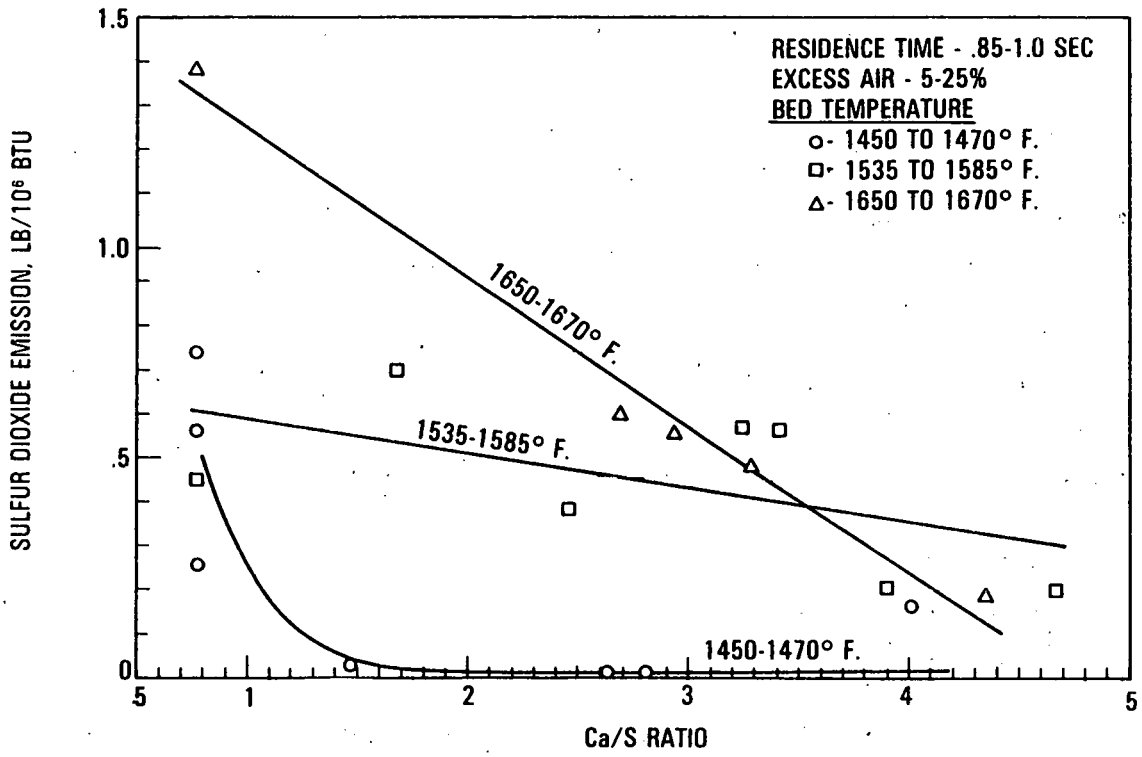

Figure 5. — THE EFFECT OF Ca/S RATIO AND BED TEMPERATURE ON SULFUR DIOXIDE EMISSIONS

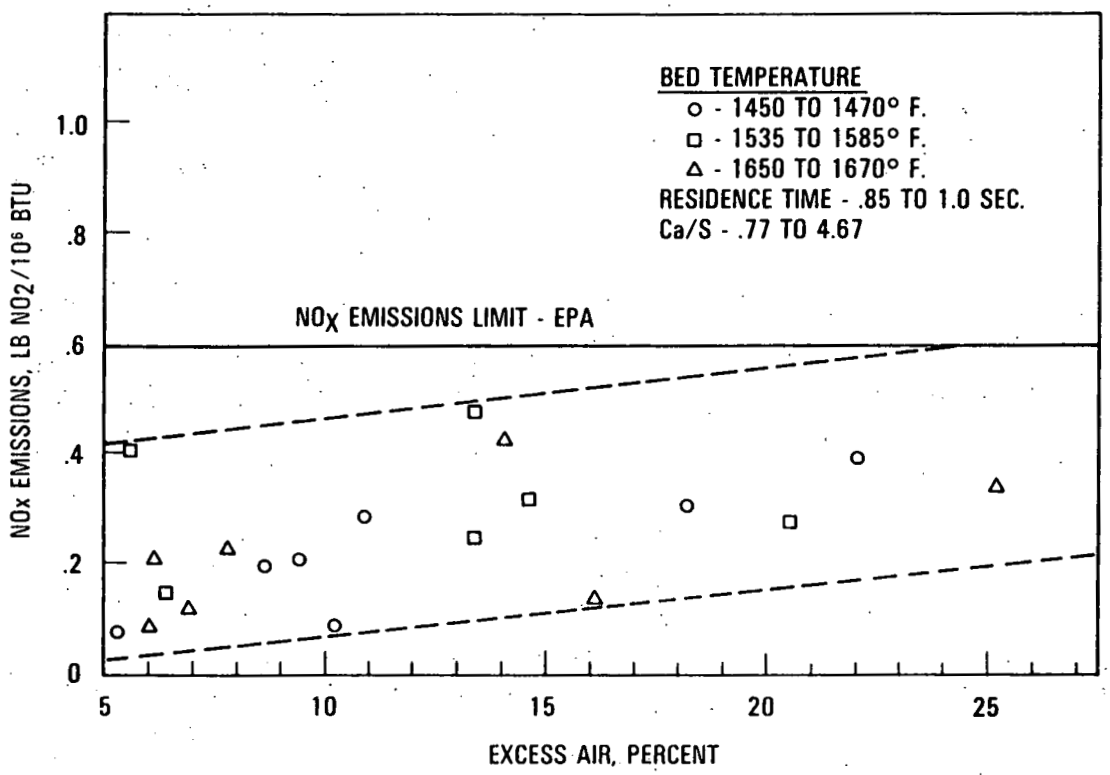

Figure 6. — THE EFFECT OF EXCESS AIR ON NOx EMISSION

Biological and Environmental Characteristics of FBC Emissions

Work carried out to examine the stack emissions of the 18-inch FBC unit at METC[9,10,11] during the burning of Rosebud coal and other fuels showed interesting comparisons. Some of the significant conclusions are shown in Tables 6 and 7.

Conclusions

- Sulfur dioxide emission can be kept below the EPA limit of 1.2 lb/10^6 Btu without any added sorbent for bed temperatures below 1500°F. More stringent limits may require the addition of limestone.
- The NO_x emission limit of 0.6 lb $NO_2/10^6$ Btu is met with excess air up to 25 percent and bed temperatures to 1670°F.
- Occasional plugging of the recycle line from the primary cyclone was the only operational problem encountered.
- Emissions from the 18-inch fluidized-bed combustor, including toxic trace elements and mutagenic activity, were comparable to or lower than those from conventional power plants.

- AFBC CAN MEET STANDARDS FOR SULFUR DIOXIDE AND NITROGEN OXIDE EMISSIONS
- AFBC PARTICLE EMISSIONS ARE COMPARABLE OR LOWER THAN FROM CONVENTIONAL POWER PLANTS
- AFBC POLYCYCLIC ORGANIC EMISSIONS APPEAR TO BE HIGHER THAN ESTIMATED FOR CONVENTIONAL POWER PLANTS AND ARE PRIMARILY VAPOR PHASE AS MEASURED
- AFBC TRACE ELEMENT EMISSIONS ARE COMPARABLE OR LOWER THAN CONVENTIONAL POWER PLANT EMISSIONS
- MUTAGENIC ACTIVITY HAS BEEN DETECTED IN SOME FLY ASH SAMPLES FROM THE AFBC STACK
- THE MUTAGENIC ACTIVITY PER MASS OF FLY ASH EXTRACTED APPEARS TO BE LESS IN THE METC FLUIDIZED BED COMBUSTOR ASH THAN THAT REPORTED FOR ONE CONVENTIONAL POWER PLANT

TABLE 6: CONCLUSIONS CONCERNING EFFLUENTS FROM 18-INCH FLUIDIZED BED COMBUSTOR AT METC.

PARTICULATE TRACE ELEMENT EMISSIONS

PLANT TYPE	EMISSION RATE OF 8 TOXIC TRACE ELEMENTS* (G/10^6 BTU)
18" AFBC BAGHOUSE	0.01
350 MW PULVERIZED COAL-VENTURI SCRUBBER	0.2
350 MW PULVERIZED COAL-HOT SIDE ESP	0.1
250 MW PULVERIZED COAL-CYCLONE	0.6

* Sb, As, Cd, Cr, Cu, Pb, Ni, Se

TABLE 7: COMPARISON OF EFFLUENTS FROM 18-INCH FLUIDIZED BED COMBUSTOR AND CONVENTIONAL POWER PLANTS.

References

1. Hammard, A. L., W. D. Metz, and T. H. Maugh, II. Energy and the Future, Am. Assoc. for Advancement of Science, 1973.

2. Mei, J. S., U. Grimm, and J. S. Halow. Fluidized-Bed Combustion of Low Quality Fuels, Texas Lignite and Lignite Refuse. MERC/RI-78/3, Morgantown Energy Research Center, Morgantown, WV, April 1978.

3. Goblirsch, G. M., R. W. Fehr, and E. A. Sondreal. Effects of Coal Composition and Ash Reinjection on Sulfur Retention Burning Lignite and Western Subbituminous Coals. Proceeding of the Fifth International Conference on Fluidized Bed Combustion, Washington, DC, December 12-14, 1977.

4. Mei, J. S., J. S. Halow, U. Grimm, and R. L. Rice. Fluidized-Bed Combustion of High Sulfur Coals. METC/RI-79/4, Morgantown Energy Technology Center, Morgantown, WV, April 1979.

5. Ulerich, N. H., R. A. Newby, M. A. Alvin, W. G. Vaux, and D. L. Keairns. Sulfur Removal System Performance for AFBC Utility Plant Burning Western Coal. Final Report Contract No. 3377-03, November 1977.

6. Shearer, J. A., I. Johnson, and C. B. Turner. The Effect of Sodium Chloride on the Reaction of SO_2/O_2 Mixtures with Limestone and Dolomites. Argonne National Laboratory Report ANL/CEN/FE-78-8 (July 1978).

7. Gasner, L. L. Enhancement of Sorbent Utilization by the Use of Additives. Proceedings of the Fluidized Bed Combustion Technology Exchange Workshop, April 13-15, 1977.

8. Rice, R. L., J. Y. Shang, and W. J. Ayers. Fluidized-Bed Combustion of North Dakota Lignite. To be published in the Proceedings of the Sixth International on Fluidized-Bed Combustion, Atlanta, GA, April 9-11, 1980.

9. Carpenter, R. L., et al. Characterization of Aerosols Produced by an Experimental Fluidized-Bed Coal Combustor Operated with Subbituminous Coal. Prepared for the Div. of Biomedical and Enviromental Res., DOE, Contract No. EY-76-C-04-1013, February 1978.

10. Mazza, M. H., D. A. Green, and M. W. Paris. Mineral Characterization of Fluidized-Bed Combustion Aerosol Ash -- Montana Rosebud Subbituminous Coal. MERC/TPR-78/1. Morgantown, WV, April 1978.

11. Staff of ITRI, Current Status of the Inhalation Toxicology Research Institutions Fluidized-Bed Toxicology Program and Low-Btu Gasifier Health Effects Program. DOE Contract No. EY-76-C-04-1013, October 1979.

Atmospheric Fluidized Bed Combustion Testing of North Dakota Lignite

G. Goblirsch, Supv. Mech. Engineer, Grand Forks Energy Technology Center/DOE
R. H. Vander Molen, Mktg. Mgr., Research, Combustion Power Company
Keith Wilson, Project Engineer, Combustion Power Company
D. Hajicek, Mech. Engineer, GFETC/DOE

INTRODUCTION

The direct combustion of low-rank coal (lignite, coal preparation plant wastes, and sub-bituminous coal) is becoming more important for both utility and industrial uses. Currently, the largest use of these coals is with mine mouth electric power generation utility plants. Some of the major difficulties in burning low-rank coal in conventional plants are: 1) the fouling/slagging of heat exchanger surfaces; 2) the expense, and reliability problems involved in the scrubbers required to control the SO_2 emissions; and 3) the sensitivity of the combustors to fuel variability (moisture, sodium, etc.,) and how it relates to emission control, unit reliability, and unit load carrying ability.

The application of the Atmospheric Fluidized Bed Combustion process (AFBC) to the direct combustion of low-rank coal has the potential to solve many of the problems associated with conventional combustion. Many of the low-rank coals contain more than sufficient alkali to react with all the SO_2 formed from the combustion of the coal sulfur. The temperatures in the combustion zone of the AFBC are at the right levels to provide maximum reaction of the SO_2 and alkali to form solid alkali sulfate wastes. Therefore, AFBC may eliminate the need for a wet scrubber resulting in lower capital costs, and improved reliability. Because of the high heat transfer rates to the unburned fuel, and the long residence time of the fuel particle in the bed, the fluid bed process burns solid fuel efficiently at temperatures as low as 1400 F to 1800 F.

Fluidized Bed Combustion Research on North Dakota Lignite has been taking place at Combustion Power Company (CPC) under contract to the Department of Energy, Grand Forks Energy Technology Center (GFETC) in a 7 sq ft combustor, This work on AFBC at CPC and GFETC has the primary objective of developing process design and emissions control data for low-rank coal applications. Some of the important problems to be looked at during the work at CPC are: 1) sulfur retention on coal ash and supplemental sorbents; 2) ash and bed agglomeration problems; 3) effect of operational conditions, and bed characteristics on heat transfer coefficient, and 4) generation of process data from a larger scale fluid bed unit. While the 7 sq ft CPC unit is not as large as an industrial unit, it does provide a third point of reference for data generated at GFETC on the 0.2 sq ft and 2.25 sq ft units. The operation of this unit is also very useful because it will allow the acquisition of process data on the low-rank coals much more rapidly than using the GFETC units alone.

The initial testing phase of the work at CPC is now complete. Fourteen tests with differing operational conditions were performed with a high sodium, North Dakota lignite. Samples of this lignite have also been burned in the 0.2 sq ft AFBC at GFETC. The first results of these tests are presented in this paper. Table I shows the important operational parameters and results of the tests performed at CPC and GFETC. Further data from these tests will be published as it becomes available.

Analysis of the coal, coal ash, and limestone used in the CPC and GFETC tests is shown on Table II.

TEST FACILITIES

GFETC 0.2 sq ft AFBC Boiler

The 0.2 sq ft AFBC used for the tests at GFETC is shown in Figure 1. The combustor shell is made from 6-in. type 316, schedule 40 stainless steel pipe. It is 10 ft high, which allows sufficient freeboard above the bed to limit elutriation. The combustor shell is enclosed in a stainless steel sheet metal skin which is filled with a loose insulation. Internal stainless steel cooling coils are the primary means for controlling temperature. Combustion air from a 7.5 hp positive displacement-type blower is electrically preheated both to provide heat for ignition and to maintain a selected air preheat temperature during a combustion run. The unit uses a flat, drilled plate for an air distributor, and a pneumatic coal injection system.

The nominal coal feed rate to the combustor is 15 lb/hr of lignite at 9 ft/sec and 20% excess air. The off-gases from the combustor are cooled by a series of heat exchangers to about 400 F. Gases are cleaned of particulate by a primary and secondary cyclone and a fiber filter before

TABLE I

LIGNITE TEST DATA SUMMARY

LOCATION & TEST AREA OF COMBUSTOR	TEST NO.	BED TEMP. (F)	BED VELOCITY	EXCESS AIR	ASH RECYCLE	CALCIUM TO SULFUR RATIO	ALKALI TO SULFUR RATIO	SULFUR EMISSION lb/10^6Btu	SULFUR RETENTION
GFETC 0.2 ft^2	101	1609	7.7 ft/sec	17.8%	No	0.93	1.31	1.08	58%
"	103 A	1604	7.1	19.1	Yes	2.73	3.11	0.43	83
"	103 B	1606	7.6	19.0	Yes	3.93	4.31	0.14	95
"	106	1599	7.7	18.0	Yes	0.93	1.31	0.95	63
"	107	1314	6.9	22.4	Yes	0.93	1.31	0.90	66
"	108	1791	9.3	21.7	Yes	0.93	1.31	1.67	36
"	110	1596	10.7	19.6	Yes	0.93	1.31	1.01	61
CPC 7 ft^2	L-101	1582	6.1	19.1	No	0.93	1.31	1.98	23
"	L-102	1611	5.8	21.1	No	4.73	5.11	0.10	96
"	L-103	1620	5.3	22.1	Yes	4.73	5.11	0.05	98
"	L-104	1608	5.0	20.4	Yes	3.03	3.41	0.05	98
"	L-105	1813	4.5	27.0	Yes	2.83	3.21	1.23	52
"	L-106	1608	4.3	20.8	Yes	0.93	1.31	1.23	52
"	L-107	1422	5.5	25.6	Yes	0.93	1.31	0.51	80
"	L-109	1605	5.9	20.9	Yes	1.83	2.21	0.54	79
"	L-110	1600	8.2	21.2	Yes	0.93	1.31	1.62	37
"	L-111	1601	5.3	21.8	Yes	1.46	1.84	1.21	53
"	L-112	1608	5.7	21.9	Yes	1.98	2.36	0.62	76
"	L-114	1618	5.9	24.6	Yes	0.93	1.31	1.18	54

NOTE: The alkali-to-sulfur ratio is calculated for the calcium and sodium ash concentration only. Earlier GFETC reports have included magnesium in this ratio.

TABLE II

TYPICAL COAL, COAL ASH, AND LIMESTONE ANALYSIS:

Coal ultimate analysis dry basis:

Carbon	63.8 %
Hydrogen	4.3
Nitrogen	1.1
Oxygen	18.2
Sulfur	1.4
Ash	11.2
Heating value	10,343 Btu/lb

Moisture samples ranged from 26% to 40%

Coal ash analysis important species:

Calcium oxide CaO	20.2 %
Magnesium oxide MgO	5.7
Sodium oxide Na_2O	9.2
Silica SiO_2	15.6
Aluminum oxide Al_2O_3	10.3

Limestone analysis important species:

Loss on ignition @ 800 C	40.6 %
Calcium oxide CaO	50.2
Magnexium oxide MgO	2.3
Sodium Oxide Na_2O	0.0
Silica SiO_2	3.6
Aluminum oxide Al_2O_3	1.4

entering the induced draft fan, which is used to control the combustor static pressure. The gases are sampled once during each test for particulate loading, both upstream and downstream of the cyclone. The stack gases are continuously monitored for oxygen, carbon dioxide, carbon monoxide, nitric oxide, and sulfur dioxide. Oxygen concentrations are determined by an amperometric-type analyzer. Carbon monoxide and carbon dioxide are monitored by infrared analyzers. Nitric oxide emissions are analyzed by a chemiluminescent type of analyzer, and the sulfur dioxide concentrations are determined on a dry flue gas basis by an ultraviolet analyzer.

GFETC 2.25 sq ft AFBC Boiler

GFETC recently constructed a 2.25 sq ft experimental atmospheric fluidized bed combustor. Figure 2 shows this new combustor in the pilot plant at Grand Forks. The combustor is a refractory-lined steel shell with a removable door which provides for easy access to the combustor. Horizontal water-cooled tubes are installed through the access door allowing the surface area of the heat removal system to be easily varied to provide for different operational conditions. The area of the heat exchange surface in the bed can be varied from 0 to 38.34 sq ft by increments of 1.6 sq ft. The nominal

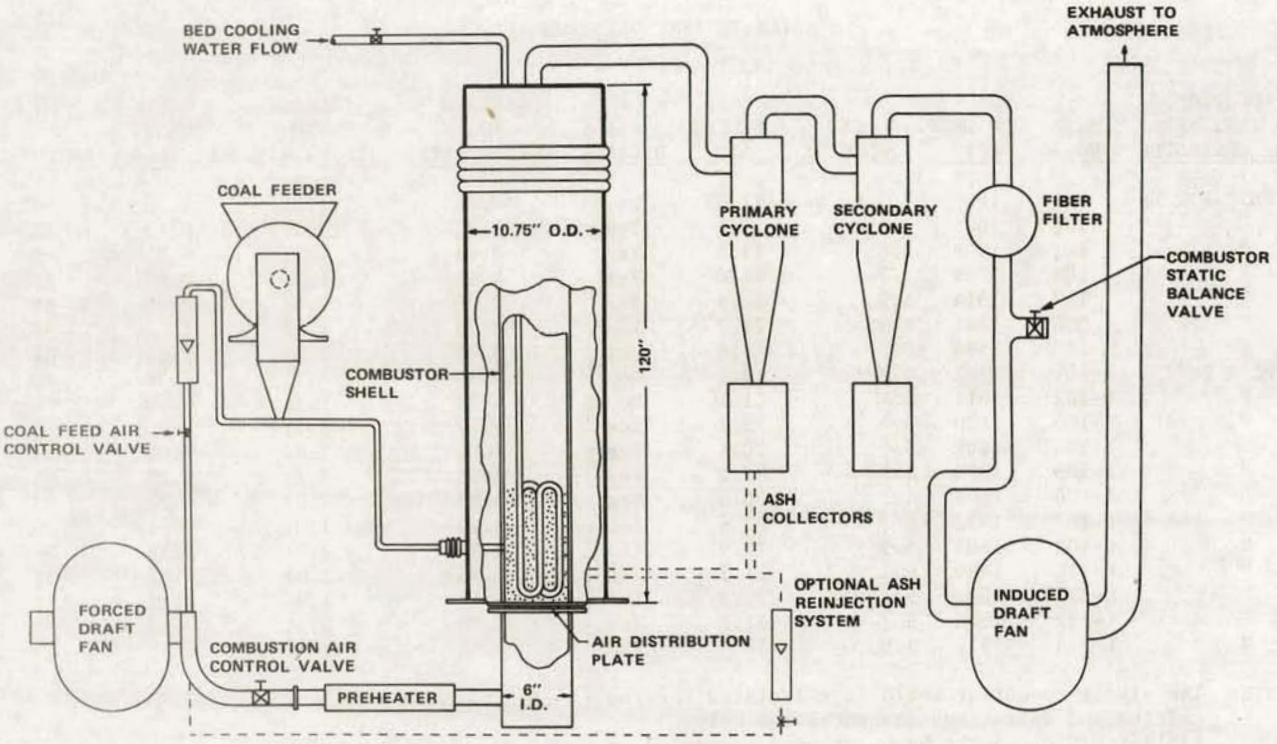

Figure 1 Schematic of GFERC's 6-inch FBC

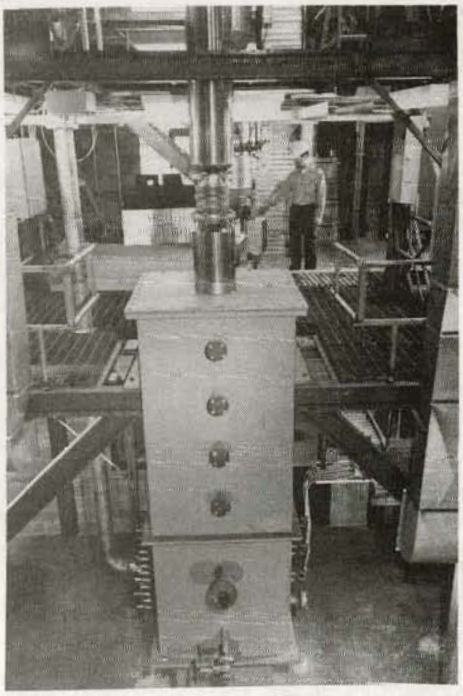

Figure 2 2.25 sq ft Fluidized Bed Combustor at GFETC

fuel feed rate to this combustor is 180 lb/hr of lignite at 9 ft/sec superficial gas velocity and 20% excess air. The combustor system has been designed to operate over a wide range of conditions, as listed below:

Average bed temp.	1300 F - 2000 F
Superficial gas velocity	3-12 ft/sec
Excess air	10%-50%
Ash reinjection(% of cyclone catch)	0-100%

This AFBC uses a flat-drilled plate distributor which is inter-changeable with other plates for different operating conditions. The unit also has complete gas analysis and operational control systems dedicated to its operation. The control systems control the percent of excess air (air-to-fuel ratio), average bed temperature (through air preheat temperature modulation), superficial gas velocity, and ash reinjection rate. The exhaust gases are continually monitored for O_2, CO_2, CO, NO_x, SO_2, total HC, and opacity. These and about 70 other operational and functional parameters are measured and recorded automatically every hour. On-line data processing is available with the use of a Tektronix 4051 mini-computer which also provides system alarm and process display data.

CPC 7 sq ft AFBC Boiler

Lignite testing is conducted in the fluid bed boiler test facility shown pictorially on Figures 3 and 4. The facility consists of a 7 sq ft atmospheric fluid bed combustor (AFBC) and related equipment. The refractory lined combustor is cylindrical with an inside diameter of 3 ft and an inside height of 16 ft. It is designed to permit several different fuel feed and heat extraction arrangements.

Lignite is crushed to 1/4" minus in a separate CPC facility and transported to the CTU by fork lift truck in 50 cu ft bins. A weigh feeder controls the fuel feed rate between 0 and 15 lb/min on manual or automatic control. From the weigh feeder, lignite enters a rotary air-lock and is pneumatically injected into the combustor. Combustor off-gases enter a cyclone that may be piped for reinjecting ash back to the combustor or for ash removal. The exhaust gases from the cyclone are cooled to about 375 F

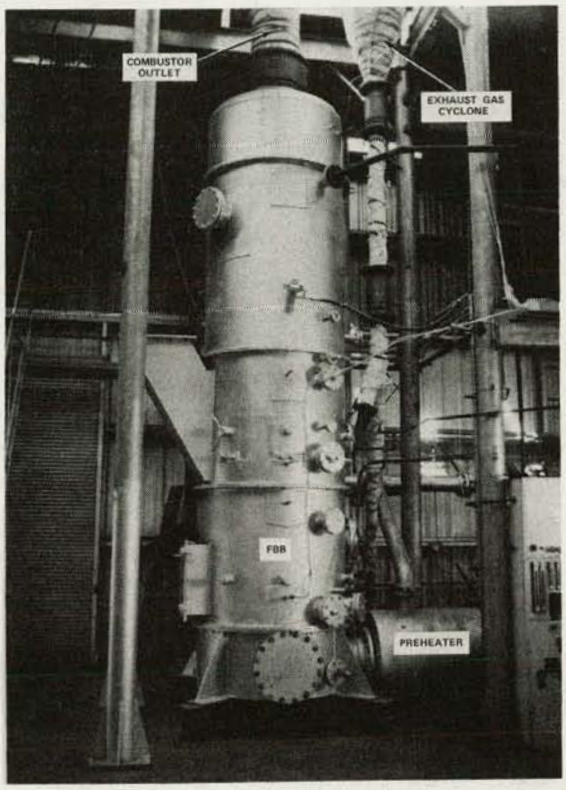

Figure 3 CTU Fluidized Bed Combustor at Combustion Power Co., Inc.

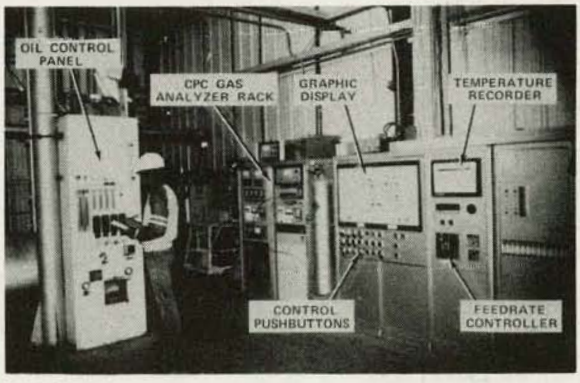

Figure 4 CTU Controls

in a spray water cooler prior to final cleanup in a pulse jet-type baghouse.

Heat is transferred to pressurized water-cooled tubes in the fluid bed. Typically, 150 psig water is heated from 200 F to 300 F. The 300 F water is then reduced to atmospheric pressure across a valve while entering a flash separator where the water drops to 212 F. Automatically controlled makeup water then reduces the recycled water to about 200 F.

During operation, temperatures are monitored in the system at 37 different points. Additional measurements of pressure and flows of the combustion air, exhaust gas, water and fuel are monitored at the control panel and recorded regularly. Exhaust gases are sampled continuously with concentrations recorded on strip chart recorders for: O_2, CO_2, SO_2, NO_x, and CO. The exhaust gases are also sampled for particulate concentration and size distribution upstream and downstream of the cyclone.

Exchanger coils can be of a horizontal and/or vertical configuration. The vertical coils are made of 3/4", schedule 40, 316 SS pipe bent on 3-in. centerlines to form the desired number of passes. Horizontal coils are made from 1¼" schedule 40, 316 SS pipe bent on 6½" centerlines to form four passes in a single plane.

DISCUSSION OF TEST RESULTS

Sulfur Retention

Tests designed to determine the sulfur retention by the alkaline ash of low-rank coals have been run on a variety of low-rank western coals at GFETC. Data from these test runs have shown that the most important parameter contolling the retention of sulfur by the alkali ash is the alkali-to-sulfur molar ratio (1)*. Results very similar to these have been reported by other researchers. Argonne National Laboratory (ANL) in 1977 reported data that was obtained from a wide variety of combustors over a wide range of operating conditions burning Illinois #6 coal in a limestone bed (2). This data shows a band of sulfur retention as a function of alkali-to-sulfur ratio which is very similar to that found by GFETC for low-rank western coal. Figure 5 shows a band of sulfur retention, which covers both GFETC and ANL data, and specific datum points obtained by CPC and GFETC on the Beulah Lignite selected for the CPC tests. In general, the correlation of the GFETC data obtained on the 6-in. unit, and the data obtained on the 7 sq ft unit is very good and agrees well with the data obtained previously by GFETC and ANL. The data for the low-rank coal falls within the banded region determined for the high sulfur Illinois coal, leading to the conclusion that the inherent alkali in the coal performs about as effectively as the added sorbents. This approximation is not exact but it does demonstrate the predominant

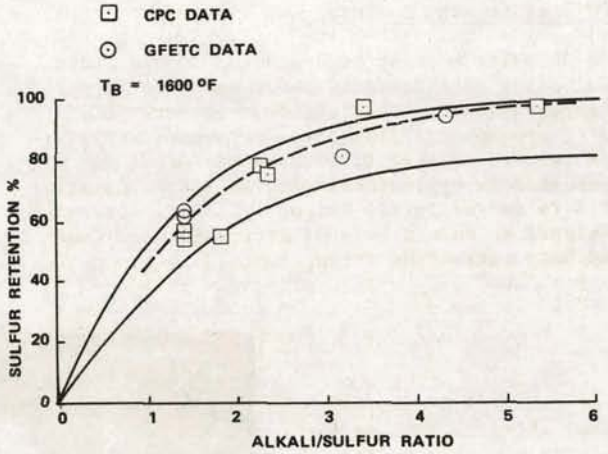

Figure 5

effect of the stoichiometric alkali-to-sulfur ratio in controlling sulfur retention. It is important to note that the alkali reported in this paper is taken to be the calcium and sodium and does not include the magnesium as reported in earlier GFETC reports.

The principal operating variables affecting sulfur capture by the alkali ash, and limestone sorbent, when burning low-rank coal are average bed temperature, and ash recycle. In addition, when burning coal which contains a high percentage of extraneous ash, superficial bed velocity becomes important.

The effects of bed temperature, and ash recycle for the tests at CPC, and GFETC on this Beulah Lignite sample, are shown in Figure 6.

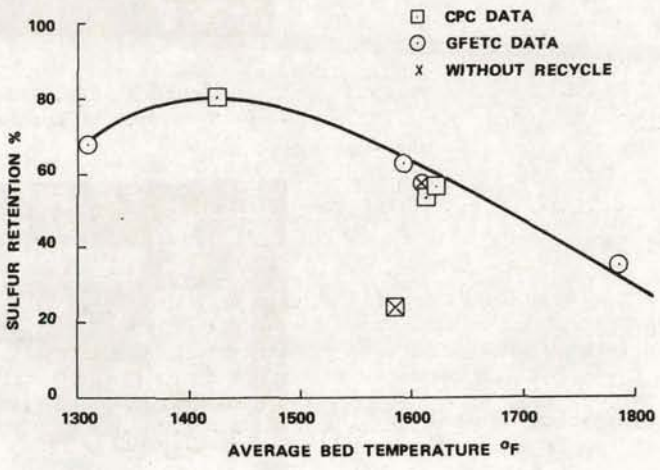

Figure 6

The retention of sulfur on the inherent coal ash alkali appears to peak for this lignite, under

these test conditions at just over 1400 F. Data presented earlier has shown that the sulfur retention with ash recycle taking place, on a different sample of the same lignite, peaked at 1500 F. One possible explanation for the difference is that the higher sodium concentration in the most recent Beulah sample blinds some of the calcium, causing the optimum sulfur capture to occur at lower average bed temperature. The sodium concentration in the CPC sample as a percentage of the dry lignite is 1.03% compared with 0.51% for the original sample of Beulah lignite tested at GFTEC. The calcium content in both samples is essentially the same.

Figure 7 shows the superficial gas velocity over the tested range of 4 to 10.5 ft/sec has a minor effect on the sulfur retention while burning Beulah lignite. This concurs with previous results on North Dakota lignite where the ash alkali are organically bound with combustible material. However, with coals that contain high concentrations of extraneous ash alkali the effect of superficial gas velocity can be quite different (3). Coals that contain high concentrations of the extraneous ash alkali show decreasing sulfur retention with increased velocity.

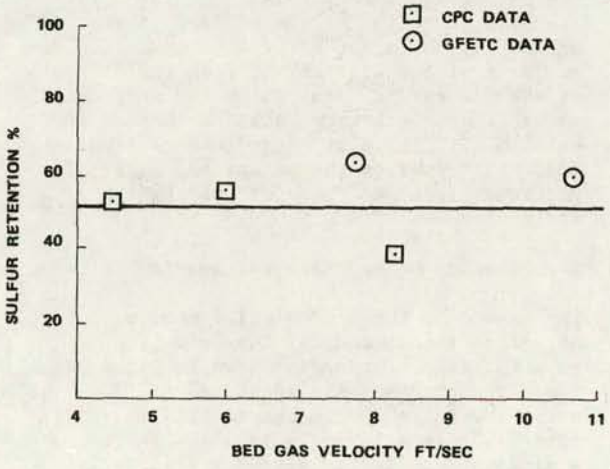

Figure 7

Figure 8 shows the emission of SO_2 as a function of the alkali to sulfur ratio in reference to the New Source Performance Standards of 90% and 70% removal. From this curve it appears that a safe total stoichiometric ratio to meet the applicable standard is about 2.8, or for this coal an added limestone calcium stoichiometric ratio of 1.5 to 1. This would yield a sulfur dioxide emission level of about 0.4 lb/10^6 Btu, or a sulfur removal of 85%. The applicable standard for this specific lignite is 0.6/10^6 Btu or approximately 75%sulfur removal.

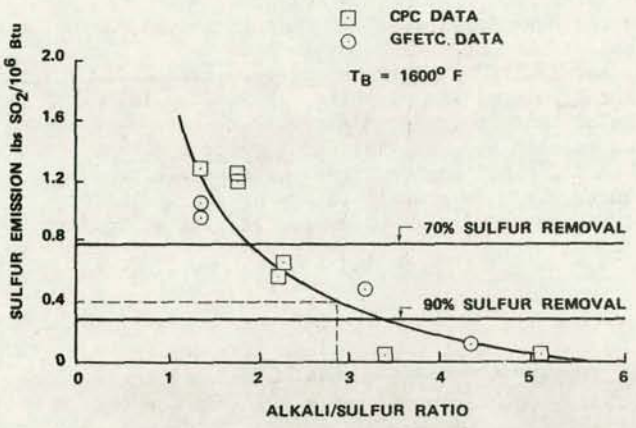

Figure 8

Ash and Bed Agglomeration

Throughout the testing program at CPC and at GFETC, occurrences of ash agglomeration arose and on occasion, serious bed agglomeration occurred. GFETC has reported (1) on some of these problems in an earlier paper. While firm information regarding the specific causes of the agglomeration has not yet been developed, the data collected to date suggests the following:

- In the range of bed temperature between 1400 F and 1800 F, higher temperature results in more severe agglomerations.
- The addition of limestone reduces the tendency to agglomerate.
- The agglomerates adhere to hot surfaces within the bed but not to the cold (350 F) water tubes.
- Recycle aggravates the problem.

The first two of the above items has been clearly apparent during operation of the equipment at CPC. The tests which were conducted at higher bed temperatures (1800 F) exhibited a high degree of agglomeration as indicated by the frequent problems with plugging of the recycle piping and difficulty in removing material from the bed. The single 1450 F test was relatively free of these difficulties but it exhibited a loss of heat transfer, similar to the 1600 F test, a recurring problem which is attributed to bed agglomeration and is discussed in a later section. The 1600 F tests all displayed some symptoms of agglomeration which were most severe when recycle was used and no limestone was injected.

The 1800 F test in which limestone was fed at a rate of Ca/S = 1.9 (L-105) was the only test

in which agglomerates were observed in the extracted bed material. The 1800 F test (L-105) which used a limestone rate equivalent to Ca/S = 0.5 was terminated after 22 hours of operation due to a total loss of fluidization. Post-test inspection of L-105 revealed minor wall deposits and free-flowing bed material which contained about 5% to 10% small agglomerates. The photos of Figures 9 and 10 show the state of the bed after L-108; approximately 80% of the bed was solidified.

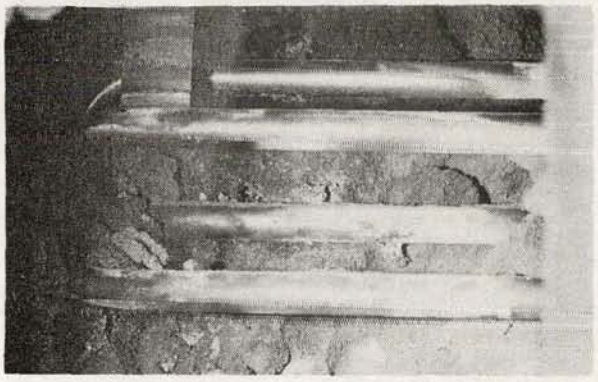

Figure 9 Second, Third, Fourth, and Fifth Passes. Large Agglomerated Mass below Exchanger

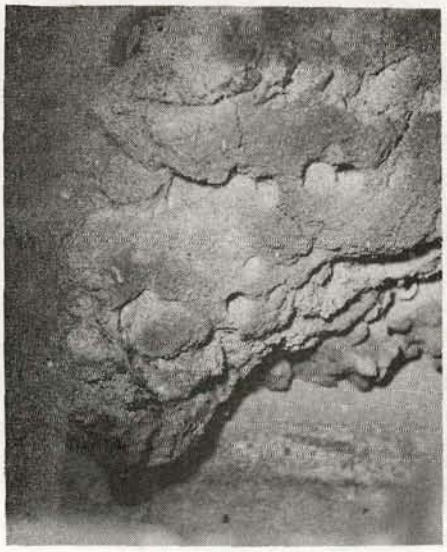

Figure 10 Large Agglomerated Mass Hanging from Upper Bed above HX1

The data from all the tests is still in the process of analysis. Some early results are discussed in the following:

- Agglomeration Analysis

  Scanning Electron Microscope (SEM) surface analysis of some of the agglomerated material from run number L-108 was taken. Figure 11A shows a cross-section of one, approximately 18 mesh, particle from the agglomerate magnified 55 times. The particle was mounted in epoxy and polished down through the surface, exposing the central core and the coating material. Several scans of the particle were made to determine relative concentrations of several important elements of the particle. Figure 11B is an SEM scan of the calcium showing an even distribution over the particle surface varying from a fraction of a millimeter to almost one millimeter thickness.

  Figures 11C and 11D show the SEM sodium and iron scans, respectively, with a relatively evenly distributed coating over the particle surface as well. The sulfur scan, not shown here, indicated essentially no sulfur in the surface coating. The SEM scan of silica shows very high concentrations in the central core, as would be expected, because the parent bed material is about 95% silica. The lack of sulfur on the surface of the agglomeration is not always the case. In the analysis of one agglomerate from the 0.2 sq ft AFBC, a random location on the surface showed a concentration equal to that of the calcium (3). In most cases, the calcium layer is formed on the parent bed material particle first and then followed by the sodium layer.

- Distribution of Bed Material Species

  The change of the bed material species of silica (SiO_2) and calcium oxide (CaO) as a function of time is shown in Figure 12 for three of the tests conducted at CPC using the Beulah North Dakota lignite. The Test L-106 (see Table I) in which there was a slow rate of increase, and a relatively low total concentration of CaO, was one of the runs in which the most severe conditions occurred. This test was terminated prior to the scheduled 80 hours because the thermocouples became covered with material agglomerate, and the heat transfer coefficient decreased so rapidly that control of the process could not be maintained. This run was performed at about 1600 F average bed temperature, with recycle of the cyclone collected ash, but without any added limestone. This test was terminated after about 53 hours of coal feed.

  The change in bed sodium oxide (Na_2O) concentration for the three tests is shown in

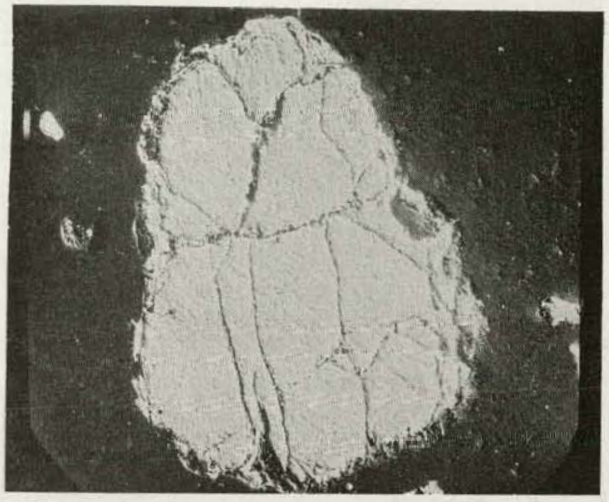

Fig. 11A Single 14-mesh Particle from Agglomerate Mounted, Polished Down, and Magnified 55 Times

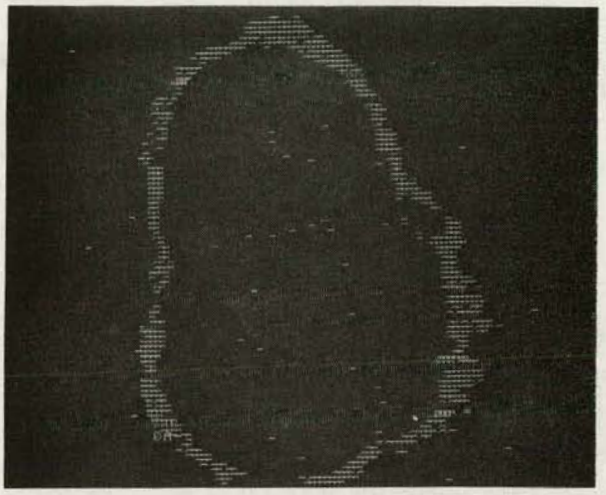

Fig. 11B Calcium Concentration Scan from Surface of Single Particle

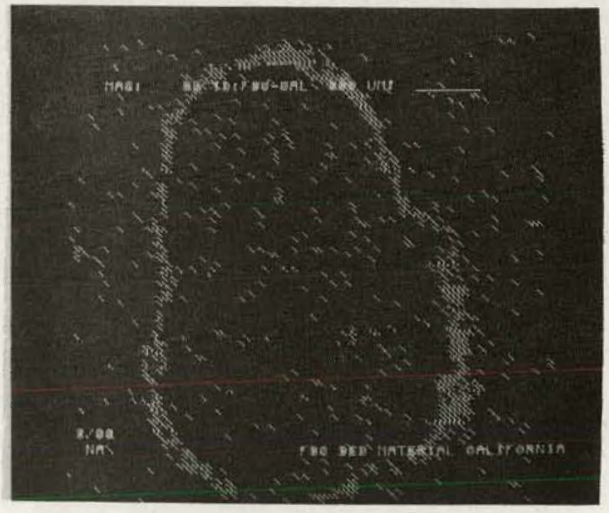

Fig. 11C Sodium Concentration Scan from Surface of Single Particle

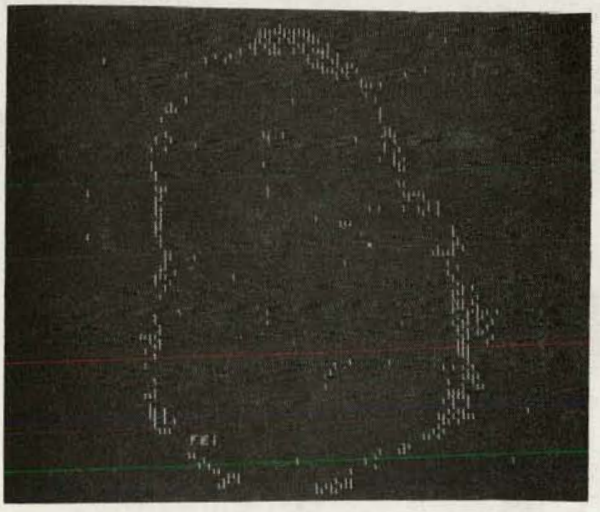

Fig. 11D Iron Concentration Scan from Surface of Single Particle

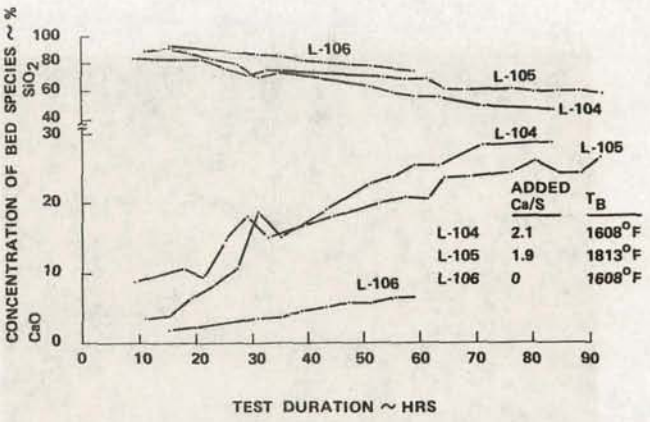

Figure 12

Figure 13. Test L-106 shows the highest rate of increase, and the highest total concentration of Na_2O. The increase in ferric oxide (Fe_2O_3) is about the same for all three tests as shown in Figure 14.

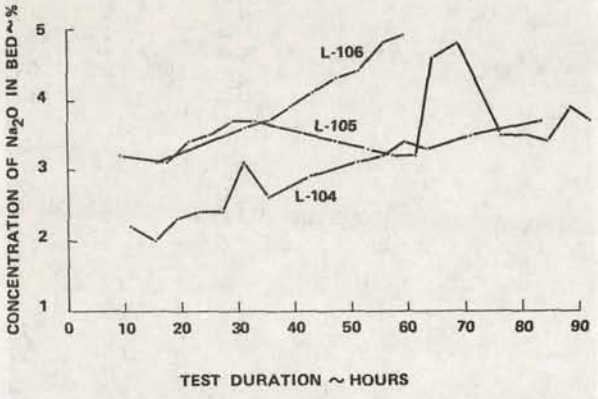

Figure 13

Runs L-104 and L-105 were both performed using limestone injection. L-104 had the higher rate of limestone addition, increasing the calcium-to-sulfur ratio by 2.1 over that inherent in the ash. Test L-104 had very light deposits on the walls of the combustor, but no indication of agglomeration was apparent during the run. This run was performed at about 1600 F average bed

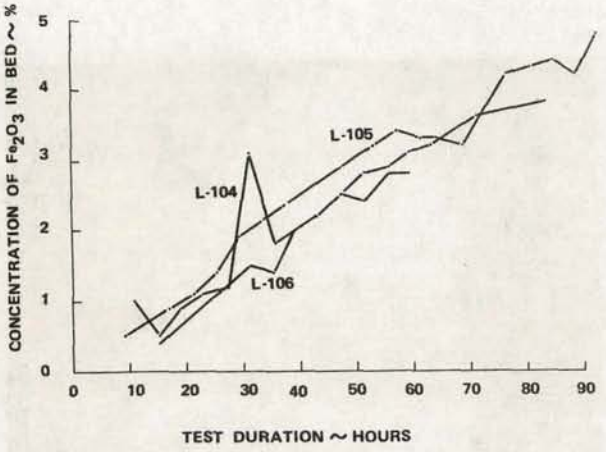

Figure 14

temperature. Test L-105 was performed at an average bed temperature of just over 1800 F. This test showed evidence of bed agglomeration but was completed to a scheduled shutdown. There was, however, a severe loss in overall heat transfer coefficient, but this was compensated for by allowing the excess air level to increase. Spheres of about 3/16" diameter, along with heavy wall deposits, were observed in the combustor after shutdown.

The high peak in sodium level between the 60th and 75th hours is not fully explained, but coincides with a similar high peak in carbon monoxide concentration in the flue gas during the same period. This high CO concentration indicates poor combustion efficiency, and a high concentration of coal in the bed which could be the cause of the high Na_2O concentrations in the bed material sample.

Heat Transfer Coefficient

Exchanger tubes were designed for operation in the fluid bed primarily to extract heat to maintain desired excess air levels at design firing rates. To monitor tube conditions and yield overall heat transfer coefficients, flow meters and thermocouples were mounted on each tube or set of tubes, allowing the computation of heat transfer to each tube, Q. Then, using the average fluid bed temperature and the tube areas, A, the overall heat transfer coefficient, U, could be calculated using the relation:

$$U = \frac{Q}{A\Delta\overline{T}}$$ where $\Delta\overline{T}$ is the log mean temperature difference.

To assure structural stability of the exchanger coils in the fluid bed, stiffeners and guides were added to the coils that, logically, alter the total heat exchange to the tubes. Overall heat transfer coefficients were based only on the outside tube area projecting inside the combustor wall. No adjustments were made for the fin effect of the stiffeners, or shielding by guides (vertical exchangers only at CPC), or for any heat transfer that may have taken place inside the refractory walls. It is suspected that these effects may be significant, especially on the short, two-pass exchangers used at CPC.

Table III shows the heat exchanger data obtained from tests with CPC's combustor and GFETC's 2.25 sq ft unit. The value designated as "high" is actually an average value over the first 5 to 10 hours of each test, while the average value is either the test average for the shorter tests or an average over the last 48 hours for the longer tests. The significance of showing the two values is that in every case, the computed coefficient decayed during the test. In some cases, the loss of heat transfer exceeded 40% in 80 hours. This loss is generally attributed to some form of agglomeration of the bed material and its attendant effect on heat transfer either by 1) increasing the mean particle size, 2) causing buildup on walls and thus blocking some tube surface area, or 3) the blockage causing a restriction in circulation of solids around the tubes. The last two causes were partly rationalized as a result of the CPC observations where post-test FBC inspection always revealed clean water tubes but sometimes deposits on walls, and by virtue of a markedly different loss in heat transfer depending on whether the tube bundle was made of vertical tubes or of horizontal tubes. The horizontal tubes always displayed less heat transfer loss than the vertical tubes which are located in close proximity to the walls and would be expected to suffer the most from wall deposits. Figure 15 shows a fairly typical trend of heat transfer coefficient for a set of horizontal tubes while superficial velocity was maintained within 0.25 ft/sec of the average value from the 25th hour to the end of the test. Other general observations regarding heat transfer are:

- Heat transfer coefficient was generally higher for the vertical tube configurations than the horizontal.
- The vertical two-pass configuration almost always had the highest value of heat transfer coefficient and the eight-pass the lowest. The simple uncluttered design of the two-pass exchanger is thought to contribute to this.
- Values of heat transfer coefficient for the configuration were as high as 69 Btu/hr-F-ft^2.

Several heat transfer correlations have been developed and have been summarized by Botterill (4). Kunii and Levenspiel (5) also present several correlations based on both the thin film

TABLE III

OVERALL HEAT TRANSFER COEFFICIENT

TEST NO.	TEST DURATION (Hrs)	AVERAGE SUPERFICIAL VELOCITY (ft/sec)	AVERAGE BED TEMP. (F)	HEAT EXCHANGE COEFFICIENT (Btu/Hr-F-ft^2)		COAL/TEST LOCATION
				High	Avg.	
1	43	6.8	1585	39.4	35.0	Decker Sub-bituminous/ GFETC
FB-2-180	28	6.7	1454	44.2	42.2	Velva Lignite/GFETC
FB-2-280	30	6.7	1515	42.0	35.3	Beulah Lignite/GFETC
L-101	80	6.1	1582	46.4	44.6	Beulah Lignite/CPC
L-102	69	5.8	1611	51.1	47.4	Beulah Lignite/CPC
L-103	80	5.3	1620	56.9	44.7	Beulah Lignite/CPC
L-104	80	5.0	1608	54.6	45.9	Beulah Lignite/CPC
L-105	80	4.5	1813	57.5	40.5	Beulah Lignite/CPC
L-106	54	4.3	1608	54.7	44.4	Beulah Lignite/CPC
L-107	80	5.5	1422	49.4	34.1	Beulah Lignite/CPC
L-109	132	5.9	1604	51.3	47.9	Beulah Lignite/CPC
L-110	66	8.4	1597	47.0	42.6	Beulah Lignite/CPC
L-111	80	5.3	1601	59.4	44.4	Beulah Lignite/CPC
L-112	80	5.7	1608	48.1	45.6	Beulah Lignite/CPC
L-114	80	5.9	1618	48.3	38.8	Beulah Lignite/CPC

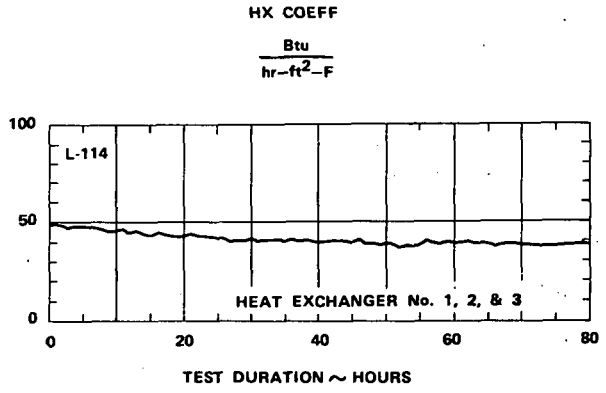

Figure 15

and packet renewal theories. Most of these correlations have been developed for small particles and low bed velocities using relatively cold bed temperatures. In the past few years, additional data has been developed in specially designed experimental programs where the primary objectives are other than heat transfer. Figure 16 displays the early correlations by Baskakov (6) and Lock (7), along with data from several recent experimental programs, as a function of particle size. CPC and GFETC data for the horizontal tubes fits the available data quite well. All data shown was obtained early in the tests, prior to the characteristic loss in heat transfer, when bed particle size was still reasonably well known.

Recycle Rates

For all but two of the tests at CPC and for many of the GFETC tests, elutriated bed solids were continuously recycled back to the fluid bed. At CPC, the recycle is accomplished using a hot cyclone which returns material directly to the bed. Sampling ports are located upstream and downstream of this cyclone and EPA-5 particulate samples are taken at each location approximately ten times during each 80-hour test. Each test has shown a consistent pattern of having a

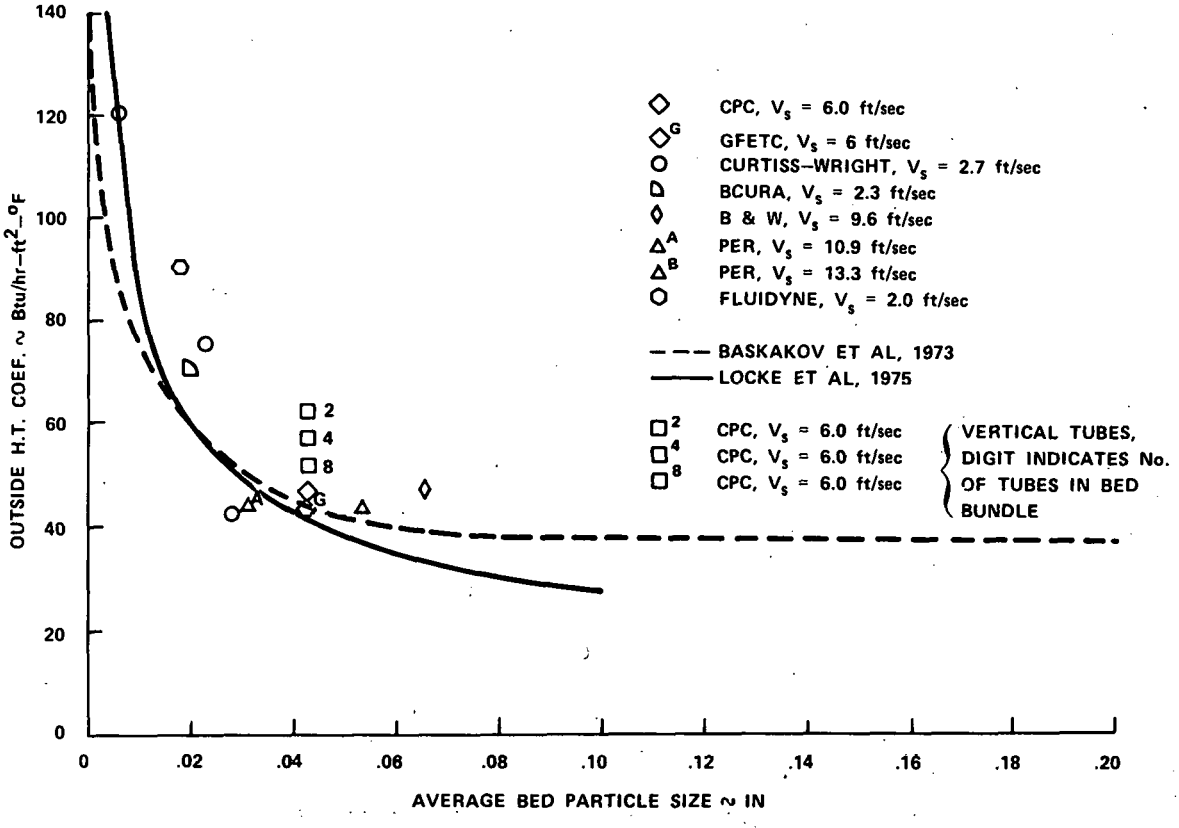

Figure 16 Fluid Bed Heat Transfer Coefficient Data

relatively high initial recycle rate (first 24 hours) dropping off to a steady lower rate during the last 48 hours. In some cases, due to decreases in superficial bed velocity, the rate continues to drop. The early high rate is attributed to the elutriation of initial bed material. The initial charge for each test was a high-purity silica sand having a predominant 20 mesh size. These early rates have been as high as 50 lb/min while the lower rates later have varied between 1 and 4.5 lb/min.

NO_x and CO Emissions

It is generally accepted that nitrous oxide emissions from a fluidized bed are strongly related to fuel nitrogen and bed oxygen level and only above 1700 F to 1800 F does bed temperature play a significant role. Most of the NO_x data obtained at CPC and GFETC on lignite is below 1700 F and is thus compared in Table IV to data obtained during a test series on eastern coal (8) at similar temperatures which was conducted at DOE's Morgantown Energy Technology Center (METC). The GFETC and CPC data are averaged while the METC NO figure was taken from a curve of NO versus oxygen which was generated from a series of individual tests. The data at GFETC and CPC range from as low as 0.2 lb/10^6 Btu to 0.4 lb/10^6 Btu.

/TABLE IV

COMPARISON OF NO_x EMISSIONS

TEST SITE	BED TEMP (F)	OXYGEN (%)	NO (lb/10^6Btu)	FUEL	FUEL N (%)
GFETC	~1600	3.5-4.0	0.342	Beulah lignite	1.10
CPC	~1600	~4.0	0.299	Beulah Lignite	1.10
METC	1500-1600	4.0	0.450	Pittswich Coal	1.15

Measured values of CO emissions during all the tests were very low, e.g., generally below 50 ppm and usually much less.

Combustion Efficiency

Combustion efficiency in AFBC can be a problem, more so than in conventional firing, because of the lower temperatures and the elutriation loss of carbon particulate at higher velocities. The solution to the problem can be approached either by capturing unburned particles and burning them in a separate fluidized bed operating at a lower velocity and higher temperature (carbon burnup cell, as at Rivesville), or by employing recycle of the collected carbon particulate back into the main bed. The extended contact time of particulates and SO_2 achieved by either method also improves sulfur retention, marginally, from the inherent coal alkali.

Combustion efficiencies were determined on five of the tests run at CPC and four tests run at GFETC by both flue gas analysis and dust loading measurements. In general, the determinations using the dust loading calculation showed higher efficiencies ranging from 98% to 99.7%. These efficiencies are in good agreement with data showed by Morgantown Energy Technology Center for Texas lignite. The flue gas calculation showed efficiencies for the five CPC tests ranging from about 83% to 92%. Figure 17 shows the efficiencies calculated by the dust loading measurements compared to METC data on Texas lignite (8).

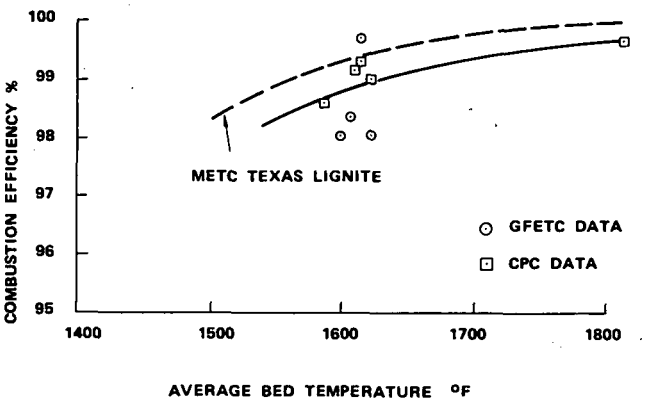

Figure 17

CONCLUSIONS

- The sulfur retention by the inherent alkali, and added limestone sorbent, perform about the same and are reasonably predictable within a range of about ±10% retention by application of alkali to sulfur ratio.
- Temperature has a substantial effect on the retention of sulfur by the inherent alkali or limestone. The temperature effect is not yet fully understood but it appears to be different for different coals and operational conditions.
- The emission of SO_2 from the fluid bed burning the Beulah lignite sample used for these tests can be controlled to meet or better the current emission standards. The injection of limestone to an alkali-to-sulfur

molar ratio of 1.5 to 1, should lower the SO_2 emissions below the current requirement of 0.6 lb $SO_2/10^6$ Btu to 0.4 lb $SO_2/10^6$ Btu, a safe 33% below the standard.

- Agglomeration of bed material, and consequent loss of fluidization quality can be a problem when burning high sodium lignite in a silica bed. There appears, however, to be several ways of controlling the problem including the injection of calcium compounds, and careful control of operating conditions.

- The heat transfer coefficients measured in the CPC and GFETC tests are comparable to data obtained by other researchers, and agree reasonably well with empirical conditions.

- The NO_x emissions measured in all of the tests on Beulah lignite are below the current New Source Performance Standard of 0.5 lb $NO_2/10^6$ Btu input.

- Combustion efficiencies for the Beulah lignite are generally quite high when ash recycle is being used. Efficiencies in the range of 98% to 99%+ have been measured in all tests using this fuel.

REFERENCES

1. Goblirsch, Gerald M. and Everett A Gondreal. "Low-Rank Coal Atmospheric Fluidized Bed Combustion Technology," Tenth Biennial Lignite Symposium at Grand Forks, ND. May 30-31, 1979 GFERC.

2. Vogel, G.F., etal. Supporting Studies in Fluidized Bed Combustion Quarterly Report, January-March 1977, Argonne National Laboratory, ANL/ES-CEN-1019 and FE-1780-7.

3. Goblirsch, Gerald M. and Harvey M. Neas. "Fluidized Bed Combustion Tests on Lignites and Bituminous Coals at the Grand Forks Energy Technology Center," DOE Symposium on Environmental Control Activities, November 28-30, 1978 Washington, DC.

4. Botterill, J.S.M. "Fluid Bed Heat Transfer," Academic Press, 1975.

5. Kunii, D., and Levenspiel, O. "Fluidization Engineering," John Wiley & Sons, 1979.

6. Bashakov, etal. Power Technology, 8, 273, (1973).

7. Lock, H.B. etal. "Fluidized Combustion in Great Britain," paper presented at Fourth International Conference on Fluidized Bed Combusiton, Mitre Corporation, McLean, VA, December 1975.

8. Mei, J.S., V. Grimm and J.S. Harlow. "Fluidized Bed Combustion Test of Low-Quality Fuels (Texas Lignite and Lignite Refuse)," MERC/RI-78/3.

FLUIDIZED-BED COMBUSTION OF NORTH DAKOTA LIGNITE

R. L. Rice, Project Leader
J. Y. Shang, Deputy Assistant Director
U.S. Department of Energy

W. J. Ayers, Technical Scientist
EG&G
Morgantown Energy Technology Center
P.O. Box 880
Morgantown, WV 26505

EXECUTIVE SUMMARY

Introduction

Combustion of coal in an atmospheric fluidized-bed combustor (AFBC) has been considered for several years by the industrial and utility community as a potential alternative to conventional methods for steam and power generation[1,2]. The major advantages of the AFBC are the removal of sulfur dioxide during the combustion process by using limestone or dolomite as a sorbent, the control of nitrogen oxide emissions by the lower combustion temperatures, the capability of burning a wide variety of fuels, the high volumetric heat release rate, and high heat transfer rates. In addition, the spent sulfur sorbents are dry and can be of directly disposed along with the coal ash.

There is a wide variety of carbonaceous fuels available (Figure 1, Coal Map) in different areas of the United States[1]. There are also variations in climate and geography. AFB combustors appear to be ideally suited to being adapted to industrial and utility uses, in all these areas, as a means of burning the local fuels in an environmentally acceptable manner. The purpose of this study was to burn North Dakota lignite in the Morgantown Energy Technology Center's 18-inch diameter combustor, to determine heat release rates, combustion efficiencies, sulfur dioxide emissions, nitrogen oxides emissions, and problems associated with burning the lignite. The North Dakota lignite deposits are part of the northern lignite field located in Western North and South Dakota, eastern Montana, northeastern Wyoming, as well as southern Saskatchewan, Canada (Figure 2). In addition to being used as fuel for combustors, the lignite has been studied in pyrolysis units as well as a source of other fuels such as methanol[3,4]. A total of 25 test periods were conducted under steady-state conditions; 12 of the steady-state periods were 5 hours long and 13 periods were 10 hours long. The combustor was operated for 5 days at a time and shutdown for weekends. During the 5 days, when one period was ended, conditions were changed and operation continued with the next period started when steady-state had been achieved at the new conditions.

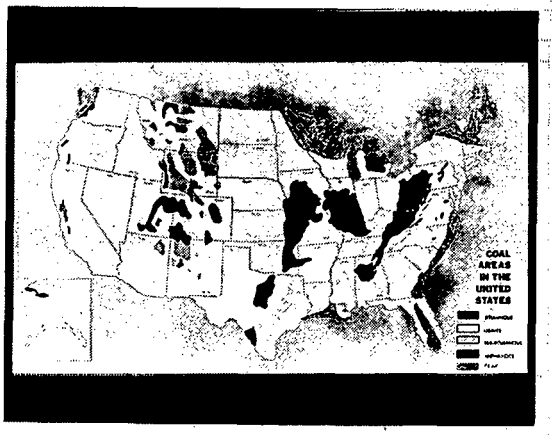

FIGURE 1

Fluidized-Bed Combustion

The fluidized-bed combustor (FBC) is a burner which can burn very low heating value fuels at relatively low temperatures (1300°F-1700°F). The fluidized-bed is a body of particles (coal, ash, sand, limestone) which is supported by gas passing through a grate-like distributor. Combustion air blown through the bed mass lifts and suspends the solid particles inducing a fluid-like behavior to the bed. After preheating the particles to ignition temperatures of 1200°F-1400°F, coal or other fuel-containing material is continuously injected and burned. At any given time, the solid material in the furnace contains only one to two percent combustible material; the balance being non-combustible solids. With this characteristic, the fluidized-bed combustor can burn materials with very low fuel value providing an advantage for the FBC over conventional combustion techniques. The use

of heat transfer tubes in the fluidized-bed combustor to extract heat for steam raising or process fluid heating is more efficient because the scouring action of the solids on the tube surface improves heat transfer. Limestone or other sulfur absorbing material may be added to the fluidized bed, if necessary, to capture most of the sulfur oxides before they can be emitted to the atmosphere.

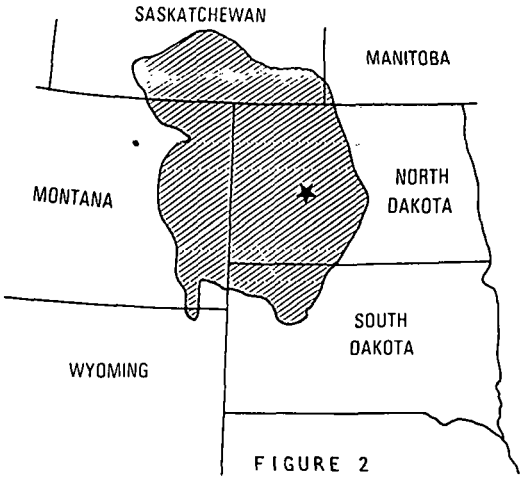

FIGURE 2

Coal and Sorbents

The coal used in these tests was lignite, run of mine, from the Beulah Mine, in Mercer County, North Dakota. The lignite was air dried and then crushed in a hammer mill to 1/4" x 0 size. The dried coal had a sulfur content of 1.4 weight percent and a heating value of 9240 Btu per pound (Table I). The sorbent used in the tests was Greer limestone sand from the Greer Quarry near Morgantown, West Virginia. The particle size of the sand was approximately 1/8" x 0. In addition to the limestone sorbent, a high-silica sand was used to build the initial bed in the combustor. The silica sand was obtained from the Tom Brown Corporation near Pittsburgh, PA. This sand is designated as 4Q rock size and is 10 x 30 mesh size.

Equipment and Operation

The Morgantown Energy Technology Center fluidized-bed combustion tests were carried out in the No. 1 atmospheric pressure fluidized-bed combustor which is depicted schematically in Figure 3. It is basically a refractory lined, cylindrical combustor having an internal diameter of 18 inches in the bed region which is 45 inches high and an expanded freeboard section of 24-inch diameter which is 27 inches high. The combustor is equipped with a horizontal, water cooled or steam cooled heat exchanger submerged in the bed which is comprised of six hairpin 1/2-inch schedule 160 type 316 stainless steel pipes. Each cooling loop is fed separately from a water or steam manifold and any number from

AIR-DRIED LIGNITE ANALYSES

		ASH BY X-RAY	
MOISTURE	13.83		
ASH	9.51	SiO_2	19.11
SULFUR	1.40	Al_2O_3	10.65
HYDROGEN	4.72	Fe_2O_3	12.55
CARBON	56.13	CaO	21.75
NITROGEN	0.25	Na_2O	7.86
OXYGEN	14.16	K_2O	0.30
		MgO	6.36
		TiO_2	0.46
VOLATILE	35.9	SO_3	15.87
HEATING VALUE	9242		

TABLE 1

one to six of these tubes can be in service. Each tube has a surface area of 0.6 square foot. These tubes are used to obtain heat transfer coefficients in the bed and additionally to control bed temperatures. Because some of them may be out of service for extended periods of times, they must be physically able to withstand the bed temperatures; alloy tubes are required.

The freeboard area is equipped with a single-pass heat exchanger with the tubes essentially horizontal in a zig-zag pattern around the periphery of the freeboard space. This heat exchanger is used to provide heat transfer coefficients and to control the exit gas temperature.

Fuel is metered from a hopper, which is suspended from a weigh cell, by a 1 3/16-inch variable speed screw. This fuel falls into a fuel injection chamber where it is entrained by compressed air at ambient temperature and transported through a 1-inch schedule 40 pipe through the base of the conical distributor to the nozzle. Velocity through the nozzle ranges from 60 to 80 fps.

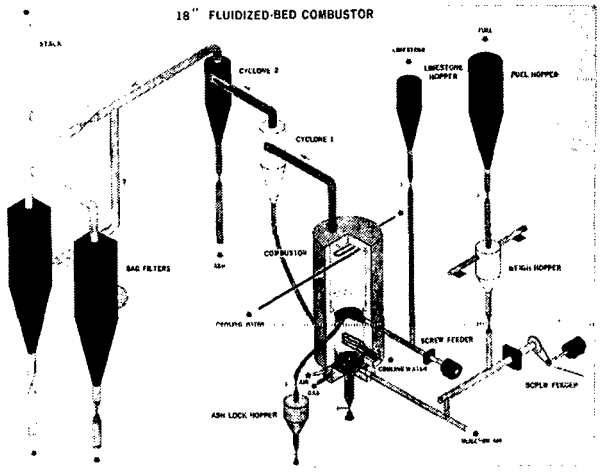

FIGURE 3

Fluidizing air comes from a plant air supply system through a pressure regulating valve and panel operated control valve to the air plenum located beneath the conical distributor. From the plenum it passes through 95 3/16-inch holes arranged in seven equally spaced concentric circles into the directional nozzles inside the air distributor. The nozzles are 1/8-inch stainless steel 90° elbows, each equipped with a drilled pipe plug on the discharge side. These elbows are welded on the distributor plate and turned at various angles all inclined toward the center of the cone. The pipe plugs are drilled to 1/8-inch on the lower four circles radially outward from the cone apex and the plugs in the outer three circles are drilled to 1/16-inch (see Figure 3A). Open area amounts to 0.27 percent of the distributor plate area. At 4.9 fps fluid velocity, maximum pressure drop through the distributor and expanded bed amounts to 3 psig.

Flue gases exit the bed through a 5-inch diameter stack and enter the No. 1 cyclone at approximately 900°F. The particulate removed in this cyclone is recycled back into the bed for additional carbon burnup. From the No. 1 cyclone the gas enters the No. 2 cyclone and the particulates removed here are weighed and analyzed. From the No. 2 cyclone, the gas enters one of two parallel bag filters and then is vented to atmosphere through a stack.

Limestone (sorbent) when needed or used is fed via a 1 3/16-inch variable speed metering screw from a weigh hopper directly into the top of the expanded bed.

Ash is extracted from the combustor through a 3-inch schedule 40 pipe and a 3-inch feed screw located at the bottom of the conical distributor, or a 2-inch adjustable overflow tube which penetrates the side wall upward at about 30° angle. The opening in the overflow tube is normally set at the 36-inch level and this is used to control expanded bed height. The overflow tube discharges into a lockhopper which is periodically emptied. The bed material is weighed and analyzed.

The stack gas is continuously sampled as it leaves the freeboard and passes through several filtering steps before being admitted to the analytical equipment. The gas monitoring (analytical) equipment includes the following instrumentation:

Compound	Principle of Operation	Instrument[1]
CO	NDIR	MSA--LIRA--Model 303
CO_2	NDIR	MSA--LIRA--Model 1300
SO_2	Flame Photometric	Meloy--FPD
$NO-NO_x$	Chemiluminescence	Thermo-Electron, Series 10
O_2	Paramagnetic	Beckman
Total HC	Flame Ionization	Beckman--Model 400

[1]The use of brand names is for identification purposes only and does not constitute endorsement by the Department of Energy.

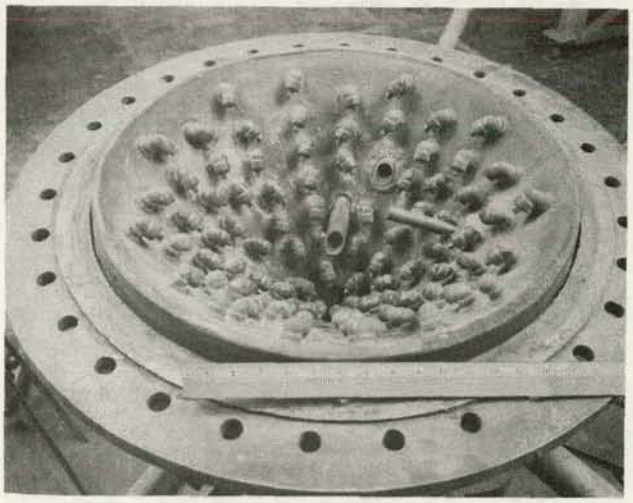

FIGURE 3A CONICAL DISTRIBUTOR PLATE

Start-Up Procedures

Start-up of the unit is accomplished by preheating the lower part of the vessel to 1400°F with premixed natural gas and air fed through the fluidizing air nozzle into the bed. When the 1400°F temperature level is reached, about 40 pounds of bed material is added at a slow rate until it is also up to temperature. When this occurs, fuel feed is started, the natural gas is shut off and the fire is self-sustaining. Feeding of bed material is continued until the desired bed level is attained (usually about 36 inches).

The entire procedure from cold start takes about 3 to 5 hours but can be done faster if necessary. Bed temperatures are maintained by three controls:

1. Bed level which is maintained by the level of the opening in the overflow tube.

2. Fuel feed rate which is controlled by the screw feeder rpm.

3. Coolant flow through in-bed heat exchangers.

Bed temperatures can be closely maintained with these controls. Superficial velocities have ranged from 2 to 4.9 ft/sec using 1/8-inch x 0-inch sorbent and 1/4-inch by 0-inch fuel. This is controlled by measuring the ambient air input readings. Sorbent material (such as limestone) is fed directly into the top of the bed by a controllable speed screw feeder. The pressure within the combustor is equivalent to the few inches of water pressure drop through the dust collecting system.

Run Conditions and Results

For the North Dakota Lignite tests, bed temperatures ranged from 1425° to 1675°F, fluidizing velocities were 2.8 to 4.1 feet per second, and excess air rates were -10 to 50 percent (see Table II). Coal feed rates were 35 to 80 pounds per hour and limestone rates were 4 to 27 lb/hr resulting in Ca/S ratios from 2 to 11. The calcium in the coal contributed a total of 0.84 to the above Ca/S ratios. The Na_2/S ratio in the coal was 0.28 and the Mg/S was 0.34 giving a total alkaline to sulfur ratio in the coal of 1.46. The high Ca/S ratios reported for the tests were due to the use of limestone for bed material, as would probably be common practice in a commercial FBC. The bed was built initially using high-silica sand but all make-up was limestone. Due to the high calcium content of the bed, very little SO_2 was emitted as shown by Table II and Figure 4, SO_2 Emission vs. Bed Temperature.

BED TEMPERATURE, °F	1425 TO 1675
FLUIDIZING VELOCITY, fps	2.8 TO 4.0
EXCESS AIR, %	-10 TO 50
COAL RATE, pph	35 TO 80
LIMESTONE RATE, pph	4 TO 27
CA/S MOLE RATIO	2 TO 11
CARBON EFFICIENCY, %	50 TO 103
SO_2 EMISSION, lb/M BTU	0.01 TO 0.63
NO_X EMISSION, lb/M BTU	0.04 TO 0.86
IN BED H.E. COEFF., BTU/hr/ft2/°F	25 TO 65
FREEBOARD H.E. COEFF., BTU/hr/ft2/°F	5 TO 14
ASH MATERIAL BALANCE, %	89.9 TO 106.5

TABLE 2

FIGURE 4

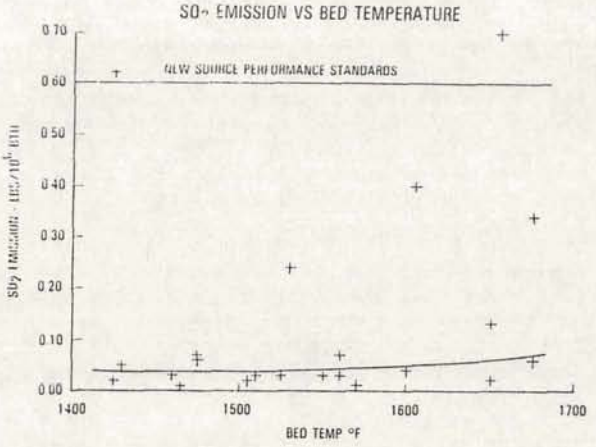

In addition, the high-calcium bed resulted in a low-calcium utilization as shown by Figure 5, Ca Utilization vs. Bed Temperature. The temperature effect is very slight on SO_2 emissions with a gradual increase at above 1550°F. The calcium utilization decreases at above 1550°F. These trends have been reported by others working on SO_2 emission control using limestone.

The carbon combustion efficiency increased with increasing temperature as shown by Figure 6, Carbon Combustion Efficiency vs. Bed Temperature. Most of the combustion efficiencies were over 96 percent (based on solids), however, a low of 50 percent was observed in one test and was due to solids losses in handling. In general, efficiencies were 98 percent or better.

The volumetric heat release rate showed little response to temperature, Figure 7, Volumetric Heat Release vs. Bed Temperature, but did show a tendency to increase with increasing fluidizing velocity, Figure 8, Volumetric Heat Release vs. Fluidizing Velocity, as would be expected due to the higher throughput.

FIGURE 5

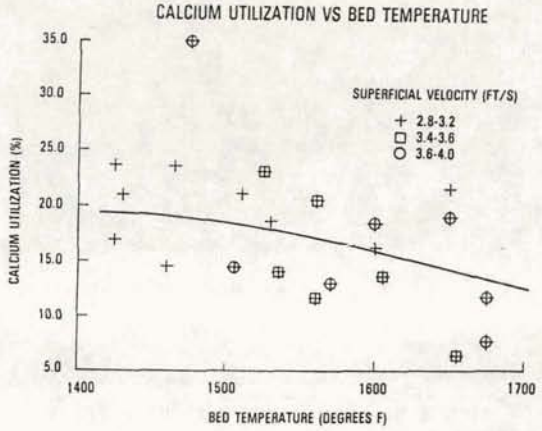

The heat release rate was based on the heat recovered and not on the coal fed. As a result the rate varied widely due to variations in heat transfer, combustion efficiency, and materials output variations. The ash distribution as it was affected by the fluidizing velocity is shown in Figure 9, Ash Distribution vs. Fluidizing Velocity. The most notable difference was in the amount of material passing to the bag filters with increasing fluidizing velocity. Almost no change occurred in the No. 2 cyclone solids output, whereas there was a decrease in the bed and No. 1 cyclone solids compensating for the increase to the bag filters.

The NO_x analyzer was not functioning during the entire testing, but during the tests in which the analyses were obtained, the NO_x emissions were within EPA limits in all cases but one. That case was the test made with 50 percent excess air.

The in-bed heat exchange coefficients ran from 25 to 65 Btu/hr-ft^2-°F. Some of the heat exchanger tubes were cooled with steam and some with water which would explain the wide range in values. The freeboard coefficients were 5 to 14. These values are lower than are usually reported and are due to the tendency of the lignite ash to form light deposits on the freeboard tubes. This could be alleviated to some degree by blowing down the tubes occasionally.

FIGURE 6

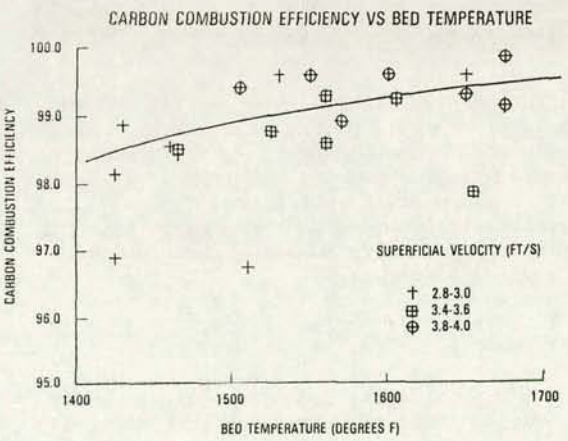

Problems

During the tests with North Dakota lignite, it was found that unusual deposits formed at times on the heat exchanger tubes (Figures 10 and 11) and at other times on the conical distributor (Figures 12, 13, and 14). These deposits were found only with the North Dakota lignite. The deposits did not occur with any other fuel including lignite from Texas[5]; however, in discussing the problem with personnel from Grand Forks E.T.C., it

FIGURE 7

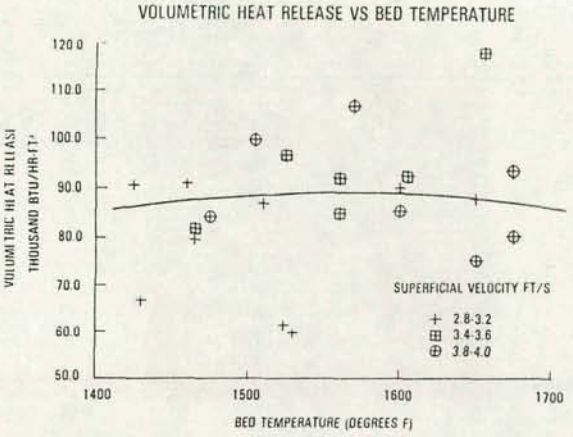

FIGURE 8

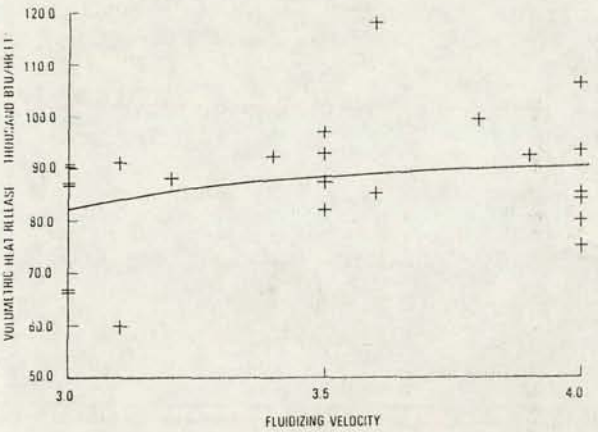

FIGURE 9

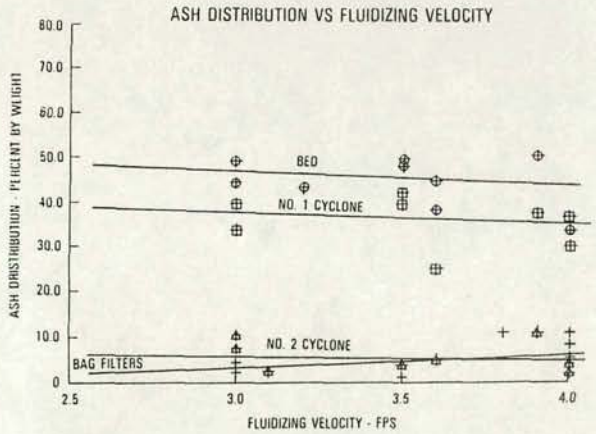

was found that they had encountered the same deposits with North Dakota lignite and in one case had found it with Texas lignite.

The deposits were deposited in thin layers and varied in appearance, as noted in Figures 10-14. In Figure 10, the deposit on

FIGURE 10 - Deposits on heat exchanger tubes

FIGURE 13 - Crust deposited above distributor plate

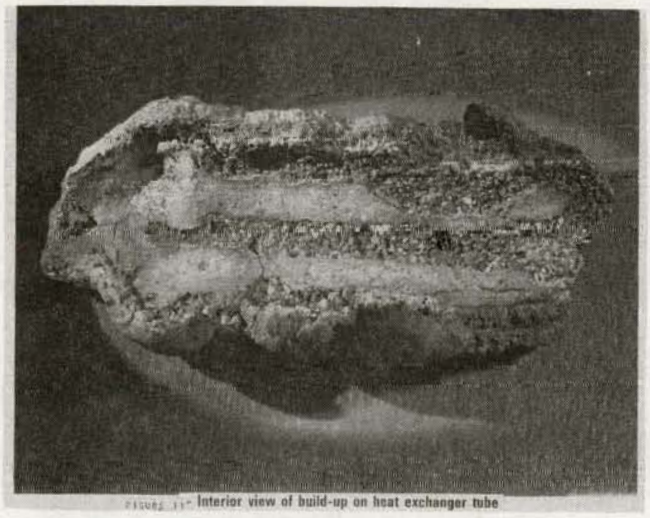

FIGURE 11 - Interior view of build-up on heat exchanger tube

FIGURE 14 Crust build-up on distributor nozzles

FIGURE 12 - Close-up of deposits formed on distributor nozzles

the heat exchanger tubes was a weakly bonded thin layer of small particles; whereas, Figure 11 shows a much thicker layer of larger particles tightly cemented together. Figure 12 shows a crust that formed over the conical distributor. The thin crust (less than ¼-inch) was located about 2 inches above the surface of the cone with a layer of loose unconsolidated bed material under the crust. The fluidizing air emerged below the crust in the lower part of the cone and flowed up through the center of the bed. A similar type of deposit was found by Combustion Power Corporation (CPC) in burning lignite in their 7 square feet combustor at Menlo Park, CA. CPC made these tests under contract to Grand Forks[6]. Another form of deposit on the distributor is shown in Figures 13 and 14. In this form, the material agglomerated into tube-like extensions of the air inlet nozzles. The tubes appeared to have been formed from a molten material that had frozen around the air jetting from the nozzles. Even with these deposits, the bed continued to operate, not showing the unbalance that occurs with clinkers in the bed.

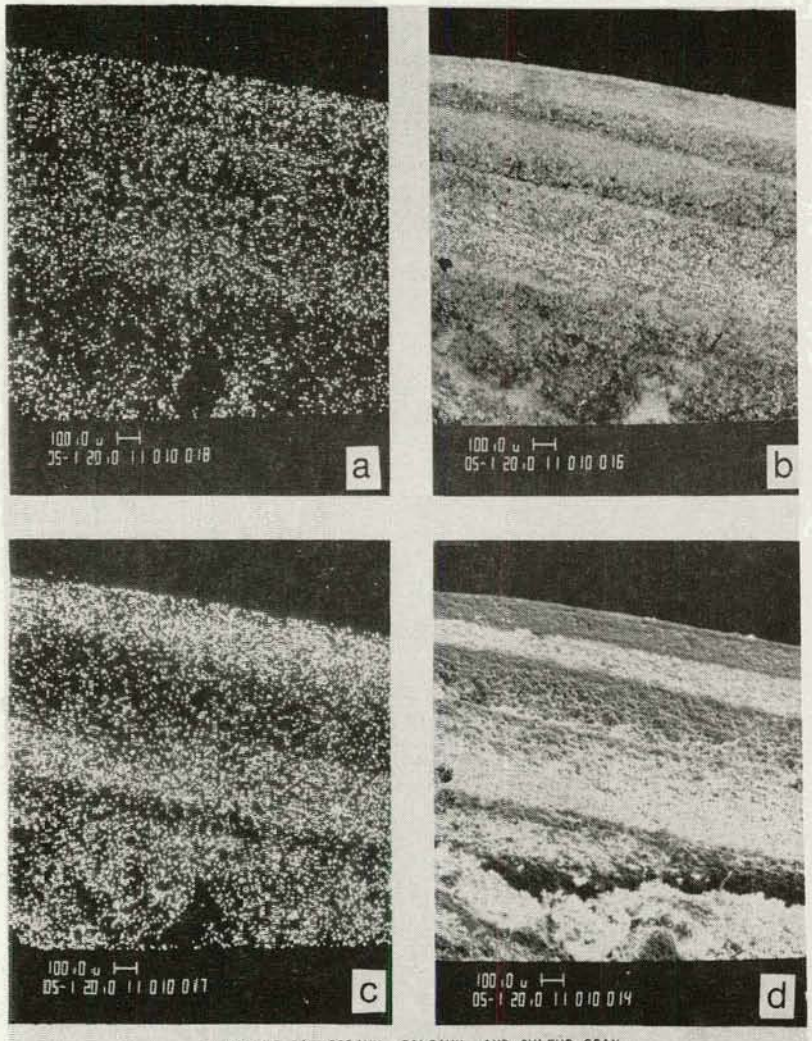

FIGURE 16 SODIUM, CALCIUM, AND SULFUR SCAN

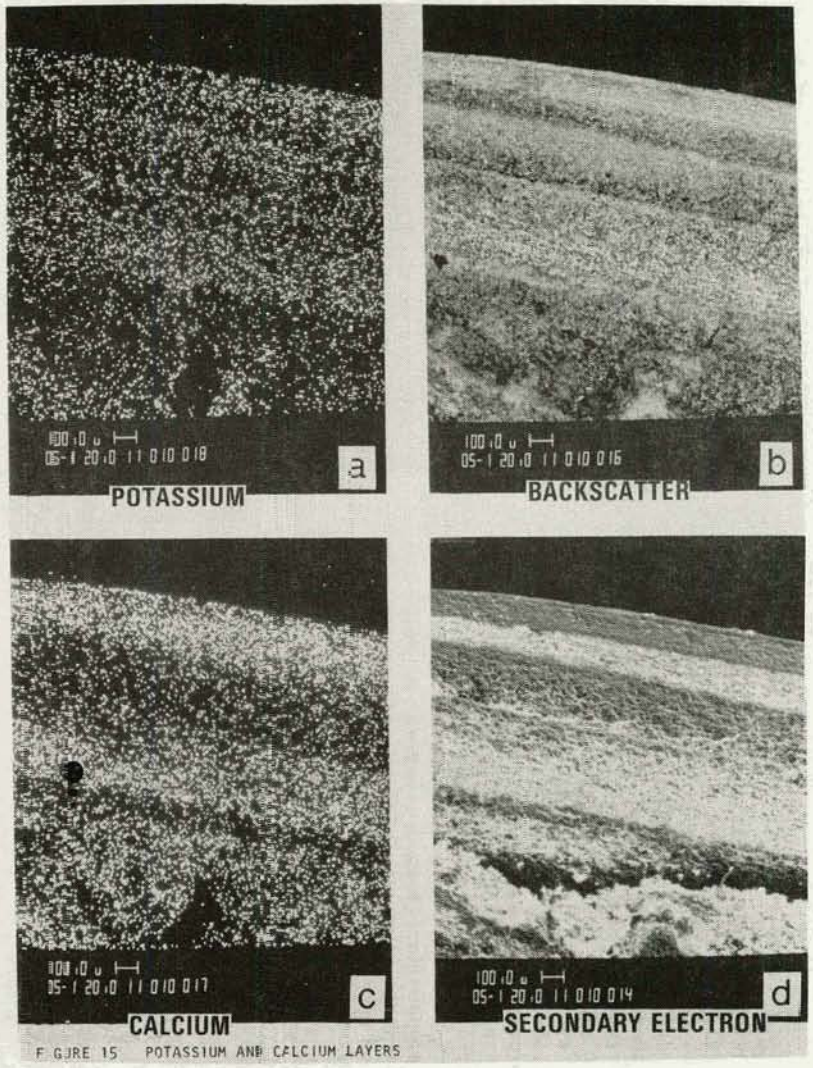

FIGURE 15 POTASSIUM AND CALCIUM LAYERS

In attempting to determine the nature of these deposits and to identify the mechanism responsible for their formation, various analyses were made. The deposits were examined by electron microscope. Figure 15, a secondary electron microphotograph, shows the layering that is characteristic of the deposits, with a total of six layers visible. Figure 16.c., another deposit, shows three layers in the backscatter image. The electron microscope was used to do an elemental scan of the samples and Figures 15.a. and c. show potassium and calcium present in the layers. The potassium is evenly distributed in all layers, whereas calcium is less in some of the layers. Figures 16.a., b., and d. show a sodium, calcium, and sulfur scan respectively. The sodium and sulfur are fairly well distributed in the sample, but again there is a variation in the calcium. In looking at the sample more closely, it appears that the calcium distribution is more a function of the pore size or density of the layer than any thing else. The most interesting feature of the microphotographs is the sodium scan in the upper left portion of 16.a. There is very little calcium or sulfur in that section, and it almost appears to be a lake of liquid sodium. It could also be another sodium salt, but it does appear to have been deposited from a liquid material.

Results from GFETC show that these deposits occur when the sodium content of the ash in the lignite exceeds three percent. They had observed these deposits in working with 6-inch FBC units. Results of work performed by Combustion Power Company, in their 7 ft^2 FB combustor in California, again show the deposits. The pictures of the CPC combustor after some of their tests showed deposits very similar to those in Figures 10 through 14.

TABLE III -- ANALYSES OF MATERIALS IN FBC TESTS

Ultimate	Deposit	N.D. Lignite	Bed Material	Texas Lignite
Moisture	--	13.83	0.12	16.42
Ash	99.53	9.51	96.64	12.52
Sulfur	3.58	1.40	3.21	1.01
Hydrogen	0.05	4.72	0.04	4.66
Total Carbon	0.16	56.13	0.84	49.13
Nitrogen	0.08	0.25	0.00	1.01
Oxygen	--	14.16	0.00	15.25
Ash:X-ray				
SiO_2	54.04	19.11	33.57	44.83
Al_2O_3	3.65	10.65	4.00	12.40
Fe_2O_3	2.98	12.55	2.58	7.49
CaO	25.28	21.75	43.94	13.10
Na_2O	3.23	7.86	1.88	0.31
K_2O	0.52	0.30	0.46	0.55
MgO	1.74	6.36	2.05	2.11
TiO_2	0.17	0.46	0.22	1.02
SO_3	3.64	15.87	8.03	12.51
CO_2	0.15	--	3.00	--

TABLE IV -- ELEMENTAL ANALYSIS OF LAYERS IN THE CRUST FOUND IN FBC TESTS

Element Layer	Si	Al	Fe	Ca	Na	K	S
1	2.9	1.4	4.3	37.1	24.3	7.1	22.9
2	-	1.6	-	11.4	39.3	6.6	45.9
3	1.9	-	1.9	13.5	40.3	1.9	40.3

Other points related to the deposits are: There are eutectics of sodium, calcium, and sulfur that melt at FBC operating temperatures. The deposits seem to occur on surfaces at 1000°F or higher. The deposits form in beds operating at 1550°F or higher, the deposits do not develop when a sodium salt is added to a low-sodium fuel but do form when the ash has a high-sodium content (greater than 3 percent). A high-silica bed seems to increase the chances of the deposits, whereas limestone tends to reduce the likelihood of deposition. Extended operating time may be a factor, as in a continuously operating combustor, if the build-up rate is related to both time and temperature. Further testing is needed to define the level of each of the effects mentioned above.

In the development of the crust, the first step is the joining of two particles into a dumbbell shape, and then the addition of other particles, leading to the buildup. The glue causing these particles to stick together contains sodium, calcium, and sulfur, which appears to have been a liquid salt.

Table III shows the ultimate analysis and the x-ray analysis of the ash of the North Dakota lignite, the bed material, and the crust. The same analyses of the Texas lignite are shown for comparison. The sodium content of the North Dakota lignite ash is 7.86 percent as compared to 0.31 percent for the Texas lignite. Using the 3 percent guideline, the North Dakota lignite would be expected to form the crust material, whereas the Texas lignite would not. This was born out in the combustion tests. Table IV shows the x-ray analyses of three layers of the material deposited on the distributor. The major constituents are calcium, sodium, and sulfur, showing that complex salts of these materials are responsible for the crusts. The variation, particularly in the calcium and sulfur ratios in the three layers, indicates that more than one salt is involved in the glue formation.

At the present time, it appears that a combustor for burning North Dakota lignite should operate at 1500°F using a bed of limestone.

Conclusion

The fluidized-bed combustion of North Dakota lignite was carried out using a variety of operating conditions, and generally met SO_2 and NO_x emission standards. The bed used was limestone as would most likely be used in a commercial FBC. The problem of ash agglomeration was identified and possible remedies suggested.

REFERENCES

1. Coates, N. H. and R. L. Rice. Sulfur Dioxide Reduction by Combustion of Coals in Fluidized Beds of Limestone. AIChE Symposium Series, Volume 70, Number 141, 1974.

2. Abel, W. T., R. L. Rice, J. Y. Shang, W. J. Ayers, Jr., and D. G. Turek. Combustion of Western Coal in a Fluidized Bed. Proceedings of the Sixth International Conference on Fluidized-Bed Combustion, Atlanta, Georgia, April 9-11, 1980.

3. Suuberg, E. M., W. A. Peters, and J. B. Howard. Product Composition and Kinetics of Lignite Pyrolysis. Industrial Engineering Chemistry, Process Design Development; Volume 17, Number 1, 1978.

4. Glass, E. C., A. L. Freeman, and T. O. Wentworth. Methanol Derivation from North Dakota Lignite and Use as a Fuel. Industrial Engineering Chemistry, Process Research Development, Volume 18, Number 4, 1979.

5. Mei, J. S., U. Grimm, and J. S. Halow. Fluidized-Bed Combustion of Low-Quality Fuels, Texas Lignite and Lignite Refuse. MERC/R1-78/3, Morgantown Energy Research Center, Morgantown, WV, April 1978.

6. Goblirsch, G., R. H. VanderMolen, K. Wilson, Sr., and D. Hajicek. Atmospheric Fluidized-Bed Combustion Testing of North Dakota Lignite. Proceedings of the Sixth International Conference on Fluidized-Bed Combustion, Atlanta, Georgia, April 9-11, 1980.

Dup

ATMOSPHERIC FLUIDIZED BED COMBUSTION OF MUNICIPAL SOLID WASTE: TEST PROGRAM RESULTS

L. C. Preuit
K. B. Wilson

Combustion Power Company, Inc.
Menlo Park, California

INTRODUCTION

Disposal of solid waste has historically been an economic cost to municipalities and industry. The least expensive means of disposal in this country has traditionally been landfill. Rapidly decreasing availability of space for landfill and rapidly increasing need for recovery of energy value of solid waste have generated considerable interest in the development of solid waste combustion technology. Mass burning incinerators, both with and without water walls for energy recovery, have seen the greatest use in combustion of municipal solid waste. Drawbacks of mass burning are low process efficiency and high emissions levels. Alternative processes include atmospheric fluidized bed (AFB) boilers, semi-suspension fired boilers, and pyrolysis processes.

AFB boilers offer the advantage of low NO_x emissions and high combustion efficiency in relatively compact equipment for the firing of municipal solid waste (MSW). Prior to the present tests, however, MSW combustion in an AFB boiler had not been demonstrated. An experimental program was designed to investigate the favorable operating regimes for a bed with steam-raising tubes, to determine the combustion efficiency, to measure the gaseous pollutants, to determine the erosion or corrosion of the tubes, and to investigate the fouling of the tubes or system internals caused by the combustion of municipal solid waste. Two 50-hour preliminary experiments were run to shake down the equipment and to identify the most favorable operating regime for a subsequent 300-hour test. This paper will describe the results of the experimental program and relate those results to the economics of a full scale cogeneration facility being considered for Stanford University.

EQUIPMENT DESCRIPTION

Testing was conducted in a 7 sq ft atmospheric fluidized bed combustor at Combustion Power Company's energy laboratory. The refractory-lined combustor is cylindrical with an inside diameter of 3 ft and an inside height of 16 ft. A view port permits observation of the bed during operation. Figure 1 diagrams the combustor facility as arranged for combustion of processed municipal solid waste (MSW). Figure 2 shows the combustor.

The combustor permits several arrangements of in-bed heat exchanger tubes so that heat extraction can be adjusted to suit desired test conditions. Primary heat extraction is through two, three, or four horizontal water tube bundles. These stainless steel tubes operate at low temperature to assure test reliability. Typically, 150 psig water is heated from 100 F to 300 F. This water is flashed to atmospheric pressure and makeup water reduces the feedwater temperature to 200 F. The water tube wall temperatures are lower than those of typical boiler tubes so that temperature-related corrosion does not occur. For the long duration test, air-cooled sample tubes were installed in the fluid bed and in the freeboard above the bed. These tubes were designed to duplicate boiler and superheater tube-wall temperatures for study of erosion and corrosion. Figure 3 shows the bed heat exchanger arrangement for the 300-hour test.

The combustor may be operated with or without recycle of elutriated bed material. During the first parametric test, the exhaust cyclone at the combustor was arranged to discharge into a collection barrel rather than returning collected particles to the bed. During the second parametric test and the 300-hour test, elutriated particles were recycled back to the bed from the cyclone. Discharge piping from the stainless steel recycle cyclone permits sampling of recycle material during operation.

Exhaust gas from the recycle cyclone passes through a spray cooler before

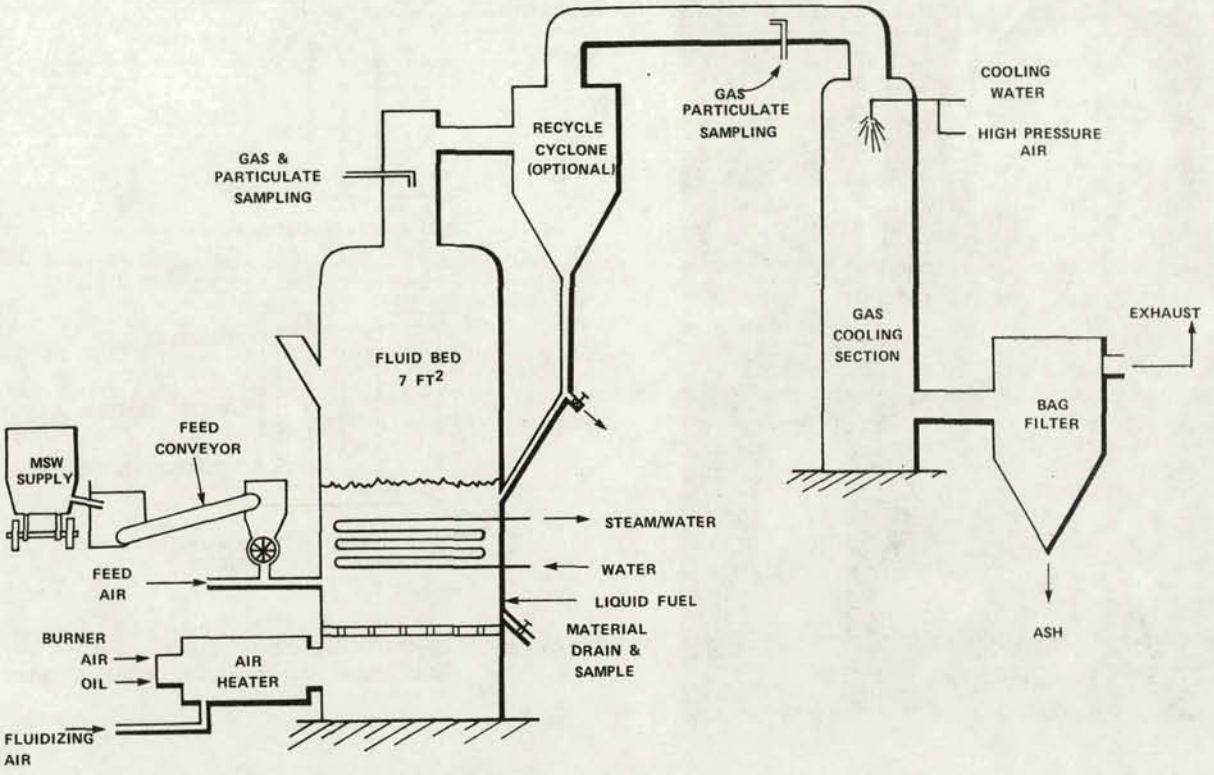

Figure 1 Fluid Bed Boiler Test Facility

final particulate cleanup in a baghouse. Stack discharge from the baghouse meets all applicable emissions regulations. Sampling ports are provided before and after the recycle cyclone, and also in the discharge stack from the baghouse.

Solid Waste Processing and Feed

Municipal solid waste is received in conventional packer trucks, each containing 3 to 6 tons of refuse. The trucks dump their contents on a covered concrete pad from which the refuse is pushed to shredder input conveyors as shown in Figure 4. The 100 hp Eidal mini-mill shredder has a nominal capacity of 5 tons per hour. Shredded solid waste is air-classified and the light fraction pneumatically transported to a storage shed to await transport to the combustor facility.

At the combustor, a live bottom bin provides short term storage and variable outfeed capability. Processed MSW is carried from the bin by the feed conveyor which is designed to provide uniform volumetric flow of the fuel. The combustor bed temperature control loop adjusts the speed of the feed conveyor, which discharges into a constant-speed rotary airlock. From the airlock, fuel is fed pneumatically through a 3-inch feed pipe to the fluid bed combustor.

Instrumentation

During combustion of processed MSW, temperatures in the system are monitored at 37 points. Data is collected for pressure and flow of combustion air, exhaust gas, cooling air and water, and fuel and oil. Exhaust gas composition is continuously monitored and concentrations

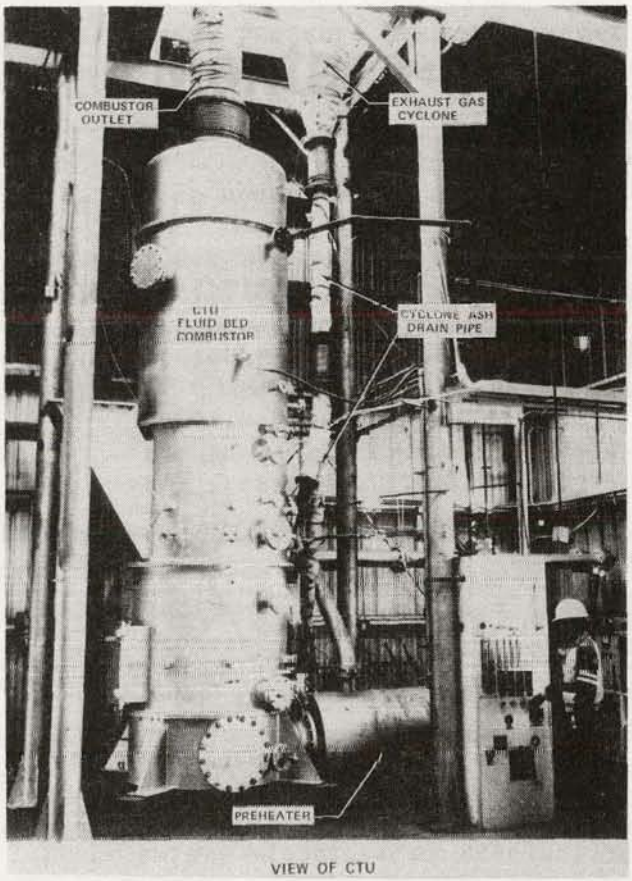

Figure 2 Fluidized Bed Combustor at Combustion Power Co.

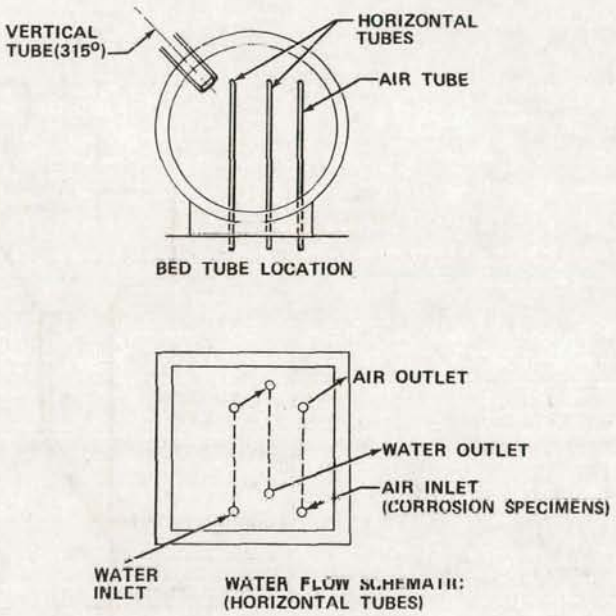

Figure 3 SSWEP 300-hour Test Bed Heat Exchanger Arrangement

of O_2, CO, NO_x, and hydrocarbons are recorded. Gas analysis is supplemented by Orsat testing at frequent intervals. Samples are taken daily for determination of HCl concentration and particulate loading. Material samples for analysis are taken daily from the bed and from the baghouse.

PARAMETRIC TESTS

Two 50-hour parametric tests were conducted to accomplish operational checkout of the system, explore the range of allowable process parameters, and identify the most desirable conditions for longer duration steady-state operation. Both parametric tests were planned to explore the same range of parameters. The first test, however, was run without recycle while in the second parametric test, elutriated material was recycled back to the bed. The first test ran 48 hours before being shut down by high pressures caused by slag buildup in the combustor freeboard and exhaust duct.

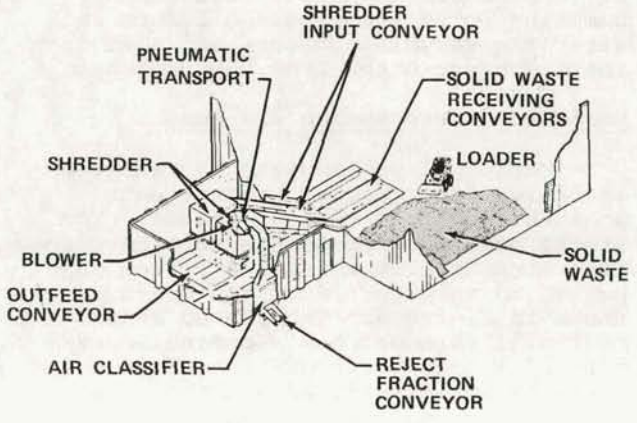

Figure 4 Solid Waste Processing Station

The second parametric test was terminated after 73 hours of operation.

Parametric Test Results

Parametric testing began with the bed depth maintained at 2.5 ft (slumped), but freeboard combustion appeared decreased when bed depth was increased to 3.5 ft (slumped). Deeper beds were used for all subsequent testing. Stable combustion was maintained within the ranges of:

Bed Temperature	1300-1410 F
Superficial Velocity	4.1-6.8 ft/sec
Excess Air[1]	50%-74%

Combustion efficiency[2] averaged 98.9%. Operation outside these ranges, particularly with excess air below 40%, resulted in undesirable freeboard afterburning and slag deposits in the combustor freeboard and exhaust ducting.

Slag deposits which formed during parametric tests were subjected to fusion-temperature analysis and found to have initial deformation temperatures of 1990 F and above. Differential thermal analysis confirmed the fusion test results. Since slag formation thus appeared to be related to high freeboard temperatures, one process condition set for the 300-hour test was a freeboard high temperature limit of 1600 F. The slag samples analyzed were, in general, calcium-rich alumina silicates.

---

[1] Excess air is calculated from:

$$EA = \frac{2.67C}{2.67C+8H+S-O} \times \frac{O_2}{CO_2+CO} \times 100\%$$

where:

EA = excess air
C, H, S, O = respective elemental dry weight %
O_2, CO_2, CO = respective gaseous dry volume %

[2] Combustion efficiency is based on unburned carbon in the flue gas and ash:

$$\eta = \frac{\frac{12}{44}a(\Delta H_{CO_2}) + \frac{12}{28}b(\Delta H_{CO}) + \frac{24}{30}c(\Delta H_{HC})}{\frac{12}{44}a + \frac{12}{28}b + \frac{24}{30}c + dH_{CO_2}}$$

where: a,b,c = respective weight concentration of CO_2,CO,HC in flue gas
and d = weight ratio of C to flue gas.

The 3-inch diameter fuel feed line was found to be very susceptible to plugging problems caused by round plastic lids of approximately 4-inch diameter. These lids were resilient enough to pass through the shredder, light enough to pass through the air classifier, but just stiff enough to cause blockage of the pneumatic feed line. Adjustment of the air classifier eliminated most of the lids and the problem with feedline plugging, but also resulted in rejection of a larger portion (near 50%) of the shredded MSW than had been desired. Larger diameter feedlines or improved shredding of the MSW would eliminate this problem in large scale equipment.

300-HOUR TEST

Operating conditions for the 300-hour test were based on results of the two parametric tests. Test objectives were to:

- Demonstrate the feasibility of burning municipal solid waste in an atmospheric fluid bed combustor with energy extraction from the bed.
- Evaluate the fluid bed media and fluidization characteristics over a 300-hour time period.
- Characterize exhaust gas emissions.
- Measure bed heat transfer coefficients.
- Gather data on erosion and corrosion of typical boiler and superheater materials at representative tube wall temperatures.

The 310 hours of operation included 298 hours of firing MSW at test conditions. The test was completed without any significant combustion-related problems, and operating conditions remained substantially constant. Upsets were caused by feedline plugs which occurred 35 times during the test. These blockages, caused by plastic lids which did not shred during fuel processing, were cleared within two to five minutes while combustor operation was maintained on oil. No material deposition or agglomeration was observed; at test conclusion the combustor and freeboard were virtually free of slag.

Fuel Analysis

Samples of the processed MSW were analyzed daily. Fuel properties were reasonably consistent throughout the test. Results of proximate and ultimate analysis on the fuel are:

PROXIMATE ANALYSIS (As Received)	Average	Range
Moisture Fraction(%)	23.6	17-26
Ash Fraction (%)	10.6	9-13
Volatiles (%)	57.6	54-64
Fixed Carbon(%)	8.2	8-9.7
Higher Heating Value (Btu/lb)	5572	5250-6050

ULTIMATE ANALYSIS (Dry Weight %)	Average	Range
Carbon	44.46	43.9-45.2
Hydrogen	5.96	5.8- 6.1
Oxygen	34.32	32.2-35.6
Nitrogen	0.67	0.63-0.80
Chlorine	0.49	0.40-0.67
Sulfur	0.13	0.09-0.17
Ash	13.97	12.0-16.0
Higher Heating Value (Btu/lb)	7352	6900- 7700

Operating Conditions

Operating conditions remained substantially constant throughout the 300 hours of test operation. Some parameters, however, changed due to a gradual decrease in bed particle size that occurred during the first half of the test. At typical steady state operating conditions, data from the last 144 hours of the test were averaged:

Bed Temp.	1392 F
Freeboard Temp.	1487 F
Superficial Velocity	4.6 ft/sec
Excess Air	44%
Bed Depth (slumped, nominal)	3.5 ft
Fluidizing Air Flow	43.0 lb/min
Fuel Feed Rate	8.2 lb/min
Combustion Efficiency	99.0%
Exhaust Material Recycle Rate	16 lb/min
Baghouse Ash collection Rate	0.9 lb/min
Bed Material Letdown Rate	4.9 lb/hr

Figure 5 shows the temperature recorder chart for a portion of the twelfth day of operation (260 through 264 hours into the test) as representative of general test conditions. Bed temperature remains constant, despite fluctuations in freeboard and exhaust temperatures caused by variations in heating value of processed MSW fuel.

Flue Gas Emissions

Emissions levels in the flue gas were considered very important to the basic program objective of demonstrating the feasibility of steam generation by firing MSW in an AFB boiler. Actual emission levels verified the potential of AFB combustion for low flue gas emission levels. Average emissions levels for the last 144 hours of test operation were:

Flue Gas Emissions	
O_2	6.7%
CO_2	13.5%
CO	200 ppm
SO_2	29 ppm
NO_x	160 ppm
Hydrocarbons (as CH_4)	40 ppm
HCl	100 ppm

Generally, each of the gaseous emissions monitored tended to exhibit constant variation. Occasional very high spikes of SO_2, CO, and hydrocarbons occurred independently of each other or any other parameter recorded. These spikes were probably due to particular constituents of the MSW fuel.

Emissions of SO_2 and NO_x are of particular concern in light of the tight regulations regarding these pollutants. Actual emissions levels were well under 1979 EPA promulgated New Source Performance Standards (NSPS) for boilers but would require emissions offset consideration to

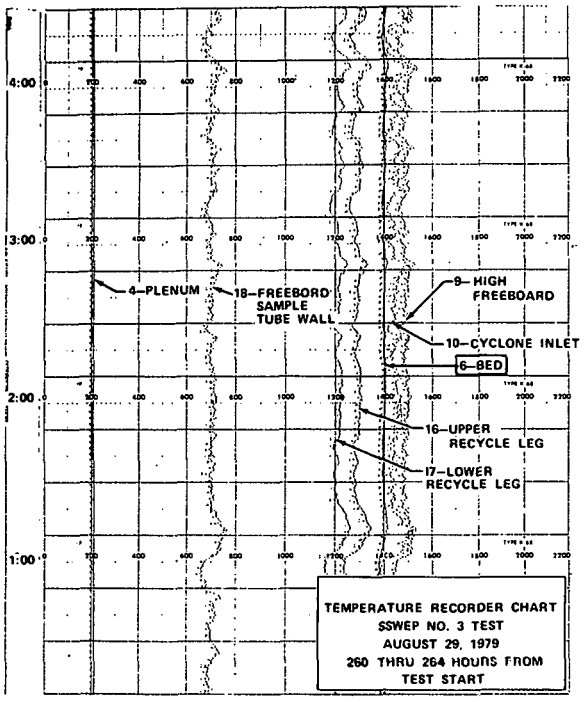

Figure 5 Temperature Recorder Chart SSWEP No.3 Test, 260 thru 264 Hours

be approved by California and local authorities. The indicated exhaust concentrations translate to approximately 0.06 lb/MMBtu fuel input for SO_2 and 0.25 lb/MMBtu for NO_x average for the last 144 hours of operation.

Bed Material

The original bed material was Monterey 16-mesh sand with an average particle size[3] between 1.0 and 1.1 mm. Daily samples were taken of bed material and of material returning to the bed from the recycle cyclone. Figure 6 shows the rapid drop in bed particle size at the beginning of the test, followed by a more gradual decline to nearly constant particle size at the end of the test. Also shown is the recycled material size which appeared unaffected by the changing bed material size. Some pieces of glass could be observed in the material samples and a few (less than 1%) pieces of agglomerated particles up to 1/4" size.

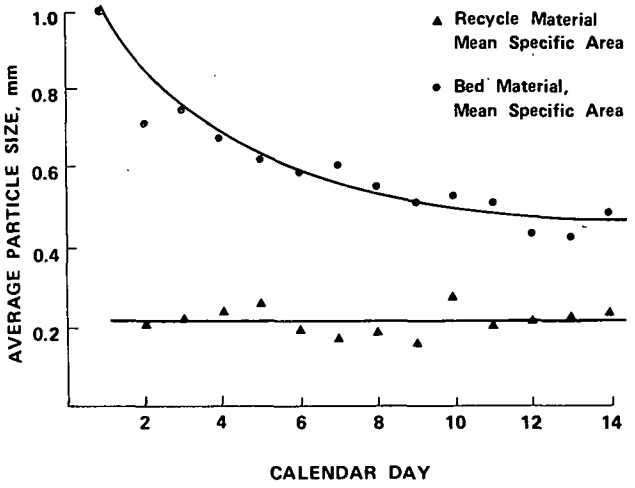

Figure 6 Bed Particle Size

Daily bed material samples were analyzed for cations and metals content by means of the emission spectroscopy scan method. The concentrations of the major constituents of the bed material were found to remain essentially constant. A number of elemental concentrations, however, increased throughout the test and accumulation of these materials appeared to be continuing up to the time the test was terminated. This accumulation of elements was the only observed phenomena which had not reached a steady state equilibrium before the end of the test. Longer test duration will be necessary to observe the effects of this accumulation.

Elements which accumulated were Ca, Fe, Mg, Ti, Na, Cu, Mn, P, Zn, and possibly Pb. Concentrations of these elements are shown for samples taken early in the test and at the end of the test. (Trace elements are not shown).

Element	Concentration Weight % 3rd Day	12th Day
Si	37.0	33.8
Al	4.0	3.8
Ca	1.8	5.5
K	2.8	2.7
Na	1.9	4.0
Fe	0.48	1.2
Mg	0.17	0.69
Ti	0.068	0.28
Ba	0.11	0.10

Heat Transfer

Water inlet and outlet temperatures as well as flow through the main heat exchanger were monitored throughout the test. That heat exchanger consisted of two four-pass, horizontal tubes arranged in bed as shown in Figure 3. Early in the test, the overall heat transfer coefficient averaged 46 Btu/hr-ft^2-F. By the end of the test, the heat transfer coefficient had increased to 58 Btu/hr-ft^2-F. The increase in heat transfer coefficient is attributed to the decrease in bed material particle size. The influence of particle size on outside wall heat transfer coefficient is predicted by Bashakov (2) or Locke (3).

Corrosion and Erosion

In addition to the stainless steel (TP316) water cooled tubes in the bed which were the primary means of heat extraction, air cooled sample tubes were installed in the bed and in the freeboard to duplicate wall temperatures of superheater tubes. No significant corrosion or erosion was observed on the water cooled tubes in the bed. Mechanical failure of the air cooled tube in the bed invalidated the sample exposure.

The freeboard air cooled sample tube was installed transverse to gas flow in the exhaust ductwork from the combustor. The tube was fabricated from sample sections of six different tube materials. The samples were exposed to 1500 F to 1600 F flue gases heavily laden with particulate (40-50 gr/acf) at a gas velocity of about 35 fps. The sample tube

[3] Particle size is calculated by the "Mean Specific Surface" method (1)

wall temperature was about 720 F. Combined corrosion and erosion resulted in substantial metal wastage of carbon steel specimens, with less wastage apparent as the alloy content increased.

As shown in Table I, metal wastage was greatest for carbon steel coupons, approximately 50%-60% of the wall facing the gas side, while wastage of the sides and tops was less than 5%. Wastage was considerably less for the low alloy steels in the same orientation. On the side facing the gas flow, the wastage was 13%-17% while elsewhere it was less than 3%. The metal wastage of the austenitic specimens (SS304, SS316, and Incoloy 825) was the lowest, being less than 6% on the side facing the gas flow and less than 1% elsewhere. Scaling and deposits were also orientation dependent, with bottoms of the coupons relatively free of scale and deposits compared to the sides and top. As expected, scale formation was thickest on the carbon steels, and the chrome-containing austenitic steels were resistant to scaling.

Residual corrosion penetration was very low on the bottoms of the carbon steel and low alloy specimens. Apparently, corroded areas and scale were removed by erosion as they formed, i.e., corrosion-erosion was a major factor in the metal wastage. Corrosion penetration on the low alloy specimens was comparatively low on the tops and sides at 5 to 10 microns. With respect to corrosion

TABLE I

PIPE THICKNESS AND MICROGRAPH MEASUREMENTS

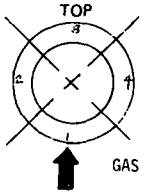

SSWEP: 300 HR TEST COUPONS
LOCATION: CTU FREEBOARD

Specimen Identification	Pipe Orientation	Pipe Thickness (Inch) *Unexposed	Exposed	% Wastage	(Residual Maximum) Micrograph Measurements Scale	Penetration M	Comments
1A1	1. Bottom	.115	.060	47.8	None(a)	6	(a) Corrosion-erosion
(Carbon Steel)	2. Left Side	.112	.113	-.9	15	10	
(SA-106B)	3. Top	.110	.116	-5.5	16	60	
(SA-210A1)	4. Right Side	.113	.110	2.7	(b)	14	(b) Spalled
3A3	1.	.116	.100	13.8	3	<2	
(1¼Cr-½ Mo-Si)	2.	.115	.116	-.9	60	10	
(SA-335P11)	3.	.118	.124	-5.1	15	10	
(SA-213T11)	4.	.120	.117	2.5	250(a)	10	(a) Scale and ash deposit
4A4	1.	.135	.113	16.3	80	<2	
(2¼Cr-1 Mo)	2.	.130	.129	.8	a.	5	a. Spalled
(SA-335P22)	3	.129	.131	-1.6	b.	10	b. Spalled
(SA-213T22)	4.	.132	.132	0	c.	5	c. Spalled
5A5	1.	.105	.100	4.8	-	35	.005" wastage
(18Cr-8Ni)	2.	.105	.105	0	100(a)	50	(a) Scale and ash deposit
(SA-312-TP304H)	3.	.105	.106	-1.0	(b)	10	(b) Spalled
(SA-213-TP-304H)	4.	.104	.104	0	200(c)	10	(c) Scale and ash deposit
6A6	1	.107	.101	5.6	8	-	.006" wastage
(16Cr-12Ni-2Mo)	2	.118	.118	0	30	10	
(SA-312-TP316H)	3	.107	.107	0	a.	-	a. Spalled
(AS-213-TP-316H)	4	.106	.106	0	b.	5	b. Spalled
7A7	1	.112	.109	2.7	20	30	.003" wastage
(Ni-Fe-Cr-Mo-Cu)	2	.113	.113	0	a.	30	a. Spalled ?
(INCO 825)	3	.117	.117	0	b.	4	b. Spalled ?
(Sb-163)	4	.118	.119	-.8	c.	25	c. Ash deposit

* Unexposed pipe remnant measurements.

under the exposure conditions, the low alloy specimens compared well with the type SS316 that showed only 5 to 10 microns of corrosion penetration, while the metal wastage of the low alloy specimens was greater. The SS304 and Incoloy 825 showed corrosion penetrations ranging from 10 to 50 microns. Apparently, corrosion was by oxidation and sulfidation as sulfur was found in most corroded regions of all coupons.

CONCEPTUAL DESIGN STUDY

An economic study was undertaken to determine the promise of the AFB boiler system as defined by results of the experiments. The complete cogeneration system was envisaged for application to the Stanford University campus with the sizing and performance of the MSW fired AFB boiler based on test results.

Proposed System

The AFB system for study was designed to meet an existing situation in which the local municipality is faced with unavailability of landfill disposal area while Stanford University is seeking to control energy costs. Municipal solid waste would be processed at a central collection location and the MSW fuel trucked to the campus boiler plant. Size of the system is set by the 800 tons per day of processed MSW derived from 1200 tons per day of raw municipal solid waste estimated to be available in 1983. The modular AFB boilers would produce 600 psia, 750 F steam for a turbine with extraction at a pressure of approximately 170 psia. The extraction steam would condense in a heat exchanger to provide heating steam for the campus. Steam not needed for campus services would flow through the condensing stage of the turbine. Thermodynamic and process studies provided estimates that the proposed system would supply all of the university steam demand and approximately 50% of the electricity needs.

A flow diagram of the proposed system is shown in Figure 7. No attempt was made to investigate the processing of the MSW; study was limited entirely to conversion of the processed MSW to thermal energy and to electricity. All ancillary equipment necessary for energy production from MSW fuel was included.

Plant Design and Cost Estimating

The plant design was broken down into 12 major cost components listed in Table II.

For each of these systems, sufficient design work was done to define a concept and to specify the necessary size of the equipment. Wherever possible, standard components were used and cost estimates obtained from vendors. A plant plan, Figure 8, and layout drawings were made and necessary buildings included to enclose turbine, boiler, and fuel receiving areas so as to be compatible with the campus site. No cost was included for the value of the land. An artist's rendition of what the plant might look like is shown in Figure 9. General performance figures for the plant are shown below.

Plant Performance

- Design firing rate for processed MSW fuel:
  Average - 800 tons/day
  Maximum - 1000 tons/day
- Yearly average plant output:
  Steam at 125 psi, 110,800 lb/hr
  Electricity - 6.7 MW
- Boiler output:
  Average - 200,000 lb/hr
  Maximum - 250,000 lb/hr
- Maximum electrical output (net): 13.8 MW
  Concurrent 125 psi steam output 91,200 lb/hr
- Fuel Storage:
  Normal - 200 tons (6 hr avg output)
  Maximum - 500 tons(15 hr avg output)
- Reserve Fuel:
  Low grade bunker oil - 35 gpm at max. output
- Reserve fuel storage: 126,000 gal, 3 days.

Environmental Considerations

Emissions data collected during the 300-hour test were converted to a pounds-per-hour basis using the flow rate of combustion products for an 800 tons-per-day plant. Below are the data reported in this form, together with the "offset" that Stanford is permitted to take if it shuts down its present oil-fired heating plant.

Emissions	Projected 800-TPD Plant	Offset from Existing plant
SO_2	2.9 lb/hr	24.1 lb/hr
NO_x	7.7	23.1
CO	8.9	5.2
Hydrocarbons	0.7	1.1

Only CO would exceed the offset available from the existing boiler. The present

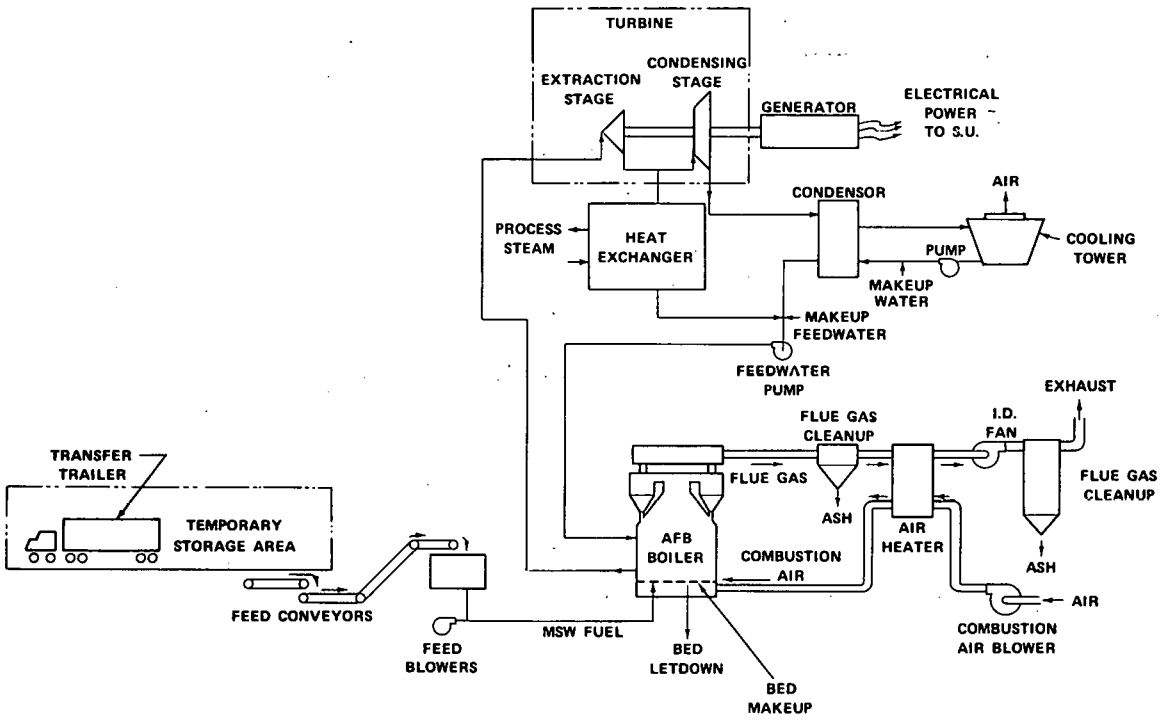

Figure 7 MSW Fired Cogeneration Plant Diagram

TABLE II

PLANT DESIGN - LIST OF MAJOR EQUIPMENT

1. Boiler System

Modules w/tubes & plenums (6)
Recycle cyclones (24)
Exhaust manifolds (2)
Evaporators (2)
Economizers (2)
Attemporators (2)
Supports & lagging
Sootblowers (6)

2. Startup System

Duct burner assembly
Booster fan
Fuel-oil pumps (dual)
Fuel-oil storage tank
Bed injectors (36)
Air manifold & dampers

3. Combustion Air System

F.D. fans & motors (2)
Intake silencers (2)
Tubular air preheaters (2)
Ductwork

4. Flue-Gas System

Multiclones (2)
Electrostatic granular filter
I.D. fan & motor
Ductwork

5. Bed Maintenance Systems

Slide gates (6)
water-cooled conveyors (2)
Blowers w/filter silencers (3)
Airlock feeders (3)

5. Bed Maintenance Systems (Cont.)

Sand storage bin
Bin discharger
Fabric filter
Transport piping
Discharge diverter valves (7)

6. Flyash Disposal System

Airlocks (6)
Screw conveyors (2)
Feeders (2)
Transport piping
Ash silo
Fabric filter
Blower w/filter/silencer (2)
Silo discharger
Discharge conveyor

7. Fuel-Feed System

Main conveyor
Distribution conveyor
Feed bins (6)
Metering conveyors (6)
Conditioners (6)
Airlocks (36)
Blowers w/filter silencers (2)
Transport piping

8. Fuel Receiving & Storage

Apron
Conditioners
Live storage bin
Fabric filter w/blower
Dust collection ductwork
Front-end loader

9. Main Steam System

Turbine & assoc. equipment
Condensor
Condensate pumps
Condensor vacuum pumps
Condensate polishing
Cooling towers
Cooling water pumps
Process heat exchangers

10. Feedwater System

Boiler feed pumps (motor) (2)
Feedwater heater
Deaerating feedwater heater
Boiler feedwater transfer pump
Deaerated feedwater storage tank
Boiler feed pumps (turb.) (2)
Feedwater piping valves

11. Electrical & Control Systems

Generator & controls
Switchgear
Transformers
Motor control center
Instrumentation & controls

12. Buildings & Site

Grading & roads, landscaping
Foundations
Structures
Enclosures
Maintenance & administration
Heating, ventilation, A.C.
Fire safety equipment
Utilities

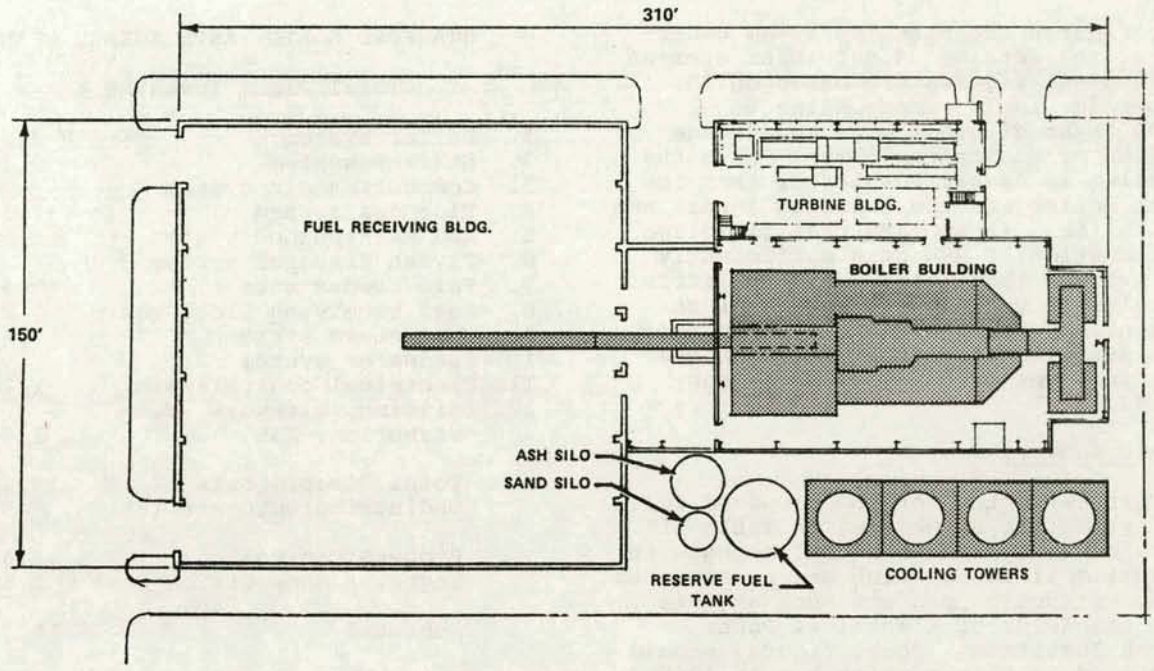

Figure 8 Solid Waste Energy Plant Plan

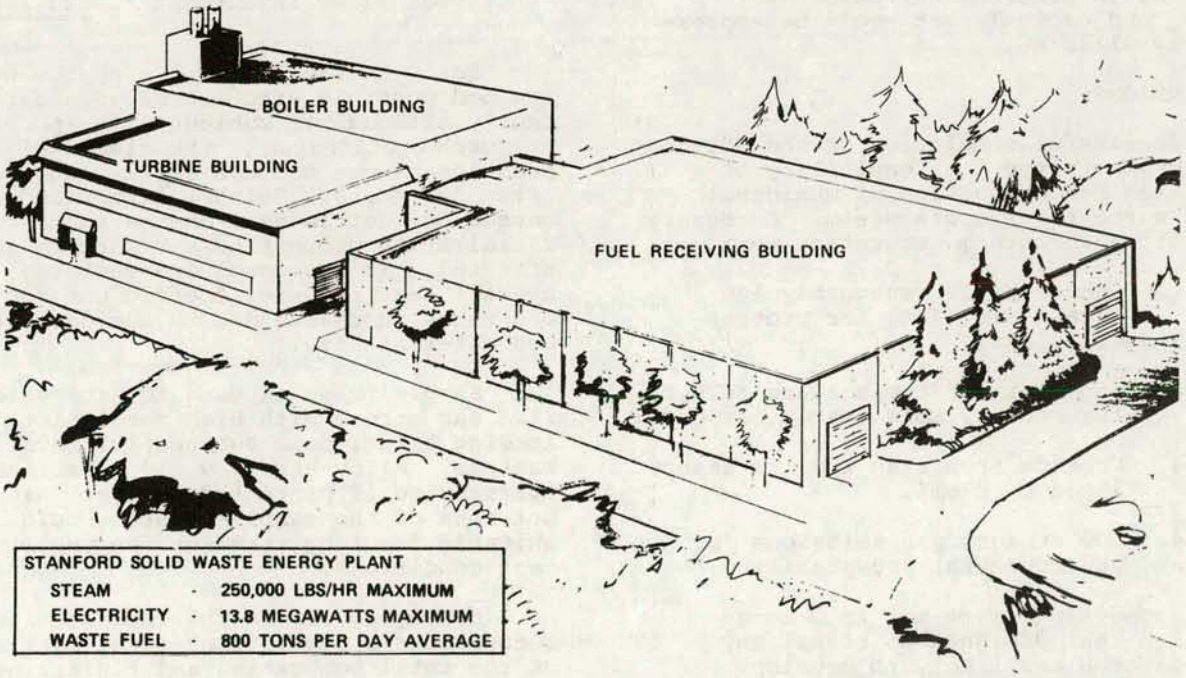

Figure 9 Artist's Rendition

Environmental Considerations (Continued)

boiler figures are based on steam generation at the rate of 80,000 lb/hr whereas the AFB plant figures are based on 800 tons per day fuel corresponding to 110,000 lb/hr of steam plus an average of 6.7 MW of electrical power. Thus the AFB boiler is nearly 40% larger than the present boiler and the emission levels are very similar. It appears that fluidized bed combustion of MSW is a sufficiently clean process that there would be little difficulty in meeting the stringent requirements of the San Francisco Bay Area Air Pollution Control District when the offset from the present boiler is considered.

Economic Summary

Cost estimates for the proposed full scale system are summarized in Table III. Each major subsystem is shown, along with the additional costs which are recommended for a construction project such as this by the standards of Electrical Power Research Institute. These figures should be compared to plants which handle 1200 tons per day of raw municipal solid waste and produce both steam and electrical power. The costs presented do not include processing or transporting the processed MSW to the point of use. For purposes of comparison, if the entire boiler steam output were converted to electricity, the plant would generate approximately 20 MW_e and capital cost would be approximately $1150/kW.

CONCLUSIONS

Successful completion of the 300-hour test demonstrated the feasibility of fluidized bed combustion of municipal solid waste to generate steam. Necessary conditions for steam generation were met:

1. Operation at reasonably low excess air (44%) for process efficiency.
2. Constant bed temperature (±20 F) for controllable system output.
3. Freedom from slag and its associated problems.
4. Low exhaust gas emissions for environmental acceptability.

These conditions were met in a long-duration test designed to reveal any process problems likely to develop.

TABLE III

STANFORD SOLID WASTE ENERGY PLANT

Total Plant Investment

1.	Boiler system	$ 2,239,700
2.	Startup system	155,200
3.	Combustion air system	798,900
4.	Flue gas system	2,382,000
5.	Ded maintenance system	84,100
6.	Flyash disposal system	79,200
7.	Fule feed system	457,800
8.	Fuel receiving bldg. equip.	252,400
9.	Main steam system	5,421,000
10.	Feedwater system	1,942,600
11.	Electrical/controls/mis.	1,204,100
12.	Building, sitework, construction, A&E	1,645,000
	Total Direct Costs	16,662,000
	Undistributed Costs (6%)	999,700
	Process Capital	17,661,700
	Engrg. & Home Office Fees	1,666,200
	Subtotal	19,327,900
	Project Contingency (Subtotal x 15%)	2,899,200
	Process Contingency (Item 1 x 5%)	112,000
	Sales Tax	777,300
	Total Plant Investment	$23,116,400

Early in the 300-hour test the average bed particle size decreased significantly although it subsequently appeared to reach equilibrium. The elemental composition of the bed was still changing after 300 hours. Neither situation caused any detrimental change in bed fluidization properties nor were emissions affected. It was concluded that the overall heat transfer coefficient for the bed tubes increased due to the decrease in bed material size.

Sample tubes exposed to high velocity flue gas stream with high particulate loading experienced substantial metal wastage. Alloy steels would be suitable for service if protected from abrasion but none of the samples tested would be suitable for long term service under test conditions.

Conveying air in the fuel feedline constitutes a significant (30%) portion of the total combustion and fluidizing

air. This air enters the bed as a point source and is not easily distributed throughout the bed. While a larger feedline is desirable to avoid feedline plugging and permit firing of less-processed fuel, greater spacing between larger feedlines may create air distribution problems in the bed. Investigation of alternate fuel feed technology is warranted.

Based on data from 300 hours of testing, projected emissions from an AFB boiler firing municipal solid waste would be low compared to an existing conventional oil fired boiler. Total plant investment for a cogeneration plant burning 800 tons per day of processed MSW fuel would be $23,116,000 corresponding to approximatley $1,150/kW if the entire steam output were converted to electricity.

ACKNOWLEDGEMENT

This work was accomplished at Combustion Power Company, Inc., under subcontract to Stanford University with the program jointly sponsored by the United States Environmental Protection Agency and Department of Energy. The generous contribution of Professor R. H. Eustis of Stanford University is gratefully acknowledged.

REFERENCES

1. Kunii, D., and Levenspiel, O., "Fluidization Engineering," John Wiley and Sons, 1979.

2. Bashakov et al., (1973). Power Technology, pp. 8, 273.

3. Locke, H.B. et al., "Fluidized Combustion in Great Britain," paper presented at Fourth International Conference on Fluidized Bed Combustion, Mitre Corporation, McLean, Virginia, December 1975.

SORBENT UTILIZATION

STATUS OF RESEARCH ON AGRICULTURAL USES OF FLUIDIZED BED COMBUSTION RESIDUE

O. L. Bennett, W. L. Stout, J. L. Hern,
and R. L. Reid

U. S. Department of Agriculture, Science & Education Administration,
Agricultural Research, in cooperation with the
U. S. Department of Energy

More than 90 percent of U.S. coal reserves are classified as high sulfur. Increased use of coal will significantly increase air pollution from SO_2, NO_x, and other potentially toxic compounds unless adequate controls are utilized. One of the most promising emission control techniques is the combustion of fossil fuel in a fluidized bed of sulfur-retaining additives.

Large quantities of limestone are used in the fluidized bed combustion (FBC) process. The resulting residue consists of various combinations of calcium sulfate, magnesium sulfate, calcium oxides and other compounds that may be contained in the limestone or scrubbed from the coal during combustion (1). Therefore, FBC residue represents a tremendous resource of elements and compounds that may prove valuable for agricultural production (5). However, this residue may also contain heavy metals that are toxic to plants, animals, and humans, if these elements enter the food chain in sufficient amounts. This could seriously limit the use of FBC residue in agricultural production.

Since 1976, an extensive research program has been conducted by the U.S. Department of Agriculture, Science and Education Administration, Agricultural Research, in cooperation with the U.S. Department of Energy to determine agricultural uses of FBC residue. The research is conducted at several locations representing most of the major soil associations and environmental conditions existing in the eastern half of the United States. The research consists of detailed chemical and physical evaluation of the FBC residue followed by extensive greenhouse, environmental growth chamber, and field studies to determine its plant nutrient supplying status. All major plant species, including corn, small grain crops, vegetables, nut crops, grass, and legume species are grown with FBC residue in these studies. Final phases of the research will cover metabolic studies using test animals and possible human feeding trials with feed and food products grown with FBC residue. The purpose of this paper is to give a summary of the nature, extent, and some of the results of this extensive research program.

CHEMICAL EVALUATION

Samples of FBC residue from several locations throughout the United States have been collected for chemical and physical evaluation (2). Chemical analysis of several samples of FBC residue are given in Table 1. A theoretical mineral balance obtained from chemical composition indicates FBC residue contains an average of 28.3 percent calcium sulfate, 33.6 percent calcium oxide, 4 percent aluminum oxide, 2.1 percent iron oxide and 1.8 percent magnesium oxide with 26 percent of the material listed as inert and identified as primary silic dioxide. This leaves 3.2 percent for trace elements and undetermined components. The chemical analysis was to determine those constitutents of FBC residue which are: 1) essential plant nutrients, 2) toxic metals, 3) possible phytotoxic elements and 4) a soil pH amendment. Essential elements are those required for plant growth and reproduction of crop species. This group consists of calcium, magnesium, potassium, phosphorous and sulfur which are required in micro amounts, and iron, manganese, molybdenum, boron, copper and zinc, which are required in micro amounts. The heavy metals listed in Table 1 are: nickle, lead, cadium, chromium, selenium and aluminum. Mercury and arsenic (not shown) would be in the same category. The micro elements in FBC residue samples vary considerably in chemical composition, but are similar to amounts of micro elements and heavy metals already present in the soil. The essential plant nutrients such as calcium, magnesium and sulfur would be highly beneficial for most acid soils. Boron may be present in sufficient amounts to be phytotoxic for some sensitive plant species. The plant availability of many of these elements, especially the micro-nutrients and heavy metals are within the range of those usually found in soils; but uptake of these elements by plants will depend on the amount applied in the FBC residue, native amounts in the soil, soil pH, interactions with other ions, and the solubility of the compound. Therefore, the application of large amounts of FBC residue over a period of time should be carefully monitored.

Laboratory studies were carried out to determine particle size distribution, porocity, water retention capacity and the effects of these physical properties on potential use of FBC residue as an agricultural liming material.

Table 1. Variations in some chemical constituents of nine samples of fluidized bed combusion waste (2), FBCW.

Constituent		FBCW Average	FBCW Range
		-------ug/g of Dry Matter------	
	Ca	380,000	240,000-460,000
Essential	Mg	7,100	5,000-112,000
Plant	K	2,500	500-8,000
Nutrients	P	430	380-500
	S	92,000	72,000-140,000
	Fe	11,000	800-16,000
	Mn	485	210-685
	Mo	0.19	0.12-0.28
	B	110	95-170
	Cu	15	12-19
	Zn	55	29-105
	Ni	21	13-29
Heavy	Pb	3.2	1.5-7.5
Metals	Cd	0.5	---
	Cr	15	9-23
Possibly	Se	0.29	0.16-0.58
Phyto-	Al	10,000	4,000-20,000
toxic			
		-------% of $CaCo_3$----------	
Soil pH Amendment	Neutralizing Potential	60	31-100

Such studies carried out at several locations indicated that particle size will significantly affect chemical reactivity. In general, the smaller size fractions have a much faster rate of reaction and release of potential nutrients for plant growth. Particle size distribution of several samples of FBC residue indicate that 27 percent of the particles were in the 1 - 2 mm size range and about 28 percent of the 1/2 - 1 mm size range (Table 2). An average of 90 percent of all of the material was less than 2 mm in size. However, the percentage spread is considerable between subsamples.

LEACHING STUDIES

In order to determine possible elemental movement through soils treated with FBC residue, column leaching studies were conducted at several locations. At Morgantown, West Virginia, studies were initiated to evaluate the effects of FBC residue liming rates on the movement of added chemical constitutents in both acid soils and mine spoils (4). This was accomplished in incorporating various rates of FBC residue in the upper portion of the soil or mine spoil material. Sufficient amounts of FBC residue were applied to bring the soil and spoil material to pH(s) of 4.6, 5.0, and 6.0. Since the soil had a higher buffering capacity than the mine spoil, this meant that higher amounts of FBC residue were applied to the soil columns than the mine spoil.

Table 2. Particle size distribution from 9 subsamples of fluidized bed combustion waste obtained from the Alexandria, WV, Pilot Plant.

Size	Mean	High	Low	CV
	--------- % --------			
> 2 mm	9.2	19.0	0.7	58
1 - 2 mm	46.6	57.9	36.0	19
0.5 - 1 mm	27.9	39.6	19.1	22
0.25 - 0.5 mm	9.4	16.9	1.1	58
0.15 - 0.25 mm	3.4	9.9	0.3	93
0.15 mm	3.5	10.9	0.4	97

Data by W. L. Stout and R. C. Sidle

Analysis of the leachate from 14 different leachings for each column, carried out at 10-day intervals, shows that of the elements analyzed in the mine spoil digest, only calcium showed any significant downward migration as a result of the FBC residue treatment. Of the heavy metals analyzed in leachate from mine spoil, all were within an acceptable range for potable water. Only percolate SO_4^{-2} and manganese concentrations were present in excess of suggested limits for potable water. However, this was true for percolate collected with FBC residue amended as well as control column. Of the elements analyzed in the percolate from soil samples, calcium increased the most due to FBC liming amendment. Mean percolate calcium concentrations for all leaching periods for the high FBC treatment were significantly higher than concentrations for either the low treatment (11.4 ppm) or control (6.7 ppm). Other elements showing downward migration in the soil column were magnesium, manganese, and sulfate. None of the other elements analyzed in the percolate showed any overall FBC residue treatment effect. These studies indicate, in general, that no environmental problems are found with respect to solute transport from liming rate applications of FBC residue on soils or strip mine spoils. Movement of calcium and magnesium into the subsoil would definitely be beneficial to many acid soils in the eastern United States.

PLANT GROWTH STUDIES

Initial studies with plant species were carried out at several locations in both the greenhouse and in environmental growth chambers. Indicator plants were used, such as: vegetable crops of swiss chard, cabbage, tomatoes, lettuce, radish and turnips, that tend to accumulate heavy metals (5). By using indicator crops, we were able to get a quick estimate of the potential availability of the heavy metals contained in the FBC residue as compared with regular limestone. In general, these studies indicated that when FBC residue was applied on a lime equivalency basis, soil pH was increased to the same level as where agricultural lime was applied. Greenhouses and growth chambers studies indicated that no

significant increases in heavy metal concentrations in plant tissue were obtained and growth rates were equivalent to those obtained with limestone. In some cases, the calcium and sulfur content of the plant material was increased significantly by application of FBC residue. For instance, studies conducted in Maryland using apple seedlings showed that FBC residue applied at rates of 1, 2, or 4 times the lime requirement on three different soils, resulted in better or equal apple seedling growth when compared to a non-calcium fertilizer control or calcium carbonate applied at the lime requirements (3). The largest growth responses were obtained when FBC residue was applied at rates equivalent to lime requirements for each soil. When FBC residue was applied at eight times the lime requirement, severe growth reduction occurred.

Greenhouse studies with pecan seedlings in Georgia indicated a significant increase in growth and calcium and magnesium concentrations in seedlings that were treated with equivalent rates of FBC residue generated from dolimite sources. Similar results were obtained using peach seedlings. The use of dolimite in the FBC process would certainly enhance the value of the FBC residue for agricultural uses because of the need for larger amounts of magnesium on most acid soils throughout the eastern United States.

Other plant species tested in environmental growth chamber and greenhouse conditions include several grass and legume species, various vegetable crops, small grain species, buckwheat and blueberries.

Field studies using most of the major agricultural crops are in progress throughout the eastern United States representing most major soil series and environmental conditions. Studies extend from Massachusetts to Georgia. Field studies are in progress utilizing apple and peaches as test crops near Amherst, Massachusetts; New Brunswick, New Jersey; Raleigh, North Carolina; Beltsville, Maryland; and peaches and pecans at Bryon, Georgia. Studies with forage and grain crops are underway in Virginia, Delaware, Pennsylvania, West Virginia, Kentucky, Maryland, and South Carolina. Vegetable and horticultural crops are being grown in many of the above states using FBC residue.

The results of several field experiments are presented to give an idea of the effect of FBC residue as compared to regular agriculture lime treatment on elemental composition of several plant species. Since no differences in yield were obtained, between FBC residue and lime treatments, only the elemental composition of various plant parts will be given. Elemental analysis of first year field results for corn, soybean, and oats are given in Tables 3 and 4. First year results for broccoli, lettuce, beets and snapbeans are presented in Table 5 for different edible plant parts, i.e., infloresence, leaves, roots and pods.

In Table 3 are given the elemental composition of corn leaves and grain, and soybean leaves and grain grown with FBC and calcium hydroxide treatments in field studies at Morgantown, West Virginia. The FBC treatment, when compared to the calcium hydroxide treatment, showed only significant increases in levels of sodium and copper in corn grain and a significant decrease in potassium in corn leaves. Soybean leaves showed increases in calcium and sodium levels and a decrease in potassium level with FBC residue applications. Soybean grain actually had significantly lower cadmium level in the FBC treatment than in the calcium hydroxide treatment. Since soybeans normally have a tendency to accumulate cadium in the grain, this is of special interest.

Oak grain did show a significant increase in cadium level with FBC applications (Table 4). Although this increased level is still within a safe range, such increases, if consistent from year to year, could limit the rate of applications of FBC to crop land. Therefore, when repeated application of FBC residue are applied to land over an extended period of time, plant uptake of heavy metals should be carefully monitored. Oat straw showed a significant increase in zinc concentrations with application of FBC residue (Table 4).

Vegetable crops showed very few differences in elemental concentrations between FBC and calcium hydroxide treatments. Zinc did have a tendency to increase in lettuce leaves. However, this increase would be more beneficial than harmful. It should be pointed out that different plant species accumulate elements at different levels (Tables 3, 4 and 5). For instance, lettuce and soybean leaves have dangerously high levels of lead, even in the calcium hydroxide check area. Therefore, it is very important to use several species to evaluate the effects of FBC on the food chain.

The final phases of the research program will involve extensive metabolic testing of various food and feed products with small animals, large animals and using human subjects. In these studies, animals will be fed plant material grown with either FBC residue or with those grown with regular limestone. Pending favorable results with the animal trials, a human nutrition study is being formulated in cooperation with the West Virginia University Animal Science Division, the Human Nutrition Department, and West Virginia University Medical Center. Complete diets will be formulated from food growth with both FBC and the calcium hydroxide treated land. These diets will include meats, poultry, and dairy products as well as fruits, vegetables, and nut crops.

SUMMARY

A comprehensive research program is in progress to evaluate the potential of using FBC

residue for agricultural uses throughout the eastern United States. The results with field, greenhouse, growth chamber and laboratory studies indicate that the material can be used effectively for food and feed productions. At the present time, we have found little evidence to indicate that this material would be detrimental to the food chain. However, studies with plants only indicate the short-term effect of FBC residue on heavy metal uptake. It is absolutely essential that studies be conducted over a long period of time with repeated applications to the soil before final conclusions can be drawn. The soil is not a static situation and is continuously changing. Repeated heavy applications of FBC residue to the soil could cause a slow building of certain toxic heavy metals, or solubility and availability to plants can change with time. Therefore, we must evaluate soil management practices relative to FBC residue applications to crop land under as many different environmental conditions as possible before final judgment is made.

LITERATURE CITED

1. Bennett, O. L., W. L. Stout, J. L. Hern, and R. C. Sidle. 1978. Potential agricultural uses of fluidized bed combustion waste. In Energy and the Environment. Proceedings, 5th National Conference, October 31-November 3, 1977, Cincinnati, Ohio. American Institute of Chemical Engineering, Dayton, Ohio, pp 84-89.

2. Hern, J. L., W. L. Stout, R. C. Sidle, and O. L. Bennett. 1977. Characterization of fluidized bed combustion waste, Composition and variability as they relate to disposal of agricultural land. Proceedings, 5th International Conference of Fluidized Bed Combustion, Washington, D.C., Vol. II, p. 821.

3. Korcak, R. F. 1980. Fluidized bed material as a liming substitute in calcium sources for apple peelings. Journal, Environmental Quality 9(1):147-151.

4. Sidle, R. C., W. L. Stout, J. L. Hern, and O. L. Bennett. 1979. Movement of chemical constituents associated with fluidized bed combustion waste in acid soils and mine spoil columns. Journal, Environmental Quality 8(2):236-241.

5. Stout, W. L. and O. L. Bennett. 1979. Fluidized bed combustion waste in food production. Proceedings, ASCE/PRC-EPRI Workshop on Solid Waste Research and Development Needs for Emerging Coal Technologies, San Diego, CA, April 23-25, 1979, pp. 170-184.

Table 3. Elemental composition of corn leaves and grain and soybean leaves and grain grown with FBCW and $Ca(OH)_2$ (1978, Morgantown, WV).

Element	Corn				Soybean			
	Leaves		Grain		Leaves		Grain	
	FBCW	$Ca(OH)_2$	FBCW	$Ca(OH)_2$	FBCW	$Ca(OH)_2$	FBCW	$Ca(OH)_2$
	Percent Dry Matter							
Ca	1.05	0.93	0.02	0.02	2.14	1.93*	0.26	0.28
Mg	0.22	0.22	0.14	0.13	0.27	0.28	0.25	0.24
K	1.92	2.05*	1.03	1.02	1.31	1.42*	1.70	1.70
N	3.16	2.85	1.54	1.65	3.77	4.24	5.79	5.97
P	0.32	0.31	0.40	0.35	0.24	0.28	0.49	0.50
S	0.43	0.45	1.49	1.48	0.28	0.30	0.33	0.33
	ug/g Dry Matter							
Na	245	243	64	59*	358	339*	256	240
Fe	162	158	23.4	19.7	148	153	73	111
Zn	45	42	38.5	36.6	41.0	45.5	45	44
Mn	75	73	4.53	2.98	102	105	31	35
Cu	16.6	14.4	3.19	2.68*	8.72	9.71	13.4	13.0
Al	59	60	31.1	29.0	43.3	59.7	16.4	43.9
Ni	1.95	2.08	1.28	1.10	5.02	4.37	3.56	3.32
Sr	12.1	9.5	0.17	0.72	26.8	21.4	5.50	5.79
Cr	1.88	1.68	1.30	1.30	3.54	3.46	0.09	0.10
Cd	0.26	0.31	0.05	0.08	1.71	1.54	0.09	0.15*
Pb	6.00	5.73	0.20	0.30	24.3	22.4	0.16	0.22
Co	1.90	1.80	0.43	0.55	19.3	17.0	0.35	0.18
N/S ratio	7.45	6.53	10.4	11.2	13.7	14.0	18.5	17.7

*Indicates that means are significantly different ($P < .05$) by Duncans Multiple Range Test.

Table 4. Elemental composition of oat herbage, grain and straw grown with FBCW and $Ca(OH)_2$ (1978, Morgantown, WV).

Element	Herbage		Grain		Straw	
	FBCW	$Ca(OH)_2$	FBCW	$Ca(OH)_2$	FBCW	$Ca(OH)_2$
	Percent Dry Matter					
Ca	0.53	0.51	0.09	0.09	0.50	0.50
Mg	0.20	0.19	0.12	0.12	0.16	0.15
K	2.00	2.05	1.15	1.16	1.82	1.61
N	0.99	1.04	2.73	2.66	1.31	1.36
P	0.37	0.38	0.48	0.48	0.19	0.17
S	0.34	0.33	0.22	0.22	0.19	0.18
	ug/g Dry Matter					
Na	275	380	108	101	397	436
Fe	723	378	603	755	511	424
Zn	50	51	49	44	25	21*
Mn	108	83	85	68	78	75
Cu	10.7	12.0	8.5	6.0	10.4	5.9
Al	1020	1362	277	200	359	542
Ni	4.0	9.3	3.1	3.1	2.3	1.9
Sr	17.5	18.0	1.72	1.56	11.6	11.1
Cr	3.45	3.00	2.68	2.58	3.00	2.70
Cd	0.87	0.87	0.10	0.04*	0.06	0.70
Pb	2.33	3.05	0.70	0.78	1.73	2.83
Co	2.53	2.45	4.98	4.88	3.55	4.17
N/S ratio	11.1	11.6	11.0	12.5	6.78	7.47*

*Indicates that means are significantly different ($P < .05$) by Duncans Multiple Range Test.

Table 5. Elemental composition of broccoli, lettuce, beets, and snap beans grown with FBCW and $Ca(OH)_2$ (1978, Morgantown, WV).

Elements	Broccoil		Lettuce		Beets		Snap Beans	
	FBCW	$Ca(OH)_2$	FBCW	$Ca(OH)_2$	FBCW	$Ca(OH)_2$	FBCW	$Ca(OH)_2$
	Percent Dry Matter							
Ca	0.46	0.51	1.53	1.63	0.16	0.16	0.48	0.48
Mg	0.17	0.19	0.27	0.26	0.27	0.22	0.20	0.19
K	2.62	2.48	3.18	2.62	2.52	2.56	2.10	2.18
N	6.14	6.18	2.85	2.72	2.50	2.37	3.01	3.13
P	0.86	0.86	0.38	0.35	0.30	0.30	0.34	0.43
S	1.55	1.56	0.33	0.31	0.16	0.14	0.21	0.20
	ug/g Dry Matter							
Na	579	619	1274	1278	436	708	182	178
Fe	91	134	927	867	69	58	73	75
Zn	80	85	40	36*	42	39	30	31
Mn	20	21	104	93	32	28	15	14
Cu	6.0	6.3	8.2	7.7	11.4	10.3	6.6	7.0
Al	17	15	1117	967	13.2	13.7	30	32
Ni	2.26	2.19	1.46	1.48	0.80	1.22	2.48	2.25
Sr	11.6	14.3	23.6	26.0	9.06	8.18	6.01	6.06
Cr	1.16	1.57	3.37	3.34	1.67	1.54	1.43	1.48
Cd	0.08	0.09	0.67	0.69	0.27	0.39	0.10	0.04
Pb	1.71	0.63	8.50	8.45	0.31	0.13	0.55	0.35
Co	0.87	0.88	0.38	0.62	0.41	0.69	1.18	1.25
N/S	3.96	3.96	9.30	9.35	15.5	17.3	14.3	16.1

*Indicates that means are significantly different ($P < .05$) by Duncans Multiple Range Test.

Questions to O.L. Bennett:

Q: (Participant not identified)

Could you elaborate on the use of fluidized bed waste in combustion with organic waste?

A: One thing we have found when working with organic waste is that we have been able to use it to move calcium, zinc, etc., into the soil. It is extremely useful when supplementing deficient soils. In general, we have found that if we keep pH within the desired range, the heavy metals do not move in the soil. In the case of bark, which is a kind of inert material, we got immediate benefits from the use of FBC waste. With composted garbage and sewage there was little initial effect.

Q: (Participant not identified)

Do you see this material in wide use in agriculture?

A: We visualize that if the fluidized bed combustion process is widely used, this material may be the major source of lime for agriculture in the eastern U.S., and any part of the world where agricultural lime is needed. It could be a very important commercial substance.

RESEARCH PROGRAM TO ASSESS THE IMPACT OF THE LAND APPLICATION OF FLUIDIZED BED COMBUSTION RESIDUE ON HUMAN NUTRITION

W.L. STOUT, E. FASHANDI, M.K. HEAD, R.L. REID, AND O.L. BENNETT

USDA-SEA AND WEST VIRGINIA UNIVERSITY
MORGANTOWN, WEST VIRGINIA

INTRODUCTION

The total scope of the ongoing work being done to determine the potential of FBC residue (FBCR) as an agricultural resource has been reported in the proceeding paper and elsewhere (5). The purpose of this paper is to present in greater detail the research program being conducted to evaluate the possiable effects, detrimental as well as beneficial, of foods produced with FBCR on the nutritional status of humans.

The FBCR-human nutrition study is a co-operative effort between the United States Department of Agriculture and the West Virginia University. The study is funded by the United States Department of Energy. Co-operating divisions within West Virginia University represented in the study are animal and veterinary sciences, family resources, plant sciences, and the West Virginia University Medical Center. The scientific diciplines represented in this effort include agronomy, animal nutrition, chemistry, foods and nutrition, horticulture and soil science.

RESEARCH APPROACH

Past research has shown that the most promising agricultural usage of FBCR is as a liming material for acid soils (3,4,5). However, FBCR does contain several heavy metals in micro amounts that could be detrimental to animals and humans if the metals were allowed to enter the food chain in sufficient amounts (5). To address this concern, a series of studies were started in the spring of 1978 to evaluate the effect of cropland application of FBCR on the food chain.

These studies are sequenced so that if FBCR application appears to be detrimental to the food chain the program can be terminated before reaching the human phase (Figure 1). There are three points in the program at which all data pertaining to possible heavy metal contamination in the food chain will be analyzed and reviewed, If, at these points, there appears to be some danger of heavy metal accumulation, the flow of the project will be stopped.

INITIAL STUDIES

In the spring of 1978 field plots were treated with FBCR and hydrated agricultural lime ($Ca(OH)_2$. Hydrated lime was selected as a control because the CaO in the FBCR readily hydrates to $Ca(OH)_2$. Thus the reaction rate in the soil and the resulting soil pH change for both liming materials will be similar. This is very important since previous work has shown that the increased soil pH brought about by FBCR application influences heavy metal uptake more than the metals contained in the FBCR (4).

The primary objective of this phase was to determine the effect of land application of FBCR on the quality of food for human and animal consumption. The main quality factors that we were concerned with were heavy metal levels in the plant tissue. Heavy metals in the food chain are of particular concern since their accumulation in animal organs can cause metabolic diseases such as hypetension and cancer (1,2). Sulfur levels in plant tissue are also of interest since sulfur is a necessary component of cystine and methonine, amino acids essential to humans.

Details of the study and results of the analyses of the plant material grown in these studies have been previously reported (5). These results show that there was no significant increase in heavy metal accumulation in ediable portions of vegetable species grown on areas treated with FBCR. However, the cadnium level in oat grain grown on FBCR treated areas (0.10 ug/g) was significantly higher than that of the oat grain grown on $Ca(OH)_2$ treated areas (0.04 ug/g). Though this increase is statistically significant, these levels are still within a safe range. In contrast to the oat data, cadnium level of soybeans grown on $Ca(OH)_2$ treated areas (0.15 ug/g) is significantly higher than that of the soybeans grown in the FBCR treated areas (0.09 ug/g). This indicates that we are working at near background levels at least as far as cadnium is concerned.

Corn, oat, and soybean grains were grown in quantities sufficient to formulate diets for rats and hamsters (Tables 1). Chemical analysis indicated that the heavy metal levels in these diets were very low (Tables 2, 3). Cadnium and lead levels in the experimental rat diets were the

FIGURE 1 - Flow Diagram Of FBCR-Human Nutrition Study, Morgantown, WV

YEARS	TASKS
1978-1979	Vegetable production feed grain production small animal trails.
1979-1980	Vegetable & fruit production feed grain production. Production of animal products Swine metabolic trial
	Review, & Decision
1980-1981	Vegetable & fruit production Feed grain production Production of dairy products Production of animal products
1981	Human metabolic trials

TABLE 1 - Percentages Of Feed Grains In Rat And Hamster Diets

Soybean & Corn diets	48.5%	Soybeans
	48.5%	Corn grain
	3.0%	Vitamin Supplement
Soybean & Oats diets	48.5%	Soybeans
	48.5%	Corn grain
	3.0%	Vitamin Supplement

TABLE 2 - Heavy Metal And Sulfur Levels In Rat Diets Composed Of Grains Grown On Lime And FBC Residue (FBCR) Treated Lands. All Data On A Dry Matter Basis.

Treatment	Diet	Elements						
		Cd	Cr	Cu	Ni	Pb	Zn	S
		ug/g						%
Lime	Soybean & Corn	0.12	1.87	8.38	1.62	0.20	37.4	0.246
FBCR	Soybean & Corn	0.12	1.25	8.48	1.37	0.20	36.3	0.222
Lime	Soybean & Oats	0.12	1.75	16.0	2.62	0.20	44.3	0.268
FBCR	Soybean & Oats	0.12	3.37	30.4	2.50	0.20	50.9	0.288
Commerical	Rat Row	0.12	4.62	14.2	2.12	0.20	78.0	0.336

TABLE 3 - Heavy Metal And Sulfur Levels In Hamster Diets Composed Of Grains Grown On Lime And FBC Residue (FBCR) Treated Lands. All Data On A Dry Matter Basis.

Treatment	Diet	Elements						
		Cd	Cr	Cu	Ni	Pb	Zn	S
		ug/g						%
Lime	Soybean & Corn	0.12	2.75	9.30	1.88	0.20	38.9	0.250
FBCR	Soybean & Corn	0.12	2.25	8.36	1.37	0.20	37.8	0.270
Lime	Soybean & Oats	0.12	3.25	16.5	2.87	0.20	45.8	0.268
FBCR	Soybean & Oats	0.12	5.12	10.6	3.25	0.20	44.9	0.258

same or lower than the commerical rat diet (Table 2). Chromium and copper levels in the FBCR-Soybean & Oat diet were somewhat higher than that of the comparable lime formulation. Other differences in metal levels in the rat diets were a function of the grains used to formulate the diets. Although there was no commerical diet for hamsters available for comparison, analysis indicated that the heavy metals in the hamster diets were also low (Table 3). The chromium level increased in the FBCR-soybean & oats hamster diet as it did in the comparable rat diet.

Weanling rats and hamsters were fed these diets for periods of six weeks. During this time weight gain data were taken every four days. Also during the trial feces and urine were collected for analysis. At the end of the trials the animals were sacrificed and appropriate organs removed for analysis. Also, several animals from each diet were homoginized for whole body analysis.

Data from this study is just now becoming available. Weight gain data indicate the the rats gained weight equally on all diets (Table 4). Hamsters on the FBCR-soybean & corn diet performed better than these fed to the comparable lime formulation. This was due to a longer period of weight loss at the beginning of the study in hamsters on the lime diet.

Whole body analysis for chromium, copper, and sulfur is available for both rats and hamsters (Tables 5, 6). There was no difference in whole body chromium levels in rats fed any of the diets or rats analyzed before the trial. The only increase in whole body copper levels in rats was in the lime-soybean & oats diet (Table 5). Whole body sulfur levels were the same for all fed the experimental diets and higher for rats fed the control diets and the pretreatment rats.

Whole body chronium and sulfur levels in hamsters were the same for all diets and the pretreatment animals (Table 6). The only increase in whole body copper levels for an experimental diet was for the lime-soybean & corn diet.

Cadnium and lead are two heavy metals of particular concern. In whole body tissue of rats and hamsters the elements were generally below our detection limits for flame atomic absorption. These levels are 0.25 ug/g and 2.5 ug/g for cadnium and lead respectively in the dry animal tissue.

Presently mineral (element) balance and mineral (element) retention in both rats and hamsters are being calculated by the following equations:

Mineral balance = Total intake of mineral in feed (Total mineral excreated in urine + total mineral excreated in feces)

And

%Mineral retension = (mineral balance/ total intake of mineral in feed) x 100.

These calculations will determine if the application of FBCR to croplands can affect the utilization of minerals (elements) by animals consuming feeds grown on these lands.

EXPANDED STUDIES PHASE

In 1979, at Morgantown, WV food production studies were expanded to include hay and pasture areas for cattle and sheep and increased areas for begetables, fruit, corn, and soybean productions (Table 7). At the same time at Georgetown, DE poultry studies were conducted in which FBCR was added as a calcium supplement directly into the diets of broilers and laying hens. Food products from existing studies at other USDA-SEA locations at Byron, GA and Beltsville, MD are also being incorporated into the study (Table 7).

Grains, vegetables, fruits, and poultry products produced in the 1979 growing season are presently being formulated into diets which will be fed to swine in a metabolism trial starting in July 1980. Swine were chosen for this study since their digestive system and metabolism closely simulate those of the human. Data collected in this study will include metabolic measurements such as blood pressure and mineral retension as well as heavy metal analysis of appropriate organs and tissues.

Presently in this pahse of the study we are preparing to produce, in the 1980 growing season, the foods necessary for the human phase of the study. Our objective is to produce a variety of experimental foods in sufficient quantities to formulate essentially all of the human diets. These diets will include vegetables, meats, wheat products, dairy and poultry products and nuts.

STATUS OF HUMAN PHASE

Status of human phase the human phase of this project is presently in the planning stages. Food is being produced, menues being planned, facilities being readied, and the data to be collected determined. In the fall of 1980, sixteen male subjects for the study will be selected on the basis of complete physical examinations and interviews.

The time of the human study is projected for January 1981. The present plans are for the study to be six weeks long. The first two weeks baseline data on the subjects will be collected. Experimental diets will be fed in the final four weeks, with fecal and urine samples being collected in the final week. Blood samples will be taken weekly throughout the study. However, the actual execution of this study is dependent on the decision reached by review of all of the project data after the swine metabolism trial is complete and all foods to be used in the diets are analyzed for heavy metals. If at that time there is any indication that heavy metals are being enhanced in the human diet the human study will be terminated.

TABLE 4 - Weight Gains Of Rats And Hamsters Fed Diets Composed Of Grains Grown On Lime And FBC Residue (FBCR) Treated Lands. All Data On A Dry Matter Basis.

Treatment	Diet	Rats	Hamsters
		--- grams ---	
Lime	Soybean & Corn	268A	23B
FBCR	Soybean & Corn	268A	36A
Lime	Soybean & Oats	294A	38A
FBCR	Soybean & Oats	291A	33AB
Commerical Rat Diet		334A	

TABLE 5 - Chromium, Cooper, And Sulfur Levels In Whole Body Tissue Of Rats Fed Diets Composed Of Grains Grown On Lime And FBC Residue (FBCR) Treated Lands. All Data On A Dry Matter Basis.

		Element		
Treatment	Diet	Cr	Cu	S
		--- ug/g ---		%
Lime	Soybean & Corn	12.9A	6.12B	0.68B
FBCR	Soybean & Corn	12.7A	6.77B	0.58B
Lime	Soybean & Oats	15.5A	14.2A	0.66B
FBCR	Soybean & Oats	14.0A	6.70B	0.67B
Commerical Rat Diet		13.8A	7.46B	0.82A
Pre Treatment		13.3A	8.56AB	0.94A

TABLE 6 - Chromium, Copper And Sulfur Levels In Whole Body Tissue Of Hamsters Fed Diets Composed Of Grains Grown On Lime And FBC Residue (FBCR) Treated Lands. All Data On A Dry Matter Basis.

		Element		
Treatment	Diet	Cr	Cu	S
		--- ug/g ---		%
Lime	Soybean & Corn	10.9A	11.9A	0.66A
FBCR	Soybean & Corn	9.6A	6.07B	0.64A
Lime	Soybean & Oats	10.8A	7.08B	0.53A
FBCR	Soybean & Oats	9.8A	6.97B	0.60A
Pre Treatment		9.6A	10.3AB	0.65A

TABLE 7 - Location Of Food Products Produced For FBCR - Human Nutrition Study

Morgantown, WV	Vegetables, Wheat flour, meat products, dairy products.
Kearneysville, WV	Apples, Peaches
Point Pleasant, WV	Strawberries
Byron, GA	Pecans, Peanuts
Georgetwon, DE	Poultry Products
Beltsville, MD	Apples

LITERATURE CITED

1. Furst, Arthur, 1968. Trace Elements Related to Specific Chronic Diseases: Cancer. In Environmental Geochemistry in Health and Disease. The Geological Society of American, Inc. Boulder, Colorado.

2. Perry, H.M. 1968. Trace Elements Related to Cardiovascular Disease. In Environmental Geochemistry in Health and Disease. The Geological Society of America, Inc. Boulder, Colorado.

3. Sidle, R.C., W.L. Stout, J.L. Hern, and O.L. Bennett. 1979. Movement of Chemical Constituents Associated with Fluidized Bed Combustion Waste in Acid Soil and Mine Spoil Columns. J. Environ. Qual. Vol. 8, No. 2, p. 326-331.

4. Stout, W.L, R. C. Sidle, J.L. Hern, and O.L. Bennett. 1979. Effect of Fluidized Bed Combustion Waste on The Calcium, Magnesium, Sulfur, and Zinc Levels in Red Clover, Tall Fescue, Oats, and Buckwheat. Agron. J. Vol. 71 No. 4, p. 662-665.

5. Stout, W.L., H.A. Menser, J.L. Hern, and O.L. Bennett. 1979. Fluidized Bed Combustion Waste in Food Production. In Solid Waste Research and Development Needs for Emerging Coal Technologies . America Society of Civil Engineers. New York, New York.

Questions to W.L. Stout:

Q: (Participant not identified)

What were the rates of application of the FBC waste?

A: It varies. Somewhere around 2 1/2 tons of calcium carbonate per acre is necessary for the soil in the areas used. Since the buffering capacity of the soil varies, the calcium oxide in the waste varies, etc. You wind up with 5-8 tons of FBC waste per acre.

Q: (Participant not identified)

Were there problems with heat when the calcium oxide hydrated in the soil?

A: No; we are talking about 5-8 tons of waste mixed into 1000 tons of soil. We're really not putting that much on.

Q: (Participant not identified)

Has there been any work done on FBC waste with fly ash in it?

A: When you start mixing the ash in, you start knocking down the percentage of the beneficial materials of the entire mixture. Boron toxicity may also come up.

FLUIDIZED-BED COMBUSTION RESIDUE DISPOSAL: ENVIRONMENTAL IMPACT AND UTILIZATION

C. C. Sun
C. H. Peterson

Westinghouse R&D Center
Pittsburgh, PA

INTRODUCTION

Fluidized-bed combustion (FBC) is an emerging technology aimed at utilizing coals in a manner protective of the environment. Environmentally acceptable disposal or utilization of partially reacted limestone or dolomite and coal ash from AFBC and PFBC is required. Westinghouse has been contributing to the development of FBC solid residue disposal technology and utilization.[1-4] This paper provides perspective on some of the available choices in direct disposal of the residues as well as on residue processing options for utilization or disposal.

Laboratory tests were performed to determine the environmental impact of unprocessed and processed residues from both AFBC and PFBC plants, based on residue characterization, leaching tests, and activity tests. The results are compared with criteria based on drinking water standards (DWS), the Resource Conservation and Recovery Act (RCRA), and the properties of reference materials. Spent sorbent processing options are reviewed, and screening tests have been performed to evaluate selected alternatives. Fixation of solid residue is examined in this paper. Development work must recognize several constraints which include economics, market size, legal requirements (which may be federal, regional, or local), and various property and performance criteria that may limit utilization options.

An assessment of the potential environmental impact and a view of the choices based on the results of the experimental investigations are presented.

RESIDUE CHARACTERIZATION FOR DIRECT DISPOSAL

Two major types of solid residue result from an FBC system: bed overflow material and entrained (carry-over) material. The former consists largely of partially reacted limestone or dolomite sorbent (calcium sulfate [$CaSO_4$], calcium oxide [CaO], calcium carbonate [$CaCO_3$], magnesium oxide [MgO]) mixed with coal ash; the latter consists of finer particles of sorbent, char, and coal ash entrained from the bed. The entrained particles are collected at different stages of the particulate control system - primary, secondary, and third-stage cyclones - as well as baghouses or other filtering devices, for example. These two types of materials may be disposed of separately or as a mixture.

Evaluation of the environmental impact of direct disposal has been carried out by considering

- The effect of FBC design and operating conditions on residue leachate and thermal activity
- The effect of coal and sorbent characteristics on leachate and thermal activity
- The effect of the disposal environment including surface water and soil characteristics
- Reference materials, including conventional power plant ash, FGD residues, and natural gypsum.

A review of the results in each of these areas is presented. Perspective on the disposal requirements determined by RCRA criteria - hazardous vs nonhazardous - is presented in the next section.

Samples Investigated

The environmental impact tests were performed on over 40 samples of bed overflow and entrained materials obtained from experimental and pilot-scale FBC units operated by Argonne National Laboratories (ANL), Exxon, Pope, Evans and Robbins (PER), Morgantown Energy Research Center (MERC), Babcock and Wilcox, Inc. (B&W), Battelle Columbus Laboratories, Combustion Power Company, and the National Coal Board (Leatherhead, England). The FBC residues investigated during this work include bed overflow material and entrained material from both pressurized and atmospheric units operating with either once-through injection of sorbent (with or without carbon burnup) or with sorbent regeneration. For comparison six flue gas desulfurization (FGD) residues (untreated, oxidized, and fixed) and two natural gypsum samples were tested during this investigation.

Chemical, physical, and morphological characterization of the bed overflow and entrained material was carried out. The methods employed included optical microscopy, scanning electron microscopy (SEM), energy dispersive analyses by X-ray (EDX), electron microprobe analysis (EMA), X-ray diffraction, thermogravimetric analysis (TGA), emission and atomic absorption spectroscopy,

and wet chemical methods. Table 1 summarizes how the residues are proportioned between sorbent-based and coal ash constituents for the different stream sources of FBC solid residue (bed overflow, entrained material) investigated in this study. Table 2 summarizes the calcium distribution range of the partially reacted sorbent in these residues. Minor and trace species in the FBC solids are discussed in the next section.

Table 1

DISTRIBUTION OF SORBENT/COAL ASH BETWEEN THE FBC BED OVERFLOW AND ENTRAINED MATERIAL

Dwg. 7721A98

Residue Source	Sorbent, wt %	Coal Ash, wt %
Bed Overflow Material	60-90	10-40
Entrained material collected by the particulate control device, (e.g., cyclone)	20-50	50-80
Entrained material collected by the particulate control device, (e.g., 3rd stage cyclone or fabric filter)	10-40	60-90

Table 2

SUMMARY OF COMPOSITION OF PARTIALLY REACTED SORBENT FROM FBC SYSTEMS

Process	Composition (Ca-based molar fraction)			
	$CaSO_4$	CaO	$CaCO_3$	CaS
AFBC, Once-through	0.10-0.50	0.50-0.90	0-0.10	<0.01
PFBC, Once-through	0.10-0.7	0-0.30	0.10-0.80	<0.01
PFBC, Regenerative	0.10-0.40	0.60-0.90	0-0.10	<0.01
PFBC, Adiabatic	0.40-0.70	0-0.30	0-0.30	<0.01

Dwg.7721A88

Leaching Tests

In the study covered in this paper, leachates were induced by the shake tests developed by Westinghouse except where otherwise specified, e.g., RCRA/extraction procedure (EP) test. An automatic shaker at 70 excursions per minute was used to agitate the FBC/leaching medium mixtures. Among the variables investigated were solid/liquid ratio, sample mixing time, and pH of the leaching medium. The leachates resulting from this operation were tested for pH, specific conductance, total dissolved solids (TDS), calcium, magnesium, sulfide, sulfite, sulfate (SO_4), minor and trace metal ions, anions, and total organic carbon (TOC). Three types of leaching media were used in the shake tests - deionized water, CO_2-saturated water (pH=4) to simulate typical surface water at a disposal site, and sodium acetate-acetic acid buffer solution (pH=4.5) to simulate a typical acidic leaching environment when disposed of with municipal or other acidic wastes.

The shake tests are severer than conditions anticipated under actual land disposal; results from the shake tests are expected to project the worst case. Two shake procedures have been employed. These are described below.

- Continuous shake test. It establishes equilibrium conditions between the solid and its aqueous surrounding and provides the worst possible case with respect to contaminant release. Typically, a 1:10 solid-to-liquid ratio is used, and the mixture is shaken for up to 400 hours.

- Intermittent shake test. A series of ten to fifteen cycles of a 72-hour shake test was adopted as part of the leachability study to show leaching rate as a function of time over a long period under worst case conditions. Leachates are analyzed at the end of each interval, and a fresh charge of leaching medium is added for each 72-hour leach cycle. Typically, a 1:3 solid-to-liquid ratio is used.

In addition to the Westinghouse shake tests, the EPA's extraction procedure (EP) developed under RCRA[5] was performed to determine if FBC residues are hazardous or nonhazardous and is discussed in the next section.

Activity Tests

No standard EPA activity test exists that can be applied to FBC residues. Under Sec. 3001 of RCRA, EPA's Office of Solid Waste (OSW) has proposed some general tests to determine whether a waste is hazardous because of reactivity. These tests concentrate on hazardous properties such as explosiveness and chemical and mechanical instability, however, and do not apply to residual CaO activity in FBC residue.

The heat release activity of FBC residue was measured calorimetrically in this study. The temperature rise of a solid/water system containing free CaO is a function of solid/water ratio. Two solid/water ratios were used in this study (4/1 and 3/20) with the advantage of higher sensitivity in the one and better reproducibility in the other.

Results

Table 3 summarizes the environmental parameters investigated and compares the potential environmental concerns of FBC solids with conventional FGD residues. To provide comparison, those leachate parameters passing natural gypsum but exceeding the drinking water standard (DWS) are singly crosshatched, and those exceeding both are doubly crosshatched. Major concerns for FBC

Table 3

Dwg. 2618C33

PRELIMINARY COMPARISON OF ENVIRONMENTAL IMPACT OF THE FBC AND FGD SOLID AND LIQUID WASTE DISPOSAL[a]

Process	Sample	Sorbent Type	Environmental Parameters: Heat Release[b,c] (spontaneous temp rise) 3 g/20 ml	Trace Metal	TDS	Total[b] Organic Carbon	pH	Calcium	Magnesium	Sulfate	[b] Sulfite	[b] Sulfide
Pressurized FBC, Once-through	Bed material, leachate	Limestone	< 0.2°C		▨	< 30 ppm	▨	▨		▨		
Pressurized FBC, Once-through	Bed material leachate	Dolomite	< 0.2°C		▨	< 30 ppm	▨	▨		▨		
Pressurized FBC, Regenerative	Bed material leachate	Dolomite / limestone	0-3°C		▨	< 30 ppm	▨	▨		▨		▩
Atmospheric FBC, Once-through	Bed material leachate	Limestone	5 to 15°C		▨	< 30 ppm	▨	▨		▨		
Atmospheric FBC, Once-through	Carry-over material, leachate	Limestone	0-3°C	(d)	▨	< 30 ppm	▨	▨		▨		
Pressurized FBC, Once-through	Carry-over material, leachate	Limestone / dolomite	< 0.2°C	(d)	▨	< 30 ppm	▨	▨	(d)	▨		
Pressurized FBC, Once-through	Processed compacts from bed carry-over mixtures, leachate	Dolomite / limestone	< 0.2°C		▨	< 30 ppm	▨	▨		▨		
FGD	Liquor of untreated sludge	Lime / limestone		▩	▩	< 30 ppm	▩	▩	▩	▩	▩	
FGD	Liquor of oxidized sludge	Lime / limestone		▩	▩	< 30 ppm		▩	▩	▩		
FGD	Leachate of dried, untreated sludge	Lime / limestone	< 0.2°C	▩	▩	< 30 ppm	▩	▩	▩	▩		
FGD	Leachate of dried oxidized sludge	Lime	< 0.2°C	▩	▩	< 30 ppm		▨	▨	▨		
FGD	Leachate of dry stabilized sludge	Lime	< 0.2°C		▨	< 30 ppm		▨		▨		
Gypsum	Leachate	Natural	< 0.2°C		▨	< 30 ppm		▨		▨		

▩ Do not meet either the drinking water or gypsum leachate criteria

▨ Pass gypsum leachate criteria but not Drinking Water Standards

☐ Pass both drinking water and gypsum leachate criteria

(a) Based on data from currently available FBC and FGD residues
(b) No existing criteria
(c) Subjected to the specified procedures, i.e., 3 g solid added to 20 ml H_2O
(d) All except two carry-over fines pass Drinking Water Standards (total of 30 samples tested)

residue disposal are the high pH, TDS, sulfate, and calcium levels in the leachate; the thermal activity; and the large quantity of solid to be disposed of.

The pH, calcium, and TDS levels of an FBC leachate depend largely on the amount of unutilized CaO present in the solid. Higher pH, calcium, and TDS levels are found in the leachates of residues with lower CaO utilization. On the average, the leachate of AFBC residue has a higher pH, calcium, and TDS level than that of PFBC residue, which generally contains less CaO. Similarly, the leachate of spent limestone sorbent contains higher concentrations of calcium, TDS, and pH than that of spent dolomite.

Trace element levels in FBC leachate are low. With only two exceptions (one AFBC bagfilter sample and one PFBC third-cyclone catch), leachates of all

FBC residues (>40 samples) tested throughout this and previous studies met all the existing DWS. Trace elements are more concentrated in the entrained material and in its leachate than in that of bed overflow material. The bed overflow material, on the other hand, consists predominantly of sorbent-based components; its leachate, therefore, has higher pH, calcium, and TDS levels. In general, leaching property is a function of leachate pH: higher levels of trace elements exist in leachates having a lower pH.

The total organic carbon level in FBC leachates is low. All (>40 samples) except one (TOC = 30 ppm for leachate of an AFBC bagfilter sample) were below or near the detection level (<10 ppm).

Substantial heat can be released from FBC residue upon its initial contact with water and may require special handling and disposal procedures to minimize this thermal activity. The thermal activity is largely dependent on the amount of CaO present in the residue and is also a function of the operating conditions of the process, which may result in either calcined or uncalcined sorbent in the form of CaO or $CaCO_3$. Thermal activity is higher for the AFBC than for the PFBC residue, higher in bed overflow material than in entrained material.

The thixotropic character and the chemical oxygen demand (COD) due to the presence of large amounts of sulfite and the potential environmental impact due to trace elements are major environmental concerns for disposal of untreated FGD sludges. Leachate TDS, calcium, and SO_4 are concerns for both FBC and FGD residue disposal (also for natural gypsum if it were to be disposed of). Leachate pH is a concern for disposal of FBC solids and untreated FGD sludges.

Leaching characteristics are a function of final leachate pH. The effect of using CO_2-saturated water as the leaching medium is not pronounced for FBC residues because the resultant leachate pH is almost as high as in the deionized water leachate (pH = 9 to 12). Acetate buffer, however, results in a leachate with lower pH, arsenic, selenium, vanadium, fluoride, chloride, and SO_4, but increased boron, calcium, cadmium, cobalt, iron, potassium, magnesium, manganese, sodium, silicon, and strontium. These results suggest that care should be exercised in selecting the FBC residue disposal site to avoid persistent acid leaching conditions.

Soil Attenuation

Since the potential environmental impact of land disposal depends not only on the waste characteristics but also on site-specific factors such as hydrogeology and soil types, an investigation of soil attenuation was carried out, with the initial effort directed toward developing screening tests and determining attenuation by selected pure clay types (montmorillonite and kaolinite). The preliminary methods developed were continuous and intermittent shake tests parallel to those discussed in the previous section in order to utilize the abundant data on FBC leachates prior to their interaction with soils. Preliminary results on the attenuation effects of montmorillonite and kaolinite are shown in Figure 1. Attenuation effects (in some cases desorption effects) are seen on leachate pH, specific conductance, SO_4, calcium, sodium, and silicon.

Preliminary results demonstrate that the interaction between the leachates and the underlying soils can be an important factor affecting the environmental impact of land disposal.

Assessment

General trends have shown that the physical, chemical, and leaching properties of FBC residue before or after fixation are superior to those of the untreated FGD sludge for disposal and are comparable to those of the chemically and physically stabilized FGD residue from a conventional power plant. On the basis of our findings, we have concluded that the environmental impact of residue disposal will not be an obstacle to the commercialization of the FBC process.

IMPACT OF THE RESOURCE CONSERVATION AND RECOVERY ACT

The Resource Conservation and Recovery Act (P.L. 94-580, 1976) attempts to create a comprehensive scheme for regulating solid waste - hazardous and nonhazardous* - disposal. The assessment of the impact of the RCRA on FBC has been presented in a separate EPA report.[6] The key provisions of RCRA that could have the greatest impact on FBC residue disposal are Subtitle C on hazardous waste management, in particular the hazardous waste identification criteria under Sec. 3001, and Subtitle D, which regulates disposal of nonhazardous waste.

Impact of Hazardous Waste Identification Criteria on the Classification of FBC Residue (Subtitle C)

RCRA Sec. 3001 of Subtitle C requires EPA/OSW to promulgate criteria for identification of hazardous waste which OSW began to develop in 1977. On December 18, 1978, EPA formally proposed in the Federal Register[5] RCRA Sec. 3001 regulations which were scheduled to be promulgated in April 1980. An extraction procedure (EP) was proposed to determine the toxicity of a waste with 10 x the National Interim Primary Drinking Water Regulations (NIPDWR) of heavy metal elements as the hazardous criterion. According to the proposed Sec. 3001, a waste can be classified as hazardous either by being on EPA's hazardous lists or by possessing any of the proposed hazardous characteristics (Figure 2). The FBC residue is not on the lists and, therefore,

*Nonhazardous is used to identify a solid waste that does not qualify as hazardous; it is not used to imply an absence of environmental impact.

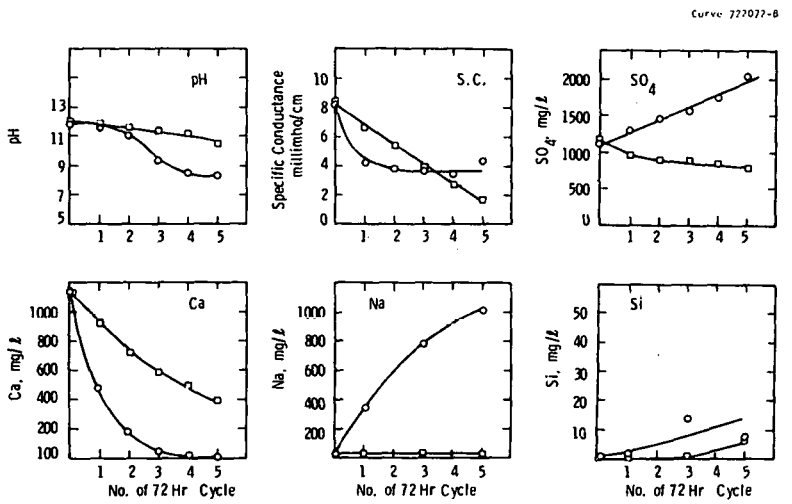

Figure 1 - Attenuation Effect of FBC Leachate by Montmorillonite (O) and Kaolinite (□) with Fresh Clay Materials for Each 5 x 72-hr Cycle

whether it is hazardous must be determined according to the criteria specified for the proposed hazardous characteristics - ignitability, corrosivity, reactivity, and toxicity. Of the four characteristics toxicity, for which EPA has proposed an EP and hazardous criteria (10 x NIPDWR), causes the most concern for FBC residue. Because of the large volume of waste and the limited data on their potential hazard, EPA has proposed a list of "special wastes" under Sec. 3004; "utility waste" is among these five special wastes. Should any FBC waste be determined as hazardous according to Sec. 3001, we would expect it to be classified as a utility waste under the special waste category and to be regulated with partial exemption from the cradle-to-grave regulations under hazardous waste management Sec. 3002 to 3005.

FBC residue is not ignitable, corrosive, or reactive according to the currently proposed criteria. To determine if it is toxic, 17 FBC residues representing different process variations, (AFBC and PFBC/PFBC adiabatic combustor, bed overflow/entrained material, with/ without carbon burnup cell, once-through/regenerative, limestone/-dolomite sorbent) together with reference materials (FGD residues, conventional ash, and raw sorbent) were tested using the RCRA/EP test. Results (Table 4) which showed the EP leachates to have silver, arsenic, barium, cadmium, chromium, mercury, lead, and selenium below ten times the primary DWS indicated the FBC residue should be classified as nontoxic and, thus, nonhazardous. The only exception in the EP leachate from 17 FBC residues is the leachate from a PFBC run with sorbent regeneration which had an average arsenic concentration of 0.94 ppm (the criterion for arsenic is 0.5 ppm). Although lower than the criteria, the level of chromium was much higher in three EP leachates than in all others - AFBC and PFBC fines (<15 μm) from the third cyclone and bagfilter and PFBC regenerator bed material had chromium concentrations in their EP leachates (0.15 to 0.4 ppm) much higher than the others and were close to the criterion for chromium, 0.5 ppm. Future investigations, therefore, should emphasize samples from these sources.

As there is no reason to believe that the FBC residues could contain chlorinated organic pesticides and herbicides, EP analyses for Lindane, Methoxychlor, Toxaphene, 2.4-D and 2.4.5-TP Silvex which were also proposed in Sec. 3001 were not performed.

Bioassays and testing for radioactivity are not included in the currently proposed identification methods for hazardous characteristics (ignitability, corrosivity, reactivity, and toxicity) and thus were not carried out in our investigation on FBC residues. However, EPA is considering expanding the hazardous characteristics to include radioactivity, genetic activity, bioaccumulation, and additional aspects of toxicity (Advanced Notice for Proposed Rulemaking, Federal Register, December 18, 1978).[5] There is still much uncertainty about, for

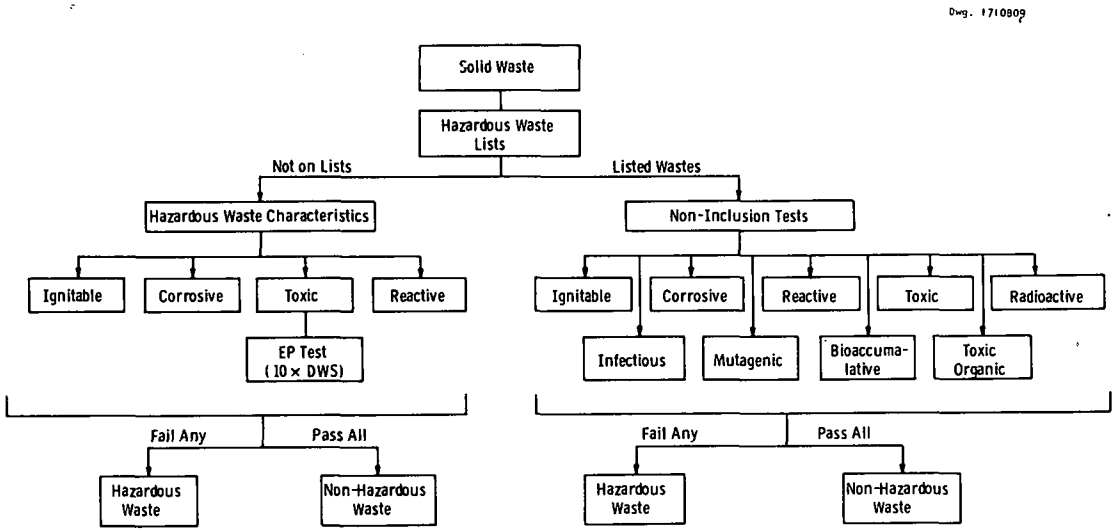

Figure 2 - Hazardous Waste Identification Mechanism

example, the compatibility of biological testing with the acetate-based EP leachate, the reliability of the various specified procedures (mutagenicity, bioaccumulation, aquatic toxicity, and phytotoxicity), and the interpretation of the results. Preliminary results from Oak Ridge National Laboratory (ORNL)[7,8] showed that FBC residue exhibited negative results in mutagenicity, in aquatic and phytotoxicity, and in metal elements, agreeing with our conclusion that the FBC residue is nonhazardous. ASTM D19.12 also carried out bioassay tests; results are less conclusive due to difficulties encountered in sample preparation, test procedures, and interpretation of test results.[9]

Impact of Nonhazardous Waste Disposal Regulations on FBC Residue Disposal (Subtitle D)

Since FBC residue appears to be nonhazardous according to the current RCRA Sec. 3001 definition, it would not be subject to the cradle-to-grave regulation under RCRA Subtitle C--Hazardous Waste Management. Instead, it would be regulated as a "Sanitary landfill" residue under Subtitle D--state and regional solid waste plans--which is almost as stringent in regulating site selection and disposal facility design, operation, and monitoring but is more relaxed in the requirements for the generation, transportation, and manifest system of the solid waste.

According to the current regulations promulgated on September 13, 1979,[10] eight criteria, including site selection and leachate monitoring, apply to the nonhazardous solid waste sanitary landfills, where FBC waste would most likely be disposed of. The most important issues among them that can affect the FBC residue disposal are the standards for ground-and surface water. Compliance with the RCRA and NPDES under the Clean Water Act (CWA) is required of sanitary landfill. Efforts by EPA are under way to consolidate the solid waste permit system. Since effluent guidelines for FBC units and FBC residue disposal facilities are currently unavailable, the best engineering practices for designing, operating, and managing the disposal facility will be needed to avoid potential adverse environmental effects. Table 5 shows leachate characteristics of a typical FBC residue generated by a 200-hr continuous shake test (which is based on equilibrium conditions and represents the worst-case leachates) and compares them to the NIPDWR and secondary drinking water standards (NSDWR).

Because FBC leachates meet the primary DWS, which consists of eight heavy metals, fluoride, and NO_3, the FBC residue disposal is expected to meet the current standards for sanitary landfill - groundwater at the "disposal facility boundary" meeting the NIPDWR. Should the secondary DWS (NSDWR) be included as they are currently proposed (Federal Register, September 13, 1979),[10] however, FBC leachate pH would be a major concern. A typical FBC leachate pH ranges from 9 to 12, while the pH of NSDWR is 6.5 to 8.5. The total dissolved solids and SO_4 are within 10 x DWS if a dilution/attenuation factor of 10 is assumed. The potential role of soil attenuation in controlling FBC leachate pH, TDS, SO_4, and calcium has been discussed in a previous section. Site selection and design of the disposal facilities are two important factors in preventing potential groundwater contamination.

Contamination due to trace metal elements and microbiological activity is not expected because the worst-case FBC leachate meets DWS. Radioactivity, if any, should be similar to that of a conventional power plant residue.

Other Aspects of the Impact of RCRA on FBC

RCRA may affect not only the technology and cost of FBC development, but also the siting of potential FBC facilities. The key aspects of the act that would influence siting are provisions for hazardous and solid waste disposal (Subtitles C and D) and provisions for resource recovery (Subtitle E). The potentially increased costs of

Table 4

Dwg. 1712859

LEACHATE CHARACTERISTICS (TRACE ELEMENTS) FROM RCRA/EP TEST

	Trace Elements, mg/ℓ									
Sample	Ag	As	Ba	Cd	Cr	Hg	Pb	Se	F	NO_3 (as N)
Battelle Bed	<0.02	0.001	<1	<0.01	0.09	<0.0005	<0.04	0.001	<1	<5
Battelle Carry-over, cyclone	<0.02	0.001	1	<0.005	0.06	0.0007	<0.04	<0.001	<1	1.6
MERC Carry-over, bag filter	<0.02	0.004	<1	<0.005	0.4	0.0008	<0.04	0.01	<1	15
PER Carry-over, CBC residue	<0.02	<0.001	<1	<0.01	0.04	0.0007	<0.03	<0.001	-	-
Argonne C_2/C_3 Bed	<0.02	0.023	<1	<0.01	0.02	<0.0005	<0.04	0.003	1.7	<5
Leatherhead Carry-over, Primary cyclone	<0.04	0.002	<1	<0.01	<0.05	0.0005	<0.04	0.007	<1	<1
Leatherhead Carry-over, 2nd cyclone	<0.04	0.012	<1	<0.01	<0.05	0.0021	<0.04	0.008	<1	<1
Exxon No. 73 Bed	<0.04	0.002	<1	<0.01	<0.05	<0.0005	<0.04	0.003	<1	<1
Exxon No. 73 Carry-over, 2nd cyclone	<0.04	0.002	<1	<0.01	0.06	0.001	<0.04	0.020	<1	<1
Exxon No. 73 Carry-over, 3rd cyclone	<0.04	<0.001	<1	<0.01	0.35	0.0022	<0.04	0.017	<1	<1
Exxon No. 67 Carry-over, 3rd cyclone	<0.02	0.007	<1	0.045	<0.02	0.0008	<0.04	0.005	<1	<1
Exxon No. 105 Combustor Bed	<0.02	<0.001	<1	<0.01	<0.05	0.0006	<0.05	<0.001	-	-
Exxon No. 105 Regenerator Bed	<0.02	<0.001	<1	<0.01	0.15	0.0015	<0.01	0.004	-	-
Exxon No. 105 Carry-over, 2nd cyclone	<0.02	0.68 to 1.13	<1	<0.01	<0.05	0.0019	<0.05	0.008	-	-
Exxon No. 105 Carry-over, 3rd Cyclone	<0.02	0.004	<1	<0.01	<0.05	0.0012	<0.05	0.007	-	-
Exxon No. 105 Regenerator Carry-over	<0.02	<0.001	<1	<0.01	<0.05	0.0014	<0.05	<0.001	-	-
Combustion Power P-403 Carry-over, baghouse	<0.02	<0.001	<1	<0.005	<0.02	0.0009	<0.04	<0.001	-	-
Untreated FGD Residue	<0.04	0.069	<1	<0.01	<0.05	0.0013	<0.04	0.017	4.2	≤1
Stabilized FGD Residue	<0.04	0.058	<1	<0.01	<0.05	0.001	<0.04	0.08	1.7	≤1
Fly Ash No. 1	<0.02	0.065	<1	<0.005	<0.02	0.0006	<0.04	0.02	<1	<1
Fly Ash No. 2	<0.02	0.005	<1	<0.01	0.03 to <0.05	0.0013	<0.03	0.009	-	-
Bottom Ash	<0.02	<0.001	<1	<0.01	<0.03	0.0011	<0.03	<0.001	-	-
Reference, dolomite sorbent	<0.02	<0.001	<1	<0.005	<0.02	0.0009	<0.04	<0.001	<1	<1
Reference, natural gypsum	<0.02	0.001	<1	<0.005	<0.02	0.0011	<0.04	<0.001	<1	1.4
Criterion, 10x NIPDWR	0.5	0.5	10.0	0.1	0.5	0.02	0.5	0.1		

- = not analyzed

▨ = exceeds 10 X NIPDWR

transportation and disposal of the waste brought on by RCRA as well as the marketability and transportation costs of the products (should FBC residue be utilized) will play an important role in siting FBC facilities. Also, in light of the public awareness created by RCRA, public support or opposition is becoming increasingly more important in siting decisions for fossil-fuel energy facilities, such as FBC, that create large quantities of solid wastes.

The economics of FBC systems are affected by the total cost of sorbent,[11] including purchase, transportation, and disposal. The major increase in disposal cost potentially resulting from RCRA is expected to be associated with disposal site selection and transportation. The response of FBC economics to total sorbent cost may lead FBC developers to consider more seriously alternatives that reduce the total amount of sorbent required (i.e., Ca/S ratio),[12] and potential residue utilization. In summary, RCRA may have a sufficient technical and cost impact on FBC residue disposal to require engineering and economic evaluation of residue disposal to be incorporated into the development of successful FBC systems.

FBC RESIDUE PROCESSING FOR DISPOSAL OR UTILIZATION

The quantity of FBC residue from large-scale industrial and utility applications makes the utilization of the residue attractive from the environmental and resource utilization perspective.[13] For a 4 percent sulfur, 10 percent ash coal the total residues are in the range of 1/4 to 1/2 lb/lb

Table 5

Dwg. 1712B57

COMPARISON OF A TYPICAL FBC LEACHATE WITH THE DWS (Leachate Generated by 200-hr Shake Method)

Substance	FBC Leachate, mg/ℓ	DWS, mg/ℓ	
		NIPDWR	NSDWR
Al	0 to > 2		
Ag	< 0.05	0.05	
As	< 0.05	0.05	
B	0 to > 5		
Ba	< 1	1.0	
Be	< 0.02		
Bi	< 0.04		
Ca	> 500		
Cd	< 0.01	0.01	
Co	< 0.1		
Cr	< 0.05	0.05	
Cu	< 1		1.0
Fe	< 0.3		0.3
Hg	< 0.002	0.002	
Mg	< 30		
Mn	< 0.05		0.05
Mo	< 5		
Na	0 to > 100		
Ni	< 0.1		
Pb	< 0.05	0.05	
Sb	< 0.5		
Se	< 0.01	0.01	
Si	0 to 30		
Sn	< 1.0		
Sr	0 to > 10		
Ti	< 2		
V	< 1		
Zn	< 3		5.0
Zr	< 1		
SO_3	< 10		
SO_4	1000-2000		250
Cl	< 250		250
F	< 2.4	2.4	
NO_3 (as N)	< 10	10.0	
TOC	< 30		
pH	9 to 12		6.5-8.5
TDS	2000 to 4000		500
Specific Conductance millimho/cm	0.5 to 10.0		
Color	None		15 color units
Odor	None		3 threshold odor number
Foaming Agents	None		0.5
Radioactivity	Not determined	5 pCi/ℓ Ra 226 & 228	
Biological Activity	None	4 coliform/ 100 mℓ	

▨ - exceeds DWS

coal. On a volume basis this is equivalent to 75 to 150 acre-feet per year from a 200 MWe plant.

Utilization of the residues could be preferable to disposal since the former should provide better environmental protection, improved resource utilization, and energy conservation. Options have been identified previously[4] and include landfill, soil stabilization, road base construction, aggregate, and cement manufacture. This list of end uses includes only those for which a secondary residue is not created. All of them have the advantage of filling a need that is widely distributed geographically, thus reducing the constraint of transportation costs. Landfill constitutes a base option insofar as its structural and other requirements are expected to be more easily met than those of the other options. Soil stabilization, aggregate, and road base construction appear to be large markets, although the last appears more constrained by its specificity. Cement manufacture also has at least one compositional constraint: its sulfate content.

Whether FBC residues are utilized or deposited in the environment, contact with water may result in leachates containing excessive amounts of $CaSO_4$ and $Ca(OH)_2$. Trace elements, however, do not appear to be a problem, although in acid environments they may be. Consideration of these findings led to work reported previously in which the concept of forming the granular residues into larger masses was proposed.[3] The underlying principle is reduction of the surface-to-volume ratio on the hypothesis that the leach rate should be directly related to surface area. Disposal to the environment implies contact with the soil and natural waters and, hence, generation of leachates that may permeate such soil and then enter groundwater systems. Various barriers to such movement have been proposed, such as clay liners and synthetic membrane liners. The performance of all of these, however, is subject to question. Thus, one is led again to consider fixation of the residues in larger masses to protect the environment.

The previous work showed not only that FBC residues could be processed to larger sizes (5-cm cubes, in this case), but that these cubes also had significant compressive strength (up to 15 MPa or 2175 psi).

An immediate question is whether these larger masses would retain structural integrity under environmental conditions. The worst case would be reversion to granular form. Lesser forms of degradation would be cracking and spalling. Ideally, such changes would occur not at all or over a long period of time so that the rate of exposure of new surface to leaching would be acceptably slow.

A second question is whether the rate of leaching from these larger masses is indeed lower than that of the as-produced granular form. This question will be addressed first.

Leach Rate with Processed Residue

Further perspective on the environmental impact of converting FBC residues to larger masses is obtained by analysis of selected data on leaching of raw and processed residues from Run 27 at the Exxon miniplant.[3] The test specimens are described in Table 6. The data on intermittent leaching, in which test materials were agitated in water for fifteen 72-hour periods using fresh deionized water for each period, were used to calculate the amounts of calcium extracted in terms of milligram moles per period.[3] These were cumulated and plotted against time, expressed as number of extraction periods, as shown in Figure 3 for specimen IlD. This was for a 5-cm cube containing about 36 wt % carry-over on total solids, which was an estimate of the production proportions of entrained and bed overflow material with a pilot plant. Such leaching data may be considered a simulation of

Table 6

Dwg. 7721A93

CONSTANTS IN THE EMPIRICAL CORRELATION OF CUMULATIVE CALCIUM LEACHED VERSUS NUMBER OF EXTRACTIONS

Specimen Number	Description of Specimens				Constants		
	Carry-over, total solids	Water, total solids	Curing Time, days	Form	L_0	b_1	b_2
11D	0.358	0.445	7	5-cm Cube	27.954	0.29718	2.266
114D'	0.100	0.300	60	5-cm Cube	27.371	0.30930	1.934
114d	0.100	0.300	60	Crushed Cube	26.637	0.22848	7.113
SBM[a]	–	–	–	Raw Granule	11.746	0.29062	1.458

[a]Spent bed material from Run 27, Exxon miniplant

repeated rainfalls on residues placed in the environment, if one assumes a fixed water/residue ratio and 100 percent efficiency of contacting.

The data are presented on a normalized basis in Figure 4, which was obtained by dividing each of the ordinate values of Figure 3 by the weight of the specimen involved. Figure 4 shows the substantial reduction in leaching obtained by fixation (Samples I1D and II4D' vs SBM). It also shows that crushing the cubes results in material from which more calcium can be leached than from the raw residue.

Empirical equations of the following form were fitted to the curves of Figure 3:

$$L_T = L_0 (1 - e^{-b_1 N}) + b_2 N$$

where L_T = total calcium leached after N extractions, mg-moles, N = number of 72-hour extractions and L_0, b_1, and b_2 are constants. The data for four sets of results are shown in Figure 3. At 1080 hours of leaching, leach rates had decayed to a linear form:

$$\frac{dL_T}{dN} = L_0 b_1 e^{-b_1 N} + b_2 \sim b_2 .$$

Fixation may aid environmental protection, provided the constant b_2 is small enough. Table 6 summarizes numerical values for the constants for the four different test materials.

To facilitate comparisons, normalized rates at two different times were calculated: the initial rate and the rate at 1080 hours (15 extractions). The results are in Table 7 in terms of mg-moles Ca/g sample-hr. As to initial rates, forming the residues into 5-cm cubes reduced the leach rate by a factor of 3. Crushing the cube to powder resulted in an increase in leach rate, but only to about 80 percent of that of the unprocessed material. As to long-term rates, in all four cases attenuation with time was demonstrated, with

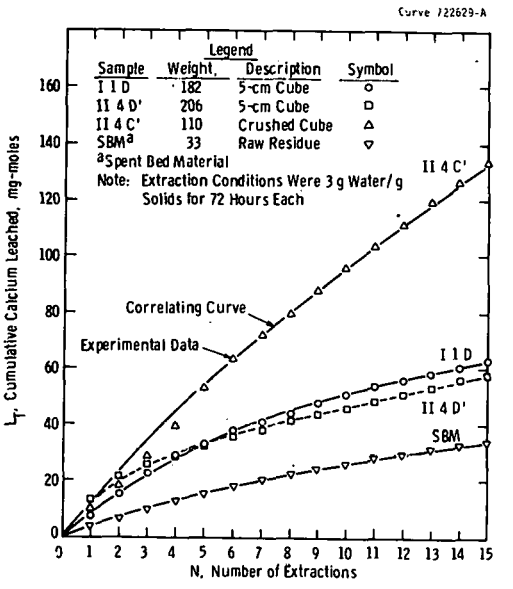

Figure 3 - Leaching of Calcium from Exxon Spent Sorbent/Carry-Over Compacts

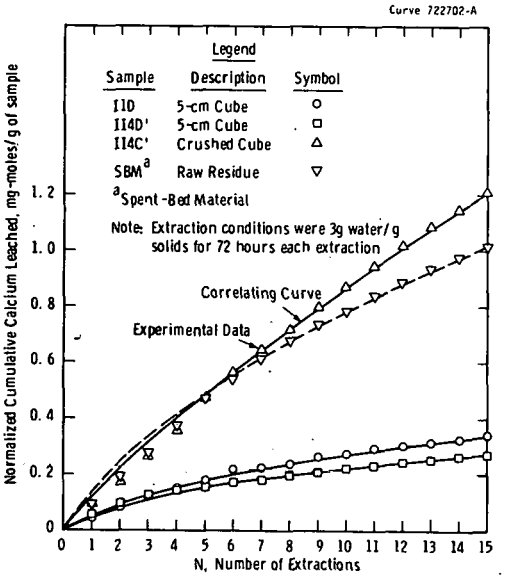

Figure 4 - Leaching of Calcium from Exxon 27 Spent Sorbent/Carry-Over Compacts

the greatest reduction (factor of 5) occurring for specimen II4D', which had been cured the longest (60 days) before testing.

The average particle size for spent-bed material as received was about 1200 μm. It should, therefore, have had about 40 times the surface area of a 5-cm cube, yet its leach rate was only three

Table 7

CALCULATED LEACH RATES FOR PROCESSED FBC RESIDUES

Dwg. 7721A94

	Sample		Identification	
	14D	II 4D'	II 4C'	SBM
Sample weight, g	182	206	110	33
Leach water, g/extraction	546	618	330	100
Sample Composition, wt %				
Spent-bed material	44.4	69.2	69.2	100.0
Carry-over	24.8	7.7	7.7	–
Water	30.8	23.1	23.1	–
	100.0	100.0	100.0	100.0
Total Ca	11.6	15.7	15.7	21.8
Leach Rate, μg moles Ca/g sample-hr				
0 hours	0.807	0.701	1.667	2.050
1080 hours	0.180	0.136	0.923	0.632
Leach Rate, mg moles Ca/m^2- hr				
0 hours	11.75	11.56	–	–
1080 hours	2.62	2.24	–	–

to five times as great. It is possible that grinding the spent-bed material as one of the processing steps may make the material more susceptible to leaching, even after fixation, or that mass transfer resistances are not controlling the overall leaching process.

These results can be used to provide perspective on the limiting leach rate from unprocessed and processed materials. To illustrate the differences with an idealized case, one may visualize a mass 10 m high by 100 m long by 100 m wide, which might be accumulated in one year from operation of a 200 MWe FBC plant. We assume the mass to be essentially impermeable. We also assume that no significant fissuring of the slab will occur. The area effectively contacted by continuous water flow is probably only the top and at most the four vertical sides: 14,000 m^2. One may visualize a stagnant layer of saturated leachate along the bottom face. Using a leach rate of 2.24 mg-moles calcium/m^2-hr from Table 6, the calculated amount of solute lost from the mass is 4.3 kg/hr, expressed as $CaSO_4$. This rate should attenuate with time for two reasons: the surface area should decrease, and, since the mass is not all soluble calcium, diffusional resistance should increase. If, however, the rate did not decrease from that at 1080 hours and the mass was all $CaSO_4$, complete solution would require 3500 years. In contrast, the unprocessed residue if contacted continuously with water would be dissolved in less than two years since the calculated solution rate is 11.2 Mg/hr.

There is another important constraint, however: the quantity of rainfall available. Any residue deposit will presumably be designed so that precipitation on contiguous areas will be diverted from contact with the deposit. The average rainfall in the U.S. is 1.5 m/yr. If we assume that a saturated solution of $CaSO_4$ (3000 ppm) is formed, complete solution of the above mass would require 3000 years, with unprocessed or processed material.

A further constraint is the effectiveness of leaching. The laboratory data at 1080 hours indicate a concentration of perhaps only 100 mg Ca/ℓ for the processed residue which is equivalent to 340 mg $CaSO_4$/ℓ. This is well below 10 x DWS (2500 mg/ℓ) and with modest improvement could be within the DWS itself. Without fixation the concentration would be six times greater but still unsaturated and below 10 x DWS.

Placing FBC residues in the environment in any form, therefore, means making a source of substances such as $CaSO_4$ and $Ca(OH)_2$ available for leaching by environmental waters for a very long time. The significance of processing the residues to monolithic masses is that the rate of leaching is reduced by reducing the effectiveness of contacting.

Actual results will depend on specific site conditions and further tests to determine fixed material performance. The available data however, demonstrate the potential for reducing the leachate rates into the groundwater. Thus, processing of residues into monolithic masses offers an option that can reduce the environmental impact if required by specific site considerations or regulations.

Environmental Stability

As a partial answer to the question of environmental stability, one test, freeze-thaw (F/T) resistance, was selected. Other tests were considered but were assigned a lower priority. Wetting and drying would be included to some extent in F/T testing. Autoclave expansion, to check for deleterious effects of hydration, was considered a severe test by Paul Brown of the National Bureau of Standards,[14] and it was therefore deferred as probably less representative of field conditions than F/T. Sulfate resistance was also deferred, but on the basis of being less significant geographically than F/T resistance.

The actual test procedure was adapted from ASTM C-666, Resistance of Concrete to Rapid Freezing and Thawing.[15] Specimens were placed in an insulated chamber (see Figure 5) through which was circulated air that was alternately cooled by dry ice and heated by electricity. Cycle times averaged 36 minutes for freezing and 78 minutes for thawing.

The test specimens were 1.8 cm in diameter and 3.7 mm long and were cut from longer cylinders prepared by isostatic pressing, a procedure for exerting a hydrostatic pressure of 138 MPa (20,000 psi) for 60 s uniformly over the surface of a powder placed in a special mold. The powders used were various FBC residues previously ground to 100 percent through 63 μm (No. 230 U.S. Sieve). (We had intended to test spent bed material and carry-over blended in production proportions, but at the time

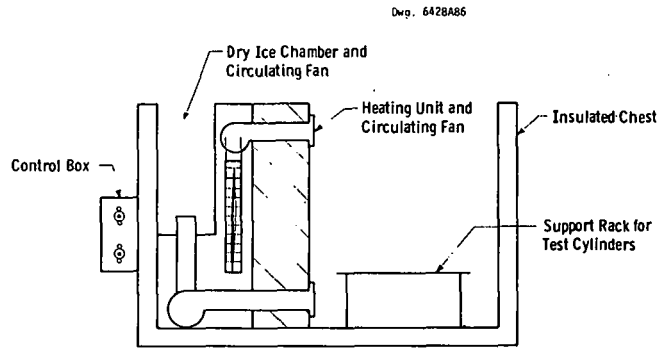

Figure 5 - Schematic of Freeze/Thaw Chamber

of testing only the Exxon miniplant could supply both of these materials. As an alternative to carry-over, fly ash from the Duquesne Light Company was tried as a substitute for carry-over, but the specimens crumbled on curing.) These initial tests, therefore, were carried out on pressed bed material only. Bed materials from three pilot plants were used: Exxon, Babcock & Wilcox, and Pope, Evans and Robbins. Control specimens were carried through the test period outside the freeze-thaw chamber. Portland cement alone and in admixture with river sand was used to make reference specimens. Outside control specimens of these materials were also used.

Following isostatic pressing, the specimens were cured under water for 24 hours, cut to the desired lengths, and then cured further under water for a total of 14 days.

The effect of freeze-thaw cycling was observed by measurement of the comprehensive strength of the cylinders in triplicate at four different exposure times: 0, 12, 36, and 300+ cycles. The data summarized in Table 8 are for the final values of compressive strength and may be expressed as follows.

1. The Portland cement specimens showed the greatest resistance to freeze-thaw cycling (FTC) as judged by compressive strength. Exposure to FTC was associated with development of 8.2 percent lower compressive strength relative to the controls.

2. The Portland cement/river sand test specimens developed the next highest compressive strength. Exposure to FTC was associated with development of 8.6 percent greater compressive strength relative to the controls, which is in contrast to the response of the cement specimens.

3. Compressive strengths for the pilot-plant test specimens were comparable to those for the cement/sand specimen.

4. Exposure to FTC was associated for all three plant specimens with development of greater compressive strengths than in the unexposed controls. This is also in contrast to the response of the cement specimens.

Table 8

EFFECT OF FREEZE-THAW EXPOSURE ON THE COMPRESSIVE STRENGTH OF ISOSTATICALLY PRESSED CYLINDERS OF FBC SPENT BED MATERIAL

Specimen	Control Specimens		Exposed Specimen		% Change in Strength
	MPa	psi	MPa	psi	
Portland Cement	101.8	14767[b]	93.4	13550[b]	- 8.2
Portland Cement + River Sand	75.1	10897	82.2	11927	+ 8.6
B&W	75.3	10917	76.3	11070[c]	+ 1.4
Exxon	56.8	8237	83.7	12140	+ 47.4
PER	66.0	9567	82.5	11960	+ 25.0

a All specimens were carried through 317 cycles except as noted

b 172 cycles

c 342 cycles

In all cases development of compressive strength was monotonic. Figure 6 is a typical curve. At the end of the test period, none of the specimens showed any evidence of deterioration. We concluded that the process of grinding spent bed material to -63 μm, compressing it dry at 20,000 psi for 1 minute, and then curing under water for 14 days resulted in specimens with 1) higher compressive strength than for ordinary concrete and 2) substantial resistance to freeze-thaw cycling. For commercial application, briquetting may be a more practical way of applying pressure rather than the batch type isostatic pressing.

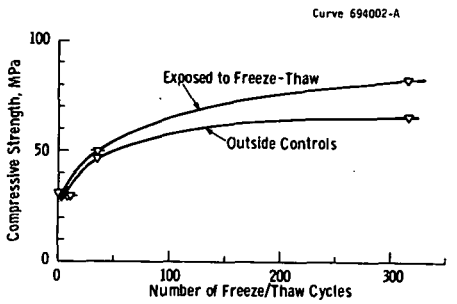

Figure 6 - Freeze-Thaw Resistance of Isostatically Pressed Cylinders of PER Spent FBC Sorbent

CONCLUSIONS

The foregoing data and analyses support the following conclusions with respect to environmental impact:

- FBC residue disposal will not be an obstacle to commercialization of FBC.
- FBC residues are nonhazardous on the basis of RCRA tests.

- The potential concerns in FBC residue disposal are:
  - Their chemical impact: pH, TDS, SO_4, Ca
  - Their thermal activity.
- Low-temperature processing reduces environmental impact since:
  - Stable compacts are formed.
  - Fixation reduces both the concentration of solutes and their rate of leaching.
- Low-temperature pressed residues have the potential for utilization (e.g., aggregate). This processing also protects the environment. Tests have demonstrated compressive strengths of 76 to 84 MPa following >300 freeze-thaw cycles.
- Disposal options are available for meeting specific applications, site requirements, and environmental impact constraints.

REFERENCES

1. Keairns, D. L., et al., Fluidized Bed Combustion Process Evaluation, Phase II - Pressurized Fluidized Bed Coal Combustion Development, Report to EPA, Westinghouse Research and Development Center, September 1975, EPA-650/2-75-027c, NTIS PB 246-116.

2. Sun, C. C., C. H. Peterson, R. A. Newby, W. G. Vaux, and D. L. Keairns, Disposal of Solid Residue from Fluidized-Bed Combustion: Engineering and Laboratory Studies, Report to EPA, Westinghouse Research and Development Center, Pittsburgh, PA, March 1978, EPA 600/7-78-049, NTIS PB 283-082/6ST.

3. Sun, C. C., C. H. Peterson, and D. L. Keairns, Experimental/ Engineering Support for EPA's FBC Program: Final Report, Volume 3, Solid Residue Study, Report to EPA, Westinghouse Research and Development Center, Pittsburgh, PA, January 1980, EPA 600/7-80-015c.

4. Sun, C. C., C. H. Peterson, and D. L. Keairns, Environmental Impact of FBC Residue Disposal. Proceeding of the 5th International Conference on Fluidized Bed Combustion, Washington, DC, December 12-14, 1977, McLean, VA: The Mitre Corporation, 1978.

5. Environmental Protection Agency, Hazardous Waste: Proposed Guidelines and Regulations and Proposal on Identification and Listing, Federal Register, December 18, 1978.

6. Sun, C. C., R. A. Newby, and D. L. Keairns, Impact of RCRA on FBC Residue Disposal, Report submitted to EPA, Westinghouse Research and Development Center, Pittsburgh, PA, April 1980, Contract 68-02-3110.

7. Epler, J. L., et al., Toxicity of Leachates, Report to DOE and EPA, Oak Ridge National Laboratory, Oak Ridge, TN.

8. Francis, C. W., M. P. Maskarinec, J. L. Epler, and D. K. Brown, The Utility of Extraction Procedures and Toxicity Testing with Solid Wastes, submitted to: Annual Symposium on Solid and Hazardous Waste, Chicago, IL, March 17-20, 1980.

9. Hanson, D. M., Testing Program for Assessment of Hazardous Waste Characteristics Under Section 3001 of the Resource Conservation and Recovery Act, in ASTM D19.12 Presentation, presented at Ft. Lauderdale, FL, January 1980.

10. Environmental Protection Agency, Criteria for Classification of Solid Waste Disposal Facilities and Practices; Final, Interim Final, and Proposed Regulations, Federal Register, September 13, 1979.

11. Newby, R. A., N. H. Ulerich, E. P. O'Neill, D. F. Ciliberti, and D. L. Keairns, Effect of SO_2 Emission Requirements on Fluidized-Bed Combustion Systems: Preliminary Technical/ Economic Assessment, report to EPA, Westinghouse Research and Development Center, Pittsburgh, PA, October 1978, EPA-600/7-78-163.

12. Newby, R. A., et al., An Assessment of Advanced Sulfur Removal Systems for Electric Utility AFBC, presented at the 6th International Conference on Fluidized Bed Combustion, Atlanta, GA, April 9-11, 1980.

13. Peterson, C. H. and D. L. Keairns, Processing FBC Spent Sorbent for Improved Resource Utilization and Reduced Environmental Impact. Presented at the Sixth National Conference on Energy and the Environment, Pittsburgh, PA, May 1979.

14. Brown, P. W., et. al., Energy Conservation through the Facilitation of Increased Blended Cement Use, Prepared for ERDA, Institute for Applied Technology, National Bureau of Standards, Washington, D.C., Interim Report July 1-Dec. 1, 1975, NBSIR 76-1008, NTIS PB 251-218.

15. ASTM Annual Book of Standards, Part 10, 1973, American Society for Testing and Materials, Philadelphia, PA.

NOMENCLATURE

AFBC	- atmospheric fluidized-bed combustion
ANL	- Argonne National Laboratory
B&W	- Babcock & Wilcox
COD	- chemical oxygen demand
DWS	- drinking water standard
EDX	- energy dispersive analysis by x-ray

EMA - electron microprobe analysis

EP - extraction procedure

FBC - fluidized-bed combustion

FGD - flue-gas desulfurization

F/T - freeze/thaw

FTC - freeze-thaw cycling

L_{O,b_1,b_2} - constants

L_T - total calcium leached, mg-moles

MERC - Morgantown Energy Research Center

N - number of 72-hr extractions

NIPDWR - National Interim Primary Drinking Water Regulation

NSDWR - National Secondary Drinking Water Regulations

ORNL - Oak Ridge National Laboratory

OSW - Office of Solid Waste

PER - Pope, Evans and Robbins

PFBC - pressurized fluidized-bed combustion

RCRA - Resource Conservation and Recovery Act

SEM - scanning electron microscopy

TDS - total dissolved solids

TEP - toxic extraction procedure

TGA - thermogravimetric analysis

TOC - total organic carbon

ACKNOWLEDGEMENT

This work was performed under Contract 68-02-3110 and 68-02-2132 for IERL of EPA. We should like to acknowledge the contributions of D. B. Henschel, the contract officer. We should also like to acknowledge the project management and consultation of D. L. Keairns and R. A. Newby of Westinghouse Research and Development Center.

Our special thanks go to J. T. McAdams and L. Thomas for their technical assistance in carrying out the laboratory experiments. We also express our appreciation to many members of the Analytical Chemistry, Physical Metallurgy, Biology, and Ceramic Departments within the Westinghouse Research and Development Center for their valuable contributions in sample preparation and characterization.

UTILIZATION OF THE BY-PRODUCTS FROM FLUIDIZED BED COMBUSTION SYSTEMS

L. John Minnick, Research Consultant
Richard H. Miller, Valley Forge Laboratories, Inc.
Devon, Pennsylvania

The current interest in the United States to find commercial uses for process waste is a result of a number of major national concerns that have emerged during the last decade. These include the need to keep America self-sufficient by cutting down on imported raw materials, to provide alternate materials to compensate for the rapid depletion of virgin resources, to establish commercial programs to provide a reduction in energy requirements, and alleviation of serious health and environmental problems resulting from unmanaged disposal practices.

Fortunately, numerous technologies are available to assist in resolving these concerns, particularly as relating to use and conservation of large scale process waste from utilities (fly ash, bottom ash, lime/limestone scrubber sludge). This would also encompass the use of by-products from fluidized bed combustion, iron and steel production, mining of basic materials, and incineration.

This paper is directed primarily to applications of available technologies to the by-products produced from atmostpheric fluidized bed (AFB).

Just what are these by-products? They are the spent bed material (hereafter referred to as AFB residue) and fly ash. The AFB residue is a granular material with a salt and pepper appearance (Figure 1). Some particles are readily friable and can be crushed with moderate finger pressure. The typical gradation, shown in Figure 2, is similar to that of a fine aggregate (ASTM C-33). Other significant characteristics of the material are its free lime content, level of reactivity, and cementitious properties. The free lime content may be as much as 30 percent by weight. In most cases, the lime is very reactive and responds to the addition of water in much the same manner as a quicklime. Heat is generated and moisture is driven off in the form of steam. Previously reported information on the cementing potential* as demonstrated by the compressive strength of compacted cylinders showed that strengths as high as 4000 psi were obtained after 28 days of curing.

The fly ash is a considerably finer material with up to 98 percent passing the #200 sieve in some samples. It is relatively inert when compared to the spent bed material although some recent samples contained approximately 32 percent of CaO and were moderately reactive.

There are numerous potential applications for the AFB residue and/or fly ash. They include the following:

CONSTRUCTION APPLICATIONS

- Land reclamation
- Synthetic aggregates
- Structural compositions -

Road base	Masonry units
Embankments	Fish reefs
Dikes	Jetties
Structural fill	Gabions
Pond & lagoon Liners	Cement Replacement

CHEMICAL USES

- Treatment of trade waste
- Treatment of municipal waste
- Acid mine drainage control
- Sorbent for SO_x scrubbers
- Reagent for stabilizing industrial sludges
- Hydrated lime replacement

*R.H. Miller, Sr., "Potential Uses for the Residue from the Fluidized Bed Combustion Process", Proc. of Fifth Int'l Conference on Fluidized Bed Combustion, sponsored by U.S. Dept. of Energy, 1977 pp. 800-816

OTHER USES

- Co-disposal with other process waste
- Conditioning of materials for waste disposal to provide low permeability and general environmental acceptance as means of managing hazardous materials.

AFB RESIDUE AS A COMPONENT OF MASONRY UNITS

On two occasions, masonry block were manufactured at a commercial block plant. On January 28, 1978, approximately seven hundred 8" by 8" by 16", 2 core, blocks were made in a Besser machine at the Kurtz Brothers plant in Ephrata, Pennsylvania. On January 26, 1980, approximately 250 additional blocks were made, again with a Besser machine, at the Calcite block plant in Lebanon, Pa. Some of the blocks that were produced during these trial production runs are shown in figures 3 and 4.

High quality blocks were made from compositions in which approximately 40% of the aggregate was replaced with a combination of AFB residue and bituminous coal fly ash. These blocks were lighter in color and had a finer texture than those made from control mixes. In addition, their compressive strength one year after was twenty-five percent higher than the controls. Composition and compressive strength data for these mixes are given in Table I.

The Alexandria AFB residue that was used in the second masonry block production run was pretreated. The pretreatment is described in the section "Pretreatment of AFB Residue" later in this report. The pretreated residue was stored in an aggregate bin at the block plant and subsequently weighed and batched with conventional equipment. With a moisture content between 4 and 19 percent, the residue resembles and handles like a moist, fine aggregate.

Blocks were produced from a number of compositions in which various percentages of aggregate, AFB residue, bituminous coal fly ash, and cement were used. The compositions and properties of the more successful mixes and the controls are shown in Table II. The properties of the block were compared with the ASTM Standard Specifications for Hollow-Load Bearing Concrete Masonry Units and Non-Load Bearing Concrete Masonry Units, ASTM C90 and C129 respectively. The comparisons are shown in Table III.

It is evident that acceptable masonry units can be made utilizing AFB residue in the mix. As with the use of conventional materials, the properties of the resulting blocks depends upon the design of the mix.

UTILIZATION OF AFB RESIDUE IN A VENTURI SCRUBBER

AFB residue was used successfully as the sorbent in a wet scrubbing system to remove SO_2 from the flue gases from a chain grade stoker fired boiler. The boiler burned Illinois bituminous coal and was rated at 80,000 lbs. of steam per hour. A diagram of the scrubbing system is shown in Figure 5. SO_2 removal efficiencies of up to 88.9% were achieved. Scrubbing of the flue gas with commercial lime resulted in 90% SO_2 removal. It is believed that higher efficiencies can be obtained if the availability of the reactive lime in the AFB residue is improved. Crushing of the residue prior to use will produce this improvement.

A five percent solids stream was bled off from the scrubbing system and sent to a five foot diameter thickener where the solids were increased to ten percent. This slurry was then pumped to a rotary vacuum filter where the solids content was increased to thirty-six percent. The composition of the resulting sludge is shown in Table IV.

The only significant difference between the composition of this sludge and that resulting from the usual lime scrubbing is that it has somewhat more unreacted CaO than the usual lime sludge.

The sludge from the scrubber was then mixed with various combinations of AFB residue, grits*, and fly ash to form a stable composition that could serve as a structural fill. Compressive strength of cylindrical samples averaged 20 to 35 lbs. per sq. in. when the sludge was combined with the grits or the AFB residue. When fly ash was added, the strength was increased to 40 to 60 lbs. per sq. in. Comparable strengths would be obtained for a hard clay (60 psi), a very stiff clay (35 to 40 psi), and a stiff clay (20 psi).

Prior to introducing the AFB residue into the scrubbing system it was slaked in a tank equipped with a lightning propeller type mixer. Steam was also used to help agitate the mixture as the residue

*Grits is the coarse fraction of the AFB residue that settled out when the residue was put into slurry form.

was added slowly to the water. During this procedure the heavier particles (grits) settled out. The slurry was pumped off and used as the sorbent. The grits contained unextracted lime as evidenced by a temperature rise up to 212° F due to continued slaking after they were removed from the tank.

This demonstration showed that the AFB residue used as the sorbent performed in a manner identical to a system using hydrated lime. If the AFB residue were used in the same condition as when it exits the boiler, as much as three times the lime requirement might be needed to accomplish the scrubbing. Beneficiation of the residue, however, would result in a much improved efficiency. Beneficiation would include crushing, slaking, and subsequent separation of the lime-rich fraction.

PRETREATMENT OF AFB RESIDUE

The feasibility of processing large quantities of AFB residue on a production scale was demonstrated at the ash processing facility of the American Admixtures Corporation in Chicago, Illinois. This facility is routinely used to process high calcium lignite and sub-bituminous fly ash prior to distribution to the ready mix concrete industry in the Chicago area. The process involves the addition of water to the ash, stockpiling, and then recrushing.

Several pilot runs were made using approximately 2½ tons of AFB residue for each run. Between 25 and 32 percent water was added to a residue that had been stored under cover for several months. The addition of water was accompanied by a sudden generation of heat that caused steam to be formed. The consistency of each mixture, following the addition of water, was that of a slurry. Hydration continued, however, and the final product was quite similar to a moist sand. A slightly larger (3½ tons) batch of residue was put through a crusher before the water was added. The crusher reduced the particle size of the residue until there was 100 percent finer than the #10 sieve. The addition of 20 to 25 percent moisture to the crushed material then produced the same result as before.

The processed material was then returned to a stockpile for future use.

The type of equipment required for this operation is consistent with that generally used in mixing plants. Figures 6 and 7 show a stockpile and a close-up of the AFB residue as it appeared after being brought from storage. It is necessary to use a pneumatic blower truck to load the residue into a silo. Figure 8 shows the residue being dumped into a hopper from which it is loaded into the blower truck by way of a conveyor (Figure 9). From the blower truck, the residue goes to the silo and thence to a pugmill where the water is added. The processed residue is then transported by a conveyor (Figure 10) to either further treatment (such as a crusher), to a stockpile, or into a truck for distribution. Figure 11 shows a small stockpile of AFB residue immediately after it was processed. Steam coming from the pile is clearly visible.

Similar processing was done at the plant of John D. Tonkovich and Son, Inc. in Shadyside, Ohio. This plant has been used for preparing lime/fly ash/aggregate mixtures for road base. The mixing operation employs a Barber-Greene pugmill with a capacity of 400 tons per hour. A third processing demonstration was performed utilizing a concrete mixing truck. Water was added and mixed with approximately 5 tons of AFB residue in several experimental batches. The processing was accomplished successfully, with several of the batches, but the almost explosive generation of heat and steam accompanying the addition of water again emphasized the necessity for careful control of the operation. In the first trial, approximately 5 barrels of AFB residue were loaded into the mixing truck. Forty percent of water by weight at 110° F were added and after one minute, a large volume of steam issued from the truck and continued for several minutes. After five minutes of continuous mixing, the mix temperature was 180°F. and the moisture content of the residue was 18 percent. The mixing of the second batch was much the same as the first, except that the moisture content after five minutes was 4.8 percent. In the third batch, water was added after the initial five minute mixing period in order to increase the moisture content of the processed residue to between 10 and 15 percent. This addition of water considerably increased the cohesion of the mass so that it was impossible to remove from the truck by ordinary means. A fourth batch was processed, after cooling down the truck, with no apparent difficulty.

ROAD BASE

The cementitious property of AFB residue suggested, at an early date, that an ideal use for the material (in combination with fly ash and aggregate) would be as a stabilized road base or a structural fill. Its use as a stabilized base involves the mixing of the component materials with a controlled amount of water; depositing it in a non-plastic condition on a prepared

subgrade; compacting it to a predetermined density and covering with one or more layers of bituminous concrete depending on the particular application. As a structural fill, AFB residue can be used alone or in combination with a wide variety of other materials, such as: fly ash, soil, and sludge. In this way, it has potential for use in land reclamation, for highway and airfield construction, and in other situations where a fill capable of supporting substantial loads is required.

Compressive strengths of as much as 4000 psi at 28 days were obtained from some compositions. This indicated that there was ample strength for many structural applications, including road bases. In addition, the compositions showed that there was a substantial increase in strength at 28 days compared to the strength at 7 days - a characteristic typical of portland cement concrete. Freeze-thaw testing also showed excellent durability of the material. Less than one percent of the material was lost by wire brushing after twelve freeze-thaw cycles and a residual strength of 1700 psi was maintained. One characteristic that was not detected in early laboratory work was a tendency for detrimental expansion to occur for mixes with high residue content or with a high ratio of AFB residue to fly ash. Unfortunately, this property caused what appeared otherwise to be a successful road base demonstration to be aborted.

In the Fall of 1978, a 190 ft. long section of 6-inch road base, 25 ft. wide, was placed on State Route 3, five miles west of Bellaire, Ohio. Except for one small section that was placed with material that was too wet, the construction was carried out without difficulty. The operation involved processing of the AFB residue; mixing of the residue with bituminous coal fly ash, and aggregate; placing and spreading on the roadway, and compacting and finishing to final grade. Three experimental mixes were used. The composition of these mixes and the compacted densities are shown in Table V. The compressive strengths of the mixes that were determined prior to the construction are shown in Table VI.

The processing* of the AFB residue and the mixing of the residue, fly ash, and aggregate was done in a pugmill in a conventional mixing plant (see Figure 12). In this particular demonstration, the residue and aggregate were premixed and stockpiled (see Figure 13). The fly ash and water were added in a second step.

*Adding water to hydrate the lime in the residue.

The first 60 tons of experimental base material were placed on October 25, 1978 using a Barber-Greene asphalt paving machine (see Figure 14). This involved approximately 40 tons of Mix A and 20 tons of Mix B. Some initial difficulties were encountered with moisture control of Mix A at the mixing plant. This resulted in the production of approximately 20 tons of material which contained excessive water, with moisture contents ranging from 12 to 16 percent. Some of this material was placed in the field in an overly wet condition and could not be compacted. The remaining 40 tons of material were blended at optimum moisture content and were well compacted. A 10 ton three wheeled steel roller and a 12 ton vibratory roller were used to compact the base material during the first day of demonstration.

Due to scheduling of other work at the project site, the installation of the remaining 100 tons of experimental road base material was completed on November 8, 1978. This involved the production and placement of approximately 40 tons of Mix B and 60 tons of Mix C. These compositions were blended at, or very near, the optimum moisture content of the respective mixtures and were compacted in the field by means of the 12 ton vibratory roller. The placement of each of these mixes was accomplished by means of a motor grader with a movable spreading blade, instead of using a paving machine.

Because of the relative ease of installing the material on the second day of the demonstration, it was concluded that dumping and spreading of these compositions is a more suitable means of placement than the use of a paving machine, although a spreader box mounted behind a dump truck may also prove to be a practical method for installing such mixtures in the future.

Several weeks after placing the base, one of the compositions developed linear expansion similar to that which occurs with steel slag aggregate that has not been adequately cured before use. The problem mixture evidently had not been preconditioned sufficiently to allow the mixture to completely stabilize. Similar experience has been noted in structural compositions, using pulverized coal fly ash derived from lignite and sub-bituminous coal. In order to properly precondition the latter material before use, the fly ash is first blended with water, then allowed to "cure" for several weeks in a stockpile, after which it is pulverized to a uniform fineness.

An extensive laboratory program, which included observation of expansion bars, large and small field plots, and test cylinders has been undertaken to study the

expansion characteristics of a number of AFB bed materials. This program led to the following observations:

- compositions with ratios of AFB residue to fly ash of 3:7 or less (1:4, 1:9, etc.) show no detrimental expansion*
- exposure to free water is necessary in order for excessive expansion to occur
- expansion bars made from AFB residue that was processed at the American Admixtures plant show many compositions that have low expansion characteristics
- expansion bars that were maintained free of direct contact with water for a longer time after molding show considerably less expansion than their counterparts
- expansion measurements of 1' x 4' x 6" test pads verify that compositions containing a ratio of AFB residue to fly ash greater than 3:7 (1:2, 1:1, etc.) will expand more than 0.1 percent.

As a result of these observations, some large test pads (approximately 10 ft. by 40 ft.) were constructed in Canton, Ohio. These pads were made for the purpose of evaluating the expansion characteristics of mixes that were believed to have good dimensional stability. The results of these are not yetavailable. Further field evaluation of road base compositions will be affected by the findings.

CURRENT AND FUTURE ACTIVITIES

The continuing demonstration of the potential for commercial use of the by-products of the fluidized bed combustion process has many facets. A few additional applications that are being further developed at the present time are: synthetic aggregate, masonry units, and treatment of trade wastes. The following is a brief description of these efforts:

- Synthetic Aggregate - preliminary studies have indicated that briquettes can be manufactured using various combinations of residue and fly ash. Briquettes are to be made using commercially available equipment. Several tons will be produced so that they can be fully evaluated as a stockpiling medium and as a conventional aggregate substitute.
- Masonry Units - additional hollow core blocks are to be manufactured using mix compositions that have been shown to be acceptable. Two walls are to be constructed to evaluate response to weathering, construction considerations, and any mass action that might occur because of the combination of units. The structural properties of several test panels will also be studied.
- Treatment of Trade Wastes - various trade waste sludges are being stabilized with additions of AFB residue and fly ash.

Application of the by-products in structural fills and road bases will be further demonstrated following the present phase of an extensive expansion study which is scheduled for completion in late May 1980.

*For the present, a linear expansion in excess of 0.1% is considered to be detrimental.

TABLE I.

MIX AND COMPRESSIVE STRENGTH DATA
ON 8"x8"x16", 2 CORE, MASONRY UNITS

	Mix Composition % by Dry Weight				Compressive Strengths psi - gross area	
	Aggregate	Fly Ash	AFB Residue	Cement	30 Days	1 Year
Experimental Mix #1	55.5	5.8	29.2	9.5	1070	1253
Experimental Mix #2	52.4	11.0	27.6	9.0	1453	1355
Control #1	90.1	1.8	--	8.1	762	1015
Control #2	90.1	1.8	--	8.1	879	1065

TABLE II.

COMPOSITIONS AND PROPERTIES OF MIXES USED IN
PRODUCTION OF MASONRY BLOCK (JANUARY 26, 1980)

	Mix No.				
	1*	2	4**	5	7
Composition (% dry weight basis)					
Aggregate	92.6	56.4	90.4	59.4	-
AFB Residue	-	28.2	-	28.5	78.1
Fly Ash	-	6.4	2.5	6.2	17.1
Cement	7.4	8.9	7.1	5.7	4.7
Dry Weight of Each Material (lbs. per block)					
Aggregate	36.5	19.4	32.4	20.1	-
AFB Residue	-	9.7	-	9.7	17.7
Fly Ash	-	2.2	0.9	2.1	3.88
Cement	2.92	3.06	2.55	1.93	1.07
Dry Unit Weight - pcf	134.2	112.5	134.0	112.1	86.9
Absorption - %	6.54	14.79	7.05	16.00	27.70
Compressive Strength					
psi on net area	2420	1760	3110	1120	1110
psi on gross area	1360	1000	1590	590	590

*Control

**Control with fly ash

TABLE III

COMPARISON OF MASONRY UNIT (BLOCK)
ASTM STANDARDS (C90 and C129)*

Mix No.	Description	Remarks
1	Control	Meets compressive strength and absorption requirements of C90 and C129 for normal weight block-general use.
2	Natural aggregate partially replaced by AFB residue. Normal cement content plus fly ash.	Meets compressive strength requirements of C90 and C129 for medium weight block - general use and the absorption requirements for C90 and C129 for medium block-limited use.
4	Control with fly ash added.	Meets compressive strength and absorption requirements of C90 and C129 for normal weight block - general use.
5	Mix 2 with one-third less cement.	Meets compressive strength and absorption requirements for C129 for medium weight block.
7	AFB residue, fly ash, and cement.	Meets compressive strength and absorption requirements for C129 for lightweight block.

*ASTM C90 Standard Specification for Hollow-Load Bearing Concrete Masonry Units.

*ASTM C129 Standard Specification for Non-Load Bearing Concrete Masonry Units.

TABLE IV.

COMPOSITION OF SLUDGE FROM FLUE GAS SCRUBBING SYSTEM - percent by weight

$CaSO_3 \cdot 1/2\ H_2O$	45.92
$CaSO_4 \cdot 2H_2O$	9.52
$MgSO_4 \cdot H_2O$	8.16
$CaCO_3$	5.10
CaO (unreactive)	15.57
SiO_2	1.12
R_2O_3	6.70
Other	7.91

TABLE V.

OHIO ROAD BASE COMPOSITIONS AND COMPACTED DENSITIES

Mix	Composition	Plant Test Results			Field Test Results		
		Wet Density[1]	Dry Density[1]	Moisture	Wet Density[1]	Dry Density[1]	Moisture
A	40% Aggregate[2] 30% Alliance AFB Residue 30% Fly Ash[3]	120.8	106.5	13.2%	120.9	111.0 (104.2%)	10.8%
B	75% Aggregate 15% Alliance AFB Residue 10% Fly Ash	135.0	124.9	8.2%	131.7	121.5 (97.4%)	8.4%
C	75% Aggregate 15% Battelle AFB Residue 10% Fly Ash	143.0	133.2	7.3%	142.6	133.0 (99.9%)	7.6%

[1]Density values expressed in terms of pounds per cubic foot. Plant test results based on average of three compacted specimens, using the ASTM C 593 compaction procedures. Field test results based on an average of all in-place density values.

[2]The aggregate was a siliceous gravel from eastern Ohio conforming to the Ohio Department of Transportation Specification for 301 Aggregate.

[3]The source of the fly ash was the Ohio Edison Co. which burns coal from eastern Ohio or western Pennsylvania.

TABLE VI.

COMPRESSIVE STRENGTH OF
ROAD BASE COMPOSITIONS USED IN OHIO DEMONSTRATION

Composition of Mix	Compressive Strength (psi)[1]				
	7 Days @ 73° F	28 Days @ 73° F	7 Days @ 100° F	28 Days @ 100° F	Vacuum Saturated
75% Aggregate 15% AFB Residue 10% Fly Ash	838	2474[2]	1252	2784	1483
40% Aggregate 30% AFB Residue 30% Fly Ash	873	1317[2]	1578	1925	1259
75% Aggregate 15% AFB Residue 10% Fly Ash	222	922	888	2479	784

[1]All compressive strengths are the average of three individual values, unless otherwise noted.

[2]Compressive strength based on the average of two individual values.

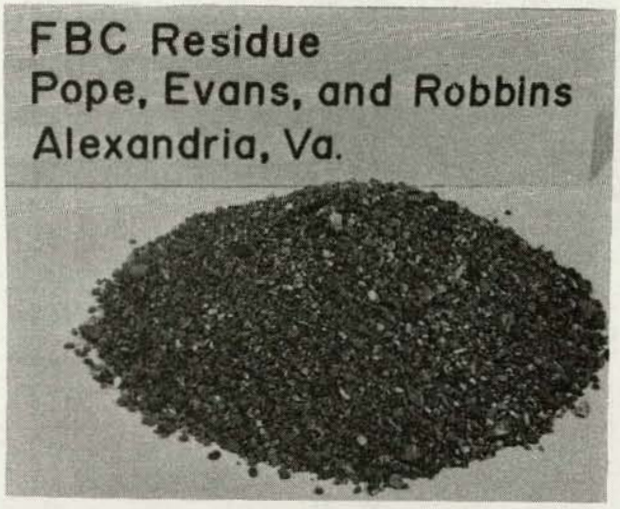

Figure 1 - Fluidized Bed Residue

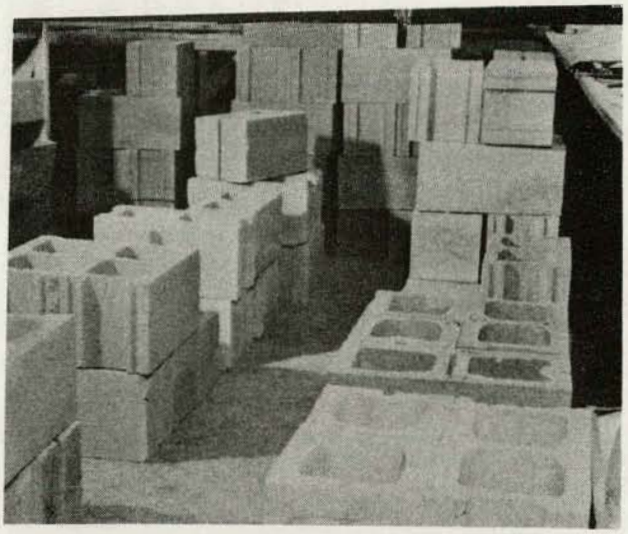

Figure 3 - Structural Masonry Units - Light Colored Block in Foreground Made with AFB Residue

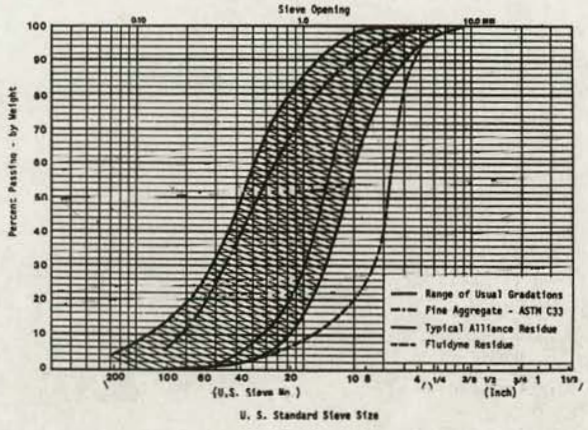

Figure 2 - Gradation of Fluidized Bed Residue

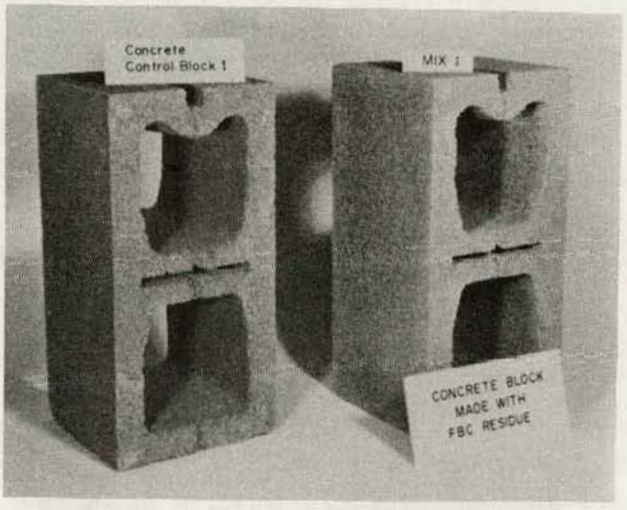

Figure 4 - Structural Masonry Units Made at Commercial Block Plant

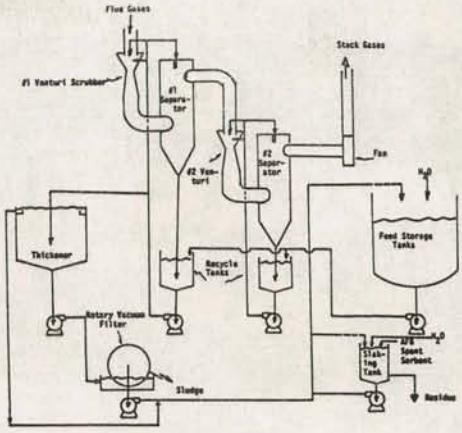

Figure 5 - Southern Illinois University Pilot Plant Scrubbing System

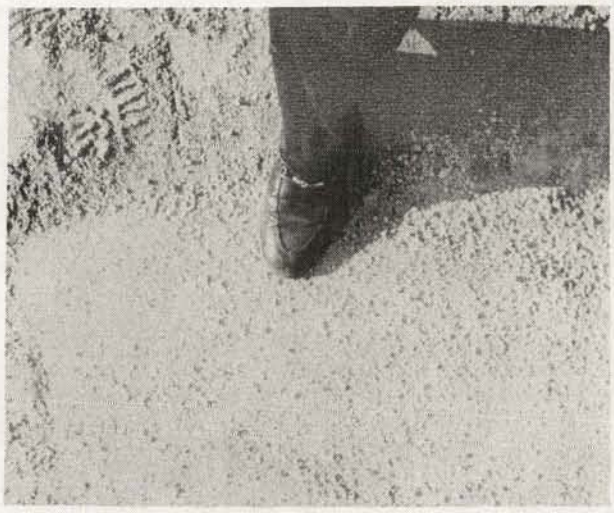

Figure 7 - Close-up of AFB Residue

Figure 6 - Stockpile of AFB Residue

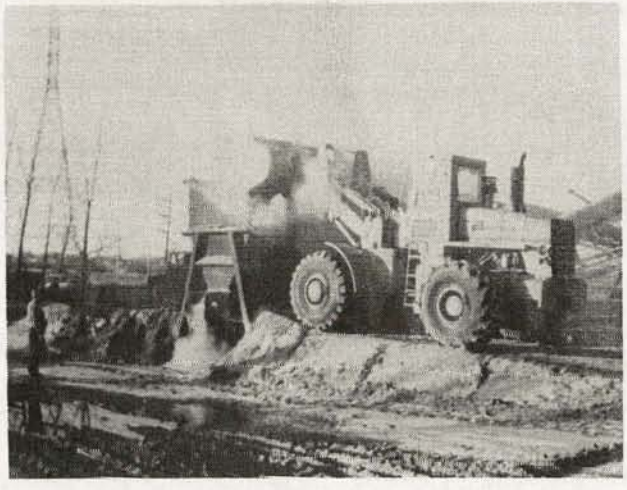

Figure 8 - Discharging of AFB Residue into Scalping Screen Hopper

Figure 9 - Loading of AFB Residue into Blower Truck

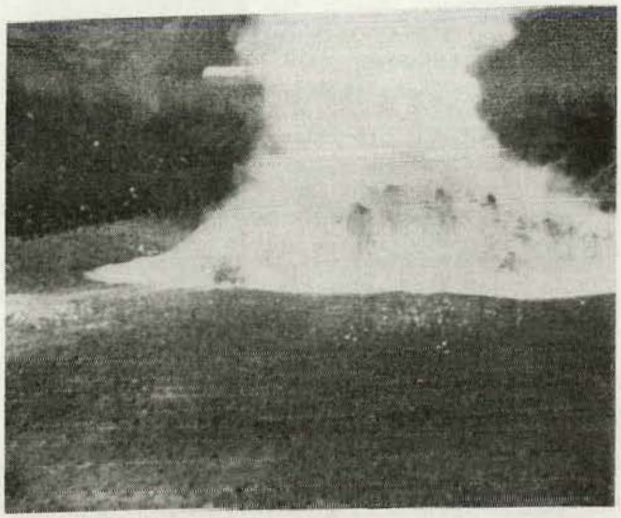

Figure 11 - AFB Stockpile Immediately After Processing

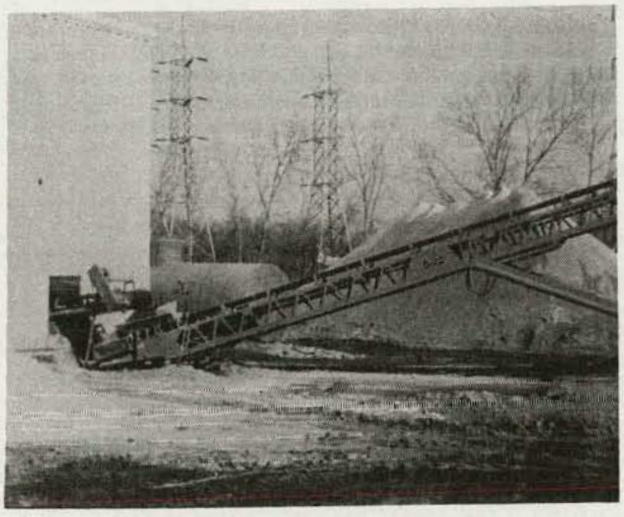

Figure 10 - View of Stacking Conveyor from AFB Conditioning Plant

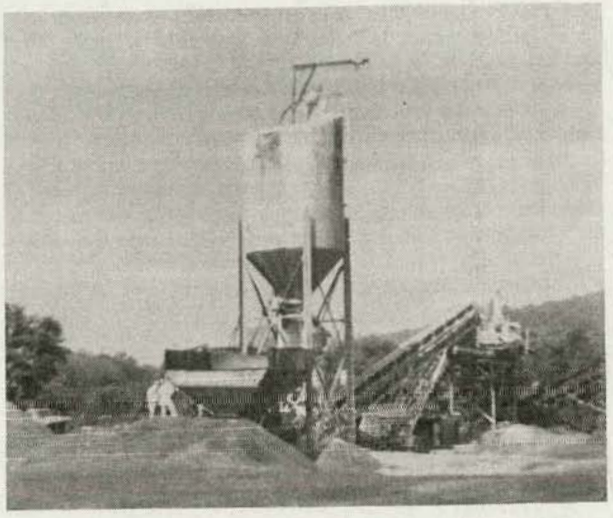

Figure 12 - View of Stabilization Plant

Figure 13 - Stockpile of Premix Blend of Alliance Residue and Aggregate

Figure 14 - Spreading of AFB Composition on Prepared Subbase

LABORATORY AND FIELD STUDIES OF PRESSURIZED FBC WASTE LEACHATE GENERATION AND ATTENUATION

T. W. Grimshaw, D. N. Garner, W. F. Holland; Radian Corporation, Austin, Texas 78766
D. A. Kirchgessner; EPA Industrial Environmental Research Laboratory, Research Triangle Park, N.C. 27711

Although fluidized bed combustion (FBC) is an emerging coal utilization technology that holds great promise in terms of energy conversion efficiency and minimal air pollutant emissions (especially SO_2), the solid residues generated by the process may pose a hazard to the environment. As with other types of solid wastes FBC residues are of particular concern with respect to the hydrologic environment.

The EPA Industrial Environmental Research Laboratory at Research Triangle Park, North Carolina, conducts environmental assessment and related investigations of emerging energy conversion technologies to facilitate the parallel development of environmental control technologies for the conversion processes. The investigation reported here is a major part of the IERL-RTP effort with respect to FBC.

The objectives of this program are two-fold: (1) analysis of the characteristics of FBC wastes and their interaction with natural environmental media; and (2) development of a methodology for providing environmental protection at future FBC waste disposal sites on a case-by-case basis. The general procedure of the investigation is to utilize the approaches and data from previous general solid waste studies and from studies specific to FBC solid wastes, to perform additional laboratory and field analyses specific to FBC solid wastes, to establish a rigorous correlation between laboratory and field results, and to develop a step-by-step method which can be applied at future disposal sites.

The structure of the program is strongly influenced by the Resource Conservation and Recovery Act of 1976 and related regulations that are presently being developed by EPA. Preliminary analyses reported by IERL-RTP indicate a strong likelihood that FBC wastes will be classed as non-hazardous under the provisions of RCRA. Consequently, much effort in this study has gone into defining the characteristics of FBC waste leachates and the interaction of the leachates with geologic materials. However, the eventuality of a hazardous classification of some FBC wastes, which would mean hydrologic isolation of future wastes with the use of liners, is also addressed. This part of the study is directed toward investigation of the interaction of FBC wastes and candidate liner materials.

This report will review the methods being used, state the progress during the first year of investigation, and report the results for pressurized FBC (PFBC) wastes. Although studies have been completed only for PFBC wastes at this time, two atmospheric FBC (AFBC) wastes will be included in the investigation before completion of the program.

METHODS OF ANALYSIS

Several program elements have been established to achieve the multiple objectives of this investigation:

- Information Services,
- FBC Waste Acquisition,
- Field Studies,
- Laboratory Studies,
- Chemical Analyses,
- Data Management and Interpretation, and
- Methodology Development.

Information Services

The purpose of the information services task is to secure published and unpublished literature relating to FBC and to general solid waste investigations. An abstract file has been compiled through the use of on-line literature files, and a current awareness service is provided to the program team members.

FBC Solid Residue Identification and Acquisition

The objective of this task is to identify those FBC test units that are producing wastes that are as representative as possible of wastes that will be generated in future commercially viable FBC plants. Once candidate wastes have been identified and acquired, the operational parameters that existed when the waste was produced are carefully defined. It is assumed that the solid waste streams (bed draw and cyclone catch) from the FBC units will be combined before disposal. Wastes from three types of operations are sought for this program: (1) PFBC; (2) AFBC with recycle mode of operation; and (3) AFBC with carbon-

burnup cell (CBC) mode of operation.* At present, PFBC wastes have been obtained from the Exxon Miniplant at Linden, New Jersey, and AFBC-with-recycle wastes have been obtained from the EPRI/B&W pilot plant at Alliance, Ohio. It is presently uncertain that AFBC-with-CBC wastes will be available within the timeframe of this study. Consequently, the third waste type for this program has not yet been determined.

Field Studies

The major effort of the field studies task consists of the installation of 18 large cylinders (four-inch diameter and seven-inch length) containing both representative FBC wastes and representative geologic materials. Most of the field work is accomplished at a site near Morgantown, West Virginia, which was selected because of its representative location in the northeastern United States and the availability of an EPA field station (Mine Drainage Control Facility at Crown, West Virginia).

The objective of the field studies task is to simulate field conditions of a sanitary landfill as closely as possible. In the interest of controlling extraneous variables, "quasi-field" conditions have been achieved. Rainfall, underground (near surface) temperature, and the unsaturated conditions are what would be expected in a typical landfill. However, the field cells are in hydrologic isolation from the environment in order to control water chemistry variables.

The field cell geometry (Figure 1) includes an upper 1 foot of disposal media, 1.5 ft. of FBC waste, 0.5 ft. of sand for sample collection, 3 ft. of disposal media, and a lower 1 ft. of sand for sample collection. The upper sample point is for the collection of leachate after generation from the FBC waste but before attenuation. The lower sample point yields leachate which has been attenuated by the disposal media. The arrangement of the cells in the field (Figure 2) consists of three sets of six cells with a central large cylinder for each set to collect leachate samples. Each cell is connected to the central cylinder with steel pipes which contain sampling tubing. The central cylinder contains vacuum pumps, sample flasks, and a drum for bottom drain leachate storage. Field cell operation consists of sampling for leachate at the upper and lower points on the basis of a predetermined schedule which is modified as necessary to allow for rainfall occurrence, which controls leachate availability at the sample point.

The field studies task also includes the identification and acquisition of representative geologic materials (disposal media). The objectives in selecting the geologic materials were to include a mix of representative disposal media as well as a range of natural geochemical conditions. Six materials were selected from locations near the Morgantown field site: (1) shale, sandstone, and interburden from a coal mine near Morgantown; (2) alluvium from the Ohio River Valley; (3) glacial

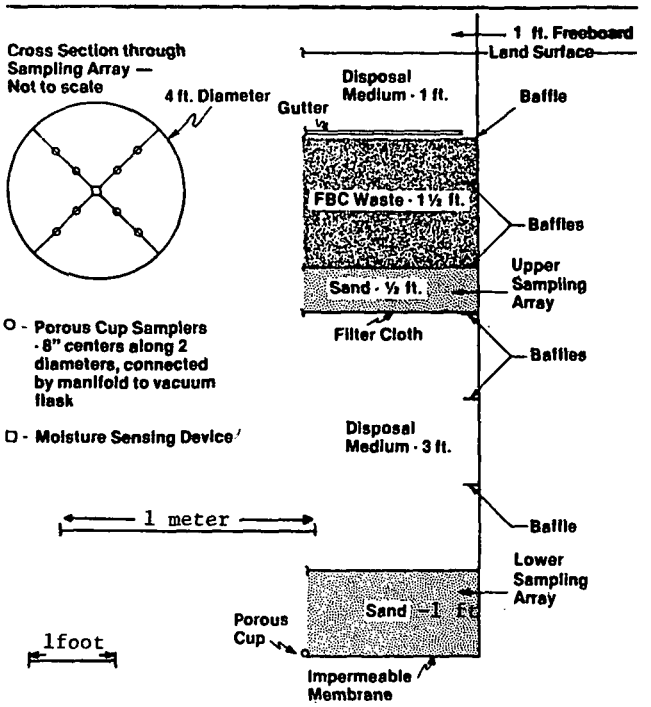

Figure 1. Field Cell Geometry

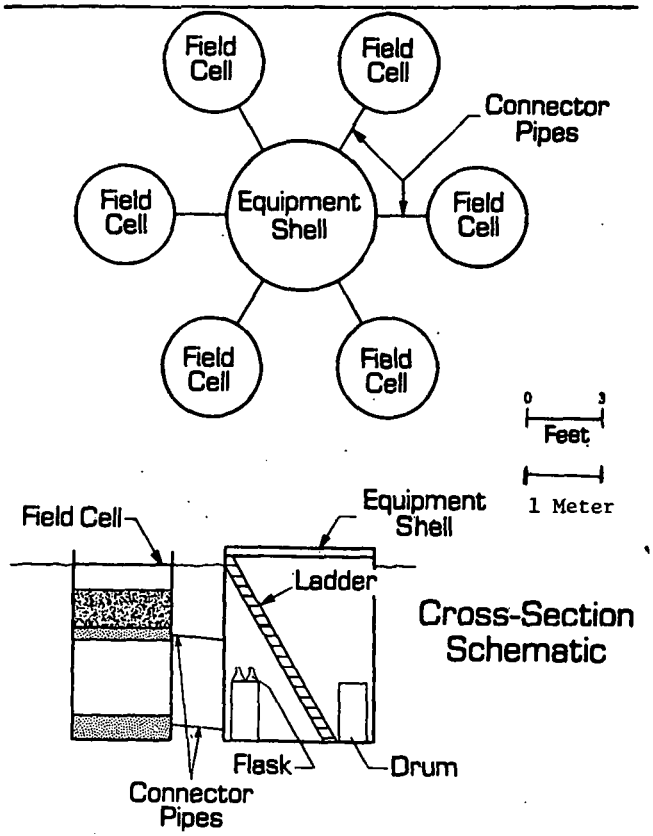

Figure 2. Field Cell Arrangement

till from near Columbus, Ohio; and (4) limestone from a quarry near Morgantown.

The installation of field cells containing all possible combinations of wastes and disposal media is both costly and unnecessary. Therefore, a partial matrix of combinations of wastes and disposal media is used to assess a range of conditions (Figure 3). Of the total of 17 cells included, 2 contain disposal media only and serve as control cells. The remaining 15 contain both FBC wastes and disposal media. Two of these 15 cells contain duplicate FBC wastes and disposal media to provide additional control for field experiments.

	PFBC	AFBC with Recycle	To Be Determined	Control (No Waste)	Total
Shale	2	1	–	1	4
Sandstone	1	–	1	–	2
Interburden	–	1	1	–	2
Alluvium	1	2	1	1	5
Glacial Till	1	–	1	–	2
Limestone	1	1	–	–	2
Total	6	5	4	2	17

Figure 3. Matrix of FBC Wastes and Disposal Media in Field Cells

Laboratory Studies

The two principal components of the laboratory studies are physical characterization of the FBC wastes and disposal media and the laboratory leachate generation and attenuation studies. The primary purpose of the physical characterization of the waste and disposal media is to aid in the interpretation of the chemical behavior of the materials during leachate generation and attenuation.

Physical characterization of FBC wastes includes X-ray powder diffraction patterns of whole samples, scanning electron microscope analysis, electron microprobe analysis at two depths in the particles, particle size (texture) analysis, specific surface area determination, and specific gravity analysis. For the disposal media, physical characterization includes X-ray powder diffraction patterns of whole samples, X-ray powder diffraction patterns of the clay-size fraction, particle size (texture) analysis of unconsolidated materials, thin section analysis by polarizing microscope of the consolidated materials, scanning electron microscope analysis, electron microprobe analysis, and specific surface area determinations.

The main thrust of the laboratory studies is on the generation of leachate from FBC wastes and subsequent attenuation of the leachate by the disposal media. Several phases of leaching and attenuation under natural conditions are accounted for in a 6-step protocol (Figure 4) for batch equilibration testing (shake tests).

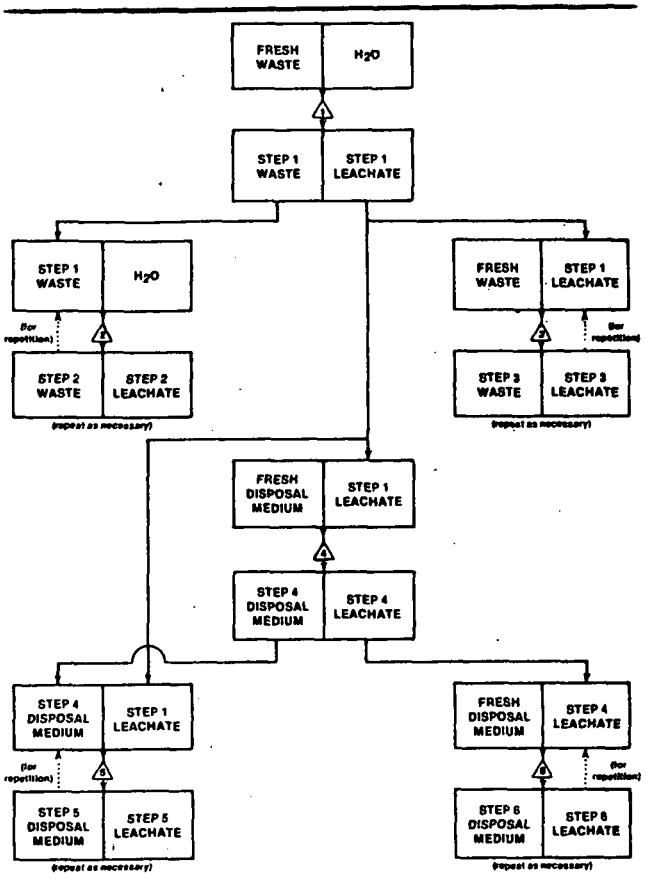

Figure 4. Multi-Step Laboratory Leaching Protocol

Step 1 of the protocol includes initial leaching of the FBC wastes by deionized water. This step corresponds to the initial leaching as in the upper part of a landfill body during the early life of a landfill. Step 2 includes secondary leaching of the FBC wastes by using fresh deionized water eluant. This step is intended to mimic the behavior of wastes in the upper part of the landfill after leaching has progressed for some time. Step 3 is intended to give a measure of the ability of leachate from Step 1 to take up additional contaminants upon exposure to fresh wastes. This step is intended to model the behavior of the lower part of a landfill as it is leached by leachate generated in the upper part of the landfill. Step 4 provides a measure of the attenuation of fresh leachate (from Step 1) as it is exposed to fresh disposal media. This step models the response of the substrate below a landfill during the early life of the landfill. Step 5 measures the secondary attenuation of fresh leachate by disposal media that have been previously "burdened" with fresh leachate. This step indicates the ability of disposal media to continue to attenuate leachate after it has been previously exposed to leachate. This step thus models the disposal media below a landfill during the later life of the landfill. The final step, Step 6, measures the secondary

attenuation of attenuated leachate by fresh disposal media in order to determine the increment of attenuation of contaminants in the leachate as the leachate moves through fresh disposal media. This step accounts for the response of the disposal media at some distance below the landfill, which is exposed to leachate that has already been exposed to disposal media at higher levels.

Several variables have been fixed during the conduct of the protocol: (1) the extracting liquid (eluant) is deionized water; (2) extraction times are 1 day, 2 days, and 7 days; (3) the solid-to-liquid mass ratio is 1:10 (25 g per 250 ml H_2O); (4) the waste and disposal media are ground prior to leaching to ensure homogeneity and reproducibility; and (5) agitation is maintained at specified constant parameters. The instrument selected for agitation is the Rugged Rotator; the parameters of operation are 6 revolutions per minute at 70° to the horizontal. These parameters provide good mixing of the wastes with the eluant but with minimum particle abrasion.

Twenty-one chemical parameters have been selected for routine analysis of the leachate (Figure 5). The same parameters are analyzed in leachates generated in both field and laboratory studies. The parameters were selected on the basis of previous studies of FBC wastes and preliminary analysis of FBC waste leachates for this program. In addition to the 21 routine parameters, 10 additional parameters are checked in initial analyses of each FBC waste: arsenic, beryllium, copper, lead, magnesium, manganese, molybdenum, silicon, strontium, and titanium. Most elemental analyses are made by the Inductively Coupled Argon Plasma Emission Spectroscopy (ICPES) Method. Atomic absorption spectrometry (AAS) is used for analyses for lithium, lead, mercury, selenium, and arsenic. Other methods are used for fluorine, total organic carbon, total dissolved solids, pH, and sulfate.

Aluminum	Fluoride	Silver
Barium	Iron	Sulfate
Boron	Lithium	Vanadium
Cadmium	Mercury	Zinc
Calcium	Nickel	pH
Chromium	Potassium	TDS
Cobalt	Selenium	TOC

Figure 5. Chemical Parameters Selected for Routine Analysis

Control columns containing disposal media have been set up in the laboratory to fill in gaps in the field cell matrix. These laboratory columns provide an inexpensive substitute for control cells in the field. The laboratory columns receive the same moisture input as the field cells, but on a delayed schedule to match the rainfall input in the field cells. Leachate is collected from the laboratory columns on a similar schedule to the field cells and is analyzed for the same parameters.

In order to address the eventuality that some FBC wastes will be classed as hazardous and will therefore have to be isolated from the hydrologic environment, studies are being conducted of the compatibility of several candidate liner materials with FBC wastes. These investigations are being conducted to assess the deterioration of the candidate liners when exposed to 7-day FBC leachate. The liner materials included in the investigation are: (1) Neoprene; (2) polyvinyl chloride (PVC); (3) chlorinated polyethylene (CPE); (4) Hypalon; (5) butyl rubber; (6) EPDM rubber; and (7) sodium bentonite. For all candidate liner materials except the bentonite, strips of the material are immersed in 7-day leachate over a period of approximately 12 months. Individual strips are removed from the leachate at specified intervals and tested for tensile strength and by scanning electron microscope observation of the liner surface. In addition, the total organic carbon content of the leachate is monitored regularly. The bentonitic clay is also exposed to FBC waste leachate and is studied by scanning electron microscope observation of the clay particles, by X-ray diffraction analysis, and by monitoring the aluminum content of the leachate.

Data Analysis and Interpretation

The primary purpose of this task is to receive and store the results of the chemical analyses of FBC waste leachates before and after attenuation by the disposal media. All chemical analytical data are stored in and manipulated by SAS (Statistical Analysis System). Software is written for the SAS system to produce the desired data plots. Different types of data plots are presented for each step of the multi-step laboratory leaching protocol. The data plot for laboratory leachate generation (Figure 6) shows initial leachate generation in Protocol Step 1 followed by additional leaching of the wastes by fresh water during Step 2 repetitions. The plot shows concentration of the chemical parameter on the ordinate as a function of leachate volume on the abscissa. The leachate volume on the abscissa is normalized by dividing the leachate volume by the mass of waste to which the leachate has been exposed. The resulting abscissal unit is volume-to-mass ratio, where units are ml/g. Concentration is measured after each step of the protocol (or after a repetition of a step), such that the volume-to-mass ratio increases by 10 between measurements of concentration.

In order to express laboratory secondary leachate generation, which results from exposure of leachate from Protocol Step 1 to additional fresh waste, the concentration of the chemical parameter of interest is again depicted as a function of volume-to-mass ratio (Figure 7). The result of Protocol Step 1 is indicated as the farthest point to the right on the plot, and repetitions of Step 3 are shown as data points to the left of the Step 1 data point.

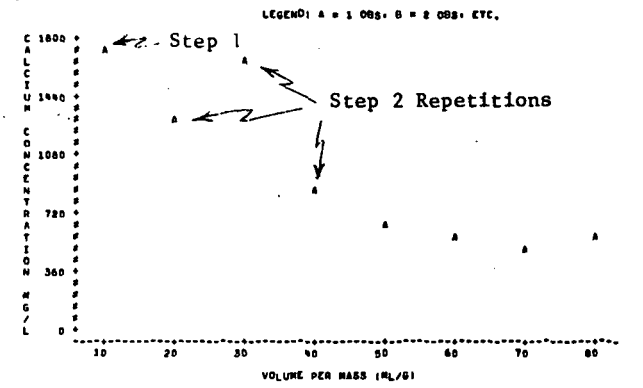

Figure 6. Derived Data Plot for Laboratory Leachate Generation

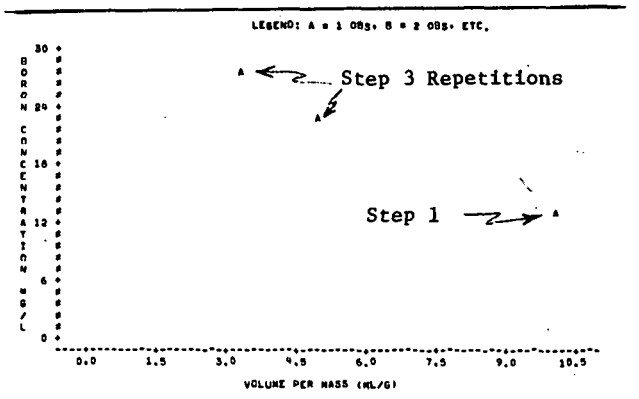

Figure 7. Derived Data Plot for Laboratory Secondary Leachate Generation

The SAS data management system is also used to generate plots of laboratory leachate attenuation. Laboratory fractional attenuation is calculated by the following equation:

$$A_L = \frac{C_a - C_b}{C_a}$$

A_L = fractional attenuation

C_a = Step 1 leachate concentration

C_b = concentration after exposure to disposal media.

The laboratory fractional attenuation provides a measure of the decrease in concentration of Step 1 leachate after the leachate has been exposed to the disposal media. Fractional attenuation values between 0 and 1 indicate contaminant removal by the disposal media. Fractional attenuation values less than zero indicate that contaminants have been mobilized from the disposal media by the leachate. The SAS data plot for laboratory fractional attenuation (Figure 8) shows fractional attenuation on the ordinate as a function of volume-to-mass ratio on the abscissa. The first data point on the left side of the data plot is the result of Step 4 of the Protocol. Subsequent points are generated by repetitions of Step 5 of the Protocol. A separate data plot is required for each chemical parameter, FBC waste, and disposal medium.

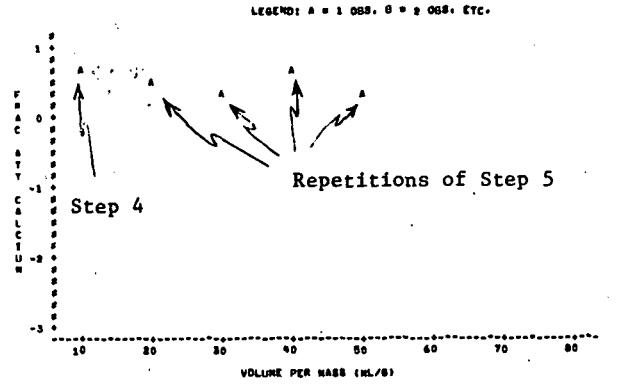

Figure 8. Derived Data Plot for Laboratory Leachate Attenuation

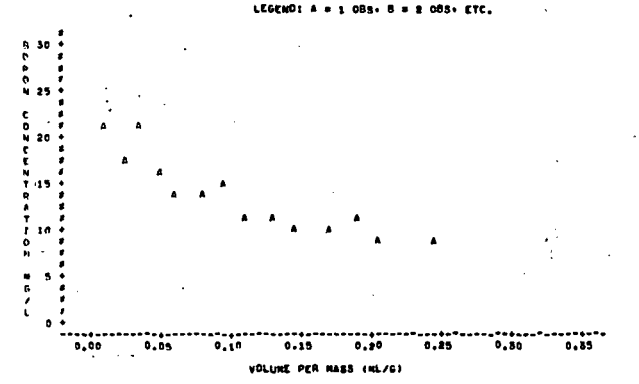

Figure 9. Derived Data Plot for Field Cell Leachate Generation

The SAS data plot for leachate generation in field cells is quite similar to the data plot for laboratory leachate generation (Figure 9). The plot depicts concentration on the ordinate as a function of volume-to-mass ratio on the abscissa. The concentration on the ordinate is from the analysis of leachates collected from the upper sample point of the field cell. The PFBC field cells have been in operation only since August 1979, so the quantity of leachate generated thus far is relatively small. Consequently, the volume-to-mass ratios for the field cells are generally much lower than for the laboratory studies. A separate data plot is again required for each chemical parameter and for each field cell.

The SAS data plots for leachate attenuation in field cells are derived in a similar fashion to the fractional attenuation plots for laboratory attenuation studies. The equation for calculating field fractional attenuation is similar to the laboratory equation:

$$A_F = \frac{C_u - C_l}{C_u}$$

A_F = field fractional attenuation

C_u = leachate concentration, upper sample point

C_l = leachate concentration, lower sample point

Field fractional attenuation data plots (Figure 10) depict fractional attenuation on the ordinate as a function of volume-to-mass ratio on the abscissa. Positive values again indicate attenuation and negative values signify contaminant mobilization from the disposal media by the leachate.

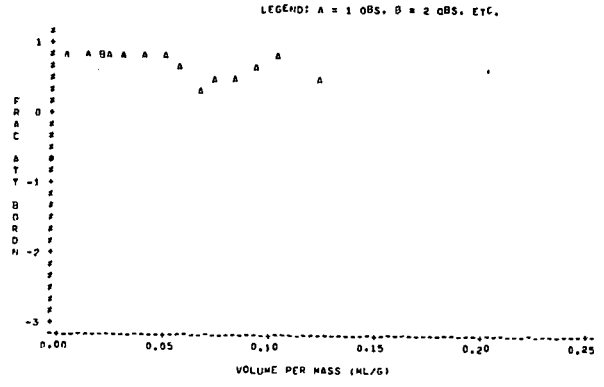

Figure 10. Derived Data Plot for Field Leachate Attenuation

PROGRESS SUMMARY

Of the 3 candidate FBC waste types that have been identified, 2 have been acquired. All 6 candidate disposal media have been obtained from the Morgantown area. The PFBC wastes from the Exxon Miniplant have been analyzed by the multi-step laboratory leaching protocol. Physical characterization studies have been completed for the PFBC wastes and the disposal media. The field cells containing PFBC wastes are in place, and the initial leachate samples have been collected and analyzed. Studies have been initiated in the laboratory and in the field for the AFBC-with-recycle wastes from the EPRI/B&W pilot plant at Alliance, Ohio. The third waste is yet to be identified and acquired. The control (waste only) field cells have been installed, and the laboratory control columns containing disposal media have been put into operation. One of the 2 planned field permeameters has also been put into operation.

The most significant results obtained thus far are from the multi-step laboratory leaching protocol and from the field cell leachate collected from the upper and lower sample points. The remainder of this report will focus on the findings of laboratory and field studies of generation and attenuation of leachate from PFBC wastes.

LABORATORY STUDIES FOR PFBC WASTE LEACHATE GENERATION AND ATTENUATION

As noted, the multi-step laboratory leaching protocol includes studies of the generation of leachate from PFBC wastes and the subsequent interaction of the PFBC waste leachates with each of the 6 disposal media. Of the 21 chemical parameters that are routinely analyzed, 3 are selected here to show a range of typical behavior: calcium, boron, and sulfate. Trends have been observed and will be commented upon, but interpretation of the chemical basis for the trends observed remains to be accomplished later in the program.

Laboratory Leachate Generation

Leachate generation trends are described by a plot of the analytical results of Step 1 and Step 2 of the multi-step laboratory leaching protocol. The results for calcium are shown in Figure 11.

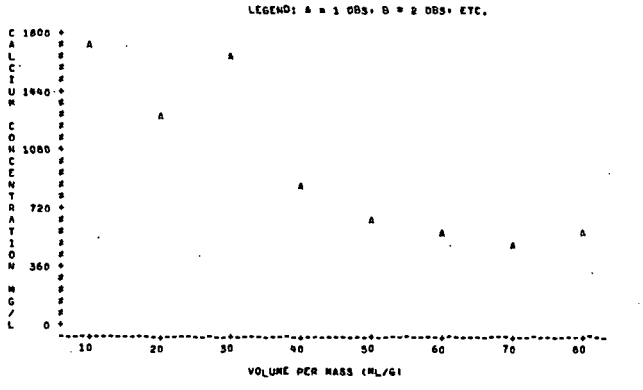

Figure 11. Calcium Trends in Laboratory Leachate Generation

This plot shows that the initial calcium concentration from leaching of fresh PFBC wastes is just below 1,800 mg/ℓ. Successive leaching of the wastes in Step 2 results in smoothly decreasing calcium concentrations, although there is a single anomalous data point at 30 mℓ/g. The calcium concentration appears to be leveling off at about 500 mg/ℓ with increasing leaching of the waste. When fresh waste is added to leachate generated from Step 1 of the protocol (Figure 12), the calcium concentration does not change markedly. The

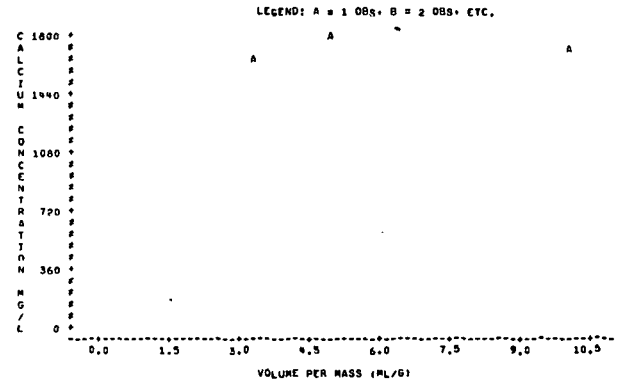

Figure 12. Calcium Trends in Laboratory Secondary Leachate Generation

inital Step 1 concentration of just below 1,800 mg/ℓ (indicated by the data point at the far right of the data plot) does not change when additional fresh PFBC waste is added to the leachate in repetitions of Step 3 of the protocol as depicted from right to left on the plot. Apparently the leachate is unable to take up any additional calcium after the initial leaching of fresh waste.

During primary leaching, boron shows trends similar to the calcium trends (Figure 13). Initial concentrations from Step 1 are about 14 mg/ℓ and there is apparently a smooth decrease in concentration to about 2 mg/ℓ with increased leaching. An anomalous data point again appears at volume-to-mass ratio of 30 mℓ/g. Boron trends are markedly different from calcium trends, however, when leachate is exposed to additional fresh PFBC wastes as shown in Figure 14. The initial 14 mg/ℓ concentration from Step 1 increases to about 23 mg/ℓ and then to 28 mg/ℓ as the leachate is exposed to additional fresh waste and the volume-to-mass ratio decreases.

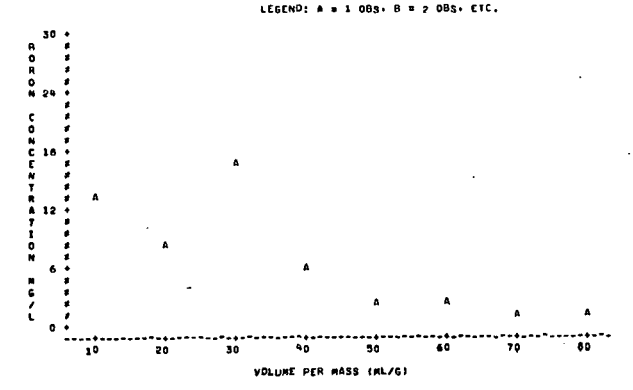

Figure 13. Boron Trends in Laboratory Leachate Generation

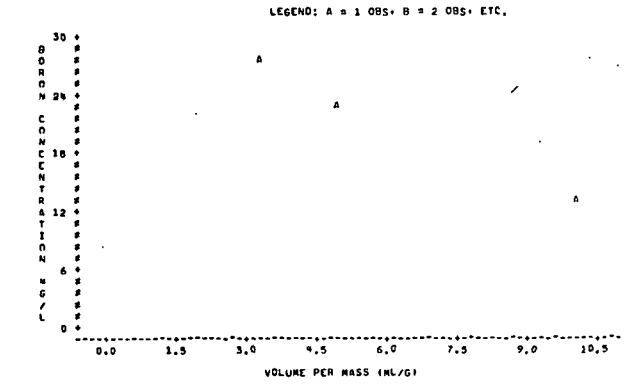

Figure 14. Boron Trends in Laboratory Secondary Leachate Generation

Sulfate concentrations in fresh Step 1 PFBC waste leachate are about 1,300 mg/ℓ (Figure 15). Additional leaching of the waste by fresh eluant does not result in a decrease in sulfate concentration in the leachate as is the case for calcium and boron. Also, there apparently is not an increase in sulfate concentration when the leachate is exposed to fresh waste (Figure 16). The concentration remains at a relatively constant 1,200 to 1,400 mg/ℓ level with decreasing volume-to-mass ratio.

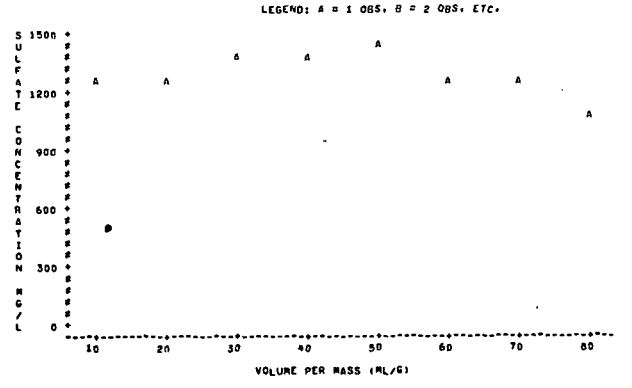

Figure 15. Sulfate Trends in Laboratory Leachate Generation

Laboratory Leachate Attenuation

The attenuation of leachate by exposure to disposal media under laboratory conditions is accounted for in Protocol Steps 4, 5, and 6. The general trend of attenuation of calcium in laboratory studies of PFBC waste leachate attenuation is one of continued (and even increasing) attenuation as the disposal medium is exposed to fresh leachate. When the leachate is exposed to sandstone,

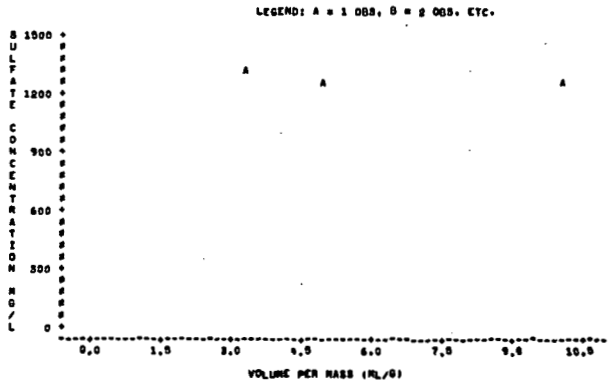

Figure 16. Sulfate Trends in Laboratory Secondary Leachate Generation

for example, initially the fractional attenuation has a value of about 0.3 (Figure 17). As the volume-to-mass ratio increases, the fractional attenuation value rises to 1.0 at 60 mℓ/g. A similar pattern is observed when the leachate is exposed to interburden (Figure 18). The initial fractional attenuation value is about 0.4 and increases gradually to 1.0 at a volume-to-mass ratio of 60 mℓ/g.

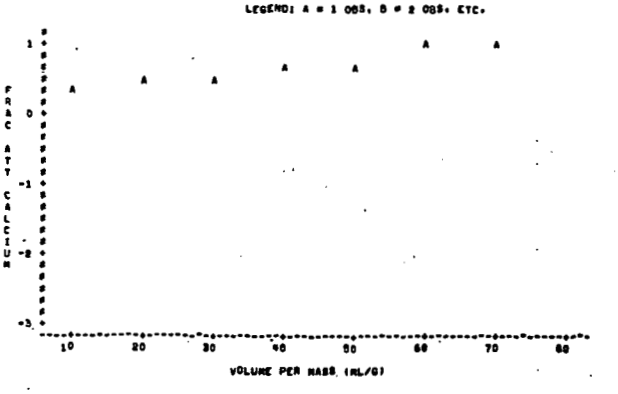

Figure 17. Calcium Trends in Laboratory Leachate Attenuation by Sandstone

Boron, unlike calcium, shows nearly complete attenuation for all disposal media. For example, boron is completely attenuated by shale (Figure 19) at all volume-to-mass ratios analyzed. Only limestone (Figure 20) shows a departure from the trend of complete attenuation. When the PFBC waste leachate is exposed to the limestone disposal media, there is a decrease in attenuation from 1.0 at 10 mℓ/g to about 0.8 at 50 mℓ/g.

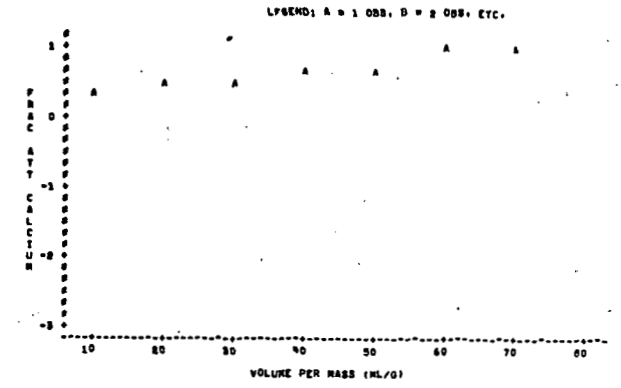

Figure 18. Calcium Trends in Laboratory Leachate Attenuation by Interburden

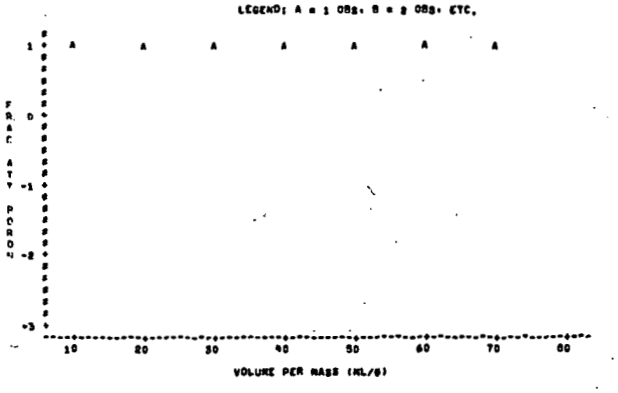

Figure 19. Boron Trends in Laboratory Leachate Attenuation by Shale

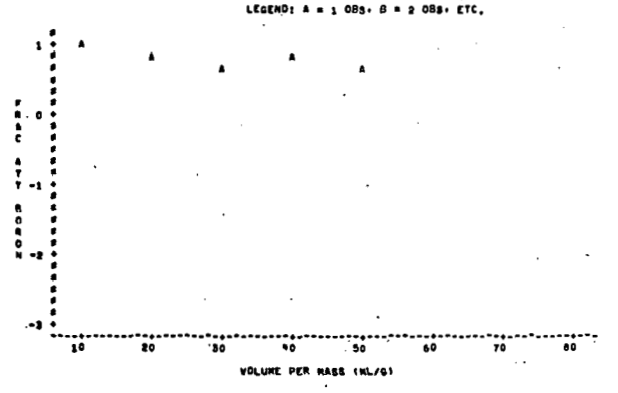

Figure 20. Boron Trends in Laboratory Leachate Attenuation by Limestone

Sulfate shows a much different attenuation pattern, in that only minimal attenuation is observed by any disposal media. A typical pattern is shown by glacial till (Figure 21), where the attenuation reaches a maximum of about 0.25 and then decreases to zero. All other disposal media tested show a similar pattern of little or no attenutation, although there is no contribution of sulfate by any of the disposal media.

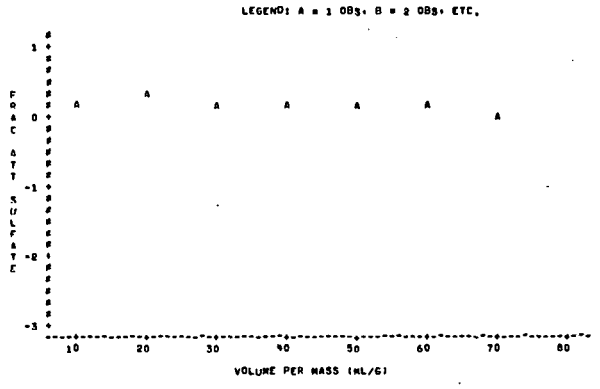

Figure 21. Sulfate Trends in Laboratory Leachate Attenuation by Glacial Till

FIELD STUDIES OF PFBC WASTE LEACHATE GENERATION AND ATTENUATION

The patterns of PFBC waste leachate generation and attenuation in field cells are observed from analyses of leachates collected from the upper sample point and the lower sample point of the cells. The leachate generation phase is represented by leachate collected from the upper sample point. All PFBC field cells are quite similar in their construction down to this upper sample point, with the exception of the upper 1 ft. of disposal medium. The leachate attenuation phase, which is ascertained by analyses of leachates from the lower sample point, is different for each field cell containing a different disposal medium. As noted above, the volume-to-mass ratios are generally much smaller in the field cells than in the laboratory studies because of the short period of operation of the field cells.

Field Cell Leachate Generation

In leachates from the upper sample point of field cells containing PFBC wastes, calcium concentration trends as a function of volume-to-mass ratio are quite similar for all field cells. Concentration values begin in the 100 to 400 mg/ℓ range and increase gradually with increasing volume-to-mass ratio. The field cell containing shale is a typical example; the concentration begins at 200 to 300 mg/ℓ and increases gradually to a maximum of about 500 mg/ℓ and then begins to level off (Figure 22). The field cell containing

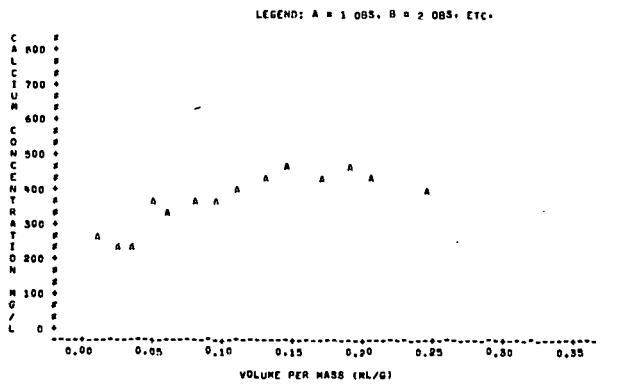

Figure 22. Calcium Trends in Leachate Generated in Field Cell Containing Shale

sandstone shows a similar pattern with an initial concentration of 300 to 400 mg/ℓ increasing to about 600 mg/ℓ and then leveling off at about 500 mg/ℓ (Figure 23).

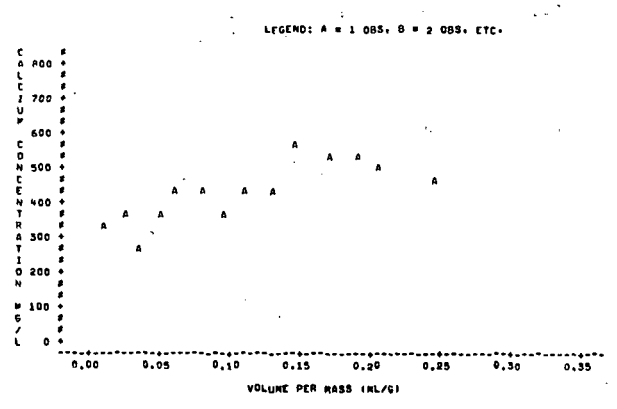

Figure 23. Calcium Trends in Leachate Generated in Field Cell Containing Sandstone

Boron shows a much different pattern from calcium during PFBC waste leachate generation in the field cells. All field cells show a similar pattern of smoothly decreasing boron concentration with increasing volume-to-mass ratio. The field cell containing limestone, for example, has initial values of 20 to 25 mg/ℓ which decrease to about 5 mg/ℓ at higher volume-to-mass ratios (Figure 24). A similar pattern is displayed by the field cell containing shale (Figure 25), which has initial concentration values of 25 mg/ℓ decreasing to about 7 mg/ℓ.

Sulfate shows a similar pattern to boron, but it is somewhat less consistent. A typical trend

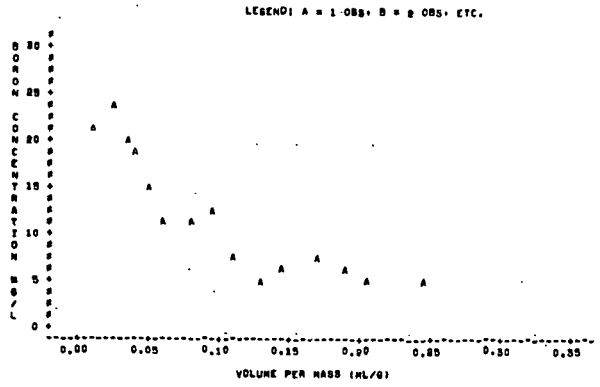

Figure 24. Boron Trends in Leachate Generated in Field Cell Containing Limestone

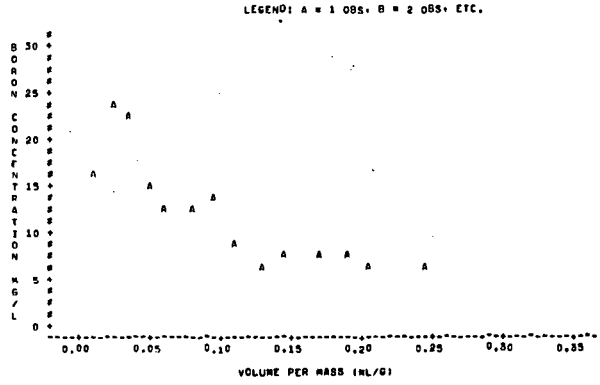

Figure 25. Boron Trends in Leachate Generated in Field Cell Containing Shale

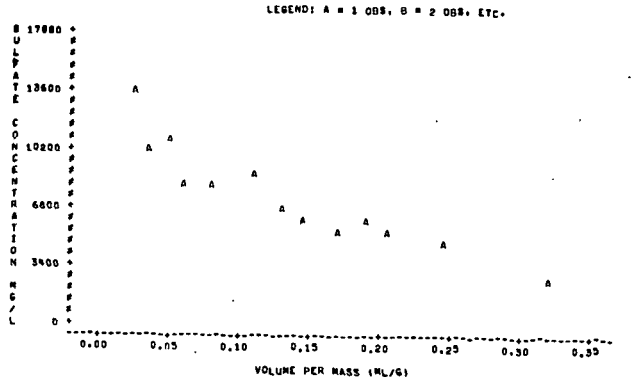

Figure 26. Sulfate Trends in Leachate Generated in Field Cell Containing Shale

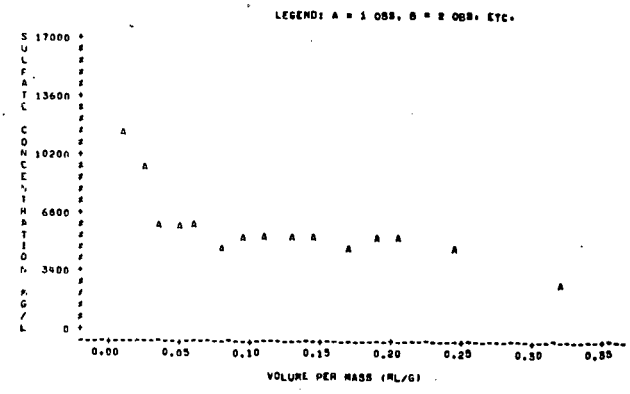

Figure 27. Sulfate Trends in Leachate Generated in Field Cell Containing Alluvium

is shown by the field cell containing shale (Figure 26), which shows an initial leachate concentration of 26,200 mg/ℓ decreasing to about 3,400 mg/ℓ at higher volume-to-mass ratios. The trend is similar for other field cells, as exemplified by the cell containing alluvium (Figure 27), in which the sulfate concentration is initially about 12,000 mg/ℓ and decreases to about 4,500 mg/ℓ. The final data point indicates a further decrease to about 3,400 mg/ℓ.

Field Cell Leachate Attenuation

The leachate attenuation data from the field cells present the least consistent patterns of any of the laboratory or field data. Such inconsistency may reflect the early stage of operation represented by the data collected thus far. It is expected that the behavior of the field cells will become more smooth and consistent as time progresses.

The calcium concentrations in leachate exposed to disposal media in the PFBC field cells exhibit a variety of behavior, ranging from moderately good attenuation on one extreme to strong contribution of calcium to the leachate by the disposal media on the other extreme. Good attenuation of calcium in the field cell containing alluvium is shown in Figure 28. The fractional attenuation values range from nearly 1.0 at lower volume-to-mass ratios and to about 0.4 at higher volume-to-mass ratios. An example of strong contribution of calcium to the leachate by the disposal media is exhibited by the field cell containing limestone (Figure 29). Calcium contribution is particularly strong in the early phases of cell operation (low volume-to-mass ratios) when the fractional attenuation is almost -2.0. However, the contribution decreases with increasing volume-to-mass ratio of about -0.25.

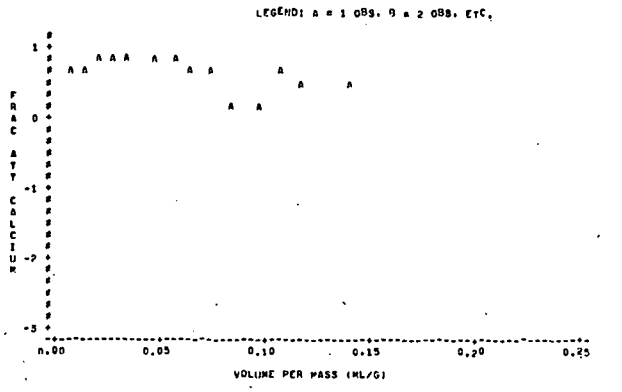

Figure 28. Calcium Trends in Leachate Attenuated in Field Cell Containing Alluvium

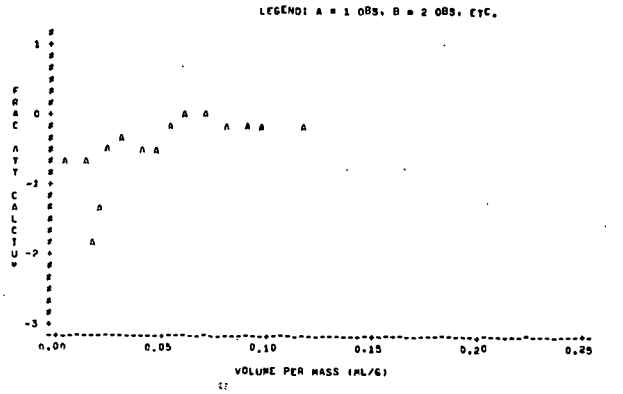

Figure 29. Calcium Trends in Leachate Attenuated in Field Cell Containing Limestone

Boron is strongly attenuated by almost all the disposal media in the PFBC field cells. A typical example is the field cell containing glacial till (Figure 30), which displays a fractional attenuation of nearly 1.0 at all volume-to-mass ratios. The field cell containing limestone is the only exception to the rule of strong boron attenuation (Figure 31). In that field cell, fractional attenuation begins at about 0.7 and decreases steadily to about 0.3.

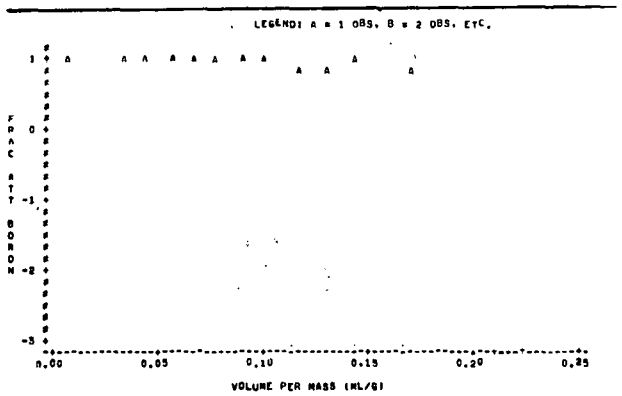

Figure 30. Boron Trends in Leachate Attenuated in Field Cell Containing Glacial Till

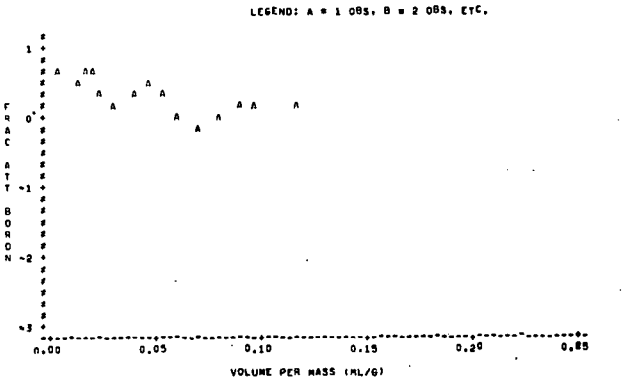

Figure 31. Boron Trends in Leachate Attenuated in Field Cell Containing Limestone

Sulfate, like calcium, shows rather inconsistent behavior in PFBC field cell leachate attenuation characteristics. This behavior ranges from relatively good attenuation (at least initially) as shown in the field cell containing alluvium (Figure 32) to very poor attenuation and even some contribution of contaminants as shown in the field cell containing sandstone (Figure 33).

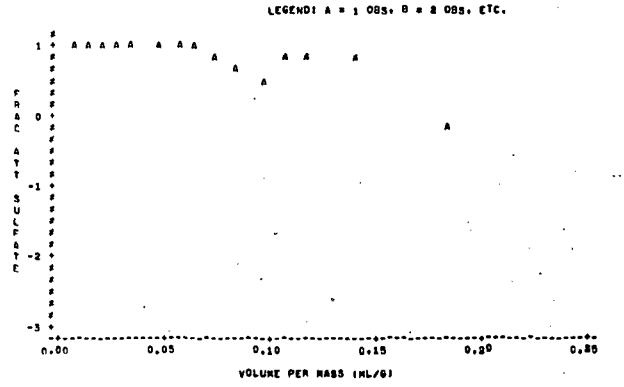

Figure 32. Sulfate Trends in Leachate Attenuated in Field Cell Containing Alluvium

CORRELATION OF LABORATORY AND FIELD STUDIES

A major objective of this program is an attempt to correlate the results obtained in the laboratory and the field studies. If this correlation can be achieved, then waste leaching behavior under field conditions can be predicted on

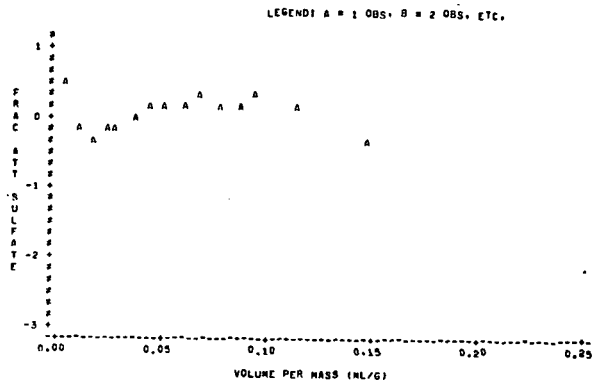

Figure 33. Sulfate Trends in Leachate Attenuated in Field Cell Containing Sandstone

the basis of fast, low-cost laboratory studies. An eventual goal is to establish the correlation on a sound, statistically valid basis. The necessary statistical work to accomplish this goal has not yet been done, but initial attempts to correlate have been made. Separate correlations are being attempted for the leachate generation phase and the leachate attenuation phase. The correlation must be established separately for each chemical parameter. The initial correlation efforts have focused on 7 example parameters: calcium, boron, sulfate, strontium, magnesium, zinc, and total dissolved solids.

Correlation of Leachate Generation Results

The initial attempt to establish correlation during the leachate generation phase consists of a plot of the cumulative mass of the contaminant species released per gram of waste on the ordinate and the volume of leaching liquid (eluant) per gram of waste on the abscissa (Figure 34). The units of the ordinate are grams of species "X" per gram of waste, and the units of the abscissa are milliliters of eluant per gram of waste. The plots are made on a log-log scale for the laboratory and field data. Initial results indicate that the correlation is quite good, at least for the initial phases of field cell operation. All parameters appear to correlate quite well from laboratory to field studies with the exception of magnesium. Correlation for the other 14 parameters included in the routine analyses of leachate will be attempted in the future.

Correlation of Leachate Attenuation Results

The correlation of laboratory to field studies during the leachate attenuation phase is conducted similarly to the correlation for the leachate generation phase. A log-log plot is made of the cumulative mass of species attenuated per gram of disposal medium on the ordinate as a function of the volume of eluant per gram of medium on the

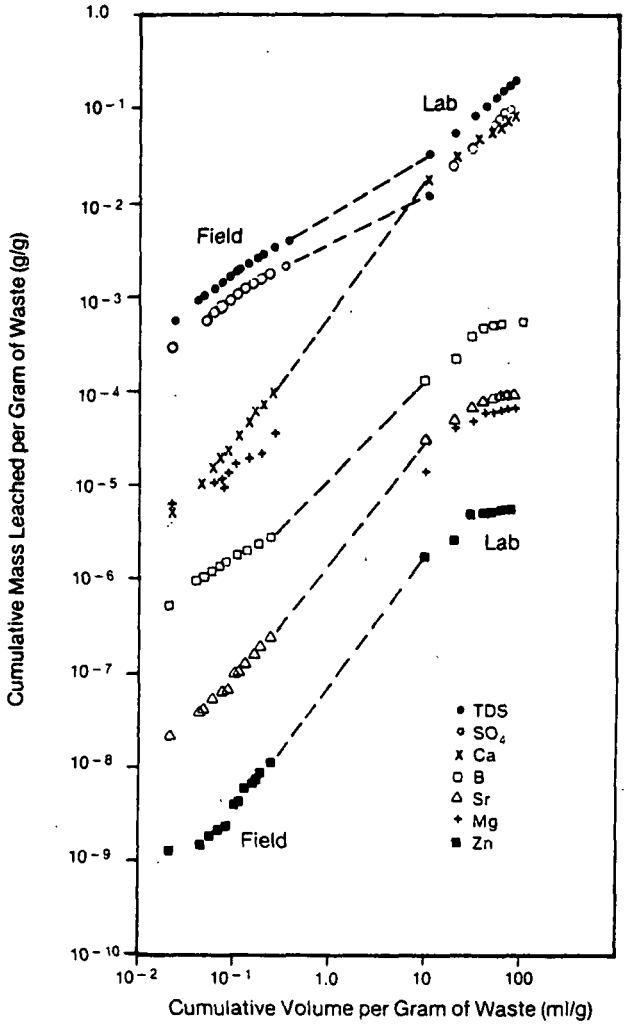

Figure 34. Correlation of Laboratory and Field Leachate Generation Data

abscissa (Figure 35). This plot shows a good correlation for 3 of the example parameters: total dissolved solids, sulfate, and boron. Magnesium is not as consistent. Calcium, strontium, and zinc do not show a correlation because they are attenuated in laboratory studies and are mobilized in field cell studies.

COMPARISON OF LEACHATE CHARACTERISTICS WITH WATER QUALITY CRITERIA AND REGULATIONS

Studies described in the preceding paragraphs provide insight into the trends of PFBC waste leachate concentration during the generation and attenuation phases. This information will be vital to predicting the behavior of FBC wastes in future landfills. In order to provide a measure of the strength of FBC waste leachates, comparisons have

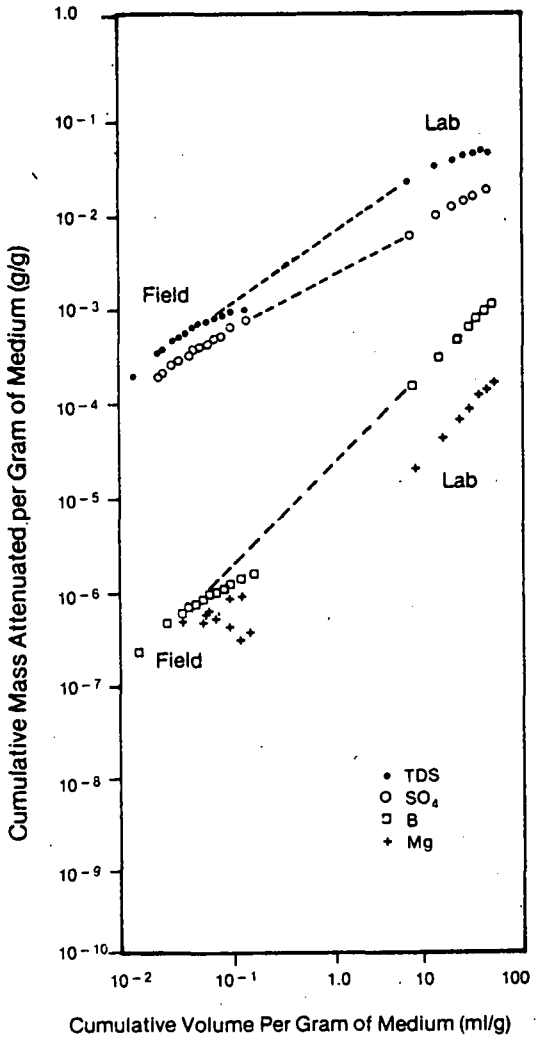

Figure 35. Correlation of Laboratory and Field Leachate Attenuation Data

been drawn between the leachate concentration and four sets of water quality standards, criteria, and goals:

- National Interim Primary Drinking Water Standards;
- National Secondary Drinking Water Regulations;
- Multi-Media Environmental Goals; and
- Quality Criteria for Water (EPA, 1976).

The first step in drawing these comparisons is to obtain volume-weighted averages of concentrations for all 21 chemical parameters included in routine analysis. Step 1 (primary leaching) and Step 4 (primary attenuation) leachates are included in this analysis. For each parameter, a Discharge Severity (DS) is then obtained by calculating the ratio of the volume-weighted concentration of the parameter to the corresponding standard or criterion. The DS thus determined is classed into 3 categories for each set of standards and criteria: (1) DS less than 1; (2) DS between 1 and 10; and (3) DS greater than 10.

The DS categories for all 21 chemical parameters included in routine analyses are shown for the Primary and Secondary Drinking Water Standards in Figure 36. Each of the parameters is categorized for both the leachate generation and attenuation phases for the laboratory studies and field studies. The results of this categorization show that, in the laboratory phase of investigation, cadmium appears to be of greatest concern. In the field studies, manganese, sulfate, and TDS are apparently of greatest concern.

Category 1 Parameters
(DS <1)

Laboratory Leachate		Field Cell Leachate**	
Generation	Attenuation	Generation	Attenuation
As, Ba, Cd, Cl, Cu, F, Fe, Pb, Mn, Hg, Ag, Zn	Ba, Cl, Cu, F, Hg, Zn	Ba, Cd, Cl, Cu, F, Ag, Zn	Ba, Cd, Cu, F, Fe, Ag, Zn

Category 2 Parameters
(1 < DS < 10)

Laboratory Leachate		Field Cell Leachate	
Generation	Attenuation	Generation	Attenuation
Cr, Se, SO_4, TDS	As,* Cr, Fe, Pb,* Mn, Se,* Ag, SO_4, TDS	Cr, Fe	Cl, Ca

Category 3 Parameters
(DS > 10)

Laboratory Leachate		Field Cell Leachate	
Generation	Attenuation	Generation	Attenuation
	Cd	Mn, SO_4, TDS	Mn, SO_4, TDS

*Tabular position determined by detection limit.
**As, Pb, Hg, Se not determined for field cell leachates.

Figure 36. Discharge Severity for Drinking Water Regulation Parameters: PFBC Waste Leachates

When the Discharge Severities of all 21 chemical parameters are tabulated with respect to the Discharge Multi-Media Environmental Goals (DMEGs, which apply to discharge, not ambient concentration), it is apparent that more parameters may potentially be of concern (Figure 37). Discharge Severities for the DMEGs are calculated by obtaining the ratio of the volume-weighted concentration to the lower of the health and ecology DMEG values. In the laboratory studies, calcium is of greatest concern in the leachate generation phase. In

laboratory attenuation, calcium, cadmium, cobalt, nickel, potassium, and silver are of greatest concern. Field studies show that calcium, magnesium, nickel, and potassium are of the greatest potential concern in both the leachate generation and attenuation phases.

Category 1 Parameters
(DS < 1)

Laboratory Leachate		Field Cell Leachate**	
Generation	Attenuation	Generation	Attenuation
Al, As, Ba, B, Cr, Co, Cu, Pb, Li, Mg, Mn, Hg, Mo,† K, Se, Ag, Sr, Tl, V	Ba, B, Cr, Li, Mg, Hg, Sr, Tl, U‡	Al, Ba, B, Cr, Co, Cu, Mo, Sr, Ti, Zn	Al, Ba, B, Cr, Cu, Mo, Sr, Tl

Category 2 Parameters
(1 < DS < 10)

Laboratory Leachate		Field Cell Leachate	
Generation	Attenuation	Generation	Attenuation
Cd,* Ni,* Zn	Al, As,* Cu, Pb,* Mn, Se,* V, Zn	Cd,* Li, Mg, Ag, V	Cd,* Co, Li, Mg, Ag, V, Zn

Category 3 Parameters
(DS > 10)

Laboratory Leachate		Field Cell Leachate	
Generation	Attenuation	Generation	Attenuation
Ca	Ca, Cd, Co, Ni, K, Ag	Ca, Mn, Ni, K	Ca, Mn, Ni, K

*Tabular position determined by detection limit.
**As, Pb, Hg, Se, U not determined for field cell leachates.
†Mo not determined for laboratory attenuation.
‡U not determined for laboratory generation

Figure 37. Discharge Severity for Discharge Multi-Media Environmental Goal Parameters: PFBC Waste

For the Quality Criteria for Water (QCW), most of the 21 parameters analyzed for are subsumed by the Discharge Multi-Media Environmental Goals. The only parameter not addressed in the DMEGs, and that has a DS greater than 10, is boron. As in the DS determinations for DMEGs, the "worst-case" (lowest value) of concentration for each parameter was used in deriving DS values for the QCW.

SUMMARY AND CONCLUSIONS

This report has presented the interim results of a comprehensive program for the investigation of the hydrologic implications of disposal of solid residues from FBC. The results reported have included principally: (1) laboratory studies of leachate generation and attenuation; (2) field studies of leachate generation and attenuation; (3) preliminary attempts to correlate the laboratory and field results; and (4) comparison of leachate chemistry with several water quality standards and criteria.

The studies conducted to date have included only one of 3 planned FBC waste materials--pressurized FBC wastes. A variety of PFBC waste leachate generation and attenuation patterns have been noted for three representative parameters--calcium, boron, and sulfate. There appears to be a strong possibility of correlating laboratory and field results, at least for many chemical parameters. The leachate content of all 21 parameters included in the investigation has been compared to water quality standards and criteria. Cadmium, manganese, sulfate, and TDS appear to be of potential concern with respect to drinking water standards.

Much interpretive work remains to be accomplished for the program. For the most part, only observed trends in chemical behavior have been reported, but the causes of the observed trends have not yet been analyzed. The attempt to correlate laboratory and field results remains to be placed on a sound statistical basis. Also remaining to be accomplished in the program are parallel studies with two additional FBC wastes representative of different operating conditions and development of the methodology for case-by-case application of future FBC waste disposal sites.

ACKNOWLEDGEMENTS

Although the results reported here are presented by four individuals, the program is being conducted as a team effort in the true sense of the word. Acknowledgements are given to the following task leaders:

A. G. Lamkin, Laboratory Studies,

W. M. Little, Field Studies,

R. M. Mann, Chemical Analysis, and

H.J. Williamson, Data Management and Interpretation.

D. L. Jernigan, now at American Technological University, Killeen, Texas, was instrumental in development of the laboratory protocol and the direction of the program as a whole.

This project has been funded at least in part with federal funds from the U. S. Environmental Protection Agency under Contract #68-02-3103. The content of this publication does not necessarily reflect the views or policies of the U. S. Environmental Protection Agency, nor does mention of trade names, commercial products or organizations imply endorsement by the U. S. Government.

Metric Equivalents:

1 inch = 2.54 centimeters

1 foot = 0.305 meters

USE OF FLUIDIZED BED COMBUSTION SPENT SORBENT IN ENERGY FORREST PRODUCTION AND AGRICULTURE

D.A.A. Arthursson

Arthurssonlaboratoriet ALAB
Enkoeping 3, Sweden

K. Valdmaa

Swedish University of Agricultural Sciences
Upsalla, Sweden

An analytical and applied study for use of fluidized bed combustion spent sorbent to correct low soil pH levels and to provide essential nutrients is carried out in a proposed six years programme since 1977. The potential value of fluidized bed combustion spent sorbent to substitute present use of limestone and dolomite is identified (figure one). The government grant to this programme was proposed by the Swedish District Heating Association, the National Board of Economic Defence and the National Industrial Board.

Bed spent sorbent and filter spent sorbent are generated at a hot water district heating boiler station.[1] Calcium-Sulphur mole ratio 1,5 to 2,0 with a local dolomite as sulphur acceptor is used (figure two). Bed spent sorbent is drained from the hot bed through a fluidized bed reactor for complete oxidation and cooling to a temperature lower than 100°C. Filter spent sorbent is separated from flue gas at a temperature below 200°C by fabric filters. The spent sorbents are sepaately collected in two silos and removed offsite by truck to fields (figure three).

Until 1976 we studied ecologically significant fragments of heavy metals in soils and fluidized bed combustion spent sorbents. Effects on plants by fluidized bed combustion spent sorbents treated pot soils started 1977 (figure four). Treatments applied to field and pot soils are the following:

A No treatment
B Bed spent sorbent treatment to 70% of base saturation
C Filter spent sorbent treatment to 70% of base saturation
D Dolomite meal treatment to 70% of base saturation
E Limestone meal treatment to 70% of base saturation
F Bed spent sorbent treatment to 110% of base saturation
G Filter spent sorbent treatment to 110% of base saturation
H Dolomite meal treatment to 110% of base saturation
J Limestone meal treatment to 110% of base saturation

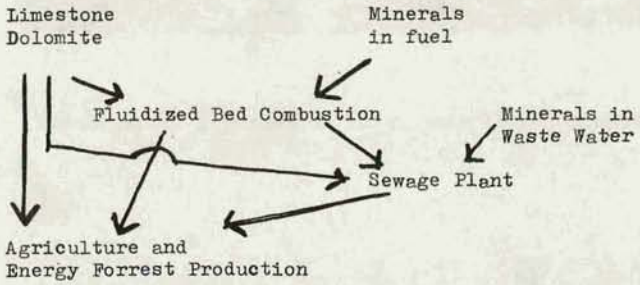

Figure one: Distribution of limestone and dolomite and use of fluidized bed combustion spent sorbent.

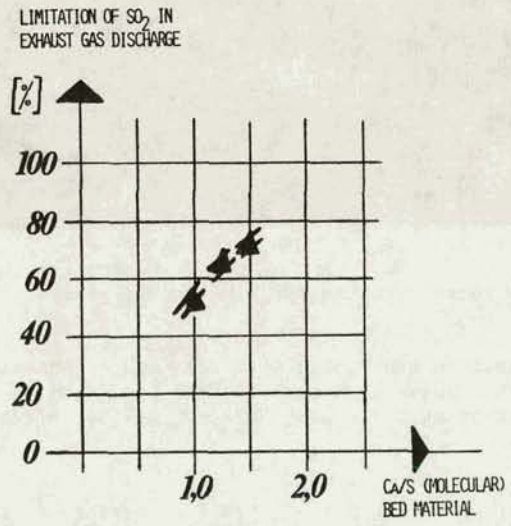

Figure two: Limitation of sulphur in exhaust gas emission when firing with oil with 3,6% sulphur content (by weight) as a function of the Ca/S molecular ratio for a bed material of 0,5 - 3,0 mm Sala dolomite.

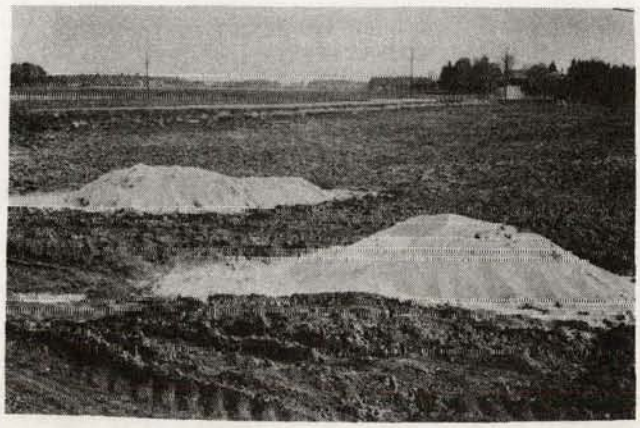

Figure three: Bed spent sorbent and filter spent sorbent at the field "Lado."

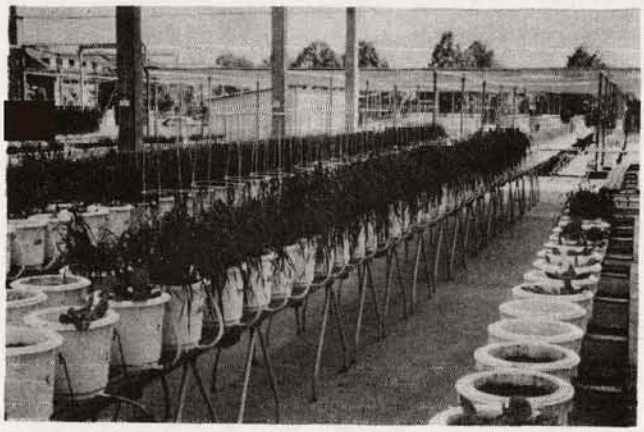

Figure four: Treatments of pot soils started 1977.

Results from two fields L (Lado) and A (Andersson) for the years 1978 and 1979 are presented as 100% production at field plot L78/A, L79/A, A78/A and A79/A.

Field Production	L78 %	L79 %	A78 %	A79 %
A	100	100	100	100
B	107	98	106	104
C	106	113	107	102
D	104	101	100	104
E	105	112	99	104
F	103	108	107	101
G	108	129	107	98
H	99	104	99	105
J	110	116	94	107
Error (A)	4,6	4,2	2,7	2,9

L978 was a year when more rainwater was added to the soils than a normal year as 1979. In the field each plot has four replicates with a gross area of 90 m^2 (6 x 15m). The crops are those in the rotation of the farm (1978 and 1979 barley). In the pot trials the respective treatments have two pots of each soil (L and A) with three different crops, wheat, barley an oilseeds (green matter of winter rape). All liming agents are spread evenly over the surface of the field plots and are mixed into the topsoil by rotary cultivation. In the pot trials the liming agents are mixed with the entire soil in the pot. Fertilisers are supplied to all treatments annually at sowing in amounts that correspond to the normal applications to the crops.

Soil samples are taken and analysed for their liming requirement according to the research plan and for chemical composition. Each sample is analysed for soil type, dry matter, organic carbon, pH, Kjeldahl-N, NO_3-N, Am-N, P-AL, K-AL, Ca-AL, Mg-AL, S, Fe, Mn, Cu, Pb, Hg and the degree of base saturation. Samples are taken of plant parts and analysed to define circulation of elements (soil to plant) for macro-micro nutrients balance.[2,3,4,5]

Presently research is being initiated to used forrest soils treated with sewage plant sludge and fluidized bed combustion spent sorbent. Observations from pot and small scale field treatments of soil for energy forrest production have identified this potential utilization of spent sorbent. The proposed research programme will involve a detailed chemical and physical analysis of the material and extensive greenhouse, growth chamber and field studies.

In our six years research programme observations until now are that fluidized bed combustion spent sorbent corrects low soil pH levels and provides essential nutrients to crops. Potential long term effects of fluidized bed combustion spent sorbent uses are expected to be identified within the next three years.

References:

1. Institute of Energy Symposium series No. 3, pp. 1719.

2. Plant and Soil 45, pp. 445-459.

3. Swedish J. agric. Res. 6, pp. 19-25.

4. Swedish J. agric. Res. 7, pp. 7-20.

5. Andersson, A. "Heavy metals in soil environment:

on their retention, distribution and amounts, on the influence of fertilization measures, and on methods of analysis," Swedish University of Agricultural Sciences, Feb. 25, 1977.

ENVIRONMENTAL EMISSIONS

NO_x AND SO_2 EMISSIONS

NO FORMATION AND REDUCTION IN FLUIDIZED BED COMBUSTION OF COAL

J. M. Beer, A. F. Sarofim, and Y. Y. Lee

Department of Chemical Engineering
Massachusetts Institute of Technology
Cambridge, Massachusetts 02139

I. Introduction

Fluidized combustion shows potential of becoming the method of choice for burning coal and other low grade fuels in industrial and utility boilers. The industrial development is in the initial stages of commercialization; package boilers of up to 100,000 lb/h steam capacity are under construction, and 200 to 600 MW utility boilers will be constructed during the 1980s both in the United States and abroad.

Unlike pulverized coal combustion which was developed gradually during the last fifty years, fluidized combustion has to be brought to the stage of industrial application within one decade, and these plants will have to fully comply with present day stringent requirements on pollutant emission and combustion efficiency before any significant industrial experience is gained with their operation. It follows that there is an urgent need for research to create - though the better understanding of the processes of combustion and pollutant emission - a sound base for fluidized combustor design. Nitrogen oxides emission from fluidized bed combustors (FBC) is generally lower than from other coal combustion systems such as stokers or pulverized coal combustors. The relatively low NO_x emission is due to a special combination of NO forming and reducing processes in the fluidized bed combustors. There is great interest in the quantitative description of these processes in a mechanistic mathematical model. Such a model is necessary to describe the complex interaction of factors influencing combustion efficiency, sorbent utilization, sulfur retention, and NO_x formation and reduction; information required for a strategy of design optimization by combustion process modification.

Experimental results from M.I.T.'s 2' x 2' pilot plant studies have shown consistently a buildup and subsequent reduction of NO concentration along the height of the bed and freeboard. The NO_x profiles in Fig. 1 illustrate the effectiveness of the NO destruction processes as they reduce the NO concentrations from typical values of 600 to 1000 ppm in the bed to a level of 200 to 300 ppm on top of the freeboard.

The purpose of the present study is to develop a mechanistic NO_x model based on considerations of the evolution and subsequent transformations of fuel-nitrogen leading to the formation of NO_x, N_2 and NH_3 as products. Previous studies [1,2,3] have shown that under FBC operating conditions about 90% of the NO_x formed originates from nitrogen organically bound in the fuel ("fuel-NO"), with the rest produced by the fixation of atmospheric nitrogen ("thermal NO"). For the development of a mechanistic NO_x model, it is then necessary to understand the chemical pathways of the coal nitrogen as it is converted into the above mentioned products.

Fig. 2 is a schematic diagram showing the transformations of coal nitrogen including the formation and destruction of NO_x in the fluidized combustion process. Upon injection into the fluidized bed, the coal thermally decomposes into volatiles and the residual char. NO is generated both during the volatile and the char combustion. The nitrogen left in the residual char decreases as the devolatilization temperature increases. On the other hand, NO is reduced to N_2 by reactions with nitrogenous fragments in the volatiles and carbon monoxide, and also by the heterogenous reaction with char[4,5]. Little data on the composition of the nitrogenous products of devolatilization are available. It is known, however, that under coking conditions, the upper temperatures of which are in the range of interest to fluidized bed operation, ammonia accounts for a major fraction of the fixed nitrogen compounds in the volatiles. The volatile nitrogen compounds will therefore be approximated by ammonia in the discussion that follows. Fig. 3 shows the locations where the above mentioned reactions are occuring in the fluidized bed. Devolatilization of coal and the formation of NO takes place readily near the distributor where the O_2 concentration is high. Nonetheless, the NO concentration should gradually decrease along the height of the bed and the freeboard because of the NO reducing reactions in the emulsion phase and the freeboard.

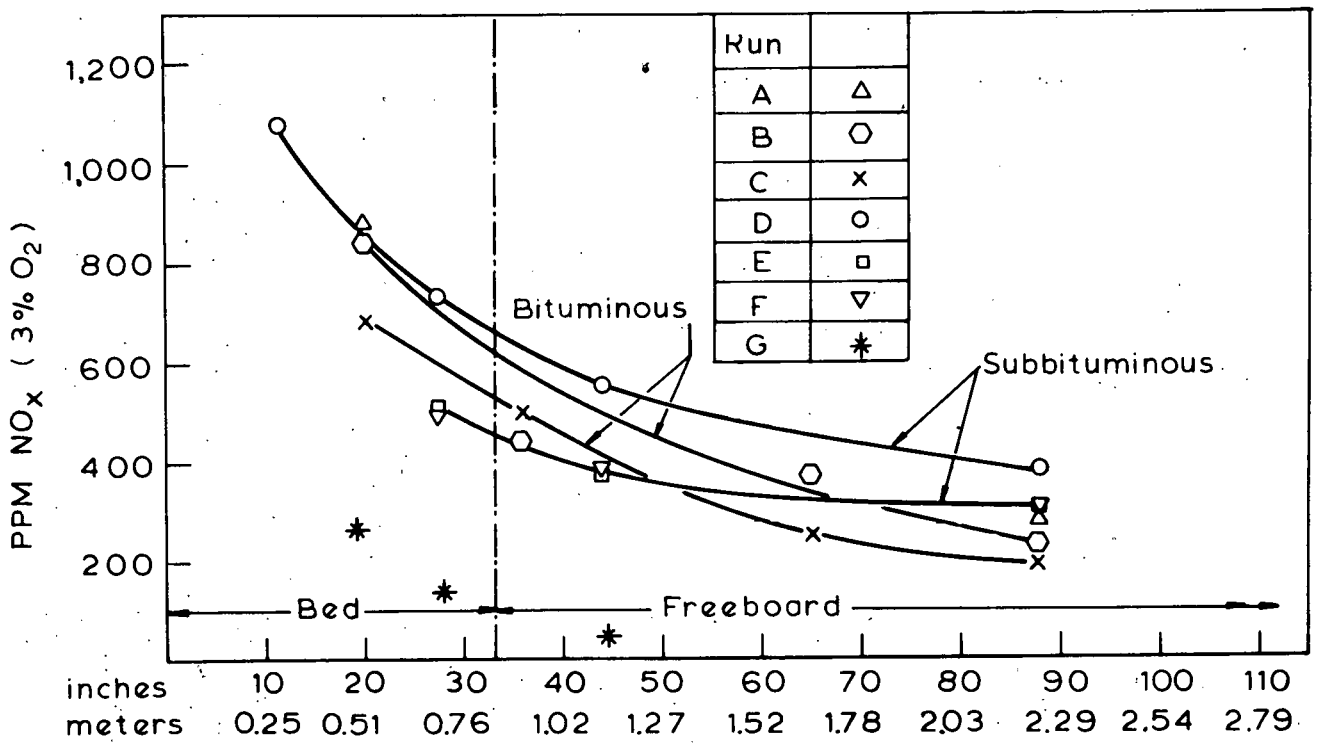

Fig. 1. NO_x concentration along the height of the bed and freeboard.

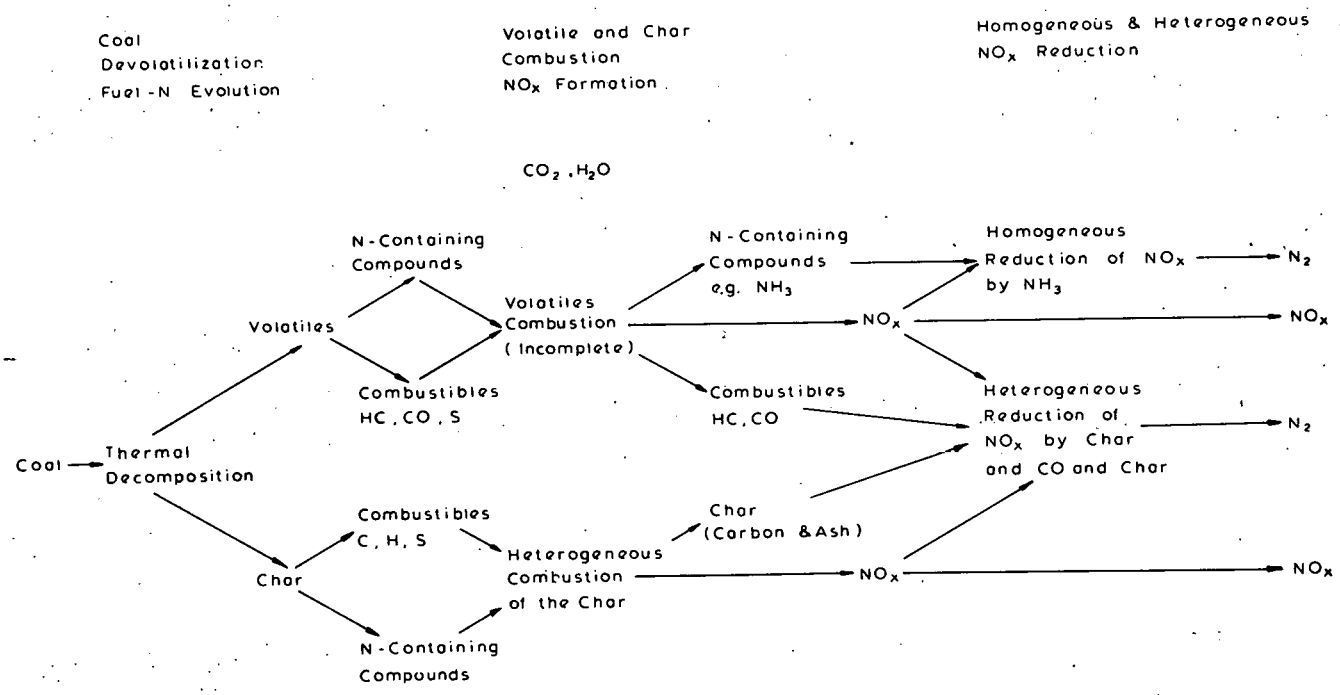

Fig. 2. Schematic of the transformations of coal nitrogen including the formation and destruction of NO_x in the fluidized combustion process.

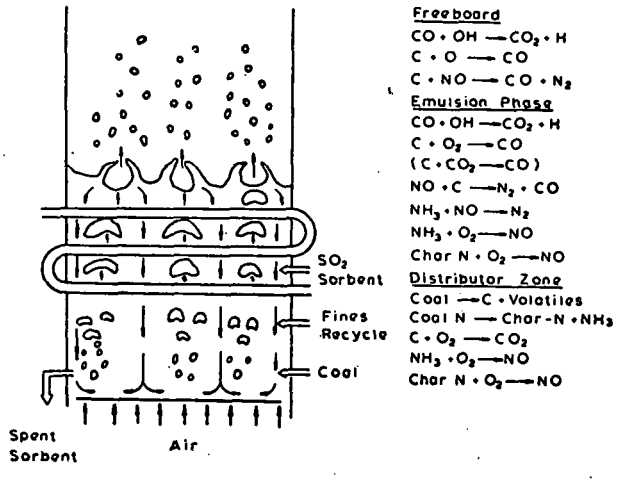

Fig. 3. Reactions occuring in fluidized bed combustor.

The development of a strategy for the control of NO_x emission by combustion modification requires a model capable of predicting the conversion of fuel-N in the bed and the freeboard for a range of operating conditions. The optimal conditions determined for NO_x emission will then have to be tested for their effects upon FBC performance, combustion efficiency, sulphur retention, etc. A brief summary of previous NO_x modeling efforts is shown in Table 1. Pereira and Beér[6] (1976) presented a model which used De Soete's kinetics for the homogeneous reactions of the coal-nitrogen but neglected the heterogenous NO-char reduction reaction. Horio et al.[7] (1977) neglected the release of coal nitrogen in the form of volatiles and its subsequent reactions. Wen et al.[8] (1979) did not consider the reaction between NO and nitrogeneous fragments in the volatiles. However, Wen et al. have taken into account the dependence on temperature of the partial release of fuel-nitrogen as volatiles. These models predict values for NO emission of

TABLE I. PREVIOUS STUDIES ON NO_x MODELING

INVESTIGATORS	2 PHASE		HOMOGENEOUS REACTIONS	HETEROGENEOUS REACTIONS	COAL DEVOLATILIZATION	DISTINGUISHING THE RELEASE OF FUEL-N AND TOTAL VOLATILE
	EMULSION	BUBBLE				
Pereira and Beér (1976)	Well-Stirred and Plug-Flow	Plug-Flow	$NH_3 + O_2 \rightarrow NO$ $NH_3 + NO \rightarrow N_2$	Not Considered	Either near the Distributor or Uniformly Distributed	No
Horio et al. (1977)	Well-Stirred	Plug-Flow	Not Considered	$NO + C \rightarrow N_2$	Uniformly Distributed	No
Wen et al. (1979)	Plug-Flow	Plug-Flow	Not Considered	$NO + C \rightarrow N_2$	Partial Release At The Distributor With Remainder Uniformly Released	Fuel-N Release Dependent On Bed Temperature

the same order of magnitude as that of experimental results. Only Wen's model, however, predicts a peak in the longitudinal concentration profile of NO in the bed as is observed experimentally. The NO concentration distribution depends strongly upon the nature of fluidization in the bed. This is dagramatically shown in Fig. 4.

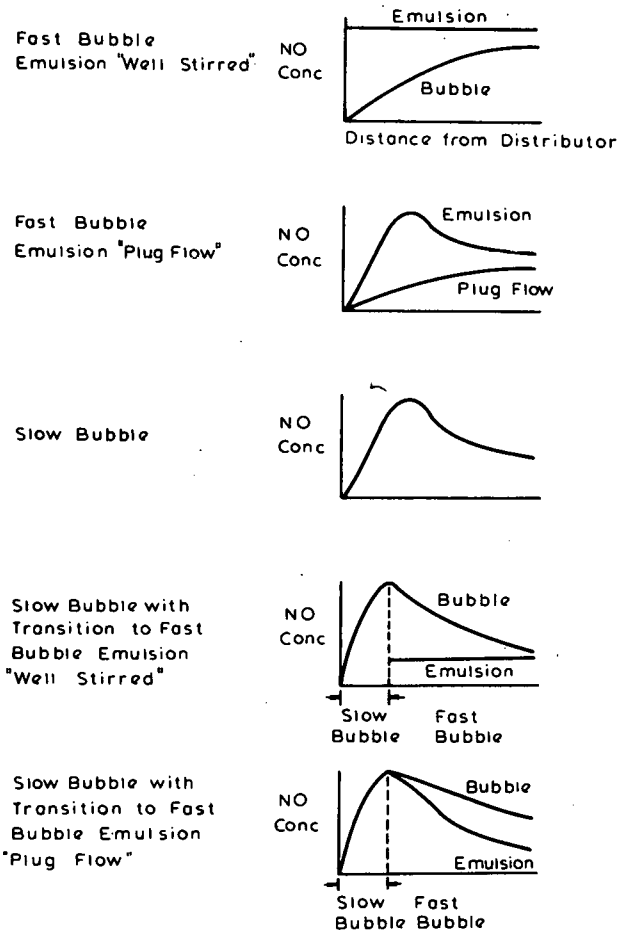

Fig. 4. The effect of mode of fluidization upon the NO concentration distribution.

It can be seen that the NO_x profiles are strongly influenced by the fluid mechanics near the distributor plate. If the air in excess of that needed for minimum fluidization by-passes the emulsion flow in fast bubbles (the classical Davidson-Harrison tho-phase model) the bubbles will have a lower NO_x concentration than the dense phase. If, however, the particle size is large and the bubble velocity is slower than the emulsion phase velocity (slow bubbles), then the NO formed near the distributor will flow through the beds in the bubbles; the extent to which the NO_x in these slow bubbles will be reduced by char in the dense phase will depend upon the exchange between the bubble and dense phases higher in the bed. If the bubble velocity increases, as a result of bubble coalescence to a value exceeding the emulsion gas velocity then a transition from a "slow " to a "fast" bubble regime will occur. Depending upon particle size and fluidizing velocity the different hypothetical profiles sketched in Fig. 4 may be approached in different FBC configurations. The sensitivity with which the NO concentration distribution in the bed responds to variations in gas flow patterns illustrates the importance of a realistic fluidization model as one of the components of the NO_x model development.

II. Components of the proposed model.

Fluid Mechanics

The model is based on the three-section characterization of the bed currently being used in the MIT system model. Above the distributor plate, an inlet zone I of variable height, HT, is assumed to exist in which the gases travel in plug flow, and oxygen bypassing due to bubble formation is unimportant. This region corresponds to the "slow bubble" regime in a fluidized bed and it leads into a section that comprises the rest of the bed. This upper section corresponds to the "fast bubble" regime of the bed where the two phase theory of fluidization[9] is applicable. It has a bubble phase B where gases travel in plug flow and carry no solids and an emulsion phase E in which the gas is assumed to have uniform properties. The gas flow rate through the emulsion phase is assumed to be that corresponding to minimum fluidization augmented by the flow in the bubble cloud, and the remaining fluidizing gas flow is assumed to pass through the bed in the form of bubbles.

Coal Devolatilization

Previous studies by Borghi et al.[10] have investigated the phenomenon of volatile release in coal combustion. The kinetic expression for volatile release proposed by Anthony et al.[11] was used. The rate expression is based on the assumption of parallel first-order irreversible reactions having the same pre-exponential factor, and activation energies that can be approximated by a Gaussian distribution. It was assumed that the rate of reaction of oxygen with volatiles was infinitely fast. The char oxidation was modeled using a modification of the Smith and Tyler model [12] for the reaction of a porous brown coal. In Fig. 5, the unburned fraction of volatiles and char are plotted versus time for a 3 mm particle exposed to an oxygen concentration of 8% and at temperatures of 1023 and 1323° K. Since the times for devolatilization are approximately two orders of magnitude shorter than the corresponding char

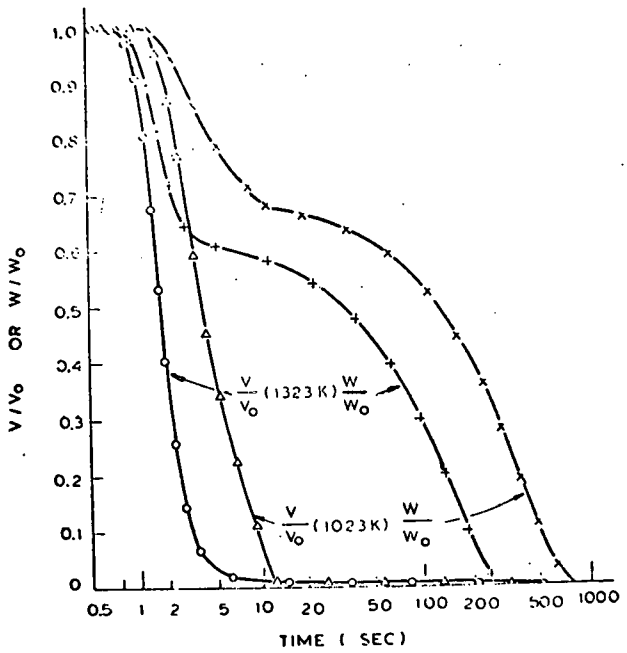

Fig. 5. Burnout and devolatilization histories of particles with ignition of volatiles. R = 0.15 cm, C_{O_2} = 0.08 atm.

burnout times, the volatiles can be assumed to be instantaneously released. However, the volatile release times are comparable to the solid circulation times and, hence, the volatile release will be distributed throughout the fluidized bed in a pattern dependent upon coal feed position and solid circulation velocities.

Char Particle Temperature Overshoot

Knowledge of the particle temperature is important for the calculation of the volatile nitrogen release. A single carbon particle burning model has been developed[13] to calculate particle temperature. The model assumes that O_2 diffuses from the bulk air stream in the particulate phase to the carbon surface where it reacts to form CO. The CO produced at the surface diffuses away from the the particle and reacts with the incoming O_2 to form CO_2 in the boundary layer. The CO_2 formed can diffuse back to the particle surface and reacts to form CO. Both radiation heat loss and stefan flow are considered. Since the carbon oxidation at the particle surface is exothermic the surface temperature would be higher than the ambient temperature. Figures 6 and 7 show the particle temperature overshoot versus the ambient temperature for the case of a 1 mm particle under 3.5% O_2 and 21% O_2 concentration in the surrounding respectively. The upper and lower curves represent the temperature overshoot for the limiting cases when CO_2 and CO are the products of combustion. In the operating temperature range of a fluidized bed combustor (1000-1200° K) the overshoot varies from 30°K for low O_2 concentration to 500°K for high O_2 concentration. The higher temperature overshoot occurs near the distributor where the O_2 concentration approaches that of the inlet air.

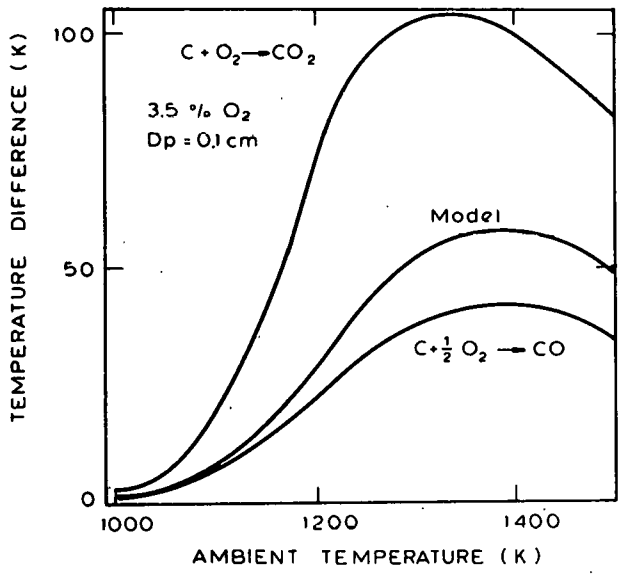

Fig. 6. Char particle temperature overshoot (3.5% O_2)

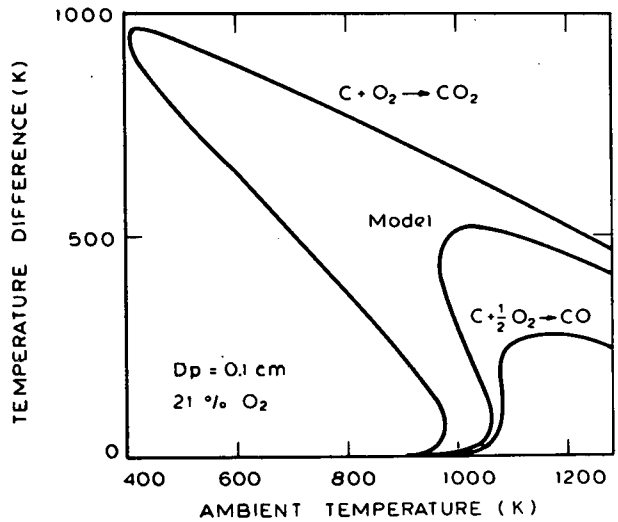

Fig. 7. Char particle temperature overshoot (21% O_2)

Fuel-Nitrogen Release

The yield and composition of the volatiles depend primarily on the coal type and the particle temperature. The volatile yield would determine the proportions of the fuel-nitrogen that undergoes the respective routes of chemical transformations of the volatile nitrogen and char nitrogen compounds. Pohl et al. [14] have made measurements on the percentage retention of nitrogen in char produced by heating samples of coal in crucibles until the weight approached a constant value. The results of the nitrogen evolution and dry weight loss are summarized in Fig. 8. In the operating temperature range of a fluidized bed (1000-1200°K), the volatile nitrogen evolved is shown to be 18 to 38% for bituminous coal. However, with the temperature overshoot near the distributor, the volatile nitrogen released would be 75 to 90%. This occurrence is in agreement with the experimental results which showed a rapid buildup of NO concentration near the distributor. It is also shown in Fig. 8 that most of the dry weight loss occurs at a higher temperature. Solomon [15] (1977) has performed experiments on 13 different coal types and reported that coal nitrogen is contained almost entirely in tightly bound rings which are released without breakage in the tar during the initial stage of devolatilization and the remainder released at higher temperatures when rings are ruptured. First order rate constants for the nitrogen evolution reaction are used to obtain the curves in Fig. 9., which is a plot of fraction of nitrogen evolved versus time. It is shown that in 50 seconds, 40% of volatile nitrogen is evolved, at 1000° K whereas 84% would be evolved at 1600° K, the difference in the fraction of fuel-N evolved as volatiles between Pohl's and Solomon's data may be due to the difference in types of coal. A major portion of the volatile N is expected to be released during the high temperature excursions that particles undergo each time they circulate through the distributor.

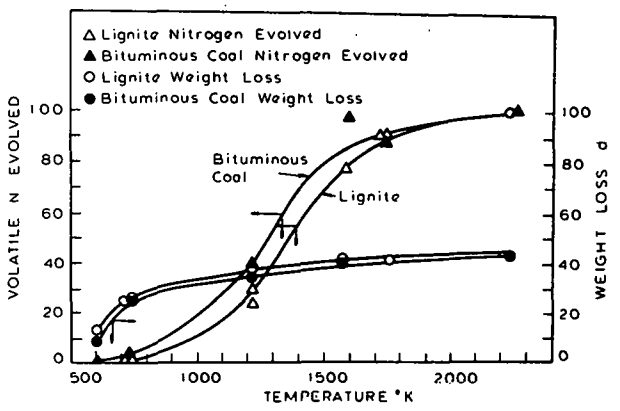

Fig. 8. Asymptotic volatile nitrogen evolved and weight loss crucible experiments.

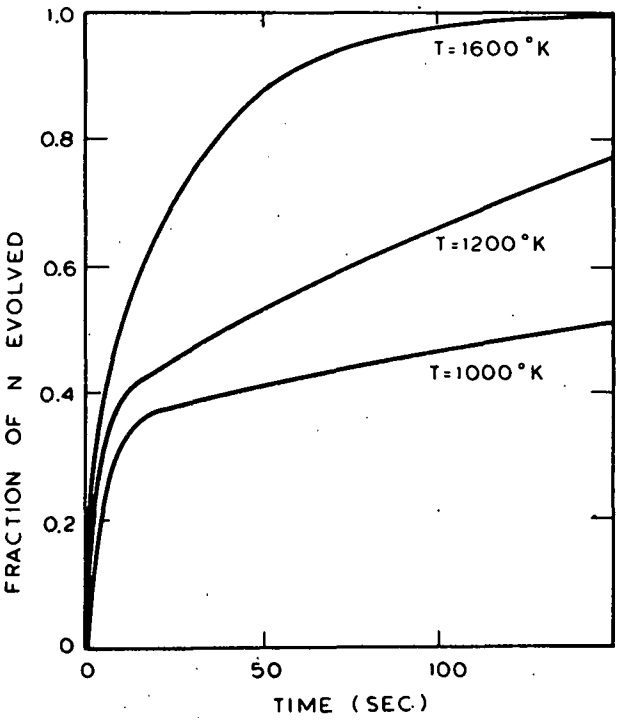

Fig. 9. Fraction of nitrogen evolved vs time (based on kinetic parameters by Solomon [15])

Volatile - N Reactions

A kinetic mechanism of the oxidation of the volatile-N to form NO and the destruction of the formed NO by the nitrogeneous compounds in the volatiles has been proposed by De Soete[16]. It involves the parallel-consecutive reactions in which NO is formed during oxidation of the fuel-N fragments and is subsequently destroyed by the same fragments:

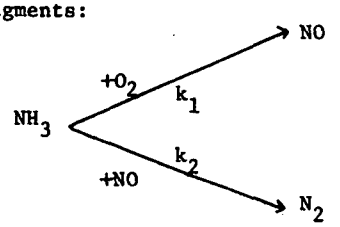

The rate constants of the two reactions are given below:

$$k_1 = 2.544 \times 10^3 \, T \exp(-15098/T) \ cm^3/mole \ s$$

and

$$k_2 = 6.564 \times 10^{11} \, T^{0.5} \exp(-13588/T) \ cm^3/mole \ s$$

In the model, the volatile nitrogen evolved is assumed to be NH_3. De Soete's global kinetics have been preferred to the more detailed mechanistic model of NH_3 oxidation because of computational savings.

NO-Char Reaction

Researchers[4,17,18] have investigated the NO-carbon reaction and most of them concluded that the reaction is first order with respect to NO concentration. The products of the reaction are CO, CO_2 and N_2. The value of the activation energy for the temperature range of 400 to 900°C and for carbonaceous solids such as coal chars, activated carbons and graphite is within the range of 8.2 to 26.6 kcal/mole.[19]

A number of experimental studies were carried out on the NO-char reactions using fixed bed[20] and fluidized[21] bed reactors in which the kinetic parameters of the reaction were determined. The rate constants of NO-char reaction plotted as a function of inverse temperatures for several experimental studies [20,21,22,23] are shown in Fig. 10. In our NO_x emission model, the rate constant proposed by L. K. Chan's data was selected; it can be represented by

$$k = 5.949 \times 10^{-6} T \exp(-19500/RT) \text{ m/s.}$$

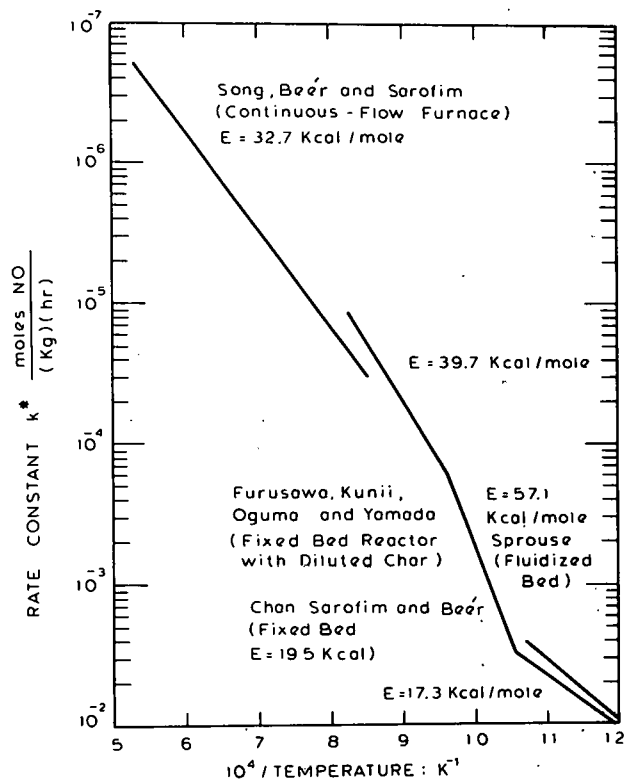

Fig. 10. Comparison of rate constants for nitric oxide reduction by char.

III. The Component Models and Assumptions

The components of the NO_x model have been discussed above. These, together with their sources, and the most important assumptions are summarized below:

- coal devolatization is approximated by parallel first order reactions (Anthony-Howard[14]).
- coal combustion is modeled allowing both volatile and char combustion (Borghi[10]).
- coal-nitrogen distribution between volatiles and char is determined from the data of Pohl[14].
- char particle temperature overshoot is calculated from a single particle combustion model of Y.Y. Lee.[13]
- volatile nitrogen reactions are modeled using the global kinetics for NH_3/O_2 and NH_3/NO of De Soete.[16]
- NO-char reaction kinetics are taken from the correlation by L. K. Chan.[20]
- The flow is approximated by slow bubbles (plug flow) near the distributor with the remainder of the bed modeled as two-phase with gas in the emulsion phase well-stirred, and in the bubble phase in plug flow.
- the volatile nitrogen is assumed to be evolved in the slow bubble region and the char nitrogen oxidation is assumed to parallel the combustion of the char.
- NH_3 oxidation in the bubble phase is assumed to be instantaneous.

IV. Mathematical Structure of the Model

Mass balances for NH_3 (subscript 1) and NO (subscript 2) in the slow bubble and the fast bubble regime of the bed are shown in Fig. 11 and 12 respectively. The equations obtained from the mass balances are summarized in Table 2. The symbols used in the equations are listed at the end of this paper.

The rate at which NO is destroyed by a char particle is obtained from equating the NO flux to a particle with the amount reacted on the outer surface and in the pores and assuming that the pores are cylindrical in shape and extend to the

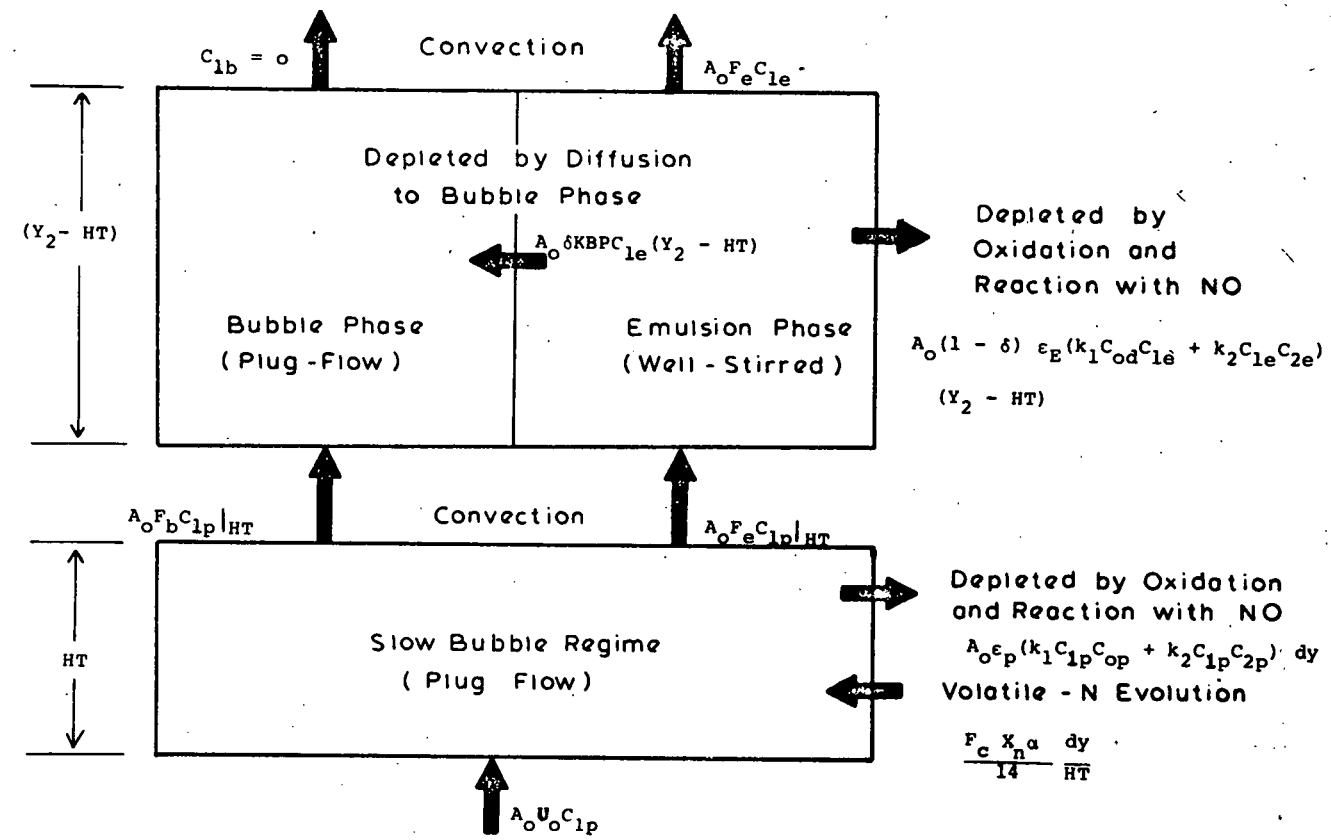

Fig. 11. Mass balance of volatile -N (NH_3)

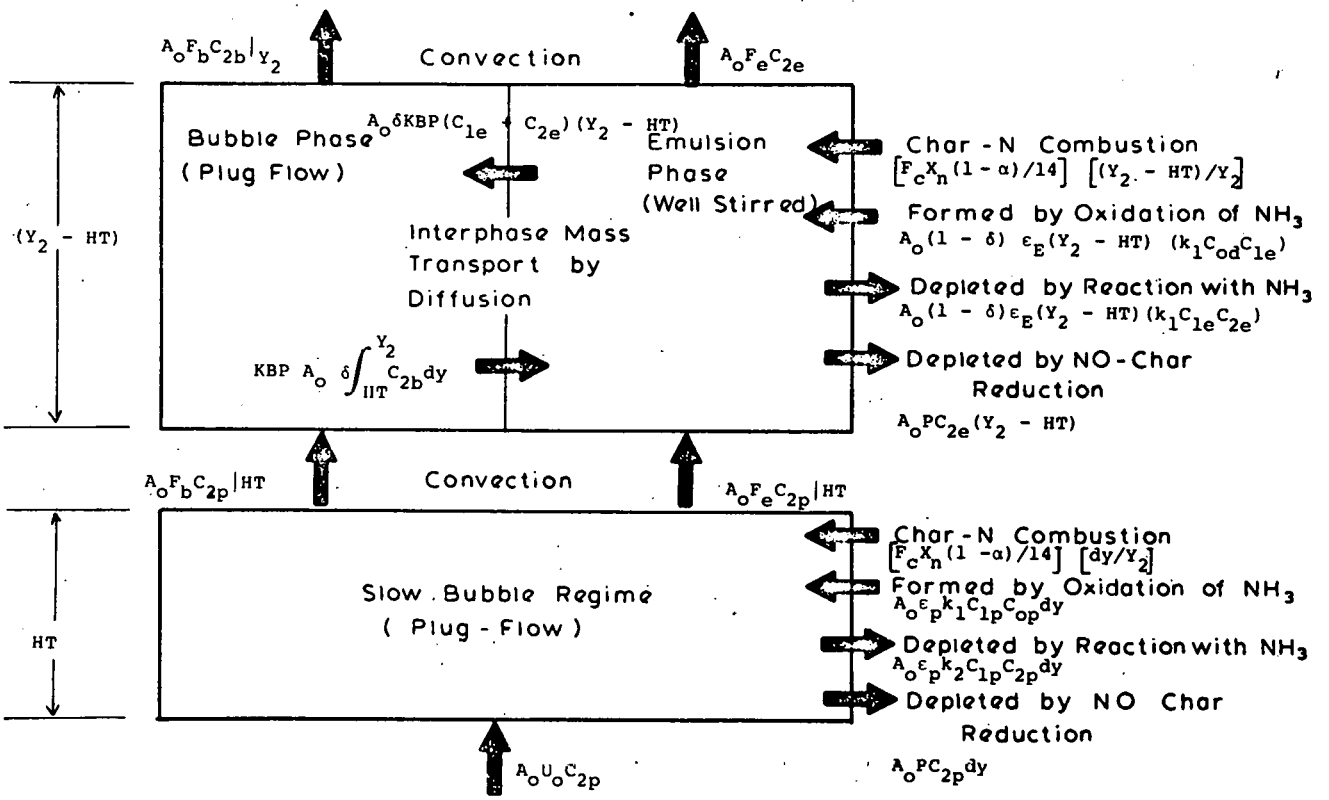

Fig. 12. Mass balance of NO.

TABLE 2. EQUATIONS OBTAINED FROM MASS BALANCES OF SPECIES 1 AND 2.

	SPECIES	EQUATION
Transition Height Region (Plug-Flow)	1	$\frac{dC_{1p}}{dy} = \frac{F_c X_n^{\alpha}}{14(HT)} \frac{1}{A_o U_o} - \frac{C_{1p}\varepsilon_p}{U_o}\left[k_1 C_{op} + k_2 C_{2p}\right]$
	2	$\frac{dC_{2p}}{dy} = \frac{F_c X_n (1-\alpha)}{14(Y_2)} \frac{1}{A_o U_o} + \frac{\varepsilon_p C_{1p}}{U_o}(k_1 C_{op} - k_2 C_{2p}) - \frac{PC_{2p}}{U_o}$
Bubble Phase (Plug-Flow)	1	$C_{1b}(y) = 0$
	2	$\frac{dC_{2b}}{dy} = \frac{\delta KBP}{F_b}[(C_{1e} + C_{2e}) - C_{2b}]$
Emulsion Phase (Well-Stirred)	1	$C_{1e} = \frac{F_e C_{1p}\vert HT}{F_e + (Y_2 - HT)\,\delta KBP + (1-\delta)\,\varepsilon_E (Y_2 - HT)(k_1 C_{od} + k_2 C_{2e})}$
	2	$C_{2e} = \frac{\frac{F_c(1-\alpha)X_n(Y_2-HT)}{14A_o Y_2} + C_{2p}(HT)(U_o - F_b K_6) + C_{1e}[(Y_2-HT)(1-\delta)\varepsilon_E k_1 C_{od} + KBP\delta + F_b(K_6-1)]}{[U_o - F_b K_6 + (Y_2 - HT)P] + (Y_2 - HT)(1-\delta)\,\varepsilon_E k_2 C_{1e}}$ where $K_6 = \exp\left[\frac{KBP\delta}{F_b}(HT - Y_2)\right]$

center of the particle. The following equation is obtained:

$$-4\pi R_p^2 D_g \frac{C_s - C_\infty}{R_p} = 4\pi R_p^2 (1-\theta)\, kC_s + 4\pi R_p^2 \theta k C_s \frac{\tanh\left(\sqrt{\frac{2k}{Dh}}\, R_p\right)}{\sqrt{\frac{2k}{Dh}}\, R_p}$$

This may be used to define a rate coefficient P for the NO reduction per unit volume of bed and per unit concentration of NO. P is given by

$$P = D_g 4\pi R_p n \frac{K_3}{1 + K_3} \frac{1}{A_o Y_2}$$

where

$$K_3 = \frac{(1-\theta)\, kR_p + \theta k\left(\frac{1}{K_2}\right)\tanh(K_2 R_p)}{D_g}$$

and

$$K_2 = \sqrt{\frac{2k}{Dh}}$$

In the mass balance calculations on NH_3, it is assumed that all ammonia transferred to the bubble reacts instantaneously and that therefore no ammonia is present in the bubble phase. It is also assumed that no combustion takes place in the bubble phase.

The program developed solves for the concentrations in the distributor zone first, then in the bubble and emulsion phases. The average NO and NH_3 concentrations along the height of the bed are calculated by weighing the concentrations in the bubble and the emulsion phase by their respective flow rates.

V. Results.

Fate of Fuel-Nitrogen

The percentage distribution of fuel-nitrogen in each step of the reaction pathway is shown in Fig. 13. For the case considered, 70.6% of the fuel-N evolved as volatiles (in the form of NH_3) and 29.4% formed NO through char combustion. Only 0.15% of the NO reacted with the NH_3 to form N_2, whereas 64.45% of the NO formed either from volatile-N or char-N are reduced by the NO-char reaction to form N_2. The ratio of NO formed from volatile-N to that formed from char-N is approximately 1.6 which is comparable with the experimental result obtained by Pereira et al. in a 7.5 cm fluidized bed. 8% of the fuel-N escaped from the bed in the form of NH_3 and this magnitude of NH_3 concentration has been reported by Furusawa et al.[3] Furthermore, the total NO found is 26.4% of the fuel-N in coal. From the results obtained, it is shown that NO-char reaction has a major effect on the reduction of NO emission from the bed.

Longitudinal profile of NO concentration in the bed.

Fig. 14 shows the typical shape of the NO vertical concentration profile in the bed. The profile shows a buildup of the NO concentration up to the height at which the transition from the "slow bubble" to "fast bubble" regime occurs and a subsequent decay of the NO concentration in the fast bubble region. The sudden jump of NO concentration at the transition height in the bubble phase is due to the assumption that NH_3 oxidation occurs instantaneously at the bubble interface. It is predicted that the NO concentration in the bubble is higher than that in the emulsion phase. These predictions are supported by the experimental result obtained from the M.I.T. 2' x 2'

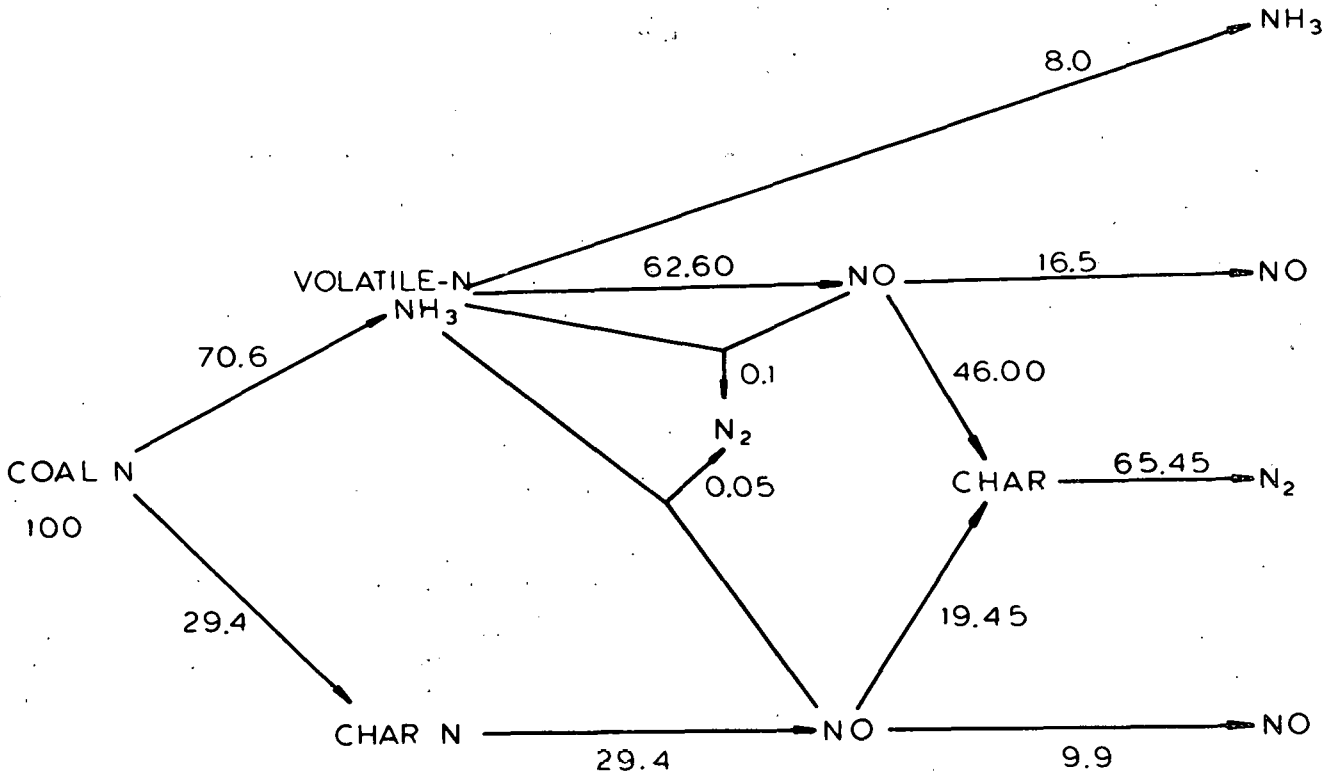

Fig. 13. Pathways for bound nitrogen in a fluidized bed combustor.
M.I.T. 2' x 2' bed (Run A) U_o = 0.87 m/s DPART = 0.762×10^{-3} m
EXAIR = 0.323 ROS2 = 0.246×10^{-3} m
TGAS = 1033°K BEDH = 0.796 m

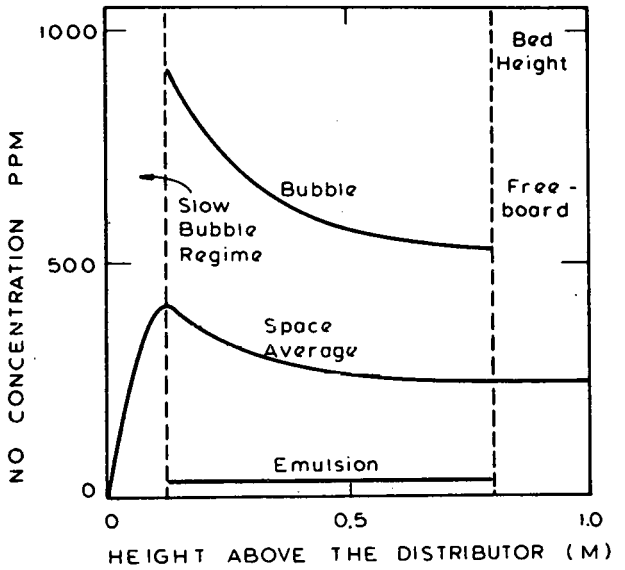

Fig. 14. Typical shape of NO concentration longitudinal profile.

2' x 2' BED (RUN B)
U_o = 0.98 m/s
DPART = 0.765 x 10^{-3}m
ROS2 = 0.273 x 10^{-3}m
TGAS = 1105.2°K
EXAIR = 0.19

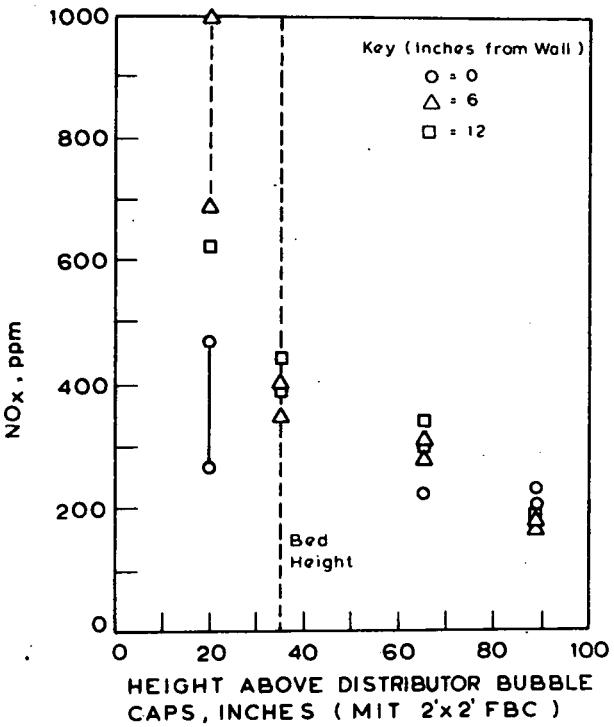

Fig. 15. NO_x concentration profiles.

pilot plant. Fig. 15 is a plot of NO concentration along the height above the distributor bubble caps. These studies have shown a much higher NO_x concentrations 6" from the wall than near the wall; the radial position of peak concentration is consistent with the observation that the bubbles are bursting at the top of the bed at locations about 6" from the wall. The good qualitative agreement between NO_x distributors calculated and measured in the fluidized bed reflects favorably on the chosen combination of the fluidization and NO_x conversion components of the model.

Parametric Studies

The first test of the model was made in the form of parametric studies. In these calculations the effects of changes in operating conditions upon the NO_x exit concentration from the bed were determined. The independent variables that were individually varied were gas superficial velocity, gas temperature, excess air ratio, sorbent size and coal particle size. The results of these studies have shown the same trends as the experimental studies of Pereira et al.: increase of gas velocity, gas temperature, excess air ratio and coal particle size and the decrease in sorbent size would increase the NO_x exit concentration from the bed. Figs. 16 and 17 show the effect of gas temperature and coal particle size on the NO_x concentration profile in the bed, respectively.

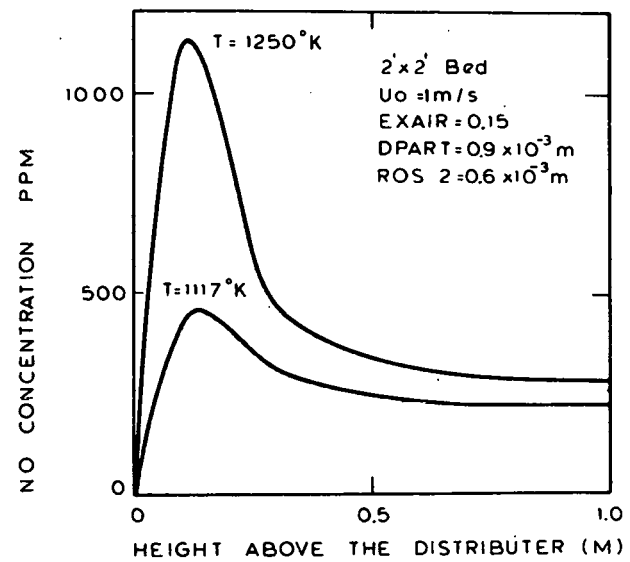

Fig. 16. Effect of bed temperature on NO emission.

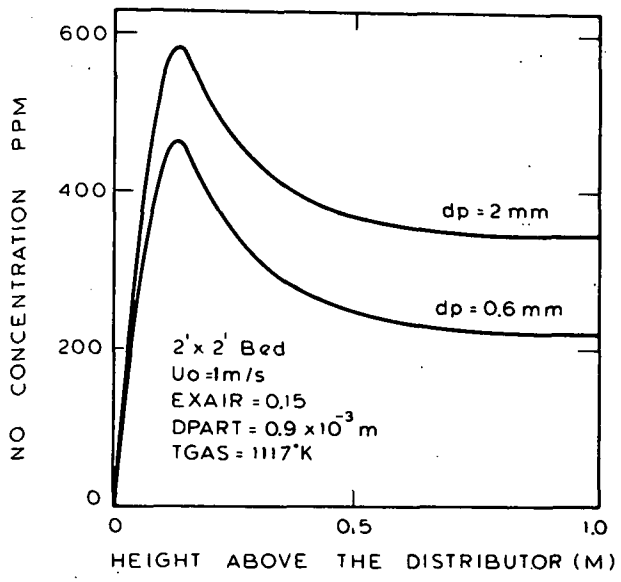

Fig. 17. Effect of coal particle size on NO emission.

Model Limitations

The limitations in the present model are due to the uncertainties in the simplifying assumptions made for the various component models. Future research and subsequent refinements of the model can be done in the following areas:

- Finite kinetic rate of the $NH_3 + O_2$ reaction in the bubble phase should be incorporated into the model despite the mathematical complication involved.
- With further research in the catalyzed NO/CO reactions, these reactions should be included in the model. This would require the determination of the rate parameters of the catalyzed reactions and the simultaneous development of the NO and CO emission model.
- Experiments should be performed to obtain the fuel-N split between the volatile-N and the char-N in a fluidized bed. These data can then replace Pohl's data as input to the model.
- Further information is needed on reactions of the NH_3 including its thermal decomposition in the fluidized bed.
- An improved solid-mixing model is needed in order to provide a better picture of the volatiles distribution in the bed.
- Reactions for the thermal fixation of nitrogen are needed to account for this small (about 10%) source of the total NO_x emitted by FBC's.

Conclusions

A detailed mechanistic model of NO_x formation and destruction in the fluidized bed which is based on the kinetics of coal-nitrogen transformations was developed. It can serve as a dependable guide for designing critical experiments and a base for the development of a predictive NO emission model. The important features of this study can be summarized as follows:

1) Mechanistic understanding.

   i) From the development of a single char particle burning model it has been found that under 21% O_2 ambient condition there can be a substantial particle temperature overshoot of around 500°K for a 1 mm particle. This temperature overshoot can occur in the region near the distributor where the O_2 concentration is high. This, in turn, affects the fraction of volatile-N release and its release near the distributor.

   ii) From the calculated results, NO-char reaction can account for the major effects of the NO destruction mechanism.

   iii) The nature of fluidization has an important effect in determining the spatial distribution of NO_x concentration in the bed, e.g., whether the bubble or emulsion phase has a higher NO_x concentration.

2) The model was used for calculations following the pathways of fuel-nitrogen. The results obtained on the proportions of NO_x - N_2 and NH_3 emitted as a function of operating parameters show reasonable agreement with experimental data.

3) Parametric studies show also that the model is capable of accounting for the effects of temperature, coal particle size, excess air ratio and sorbent size upon the NO_x concentration distribution in and eventual emission from the fluidized bed.

Acknowledgement

This research has been supported by a Grant from the U.S. Environmental Protection Agency for experimental studies on NO_x emission from fluidized bed combustor and by a contract from the U.S. Department of Energy for AFBC modeling. The financial support is gratefully acknowledged.

NOMENCLATURE

A_o	Cross-Sectional Bed Area, m^2
BEDH,Y2	Expanded Bed Height, m
C_i	Concentration of Gaseous Species i, kg-mol/m^3.
D	Pore Diffusion Coefficient, m^2/s
D_g	Molecular Diffusion Coefficient, m^2/s
EXAIR	Excess Air Ratio
F_c	Coal Feed Rate, kg/s
F_j	Gas Flow Rate per Unit Area through Phase j, m/s
h	Pore Radius of Char Particle, m
HT	Transition Height, m
k	Rate Constant of NO-Char Reaction, m/s
k_1	Rate Constant of $NH_3 + O_2$ Reaction, kg mol/m^2s
k_2	Rate Constant of NH_3 + NO Reaction, kg mol/m^2s
KBP	Interphase Mass Transfer Coefficient 1/sec
P	Reduction Efficiency Factor of NO-Char Reaction, 1/sec
R_p,ROS2	Radius of Coal Particle, m
T,TGAS	Gas Temperature, °K
U_o	Gas Superficial Velocity, m/s
X_n	Weight Fraction of Nitrogen in Coal

Greek Symbols

α	Volatile Nitrogen Content by Weight
δ	Bubble Fraction
ϵ	Void Fraction
θ	Void Surface Fraction of a Char Particle.

Subscripts

1	NH_3
2	NO
b	Bubble Phase
e,E,d	Emulsion Phase
o	Oxygen
p	Transition Height Region
s	Char Particle Surface
∞	Ambient

LITERATURE CITATIONS

(1) Jonke, A.A., (1969) Argonne National Lab. Publication No. ANL/ES-CEN 1001.

(2) Pereira, F.J., Beér, J.M., Gibbs, B.M. and Headley, A.B., 15th Symposium (International) on Combustion, The Combustion Institute, Pittsburgh (1974).

(3) Furusawa, T., Honda, T., Takamo, J. and Kunii, D., 2nd International Conference on Fluidization, Cambridge University Press (1978).

(4) Pereira, F.J. and Beér, J.M., Ph.D. Thesis, University of Sheffield (1975).

(5) Pereira, F.J. and Beér, J.M., Second European Symposium, French Section, Orleans, France (1975).

(6) Pereira, F.J. and Beér, J.M., Proceedings of the 2nd Engineering Foundation Conference on Fluidization, Cambridge University Press (1978).

(7) Horio, M., Mori, S., Muchi, I., 5th International Conference on Fluidized Combustion, Washington, D.C. (Dec. 1977).

(8) Wen, C.Y., Krishnan, R., Rengarajan, P., "Simulation of Fluidized Bed Coal Combustors", NASA CR-159529.

(9) Kunii, D and Levenspiel, D., Fluidization Engineering, John Wiley & Sons, Inc. (1969).

(10) Borghi, G., Sarofim, A.F. and Beér, J.M., Paper presented at A.I.Ch.E. 70th Annual Meeting, New York (Nov. 1976).

(11) Anthony, D.B., Howard, J.B., Hottel, H.C. and Meissner, H.P., Fifteenth Symposium (International) on Combustion, p.1303, The Combustion Institute, Pittsburgh, PA (1975).

(12) Smith, I.W. and Tyler, R.G., Combustion Science and Technology , 9, 87 (1974).

(13) Sarofim, A.F., Georgakis, C. and Lee, Y.Y., (paper to be submitted).

(14) Pohl, J.H. and Sarofim, A.F., "Devolatilization and Oxidation of Coal Nitrogen", paper presented at the 16th (International) Symposium on Combustion, Cambridge, MA (1976).

(15) Solomon, P.R., "The Evolution of Pollutants During the Rapid Devolatilization of Coal", Report No. R77-952588-3, United Technologies Research Center (1977).

(16) DeSoete, G., "An Overall Mechanism of NO Formation From Ammonia and Amines Added to Premixed Hydrocarbon Flames", The Combustion Institute, European Combustion Symposium, Sheffield, England (1973).

(17) Edwards, H.W., A.I.Ch.E. Symposium Series 125, 68 (1972).

(18) Shelef, M. and Otto, K., Journal of Colloid and Interphase Science 31, No. 1 (Sept. 1969)

(19) Sarofim, A.F. and Beér, J.M., "Modelling of Fluidized Bed Combustion", 17th Symposium (International) on Combustion, The Combustion Institute, Pittsburgh, PA (1978).

(20) Chan, L. K., "Nitric Oxide Reduction by Char in a Fixed Bed Reactor", M. S. Thesis, Chemical Engineering Department, M.I.T. (1977).

(21) Sprouse, A. M., "Reduction of Nitric Oxide by Coal Char in a Fluidized Bed", M.S. Thesis, Department of Chemical Engineering, M.I. T. (1977).

(22) Song, Y. H., Beér, J. M. and Sarofim, A.F., "Fate of Fuel Nitrogen during Pyrolsis and Oxidation," Proceedings of the Second Stationary Source Combustion Symp., EPA-600/7-77-07ed, 79 (1977).

(23) Furusawa, T., Kunii, D., Oguma, A., Yamada, N., Proceedings of the Society of Chemical Engineers, Japan, vol. 4, No. 6, pp. 562-566 (1978).

Questions to M. J. M. Beer:

Q: Krishna Pele

Have you considered the effect of pressure in your model?

A: We have no evidence, but we think that under PFBC conditions, interface mass transfer is greatly improved.

Q: (Participant not identified)

Do you assume no CO reduction?

A: We believe that CO plays a role in the reduction.

Q: Henry Withers, TVA

We would like to introduce an idea. Is it possible that we could put our in-bed tubes in choke rows and gain some staging and more turbulence?

A: I would agree with this. The tube arrangement is very important.

NO_x CONTROL THROUGH STAGED COMBUSTION IN FLUIDIZED-BED COMBUSTION SYSTEMS

T. E. Taylor

Foster Wheeler Development Corporation
Livingston, New Jersey 07039

INTRODUCTION

As the fluidized-bed combustion process becomes more widely accepted, new applications arise which, through either unusual feed composition or more stringent emissions regulations, exceed the current process emissions control capabilities.

Over the course of several years, it has become evident that the existence of more than trace amounts of carbon monoxide in the off-gas, or the operation which promoted CO in the off-gas, was effective in the reduction of NOx emissions from a fluid bed. These observations were sometimes dramatically demonstrated when coal feeding problems resulted in a fuel-rich mixture and therefore substoichiometric operation. Under these conditions, emissions of the oxides of nitrogen were observed to fall to levels below 20 ppm by volume. The CO and hydrocarbons emissions which resulted were, of course, far higher than could be tolerated in continuous operation. It was believed, however, that these could be lowered to acceptable levels with overfire air using the staged combustion approach. While it was never determined whether CO was entering into a destructive reduction reaction with the NO_x or whether the reduced emissions were due to a low oxygen partial pressure, the results were extremely encouraging. Utilization of this phenomenon in a fluidized-bed combustion process for NO_x reduction had never been seriously considered until this time because of the hereto acceptable emissions and the possible adverse effects of partially reducing conditions on sulfur capture and tube metal wastage. The advent of "offset" emissions regulations and the economic attractiveness of specialty fuels, however, have necessitated reevaluation of the staged combustion process.

PROGRAM OBJECTIVES

A pilot-plant test program was formulated to provide preliminary data for the evaluation of the process. Objectives of this program were:

1) Confirmation of the validity of NO_x reduction through staged combustion
2) Documentation of the stoichiometry requirements of each stage of the process
3) Documentation of combustion efficiency, sulfur capture and gaseous emissions
4) Determination of the effect of the process on bed chemistry.

DESCRIPTION OF TEST FACILITY

The test program described in this paper was performed on the fluidized-bed combustion facility at the Foster Wheeler Development Corporation (FWDC). A photograph and schematic of the test facility are presented in Figures 1 and 2. A description of the facility follows.

The fluidized-bed combustor consists of a refractory-lined carbon steel shell about 15 ft high. A constant cross-section of 20 in. x 20 in. is maintained over the entire height. The 3-layer refractory lining consists of 7 in. of lightweight castable, 2 in. of medium-weight castable, and a 1/4-in. layer of high-alumina erosion-resistant mortar. Operation of the bed can be seen through three quartz windows.

The present configuration (Figure 2) is capable of operating at the following conditions:

	Range	Design
Superficial velocity (ft/s)	4-12	10
Bed temperature (^oF)	1500-2100	1650
Excess air (%)	0-100	15
Coal rate (lb/h)	100-500	250
Ca/S ratio	0-20	4

Fluidizing air enters the furnace via a drilled, stainless-steel distributor plate (Figure 3) located above the plenum chamber. This plate has been designed for a 20-in. water pressure drop at design conditions. An alternate plate of the same design is available for high-velocity runs. Bed material was removed through a centered gravity tap. Four thermocouples on the plate permitted continuous monitoring of the plate temperature. Additional thermocouples at 1/2-, 1-, 2-, 4- and 6-in. intervals above the distribution plate provided the bed temperature profile above the plate. Addition of overfire air is accomplished using a sparger pipe located in the freeboard zone (Figure 4).

Air is supplied to the distribution plate, materials feeders and overfire air ports by a positive-displacement-type compressor rated at 1000 aft^3, 18 lb/in^2g. Air-stream flow rates are measured with orifice plate meters located in the air-supply lines.

Two multiple-pass tube bundles are used to remove heat -- one in the bed zone, the other in the convection zone. The lower bundle, which is fabricated from 1-1/2-in. O.D. 310 stainless-steel tubes, is cooled with pressurized water at 350 lb/in^{2}g. Downstream of the bundle, the coolant is flashed into a storage tank where the steam produced is vented and the water recovered is recycled. A temperature flow-control system maintains the bundle outlet below the saturation temperature. The upper bundle, located above the 8-ft freeboard, is constructed of 3/4-in. O.D. 304 stainless-steel tubes. Its multiple-pass, compound-flow design permits reduction of the flue-gas temperature to about 800°F.

After leaving the combustor, combustion products are passed through a single-stage cyclone separator. From the cyclone exit, the gas can be passed through one or two dilution flow misters and baghouse filters or be vented directly outside. The product gases are sampled upstream of the cyclone, and following cooling, filtering and dehumidifying, are passed through real-time gas analyzers, where concentrations of oxygen, carbon monoxide, sulfur dioxide and nitrogen oxides are determined. A spare sample point is available for batch gas analysis of hydrocarbon and carbon dioxide.

Startup of the unit is accomplished with a pressurized oil burner which discharges 1850°F gas directly into the bottom of the bed.

Coal and bed materials are metered from their bulk hoppers to the common-feed air lock by variable-speed screw feeders. Load-cell systems monitor the weight of each feedstock component. After mixing in the air lock, the feed is pneumatically transported to the center of the furnace at a point approximately 2 in. above the distribution plate. The 1000-lb capacity coal weigh hopper is serviced by a sizing and handling system.

Overbed coal firing is accomplished with a load-cell-monitored variable-speed screw feeder which feeds the coal approximately 6 ft above the surface. This method models the coal free-fall time encountered with spreader-stoker firing.

Spent bed material and ash are removed from the bottom of the furnace via a 3-in. standpipe with a ball-valve-controlled output.

Temperature of the combustor, inlet and outlet streams, and some of the peripheral equipment is monitored and recorded on two multipoint recorders.

Pressure-drop data from the bed are monitored on a strip-chart recorder powered by a differential-pressure transmitter that is connected across the furnace.

The facility is equipped with a fluidized-bed coal dryer, which is capable of reducing surface moisture of the coal down to 1 percent prior to feeding it to the coal crusher.

Recycle operation (Figure 5) is made possible by a diverter valve on the cyclone dipleg which permits fines to be directed either to a screw feeder or waste. The recycle screw feeder is of the variable-speed type. It supplies a dense-phase pneumatic transport line which conveys the fines into the bed.

TEST PROGRAM

Program Outline

To provide data for a preliminary assessment of staged combustion for NO_x reduction, a series of eight batch tests, followed by a 50-hour continuous performance test, were carried out. The eight batch tests verified the significant parameters for the process and established guidelines for operating limits. From these data, conditions for the 50-hour run were chosen.

Target Emissions Limits

Emissions levels of 100 ppm NO_x and 60 ppm SO_2 (corrected to 3 percent O_2) were selected as goals for the test program. Selection of these limits was guided by both current and proposed emissions limits and offset regulations.

Fuel and Sorbent

A western bituminous coal was used in this test series. The nominal 1 percent sulfur content was found to vary from 0.6 percent to 1.1 percent. Coal preparation consisted of drying and crushing the 1-1/2 in. x 0 as received coal to 1/4 in. x 0 for inbed feeding. Limestone for the tests was obtained from a commercial quarry in Apex, Nevada. Chemical analyses of the coal and limestone appear in Tables 1 and 2, respectively.

Batch Test Procedures

The general procedure for testing each set of conditions consisted of the following steps: First, the combustor was stabilized at a given superficial velocity and residual O_2. Next, the coal feed rate was slowly increased to a point where NO_x was reduced to the target level (60 ppm to 70 ppm). Normally, this resulted in a residual O_2 concentration of 0.4 percent and a CO concentration of 0.6-1.2 percent. Finally, overfire air was added until the CO emissions reduction was maximized without exceeding the NOx maximum emissions level (100 ppm).

Minor adjustments were then made as necessary to maintain both bed temperature and target emissions.

50-Hour Test Procedure

Startup and initial staged combustion adjustments were accomplished using techniques similar to those used in the batch tests. During the beginning of the 20-hour stabilization period, however, previously identified optimum operating conditions were reconfirmed. Following stabilization, several data sets were obtained during the 30-hour test period.

RESULTS

The test data from this program have been divided into two sections, batch test results and those from the 50-hour continuous operation test. Data obtained during the batch test portion of the program were used to verify test procedures and identify optimum ranges for the primary operating variables. Because much of these data were obtained at nonequilibrium conditions, the results are qualitative and therefore will not be presented. Of more significance are the data from the 50-hour test where thermal, physical and chemical equilibria were approached. Two test periods (Runs 63 and 64) of 8- and 6-hours' duration, respectively, have been selected for review. Results from these test periods appear in Tables 3, 4 and 5. Discussions of these and other related results appear in the following sections.

Gaseous Emissions

Table 3 presents a summary of the operating conditions maintained during the 50-hour staged combustion test and the average emissions which resulted. To permit direct comparison of the results to the target limits, reported values have been corrected to 3 percent residual O_2. Examination of these results will show that the average value maintained during both tests for both NO_x and SOx was below target limits. Instantaneous values of SOx in Run 63 did, in some cases, exceed the 60 ppm limit. This problem was eliminated by slight changes in the operating conditions as can be seen in the results from Run 64.

Carbon monoxide emissions averaged 0.06 and 0.08 percent, or 600 and 800 ppm, respectively. Further refinement of the operating conditions by means of changing the residual O_2 level residence time and freeboard temperature profile has resulted in lower emissions during subsequent test series.

A better idea of the NO_x and SO_x reduction picture can be obtained in Figures 6 and 7. These graphs present the actual measured NO_x and SO_x concentrations at 10-minute intervals for Runs 63 and 64. Reference lines representing the target limits for these pollutants have been corrected to the residual O_2 maintained during the test. As can be seen in all cases, the NO_x emissions are well within the target limits.

Limestone feed rates maintained during the tests appear in Table 4. Even though the Ca/S mole ratios of 6.03 and 4.75 appear a little high, the actual lime usage rate is well within commonly encountered bounds for higher sulfur coals. This is more easily observed by examining the ratio of lime feed/coal feed. As an example, a 4 percent sulfur coal requiring a Ca/S mole ratio of 3:1 would require a lime/coal weight ratio of 0.38. Thus, although the mole ratio may look high, because of the low sulfur content of the coal, the actual lime usage rate is within limits experienced in atmospheric fluidized-bed steam generators.

Combustion Efficiency

Combustion efficiency determined during the two combustion checks (Runs 63 and 64) was found to be 96.7 and 94.9 percent, respectively, based upon carbon combustion. A benchmark combustion efficiency average of 97 percent was established during conventional runs on the test fuel at similar operating conditions. Table 5 presents an accounting of the distribution of the carbon combustion efficiency losses for each run. As might be expected, the cyclone fines represent the largest single loss amounting to 66.16 percent and 76.21 percent, respectively, of the total carbon loss in each run. Therefore, it would appear that the largest gain in efficiency could be realized by reducing the cyclone loss.

Process Stoichiometry

The distribution of combustion air between the bed and the overfire air distributors is tabulated in Table 4. In each case, an initial stoichiometry of approximately 85 percent was necessary to provide the required reduction in NOx emissions. Measurements of CO prior to introduction of overfire air showed that the resultant CO emission was 0.6-1.2 percent by volume, with an average value of 0.8 percent. Optimum reduction of CO emissions without large increases in NO_x emissions occurred at an overall stoichiometry of approximately 104 percent. This resulted in a residual O_2 level of 0.8 percent and 0.7 percent, respectively. During the original batch tests equivalent NO_x emissions reductions were accomplished with a higher overall excess air rate which resulted in lower CO emissions.

Bed Chemistry

Of great concern during the staged firing tests was the formation of calcium sulfide (CaS) in the partially reducing zones of the bed. This compound, whose formation is favored over calcium sulfate ($CaSO_4$) in reducing atmospheres, decomposes in water, producing hydrogen sulfide gas (H_2S) and calcium oxide (CaO). Thus, if present in large quantities in the waste bed material, it can create disposal problems.

To determine the severity of this potential problem, hot samples were removed from the bed and cooled in a sealed container prior to analysis. Similarly, samples from the cyclone and baghouse were also collected for analysis. The results of these analyses appear in Table 8.

As expected, all three samples contained varying amounts of calcium sulfide. Of greatest concern is the composition of the bed material which will make up the majority of the waste stream. Sulfide contents of the bed material samples were found to be approximately 30 percent of the total sulfur captured. However, they amounted to only 1.45 percent and 1.23 percent on a total basis.

In hope of finding a method to convert the sulfide back to sulfate prior to disposal, the kinetics of these reactions were reviewed. It was

determined that, if the sulfide-containing bed material could be exposed to oxygen concentration in excess of approximately 10 percent at bed temperature, conversion of the sulfide to sulfate would occur. To test this hypothesis, pure calcium sulfide powder was tested in a thermogravimetric analyzer under several different oxygen concentrations and at several different temperatures. Preliminary results show that a conversion rate of 8 to 10 percent can be expected with air at 1650°F. This level of conversion is certainly high enough to eliminate sulfur problems at the levels listed in Table 8.

The application of this reaction to a commercial device might take the form of the sketch in Figure 8. Removal of bed material would be accomplished in a normal fashion through an insulated duct. Air would be introduced through a sparger ring at the lower extremity of the duct just above the solids-flow metering device. The counter-flow of the air and solids would result in a cooling of the solids and heating of the air to near-bed temperature. As the air temperature exceeded approximately 1200°F, conversion of CaS to $CaSO_4$ would begin. Some control over the conversion rate would be possible by metering of the air and solids flowrates. Further refinement of this device might include the addition of a heat exchanger for better temperature control.

CONCLUSIONS

The test program has demonstrated that:

1) Significant reductions can be obtained in NO_x emissions through staged combustion without detrimental effects on combustion efficiency or sulfur capture.

2) Although a partially reducing atmosphere is maintained in the bed, the primary sulfur reaction results in sulfate formation.

3) Conversion of calcium sulfide (CaS) formed during combustion to calcium sulfate appears feasible.

TABLE 1

FUEL BULK ANALYSIS

Proximate	Percent
Fixed Carbon	39.17
Volatile Matter	46.25
Ash	9.45
Moisture	5.13
Ultimate	**Percent**
Carbon	64.95
Hydrogen	5.32
Oxygen	13.15
Nitrogen	.99
Sulfur	1.01
Ash	9.45
Moisture	5.13

TABLE 2

BULK LIMESTONE ANALYSIS
(CALCINED)

	Percent
CaO	52.65
MgO	0.40

TABLE 3

STAGED COMBUSTION TEST RESULTS

RUN #	Average Bed Temp. (°F)	Superf'l Velocity (ft/s)	η_C Based on Carbon (%)	Emissions Corrected to 3% O_2								
				SO_x (ppm)			NO_x (ppm)			% CO		
				Avg.	Low	High	Avg.	Low	High	Avg.	Low	High
78-63	1556	4.06	96.7	33	0	99	69	53	89	.06	.02	.13
78-64	1549	3.99	94.9	8	0	18	76	54	89	.08	.02	.23

TABLE 4

STAGED COMBUSTION AIR DISTRIBUTION

RUN #	Coal Flow (lb/h)	Primary Air (lb/h)	% Stoich. Air	% CO Prior to Overfire Air	Overfire Air (lb/h)	Cumul. % Stoichiometric Air	% O_2 in Off-Gas
78-63	111.25	801	85.30	0.8	178.70	103.90	0.80
78.64	108.40	793	86.39	0.8	156.58	103.45	0.70

TABLE 5

CARBON LOSS ACCOUNTING

	Combustion Efficiency % Loss	% Total Loss
Run 78-63		
Baghouse	0.647	19.42
Cyclone Dust	2.206	66.16
CO in Off-Gas	0.480	14.42
	3.333	100.00
Run 78-64		
Baghouse Dust	0.639	12.65
Cyclone Dust	3.881	76.21
CO in Off-Gas	0.563	11.14
	5.053	100.00

TABLE 6

STAGED COMBUSTION MASS FLOW

Flow (lb/h)	Run 78-63	Run 78-64
Coal	111.3	108.4
Limestone	37.0	28.6
Cyclone	25.9	23.8
Baghouse	3.2	5.0
lb Lime/lb Coal	.33	.26
Ca/S Mole Ratio	6.03	4.75

TABLE 7

INPUT AND OUTPUT STREAM ANALYSES

	% Carbon	% Hydrogen
Run 78-63		
Coal	64.14	5.42
Baghouse	14.62	.87
Cyclone	6.08	.58
Run 78-64		
Coal	68.0	6.03
Baghouse	9.42	.33
Cyclone	11.93	.36

TABLE 8

ANALYSIS OF SULFUR COMPOUNDS
IN COMBUSTOR EFFLUENT STREAMS

	CYCLONE SAMPLE			BAGHOUSE SAMPLE			BED SAMPLE		
RUN #	Total Sulfur (%)	Sulfate Sulfur (%)	Sulfide Sulfur (%)	Total Sulfur (%)	Sulfate Sulfur (%)	Sulfide Sulfur (%)	Total Sulfur (%)	Sulfate Sulfur (%)	Sulfide Sulfur (%)
78-63	*	*	*	*	*	*	4.89	3.44	1.45
78-64	1.91	1.60	.31	1.66	.96	.70	3.89	2.66	1.23

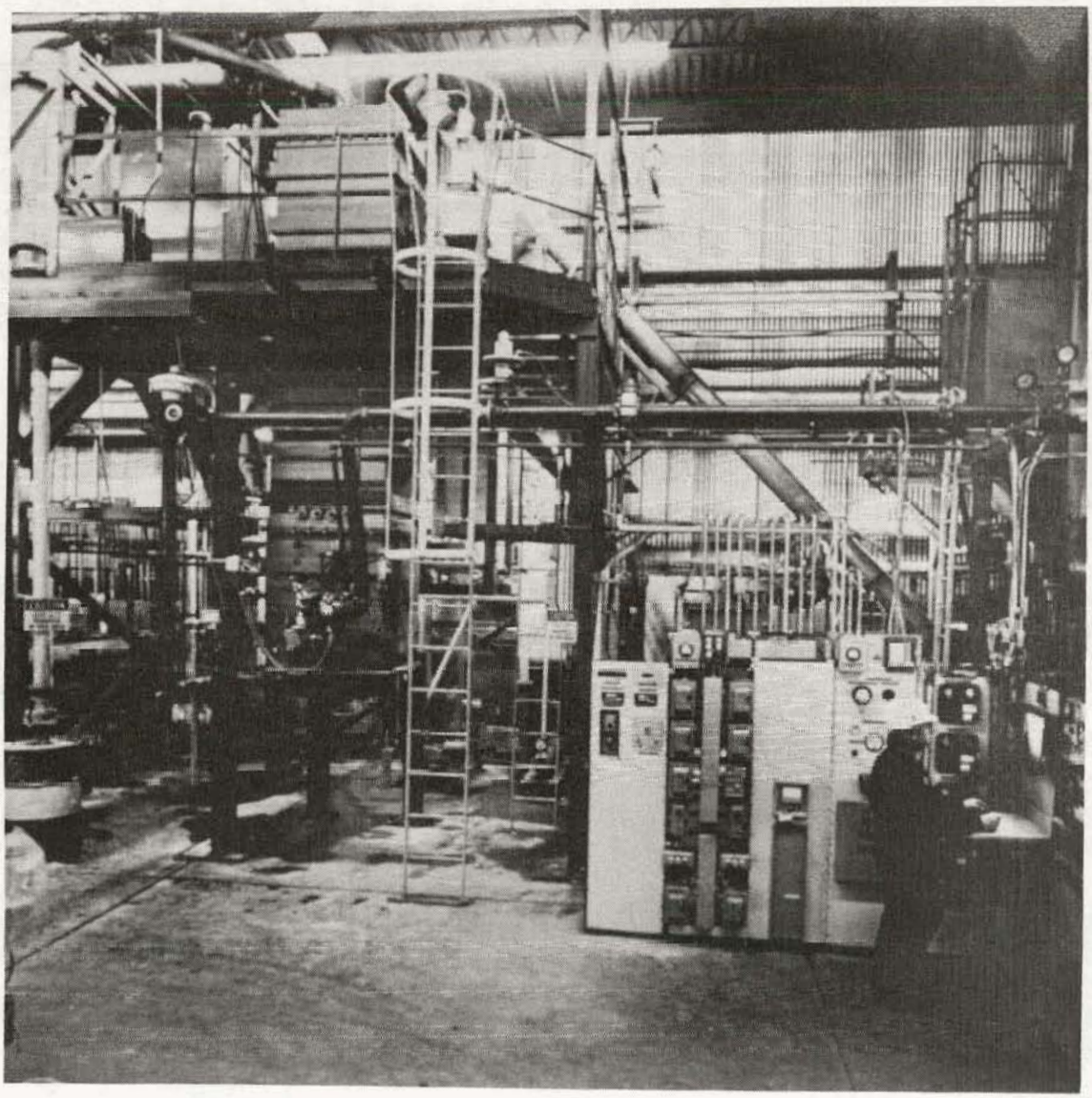

FIGURE 1 20 IN. X 20 IN. ATMOSPHERIC FLUIDIZED-BED PILOT PLANT

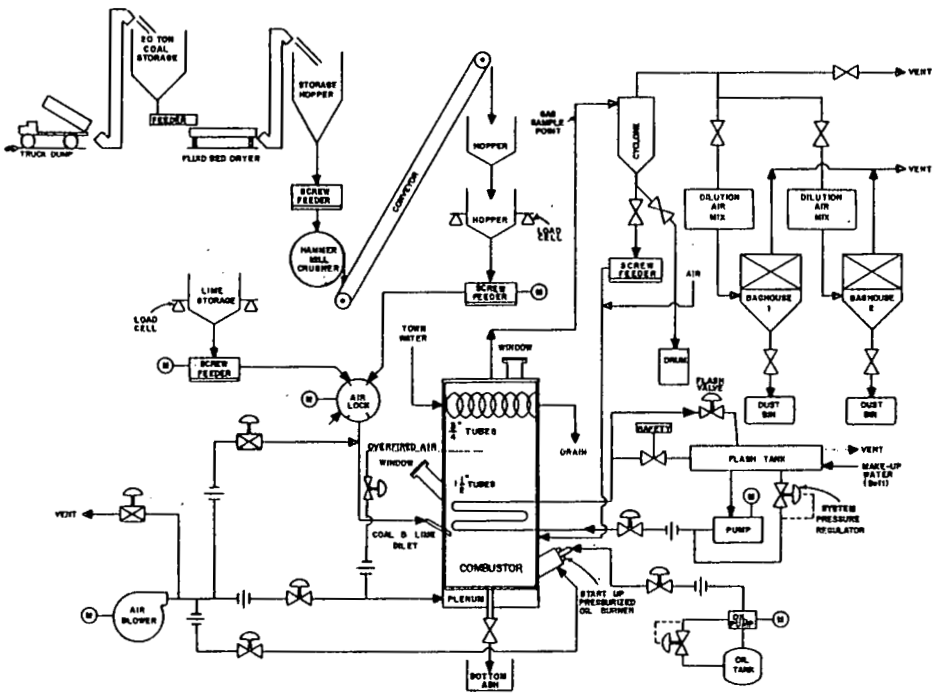

FIGURE 2. FLOW SHEET 20" x 20" FLUID BED PILOT PLANT

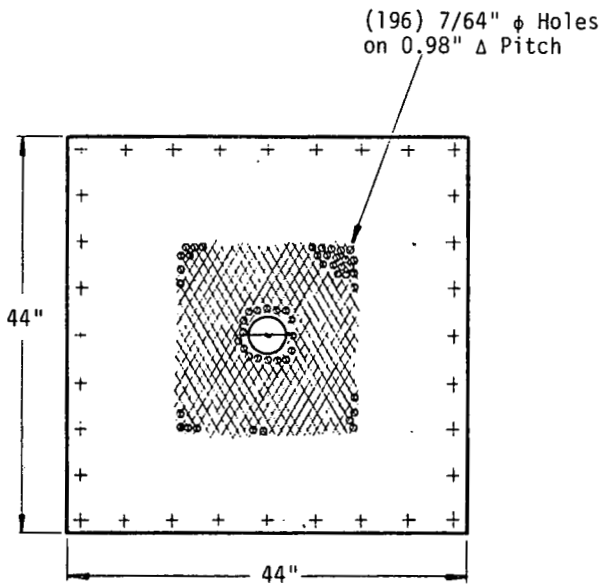

FIGURE 3. PERFORATED DISTRIBUTION PLATE

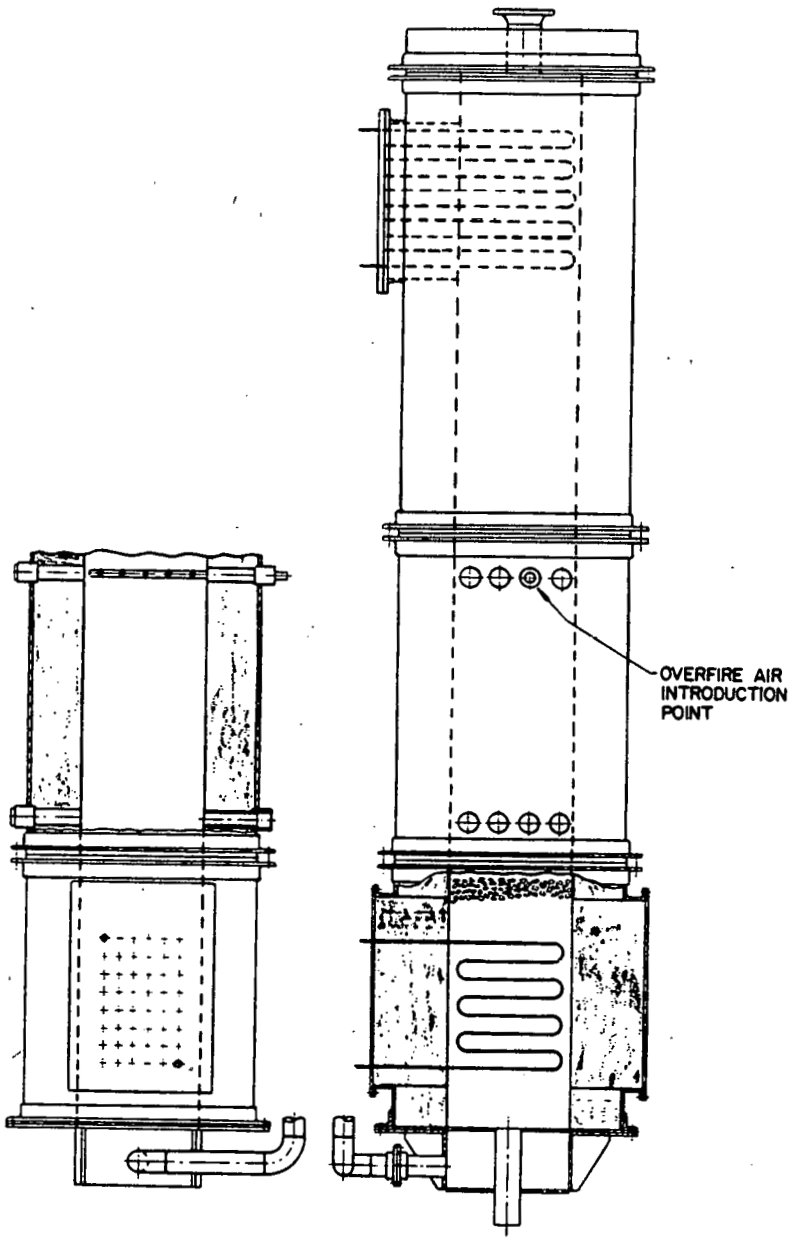

FIG. 4 ELEVATION VIEW OF OVERFIRE AIR INTRODUCTION POINT

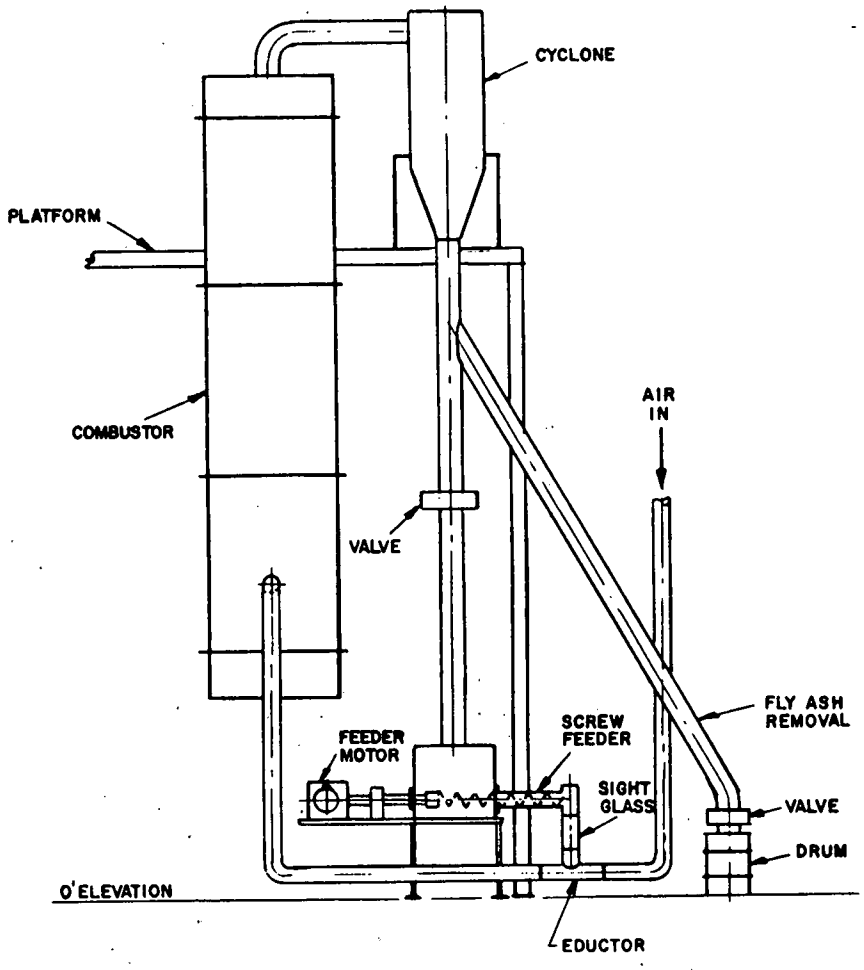

FIGURE 5. RECYCLE SYSTEM

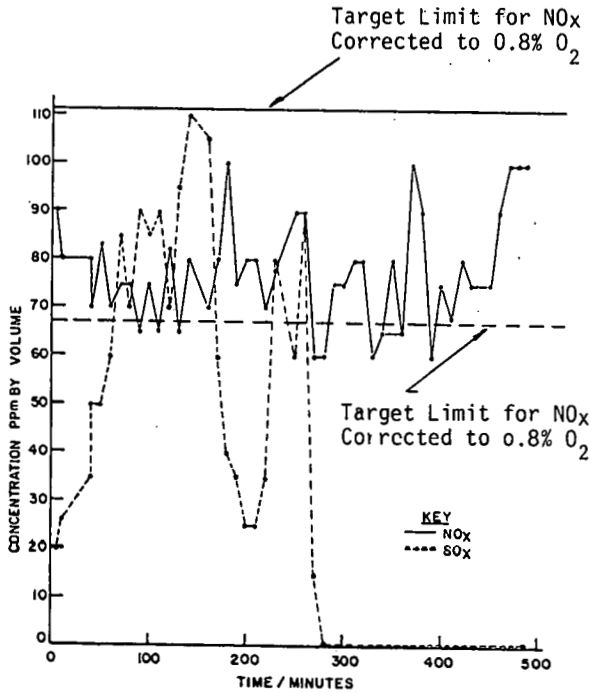

RUN 63

FIG. 6 STAGED COMBUSTION TEST
NO_x & SO_x EMISSION DATA

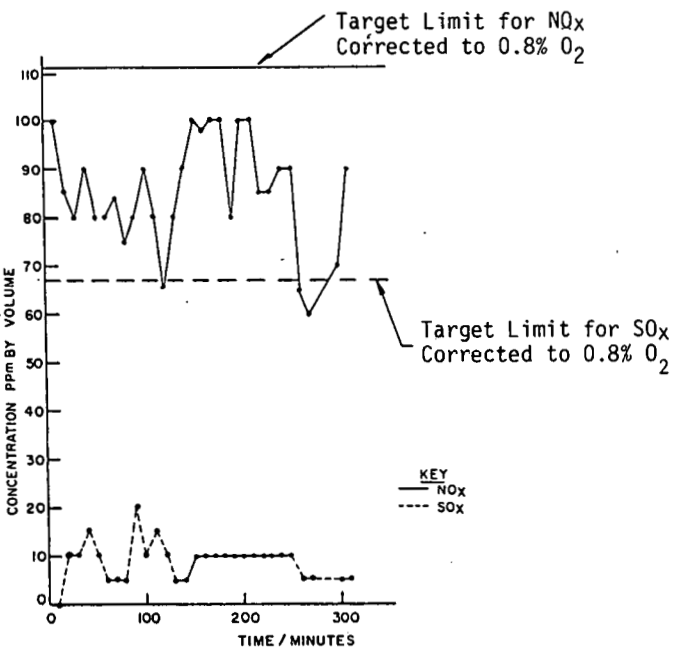

RUN 64

FIG. 7 STAGED COMBUSTION TEST
NO_x & SO_x EMISSION DATA

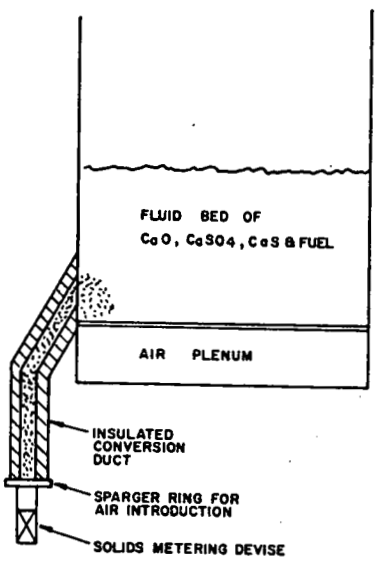

FIG. 8 DEVICE FOR CONVERSION OF CaS TO CaSO4
DURING REMOVAL OF BED FROM FBC

Questions to T.E. Taylor:

Q: Bruce Henschel, EPA

How far above the top of the bed did you inject the secondary air?

A: Four feet.

Q: Dick Sadoski, Riley

What was the NO_x levels without staged combustion?

A: 250-300 ppm.

Q: Bob Libeck, Conoco

Have you had any data on a higher sulfur fuel to indicate what the Ca-S ratio might be?

A: We ran a 2 1/2 sulfur coal and we needed Ca-S of 4 or 5 to 1.

Q: (Participant not identified)

Did you lose 2-4% efficiency when you went to two stage combustion?

A: About 1% loss.

RESEARCH AND DEVELOPMENT OF NOx EMISSION ABATEMENT IN A FLUIDIZED BED COAL COMBUSTER IN JAPAN

M. Horio*, S. Mori**, T. Furusawa***, S. Tamanuki****

*Department of Metallurgical Engineering, Nagoya Univeristy
**Nagoya Institute of Technology
***Department of Chemical Engineering, University of Tokyo
****Japan Coal Mining Research Center

Introduction

Japan, which has one of the greatest densities of population, consumption of energy, and industrial production, is required to enforce the world's most stringent environmental regulations. Japan's major research needs are concentrated on NOx emission control, sulfur dioxide removal and ash disposal and utilization. The need for research into the development of nitric oxide emission control techniques has been especially emphasized in Japan compared to European countries and the U.S. The development target for controled NOx emission levels in a fluidized bed coal-fired boiler is recognized to be 50ppm. Thus extensive investigations concerning the abatement of NOx emissions are being carried out. We are now at the stage of development which can almost clear this difficult target. The objective of this report is to review the fundamental research results concerning NOx destruction which have been obtained at Japanese universities and governmental institutes. In addition, the present status of R & D of combustion modifications, which includes the results obtained by four major developers of fluidized-boilers, Hitachi-Babcock, Inshikawajima, Kawasaki, and Mitsubishi, will be presented. These developments are promoted by the Japan Coal Mining Research Center.

1. Fundamental results obtained by small experimental rigs

1.1 Evaluation of the relative contribution of thermal and fuel "NO" to total "NO" emission and the mechanism of thermal "NO" formation

The initial series of experiments was carried out to investigate the relative contribution of thermal and fuel "NO" to total "NO" emission. This can be measured by substituting an inert component, argon, for the nitrogen component of the fluidizing gas.

Figure 1 represents the results of the first series of experiments with coal. Both thermal and fuel "NO" appeared to increase markedly with increased excess air. The fuel contribution completely dominated the total "NO" emission. It was found that the emission of thermal "NO" was not detected when the combustion temperature was lowered to 800°C or below. Thermal "NO" was observed even in the case of char combustion. This indicated that the formation of thermal "NO" could not only be attributed to the combustion of volatiles but also to the combustion of char. The rate of nitrogen fixation reaction was known to be low over the temperature range of fluidized-bed combustion. Our experimental examination, in which only air was fed without involving combustion, indicated that the level of nitric oxide emission was 0.3ppm at 1000°C. Therefore, the experimental fact that approximately 10% of the total "NO" emission is due to nitrogen fixation reaction cannot be satisfactorily explained. A possible explanation is given below. The temperature of the particles which have direct contact with fresh air supplied through the distributor, or the temperature of volatiles combustion, is several hundred degrees higher than the mean bed

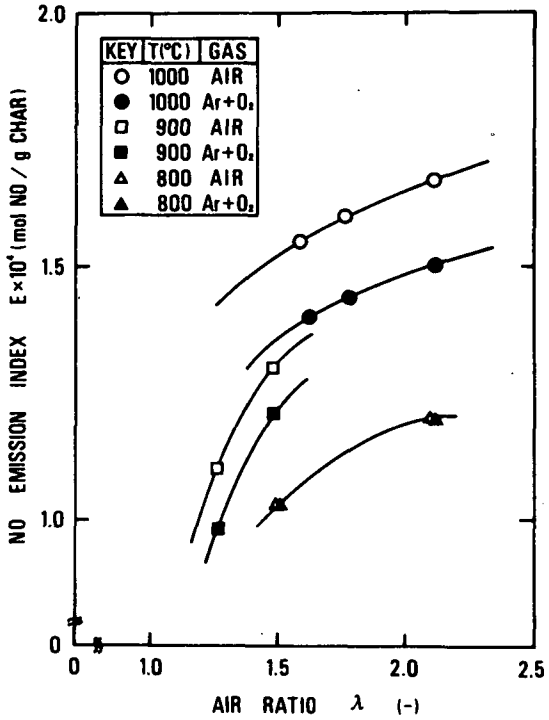

Fig. 1 Relative contribution of fuel and thermal nitric oxide for combustion (Char I)

temperature measured by the thermocouple. Visual observation by use of a two-dimensional fluidized bed combustor of carbon, also indicated that the dispersed particles within the bubble were ignited and formed local hot spots. Related discussions are found elsewhere.[1] The scope of the experiment is shown in Table 1. The carbonaceous materials employed for the present series of experiments are shown in Table 2.

Table 1 Scope of experiment

Inert particles: Microspherical particles SiO_2:8.93%·Al_2O_3:90.61%·Fe_2O_3:0.46%	
Surface mean particle diameter:	580 microns
Bulk density:	0.57 g/cm^3
Total amount:	113 g
Temperature of fluidized bed:	700-1000°C
Static height of bed:	10 cm
Bed diameter:	5 cm
Diameter of coal and char particles:	500-710 microns
Flow rate of fluidizing air and simulated air:	4.2-8.1 l/min
Feed rate of fuel particles:	0.5-1.7 g/min

Table 2 Proximate and ultimate analyses of coal and char particles

Proximate analysis [wt%]

	Volatile matter	Fixed-carbon	Ash	Moisture
Char I*	3.83	54.09	19.80	22.28
Char II**	2.74	66.00	24.47	6.69
Char III***	10.80	65.04	19.84	4.32
Coal ****	43.3	39.1	12.7	4.9

Ultimate analysis [dry%]

	C	H	N	S	O	Ash
Char I*	69.21	0.59	0.54	0.27	3.91	25.48
Char II**	71.66	1.03	0.61	0.01	0.34	26.35
Char III***	70.99	2.77	1.27	0.02	4.21	20.74
Coal ***	66.9	5.4	1.4	0.1	13.2	13.0

* Char I: produced from Liddell coal/ Australia
** Char II: produced from Taiheiyo coal pyrolysis temperature :800°C
*** Char III: produced from Taiheiyo coal; pyrolysis temperature: 600°C
**** Coal: Taiheiyo coal

1.2 The effects of volatiles components on "NO" emission

Fundamental investigations concerning the effects of stoichiometric ratio and combustion temperature on the "NO" emission by use of various types of char were carried out at the University of Tokyo.[3] The experiments, which were carried out over a temperature range which included higher temperatures of less practical importance, produced the following significant results. The level of "NO" emission for char and coal under a deficiency of oxygen was strongly influenced by the level of volatiles contained in the fuel. Typical results are shown in Fig. 2. This indicated that "NO" emission from char is radically reduced as the air feed ratio is reduced, where as the results obtained from the coal combustion in the same combustor indicated that a significant level of "NO" emission under reducing atmosphere was observed. Such a radical reduction of "NO" emission from char as the air feed ratio approaches unity has not been thoroughly investigated up until now. Jonke et al.[2] reported that "NO" emission from coal under reducing conditions was higher at lower bed temperature. This indicated that the "NO" emission levels under reducing conditions were significantly affected by the type of fuel. The "NO" emission level from fuels with less volatile contents is similar to the "NO" emission level from fuels with volatile contents at higher combustion temperature. It was discovered in the

subsequent series of experiments that staged combustion of char was a potential combustion modification for reducing "NO" emission.[3,5] The conversion of fuel N to "NO" is illustrated in Fig. 3.

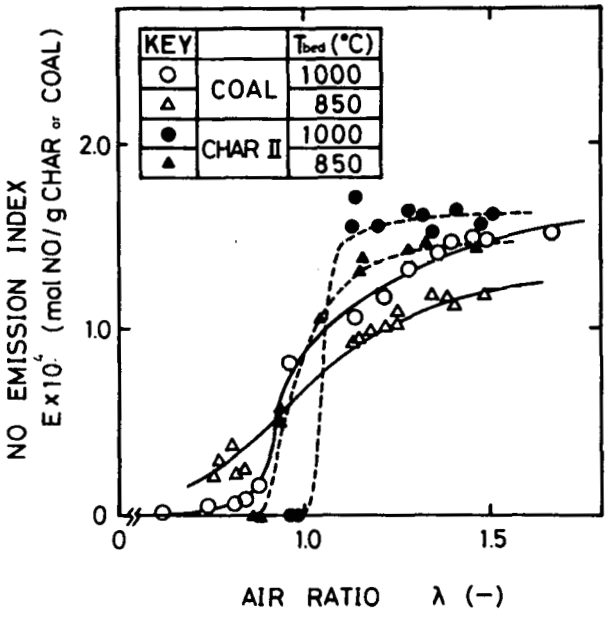

Fig. 2 The dependence of nitric oxide emission from combustion of coal and char II on the stoichiometric ratio

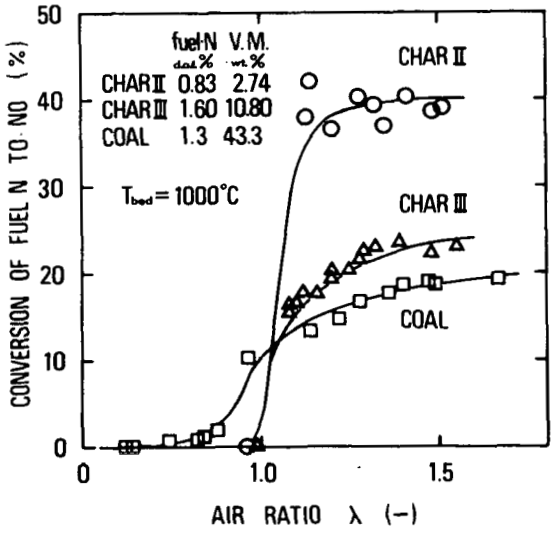

Fig. 3 Conversion of fuel N to "NO"

1.3 Formation of nitrogenous compounds and possibilities of staged combustion

In the previous paragraph, it was shown that emission of nitrogen oxides was significantly reduced when the bed was kept in a reducing condition. In order to obtain good results from staged combustion, the "NO" formed with the injection of secondary air, from nitrogenous compounds other than "NO", should be lowered. Typical nitrogenous compounds produced in substoichiometric combustion are NH_3, HCN, and $(CN)_2$, and the previous experiments indicated that the NH_3 emission level from the primary stage was one of the most important factors which control the total "NO" emission. The levels of ammonia emission from this experimental combustor, measured by detector tube method, are shown in Fig. 4. Figure 4 indicates that ammonia was not detected under an excess air condition. NH_3 emission from both char and coal was reduced by raising the combustion temperature.[4] The ammonia produced in substoichiometric combustion of coal might be mainly attributed to volatile components, whereas the ammonia from char was produced from fuel bound nitrogen in the presence of oxygen or free moisture.[4] It is remarkable to note that a significant reduction of NH_3 emission was also observed in the combustion of char. The emission level of ammonia from char is significantly lower than the emission level of "NO" from the same char under an excess air condition.[4] This may correspond to the lower hydrogen content of char. The results demonstrates that a significant reduction of "NO" emission will be achieved by staged combustion of char. The hydrogen content of char can be reduced by raising the pyrolysis temperature of the coal.[6]

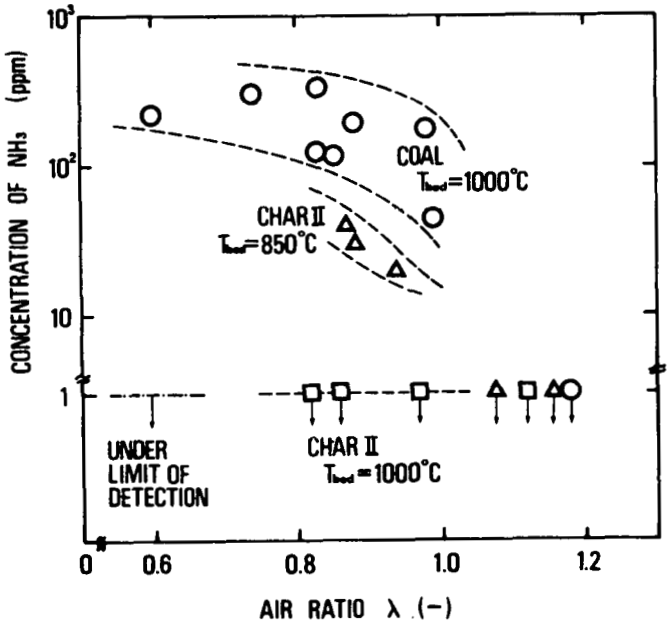

Fig. 4 Ammonia emission from combustion of coal and char

1.4 Preliminary experiments of staged combustion

A series of experiments was carried out to check the possibilities of staged air firing.[3] In this mode of combustion, the air used for combustion was separated into the primary air stream supplied for fluidization through the distributor, and the secondary air stream injected above the bed surface into the freeboard. All fuels were injected into the primary stage, so that the bed could be operated under a deficiency of air to prevent "NO" formation. The overall stoichiometric condition was maintained at excess air condition. The secondary air was injected at several levels above the bed surface. The extent of the reduction of "NO" emission in the present combustor was calculated by use of the "NO" emission index for conventional operation.[3]

Experimental results indicate that an approximately 90% reduction of "NO" emission was achieved and that staged combustion of char is a prospective combustion modification, while the maximum level of "NO" reduction observed in the staged combustion of coal remains in the range of data in previous investigations. The main difference concerning "NO" reduction in staged air firing may be attributed to the difference of emission levels of nitrogenous compounds produced and coming from the primary stage.

1.5 Mechanism of "NO" reduction in sub-stoichiometric fluidized-bed combustion

The possible reaction which suppresses the emission of "NO" might be considered as the reduction of "NO" by carbonaceous materials. Beér et al.[7] also reported that a significant reduction of "NO" emission from fluidized-bed combustion of coal could be attributed to the reaction between char particles or volatiles and "NO". In order to estimate the effects of this reaction, the steady state concentration of carbon particles during the present experiment was measured.

After terminating the feed of fuel solids, the amount of carbon dioxide and monoxide originating from the remaining carbon particles was measured by means of the gas bag method. The results obtained are compared with the level of "NO" emission in Fig. 5. These results indicate that "NO" emission was inversely related to the steady state carbon concentration. Furthermore, the steady state carbon concentration within the bed was found to be considerably small. If the "NO" is reduced by the reaction with char, the reaction rate should be extremely high.

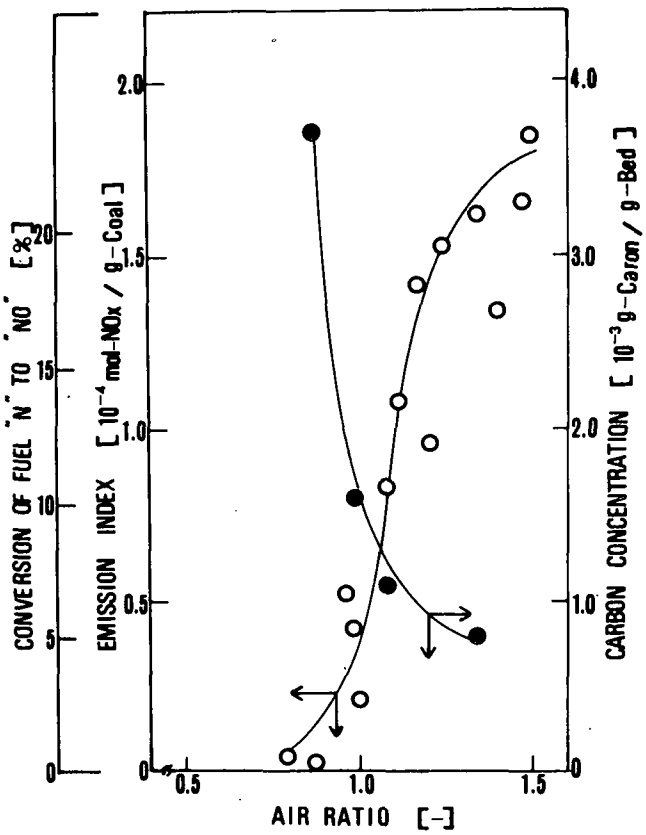

Fig. 5 NOx emission level with respect to steady state carbon concentration from the experimental rigs

To verify the explanation given above, char particles were injected into the fluidized-bed of inert particles fluidized by a gas mixture containing 860ppm "NO" of nitrogen. The concentration of "NO" was extremely low, therefore, the holdup of the carbon particles could be assumed constant during the experiments. The experimental results strongly indicate that char was very effective in reducing "NO" emission. Even when the bed was operated with a deficiency of oxygen, the local stoichiometric ratio in the vicinity of the coal feed point was much larger than unity, therefore, local "NO" emission is comparable with that of $\lambda > 1$. The "NO" produced in the lower part of the bed can be supposed to be reduced to zero by chemical destruction higher in the bed.

1.6 Rate of reduction of nitric oxide by char[8]

The importance of the reaction between the NOx and the char which is present either within the bed or in the freeboard was suggested in previous sections. A

diluted fixed bed isothermal tubular reactor was employed to determine the reaction rate constants over the temperature range which is important in fluidized bed combustion and for which no data have yet been published.

Two different fuels were used in these experiments: Char, which was produced by carbonization at 800°C of the non-coking Taiheiyo coal, (Char II, Table 2) and activated carbon manufacture by petroleum cokes. These particles were mixed with inert particles of a similar size, and then packed into a silica-glass reactor tube. Tests using a char-free bed showed that the MS particles are inert as far as the decomposition of "NO" is concerned.

As the reaction proceeds, the reduction of "NO" by char or activated carbon will decrease as a result of the decreasing holdup of the carbon. Since the "NO" concentrations used in these experiments were very low, the difference between the amounts of carbon present before and after the experiments was neglegibly small, so that the carbon concentration could be assumed to be constant. Previous investigations, done at a lower temperature range, have reported that the reaction between carbon and "NO" is first order with respect to "NO" and on this basis the analysis was done by assuming that the reaction is first order with respect to "NO".

It can be seen from the experimental results that there was a linear relationship between the residence time and $-\ln(1-X)$ where X denotes the extent of reaction within the range of these experiments. This fact, taken in conjunction with the fact that film resistance is negligible, shows that the reduction of "NO" by char or activated carbon is a first-order reaction with respect to "NO" concentration. This indicates that the order of the reaction obtained by Smith et al.[18] for the reduction of "NO" by an ashless sugar charcoal can be extended to a higher temperature range, used for the fluidized bed combustion. Figure 6 represents the Arrhenius plot. It can be seen from this figure that, both in the case of char and also in the case of activated carbon, there was a large increase in the activation energy at temperatures above about 680°C. At lower temperatures, the activation energy in both cases was around 15-16 kcal/mole and independent of the ash content. Between 450°C and 600°C, the activation energy was around 15.0-18.3 kcal/mole, in agreement with the previous results; while above 680°C, the activation energies were approximately 59 kcal/mole in the case of char and 40 kcal/mole in the case of activated carbon. The reason for the increase in the activation energy above 680°C has not been clear, but it might be attributed to a change in the reaction mechanism, since in both cases--char and activated carbon--the activation energy increased.

The gaseous reaction products that were formed at each temperature were analyzed. It was found that at lower temperatures, N_2 and CO_2 were formed, while at temperatures above the temperature corresponding to the increase in the activation energy, N_2, CO, and CO_2 were formed. As the temperature was raised, the amount of CO_2 that was formed decreased, while the proportion of CO in the reaction products increased. (Figure 6 is located at the end of the manuscript)

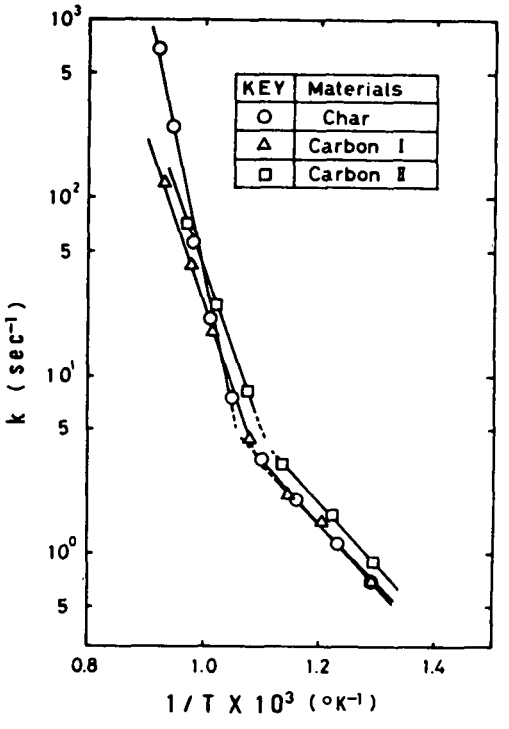

Fig. 6 Temperature dependence of reduction rate of nitric oxide [k:sec^{-1}]

1.7 Rate of "NO" reduction by char under an excess air condition[9]

The kinetic information which is applicable to a system operated under an excess air condition is definitely needed in order to analyse the mechanism of "NO" abatement. Since the rate of char oxidation is high, experimental conditions employed for the fixed bed reactor were restricted to a lower oxygen concentration and/or lower temperature, where the carbon concentration could be assumed constant for the time interval required by the experiment. The previous kinetic studies carried out

without involving char combustion by oxygen indicated that the reaction was first order with respect to "NO". Therefore, it was assumed that the "NO" destruction accompanied by oxidation of char was also first order with respect to "NO" concentration. The experimental results indicated that the reaction in the presence of oxygen can also be expressed as a first order reaction with respect to "NO" concentration. These results, together with the previous results not accompanying the oxidation reaction, are shown in Fig. 7. Alpha, (α) in Fig. 7 denotes the ratio of oxygen to "NO" at the inlet. The reaction was significantly accelarated by the coexisting oxygen, especially in the lower temperature range. The increased rate was also observed for activated carbon. Therefore the occurence of the phenomena is not restricted to char carbon. It is remarkable to note that the rates obtained for the different ratios of "NO" to oxygen by changing the gas flow rate, but by keeping both the ratio of oxygen to "NO" and the amount of carbon particles charged constant, can be approximately expressed by a single straight line in an Arthenius plot. The activation energies obtained coincides approximately with the reported data. Additions of oxygen increased the rate of "NO" destruction significantly over a lower temperature range in which the desorption of carbon-oxygen surface complexes controls the overall rate. It is known that the desorption in the absence of oxygen proceeds with the reaction between the surface complexes and gaseous "NO". The

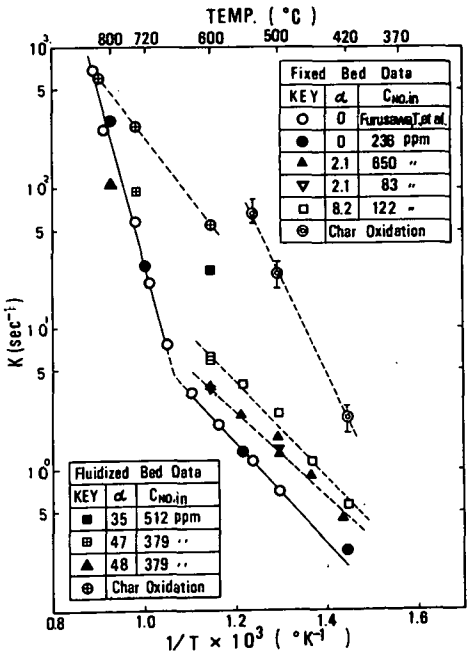

Fig. 7 The effects of oxygen on reduction rate of nitric oxide: Fixed bed and fluidized bed data

mechanism of the accelerated desorption of oxygen surface complexes on carbon surfaces of various natures was discussed in detail by R.N. Smith and colleagues.[18] To discuss the mechanism in detail is not of our research concern. Over a range of higher temperatures (above 680°C), the effects of the added oxygen on the rate of "NO" destruction was not detected by the fixed bed experiment. It may be because the oxygen was consumed rapidly at a certain short distance from the inlet. To support this explanation, the oxidation rate of char was investigated briefly by the same procedure previously described, at temperatures ranging from 425°C to 535°C. The results can be expressed as a first order reaction with respect to oxygen concentration. The results obtained are also shown in Fig. 7. The oxidation rate is approximately a hundred times faster than the "NO" reduction rate by char. Therefore the effects of oxygen on the increase of "NO" reduction rate of a range of higher temperatures could not be investigated by fixed-bed reactor, since carbon concentration could not be assumed constant. The rate over the range of temperatures in which the desorption of carbon-oxygen surface complexes is controlling the overall rate was expected to depend on the ratio of "NO" to oxygen and also on the initial concentration. Experimental results obtained at different initial concentrations of oxygen, with the ratio of oxygen to "NO" constant, indicate that the rate does not appear to depend on the initial concentration but on the ratio of oxygen to "NO". These results support that both of the reactions are first order with respect to gaseous reactant over a lower concentration range of oxygen. Since the oxidation rate of char is considerably higher than the "NO" decompostion by char, a fluidized bed reactor with a continuous feed of carbon was used to analyze the rate for higher oxygen concentration; namely, a large value of α and a higher temperature. Furthermore, the reduction of "NO" in a simulated combustion product was studied. Typical results are shown in Fig. 8.[9]

A remarkable result from these experiments is that a significant reduction of "NO" was realized even under an excess air condition in which oxygen remained in the outlet flow.[9] Furthermore, an increased rate of "NO" reduction was observed in the presence of oxygen at both 600°C and 750°C. The rate was not significantly reduced by the presence of oxygen at 800°C. At 853°C the rate of "NO" destruction was reduced by coexisting oxygen. The reduction of "NO" by use of a simulated gas containing oxygen produced fuel "NO", originated from the simultaneously occuring combustion of char. Thus the observed outlet concentration was partly reduced "NO" from the inlet plus partly reduced "NO" originating from

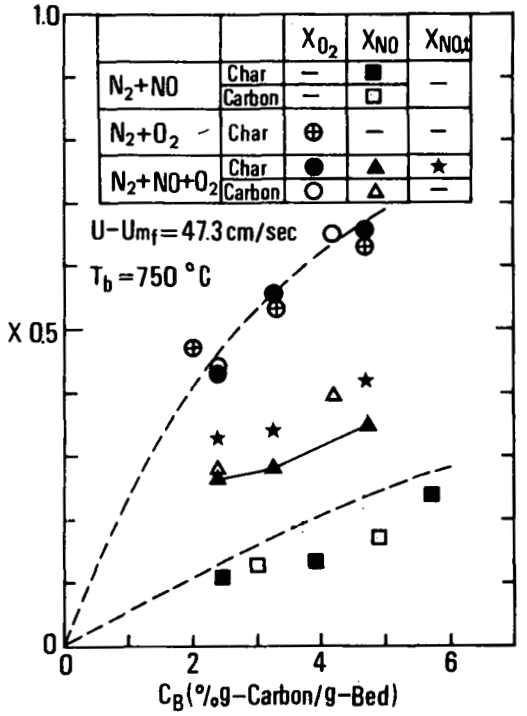

Fig. 8 Conversion of "NO" and oxygen versus carbon concentration within the fluidized bed

fuel nitrogen. In order to evaluate the relative magnitude of "NO" reduction and "NO" formed by the combustion, X_{NO}, t was evaluated at 750°C, 800°C, and 850°c by measuring the fuel "NO" concentration and subtracting it from the observed outlet concentration, where the denominator remained the same as that used for the evaluation of X_{NO}. The effect of fuel "NO" formed by the combustion of char on the reduction of "NO" was found to be less significant in this investigation.

The simplified bubbling bed model by Kunii and Levenspiel was used to evaluate the reaction rate in the presence of oxygen.[10] First, the effective bubble diameter was calculated as an adjustable parameter by curvefitting the experimental data obtained in the absence of oxygen to the curve calculated theoretically by the above model and the kinetic data shown previously. Then the increased rate in the presence of oxygen was evaluated by changing the rate, but by keeping the other parameter, including the effective bubble diameter, constant. The rate obtained at 600°C, α=35.0, and u/u_{mf}=5 was 11.3 times greater, and the rate obtained at 750°C, α=47.0, u/u_{mf}=8 was 2.0 times greater than the rate observed in the absence of oxygen. The data obtained by the present experiment may be considered to be an approximate value of the rate for higher oxygen concentrations; namely, a large value of α and a higher temperature, where the reaction rate was not evaluated by conventional procedures. Furthermore, in a fixed bed operation, oxygen is consumed soon after entering the bed in a small area near the inlet, and the reduction of "NO" in the absence of oxygen proceeds in the remaining major portion of the bed. In a fluidized bed operation, oxygen is continuously supplied from by-passing bubbles to the dense phase where "NO" reduction is carried out. This is schematically illustrated in Fig. 9.

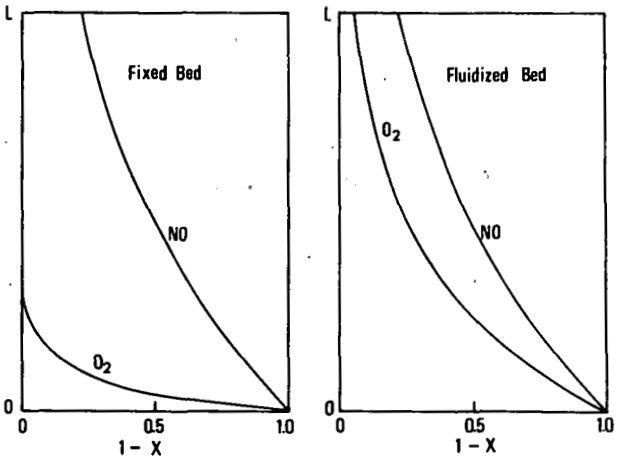

Fig. 9 The extent of "NO" reduction and oxygen consumption at various heights of the beds

2. Development of a low "NOx" combustion system

The preceding sections reviewed the basic phenomena which were observed by small experimental rigs at the University of Tokyo. In this section the results obtained by the fluidized bed combustor test plants indicated in Table 3 are briefly discussed.

Table 3 Experimental Research on FBC in Japan

University of Tokyo	2x50mmφ, 78mmφ 2 stage, secondary air into freeboard
Ishikawajima-Harima Heavy Industries	300mm 2 stage + Flue gas recycle
Kawasaki Heavy Industries	500mm Secondary air into freeboard 200mm

Table 3 (continued)

Babcock-Hitachi	550mm Secondary air into freeboard 350mm (CBC)
Mitsubishi Heavy Industries	600mmϕ Secondary air into freeboard
Gov. Ind. Dev. Lab, Hokkaido	108+133mmϕ 2 stage

The findings by the small rigs strongly indicated that overall "NO" emission was determined by the relative importance of the "NO" formation rate and the "NO" decomposition rate within the bed as well as the freeboard. Therefore, the development of a "NO" emission free combustion system should be concentrated on the development of an effective modification which would impede "NOx" formation and promote "NOx" destruction. The combustion modifications proposed so far are shown in Table 4

The pressurized operation which has been extensively developed in the U.S. and Europe is a future target for development in Japan. The mechanism of "NOx" abatement has not been well investigated in this operation. However, recent advances in fluidized bed engineering indicate that the decreased density difference between gas and solids reduced the mean bubble size, followed by a decreased bubble frequency. The increased fraction of gas penetrating through the emulsion phases was considered to imporve the contact efficiency. This might be related to the increased decomposition of "NO". A higher efficiency is achieved by the pressurized operation when energy is recovered from compressed combustion products. Thus, the development of corrosion resistant turbine blades and hot gas purification of higher efficiency is absolutely necessary in order to appreciate the merits of the pressurized operation. The urgen need for development of a NOx free combustion system in Japan has promoted the development of alternative modifications, which decrease NOx emission without involving the pressurized operation.

Once such alternative is a two stage fluidized bed operation. Kunii proposed such a system which induces a "NO" destruction reaction by use of in situ formed char.[10] In this concept, the combustor consists of a primary bed and a secondary bed, which is situated on top of the primary bed. The primary stage of the bed is maintained under an excess air conditions so that the nitrogenous contents of coal could be converted into "NO" or nitrogen. The "NO" produced in the primary stage is destroyed in the secondary stage by the unburnt carbon particles entrained from the primary stage. Thus the secondary stage was used to increase the combustion efficiency by catching the entrained carbon fines, as well as to reduce "NO" by carbon fines fixed by the secondary stage. The limestone or dolomite employed for sorbent of sulfur dioxide is first supplied to the secondary stage and then sent to the primary stage by displacement. Recycled char can be injected into the second stage as needed. The basic kinetic information required to

Table 4 Comparison of various combustion modifications

Modifications	Mechanism	Merits	Demerits
Pressurized operation	Possibly improved contact efficiency or promoted decomposition	High efficiency	Innovative development of energy recovery from pressurized dirty gasses is required
Staged air firing of coal	Secondary air injection after decaying nitrogenous compounds formed under a deficiency of air	Simple mechanical arrangement	Increased size of freeboard, consequently increased equipment size
Staged air firing of char	Retarded formation of nitrogenous compounds by decreasing hydrogen contents by carbonization	High level of NOx abatement	Carbonizaiton plant required & marketing of tar and gas products
Stage fluidized bed	Promoted conversion of fuel-N into nitrogen in the primary stage followed by the decompostion of "NO" by char in the secondary stage	Increased combustion efficiency	Complex mechanical arrangement

evaluate the potential function of the proposed concept to control "NOx" emission are based upon a "NO" destruction reaction by char under an excess air condition. This has been explained in the previous section.

The Governmental Industrial Development Laboratory in Hokkaido, (G.I.D.L.H.)[12,13] proposed a similar staged fluidized bed. In this concept the primary stage is maintained as substoichiometric so that the decomposition of "NO" might be enhanced. Previously this was shown to be unnecessary. Sulfur sorbent is supplied only into the secondary stage. Therefore, the separation of sorbent from ash is not required in this system. Both concepts require special engineering consideration for the design of their gas distributors. The details of this concept will be reported elsewhere at these proceedings.

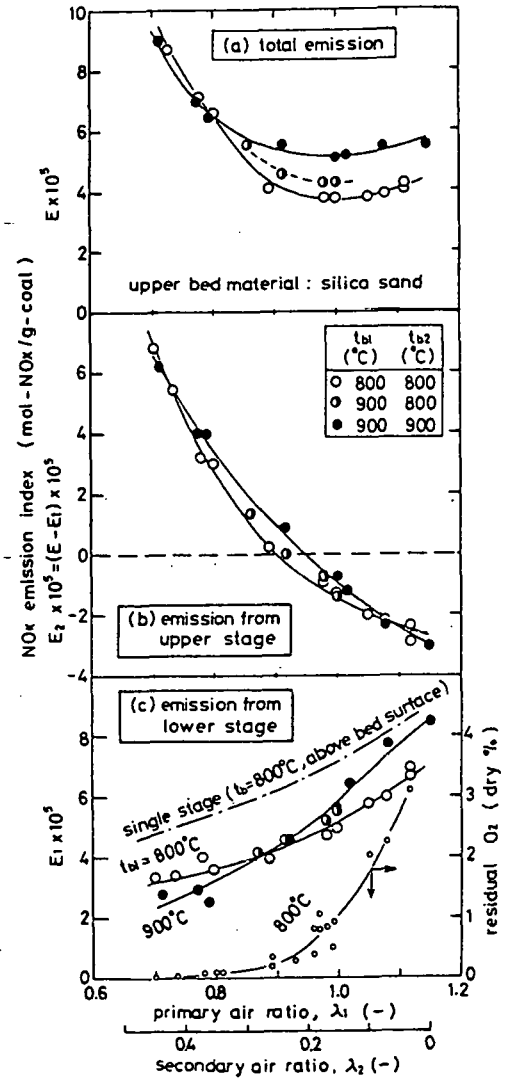

Fig. 10 Effects of bed temperature and primary air ration on NO_x emission at total air ratio of 1.15[12,13]

Figure 10 shows the results of two-stage fluidization by G.I.D.L.H. Increasing the primary air ratio, NOx emission (E_1) from the lower bed increases as shown in (c). NOx generation from the upper bed (E_2) decreases with increasing primary air ratio. When the primary air ratio becomes larger than 0.9, NOx generated in the lower bed is reduced effectively in the upper bed as shown in (b). Thus the total NOx emission (E) from the combustor has a minimum value of approximately λ = 1.0 as shown in (a).

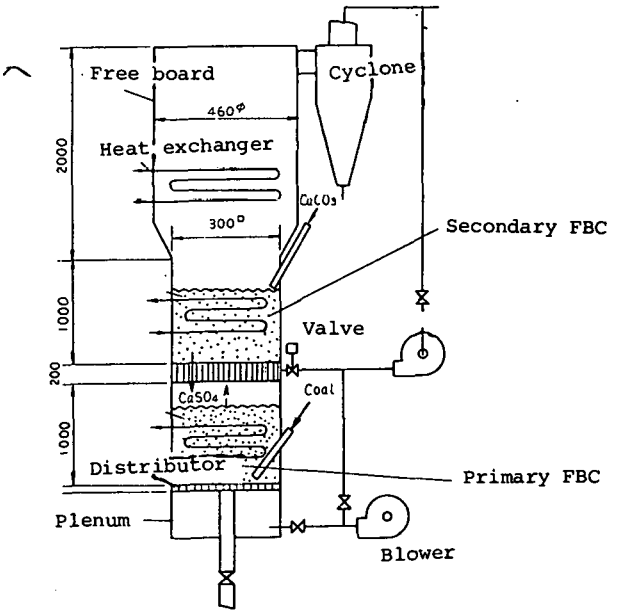

Fig. 11 Test plant of Ishikawajima-Harima Heavy Industries

The 300 x 300mm test plant of Ishikawajima-Harima Heavy Industries with a two-stage fluidized bed is shown in Fig. 11.[17] The proposed mechanism of NOx emission control in this plant differs from the two-stage fluidized bed proposed by Kunii and G.I.D.L.H. Here, the catalytic effect of sorbert for NOx reduction is emphasized. The primary bed, which is operated at 950°C under a deficiency of air, is used for the primary combustion of coal as well as NOx reduction by carbon monoxide, which is catalyzed by the sorbent ($CaO/CaSO_4$) falling from the secondary bed. The secondary bed, operated at 730°C, is used for the secondary combustion and desulfurization. The lime stone as sorbent, recycled flue gas, and the secondary air are supplied at this stage. Complete combustion can be achieved in the free-board above the secondary bed.

The results from the Ishikawajima-Harima Heavy Industries plant are shown in Fig. 12.[17] These results were obtained at

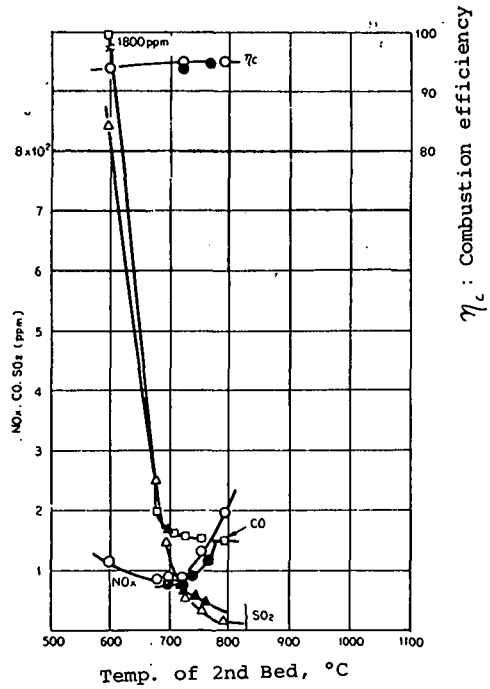

Fig. 12 NOx and SO_2 emission levels from Ishikawajima-Harima Heavy Industries two stage combustion system

optimum operational conditions as follows; primary air ratio = 0.92, flue gas recycle ratio = 0.4, primary bed temperature =950°C, and heat release = 1.06 x 10^6kcal/m^2hr. It was indicated from these results that there exists and optimum temperature for the secondary bed. A 82% NOx reduction 95% desulfurization and 95% combustion efficience were obtained at the secondary bed temperature of 730°C and λ = 1.3.

Two stage air firing by a secondary air injection into the freeboard has been adopted by Kawasaki Heavy Industries,[16] Babcock-Hitachi Corporation,[15] and Mitsubishi Heavy Industries.[14] Mitsubishi's 600mmϕ ID test plant is shown in Fig. 13. In this plant, limestone and inert sand are fluidized by the primary air through the distributor and the secondary air is injected into the freeboard. The operation conditions were as follows; bed temperature = 850°C, gas volocity = 2.4 m/sec, bed height = 1.4m, and injection height of the secondary air = 2.35m from the distributor. The stoichiometric air ratio of the primary air was held to between 0.8 and 1.2, that of the secondary air was adjusted so that the total air ratio was 1.23.

Higher NOx reduction was observed when coal which has a larger ratio of fixed carbon content to volatile matter content was used.[14] This coincides well where higher NOx reduction could be achieved by the staged air firing of char. This strongly suggest that higher NOx reduction may be realized by staged air firing of coals which are less volatile.

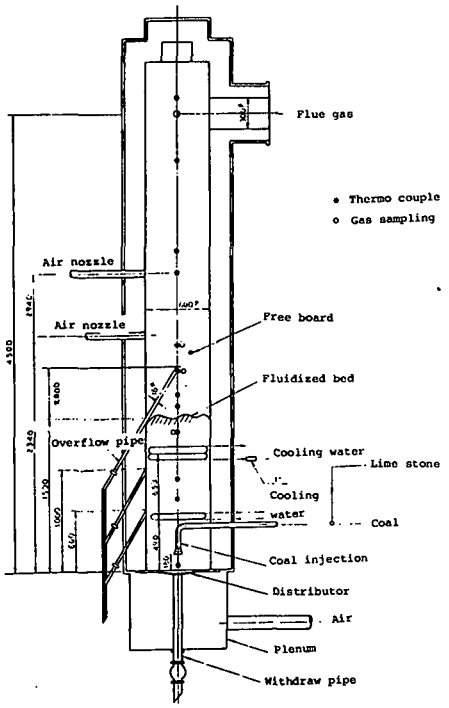

Fig. 13 Mitsubishi Heavy Industries' FBC test plant

The effects of changes in the injection height of the secondary air on "NO" reduction has been thoroughly investigated by Kawasaki Heavy Industries.[11, 16] Their detailed results will be reported elsewhere at these proceedings. "NO" destruction under an excess air condition within the freeboard was observed. The dependence of total "NO" emission levels on the various positions of the secondary air injection is illustrated in Fig. 14. As the height of the secondary air feed above the bed surface is raised, the "NO" emission level is sharply decreased. The minimum "NO" emission attained by the secondary air injection at more than one meter above the bed surface was around 60ppm with a heat release rate of 4.6 x 10^9 J/m^2h.

The condition which attains the lowest "NO" emission must be matched to the optimal condition of desulfurization. The desulfurization can also be sufficiently achieved in the bed which is operated under a deficiency of oxygen. Using standard size Japanese commercial limestone, the Ca/S ratio should be larger than three

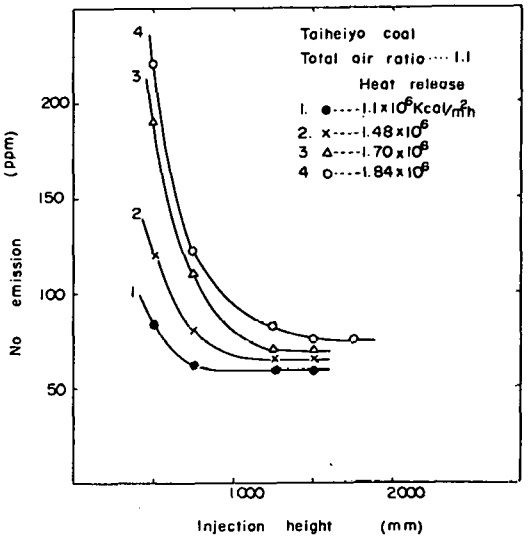

Fig. 14 "NO" emission versus secondary air injection point (Kawasaki Heavy Industries)

even under oxygen rich combustion of coal. This rather low desulfuization efficiency can be explained by the relatively high level of elutriation loss of limestone due to the low strength of Japanese high quality limestone. Thus we are nearly at the stage of development which will clear the 60ppm level of NOx emisson demanded by strict environmental needs. More extensive investigations are required for the simultaneous control of NOx and SOx emissions.

3. Concluding remarks

Various fundamental phenomena observed in Japan which control NOx emission from fluidized bed conbustion of coal are reviewed. In addition the present status of R & D of combustion modifications proposed for reduction of NOx emission are briefly reviewed. The target level of 60ppm NOx emission is now being cleared. More extensive investigations are needed to match the conditions required for NOx reduction to the optimal desulfurization condition.

Acknowledgement

Most of the fundamental research was carried out in cooperation with Professor D. Kunii (University of Tokyo) under the sponsorship of Science Research Grants from the Ministry of Education, Japan, Grants NO 311604 and NO 411003. In addition, T. Furusawa received grant NO 455363 from the same body.

The authors would like to thank Professor D. Kunii and Professor I. Munchi (University of Nagoya) for their encouragement.

Finally, the authors wish to express their thanks to Mr. H. Terada (Babcock-Hitachi), Mr. H. Tsuji (Ishikawajima-Harima Heavy Industries), Mr. S. Shirakawa and Mr. K. Taota (Mitsubishi Heavy Industries), Mr. M. Tomita (G.I.D.L.H.), Mr. T.Yawata (Chiyoda Chemical Engineering Construction), and Mr. J. Tatebayashi (Kawasaki Heavy Industries), for their valuable comments.

Literature cited

1) Aoyagi, M. and D. Kunii: Chem. Eng. Comm. 1, 23 (1974)
2) Jonke, A.A., G.J. Vogel, E.L. Carls et al: Chem. Eng. Prog. Symp. Series 68, NO 126, 241 (1972)
3) Furusawa, T., T. Honda, J. Takano and D. Kunii: J. of Chem. Eng. Japan 11, 377 (1978)
4) Furusawa, T., N. Yamada, T. Sendo and D. Kunii: J. of Chem. Eng. Japan 12, 71 (1979)
5) Furusawa, T., T. Honda, J. Takano and D. Kunii: Fluidization, Proceedings of 2nd Eng. Found. Conf. Cambridge University Press (1978)
6) Nagashima, I., N. Yamamoto, T. Fujikawa T. Furusawa and D. Kunii: Int. Chem. Eng. 18, 654 (1978)
7) Gibbs, B.M., F.J. Pereira and J.M. Beer: 16th Symposium on Combustion, Cambridge, 461 (1976)
8) Furusawa, T., D. Kunii, N. Yamada and A. Oguma: Int. Chem. Eng. 20, 239 (1980) or Kagaku Kogaku Ronbunshu 4, 562 (1978)
9) Kunii, D., K.T. Wu and T. Furusawa: Chem. Eng. Sci. 35, 170 (1980)
10) Kunii, D., T. Furusawa and K.T. Wu: 1980, International Fluidization Conference ed. J.R. Grace and J.M. Matsen, Plenum Publishing Corp. New York (1980)
11) Okada, Y., J. Tatebayashi and R. Yamamura: Paper presented at 72th annual meeting of A.I.Ch.E. (Nov. 1979, San Francisco U.S.A.)
12) Hirama, T., M. Tomita, T. Adachi, H. Yamaguchi and M. Hirio: unpublished paper
13) Hirama, T., M. Tomita, T. Adachi, M. Horio: unpublished paper
14) Takahashi, T., T. Kondo and S. Fujima: Symp. of Coal Mining Research Center Japan, 11 (Aug. 1979, Tokyo)
15) Fujiwara, N., H. Terada and K. Sakamoto: ibid., 24.
16) Tatebayashi, J.: ibid., 41
17) Tsuji T.: ibid., 52
18) Smith, R.N., J. Swinehart and D. Lesnini: J. Phys. Chem. 63, 44 (1959)

CONTROL OF SULFUR DIOXIDE AND NITROGEN OXIDE EMISSIONS BY BATTELLE'S MULTISOLID FLUIDIZED-BED COMBUSTION PROCESS

H. Nack, K. T. Liu* and C. J. Lyons

Battelle, Columbus Laboratories
* Gulf Science & Technology Co.

Introduction

This paper describes Battelle's Multisolid Fluidized-Bed Combustion Process, and in particular, its application to NO_x control. The process is described in the single-stage and in the two-stage combustion modes. Then a summary of the results of a preliminary program conducted in a small pilot hot model is presented, and some of the major factors influencing reduction of NO_x emissions using staged combustion are discussed.

Description of Process

In the single-stage multisolid fluidized-bed combustion process, a recirculating bed is superimposed on a dense fluidized bed as shown in Figure 1. The multisolid fluidized-bed combustion system has the following characteristics:

1. The combustor operates at superficial gas velocities of 30-40 ft/sec
2. The dense bed is an intensive mixer and flame holder.
3. The freeboard is maintained at optimum temperature to promote reactions of interest.
4. Ground limestone presenting high surface area for reaction with SO_2 is fed into the bed to capture sulfur.
5. Sulfated limestone, ash, and recirculating bed material are blown out of the dense bed and collected downstream.
6. There are no heat exchanger surfaces in the dense bed region, and the dense bed temperature is controlled by the feed rate of cooled recirculating bed solids.
7. About two-thirds of the heat duty is transferred in the low velocity fluidized-bed heat exchanger or boiler. The flue gases are cooled in a convective boiler.

The external heat exchanger is a conventional fluidized bed operated at a velocity of about one foot per second to minimize erosion of immersed heat exchanger tubing.

A small pilot hot model with a heat release rate of 400,000 Btu per hour, has been operated for almost 4,000 hours burning solid fuels. A 4,000,000 Btu per hour pilot plant has been operated for about 1,500 hours. These studies[1,2,3] demonstrated a number of significant features of the multisolid process, including:

1. Capability of burning as-received wet, lump stoker coal
2. High SO_2 retention approaching 100 percent
3. Low limestone consumption
4. Combustion efficiency from 96 to 99 percent
5. Three to one turndown at 18 percent excess air and excellent load follow
6. Minimum potential for erosion/corrosion of heat exchanger tubes
7. Rapid startup and shutdown due to absence of tubes in combustor.

In prior work, emphasis was placed on control of SO_2 emissions. NO_x emissions were typically in the 300 to 400 ppm range which was adequate to meet Federal New Source Performance Standards. However, means for further lowering levels of nitrogen oxide and SO_2 emissions have been the subject of much study.

For the multisolid process, staged combustion was selected as the preferred method for simultaneously controlling NO_x and SO_2 emissions to low levels. This decision was based on the absence of heat exchanger surfaces in the combustor, the presence of a circulating bed to control heat absorption, and the capability to remove heat in the freeboard.

As shown in Figure 2, the staged combustion technique involves operating the lower region of the combustor under fuel-rich conditions by introducing a limited amount of "primary air" into this region. The upper zone of the combustor is operated with excess air by introducing secondary air at one or more vertical locations above the lower region. The nitrogen oxides released during combustion are reduced to gaseous nitrogen in the lower region by reacting with char and/or carbon monoxide. The secondary air serves to complete combustion of char and carbon monoxide and reduced species in the upper region. The temperature of the dense bed is controlled by the rate of cooled recirculating bed material (sand) at the lower recycle leg, while the freeboard temperature is controlled by the upper recycle stream.

BATTELLE MULTI-SOLID FLUIDIZED-BED COMBUSTOR

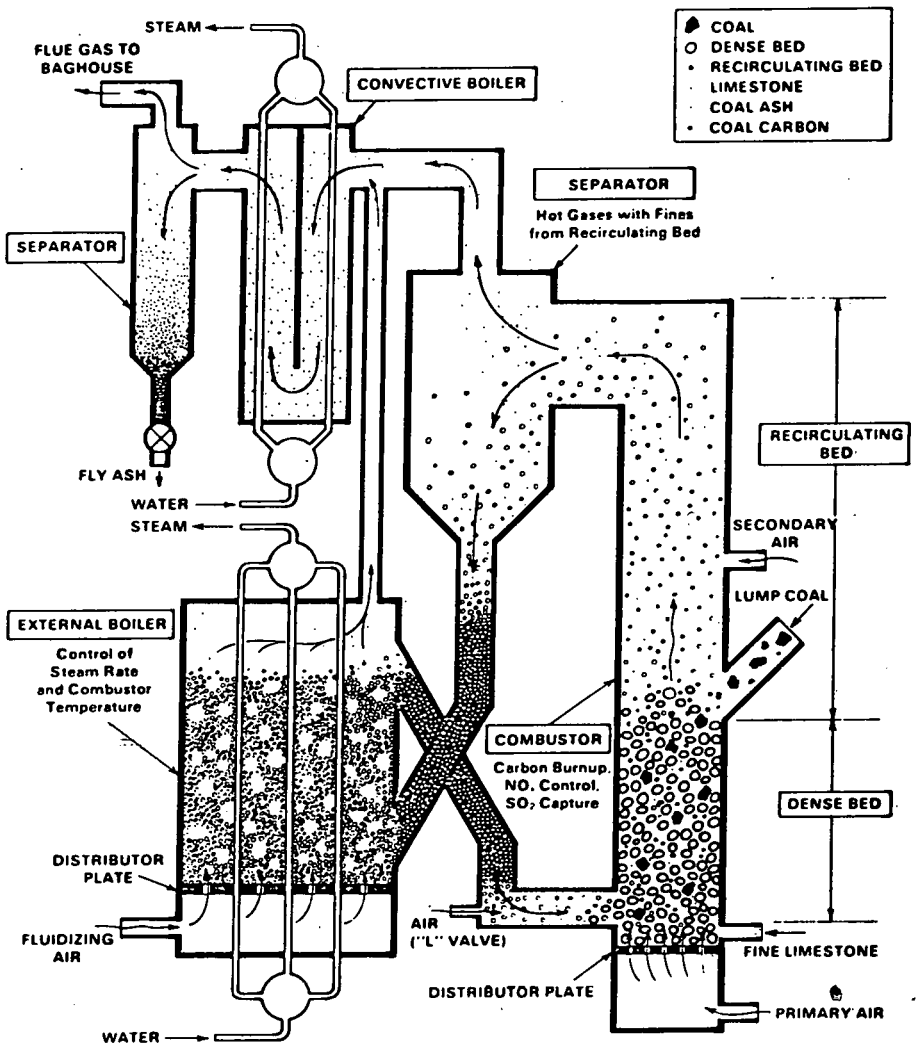

FIGURE 1. BATTELLE'S MULTISOLID FLUIDIZED-BED COMBUSTION PROCESS WITH EXTERNAL BOILER CONFIGURATION

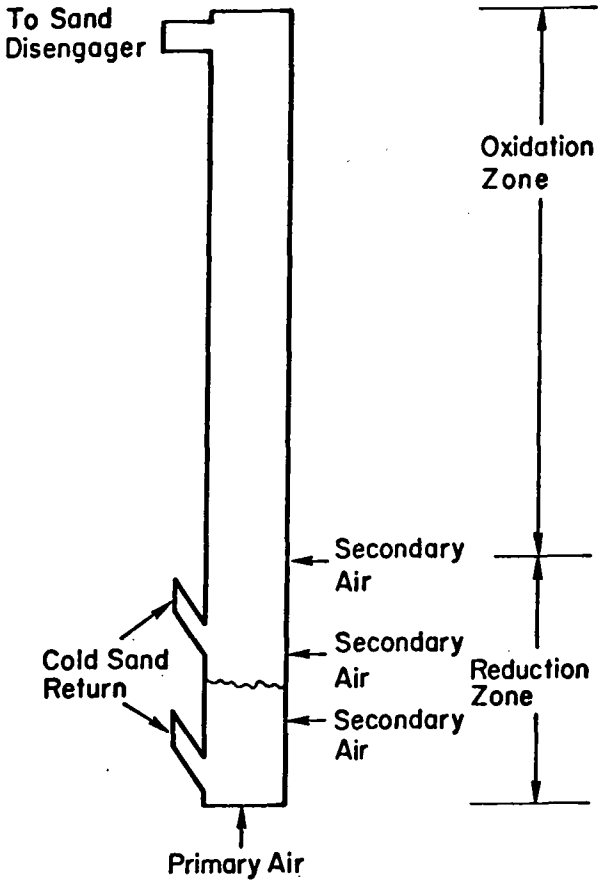

FIGURE 2. STAGED COMBUSTION IN MULTISOLID FLUIDIZED-BED COMBUSTION SYSTEM

Equipment

A preliminary study was conducted in the small hot model to investigate the staged combustion technique. This unit is shown schematically in Figure 3. The insulated combustor is made of stainless-steel pipe with the bottom section 5 feet high (measured from the air distributor plate) and 6-3/8-inch I.D. The freeboard is expanded to 8-1/4-inch I.D. for a distance of 15 feet.

For staged combustion operation, secondary air can be introduced at various vertical locations on the combustor. Normally, only one or two secondary air injection points were used at any given time.

The entrained bed solids recirculation system is comprised of a 12-inch-diameter primary cyclone, a solid recycle hopper and two solids recycle legs. In this small unit, the recirculation system is only partially insulated to permit heat loss to the surroundings, simulating an external heat exchanger. Each recycle leg is equipped with a knife-gate slide valve to regulate solids flow rate. These two solids recirculation legs enter the combustor at 2 inches and 48 inches above the distributor plate, respectively. The recycle rates are adjusted to control temperatures in the dense bed and freeboard regions. Under typical operating conditions, the primary cyclone is capable of collecting essentially all of the entrained bed particles and most of the limestone and unburnt carbon above 10 to 20 microns in size.

Fuel and limestone are either premixed at a predetermined ratio before feeding or are fed separately to the combustor at specified rates. A pneumatic injection line is used to introduce the fuel and limestone into the combustor at a point about 2 inches above the distributor plate. A natural gas burner for preheating the dense bed during startup is located upstream of the distributor plate.

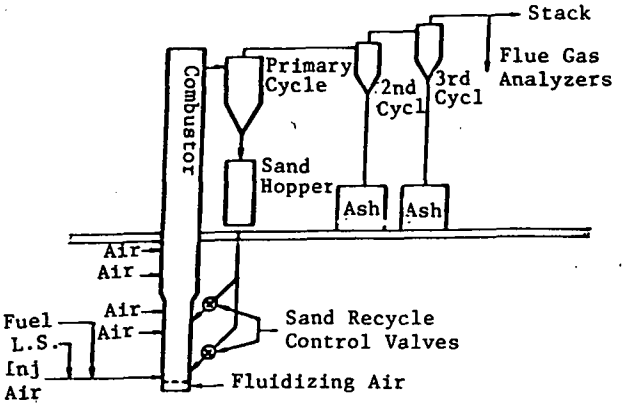

FIGURE 3. SCHEMATIC OF 6-INCH MS-FBC EXPERIMENTAL UNIT

Results

A series of experiments was conducted, with the objective of demonstrating that significant NO_x reduction could be achieved in the multisolid system using staged combustion. In addition, we hoped to identify important process parameters affecting both NO_x and SO_2 emissions under staged combustion conditions.

Illinois No. 6 coal and a petroleum coke were used as fuels in this study. The analyses of these fuels are shown in Table 1. The sulfur sorbent was a Piqua, Ohio limestone, minus 325 mesh in size, containing 83.6% $CaCO_3$.

The operating ranges used in this series of experiments are shown in Table 2.

Control of the primary air/stoichiometric air ratio is an important parameter in reducing NO_x emissions. This ratio is defined as the ratio of the air introduced through the bottom

TABLE 1. CHEMICAL ANALYSIS OF COAL AND PETROLEUM COKE

COMPONENT	ILLINOIS NO. 6 COAL	WEIGHT PERCENT (AS-FED) PETROLEUM COKE
C	61.9	86.9
H	4.2	3.8
O	8.8	1.8
N	1.2	2.6
S	4.0	1.8
ASH	9.4	0.4
MOISTURE	10.5	2.9
TOTAL	100.0	100.0
VOLATILE, % (MF)	36.0	10.5
HHV, BTU/LB	11090	14920

TABLE 2. TYPICAL RANGES OF OPERATING CONDITIONS

COMBUSTION TEMPERATURE:	1590-1650 F FOR COAL 1710-1730 F FOR PETROLEUM COKE
SUPERFICIAL GAS VELOCITY:	21-30 FT/SEC
Ca/S RATIO:	UP TO 4.0
EXCESS AIR:	40 PERCENT MAXIMUM
PRIMARY AIR/STOICHIOMETRIC AIR RATIO:	0.32 TO 1.4
DENSE BED MATERIAL:	IRON ORE (6 X 12 OR 10 X 16 MESH)
ENTRAINED BED MATERIAL:	SILICA SAND (20 X 70 MESH TYPICAL)
DENSE BED HEIGHT (SETTLED):	20 INCHES

of the dense bed and the calculated stoichiometric air. NO_x emissions was found to decrease significantly with decreasing air ratio. This is shown in Figure 4 burning coal and in Figure 5 when burning petroleum coke. The results indicate that to decrease NO_x emissions to roughly the 100 ppm level, the primary air/stoichiometric air ratio should be maintained at about 0.4 to 0.6.

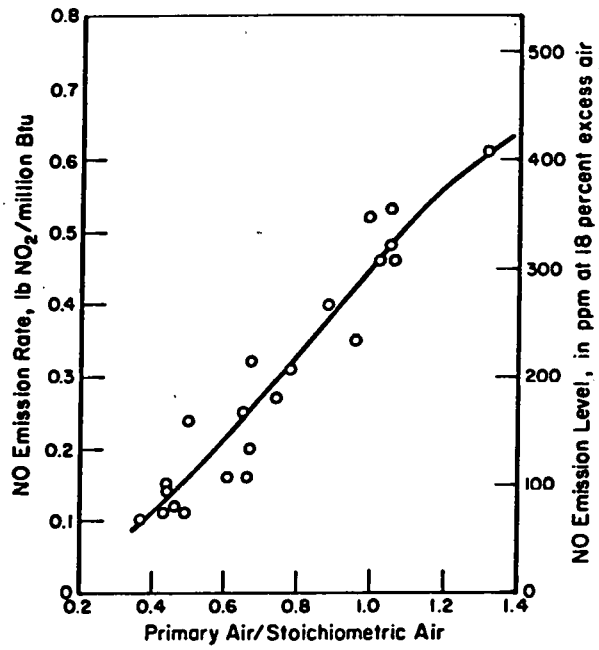

FIGURE 4. EFFECT OF PRIMARY AIR/STOICHIOMETRIC AIR RATIO ON NITROGEN OXIDES EMISSIONS (COAL)

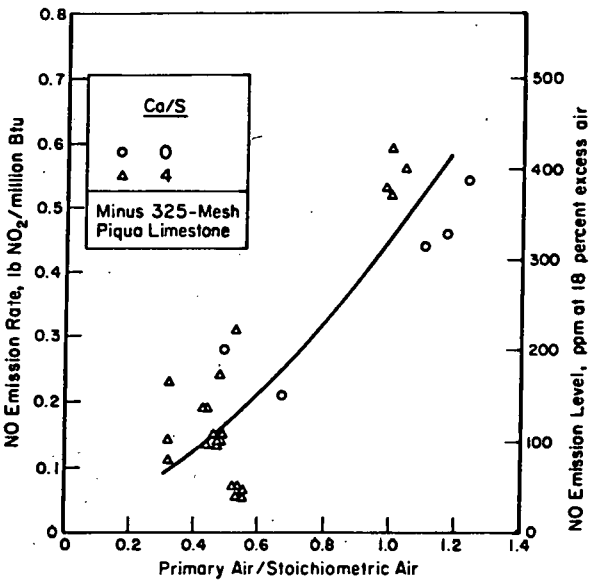

FIGURE 5. EFFECT OF PRIMARY AIR/STOICHIOMETRIC AIR RATIO ON NITROGEN OXIDES EMISSIONS (PETROLEUM COKE)

The residence time of the gas in the reducing zone is another important parameter in controlling NO_x emissions. The gas residence time is arbitrarily defined as the calculated time interval for the gas to travel from the distributor plate to the point where the lowest secondary air jet is located. As one might expect, longer residence time in the fuel-rich zone should increase the reaction between NO_x and char or carbon monoxide, thus yielding lower NO_x emissions. The experimental results obtained as shown in Figure 6 verify this. It can be concluded that in this system, NO_x can be reduced to 100 ppm with 1.0 sec residence time and 50 ppm with a residence time of about 1.5 sec.

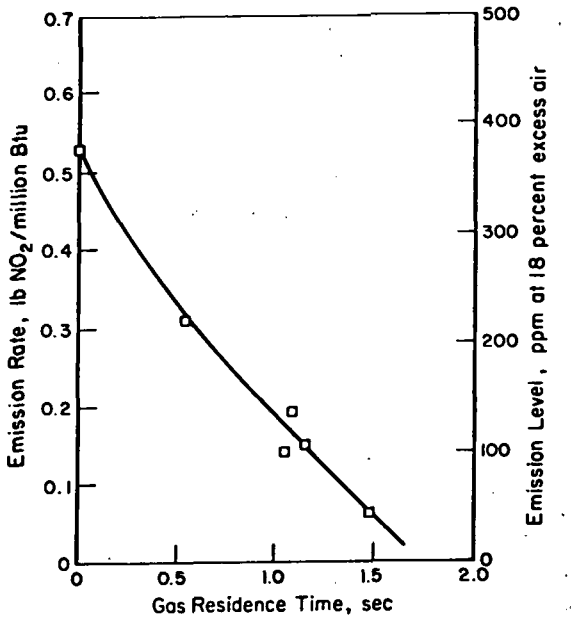

FIGURE 6. EFFECT OF GAS RESIDENCE TIME ON NITROGEN OXIDES EMISSIONS (PETROLEUM COKE)

Operation of the small pilot combustor in the staged combustion mode resulted in reduced sulfur retention at an equivalent limestone rate as shown in Figure 7. It appears that the creation of a reducing zone in the combustor shortens the effective length of the oxidizing region, reducing the degree of the $CaO-SO_2-O_2$ reaction to form $CaSO_4$. Thus, for a combustor of limited height, there will be a compromise between SO_2 and NO_x performance, and high levels of reduction will be obtained at a price. In a larger system, increased residence time could be provided to reduce the limestone consumption. In addition, recycle of flyash (which was not used in this study) has been shown to improve sulfur retention performance.

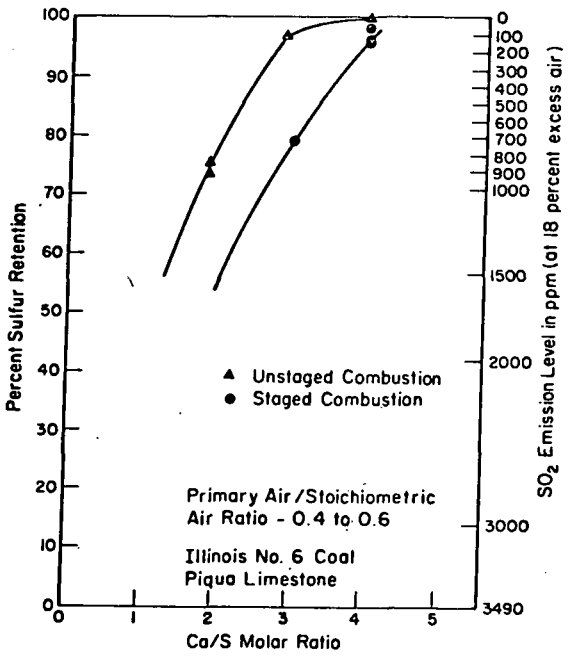

FIGURE 7. EFFECT OF STAGED COMBUSTION ON SULFUR RETENTION

Conclusions

The following conclusions were drawn on the application of staged combustion in the multi-solid fluidized-bed process.

1. The system is very effective in reducing NO_x emissions to low levels. Experimental results have shown that a level of 100 ppm or lower can be achieved as compared to 300-400 ppm with unstaged combustion.
2. Under the proper conditions, SO_2 and NO_x emissions can be simultaneously reduced to low levels.
3. NO_x emissions decreased with decreasing primary air/stoichiometric air ratio and increasing gas residence time in the reducing zone. To reduce NO_x to 50 to 100 ppm, the air ratio was in the 0.4 to 0.6 range, and the gas residence time in the reducing zone between 1.0 to 1.5 seconds.
4. Under a given set of conditions, sulfur retention is proportional to gas residence time in the oxidizing zone.
5. The system is sufficiently flexible so that by adjustment of design parameters, stringent emissions control requirements can be met.

The results of this preliminary study are very encouraging. Additional experiments will be conducted in the near future in two larger pilot units, one at Battelle and the other at Struthers Wells Corporation. Plant scale tests will be made in a 50,000 pounds of steam per hour prototype boiler to be constructed by Struthers Wells for the North American Production Division of the Conoco Oil Company. This unit is expected to be operational in about 1 year.

References

1. Nack, H., K. T. Liu and G. W. Felton, "Battelle's Multisolid Fluidized-Bed Combustion Process", paper presented at the 5th International Conference on Fluidized-Bed Combustion, Washington, D.C., December, 1976.
2. Liu, K. T., G. W. Felton, A. E. Weller, and H. Nack, "Multisolid Fluidized-Bed Combustion - Initial Pilot Plant Results", paper presented at the 86th AIChE Meeting, Houston, Texas, April, 1979.
3. "Fluidized-Bed Combustion - Industrial Application Demonstration Projects, Battelle's Multisolid Fluidized-Bed Combustion Process", End-of-Phase Report to U.S. Department of Energy, Contract No. EX-76-C-01-2472, October, 1979.

Questions to Herman Nack:

Q: Jeff Kennedy, Acurex

One of your curves showed NO_x going down with decreasing primary to stoic air ratio and your next slide showed staged combustion versus non-staged combustion and SO_2 limits and SO_2 reduction. What primary stoiciometric air ratio was the staged combustion done at on that second curve?

A: That was at about .6.

Q: Al Wormser, Wormser Engineering

It seemed like your NO_x figures went all the way down to zero at a sufficiently low stoiciometric ratio and you said at the last that you like to run as low as 100 ppm on NO_x. Am I missing something, or do you choose to run at 100 ppm by choosing your stoiciometric ratio, or is that the lowest limit you can reasonably expect to get?

A: We showed actual data of the study, of about 40 ppm at a little less than .4 primary air-stoiciometric air ratio. We did not pick any magic number like 100 ppm; we tried to just develop some relationship to indicate what we could do under what specific conditions. So, the answer to your question is, we probably could go down to 40. When you try to get below that, you get into difficulty in lack of oxygen for heat for the gasification reaction.

SIMULTANEOUS NO_x AND SO_2 EMISSION REDUCTION WITH FLUIDIZED BED COMBUSTION

J. TATEBAYASHI, Y. OKADA, K. YANO and S. IKEDA

KAWASAKI HEAVY INDUSTRIES, LTD.

1. INTRODUCTION

With the oil crisis of 1975 as a turning point, regarding coal as an important alternative to petroleum in the course of seeking easy-to-obtain and efficient energy sources became a world-wide trend.

To utilize coal more effectively, research and development of various combustion techniques have been intensively conducted in various countries. Among the methods tested are pulverized coal combustion, which is now conventionally available, fluidized bed combustion, gassification and liquefaction, each of whose completion is yet to be attained. Fluidized bed combustion (FBC) has attracted the greatest attention for a number of reasons, among them being: (1) it is an application of the existing coal combustion techniques and thus practicability is seen as great; (2) it assures low-pollution combustion; and (3) it cuts down on power generation costs. In the U.S., U.K. and West Germany, pilot plants are already operating.

In Japan, where environmental protection regulations are among the strictest to be found anywhere, the cost of environmental protection (removal of NO_x and SO_2 emission) in a power generation plant is high; in pulverized coal combustion, for example, the cost of de-NO_x and desulfurization facilities accounts for about 20% of the total power generation cost. In addition, Japan produces only a small amount of coal, so almost all of its coal demand must be met with a supply from overseas, both at present as well as in the future. Therefore, especially in Japan, the completion of the fluidized bed combustion boiler is met with great expectations because it is advantageously applicable to a variety of coal types while assuring low-pollution combustion.

Kawasaki Heavy Industries (KHI) first began the basic research and development of FBC technology in 1975. Since then various tests have been conducted using different fuels: C heavy oil, COM (coal-oil mixture) and coal. Through these tests were sought combustions with lowered pollutant emission levels. In 1978, KHI joined a cooperative effort, the Fluidized Bed Combustion Boiler Development Project, under the auspices of the Japanese Government. As major participants in this Project, we are now engaged in the planning of a pilot plant with evaporation of 20 tons per hour, to be completed in 1981.

Until today, a great volume of outstanding experimental reports and results of research on low-pollutant emissions in the FBC have been published from various parts of the world.[1] It is necessary in Japan, however, to conduct research and development of our own because:

1) Japanese environmental regulations are expected to be extremely strict—NO_x and SO_2 emission levels will be restricted to less than 100ppm, and to a few score ppm in the final stage; and
2) almost all the types of coal expected to be used in Japan in the future will contain less than 1.5% S content and 1 to 2% N content.

Therefore, we at KHI first engaged in a study of the effects of various parameters on NO_x and SO_2 emissions in FBC, and succeeded in clarifying them.[2,3] Based on these results, we conducted a series of two-stage combustion tests to attain effective NO_x and SO_2 emission controls. As a result, we successfully brought NO_x and SO_2 emission levels down to within 100ppm.

This paper reports the effects of various parameters on NO_x and SO_2 emission in the fluidized bed combustion of coal.

2. EXPERIMENTAL EQUIPMENT AND PROCEDURES

2.1 Experimental Equipment

In the combustion test, two test combustors were used, with inner measurements of 200mm and 500mm square respectively. Fig. 1 shows the general view of the 500mm-square FBC facilities. This experimental equipment consists of (1)

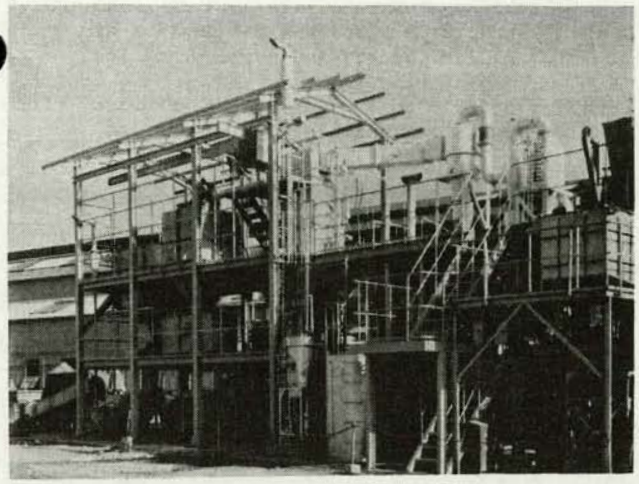

Fig. 1 General view of 500mm-square fluidized bed combustion facility

pre-treatment system comprising dryer, crusher, screen storage bunker and feeder of coal; (2) fluidized bed combustor; (3) water supply and steam system of 0.5 ton/h evaporation comprising water softener, deaerator, feed pump and water separator; (4) air-flow system consisting of FCF and IDF; and (5) dust collector system made up of cyclone and bag filter.

Shown in Fig. 2 is a cross sectional view of the 500mm-square combustor. Coal and sorbent are fed pneumatically into the combustor at the bottom.

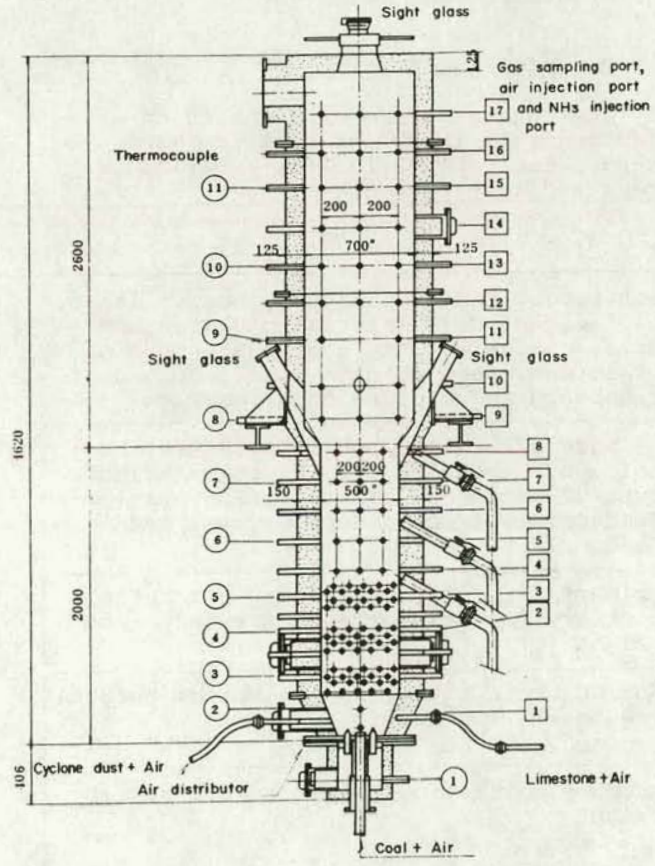

Fig. 2 General arrangement of 500mm-square coal-fired fluidized bed combustor

2.2 Experimental Procedure

PROXIMATE ANALYSIS (as moisture free)			(w/w %)
Type of coal	Taiheiyo	Miike	Takashima
Moisture	5.4	2.7	2.3
Ash	11.5	19.8	24.5
Volatile matter	43.9	36.5	33.3
Fixed carbon	39.2	41.1	39.9
ULTIMATE ANALYSIS (dry basis)			(w/w %)
Type of coal	Taiheiyo	Miike	Takashima
C	66.2	66.2	60.6
H	5.6	5.1	4.6
N	1.07	0.88	1.05
S	0.4	2.82	1.14
HEAT VALUE (as moisture free)			(kcal/kg)
Type of coal	Taiheiyo	Miike	Takashima
Higher heat value	6580	6480	6080
Lower heat value	6260	6200	5820

Table 1 Analysis of sample coals

Three different types of coal were employed as sample coal. Table 1 shows typical composition analysis results of the sample coals. In consideration of the application of the test results to a practical FBC boiler design, coal particles were screened, without omission of undersize specimens, into the following diameter groups: 0 to 2mm, 0 to 4mm and 0 to 6mm. As sample sorbent, natural limestone, consisting of 98.8% $CaCO_3$, 0 to 2mm in diameter was chosen. Quartz sand consisting of 94% SiO_2 or limestone, 0.3 to 1.4mm in diameter was employed as material for forming the fluidized bed.

Each combustor had many sampling ports in its walls; through them secondary air and NH_3 gas were injected into the combustor in a staged combustion test. Choosing the proper ports among them allowed change in the air or NH_3 gas feed positions.

To reduce NO_x and SO_2 emission, a baffle screen was installed in the freeboard. Photo of the test screen is shown in Fig. 3.

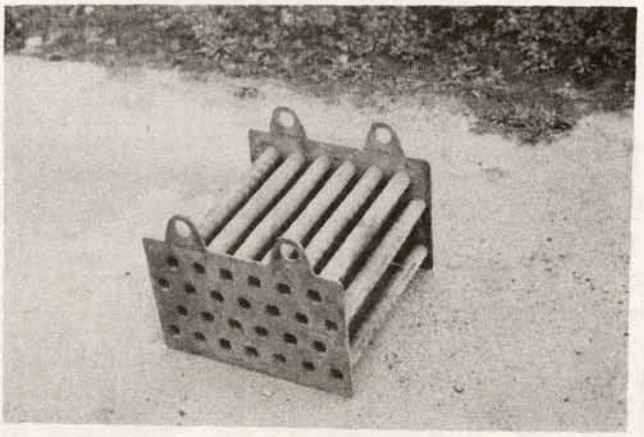

Fig. 3 General view of experimental baffle screen

Samples of emission gas analysis were taken from the cyclone or economizer outlet and analyzed by magnetic O_2 analyzer, chemical luminescence NO_x analyzer, NDIR-type CO and SO_2 analyzer. Further, as necessary, the samples were analyzed using gas chromatography and chemical analysis of liquid absorption. All the outputs obtained above and other signals including air, water and steam pressure, temperature and flow rate were recorded by the digital data collector.

Combustion efficiency ηc, desulfurization efficiency ηs and NO_x concentration which appear in this paper were obtained by using the following formulas:

$$\eta c = (1 - \frac{8100 \times C \times D}{B \times H\ell}) \times 100 \quad (\%)$$

where B = coal feed rate (kg/h)
$H\ell$ = low heat value of sample coal (kcal/kg)
C = carbon concentration in cyclone-collected ash (weight fraction), and
D = quantity of cyclone-collected ash (kg/h).

$$\eta s = (1 - \frac{(SO_2)\ \text{meas.}}{(SO_2)\ \text{theo.}}) \times 100 \quad (\%)$$

where (SO_2)meas. = measured SO_2 concentration in emission gas (ppm), and
(SO_2)theo. = total SO_2 concentration calculated on the assumption that all the sulfur content in the coal was converted to SO_2 (ppm).

$$NO_x = \frac{21 - 6}{21 - (O_2)} \times (NO_x) \quad (\text{ppm})$$

where (O_2) = measured O_2 concentration in emission gas, and
(NO_x) = measured NO_x concentration in emission gas.
This formula gives the NO_x concentration on the basis of O_2 content in emission gas being 6%.

2.3 Experimental Items

We conducted the experiments on emission controls in FBC of coal in three steps. See Table 2 for the experimental items and test parameters.

STEP I Normal combustion test	Effects of various parameters on NO_x emission, ηs and ηc under normal combustion conditions	air ratio, bed temperature, heat release, bed height, Ca/S mole ratio, limestone size, coal size, typ e of coal, type of limestone, feed point of coal, height of freeboard and cyclone dust recycle
STEP II Low-pollution test	Effects of various parameters on NO_x emission, ηs and ηc under two-stage combustion conditions	primary air ratio, bed temperature, heat release, secondary air injection height, type of secondary air injection nozzle, feed point of coal, type of coal and Ca/S mole ratio
	Effects of various parameters on NO_x emission under three-stage combustion conditions	primary air ratio, secondary air ratio, tertiary air ratio, staged air injection height
	Effects of various parameters on NO_x emission with NH_3 injection	$NH3/NO_x$ mole ratio, NH_3 injection height, freeboard temperature
STEP III Advanced low-pollution test	Effect of baffle screen on NO_x emission, ηs and ηc under two-stage combustion conditions	primary air ratio, baffle screen setting height

Table 2 Test items and parameters

3. EXPERIMENTAL RESULTS AND DISCUSSION

3.1 Normal Combustion Test

Among various parameters affecting combustion characteristics in normal combustion, such as combustion efficiency, desulfurization efficiency and NO_x emission, those which have the greatest effects are air ratio, bed temperature, heat release, Ca/S mole ratio and type of coal. Coal size, bed height, type of limestone and coal feed position are of much less importance. Qualitative effects of these parameters on normal combustion are listed in Table 3.

Parameter		Variation	NO	ηs	ηc
Air Ratio	—	0.8 → 1.4	↗	↗	↗
Bed Temperature	°C	750 → 900	→	↘	→
Heat Release	$Kcal/m^2h$	0.5 → 2.2 $\times 10^6$	→	↘	↘
Bed Height	m	0.6 → 1.4	→	↗	→
Ca/S Mole Ratio	—	0 → 6	→	↗	→
Size of Limestone	—	Fine → Coarse	→	↘	→
Kind of Coal	—	Taiheiyo Coal → Miike Coal	↘	↗	↘
Size of Coal	mm	-0.25 → 1~2	↘	→	↗
Feed Point of Coal	m	From distributor 0.05 → 0.6	→	↘	→
Height of Freeboard	m	0.4 → 2.4	↘	→	↗
Cyclone Dust Recycle	—	No. → Yes.	→	↗	↗

Table 3 Parameter survey of ηc, ηs, and NO_x emission in normal combustion

Effect of air ratio

Shown in Fig. 4 is the effect of air ratio on normal combustion. Its effect on NO_x emission was remarkable; as the air ratio became smaller, NO_x emission simply dropped. In the range of 1.0 or less air ratio, NO_x emission remained small but some emission of NH_3 and HCN was observed. Both desulfurization efficiency and combustion efficiency drew downward curves as the air ratio decreased.

Effect of bed temperature

NO_x emission increased as the bed temperature rose. Desulfurization efficiency reached its maximum level at the bed temperature of 800 to 830°C, then suddenly dropped as the temperature exceeded 850°C. This pattern applied to all the four types of limestone, each with different origins, used in our tests. Combustion efficiency meanwhile increased as the bed temperature rose; there was no remarkable boost, however.

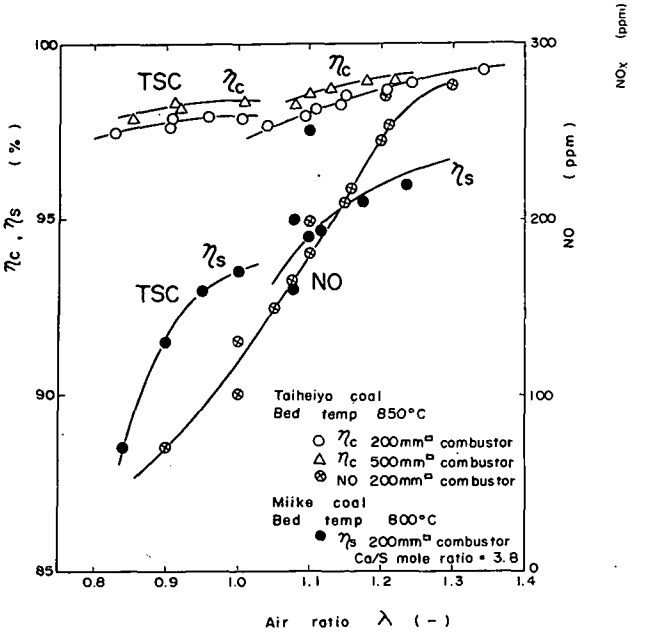

Fig. 4 Effect of air ratio on ηc, ηs and NO emission in normal combustion

Effect of heat release

Heat release means the thermal input per unit time and per bed area. We conducted the combustion tests by changing the heat release rate within the parameters 0.5×10^6 kcal/m^{2}h and 2.2×10^6 kcal/m^{2}h. The effect of heat release on NO_x emission was small. But an increase in heat release had a negative impact on desulfurization efficiency. This is partly because the increase in heat release speeded up gas flow velocity, thereby hindering sufficient contact between sorbent and SO_2, and partly because the increase caused more active combustion of elutriated coal in the freeboard, accelerating the generation of SO_2 therein. Combustion efficiency also decreased as the heat release rate increased. This is attributed to the fact that elutriation of unburnt coal particles was accelerated by the increase in gas flow velocity. The degree of such an effect varied depending on the coal particle distribution.

Effect of Ca/S mole ratio

The Ca/S mole ratio had a great influence on desulfurization efficiency. As the mole ratio decreased to less than 2, desulfurization efficiency suddenly dropped. As the ratio increased, desulfurization efficiency was enhanced, but at a ratio greater than 6, it leveled off. We believe this is because SO_2 is released from the freeboard even though the Ca/S mole ratio increased. With the increase in the mole ratio, NO_x emission rose a little, but no difference was observed in combustion efficiency.

Effect of bed height

No noticeable effect could be observed in NO_x emission when the bed height was varied. Desulfurization efficiency showed an upward curve with the increase in bed height, but the curve soon levelled out. One of the reasons for this is believed to be SO_2 generation in the freeboard. Combustion efficiency, too, was improved a little by the increase in bed height, but further improvement could not be expected.

Effect of coal size

In the test, Taiheiyo Coal was screened into four particle sizes: 0 to 0.25 to 0.5mm, 0.5 to 1.0mm and 1.0 to 2.0mm. Each group of coal particles was subjected to the combustion test. NO_x emission was greatest when coal particles were between 0.25 and 0.5mm in diameter. Coal size had an effect on combustion efficiency: the greater the coal particle diameter, the higher the combustion efficiency. With 1- to 2mm-diameter coal particles, combustion efficiency was as high as 99.5%. Combustion efficiency with particles 0 to 0.25mm in diameter and that with particles 0.25 to 0.5mm were equal.

3.2 Low Pollution Test

It can be generally said that NO_x emission with FBC of coal is less than that with pulverized coal combustion. But the reduction by normal FBC is not enough to fulfill strict Japanese environmental protective regulations requiring less than 100ppm NO_x emission and even around three score ppm in the final stage. To meet such requirements, we conducted a two-stage combustion test, a three-stage combustion test and a NH_3 injection test mainly for further suppression of NO_x emission, and clarified the effects of various parameters on NO_x emission, desulfurization efficiency and combustion efficiency in each case.

1) Two-stage Combustion Test

It has been found that, in two-stage combustion, such parameters as primary air ratio, secondary air injection height, heat release and bed temperature have a great effect, and that the others do not. In Table 4 are shown the qualitative effects of various parameters.

Effect of primary air ratio

The effect of primary air ratio in two-stage combustion is shown in Fig. 5. The greatest effect was observed in NO_x emission. NO_x emission quickly dropped as the primary air ratio was decreased; the emission was minimized at a primary air ratio of 0.95. As the primary air ratio was decreased still further, NO_x emission started to rise. Throughout the testing, the primary air ratio at which NO_x emission was minimal varied a little depending on other factors, such as heat release, secondary air injection height and coal type; but in any case, the primary ratio lay between 0.9 and 1.0. The reason for this, we believe, is that the reducing reaction of NO_x which had been produced in the primary combustion zone, caused by NH_3, CO and char and taking place in the bed and freeboard, and the NO_x forming reaction occurring in the secondary combustion zone when NH_3 and char burn, are closely affected by the in-bed combustion

Parameter		Variation	NO	η_s	η_c
Primary Air Ratio	—	0.8 → 1.05	↘	↗	↗
Total Air Ratio	—	1.05 → 1.25	↗	→	→
Bed Temperature	°C	750 → 900	↗	↘	→
Heat Release	$Kcal/m^2h$	$0.8 \rightarrow 2.2 \times 10^6$	→	↘	↘
Secondary Air Injection Height	m	From Bed Surface 0.25 → 1.75	↘	↘	↘
Secondary Air Injection Nozzle	—	Single-port → Multi-port	↗	→	→
Feed Point of Coal	—	From distributor 0.05 → 0.6	↗	↘	→
Kind of Coal	—	Taiheiyo Coal → Miike Coal	↘	↗	↘
Ca/S Mole Ratio	—	0 → 3.8	→	↗	→

Table 4 Parameter survey of ηc, ηs, and NOxemission in 2-stage combustion test

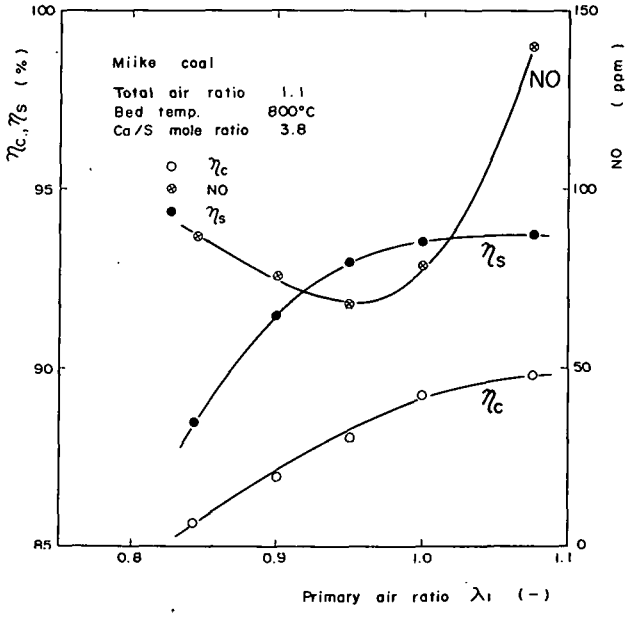

Fig. 5 Effect of primary air ratio on ηc, ηs and NO emission in two-stage combustion

efficiency and the freeboard temperature profile.

Desulfurization efficiency simply dropped as the primary air ratio was decreased; the lowering curve started a sharp descent as the ratio reached less than 0.9. This drop in desulfurization efficiency in two-stage combustion of coal was much more moderate than that obtained in FBC of heavy oil that had been conducted before. This is because, compared with heavy oil, coal burns at a slower rate, and its bed residence time is long enough to allow itself to spread throughout the bed uniformly as particles. Further, it has the opportunity to come into contact with air which rises through the bed in the shape of bubbles. This accelerates combustion, sulfur release and desulfurization, all at the same time. As a result, the by-pass of SO_2 gas is decelerated and the drop in desulfurization efficiency of coal-fired FBC is suppressed to a small degree compared with that of FBC of heavy oil.

As for combustion efficiency, it dropped as the primary air ratio was decreased; but the drop itself was not too great.

Effect of secondary air injection height

The effect of secondary air injection height upon two-stage combustion of coal is given in Fig. 6. The greater the secondary air injection height, the smaller the NO_x emission. There was a point, however, where NO_x emission would not further decrease even if the air injection height continued to be raised. This indicates the necessity in two-stage combustion for providing sufficient freeboard height so that NO_x can be reduced to a sufficient extent by NH_3, CO and char. It was also found that the above-mentioned point where NO_x emission would not further decrease was different in the 200mm-square combustor and the 500mm-square combustor; two-stage combustion with the 500mm-square combustor required the greater secondary air injection height to achieve the same NO_x emission level. We believe this is because of the difference in mixing and temperature profile in the two combustors' freeboard.

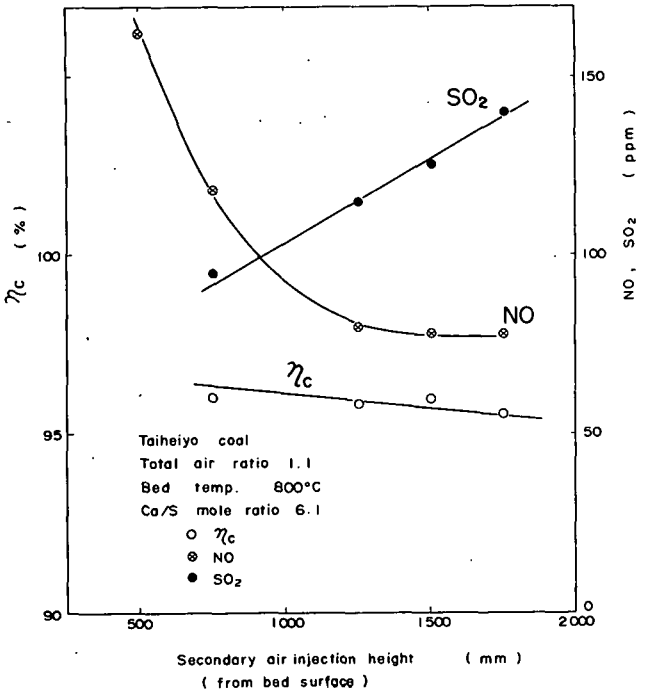

Fig. 6 Effect of secondary air injection height on ηc, ηs and NO emission, in 2-stage combustion

In contrast to NO_x emission, SO_2 emission increased as the secondary air injection height was increased. In our opinion, heightening the secondary air injection position shortens the time for an elutriated sorbent to engage in desulfurization in the freeboard where the air ratio is high and desulfurization actively takes place.

Combustion efficiency dropped as the secondary air injection height increased; but the drop was small.

Effect of heat release

Given in Fig. 7 are the results of the combustion test, where the effect of heat release was studied with the primary air ratio and secondary air injection height set at such levels as to minimize NO_x emission. From this we have found

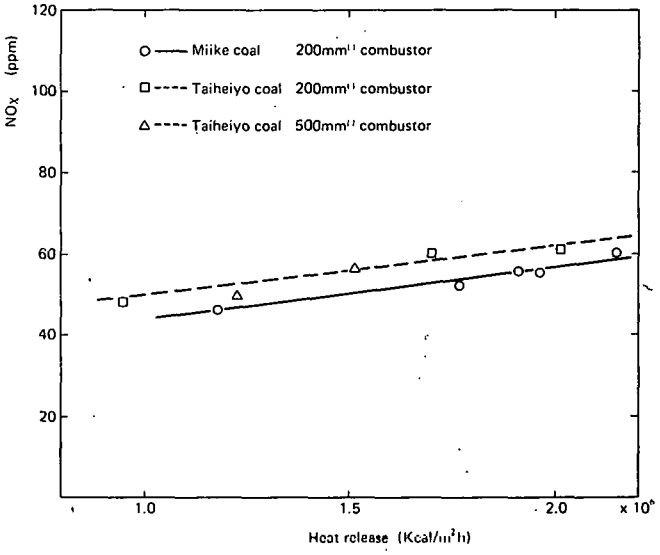

Fig. 7 Effect of heat release on optimum NO emission in two-stage combustion

that an increase in heat release causes a rise in NO_x emission level. As in normal combustion, desulfurization efficiency and combustion efficiency dropped as heat release increased.

Effect of bed temperature

NO_x emission drew an upward curve as the bed temperature rose; but the increasing speed varied depending on the secondary air injection height. When the secondary air injection height was low and consequently NO_x emission was great, bed temperature had a great influence on the emission; on the other hand, when the secondary air injection height was great and NO_x emission was near the minimum point, the effect of bed temperature was small. As in normal combustion, desulfurization efficiency in two-stage combustion was greatly affected by the bed temperature. But the optimum bed temperature where desulfurization efficiency was maximum was lower in two-stage combustion than in normal combustion. Desulfurization efficiency simply decreased as the bed temperature rose, within the limited conditions of our study (775° to 875°C).

It must be noted, however, that the desulfurization efficiency cited above is not the true desulfurization efficiency, but an apparent one obtained on the basis of the total sulfur content in the fuel. Actually, the in-bed desulfurization consists of the following three processes:

(1) calcination of limestone(sorbent),
(2) release of sulfur from coal, and
(3) desulfurizing reaction between CaO and SO_2.

As the bed temperature has an effect on each of the above three processes, it is extremely difficult to clarify the true cause of the effect of the bed temperature on desulfurization efficiency.

2) Three-Stage Combustion Test

Finding that two-stage combustion is extremely effective in reduction of NO_x emission, we conducted a series of three-stage combustion tests with air injected in three steps: primary, secondary and tertiary. In this case, too, as in two-stage combustion, NO_x emission was minimized at a primary air ratio between 0.9 and 1.0. But the NO_x emission level in three-stage combustion remained greater than that in two-stage combustion throughout the testing, except at extremely high heat release ratios and at very small primary air ratios.

3) NH_3 Injection Test

To know the non-catalytic de-NO_x reduction effect of NH_3 gas, NH_3 was injected into fluidizing air, coal carrier air, fluidized bed or freeboard. When the NH_3 gas was fed into the fluidizing air, coal carrier air or into the bed, the NO_x emission level was higher than that obtained when no NH_3 was fed. But when NH_3 gas was injected into the upper part of the bed or into the freeboard, the NO_x emission level decreased. As long as NH_3 gas was injected into the freeboard, NO_x emission dropped as the NH_3 injection height was raised, or as the NH_3/NO_x ratio increased. But since the temperature in the freeboard in FBC is comparatively low, i.e., 750 to 850°C, more NH_3 remains unreacted and emitted as the NH_3/NO_x mole ratio is increased. Typical de-NO_x efficiency in the test was approximately 50% at 1.0 NH_3/NO_x mole ratio.

3.3 Advanced Low Pollution Test

It is now clear that two-stage FBC is extremely effective in the suppression of NO_x emission, as mentioned above. It is also true, however, that this two-stage combustion is accompanied by decreased desulfurization efficiency and requires great freeboard volume. These factors pose difficulties for putting FBC into

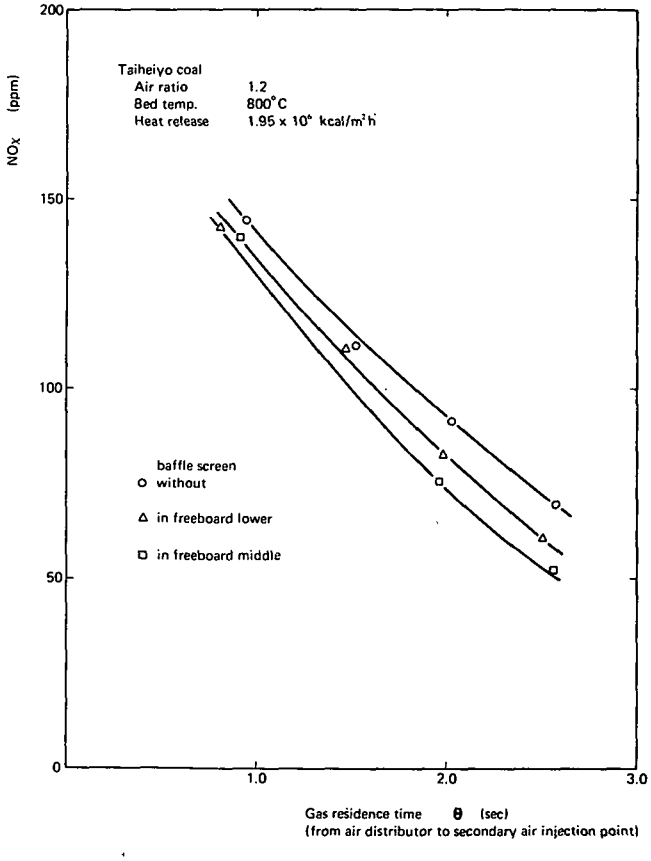

Fig. 8 Effect of baffle screen on NO_x emission

practical use. To eliminate such demerits of two-stage FBC, we conducted a series of combustion tests with a baffle screen in the freeboard.

Shown in Fig. 8 is the effect of the baffle screen upon NO_x emission. Taiheiyo Coal was chosen for the test, and the correlation between NO_x emission and the time duration for gas remaining between the air distributor and the secondary air injection position (gas residence time), was sought. The test results in Fig.8 clearly display the remarkable effect of the baffle screen on NO_x emission suppression. It also suggests that the scale of the effect varied, depending on where the baffle screen was installed. The effect was greater when the screen was located in the mid-section of the freeboard than when it was at the bottom.

With the secondary air injection height kept constant, installation of a baffle screen decreased NO_x emission and shortened the gas residence time until the same NO_x emission level was achieved by approximately 0.5 second.

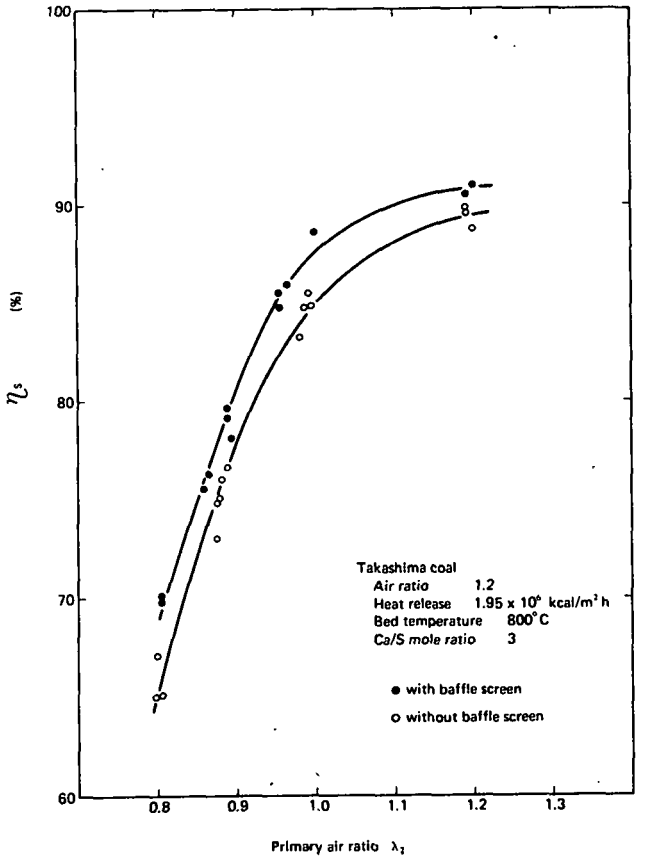

Fig. 9 Effect of baffle screen on desulfurization efficiency

Fig. 9 gives the effect of the baffle screen on desulfurization efficiency. In the test, Takashima Coal was employed and a baffle screen was installed in the mid-section of the freeboard. As a result, desulfurization efficiency was enhanced by 2 to 5% at any primary air ratio. The reason for such a favorable effect of the baffle screen on NO_x and SO_2 emission is, we believe, that the "unmixedness" in the freeboard peculiar to FBC, is eliminated by the mixing effect of the screen. This elimination of the "unmixedness" accelerates mixing of gas and gas, and gas and particles, thereby activating various reactions in the freeboard. The FBC "unmixedness" mentioned above usually occurs as a result of the co-existence of an emulsion phase and bubble phase in the bed and/or when gas flow in the freeboard is slow. As a result, it has been found that by optimizing the structure and position of the baffle screen, it is possible to reduce both NO_x and SO_2 emissions and freeboard volume simultaneously.

3.4 Relation between NO_x Emission and SO_2 Emission

A series of parameter surveys conducted so far indicates that many of the combustion conditions favorable for suppression of NO_x emission and for abatement of SO_2 emission are incompatible. It also suggests, on the other hand, that it is possible to suppress both NO_x and SO_2 emission simultaneously to within levels tolerated by environmental regulations, by setting such parameters as bed temperature, primary air ratio, secondary air in-

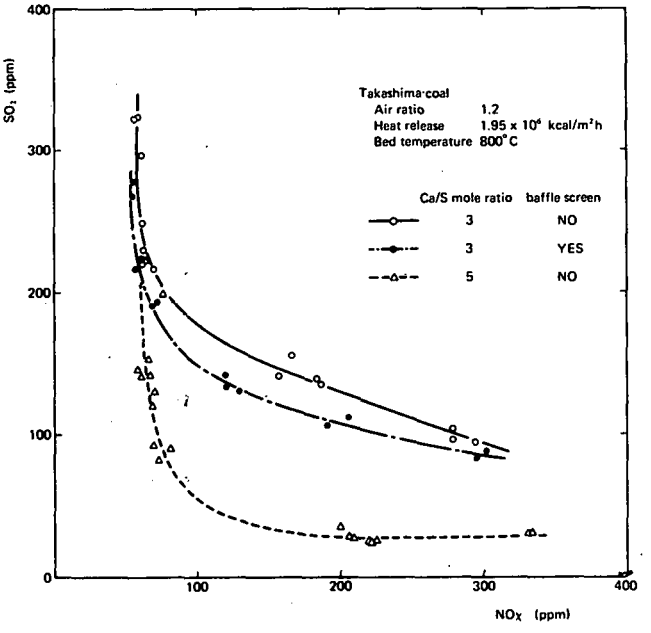

Fig. 10 Correlation between NO_x and SO_2 emissions in 2-stage combustion

jection height and heat release, to their respective optimum levels. As the optimum levels of these parameters vary depending on environmental regulations, which themselves vary according to the particular area where the boiler is to be constructed and FBC boiler capacity, they should be determined after careful consideration from the aspects of efficiency and economy on a case-by-case basis.

Given in Fig. 10 is the correlation between NO_x and SO_2 emissions in two-stage combustion. This correlation was obtained in a test using Takashima Coal, a type of coal with the same fuel S and N contents as the types most likely to be used in Japan in the future. As can be seen from the figure, SO_2 emission starts to increase with the NO_x emission level at around 100ppm, then suddenly shoots up at around 60 to 70ppm NO_x emission. The effect of the baffle screen on suppression of NO_x and SO_2 emissions was remarkable; with the Ca/S mole ratio constant, the SO_2 and NO_x emission levels with the baffle screen installed were lower than those with no screen. At a Ca/S mole ratio of 5 and without the baffle screen, both the NO_x and SO_2 emission levels were suppressed to less than 100ppm (see Fig. 10). Fig. 10 was obtained by setting the heat release rate at 1.95×10^6 kcal/m^2h. We believe that by decreasing the heat release rate more than that and/or by installing a baffle screen, the range where both SO_2 and NO_x emission levels are kept under 100ppm, can still be widened and that it will be possible to maintain less-than-100ppm levels at small Ca/S mole ratios. The correlation between NO_x emission and SO_2 emission varied depending on such parameters as heat release, secondary air injection height and mixing effect of the baffle screen. The correlative variations are shown in Table 5.

Mode of correlation change	Change in parameters
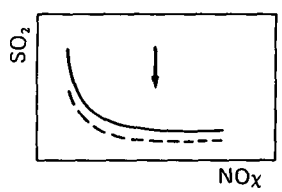	Ca/S mole ratio increase coal sulfur content decrease
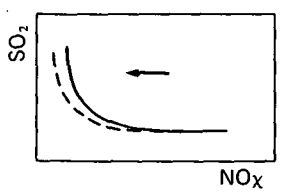	coal nitrogen content decrease
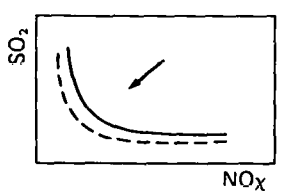	heat release decrease bed temperature decrease baffle screen mixing strength increase
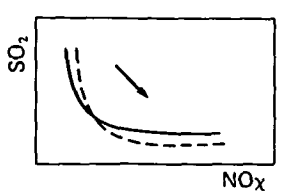	secondary air injection height decrease

Table 5 Change in correlation between NO_x emission and SO_2 emission

4. CONCLUSIONS

In this paper, we have studied and successfully clarified the effects of various parameters on FBC NO_x and SO_2 emissions. As a result, we have found that many of the conditions effective for the suppression of NO_x emission and those for the abatement of SO_2 emission are incompatible, but that it is possible to suppress both NO_x and SO_2 emissions to considerably low levels by employing a two-stage combustion and setting the parameters at their respective optimum levels.

After achieving these test results, we believe that we have proved the probability of simultaneous suppression of NO_x and SO_2 emission below 100ppm in FBC, and of completion of a fluidized bed combustion boiler able to attain economical power generation without the need for de-NO_x and desulfurization facilities and yet able to operate while satisfying the strict Japanese environmental regulations. We also believe that the remarkable low-pollution performance of the FBC boiler will be demonstrated in the 20 ton-per-hour evaporation pilot plant, to be completed in 1981.

We are now determined to further suppress NO_x and SO_2 emissions to even lower levels, to a few score ppm.

ACKNOWLEDGEMENTS

Part of this work was carried out under a grant from the Japanese Ministry of International Trade and Industry. We are also grateful to the Coal Mining Research Center for its useful help in various forms.

REFERENCES

1) A.A. Jonke et al, "Pollution Control Capabilities of Fluidized-bed Combustion", AIChE, Sym. Ser. 68-128.

2) Y. Okada et al, "Experimental Emission Control on Fluidized-bed Combustion of Coal", AIChE, 72nd Annual Meeting, 1979.

3) J. Tatebayashi et al, "Fluidized Bed Combustion of Coal", 2nd Miami International Conference on Alternative Energy Sources, 1979.

THIS PAGE

WAS INTENTIONALLY

LEFT BLANK

SULFUR CAPTURING EFFECTIVITY OF LIMESTONES AND DOLOMITES IN FLUIDIZED BED COMBUSTION

Heinrich Münzner, Bernhard Bonn

Bergbau-Forschung GmbH, Essen

Introduction

The use of limestone or dolomite as a sulfur capturing additive in fluidized bed combustion (FBC) is a well established technique and its efficiency is, in fact, one of the advantages of FBC over conventional combustion technology. However, it is well known, that limestones of different origin vary considerably in sulfur capturing effectivity (1). This has in several careful studies been investigated and one of the reasons for these differences has been found to be different porosity of the stones (2). Yet a formal relationship between porosity or any other characteristic property and sulfur capturing effectivity of the additive has so far not been established. Thus in this work we looked for guidelines for the selection of natural additives in technical scale fluidized bed combustors.

From the operator's point of view the selection of an additive will be made according to

- effectivity
- cost and
- availability.

High effective additives not only save cost in buying but also in reduced size of handling equipment and substantially reduced amount of waste for disposal. In terms of buying cost a locally occurring natural additive without special pretreatment or even preparation would be preferable. This would also be advantageous from the view-point of availability.

Therefore, tests were begun to evaluate the reduction in SO_2-emission using in all 25 limestones and dolomites from different deposits of different geologic periods and from all over Germany.

Experimental

The experiments were run in a laboratory combustor of 6 cm diameter and 0.6 m bed height. By means of a wire spiral serving as a bubble breaker smooth fluidization was obtained. In previous experiments the influence of various operating parameters on combustion were studied and several different coals were examined (3). Also the results from the laboratory combustor had been compared to results from an atmospheric FBC test rig of 0.32 m^2 cross-section to obtain a criterium for the reliability and importance of the lab results for practical operation on a larger scale. It was found, that if the conditions for the lab combustor and for the larger test rig combustor were chosen as to have the same heat release rates per m^2 of distributor grid, equal gas residence times (by means of variation of bed height) and a suitable ratio of fluidizing velocity and coal grain size then combustion efficiency and sulfur capture in both combustors yielded quite similar results (4).

From this experience the most characteristic operating conditions and a suitable standard coal were selected for the comparative additive investigation. We are, therefore, confident that our results enable us to draw more generally applicable conclusions.

The sulfur capturing effectivity of an additive results mainly from two factors. Firstly, the properties of the individual grains control the reaction rates of the chemical and diffusional steps of the SO_2-absorption. Secondly, the concentration of active additive particles in the fluidized bed determines the total absorption. Since, however, large particles (i.e. those which will not be elutriated) accumulate in the bed overall sulfur capturing effectivity of such large additive particles results from two counter-current effects: first the saturation of the individual additive particles in the course of the reaction and second the slow increase in concentration in the bed. In order to study these effects separately, it was decided to investigate the effectivity of the stones in three size fractions:

- small particles, which will be rapidly elutriated and thus have only a relatively short residence time in the bed,

- large particles, which will not be elutriated and thus stay on in the fluidized bed for the rest of the test run (except for loss by means of disintegration or attrition). Test duration was confined to times where no bed material had to be taken off.

- particles of intermediate size for which elutriation plays an important rôle.

For these fractions the sulfur capturing effectivity of each of the stones was determined separately in actual combustion tests. Also a pore size distribution of the raw stones was measured using the Hg-porosimeter technique and for the small particles fraction a grain size distribution (gradation) was evaluated. For the larger particles determinations of elutriation loss and stone utilization of elutriated material as well as of material retained in the bed were made.

Results and Discussion

This is not the place to discuss all the details of the measurements. Rather, it seems appropriate to deal with the most conspicuous findings only in some examples and then present more general conclusions.

Elutriatable Additive

To start with the results for the small particles fraction are most suitable since effects arising from accumulation of additive in the bed do not occur. From the layout of the lab combustor all particles smaller than 100 μm have only a very short residence time and will be rapidly elutriated. Therefore, the stones have been ground to grain size below 100 μm and the coal and the bed material (coal ash) have been sized to grain sizes above c. 200 μm. Steady desulfurization conditions were achieved in approx. 0.5 h time after feeding a new coal/additive-mixture and thus sulfur capture effectivity could be determined for several coal/additive ratios in reasonable time. In Fig. 1 the results for 5 different stones, all from the Triassic period, are presented using standard conditions and standard h.v. bituminous A coal. On the abscissa the mass ratio of stone additive and coal has been used. This quantity is, from the operator's point of view, the most significant one. It is obvious, that part of the different sulfur capturing efficiency of the stones is due to differences in purity, i.e. different content of the active substance. Therefore, in a new diagram the Ca/S ratio has been chosen as abscissa scale (Fig. 2).

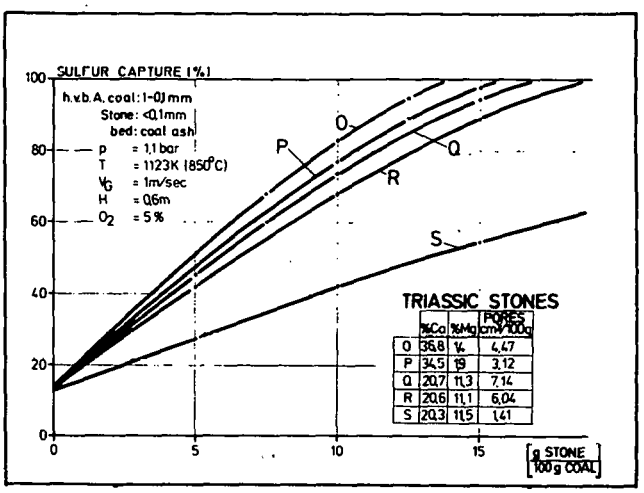

FIG. 1: Sulfur Capturing Effectivity of Triassic Stones

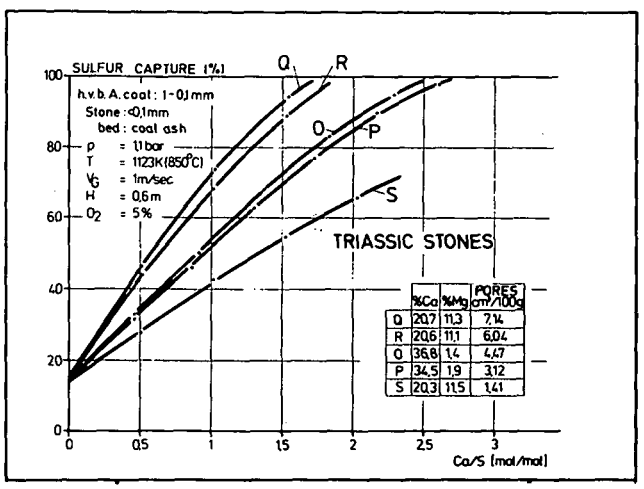

FIG. 2: Sulfur Capturing Effectivity of Triassic Stones

Now the dolomites Q and R turn out to be more effective than the limestones O and P which were better in Fig. 1. From the specific pore volume of the stones listed up in Fig. 2 as well it can be concluded, that porosity of the additive, i.e. availability of the active constituent not only on the surface but also in the core of the particle is next to purity one of the most important factors. Strictly, pore size or, better, pore size distribution is even more important than overall porosity (cf (2)). For the Triassic stones investigated here pore size distribution

is, however, not markedly different (Fig. 3).

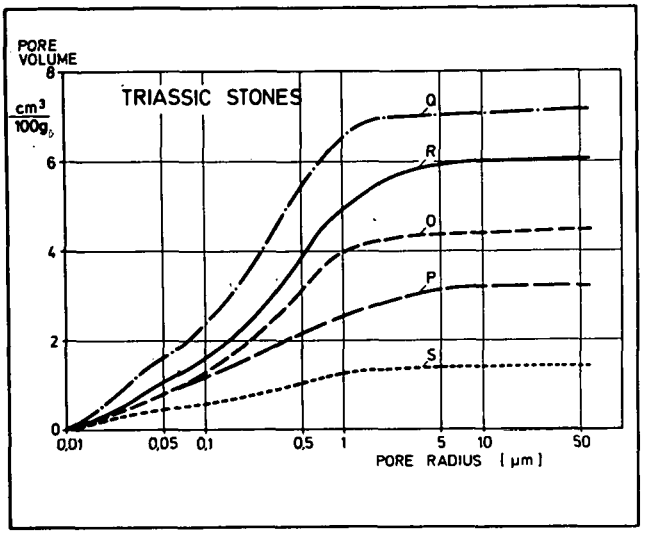

FIG. 3: Pore Volume vs. Pore Radius for Triassic Stones

Accessibility of the Ca is also determined by the grain size of the particles. Fig. 4 shows that the high effectivity of stones Q and R and correspondingly the comparatively low performance of dolomite S is influenced by the grain size distribution (gradation) of the stones. Dolomites Q and R consist of a large fraction of very fine material, whereas dolomite S is substantially coarser than the other stones. Since all of the stones have been prepared in precisely the same way (crushing, milling, sieving) a different grain size distribution reflects the physical properties of the individual stones rather than differences in stress during diminution.

Corresponding test series were run also with stones originating from other geologic periods yielding similar results and trends. In Fig. 5 the sulfur capturing effectivity of the most active limestones from each group of stones is presented. Greek marble, although the purest stone with the highest Ca-content, turns out to be the least efficient additive. This is due to its very low porosity and to the fact that the stone because of its well crystallized structure yielded a rather flat grain size distribution curve and much more coarse material than the other stones. The small advantage of higher Ca-content is thus by far outweighed by the low accessibility of the sulfur trapping constituent of the additive for SO_2 and oxygen.

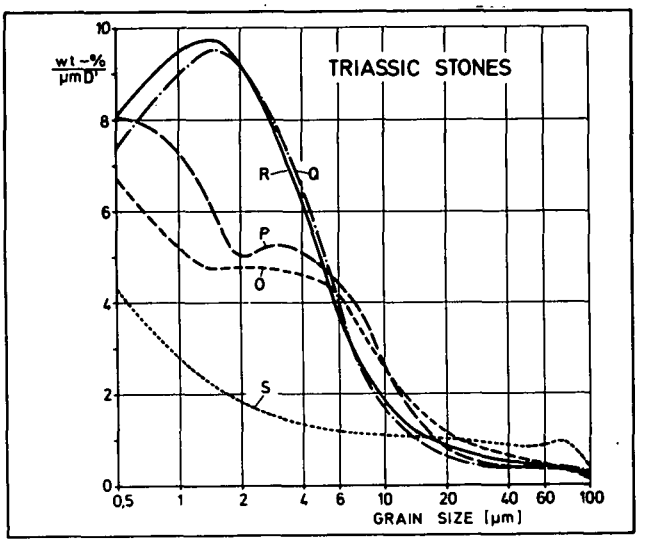

FIG. 4: Gradation of Triassic Stones

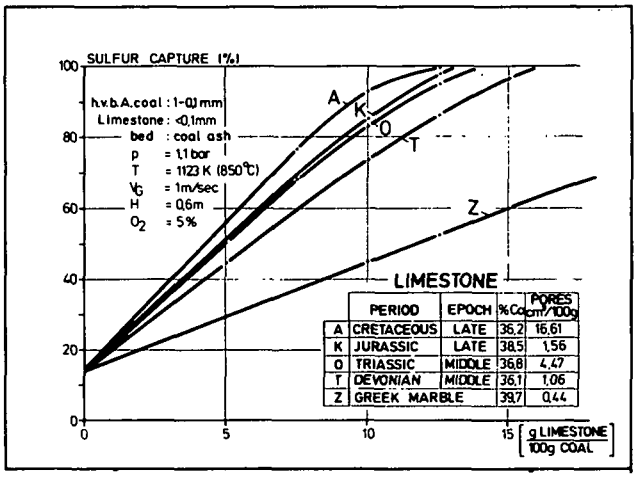

FIG. 5: Sulfur Capturing Effectivity of Limestones from Different Geologic Periods

In this diagram the mass ratio of additive and coal has been used again. In terms of Ca/S-ratio the difference between limestone A and the other stones would increase a bit which is due to the much larger fraction of very fine material in the stone employed and to its much higher porosity. Stones K and O show quite a noticeable difference in porosity and although their grain size distributions were quite similar, there is no correspondingly marked difference in sulfur capturing effectivity, even if the small difference in purity is accounted for. Stone T consisted of a somewhat larger fraction of coarse material than the other stones which in conjunction with its low porosity explains its lower performance.

In Fig. 6 results for all the dolomites studied are summarized. Apparently there exist two groups, viz. stones Q and R on the one hand and stones Y, N and S on the other. In terms of Ca/S-ratio the curves for stones N and S nearly coincide. The grain size distribution revealed that stones Y, N, and S are much coarser than stones Q and R and thus smaller mean grain size and higher porosity lead to the higher efficiency of stones Q and R as compared to the other dolomites. Stone Y showed higher attrition than the other stones. This is believed to provide for its slightly better performance compared to stones N and S. It may, therefore, be concluded that small differences in porosity do not reflect significantly in sulfur capturing effectivity or are easily overrun by other effects. Highly porous additives, on the other hand, do absorb substantially better than others.

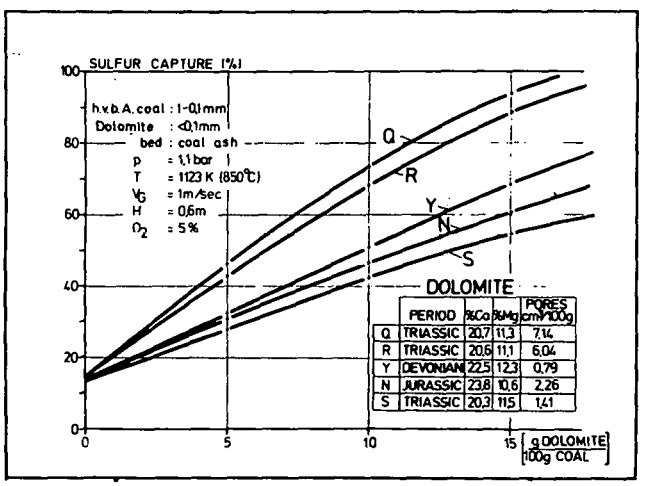

FIG. 6: Sulfur Capturing Effectivity of Dolomites from Different Geologic Periods

Nonelutriatable and partly elutriatable Additive

Considering next large particles, i.e. those which are not being elutriated from the bed (at the conditions of our lab combustor this applies for particles > 0.5 mm), the previously used presentation of sulfur capture vs. limestone/coal mass ratio cannot be employed since steady state conditions could only be achieved in most cases after excessively long test durations. Therefore, in Fig. 7 sulfur capture is plotted vs. test duration at constant Ca/S-ratio in the feed mixture. Because of accumulation of the additive (partly or totally spent) in the bed the actual Ca/S-ratio increases slowly but cannot be determined precisely. In a large FBC unit with regular bed overflow a steady ratio of additive to coal will develop eventually after long operation time. In this paper the shape and trend of the curves obtained in 10 h-test runs will be discussed and it is believed that sufficiently reliable conclusions can be drawn also for long term operation. Typical for all the curves is the initial steep increase in sulfur capture and the consequent more or less flat course of the curves. The steep increase is due to transient conditions before quasi steady conditions are established. After approximately 2 to 4 h test duration, however, the constant feed rate of fresh additive and the assumed constant or nearly constant "end activity" of the stone in the bed lead in conjunction with the constant accumulation rate of stone to the slow increase in the flat part of the curve. The rather large differences in sulfur capturing effectivity of the limestones as expressed by the distance of the curves reflects quite clearly the importance of the porosity of the stones.

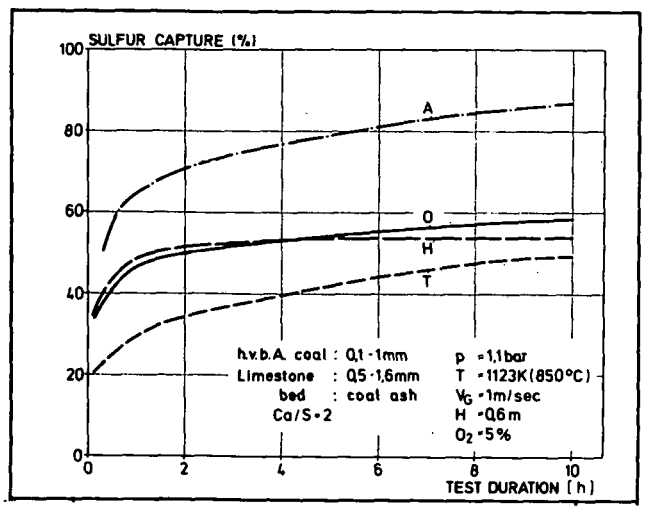

FIG. 7: Sulfur Capturing Effectivity of Limestones (0.5 - 1.6 mm)

A pecularity can be seen with stone H, which after about 2 h exhibits nearly constant sulfur retention. Since the feeding rate for fresh stone is constant, only the "end activity" or the rate of accumulation can be responsible for this behaviour. This activity will be determined essentially by the diffusion rate of SO_2 and O_2 through the outer layer of $CaSO_4$ formed on the freshly calcin ed stone. The diffusion rate, however, will be largely dependant on porosity and pore size distribution, which do not differ significantly for stones H and O. Stones H and O differ, however, markedly

in their disintegration and attrition rate. Whereas from stone H 80 % were left in the grain size fraction > 0.5 mm after the experiment, from stone O only 68 % were left over. From the disintegrated stones O 18 % were still in the bed material, but with grain size < 0.5 mm and 14 % was elutriated. The higher disintegration rate of stone O, thus, always exposes new, fresh surfaces which can absorb SO_2 and lead to an, though small, activity in sulfur capture, whereas stone H apparently loses sulfur capturing activity because of plugging after a short residence time in the bed and the attrition mechanism is not sufficient to contribute significantly to retaining sulfur capturing activity.

Looking at these same stones at the intermediate size fraction (Fig. 8) the most obvious finding is the higher sulfur capturing effectivity of all stones. This must be due to the increased surface area per mass unit of the stones. Since part of the additive will be elutriated in the course of the experiment the rate of accumulation of stone in the bed must be smaller than for the coarse material of Fig. 7. Nevertheless the slope of the curves is greater indicating a higher "end activity" of the stones. Since the material is the same, i.e. pore size distribution and porosity unchanged, the shorter diffusion path length is apparently the reason for this effect. Attrition is less important than for the coarser stone, but again stone O performs, on the long run, better than stone H.

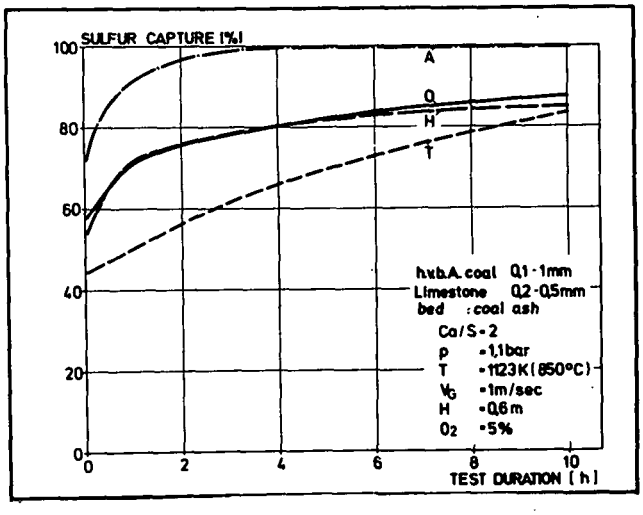

FIG. 8: Sulfur Capturing Effectivity of Limestones (0.2 - 0.5 mm)

Among the dolomites stone Q was the best and stone S was the least efficient one of the fine grain samples. Fig. 9 shows the performance of the coarse dolomites which are not elutriated. Here also the different porosity is reflected in a difference in sulfur capturing effectivity. The comparatively high "end activity" of the dolomites as expressed in the slopes of the curves is apparently due to the less dense Ca SO_4 layer round the particles, since the Mg-content of the dolomite does not absorb SO_2 and thus serves as a diluent. Attrition is somewhat different for these dolomites (stone Q: 15 % loss; stone S: 24 % loss within the size fraction > 0.5 mm during the experiment), however, the influence on the "end activity" cannot be quantified.

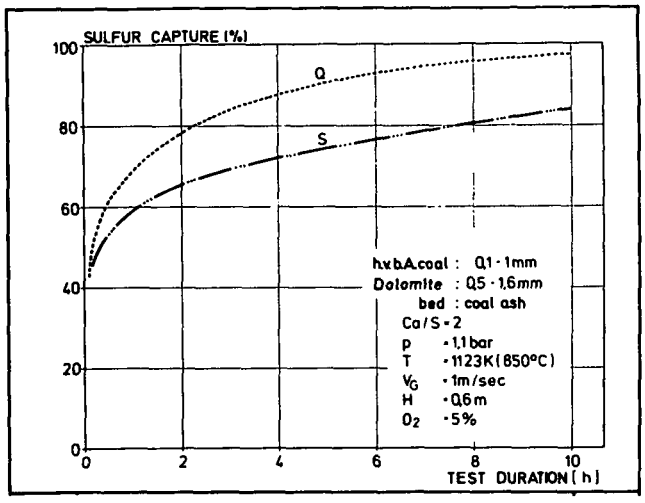

FIG. 9: Sulfur Capturing Effectivity of Dolomites (0.5 - 1.6 mm)

For the dolomite size fraction 0.2 - 0.5 mm (Fig. 10) nothing unexpected was found. Again the larger surface of the additive leads to increased effectivity, both stones are very active sorbents.

Conclusions

From the preceding discussion it is quite clear that the grain size of the additive plays a very important rôle for its effectivity. For this reason much narrower grain size bands were sieved out from limestone and dolomite samples and sulfur capturing effectivity was measured in much the same way as before. The results obtained revealed the facts discussed before in a very clear manner and Fig. 11 can serve to illustrate the conclusions to be drawn.

- Next to purity porosity is the most important parameter of influence on sulfur capturing effectivity.

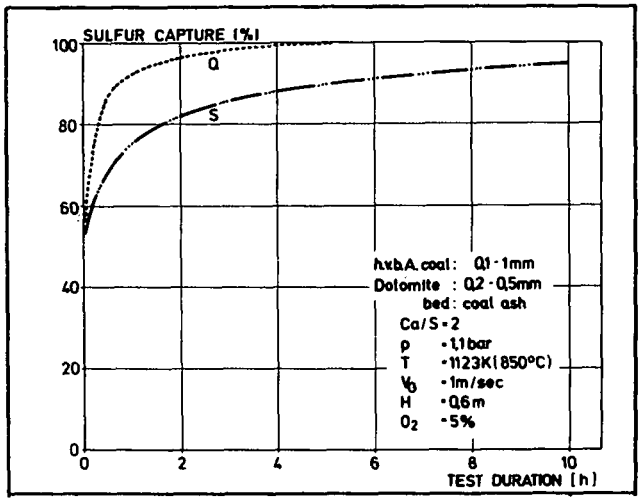

FIG. 10: Sulfur Capturing Effectivity of Dolomites (0.2 - 0.5 mm)

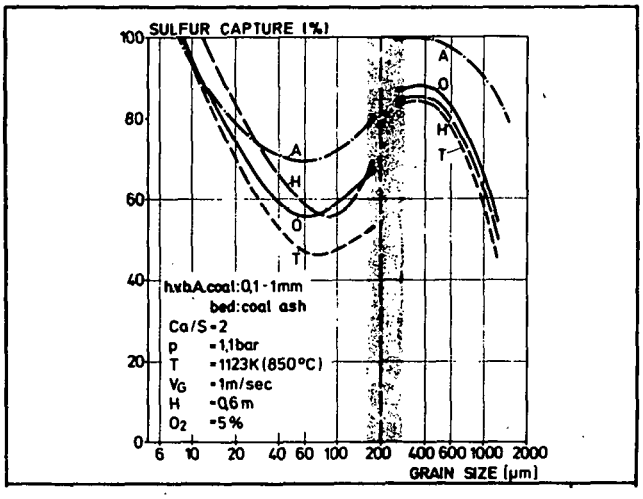

FIG. 11: Sulfur Capture vs. Grain Size for Various Limestones

- For highest effectivity the additive should be as fine as possible. If pulverized stone is being employed the residence time in the bed is short and mean grain sizes below c. 20 µm are required in order to obtain good stone utilization. If coarser stone is preferred the mean grain size should be just only a little bit above the size were elutriation begins.

- Attrition and disintegration of the stones can serve to improve sulfur capturing effectivity substantially, especially of coarse stones.

- Dolomites are on a Ca/S-basis usually more effective than limestones (Fig. 12). Because of their Mg-ballast, however, in terms of the mass ratio limestones can be, but are not always, more economic.

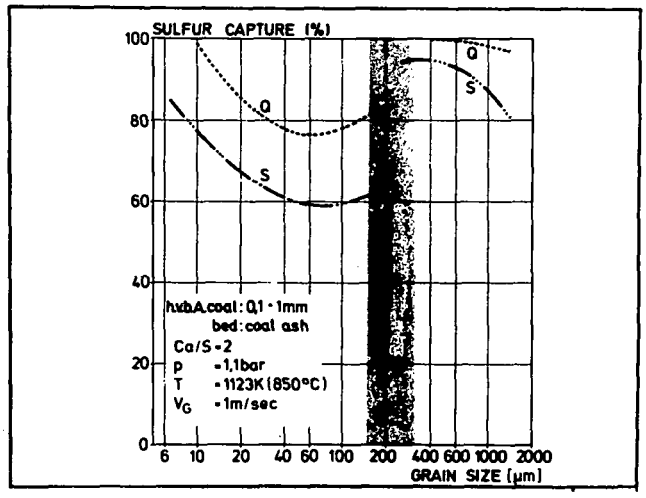

FIG. 12: Sulfur Capture vs. Grain Size for Dolomites

- Geologic age can serve as a first, very rough, clue to the effectivity of the stones: the older the stone, the lower its porosity and the lower is the stone utilization. This does not obtain for each stone but is rather only a rule-of-thumb.

- Choosing an elutriatable additive will yield a bed overflow which is essentially free from additive and a fly ash containing all of the spent stone. On the other hand, by choosing a non elutriatable additive the fly ash will contain only the disintegration and attrition loss of the additive whereas the bulk of the additive is withdrawn with the bed overflow. By proper selection of the type and the mean grain size of the additive either choice can be made without sacrifying sulfur capturing efficiency. This can be especially important with respect to the utilization or disposal of the FBC-waste.

Acknowledgement

Sponsorship of the Bundesministerium für Forschung und Technologie (grant No. ET 1024 B) is gratefully acknowledged.

References

(1) e.g.: R.B. Snyder, W.I. Wilson, and I. Johnson
Proc. 5th Int'l Conf. Fluidized Bed Combustion, Wash., D.C.,
12-14 Dec. 1977, Vol. II, p. 748

The MITRE Corp., McLean, Va., M78-68

(2) e.g.: J. Shearer, C. Turner, and I. Johnson
Proc. 5th Int'l Conf. Fluidized Bed Combustion, Wash., D.C.,
12 - 14. Dec. 1977, Vol. II, p. 776
The MITRE Corp., McLean, Va., M78-68

(3) H. Münzner
VDI-Ber. 286 (1977) p. 97

(4) H. Münzner
VDI-Ber. 345 (1979) p. 319

AGGLOMERATION METHODS OF IMPROVING FBC SORBENT UTILIZATION AND COMBUSTION EFFICIENCY

P. G. Dunne* and L. L. Gasner

UNIVERSITY OF MARYLAND
College Park, MD 20742

Background

Fine powders can be agglomerated into large particles. The technology for accomplishing this is widely used in the taconite and food industries. These agglomerates possess two distinctive qualities:

1. The agglomerates can retain much of the high chemical reactivity of their component fine particles. In particular the high reactivity due to the high surface to volume ratio of the fine particles can be largely retained in the agglomerates. This favorable access to internal particle surfaces is due to the inherently large macropores of agglomerated particles.

2. Hydration of the $CaO/CaSO_4$ leads to changes in its crystal structure which improve sulfur capture capability.

3. The overall particle size of the agglomerates can be adjusted to give optimum fluidization characteristics while retaining the component fine particles in the bed. Spherical, optimum sized particles would replace the conchoidal fractured, widely sized particles occurring naturally.

Other advantages are shown in Figure 1.

Application of agglomeration technology to fluidized bed comubustion could possibly be applied to four materials, either alone or in combination. These are either the raw materials or recycled materials. Raw materials could be agglomerated offsite, possibly by the material suppliers. The four materials are as follows:

1. Limestone could be pulverized and agglomerated by the limestone supplier. This would yield a stone of high macroporosity providing high reactivity and chemical saturation of the limestone to the core of the particle. Less reactive limestones could have agglomerates tailored to have a more favorable internal pore structure and reactive internal surfaces such that these limestones would compare favorably with other, more reactive, limestones.

2. Coal fines could be agglomerated such that they would be retained in the fluidized bed until combustion was complete. This would provide for enhanced combustion efficiency and it could be accomplished by the coal supplier at the mine.

3. Flyash including electrostatic precipitator or baghouse dust could be agglomerated and recycled back to the combustion zone. This would eliminate any solids discharge from the unit with the exception of spent bed drainage. Combustion efficiencies could be enhanced to the point where uncombusted gas phase carbon represents essentially all of the carbon lost. Agglomeration of flyash and dust, could eliminate the carbon burn-up cell required by current technology.

4. Spent bed material could be screened, pulverized, agglomerated and reinjected into the bed. This would improve limestone utilization, while simultaneously taking advantage of the greater friability of the spent bed material. Alternately, if a binder is necessary in any of the above proposed agglomerates, pulverized spent bed may be an ideal binder.

In summary, agglomeration processes are established technology that offer control of external particle size and internal reactivity independently. Possible uses in fluidized bed combustion are for agglomeration of raw materials (limestone, coal fines) or recycled materials (flyash, spent bed). Possible advantages are improved utilization of limestone, improved rates of reaction, and improved combustion efficiency.

An agglomeration device consists of a

* Current address: Pope, Evans & Robbins, Inc. 320 King St., Alexandria, VA

rotating drum or pan with a powder feed device, a fog type water spray nozzle and a plow. The drum or pan may be inclined at an angle such that the fully formed agglomerates overflow after the appropriate residence time. A fogging spray nozzle adds surface hydration to the particles. The location of the spray nozzle depends upon whether the primary purpose of the moisture is nucleation or buildup of the agglomerates. The plow is provided to prevent agglomeration unto the equipment surfaces.

Nucleation generally occurs by the adhesion of several fine particles to a water droplet. The nucleated aggregate rolls due to rotation of the equipment, picking up individual grains on its surface such that it grows in diameter. After a point the agglomerate has traveled to a location where individual grains are not present. Growth continues, however, since large agglomerates crush smaller ones which then add to the outer surface of larger agglomerates. The system thereby eliminates its own fines. Large particles tend to be buoyed to the upper surface where overflow occurs and where growth is much slower. Therefore, both large and small agglomerates are eliminated and a narrow particle size distribution is obtained. Taconite ore, for example, is produced in a - 1/2" + 1/4" size such that all particles are within a factor of two of each other. In this case the oversize and undersize are screened out and recycled. However, when a rotating pan is used a very narrow particle size distribution is frequently obtained without any agglomerate screening.

The final agglomerate contains moisture which usually is removed by drying to form strong free flowing pellets, capable of being handled and stored in deep bins. Alternately, the agglomerates can be injected directly into the combustion zone eliminating the drying step.

The mechanism of agglomeration entails a particle-particle bond which gives strength to the agglomerate. These bonds are hydration forces or van der Waals forces in the newly formed agglomerate. In order to have high strength, however, the cured particle must develop stronger bonds. This is frequently accomplished by adding small amounts of a slightly soluble "binder" which becomes solid upon evaporation of the liquid. Effective binders which have been used include $CaCO_3$, CaO, $CaSO_4$, salts and clays. It appears as though the natural calcium components in the limestone and spent bed and the natural clays in flyash may in some cases act as an adequate binder.

Certain parameters are important for scale up of an agglomeration process. The capacity of a unit is about proportional to the square of the diameter. The collar height required is approximately proportional to the square root of the diameter. The speed of rotation is approximately proportional to the reciprocal square root of the diameter. This type of information must be obtained experimentally in order to approximate the size and power consumption of a large scale unit.

Experimental Program

The application of agglomeration process technology to fluidized bed combustion processes could yield many significant advantages. Sorbent and spent sorbent agglomeration techniques could significantly enhance sulfur capture rates and increase sorbent utilization. Coal fines, flyash and collected dust agglomeration could increase carbon utilization and combustion efficiency. The assessment of these alternatives requires the development of certain basic performance data. The current investigation was the first exploratory step in developing this data. Primary emphasis was given to flyash agglomeration with spent bed as a binder. The acceptable operating ranges of some of the most important variables were identified. The ranges of performance enhancement which can be expected could be estimated.

1. The literature was surveyed to determine agglomeration principles and past experience with similar systems.

2. Eighteen different types of agglomerates were prepared from three materials (flyash, low iron spent bed (GSB), and high iron spent bed (RSB)) using horizontal drum techniques. Agglomeration formulations specifying some of the important parameters (final agglomerate size, process operating conditions, required quantities of binder and water) were identified.

3. The agglomerates prepared were physically characterized by size and cold strength measurements. The most important parameter was the general suitability for use in a fluidized bed combustor.

4. Sulfur capture reactivity and capacity were determined in a TG apparatus.

5. Attrition, decrepitation, combustion efficiency and suitability for fluidized bed combustion environments were determined in a cold 2" laboratory fluid bed unit and in a hot 8" laboratory fluid bed unit.

6. The results of the above experiments were analyzed to suggest the agglomerates

of greatest potential. Some other information which could be useful in agglomeration process assessment was also found.

Methods and Materials

1. Materials Studied

Three materials were studied in this investigation: flyash (FA), high iron spent bed (RSB), and low iron spent bed (GSB). The difference between the two spent beds is that the red variety was produced from a coal with a high iron content in the ash. The flyash, as well as both spent bed materials, were steady state products obtained from the Pope, Evans and Robbins Pilot Fluidized Bed Facility in Alexandria, VA using Sewickley Coal and Greer Limestone. When used in agglomeration, the flyash received no pretreatment, whereas the spent bed materials were pulverized to fines. The mean size of the flyash was about 120μ. After pulverization the mean size of the spent bed materilas used was about 320μ. Chemical compositions based upon non-agglomerated samples of the three materials are shown in Table 1.

2. Apparatus

The batch-agglomerating drum which was employed was constructed of plexiglas, 9-1/2 in. O.D. and 9 in. deep with 1/4 in. wall thickness. A 5 in. O.D. hole centrally located in the front face of the drum served as a means of access to the samples during runs. Four equally spaced lifter rods of 1/8" O.D. plexiglas were attached lengthwise around the internal periphery to impart a tumbling action and to prevent a sliding motion of the charge during operation. A hinged scraper was constructed to keep the inside surface of the drum clean.

The drum revolved with its axis horizontal. The shaft was driven by a 1/4 h.p. electric motor through a variable speed drive. A timer was placed into the system to serve as a revolution counter. The range of speeds was from 0 to 30 rpm, depending upon the phase of the investigation. In all cases the following was the general method of preparation of agglomerates: A weight of sample of known composition was thoroughly mixed with a measured amount of tap water and the contents thoroughly mixed. The moist powder was rubbed through a 6 mesh (3.3 mm opening) sieve to break up any lumps formed during mixing. The scraper was placed in position, the sample added to the drum, speed of rotation selected and drum rotation initiated. Rotation was stopped at a preselected time and the agglomerate sample was removed.

Two small fluidized beds were used in this study. They were a 2" I.D. x 3' cold abrasion test cell and an 8" I.D. x 18" hot fluidized bed. A calibrated orifice was used to monitor the adjustable air flow rate to either bed. A propane cylinder was attached to the hot bed with a rotameter used to monitor and control the propane flow rate into the air stream. Just preceeding the entrance of the upward flow of propane and air to the hot bed a diffuser was placed in the line to assure evenly distributed gas mixing and flow to assure an even flame distribution in the bed. Temperature was measured by a chromel-alumel thermocouple placed within the hot fluidized bed.

3. Pellet Characterization Tests

The desirable properties of an agglomerate have been the subject of intense investigation since the earliest days of production. The major problem is that quality tests devised by manufacturers do not accurately simulate actual conditions to which the agglomerates will be exposed. Thus, it is normally difficult to correlate quality tests to actual agglomerate performance. However, it is believed that the quality tests used in this study are as close to actual fluidized bed conditions as is attainable in a bench scale test environment. The following were the tests employed:

A. The Drop Test

The drop test is designed to assess the ability of agglomerates to withstand impacts encountered in processing, for example, at conveyor belt transfer points. It is also one of the standard specifications required by a manufacturer if agglomerates are to be ordered.

A typical test is to drop the agglomerates from a height of (a) 12 in. (300 mm) and (b) 18 in. (450 mm) to a stainless steel surface and to observe the average number of drops the agglomerate can withstand before breaking. A sample of agglomerates is tested and a statistical result derived. Satisfactory values of 15 and 6 drops from heights of 12 in. and 18 in. respectively are quoted in the literature for taconite ore agglomerates.

B. Cold Abrasion Test

This test was used to evaluate the abrasion properties of dried agglomerates in a fluidized bed environment. The 2" fluidized bed was packed with - 12 + 20 mesh limestone as typically used in an actual atmospheric fluidized bed combustor. The bed was fluidized and a weighed sample of pellets added for a known period of time. The test conditions

Table 1. Chemical Analysis of Materials Used in Agglomeration Studies

Component	%C	%H	%S	%Ca	%Fe	% Ash
Flyash	50.29	1.89	2.20	12.82	2.13	43.27
GSB	0.30	0.63	9.33	31.90	1.58	94.00
RSB	1.07	0.42	8.66	33.56	15.10	91.89

were held constant for each run. After a set time period, the bed was removed and the remaining whole agglomerates gathered and reweighed to determine the abrasion loss with time.

C. Hot Abrasion Test

The goals of this test were twofold. First, the test would measure the abrasion resistance under actual hot fluidizing conditions. Thus, the test was run in the same manner as the cold abrasion test but an 8" O.D. hot fluidized bed combustor was used at a temperature of approximately 850°C. After a preset time a bed drain port was opened allowing immediate drainage of the bed. Any pellets found were weighed to determine the hot abrasion loss. A loss on ignition, LOI, value was obtained for the recovered agglomerates to determine the burnout as a function of time in the hot fluidized bed.

D. The Char Test

The char test (or loss on ignition, LOI) was used to determine the amount of combustible material present in an agglomerate. The test was performed on dry, untested agglomerates and also on those removed from the hot bed as described above. Ceramic combustion boats were dried in an furnace, stored in a dessicator and tared. The boats were then weighed empty and then, again, containing agglomerates. Agglomerates were added, the boats were weighed and placed in a furnace for two hours at 1000°C. Upon removal and cooling the boats were reweighed and the weight % combustibles determined.

E. Sulfur Capture Capacity

The sulfation capacity of the agglomerates was measured at 850°C by a modified Dupont Model 950 Thermogravimetric Analyzer, TGA. A TGA is a calibrated electronic balance attached to a dual chart recorder monitoring both the weight of the sample and the temperature of its surroundings. Following calcination in N_2, the gaseous atmosphere was changed to 0.1% SO_2 and about 5% O_2 in N_2. Sample weight as a function of time was recorded until apparent saturation and sulfur capture as a function of time was calculated.

Results and Discussion

The agglomerates examined fell into one of eighteen possible categories. The amount of each spent bed binder added to flyash was varied from 0 to 100% by weight in 25% intervals. Thus, nine possible compositions existed among the flyash and the two spent bed binders. Another criteria was size of the agglomerate. Each composition after agglomeration was divided into two sizes; "large" being - 0.371" + 0.223" representing the 1/4" size and "small" being - 0.223" + 0.0937" representing the 1/8" size.

More than 1200 individual tests were carried out in order to achieve statistical validity of the results. A rather brief description of the major results achieved is described in the following paragraphs.

1. Results of Drop Test

No agglomerate type was fully characterized unless it passed the selected drop test criterion to insure mechanical strength. All agglomerates containing flyash alone were unacceptable in mechanical strength. The strength of flyash/spent bed agglomerates was unacceptable unless spent bed was the majority component. Nevertheless, both types of spent bed tested were found to serve as appropriate binders, perhaps due to their inherent cementitions properties. The fact that the two spent bed types tested showed significantly different suitability as a binder whereas they were both derived from Greer limestone and Sewickley coal shows that the chemistry of pellet strength is an important parameter and is not fully understood. Typical results will be given here for only the 75% and 100% mixtures of RSB and GSB with 25% and 0% flyash, respectively. In this way the properties of both agglomerated flyash with spent bed and of spent bed alone may be seen.

2. Cold Abrasion Test Results

The cold abrasion tests showed the same results as the drop tests. The 100% flyash agglomerates did not survive the cold abrasion tests, being entirely fragmented and elutriated within 10 minutes. Those agglomerates which demonstrated

acceptable wet cold strength contained 50% or more of spent bed. These results are important in considering the suitability of the agglomerates to survive subsequent processing steps and materials handling equipment. It was observed that agglomerates stored in the ambient room air showed some surface cracks and decrease in strength after 4 to 8 days. This is, perhaps due to reaction with humidity or carbon dioxide in the air. It was found that oven drying-curing did not increase the strength of the agglomerates.

3. Hot Bed Test Results

In order to calculate the per cent combustible burnout of the spent bed - flyash particles, the amount of total combustibles was determined by the char test, LOI. Hot bed testing was performed on twenty agglomerate samples selected from the same test batch as was used in the cold testing. Four runs were done for each composition and size at 2-1/2, 5, and 7-1/2 mins. agglomerate residence time in the hot fluidized bed at 850°C. The zero and five minute runs were performed in duplicate as a reproducibility test.

An important aspect of the hot bed tests were the observations made during the runs. Fifteen to thirty seconds following the addition of any flyash containing agglomerate to the bed, the pellets became a clearly more brillant orange color than the surrounding hot bed. They randomly appeared and disappeared from the bed's upper surface. That combustion was actually occurring was substantiated by the examination of several 50% RSB and GSB agglomerates removed after 2-1/2 minutes in the hot bed. Cutting the agglomerate in half revealed an interior consisting of three concentric regions. Region I was a dark gray core of unburnt carbon which was small relative to the overall agglomerate diameter. Region III, the most prominent, consisted of entirely ash. It was light in color and pitted at the surface but never to the core. Between the ash region and the unburnt core was Region II appearing as a narrow gold colored ring.

The result of ultimate importance from the hot bed tests was the total combustion burnout obtained. The burnout as a function of time in the bed versus agglomerate composition and agglomerate size was determined. Typical results shown in Table 2 show that 90% burnout was possible in 2-1/2 min. in most cases. Thus, despite the fact that not all flyash/spent bed aggomerates showed long abrasion lives in the hot bed, only 2.5 to 5 minutes was required for 90% of the combustible to burnout. Again, 100% flyash agglomerates and those where flyash was the predominant component, did not last 2.5 mins. in the bed, but the observation of them in the bed as brilliant orange spheres indicates combustion to some extent occurred.

The last 2 - 6% of the possible loss on ignition, LOI, was lost very slowly, if at all. It is suggested that the early weight loss contained essentially all of the combustible carbon and that the remaining few percent consisted of the sulfur which combusted, was captured, and retained if combustion occurred within a 50% spent bed pellet. It was shown by material balance that even when combustion occurred extremely rapidly within the pellet the emitted SO_2 was retained as the surfate. If any regeneration occurred by CO at the interior combustion front, the SO_2 generated was apparently quantitatively recaptured as it diffused out through the oxidizing shell.

These results show that agglomeration and recycle of flyash can be used as a substitute for a carbon burnup cell, that even ESP dust can be recycled this way to get essentially complete combustion, and that combustion within the pellet occurs so rapidly that eventual attrition of the pellet need not adversely affect combustion efficiency. It is suggested that obtaining the additional 1 - 2% overall combustion efficiency from the ESP dust and from the more complete combustion of flyash along with the elimination of the CBC, an agglomeration process can manyfold pay for itself.

4. Sulfur Capture Capacity Test Results

An important characteristic of the agglomerates studied was enhanced sulfur capture capacity and rates. Both of the spent bed sorbents used in this testing, RSB and GSB, came from SO_2 saturated steady state beds. However, pulverization of large bed particles exposed the unreacted sorbent at the core, agglomeration increased the surface-to-volume ratio and the hydration increased the available pore volume. All three of these effects combine to yield enhanced sulfur capture.

As a basis for comparison a sample of Greer limestone of the size range normally used in a fluidized bed was tested in the TGA. When placed in the 850°C surroundings and the atmosphere adjusted to 20% O_2, 80% N_2 the limestone was completely calcined in approximately 12 mins. After showing no weight loss for a 7 minute period, the gaseous environment was changed to one of 5% O_2, 0.1% SO_2 in N_2. Whole pellet samples of agglomerate were run in the same manner. The initial weight loss on calcination for agglomerates includes combustibles, CO_2 and

Table 2: Typical Combustion Efficiency of (Burnout Fraction) of GSB Agglomerates as a Function of Time in Bed and Size

Composition	Run Time	Combustion Efficiency
50% GSB/Large	2.5	0.98
	5	0.98
	5	0.99
	7.7	0.99
50% GSB/Small	2.5	0.93
	5	0.99
	5	1.00
	7.5	1.00
75% GSB/Large	2.5	0.83
	5	0.99
	5	0.97
	7.5	0.98
75% GSB/Small	2.5	0.70
	5	0.87
	5	0.94
	7.5	0.94

moisture loss. The initial weight loss prior to sulfation was much more rapid for agglomerates than for limestone particles. In most cases the initial weight loss was complete in 2.5 to 4.0 mins, thus confirming the burnout results seen in the hot bed combustion tests. In addition, not only was sulfur capture increased, but the rate of capture was significantly enhanced. Increases in rate of sulfur capture per unit area of particle surface of up to 200 fold were observed when comparing agglomerates to limestone. In order to compare the agglomerates to the Greer limestone, plots were made of the normalized weight vs. time in the SO_2 environment. The normalized weight is defined as the sulfated weight divided by the actual initial weight prior to calcination. These plots for the 75% GSB and the 100% RSB agglomerates as well as the Greer limestone sample are shown in Figures 2 and 3. Qualitatively, these figures show two points. The agglomerates, in all cases, captured more sulfur per initial weight than the limestone. Secondly, not only did they capture more sulfur but they did so more rapidly, reaching saturation points sooner than did the limestone. Sulfur capture was found to approximately double when compared to the original "steady state saturated" limestone bed material. Also, the time to 90% saturation was dramatically less in the agglomerate testing compared to the nearly 6 hrs seen in the Greer limestone test. It is speculated that the reason for this was the larger surface-to-volume ratio of the agglomerates and the elimination of the diffusion dependence of the SO_2 capture reaction due to increased pore volume obtained by agglomeration. It is indicated, therefore that agglomeration technology could result in a decrease in limestone consumption by a factor of about 2 or, perhaps, even more for stones that are inherently less reactive than Greer limestone. Also this technology may change the emphasis in limestone selection. It may be possible to "engineer" any limestone to a "spec" reactivity and capacity merely by manipulating agglomeration variables (grain size, particle density, etc.). In some cases the coal ash may play a dominant role as binder and catalyst. Also if added catalysts are found to be desireable they could be included in the formulation. Decrepitating stones would now be acceptable.

A final note is in order about processing costs. Pulverizing costs are expected to be nominal if this process were used due to the friable nature of spent bed and the already acceptably sized flyash. The taconite industry uses large ball mills and claims processing costs of less than $1.00/ton to pulverize this very hard ore to extremely fine mesh size. Even at a much smaller scale this should be the upper limit for spent bed-flyash mixtures. Ball mills and agglomeration drums are standard, off-the-shelf, established technology that do not require further development. They are low maintenance, highly reliable pieces of equipment. The milling and agglomeration process itself is easy to run with little attention and is self correcting of operator inattention. The overall process is self correcting in that if the agglomerates produced are insufficiently strong, they will become high-calcium flyash that will have greater strength on the next pass. The primary cost of the process concerns the heat loss of evaporation of the added water. A "worst case" estimate assuming 1000 lb H_2O/ton dry pellets would yield a loss of about one million BTU/ton dry pellets. Another possible cost item is a supplementary binder such as a clay added to the extent of, perhaps, 1 - 3%. It can

be roughly estimated that the quantity of agglomerates produced in this way in a large scale facility would be about one half ton per ton of high sulfur coal. These agglomerates would cost $2 - 4/ton dry basis to produce or about $1 - 2/ton of coal. The overall effect would be 99+% combustion efficiency, elimination of the CBC, and plant Ca/S ratios of up to 1.5 for high sulfur coals and 1.0 or less for low sulfur coals.

Conclusions

From this inital study to evaluate agglomeration process applications to fluidized bed combustion processes the following conclusions were drawn:

1. Based on drop tests and cold fluidized bed abrasion tests flyash alone is not a suitable agglomerate. A binder is needed.

2. Spent bed, in two forms, served as appropriate binders for flyash. Based on agglomerate characterization tests performed, the spent bed added must be in excess of 50% by weight.

3. Total combustibles burned could be significantly increased by agglomeration techniques. Results of hot fluidized bed testing showed that more than 90% of the combustible material in the agglomerate burned in 2.5 - 5.0 mins. In cases where flyash was the predominant component of the agglomerate the burnout could not be measured due to rapid elutriation. However, observation indicates that the pellets did combust before elutriating.

4. TGA studies confirmed that rapid combustion of the flyash element of the agglomerates. Further, samples made by pulverizing "steady state saturated" spent bed agglomerating it alone and with 25% flyash showed approximately a doubling of initial sulfation capacity.

5. Not only was the sulfur capture capacity of saturated limestone increased but the rate at which SO_2 was captured was greatly enhanced through pulverization and agglomeration.

6. Agglomeration technology could be readily applied to fluidized bed combustion processes. This could lead to improvements in combustion efficiency, sulfur capture and overall process economics.

Acknowledgement

The authors wish to gratefully acknowledge the support and contributions to this work of the Electric Power Research Institute; Westinghouse Research and Development Corp.; Pope, Evans and Robbins, Inc.; the U.S. Department of Energy and the College of Engineering of the University of Maryland.

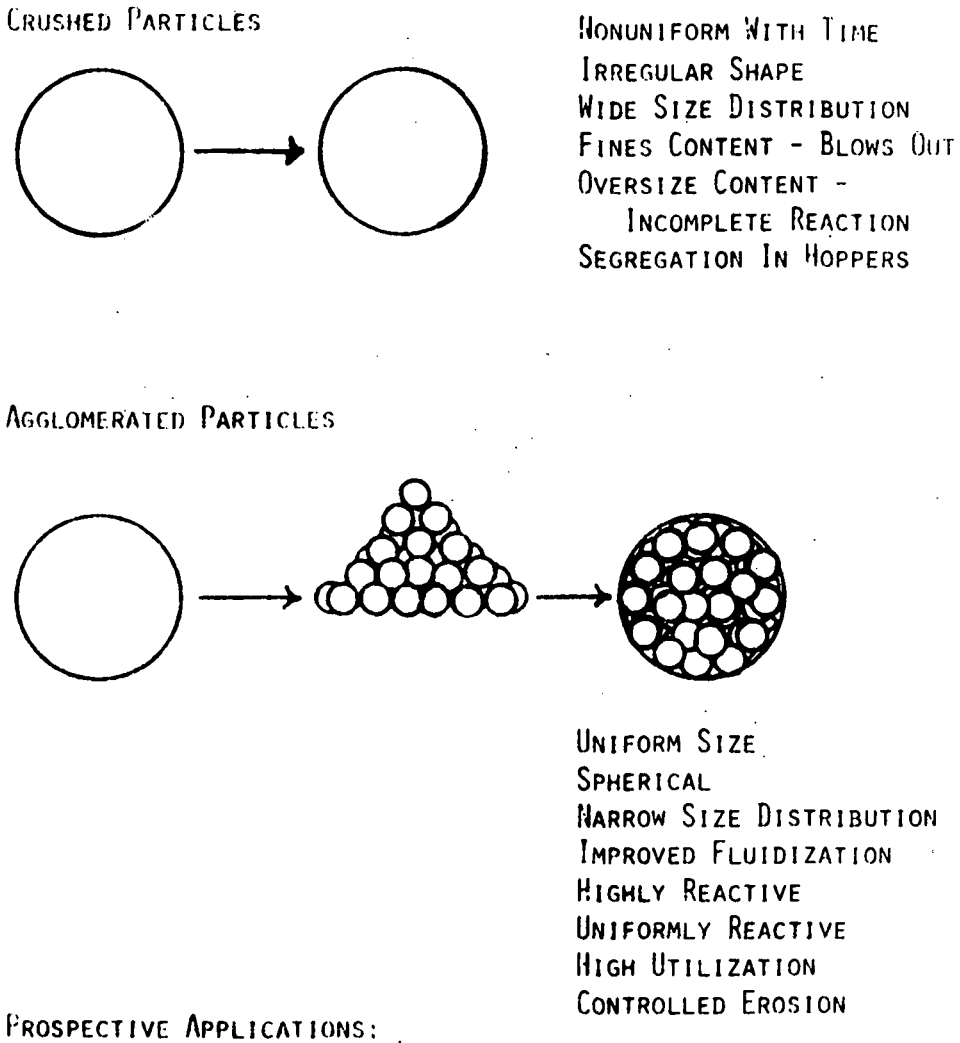

Figure 1. Schematic Noting Advantages and Disadvantages of Conventional Crushed Particles Versus Agglomerated Particles

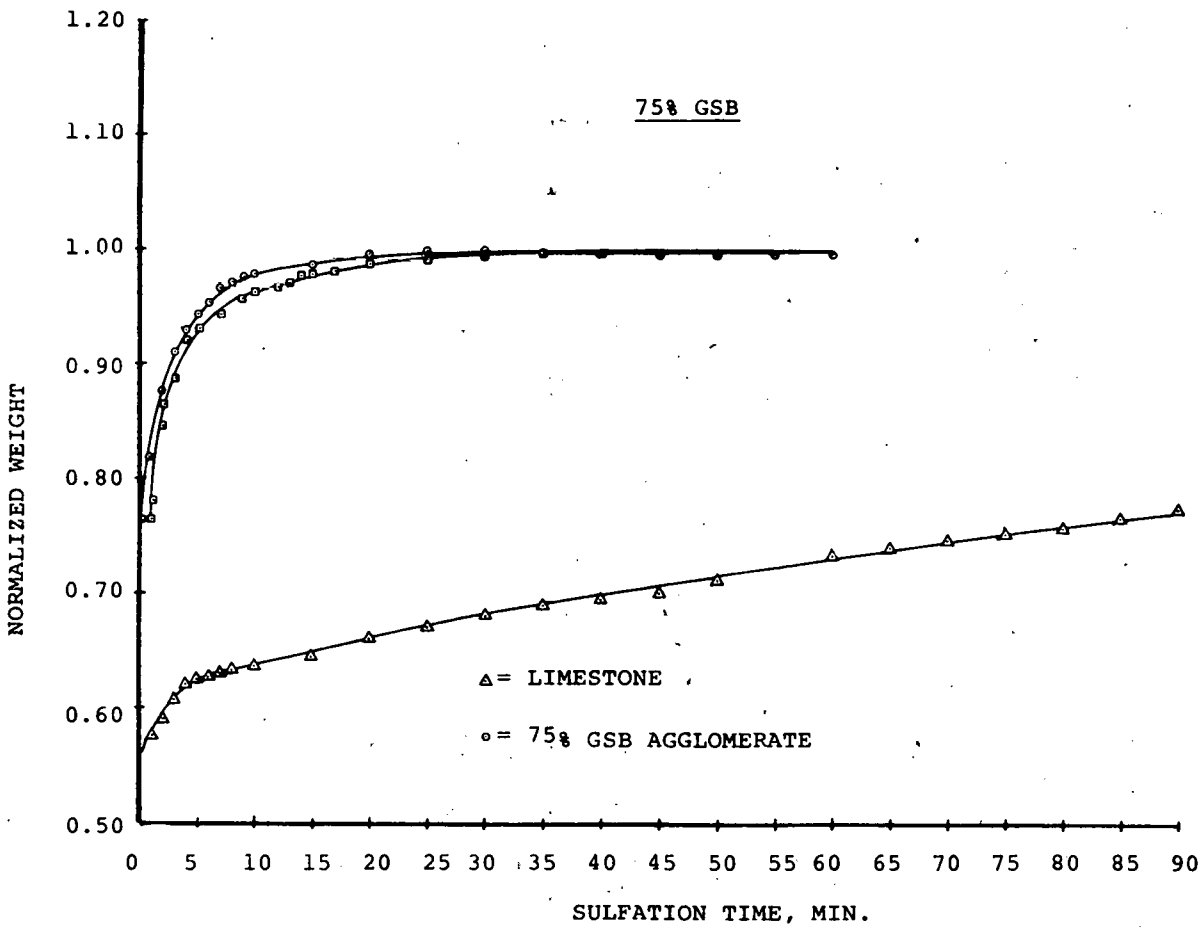

Figure 2. Typical TGA Sulfur Capture Results for 1/8" Diameter 75% GSB - 25% Flyash Agglomerates

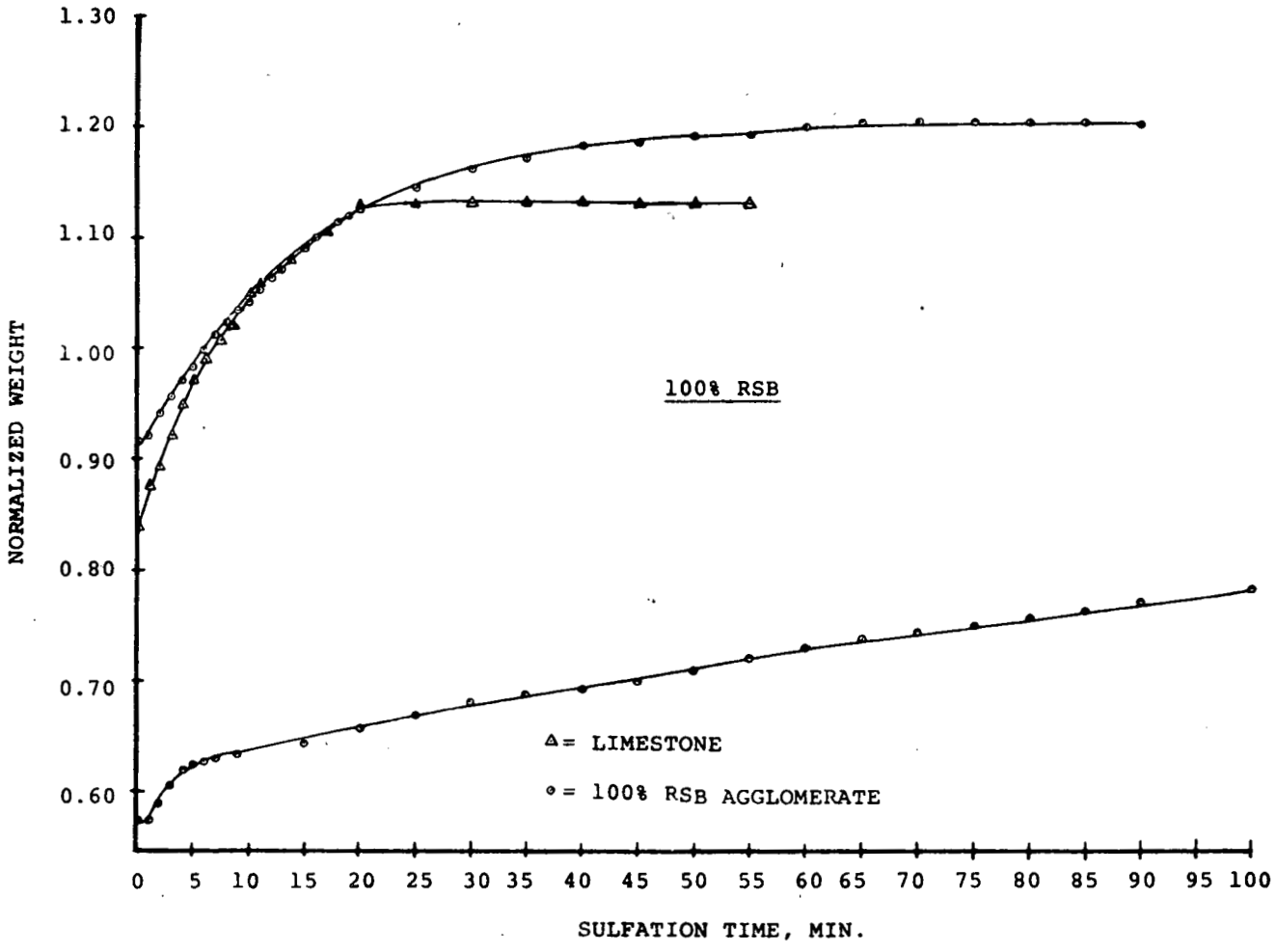

Figure 3. Typical TGA Sulfur Capture Results for 1/8" Diameter 100% RSB Agglomerates

Question to Paul Dunne:

Q: (Participant not identified)

A curing process will help make the pellets more acceptable.

A: One of the things which we did try was curing for 24 hours at an elevated temperature. Our limited tests showed no difference in results.

HYDRATION PROCESS FOR REACTIVATING SPENT LIMESTONE AND DOLOMITE SORBENTS FOR REUSE IN FLUIDIZED-BED COAL COMBUSTION

J. A. Shearer, G. W. Smith, D. S. Moulton, E. B. Smyk,
K. M. Myles, W. M. Swift, and Irving Johnson

Argonne National Laboratory
Argonne, Illinois 60439

Introduction

Fluidized-bed combustion (FBC) has been shown to be an environmentally acceptable and economic process for utilizing this country's plentiful coal reserves for producing steam and/or electric power. As a result of the renewed interest in coal as a major energy source, considerable attention is being focused on FBC since it can offer potentially high efficiency and low capital costs.[1] In the FBC process, crushed coal is burned at 800-900°C and 100-1000 kPa pressure in a fluidized-bed of SO_2 sorbent such as limestone or dolomite. The bed sorbent material transfers heat to the boiler tubes and its CaO component reacts with the potentially harmful SO_2 released from the coal to form $CaSO_4$. FBC process disadvantages are the incomplete utilization of CaO in the sorbent and the resultant increase in cost and environmental impact of (1) extensive quarrying and (2) disposing of solid waste (i.e., spent sorbent). Regeneration and reuse of spent limestone and dolomite sorbent or, alternatively, an increase in utilization of CaO can reduce this cost and environmental impact. A new method for significantly reducing this impact is discussed in this paper.

In this new method, partially sulfated spent sorbent containing some residual CaO is hydrated to reactivate it for further sulfation, thereby increasing the overall calcium utilization.[2,3] In this process, the partially-sulfated overflow material from a combustor is treated with water and reintroduced to the combustor where it reacts to pick up additional SO_2. Early research for the dry limestone injection process[4,5] and other work[6] shows that the hydrated lime is, in general, a highly reactive species for SO_2 sorption. However, the economics of production along with the attrition and elutriation of soft $Ca(OH)_2$, preclude its use as a sorbent for fluidized-bed coal combustion. The formation of $Ca(OH)_2$ in a partially sulfated sorbent, however, produces a material with sufficient physical integrity, due to the outer sulfate layer, and high reactivity which make it suitable as a sorbent feed material. The work presented below details laboratory observations on a number of sorbents reacted in tube furnaces as well as verification of the effectiveness of the method utilizing a typical limestone sorbent in a process-development unit (PDU) scale atmospheric fluidized-bed combustor (AFBC). Early kinetic results of the hydration reaction are included as well as flowsheets illustrating the process as a continuous operation.

Tube Furnace Sulfation-Hydration Procedure and Results

A series of studies were performed on various limestones and dolomites using horizontal tube furnaces. One-gram samples were sulfated at 850°C with a simulated flue gas of 0.3% SO_2, 5% O_2, 20% CO_2, and the balance N_2. The resultant spent sorbent was fine-mist sprayed with more than sufficient room temperature water to hydrate all available CaO. After air drying, the water content was determined by weight loss measurements after 15 minutes at 850°C. The hydrated sorbent was then resulfated during which simultaneous dehydration occurred. Chemical analyses of the sulfated and resulfated sorbents were performed to determine the extent of sulfation. Figures 1 and 2 show bar graphs of percentage conversion of CaO to $CaSO_4$ for the untreated and hydrated/resulfated limestones (Fig. 1) and dolomites (Fig. 2). The results show a marked increase in the total sulfation capacity for all the sorbents studied. Stones having a lower initial calcium conversion benefited most in terms of increased sulfation due to a single water treatment.

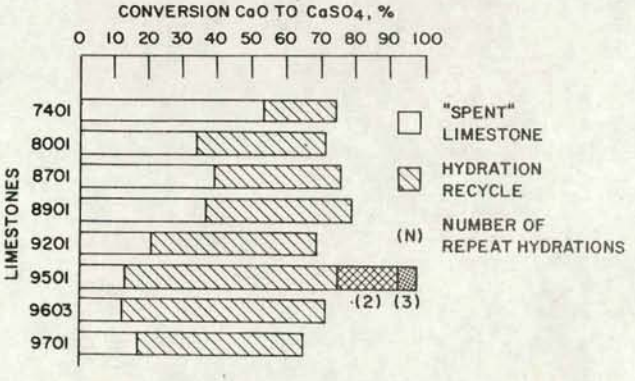

Fig. 1. Increased Sulfation of Several Limestones by Hydration of Partially Sulfated Material. Sulfated 6 h at 850°C in 0.3% SO_2, 5% O_2, 20% CO_2, and the Balance N_2.

Also included are three experiments in which a limestone (Fig. 1, 9501) and two dolomites (Fig. 2., 5501 and 5601) were subjected to several successive hydration-sulfation cycles to determine the maximum utilization of the available calcium oxide. These results show that there is a potential for complete sulfation even in the stones with poor initial reactivity.

Scanning electron microscope (SEM) photography of these materials was used to verify a proposed model for the reaction. An SEM photograph of a typical partially sulfated limestone contrasts sharply with the resultant porosity changes due to the hydration treatment shown in Figure 3. The untreated partially sulfated limestone has a dense outer sulfate layer that seals off the fine-pored interior. Hydration by water and subsequent dehydration causes a recrystallization of CaO and a growth of pores within the stone.

Proposed Mechanism of Sulfation Enhancement by Hydration

Based upon laboratory experiments, porosity measurements and SEM photographs, a proposed model has been developed which is schematically illustrated in Figure 4. Starting with unreacted limestone and dolomite, the material is introduced into a coal combustor where calcination and sulfation occur simultaneously, producing a product with a dense $CaSO_4$ layer surrounding a core of residual CaO with a pore structure characteristic of the particular stone. Upon partial hydration of this unreacted CaO, particle expansion occurs due to the formation of $Ca(OH)_2$ whose molar volume is larger than the molar volume of CaO. The surface layer of $CaSO_4$ is apparently unaltered other than being subject to cracking from the particle interior expansion. After water treatment, the now partially hydrated material is reintroduced to the combustor where dehydration and sulfation occur simultaneously. The gas permeability of the treated material greatly increases due to an increase in

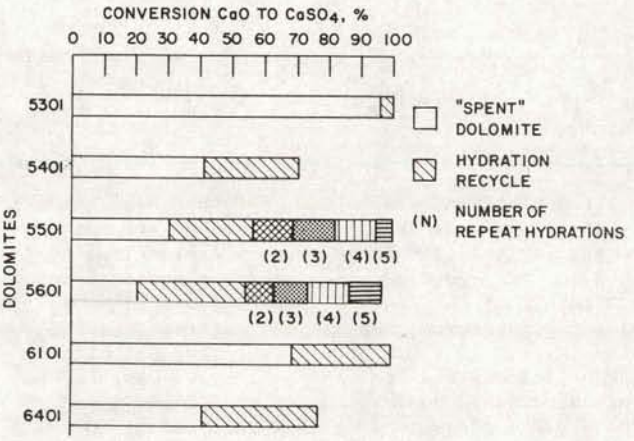

Fig. 2. Increased Sulfation of Several Dolomites by Hydration of Partially Sulfated Material. Sulfated 6 h at 850°C in 0.3% SO_2, 5% O_2, 20% CO_2, and the Balance N_2.

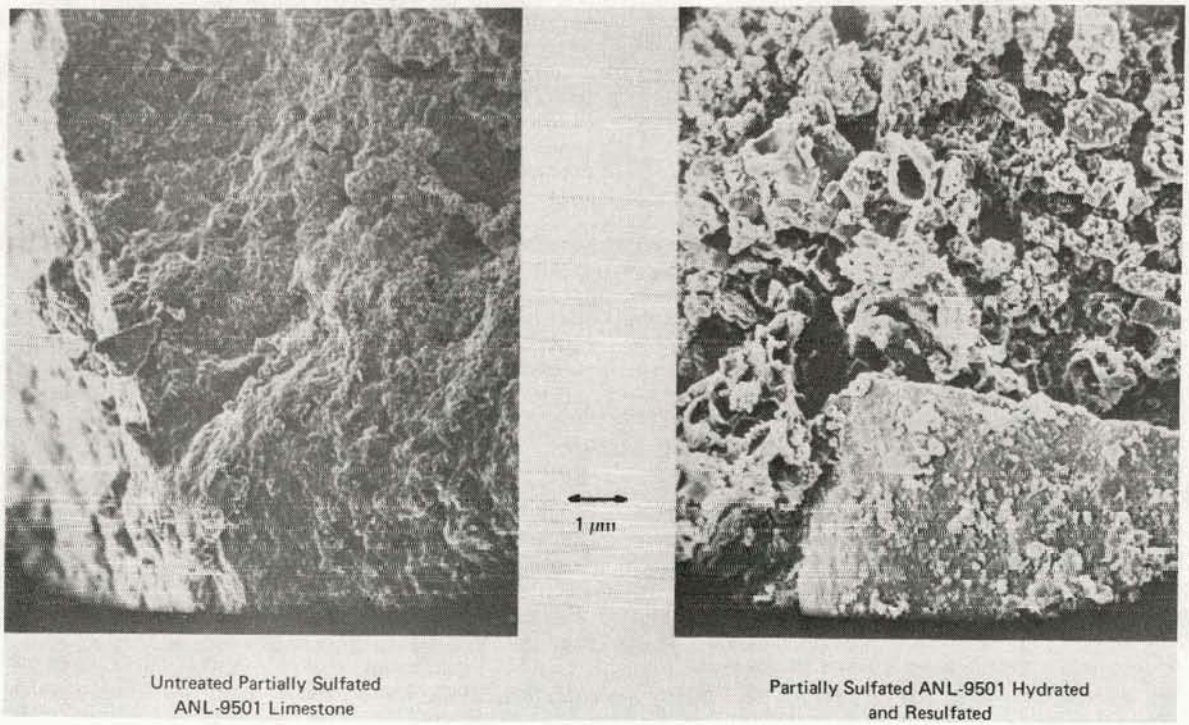

Fig. 3. The Effects of Hydration and Resulfation of a Partially Sulfated Limestone (ANL-9501) from an Atmospheric Fluidized-Bed Coal Combustor at 850°C.

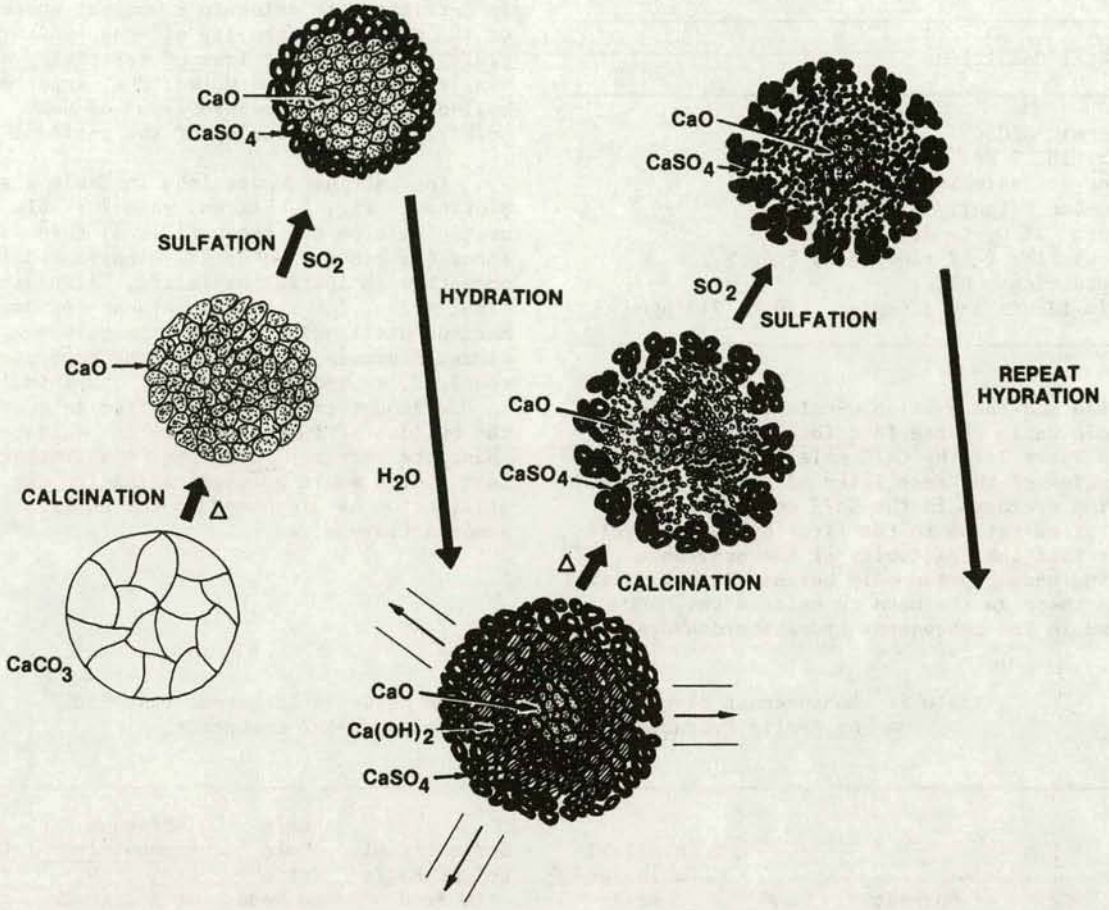

Fig. 4. Schematic Model of the Enhancement of Limestone Sulfation by Hydration.

average pore size, an increase in total porosity and an increase in surface area due to recrystallization of the CaO.[7,8] Sulfation proceeds until sufficient $CaSO_4$ has formed to seal off any remaining CaO from further reaction. The water treatment may be repeated successively to achieve very high levels of sulfation with a resultant decrease in total amount of solid material necessary to remove the SO_2 from the flue gas to meet emission standards.

Fluidized-Bed Combustor Sulfation-Hydration Procedure

The PDU-scale cyclic hydration-sulfation experiments of Grove limestone (9501) were performed in a 15-cm-ID AFBC with a high-sulfur coal. Each cycle was conducted as one long-term run. The steady-state operating conditions for the series of cyclic hydration-sulfation experiments are given in Table 1.

In these experiments, the duration of steady state ranged from 85 h for the initial sulfation of Grove to 2 h for the fifth cycle. The SO_2 levels in the dry off-gas correspond to a nominal 85% sulfur retention in the sorbent. For each cycle, a starting bed of 7 to 9 kg of the appropriate feed sorbent was first sulfated until the dry off-gas contained approximately 800 ppm SO_2. Then an additional bed equivalent of feed sorbent (7-9 kg) was gradually fed to the combustor; during this time, the SO_2 level in the off-gas reached a steady-state level of 700 ppm. After each cycle, the steady-state bed overflow and the final-bed products were mixed together, spray-hydrated by hand, and dried with heat lamps and forced air. Approximately 20 wt % distilled water was added to the products of the initial sulfation and the first two hydration cycles, 15 wt % was added to the products of the third cycle, and 10 wt % was added to the products of the fourth cycle. After each sulfation, hydration, and drying sequence, the material was sampled for analysis before being used as feed for the next cycle.

AFBC Sulfation-Hydration Experimental Results

The cyclic studies in the AFBC were designed to sequentially reproduce the operations that would be required in a commercialized continuous cycling system. The steady-state product

Table 1. Steady-State Operating Conditions for the PDU-Scale Cyclic Hydration-Sulfation Experiments

Experimental Conditions
Temperature: 850°C
Pressure: 101.3 kPa (1 atm)
Fluidizing-gas velocity: 1 m/s
Fluidized-bed height: 810 mm
Excess air: 3% O_2 in dry off-gas
Coal: Sewickley (-12 +100 mesh) 5.46 S
Sulfur retention: 85%
Sulfur dioxide in dry off-gas: 680 to 715 ppm

composition and the available-calcium to sulfur (Ca/S) mole ratio in the feed for each cycle are listed in Table 2. The Ca/S mole ratio provides an indication of the reactivity of the feed limestone. The decrease in the Ca/S mole ratio from the initial sulfation to the first hydration cycle indicates that the reactivity of the available calcium increased, presumedly because in the initial sulfation there is the need to calcine the $CaCO_3$ to CaO and in the subsequent hydration/dehydration structural changes caused by the water treatment create a large-pore structure. For the water-treated sorbents, a nominal Ca/S mole ratio of 2 is sufficient to maintain a nominal concentration of 700 ppm SO_2 in the dry off-gas. After the fifth cycle, a significant loss of reactivity of the available calcium was noted; due, apparently, to a buildup of an impermeable layer of $CaSO_4$ and, possibly, to a sintering of the residual CaO.

The calcium conversions in Table 2 are also plotted in Fig. 5. After cycle 2 (Table 2), 68% of the calcium had been utilized; this is three times the conversion of 22% experienced in the once-through initial sulfation. Although after five cycles, the sulfated sorbent approached a maximum utilization of approximately 90%, a significant increase in the amount of sorbent also was required, as indicated in Fig. 5. This increase in the amount of sorbent required is a result of the buildup of inert $CaSO_4$ in the sulfated stone. Thus, the increase in sorbent requirements in the last cycles would preclude attaining the maximum utilization as discussed in the section about process flowsheets.

Table 2. Enhancement of the Sulfur Retention of Grove Limestone (ANL-9501) by Cyclic Hydration Treatments (Fluidized-Bed Combustor)

Hydration Cycle	Sorbent	Available Ca in Feed,[a] wt %	Sorbent/Coal Weight Ratio in Feed	Ca/S Mole Ratio[b] in Feed	Product Composition[c] Ca, wt %	Product Composition[c] S, wt %	Calcium Conversion to $CaSO_4$,[d] %
Initial Sulfation	As-received	38.2	0.59	3.3	46.7	8.3	22
1	Hydrated Initial Sulfation 10.4 wt % H_2O	30.6	0.47	2.1	32.1	12.7	49
2	Hydrated Cycle 1 Product 6.4 wt % H_2O	15.3	0.90	2.0	26.5	14.3	68
3	Hydrated Cycle 2 Product 4.2 wt % H_2O	8.3	1.31	1.6	24.1	15.3	79
4	Hydrated Cycle 3 Product 3.8 wt % H_2O	4.8	2.98	2.1	23.3	16.1	86
5	Hydrated Cycle 4 Product 1.1 wt % H_2O	3.1	8.40	3.9	24.1	16.8	87

[a] [(analyzed total grams Ca - analyzed grams Ca as $CaSO_4$) ÷ total grams sample] x 100.

[b] (analyzed total moles Ca - analyzed moles Ca as $CaSO_4$) ÷ moles S in coal.

[c] As chemically analyzed.

[d] (analyzed moles S ÷ analyzed moles Ca) x 100.

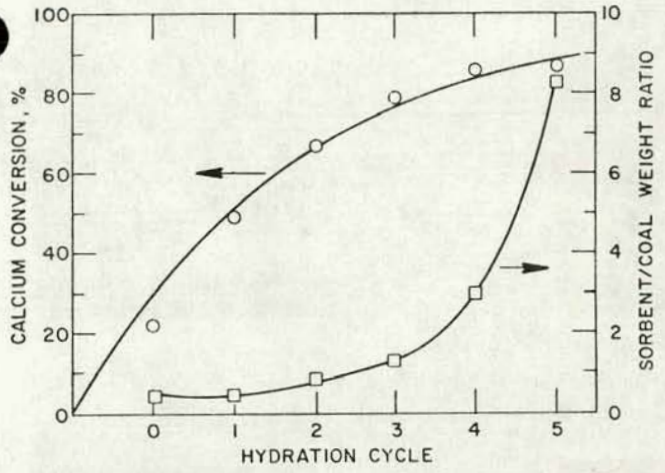

Fig. 5. Calcium Conversion of the Steady-State Product as a Function of Hydration Cycle. (Hydration cycle zero represents the initial sulfation.)

SEM and Porosity Analyses of Sulfated Stones

The SEM photographs of sulfated and hydrated stone from the combustor (Fig. 6) support the mechanism detailed in Fig. 4. The photographs at 132x and 330x show the cracking of the outer shell of $CaSO_4$. The outer sulfate shell, however, maintains sufficient physical integrity to hold the particle together. Thus, the outer sulfate shell provides a structure within which the $Ca(OH)_2$ can recrystallize as shown in the 1320x, 660x and 3300x photographs. In addition, the cracks in the outer shell provide a convenient diffusion path for the SO_2 to reach the reactivated CaO formed by dehydration.

The effects of repeated cycling are shown in Fig. 7 and Fig. 8. As can be seen in the SEM photographs, Fig. 7, a more open pore structure develops during the first three hydrations. After three hydrations, however, the increasing amount of $CaSO_4$ formed begins to close off the pores accounting for the drop in reactivity shown during the last cycles in the AFBC. The formation of a large-pore structure that closes with repeated sulfation is also indicated by the porosity measurements shown in Fig. 8. It should also be noted that most of the increased porosity results from large pores ($\geq$0.3 μm) which have been shown to contribute most to sulfur capture without premature blockage by $CaSO_4$.[9]

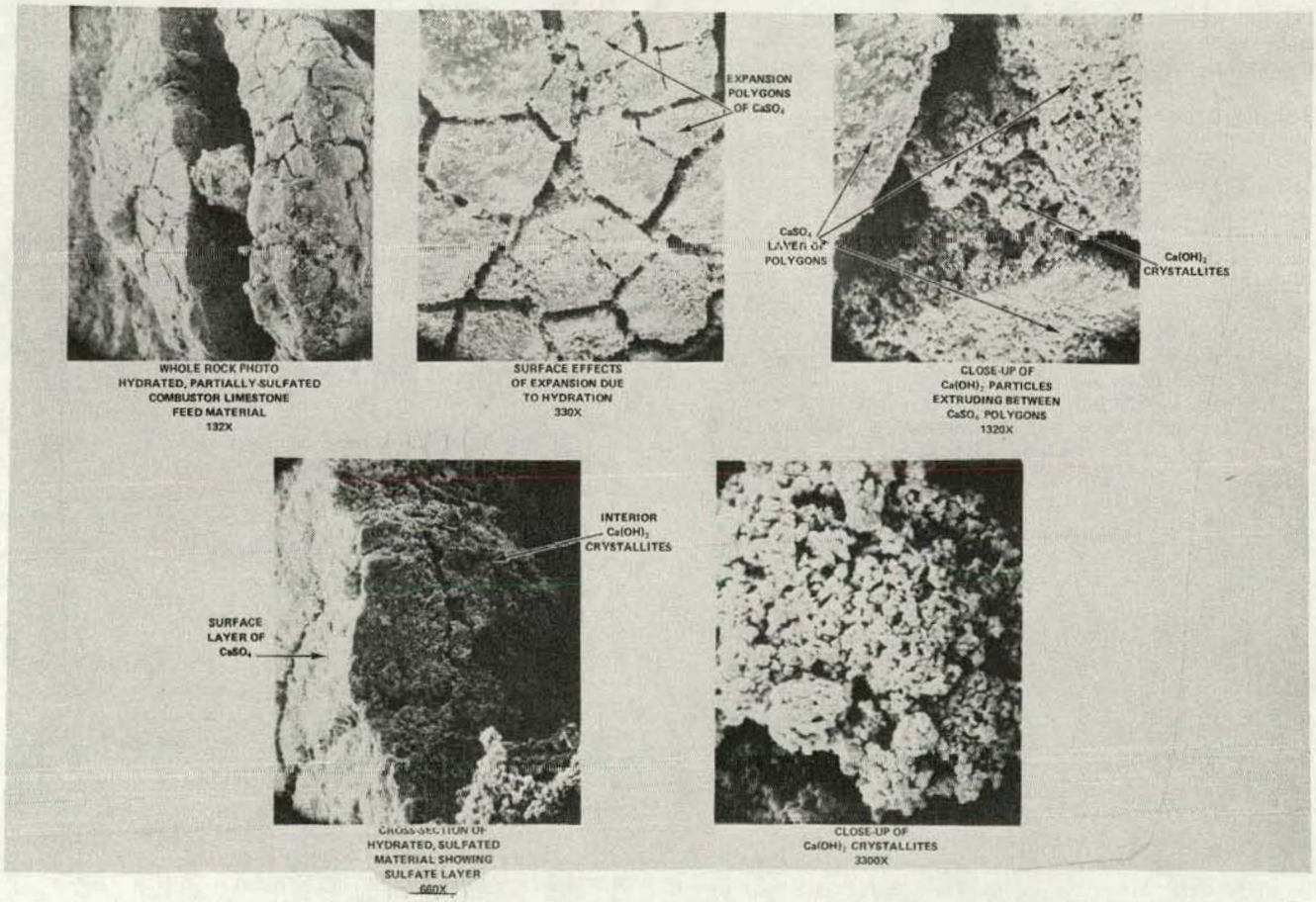

Fig. 6. Partially Sulfated Fluidized-Bed Combustor Limestone Additive (ANL-9501) Overflow Showing Physical Effects of Hydration.

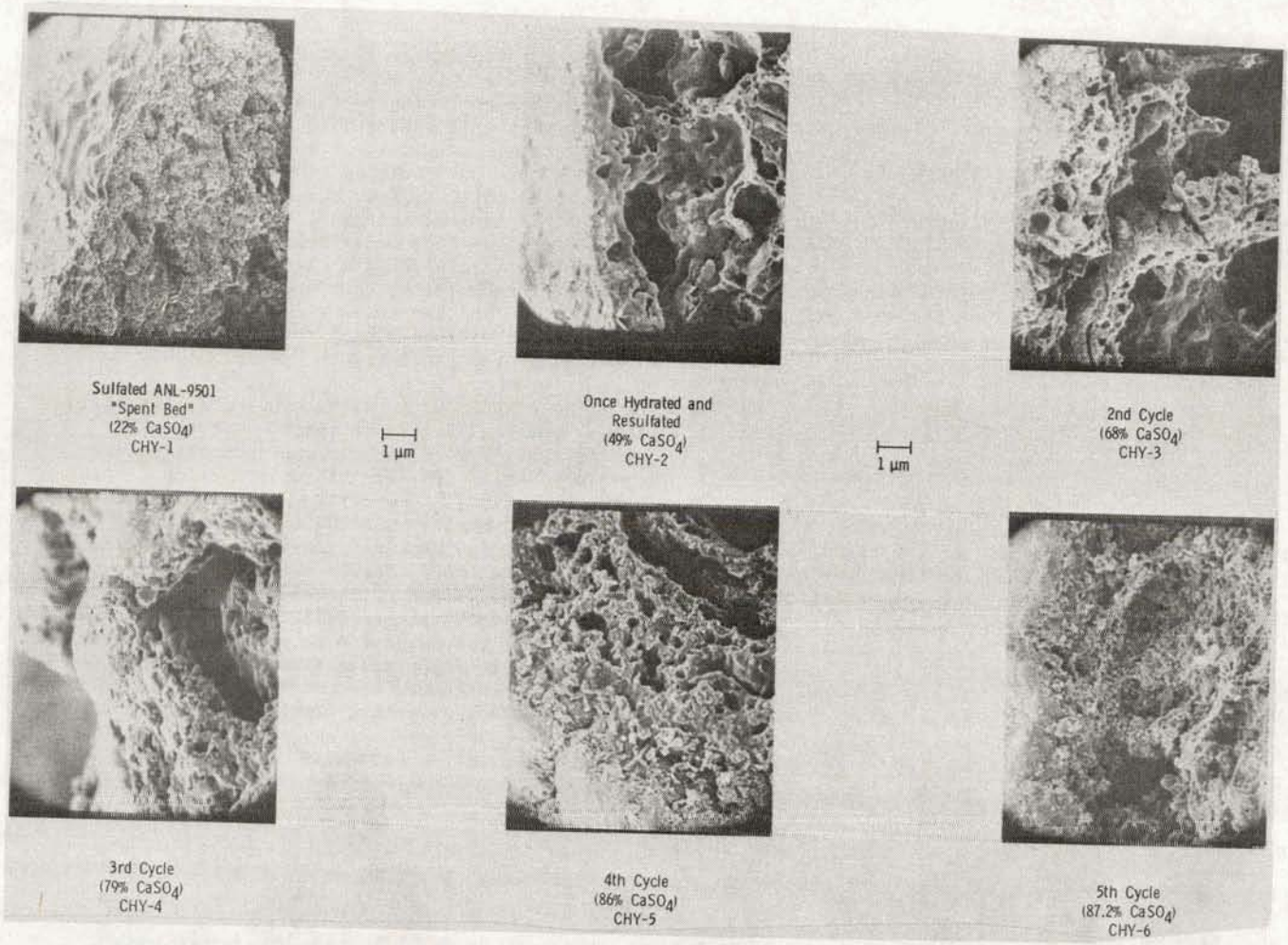

Fig. 7. Cross-Sections of a Series of Water-Treated Steady-State Samples of ANL-9501 from a PDU-Scale Atmospheric Fluidized-Bed Combustor at 850°C

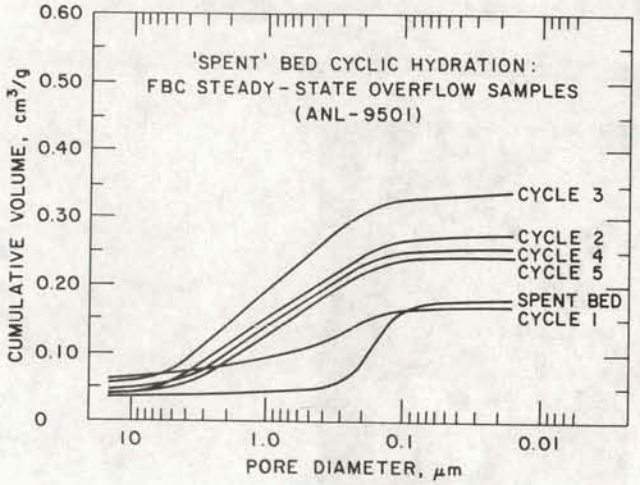

Fig. 8. Porosity Distribution Curves of FBC Overflow Samples of Limestone ANL-9501 from a Series of Cyclic Hydration-Sulfation Experiments of 850°C.

Kinetic Studies of the Hydration of Partially Sulfated Limestones

The kinetic measurements were made in a temperature controlled steam-air flow system with a standard TGA for recording weight change as the sample absorbed moisture. Fluidized bed hydration experiments were made in a 7.5 cm hydrator operated between 100 and 200°C and 1.2 to 2 U_{mf}. About 3.2 kg of spent sorbent were hydrated batch wise with a steam-air mixture in each run.

Some of the spent sorbents were obtained from fluidized-bed combustor runs, and others were batch sulfated in a simulated combustion atmosphere to obtain uniformly sulfated material. Sorbents used in these studies include batch sulfated Lowellville (ANL-9202) and Greer limestone (ANL-8001), and two Grove limestone (ANL-9501) sorbents, one combustor-sulfated at Argonne and the other combustor-sulfated in the Pope, Evans, and Robbins (PER) fluidized-bed combustor at Alexandria, Virginia.

The rate of sorbent hydration was affected by the following factors: (1) steam-concentration, (2) temperature, (3) conversion to calcium hydroxide, and (4) the extent of sulfation and the past history of the stone.

The results of a series of TGA runs which were made varying only the steam concentration, are shown in Fig. 9. There is clearly an advantage in using higher steam concentrations. Analysis of the data shown in Fig. 9 and similar experiments indicates that for much of the reaction, the hydration rate was about 1.5 order in steam concentration. Experiments are underway to see if this result can be extended to a variety of other spent sorbents.

The effect of temperature on the hydration rate was somewhat unexpected. Figure 10 shows results of a series of TGA runs in which the temperature was varied between 100 and 300°C. The runs all started out at about the same rate, but rates of the high temperature runs decreased rapidly while the rates of the low temperature runs remained high or actually increased slightly until a much larger conversion had been achieved. Hydration at

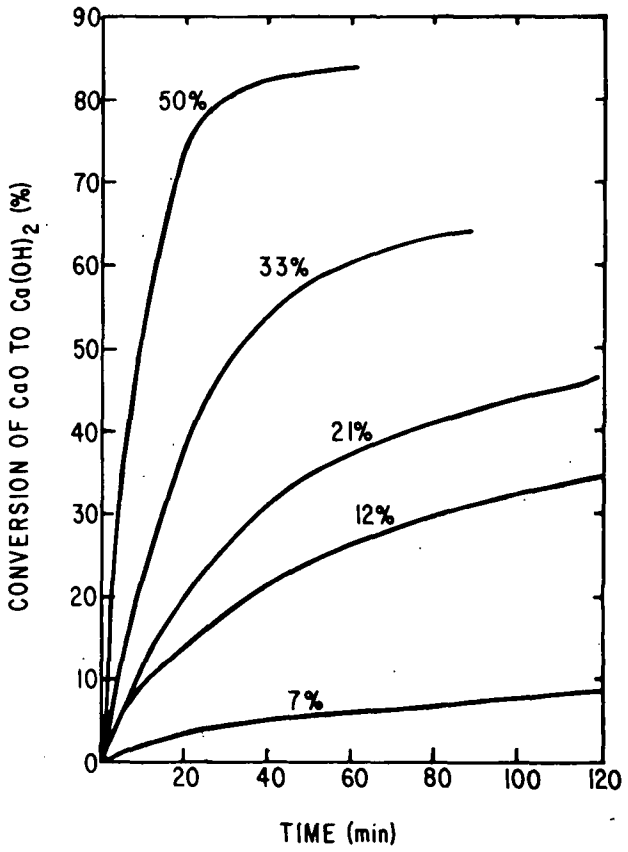

Fig. 9. Conversion Versus Time for Steam Hydration at 200°C. The Sorbent was ANL-9501 Sulfated to 5.8% S by PER in a Fluidized-Bed Combustor. The Numbers Refer to the Percent Steam.

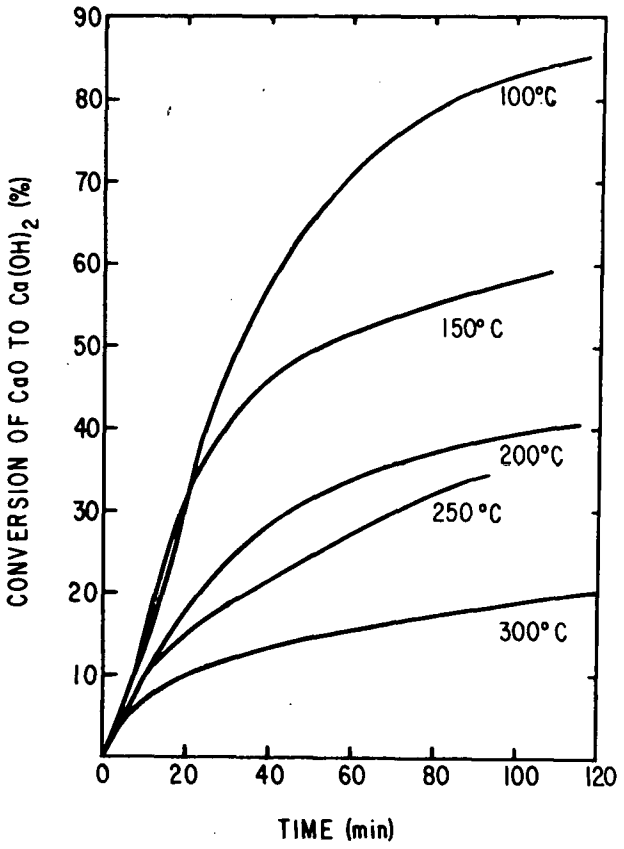

Fig. 10. Conversion Versus Time for Hydration in 12% Steam at the Temperatures Indicated. The Sorbent was ANL-9202 Batch Sulfated to 8.7 % S in a Simulated Combustion Gas.

the lower temperatures appeared to increase the pore volume more rapidly than hydration at higher temperatures, but the reason for this effect is not known.

Kinetic runs were also made with samples of the overflow from the sulfation-hydration experiments, and the results are shown in Fig. 11. As the extent of sulfation increased, the hydration reaction rate decreased. This may be related to the diffusional path travelled by the steam in penetrating the calcium sulfate layer which surrounds the calcium oxide. The sulfate layer would be thicker for the more extensively sulfated sorbents, and the diffusional path would be longer causing the rate to be slower. Another possible explanation may involve pore blockage by foreign material.

Grove sorbent which had been sulfated in the PER combustor was hydrated in a fluidized bed. Two runs were made in which 22% and 56% conversion were achieved. Samples from each run were subsequently sulfated in a TGA at 850°C using a simulated combustion gas containing 0.3% SO_2, 5% O_2, 20% CO_2,

and the balance N_2. The results shown in Fig. 12, along with a non-hydrated sample for comparison, indicate that the sorbent reactivation effect increases with the conversion of CaO to $Ca(OH)_2$ achieved in the hydration. A similar result is indicated in Fig. 13 which shows the increase in sulfation achieved in a standard tube furnace sulfation described earlier in the paper for samples of a sorbent which had been previously hydrated to different levels of conversion to $Ca(OH)_2$.

Hydration Process Design

Since the dehydration reaction (which occurs in the combustor) is endothermic, the heat available to generate steam would decrease. Thus, a process for hydrating the partially sulfated sorbent should be capable of recovering the exothermic heat of hydration ideally resulting in no net energy loss in the hydration-dehydration reactions. When partially sulfated sorbent leaves the combustor, it is at a temperature of about 870°C. A significant amount of heat must be removed from this sorbent in order for it to be discarded at ambient temperature. Thus, it would be advantageous to also develop a process to recover this heat.

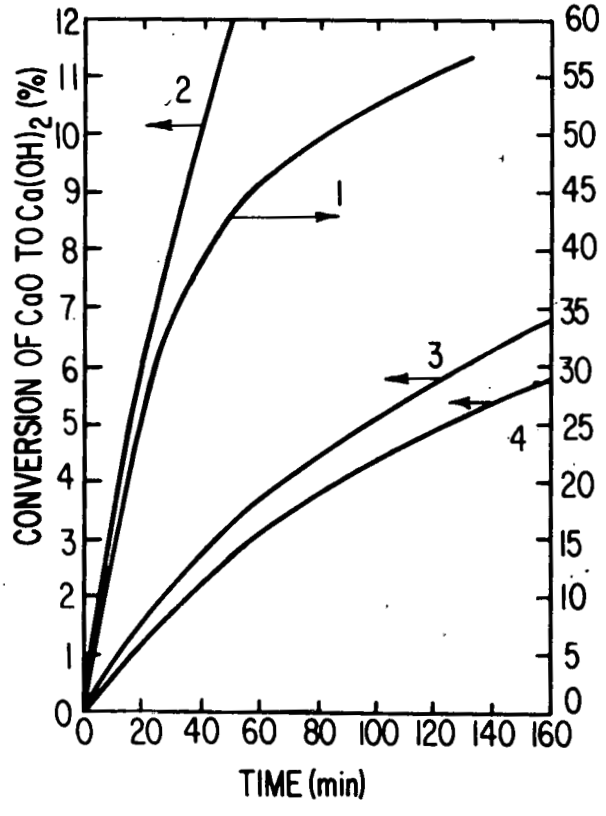

Fig. 11. Conversion Versus Time for Hydration in 12% Steam at 200°C. The Sorbent was ANL-9501 Used in a Series of Combustion-Hydration Cycles. The Number of Prior Combustion Usages is Indicated.

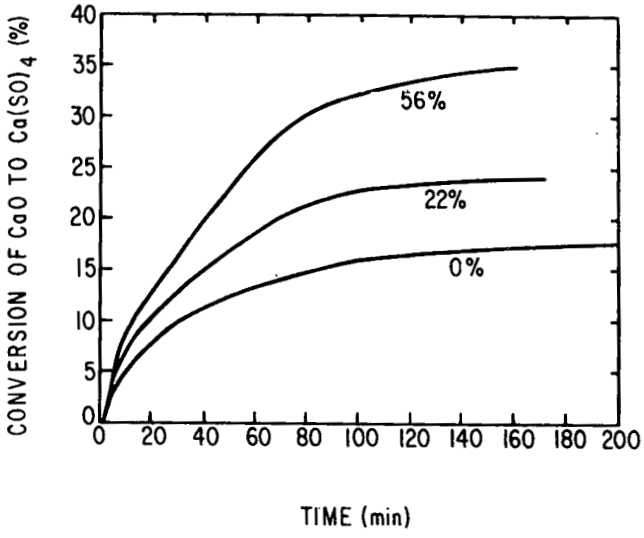

Fig. 12. Conversion Versus Time for Sulfation in a Simulated Combustion Gas. The Numbers Refer to the Conversion of CaO to $Ca(OH)_2$ Attained Previously with Steam in a Fluidized-Bed Hydrator.

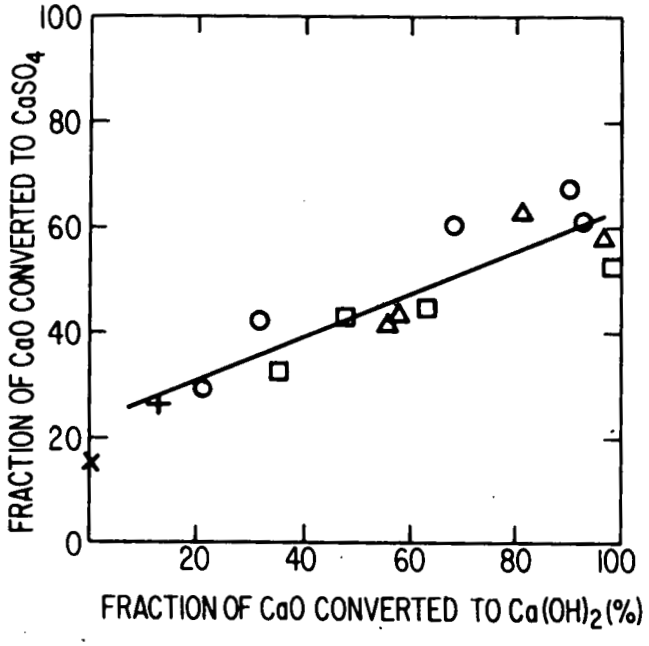

Fig. 13. Increase in Calcium Utilization During a Resulfation Which Followed Partial Hydration at Various Temperatures: +, 23°C; ○, 110°C; △, 200°C; and □, 300°C. The X Indicates the Initial Sulfation.

The fluidized-bed cooler-hydrator (FBCH) performs both functions. Combustion air is sent through a fluidized-bed of partially sulfated sorbent along with water. Thus, both the sensible heat contained in the sorbent as well as the heat of hydration are transferred to the combustion air which is thereby preheated increasing the overall efficiency of the combustion cycle.

In presenting a process flow sheet, certain baseline conditions will be assumed for the calculations as shown in Table 3. Reactivity data for the flow sheet are calculated from the cyclic sulfation-hydration experiment run with Sewickley coal and Grove limestone for six sulfations and five hydrations mentioned in the PDU experimental section. Further experimental work may result in modification of the values of some of these parameters. In particular, the effect of solids residence time in and the operating temperature of the hydrator on overall performance of the system will be investigated.

Table 3. Baseline Conditions for Process Flow Sheet

COMBUSTOR

600 MW AFBC
Coal - 12,500 Btu/lb, 12% Ash, 3.5% S
Sorbent - Grove Limestone, 95.5% $CaCO_3$
Plant Efficiency - 38%
SO_2 Retention - 80%

HYDRATOR

Solids Residence Time - 1 h
Superficial Gas Velocity - 1.8 m/s
Solids Specific Gravity - 1.3
Air Inlet - 20°C
Air Outlet - 150°C
Solids Inlet - 870°C
Solids Outlet - 150°C

As mentioned previously, a means of regeneratively cooling the spent sorbent would increase the overall efficiency of the process. There is also some concern about disposing of untreated spent sorbent as it contains free lime which would generate considerable heat if hydrated by natural water (rain or groundwater) in a landfill. Thus, it would be more environmentally acceptable to hydrate the spent sorbent before final disposal. Combining these two functions in one unit, one can present a process flow sheet which utilizes an FBCH with a once-through sorbent path, i.e., the sorbent is cooled and hydrated but not returned to the combustor for reuse. In a 600-MW AFBC, this system would recover about 21.1 MW of heat (and thus increase cycle efficiency by more than one percentage point) in addition to making the waste product more environmentally acceptable.

Since the hydration process reactivates the sorbent for further sulfation, the sorbent may be reused by injecting it into the combustor. Figure 14 presents this process flow sheet. Sorbent is continuously cycled between the combustor and hydrator with some fresh sorbent being constantly added as well as some spent sorbent being constantly drawn off. The process is characterized by defining a fresh mass ratio of combustor feeds (FFMR), i.e.,

$$FFMR = \frac{\text{Fresh feed}}{\text{Fresh feed + recycle feed}}$$

Low FFMR's mean that little fresh sorbent is being used while high FFMR's signify that mostly fresh sorbent is being fed to the combustor. The performance and dimensions of the system vary with changes in FFMR. Less fresh sorbent is used when utilizing a low FFMR, but the size of the FBCH must be larger.

The method used to calculate the flows assumes a backmix system and is the same as used previously to generate regeneration system process flow sheets. The method utilizes the experimentally determined properties (composition, reactivity) of the sorbent after successive sulfation and hydration steps and a calculated steady-state cycle number (age) distribution in the system as a function of FFMR. The derivation of this method has been described previously.[10] Suffice it to say, that the equation is:

$$g_n = \alpha(1 - \alpha)^{n-1}, \quad 1, 2, \ldots, \infty$$

where g_n = fraction of the total charge which is in cycle n
n = the cycle number of interest
α = FFMR

Performing this analysis for an FFMR of 0.25 the following cycle distribution in the combustion at steady state is as follows:

Cycle #1	25.0%
Cycle #2	18.8%
Cycle #3	14.1%
Cycle #4	10.5%
>Cycle #4	31.6%
	100.0%

Referring to Table 2, one sees that the material in Cycle #4 is not very active and that material beyond cycle #4 is essentially inert. Therefore, at an FFMR of 0.25, over 40% of the material in the system is inert. One of the difficulties, therefore, in getting good sorbent utilization (i.e., low FFMR) is the necessity for circulating large amounts of inert material.

One way to circumvent this difficulty is by designing the system to more nearly approximate a plug flow situation. A flow sheet for this type of system is presented in Fig. 15. The process is continuous, but sorbents of different sulfation/hydration cycle numbers are not mixed. The sorbent proceeds through a series of backmixed reactors; this system approaches the characteristics of a plug flow reactor. Table 4 shows the calculated performance and dimensions associated with "plug flow" systems utilizing two, three, and four cycles. Table 5 compares the backmix mode with the plug

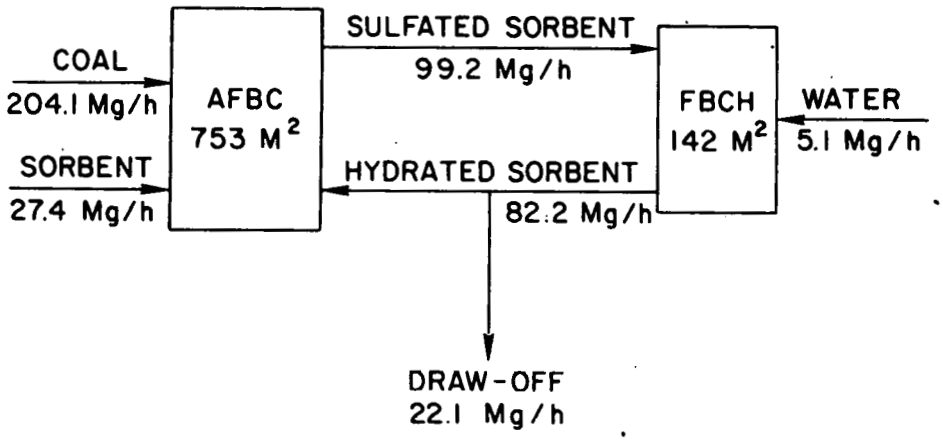

Fig. 14. Backmix Mode Hydration Process (FFMR = 0.25)
Total Waste = Draw-off + Overhead sorbent + Overhead ash
55.8 Mg/h = 22.1 Mg/h + 12.7 Mg/h + 21.0 Mg/h

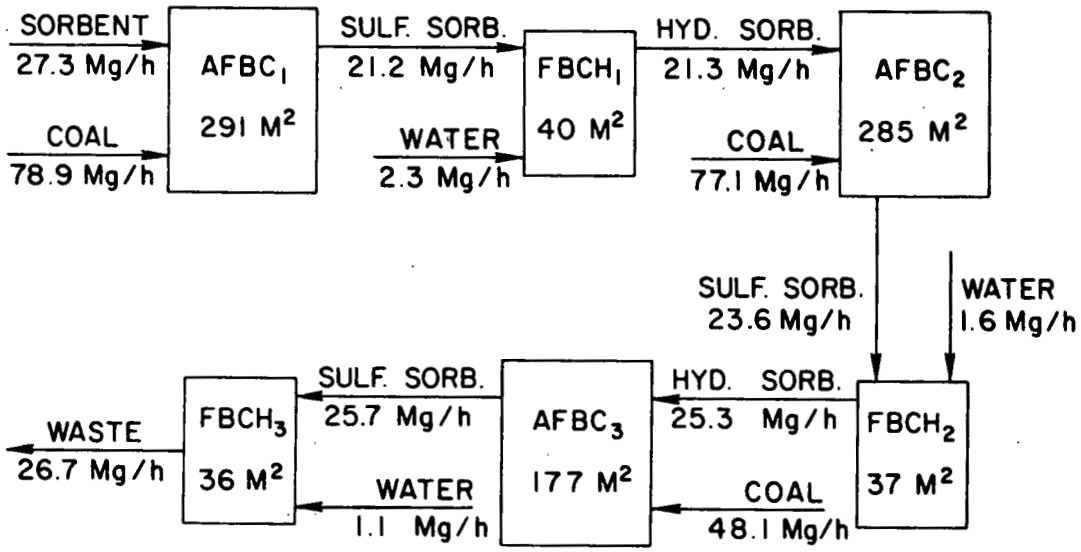

Fig. 15. Plug Flow Mode Hydration Process (3 Cycles)
Total Waste = Waste + Overhead sorbent + Overhead ash
53.8 Mg/h = 26.7 Mg/h + 8.3 Mg/h + 18.8 Mg/h
Sorbent saved - 61%, Waste saved - 33%, Additional hydrator area - 11% (vs. once-through)

Table 4. Calculated Performance and Dimensions of Plug Flow Mode Hydrators of Various Cycle Configurations

Steam	Once-Through	2	3	4
Fresh Feed, Mg/h	70.7	35.7	27.4	23.3
Cooler-Hydrator Feed, Mg/h	54.8	58.5	70.3	77.5
Net Water Feed, Mg/h	5.72	4.90	4.94	4.90
Sorbent Utilization, PCT	26.3	52.0	67.9	79.5
Bed Area, m^2	101	99	113	118
Cooler-Hydrator Heat Duty, MW	21.1	20.8	23.1	24.6
Total Waste (no ash) Mg/h	55.8	34.7	29.0	27.1

Table 5. Plug Flow vs. Backmix Mode for Hydration Process

Fresh Feed		Plug Flow Mode	Backmix Mode	Hydrator Area, m^2	
Mg/h	PCT of Once-Through	(# Cycles)	(FFMR)	Plug Flow	Backmix
35.7	50.5	2	0.45	99	115
27.4	38.7	3	0.25	113	142
23.3	33.1	4	0.13	118	191

flow mode. As can be seen, the plug-flow mode is considerably more efficient than the backmix mode inasmuch as a given fresh sorbent savings can be realized in the plug flow mode with smaller equipment and lower circulation rates. For example, a plug flow mode system with three cycles (Fig. 15) and a backmix mode system with an FFMR of 0.25 (Fig. 14) require the same quantity of fresh sorbent (27.4 Mg/h, or 38.7% of what a once-through system would require) but in the plug flow mode, the hydrator bed area required is considerably smaller than in the backmix mode (113 m^2 vs. 142 m^2). This should translate to lower costs with the plug flow mode design.

Conclusions

In the removal of SO_2 from the combustion gas of fluidized-bed combustors, hydration of residual CaO in partially sulfated limestone and dolomite sorbents appears to be an extremely promising technique for increasing calcium utilization by increasing the SO_2 removal capacity of the sorbents. Experiments have shown that the technique is generally applicable to a variety of limestones and dolomites but is relatively more effective on stones with less initial calcium conversion.

A probable mechanism accounting for the enhanced sulfation results from changes in pore-size distribution resulting from the formation of $Ca(OH)_2$ during hydration and recrystallization of CaO when the stone is dehydrated in the combustor. According to this mechanism, sulfation of the stone proceeds to a point where further reaction of SO_2 is prevented by buildup of the $CaSO_4$ reaction layer. Treatment with water partially hydrates the residual CaO to form $Ca(OH)_2$, with a resultant expansion of the CaO particles thereby cracking the surface layer. Upon dehydration of the $Ca(OH)_2$, a completely new pore structure develops having a greater total porosity and much larger average pore diameters than in untreated spent sorbent, as well as a smaller crystallite size. The resulting increase in gas permeability, coupled with the increase in surface area of the finely crystallized CaO, allows further sulfation to occur.

Results from kinetic studies indicate that hydration was about 1.5 order in steam concentration with low temperature hydration producing more complete conversion. In the temperature range 100-300°C, the hydration rate was somewhat faster at the lower temperature. The sorbent reactivation due to hydration increases with the extent of conversion of CaO to $Ca(OH)_2$.

Based on the above experimental observations a process design study indicates that a plug flow mode of successive hydration-sulfation steps is more efficient than a backmix mode wherein the hydrated material is recycled into the combustor continuously.

The increased calcium utilization due to the hydration treatment, as shown in the tube furnace experiments and verified in the PDU-scale combustor experiments, directly leads to a significant reduction in (1) the quantities of limestone required to reduce SO_2 levels in FBC off-gas to EPA emission standards, (2) the quantities of solid waste produced, and (3) the costs associated with satisfactorily managing these environmental impacts. Thus, this simple noncorrosive process may make heretofore poorly reactive limestones and dolomites economically attractive.

Acknowledgments

The authors are pleased to acknowledge the support of A. A. Jonke, D. S. Webster, and L. Burris of the Chemical Engineering Division, Argonne National Laboratory, Argonne, Illinois. Analyses were performed by C. B. Turner, J. J. Stockbar, and T. J. Prettyman. The fluidized-bed combustor was operated by R. W. Mowry, J. R. Falkenberg, A. R. Pumphrey, and S. D. Smith. This work was performed under the auspices of the U.S. Department of Energy and the U.S. Environmental Protection Agency.

References

1. A. A. Jonke, W. M. Swift, and G. J. Vogel, Fluidized-Bed Combustion: Development Status, Trans. Metall. Soc. AIME, 258: 159 (1975).

2. Irving Johnson, J. F. Lenc, J. A. Shearer, G. W. Smith, W. M. Swift, F. G. Teats, C. B. Turner, and A. A. Jonke, Support Studies in Fluidized-Bed Combustion Quarterly Report, April-June 1979, Argonne National Laboratory Report ANL/CEN/FE-79-8.

3. Irving Johnson, W. Boyd, S. H. Lee, J. F. Lenc, K. M. Myles, T. J. Prettyman, J. A. Shearer, A. A. Siczek, G. W. Smith, W. M. Swift, W. I. Wilson, and A. A. Jonke, Support Studies in Fluidized-Bed Combustion Annual Report July 1978 - July 1979, Argonne National Laboratory Report ANL/CEN/FE-79-14 (in press).

4. H. L. Falkenberry and A. V. Slack, "SO_2 Removal by Limestone Injection", Chem. Eng. Prog. 65(12): 61-66 (1969).

5. R. W. Coutant, R. E. Barrett, and E. H. Lougher, "SO_2 Pickup by Limestone and Dolomite Particles in Flue Gas", Trans. ASME. Series A Engineering for Power 92: 113-122 (1970).

6. A. E. Potter, "Sulfur Oxide Capacity of Limestones", Am. Ceram. Soc. Bull. 48(9): 855-858 (1969).

7. M. A. Hepworth and J. Rutherford, "Fabrication of High-Density Calcium Oxide Ceramics", Am. Ceram. Soc. Bull. 43(1): 18 (1964).

8. P. J. Anderson, R. I. F. Horlock, and R. G. Avery, "Some Effects of Water Vapor during the Preparation and Calcination of Oxide Powders", Proc. Brit. Ceram. Soc. 3: 33-42 (1965).

9. J. A. Shearer, Irving Johnson, and C. B. Turner, The Effects of Sodium Chloride on the Reaction of SO_2/O_2 Mixtures with Limestones and Dolomites, Argonne National Laboratory Report ANL/CEN/FE-78-8 (June 1978).

10. J. C. Montagna, et al., Fluidized-Bed Regeneration of Sulfated Dolomite from a Coal Fired FBC Process by Reductive Decomposition, Argonne National Laboratory Report ANL-77-16 (April 1977).

Questions to John A. Shearer:

Q: (Participant not identified)

You show a draw-off the hydrated sorbent. What is the basis for deciding how much to draw off?

A: That would depend on the system. In the back mix system, you cannot selectively draw off material. That is why the plug flow system is more efficient.

Q: (Participant not identified)

What are the relative attrition characteristics of steam hydrated versus water hydrated?

A: I would guess water hydration produces more attrition.

Q: (Participant not identified)

What was the apoproximate percentage, by weight, of water added?

A: For the first cycle in the combuster experiments it was about 20%. This amount decreased with subsequent cycles.

NATURAL SORBENT ATTRITION STUDIES RELATED TO FLUIDIZED BED COAL COMBUSTION

J. Franceschi, A. Kolar, G. Miller, V. Zakkay, C. Ho,
W. Skelley and S. Hakim

NEW YORK UNIVERSITY
Antonio Ferri Laboratories
Westbury, N.Y. 11590

1. INTRODUCTION

Atmospheric fluidized bed coal combustion is a rapidly developing technology which has the capability of burning high-sulfur coal in an efficient and environmentally acceptable manner. This technology involves burning coal in a bed of sulfur adsorbing stones, fluidized with air, to allow the harmful sulfur dioxide produced during combustion to react with the adsorbent forming disposable sulfates (to limit the atmospheric SO_2 emission to within EPA standards). In addition, the high heat transfer rates in fluidized combustors result in reduced boiler sizes relative to conventional systems.

The performance of this technological process is strongly dependent on the proper selection of the sulfur adsorbent, either natural or synthetic. Limestone ($CaCO_3$) and Dolomite ($CaCO_3 + MgCO_3$) are the two natural sorbents which have been proposed for use in commercial fluidized bed coal combustors, and are presently being employed in pilot plants and demonstration units. Two important characteristics which govern the sorbent selection are its sulfur retention capacity and heat transfer effectiveness. These features differ from sorbent to sorbent, and for a given sorbent they are very strongly influenced by the particle diameter. It is well known that sulfur retention during combustion in the bed depends on the pores present on the stone surface. The particle diameter dictates the exposed stone surface area, and the number and size of pores available for utilization, thus exerting overall control over the sulfur retention mechanism. It also has been established that the heat transfer from a bed particle to any immersed heat exchanger surface decreases with increasing particle diameter up to 1mm and then increases for larger (>1mm) particle diameters. These two particle size-dependent mechanisms make it imperative for the fluid bed designers to have a knowledge of the particle diameter in the bed.

It is noted, however, that the sorbent particles in the bed do not continue to have the same diameter as when they were fed through the sorbent feeder. This change in particle size occurs due to the phenomenon of attrition which the particles are subjected to while in the bed. The sorbent particles are known to disintegrate, at the point of feeding into the combustor, due to the thermal shock they experience. The particles are further subjected, continuously, to such size reducing mechanisms as grid jet interaction, chemical reactions, crushing, and high and low energy collisions with other particles and solid surfaces. The solid surface may be the combustor wall itself or that of any immersed heat exchanger. This phenomenon of attrition is characterized by two significant effects. The first effect is that the particles lose their surface material (abrasion) or actually break up forming smaller particles and shrinking in size during their residence time in the bed thus reducing the average bed particle diameter. The second effect is that the abraded surface material, which is in a fine powder form (the degree of fineness depending on the material strength, hardness and operating conditions), increases the fines composition of the bed. The super fines, defined as that fraction of the bed particles whose terminal velocity is smaller than the operating gas velocity, are blown out of the bed, this phenomenon being called elutriation. Elutriation of super fines dictates the free board height and the sizing of the downstream particulate control devices, affects the average bed particle diameter, and necessitates sorbent make-up to maintain the overall bed heat transfer and sulfur retention performances. A summary of the causes, characteristics and effects of attrition is presented in Table I.

It is obvious, therefore, that it is very important to measure the attrition rates of candidate sorbents under various operating conditions in order to facilitate comparison and proper selection. However, it must be emphasized that the term "attrition rate" has been used in the literature to date with varying connotations. A close look at the combined attrition-elutriation process would prompt one to differentiate between three rate parameters, interdependent in some complex fashion, which must be determined. These are the particle shrinkage rate, the rate of fines production and the rate of elutriation. Most of the attrition studies so far have reported attrition rates in terms of either fines production or loss by elutriation. The particle shrinkage rate, though referred to in theoretical investigations, has not attracted the attention of experimental researchers as much as it should. Even though the rates of fines production in the bed and superfine elutriation from the bed serve as indicators of attrition, they do not represent the

complete attrition process in the absence of information on particle shrinkage. This information on particle diameter-time history will assist the designers and operators of fluidized bed combustors in determining the correct initial particle diameter for a given system and predicting the instantaneous bed particle diameter for process calculations. In the present investigation, therefore the term attrition rate is used to mean the particle shrinkage rate, i.e., the actual rate of change of bed particle size (represented by the volume/surface mean diameter) with time.

where K is an experimentally determined abrasion rate constant whose dependency on system operating and geometric conditions in unknown. A knowledge of this dependency is essential for their model to predict the average particle diameter, D_p. They used this parameter, K, only as an input into an overall elutriation model which was solved by iteration. Results of experiments on silica sand (2) showed that attrition in the cyclones and ducts does not affect the elutriation rate constant estimates. Of more relevance, studies on various limestones and dolomites (3) reveal that

TABLE I

ATTRITION IN FLUIDIZED BED COMBUSTORS

CAUSES	CHARACTERISTICS	AFFECTED PARAMATERS
1. High velocity jet-particle interaction at the distributor.	1. Particle shrinkage and change of average diameter in the bed.	1. Quality of fluidization. 2. Heat transfer effectiveness. 3. Sulfur sorption capacity (sorbent utilization).
2. Crushing of particles near the distributor due to bed overburden.		
3. Particle-particle, particle immersed surfaces and particle containing vessel wall collisions and abrasion in the bed.	2. Production of fines	1. Material elutriation from bed. 2. Sorbent feed rate. 3. Particulate loading in atmospheric emission. 4. Efficiency of downstream particulate control devices.
4. Thermal shock and particle heating in the bed.		
5. Chemical reactions in the bed.		
6. High velocity particle impingement at the cyclone.		5. Erosion of downstream gas turbine components.
7. Transport of particles in the duct system.		

ATTRITION RATE PARAMETERS

1. Particle Shrinkage Rate, $\dot{D}_p$
2. Rate of Fines Production, M
3. Elutriation Rate Constant, K^*

2. PREVIOUS WORK

A survey of attrition research was conducted revealing that attention has been directed at only one characteristic of attrition; viz. the production of fines from coarse sorbent feed material and their subsequent elutriation (1,2,3). The other important characteristic, the rate of size reduction of the feed material itself, has been completely neglected. The authors of Refs. 1 and 2 list several proposed correlations for elutriation rate constants with and without attrition-caused elutriation. Merrick & Highley (1) derive a theoretical model for particle size reduction based on the Rittinger's law of abrasion, of the form

$$\dot{D}_p = \frac{dD_p}{dt} = -\frac{K}{3}(U-U_{mf})D_p \qquad (1)$$

the rate of production of fines is dependent upon whether oxidizing or reducing condition exists in the bed. Also the resistance to powder formation depends on whether the sorbent is calcined, half-calcined, sulfated or sulfided. Apriori prediction of the rate and amount of powder formation was not feasible.

Experiments on Tymochtee dolomite (4) indicate that the attrition rates (measured as percent of bed material elutriated in a 10 hour run) are high initially for up to 1 hour and then decrease rapidly, attaining a steady state in about 2-4 hours. The attrition rates are also dependent on superficial gas velocity and bed depth. Tests on limestone (4) show that attrition rates could be correlated with the impurity (Al, Si, Fe) concentration in the stone, the higher the impurity levels, the lower the attrition rates.

Further studies at Argonne National Laboratory (5) on two limestones and a dolomite indicate that attrition rates are independent of calcination, generally decrease with sulfation and are affected by temperature. The extent and rate of sulfation is also important. Physical properties such as particle shape, size and defects may also significantly affect attrition rates.

Recently, a test program has been initiated at Westinghouse to study the attrition mechanisms in detail in order to facilitate theoretical modelling, and to develop a universal attrition testing apparatus (6). Tests have been conducted on several types of limestone and dolomite in three different bench type fluidized beds of 3.5 cms, 7 cms, and 10 cms diameter at temperatures up to 900°C in the bubbling regime. Results indicate that attrition, defined as powder formation, depends on the stone type, bed atmosphere, and extent of sulfation and calcination. Furthermore, thermal shock leads to higher rates of attrition than does gradual heating, operating bed pressure does not influence attrition and the effect of particle diameter is as yet uncertain. A bubbling bed attrition model (6) has been proposed which implies that attrition rate is a strong function of excess gas velocity, location in the bed, stone density, and strength.

3. RATIONALE FOR EXPERIMENTAL PROGRAM

While a considerable amount of attrition data has been gathered to date, there have been no studies on actual particle shrinkage as a function of time in the fluidized bed, not even on a laboratory scale. Most of the elutriation data has been collected only on bench scale apparatus, as well as the data on attrition tendencies. The results of the Westinghouse research indicate that attrition is independent of operating pressure, but this may be true only for shallow bubbling beds and not for deep slugging or turbulent beds, especially at large excess gas velocities. Furthermore, except for a theoretical expression for average bed particle diameter (1) which assumes the unknown particle shrinkage rate as input, there is no experimentally correlated relation for particle diameter as a function of time and the relevant operating parameters.

A knowledge of particle shrinkage rate is essential to; (1) estimate instantaneous average bed particle diameter in order to assess the quality of fluidization, bed heat transfer and sorbent utilization rates, (2) estimate material elutriation rates for proper design of sorbent feed and particulate control devices, (3) provide input into elutriation models and (4) aid in the selection of a suitable sorbent, with a proper initial particle diameter, for a fluidized bed system.

It is to be expected that bed geometry, the presence of bed internals, reinjection of fines from cyclones, continuous sorbent feeding and spent material removal from the bed will all influence the average bed particle size and elutriation rates in different and varying degrees. The additional influence of such operating parameters on the attrition rate tends to make the overall attrition and elutriation processes quite complex, imposing restrictions on the simultaneous inclusion of all parameters in a study. Certain assumptions and parameter isolation are required for a step by step solution of this formidable problem.

The New York University Antonio Ferri Laboratories has begun research in attrition effects in a fairly realistic size facility with the philosophy of obtaining data which would be useful for industrial application. One of the aims is to provide a working correlation for the attrition rate of various sorbents, and also for the instantaneous average bed particle size. Attrition testing is in progress on a one-foot Gas Fired Batch Combustor (GFBC). This work is expected to be complemented by studies in the one-foot Coal Fired Batch Combustor (CFBC). As an initial step, in-bed tests have been conducted on several kinds of natural sorbents in the GFBC, without internals and fines reinjection, and the results are reported within. It is understood that the results reported (which are without sulfur adsorption and are at lower temperatures than realistic) must be utilized for qualitative not quantitative, content. Results of a test in the CFBC are also presented. This represents an initial step in the program, as extensive data from our coal burning unit will be available in the near future.

It must be appreciated that the attriting quality of a sorbent is dependent upon its hardness and strength. In turn, these properties are considerably affected, during the sorbent residence time in the bed, by the operating conditions. A study of the time-history of stone strength while in the bed demands out-of-bed tests to be performed on samples removed from the bed. At present there is no single accepted method to determine the crushing strength of a sample of a wide particle size distribution. In the present investigation, a test unit for out-of-bed testing has been fabricated based on the suggestions by Zenz (7) and results of tests conducted on this unit are also reported in this paper.

4. EXPERIMENTAL FACILITY & EQUIPMENT

The fluidized bed and test equipment used for the reported work is comprised of a one foot gas fired batch combustor, a particle sampling device, a Ro-Tap sieve shaker, and a crushing strength tester.

A detailed description of the gas fired batch combustor (GFBC) consisting of a combustor, air system, and gas system can

be found in Ref. 8. Figure 1 contains a line diagram of the GFBC general arrangement. The various components of the GFBC and auxilliary equipment are briefly described in the following subsections.

a) The Combustor

The combustor is comprised of three sections namely; the lower combustion chamber, the fluidized bed, and the freeboard section. The combustor is constructed from 1' OD standard pipe 12' in length with the bottom 2' forming the lower combustion chamber and the remaining 10' being the fluidized bed and the freeboard sections. Each section is fitted with 150# slip-on flanges. The sections are connected together and capped from below with a 150# blind flange on which the gas burner is situated and through which the fluidizing air enters. The vertical gas burner is fabricated from a 4" OD ceramic lined stainless steel pipe 10.5 inches high centered and fastened to the lower 1' blind flange. Air and gas (either propane or methane) burn in this tube on ignition by a spark plug. Fluidizing air enters the 4" annulus around the gas burner and flows through a baffled turbulent promoter, mixing with the hot gases before passing upward through the distributor grid. The freeboard section is closed from above by a 150# blind flange through which a 6" OD standard pipe exhausts the hot gases via a 6" plug valve used to control the bed pressure up to 7 atmospheres. From the combustion chamber the hot fluidizing air is uniformly distributed to the fluidized bed by a sandwich type grid made from three Inconel screens (a No. 18 mesh sandwiched between two No. 6 mesh screens) encased in a 1' flange. Eighteen ports of four inch diameter (nine on each side of the vessel), located at one foot intervals along the height of the fluidized bed and freeboard sections, provide (1) penetrations for in-bed analysis probes such as bed pressure and temperature sensors, (2) access to particle loading and bed maintenance operations and (3) visual observation of bed movement.

b) Air System

A compressed air system storing 2500 ft^3 bulk air at 2000 psia facilitates testing at atmospheric and pressurized bed conditions. Compressed air is fed to the combustor via a pressure regulated flow control valve (actuated from the control board) and a venturi meter. Control board indication of system flow rate is used to determine superficial gas velocity.

c) Gas System

Bulk propane or methane is stored in pressurized tanks connected to one main supply header where the pressure is regulated to burner operating conditions. The burner, situated on the lower blind flange, supplies heat to the primary fluidizing air which flows through the grid heating the bed. All gas equipment components are actuated from the control board where the combustion chamber temperature is indicated.

d) Particle Sampling Device and Size Analyzer

The particle sampler, Fig. 2, was fabricated using a double shell arrangement. The outer shell material is 2" schedule 40 stainless steel pipe while the inner particle transport tube is made of 1" stainless steel tubing. Pressurized air is fed through the annulus providing transport air to the inner tube for particle removal via the 3/16" nozzle. The particles are transported from the outer shell penetration through the inner tube to a cyclone separator. At the cyclone, particles are removed from the transport air and collected in the underflow sample jar. The sampling device enters the bed through a port where it is fastened in place by a flange and sealed with an inconel-asbestos packing.

A CE-Tyler Ro-Tap sieve shaker (Model B) was used, in conjunction with a set of U.S. Standard Series sieves ranging from 44 to 4000 micron, to determine the size distribution and the average particle diameter of bed samples.

e) Crushing Strength Tester

The crushing strength tester consists of a 9" long 2" standard pipe section fastened to a ½" steel plate. A 2.060" OD plunger 9¼" long slides into the pipe section applying the required load to the particles below as shown in Fig. 3.

5. EXPERIMENTAL PROCEDURE

The required type of sorbent (limestone or dolomite) was loaded into the experimental facility to a predetermined level, the range of which was selected to include both the shallow and deep beds, of 21", 33", or 45" above the distributor. The sorbent bed, whose size distribution is known, was gradually heated by the hot gases formed in the lower combustion chamber maintained between 800°F to 1100°F depending on the final bed temperature required. The air flow was controlled so as to achieve the required bed temperature in the shortest possible time without excessive elutriation from the bed or flame quenching. The time required to obtain the bed temperature at the required superficial velocity varied from 15 minutes to 1 hour depending on the initial bed height. During this heating

period, samples of bed material (approximately 300 grams) were extracted with the help of the particle sampling probe. Once the test bed temperature was reached, the combustion chamber temperature and air flow were maintained constant and bed samples were taken every 15 minutes. The system constraints were such that a test could be run continuously in the range from 2 to 4 hours. Since the bed height continuously decreased during a run due to elutriation, the final bed height was also noted.

Several preliminary runs with a 45" cold bed at 4 fps showed that there was no significant change in average bed particle size with time. These runs also indicated that the height of the particle removal probe above the grid did not affect the results (which may not be true for beds at higher temperatures and velocities). As an initial step, however, the particle sampler was located 10" above the distributor with the collecting port coaxial with the bed. This position was used for all subsequent tests since attrition is expected to be high in the distributor jet zone of the bed.

The labelled samples taken from the bed were then processed through the particle size analyzer to determine the average particle size given by

$$D_p = \frac{1}{\Sigma \frac{x_n}{d_{p_n}}}$$

Each sample was then transferred to the crushing strength tester where a 500 pound load (resulting in a pressure of 150 psig) was applied gradually over a period of 30 secs and held constant for one minute. The crushed sample was again sieved to obtain the average particle diameter to determine the crushing index.

The sieved data was reduced on a PDP-11 computer facility to determine the average and mass median particle diameters, change of average diameter with time, and its rate of change.

Table II lists the operating variables for the various GFBC experimental runs. The first of a series of proposed tests was conducted on the one-foot CEBC to investigate attrition at coal combustion conditions. The test was run using a 30" initial bed height with a bed temperature of 1550°F and a superficial velocity of 7 fps. The sorbent (Newton #2 limestone) was initially heated to 1000°F with propane gas heaters prior to coal (Pennsylvania Bituminous) feeding. Bed samples were removed: (1) upon initial fluidization, (2) during bed pre-heating (70°F - 1000°F) and, (3) during coal combustion (1350-1550°F). Sieving and data reduction was carried out as outlined for the GFBC experiments.

6. RESULTS AND DISCUSSION

a) Effect of Particle Diameter

Of all the system variables involved in the attrition phenomenon, few are as little understood as the particle diameter (with regard to its influence on the process). It is to be noted that the influence of initial particle diameter, D_{pi}, will be different from that of the instantnaeous D_p, for otherwise identical operating conditions. It is useful here to re-emphasize that in this study the magnitude of attrition is measured by the particle shrinkage rate, $\dot{D}_p$. This is necessary in view of the fact that the D_p influence on the three attrition rate parameters ($\dot{D}_p$, $\dot{M}$ and K^*) is different.

According to findings to date, the rate of production of fines, $\dot{M}$, is directly proportional to the mass of coarse material in the bed, M, and excess gas velocity, U_x, but is independent of D_p, as given by,

$$\dot{M} = -\frac{dM}{dt} = K U_x M \qquad (2)$$

If, on the other hand, attrition is measured by the percentage production of fines, R, then it is independent of both M and D_p, as given by,

$$R = KU_x \qquad (3)$$

R is thus directly proportional only to the excess gas velocity. However, Tarman and Punwani (9) concluded from their experiments on siderite at room temperature that R is inversely proportional to D_{pi}. This apparent anomaly was sought to be explained by Ulrich, et. al. (6) who suggested that in the experiments of (9) the superficial velocity U was maintained constant for various initial particle sizes, and not the excess gas velocity, U_x. The result, therefore, was that R varied as $1/D_{pi}$, since U_x varied as $1/D_{pi}$ and R varied as U_x. However, this explanation, assumes that; (1) U_x in Equation (3) is excess gas velocity U_x based on D_{pi} and (2) U_{mf} is directly proportional to the first power of D_{pi}, both of which are open to question. Vaux (11) has proposed a bubbling bed attrition model, Equation (4), in which R varies directly with U_x and directly with depth of bed measured from the bed surface. Also, R is independent of D_p

$$\frac{R}{U-U_{mf}} = \frac{g\rho}{g_c\sigma} Z \qquad (4)$$

An expression for particle shrinkage rate, $\dot{D}_p$, has been derived by Merrick and Highley (1) for input into an elutriation model based on Rittinger's law

TABLE II

GFBC ATTRITION TESTS

TEST #	SORBENT TYPE & SIZE	SAMPLER PROBE POSITION (INCHES ABOVE DISTRIBUTOR)	L_{mf} INCHES	U (fps)	T (^{o}F)	TIME (HOURS)
1-2-3	Newton #3 Limestone (1.4 mm)	10,22,34	45	4	50	4 to 5
4 to 16	Newton #3 Limestone (1.4 mm)	10	21,33,45	4,7	300,600	3 to 6
19	Newton #2 Limestone (2.45 mm)	10	33	7	600	4
21	Chas. Pfizer #10 Dolomite (1.2 mm)	10	33	7	600	5
23	Chas. Pfizer #6 Dolomite (1.8 mm)	10	33	4	600	4

of abrasion, Equation (2) and is given by,

$$\dot{D}_p = \frac{-K}{3} U_x D_p \qquad (5)$$

This is a first order differential equation in D_p whose solution is,

$$D_p = D_{pi} e^{\frac{-K}{3} U_x t} \qquad (6)$$

which indicates an exponential decrease of D_p with time. Merrick and Highley, though, did not experimentally measure the D_p-time history to confirm this relation. Instead, the validity of the expression was inferred by the success of the elutriation model for which Equation (5) was an input. The physical interpretation of Equation (6) is as follows. The particles which are generally irregular in size and shape lose material by abrasion at a fast rate initially (high $\dot{D}_p$) until the projections, rough edges and defects are rounded off. They then generally become resistant to shrinkage by abrasion leading to a decrease in $\dot{D}_p$. However, the particles at this stage are still prone to shrinkage by break-up due to collisions and very mild abrasion, and hence a finite shrinkage rate persists.

An interesting observation from Equation (5) is now in order. The U_x in the equation has been interpreted, in the literature to date, to mean the excess gas velocity based on the initial diameter, D_{pi} and not the instantanepus D_p. The fact that the U_{mf} of particles is continuously changing (generally reducing) because of the continuous particle shrinkage due to attrition has been generally overlooked (probably because of its inherent complexity). Thus, when U is being held constant in practice, U_x is actually increasing. Assuming U_x to be a constant in Equation (5) is therefore incorrect (except for large U_x) and referring to a "constant U_x" is not realistic. However, one could use the initial U_x as a reference. Even though this is welcome from a practical standpoint, it would grossly misrepresent the physical rationale behind the model. According to the original Rittinger model, particle abrasion is due to the energy input into the particles represented by U_x. Then, at any instant during the attrition process, the energy input is proportional to the instantaneous U_x which is a function of the instantaneous D_p. By utilizing a value of initial U_x in the equation, one could inadvertently miss the particle diameter effect involved in the U_{mf} term and thus force the first power D_p dependency.

While Merrick and Highley assumed an exponential variation of D_p with time, Gonzales and Otero (12) proposed an empirical relationship wherein the variation follows a power law. The $\dot{D}_p$-D_p relationship was given by,

$$\dot{D}_p = - C D_p^{2.6} \qquad (7)$$

where C is a constant depending on system condition. They showed that C is independent of U and U_x, implying that gas flow has no effect on shrinkage rate, contradictory to the Merrick and Highley model. The solution to Equation (7) is of the form,

$$D_p^{-1.6} = D_{pi}^{-1.6} + 1.6\ C\ t \qquad (8)$$

exhibiting a linear variation of $D_p^{-1.6}$ with time and a power law variation of D_p with time.

To sum up, the available data, while agreeing on the general decrease of D_p with time, fail to establish; (1) the manner of decrease, whether exponential, power law or any other, and (2) the role of U or U_x. Simply stated, the type of influence D_p has on the particle shrinkage rate, $\dot{D}_p$, is still uncertain at this time.

In an attempt to examine the D_p effect in the present investigations, data from typical tests were plotted according to models similar to Equations (5) and (8), Fig. 4. It is seen that for the operating conditions of these tests, both models are satisfactory with the least square fit-straight lines having correlation coefficients on the order of 0.9. It is difficult to give a completely acceptable explanation for such a result at the present time. However, the apparent agreement with the Merrick and Highley model may have a plausible explanation. The model is more appropriate to a bubbling bed, where most of the particle size reduction is due to abrasion, because of the assumption of U_x being the effective energy input to the particles. The model therefore is not expected to exhibit an exponential variation of D_p unless U_x is the initial value, which is anyway incorrect. On the other hand if it is considered that U is a suitable representation of the energy input, especially because of the slugging, sometimes severe, experienced in the present series of tests, it is conceivable that

$$\dot{D}_p = -\frac{K}{3}\ U\ D_p$$

and (9)

$$D_p = D_{pi}\ e^{-\frac{K}{3}Ut}$$

thus giving an exponential variation, which is represented by a straight line on the semi-log plot as shown in the figure.

This brings us to the question of what, then, is the actual D_p dependency in the Merrick and Highley model. This can be ascertained by considering the D_p influence on U_{mf}. According to Kunii and Levenspiel (13), the influence is different for small and large particles, as given by,

$$U_{mf} = A\ D_p^2 \qquad \text{for } Re < 20 \qquad (10a)$$

and

$$U_{mf} = B\ D_p^{\frac{1}{2}} \qquad \text{for } Re > 1000 \qquad (10b)$$

In the intermediate Reynolds number range, the Ergun relation holds. Hence we can write

$$\dot{D}_p = -\frac{K}{3}\ (U - A\ D_p^2)\ D_p \qquad \text{for } Re < 200 \qquad (11a)$$

and

$$\dot{D}_p = -\frac{K}{3}\ (U - B\ D_p^{\frac{1}{2}})\ D_p \qquad \text{for } Re > 1000 \qquad (11b)$$

The conclusion, therefore, is that $\dot{D}_p$ dependency on D_p may not be as given by Equation (5) but as given by Equation (9) or Equation (11). Also the power law model of Gonzales and Otero may be satisfactory except for a physical anamoly of U or U_x being of no consequence.

It has to be noted here that Equation (3) predicts a constant R for a "constant U_x". The interpretation is that if two systems are operated with identical U_x values, R would be the same. However, if we consider a single system, we know that U_{mf} is continuously decreasing. This would imply an increase in R with U_x, if U is held constant (as is generally done in practice). Then R is an increasing function of U_x, which is not borne out by experiments. To the contrary, Ulrich, et. al. (6) fit a curve of the form

$$R = 0.0407 + 3.82\ e^{-0\text{-}5789t} \qquad (12)$$

for Grove 1359 at 875°C and initial U_x of 20 cm/s. This would imply that the coefficient of the exponential term, the abrasion rate constant, is a strong function of time.

The effect of initial particle diameter, D_{pi}, may be seen in Figs. 5 and 6 which show D_p and $\dot{D}_p$ as functions of time for Newton Limestone #2 (D_p = 2.85 mm) and Newton Limestone #3 (D_p = 1.4 mm) at identical operating conditions. The difference in the initial particle shrinkage rates (about 30 μ/min) is striking. During an operating time of about 100 minutes, it is evident that the larger particle has a higher $\dot{D}_p$. The experimental conditions were such that the larger limestone was subjected to a smaller initial U_x than the smaller limestone. In spite of this, we see a higher $\dot{D}_p/D_{pi}$ for the larger particle. Although at first glance it is surprising, it must be appreciated that larger particles are more prone to abrasion and break-up than small particles thus causing a significant difference in $\dot{D}_p/D_{pi}$. Furthermore, the $\dot{D}_p$ for the larger particle has a higher reduction rate than that for the small particle. Another interesting observation, in combination with the D_p vs t curve, is that the D_p dependency on $\dot{D}_p$ is not a function of the past history of D_p. In other words, the $\dot{D}_p$ at an instantaneous D_p does not depend on how D_p was attained, i.e., the attrition

mechanism has a "poor memory".

The idea that larger particles shrink faster leads to several interesting observations. In a material sample of wide size distribution, the shrinkage rate would be controlled by the coarse fraction. This suggests that if two samples have the same average diameter but different size distributions, the one with a larger coarse fraction would attrite faster. This would then raise the question of whether D_p is a suitable parameter, or is it enough to compare attrition rates. Furthermore it would also mean that a sample of uniform spherical particles with diameter D_p would behave differently from a sample with a wide size distribution having the same value of average D_p. The assumption of Merrick and Highley that K is the same in the two equations,

$$\frac{dD_p}{dt} = -\frac{K}{3} U_x D_p \qquad (5)$$

and

$$\frac{dd_p}{dt} = -\frac{K}{3} U_x d_p \qquad (13)$$

is open to question. The abrasion rate constant, K, may be significantly different for the various size fractions in the given sample, and the sample as a whole has a different K value which is dependent on individual K values of the fractions. S_o, unless K is a function of D_p and t, the application of the Equations (5) and (13) to beds of wide size distribution becomes tenuous.

As a consequence of the above discussion one must conclude that elutriation data is an insufficient representation of the attrition process and is inaccurate for the prediction of D_p. In-bed particle size measurements are essential for the proper understanding of the attrition phenomenon and an accurate prediction of average bed particle diameter, D_p.

b) Effect of Superficial Velocity, Bed Temperature and Bed Height

Figures 7 and 8 present the variation of particle shrinkage rate with time for shallow (21") and deep (45") beds, with the superficial velocity (4 and 7 fps) and bed temperatures (300 and 600°F) being the variable parameters. It should be pointed out that the ordinate in the figures is $-\dot{D}_p$. A positive value of this parameter indicates particle size reduction, a negative value indicates a particle size increase and a zero value indicates a constant particle size. The numerical value itself indicates the actual rate (μ/min) at which this particle size change is occuring.

A general feature of Fig. 7 for a shallow bed is that the particles have high attrition rates during heat up, which reduce gradually and attain an approximately constant value, after about 100 minutes. As has been mentioned earlier, this is due to the particles losing their rough edges, projections and defects quickly, before becoming rounded off, increasing their attrition resistance in the process. It is interesting to note that this type of behavior has its counterpart in the elutriation process where the elutriation rate approaches a constant value in time, after a high initial value.

Two distinct features of the D_p behavior to be noted from the figures are: (1) higher temperatures result in higher attrition rates, at a constant superficial velocity for the temperature range tested, and (2) lower superficial velocity results in higher attrition rates, at a constant temperature. Also, the effect of velocity is more pronounced at higher temperatures while the effect of temperature is more pronounced at lower velocities. After the initial large differences, the attrition rates, for all operating conditions, appear to approach the same value. This would lead one to conclude that the effects of velocity and temperature become negligible with time.

The temperature effect is as expected. At higher temperatures, the particles are relatively weak, and are more susceptible to abrasion and break-up than those at lower temperatures. However, the velocity effect appears not to conform to the notion of particle shrinkage being directly proportional to excess gas velocity. A possible explanation would be as follows. Two of the main causes of attrition are grid jet interaction near the distributor and particle collisions in the bed. The former is definitely a function of velocity, but the sandwiched screen type distributor used in the present investigation is expected not to generate high velocity jets (which would be more prominent in a tuyeres or simple perforated plate type distributors) and therefore the jet effect may be considered negligible. Additionally, it is known that a bed would expand more at a higher velocity. The higher bed expansion tends to increase the bed porosity, thus reducing the particle collission cross section, which in turn results in a lower attrition rate.

Figure 8 shows the D_p behavior for a deep bed. The general trend is similar to that for a shallow bed. There appears to be no appreciable difference in the effect of velocity at the lower temperatures while at the higher temperatures there appears to be an effect. The initial larger D_p value for the higher velocity is, however, opposite to what we noted earlier for a shallow bed. It is difficult to clearly explain this effect, except that a complex combination of the bed expansion effect and crushing-induced attrition tendencies of the deep bed, in some way, produce this result.

It is useful to note from all the above data that the particles shrinkage rate is in the range of 0 to 20 μ/min (for an initial particle size ≈ 1400 μ), the highest values occurring immediately after the attrition process begins. Of course, this particle shrinkage range is for lower temperatures that a particle would experience in an actual coal

combustor (at 1500°F), where the particle shrinkage rate could be expected to be higher (as discussed in the coal combustion test result below).

The bed height influence on attrition rate is shown in Figs. 9 and 10 for a constant superficial velocity (4 fps) and two bed temperatures (300 and 600°F). It is seen that there is a higher initial attrition rate in a shallow bed at both the temperatures tested. While there is a distinct increase in attrition for a shallow bed when the temperature is increased, there appears to be no effect on the deep bed value. The only plausible reason appears to be that at the same gas velocity, a shallow bed is far more active than a deep bed (even though the bed may be more expanded) thus increasing the number of particle collisions and causing higher attrition. More tests are needed to obtain a clear picture of this phenomenon.

c) Composition of Bed Fines

The buildup of fines in the bed became evident from comparisons of the initial and final bed sample size distribution (individual weight fraction, x, and cumulative weight fraction, P) plots, those in Figures 11 and 12 being typical. Since this phenomenon strongly influences the elutriation characteristics of the stone, affecting the design of downstream particulate control devices, results from several tests comparing bed fines buildup (< 323 micron) from in-bed samples were analyzed. Figure 7 describes the fines concentration as a function of time, for two velocities (4 and 7 fps) and two bed heights (21 and 33 inches) at a bed temperature of 600°F. It can be seen that for both bed heights, the lower velocity has a larger fines buildup. This may occur from the fact that at higher velocities the elutriation rate is larger thereby resulting in less fines buildup in the bed. The effect of bed height is evident by comparing the shallow (21") and transitional (33") bed curves at the same velocity. The lower fines buildup exhibited in the deeper bed may be due to higher elutriation. Finally, the effect of velocity is more pronounced in the shallow bed and the effect of bed height is more pronounced at the lower velocity.

An interesting point with respect to the earlier discussion on particle diameter can be made by considering the initial and final weight fractions in Figs. 11 and 12. Note that while the initial distribution is basically a normal type one, the final distribution is extremely skewed. The entire upper spectrum has been removed and the lower spectrum does not exhibit a normalized trend. This points out the problem of developing models for average bed particle diameter for a non-uniform initial size distribution.

d) Coal Combustion Test

In order to assess the effect of the higher bed temperatures, experienced during coal combustion, on attrition, a test was run utilizing the CFBC described in Section 5. This test (#30) was similar to test #19 (600°F, 7 fps., 33" bed) conducted on the GFBC except that an initial 30" bed was brought to a temperature of 1550°F. Figures 14 and 15 show D_p and D_p as functions of time for test #19 and #30. It should be noted that in test #30 the bed particles have already attrited to a constant particle size of 700 micron before coal feeding (Point B) was initiated. Once attaining the combustion temperature of 1500°F, there seems to be no further decrease in particle size.

Although the initial particle size is different for the two tests, the trend is similar, with the coal test attriting to a lower constant particle size. This lower plateau for test #30 may be attributed to the ability of the CFBC to attain higher bed temperatures faster (higher rate of heating) that the GFBC (Point A-745°F in 30 min. and Point C-600°F in 60 min.) and also to the coarser refractory lining, fines reinjection capability, and coal injector jet impingement geometry associated with the CFBC design.

Since D_{pi} is higher for test #19 than for #30 it would be expected that D_p would also be larger. However from Figure 15 it can be observed that test #30 has a higher D_p for the first 30 minutes. This must be due to the higher rate of heating in test #30, since all other operating conditions are similar. After this period of higher attrition, the average particle size would reach a constant value lower and earlier than in test #19 and remain so for the rest of the sorbent's residence time during combustion (especially since sulfation decreases attrition).

In an actual coal combustor, the particles in fact are subjected to a very high rate of heating (thermal shock) during which they would have a higher D_p than in test #30. Since the average residence time in pilot units ranges from 5 to 20 hours, this would mean that the major part of particle attrition occurs within a small fraction of the particles total residence time. This is an extremely important point, since it may mean that if one can predict initial in-bed attrition, one can make a definitive statement with respect to the average bed particle size at steady state conditions.

e) Comparison of Limestone and Dolomite

Figure 16 shows D_p as a function of time for limestone and dolomite at identical operating conditions (L_{mf} = 33", T = 600°F, U = 4 fps.). Since the limestone has a D_{pi} larger than the dolomite it is also expected that the limestone will have a higher initial D_p as discussed in earlier sections. However, it is observed from the figure that the dolomite exhibits higher initial rates. It can be concluded from this data that dolomite is softer, although further testing under various operating conditions is required to substantiate this finding.

f) Crushing Resistance Index

As has been previously mentioned, the crushing of bed particles from bed overburden is a major

cause of attrition. It is evident that this attrition phenomenon occurs in a region within a few inches above the grid where the particles are most prone to be crushed by the bed weight. When a particle, during its continuous random motion in the bed, arrives in this zone it is subjected to the full weight of the bed mass above (overburden). This weight may be on the order of a few hundred pounds (depending on the bed diameter and height).

As discussed before, a method of assessing the stones strength from out-of-bed tests in the crushing strength is being developed and tested. This method (explained at the end of Section V) of sieving-crushing-sieving considers the change of average particle size for the different samples as a function of time to be a direct representation of the stones varying strength. The Crushing Resistance Index is defined as:

$$CRI = 1 - \frac{\Delta D_p}{\Delta D_{p_r}}$$

where ΔD_p is the difference in average particle size of the sorbent before and after crushing as a function of time, and ΔD_{pr} is the difference in average particle size at time zero. A plot of the CRI as a function of time is shown in Figure 17.

A plot of CRI and $\dot{D}_p$ as functions of time for the shallow and deep beds is shown in Fig. 17. It is seen that the CRI increases nonlinearly with time, for both beds. This increase may be attributed to the production of smaller particles due to attrition, smaller particles being more resistant to crushing. It is also noted that the rate of increase of CRI decreases with time which may be directly attributed to the decrease in the rate at which smaller particles are formed, as represented by the decrease in D_p. Also, it is observed that the CRI and its rate of increase are slightly higher for a deep bed. This is due to the fact that (1) the initial D_{pi} for the deep bed was slightly less (1212μ) than for the shallow bed (1298μ) producing a higher initial crushing strength and (2) the initial D_p values were larger for a deep bed, producing smaller particles at a faster rate. The higher initial values of D_p for the deep bed (even though the initial D_{pi} is smaller) may be due to the faster break-up of particles by the crushing tendencies of the deep bed because of its larger bed accentuated mass.

7. CONCLUSIONS

1) Elutriation rate and production of fines are insufficient attrition parameters. In-bed particle attrition tests to determine particle shrinkage rates are essential in order to predict the instantaneous average bed particle diameter for design and process calculations.

2) Higher initial particle diameters result in higher initial attrition rates. The experimental data suggest that the particle shrinkage rate, $\dot{D}_p$, is initially high and decreases gradually with time. It also has a poor memory of the past time history of D_p. The influence of instantaneous particle diameter is as yet unconfirmed. The available models need closer scrutiny and proper interpretation before a realistic model for attrition ($\dot{D}_p$) is finalized.

3) Higher temperatures result in higher attrition rates within the present experimental range. The velocity effect on $\dot{D}_p$ is significantly influenced by its simultaneous effect on the bed expansion ratio which modifies the particle collision mechanism. This process may be similar to the effect of velocity on heat transfer, which exhibits an inflexion point at maximum heat transfer. A shallow bed exhibits higher attrition rates as compared to a deep bed, at identical operating conditions, due to its more vigorous fluidization. This may be contrasted to the higher elutriation rates for the deeper bed.

4) Shallow beds and lower velocities result in higher fines build up in the bed.

5) Higher rate of heating results in higher attrition rates. Thermal shock (very high rate of heating) is the major cause of attrition in actual coal combustors, this effect occurring in a small fraction of the total solids residence time.

6) A Crushing Resistance Index (CRI), for a bed of wide size distribution, has been defined. The observed increase of CRI with time may be a result of the decreasing particle size inherent to the attrition process.

7) The local fluid mechanics plays an important role in the overall attrition-elutriation process. Studies on large scale units are therefore essential in order to realistically quantify the parametric effects.

NOMENCLATURE

A,B	Constants in Equations (10) and (11)
C	Constant in Equation (7)
D_p	Volume/surface average particle diameter
D_{pi}	Initial average particle diameter
$\dot{D}_p$	Rate of change of average particle diameter
d_{p_n}	Average particle diameter of the nth size fraction
g	Acceleration due to gravity
g_c	Gravitational constant
K	Abrasion rate constant
K^*	Elutriation rate constant
L_{mf}	Settled bed height
M	Mass of coarse particles in the bed
$\dot{M}$	Rate of fines production
P	Cumulative weight fraction
R	Percentage rate of fines production, - M/M
T	Bed temperature

t	Time
U	Superficial gas velocity
U_{mf}	Minimum fluidizing velocity
U_x	Excess gas velocity, $U-U_{mf}$
x_n	Weight fraction of nth size fraction
Z	Bed depth measured from bed surface
σ	Stone strength
ρ	Stone density
ΔD_p	Change in average particle diameter
ΔD_{p_r}	Reference change in average particle diameter taken as that at time = 0

REFERENCES

1. Merrick, D. and Highley, J., "Particle Size Reduction and Elutriation in a Fluidized Bed Process," Recent Advances in Air Pollution Control, AIChE Symposium Series, No. 137, Vol. 70, pp. 366-378, 1974.

2. Colakyan, M., Catipovic, N., Jovanovic, G., and Fitzgerald, T., "Elutriation From a Large Particle Fluidized Bed With and Without Immersed Heat Transfer Tubes," 72nd Annual Meeting of AIChE, San Francisco, November 25-29, 1979.

3. O'Neill, E.P. and Keairns, D.L., "Selection of Calcium-Based Sorbents for High-Temperature Fossil Fuel Desulfurization," Fluidization Theories and Applications, AIChE Symposium Series, No. 161, Vol. 73, pp. 100-107, 1977.

4. Vogel, G.J., et al., "Supportive Studies in Fluidized-Bed Combustion," Argonne National Laboratories, Annual Report, June 76-June 77, ANL/CEN/FE-77-3.

5. Johnson, I., et al., "Support Studies in Fluidized Bed Combustion," Argonne National Laboratories, Quarterly Report, April-June 1978, ANL/CEN/FE-78-4.

6. Ulrich, N.M. et al., "Experimental/Engineering Support for EPA'S FBC Program," Final Report, Vol. I, Sulfur Oxide Control, Interagency Energy/Environment R & D Program Report, Westinghouse Research and Development Center, EPA-600/7-80-015A, January 1980.

7. Zenz, F.A., "Studies of Attrition in Fluid-Particle Systems I and II," NSF Workshop on Fluidization and Fluid Particle Systems: Research Needs and Priorities, Renssaler Polytechnic Institute, Troy, New York, Oct. 17-19, 1979.

8. Fluid Dynamics Of A Fluidized Bed Packed with Heat Exchangers, Annual Report (February 1976-January 1977) to ERDA, New York University Antonio Ferri Laboratories.

9. Tarman, P.B. and Punwani, D.V., "Development of the Steam-Iron System for Production of Hydrogen for the Hygas Process," Interim Report No. 2 to ERDA, IGT, Chicago, July 1974 - June 1975, FE-1518-34.

10. Ulrich, N.M. et al., Experimental/Engineering Support for EPA'S FBC Program, Final Report, Vol. I, Sulfur Oxide Control, Interagency Energy/Environment R & D Program Report, Westinghouse Research and Development Center, EPA-600/7-80-015A, January 1980.

11. Vaux, W.G. and Keairns, D.L., "Particle Attrition in Fluid-Bed Processes," International Fluidization Conference, Henniker, New Hampshire, August 3-8, 1980.

12. Gonzales, V. and Otero, A.R., "Formation of VO_3 Particles in a Fluidized Bed," Powder Technology, 7(3), pp. 137-143.

13. Kunii, D. and Levenspiel, P., Fluidization Engineering, R. Kreiger Publishing Company, New York, 1977.

ACKNOWLEDGEMENT

The work reported herein was supported by the Department of Energy under Contract EF-76-C-01-2256. The authors gratefully acknowledge Mr. J. Garn of The Pfizer Company, Gibsonberg, Ohio and Dr. Vaux of Westinghouse for their assistance and technical expertise.

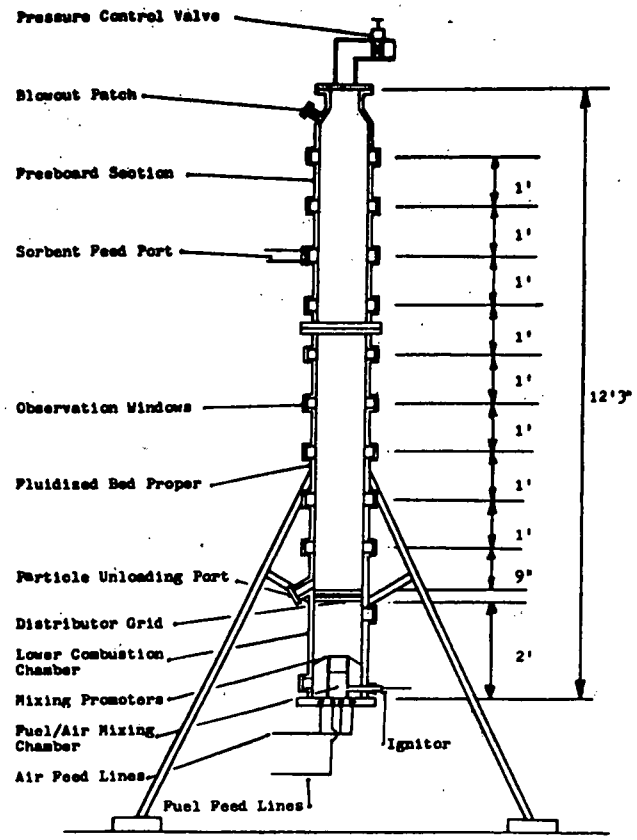

Fig.1 Gas Fired Batch Combustor (GFBC)

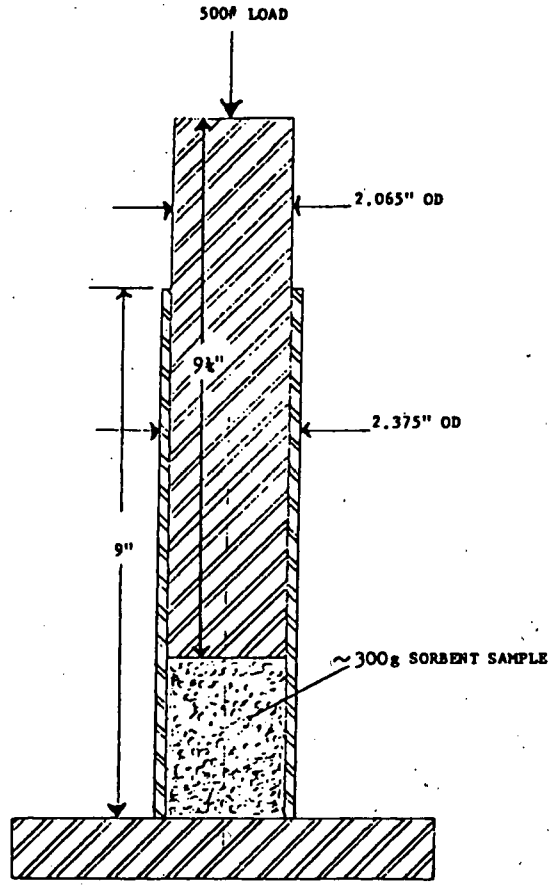

Fig. 3 Crushing Strength Tester

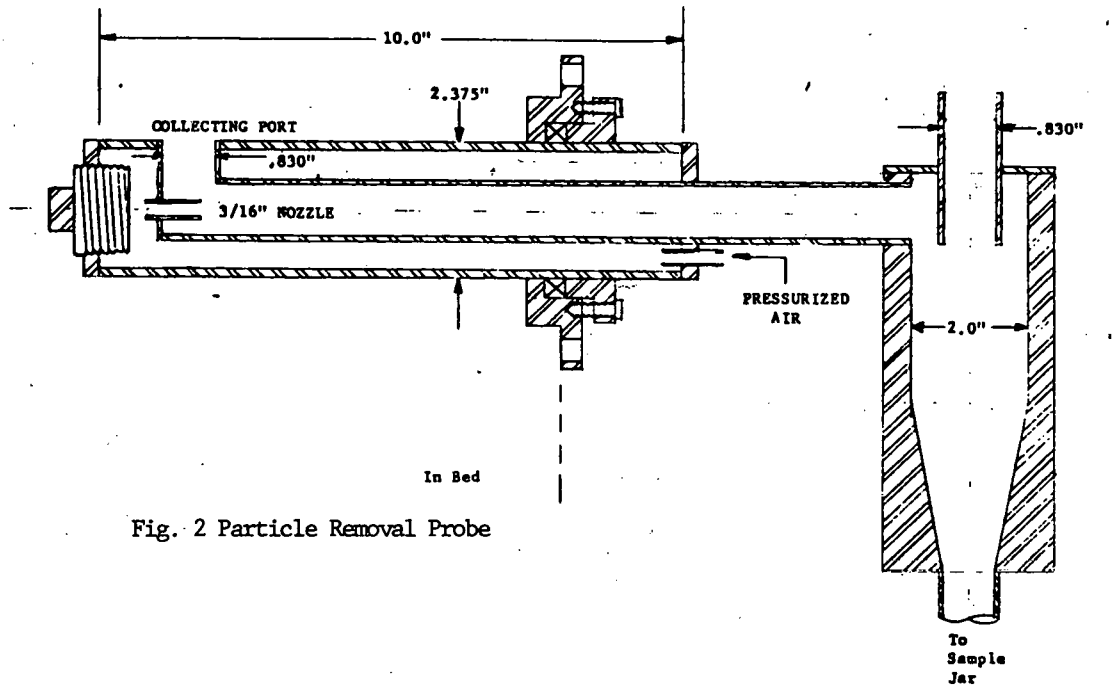

Fig. 2 Particle Removal Probe

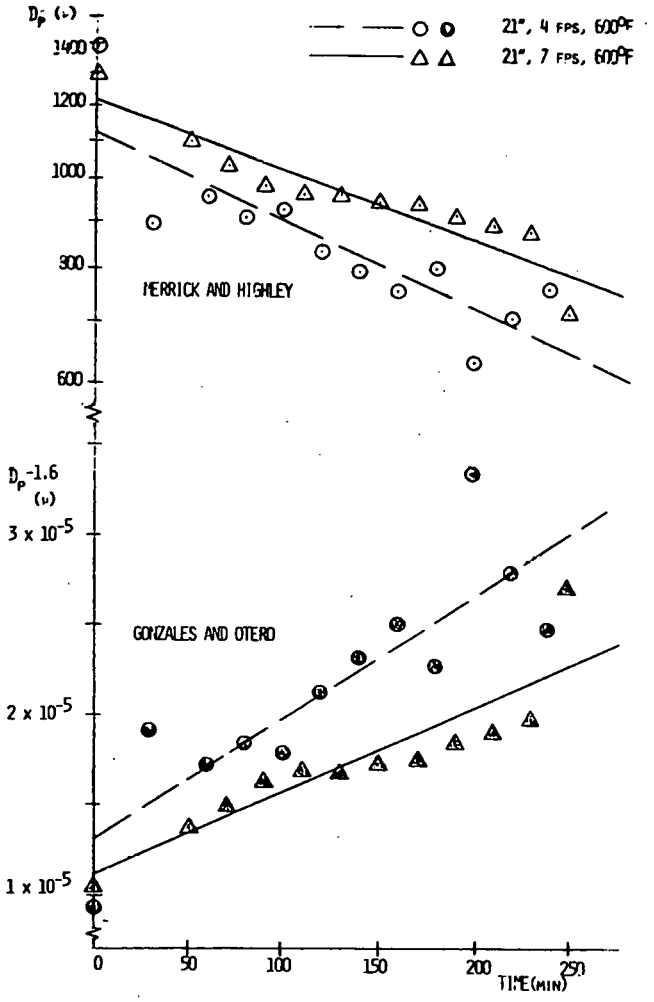

Fig 4. Comparison of Models

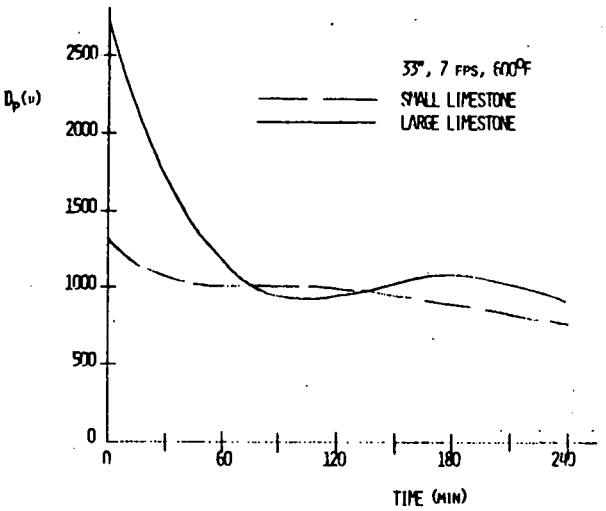

Fig. 5 Effect of Initial Particle Diameter

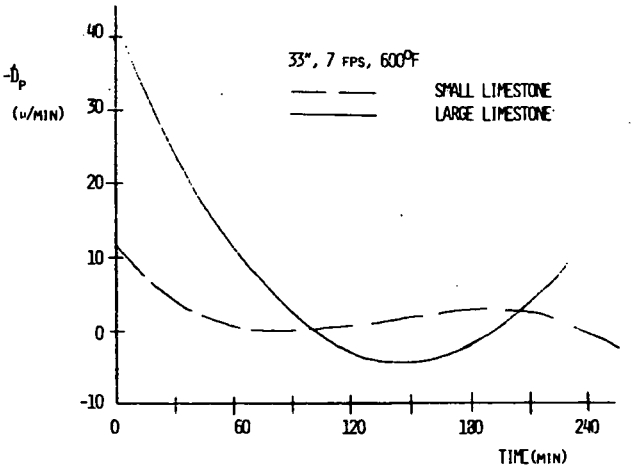

Fig. 6 Effect of Initial Particle Diameter

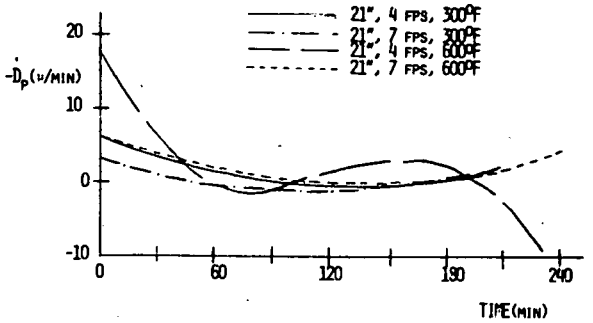

Fig. 7 Effect of U and T - Shallow Bed

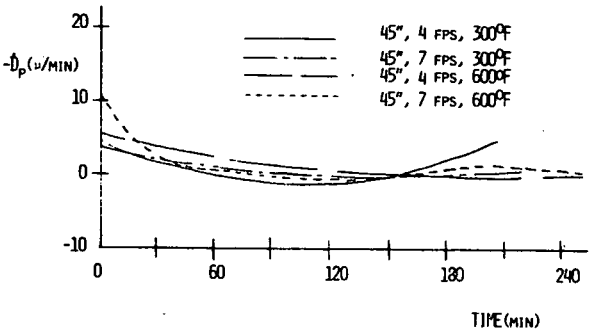

Fig. 8 Effect of U and T - Deep Bed

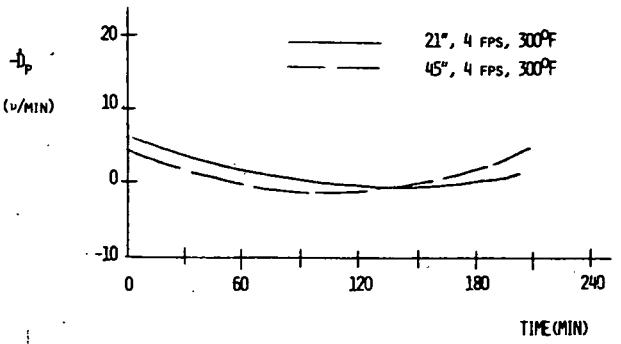

Fig. 9 Effect of Bed Height

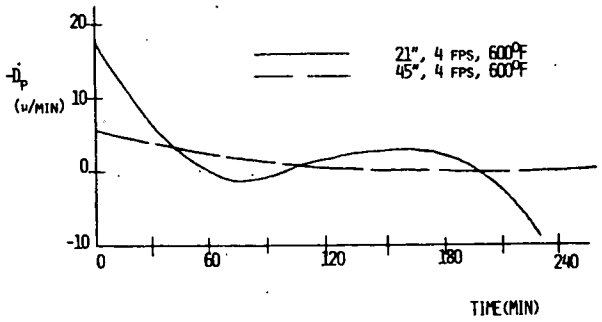

Fig. 10 Effect of Bed Height

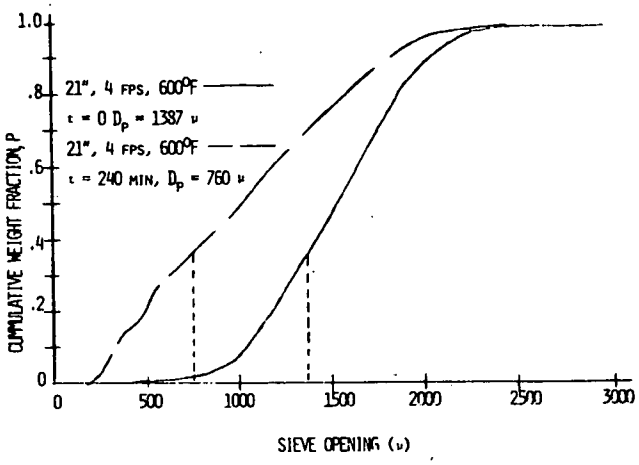

Fig. 11 Initial & Final Cum. Wt. Frac.

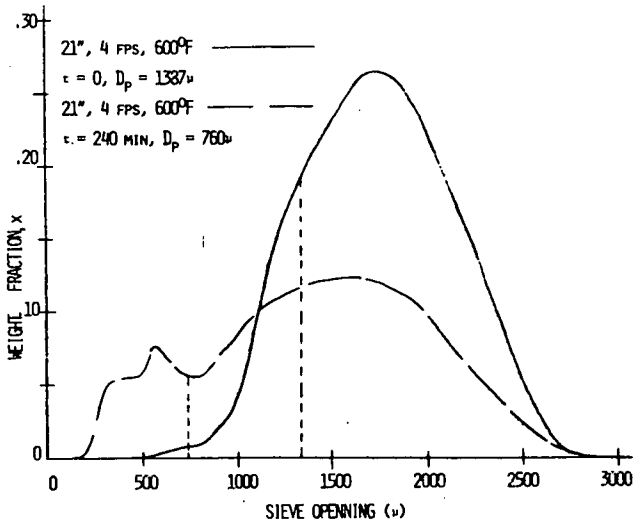

Fig. 12 Initial and Final Weight Fraction

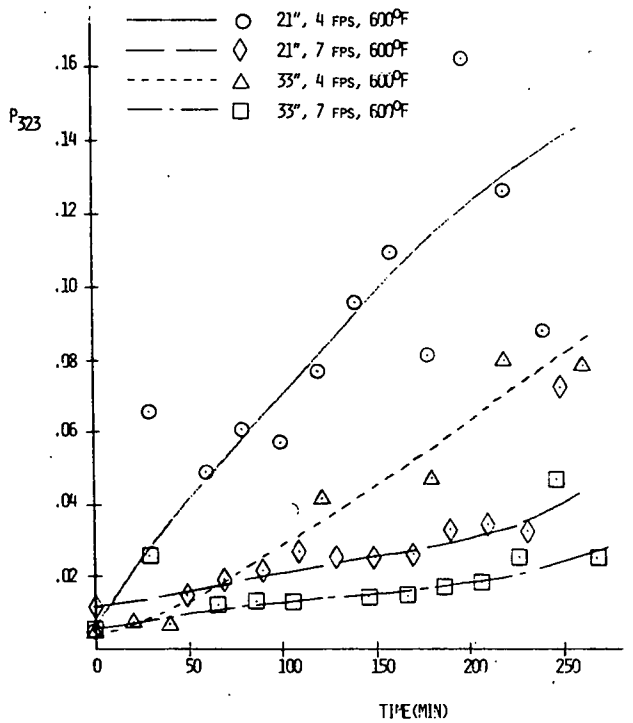

Fig. 13 Effect of Velocity & Bed Height on Build-up of Fines (<323μ)

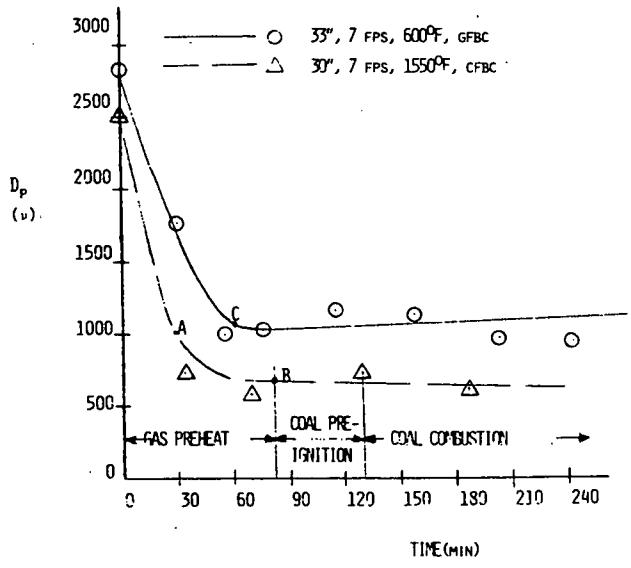

Fig. 14 Comparison of Gas-Fired & Coal-Fired Tests

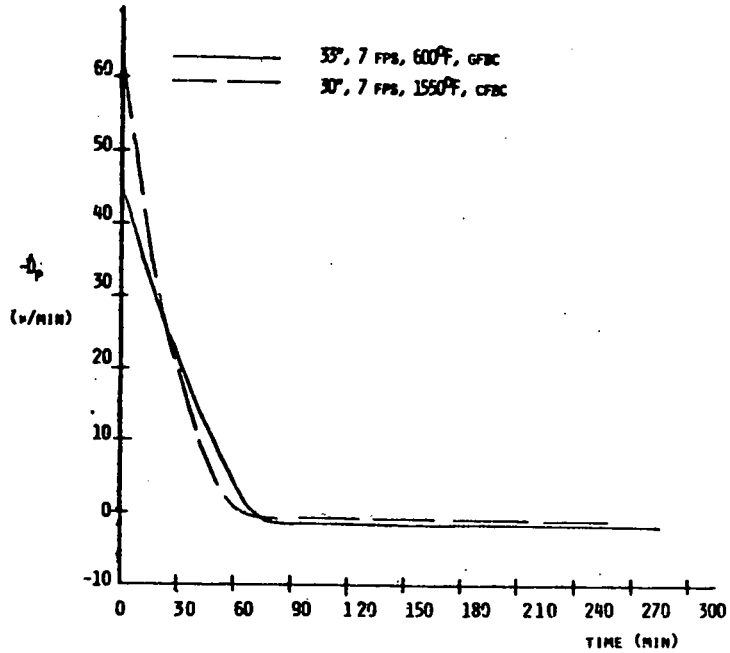

Fig. 15 Comparison of Gas-Fired & Coal-Fired Tests

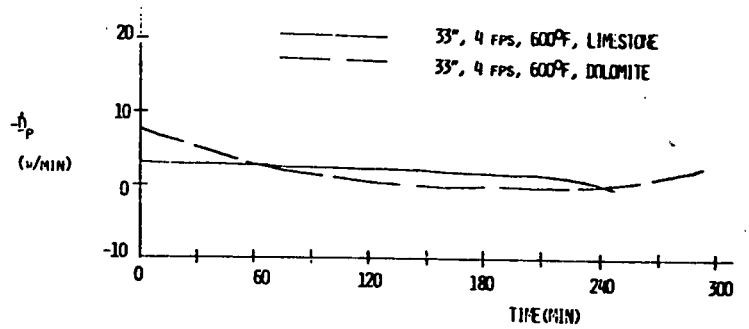

Fig. 16 Comparison of Sorbent Material

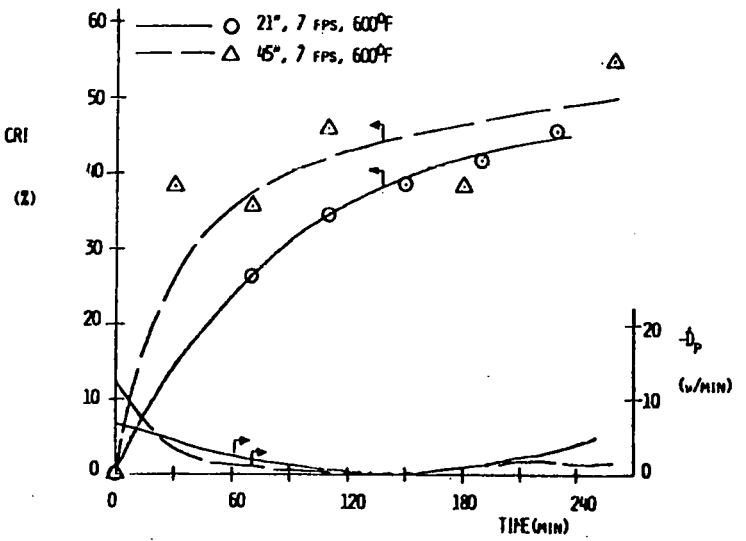

Fig. 17 Crushing Resistance Index - Trends

Question to Gabe Miller:

Q: (Participant not identified)

It is very difficult for us to get a controlled size limestone out of the field. After you are finished with limestone, when are you going to attack coal ash?

A: Incidentally, all these tests were with limestone right from the bag. We don't have any control of what comes in. That is why, at this point, we wouldn't have attempted to derive a correlation.

AN ASSESSMENT OF ADVANCED SULFUR REMOVAL SYSTEMS FOR ELECTRIC UTILITY AFBC

R. A. Newby, D. M. Bachovchin, C. H. Peterson,
N. D. Rohatgi, N. H. Ulerich, D. L. Keairns

Westinghouse R&D Center
Pittsburgh, PA

INTRODUCTION

Conventional once-through sorbent operation of atmospheric-pressure fluidized-bed combustors (AFBC) is expected to require calcium-to-sulfur (Ca/S) ratios of greater than about 2.5 in order to satisfy EPA New Source Performance Standards (NSPS) for utility boilers. High sorbent consumption rates are both an economic concern (the cost of sorbent contributes significantly to the cost of electricity, and the sorbent calcination energy significantly affects reduced plant efficiency) and an environmental concern (resource mining and delivery and spent sorbent disposal).

A multitude of techniques for reducing sorbent consumption have been conceived. In this paper we have identified and evaluated the process design, power plant performance, and cost of advanced processing techniques applied to AFBC for the purpose of reducing the consumption of sorbents. This effort is the basis for recommending the development and demonstration of one of these processes integrated with an AFBC development unit. The program was sponsored by the Electric Power Research Institute (EPRI) and was carried out in cooperation with the Babcock & Wilcox Company (B&W). The details of this work are reported in two annual reports to EPRI.[1,2]

SUMMARY

The objective of this study was to identify and evaluate the technical and economic potential of processes that minimize the consumption of sorbent in AFBC. We selected three advanced sulfur removal concepts for evaluation (sorbent pretreatment, agglomeration of carry-over material with recycle, and sorbent regeneration); three sorbent pretreatment alternatives (precalcination, salt addition, and heat treatment); and two configurations of a sorbent regeneration process.

A methodology that would allow comparison of the advanced process concepts was developed. Babcock & Wilcox specified the reference AFBC plant design parameters on which the evaluation was based. Two reference coals (western and eastern) and two reference sorbents were considered.

With the advanced processes and a 90 percent sulfur removal requirement sorbent consumption (for the eastern coal-fired AFBC plant design considered) can be reduced by 26 to 83 percent. Sorbent consumption can also be reduced for the western coal-fired AFBC plant, but the economic incentives do not support application of the advanced systems. Specific reductions in sorbent requirements depend greatly on the specific sorbent and the process.

The capital cost of the advanced processing option to break even with the once-through AFBC system can be from $150 to 300/kW (1978) with sorbent costs of $20/ton. Improved once-through operation (fines recycle, fine bed-particle size, etc.) will reduce the potential economic incentive to develop these advanced processes. Solid residue for disposal can be reduced to less than that produced from lime-scrubber systems.

The advanced sulfur removal systems considered are potentially economically and environmentally attractive, and we recommend further development. The agglomeration process (the recycling of pelletized coal ash and spent sorbent material) is the most attractive option for development. The technical uncertainties and developmental needs have been identified for each process.

SELECTION OF ADVANCED SULFUR REMOVAL CONCEPTS

The initial task in this study was to identify concepts for processes that would reduce the consumption of sorbent in AFBC and to select a few outstanding concepts to be evaluated. Nine broad groups of concepts were identified that would potentially reduce FBC sorbent consumption rates:

Once-through Concepts

1. Alternative once-through sorbents
2. Improved sorbent properties by pretreatment
3. Improved sorbent properties by in-situ combustor treatment
4. Sorbent recycle after posttreatment.

Regenerative Concepts

5. Alternative regenerative sorbents

6-9. Several sorbent regeneration schemes that potentially reactivate the sorbent chemically.

Techniques for treating the spent sorbent to produce a valuable by-product or an environmentally acceptable waste were not considered.

Altogether, some fifty concepts were proposed. The concepts identified were qualitatively ranked according to several factors:

- Availability of data
- Nature of the technology - largely conventional, developmental, conceptual, etc.
- Potential to reduce sorbent consumption
- General applicability (i.e., usable only in specific cases, such as with specific sorbents)
- Potential impact on plant cost, complexity, reliability, operability, electric utility acceptability, and environmental impact
- Nature of disadvantages - increased AFBC development time, increased corrosion, etc.
- Nature of advantages - increased combustion efficiency, reduced impact of sorbent properties variability, increased range of combustor operating conditions, etc.

The screening has resulted in the selection of three groups of concepts for evaluation:

1. Regeneration of the sorbent
   a. Reductive decomposition
   b. Once-through/regenerative combination
2. Pretreatment of the sorbent
   a. Precalcination
   b. Additive exposure
   c. Thermal exposure
3. Agglomeration processes (overhead fines agglomeration and recycle)

BASIS FOR PROCESS EVALUATION

Two coals were designated for consideration in this study, a high-sulfur (4.0 wt %) Illinois coal (heating value of 10,100 Btu/lb, 16.1 wt % ash), and a Wyoming Powder River subbituminous coal (0.48 wt % sulfur, 6.4 wt % ash, heating value of 8,020 Btu/lb). Current NSPS require 90 percent sulfur removal for the Illinois coal and 70 percent for the Wyoming.

Two sorbents were considered for each process case except agglomeration. No second sorbent was considered for tho agglomeration process because we lacked data and assumed an insensitivity of this process to sorbent type. Greer limestone was considered for all three processes, and a second specific sorbent was selected for each process on the basis of the data available. In addition, an unspecified sorbent was considered for parametric studies.

Babcock and Wilcox provided combustor operating conditions, sorbent feed size distribution, Greer limestone composition, specific assumptions for elutriation rates, combustion efficiencies, and sulfur release efficiencies in the main beds and carbon burnup cell (CBC). Operating conditions and performance assumptions for the fluidized-bed combustor are shown in Table 1. The items shown are those required for projecting the sorbent consumption rate for each process.

DETERMINATION OF BASE CALCIUM-TO-SULFUR RATIOS

Projections of sorbent requirements for once-through AFBC operation and AFBC operation with the advanced sulfur removal systems were developed using a consistent basis. The projections of Ca/S molar feed ratios required to satisfy current NSPS were derived by using a model for fluidized-bed desulfurization and kinetic rate constants obtained from laboratory thermogravimetric (TG) data.[3,4] Data developed by Westinghouse, Argonne National Laboratory (ANL), and the University of Maryland were applied. The key uncertainties in the assumed combustor performance parameters were identified and the sensitivity of the projections to these uncertainties considered. Calcium-to-sulfur molar feed ratios representing likely values within the range projected were selected for each process.

Table 2 summarizes the base Ca/S ratios determined for once-through operation and for the advanced sulfur removal systems. These specific values were applied in process material and energy balances, along with parametric values of the Ca/S ratio for an unspecified sorbent.

SORBENT PRETREATMENT

Available data on these sorbent pretreatment processes were reviewed to identify key parameters, define ranges of operating conditions, and determine various process options. Material and energy balances and auxiliary power requirements were calculated for the three selected pretreatment processes.

Background

Precalcination

Existing data show that significantly improved sorbent utilization can be obtained by controlling calcination of the sorbent prior to sulfation. To date, ANL and Westinghouse have defined the following parametric ranges:[5]

1. Limestone studied = Greer, Carbon (Lowellville), Grove (1350) and Pfizer dolomite (1337)

Table 1

FLUID-BED COMBUSTOR ASSUMPTIONS

	Once-through	
	Illinois	Wyoming
Main Beds		
Temperature °C (°F)	843 (1550)	843 (1550)
Velocity, m/s	2.44	2.44
Bed Depth, m	1.22	1.22
Excess Air, %	15	15
Bubble Volume, %	40	40
Inert Volume, %	10	51
Tube Volume, %	10	10
Sorbent Attrition Rate, % of Feed	15	15
Sorbent Elutriation Rate, % of Feed[A]	35	35
Bed Particle Size, μm (Surface Mean)	900	900
Ash Elutriation Rate, % of Feed	75	75
Sulfur Release, % of Total	88	92[G]
Sulfur Absorbed, % of Released	91.6	72.4[G]
Sulfation of Overhead Sorbent, %	22	30
Sulfation of Coal Ash CaO, %	0	30
Carbon Burnup Efficiency, %	85	85
Carbon Burnup Cell		
Temperature, °C (°F)	1093 (2000)	1093 (2000)
Velocity, m/s	2.44	2.44
Bed Depth, m	1.22	1.22
Bubble Volume, %	40	40
Inert Volume, %[B]	85	85
Tube Volume, %	0	0
Excess Air, %	50	50
Sorbent Elutriation, % of Feed[A]	100	100
Ash Elutriation, % of Feed	100	100
Bed Particle Size, μm[B]	900	900
Sulfur Release, % of Total Feed	88	88
Sulfur Absorbed, % of Released	75	37
Sulfation of Coal Ash CaO, %	0	
Carbon Burnup Efficiency, %	88	88
Sulfur Feed to CBB, % of Total	12	8.0

Dwg. 2626C44

Table 2

PROJECTED PERFORMANCE (Ca/S RATIOS) OF THE SULFUR REMOVAL SYSTEM

Once-through	Eastern Coal	Western Coal
Greer Limestone	4.2	0.7
Grove Limestone	6.3	1.0
Tymochtee Dolomite	3.0	0.4
SORBENT REGENERATION		
Reductive Decomposition with Sulfur Recovery		
Greer Limestone	a	b
Tymochtee Dolomite	0.6	b
Reductive Decomposition with Spent Sorbent Sulfation		
Greer Limestone	a	b
Tymochtee Dolomite	1.5	b
SORBENT PRETREATMENT		
Precalcination		
Greer Limestone	3.1	0.5
Grove Limestone	3.7	0.6
Salt Exposure		
Greer Limestone	2.3	0.4
Grove Limestone	1.1	0.2
Heat Treatment		
Greer Limestone	2.0	0.3
Grove Limestone	3.7[c]	0.6[c]
AGGLOMERATION		
Greer Limestone	1.4	0.3

a - Cannot achieve 90% sulfur removal with Greer limestone (due to high loss of activity on recycling) at a reasonable Ca/S ratio.
b - Cannot achieve reasonable Ca/S ratios due to high ash accumulation.
c - Heat treatment does not improve Grove limestone performance relative to precalcination.

2. Calcination temperature = 815°C - 935°C

3. CO_2 atmosphere = 15% - 60% (at atmospheric pressure)

4. Retention time (at calcination conditions) = 0 hr - 4 hr

5. Heating rate = only qualitative results are available, but higher heating rates before and during calcination seem to produce stones of lower porosity and less reactivity.

These parameters can act individually or collectively to change the activity (percent utilization) of the calcined sorbents. Sorbent utilization generally improves with increasing calcination temperature, increasing CO_2 partial pressure, and increasing retention time. The optimum calcination conditions remain specific to each sorbent type and must be determined experimentally.

Use of Salt Additives

As early as 1968, Pope, Evans and Robbins successfully used alkali salts to enhance the sulfur capacity of limestone sorbent in the fluidized-bed

combustion of coal. They found that solid salt particles, fed in small amounts to the combustion zone, would drastically reduce the level of SO_2 emissions from fluidized-bed combustors with limestone beds. Argonne National Laboratory has carried out work to determine the effects of salt additives on the operation of fluidized-bed combustors with regard to SO_2 retention and potential corrosion in the combustor system. Preliminary results have indicated that salt additives in small amounts (up to 1 mole %) could enhance the reactivity and capacity of sorbents. Researchers reported that most salt additives (NaCl, $MgCl_2$, and $CaCl_2$) affected the pore size distribution of sorbents during calcination by accelerating the rate of sintering and crystal growth.[6]

Argonne National Laboratory has studied 15 different limestones and 11 salt additives in various combinations to determine optimum salt concentrations and sorbent-salt combinations. Its investigators concluded that because most of the salts tested have measurable effects (either positive or negative), all are potential sulfation-enhancers at proper salt concentrations. The salt used and its optimum concentration depend on the composition and morphology of the original sorbent stone. The maximum sulfations achievable for a particular stone and salt combination must be determined experimentally.

Heat Pretreatment

Argonne National Laboratory is currently studying the enhancement of limestone reactivity by heat treatment.[7] Investigators heat treated five limestones - Greer, Grove (or 1359), Germany Valley, Chaney, and 2203 - at various conditions to determine the percentage increases in calcium utilization. They identified and studied the following parameters:

1. Limestone source = Greer, Grove, Germany Valley, Chaney, and 2203
2. Calcination temperature = 900-1100°C
3. Calcination atmosphere = 20% CO_2 - balance air
4. Heat-treatment temperature = 1000-1200°C
5. Time of heat treatment = 5 - 180 minutes
6. Heat-treatment atmosphere = air, 20% CO_2 - balance air.

Preliminary results indicated that heat treatment seemed to be beneficial for some stones and not for others. Greer, Germany Valley, and 2203 showed increased utilization after heat treatment at 1000°C for 15 minutes, as compared with calcination and sulfation at 900°C, while Chaney and 1359 resulted in no change in calcium utilization after heat treatment.

Selection of Process Configuration

A schematic diagram of the selected process configuration for the pretreatment of sorbents is shown in Figure 1. This simple configuration allows the pretreatment system to operate independently of the AFBC boiler system. The main streams connecting the two systems are the pretreatment system coal feed, the lime product stream, and the pretreatment system effluent gas flow. Various options exist: the pretreatment coal can be drawn from the same silos that feed the AFBC boiler main beds or from silos built especially for the pretreatment system. The product lime can be mixed with the combustion coal before entering the main beds or it can be introduced directly into the beds via a system of lime distributors. The cooled effluent gas from the pretreatment system can be combined with the flue gas from the main beds and passed through the hot electrostatic precipitators.

The pretreatment system includes primarily a staged fluidized-bed calciner, an air blower, an optional lime-storage reservoir, and, when needed, a salt additive silo and a salt feeding system. The staged fluidized bed has been successfully used by Dorr-Oliver, Inc., in a Fluosolids lime kiln for the commercial calcination of limestone.[8]

In the precalcination option (Figure 2), at steady state, the crushed and sized limestones (stream S1) are fed to the preheating stages and are heated by the hot effluent gases from the calcination stage. The cooled gases (stream G6, S6) that leave the preheating stages combine with the flue gas from the main fluidized-bed combustor. The heated stones enter the calcination stage where lime and CO_2 are formed from the decomposition of limestone. Coal (stream S2) is fed directly into the calcination stage where its combustion in air provides the energy required for the endothermic calcination reaction. The CO_2 evolved during coal combustion and limestone calcination retards the reaction to allow the formation of adequate lime pore sizes, necessary for improved stone utilization during sulfation in the main atmospheric fluidized-bed combustors. Combustion air (stream G5), supplied by an air blower, is preheated by the outgoing lime product in the cooling stages of the calcination unit. The cooled lime (stream S7) is fed directly to the main fluidized-bed combustors or stored in a reservoir. The presence of a lime-product reservoir permits the calciner to operate independently of the main combustors.

In the option using precalcination with salt additive, the alkali salts (stream S4, G4) are introduced into the precalcination stage where they help accelerate the rate of sintering and crystal growth and increase the extent of calcination in calcite. A large fraction of the salt vaporizes into the gas stream and passes through the preheating stages. As the temperature decreases from one preheating stage to the next, condensation of the salt vapor on the sorbents occurs. The condensed salt is carried by the sorbents to the calcination

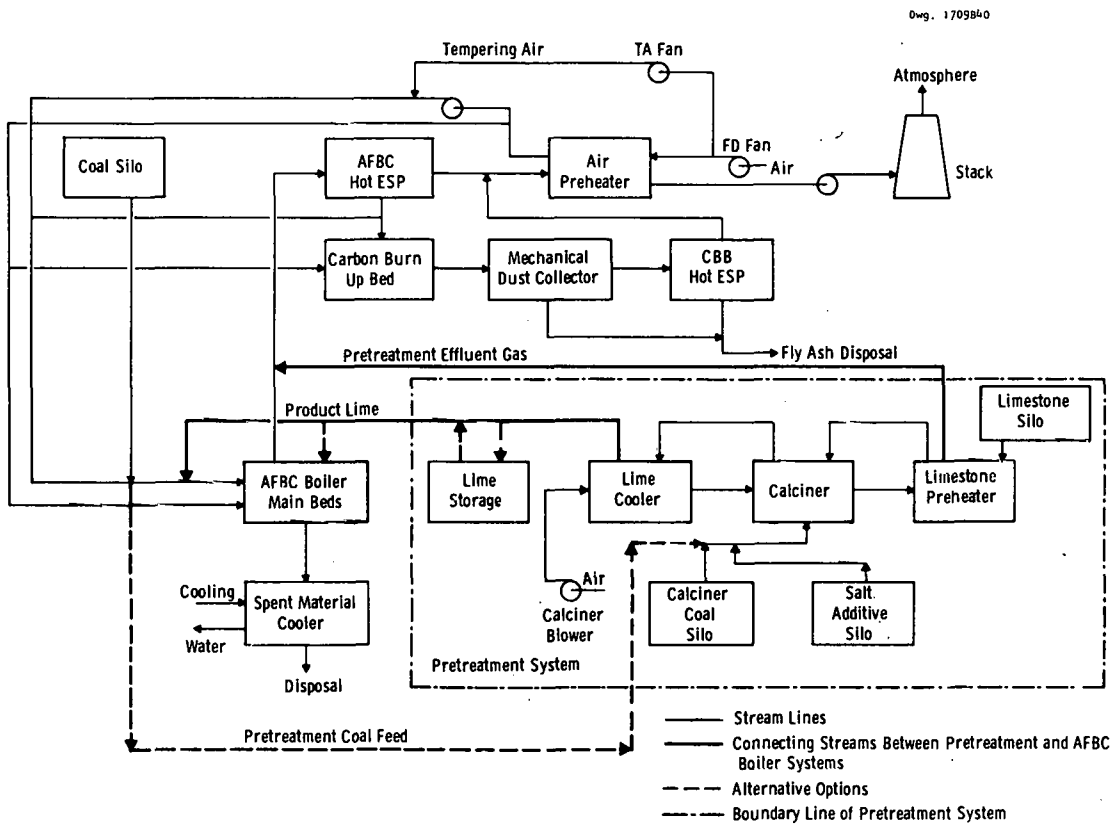

Figure 1 - Process Configuration for the Pretreatment of Sorbents

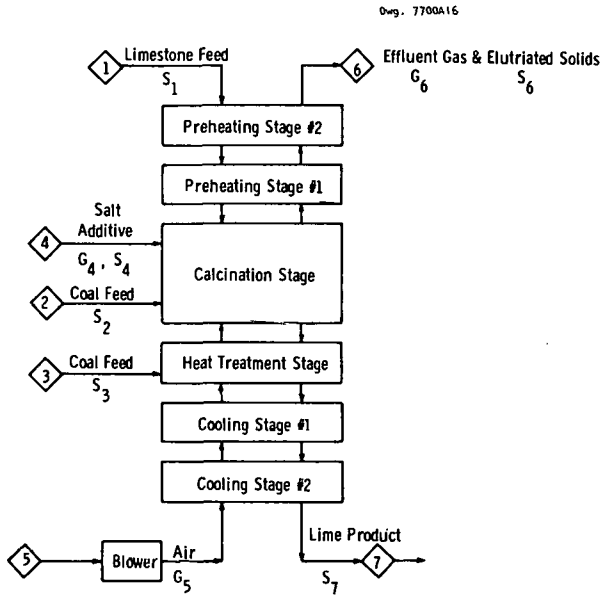

Figure 2 - Schematic Flow Diagram of the Staged Fluidized Bed in the Pretreatment System

stage where it again evaporates. In this manner there is always an inventory of salt in the fluidized bed, and only a small fraction of the salt feed escapes in the effluent gas stream.

In the option using precalcination with heat treatment, the calcined sorbents are transferred from the calcination stage to the thermal treatment stage, where the combustion of additional coal (stream S3) keeps the sorbents at the required treatment temperature.

Selected Operating Conditions

Operating conditions were selected for the development of material and energy balances around the calcination unit. They do not constitute the optimum conditions for the calcination reaction but, rather, represent a set of effective operating conditions based on available experimental data. The major conditions are as follows:

Calcination Temperature and CO_2 Pressure

The calcination temperature is set at 1562°F for all the cases considered. In the precalcination unit, where CO_2 is supplied by coal combustion and stone calcination, material balances suggest a typical CO_2 concentration of 30 to 35 percent of the total effluent gas. With this CO_2 partial

pressure the temperature was chosen to yield an adequate ratio of CO_2 partial pressure over CO_2 equilibrium pressure.

Sorbent Retention Time in the Calcination Stage

The average retention times necessary to achieve 100 percent calcination have been calculated for Greer and Grove limestones on the basis of a simplified calcination model Westinghouse developed: about 2.5 hours for Greer and 1.5 hours for Grove. Experimental results, however, show that the actual time needed for complete calcination is usually greater than estimated, thus suggesting a value of 3 hours for the average sorbent retention time in the calcination stage.

Temperature and Time of Heat Treatment

On the basis of the limited available data, the temperature and time of heat treatment, when applied, are set at 1000°C (1832°F) and 0.5 hr.

Concentration of Salt Additive

The concentration of salt additive, NaCl, when applied, is 1 percent of the sorbent weight for the hypothetical stone and for Greer limestone and 0.5 weight percent for Grove limestone. These concentrations have been chosen to provide maximum sorbent utilization, based on available experimental data. Since much of the data deal with sodium chloride, NaCl is the selected salt additive.

Material and Energy Balance Assumptions

The following general assumptions were made in the material and energy balance calculations:

- The fraction of calcium that is calcined to the calcination stage is 0.99.
- The fraction of limestone elutriated is 0.04.
- The fraction of char attrited is 0.1.
- Sulfur retention in the calcination stage is 0.98.
- Excess air in the calcination unit is 15%.
- The ash released during coal combustion is divided into two streams = 60% of the total weight of ash carried over in the effluent gas stream and 40% discharged along with the lime product.
- The inventory of salt available in the calciner, due to constant evaporation and recondensation, is equal to 90 percent of the salt feed. Of the remaining, 36.7 percent is retained in the ash, 54.7 percent is in the sorbent (mostly as silicates), and 8.6 percent is carried out by the effluent gas stream.

Material and energy balances for the hypothetical stone were calculated by using a range of values for the parameter Ca/S.

AGGLOMERATION

The agglomeration process pelletizes fluidized-bed boiler carry-over with the aid of spent bed material and returns the pellets to the combustor to complete the combustion of carbon and more fully utilize the lime. Thermogravimetric data on 2380 to 5664 μm diameter agglomerates reported by the University of Maryland were applied to make performance projections.[9,10]

Process Description

Figure 3 shows a simplified process flow diagram of the agglomeration process with its interconnections to the main FBC process. Spent bed material (fresh sorbent feed plus spent agglomerates) is withdrawn and cooled to 150°F. Indirect cooling and direct-contact air cooling, but not water spraying, are possible alternatives. The oversize material (the agglomerates) is separated by mechanical screening and stored for disposal. Undersize material (<3000 μm) is transferred to a grinding system, represented by a mill, a sieve, and an elevator, in which 100 percent of the solids are reduced to <125 μm. The material is blended with electrostatic precipitator fines, cooled to 150°F, and fed to a pelletizer. The water added for pelletizing also permits cementitious reactions to occur. The pellets are allowed to grow sufficiently to be distinctly different in size range from the spent bed material. The pellets are assumed to have sufficient strength to withstand subsequent handling and processing. The procedure permits mechanical separation of the spent bed material from the recycled pellets.

The pellets are cured in a suitable chamber, which may be visualized as an enclosure through which the pellets are moved on conveyor belts. The curing environment is atmospheric-pressure steam. The residence time is taken as eight hours for initial estimates.

The cured pellets are sieved, oversize ones are returned to the mill, and fines are returned to the blender. The midfraction is recycled to the combustor.

Material Balance Assumptions

Table 3 summarizes key process material balance assumptions. The process is visualized as occurring in two passes to facilitate defining process parameters. In the first pass fresh limestone (Greer limestone) and coal are fed to the combustor. All of the bed material drawn off is combined with the precipitator catch and fed to the pelletizing section. The pellets made constitute the second pass feed to the combustor.

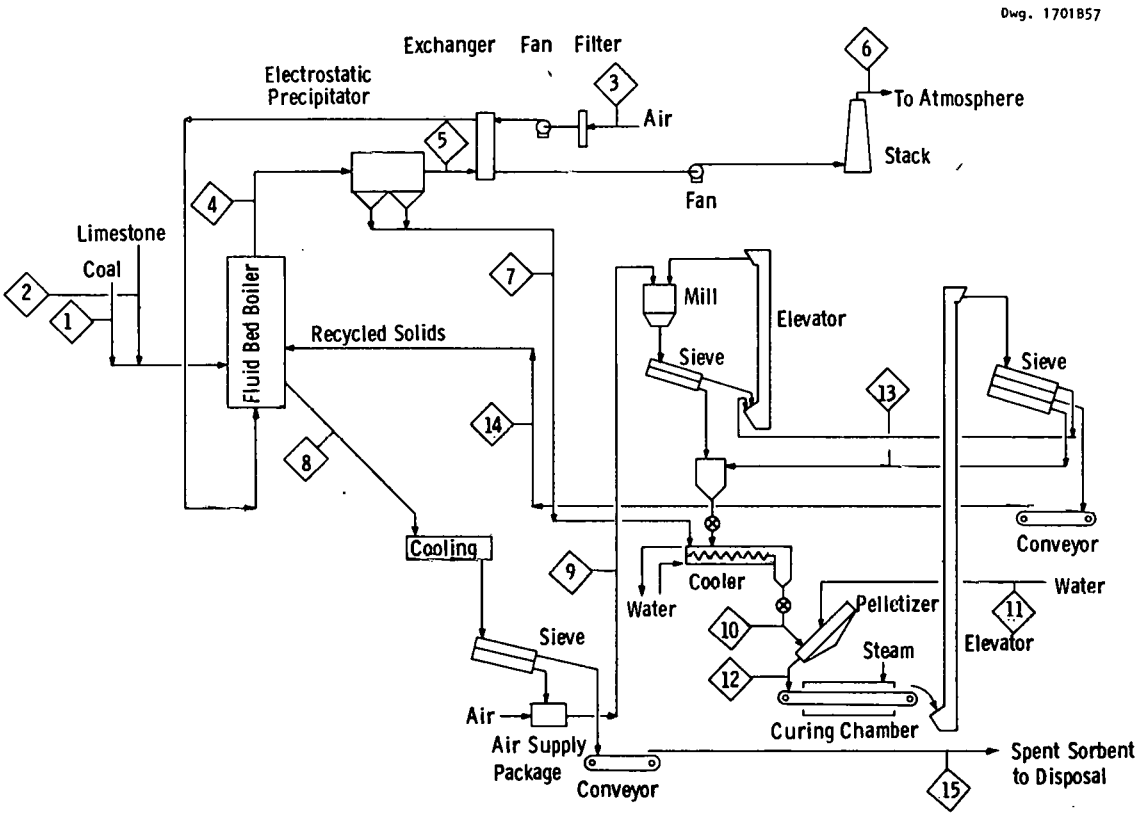

Figure 3 - Process Flow Diagram for Atmospheric Pressure Fluidized-Bed Combustion Showing Recycle of Main Bed Carry-over after Pelletization

While the University of Maryland data indicate high reactivity for the pellets of Greer limestone and high carbon burning rates, further work is needed in the laboratory to confirm certain key assumptions:

- FBC residues can be ground to 100 percent through 125 μm, pelletized with the aid of water, and cured in 8 hours or less to a product that can be recycled through the combustor bed with no more than a 10 percent attrition loss.
- These pellets will have sufficient chemical reactivity to permit absorbing the necessary amount of SO_2 to meet EPA emission standards.
- Residual carbon can be burned off to achieve the overall target of 99 percent utilization.
- First-pass sorbent can be separated mechanically from the spent second-pass pellets.
- Fluidization dynamics will not be seriously affected by the pellet recycle.

SORBENT REGENERATION

Two processes were considered for the reduction of AFBC sorbent requirements by the continuous regeneration of sorbent. These were a one-step reductive decomposition and a once-through/regenerative hybrid scheme.

A kinetic model of the basic reductive decomposition reactions was developed. This model and the Westinghouse sulfur capture model were used to produce computer simulations of the processes. The model accounts for regeneration and sulfur capture activity loss with prolonged sorbent residence time. Using the simulation, we conducted parametric studies of the effects of major variables.

The regeneration concepts we selected for study were:

- Reductive decomposition. The $CaSO_4$ generated in the combustor is reduced by the following reactions in the regenerator, with CO and H_2 being generated by partial combustion of coal:

$$CaSO_4 + CO \longrightarrow CaO + SO_2 + CO_2 \quad (1)$$

$$CaSO_4 + H_2 \longrightarrow CaO + SO_2 + H_2O \quad (2)$$

Table 3

PROCESS MATERIAL BALANCE ASSUMPTIONS

First-Pass Material		
Coal carbon combustion	88%	
Coal sulfur release	99%	
Calcium sulfation	14.8% (eastern coal)	19.0% (western coal)
Second-Pass (pelletized solids)		
Unconverted carbon	1% of total feed carbon	
Attrition loss	10%	
Pellet size	3000-6000 μm	
Water rate	15% of total weight	
Curing time	8-12 hr at 150-180°F with atmospheric-pressure steam	

Sulfur dioxide is removed from the off-gas by a commercially available process.

- Once-through/regenerative combination. Regeneration occurs in the same manner as above, but SO_2 is removed by the virtually complete sulfation of the spent CaO (increased in reactivity by particle size reduction).

Data Assessment

A detailed literature review of sorbent regeneration is given by Swift et al.[11]

Argonne National Laboratory[12,13] experimentally studied the one-step regeneration reactions given by equations (1) and (2). The tests were made over a temperature range of 1000 to 1100°C, with a particle size of about 1100 μm. In a 7.62-cm id reactor at 1.8 atm, researchers reduced Tymochtee dolomite (sulfated to 10.2 wt % S), using methane as the fuel. The dolomite had been sulfated in a fluid-bed combustor, and the regenerator had a bed depth of 0.46 m, the lower half of which was an oxidizing zone. They achieved 15 to 89 percent regeneration. Tymochtee dolomite and Greer limestone also were regenerated using coal in a 10.8-cm regenerator at 1.5 atm. Regeneration approached 95 percent under some conditions.

On the basis of these data, we were able to develop kinetic expressions for the regeneration reactions. The shell-burning model used in the development predicts that rates are inversely proportional to particle size.

Argonne also made cyclic combustion-regeneration tests to examine sorbent activity loss with time. Tymochtee dolomite was continuously fed as sorbent to a 6-in-diameter pressurized combustor at 8 atm. At the conclusion of each test the sulfated dolomite was fed to the above-mentioned regenerator at 1.5 atm and 1100°C. This quasi-continuous method was continued for ten cycles. The method permitted tight residence time distributions determinable at any point in the series. Loss of both combustion and regeneration activity was recorded. Similar tests were made with Greer limestone using a 3-atm combustor. Again, declining activity was apparent. We developed expressions for sorbent sulfation and regeneration activity loss based upon a first-order catalyst deactivation model.

Process Development

One-Step Reductive Decomposition

In the regenerator vessel $CaSO_4$ is reduced in a fluid bed following reactions 1 and 2 above. The fluid bed is maintained at as high a temperature as possible without agglomerating the bed material. At high temperature equilibrium and kinetics permit essentially complete conversion and maximization of the SO_2 concentration in the regenerator exhaust gas, necessary for lowering sulfur removal system costs. Reducing-gas for reactions 1 and 2 is supplied by partial combustion of coal in the regenerator.

The conceptual flow sheet for the basic reductive decomposition scheme is shown in Figure 4. The regenerator operates at 1000 to 1100°C and consists of a fluid bed vertically divided into oxidizing and reducing zones of approximately equal volume. The reducing zone features reactions 1 and 2 above, which are endothermic. The oxidizing zone serves to: produce reducing gas for the $CaSO_4$ decomposition, supply heat for the endothermic regeneration reaction and for heating the solid and gaseous reactants to the regeneration temperature, and consume CaS generated in the reducing zone when solids are mixed downward.

The regenerator off-gas is used to preheat the fluidizing air via indirect heat exchange. A greater heat exchange will require that less coal be consumed in the regenerator and will improve regeneration efficiency. The off-gas then goes to the primary sulfur capture plant which may be, for example, the commercial Allied Chemical process or the still developing Foster-Wheeler RESOX process. Inefficiency in primary sulfur recovery may require a secondary sulfur capture plant, such as the

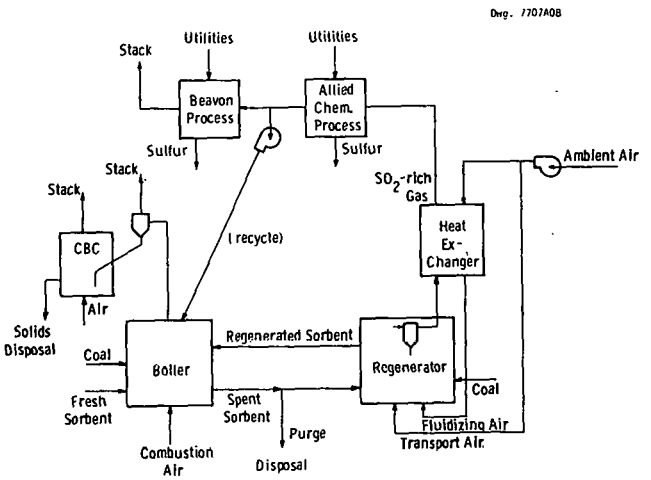

Figure 4 - Reductive Decomposition - Basic Flow Scheme

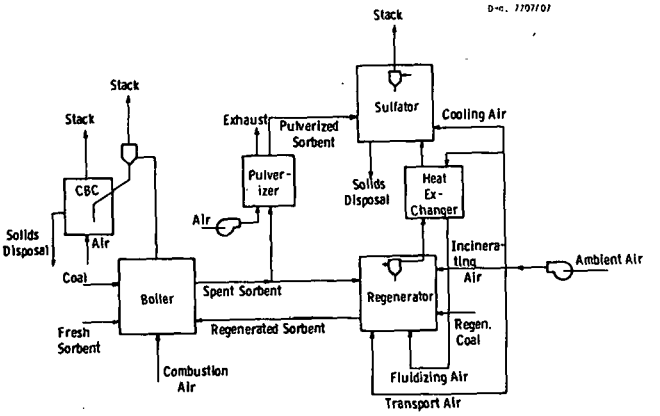

Figure 5 - Once/through Regeneration Combination Scheme

Beavon process of the Ralph M. Parsons Co. Alternatively, the regenerator gas may at this point be recycled to the boiler, increasing combustor sulfur load but eliminating the cost of the secondary sulfur plant.

Sorbent may be purged before and/or after regeneration. The former choice minimizes CaS and CaO emissions and reduces the load on the regenerator. The latter choice may permit higher SO_2 concentrations in the gas going to sulfur recovery.

Other parameters, for a given plant size, include regenerator bed area, temperature, bed depth, fluidizing air preheat, and fluidizing velocity. The fluidizing air rate determines the coal rate necessary to maintain the bed at the chosen temperature. Combustor operating conditions such as bed depth, fluidizing velocity, and sorbent recycle rate are important. Successful regeneration may require system optimization of these variables. The entrainment control system in the combustor determines sorbent losses and sets the lower limit on sorbent makeup rate.

Once-through/Regenerative Combination

The reductive decomposition regenerative/once-through scheme is illustrated in Figure 5. The purpose of this scheme is to eliminate the costly primary SO_2 package in the basic scheme by disposing of highly sulfated sorbent. This choice would limit the minimum achievable Ca/S mole ratio to something greater than 0.9 for the eastern coal and 0.7 for the western coal.

The success of this scheme will depend on the virtually complete sulfation of sorbent in a separate sulfation step. The sorbent may come from either before or after the regeneration step, and disposal may be made solely from the sulfator. The former case will again allow a lower load on the regenerator, while the latter may permit higher rates because of increased SO_2 gas concentrations.

High conversion in the sulfator requires either a long residence time or reaction rate enhancement, which would most likely be achievable by particle size reduction.

Parametric Study of Basic Process

Computer models of the processes were developed. The basic process simulation was used for an initial parametric study. We assumed that elutriated sorbent and combustibles are efficiently returned to the bed. We also assumed 75 percent of the coal ash was eventually removed by elutriation from the combustor. This is important because ash collects in the recirculating system and can significantly dilute the bed material.

The base conditions for the regeneration system are as follows:

Temperature	1100°C (2012°F)
Pressure	1.38 atm
Area	40 m^2 (430 ft^2)
Depth	1.0 m (3.3 ft)
Regenerator air preheated to	927°C (1700°F)

Fresh sorbent: Tymochtee dolomite

75% of coal ash removed by elutriation

5% regenerator carbon loss

No tail-gas recycle

Calcium-to-Sulfur Mole Ratios. Figure 6 shows how overall sulfur capture and regenerator gas SO_2 concentration vary with regenerator coal rates at several makeup Ca/S ratios. As expected, the higher Ca/S values yield better performance. The plateaus at higher coal rates in the top half of Figure 6 correspond to virtually complete regeneration.

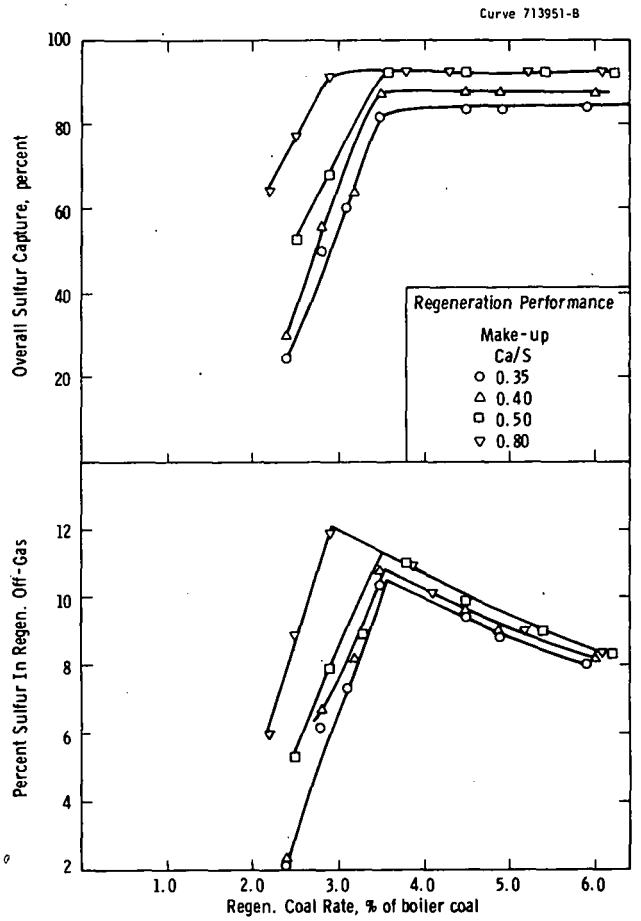

Figure 6 - Regeneration at Various Makeup Ca/S

At low makeup ratios regeneration can be pushed to completion, but performance is limited by the sulfur-capture rate in the combustor. Increasing solids residence time in the combustor is counterproductive after a point because sorbent loses activity with prolonged exposure to combustor conditions.

Regenerator Design Parameters. Figure 7 shows the effect of regenerator bed area. As expected, the larger bed is more effective unless complete conversion is obtained. This is also the case with regenerator bed depth (Figure 8).

At least under some conditions, better performance can be obtained at lower temperatures. This

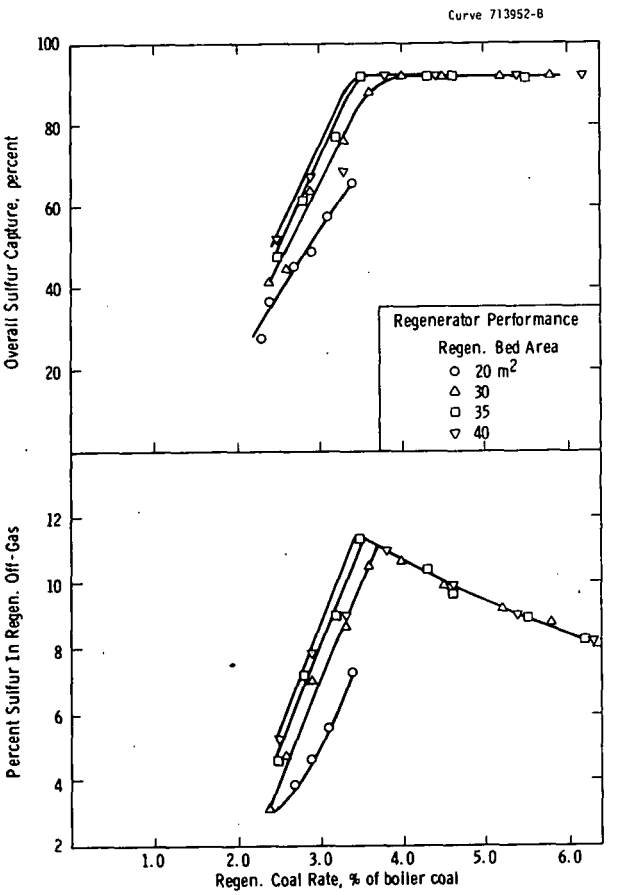

Figure 7 - Regeneration at Various Regenerator Bed Areas

is because more air must be used under fuel-rich conditions, at a given coal rate, to obtain a higher temperature, increasing the amount of CO_2 and H_2O at the expense of the reducing gases CO and H_2. Operation near 1100°C is nonetheless encouraged to avoid equilibrium limitations.

The effect of increasing regenerator air preheat is to reduce the air requirement at a given coal rate, increasing the reducing-gas concentrations. Preheat should be maximized, subject only to economic constraints.

Combustor Parameters. Changing combustor bed depth and superficial velocity, respectively, will influence regenerator performance. The depth effect, better performance at lower depth, is the result of activity loss with residence times that are too long. The velocity effect seems to go through a maximum. There is a trade-off here between detrimental added residence time (larger bed area) and the more efficient contact made at lower velocity.

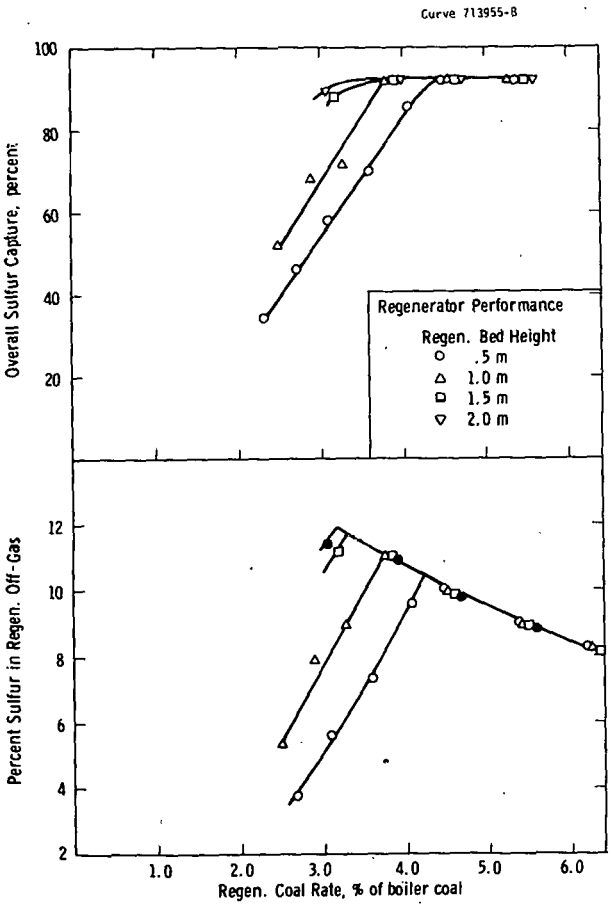

Figure 8 - Regeneration at Various Regenerator Bed Depths

Flow Sheet Options. Performance is insensitive to sorbent withdrawal location. Withdrawing after the combustor appears marginally favorable except at complete regeneration.

Another process option is to bypass the second-stage sulfur recovery plant and recycle regenerator gas to the combustor. This procedure results in slightly lower overall efficiency but higher acid gas concentration in the regenerator off-gas. A somewhat higher makeup or total Ca/S requirement will be the price for eliminating the extra equipment.

Ash Recycle. In any recycle system inerts tend to build up to an equilibrium concentration greater than would exist for once-through systems. In the present case coal ash will collect in the recycle loop, causing significant dilution of bed material unless the ash is largely permanently removed by elutriation. Because elutriated fines should be returned to the combustion system to minimize char and sorbent losses, ash will also be kept in the system.

The dilution of bed material will reduce contact efficiency and sorbent residence time, which will be detrimental to process performance.

We were unable to apply sorbent regeneration successfully to the western coal because the low sorbent rates per unit of coal ash fed result in great dilution of the boiler and regenerator beds with unreactive material. The result is low boiler sulfur-capture performance. The large quantity of recirculated ash per mole of $CaSO_4$ fed to the regenerator requires excessive coal and air rates to be heated to reaction temperature. Achieving a high SO_2 concentration in the regenerator off-gas, therefore, is impossible. Adequate performance could be achieved only by increasing the sorbent makeup rate nearly to the level needed for once-through operation and reducing the recycle rate to a very low level.

Material Balances

For comparison of the various sulfur removal system options, material balances were generated for a variety of regenerative systems with requirements for 90 percent sulfur removal for eastern coal. Assumptions were as listed above except that we assumed that coal ash elutriation rate would be proportional to the fraction of ash in the combustor beds rather than be simply a fixed fraction of the feed rate.

Complete searches for optimum conditions were run for Greer limestone and Tymochtee dolomite for both processes. The result for Greer limestone was that while we could readily obtain 85 percent sulfur removal at favorable conditions (Ca/S makeup ratio of (~0.5), we could not obtain 90 percent except at very high makeup (~2.0) and recycle ratios, in which case regenerator exhaust gas contained 3 percent or less SO_2. This inability to achieve 90 percent sulfur removal is because of sorbent activity loss at low makeup rates, while sulfation kinetics asymptotically approach complete capture of sulfur released in the main beds. The regenerator heat load with high sorbent recirculation rate is excessive, calling for more coal, more air, and more dilution. The sulfur recovery prospects would be very unfavorable. For these reasons we considered use of Greer limestone unfeasible and did not generate material balances. Note, however, that sulfur capture exceeded 85 percent over a wide range of conditions, and that within data and correlation error Greer limestone might be capable of achieving 90 percent sulfur capture.

Tymochtee dolomite, on the other hand, proved capable of achieving 90 percent sulfur capture over a wide range of conditions, such as regenerator fluidizing velocity, air preheat, bed area, and bed depth. For the once-through/regenerative hybrid scheme, variables included the above as well as sulfator vessel variables - velocity, bed depth, bed area, and reduced particle size.

EVALUATION

The overall performance factors for the processes investigated have been compared. The Ca/S

feed ratio, the solid waste production rate, the power plant efficiency, the technical uncertainties associated with the processes, and the break-even cost for the advanced sulfur removal systems are key factors in the evaluation.

Calcium-to-Sulfur-Feed Ratio

Figures 9 and 10 display the projected Ca/S ratios for the three sorbents considered (Greer limestone, Grove limestone, and Tymochtee dolomite) used as once-through sorbents and in each of the six advanced processes. There is a significant reduction in Ca/S ratio relative to the once-through case for each sorbent for both the eastern and western coals.

For the three pretreatment processes it is interesting to observe that Greer and Grove limestone behave much differently. Grove is very reactive on exposure to salt, but its performance when heat treated, relative to its precalcination performance, is not improved. We expect, however, that all sorbents will exhibit large differences in

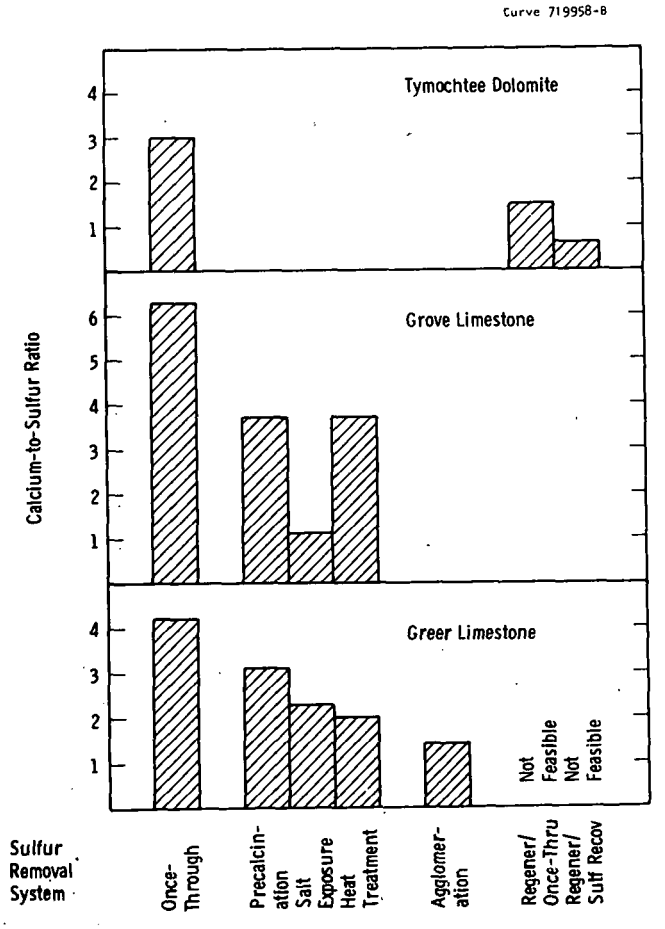

Figure 9 - Projections for Eastern Coal - 90% Sulfur Removal

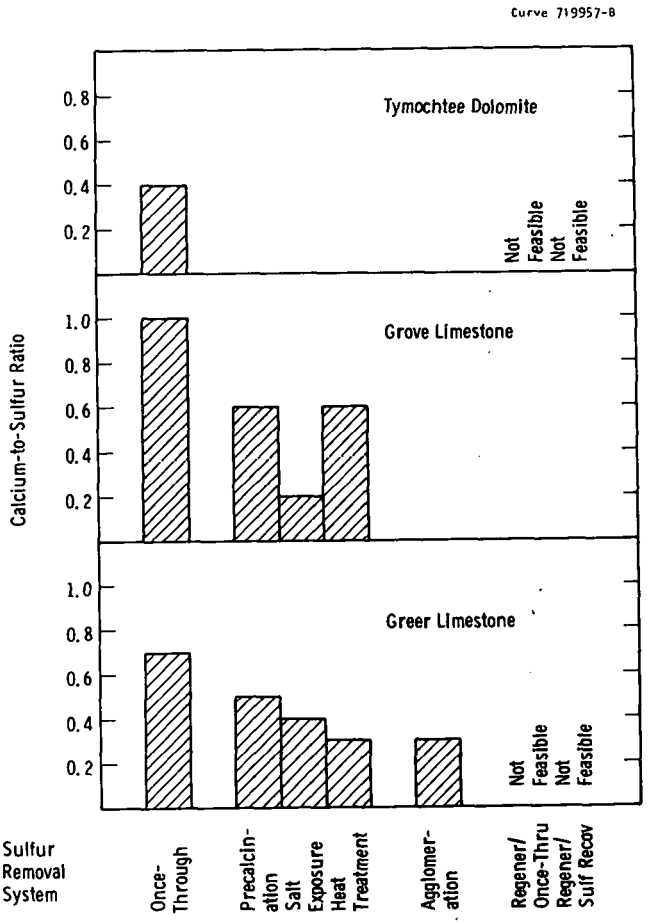

Figure 10 - Projections for Western Coal - 70% Sulfur Removal

their relative performance following precalcination, salt exposure, and heat treatment, due to differences in their physical structure and their chemical impurities.

Solid Waste

The production of solid waste for each of the advanced sulfur removal systems is illustrated in Figures 11 and 12, on a per-ton-of-coal-fed basis. The reduction in total solid waste relative to that produced in the once-through case is not as great as the reduction in Ca/S ratio because of the contribution of the ash in the coal. This is especially significant for the western coal, where no reduction in solid waste is apparent because of the large ash-to-sulfur ratio in the coal.

Plant Efficiency

Figure 13 shows the plant net efficiency of conversion of coal energy into electricity as a function of the Ca/S ratio. Specifically, shown are curves representing the hypothetical sorbent

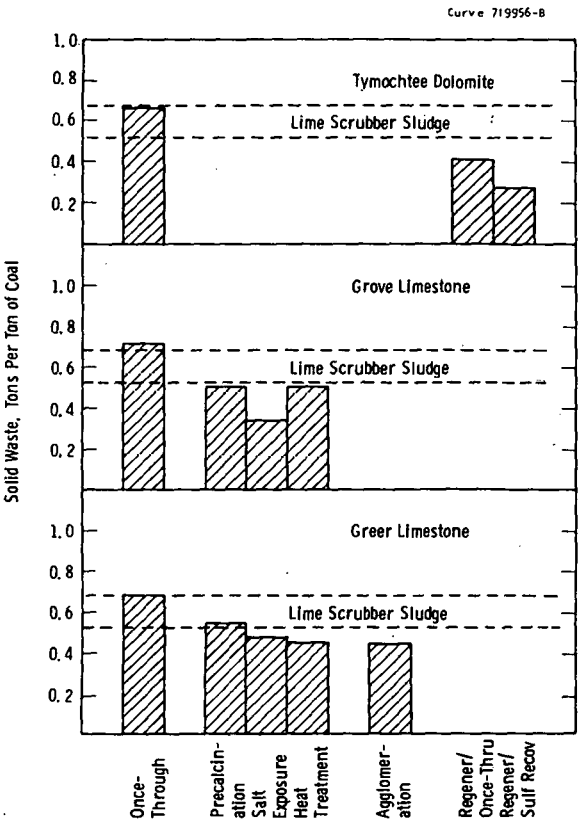

Figure 11 - Solid Waste Production for Eastern Coal - 90% Sulfur Removal

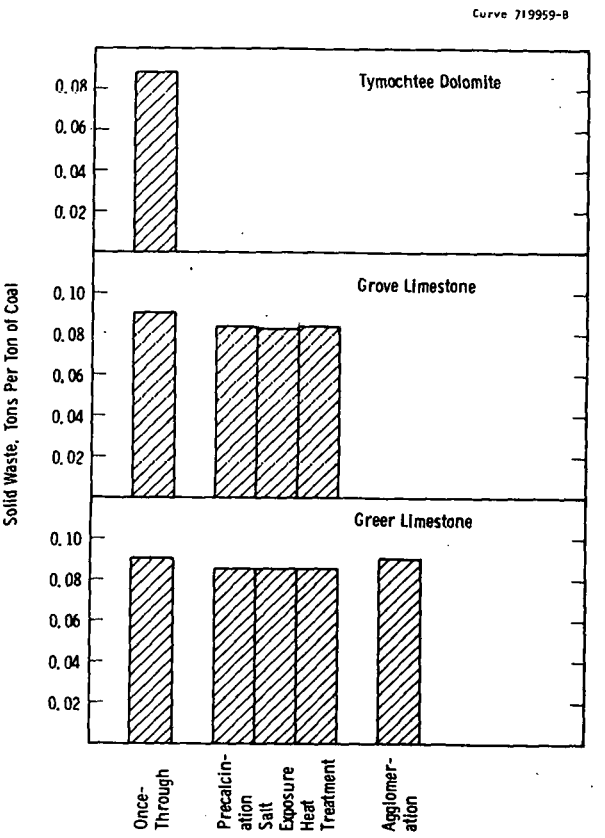

Figure 12 - Solid Waste Production for Western Coal - 70% Sulfur Removal

case for once-through operation and for each of the advanced sulfur removal processes, and points representing the three specified sorbents at their projected Ca/S ratios. The curves have been chosen to cover the potential range of Ca/S ratios that could be found in practice. The plant efficiency is very sensitive to the Ca/S ratio for the eastern coal. Here the increase in plant efficiency resulting from reduced Ca/S ratio becomes smaller as the advanced sulfur removal system becomes more complex (i.e., greater auxiliary fuel and energy consumption is associated with the more complex processes). Thus, a once-through FBC operation with Ca/S ratio of about 3 would have about the same plant efficiency as a regenerative FBC operation with a Ca/S ratio of about 1.0 or an agglomerative FBC operation with a Ca/S ratio of about 1.6.

Also note that the hypothetical sorbent has a relatively pure assumed composition while the Greer limestone and the Tymochtee dolomite are highly impure. Thus, the plant efficiencies for Greer limestone and Tymochtee dolomite lie beneath the plant efficiency for the hypothetical sorbent at equal values of the Ca/S ratio. This is a significant reduction in plant efficiency for the dolomite.

In contrast to the eastern coal case, the plant efficiency for the western coal is nearly insensitive to the Ca/S ratio and the advanced sulfur removal process. Little benefit is realized by reducing the Ca/S ratio, just as was seen for solid waste production.

Technical Uncertainties

Each of the advanced sulfur removal processes has associated with it several technical uncertainties that could result in performance that is in reality different than that assumed in the process evaluation. Table 4 lists the major technical uncertainties for each of the advanced processes. The data base for all of the processes is limited and is taken from small-scale testing. The agglomeration process has the most limited data base and possibly the greatest impact on the combustor dynamics. On the other hand, the other processes are known to be sensitive to the sorbent type used, while the agglomeration process may not be greatly sensitive to sorbent type. Low sensitivity to sorbent type is felt to be a potential advantage because it provides ease of sorbent selection and lower variability in process design. The complex regenerative processes are based on processing steps that have technical feasibility problems,

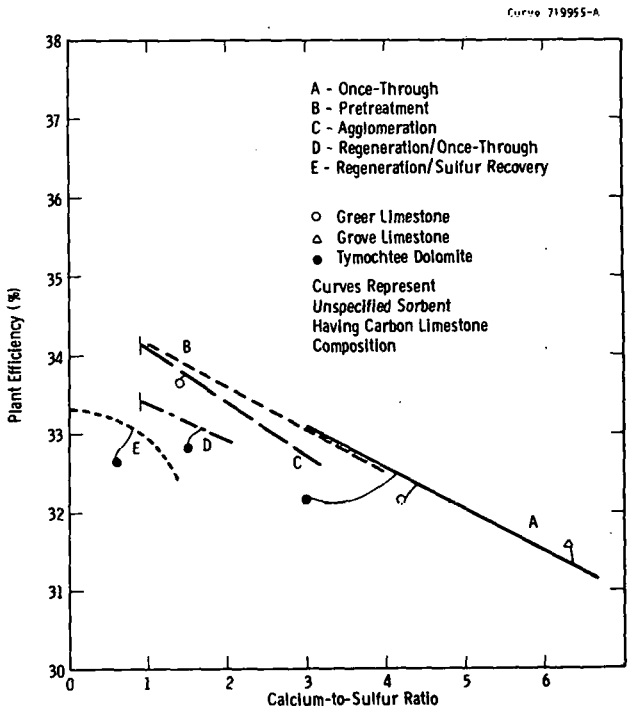

Figure 13 - Plant Efficiency for Eastern Coal AFBC - 90% Sulfur Removal

such as those associated with the high-temperature transport of solids between the combustor beds and the regenerator vessels and sulfur recovery from SO_2 streams.

The technical uncertainties listed must be addressed if future development of any of these processes is undertaken. These areas require commercial process design investigations in parallel with small-scale development unit testing.

Break-Even Cost Analysis

We performed an analysis of the break-even cost for each process to indicate how much capital investment margin is available to trade off against reduced Ca/S ratio and increased plant efficiency.

The break-even cost is defined in this analysis as the total capital requirement ($/kW) that can be invested in equipment (for the advanced sulfur removal system and for modifications to the power plant equipment) and result in the same power cost (mills/kWh) as for a once-through AFBC power plant. In developing an expression for the break-even cost, we followed the economic premises specified by EPRI for electric power generating systems.

Figure 14 relates the break-even cost for each of the six advanced processes and the three fied sorbents at their projected Ca/S ratios to the cost of the sorbent. Obviously, for the eastern coal the break-even cost is very sensitive to the cost of sorbent, the advanced process, and the sorbent type. The break-even cost is also significant

Table 4

TECHNICAL UNCERTAINTIES

Precalcination

- Limited, small-scale data; is the process of sufficient general interest?
- Can sufficient control of a precalcination device be obtained in commercial practice?
- What impact on sorbent attrition, sorbent feed system?

Salt Exposure

- Same items as precalcination
- Corrosion impact

Heat Treatment

- Same items as precalcination

Agglomeration

- Extremely limited data base; impact of sorbent type?
- Physical integrity of agglomerates, sulfur removal, and combustion efficiency vs. preparation technique unknown
- Efficiency of agglomerate-particle separation process unknown
- Impact on combustor dynamics (heat transfer, etc.) and disposal unknown
- Impact of sorbent/ash ratio

Regeneration/Once-through

- Limited, small-scale data
- Ash sintering
- Sensitivity of process to sorbent type, ash accumulation, sulfur removal requirement
- Environmental impact unknown
- High-temperature solids circulation

Regeneration/Sulfur Recovery

- Same items as regeneration/once-through
- Sulfur recovery efficiency
- Quality of the recovered sulfur
- Impact of SO_2 recycle to combustor
- Plant control integrated with sulfur recovery
- Impact of plant complexity on utility customers
- May be sensitive to attrition

relative to the capital investment of the once-through power plant, indicating that the potential savings due to reduced sorbent cost and increased plant efficiency merit a large capital investment for an advanced sulfur removal system. Obviously, using the Grove limestone with salt exposure provides the largest break-even cost (the once-through Ca/S ratio was 6.3, while the value with salt exposure was 1.1). The break-even cost for such a case is not meaningful because the once-through FBC power plant would generate electricity at an unacceptable cost, and another sorbent would be selected for the once-through plant.

Another way of looking at the break-even cost that is more realistic is shown in Figure 15. Here, the relative break-even cost is shown for each of the advanced processes and for once-through

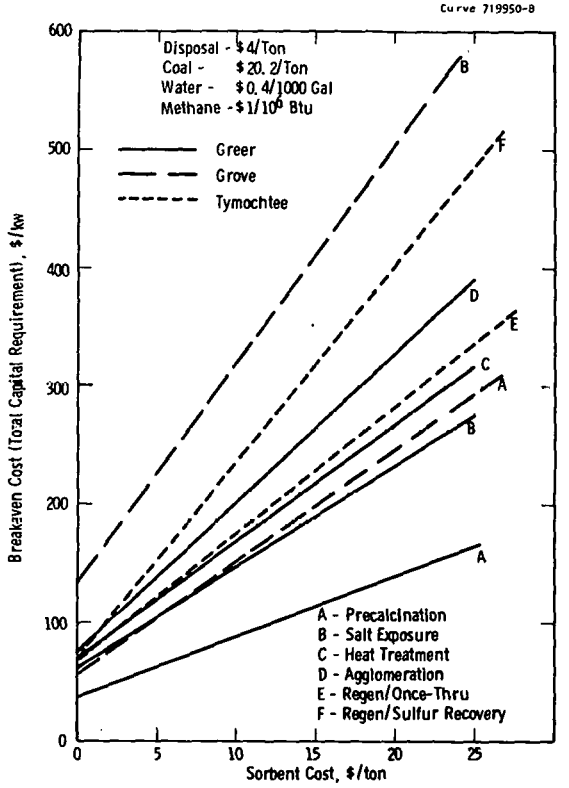

Figure 14 - Break-Even Cost for Eastern Coal

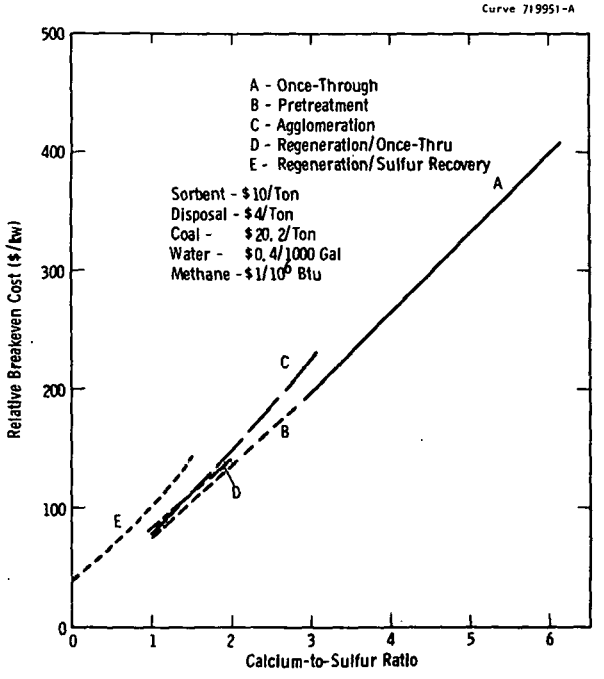

Figure 15 - Relative Break-Even Cost for Eastern Coal, Unspecified Sorbent

operation as a function of the Ca/S ratio (for the hypothetical sorbent). This figure is restricted to eastern coal and fixed sorbent cost. The break-even cost is the difference between the relative break-even cost of the once-through plant and the advanced system, each at its appropriate Ca/S ratio. The figure does not consider, however, the effect on delivered-sorbent costs of using different sorbents for the advanced process and the once-through operation. These costs could be significantly different.

For any given FBC power plant site a large number of sorbents may be available, each having a different performance in a once-through operation and in each of the advanced sulfur removal processes, and each having different delivered cost. The sorbent and sulfur removal process resulting in the lowest cost of electricity will then be very site specific, and will also depend on the nature of the coal burned (sulfur content, ash content, sulfur removal activity of the coal-ash). If a process such as agglomeration is insensitive to sorbent type, then in most cases a near optimum sorbent would simply be the cheapest delivered sorbent applied to the agglomeration process.

CONCLUSIONS

Key conclusions reached in the assessment are as follows:

- Large reductions in the Ca/S ratio are possible for eastern and western coals (depending on the specific sorbent) using the advanced sulfur removal processes. The more complex process, in general, yields the greatest reduction.
- Significant reduction occurs in the sorbent feed rate and solid waste rate for eastern coal.
- No significant reduction is realized in sorbent feed rate or solid waste rate for western coals.
- A significant increase in plant efficiency is possible for eastern coals using the advanced sulfur removal processes.
- No significant increase in plant efficiency will be obtained for western coals.
- A large break-even cost margin is available for the advanced processes with eastern coal. This margin is sensitive to sorbent type, sorbent cost, disposal cost, coal cost, and Ca/S ratio.
- Western coals provide insignificant potential cost advantages to the advanced sulfur removal systems.

- A given AFBC power plant site can use a large variety of sorbents (each of different type and cost) and sulfur removal processes. A trade-off between cost and performance of the sorbent exists. No single process will always provide the optimum situation with respect to the cost of electricity.

We recommend that, with the potential advantages of the agglomeration process (low-temperature processing, elimination of the CBC, possible insensitivity to sorbent type, possible disposal advantages), agglomeration should be pursued in further design studies and experimental programs.

REFERENCES

1. Newby, R. A., et al., Sulfur Removal System Assessment, Annual Report to B&W and EPRI, Westinghouse Research and Development Center, Pittsburgh, PA, December 1978.

2. Newby, R. A., et al., Sulfur Removal System Assessment, Annual Report to B&W and EPRI, Westinghouse Research and Development Center, Pittsburgh, PA, December 1979.

3. Newby, R. A., N. H. Ulerich, E. P. O'Neill, D. F. Ciliberti, and D. L. Keairns, "Effect of SO_2 Emission Requirements on Fluidized-Bed Combustion Systems: Preliminary Technical Economic Assessment," Report to EPA, Westinghouse Research and Development Center, Pittsburgh, PA, August 1978, EPA-600/7-78-163, NTIS PB 286 871/7ST.

4. Ulerich, N. H., R. A. Newby, and D. L. Keairns, "Sorbent Requirements for a Gulf Coast Lignite-Fired Atmospheric Fluid-Bed Combustion Power Plant," Report to EPRI, Contract No. RP 1179-1, Westinghouse Research and Development Center, Pittsburgh, PA, October 1978.

5. Ulerich, N. H., E. P. O'Neill, and D. L. Keairns, "The Influence of Limestone Calcinations on the Utilization of the Sulfur-Sorbent in Atmospheric Pressure Fluid-Bed Combustors," Final Report, Contract No. EPRI FP-426, Westinghouse Research and Development Center, Pittsburgh, PA, August 1977.

6. Shearer, J. A., I. Johnson and C. B. Turner, "The Effect of Sodium Chloride on the Reaction of SO_2/O_2 Mixtures with Limestones and Dolomites," Report to DOE and EPA, Argonne National Laboratory, Argonne, IL, June 1978, ANL/CEN/FE-78-8.

7. Johnson, Irving, et al., "Support Studies in Fluidized-Bed Combustion," Report to DOE and EPA, Argonne National Laboratory, Argonne, IL, January-March 1978, ANL/CEN/FE-78-3.

8. Perry & Chilton, Chemical Engineer's Handbook, Fifth Edition, New York: McGraw Hill Book Company, p. 20-72.

9. Dunne, P., and L. L. Gasner, "A Preliminary Investigation of the Application of Agglomeration Technology to Fluidized Bed Combustion Processes," Department of Chemical Engineering, University of Maryland, Masters Thesis, July 1978.

10. Gasner, L. L., and P. G. Dunne, Agglomeration Methods of Improving Fluidized Bed Combustion Sorbent Utilization and Combustion Efficiency, The 6th International Conference on Fluidized Bed Combustion, Atlanta, GA, April, 1980.

11. Swift, W. M., et al., "Decomposition of Calcium Sulfate - A Review of the Literature." Report to ERDA, Argonne National Laboratory, Argonne, IL, December 1976, ANL-76-122.

12. Montagna, J. C., et al., "Fluidized-Bed Regeneration of Sulfated Dolomite from a Coal-Fired FBC Process by Reductive Decomposition," Report to ERDA, Argonne National Laboratory, Argonne, IL, April 1977, ANL-77-16.

13. Jonke, A., et al., "Supportive Studies in Fluidized-Bed Combustion," Report to EPA, Argonne National Laboratory, Argonne, IL, December 1977, EPA-600/7-77-138.

ACKNOWLEDGEMENT

We are grateful for the continued financial support of the U.S. Environmental Protection Agency, IERC, and the perspective and contract direction of D.B. Henschel provided throughout the development of this model technique.

Dup

REGENERATIVE PORTLAND CEMENT SORBENTS FOR FLUIDIZED-BED COMBUSTION OF COAL

A.S. Albanese, D. Sethi, and M. Steinberg

Process Sciences Division
Department of Energy and Environment
Brookhaven National Laboratory
Upton, New York 11973

INTRODUCTION

Fluidized-bed combustion (FBC) is a relatively new technique for burning high sulfur coals cleanly, at a projected cost comparable to conventional combustion systems. In a typical fluidized-bed design, sized and dried sorbent is blended with the feed coal and fed to the fluidized-bed in proportion to the coal feed. For limestones, dolomite or other calcium bearing sorbents, this proportion is usually specified in terms of calcium (sorbent) to sulfur (coal) feed ratio. The calcium to sulfur feed ratio is set by the required or desired sulfur dioxide emission limit. Fluidization of the bed is effected by passing air up through the sorbent at superficial velocities ranging from about 3 to 12 ft./sec. Sulfur dioxide formed by the oxidation of the sulfur contained in the feed coal reacts with and remains an integral part of the sorbent, thus reducing the quantity of sulfur emitted to the atmosphere by the combustor flue gases. Fly ash and elutriated sorbent fragments are removed from the combustion gases by dust collection equipment, and heat is extracted from the system by banks of steam tubes located within the combustor. Bed depth is maintained at an approximately constant level by withdrawing spent sorbent from the bed at rates proportional to the fresh sorbent feed.

A potential problem in commercialization of fluidized-bed combustion is that vast amounts of spent sorbent will be generated by these systems if the sorbent is used on a once-through basis, especially if high sulfur coals are burned and if air pollution emission limits continue to become increasingly stringent. Although relatively inexpensive sorbents are available (e.g. limestone) and although the resulting dry sorbent wastes are perhaps easier to handle and store than the sludge produced in the scrubbers of conventional combustion systems, they do represent a potential environmental hazard. Thus, it may become necessary, particularly if a large number of FBC plants are built, to regenerate and recycle the sorbent.

Limestone and dolomite, which occur naturally and in plentiful supply, can be used on a once-through basis. However, cyclic use of these materials does not appear to be feasible because of the high regeneration temperatures required, their loss in reactivity with repeated use and their poor resistance to attrition. Furthmore, SO_2 reactivity and attrition resistance is dependent upon the origin of these materials. A low cost, regenerable FBC sorbent is definitely needed.

The requirements of a sorbent for regenerative service are: (1) it must be capable of reducing the SO_2 concentration of the FBC flue gas to within the acceptable EPA emission limits, (2) it must not lose its SO_2 reactivity in cyclic sulfation/regeneration service, (3) it must be capable of producing a relatively high SO_2 concentration during regeneration, (4) it must have good attrition resistance, and (5) its cost must not be prohibative. Calcium silicate cement pellets, e.g. Portland III pellets, appear to meet these requirements better than any other low cost regenerable sorbent under development today.

A considerable amount of basic work on SO_2 sorption with pure calcium silicate compounds of various crystal structure has indicated that the reactivity and regenerability of the silicates are much better than lime and limestone.[1] It is upon this work that portland cement was chosen as the most practical sorbent for FBC application.

DESCRIPTION AND COMPOSITION OF PORTLAND CEMENTS

Portland cement is a readily available, widely used construction material. It may be defined as a product obtained by intimately mixing together calcareous and argillaceous, or other silica, alumina, and iron oxide-bearing materials, burning them at a clinkering temperature (about 1400°C), and grinding the resulting clinker.[2] A great variety are used throughout the world. Analyses of some American Portland Cements are given in Table 1.

In the present work, several types of portland cements were screened by performing thermogravimetric (TGA) sulfation experiments on cements powders. Sulfation was carried out for a two hour period at 900°C and 1 atm. using a simulated combustion gas containing 0.25% SO_2, 5% O_2, 15% CO_2 and the balance N_2. The results of these experiments are presented in Figure 1 which indicates that Portland Type III cement (PC III)

is intrinsically the most reactive towards SO_2, PC I is second best, PC II third while PC V is the least reactive.

PC III is a rapid-hardening cement similar in composition to Type I, but normally ground to a finer extent. Type II is slightly slower in rate of strength development than Type I and has additional specification limitations on its chemical composition. Type IV, which was not tested, is a cement whose chemical composition is adjusted to reduce the heat of hydration. Type V is a sulfate-resisting cement and has increased resistance to sulfate-bearing waters.[2]

Because of its wide commercial availability and its high affinity for SO_2, we have concentrated our development efforts on preparing and evaluating PC III pellets for fluidized-bed combustion (FBC) service.

Table 1.

Composition of Some American Portland Cements

ASTM Type	CaO	MgO	Al_2O_3	Fe_2O_3	SiO_2	TiO_2	Na_2O	K_2O	SO_3	free CaO	C_4AF	C_3A	C_3S	C_2S
I	63.8	3.7	5.6	2.4	20.7	0.23	0.21	0.51	1.6	0.4	7	11	55	18
	63.1	2.5	4.7	3.0	22.1	0.21	0.06	1.30	1.7	0.2	9	7	47	28
	65.8	1.1	4.7	2.1	22.2	0.30	0.04	0.19	1.6	1.6	6	9	54	23
	62.8	1.7	6.7	2.5	21.1	0.39	0.95	0.51	1.8	2.0	8	14	33	35
II	61.4	3.1	4.8	4.8	20.8	0.21	0.06	1.30	1.8	0.9	15	5	44	26
	64.9	1.9	4.0	2.1	24.0	0.23	0.23	0.55	1.7	1.5	6	7	41	38
III	65.6	1.4	5.2	2.5	20.0	0.27	0.21	0.44	2.3	1.8	8	10	63	10
	63.3	4.3	5.1	2.0	20.3	0.21	0.19	0.28	2.5	1.9	6	10	51	19
IV	59.6	3.0	4.6	5.0	22.9	0.23	0.06	1.19	1.3	0.4	15	4	25	47
	63.6	1.1	3.7	3.1	25.2	0.19	0.33	0.01	1.9	0.4	9	5	31	49
V	64.3	1.7	3.1	3.3	24.6	0.19	0.08	0.22	1.4	0.5	10	3	45	36
	62.6	2.5	1.9	1.3	26.1	0.12	0.10	0.15	2.0	1.8	4	3	35	48
	63.3*	1.2	3.3	4.7	23.1	—	0.08	0.37	1.7	—	14	1	49	30

*Corrected for free CaO

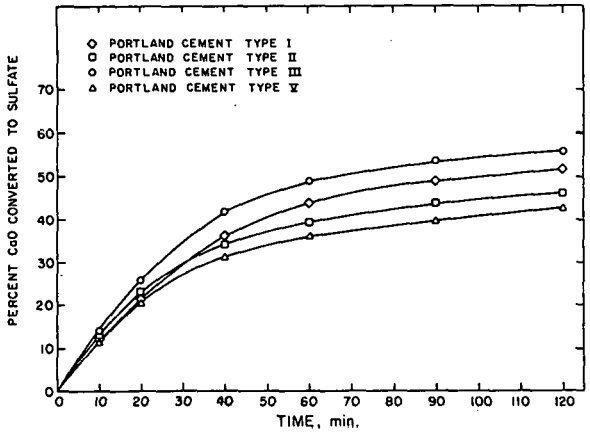

FIGURE 1. SULFATION RATES OF PORTLAND CEMENT USING GAS CONTAINING 0.25% SO_2, 5% O_2, AND 15% CO_2 IN N_2 AT 900°C.

THERMODYNAMIC ANALYSIS OF SORPTION REACTIONS

The SO_2 sorption reactions for calcium silicates may be summarized as follows:

$$Ca_xSiO_{x+2} + x(SO_2+1/2O_2) = xCaSO_4 + SiO_2 \quad (1)$$

where x is 1 for mono-, 2 for di-, and 3 for tricalcium silicate. A thermodynamic analysis of this reaction has been performed by R.T. Yang and F. King.[3] Their results are presented in Figure 2 which is a plot of the log of the equilibrium partial pressure of SO_2 in atmospheres (P_{SO_2}) versus temperature in degrees Kelvin. The plot was prepared assuming that the partial pressure of O_2 (P_{O_2}) is 0.05 atm. which corresponds to the concentration of O_2 expected in the flue gas of atmospheric fluidized-bed combustors; for pressurized combustion, the P_{SO_2} curves would be shifted downward, improving the situation. The above sorption equation represents the most unfavorable case with respect to P_{SO_2} because the products of the reaction ($CaSO_4$ and SiO_2) are assumed to be in uncombined form; less free energy would be required to form $(CaSO_4)_x \cdot SiO_2$ and therefore lower equilibrium partial pressures would result.

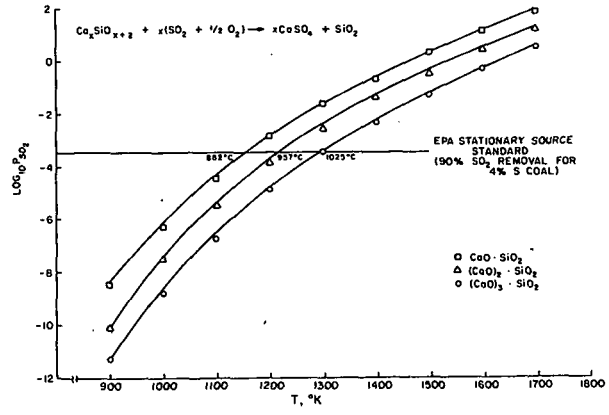

FIGURE 2. THERMODYNAMIC EQUILIBRIA FOR SULFATION OF CALCIUM SILICATES.

The horizontal line in Figure 2 represents the recently promulgated EPA stationary source standard of 90% removal for 4% sulfur coal. The points at which the P_{SO_2} curves intersect this line give the limiting temperatures for effective SO_2 removal. Thus, monocalcium silicate is suitable (thermodynamically) up to a temperature of about 900°C, dicalcium silicate is good up to a temperature of about 950°C, while tricalcium silicate can be used to 1025°C. 73 to 86% of the silicates present in commercial PC III is tricalcium silicate; the remainder is dicalcium silicate. No monocalcium silicate is present. Therefore, PC III should be suitable for service at temperatures well above 900°C, if desired.

EFFECT OF TEMPERATURE ON SULFATION RATE

The effect of temperature on the sulfation capacity of 16/20 mesh PC III pellets containing 5% amorphous SiO_2, was determined by atmospheric TGA experiments and is shown in Figure 3. The pellets where prepared by the procedure described below. The optimum temperature for sulfation is somewhere between 950°C and 1050°C. For a temperature lowering of about 65°C from the optimal temperature interval, the sulfation capacity is decreased by about 15%, whereas a temperature increase of 50° results in a sulfation capacity lowering of around 35%. The optimum temperature range for SO_2 absorption using natural limestone is between 830°C and 900°C.[4] The higher observed optimum temperature for sulfation of PC III is an advantage over limestone, because combustion and power cycle efficiencies tend to increase as bed temperature increases.

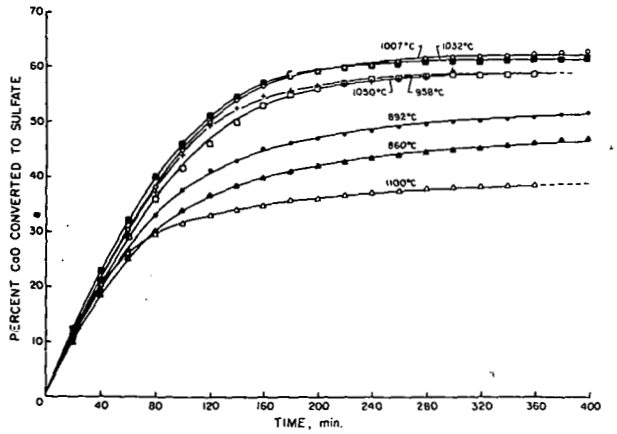

FIGURE 3 THE EFFECT OF TEMPERATURE ON SULFATION RATE AT 1 ATM., FOR PORTLAND TYPE III PELLETS WITH 5% AMORPHOUS SiO_2 ADDED.

THERMODYNAMIC EQUILIBRIA IN REDUCTIVE DECOMPOSITION

Regeneration of the $CaSO_4$ produced by the desulfurization reaction when a limestone sorbent is used can be accomplished by reacting the sulfate with an appropriate reducing medium. With a CO reducing gas, the overall reaction is:

$$CaSO_4 + CO = CaO + CO_2 + SO_2 \qquad (2)$$

which proceeds according to the following two sequential steps:

$$CaSO_4 + 4CO = CaS + 4CO_2 \qquad (3)$$
$$3CaSO_4 + CaS = 4CaO + 4SO_2 \qquad (4)$$

Experimental evidence indicates that the second step, Reaction (4), is rate controlling and determines the maximum concentration of SO_2 that can be produced during regeneration. Thermal decomposition of $CaSO_4$ in the absence of a reducing medium is theoretically possible but is not feasible because temperature requirements are prohibitively high, i.e., the sorbent becomes deactivated during regeneration due to sintering.

The reactions for regenerating sulfated calcium silicates are similar to those for regenerating calcium sulfate and may be indicated as follows:

$$xCaSO_4 + SiO_2 + xCO = (CaO)x\cdot SiO_2 + xCO_2 + xSO_2 \qquad (5)$$
$$xCaSO_4 + SiO_2 + 4xCO = xCaS + SiO_2 + 4xCO_2 \qquad (6)$$
$$3xCaSO_4 + xCaS + 4SiO_2 = 4(CaO)x\cdot SiO_2 + 4xSO_2 \qquad (7)$$

where x takes on integer values of from 1 to 3. As in the case of lime, Reaction (7) controls the rate of regeneration and thus the maximum concentration of SO_2 which can be achieved during regeneration.

Figure 4 and Table 2 show the equilibrium partial pressures of SO_2 (P_{SO_2}) for the reductive decomposition of sulfated mono-, di- and tricalcium silicates and for calcium sulfate based on Reactions (7) and (4), respectively.

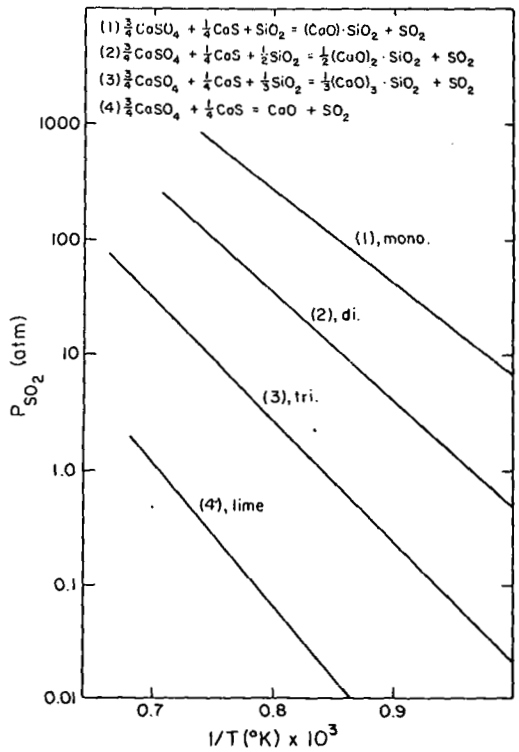

FIGURE 4. THERMODYNAMIC EQUILIBRIA FOR REPRODUCTIVE DECOMPOSITION OF SULFATED CALCIUM SILICATES AND LIME.

Table 2.

Equilibrium Partial Pressure of SO_2

(1) 3/4 $CaSO_4$ + 1/4 CaS + SiO_2	= $CaO\cdot SiO_2$ + SO_2	(mono)
(2) 3/4 $CaSO_4$ + 1/4 CaS + 1/2 SiO_2	= $1/2(CaO)_2\cdot SiO_2$ + SO_2	(di)
(3) 3/4 $CaSO_4$ + 1/4 CaS + 1/3 SiO_2	= $1/3(CaO)_3\cdot SiO_2$ + SO_2	(tri)
(4) 3/4 $CaSO_4$ + 1/4 CaS	= CaO + SO_2	(lime)

	Pressure (atm.)			
T(°C)	(1)	(2)	(3)	(4)
900	110	12	0.8	0.015
950	200	25	1.8	0.04
1000	370	50	4.2	0.10
1050	650	96	8.6	0.24

At 900°C, the equilibrium partial pressure of SO_2 is 110 atm. for mono-, 12 atm. for di- and 0.8 atm. for tricalcium silicates, but only 0.015 atm. for lime. At 1000°C, they are 370, 50, 4.2, and 0.1 atm., respectively. Therefore, thermodynamic equilibrium will not limit the concentration of SO_2 achievable in the regenerator off-gas if a calcium silicate sorbent such as PC III is used. Higher concentrations will result in more economical conversion of SO_2 to sulfur or sulfuric acid. Furthermore, sulfated silicates can be regenerated under pressure. Therefore, for pressurized fluidized-bed combustion systems, the regenerator and combustor can be operated isobarically, facilitating the transfer of solids between combustor and regenerator.

SULFATION/REGENERATION CYCLING EFFICIENCY

The results of a typical isothermal sulfation/regeneration experiment conducted at a temperature within the optimal sulfation temperature range (982°C) are presented in Table 3. Sulfation procedure was identical to that described previously. Regeneration was conducted using 5% CO, 15% CO_2 and 80% N_2. The gas flow rate for both sulfation and regeneration was 500 SCCM. Sulfation rates were monitored for 2 hours. Regeneration approached equilibrium value after about twenty minutes at the above mentioned flow rates. After this time interval, the sample was treated with 5% O_2, 15% CO_2 and the balance N_2 until no weight increase was observed. This was done to correct for the weight reduction due to reducibles, such as metal oxides, in the PC III.

Table 3.

Isothermal Sulfation/Regeneration Cycling of PC III +5% Amorphous SiO_2 + 6.1% H_2O[a] at 982°C and 1 atm.

Cycle #	Sulfation,[b] %	Regeneration[c] %
1	55.3	93.9
2	47.6	93.8
3	46.1	94.7
4	46.8	94.6
5	46.4	94.9
6	46.6	94.6
7	45.9	94.2
8	45.2	91.0
9	39.9	94.8
10	45.6	95.1

[a] See Text for pellet preparation details.
[b] Integrated sulfation over a 2 hour period.
[c] Procedure for this evaluation described in text.

Ignoring the caveat of a much higher sulfation capacity for cycle number 1, it is reasonable to conclude that the two hour sulfation capacity of about 45 percent or better and the equilibrium approaching regeneration value of about 95 percent do not deteriorate with cycling. No change in reactivity after repeated cycling of the same material indicates no sorbent sintering activity and no pore destruction. Experiments wherein the regeneration was carried out at a temperature 50°C lower than sulfation, within the 950 and 1050°C optimal temperature range, showed no significant difference from the data reported in Table 3. This implies that any minor energy loss in the desired isothermal transfer of the hot sulfation pellets from combustor to regenerator will not necessitate additional energy expenditure in this step. The higher initial sulfation capacity cannot be accounted for as due to the formation of $CaSO_4$ by sulfation of free lime (~2%) in PC III. It most likely results from the sulfation of metal oxides such as Al_2O_3, which may not be capable of regeneration at the temperatures used in this study. Such an explanation could account for the observed limiting regeneration efficiency of 0.95 as shown in Table 3. Experiments are currently underway to elucidate the mechanism of regeneration.

PRESSURE DEPENDENCE ON SULFATION CAPACITY

Pressurized TGA experiments were undertaken to determine the effect of high CO_2 partial pressure (P_{CO_2}) on the sulfation capacity of PC III. This was done to establish the viability of this sorbent for pressurized fluidized-bed combustion. The experimental data on PC III + 5% SiO_2 pellets given in Figure 5 for all three pressures of 1, 5 and 10 atms represent the mean values of seven experiments in each case.

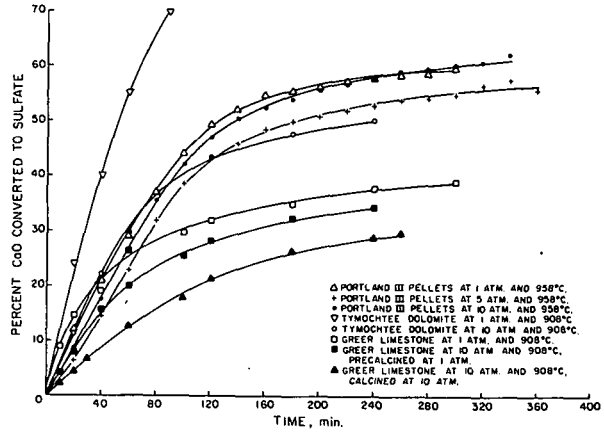

FIGURE 5. SULFATION RATES OF 16/20 MESH PORTLAND TYPE III PELLETS, GREER LIMESTONE AND TYMOCHTEE DOLOMITE AT VARIOUS PRESSURES AND TEMPERATURES.

The three curves are within one standard deviation of each other; thus, the sulfation capacity of PC III is essentially independent of pressure up to at least 10 atm. For comparison we have also plotted, on this figure, previously obtained data on sulfation rates at 1 and 10 atm. for Greer limestone and Tymochtee dolomite under

their optimal sorption activities. The decrease in the sulfation capacity at the higher pressure for both of these materials is due to the fact that calcination of $CaCO_3$ at a P_{CO_2} of 1.5 atm. is noticeably less effective than at P_{CO_2} of 0.15 atm.[4] Therefore, PC III in comparison to limestones appears to be a superior sorbent for not only atmospheric fluid-bed application, but also for pressurized combustion (PFBC) where higher combustion, power cycle and sulfur retention efficiencies, reduced reaction vessel size, and lower NO_x emissions represent important system advantages.

REGENERATION OF SULFATED PORTLAND III PELLETS AND GREER LIMESTONE

TGA regeneration experiments were run on sulfated Portland III pellets (16/20 mesh, 5% SiO_2, 6.1% H_2O) and sulfated Greer limestone to determine the extent of regeneration under several sets of operating conditions. The Portland III pellets were sulfated and regenerated isothermally and isobarically. The Greer was precalcined at 900°C and 1 atm. using 5% O_2, 15% CO_2 and 80% N_2. Sulfation and regeneration were carried out using the same gas compositions as in the cyclic sulfation/regeneration runs described above. The results of our experiments are summarized in Table 4. The rates of regeneration, which are approximate, are given in the last column of the table as SO_2 rate in mg/min. They were estimated from the entire linear portion of the TGA regeneration curves.

Table 4.

Regeneration of Sulfated Portland III and Greer Limestone.

Material	Sulfation, %	Regeneration Temp., °C	Regeneration Pres., atm.	Weight Loss, mg.	Time,[a] min.	Regeneration, %	SO_2 Rate mg/min.[a]
Portland III[b]	49.5	957	1	18.1	22	84.3	0.65
	59.0	1050	1	22.7	22	86.6	0.83
	38.8	1100	1	16.0	14	94.6	0.91
	58.9[c]	958	10	22.9[c]	26[c]	91.0[c]	0.70[c]
Greer[d]	21.0[e]	950	1	3.9	22	37.6	0.41
	18.1[e]	1000	1	5.1	13	55.3	0.31
	18.0[e]	1050	1	6.6	10	73.7	0.53

[a] Over linear portion of regeneration curve.
[b] 16/20 mesh pellets, 5% SiO_2 and 6.1% H_2O.
[c] Average value for 12 sulfation/regeneration runs.
[d] 16/20 mesh particles.
[e] Calcined at 900°C using 80% N_2, 15% CO_2 and 5% O_2.

At a system pressure of 1 atm., the regeneration rates and efficiencies of both the Portland III pellets and Greer increase with increasing temperature, over the temperature ranges considered, which is consistent with the endothermic nature of the regeneration reactions. However, Portland III pellets regenerate much more efficiently than Greer.

The rate and extent of regeneration of sulfated Portland III at 10 atm. are comparable to those at 1 atm., for a regeneration temperature of about 957°C. Therefore, considering its sulfation capability, its high SO_2 equilibrium partial pressure in reductive decomposition, and its regeneration efficiency at 10 atm. pressure, it appears that Portland III pellets would be suitable not only for pressurized-fluidized bed (PFB) service but also for isobaric sulfation/regeneration operation. Operating a commercial regenerative PFBC system isobarically would facilitate transfer of solids between the fluidized-bed combustor and sorbent regenerator.

ATTRITION OF PORTLAND III AND GREER

A small scale fluidized-bed was used to determine the rates of attrition of PC III pellets (16/20 mesh) and Greer lime. The Portland pellets were made by the procedure described below. They were cured for 28 days at room temperature in an atmosphere of 100% humidity and had an initial water content of 7.6%. Both sulfated and unsulfated PC III were tested in various gas mixtures.

Two sets of runs were made on Greer. One set on 16/20 mesh calcined Greer limestone, and a second on partially sulfated Greer that was supplied by Argonne National Laboratory (ANL). Limestone calcination was effected at 850°C and 1 atm. using air. The partially sulfated Greer was obtained from the cyclone above ANL's fluidized-bed pilot unit and had a wide particle size distribution. A grab sample of the Argonne material was screened and the faction less than 40 mesh discarded; the +40 mesh cut was used in our tests. This size cut appeared to be more representative of the material than a 16/20 mesh cut.

All experiments were run at 1 atm. and 1000°C in an electrically heated, 30 mm. I.D. by 30 cm. long quartz tube. Fluidization gases were preheated and then passed through a coarse frit which served as bed support and gas distributor. A total flow of 7500 SCCM was used in all tests, which corresponds to a superficial bed velocity of 75.5 cm/sec (2.5 ft/sec) at operating conditions. A 20 g. sample (after pre-conditioning) of each material was tested. This amount of material filled the quartz tube to a height of about 20 mm. under static bed conditions and to between 25 and 30 mm. when the bed was fluidized.

Before starting each attrition run, a sample of the test material was heated to 1000°C for 10 minutes in the reactor tube. A small amount of air was then pulsed through the bed every minute to mix the bed (Portland or Greer) and drive off any moisture and volatiles. The material was allowed to cool, and subsequently removed with a vacuum trap. A 20 g. batch of this pre-conditioned material was loaded into the

quartz tube, and brought to 1000°C within 5 to 8 minutes. Following this, gas flow was initiated. At the end of 1 hour, the gas flow was stopped and the electric heater turned off. The sample was allowed to cool for about 5 minutes, then removed from the quartz tube, weighed, and put back. The difference between the initial and final weights of the sample was taken as the amount of material elutriated from the bed due to attrition. The procedure was repeated for 8 cycles (8 hours).

For a superficial velocity of 2.5 ft/sec, it is roughly estimated (by terminal velocity calculations) that only particles less than 0.16 mm diameter would be elutriated from the fluidized bed when using air at 1000°C as fluidizing medium. The particle size in our experiments was between 0.85 and 1.00 mm for the 16/20 mesh materials and greater than 0.40 mm for the partially sulfated Greer. Thus, it is appropriate to attribute the weight loss to material attrition.

The results of our experiments are presented in Figure 6 for the 16/20 mesh Portland III pellets and in Figure 7 for Greer. For unsulfated Portland III, the lowest attrition losses occurred when air was used as fluidizing medium, and amounted to 4% of the original weight of sample after 8 hours of operation. The corresponding loss in oxygen was 5%, whereas, about 6% loss occurred when either nitrogen or a mixture of 95% air and 5% CO_2 was used. Fully sulfated PC III showed about a 6% loss after 8 hours in air, which is 1.5 times higher than for the unsulfated material.

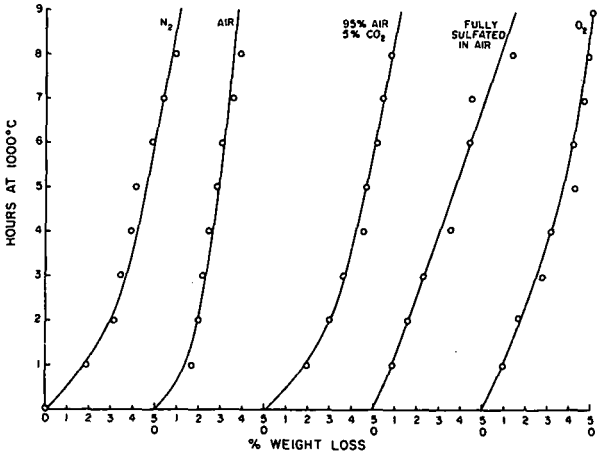

FIGURE 6. ATTRITION RATES OF 16/20 MESH PORTLAND III CEMENT (7.6 % H_2O) IN A 30mm DIAMETER FLUIDIZED-BED OPERATED AT 1000°C, 1 ATM. AND A FLOW RATE OF 7500 SCCM (SUPERFICIAL VELOCITY = 2.5 FT./SEC.).

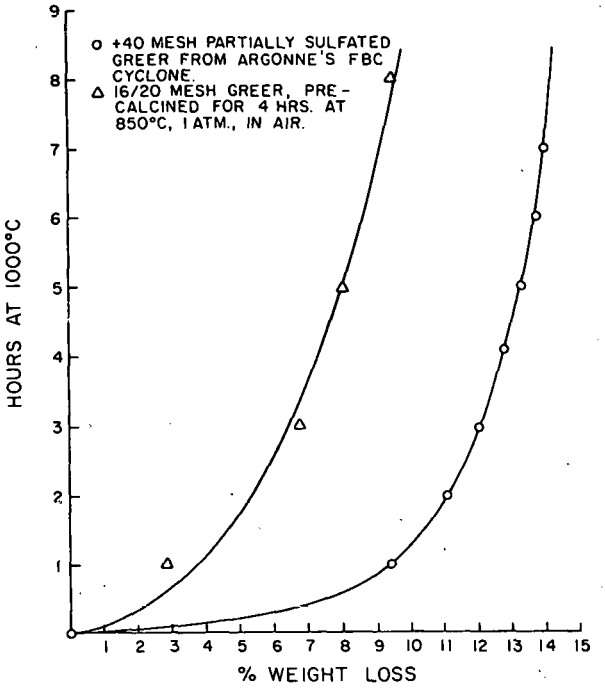

FIGURE 7. ATTRITION RATES OF GREER LIMESTONE IN A 30mm DIAMETER FLUIDIZED-BED OPERATED AT 1000°C, 1 ATM., AND AN AIR FLOW RATE OF 7500 SCCM.

The 8 hr. attrition loss for precalcined 16/20 mesh Greer in air was 9.4%, or 2.4 times greater than for unsulfated PC III. The loss for the +40 mesh, partially sulfated Greer was about 14% after 8 hours of fluidization by air. This is 3.5 times greater than that obtained on unsulfated PC III and 2.3 times greater than for sulfated PC III. Thus, although these losses are not necessarily indicative, in an absolute sense, of what will actually occur in commercial size equipment, they do give a relative indication of the superior attrition resistance of PC III pellets over natural Greer limestone. Furthermore, recent attrition data (which are not presented herein), indicate that cyclic sulfation/regeneration usage tends to strengthen PC III pellets.

It should be pointed out that attrition losses are important not only from the point of view of total material attrition and economics, but also in establishing the extent of submicron fluid bed material ejection into the atmosphere. Polycyclic aromatic hydrocarbons, analogous heterocyclic compounds and/or adducts of sulfur oxides have been reported to be present in the airborne particulate matter from coal combustion.[5] Most of this particulate matter which is not trapped by the dust collectors is probably coal fly ash. Nevertheless, it can be expected to contain some sorbent material onto which the above mentioned organics may be deposited. These compounds are suspected mutagens and carcinogens.[6] The flyash with

adsorbed SO_2 through heterogeneous photo-oxidation can give rise to SO_3 with nontrivial quantum yields followed by H_2SO_4 aerosol formation. Other sulfur containing compounds such as dimethyl sulfate have been observed in flyash and in other particulate matter from coal combustion.[5]

PREPARATION OF PORTLAND CEMENT PELLETS

The PC III pellets used in our experiments are currently prepared at Brookhaven National Laboratory, on a small batch basis, using a vertically mounted drum pelletizer 5 in. deep by 18 in. in diameter. The drum is driven by a small electric motor which operates at a speed of about 50 rpm.

The cement powder is first mixed with a fine spray of water to bring its moisture content to a maximum of 10% by weight. The powder must be pre-moistened before it is placed into the pelletizer drum or it will slide and not tumble when the drum is rotated. The conditioned powder is uniformly fed into the pelletizer pan and intermittently sprayed with a light mist of water. During operation, the cement particles remain at the bottom of the pan as the drum surface rotates around them. The continuous rolling and tumbling of powder results in the formation of nuclei. Seed formation and growth is accomplished by the continuous layering of fines and liquid on the rolling bed of cement particles. If pellets of a wide size distribution are desired, the operation is continued until the desired size distribution is achieved (within the constraints of the equipment). In our experiments, we used pellets of a narrow size distribution (16/20 U.S. mesh). Therefore, once the particle nuclei were formed, the machine was turned off and emptied and the seed pellets were screened to a uniform size, smaller than the desired diameter of the finished pellets. The seeds were then re-fed into the pelletizer and the agglomeration procedure continued until the 16/20 mesh size was attained.

The initial water content of each batch of pellets is determined by weighing a representative sample of the batch and then re-weighing after drying in a vacuum oven at 100°C for one hour. Initial water content between a range of 2 to 8%, does not appear to affect the sorption capacity of Portland III pellets nor does addition of minor quantities of other additives such as SiO_2; however, they may affect other properties of the agglomerates (e.g., attrition resistance). The finished pellets are kept at 100% humidity for 28 days (curing period). After curing, the pellets are removed from the curing apparatus and lightly hammered to separate particles that are stuck together.

CONCLUSIONS

1) Portland cements are commercially available construction materials that contain high concentrations of calcium silicates. The silicates are highly reactive towards SO_2 at temperatures and pressures encountered in atmospheric and pressurized FBC's.

2) Of the Portland cements tested, PC III appears to have the highest sulfation capacity when sulfated by SO_2 at FBC conditions.

3) A thermodynamic analysis of the sulfation of calcium silicates indicates that they are capable of reducing the concentration of SO_2 in FBC combustion gases to within the current EPA emission limits.

4) The optimum temperature for sulfation of 16/20 mesh PC III pellets is about 1000°C in comparison to about 875°C for natural limestones. The higher observed optimum temperature is an advantage because combustion and power cycle efficiencies tend to increase as bed temperature increases.

5) The reactions for regenerating sulfated calcium silicates are similar to those for regenerating calcium sulfate. However, the equilibrium partial pressures of SO_2 in the reductive decomposition of sulfated silicates are much higher than for sulfated lime. This implies that higher SO_2 concentrations will be attainable in the regenerator off-gas which will result in more economical conversion of SO_2 to sulfur or sulfuric acid.

6) The sulfation capacity and regeneration efficiency of PC III pellets do not deteriorate with repeated sulfation/regeneration cycling. This indicates that PC III pellets are suitable for use in regenerative systems.

7) The sulfation capacity of PC III is independent of pressure up to at least 10 atm. The capacities of Greer limestone and Tymochtee dolomite, on the other hand, are significantly reduced when operating pressure is increased from 1 to 10 atm. Therefore, PC III appears to be suitable sorbent for pressurized as well as atmospheric fluidized-bed combustion systems.

8) The rate and extent of regeneration of sulfated PC III pellets at 10 atm. is comparable to those at 1 atm., for a regeneration temperature of 957°C. Regeneration rates of PC III pellets are appreciably higher than those of limestone.

9) The results of small scale, hot, fluidized-bed attrition tests indicate that sulfated and unsulfated 16/20 mesh PC III pellets are significantly more attrition resistant than unsulfated and sulfated lime particles.

10) We have demonstrated that reactive, regenerative, attrition resistant PC III can be made by low energy agglomeration techniques which are currently practiced industrially.

ACKNOWLEDGEMENT

The authors wish to thank G. Farber, F.B. Kainz and J. Pruzansky for their help in performing the experiments described herein.

REFERENCES

1. R.T. Yang and M.S. Shen, "Calcium Silicates: A New Class of Highly Regenerative Sorbents for Hot Gas Desulfurization" AIChE Journal 25, No. 5 811 (1979).

2. F.M. Lea, "The Chemistry of Cement and Concrete", 3rd Ed., Edward Arnold Ltd., London (1970).

3. M. Steinberg and R.T. Yang, "Regenerative Process for Desulfurization of High Temperature Combustion Gases", Progress Report No. 1, May 1 - June 30, 1976, Brookhaven National Laboratory, N.Y.

4. M.S. Shen, J.M. Chen, and M. Steinberg, "The Optimal Temperature of Sulfur Retention", Thermochimica Acta, in press.

5. M.L. Lee et al. "Dimethyl and Monoethyl Sulfate: Presence in Coal Fly Ash and Airborne Particulate Water", Science, 207, 186 (1980).

6. See for example; G. Loproth, Chemosphere, 1, 791 (1978).

Question to A.S. Albanese:

Q: (Participant not identified)

What is the typical SO_2 in the flue gas after regeneration?

A: We have only done TGA experiments. Our next step is to run a fluidized bed regenerator.

MODELING

AN IN-SITU MODEL OF FLUIDIZED BED COAL COMBUSTION

S. RAJAN AND B. DEY

SOUTHERN ILLINOIS UNIVERSITY, CARBONDALE, ILLINOIS

INTRODUCTION

Modeling of fluidized bed combustors has its utility in simulating the performance and emissions characteristics of the bed, and in facilitating parametric design studies relevant to the scale-up of fluidized bed combustors. Models permit the evaluation of the relative importance of the various physical, chemical and fluid mechanical phenomena occuring in the bed so that the combustor may be designed and operated for maximum efficiency. This information can be obtained with a minimum of cost and experimentation provided the model is physically realistic.

Models of fluidized bed combustion available in the literature may be broadly classified into three categories. Into the first category fall those studies which investigate the rate of reaction of single carbon particles in a fluidizing atmosphere. Notable among the single carbon particle studies are the works of Avedesian and Davidson[1], Basu, Broughton and Elliot [2] and Campbell and Davidson[3]. These studies are empirical in nature and provide useful rate equations for inclusion in numerical modeling studies. An example of a mathematical model of coal particle combustion, utilizing empirical correlations such as these is given by Baron et.al.[4].

A second class of fluidized bed combustor models concern the combustion of coal in a simulated fluidizing atmosphere. Among these are the so called mechanistic models, examples of which may be found in the works of Horio and Wen [5,6], Baron et.al.[7], Chen and Saxena [8]and others. These incorporate the additional features of bubble dynamics, interphase heat and mass transfer, chemical reaction etc., in a mechanistic way into the model of fluidized bed coal combustor.

A third group of models are the system models. These studies investigate the dynamics of the total fluidized bed plant as a system, of which the fluidized bed combustor is a component. An example of a system model is given by Berkowitz et.al.[9]. These three categories of models concentrate on different aspects of fluidized bed coal combustor performance prediction, and are based on different approaches to the study of fluidized bed combustion, although there is some overlap between the various categories of models.

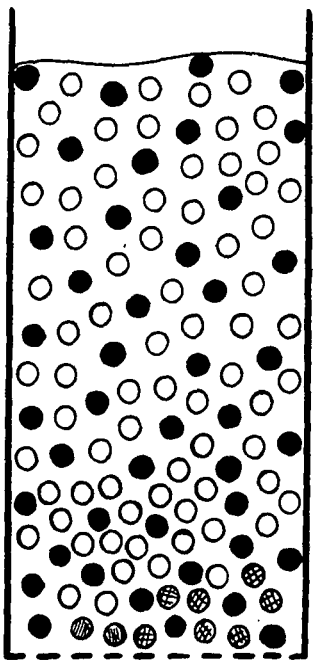

FIGURE 1. UNIFORMLY FLUIDIZED BED

The present in-situ model of fluidized bed coal combustion follows still another approach to the study of fluidized bed coal combustors. The present approach differs from existing ones, in that it yields a field description of the processes occuring during the fluidized bed combustion. In this model, the details of the flow such as heat and mass transfer between solid and gas, mixing of gas and particles, entrainment of solid particles, distribution of gas density and temperature are the natural outcome of the numerical calculations of the spatial and temporal distributions of the important process variables. Also, the important properties such as rate and extent of volatiles release and combustion, particle size, fluidized

bed size etc. can be easily incorporated in the model.

MODEL DESCRIPTION

The in-situ model of fluidized bed coal combustion, as developed in this paper, is applied in this initial study, to uniformly fluidized beds devoid of any gas bubbles, figure 1. Furthermore, the combustion of coal is investigated from the instant the coal is introduced into the bed till the time it appears at the upper bed surface. The coal, as it enters the fluidized bed at the bottom, is assumed to be at room temperature. As it is transported upwards through the bed, it first picks up heat from the hot surrounding gases and begins to devolatize. The volatiles are assumed to burn instantaneously, part of the heat released by the combustion of these volatiles contributing towards the total energy of the surrounding gas phase, while the rest of the energy release due to volatiles combustion goes to increase the particle temperature. As the coal particles are transported through the bed a point is reached where all the volatiles are completely released. At this point the remaining char begins to burn, releasing heat and adding mass to the gas phase. This interphase heat and mass transfer is treated in a similar manner as the combustion of the volatiles.

In addition to volatiles release and char combustion, the coal and limestone particles in the bed experience an upward drag force as the fluidizing gas flows upwards in the intersticial voids between the particles. This imparts an upward velocity to the particles which determines the residence time of the particle in the bed for the case of uniform fluidization studied in this paper. Thus it is possible to follow the combustion history of the coal particles as they progress through the bed.

Another feature of the present model is that the bulk of the bed material loses heat to the walls of the container which is assumed to be circular and at constant temperature. Thus the present in-situ model describes the combined interaction of the heat transfer, chemical reaction and fluid mechanical processes that actually take place during the fluidized bed combustion of coal. The model therefore seeks to be physically realistic.

Mathematically, this is accomplished through a continuum mechanical description of the various processes occuring in the fluidized bed. This continuum mechanical formulation of the problem as employed by Anderson and Jackson[10], Krier, Rajan and Van Tassell[11], Pritchett, Blake and Garg[12] and others, employs various spatial averaging techniques. These spatial averaging techniques convert point variables describing the various thermohydrodynamic processes on a microscale of the order of particle size, to averaged variables which represent the processes on a scale large in comparison to the particle size, but small in comparison to the fluidized bed reactor. Invariably these techniques utilize some form of weighting function as described by Anderson and Jackson[10].

The continuum mechanical formulation of the combustion of coal in a uniformly fluidized bed yields six partial differential equations of the mixed hyperbolic-parabolic type. These six partial differential equations for the conservation of mass, momentum and energy of the solid particulate phase and the gas phase are solved to obtain the local gas density, gas temperature, gas velocity, coal particle solidity, temperature and velocity at different locations in the bed. Since the formulation, as used in this investigation, is one dimensional and non-steady, the solution of the six governing partial differential equations yields the above mentioned physical variables along the bed height at various times from the start of the calculation. In this paper the steady state solution of the differential equations is obtained as the long time limit of the unsteady formulation. Full details of the governing equations and the solution method will appear elsewhere.

AUXILIARY RELATIONSHIPS

The continuum mechanical formulation used in the present study of the in-situ combustion of coal in a uniformly fluidized bed incorporates the following physico-chemical processes:

Heat transfer between gas and particles

Interactive drag force between particles and gas

Heat transfer between bulk of material in bed and container walls

Devolitization kinetics of coal particles

Char combustion and heat release

These physico-chemical processes are evaluated and incorporated into the governing partial differential equations on the basis of established empirical auxiliary relationships. Thus the heat transfer between the gas and particles is calculated from the equation

$$\dot{Q} = h\ (Tg - Tp) \quad \ldots\ldots\ldots\ldots\ldots\ldots (1)$$

where the heat transfer coefficient h includes both the convective and radiative coefficients. The convective heat transfer coefficient is evaluated from the Gelperin and Einstein[13] correlation

$$Nu_p = 2.0 + 0.4\ Re_p^{0.67}\ Pr_f^{0.33} \quad \ldots\ldots (2)$$

The radiative component of the total heat transfer coefficient in equation (1) is obtained from the usual Stefan-Boltzmann law.

The drag force correlation between gas and particles, which enters into the momentum conser-

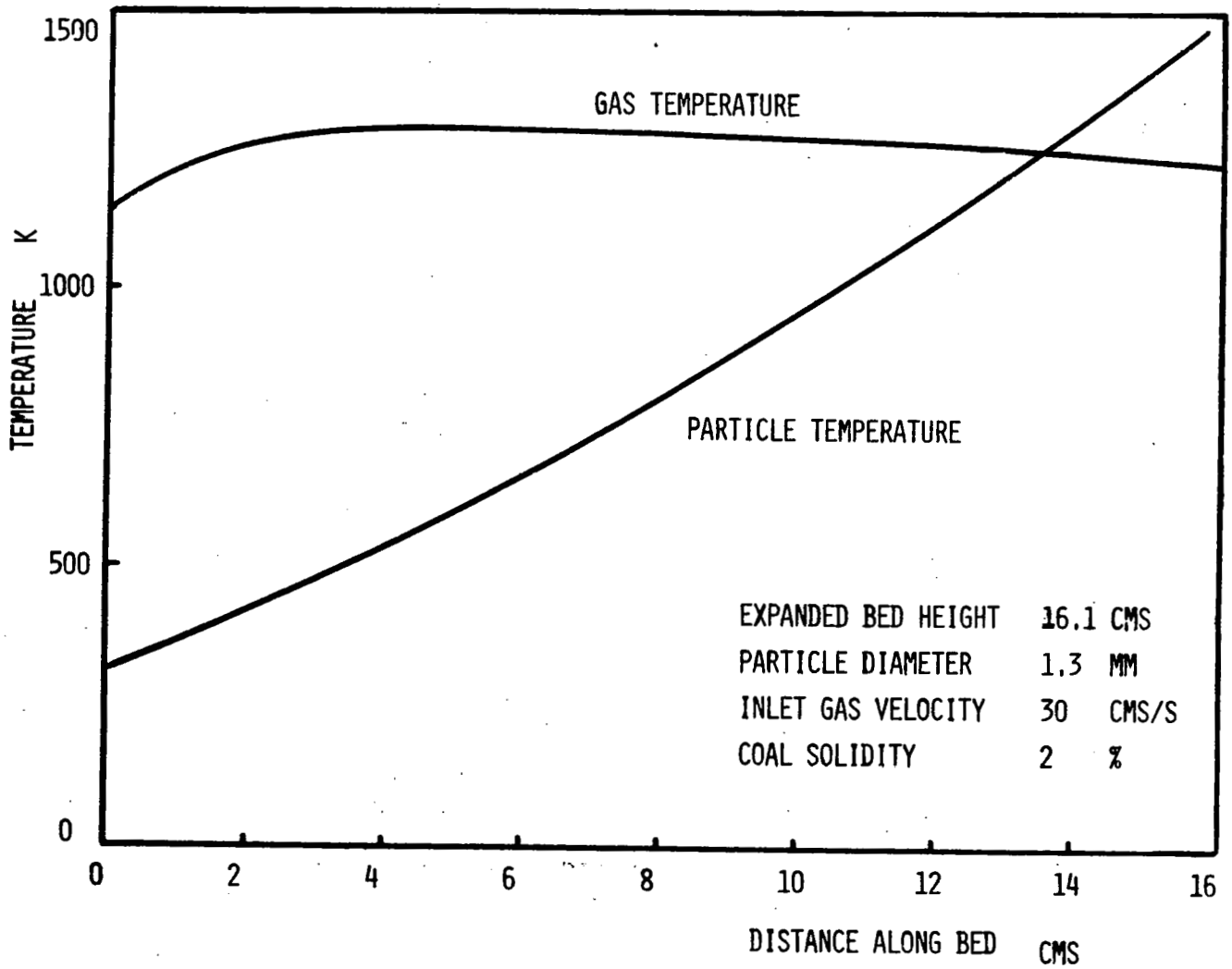

FIGURE 2. GAS AND PARTICLE TEMPERATURE VARIATION ALONG BED HEIGHT

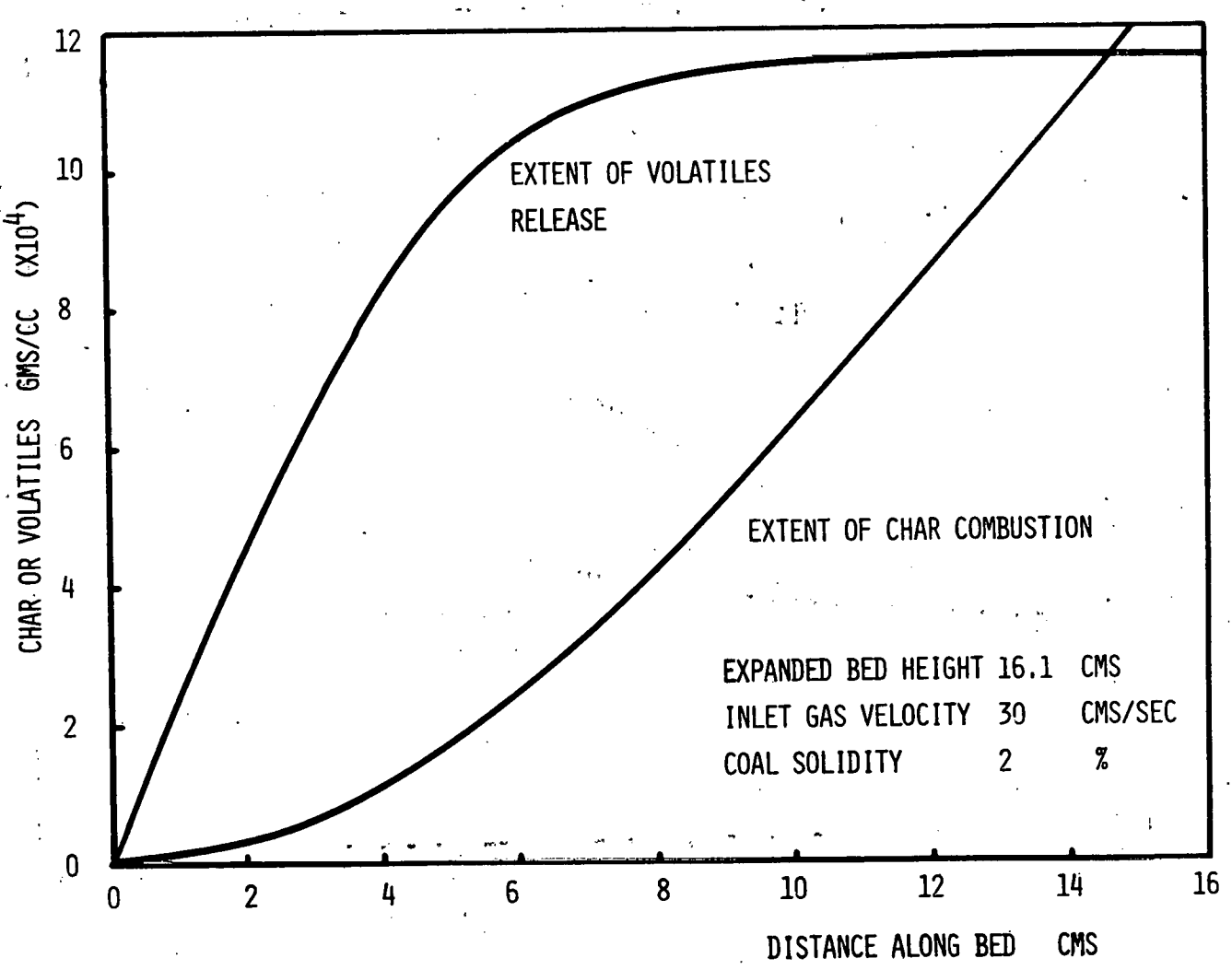

FIGURE 3. VARIATION OF CHAR AND VOLATILES COMBUSTION ALONG BED HEIGHT

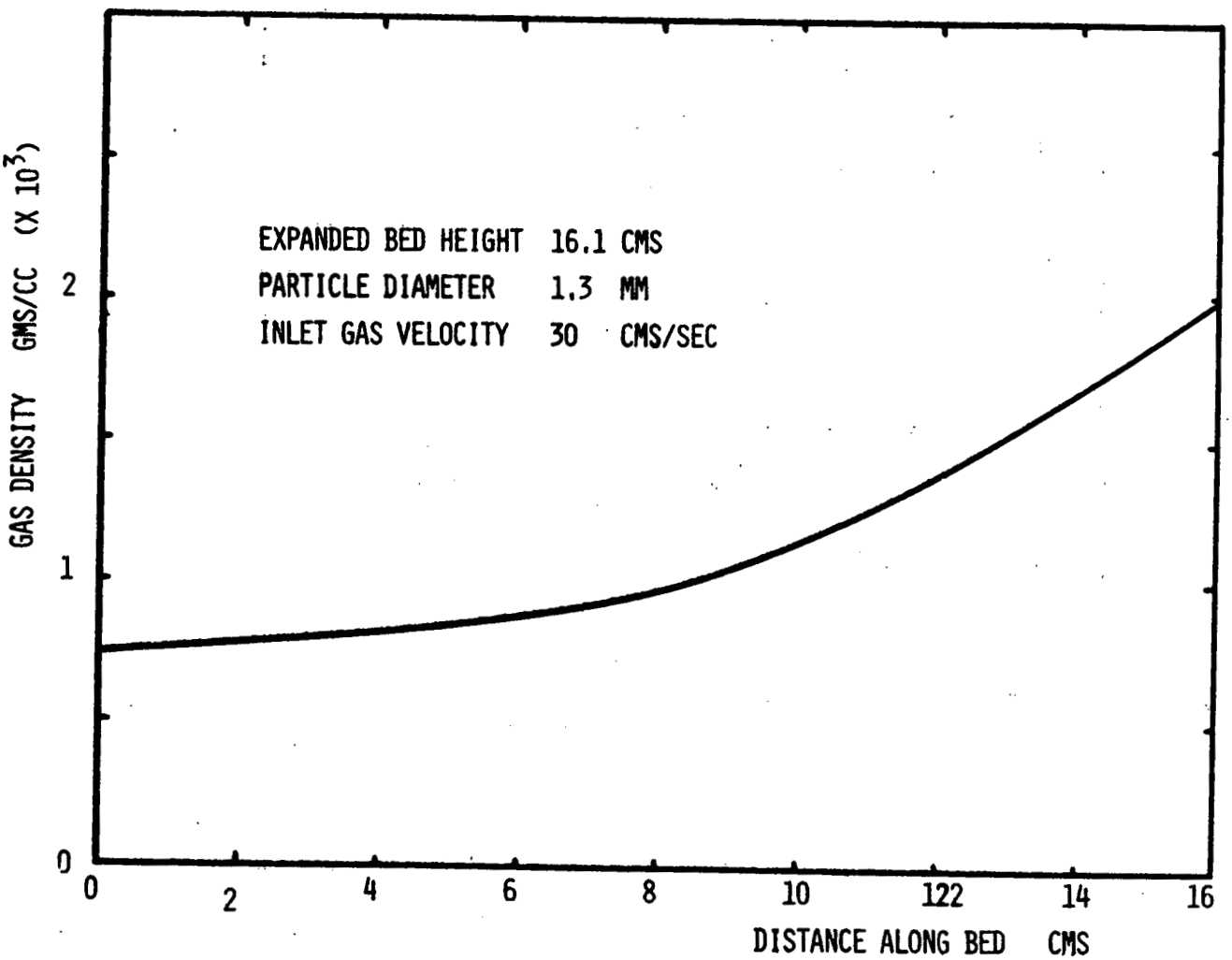

FIGURE 4. VARIATION OF GAS DENSITY ALONG BED HEIGHT

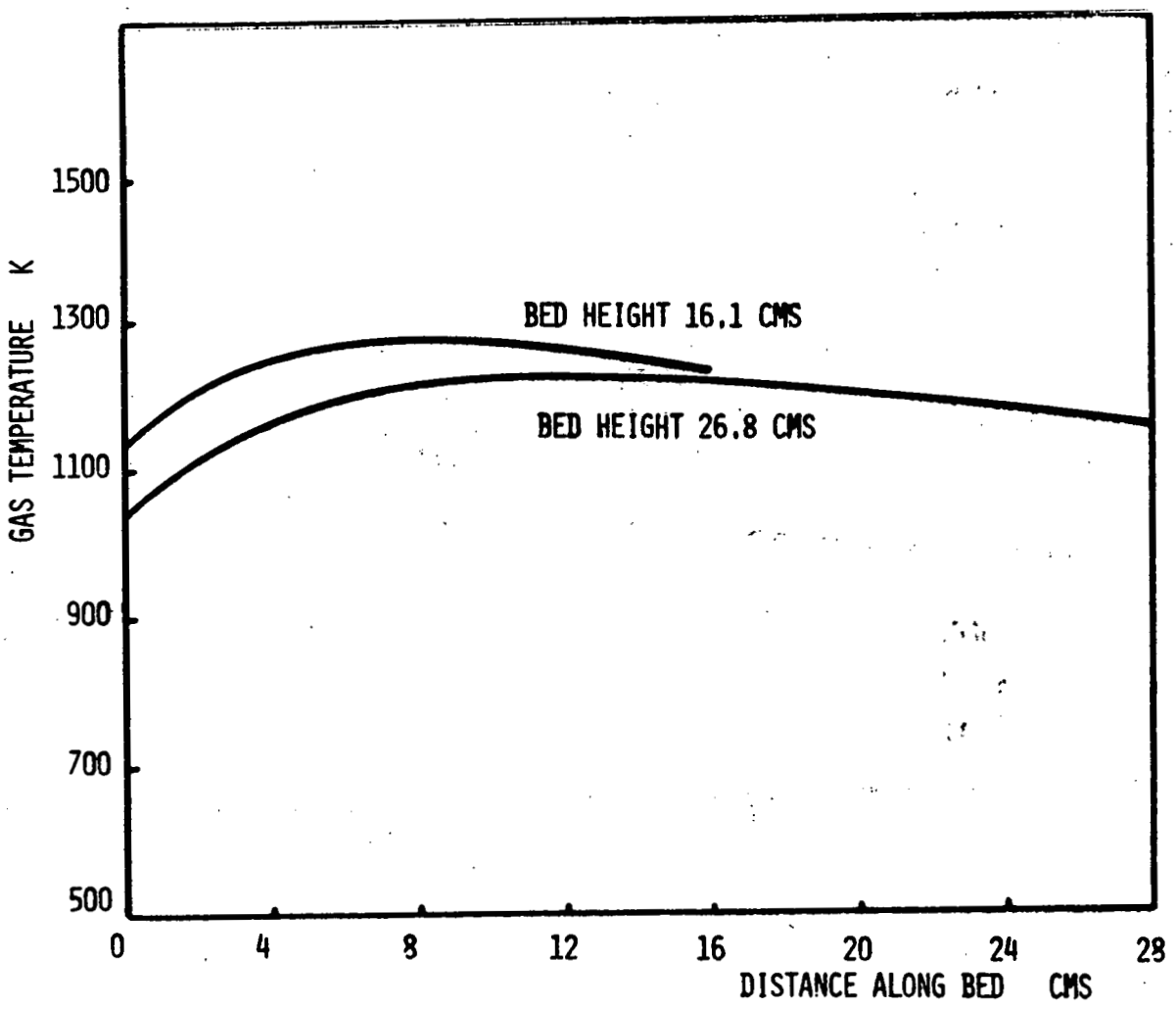

FIGURE 5. INFLUENCE OF BED HEIGHT ON GAS TEMPERATURE

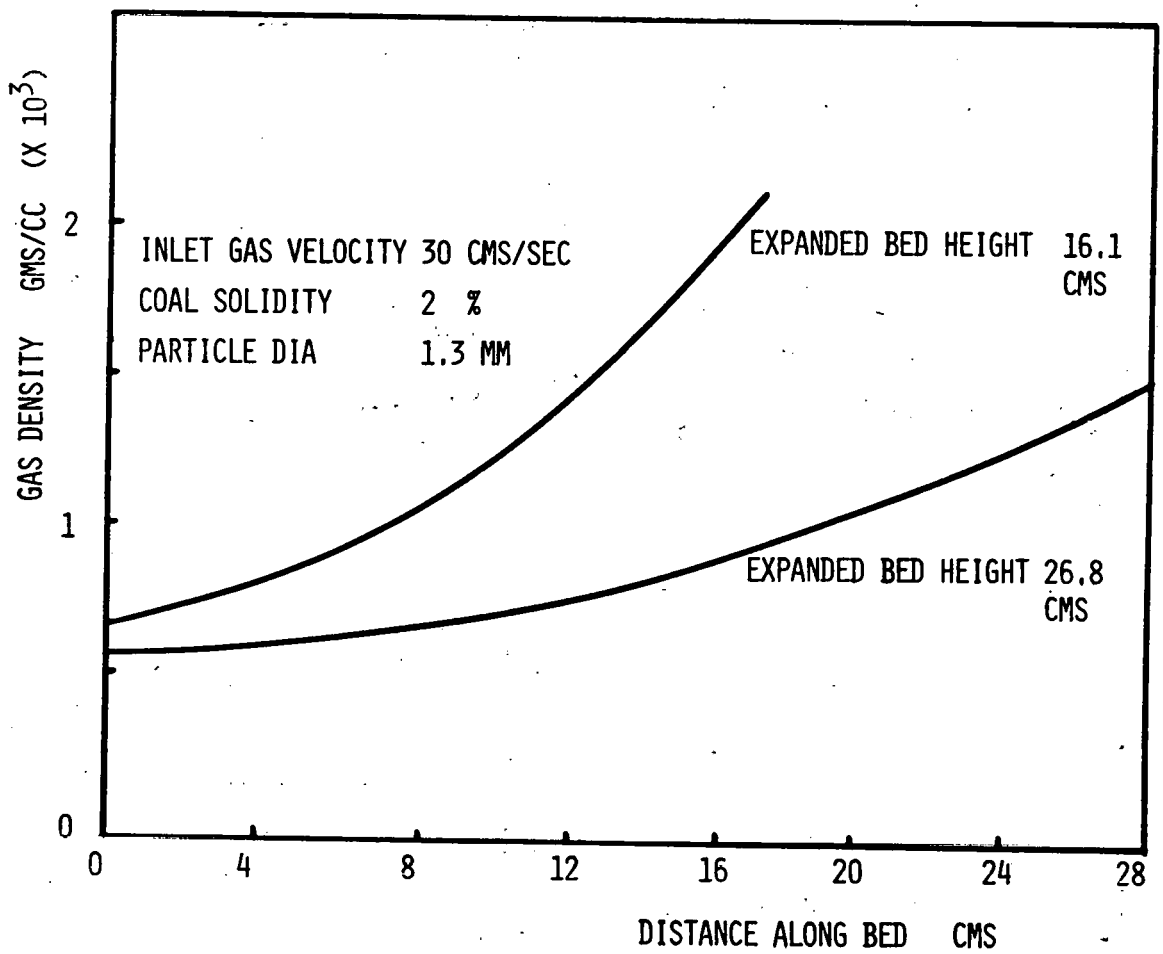

FIGURE 6. INFLUENCE OF BED HEIGHT ON GAS DENSITY

vation equations for the gas and particles, is given by the Ergun [14] equation

$$F \triangleq - g_o \varepsilon \frac{\partial p}{\partial x}$$
$$= \rho \frac{(Ug-Up)|Ug-Up|}{d_p} (1- \varepsilon)[\frac{150(1-\varepsilon)}{\varepsilon Re_p} +1.75] \quad ..(3)$$

This drag force exerted on the particle causes the velocity of the particle to increase continuously from the bottom of the bed as it travels progressively to the top. The residence time of the particle is therefore a function of this drag force, for a uniformly fluidized bed without backmixing.

When the coal particle first enters the fluidized bed its temperature is assumed to be the same as the ambient temperature. This would be the case if the carrier stream of air was not preheated, and is a reasonable assumption for calculation purposes. On entering the bed the coal particle now absorbs heat from the hot surrounding gas and as its temperature begins to rise, devolitization sets in. The devolitization kinetics of the coal particles is based on the empirical work of Badzoich and Hawksley[15]. The weight loss of coal ΔW due to volatiles release is given by the Badzoich and Hawksley model as

$$\Delta W = \Delta W_{max} [1-\exp(-kt)] \quad .....(4)$$

$$\text{where } k = A \exp(-B/T_p) \quad .....(5)$$

Combustion of char is considered to be both diffusionally controlled and chemically controlled. The rate of char reaction is given by

$$R = K P_{O_2}^N, \quad N = 1 \quad .....(6)$$

$$K = \frac{1}{\frac{1}{K_s} + \frac{1}{K_D}} \quad .....(7)$$

$$\text{Diffusional rate } K_D = 2.37 \phi D/d_p R' T_a \quad .(8)$$

$$\text{Chemical rate } K_s = 860 \exp(-18000/T_p) \quad .(9)$$

Char combustion is initiated in the model when the particle temperature reaches 450°K or upon complete release of the volatiles, which ever occurs earlier.

METHOD OF CALCULATION

The six partial differential equations for the conservation of mass, momentum and energy of the gas and coal particles are cast in finite difference form with the aid of suitable numerical schemes. Numerical experimentation is still in progress to determine the optimum scheme for fluidized bed coal combustion calculations. The initial results presented here are obtained by using the Lax Wendroff two step explicit scheme. The steady state solution is obtained as the long time limit of the finite difference formulation.

RESULTS

The in-situ model of coal combustion permits the study of the interactive influence of the various physical and chemical processes occuring locally, and temporally, as they occur in the fluidized bed. Sample results are presented here for a uniformly fluidized bed whose fixed bed height is 16 cms, and expanded bed height is 16.1 cms. The coal particle diameter for this calculation is 1.3 mm and the gas velocity at the distributor plate or inlet to the fluidized bed is 30 cms/second. The coal solidity at the bottom of the bed is 2 percent, that is, two percent of the bed volume at the bottom of the bed is occupied by the coal particles.

Figure 2 shows the variations of particle and gas temperatures along the bed height or height above the distributor plate. It is seen that gas temperature close to the distributor plate falls off slightly. This is because at this region the coal particle temperature is close to ambient temperature and the heat transfer from gas to particles is quite significant. As the particle heats up and begins to devolatize and burn, it releases heat to the gas which in turn causes the gas temperature to rise a little further along the bed height. However, due to the gas motion, the gas is constantly carrying away a significant amount of energy into the freeboard, and its temperature remains reasonably constant throughout the bed. This influence of convective energy transfer is seen by the slight fall in gas temperature towards the top of the bed. Horio and Wen[6] report similar gas temperature profiles for large values of axial dispersion constant of solids.

The particle temperature calculated from the in-situ model is also shown in figure 2. It increases monotonically from ambient temperature at the bottom of the bed to about 150°C above the gas temperature at the top of the bed. This trend has also been observed experimentally.

Figure 3 shows the variation of volatiles release and char combustion along the bed height. The coal particles used in this study were specified to contain 40 percent volatiles, 55 percent char and 5 percent miscellaneous non-combustible components. It is seen from figure 3 that although the coal enters the bed at room temperature, devolitization is almost complete at a height of about 6 cm or slightly less than a third of the bed height. This is shown by the fact that the extent of volatiles released increases continuously till it reaches 40 percent of the coal weight in the bed and then levels off. On the other hand, the extent of char combustion continues to increase steadily, until at the time the particle reaches the top of the bed about 90 percent of the char has been burnt.

Figure 4 shows the variation of gas density along the bed height. The gas density increases gradually for about half the bed height, whereupon it continues to increase but at a faster rate due to the rapid rate of char combustion. This increase in gas density is the direct effect of the mass transfer from the solid coal phase to the gas phase through the combined process of devolitization, volatiles combustion and char com-

bustion.

INFLUENCE OF BED HEIGHT

Figure 5 shows the gas temperature profiles for values of the expanded bed height of 16.1 cms and 26.8 cms. All other parameters were kept the same as in figures 2 - 4. The calculations show that the gas temperature in the bed is slightly higher for the shorter bed. This is in part due to the increased heat transfer from the taller bed to the surrounding walls of the container. Since the coal solidity is the same at inlet to the fluidized bed, roughly the same amount of energy is supplied to the bed from the combustion of the coal. Hence, the bed with the lower wall losses has the higher gas temperature. These higher gas temperatures are reflected in the higher gas density in the shorter bed due to the mass transfer from volatiles and char combustion, figure 6.

CONCLUSIONS

The in-situ model of fluidized bed coal combustion presented in this paper enables the detailed physical and chemical processes and transport phenomena to be included in the model formulation. The model permits the study of a number of parameters important to the efficient design and operation of fluidized bed coal combustors. It permits the evaluation of the relative importance of the various physical, chemical and fluid mechanical phenomena associated with fluidized bed combustion of coal. Sample results are presented. Further development of the model is in progress.

ACKNOWLEDGEMENT

This research is partly supported by the Coal Extraction and Utilization Research Center, Southern Illinois University, Carbondale, Illinois.

NOTATION

- A = pre-exponential factor in rate constant for volatiles release
- B = constant, rate equation for volatiles release (5)
- d_p = particle diameter
- D = diffusion coefficient of oxygen through other species
- F = drag force
- g_o = gravitational constant
- h = film heat transfer coefficient
- k = rate constant for volatiles release
- K = rate constant for char combustion
- K_D = rate of char combustion controlled by diffusion
- K_s = rate of char combustion controlled by chemical kinetics
- Nu_p = Nusselt Number based on particle diameter
- p = pressure
- Po_2 = oxygen partial pressure
- Pr_f = Prandtl Number
- $\dot{Q}$ = rate of heat transfer
- R = first order reaction rate for char combustion
- R' = Universal gas constant
- Rep = Reynolds Number based on particle diameter
- t = time
- T_a = average gas temperature surrounding particle.
- Tg = gas temperature
- T_p = particle temperature
- Ug = gas velocity
- Up = particle velocity
- ΔW = incremental weight loss due to volatiles release
- ΔW max = maximum possible weight loss due to volatiles release
- x = distance

Greek Letters:

- ε = porosity
- ρ = gas density
- ϕ = stoichiometric factor
  - = 1 if CO_2 is main product
  - = 2 if CO is the main product

REFERENCES

1. Avedesian, M.M., and Davidson, J.F., Combustion of Carbon Particles in a Fluidized Bed. Trans. I Chem E, Vol. 51, 1973.
2. Basu, P., Broughton, J., and Elliot, D.F., Combustion of Single Coal Particles in Fluidized Beds. Inst. of Fuel Symp Series, No. 1, Paper A3, 1975.
3. Campbell, E.K., and Davidson, J.F., The Combustion of Coal in Fluidized Beds, Inst. of Fuel Symp Series, No. 1, Paper A2, 1975.
4. Beer, J.M., Baron, R.E., Borghi, G., Hodges, J., and Sarofim, A.F., A Model of Coal Combustion in Fluidized Bed Combustors, Proc. Fifth International Conference on Fluidized Bed Combustion, The Mitre Corporation, 1978.
5. Horio, M., and Wen, C.Y., Analysis of Fluidized Bed Combustors: Part I. Combustion Efficiency and Temperature Profile, AIChE Symposium Series Vol. 74, No. 176, 1978.
6. Horio, M., and Wen, C.Y., Analysis of Fluidized-Bed Combustion of Coal with Limestone Injection, Fluidization Technology, Vol. II, Ed. D.L. Keairns, Hemisphere Publishing Corporation, 1976.
7. Baron, R.C., Hodges, J.L., and Sarofim, A.F., Mathematical Model for Predicting Efficiency of Fluidized Bed Steam Genrators, AIChE Symposium Series, Vol. 74, No. 176, 1978.
8. Chen, T.P., and Saxena, S.C., A Mechanistic Model Applicable to Coal Combustion in Fluidized Beds, AIChE Symposium Series, Vol. 74, No. 176, 1978.
9. Berkowitz, D.A., Ray, A., Sumaria, V., and Wilson,M., Proc. Fifth International Conference on Fluidized Bed Combustion, The Mitre Corporation, 1978.
10. Anderson, T.B., and Jackson, R., Ind. Eng. Chem. Fundamentals, Vol. 6, 1967.

11. Krier, H., Rajan, S., and Van Tassell, W.F., Flame Spreading and Combustion in Packed Beds of Propellant Grains, AIAA Journal, Vol. 14, No. 3, 1976.

12. Pritchett, J.W., Blake, T.R., and Garg, S.K., A Numerical Model of Gas Fluidized Beds, AIChE Symposium Series, Vol. 74, No. 176, 1978.

13. Gelperin, N.I., and Einstein, V.G., Heat Tranfer in Fluidized Beds, in Fluidization, ed. J.F. Davidson and D. Harrison, Academic Press 1971.

14. Ergun, S., Fluid Flow Through Packed Columns, Chem. Eng. Prog., Vol. 48, 1952.

15. Badzoich, S., Hawksley, P.G.W., and Peter, C. W., Kinetics of Thermal Decomposition of Pulverized Coal Particles, Ind. Eng. Chem. Process Design and Develop. Vol. 9, 1970.

Questions to S. Rajan:

Q: S.C. Suesena, University of Illinois

You did not consider bubbles in the fluid bed?

A: Not in this simplified model. I should mention some of the boundary conditions for our calculations. At the moment the particle is introduced into the bed, we consider it to be at room temperature, whereas the gas is at a much higher temperature. So the boundary condition at the bottom of the bed is that the coal particle is at room temperature. We fix a temperature for the gas at the start of calculation. The tme solution yields a bed temperature with all of the forces interacting. That is why the particle temperature continues to increase as it travels through the bed.

Q: (Participant not identified)

In attempting to apply some of this theoretical work to the actual problems which we have in designing fluidized beds, there is also a problem with omissions made in any specific model. As you develop this model are there any plans to include particle swelling increase in active burning surface at the boundary of the particle? It is very difficult to instantaneously inject fuel into a bed. So you have to consider a zone for the injected fuel.

A: These were things that I hoped would come up in the discussion. I will comment on your second point first. You are correct about the need for a fuel zone model. These are some of the things that we hope to do as we progress with the model. Particle swelling is already taken into account in the present model. One problem with these models is that computing time increases greatly as you add complexities, that is why we try to stay with a basic model. We do plan to have add-on packages to the basic model to accommodate specific needs.

A RADIATIVE PACKET MODEL FOR HEAT TRANSFER IN FLUIDISED BEDS

Krishna K. Pillai

NCB, Coal Utilisation Research Laboratory,
Leatherhead, England.

ACKNOWLEDGEMENT

The work reported in this paper was performed at The University of Aston in Birmingham, England.

INTRODUCTION

Numerous mathematical models (1-12) have now been postulated for the prediction of heat transfer rates to surfaces immersed within fluidised beds. None is definitive, yet the most successful models are those which consider the periodic, unsteady-state heat transfer between the bed and the surface. In general, these models consider transient conduction alone and apply only to non-radiative situations (bed temperatures less than 600°C).

Models can broadly be divided into:

1. Single particle models; where the fluidised bed is considered to consist of a coninuous gas phase containing a discrete solid phase made up of single particles.
2. Emulsion packet models; where the fluidised bed is considered to consist of a continuous emulsion phase containing a discrete gas phase. Here the emulsion phase is taken to be the solid particles together with the attendant gas flow required for incipient fluidisation, while the discrete gas phase consists of particle-free gas bubbles.

All models are necessarily 'surface renewal' models in that they consider transient conduction, between the surface and, either single particles or the emulsion packet, to take place only during the period when a particle or an emulsion packet is resident at the surface. The renewal mechanism itself is usually attributed to bubble frequency and/or motion.

SINGLE PARTICLE MODELS

These models, based on the Botterill and Williams single particle model (1), consider single spherical particles coming into contact with the immersed surface; transient conduction then taking place through a gas film at the point of contact until the particle is replaced by another. Using relaxation techniques the transient heat conduction equations are solved numerically. Such model solutions can be made to agree with experimental data obtained at controlled residence times by choosing an appropriate thickness for the gas film separating the particle from the surface. The major drawback of these models (2-6) lies in that the assumed gas film thickness is purely arbitrary, and is not based on direct experimental evidence. Furthermore, such models cannot be expected to be accurate in situations where the temperature penetration depth may exceed the diameter of a single particle. Though variations of the single particle model have attempted to take surrounding particles into account, the increasing complexity has not

eliminated the need for a gas film of arbitrary thickness. Moreover the agreement with experimental data is good only at low particle residence times (small Fourier Number), a condition not generally associated with fluidised bed coal combustors.

EMULSION PACKET MODELS

Emulsion-phase packet models are all based on the Mickley and Fairbanks conception of a packet (8), as originally proposed in Fairbanks' thesis (7). Here transient conduction is considered to take place between the surface and an emulsion-phase packet which comes into contact with the surface for a short time and then returns to the body of the bed. The packet is defined as a semi-permanent grouping of particles having uniform thermophysical properties which are equal to those of the incipiently fluidised bed. The packet is assumed to be rigid with no relative motion between the particles making up the packet. The packet is further assumed to be stationary during it's residence time at the surface. Packet models then generally use a constant surface temperature or a constant surface flux boundary condition to solve the conduction equations. Thus instantaneous Nusselt Numbers are obtained as a function of the prevailing Fourier Number.

$$Nu_i = f(Fo) \qquad (1)$$

where

Nu_i = Instantaneous Nusselt Number
$= h_i d_p / k_f$

Fo = Fourier Number
$= a_e t / d_p^2$

h_i = Instantaneous heat transfer coefficient

d_p = particle diameter

k_f = gas-phase thermal conductivity

a_e = emulsion-phase thermal diffusivity

t = time

The time-mean value of the Nusselt Number can then be obtained by assuming some mean particle residence time or residence time distribution, and integrating the instantaneous Nusselt Number over the time period.

The major inaccuracy of these models lies in that the thermo-physical properties of the packet are not, in fact, uniform. The existence of a surface brings about a variation in the particle packing at the surface, and the resultant effects of the voidage variation on the packet properties are not taken into account. Thus, such models effectively assume that the temperature penetration into the packet is much larger than the depth of the property boundary layer at the packet/surface interface. Consequently, such models may be expected to have validity at long residence times (large Fourier Number), but will fail at short residence times (small Fourier Number).

Various extensions and modifications of the basic packet model have now been put forward, and the most successful to date has been the Kubie-Broughton variable property boundary layer model. Here the variable packet properties brought about by the voidage variation at the packet/surface interface are taken into account. Kubie (11) approximates the voidage variation by a simple geometrical function which has now been experimentally verified (13). The voidage within the packet is taken as a function only of x, the normal distance from the constraining surface.

For $z \leq 1$

$$\varepsilon(z) = 1 - 3(1-\varepsilon_b)\ (z - 2z^2/3) \qquad (2)$$

For $z > 1$

$$\varepsilon(z) = \varepsilon_b \qquad (3)$$

where

$z = x/d_p$

$\varepsilon(z)$ = voidage at z

ε_b = voidage in the bulk of the bed

Kubie and Broughton (12) then show that all the thermo-physical properties of the packet can be represented as simple functions of the voidage and the local packet temperature. The one-dimensional transient conduction equations are solved numerically using a constant flux boundary condition, and the solutions show very good agreement with experimental data obtained at controlled residence times. This model effectively assumes that the property boundary layer does not exceed beyond one particle diameter, but, as has been shown in (13), this is a very good approximation of the real situation. Thus no physically unjustified concepts are required and, within the conductive regime, this is the most useful model proposed so far.

A RADIATIVE PACKET MODEL

The model proposed here is based on the Mickley Fairbanks conception of heat transfer to emulsion packets which periodically come into contact with the immersed surface. Here, too, the packet is defined as a semi-permanent grouping of particles which, during it's contact time with the surface, is rigid and stationary with no relative movement between particles. Based on the Kubie-Broughton concept of variable packet properties at the constraining surface, the interior of the packet is considered to be a simple gas/solid system (Figure 1). The area voidage ε, within the packet is taken to be constant along any plane parallel to the surface and hence is a function only of x, the normal distance from the surface. Thus the proportion of solid area $Y(x)$, at any point is given by

$$Y(x) = 1 - \varepsilon(x) \qquad (4)$$

and the packet interior takes up the form illustrated in Figure 1. The cross-sectional area of the solid phase along a plane parallel to the constraining surface is given by

$$A(x) = A_p\, Y(x) \qquad (5)$$

where

A_p = cross-sectional area of the packet.

It is further assumed that the temperature within the packet varies only with time and the distance x. Along any x-plane therefore, the temperature within the solid phase is assumed equal to that of the gas phase. Only one-dimensional, unsteady-state heat transfer need therefore be considered.

Whether radiative transfer takes place from the packet to the surface, or from the bulk of the bed to the packet, or across the voids within the packet itself, depends upon the form of the voidage function. With the gas phase assumed to be completely transparent to radiation, the packet can be divided into regions corresponding to the directions of nett radiative heat transfer (Figure 2, Table 1). The bed and the surface are assumed to radiate as black bodies.

The model thus assumes that for conductive heat transfer the packet can be treated as being made up of successive porous slabs, each having a different characteristic area voidage. For radiative transfer the packet is treated as a solid having a shape defined by the voidage function. Assuming further that the heat capacity of the gas phase is negligible in comparison with that of the solid phase an energy balance on an elemental slab leads to the differential equation governing the packet temperature. The

TABLE 1. RADIATIVE REGIONS IN THE PACKET

REGION	NETT RADIATION	
	FROM	TO
from x = 0 to dA/dx = 0 (max)	packet	surface
from dA/dx = 0 (maximum) to dA/dx = 0 (min)	packet or bed	packet or surface
for A = constant	bed	packet or surface

equation is non-linear and must be solved numerically (14).

The boundary conditions used are:

1. At some specified value of the distance x, from the surface (10 d_p), the packet temperature T(x), is equal to the bed temperature T_b.
2. A constant surface temperature (T_w) boundary condition leading to an energy balance at the packet/surface interface. This energy balance includes:
   a. heat conduction into the surface element from the rest of the packet,
   b. heat conduction from the element to the surface,
   c. radiation from the element to the surface, and
   d. radiation from the bed to the surface through the voids in the packet.

The initial condition used is that at time zero the entire packet is at the bed temperature T_b.

Solutions along with the method of solution are detailed in Reference (14). Once the instantaneous temperature profiles within the packet are known, the instantaneous conductive and radiative fluxes from the packet to the surface are calculated. Addition of the fluxes due to conduction from the bubble phase and radiation from the bed through the bubble phase provides the total instantaneous fluxes to the surface. Time-mean values are then obtained from a numerical integration of:

$$Nu_m = \frac{1}{t_r} \int_0^{t_r} Nu_i \, dt_r \qquad (6)$$

where t_r is the residence time of the packet at the surface.

MODEL PREDICTIONS

The solutions obtained (14) have separated the conductive and radiative components of the total flux to the surface. These solutions are presented in the form of Nu-Fo plots, where the non-dimensional parameters are:

Nu = Nusselt Number = $h\, d_p / k_f$

Fo = Fourier Number = $\alpha_s\, t / d_p^2$

S = Radiation parameter
= $\sigma e\, F\, d_p\, T_b^3 / k_s$

k_r = gas/solid conductivity ratio

μ = surface/bed temperature ratio

where

α_s = solids thermal diffusivity

The suffixes have the following meanings:

ic = instantaneous conductive

ir = instantaneous radiative

mc = time-mean conductive

mr = time-mean radiative

Typical solutions are illustrated in Figure 3. The effect of the surface temperature on the radiative flux and that of the conductivity ratio on the conductive component are illustrated in Figures 4 and 5.

Since the basic solutions are merely marching solutions, comparison with experimental data requires the choice of some particular value of residence time or residence time distribution. These have been obtained using the expressions given by Gelperin and Einstein (in 15). Though there is considerable doubt as to the accuracy of these expressions, they provide a means of illustrating the predictions of the model.

By using values of residence time calculated to match the experimental conditions of a heat transfer investigation (14), model predictions for Nu_m can be obtained and compared with experimental values.

DISCUSSION

The heat transfer model described above is an extension of the Kubie-Broughton model in that radiation is now included. Voidage variation is taken into account and the concept of treating the packet as a simple gas-solid system for conduction derives from the methods often used to treat porous solids. In addition the definition of the area voidage within the packet is effectively assumed to be the shape function controlling the nett radiation emanating from the packet. The model thus considers a variable voidage packet, the conduction within which can be separated into a solid and a gaseous component, and the radiation from which comes from the solid phase through the gaseous phase.

Though this, like any other, model can only be satisfactorily tested when experimental data, obtained at high bed temperatures and under controlled residence time conditions, becomes available; some qualitative conclusions can usefully be drawn:

1. Though this model simplifies the calculation of packet thermo-physical properties by assuming a simple gas-solid system within the packet, the model solutions at non radiative temperatures are in good agreement with the Kubie-Broughton conductive solutions. This suggests that providing the property boundary layer concept is used, simple approximations for packet properties will suffice.

2. Even though the property boundary layer is only one particle diameter deep, the thermal penetration depth at typical fluidised bed residence times (0.2-2s), can be as great as three or four particle diameters. Consequently variable property boundary layer models are the only ones which, without resorting to any unjustified expedients, are inherently valid at realistic residence times.

3. The packet residence time does not appear to be significant to the radiative Nusselt Number. However, the importance of the radiative Nusselt Number increases

with increasing residence time as the conductive component decreases. This is in good agreement with the limited experimental data available for direct comparison (14).

4. Increasing the surface temperature brings about a large increase in the radiative component as would be expected. The magnitude of the increase is in good agreement with the high temperature data reported in (16).

5. The radiative Nusselt Number increases with increasing particle size but is largely unaffected by variations in the gas/solid conductivity ratio.

6. The conductive component is not very sensitive to the radiation parameter S. Thus the the temperature dependance of the conductive component is restricted to the changes in gas-phase conductivity.

7. The conductive component decreases sharply with increasing residence time.

The above conclusions are in general qualitative agreement with experimental data (14,16). The uncertainty about the residence times used (±50%) suggests that this is the major source of any disagreements between model predictions and experimental data. The assumption that the Fluidised bed behaves as a black body is now open to some question since recent work (17) indicates that the packet emissivity may be as low as 0.8. The model could thus be overestimating the radiative contribution significantly at long residence times. The model solutions indicate that the radiative and conductive components of heat transfer can be considered independant of each other.

REFERENCES

1. Botterill J S M and Williams J R, 1963, Trans I Chem E, 41, (5), 217.

2. Gabor J D, 1970, AIChemE Symp Ser, 66, (105), 76.

3. Botterill J S M and Butt M H D, 1968, Brit Chem Eng, 13, 1000.

4. Boterill J S M, Butt M H D, Cain G L and Redish K A, 1967, Proceedings International Symposium on Fluidisation, Netherlands University Press, Amsterdam.

5. Botterill J S M, Butt M H D, Cain G L, Chandrasekhar R and Williams J R, 1967, Proceedings International Symposium on Fluidisation, Netherlands University Press, Amsterdam.

6. Zeigler E N, Koppel L B and Brazleton W T, 1964, I&EC Fund, 3, (94), 324.

7. Fairbanks D F, 1953, ScD Thesis, Massachusetts Institute of Technology.

8. Mickley H S and Fairbanks D F, 1955, AIChemE Jnl, 1, 374.

9. Baskakov A P, 1964, Int Chem Eng, 4, (2), 320.

10. Baskakov A P and Berg B V, 1967, Khim Prom, 43, (6), 439.

11. Kubie J, 1974, PhD Thesis, The University of Aston in Birmingham.

12. Kubie J and Broughton J, 1975, Int J Heat & Mass Transfer, 18, 289.

13. Pillai K K, 1977, Chem Eng Sci, 32, 59.

14. Pillai K K, 1975, PhD Thesis, The University of Aston in Birmingham.

15. Davidson J F and Harrison D (ed.), 1971, Fluidisation, Academic Press, London.

16. Pillai K K, 1976, Letters J Heat & Mass Transfer, 3, 131.

17. Lewin D A, 1975, PhD Thesis, The University of Aston in Birmingham.

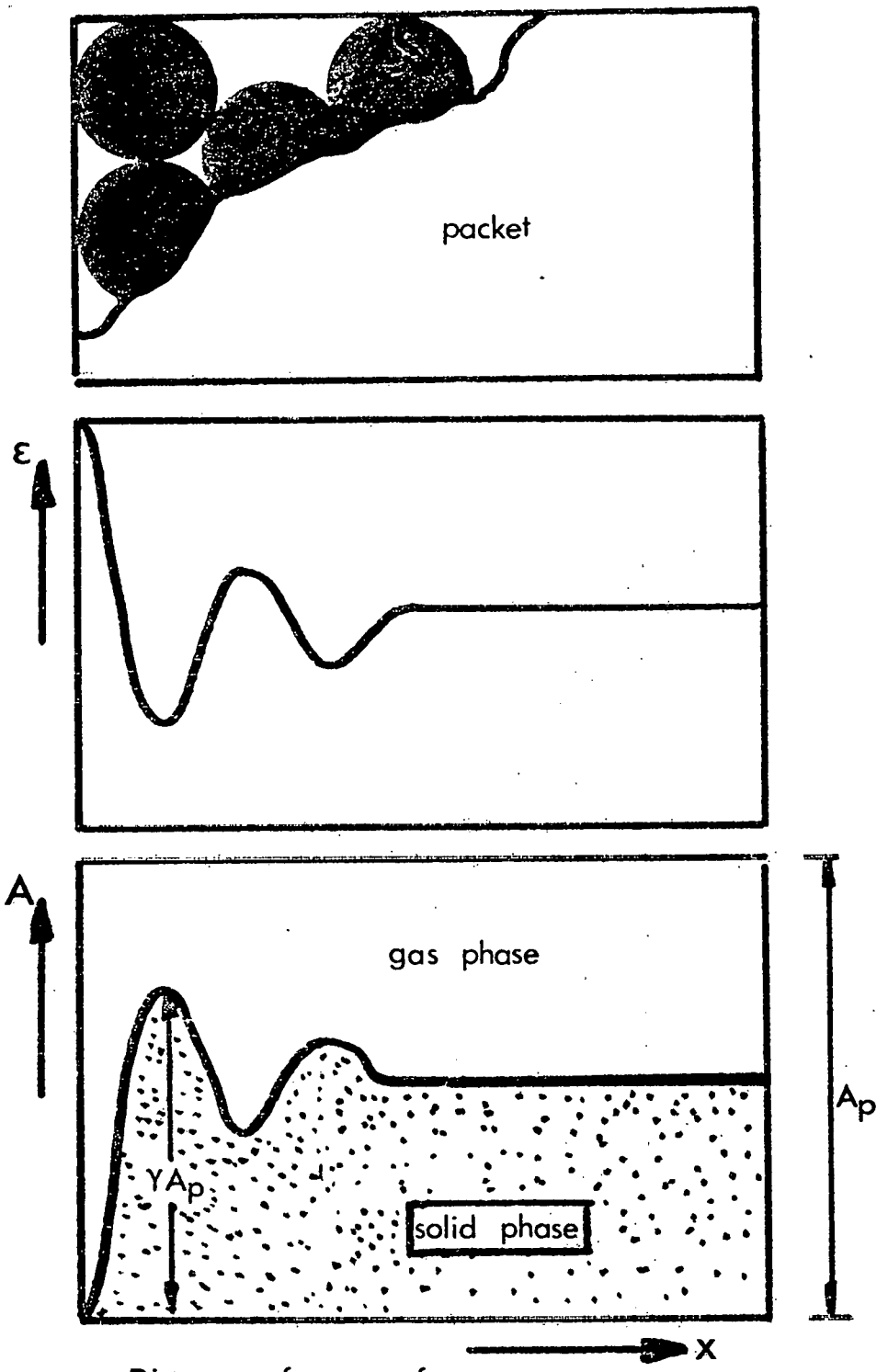

FIGURE 1. THE PACKET CONCEPT

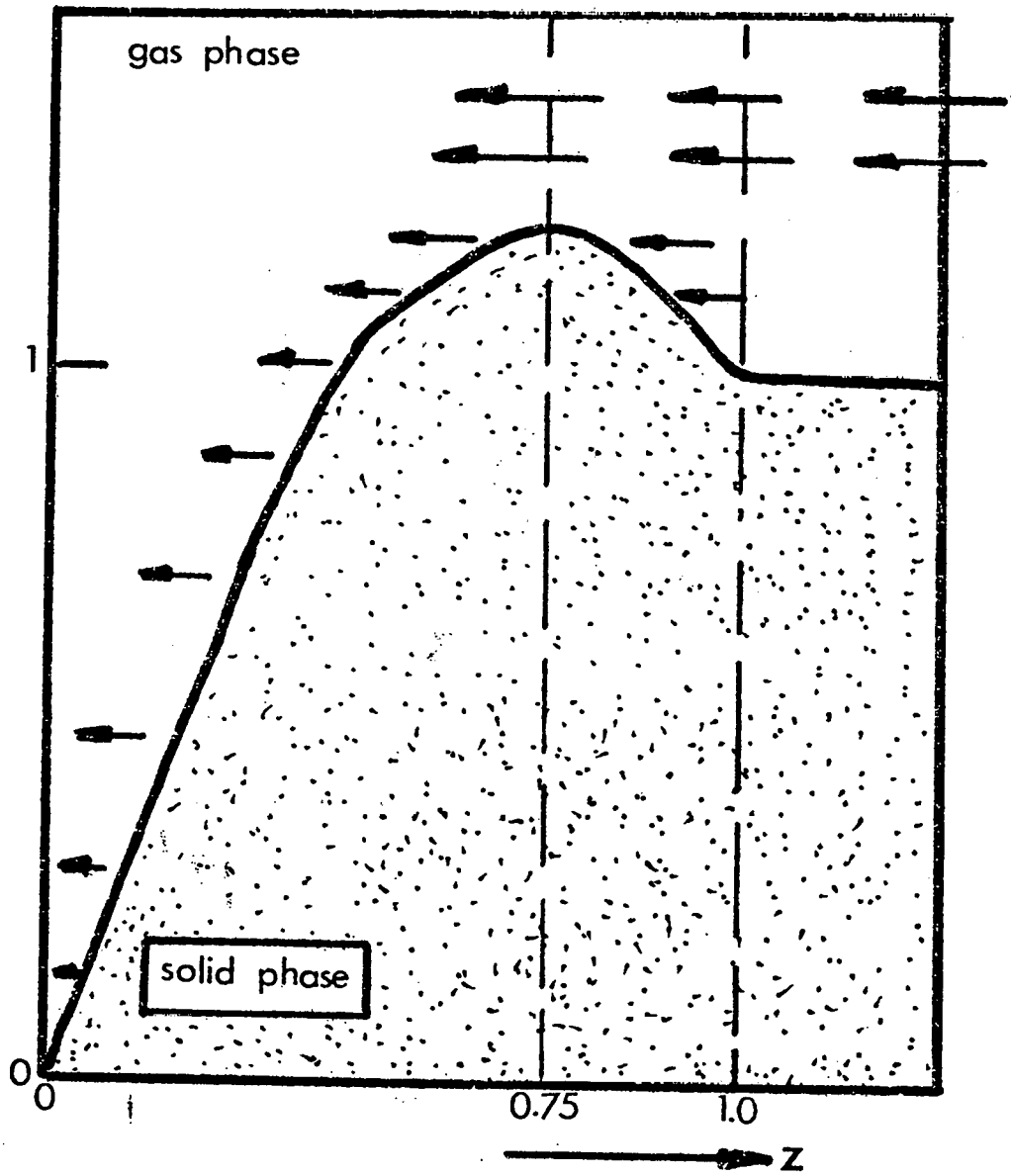

FIGURE 2. RADIATIVE REGIONS WITHIN A PACKET

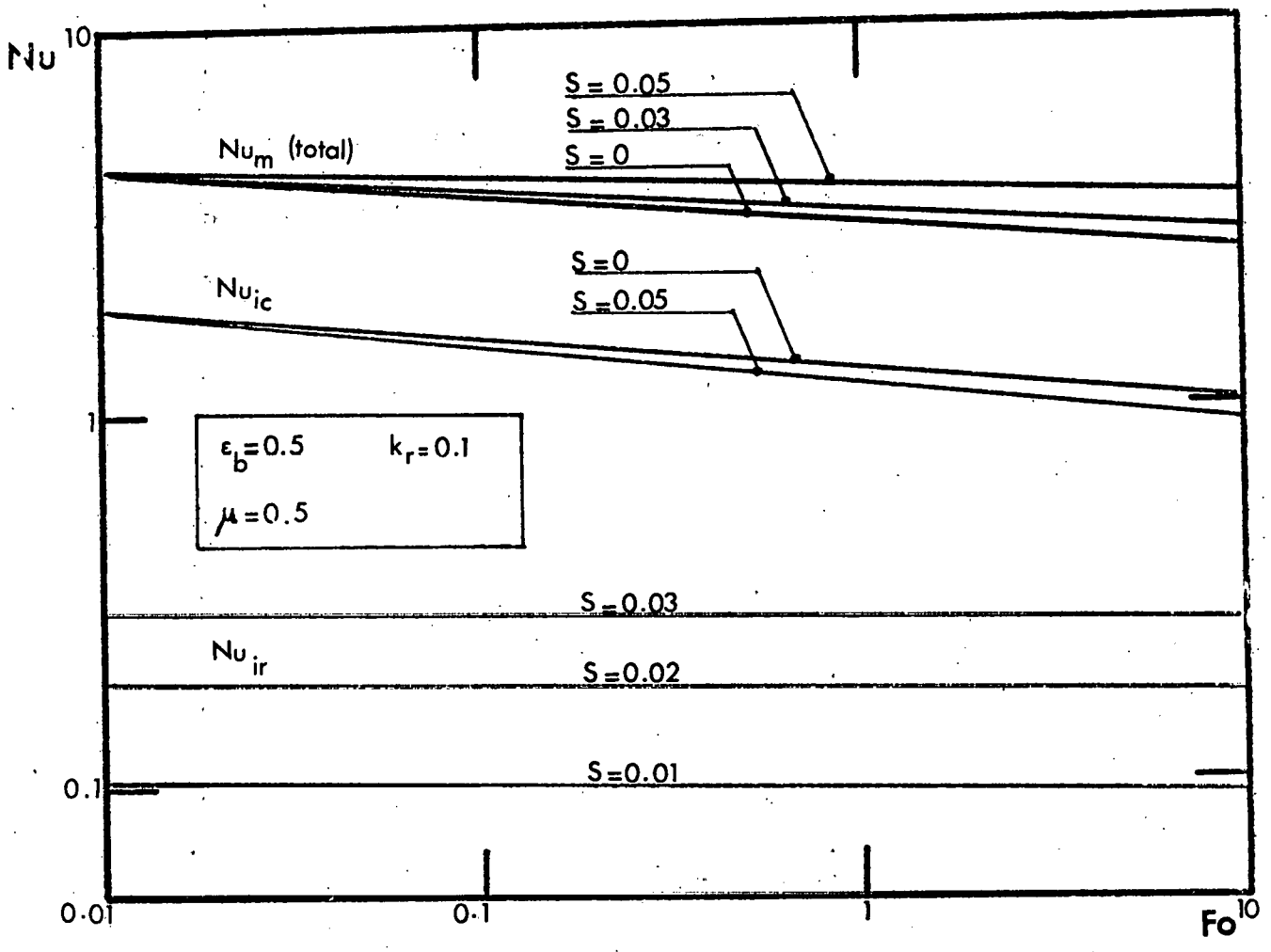

FIGURE 3. TYPICAL MODEL SOLUTIONS

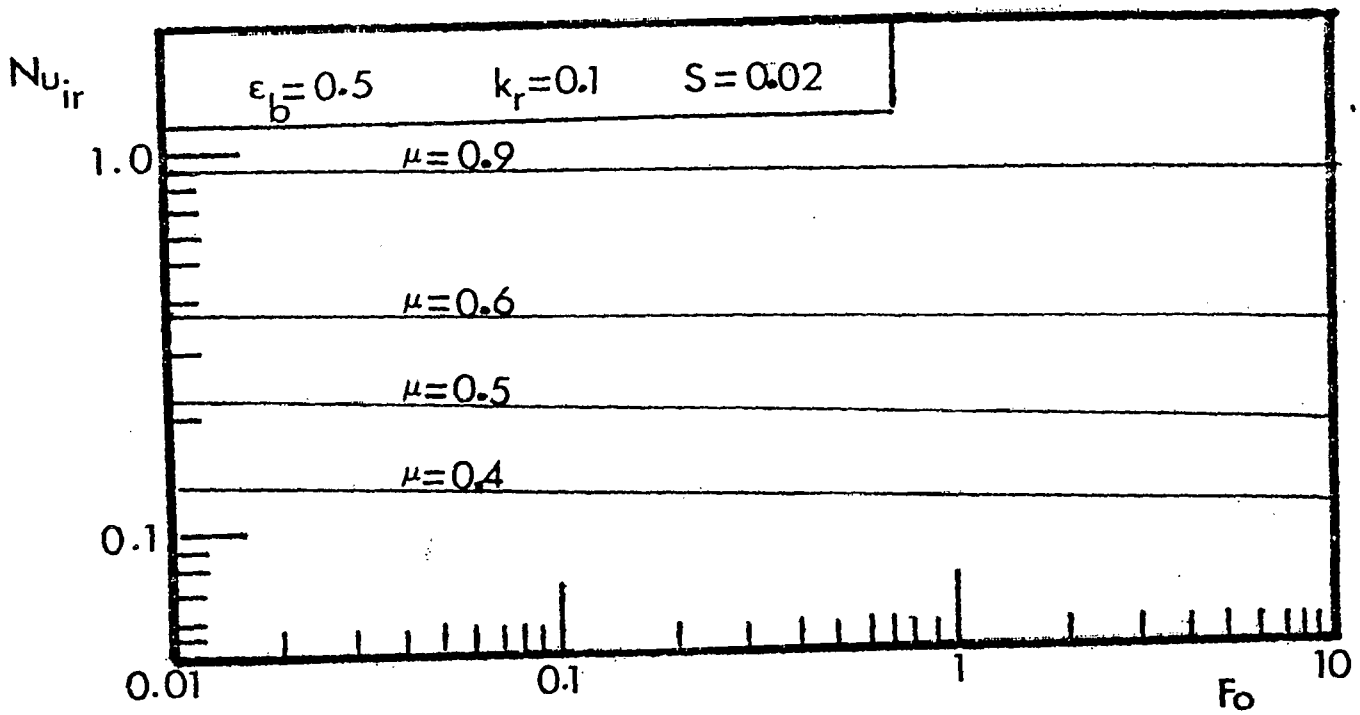

FIGURE 4. EFFECT OF SURFACE TEMPERATURE ON MODEL SOLUTIONS

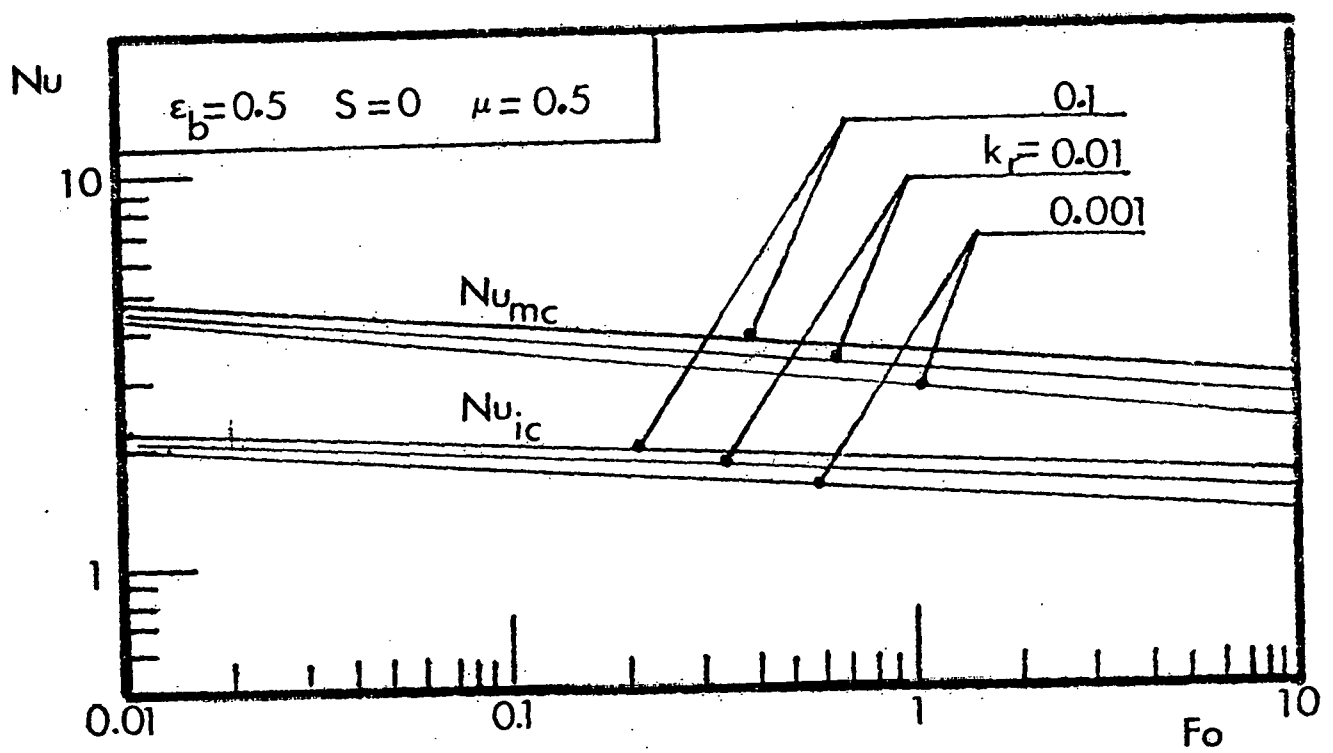

FIGURE 5. EFFECT OF CONDUCTIVITY RATIO ON MODEL SOLUTIONS

Questions to K.K. Pillai:

Q: (Participant not identified)

We have been concerned with trying to predict performance in real FBC units. If the thinking is extended into a "frosh-slosh" zone on top of the bed where you try to measure the sensible height of the bed, from a pressure gradient and call that the extended bed height, there is a very active zone above the bed which is predicted by some of the models. I think this has been born out by Pope, Evans and Robbins at Alexandria, where they measured the heat transfer height of the bed. This generally is characterized as the height of the bed over which the heat transfer conductance is maintained. When you get into the freeboard, people have modeled the freeboard forgetting that the particle and radiation equilibrium temperature is the same as the surroundings. In practicle FB combustors, we are dealing with water cooled enclosure walls that might be at 500-600°F, the gas of the bed is 1400-1600°F, and it has been assumed that the particles are in equilibrium with the gas -- which they aren't. When you do the heat balance around the particles, you'll notice that there is a described pronounced drop in the particle temperature and when you are trying to define and model the freeboard, it makes a drastic difference in the performance of the freeboard. I just wish to say that the extension of this model, a little further up, will give you some very interesting understanding of what is going on in the system.

A: It is just so difficult to describe what is happening in this "splash" zone. Again, you tend to use empirical relations for what is happening above the bed and they are more accurate than any model I can think of. In fact, for heat transfer in general, I would much rather you give me a velocity and a size and I could guess what your heat transfer coefficient is for the cooling fluid used rather than using a model to calculate it.

Q: (Participant not identifed)

I understand that the key parameter in your model is the successful prediction on the Rosenstein Distribution, and I assume that you are talking about a distribution of residence time for your controlled residence time rather than a sort of impass distribution and experimentally, I imagine that this is difficult to obtain.

A: I agree that in a real situation you need a residence time distribution because you have a particle size distribution. When we talk about doing controlled experiments to test models, we are talking about using particles of fairly narrow size range. We get instantaneous solutions and you have to use some sort of distribution to get a time average. We used one of the residence time distributions in the literature and integrated it over the time.

Q: (Participant not identified)

I seem to like all your comments, but I have a lilttle difficulty because if we see through the confusion of all these models, we can see some order in them. My suggestion is that if we go through any of them, a gas layer is physically and experimentally valid and and necessary. The question is that in the pure conduction regime, where radiation is not important, one could establish, from the existing experiments, the thickness of this air gap. Then use that thickness to go for the high temperature and radiation.

A: I must admit that I am not convinced about a gas film. If you say you have measured it, the methods were all indirect and it is a backward and circulation calculation that I do not necessarily believe, but I will keep an open mind on that.

Q: (Participant not identified)

If you consider radiation, you have a gas bubble passing the surface, is the radiation sufficient to give you a significant heat transfer as it passes?

A: We have generally assumed that there has been no radiation from the bubble. We see radiation from the bed through the bubble.

THE EFFECTS OF DEVOLATILIZATION KINETICS ON THE INJECTOR REGION OF FLUIDIZED BEDS

Ronald J. Bywater

The Aerospace Corporation
El Segundo, California

Introduction

The application of fluidization technology to the efficient and environmentally acceptable combustion of coal has brought to the forefront the large-particle (>1 mm), high superficial velocity (>1 m/sec) fluidization regime. The most notable feature of this fluidization application is that it operates in the slow bubble regime[1] such that the large particle bed is characterized as turbulent-churning[2] as distinct from the fast-bubbling, small-particle bed. The bottom-fed, shallow, atmospheric fluidized bed combustor (AFBC) envisioned for large utility scale applications is an example of a large-particle system. The special characteristics of such AFBC's contribute to a unique spatial structure which strongly influences performance and scaling. This spatial structure associated with the AFBC coal injector region and its dependence upon finite devolatilization and solids circulation rates is the subject of this paper.

Figure 1 shows a typical commercial scale AFBC whose vertical as well as lateral dimensions are 1 m. Utility scale beds, although still restricted to the 1-m height, may be many meters in lateral dimension with one coal feed per square meter. Therefore Fig. 1 also represents the 1 m^3 module upon which large-scale utility beds would be based. Upon entering the bed, the coal is transported by the solids circulation pattern, devolatilizes and, once devolatilized, undergoes char combustion. The volatiles account for as much as 50 percent of the coal heating value. Therefore, depending on comparative devolatilization and mixing times, regions of fuel- (volatiles) rich gas may exist in the vicinity of the injected coal giving rise to group combustion.

Whether or not group combustion occurs depends on how the volatiles are transported within the bed as they are formed. Some understanding of volatiles transport is provided by the experiments of Jovanovic[3] which determined the gas flow patterns associated with the slow bubble regime. Those experiments show that a tracer gas injected at the bottom of a tube-filled, large-particle bed rises as a plume. This is counter to observations in vigorously bubbling small-particle beds. These results suggest that volatiles released from injected coal rise through the bed as depicted in Fig. 1, burning in a diffusion flame with the surrounding oxygen. If the diffusion flame does not close within the bed, volatiles escaping into the freeboard will mix with air and burn, as first suggested by Park, et al.[2] in an explanation of widely varying freeboard species measurements.[4] Apparently, the spatial structure of the injector region resulting from the coupling of slow bubble regime gas flow patterns and dense volatiles release strongly impacts the AFBC behavior and, specifically, the nature of the combustion therein. This underscored the importance of volatiles evolution and, in particular, the injector region as dominant phenomena in AFBC.

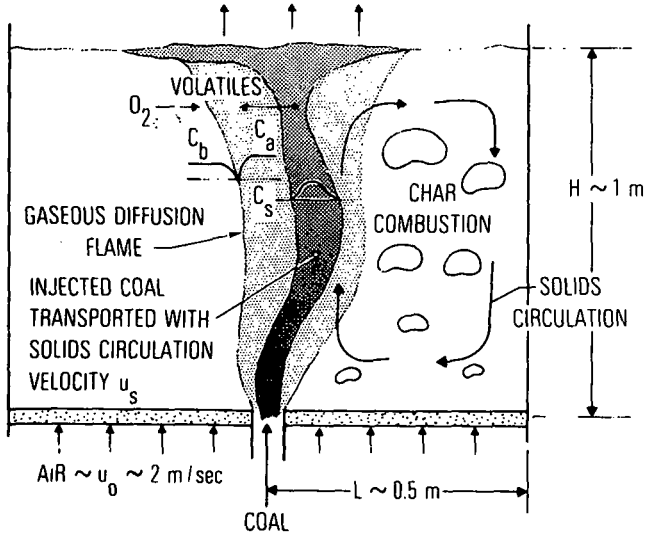

Fig. 1. Bottom-Fed Atmospheric Fluidized-Bed Combustor

Early FBC studies[5] focused on char combustion and neglected volatiles, greatly simplifying the modeling. Due to the importance of volatiles in the overall energy budget, recent studies have included some description of volatiles in models used. This was done by adopting various simplifying assumptions for devolatilization as well as solids/gas mixing rates. For example, Baron and Hodges[6] assume the volatiles to be instantaneously released and uniformly distributed throughout the bed. Park, et al., in arguing that

the general class of one-dimensional models based upon the two-phase theory of fluidization are inadequate for understanding volatiles evolution, assume that the volatiles are released instantaneously at the coal feed in order to focus upon the volatiles escape phenomenon. In most cases, these models are based upon arguments regarding the time scales of the pertinent physical-chemical processes. The present work also is based upon a review of the important time scales and concludes that finite devolatilization and solids circulation rates must be considered in the analysis of the injector region. The result is the ability to assess the importance of solids circulation for which Refs. 2 and 6 suggest significantly different times scales and, hence, vastly different modeling approaches.

The large-scale solids circulation patterns in large-particle beds have long been the subject of experimental research.[7] However, the question remains as to the significance of solids circulation for the understanding of AFBC beyond noting that the solids are well mixed on the time scale of char combustion. The present work addresses this issue by quantitatively incorporating information on solids flow patterns through the solids circulation velocity.

The following section contains the formulation of the model including a review of the pertinent time scales discussed above. Remaining sections discuss the results of the model calculations and their implications for AFBC design.

Injector Region Model

The complexity of the fluid-dynamic and chemical processes in the fluidized bed generally has dictated the need for simplified modeling with emphasis on those phenomena which most directly govern the bed behavior such as performance and scaling. The first such example was the formulation of the two-phase theory of fluidization[8] which reflected the importance of the voids in determining such bed characteristics as mass transfer and gas/solids mixing. The importance of the injector region spatial structure in determining AFBC behavior discussed in the previous section suggests that it, too, is a governing phenomenon which must be considered in AFBC modeling. Models[9-11] developed around the two-phase theory of fluidization for small particle applications generally cannot, without extensive modification, predict the structure of volatiles evolution in the injector region. There are two reasons for this. First, their transport mechanisms are representative of the fast bubble regime. Second, they generally are one-dimensional (averaged over the bed cross section), whereas a multi-dimensional description is required to resolve the important features of volatiles evolution. As a result, such models cannot predict the volatiles escape phenomenon, the species variations in the freeboard, or the excursions of gaseous fuel-air ratios within the bed, which may have a bearing on the NO_x characteristics of AFBC.

To determine the best approach to modeling the injector region, the important physical and chemical time scales will be reviewed. They are listed in Table 1. Beer[12] discusses how these time scales are related to what is considered an optimum set of operating parameters for AFBC. It is evident that the combustion times for AFBC temperatures (1100-1200°K) and particle sizes (1-10 mm), and hence overall particle residence times, are large compared to the other time scales. This suggests the approach taken elsewhere[12] of assuming the devolatized char particles to be well dispersed and burning in the presence of oxygen. The gaseous volatiles are considered to burn instantaneously under diffusion-controlled conditions. The solids circulation time is a solids mixing time to be distinguished from the overall residence time of solids in the bed and is of the same order as the gas residence time. The comparison of solids circulation times quoted in Refs. 2 and 6 with devolatilization time scales[12] is the basis for the two completely different devolatilization models used in those investigations, as discussed earlier. However, it can only be concluded from Table 1 that the two processes occur on the same time scale and, hence, are coupled and must be considered in conjunction with the gas-phase transport and combustion processes. This is the motivation for including finite rate devolatilization and solids circulation in the model to be presented herein.

Table 1. Physical and Chemical Time Scales in FBC

Physical	Chemical
Solids Residence Time - > 100 sec	Char Combustion Time - > 100 sec
Solids Circulation Time - 2 sec (MIT) 10 sec (OSU)	Devolatilization Time - 1-10 sec
Gas Residence Time - < 1 sec	Volatiles Combustion Time - $\ll$1 sec (Diffusion Controlled)

Before proceeding to the mathematical formulation of the model, a few words of clarification regarding solids circulation are in order. Solids circulation is comprised of both convective and dispersive transport. The manner in which the two combine to effect overall transport has a strong impact on chemical processes. That is, if a volume element is transported over a given distance with little mixing, then chemical processes are inhibited. Jovanovic's[3] observations of injected tracer gas rising through a bed show, for example, that the wandering of the tracer plume resulted in an apparently augmented dispersion. However, it was noted that mixing on the scale important for reactions was significantly less. Also, the quoted circulation times of 10 sec refer to the time for injected particles to become uniformly mixed throughout the bed. More important for reactions are the local velocities and dispersion rates in the vicinity where the injected particles are evolving spatially. The present model, by including finite solids velocities, mixing, and devolatilization rates, addresses this issue and is capable of assessing the comparative roles of transport and chemical mechanisms.

The physical quantities of interest in modeling the volatiles evolution associated with the coal injection process are the fraction of volatiles in the coal C_s, the gaseous concentration of volatiles released from the coal C_a, and the concentration of oxidizer C_b. Figure 1 sketches the evolution of these quantities in the AFBC. The volatiles containing solids are injected at the bottom of the bed, flow up through the bed at the solids circulation velocity, diffuse laterally and devolatilize, thereby depleting C_s from its initial injected value. The gaseous volatiles C_a are produced by devolatilization, flow up through the bed, diffuse laterally, and are depleted by combustion with the surrounding oxygen C_b.

In order to model this process in a simple manner, it is necessary to make some assumptions to represent the important physical phenomena. The gases are assumed to be in plug flow with lateral diffusion based upon the work of Jovanovic[3] and Park, et al.[2] in characterizing the slow bubble regime of large-particle fluidization. This is a key assumption which departs from the two-phase models based upon bubbles surrounded by clouds. The injected solids are assumed to be in plug flow at the solids circulation velocity in the vicinity of the injector. The solids also are assumed to diffuse laterally while undergoing devolatilization. Because solids mixing is more rapid than char combustion, the devolatilized coal particles are assumed to be well mixed and burning in the presence of oxygen. The volatiles are assumed to undergo diffusion-controlled combustion at the interface between volatiles and surrounding oxygen. The particle and gas temperatures are assumed uniform in order to simplify the initial calculations. In order to focus on the finite solids transport and devolatilization mechanisms, elutriation and char carryover are assumed to be zero.

Based on the foregoing assumptions, the injector region is modeled with a set of species equations for C_a, C_b, and C_s, expressing mass balances for the gaseous volatiles, the oxygen, and the volatiles remaining in the coal, respectively. The set treats the vertical flow and lateral dispersion of gas and solids while neglecting axial dispersion and is written as follows.

Volatiles in Coal:

$$u_s \frac{\partial C_s}{\partial x} = \frac{D_s}{r} \frac{\partial}{\partial r} \left(r \frac{\partial C_s}{\partial r} \right) - W_d \qquad (1)$$

Gaseous Volatiles:

$$u_0 \frac{\partial C_a}{\partial x} = \frac{D}{r} \frac{\partial}{\partial r} \left(r \frac{\partial C_a}{\partial r} \right) + W_a^i + W_a^h \qquad (2)$$

Oxygen:

$$u_0 \frac{\partial C_b}{\partial x} = \frac{D}{r} \frac{\partial}{\partial r} \left(r \frac{\partial C_b}{\partial r} \right) + W_b^h + W_b^i \qquad (3)$$

The symbols u_0, u_s, D, and D_s represent the superficial velocities and dispersion coefficients of the gas and solids, respectively. The origin of the (x, r) coordinate system is at the centerline of the coal injector, with x measuring the distance above the distributor and r the distance from the injector centerline. The injector radius at x=0 is denoted by r_0 and is determined by the coal mass flow and the solids circulation velocity u_s. The governing equations include reaction terms representing the devolatilization and combustion processes. The term W_d represents the reduction of volatiles in the coal C_s by devolatilization. The superscripts $(\ )^i$ and $(\ )^h$ refer to inhomogenous (solids) and homogenous (gaseous) reactions. Specifically, W_a^h is the loss of volatiles due to gas-phase combustion, while W_a^i is the production of volatiles that balances the depletion of C_s. Similarly, W_b^h and W_b^i are the oxygen losses due to combustion with volatiles and char, respectively.

Values for the gaseous dispersion coefficient are taken from Jovanovic[3] who observed that gases rising through the tube-filled bed dispersed due to particle scale motions rather than molecular and underwent a wandering motion probably due to bubble dynamics. The wandering motion when averaged over long time scales implies an apparent augmented dispersion; however, the particle scale dispersion controls the type of mixing important for reactions and is the appropriate choice for this formulation. Turbulent reacting flows exhibit a similar phenomenon in which turbulent motions apparently mix reactants on a large scale. However, it is actually the small-scale mixing which fosters reaction leading to the well-known thick turbulent diffusion flame.[13] The same

dispersion coefficient is used for both volatiles and oxygen, because the dispersion is controlled by the particle-induced gas motions rather than molecular diffusion.

Values of D_s are not as well-known as those for D. This is partly responsible for the varying estimates of solids circulation times discussed earlier. In fact, one reason for the present work is to provide a tool for investigating the dependence of AFBC behavior on D_s. Although solids tracer studies in tube-filled, large-particle beds[7] have not completely quantified D_s, they have suggested[14] that the dispersion is much smaller for solids than for gases. Therefore, D_s generally will be specified as some fraction of D and the effects of its variation observed.

The devolatilization process is highly complex and under study by many investigators.[15-16] It is comprised of many orders of chemical bond breaking requiring multistep kinetic mechanisms for accurate description.[17-18] However, for the present purposes of exploring the role of such finite rate processes, it is adequate to use simple first-order global kinetics of Arrhenius type with reasonable numerical estimates as given, for example, by Suuberg.[16] This simplification is justified for AFBC temperatures because the complex, high heating rate, physical-chemical phenomena of coal-fired MHD[15] are not in play. For the assumed uniform temperature fields, the kinetically controlled expression for W_d is

$$W_d = k_0 \exp\left(\frac{-E}{RT}\right) C_s \qquad (4)$$

The source term W_a^i, representing a mass balance between the volatiles in the coal and the gaseous volatiles released by the coal, is related to W_d by

$$W_a^i = \frac{\rho_c}{\hat{M}_a}\left(\frac{\epsilon_{mf}}{1-\epsilon_{mf}}\right) W_d \qquad (5)$$

where ρ_c is the coal density, $\hat{M}_a$ is the molecular weight of the volatiles, and ϵ_{mf} is the voidage at minimum fluidizing conditions.

The consumption of oxygen by char combustion is given by

$$W_a^i = - k C_b \qquad (6)$$

where

$$k = A_c k'$$

A_c is the char surface area per unit volume and k' is the effective char combustion rate coefficient related to the chemical rate constant k_s (m/sec) and the mass transfer coefficient k_g (m/sec) by the widely used expression

$$k' = \frac{1}{1/k_s + 1/k_g} \qquad (7)$$

The value of k_s is taken from the work of Field[19] as

$$k_s = 3.98 \times 10^4 \, T \exp\left(\frac{-35{,}700}{RT}\right) \qquad (8)$$

while k_g is obtained from the Ranz and Marshall[20] Sherwood number evaluation.

Volatiles are considered to react with oxygen according to a simple irreversible one-step combustion mechanism

$$a \text{ (fuel)} + b \text{ (oxidizer)} \xrightarrow{k_f} d \text{ (products)} \qquad (9)$$

where a, b, d are stoichiometric coefficients and k_f is the rate coefficient. Of interest here is the fast reaction limit for which k_f is considered to be large. The gas phase reaction terms W_a^h and W_b^h are related according to the stoichiometry of the above reaction as

$$\frac{W_a^h}{a} = \frac{W_b^h}{b} \qquad (10)$$

The boundary conditions for C_s, C_a, and C_b are

$$\begin{aligned} x = 0 \quad & C_a = 0 \\ & C_b = C_{b0} \\ & C_s = \begin{cases} C_{s0}, & 0 < r \le r_0 \\ 0, & r_0 < r \le L \end{cases} \\ x > 0, \quad r = 0, L \quad & \partial C_a/\partial r = 0 \\ & \partial C_b/\partial r = 0 \\ & \partial C_s/\partial r = 0 \end{aligned} \qquad (11)$$

The analysis of equilibrium combustion problems of the present type is greatly simplified by the transformation[21]

$$\beta = b\left(\frac{C_a}{C_L}\right) - a\left(\frac{C_b}{C_L}\right) \qquad (12)$$

where C_L is a reference concentration.

The governing equation set is transformed in the following manner. The equations for C_a and C_b are multiplied by b and a, respectively, and subtracted, after which the relation between W_a^h and W_b^h as well as the $(C_a, C_b) \rightarrow \beta$ transformation

are applied. Finally, application of the coordinate transformations, $r^* = r/L$ and $x^* = x/H$ where L and H are the lateral bed dimensions, results in the following equations for C_s and β:

$$\frac{\partial C_s}{\partial x^*} = \left(\frac{HD_s}{u_s L^2}\right)\frac{1}{r^*}\frac{\partial}{\partial r^*}\left(r^*\frac{\partial C_s}{\partial r^*}\right) - \left(\frac{H\Gamma}{u_s}\right)C_s \tag{13}$$

$$\frac{\partial \beta}{\partial x^*} = \left(\frac{HD}{u_0 L^2}\right)\frac{1}{r^*}\frac{\partial}{\partial r^*}\left(r^*\frac{\partial \beta}{\partial r^*}\right) + M\left(\frac{H\Gamma}{u_s}\right)C_s - S\left(\frac{H^k}{u_0}\right)\beta \tag{14}$$

where

$$M = (b\rho_c / C_L \hat{M}_a)(\epsilon_{mf}/1-\epsilon_{mf})\,(u_s/u_0)$$

$$\Gamma = k_0 \exp(-E/RT)$$

$$S = \begin{cases} 0, & \beta \geq 0 \\ 1, & \beta < 0 \end{cases}$$

The boundary conditions become

$$x = 0, \quad \beta = -(C_{b0}/C_L)$$

$$C_s = \begin{cases} C_{s0} & 0 < r^* \leq (r_0/L) \\ 0 & (r_0/L) < r^* \leq 1 \end{cases}$$

$$x > 0, \quad r^* = 0, 1 \quad \partial C_s/\partial r^* = 0$$

$$\partial\beta/\partial r^* = 0 \tag{15}$$

The coefficient of oxygen consumption due to char combustion k in Eq. (14) is related to the char particle size through, for example, the char surface area per unit volume A_c. The char particle size, in turn, is part of the solution and generally is determined by a population balance as given by Levenspiel.[22] Therefore, k must be specified as part of the solution. Through the assumption of zero elutriation and carryover, the oxygen solution can be compared to a global oxygen balance on the bed, providing a means of iterating the solution to convergence by varying k. This simplification eliminates the need for a detailed consideration of char particle size dynamics in the bed. It is important to account for the impact of char combustion on the oxygen distribution in the bed because it determines the combustion rate of volatiles and, hence, the volatiles evolution. The global oxygen balance is expressed by

$$\begin{pmatrix}\text{calculated excess}\\ \text{oxygen}\end{pmatrix} = \begin{pmatrix}\text{calculated oxygen}\\ \text{leaving bed}\end{pmatrix} - \begin{pmatrix}\text{calculated oxygen}\\ \text{to consume}\\ \text{escaping volatiles}\end{pmatrix} \tag{16}$$

This value must be consistent with the excess air specified as a bed operating parameter.

Equations (13) and (14), and boundary conditions (15), govern the group combustion of a devolatilizing coal injected into an AFBC. The solution of these equations for a range of bed parameters defines the possible regimes of group combustion which can be observed in AFBC. These various regimes and their impact upon combustor behavior will be discussed in the following section.

Discussion of Results

Three distinct combustion regimes were encountered in the solution of Eqs. (13) and (14). Which of these is actually observed depends upon the relative magnitudes of solids and gaseous transport as well as the devolatilization rate. Because the present model provides a framework for investigating the coupling of these competing phenomena, the remaining figures will quantify their role in determining AFBC behavior.

The basic calculations were performed for the bed geometry of Fig. 1 with parameter variation employed to investigate finite rate effects. A value of 0.04 was used for the parameter HD/u_0L^2 based upon Jovanovic's data for D. The coal mass flow used is 0.049 kgm/sec with a volatile matter of 43.7 percent. The value of excess air used in the calculation is 10 percent. The fraction of total combustion oxygen required for char combustion is 0.576. The bed temperature is 1116°K.

In addition to these parameters, the calculations shown in Fig. 2 employ a value for u_s/u_0 of 1/4 and D_s/D of 0.01 in the range suggested by the work of Fitzgerald.[7] For the devolatilization rate, $(H/u_s)\Gamma = 1.0$ is used. For this set of parameters, Fig. 2 shows typical radial profiles for C_s, C_a, and C_b at x/H = 0.586 selected at a convenient mid-height computational station. The solutions are normalized by their centerline values for ease of plotting. The profiles of C_s are of the expected form resulting from the devolatilization and diffusion process as the solids are carried from the injection point by the circulation pattern. The C_a profile is the result of volatiles production and concurrent diffusion outward toward the diffusion flame where it goes to zero due to combustion. The C_b profile complements the C_a profile and falls to zero at the flame, confirming the requirement under fast combustion kinetics that fuel and oxidizer cannot coexist. This flame

structure is termed "external", denoting that the gaseous diffusion flame resides outside the jet of volatiles containing solids.

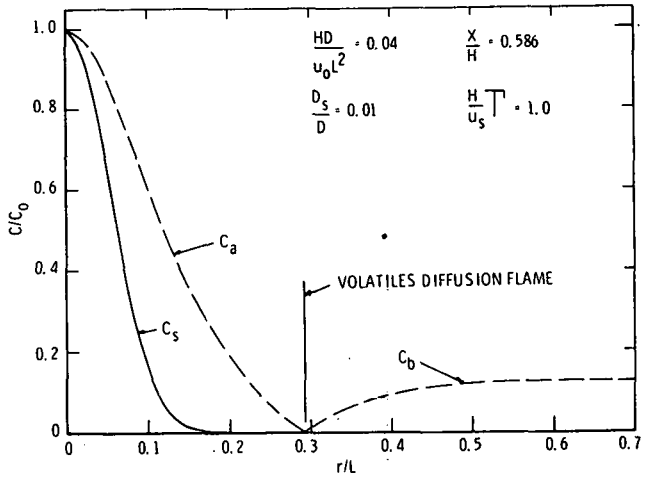

Fig. 2. Profiles of Coal Volatiles (C_s) Gaseous Volatiles (C_a), and Oxidizer (C_b) at $x/H = 0.586$ for External Diffusion Flame

Figure 3 displays calculations which differ from those of Fig. 2 by an increased diffusion ratio of $D_s/D = 0.125$. This variation is in the direction of increased circulation rates as suggested by estimates of Beer[12] in comparison with those of Park.[2] The important difference is that the gaseous diffusion flame has penetrated the solids jet. This is because the greater solids diffusion lowers the solids concentration in the outer regions of the C_s profile and, hence, the production of volatiles per unit volume. It is the volatiles production which balances the inward diffusion of oxygen. When volatiles production is large enough, it prevents penetration of the solids jet by oxygen resulting in the external flame of Fig. 2, while a reduced production rate permits oxygen to surround the devolatilizing particles in the outer edges of the jet as in Fig. 3.

A question exists as to the nature of combustion in the region outside the diffusion flame but within the C_s jet. The answer comes from close inspection of the solutions. The nonzero oxygen level in this region and the required noncoexistence of volatiles and oxygen are consistent with the absence of volatiles. Since the solids continue to devolatilize in this region, the only consistent interpretation is that the volatiles are immediately consumed by the excess available oxygen. This is an explanation within the context of the model of single particle volatiles combustion in which the volatiles burn in a diffusion flame surrounding each particle. Beér[23] has observed such single particle volatiles combustion for coal particles dropped into a hot bed. The combustion zone for the "embedded" diffusion flame case therefore extends from the diffusion flame to the edge of the C_s profile as indicated in Fig. 3.

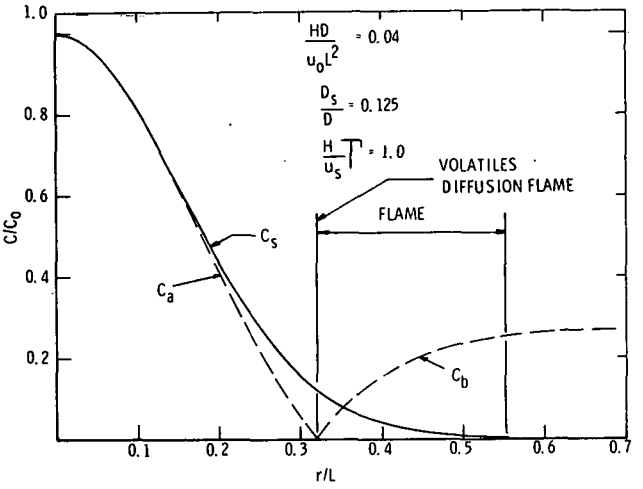

Fig. 3. Profiles of Coal Volatiles (C_s), Gaseous Volatiles (C_a), and Oxidizer (C_b) at $x/H = 0.586$ for Embedded Diffusion Flame

The final combustion regime occurs for devolatilization rates large compared to solids transport, $(H/u_s)\sqrt{\Gamma} \to \infty$, (D_s/D) finite. Figure 4 shows the calculations for this case in which the coal instantaneously devolatilizes upon entering the bed. Therefore, only gaseous volatiles are present in the bed. The combustion is once again confined to a diffusion flame, as shown by the solutions for C_a and C_b in Fig. 4.

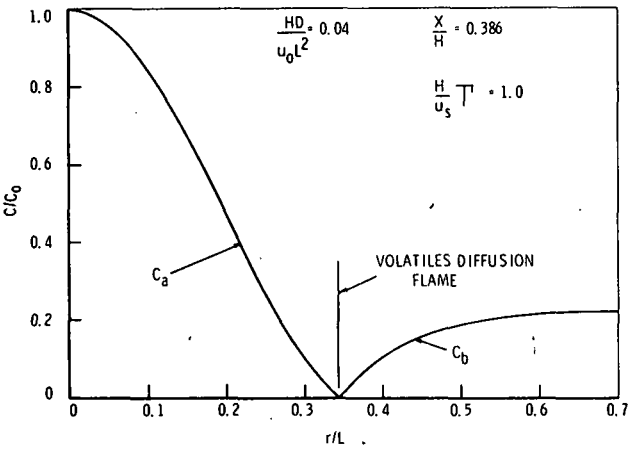

Fig. 4. Profiles of Gaseous Volatiles (C_a) and Oxidizer (C_b) at $x/H = 0.386$ for $\sqrt{\Gamma} \to \infty$

Having established the group combustion regimes associated with dense gas-solid mixtures of devolatilizing coal found in the injection regions of AFBC's, it is of interest to consider the spatial structure shown in Figs. 5 through 7. Figure 5 shows a plot of the C_s jet and the diffusion flame

surrounding the gaseous volatiles C_a in terms of (x^*, r^*) coordinates for the external flame case. Figure 6 shows the same plot for the embedded flame with the thick combustion zone indicated by a shaded region. These plots clearly show that the volatiles diffusion flames do not close within the bed allowing the core of unburnt volatiles to escape the bed. The superposition of Figs. 5 and 6 in Fig. 7 shows that the relative position of the diffusion flame does not change very much. This raises the question as to the practical importance of distinguishing the two cases. The difference lies in the level of volatiles release, with the external flame emitting more volatiles. This is because the thick single-particle combustion zone consumes more volatiles.

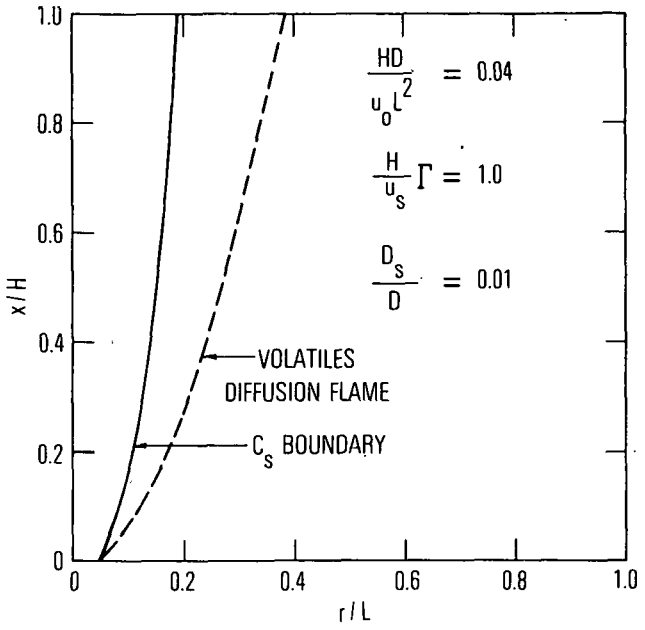

Fig. 5. Flame Structure for External Gaseous Flame

Insight into finite rate effects upon AFBC behavior can be gained by investigating the interplay of the group combustion regimes. For example, Figs. 8 through 11 display finite rate effects on volatiles escape. Figure 8 shows the conversion X_v of gaseous volatiles for the instantaneous devolatilization limit as a function of (HD/u_0L^2), where X_v is the fraction of volatiles produced at $x = 0$ that are consumed in the bed. A value of $X_v = 1$ means that the volatiles flame closes within the bed and no volatiles escape. The parameter (H/Du_0L^2) is a ratio of convective residence to diffusion times. Since the gas combustion is diffusion controlled, this parameter represents the ratio of residence to group combustion times and controls the degree of completion of combustion.

If the assumption of instantaneous volatiles release were employed as a simplified design tool, then Fig. 8 could be used as a guide, for example, to eliminate volatiles escape. Furthermore, if

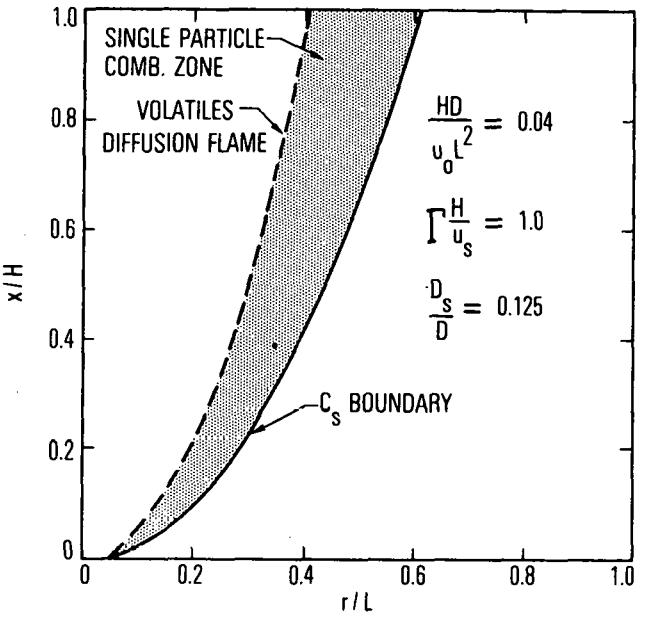

Fig. 6. Flame Structure for Embedded Gaseous Flame

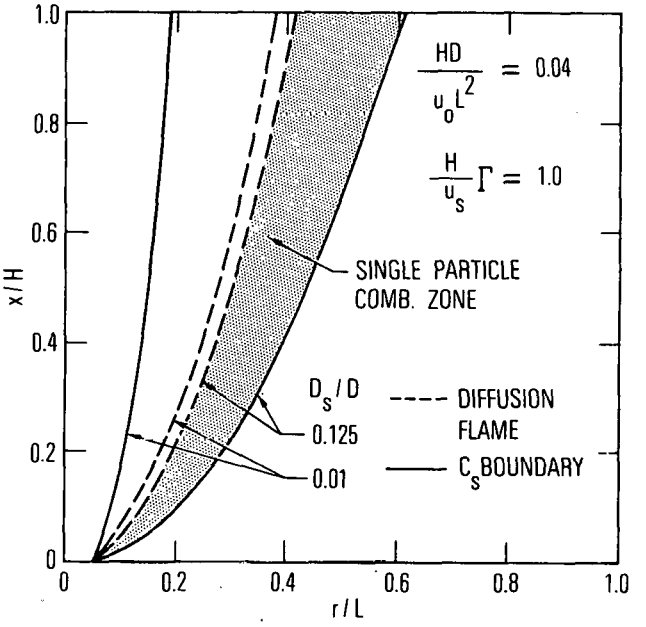

Fig. 7. Comparison of Embedded and External Flame Structure

increased bed height were employed as a solution, accepting the increased pressure loss penalty, a value of 0.12 for (HD/u_0L^2) might be selected as an optimum tradeoff. However, Fig. 9, which compares the finite and infinite rate solutions, shows that finite rate effects cause the volatiles escape to persist.

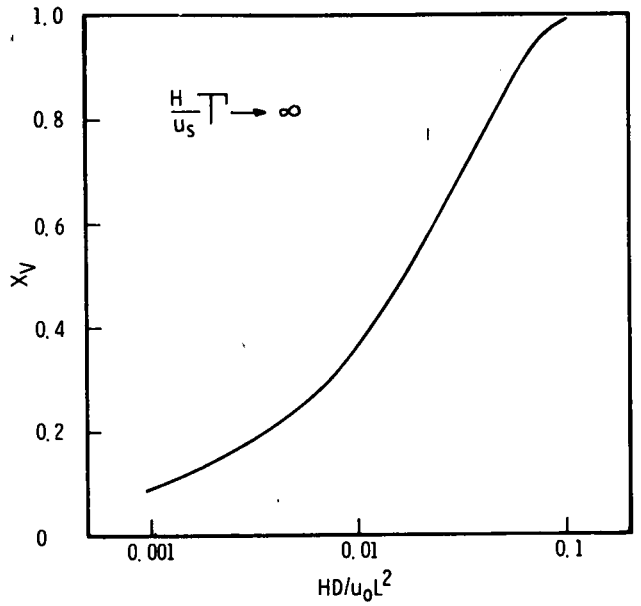

Fig. 8. Conversion X_v of Gaseous Volatiles C_a at Bed Surface

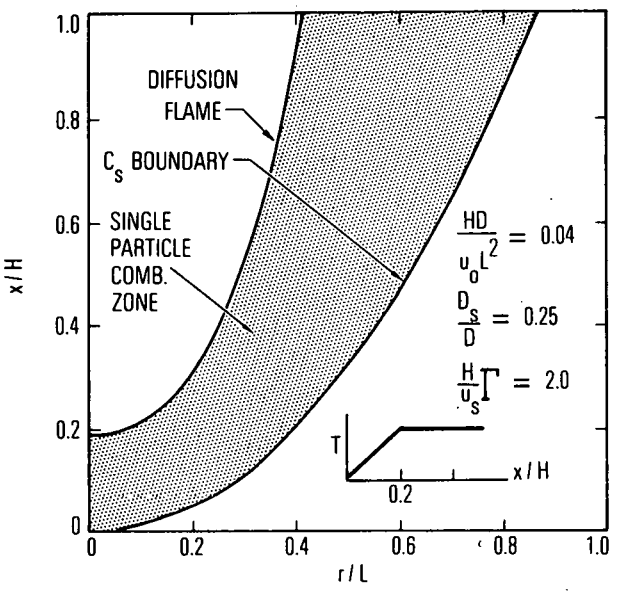

Fig. 10. Flame Structure for Finite Heating Rate

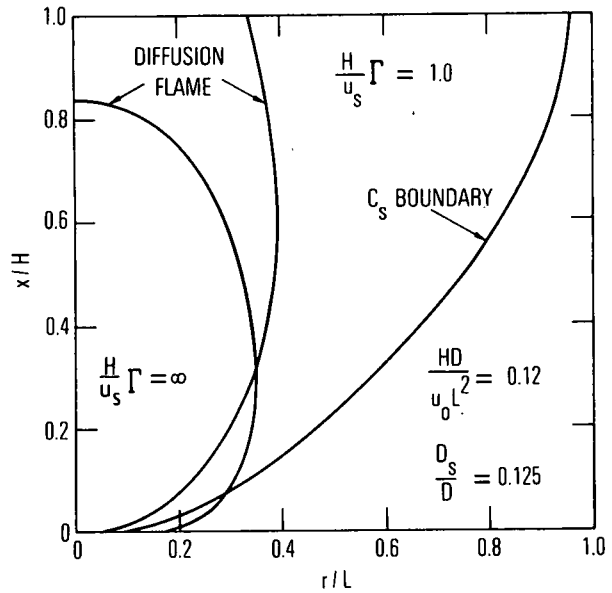

Fig. 9. Finite Devolatilization Rate Effect on Closed Flame

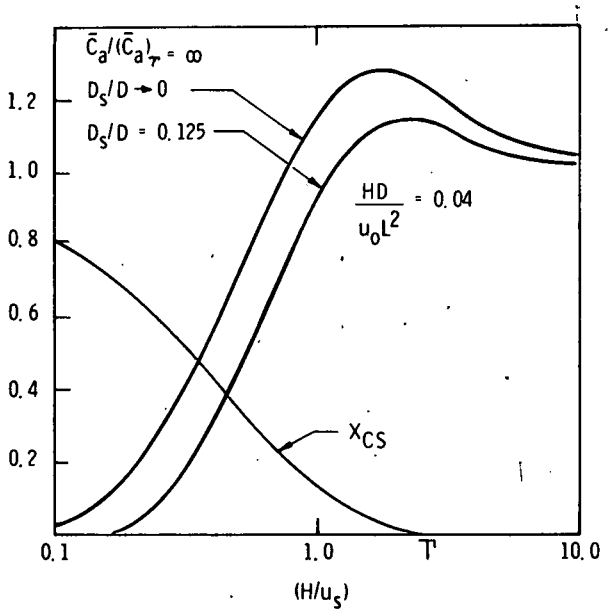

Fig. 11. Unburnt Volatiles (C_a) and Coal Volatiles Conversion (X_{cs}) at Bed Surface for Finite Γ

In the present analysis uniform particle and gas temperatures have been assumed, implying that coal particles are instantly heated to bed temperatures upon injection. This assumption is reasonable, considering solids contacting heat transfer rates, but ultimately depends upon injector design and detailed solids flow patterns. However, it is possible to relax this assumption and provide a physical trend with respect to volatiles escape by specifying a temperature variation. The result shown in Fig. 10 is that volatiles production is not large enough in some cases to exclude the oxygen from the interior of the solids jet. Therefore, the complete cross section of the jet is in the single-particle combustion regime until the solids temperature reaches a threshold at which

the increased volatiles production expels the oxygen from the interior region thereby establishing a diffusion flame. Once again, the importance of this behavior for a given set of operating conditions is that finite heating rates can result in volatiles escape when not predicted by the instantaneous devolatilization limit. This trend is best understood by considering the conceptual limit in which it takes the full length of the bed for particles to heat up to a threshold at which the volatiles are immediately released and exit the bed unburned, resulting in maximum volatiles release. The calculation of Fig. 10 is an intermediate to this limit.

Finite rate effects are summarized in Fig. 11 wherein the concentration of escaping volatiles (at x = H) averaged over the bed is normalized with respect to the instantaneous devolatilization limit and plotted for finite devolatilization and solids circulation rates. The fraction of volatiles remaining in the coal X_{cs} at x = H also is shown. For $(HT/u_s)\Gamma \sim 2.0$ and $D_s/D = 0.125$, which is in the range of parameters for the commercial scale AFBC of Fig. 1 operating at $T \sim 1100^{\circ}K$, the level of volatiles escape approaches 15 percent in excess of the infinite rate limit. For solids transport occurring only by the circulation velocity ($D_s/D \rightarrow 0$), the augmentation exceeds 25 percent. Note from the X_{cs} curve that the higher releases occur even though the solids retain a portion of the volatiles.

Concluding Remarks

Based upon the unique characteristics of AFBC's, a model has been formulated to investigate the spatial structure of the coal injection region including finite rate devolatilization and solids circulation. The purpose of this work is to provide a simplified framework for investigating the impact of finite rate processes on AFBC behavior while relaxing some of the assumptions required in previous studies to incorporate coal volatiles.

Based on the model, three distinct group combustion regimes have been identified as the: (1) external flame, (2) embedded flame, and (3) instantaneous devolatilization limit. The model correctly describes the single particle mode of volatiles combustion observed by Beer[23] and responsible for the thick combustion zone structure of the "embedded flame." Calculations in all three regimes confirm the volatiles escape phenomena for commercial scale AFBC, thought to have been observed as freeboard temperature jumps.[2]

Model predictions show, in general, that finite rate effects have the potential for enhancing the volatiles escape phenomena. In particular, the model provides the mechanism for distinguishing between solids transport by dispersion and by circulation velocity which can account for variations in quoted global circulation times.[2, 12] Calculations performed with varying ratios of solids dispersion and circulation velocity show a significant impact upon flame structure and volatiles escape. This suggests that it is indeed important to continue the study of solids circulation patterns. An immediate consequence of the importance of solids flow patterns is the need to investigate their alteration and control as well as the placement of coal injectors. The impact of the simplified heating rate calculation on volatiles escape performed herein points to a need for the investigation of injector design.

The present results underscore the importance of volatiles evolution and the spatial structure it fosters in the injector region as dominant phenomena in AFBC performance. Volatiles evolution may have implications for the NO_x emissions characteristics of AFBC. The escaping volatiles can carry fuel nitrogen fragments into the freeboard, where their conversion is likely to proceed under oxygen-rich, high-temperature surroundings as compared with the interior of the combustor. Furthermore, the spatial structure of the injector region contributes to large excursions in air-fuel ratios known to influence fuel nitrogen conversion. Finally, the jetting volatiles alter the volume of exposed char available for NO_x reduction, which is suggested to be a dominant reduction mechanism in AFBC.

The ability of the present model to identify and explain important aspects of AFBC suggests additional topics for study. The sensitivity of devolatilization to temperature with respect to the characteristic residence times of AFBC requires a coupled energy calculation for improved accuracy. The possibility of large temperature excursions associated with the gas voids[14] requires analysis with the present model and is amenable to the incorporation of certain statistical fluidization concepts.[24, 25] In summary, the present effort has provided new understanding of AFBC phenomena important for design as well as important quantitative estimates which define research needs.

Acknowledgments

This work was funded by the Advanced Technology Projects Office of the Office of Energy Research, the Department of Energy, DE-AC01-79ER/0027. The encouragement of Drs. E. Blase and R. Kostoff during the course of this work is gratefully acknowledged, as well as the challenging discussions with Professors T. Fitzgerald and O. Levenspiel of Oregon State University and Dean P.M. Chung, College of Engineering, University of Illinois Chicago Circle.

References

1. Bar-Cohen, A., L. Glicksman, and R. Hughes, "Fluid Dynamic Modelling of Fluidized Bed Combustors," Proceedings of the Fifth International Conference on Fluidized Bed Combustion, Washington, D.C., 1977.

2. Park, D., O. Levenspiel, and T.J. Fitzgerald, "A Model for Large Scale Atmospheric Fluidized Bed Combustors," 72nd Annual AIChE Meeting, San Francisco, Nov. 1979.

3. Jovanovic, G., PhD Thesis, Oregon State University, 1979.

4. Lange, H.B., T.M. Sommer, and C.L. Chen, "SO_2 Absorption in Fluidized Combustion of Coal--Effect of Limestone Particle Size," The Babcock and Wilcox Co., Final Report to EPRI, Jan. 1978.

5. Avedesian, M.M., and J.F. Davison, Trans. Instn. Chem. Engrs., 51, 1973, p. 121.

6. Baron, R.E., J.L. Hodges, and A.F. Sarofim, AIChE Symp. Ser., 74(176), 1978.

7. Fitzgerald, T., N. Catipovic, and G. Jovanovic, "Solid Tracer Studies in a Tube-Filled Fluidized Bed," Proceedings of the Fifth International Conference on Fluidized Bed Combustion, Washington, D.C., 1977.

8. Davidson, J.F., and D. Harrison, Fluidized Particles, Cambridge University Press, New York, N.Y., 1963.

9. Tung, S.E., J. Goldman, and J.F. Louis, "FBC-Modelling and Data Base," Proceedings of the Fifth International Conference on Fluidized Bed Combustion, Washington, D.C., 1977.

10. Horio, M., and C.Y. Wen, AIChE Symp. Ser., 74(176), 1978, p. 101.

11. Chen, T.P., and S. Saxena, Fuel, 56, 1977, p. 401.

12. Sarofim, A.F., and J.M. Beer, "Modelling of Fluidized Bed Combustion," 17th Symp. (Int'l) on Combustion, August 1978, University of Leeds, England.

13. Bywater, R.J., "The Calculation of a Turbulent Diffusion Flame in a Free Shear Flow with a Statistical Turbulence Model," AIAA 18th Aerospace Sciences Meeting, 14-16 Jan. 1980, Pasadena, Calif.

14. Private communication with T. Fitzgerald, Oregon State University, Corvallis, Ore.

15. Anthony, D.B., and J.B. Howard, "Coal Devolatilization and Hydrogasification," Dept. of Chemical Engineering, Massachusetts Institute of Technology, Cambridge, Mass., Oct. 1976.

16. Suuberg, E.M., W.A. Peters, and J.B. Howard, "Product Compositions and Formation Kinetics in Rapid Pyrolysis of Pulverized Coal--Implications for Combustion," XVII Symposium (Int'l) on Combustion, 1978.

17. Kobayashi, H., "Rapid Decomposition Mechanism of Pulverized Coal Particle," MS Thesis, Dept. of Aeronautics and Astronautics, Massachusetts Institute of Technology, Cambridge, Mass., 1972.

18. Anthony, D.B., J.B. Howard,, H.C. Hottel, and H.P. Meissner, "Rapid Devolatilization of Pulverized Coal," Fifteenth Symposium (Int'l) on Combustion, The Combustion Institute, Pittsburgh, Pa., 1975, p. 1303.

19. Field, M.A., D.W. Gill, B.B. Morgan, and P.G.W. Hawksley, "Combustion of Pulverized Coal," BCURA, Leatherhead, England, 1967.

20. Ranz, W.E. and W.R. Marshall, Jr., Chemical Engineering Progress, 48, 1952, pp. 141-146 and 173-180.

21. Williams, F.A., Combustion Theory, Addison Wesley, London, 1965.

22. Levenspiel, O., "Chemical Reactor Omnibook," OSU Book Stores, Inc., Corvallis, Ore., 1979.

23. Beer, J.M., A.F. Sarofim, and Y.Y. Lee, "NO Formation and Reduction in Fluidized Bed Combustion of Coal," 6th International Conference on Fluidized Bed Combustion, 9-11 Apr. 1980, Atlanta, Georgia.

24. Bywater, R.J., and R.H.C. Lee, "A Statistical Flow Model for Fluidized-Bed Reactors," AIAA 8th Fluid and Plasma Dynamics Conference, 16-18 June 1975, Hartford, Conn.

25. Bywater, R.J., "Fluidized Bed Catalytic Reactor According to a Statistical Fluid Mechanics Model," AIChE Symposium Ser., 176(74), 1978.

Questions to Ron J. Bywater:

Q: (Participant not identified)

In the early design stages of the Rivesville boiler, we had a needle injection system and we had developed a practical model for the injection zone around the needle. This is very important to the design of the tube bundles above the zone. In the design of that unit, we never anticipated the amount of fines material that would come in with the fuel. This gives you a problem in the direct char blow-through in the plume wash zone. The mushroom type injector has a number of advantages as opposed to a single point injection.

A: You bring up some good points. The obvious extension to the heat transfer, the bubbles for example, impinging in this region can cause hot spots. The indication is that a slower heating rate could aggravate this problem. What you may also want to do, as I have suggested here, is to forget about injectors and just look at circulation.

Q: (Participant not identified)

A: Have you considered the buoyancy effects of the air from a horizontal jet and its influence on mixing or the devolatilization?

A: It is not necessary that this jet is driving a circulation pattern. When the feed comes in it is drawn into a circulation pattern. The buoyancy is considered in the idea of plug flow and slow bubble regime. One of the main results of this study was that it seems the bubbles take this nicely defined jet and wave it around.

IGNITION AND EXTINCTION CHARACTERISTICS OF ATMOSPHERIC FLUIDIZED BED COAL COMBUSTORS

John P. Congalidis and Christos Georgakis

Department of Chemical Engineering and Energy Laboratory
Massachusetts Institute of Technology

1. INTRODUCTION

The analysis of the ignition and extinction characteristics of an Atmospheric Fluidized Bed Coal Combustor is one of the more important problems that need to be investigated before the full commercialization of this new combustion technology. Specifically it is of interest to explore the following question: to what extent and by how wide a margin can the steam generation rate be varied by manipulating such input variables as coal feed rate, excess air, superficial gas velocity and heat transfer area, while maintaining the operation of the combustor within prescribed bounds for pollutant emissions, combustion efficiency and bed temperature?

Most of the published models for fluidized combustion (listed in Ref. [1]) have been identified and predicted - often in satisfactory agreement with results from pilot units - the key steady state combustor characteristics such as the carbon loading, the combustion efficiency, the sulfur retention by the solid sorbent and the pollutant (mainly NO_x) emissions. The status of fluidized combustion modelling has been recently reviewed [2]. These models, however, cannot be in most instances sucessfully used to study the extinction and ignition characteristics of the combustor because they are isothermal in structure, in the sense that the bed temperature is not an output variable but must be a priori specified.

It is the purpose of this paper to present a non isothermal model which has been developed in order to study the ignition and extinction characteristics of the combustor. This model is able to predict in addition to the temperature patterns in the bed, the carbon loading, the combustion efficiency and the O_2 and CO concentration profiles in the combustor. The model can therefore be used to study the implications on the combustor performance of different designs.

2. MODEL DESCRIPTION

The input and the output variables of the proposed model are summarized in Figure 1. As Figure 2 shows the model is made up of interrelated energy and O_2 and CO mass balances between three bed regions: (i) the dilute phase consisting of gas bypassing the solids in the form of bubbles (ii) the emulsion phase consisting of the SO_2 solid sorbent (which at normal operating conditions accounts for 95% of the bed solids' inventory and of the gas in the solid interstices (iii) the burning coal particles. Following the studies by Borghi et.al. [3] we shall assume that the volatiles are instantaneously released and uniformly distributed in the bed since volatile release times are two orders of magnitude smaller than char burnout times but larger than solid circulation times.

The mass conservation equations that follow describe the processes of oxidant and combustion product transfer to and from the bubble phase, the interstitial gas and the surface of the burning char particles. They also account for the heterogeneous reaction of char consumption as well as for the homogeneous oxidation of CO in the bed. The energy conservation equations model the heat interactions associated with the above mentioned phenomena and the heat transfer to the immersed tubes for steam production; a radiative heat transfer term between the char and the sorbent particles is also introduced. Coupled with the above equations and central to the model is a population balance for the burning coal particles enabling the evaluation of the bed carbon loading and the combustion efficiency. The mass balances for O_2 and CO_2 for a single burning coal particle of radius r are shown in equations (1)-(4) of Table I. We have adopted the mechanism of direct oxidation of char by O_2 to yield CO which is further oxidized to CO_2 in the interstitial gas (subscript I) and the bubbles (subscript D). Furthermore we have lumped the chemical reaction at the external particle surface in view of the difficulty of incorporating a very detailed model of pore combustion to a model describing the overall combustor performance [4]. The energy balance for a single coal particle (Eq. 5) equates the convective (term B) and radiative fluex (term C) with the flux generated by the exothermic chemical reaction at the particle surface (term A). This same equation allows for the determination of the coal particle temperature and should be taken into account in calculating particle shrinkage rate R(r) as a function of its size once the composition and the temperature of the interstitial gas are known. The mass and heat transfer coefficients are calculated from the single particle correlations for the Sherwood and Nusselt numbers respectively (Eq.(2) and (6)). [5].

The population balance of Equation (7) determines the size distribution $P_s(r)$ of coal particles

in the bed given the size distribution in the feed $P_o(r)$ (usually of a Rosin-Rammler type) and the particle shrinkage rate. It also accounts for the two sources of combustible (coal particles) loss: (i) elutriation (the Merrick-Highley [5] correlation is used to calculate the elutriation coefficient $\kappa(r)$) (ii) carry-over in the sorbent overflow stream. A dolomite overflow stream is necessary in order to maintain a constant bed height at a given inventory of solids in the bed and is determined by balancing the dolomite and ash in the coal feed with the elutriation rate of the solid bed material. This balance also accounts for the presence of a cyclone for lines precipitation and reinjection (cyclone efficiency $\eta(r)$ although in this study we have assumed that the fines are burned up in a separate unit so that $\eta(r) \equiv 0$). Integration of this population balance determines both the size distribution $p_s(r)$ and the mass of coal particles in the bed W_s (carbon loading) and therefore the single pass combustion efficiency of the unit can be readily calculated.

Table II shows the bubble phase mass balances for O_2 and CO and the corresponding energy balance. The bubbles are assumed to move in plug flow upwards in the combustor and therefore the relationships (8) and (9) balance the convective flux (term A), the interchange flux between bubbles and emulsion (term B) and the species depletion due to the oxidation of CO to CO_2. We have accounted for bubble growth by coalescence in the bed (use of the bubble size correlation developed by Darton et.al. [7]) and therefore the bubble velocity u_D and the interchange coefficients K_{DI} and H_{DI} calculated by use of the Davidson-Harrison relationships [8]) are a function of bed depth. It should be noted that the spacing between the heat transfer tubes immersed in a bed is taken as an upper limit in the bubble size. Furthermore the two phase theory is used in order to calculate the bed height H_b given the mass of solid material in the bed W_a as well as the volumes occupied by the bubble and emulsion phases.

Table III shows the mass and energy balances for the interstitial gas and sorbent particles. (Eq. (12)-(14)). Several of the terms represent the interchange with the variable size burning coal particles and the coalescing bubbles. The assumption of a well mixed emulsion is justified because the circulation of solids within the bed is fast relative to the carbon oxidation and sorbent SO_2 reaction.

Specifically the mass balances for O_2 and CO account for the net species in-flow into the emulsion phase of the combustor from the air feed (term a), the interchange between interstitial gas and bubbles (term b), the convection to and from the burning coal particles (term c) and the depletion because of the homogeneous oxidation of CO in the interstitial gas (term d). Furthermore the oxygen contribution from the coal and the oxygen requirements for the combustion of the volatiles are appropriately accounted for (terms e and f. Eq. 12). The heat ineractions associated with these processes appear in the energy balance (Eq. (14)). This equation also takes into consideration the heat requirements for bringing the temperature of the coal and sorbent feed up to their respective values in the bed. (terms 1 and j). It also accounts for the radiative interchange between the sorbent and coal particles (term g), the endothermic dolomite calcination reaction (term k) and the heat transfer between the emulsion and the immersed tubes (term h). The heat transfer H_{ta} coefficient is calculated by use of correlations specifically developed for large solid particles which are characteristic of Fluidized Bed Coal Combustor operating conditons [9].

3. DISCUSSION OF RESULTS

The model equations are made dimensionless and the significant time constants of the system thus become apparent (cf Congalidis and Georgakis [10]). The numerical solution of the system of cquations (1)-(13) is based on the observation that the equations for the CO and CO concentrations in the interstitial gas ($C_{O_2,I}$ $C_{CO,I}$ in equations (11) and (12)) and for the temperature of the emulsion gas (T_I in equation (13))form a system of three nonlinear algebraic equations. The algorithm developed by M.J.D. Powell [11] is implemented on an HP 1000 minicomputer and is used to solve the equations of our model by adapting the stragegy shown in Fig. 3. Convergence is achieved after 25-30 interactions.

Figues 4-11 show the results from the model simulation of the combustion of a typical bituminous coal. Table IV shows the approximate and ultimate analysis of this coal and the kinetic

TABLE V: Summary of the values of the design Variables used in the model cacluations

Bed Cross Section	3.355 m^2
Excess Air Ratio	20%
Ca/S ratio	3.0
Average sorbent particle diameter	1.2 mm
Average coal particle diameter	1.2 mm
Mass of the sorbent in the bed	2200 kg
Immersed heat transfer area	15.5 m^2
Heat transfer coefficient to immersed tubes	162 W/m^2k
Steam temperature	600 K
Temperature of feed streams	298 K
Minimum Fluidization Velocity	0.41 m/s

TABLE IV: Proximate and Ultimate Analysis and Reaction Kinetics of Coal Used

Proximate Analysis (%dry)		Ultimate Analysis (%dry)	
Fixed Carbon	52.8	C	69.5
Volatile Matter	30	H	4.3
Ash	17.2	O	4.5
		S	4.5
		Ash	17.2

Coal Oxidation Rate (Field et.al.[12])

$8710 \exp\left(\frac{-35700}{RT}\right) P_{O_2}$ g C/cm^2 external surface s

CO burnout rate (Howard et.al.[13])

$$\frac{dC_{co}}{dt} = 1.3\ 10^{11} C_{co} C_{O_2}^{1/2} C_{H_2O}^{1/2} \exp\left(\frac{-30000}{RT}\right) \frac{m^3}{Kmols}$$

constants used in the calculations. Table V summarizes the values of the design variables of the combustor that remain constant when the superficial gas velocity is varied in the parametric studies.

As Figures 7-11 show the model predicts three steady states in the industrially important region of values for the design and operational characteristics. They correspond to a high (full line), intermediate (dashed line) and low reactor temperature and combustion efficiency. At the same time the respective values of carbon loading are low, intermediate and very high. The regions of high and low emulsion temperature are conjectured to correspond to stable operational regimes while the state characterized by an intermediate reactor temperature is unstable.

Figures 4,5 and 6 show the concentration profiles for O_2 and CO and the temperature distribution in the bubbles for a superficial gas velocity of 1·5 m/s and for the high bed temperature regime. It is interesting to note that the concentration of CO reaches a maximum near the distributor but as the temperature in the bubbles rises (Fig. 4) the concentration of CO quickly decreases.

The transition from the ignited (high temperature) to the extinct (low temperature) operational regime can be examined by the use of Figure 7 to 11. As the superficial gas velocity is decreased, the coal and sorbent feed rates become smaller in order to maintain constant the excess air and Ca/S ratios. Therefore the temperature of the emulsion (which is characteristic of the measured bed temperature) drops since the heat transfer area of the immersed tubes remains constant. At the same time combustion efficiency increases since lower gas velocities result in lower elutriation rates. There exists, however, a value of the superficial gas velocity ($\sim$1 m/s for the conditions of Tables IV and V) beyond which the operation of the combustor in the region of high temperatures and combustion efficiencies is no longer possible. The combustor has reached the point of extinction and further decrease in the superficial gas velocity will result in operation only along the regime of low temperature and very low combustion efficiencies. Since the particle shrinkage rate R(r) is extremely small in this unignited region a perturbation scheme is used in order to solve the population balance. The shape of the multiplicity patterns obtained leads to the conclusion that inorder to resume operation at the ignited regime it is not sufficient to simply increase the superficial gas velocity but one has to add energy to the system from outside (i.e. by use of an oil fired start-up burner).

Each point along the ignited high temperature path of Figure 7 represents a different operating point of the fluidized combustor (with corresponding values for the O_2 and CO concentrations in the interstitial gas, the carbon loading and the combustion efficiency from Fig. 8-11). The previous analysis has shown that combustor operation at a superficial gas velocity just above the critical value of 1 m/s (for the conditions of Tables IV and V) can lead to bed extinction. Another significant result of the foregoing analysis is that both the CO concentration in the emulsion phase (Figure 9) and the carbon loading (Figure 10) (the latter makes up 0·5-1% of the total solid inventory in the bed under normal operating conditions) dramatically increase as the combustor approaches extinction. This suggests that monitoring the CO concentration can be used to operate the combustor away from extinction.

This model is being currently used to study the effect of important design variables (sorbent and coal particle sizes, excess air ratio, heat transfer area) on the ignition and extinction characteristics which were previously delineated. A validation of these predictions using experimental evidence from the MIT fluidized Combusiton Facility is also planned.

References

[1] Park, D.,O. Levenspiel and T.J. Fitzgerald. Chem. Eng. Sci. 35 pp 296-301 (1980)

[2] Sarofim, A.F. and Beer J.M. 17th Symposium (International on Combustion pp 189-204. The Combustion Institute, Pittsburgh PA (1978))

[3] Borghi, G., Sarofim, A.F. and Beer, J.M. "A Model of Coal Devolatilization and Combustion in Fluidized Beds" Paper presented at AIChE 70th Annual Meeting, New York (1977)

[4] C. Georgakis "Mathematical Challenges in the Modelling of Fluidized Bed Coal Combustors" invited paper at the seventh Research Application Conference of the SIAM Institute for Mathematics and Society, to appear in Conference Proceedings, John D. Buckmaster ed.(1979)

[5] Froessling, N. Gerland. Beitr. Geophys. 52, 170 (1938)

[6] Merrick, D. and J. Highley AIChE Symposium Series No. 137, Vol. 70 p. 366 (1973)

[7] Darton, R.C. et.al. Trans. I Chem E Vol. 55, pp. 274-280 (1977)

[8] Davidson, J.F. and Harrison, D. Fluidized Particles Cambridge University Press (1963)

[9] Glicksman, L.R. and N.A. Decker "Design Relationships for Predicting Heat Transfer to Tube Bundles in Fludized Bed Coal Combustors" Paper presented at the 6th International Conference on Fluidized Bed Combustion Atlanta, GA (1980)

[10] Congalidis, J.P. and C. Georgakis, "Multiplicity Patterns of Atmospheric Bed Coal Combustors" to be submitted to Chemical Engineering Science.

[11] Powell, M.J.D. "A Hybrid Method for Nonlinear Equations" from Numerical Methods for Nonlinear Algebraic Equations ed. by P. Rabinowitz, Gordon and Breach (1970)

[12] Field, M.A. et.al. Combustion of Pulverized

Coal BCURA, Leatherhead UK (1967)

[13] Howard, J.B., Williams, G.C. and D.H. Fine 14th Symposium (International) on Combustion p. 975. The Combustion Institute, Pittsburgh, PA (1973)

This research has been supported by a grant from the U.S. Department of Energy for AFBC modelling. The financial support is gratefully acknowledged.

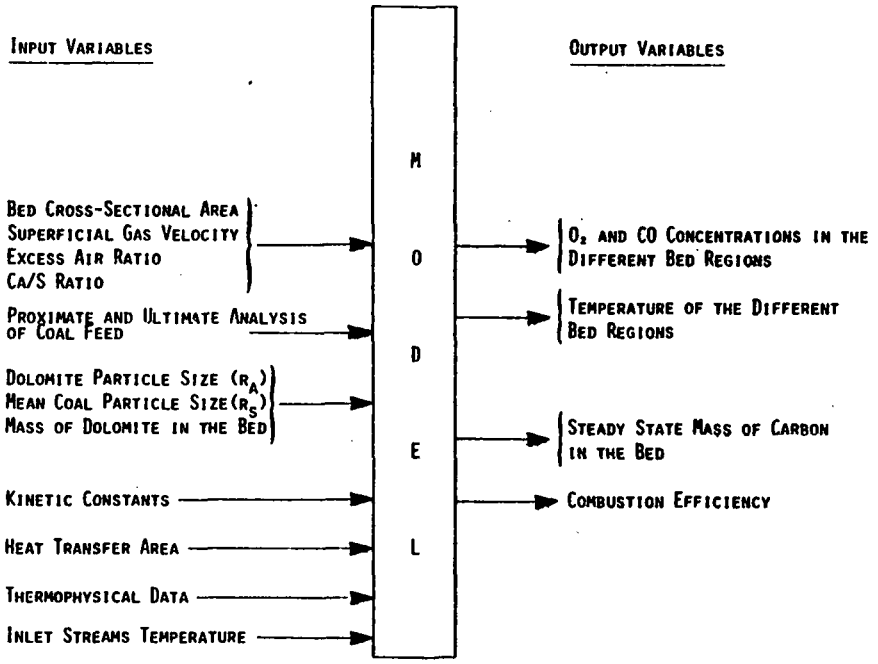

Figure 1: List of the Input and Output Variables of the Model

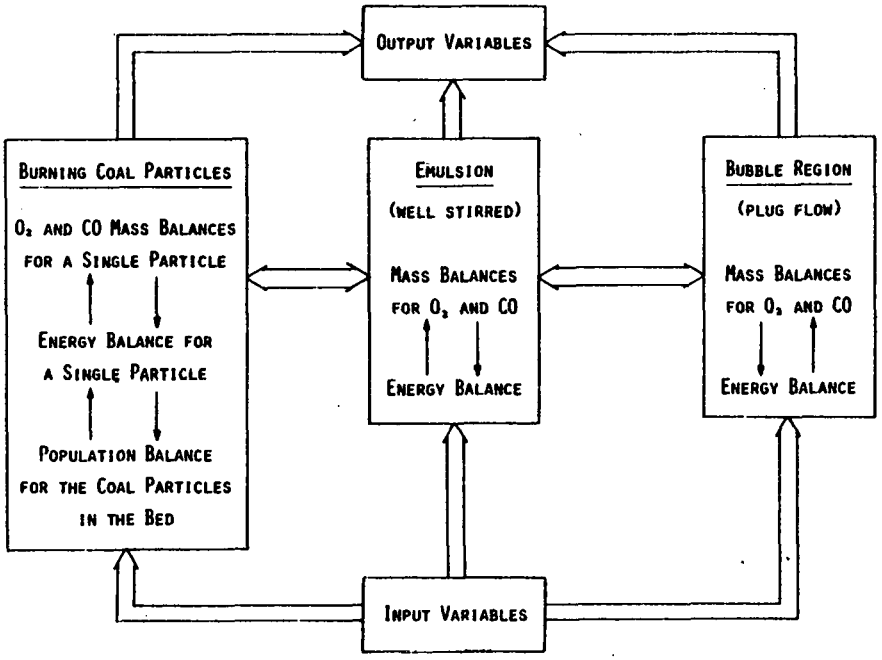

Figure 2: Schematic Representation of the Structural Characteristics of the Model

TABLE I: Equations Describing the Burning of Coal Particles

Mass Balances: (1=O_2, 2=CO)

$$K_{1I}(C_{1I}-C_{1S}) - k_1 C_{1S} = 0 \quad (1)$$

$$K_{IS}(C_{2I} - C_{2S}) + 2k_1 C_{1S} = 0 \quad (2)$$

$$K_{IS} = Sh_S \frac{D}{2r} \quad (3)$$

$$R(r) = \frac{-2M_s}{\rho_s} k_1 C_{1S} \quad (4)$$

Energy Balance

$$4\pi r^2 k_1 C_{1S}(-\Delta H_1) + 4\pi r^2 H_{IS}(T_I - T_S) + 4\pi r^2 \varepsilon_s \sigma (T_I^4 - T_s^4) = 0 \quad (5)$$

(A) (B) (C)

$$H_{IS} = Nu_s \frac{\lambda_g}{2r} \quad (6)$$

Population Balance

$$\frac{dp_s}{dr} + \left\{ \frac{F_{ov}/W_S + \kappa(r)(1-\eta(r)) + \frac{d}{dr} R(r)}{R(r)} \frac{-3}{r} \right\} p_s(r) = \frac{F_s w_c P_o(r)}{W_s R(r)}$$

$$p_s(r>R_{max,s}) = 0 \quad (7)$$

TABLE II: Equations describing the mass and heat balance in the bubble phase

Mass Balances: (1=O_2, 2=CO)

$$\frac{-d}{dz}\left(\frac{A_D u_D \rho_g}{M_{air}} y_{1D}\right) + A_D(z) K_{DI}(z)(C_{1I}-C_{1D}) - A_D(z) k_2 C_{1D}^{1/2} C_{2D} = 0 \quad (8)$$

(A) (B) (C)

$$\frac{-d}{dz}\left(\frac{A_D u_D \rho_g}{M_{air}} y_{2D}\right) + A_D(z) K_{DI}(z)(C_{2I}-C_{2D}) - 2A_D(z) k_2 C_{1D}^{1/2} C_{2D} = 0 \quad (9)$$

$$\text{at } z=0 \quad C_{1D} = C_{10} \quad C_{2D} = 0 \quad (10)$$

Energy Balance

$$-\rho_g c_{pg} \frac{d}{dz}(A_D u_D T_D) + A_D(z) H_{DI}(z)(T_I - T_D) + A_D(z)(-\Delta H_2) k_2 C_{1D}^{1/2} C_{2D} = 0 \quad (11)$$

(A) (B) (C)

$$\text{at } z = 0 \quad T_D = T_O \quad (12)$$

TABLE III: Equations Describing the Mass and Heat Balances of the Emulsion Phase

Mass Balances: (1=O_2, 2=CO)

$$0 = \frac{u_{mf} A_b \rho_g}{M_{air}}(y_{10} - y_{1I}) + \frac{F_s w_o}{M_o} - F_s w_v \xi_v + \int_o^{H_b} A_D(z) K_{DI}(z)(C_{1D}(z) - C_{1I}) dz$$

(a) (e) (f) (b)

$$+ \int_o^{\infty} K_{IS}(C_{1S}(r) - C_{1I}) \frac{3}{r\rho_s} W_s p_s(r) dr - V_I k_2 C_{1I}^{1/2} C_{2I} \quad (12)$$

(c) (d)

$$0 = \frac{u_{mf} A_b \rho_g y_{2I}}{M_{air}} + \int_0^{H_b} A_D(z) K_{DI}(z)(C_{2D}(z) - C_{2I}) dz$$

(a) (b)

$$+ \int_o^{\infty} K_{IS}(C_{2S}(r) - C_{2I}) \frac{3}{r\rho_s} W_s p_s(r) dr - 2V_I k_2 C_{1I}^{1/2} C_{2I} \quad (13)$$

(c) (d)

Energy Balance:

$$0 = u_{mf} A_b \rho_g c_{pg}(T_o - T_I) + F_s w_v(-\Delta H_v) - \int_o^{\infty} F_s c_{ps}(T_s(r) - T_{so}) p_o(r) dr$$

(a) (f) (l)

$$+ \int_o^{\infty} H_{IS}(T_s(r) - T_I) \frac{3}{r\rho_s} W_s p_s(r) dr$$

(c)

$$+ V_I(-\Delta H_2) k_2 C_{1I}^{1/2} C_{2I} + \int_o^{\infty} A_D(z) H_{DI}(z)(T_D(z) - T_I) dz$$

(d) (b)

$$+ c_{pa} F_a(T_{aO} - T_I) + F_a(-\Delta H_c) + \varepsilon_s \sigma \int_o^{\infty} \frac{3}{\rho_s r} W_s p_s(r)(T_s^4(r) - T_I^4) dr$$

(j) (k) (g)

$$+ H_{ta} A_t (T_{st} - T_I)$$

(h)

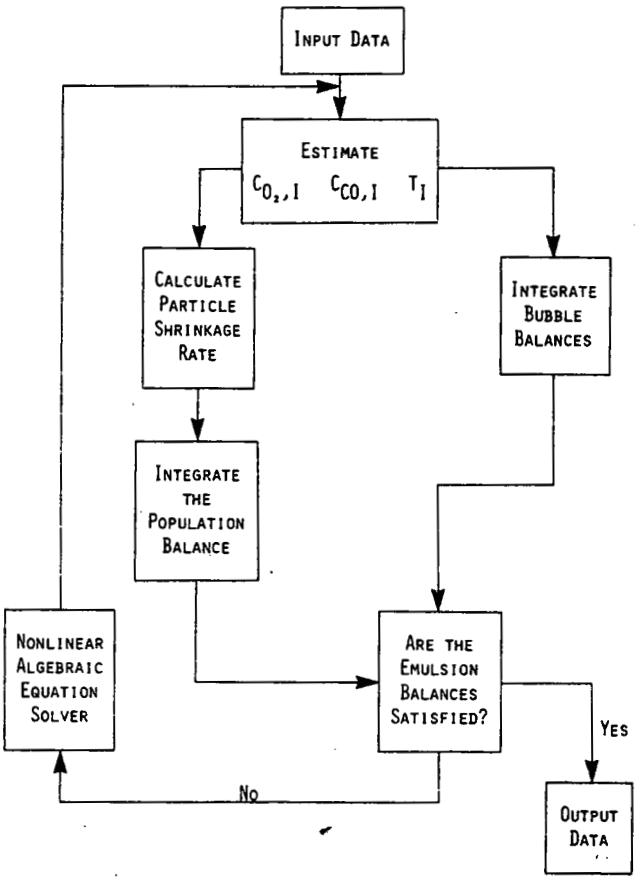

Figure 3: Schematic Representation of the Algorithm Used to Numerically Solve the Model

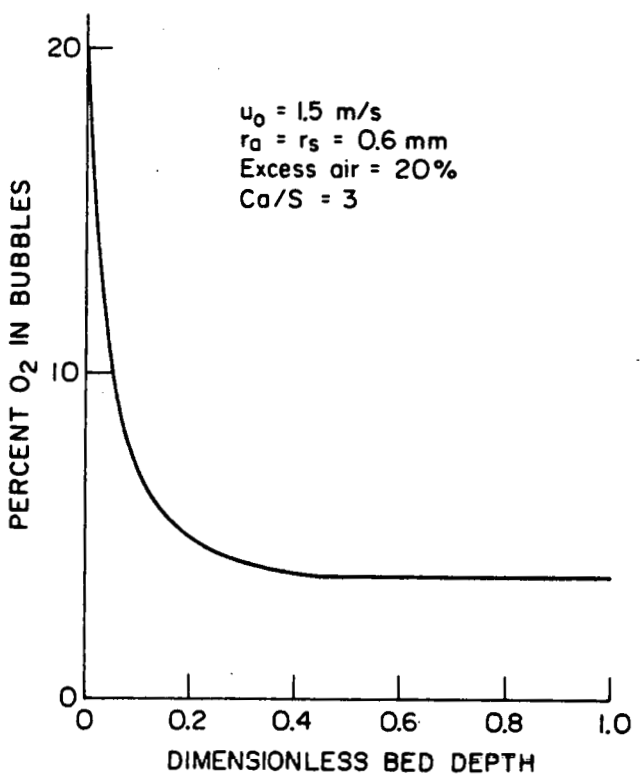

Figure 4: Variation of O_2 Percent Mole Fraction in the Bubbles with Bed Depth

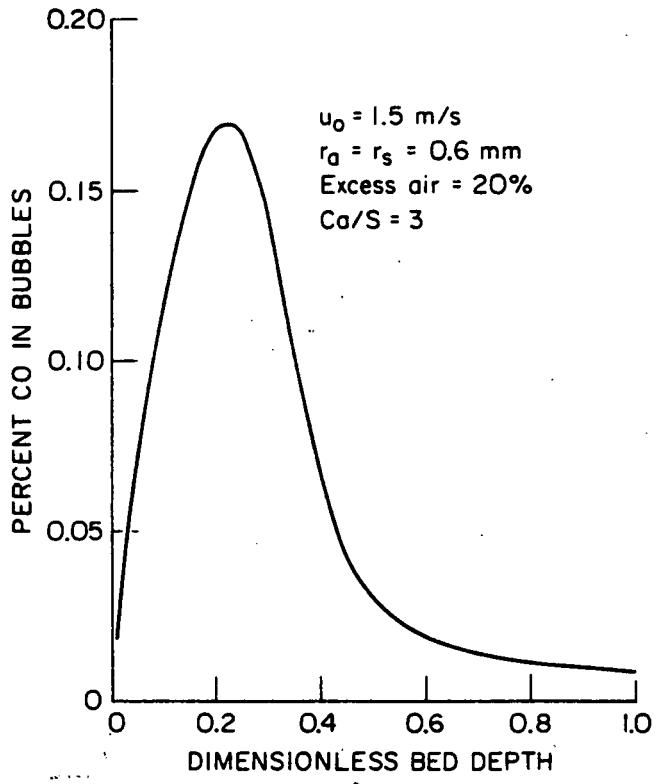

Figure 5: Variation of CO Percent Mole Fraction in the Bubbles with Bed Depth

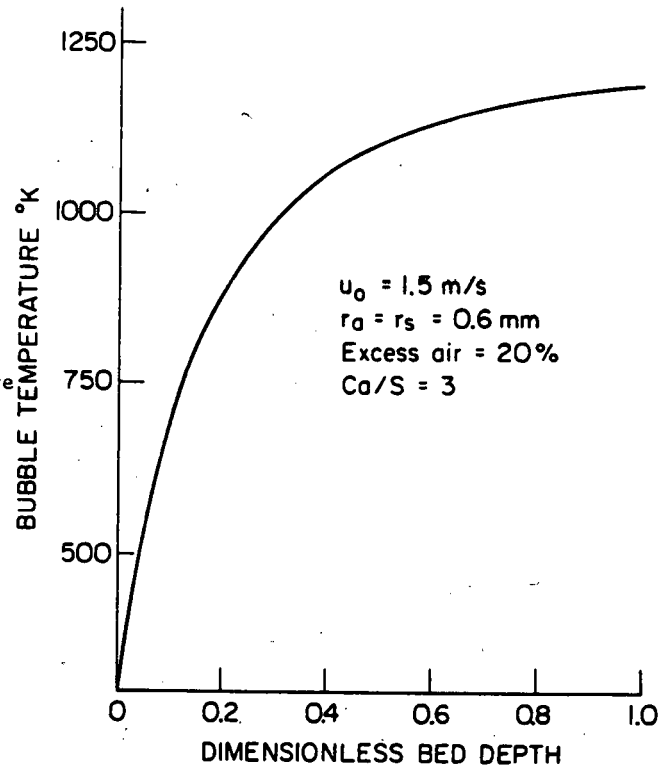

Figure 6: Variation of Bubble Temperature with Bed Depth

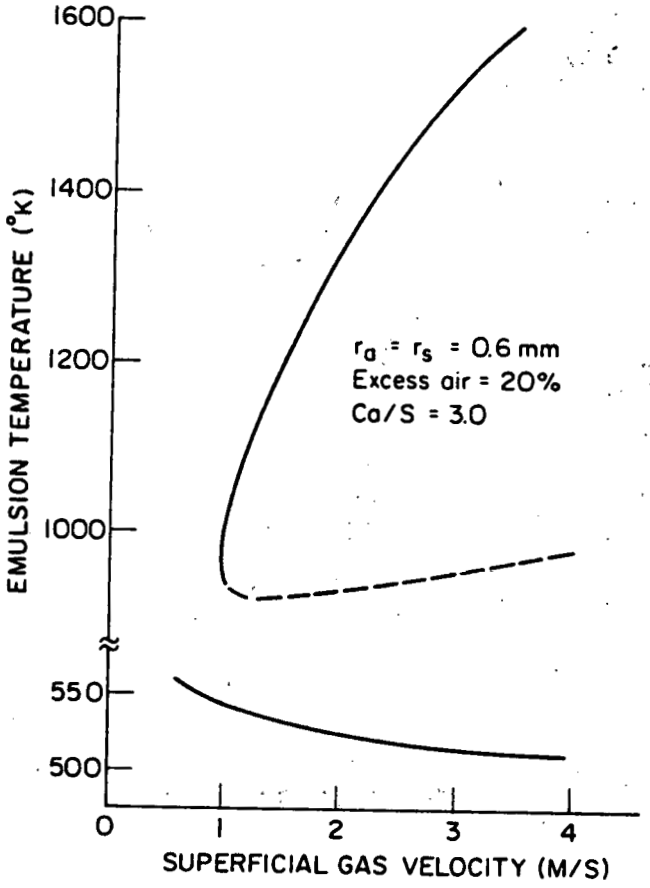

Figure 7: Dependence of Emulsion Temperature on Superficial Gas Velocity for Constant Excess Air and Ca/S Ratio

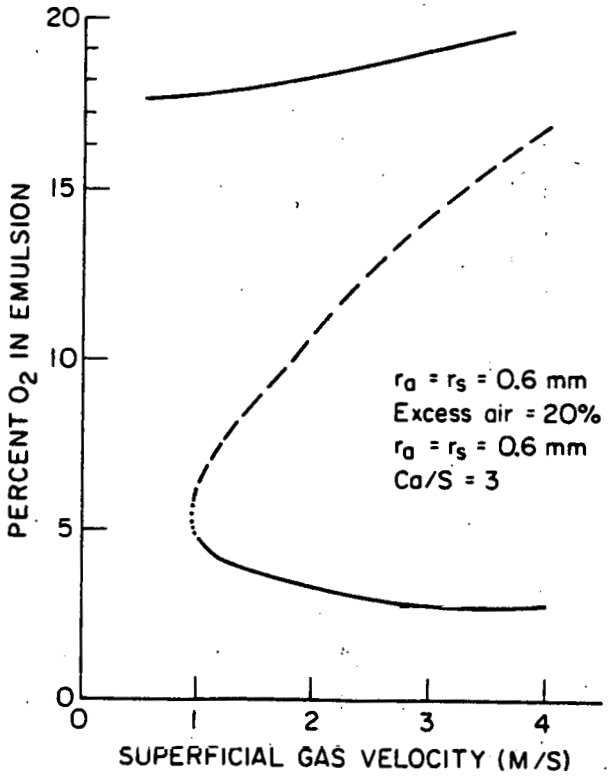

Figure 8: Dependence of O_2 Percent Mole Fraction in the emulsion on Superficial Gas Velocity for Constant Excess Air and Ca/S ratio

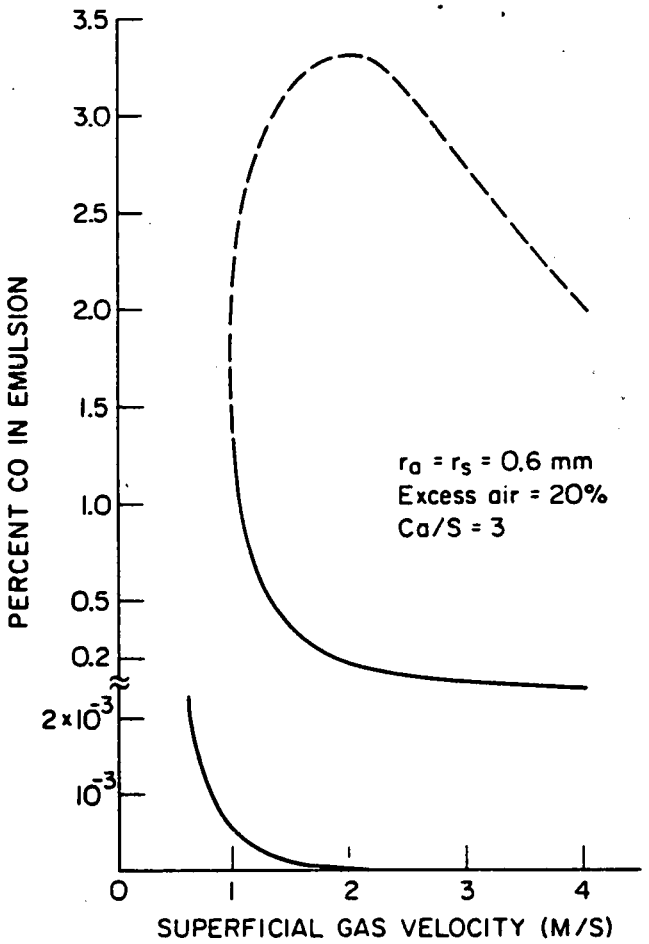

Figure 9: Dependence of CO Percent Mole in the Emulsion on Superficial Gas Velocity for Constant Excess Air and Ca/S ratio

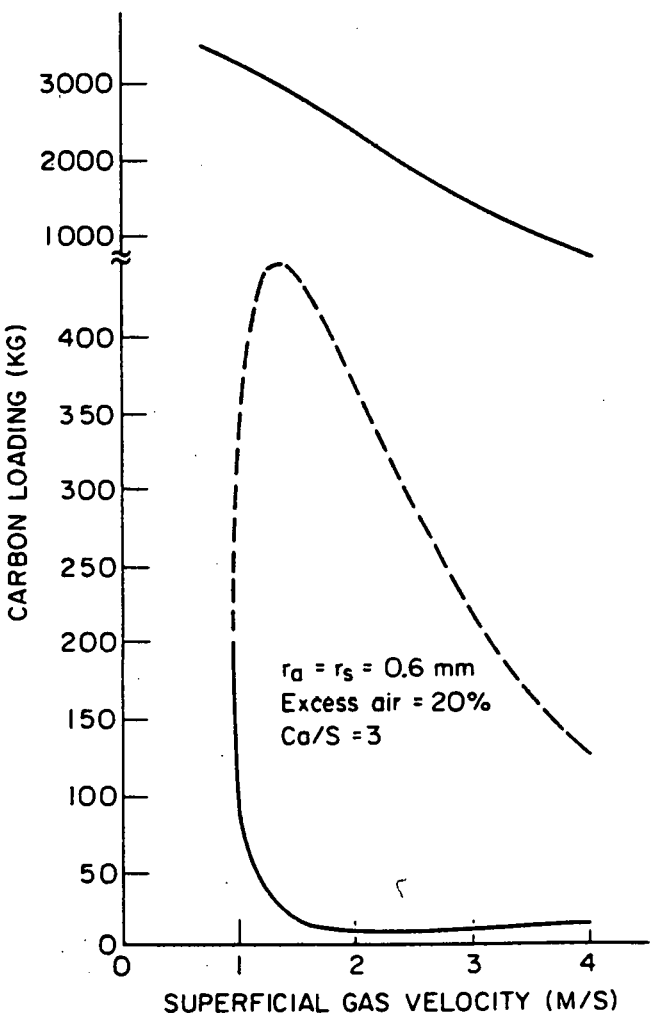

Figure 10: Dependence of Carbon Loading on Superficial Gas Velocity for Constant Excess Air and Ca/S ratio

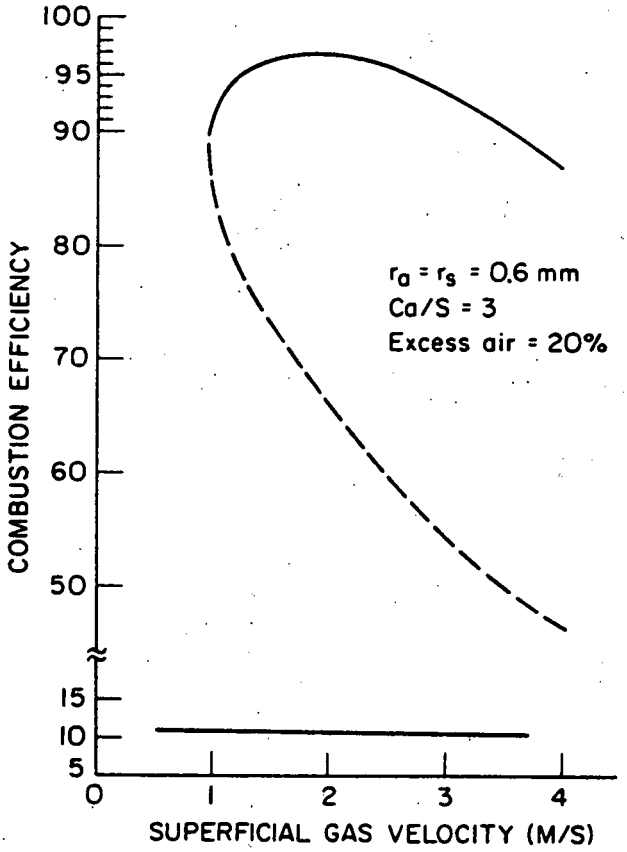

Figure 11: Dependence of Combustion Efficiency on Superficial Gas Velocity for Constant Excess Air and Ca/S ratio

Questions to C. Georgakis:

Q: (Participant not identified)

How does this study differ from the previous work by Amanson?

A: The work by Amanson, although quite elegant and systemmatic in the mathematics, did not account for some of the very important realities in the fluidized bed. Furthermore, he did not account for the presence of the dolomite. If you look at the Amanson and Gordon paper, you will notice that they automatically have 100% efficiency.

Q: (Participant not identified)

In this type of calculation and as you emphasized at the end of the talk, the combustion of carbon in the coal goes to CO and CO_2. You mentioned that carbon goes to CO for the particle and CO goes to CO_2 in the boundary layer around the particle, but you also know that there has been an increasing amount of evidence that, at the particle surface, carbon does not go alone to CO but also to CO_2. Did you consider that?

A: We did not consider that. That could be easily implemented. We were not aware of it, but we will look into that area. I think the next step, though, is to do many experiments and see how the model holds up.

Q: (Participant not identified)

Early in the FBC program, we were asked to review the instabilities that might occur with the Rivesville unit. The name mentioned at that time was Samanof's instability which had been observed in oil and pulverized coal flames. From you work, would you not conclude that a coarser particle coal system is inherantly more stable?

A: I would refrain from agreeing or disagreeing with you. We did not do enough study with sensitivity to particle size.

Q: (Participant not identified)

Are the heat transfer surfaces and their locations what keeps you from operating stably below 1 m/sec?

A: They are located in the dense bed and are thus counted in the emulsion phase heat balance.

Q: In our combustor studies, the bed temperature makes quite a difference in the initial start-up characteristics. have you investigated the initial bed temperature on the extinction characteristics?

A: This will have to be investigated through a transient model. We have started doing that, but our main problem is that the time constraints for the elements are orders of magnitude different.

A FLUIDIZED BED COMBUSTOR FREEBOARD MODEL

C. Y. Wen and L. H. Chen

Department of Chemical Engineering
West Virginia University
Morgantown, WV 26506

I. INTRODUCTION

Commercial application of the fluidized bed coal combustor (FBC) to industrial and utility boilers is rapidly becoming a realization. A race is now underway in the United States and abroad to develop and construct commercial units that will meet economic and environmental demands.

In spite of the considerable progress being made in fluidized bed coal combustion technology, a number of technical problems still remain to be resolved. One major problem having a critical impact on FBC operation is associated with freeboard phenomena and the entrainment of fines. Entrainment of carbon from the freeboard represents the main source of loss in combustion efficiency. Therefore, the recycling of entrained fines to the fluidized bed or the separate installation of a carbon burn-up cell becomes an economic necessity.

Conversely, excess fines elutriated can heavily tax the performance of cyclones and bag filters. In addition, the extent of fines loading, both carbon and limestone in the freeboard, not only significantly affects the SO_2 absorption, NO_x reduction, CO and hydrocarbon emission, etc., but also contributes to other physical phenomena such as tube heat transfer, particle attrition, yet, the phenomena of entrainment and freeboard reactions probably represent the least understood and most difficult component for modeling of a FBC.

Although many correlations on elutriation and entrainment are available in the literature, many are unreliable or are not satisfactory for prediction, design and freeboard modeling. This is mainly due to the difficulty in obtaining accurate entrainment data. Data obtained by various investigators using similar equipment and operating under similar conditions could differ considerably in some instances. Also, many of these experiments were performed using small diameter columns at relatively low velocities and small bed particles. Data from large scale beds are scarce and the effect of bed diameter on entrainment has not been established.

It is the purpose of this paper to provide a new perspective at the existing data on entrainment and elutriation and to propose a new correlation which is more reliable for simulation and modeling of the freeboard phenomena in fluidized bed combustors.

II. MODEL DEVELOPMENT

The entrainment model proposed in this paper consists of three parts. They are (1) entrainment at the bed surface, (2) disengagement of fines in the freeboard, and (3) elutriation of fines. In order to best exhibit the development of the proposed model, the following remarks will be presented; entrainment phenomena in the freeboard, entrainment rate at the bed surface, elutriation of fines above TDH, and finally, the behavior of solid particles and gas flow in the freeboard region.

1. Entrainment in the freeboard

In the freeboard region, solid particles either rise or fall, depending on the size of the particles and the gas velocity. The entrainment rate of particles has been shown to exponentially decrease along the freeboard (Large et al, 1976; Lewis et al 1962; Zenz and Weil, 1958). This decrease is assumed to result from the exponential dissipation of the effective gas velocity with freeboard height as the sharp fluctuations occurring just above the bed quickly reach average velocity as the gas leaves the surface. Also, the solid particles ejected from the bed surface into the freeboard above follow a certain velocity distribution (George and Grace, 1978; Zenz and Weil, 1958). The combination of these two effects results in an exponential decrease in the entrainment rate with respect to the height of the freeboard above the bed surface.

Thus, the entrainment rate of solids in the freeboard can be represented by the following equation which is similar to those proposed by Kunii and Levenspiel, 1969, and Large et al, 1976.

$$F = F_\infty + (F_o - F_\infty) \cdot \exp(-a\,h) \qquad (1)$$

where, F is the entrainment rate of the particles in the freeboard, h is the height above the bed and F_∞ represents the elutriation rate of the fines from the freeboard above TDH. F_o is the entrainment rate at the bed surface and the "a" is a constant representing the characteristic of the system.

Entrainment rate data available have been correlated utilizing Equation (1) by selecting an appropriate value of F_∞. Figures 1 and 2 show comparisons of the experimental data with the proposed correlations plotted on a semi-log scale for bubbling beds and slugging beds, respectively. Extrapolation

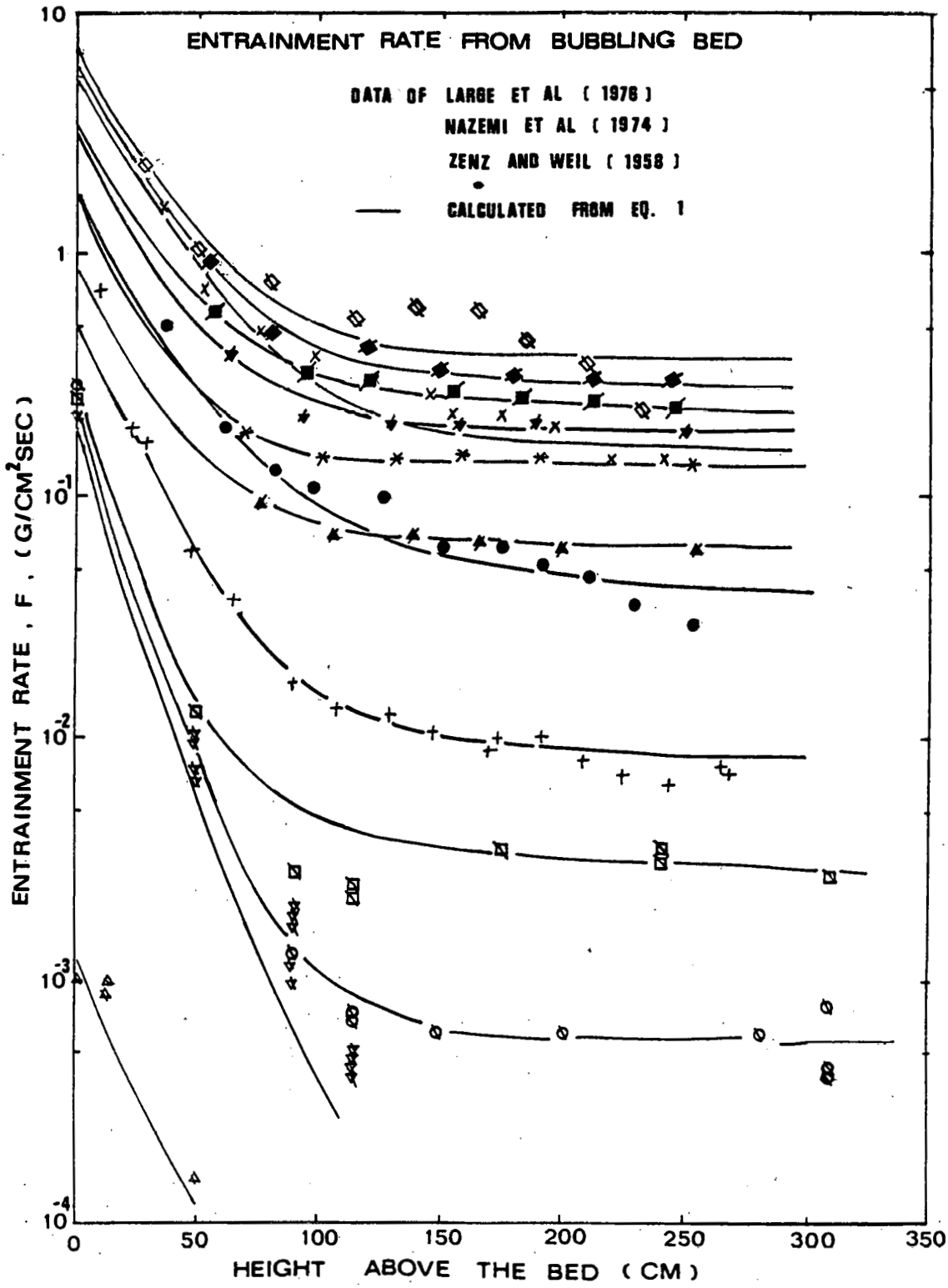

Figure 1 Comparison of Entrainment Rate Data of Various Investigators with the Proposed Model for Bubbling Beds.

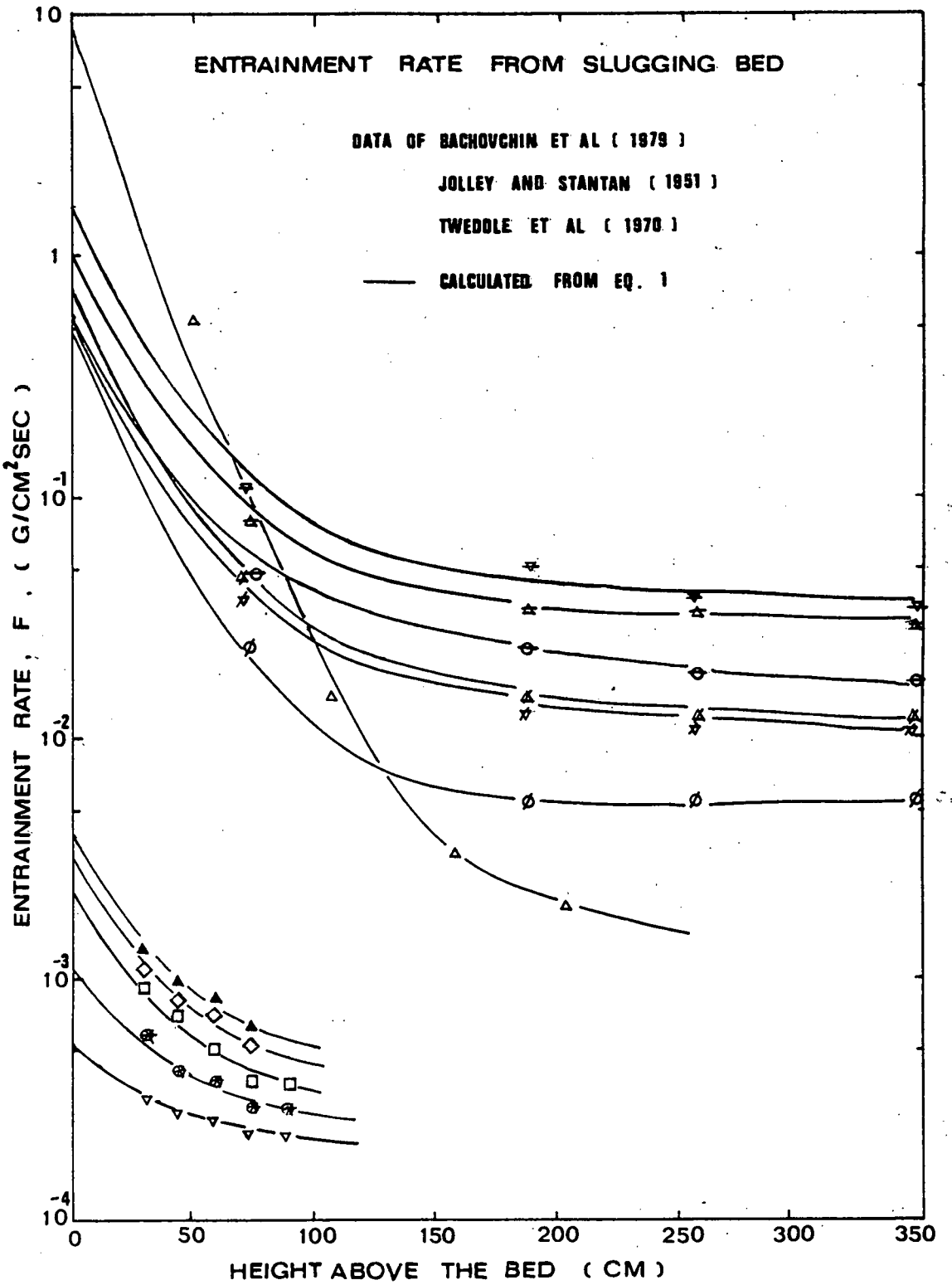

Figure 2 Comparison of Entrainment Rate Data of Various Investigators with the Proposed Model for Slugging Beds.

Table 1. Legend to Figure 1 and 2

Symbol	Investigator	$\overline{dp}$ (μm)	ρ_s (g/cm^3)	D_c (cm)	U_o (cm/sec)	a (1/cm)	a (average)
⊘	Bachovchin et	450	2.63	15.24	73	0.047	
✳	al (1979)	448				0.035	
✱		445				0.040	
⊖		450			90	0.040	0.04
✲		448				0.038	
✳		445				0.038	
	Jolley and						
▽	Stantan(1951)	76	1.33	5.08	12.19	0.022	
⊛					15.24	0.030	
□					19.05	0.037	0.035
◇					22.40	0.042	
▲					25.0	0.044	
✲	Large et al	136	2.65	61	30	0.064	
✲	(1976)	124			30	0.064	
✲		123			30	0.066	0.064
✲		123			20	0.064	
✱	Nazemi et al	59	0.84	61	9.14	0.035	
✱	(1974)				15.24	0.033	
✱					21.34	0.037	0.036
■					27.43	0.036	
✱					33.53	0.039	
△	Tweddle et al (1970)	163	1.37	16.51	76.2	0.061	0.061
+	Zenz & Weil	60	0.94	5.08x61	30.48	0.050	
●	(1958)				45.72	0.036	
×					60.96	0.042	0.042
◈					71.63	0.041	

of the curves to the dense bed surface gives the value of F_o. The value of "a" can be obtained from the slope of the straight line portion of this curve. As shown in Table 1, the value of "a" is not a strong function of the bed composition or gas velocity. Therefore, an average value of "a" is evaluated for each case. This correlation appears to agree well with the experimental data. Deviation from the experimental data is less than 50% for 95% of the cases examined as shown in Figure 3. In this figure, the average values of "a" are used in computing F. A correlation of F_∞ is presented later.

2. Entrainment at the Bed Surface

The mechanism of solids entrainment at the bed surface is not clearly understood. Although there are a number of controversies in regard to the origin of the ejected particles, the amount of particles being entrained is related to the bubbling phenomena regardless of the point of origin. Thus, it appears possible to correlate the entrainment rate of particles at the bed surface, F_o, with the bubble diameter, D_B, and the excess gas velocity, $(U_o - U_{mf})$. Such a correlation is presented in Fig. 4. The correlation equation is given by:

$$\frac{F_o}{A\, D_B} = 3.07\times10^{-9}\, \frac{\rho_g^{3.5}\, g^{0.5}}{\mu^{2.5}}\, (U_o - U_{mf})^{2.5} \quad \text{gm/cm}^5\text{.sec} \qquad (2)$$

where, A is the cross section area of the column. D_B is the bubble diameter at the bed surface and can be calculated by using an appropriate equation at different flow regime (Mori and Wen, 1975; Cranfield and Geldart, 1974). U_{mf}, the minimum fluidization velocity, is estimated by the equation of Wen and Yu,1966 . For slugging beds, column diameter, D_c, is used instead of D_B. The amount of fine particles projected into the freeboard, F_i, depends on the weight fraction of that size of fine particles present in the bed, X_i, and can be approximated by an equation having a form similar to Henry's law as: $F_i = F_o\, X_i$ (3)

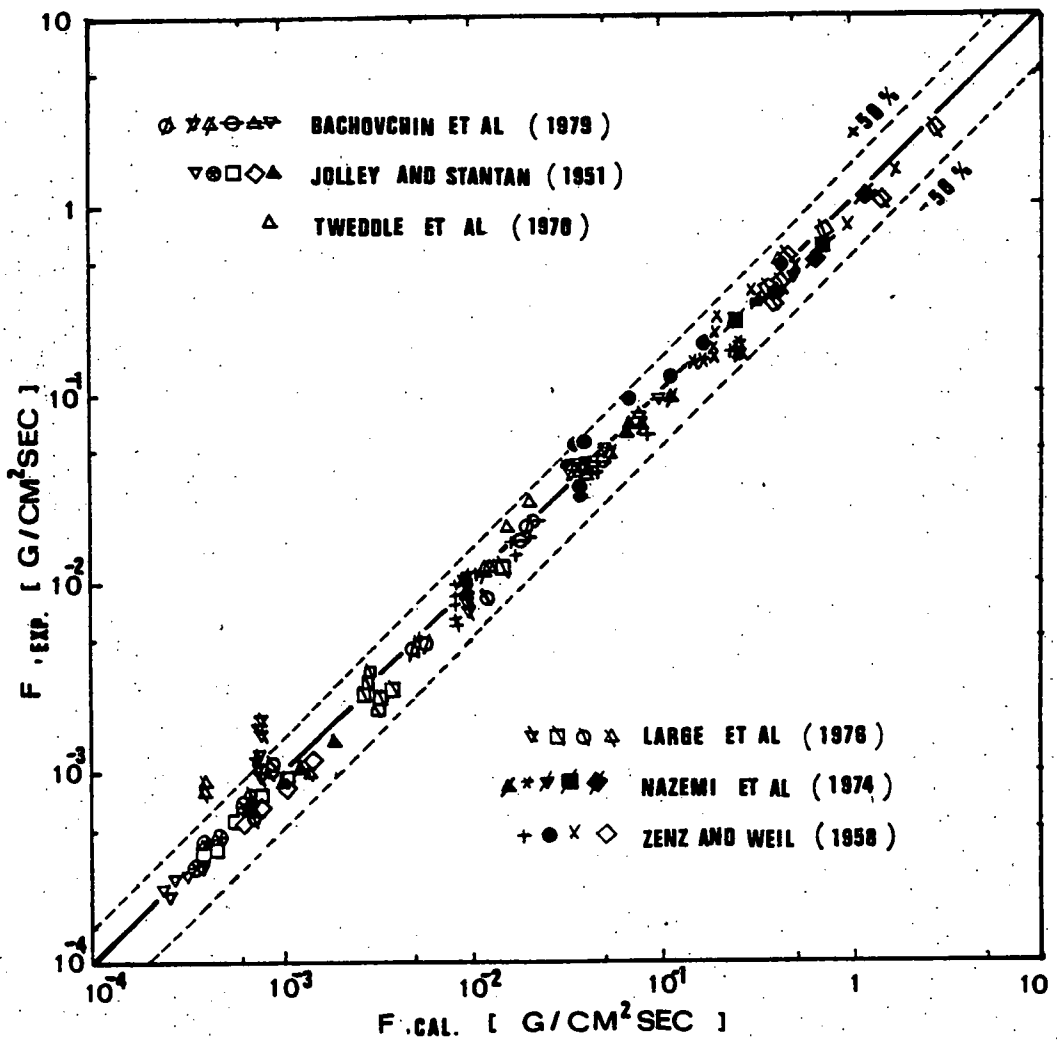

Figure 3 Comparison of Entrainment Rate Data with the Calculated Values Showing Accuracy of the Model.

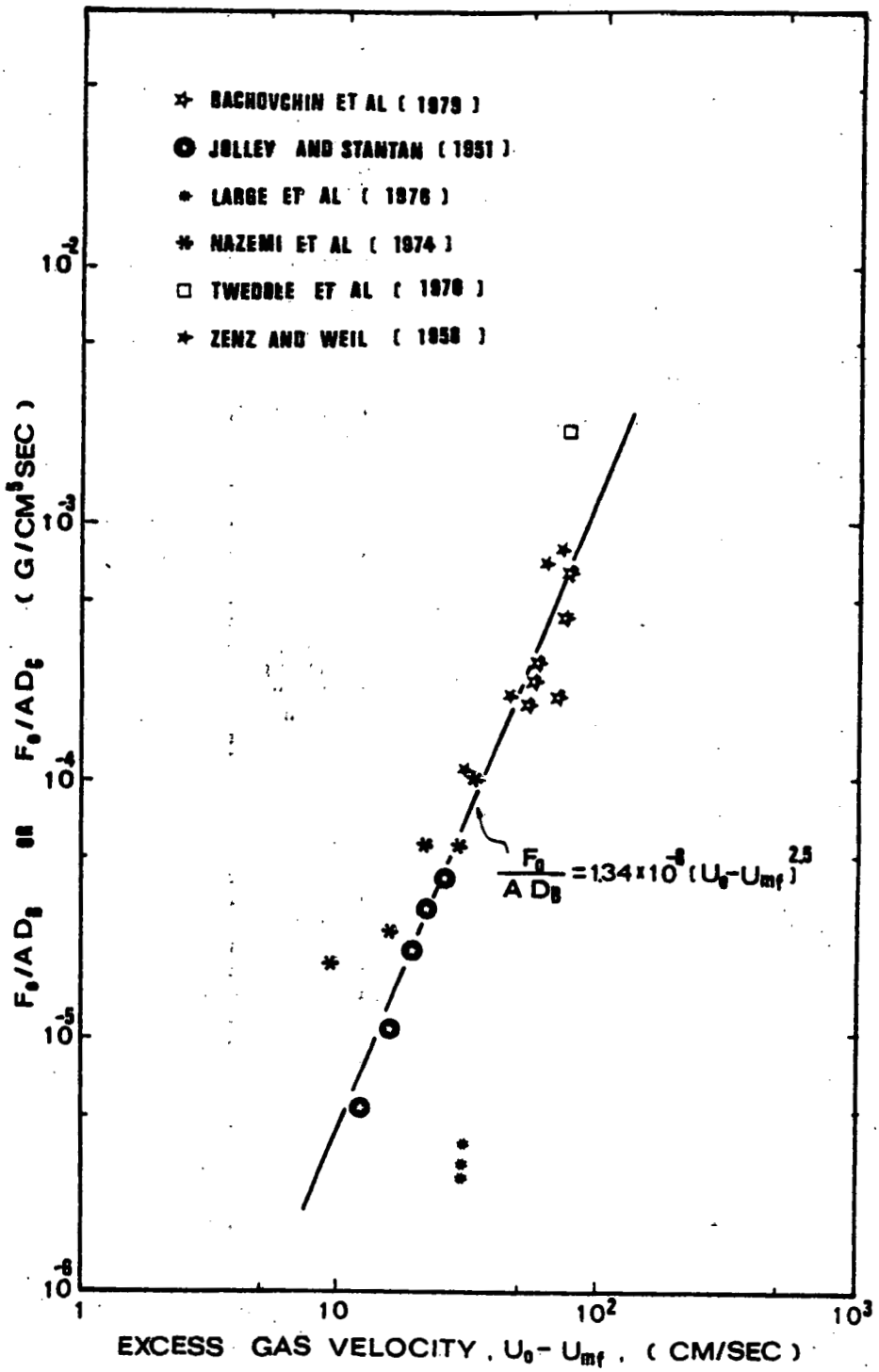

Figure 4 Correlation of Entrainment Rate Data at the Bed Surface.

3. Elutriation of Fines

Only small particles whose terminal velocity is less than the gas velocity will be carried out of the freeboard if the freeboard height is large enough. The amount of the particles elutriated, $F_{i\infty}$, is determined by both the elutriation rate constant, $E_{i\infty}$, and the weight fraction of the fine particles present in the bed, X_i, as:

$$F_{i\infty} = E_{i\infty} X_i \qquad (4)$$

The total amount of particles elutriated are calculated by summation of the amount of each particles elutriated. Thus,

$$F_{\infty} = \sum_i F_{i\infty} \qquad (5)$$

The elutriation rate constant can also be regarded as the total amount of the particles being blown away from the bed composed of particles of only one size. $E_{i\infty}$ is defined mathematically as: (Wen and Hashinger, 1960)

$$-\frac{W}{A}\frac{dX_i}{dt} = E_{i\infty} X_i \qquad (6)$$

Many correlations for determing the elutriation rate constant have been published. However, their applicabilities are limited to the range of experimental conditions under which they are employed (Yagi and Aochi, 1955; Zenz and Weil, 1958; Wen and Hashinger, 1960; Tanaka et al, 1972; Merrick and Highley, 1974; Colakyan et al, 1979; Geldart et al, 1979). Extrapolation of these correlations to different column diameters or different operating conditions often leads to very strange results. A more reliable correlation is proposed here.

When particles of a single size are elutriated above the TDH, a saturation carrying capacity of the gas stream under pneumatic transport conditions is reached. The rate of elutriation, therefore, is independent of the hydrodynamics prevailing inside the bed. A material balance of elutriating particles in such a condition can be expressed as:

$$E_{i\infty} = \rho_s (1-\varepsilon_i) U_{si} \qquad (7)$$

where ρ_s is the solid density of elutriated particles and ε_i is the voidage in the freeboard when the single size particles are being elutriated. U_{si}, the solid velocity of the given particle size, can be approximated by the difference between the gas velocity and the single particle terminal velocity as $(U_o - U_{ts})$. To calculate the voidage in the freeboard, a force balance of the particle is obtained as: (Wen, 1971; Wen and O'Brien, 1976)

$$U_{si} = U_o - U_{ts}\sqrt{\left(1 + \frac{\lambda U_{si}^2}{2g D_c}\right)\varepsilon_i^{4.7}} \qquad (8)$$

Equation 8 may be rearranged by substituting the approximate solid velocity,

U_{si}, with $(U_o - U_{ts})$ to obtain ε_i, as:

$$\varepsilon_i = \left(1 + \frac{\lambda U_{si}^2}{2g D_c}\right)^{\frac{-1}{4.7}} \qquad (9)$$

λ, the friction coefficient due to the bouncing of the particles against the wall and against each other, is correlated by the following equation.

$$\frac{\lambda \rho_s}{d_p^2} = \begin{cases} 3.06\, Rep^{-1}\, d_p^{-0.94}\, D_c^{1.4}, & Rep \leq Rep,c \\ 1.45\times10^4\, Rep^{-2.5}\, D_c, & Rep \geq Rep,c \end{cases} \qquad (10)$$

where, $Rep,c = 2.82 \times 10^2 \cdot d_p^{0.63} \cdot D_c^{-0.27}$ (11)

and $Rep = \rho_g \cdot (U_o - U_{ts}) \cdot d_p/\mu$ (12)

Figure 5 shows the comparison of this relation with the experimental data (Colakyan et al, 1979; Lin et al, 1980; Merrick and Highley, 1974; Tanaka et al, 1972; Wen and Hashinger, 1960).

At low Reynold's Number, the forces acting on the elutriating particles is dominated by the bouncing of the particles against the wall. The column diameter in this flow regime strongly affects the rate of elutriation. On the other hand, at higher Reynold's Number, the column diameter no longer affects the elutriation rate since the collisions of particles against each other now dominates the forces acting on the elutriating particles. Comparison of the calculated elutriation rate constant based on this correlation with the experimental data is shown in Figure 6. As can be seen most of the experimental data can be represented by this correlation within $\pm$ 50% deviation.

4. Solid Velocity Distribution

As previously mentioned, this model is based on the assumption that the particles ejected at the bed surface follow a certain velocity distribution function. In this section, we discuss how the velocity distribution and the velocity profile in the freeboard can be generated. As the entrained particles are carried up by the gas stream, those particles whose terminal velocity is larger than the gas velocity will reach a maximum height within the freeboard before falling back to the bed. However, those particles whose terminal velocity is less than the gas velocity, will eventually be elutriated. The initial solid velocity for large particles can be calculated from the equation of maximum projected height and the entrainment rate equation in the freeboard (Zenz and Weil, 1958; Do et al, 1972) as follows:

$$\frac{h_{max}}{d_{pi}} = \frac{\rho_s d_{pi} U_{io}}{28.1\ \mu}\left[1 - \frac{U_{ts}-U_{io}}{U_{io}} \ln\left(\frac{U_{ts}}{U_{ts}-U_{io}}\right)\right] \qquad (13)$$

and

$$F_i = F_{i\infty} + (F_{io} - F_{i\infty}) \cdot \exp(-a\, h) \qquad (14)$$

The velocity profile in the freeboard can be obtained from the following equation for the upward moving particles:

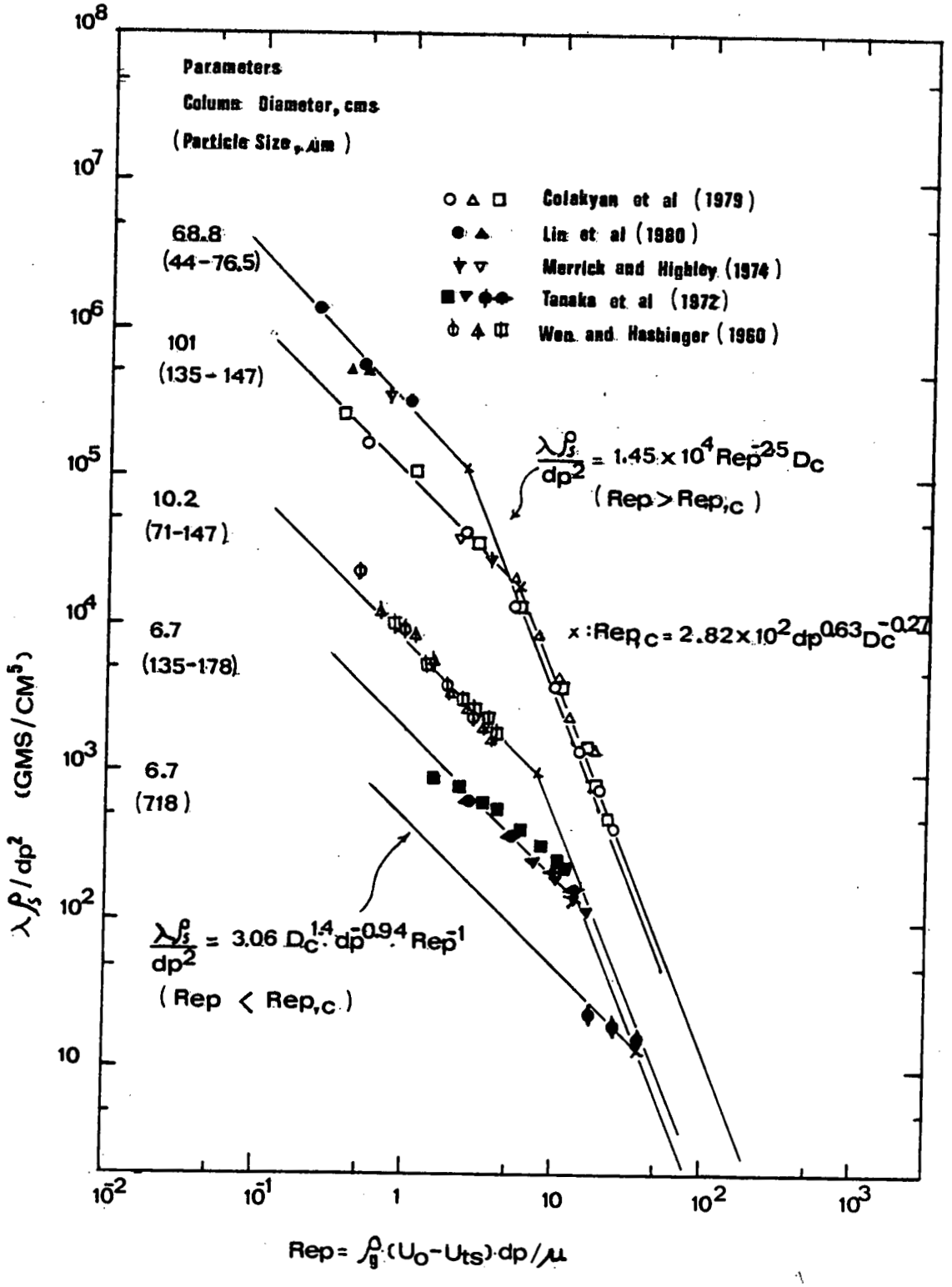

Fig. 5 Correlation of Solid Friction Coefficient Data.

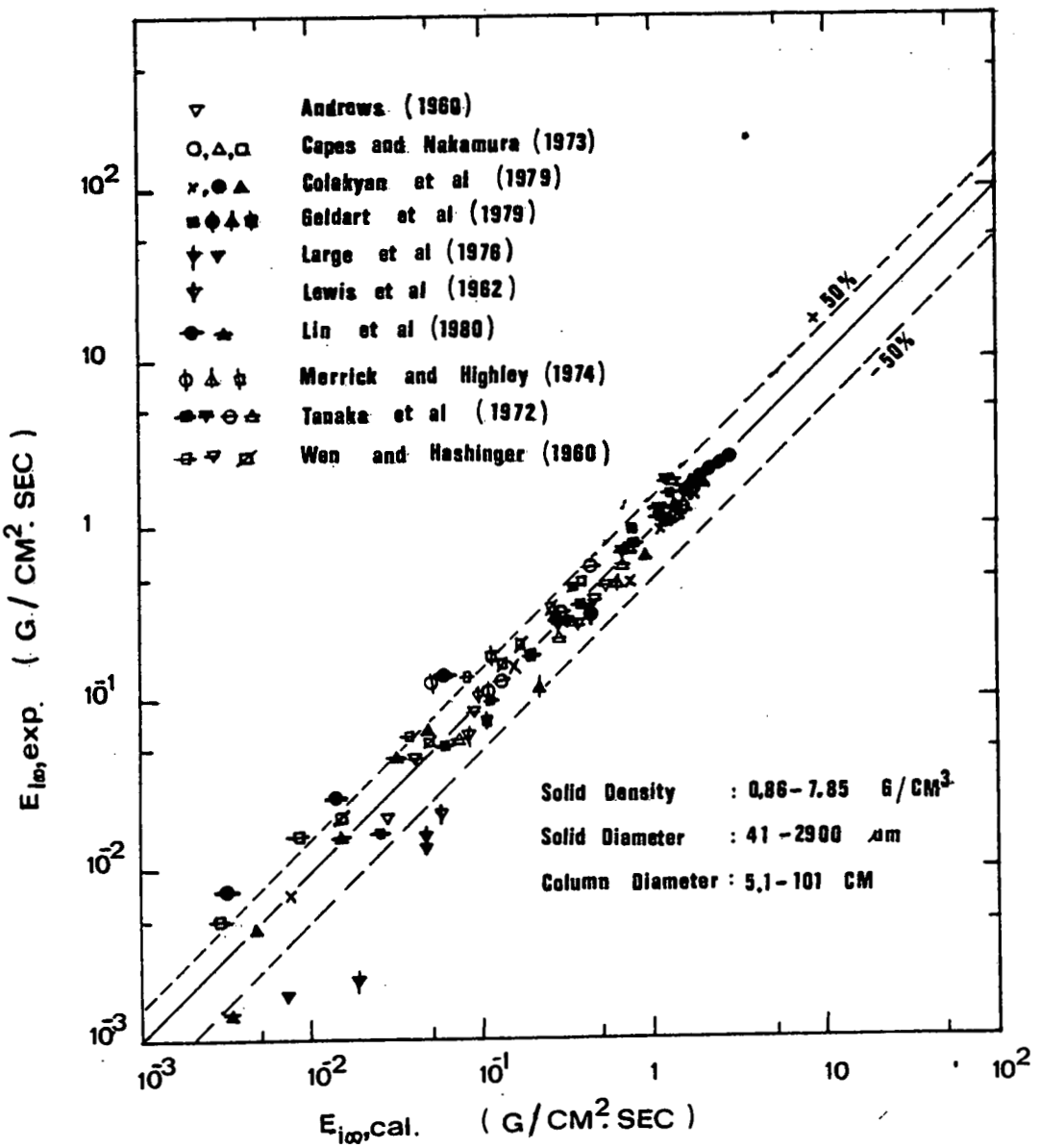

Figure 6 Comparison of Elutriation Rate Constant Data with the Calculated Values showing Accuracy of the Correlation.

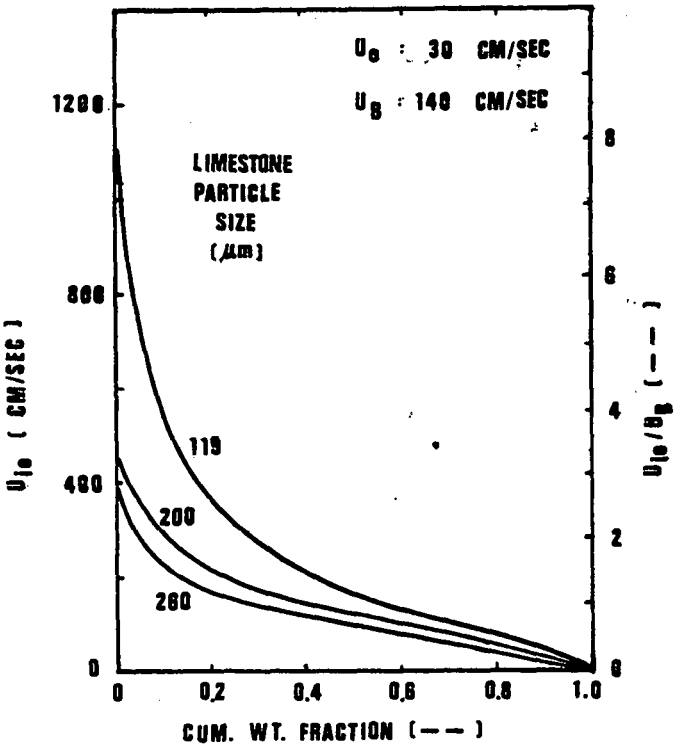

Figure 7 Solid Velocity Distribution at the Bed Surface for Limestone Particles (U_o = 30 cm/sec and U_B = 140 cm/sec)

$$\frac{d\,U_{si}}{d\,h} = -\frac{3}{4}\,\frac{C_D \rho_g\, U_{sr}|U_{sr}|}{\rho_s \cdot d_{pi} \cdot U_{si}} - \frac{(\rho_s-\rho_g)\,g}{\rho_s \cdot U_{si}} \qquad (15)$$

where $U_{sr} = U_{si} - U_g$

For the downward falling particles, the terminal velocity against the gas stream is used because of the short acceleration distance for the particles compared to the downward traveling distance.

Figure 7 shows an example of the initial solid velocity distribution for limestone. The velocity profile for the particles of 119 μm at a superficial air velocity of 30 cm/sec is shown in Figure 8. For the small particles which will not fall back to the bed, the terminal velocity relative to the gas stream is taken as the solid velocity.

The gas velocity is estimated from the interstitial velocity as:

$$U_g = U_o/\varepsilon \qquad (16)$$

Since the voidage in the freeboard is close to unity, the approximation by using the superficial gas velocity will not be expected to give a large error.

III. APPLICATION OF THE ENTRAINMENT MODEL

In this section, we present two examples to illustrate the model proposed.

1. Estimation of Elutriation Rate

Knowing the bed composition, the elutriation rate from a fluidized bed can be calculated based on Equations 4,5,8,9 and 10. As shown in Figures 9 and 10, the agreement is good for the two large fluidized bed combustors tested. In these figures, the experimental data from 6' x 6' FBC of B&W and 3' x 1.5' FBC of NCB, are compared with the calculated elutriation rate constants.

2. Calculation of Hold-up in the Freeboard

In order to simulate the solid-gas reaction in the freeboard, it is necessary to estimate the hold-up or solid concentration in the freeboard. The hold-up of the particles can be calculated by knowing the velocities and the rates of the particles flowing upward and downward.

Accordingly,
$$H_d = \sum_i \frac{F_i}{U_{si}} + \sum_i \frac{F_i'}{U_{si}'} \qquad (17)$$

where, U_{si} and U_{si}' are the solid ascending and descending velocity, respectively, and F_i and F_i' are the ascending and descending flow rates of particles. The downward flow rate of particles, F_i', can be obtained from the material balance equations as: $F_i' = (F_{io} - F_{i\infty})\exp(-ah)$ (18)

Figure 11 shows an example of the calculated hold-up along the freeboard.

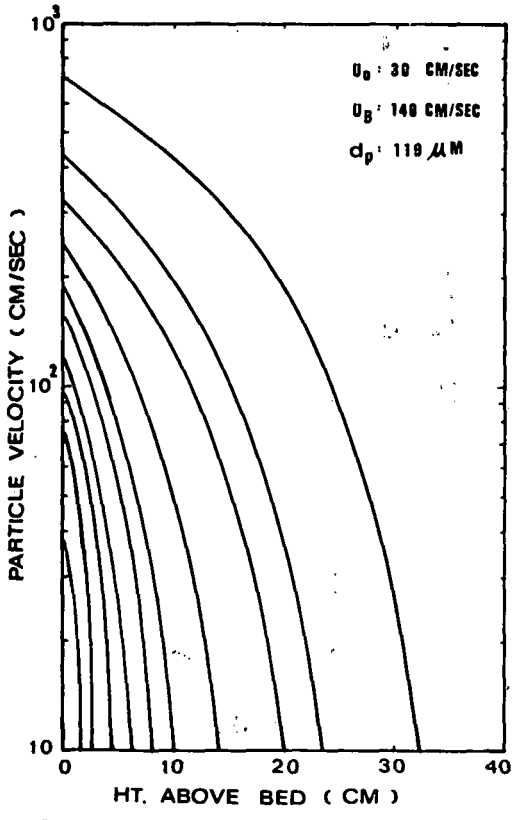

Figure 8 Solid Velocity Profile in the Freeboard (d_p = 119 μm, U_o = 30 cm/sec and U_B = 140 cm/sec)

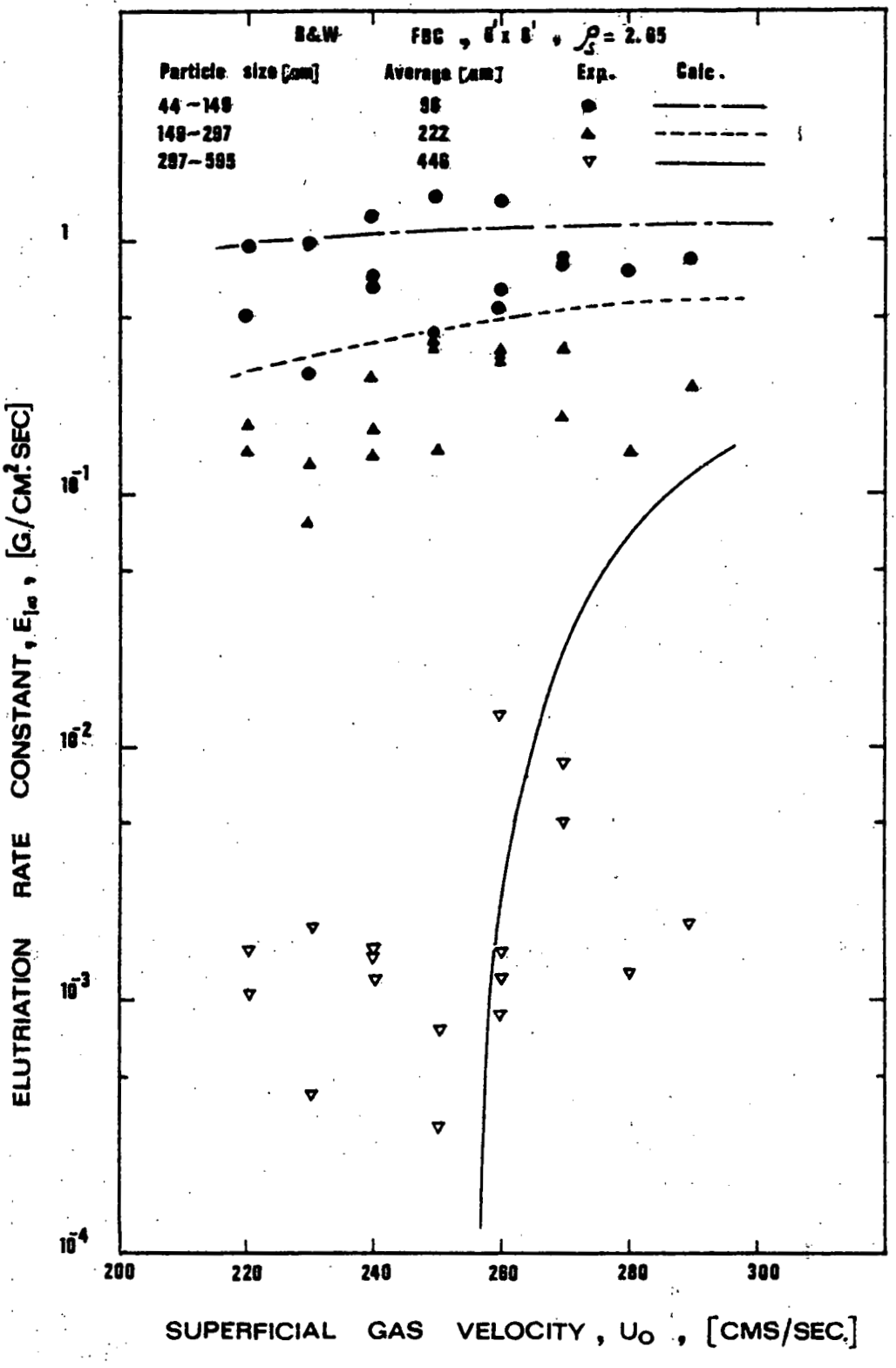

Figure 9 Comparison of B & W, 6' x 6' FBC Elutriation Rate Constants with the Calculated Values from the Proposed Correlation.

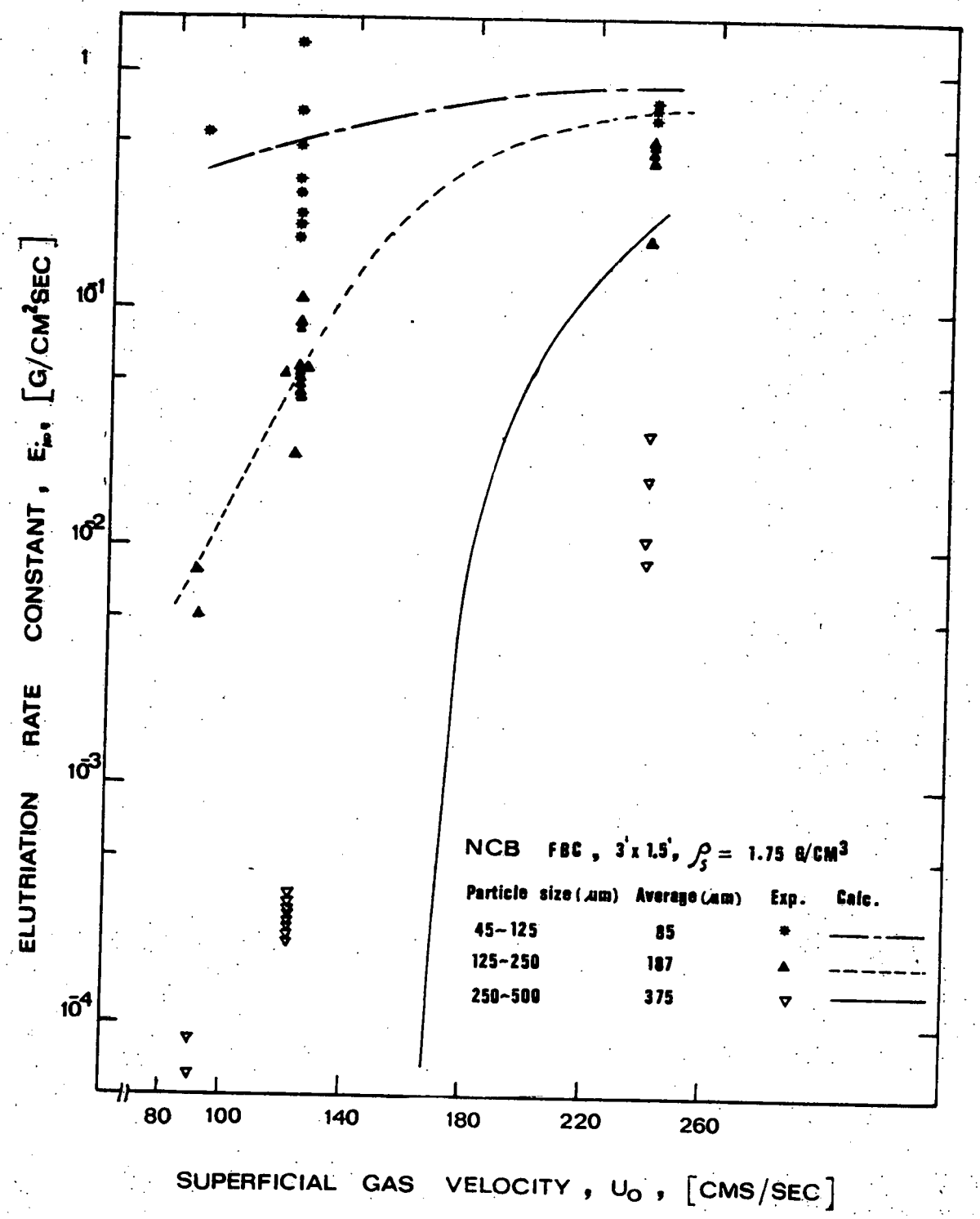

Figure 10 Comparison of NCB, 3' x 1.5' FBC Elutriation Rate Constants with the Calculated Values from the Proposed Correlation.

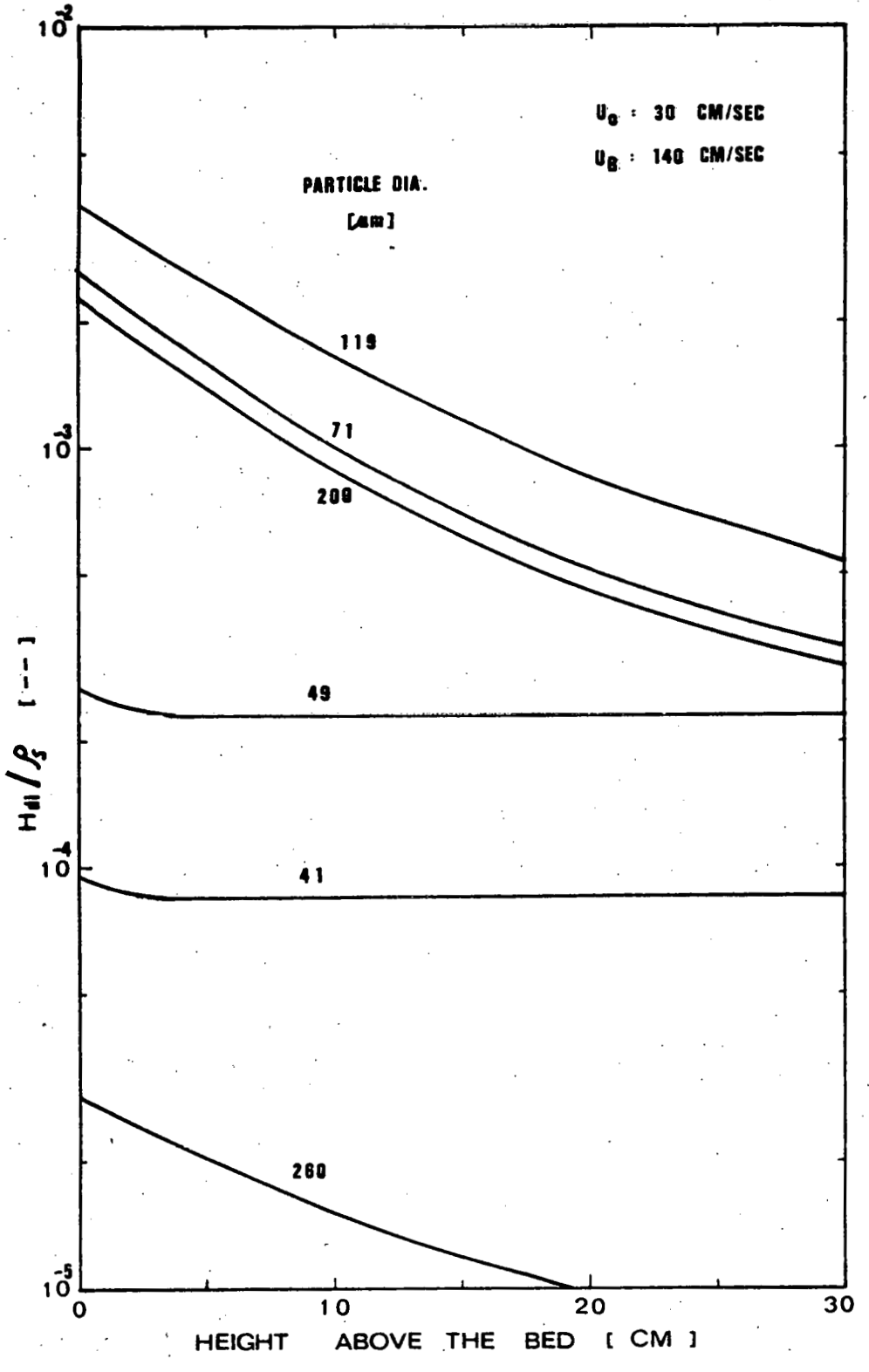

Figure 11 Solid Concentration Profile in the Freeboard
(U_o = 30 cm/sec and U_B = 140 cm/sec)

IV. DISCUSSION AND CONCLUSION

1. The entrainment model proposed here is based on the assumption that the particles ejected at the bed surface have a velocity distribution. This results from bubble eruptions and the gas jetting at the surface of the bed which ejects the particles into the freeboard at various velocities. On the other hand, the gas jets at the bed surface quickly dissipate upon leaving the surface of the bed and the gas velocity follows a flat profile. Fournol et al, 1973 have measured uniform gas velocity and entrainment rate across the radial positions in the column at heights well below TDH.

2. There is some evidence indicating the entrainment data obtained using isokinetic probes tend to give lower values than that using a funnel to collect the entrained solids. For example, the data obtained by Large et al, 1976 which are considerably lower than that of other investigators who experimented at equivalent operating conditions. Therefore, these data have been eliminated in the correlation of entrainment rate at the bed surface as presented in Figure 4. Their experimental data is again found to be considerably lower than other investigators when comparing the elutriation rate constants shown in Figure 6.

3. The value of "a" in the entrainment equation is varied from 0.035 ~ 0.064 as can be seen in Table 1. Since this value is not sensitive in the entrainment rate estimation, it is recommended that a value of 0.04 is used for the system in which no information on entrainment rate is available.

4. The entrainment model proposed here is unique as compared with other models since the value of TDH (transport disengaging height) is not required in estimating the amount of solids being entrained. Using the model proposed, the amount of solids entrained or elutriated at different heights in the freeboard can be estimated from the entrainment rate at the bed surface, F_o, and the elutriation rate, F_∞. The entrainment rate at the bed surface is calculated by knowing the size of bubbles at the bed surface, while the elutriation rate is estimated from a correlation relating to the saturation carrying capacity of gas stream which is independent of the bed hydrodynamics.

5. In calculating the elutriation rate constant, the friction coefficient, expressed as λ/D_c, is an important factor as shown in Equations 7 and 9. When the particle Reynold's Numbers are less than the critical Reynold's Number (at low solid velocity), the friction between particles and the column is important and a significant wall effect is observed. If the particle Reynold's Number is higher than the critical Reynold's Number, (at high solid velocity), the friction between particles is more important and the column diameter effect diminishes.

6. Discussion has been presented stating particles whose terminal velocity is greater than the gas velocity cannot be elutriated if the freeboard height is sufficiently high. However, it has been observed that small amounts of large particles have been collected in cyclones from several fluidized bed experiments (Merrick and Highley, 1974; Geldart et al, 1979). These observations were made at high gas velocities. It is speculated that these observations result from either (1) the height of the freeboard is not sufficiently high enough to allow coarse particles to return to the bed or (2) the channeling of the gas may have created zones of locally high velocity.

7. In comparison to bubble velocity as shown in Figure 7, the initial solid velocity is not necessarily always greater than bubble velocity. This implies that the origin of the ejected particles may not be entirely resulting from the wakes of bubbles. This point needs further investigation.

8. Since the data employed for deriving the correlation for the elutriation rate constant is based primarily on experiments utilizing air at room temperature, the correlation should not be applied to other gases at different temperatures without proper correction. Further studies are needed to improve the elutriation rate correlation for different gases at different temperatures and in the presence of tubes and/or other internals.

V. NOMENCLATURE:

a = constant in the entrainment equation (1/cm)
A = cross section area of the bed (cm^2)
C_D = drag coefficient of single particle (-)
d_p or d_{pi} = particle diameter of close cut particle i (cm)
$\bar{d}_p$ = average particle diameter in the bed (μm)
D_B = bubble diameter at the bed surface (cm)
Dc = column diameter (cm)
$E_{i\infty}$ = elutriation rate constant of particle size i ($g/cm^2 sec$)
F = total entrainment rate of the particles ($g/cm^2 sec$)
F_i = entrainment rate of particle size i ($g/cm^2 sec$)
F'_i = downward flowing rate of particle size i ($g/cm^2 sec$)
$F_{i\infty}$ = elutriation rate of particle size i ($g/cm^2 sec$)
F_o = total entrainment rate at the bed surface ($g/cm^2 sec$)
F_∞ = total elutriation rate of the particles ($g/cm^2 sec$)
g = gravitational acceleration constant (cm/sec^2)
h = height above the dense bed surface (cm)
h_{max} = maximum height the particle can be projected (cm)
H_d hold up of particles in the freeboard (g/cm^3)
H_{di} = hold up of particle size i in the freeboard (g/cm^3)
Rep = particle Reynold's Number = $\rho_g (U_o - U_{ts})\, dp/\mu$ (-)
Rep,c = critical particle Reynold's Number (-)
t = time (sec)
U = gas velocity (cm/sec)
U_{io} = initial solid velocity (cm/sec)
U_{mf} = minimum fluidization gas velocity (cm/sec)

U_o	=	superficial gas velocity	(cm/sec)
U_{gi}	=	solid velocity (upward)	(cm/sec)
U_{si}	=	solid velocity (downward)	(cm/sec)
U_{sr}	=	relative solid velocity	(cm/sec)
U_{ts}	=	single particle terminal velocity of particle size i	(cm/sec)
W	=	weight of the bed	(g)
X_i	=	weight fraction of particle size i in the bed	(-)
ε	=	voidage in the freeboard	(-)
ε_i	=	voidage in the freeboard for the system having only particle size i	(-)
λ	=	solid friction coefficient	(-)
ρ_g	=	gas density	(g/cm^3)
ρ_s	=	solid density	(g/cm^3)
μ	=	viscosity of gas	(g/cm sec)

VI. REFERENCES:

Andrews, J. M.; "Kinetic Study of Fluidized Solids Entrainment"; I&EC, 52, No. 1, 85 (1960).

Bachovchin, D. M., J. M. Beer, and A. F. Sarofim; "An Investigation into the Steady-State Elutriation of Fines From a Fluidized Bed" ; AIChE 72nd Meeting, San Francisco, (1979).

Capes, C. E., and K. Nakamura; "Vertical Pneumatic Conveying - An Experimental Study with Particles in the Intermediate and Turbulent Flow Regimes" ; Can. J. Chem. Eng., 51, No. 2, 31 (1973).

Colakyan, M., N. Catipovic, G. Jovanovic, and T. Fitzgerald; "Elutriation from a Large Particle Fluidized Bed with and without Immersed Heat Transfer Tubes" ; AIChE 72nd Meeting, San Francisco, (1979).

Cranfield, R. R., and D. Geldart; "Large Particle Fluidization"; CES, 29, 935 (1974).

Do, H. T., J. R. Grace, and R. Clift; "Particle Ejection and Entrainment from Fluidized Beds"; Powder Technol. 6, 195 (1972).

Fournol, A. B., M. A. Bergougnou, and G. G. J. Baker; "Solids Entrainment in a Large Gas Fluidized Bed"; Can. J. of Chem. Eng. 51, 401 (1973).

Geldart, D., J. Cullinan, S. Georghiades, D. Gilvray, and D. J. Pope; "The Effect of Fines on Entrainment from Gas Fluidized Beds"; Trans. I. Chem. E. 57, 269 (1979).

George, S. E., and J. R. Grace; "Entrainment of Particles from Aggregative Fluidized Beds"; AIChE Symposium Series, 74, No. 176, 67 (1978).

Jolley, L. T., and J. E. Stantan; "Fluidization in Beds of Coal and Coke Particles: Some Effect of Size of Particles and Viscosity, Density and Velocity of Gas"; J. appl. Chem. 2, Supplementary Issue, No. 1, 562 (1951).

Kunii, D., and O. Levenspiel; "Fluidization Engineering" ; John Wiley and Sons, Inc., 113 (1969).

Large, J. F., Y. Martinie, and M. A. Bergougnou; "Interpretative Model for Entrainment in a Large Gas Fluidized Bed"; International Powder Bulk Solids Handling & Processing Conference, May, (1976)

Lewis, W. K., E. G., Gilliland, and P. M. Lang; "Entrainment from Fluidized Beds" ; CEP Symposium Series, 58, No. 38, 65 (1962).

Lin, L. W., J. T. Sears, and C. Y. Wen; "The Elutriation of Char from a Large Fluidized Bed"; paper accepted by Powder Technol. (1980).

Merrick, D., and J. Highley; "Particle Size Reduction and Elutriation in a Fluidized Bed Process"; AIChE Symposium Series, 70, No. 137, 366 (1974).

Mori, S., and C. Y. Wen; "Estimation of Bubble Diameter in Gaseous Fluidized Beds" ; AIChE J., 21, No. 1, 109 (1975).

Nazemi, A., M. A. Bergougnou, and G. G. J. Baker; "Dilute Phase Hold-up in a Large Gas Fluidized Bed"; AIChE Symposium Series, 70, No. 141, 98, (1974).

Tanaka, I., H. Shinohara, H. Hirosue, and Y. Tanaka; "Elutriation of Fines from Fluidized Bed"; J. of Chem. E. of Japan, 5, No. 1, 51 (1972).

Tweddle, T. A., C. E. Capes, and G. L. Osberg; "Effect of Screen Packing on Entrainment from Fluidized Beds"; I & EC Process Des. Dev., 6, No. 1, 85 (1970).

Wen, C. Y.; "Dilute and Dense Phase Pneumatic Transport"; paper in Bulk Materials Handling, Vol. 1, edited by M. C. Hawk, Univ. of Pittsburgh, 258 (1971).

Wen, C. Y., and R. F. Hashinger; "Elutriation of Solid Particle From a Dense Phase Fluidized Bed"; AIChE J., 6, No. 2, 220 (1960).

Wen, C. Y. and W. S. O'Brien; "Pneumatic Conveying and Transporting" ; Chapter 3 in Gas-Solids Handling in the Process Industries, edited by J. M. Marchello, and A. Gomezplata, Marcel Dekker, Inc., 89 (1976).

Wen, C. Y. and Y. H. Yu; "A Generalized Method for Predicting the Minimum Fluidization Velocity" ; AIChE J. 12, No. 3, 610 (1966).

Yagi, S., and T. Aochi; paper presented at the Society of Chemical Engineers (Japan), Spring Meeting, (1955).

Zenz, F. A., and N. A. Weil; "A Theoretical-Emperical Approach to the Mechanism of Particle Entrainment from Fluidized Beds";AIChE J. 4, No.4, 472 (1958).

Question to C. Y. Wen:

Q: (Participant not identified)

In some of the larger FBC units you will find larger particles with terminal velocities five or six times larger than the superficial velocity being thrown 6-8 ft. above the bed. The fines recycling bears on this. The more fines recycled the more of these larger particles you have carried into this zone. We might look at the freeboard as a glorified distillation column.

A: Indeed, we have these large particles entrained and that shows in the data. These particles rapidly drop back into the bed.

CHAR COMBUSTION IN THE FREEBOARD REGION

S.E. Tung, T.Z. Chaung, P.K. Sharma, J. Hodges, and J.F. Louis

MASSACHUSETTS INSTITUTE OF TECHNOLOGY
Energy Laboratory
Cambridge, MA. 02139

Abstract

A model has been developed to simulate the combustion and related processes occurring in the freeboard of a fluidized bed coal combustor. This model predicts concentration profiles for both solids and the gaseous species of interest along the freeboard. Particle dynamics in the freeboard is simplified by dividing the particles in two categories: those that have their terminal velocity close to the fluidizing velocity, and others that do not. The first category of particles can be treated as combustion controlled while the second category of particles are assumed to follow Lewis' exponential decay law. Kinetic expressions based on external surface concentration are used to obtain total char burning rate. Parametric studies are reported for predicted combustion efficiency and carbon load in the freeboard.

Pilot plant FBC experience has indicated that for certain operating conditions, a significant fraction of the total heat release occurs in the freeboard region of the combustor [1]. The effect would be most pronounced under conditions of high oxygen by-pass (i.e, high gas velocity and/or small bed particle size) where the emulsion phase gas is relatively deficient and the freeboard is comparatively rich in oxygen. The observation that pilot plants do not suffer the performance degradation that would be expected under high by-pass conditions provides an additional indication that under these conditions some freeboard combustion is occurring. A model for freeboard char combustion has been formulated. Some results are presented below.

I. Model Description

The key to the freeboard combustion modeling is the prediction of carbon loading profile along the freeboard height. Once the carbon loading profile is known, then the combustion kinetics can be easily incorporated. The carbon loading in the freeboard depends principally on two factors; the initial entrainment from the bed surface and the particle residence time.

The problem of determining freeboard solids residence time is illustrated in Figure 1. It can be seen that larger particles spend comparatively little time in the freeboard since for these particles drag forces are small compared to the gravity force. As particle size is reduced, freeboard residence time increases because of an increase in drag force as compared to particle weight (a reduction in the net force acting on the particle). For some particle size (when the particle terminal velocity U_t equals superficial gas velocity U_o) the drag force will exactly balance particle weight, the net force acting on the particle will be zero and the freeboard residence time from the force balance consideration alone will be, theoretically, infinite. Smaller particles, which are capable of being elutriated from the bed, will have progessively shorter residence times. Very small particles will move with the gas with a residence time equal to H_f/U_o. One problem to deal with in the freeboard model development is the singularity in residence time when U_T equals U_o.

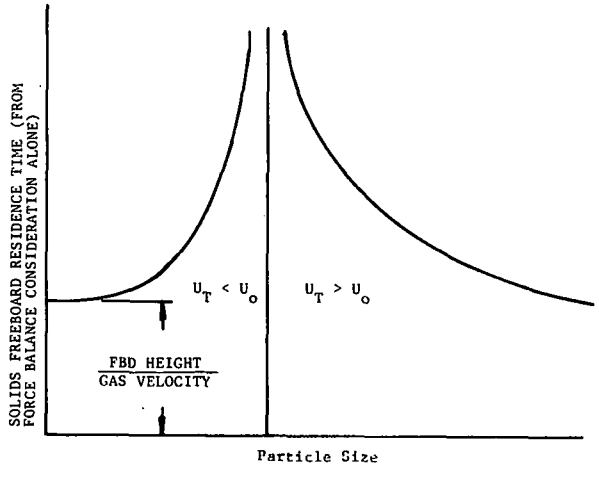

FIGURE 1. EFFECT OF PARTICLE SIZE ON FREEBOARD RESIDENCE TIME.

In the present model, char particles are divided into those that reside in a region where U_T and U_o are close to each other in magnitude (for convenience, it shall be called "critical region") and those that reside outside it. These two sets of particles are treated separately. The "critical region" is defined, by $|(U_t(i) - Ug)/Ug| < 0.15$, i.e., it includes particles whose terminal velocity is within 15 percent of the superficial gas velocity.

For particles that reside outside of the critical region, the solid density in the freeboard is assumed to experience an exponential decay. Lewis et al. [2] suggested that the following relationship holds under conditions of total reflux for solids mass density at height z in the freeboard.

$$\bar{\rho}_R = \bar{\rho}_{Ro}\, e^{-az} \qquad (1)$$

For an open freeboard, the solids mass density may be written as

$$\bar{\rho} = \bar{\rho}_{Ro}\, e^{-az} - \bar{\rho}_k \qquad (2)$$

Where $\bar{\rho}_k$ is a constant and $\bar{\rho}_{Ro}$, the density at bed top under the total reflux, can be expressed as

$$\bar{\rho}_{Ro} = \frac{E_o}{v_o} + \frac{E_o}{v_b} \qquad (3)$$

taking the sum of the contributions due to upward and downward fluxes (see Figure 2), each flux being equal to E_o under conditions of total reflux.

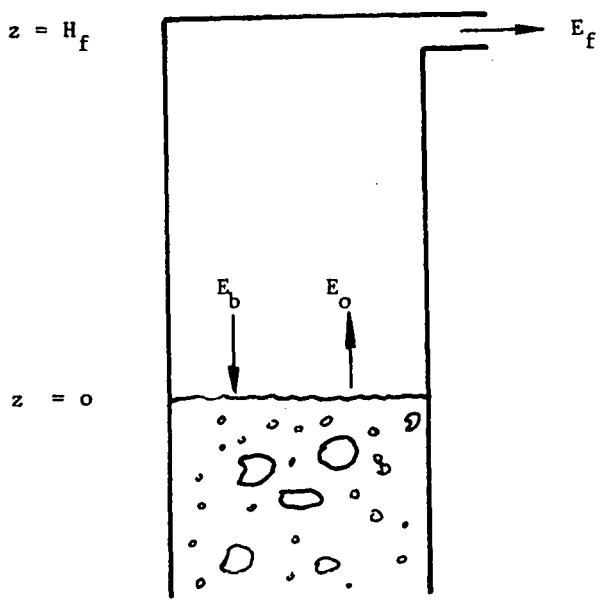

FIGURE 2. FREEBOARD SOLID FLUX.

The velocity v_o of particles entering the freeboard can be taken as equal to bubble velocity u_b while the velocity v_b of particles settling into the bed can be expressed as $(\bar{U}_t - U_o)$, where $\bar{U}_t$ is the particle terminal velocity. Further, note that for small particles (for which $\bar{U}_t < U_o$), the downward flux term is absent

Similarly, the average density at bed top for an open freeboard may be expressed as

$$\bar{\rho}_o = \frac{E_o}{v_b} + \frac{E_o - E_f}{v_b} \qquad (4)$$

where E_f represents elutriation loss per unit area and is evaluated using Merrick and Highley [3] correlation. To apply Equations (3) and (4), the density contribution for each particle size is integrated over all sizes.

The constant $\bar{\rho}_k$ in Equation (2) is obtained by applying it at the bed surface (z = 0); so that

$$\bar{\rho}_k = \bar{\rho}_{Ro} - \bar{\rho}_o \qquad (5)$$

The constant "a" being independent of the total freeboard height [4] can be more easily evaluated by assuming a freeboard with height equal to TDH (Transport Disengaging Height) where

$$a = -\frac{1}{TDH} \ln \frac{(\bar{\rho}_k)_{TDH} + \bar{\rho}_{f_{TDH}}}{\bar{\rho}_{Ro}} \qquad (6)$$

The initial flux E_o for the sorbent is obtained following George and Grace [5]. E_o for char is obtained from that for the sorbent in proportion to the weight ratio W_{coal}/W_{inert}.

For those particles that reside in the "critical region" where $\bar{U}_t \approx U_o$, the net force acting on the particle is nearly zero and such particles will tend to stay in the freeboard indefinitely. However, combustion is a competing process, which slowly reduces the particle size. Once the particle size is reduced, the resulting drag force will move the particle outside the combustor. Thus, these particles can be considered to be controlled by combustion kinetics.

A simplified population balance may be made for the particles in the critical region. It may be assumed that the rate at which these particles splash into the freeboard is the same at which they burn in the freeboard. Using the nomenclature in Kunii and Levenspiel's population balance equations, one can write

$$A_t E_o P_b(\bar{r})\,\Delta r = 3\,\frac{(\Delta W)}{\bar{r}}\,\frac{dr}{dt}\,\Big|\,\bar{r} \qquad (7)$$

where $\bar{r}$ is the radius and $\frac{dr}{dt}$ is the shrinkage rate (due to combustion) of these particles. $P_b(\bar{r})\Delta r$ represents the fraction of particles in the bed residing in the 'critical region' and ΔW is their total mass in the freeboard. The quantity ΔW can be obtained from above equation, and the mass concentration of the particles in the 'critical region' can then be obtained as

$$\bar{\rho}_c = \frac{\Delta W}{A_t H_f} \qquad (8)$$

assuming that the singularity particles are distributed uniformly throughout the freeboard. Here, H_f is freeboard height.

The total char particle mass concentration at any freeboard height is given by summing the contributions from (2) and (7). The carbon concentration profile is then integrated into the material balance of gas phase using available kinetic information to provide predictions for oxygen concentration profile in the freeboard. For estimating char combustion rate, the relatively simple expression given by Field et al. [6] is used.

In evaluating these kinetic equations, the freeboard is divided into five compartments, and each compartment is treated as a back-mix reactor. The temperature in the freeboard is assumed to be constant.

II. Results and Discussions

Oxygen Concentration and Heat Release in the Freeboard

Oxygen concentration in the freeboard is important because the extent of the freeboard combustion is determined both by carbon loading and oxygen concentration in the freeboard.

Oxygen concentration entering the freeboard is determined by means of a mass balance over the bed. A mean oxygen concentration for each of the five compartments in the freeboard is determined by making a new mass balance over the particular compartment taking into account the combustion reactions that occur. Oxygen concentration in the freeboard is thus expected to decrease with freeboard height. This decrease will be pronounced if freeboard carbon population is high. On the other hand, if freeboard carbon population is negligible, oxygen concentration in the freeboard will be nearly constant.

Figure 3 shows oxygen partial pressure variation with freeboard height for a case where about 28 percent of carbon burns in the freeboard. It is seen that the oxygen partial pressure drops from about 0.065 atm at freeboard inlet to about half this value at freeboard exit.

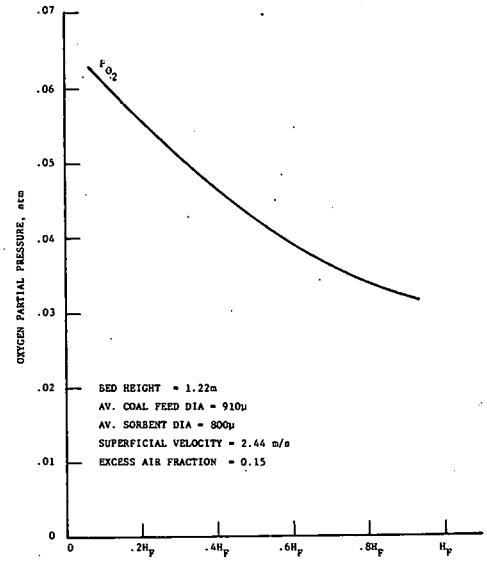

FIGURE 3. VARIATION OF OXYGEN CONCENTRATION IN THE FREEBOARD.

Heat released in the freeboard is generally proportional to amount of carbon burned in the freeboard. Some deviation from this proportionality may occur due to CO combustion and carbon-steam reaction. Thus, heat release in the freeboard depends not only on char particle concentration but also on the other factors that will influence the oxygen, CO and steam concentrations entering the freeboard.

As stated earlier, the freeboard char concentration is modeled to be made up of two types of particles: (a) the particles that follow Lewis equation which predicts exponential decay of particle concentrations along freeboard height, and (b) the particles which reside in the "critical region" and which are assumed to be uniformly distributed in the freeboard. Thus, the net particle concentration will still decay with freeboard height and so will the heat release. However, this decay will not be as sharp as one would obtain in the absence of uniformly distributed particles with long residence time.

Figure 4 shows the decrease in heat release along the freeboard height for a typical set of operating conditions. As expected, maximum heat is released near the bed surface and least near the freeboard exit.

Variation of Coal Feed Size

Parametric studies are carried out by systematic variation of coal feed size and average bed sorbent size. Both of these parameters are seen to have a significant effect on the freeboard and bed performance.

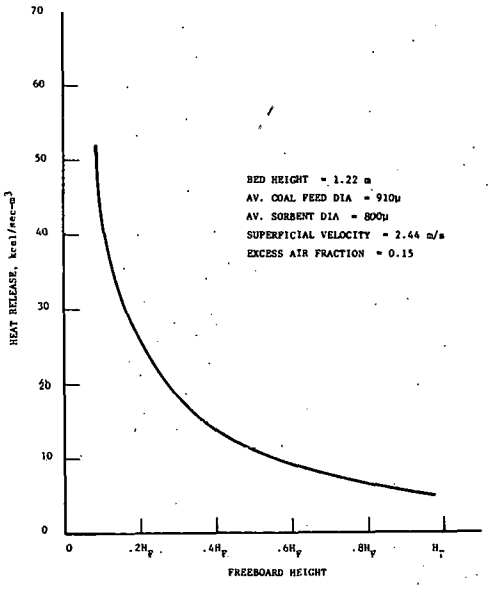

FIGURE 4. HEAT RELEASE IN THE FREEBOARD.

Figure 5 shows the ratio of freeboard to bed carbon loading as a function of average coal feed size.

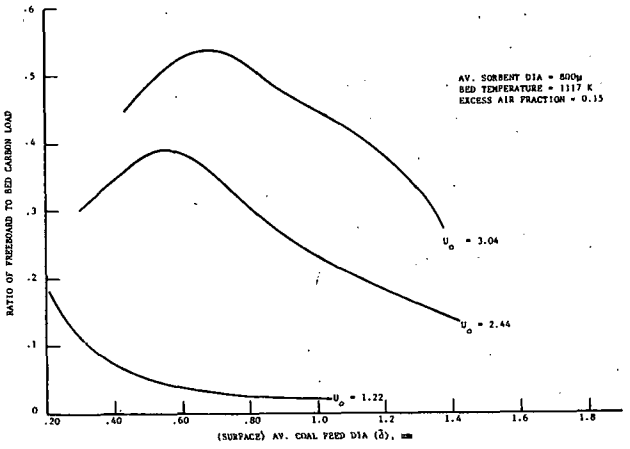

FIGURE 5. RATIO OF FREEBOARD TO BED CARBON LOAD VS AV. COAL FEED DIAMETER.

The curves typically display a maximum, which again results due to a large population of carbon particles in the bed which are close to the 'critical' size and which will tend to stay in the freeboard until burned to a small size.

Figure 6 shows the variation of the fraction of carbon that burns in freeboad, X_{CFB}, with average coal feed diameter, $\bar{d}$, for three different values of the fluidizing velocity.

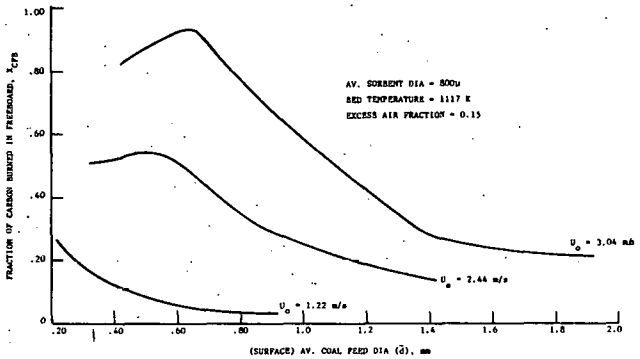

FIGURE 6. FRACTION OF CARBON BURNT IN FREEBOARD VS (SURFACE) AV. COAL FEED DIAMETER.

As the coal feed size is gradually increased, the curves typically show a maximum. The larger fluidizing velocity corresponds, as expected, to a large fraction of carbon burning in the freeboard. The maximum in these curves occurs near where terminal velocity $\bar{U}_t$ (corresponding to average coal size in bed) equals the fluidizing veloeity, U_o, i.e., near the 'critical' size. This is also expected.

It is interesting to calculate the critical size of char particles for which $\bar{U}_t = U_o$ for gas velocities of 1.22, 2.44, and 3.04 m/sec. These sizes are estimated to be about 210, 420, and 530 microns, respectively, for the three values of superficial velocity and may be compared with the maxima in Figures 5 and 6. While a close correspondence exists between these critical sizes and the respective maxima in Figures 5 and 6, the calculated critical sizes are a little smaller than the maxima in either figure. This is because the plots in Figure 5 and 6 are based upon coal feed size while the calculated values refer to average bed size which is a little smaller than the feed size.

Variation of Bed Sorbent Size

Bed sorbent size is an important factor in influencing the freeboard performance.

Figure 7 shows the variation in the respective carbon loads in the bed and in the freeboard with bed sorbent size.

The bed carbon load (shown by dashed lines) shows a maximum. This maximum probably arises due to two competing effects. As the sorbent size increases, there is a decrease in the wake fraction as well as the bubble velocity and less carbon is going to the freeboard. This will tend to increase the carbon load in the bed as is initially shown in the figure. However,

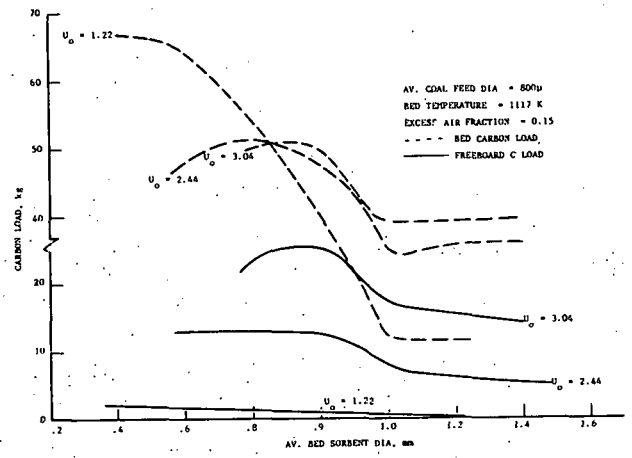

FIGURE 7. VARIATION OF BED AND FREEBOARD CARBON LOADS WITH BED SORBENT SIZE.

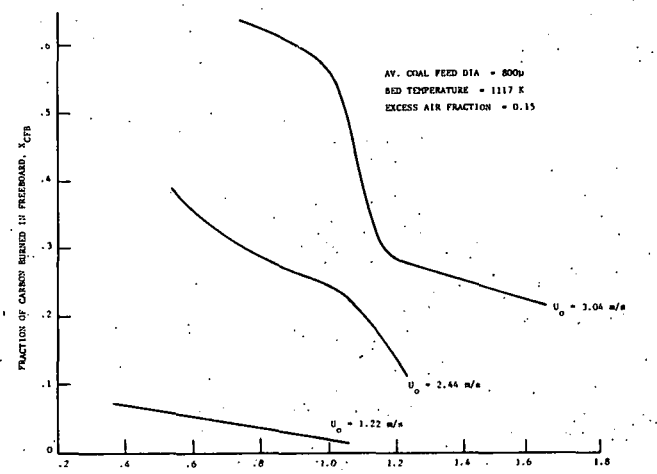

FIGURE 8. FRACTION OF CARBON BURNED IN FREEBOARD VS (SURFACE) AV. SORBENT DIAMETER.

there is the competing effect of increased oxygen flow through the emulsion phase which will cut down the bed carbon load. When this effect becomes dominating the carbon load in the bed will decrease as is shown in the later part of the curves in the figure. When the sorbent size increases to a certain magnitude, the bed may be entirely operating in a slow bubble regime. From then on, the oxygen concentration in the emulsion phase does not vary much and the carbon load in the bed will tend to level off as is shown in the figure.

The freeboard carbon load (shown in Figure by solid lines) depicts a less pronounced maximum. This is due to the fact that freeboard carbon load depends on fluidizing velocity and oxygen concentration in the freeboard in addition to bed carbon load.

The bed sorbent size can influence the freeboard combustion in at least two ways. First, an increase in sorbent size results in more oxygen flow through the emulsion phase, cutting down oxygen by passing. This results in lower oxygen concentration which, in turn, will lower freeboard combustion. Secondly, an increase in sorbent size will decrease the wake fraction as well as the bubble velocity and therefore, will decrease the initial particle flux entering the freeboard (E_o) due to bursting of bubbles. This again results in lower particle densities in the freeboard and thus lower freeboard combustion. Thus as bed sorbent size is gradually increased, both of these effects tend to cut down the freeboard combustion. This is reflected by Figure 8 which shows the variation in fraction of carbon burned in the freeboard with average bed sorbent size and superficial velocity.

For a fixed fluidizing velocity, fraction of carbon burned in the freeboard decreases significantly as sorbent size is increased. But this fraction increases when for a fixed sorbent size, fluidized velocity is increased. These trends are as expected. At 3.04 m/sec gas velocity, the decrease in fraction of carbon burned in the freeboard is less severe when the particle exceeds approximately 1.15 mm in size. This reflects that above that particle size, the bed is most probably operating in a slow bubble regime. This figure further suggests that at high gas velocity and relatively low sorbent particle size, the freeboard combustion can be very significant; but at low gas velocity and relatively high sorbent size, the freeboard contribution to combustion can be neglected.

Measurements of freeboard combustion efficiency and carbon loads are scarce. Under a certain set of conditions Babcox and Wilcox has reported a value of 9% (Series 2 Run 2A), the model computation under the same set of conditions yields a value of 13.7%.

Conclusions

The model described here represents a first approximation to an analytical model. It has been shown that the predicted results from the model appear to be quite consistent with the trends actually observed in pilot plants and demonstration units. Since many simplifying assumptions have been introduced, some measure of error in the magnitude of predicted output parameters (e.g., freeboard carbon load and combustion efficiency) must be allowed. An improved model based upon the same approach but with the elimination of some oversimplifications is now being developed and shall be reported in the near future.

Nomenclature

a	Constant in Lewis Equation
A_t	Bed cross-sectional area
E_o	Particle flux entering the freeboard by entrainment
E_b	Particle back-flux entering the bed
E_f	Particle flux leaving the combustor from the top
H_f	Total freeboard height
TDH	Transport disengaging height
U_o	Superficial gas velocity
U_T	Particle terminal velocity
v_o	Velocity of particles entering the freeboard
v_b	Velocity of particles falling back to the bed
W	Total mass
ΔW	Total mass of particles in the freeboard that reside in the "critical-size region"
z	Height above the bed surface
ρ	Particle mass concentration
$\bar{\rho}$	Average particle mass concentration
$\bar{\rho}_k$	Constant in the Lewis equation
$\bar{\rho}_{Ro}$	Average particle mass concentration at bed surface under conditions of total reflux

References

1. Modrak, T.M., T.A. Morris, and W.C. Lapple, EPRI/B&W Fluidized Bed Combustion Development Facility: Initial Test Results, Presented at the 86th National AIChE Meeting, Houston, Texas, April 1-5, 1979.

2. Lewis, W.K., E.R. Gilliland, and P.M. Lang, Chemical Engineering Symposium Series, No. 38, Vol. 58, pp 65-78 (1962).

3. Merrick, D., and J. Highley, AIChE Symposium Series, No. 137, Vol. 70, p. 336, (1974).

4. Kunii, D., and O. Levenspiel, "Fluidization Engineering", J.M. Wiley, (1969).

5. George, S.E., and J.R. Grace, AIChE Symposium Series, No. 176, Vol. 74, pp. 67-74, (1978).

6. Field, M.A., D.W. Gill, B.B. Morgan, and P.B.W. Hawskeley, "Combustion of Pulverized Coal", BCURA, Leatherhead, England, (1967).

ACKNOWLEDEMENT

The work reported here is being performed under contract with the U.S. Department of Energy. The DOE (Morgantown Energy Technology Center) Project Officer for Contract E (49-18)-2295 is Dr. J.Y. Shang whose constant support is gratefully acknowledged. One of the co-authors, Mr. T.Z. Chaung, is a thesis student of Professors J.M. Beer and A.F. Sarofim. Their permission to use materials developed under that thesis is deeply appreciated.

Question to S. E. Tung:

Q: V. N. Vedamurthy, Session Co-Chairman

My first question is on particle residence time. If you have small particles going up and immediately leaving the reactor you can calculate residence time. The large particles go up and fall back. This activity has to be taken into consideration. The second question is concerned with gas mixing. In the freeboard there must be some mixing or dispersion rather than the simple plus flow. Was that considered?

A: In this model, we tried to get out of these complicaitons by assuming, after Lewis, that the solids concentration decay was an exponential form and calculated solids loading in this way. The mixing, again, is not considered. This is a "first cut" model. We would like to develop a mechanics model which would take all of these difficulties into consideration.

A MATHEMATICAL MODEL FOR CHAR COMBUSTION IN A FLUIDIZED BED

S. C. Saxena* and A. Rehmat†

Argonne National Laboratory
Argonne, Illinois 60439

Introduction

The proper understanding of the physics and chemistry of the combustion of a char particle in a fluidized bed of inert particles is an essential step to modeling the burning of coal in a fluidized bed of ash and dolomite. One such theory has been recently developed in which the two-phase theory of a bubbling fluidized bed as given by Davidson and Harrison[1] is applied by Avedesian and Davidson[2] to the batch combustion of char and coke particles in a hot bed of ash fluidized by air. The burning rate is assumed to be primarily controlled by the transport of oxidant through the gas within the ash particles of the emulsion phase. This process is characterized by the value of the effective diffusion coefficient or dispersion coefficient, D_e. The value of D_e is less than the value of D_A, the molecular gas diffusion coefficient for the oxidant, A. A Sherwood number = $2D_e/D_A$ is defined, and its value will be two for an isolated particle burning in a stagnant atmosphere. For a carbon particle burning in a fluidized bed of ash, the Sherwood number will be less than two; amongst other factors, its actual value will depend upon voidage and tortuosity of the voids between the ash particles. Avedesian and Davidson have assumed that the value of the Sherwood number stays constant for the entire period when the char particles burn and that the particles continually become smaller.

In their calculation of burn-out time of char particles, Avedesian and Davidson[2] assumed the rate-limiting process to be diffusion resistance but neglected the resistance introduced by the formation of ash film on char particles as a result of combustion. Ash film thickness depends upon the extent of char combustion, among other factors. In a recent study, Andrei, Sarofim, and Beer[3] examined the burning at temperatures of 1023 and 1173 K of small batches of Montana lignite coal particles of 1.6 to 3.0-mm diameter in a bubbling fluidized bed of sand particles having a mean diameter of 200 μm. They concluded that the coal particles burn in a shrinking core mode and that the shrinking carbon core was surrounded by a growing layer of ash which had not abraded despite the vigorous stirring of the fluidized sand. Here, we develop a general theory of char combustion in a fluidized bed to include the mass transfer resistance through the ash layer on the surface of the char particle.

Avedesian and Davidson[2] assumed that char combustion takes place according to the two-film model[4] and that the concentrations of carbon dioxide and oxygen at the particle surface are zero. The carbon monoxide produced at the particle surface burns in a diffusion flame on the surface of a reaction sphere of radius d_p, where d_p is the diameter of the particle. The experimental work of Arthur[5], on the other hand, suggested that both carbon monoxide and carbon dioxide are produced at the surface and that the ratio of their relative rates of production in the temperature range, 753 to 1173 K, is given by

$$k_r = 2512 \exp(-51549/R_g T_o). \quad (1)$$

Here k_r is the ratio of the formation rates of carbon monoxide to carbon dioxide, R_g is the universal gas constant and is equal to 8.3 kJ/kmol-K, and T_o is the bed temperature in degrees, Kelvin. Basu et al.,[6] more recently, confirmed this conclusion. Their experimental work demonstrated that the primary combustion products are both carbon monoxide and carbon dioxide, and the oxygen did diffuse through the ash film to the carbon surface. In the temperature range, 823-923 K, k_r was large in the product gas from the fluidized bed, but the value of k_r decreased with increasing temperature above a certain critical temperature near 923-973 K. These investigations thus suggest that under certain conditions, the mode of combustion of a char particle could differ from that given by the two-film model. The model descriptions of Arthur[5] and Basu et al.,[6] are accordingly referred to as the direct oxidation model. However, we will assume that the char combustion system is adequately described by the following net reaction in a fluidized bed where coal burns in the excess of oxygen and that the concentration of carbon monoxide in the flue gas is negligibly small:

$$C + O_2 \xrightarrow{k_1} CO_2. \quad (2)$$

Here, k_1 is the reaction rate constant and its value depends on the particle temperature.

The oxygen concentration in the bubble phase is C_{AB} and that in the particulate or emulsion phase of

*Permanent Address: Department of Energy Engineering, University of Illinois at Chicago Circle, Box 4348, Chicago, Illinois 60680

†Permanent Address: Institute of Gas Technology, Chicago, Illinois 60616

the fluidized bed is C_{AP}. The particulate phase is assumed to be in the backmix condition, and hence C_{AP} is uniform throughout the bed. The gas distribution in the bubbles is described by the plug flow model, and hence a concentration gradient exists in this phase along the height of the reactor. It is then possible to develop the overall formulation of the char burn-out time, t_c, which is given in the next section and contains the following three parameters:

a. The local Sherwood number for a burning char particle which is surrounded by inert (ash and/or dolomite) particles,

b. The diffusion coefficient of oxygen, D'_{eA}, through the ash layer on the combusting particle, and

c. The number of times, X, that a bubble is swept out during its passage through the bed by the throughflow and diffusion of gases.

Theoretical Formulation

In the development of the mathematical framework to describe the combustion of a batch of char particles in a fluidized bed, the following explicit simplifying assumptions have been made.

a. The char particles are spherical, and all are initially of the same diameter, $2R_o$.

b. The combustion of a char particle leaves behind a layer of ash on its surface. The oxygen must diffuse through this ash layer in order to reach the core of the particle where reaction subsequently takes place. The thickness of the ash layer is characterized by a factor, Z, which is defined as the ratio of the volume of ash formed to the volume of char consumed by combustion reaction.

c. The gas-solid reaction of Eq. (2) takes place following the shrinking core model, which is represented in Fig. 1, and is discussed in detail by Rehmat and Saxena.[7] The rate of reaction is of the first order and is given by the following relation:

$$-r_A = k_1(T_C)C_{JO}C_{AC}. \qquad (3)$$

Here r_A is the rate of solids consumption in the reaction given by Eq. (2), $k_1(T_C)$ is the value of the reaction rate constant at T_C, the temperature of the unreacted solid core; C_{JO} is the initial concentration of oxygen at the unreacted core surface of the solid.

d. The magnitude of the diffusion coefficient of gases through the ash layer on the particle surface, D'_{eA} (T), is directly proportional to the temperature, T, i.e.,

$$D'_{eA}(T) \propto T. \qquad (4)$$

e. The formulation presented here is quite general inasmuch as all four resistances have been taken into account. These are: (1) the diffusion resistance through the inert particles surrounding a char particle, (2) the diffusion resistance through the gas film layer around the char particle, (3) the diffusion resistance through the ash layer on the unburnt core of the char particle, and (4) the finite rate constant for the heterogeneous gas-solid reaction.

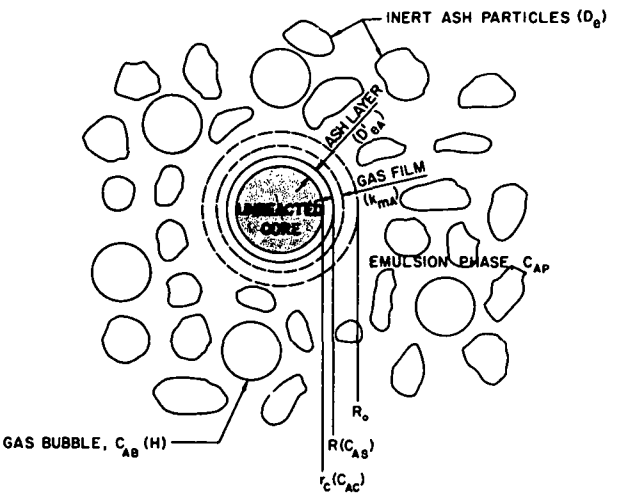

Fig. 1. Combustion of a Char Particle in a Fluidized Bed of Inert Ash Particles.

f. The forced and natural convection effects are small. This is a valid approximation as long as the particle Reynolds and Grashof numbers are less than unity. Mass transfer occurs primarily by molecular diffusion, and if it is assumed that concentration profiles are quickly established as particle size alters, we have

$$\frac{d}{dr}\left[r^2 \frac{d(D'_{eA}C_A)}{dr}\right] = 0. \qquad (5)$$

Here, D'_{eA} refers to the intraparticle diffusion coefficient through the ash layer, C_A is the molar concentration of A, and r is the radial distance from the center of the particle. The above equation is nondimensionalized by substituting

$$\xi = r/R_o, \qquad (6)$$

$$\omega_A = X_A/X_{AO}, \text{ and} \qquad (7)$$

$$U = T/T_o \qquad (8)$$

R_o is the initial particle radius, X_A is the mole fraction of component A (oxygen), X_{AO} is the value of X_A in the feed gas, air, and T_o is the temperature of the bulk gas phase. The nondimensionalized form of Eq. (5) is

$$\frac{d}{d\xi}\left(\xi^2 \frac{d\omega_A}{d\xi}\right) = 0. \qquad (9)$$

The boundary conditions are

at $\xi = \xi_s = R/R_o$,

$$\frac{d\omega_A}{d\xi} = N_{Sho}\left(\omega_{AP} - \omega_{AS}\right), \tag{10}$$

and at $\xi = \xi_c = r_c/R_o$,

$$\frac{d\omega_A}{d\xi} = \frac{\phi_1}{U_c}\ \omega_{AC} \exp\left[\frac{E_1}{R_g T_o}\left(1 - \frac{1}{U_c}\right)\right]. \tag{11}$$

Here,

$$N_{Sho} = k_{mA}R_o/D'_{eA}(T_o), \tag{12}$$

$$\phi_1 = k_1(T_o)C_{JO}R_o/D'_{eA}(T_o), \tag{13}$$

and

$$k_1(T) = k^\circ \exp\left(-E_1/R_g T\right). \tag{14}$$

Here $U_c = (T_c/T_o)$ is the reduced temperature of the unreacted core, R is the particle radius, r_c is the radius of the unreacted core whose temperature is T_c, k_{mA} is the mass transfer coefficient for the component A across the gas film; ϕ_1, defined by Eq. (13), is a parameter to characterize the ratio of the intraparticle diffusion resistance to the reaction resistance; k° is the frequency factor and is based on surface area; and E_1 is the activation energy. The quantities ω_{AP}, ω_{AS}, and ω_{AC} are the reduced concentrations of oxygen in the emulsion phase, at the particle surface and at the unreacted core of the particle, respectively.

After considerable manipulation and substitution, the solution of Eq. (9) with the boundary conditions of Eqs. (10) and (11) leads to the following relations for the oxygen concentrations at the particle surface and at the unreacted core of the particle in terms of the oxygen concentration in the emulsion phase of the fluidized bed, ω_{AP}, and other system parameters.

$$\omega_{AC} = \frac{\omega_{AP}}{D_1}, \tag{15}$$

where

$$D_1 = \left[1 + \frac{\phi_1\xi_c^2}{U\, N_{Sho}\xi_s^2} \exp\left\{\frac{E_1}{R_g T_o}\left(1 - \frac{1}{U_c}\right)\right\} + \frac{\phi_1\xi_c}{U_c}\left(1 - \frac{\xi_c}{\xi_s}\right) \exp\left\{\frac{E_1}{R_g T_o}\left(1 - \frac{1}{U_c}\right)\right\}\right],$$

and

$$\omega_{AS} = \frac{N_2}{D_2} \tag{16}$$

where

$$N_2 = \omega_{AP}\left[1 + \frac{\phi_1\xi_c}{U_c}\left(1 - \frac{\xi_c}{\xi_s}\right) \exp\left\{\frac{E_1}{R_g T_o}\left(1 - \frac{1}{U_c}\right)\right\}\right]$$

and

$$D_2 = \left[1 + \frac{\phi_1\xi_c^2}{U_c N_{Sho}\xi_s^2} \exp\left\{\frac{E_1}{R_g T_o}\left(1 - \frac{1}{U_c}\right)\right\} + \frac{\phi_1\xi_c}{U_c}\left(1 - \frac{\xi_c}{\xi_s}\right) \exp\left\{\frac{E_1}{R_g T_o}\left(1 - \frac{1}{U_c}\right)\right\}\right].$$

Further,

$$N_{Sho} = N_{Sh}(R_o/2R)\ (D_A/D'_{eA}), \tag{17}$$

and

$$N_{Sh} = (2R\ k_{mA}/D_A) = 2 + 0.6\ (N_{Re})^{1/2}\ (N_{Sc})^{1/3} \tag{18}$$

D_A is the molecular diffusivity of the component A in the gas phase and is the intermolecular diffusion coefficient. The correlation of Eq. (18) is developed by Ranz and Marshall.[8] Further, $N_{Re} = (2\rho V_{mf}R/\mu)$ and $N_{Sc} = (\mu/\rho D_A)$; ρ is the density of the fluidizing gas whose viscosity is μ, and the minimum fluidizing velocity is V_{mf}. Let n be the molar oxygen transfer rate to the particle. Then for the case where the gas film surrounding the particle is thin, we have

$$n = 4\pi R^2 D_e \left(\frac{dC_A}{dr}\right)\Bigg|_{r\,=\,R} = 4\pi R^2 k_{mA}\ (C_{AP} - C_{AS}). \tag{19}$$

The quantities C_{AP} and C_{AS} are the molar concentrations of A in the emulsion phase and at the particle surface, respectively. Rearrangement of Eq. (19) leads to the following explicit relation for k_{mA}:

$$k_{mA} = \frac{D_e\left(\frac{dC_A}{dr}\right)\Big|_{r\,=\,R}}{(C_{AP} - C_{AS})}. \tag{20}$$

Combining Eqs. (18) and (20), we get

$$D_e = \frac{N_{Sh}D_A(C_{AP} - C_{AS})}{2R\left(\frac{dC_A}{dr}\right)\Big|_{r\,=\,R}}. \tag{21}$$

Substituting this value of D_e in the first part of Eq. (19), we obtain

$$n = 2\pi R N_{SH} D_A (C_{AP} - C_{AS}) \tag{22}$$

This equation readily reduces to the combustion model of Avedesian and Davidson[2], in which the oxygen concentration at the particle surface is zero, i.e., $C_{AS} = 0$, and also the mass transfer at the gas boundary layer is assumed to take place at r = 2R instead of at r = R (as in the present case) so that

$$n = 4\pi R N_{Sh} D_A C_{AP}. \tag{22a}$$

Equation (22) will be employed here.

We now consider the combustion of char particles in a fluidized bed of inert particles at temperature, T_o. A charge of char of mass m is added to the bed fluidized by a gas of flow rate, V, and the containing oxygen of concentration, C_{AO}. In accordance with the two-phase theory of fluidization, the flow rate of gas through the bed is VA_o, with $(V - V_{mf})A_o$ the flow through the bed as bubbles which contain no solids and $V_{mf}A_o$ the flow through the emulsion phase. Here, V is the superficial gas velocity of the fluidizing gas at the mean bed temperature, A_o, is the mean cross-sectional area of the bed, and V_{mf} is the minimum fluidization velocity for the bed.

The solids in the emulsion phase are completely mixed, and consequently the oxygen concentration, C_{AP}, is a function of time but not of location. Gas is exchanged between the bubbles and the emulsion phase, and gas distribution in bubbles is described by plug flow. Consequently, the oxygen concentration in the bubbles, C_{AB}, varies with height above the distributor plate. However, the residence time of a bubble is much less than the char burn-out time, t_c, of a char particle, and therefore, the changes in C_{AB} and C_{AP} during the rise time of a bubble in the bed can be neglected since for this period, the bed is effectively in a steady state. The oxygen is being consumed by each char particle in accordance with Eq. (22).

$$\text{Rate of oxygen consumption per unit volume of the emulsion phase} = k\,C_{AP}, \tag{23}$$

$$\text{Number of char particles in the bed (N)} = \frac{m}{(4/3)\pi R_o^3 \rho_s} \tag{24}$$

Here k is the emulsion phase velocity constant and ρ_s is the density of solid particles.

$$\text{Total rate of oxygen consumption} = n\,N. \tag{25}$$

$$\text{Also, the rate of oxygen consumption in the bed} = k\,C_{AP}A_oH_o. \tag{26}$$

H_o is the height of the bed at incipient or minimum fluidization. Combining Eqs. (22), (24), and (25) we get,

$$n\,N = \frac{3mRN_{Sh}D_A(C_{AP} - C_{AS})}{2R_o^3\rho_s}. \tag{27}$$

Equations (26) and (27) lead to the following relation for the emulsion phase velocity constant,

$$k = \frac{3mRN_{Sh}D_A(C_{AP} - C_{AS})}{2R_o^3\rho_s C_{AP}A_oH_o}. \tag{28}$$

Nondimensionalization of Eq. (28) and substitution of ω_{AS} from Eq. (16) leads to the following relation:

$$k = \frac{3m\xi_s N_{Sh}D_A}{2R_o^2\rho_s A_oH_o}\,\frac{\phi_1\xi_s^2}{U_c N S_{ho}\xi_s^2}\,\frac{\exp\left\{\frac{E_1}{R_gT_o}\left(1 - \frac{1}{U_c}\right)\right\}}{D_3} \tag{29}$$

where

$$D_3 = \left[1 + \frac{\phi_1\xi_c^2}{U_cN_{Sho}\xi_s^2}\exp\left\{\frac{E_1}{R_gT_o}\left(1 - \frac{1}{U_c}\right)\right\} + \frac{\phi_1\xi_c}{U_c}\left(1 - \frac{\xi_c}{\xi_s}\right)\exp\left\{\frac{E_1}{R_gT_o}\left(1 - \frac{1}{U_c}\right)\right\}\right]$$

Substitution of defining relations for ϕ_1 and N_{Sho} leads to

$$k = \frac{3mk_1(T_o)C_{JO}\xi_c^2}{R_o^2\rho_s A_oH_oU_c}\,\frac{\exp\left\{\frac{E_1}{R_gT_o}\left(1 - \frac{1}{U_c}\right)\right\}}{D_4} \tag{30}$$

where

$$D_4 = \left[1 + \frac{\phi_1\xi_c^2}{U_cN_{Sho}\xi_s^2}\exp\left\{\frac{E_1}{R_gT_o}\left(1 - \frac{1}{U_c}\right)\right\} + \frac{\phi_1\xi_c}{U_c}\left(1 - \frac{\xi_c}{\xi_s}\right)\exp\left\{\frac{E_1}{R_gT_o}\left(1 - \frac{1}{U_c}\right)\right\}\right]$$

A dimensionless reaction velocity constant, k', is defined[2] as,

$$k' = \frac{kH_o}{V}. \tag{31}$$

The exit concentration, C_{AH}, of oxygen from the bed[1,2] is

$$\frac{C_{AH}}{C_{AO}} = \beta\exp(-X)\,\frac{[1 - \beta\exp(-X)]^2}{k' + 1 - \beta\exp(-X)} \tag{32}$$

where

$$\beta = 1 - (V_{mf}/V) \tag{33}$$

and

$$X = \frac{QH'}{U_BV_B},$$

$$= \frac{6.34H_o}{D_B(gD_B)^{1/2}}\left[V_{mf} + \frac{1.3\varepsilon_{mf}D_A^{1/2}g^{1/2}}{(1 + \varepsilon_{mf})D_B^{1/4}}\right]. \tag{34}$$

Here H' is the height of the fluidized bed, Q is the total gas exchange flow rate from each bubble, V_B is the bubble volume, U_B is the bubble velocity, D_B is the bubble diameter, g is the acceleration due to gravity, and ε_{mf} is the bed voidage at minimum fluidization. Therefore, X is the number of times the bubble volume is swept out during its time in the bed. Here it is also assumed that all bubbles are of the same size. The concentration of oxygen in each bubble as a function of height H above the gas distributor is given[1,2] by

$$C_{AB}(H) = C_{AP} + (C_{AO} - C_{AP})\exp(-QH/U_BV_B). \tag{35}$$

The combustion rate can then be obtained from an overall oxygen balance on the bed. The net rate of oxygen leaving the bed in the bubbles is represented by

$$(V - V_{mf})A_o C_{AB}(H') \tag{36}$$

$$= (V - V_{mf})A_o \left[C_{AP} + (C_{AO} - C_{AP}) \exp(-QH'/U_B V_B)\right].$$

Similarly, the net rate at which the oxygen leaves the bed from the emulsion phase is represented by

$$V_{mf} A_o C_{AP} . \tag{37}$$

The net rate of oxygen entering the bed is

$$V A_o C_{AO} . \tag{38}$$

The overall material balance of oxygen then yields:

$$V A_o C_{AO}$$

$$- (V - V_{mf})A_o \left[C_{AP} + (C_{AO} - C_{AP}) \exp(-QH'/U_B V_B)\right]$$

$$+ V_{mf} A_o C_{AP} + \begin{matrix}\text{rate of oxygen consumption} \\ \text{by the combustion reaction.}\end{matrix} \tag{39}$$

Therefore, the rate of oxygen consumption by the combustion reactions is equal to

$$V A_o C_{AO}$$

$$- (V - V_{mf})A_o \left[C_{AP} + (C_{AO} - C_{AP}) \exp(-QH'/U_B V_B)\right]$$

$$- V_{mf} A_o C_{AP} . \tag{40}$$

The derivation of Eq. (40) is based on the assumption that the heterogeneous gas-solid reactions take place uniformly throughout the bed.

The oxygen consumption is also related to carbon consumption in the bed, as indicated by Eq. (2). The number of moles of carbon in a single char particle of size R is N_s where

$$N_s = (4/3)\pi r_c^3 (\rho_c/12), \tag{41}$$

or

$$\frac{dN_s}{dt} = \frac{\pi r_c^2 \rho_c}{3} \frac{dr_c}{dt} , \tag{42}$$

where ρ_c is the carbon density of char. Also, from Eq. (3),

$$- \frac{dN_s}{dt} = 4\pi r_c^2 k_1(T_c) C_{JO} C_{AC} . \tag{43}$$

Combining Eqs. (42) and (43) gives:

$$- \frac{d\xi_c}{dt} = \frac{1}{\tau_1} \frac{\omega_{AC}}{U_C} \exp\left[\frac{E_1}{R_g T_o}\left(1 - \frac{1}{U_c}\right)\right] , \tag{44}$$

where

$$\tau_1 = \frac{\rho_c R_o}{12\, k_1(T_o) C_{JO} C_{AO}} \tag{45}$$

The rate of carbon consumption is equal to the rate of oxygen consumption, and both are equal to

$$N(\pi/3) r_c^2 \rho_c \frac{dr_c}{dt} \tag{46}$$

Combination of Eqs. (46) and (40) gives

$$- N(\pi/3) r_c^2 \rho_c \frac{dr_c}{dt}$$

$$= C_{AO}(1 - \omega_{AP})A_o [V - (V - V_{mf}) \exp(-X)]. \tag{47}$$

Substituting for N from Eq. (24) into (47), one gets after some manipulations,

$$- \frac{m\rho_c}{4\rho_s} \xi_c^2 \frac{d\xi_c}{dt}$$

$$= C_{AO}(1 - \omega_{AP})A_o [V - (V - V_{mf}) \exp(-X)]. \tag{48}$$

Substitution of ω_{AC} from Eq. (15) into Eq. (44) yields the following relation for ω_{AP}:

$$\omega_{AP} = - \frac{\tau_1 U_c (d\xi_c/dt)}{\exp\left[\frac{E_1}{R_g T_o}\left(1 - \frac{1}{U_c}\right)\right]}$$

$$\cdot \left[1 + \frac{\phi_1 \xi_c^2}{U_c N_{Sho} \xi_s^2} \exp\left\{\frac{E_1}{R_g T_o}\left(1 - \frac{1}{U_c}\right)\right\}\right.$$

$$\left. + \frac{\phi_1 \xi_c^2}{U_c}\left(1 - \frac{\xi_c}{\xi_s}\right) \exp\left\{\frac{E_1}{R_g T_o}\left(1 - \frac{1}{U_c}\right)\right\}\right] \tag{49}$$

Elimination of ω_{AP} from Eqs. (48) and (49) leads to the differential equation giving the rate of reaction of the char particle, viz.,

$$- \frac{d\xi_c}{dt} = \frac{1}{D_5} \tag{50}$$

where

$$D_5 = \tau_1 U_c \left[\exp - \left\{\frac{E_1}{R_g T_o}\left(1 - \frac{1}{U_c}\right)\right\}\right.$$

$$\left. + \frac{\phi_1 \xi_c^2}{U_c N_{Sho} \xi_s^2} + \frac{\phi_1 \xi_c}{U_c}\left(1 - \frac{\xi_c}{\xi_s}\right)\right]$$

$$+ \frac{m\rho_c \xi_c^2}{4\rho_s C_{AO} A_O [V - (V - V_{mf}) \exp(-X)]} .$$

The integration of Eq. (50) will lead to the required relationship between ξ_c and t, viz.,

$$\int_0^t dt = \int_{\xi_c}^{1} \frac{\tau_1 U_c}{\exp\left\{\frac{E_1}{R_g T_o}\left(1 - \frac{1}{U_c}\right)\right\}} d\xi_c + \int_{\xi_c}^{1} \frac{\tau_1\phi_1}{N_{Sho}} \frac{\xi_c^2}{\xi_s^2} d\xi_c + \int_{\xi_c}^{1} \tau_1\phi_1\xi_c\left(1 - \frac{\xi_c}{\xi_s}\right) d\xi_c + \int_{\xi_c}^{1} \frac{m\rho_c\xi_c^2}{4\rho_s C_{AO} A_O [V - (V - V_{mf}) \exp(-X)]} d\xi_c \quad (51)$$

If it is assumed that a thermal-pseudo-steady state condition exists so that U_c is constant, the above equation can be integrated analytically to yield the following relation.

$$t = \frac{\tau_1 U_c (1 - \xi_c)}{\exp\left\{\frac{E_1}{R_g T_o}\left(1 - \frac{1}{U_c}\right)\right\}} + \frac{\tau_1\phi_1}{N_{Sho}}\left[\frac{1 - \left\{Z + (1 - Z)\xi_c^3\right\}^{1/3}}{(1 - Z)}\right] + \frac{\tau_1\phi_1}{2}(1 - \xi_c^2) - \frac{\tau_1\phi_1}{2}\left[\frac{1 - \left\{Z + (1 - Z)\xi_c^3\right\}^{2/3}}{(1 - Z)}\right] + \frac{m\rho_c (1 - \xi_c^3)}{12\rho_s C_{AO} A_o [V - (V - V_{mf}) \exp(-X)]} . \quad (52)$$

In the above relation, the definition of Z is employed, which leads to the following equation relating ξ_s to ξ_c and which is given by Rehmat and Saxena[7]:

$$\xi_s^3 = Z + (1 - Z)\xi_c^3 . \quad (53)$$

For complete combustion or burn-out of the particle, $\xi_c = 0$ and the burn-out or combustion time, t_c, will be given by

$$t_c = \frac{\tau_1 U_c}{\exp\left\{\frac{E_1}{R_g T_o}\left(1 - \frac{1}{U_c}\right)\right\}} + \frac{\tau_1\phi_1 (1 - Z^{1/3})}{N_{Sho} (1 - Z)} + \frac{\tau_1\phi_1}{2} - \frac{\tau_1\phi_1(1 - Z^{2/3})}{2 (1 - Z)} + \frac{m\rho_c}{12\rho_s C_{AO} A_o [V - (V - V_{mf}) \exp(-X)]} \quad (54)$$

Substituting in Eq. (54) for τ_1, ϕ and N_{Sho} from Eqs. (45), (13), and (17), respectively, we get

$$t_c = \frac{\rho_c U_c R_o}{12k_1(T_o) C_{JO} C_{AO} \exp\left\{\frac{E_1}{R_g T_o}\left(1 - \frac{1}{U_c}\right)\right\}} + \frac{\rho_c R_o (1 - Z^{1/3})}{12 C_{AO} k_{mA} (1 - Z)} + \frac{\rho_c R_o}{24 C_{AO} D'_{eA}(T_o)}\left\{1 - \frac{(1 - Z^{2/3})}{(1 - Z)}\right\} + \frac{m\rho_c}{12\rho_s C_{AO}[V - (V - V_{mf}) \exp(-X)]} \quad (55)$$

The quantity $(m\rho_c/\rho_s)$ represents the mass of carbon in the charge and is denoted by m_c. If the gas-solid reaction is fast, $k_1(T_o)$ is very large and Eq. (55) simplifies to

$$t_c = \frac{\rho_c R_o (1 - Z^{1/3})}{12 C_{AO} k_{mA} (1 - Z)} + \frac{\rho_c R_o^2}{24 C_{AO} D'_{eA}(T_o)}\left\{1 - \frac{(1 - Z^{2/3})}{(1 - Z)}\right\} + \frac{m\rho_c}{12\rho_s C_{AO}[V - (V - V_{mf}) \exp(-X)]} . \quad (56)$$

With suitable changes, the above relation of Eq. (55) will give Avedesian and Davidson's model[2] as a particular case. First, the ash film resistance on the particle in Avedesian and Davidson's model is zero because the burning particle leaves no ash behind and therefore, the third term disappears. Secondly, in their model also, the gas-solid reaction is fast and therefore, the reaction rate constant $k_1(T)$ of Eq. (2) is very large. This causes the first term of Eq. (55) to disappear. Thirdly, the diameter of the reaction sphere in Avedesian and Davidson's model is twice that of the present model. With these modifications, Eq. (55) reduces to the following expression derived earlier in reference 2

$$t_c = \frac{\rho_c R_o}{48 C_{AO} k_{mA}} + \frac{m\rho_c}{12\rho_s C_{AO} A_o [V - (V - V_{mf}) \exp(-X)]} . \quad (57)$$

In the calculation of t_c from Eq. (54), the reduced temperature, U_c, of the unreacted core of the combusting particle must be known, and this can be computed from the solution of the heat balance equation with appropriate boundary conditions. The energy balance equation for a single particle suspended in a fluidized bed of constant temperature, T_o, under pseudo-steady state condition is,

$$\frac{d}{d\xi}\left(\xi^2 \frac{dU}{d\xi}\right) = 0, \quad (58)$$

The boundary conditions are as follows:

at $\xi = \xi_s$

$$-\frac{dU}{d\xi} = N_{Nuo}(U_s - 1), \tag{59}$$

and at $\xi = \xi_c$

$$-\left(\frac{R_g T_o}{E_1}\right)\left(\frac{dU}{d\xi}\right) = \frac{\phi_1 \beta_1 \omega_{AC}}{U_c} \exp\left\{\frac{E_1}{R_g T_o}\left(1 - \frac{1}{U_c}\right)\right\} \tag{60}$$

Here

$$N_{Nuo} = N_{Nu}\,(R_o/2R)\,(k_f/k_e), \tag{61}$$

$$N_{Nu} = h\,(2R/k_f), \tag{62}$$

$$\beta_1 = C_{AO} D'_{eA}(T_o)\,(-\Delta H_1) R_g / k_e E_1 \tag{63}$$

Here U_s and T_s are the reduced and absolute temperatures respectively of the outer surface of the particle, k_f is the thermal conductivity of the bulk gas, k_e is the effective thermal conductivity of the ash layer, h is the convective heat transfer coefficient, and ΔH_1 is the heat of reaction per mole of reactant. The solution of Eq. (58) leads to the following relation for the core temperature of the particle:

$$U_c - 1 = \frac{\phi_1 \beta_1 \omega_{AC} E_1}{U_c R_g T_o}\left[\frac{1}{N_{Nuo}}\frac{\xi_c}{\xi_s} + \xi_c^2\left(1 - \frac{\xi_c}{\xi_s}\right)\right]$$

$$\cdot \exp\left\{\frac{E_1}{R_g T_o}\left(1 - \frac{1}{U_c}\right)\right\}. \tag{64}$$

Comparison with Experimental Results

The general expression derived for the burn-out time, t_c, of a char particle in the batch combustion in a fluidized bed given by Eq. (55) contains four terms. These terms represent, respectively, the contributions due to the kinetics of the reaction, intermolecular diffusion of oxygen through the gas film around the char particle, intraparticle diffusion of oxygen through the ash layer left behind on the unburnt core of the char particle, and the interphase transfer of oxygen from the bubble phase to the emulsion phase of the fluidized bed. In Fig. 1, the combustion of a char particle of initial radius, R_o, is depicted with a gas film and an ash layer around the unreacted core of radius, r_c. We are interested here in the carbon-oxygen reaction, Eq. (2), which is a very fast reaction so that the contribution of the kinetics term to the carbon burn-out time is negligibly small as compared with the remaining three terms of Eq. (55). Consequently, Eq. (55) simplifies to Eq. (56), and this will be used throughout in the calculations described in this section.

The general theory of the combustion of a char particle proposed here is assessed for its appropriateness by comparison with the experimental data reported by Avedesian and Davidson.[2] These authors have considered two types of particles, char and coke, which have different carbon and ash contents. It is thus particularly appropriate to check the proposed theory because the contribution of the resistance of the ash layer on the surface of the burning carbon particle will differ in two cases. Some of the physical constants and various other parameters needed to compute the burn-out time of char and coke from Eq. (56) are listed in Table 1.

The burn-out time for the combustion of a char particle will also be computed on the two-film model which is considered in detail by Avedesian and Davidson.[2] In this model, it is assumed that there is no ash formation on the burning particle, that only carbon dioxide and no oxygen diffuses to the reacting particle surface, and that carbon monoxide burns in a diffusion flame to form carbon dioxide on the surface of a reaction sphere (zone II) whose radius is equal to the diameter of the particle. Surrounding the particle in a spherical gas annulus of thickness equal to the particle radius (zone I), it is assumed, carbon monoxide diffuses away from the particle surface, and carbon dioxide diffuses towards it to be reduced to carbon monoxide by reaction with carbon at the particle surface. The model predictions as obtained on the present theory (usually referred to as the direct oxidation model) and the predictions obtained with the two-film model will be compared and critically evaluated on the basis of the reported experimental data.[2]

In addition to the parameters listed in Table 1, other quantities are required in the calculation of t_c. The mass transfer coefficient, k_{mA}, is obtained from the Sherwood number correlation, Eq. (18), given by Ranz and Marshall.[8] The intraparticle diffusion coefficient, characterizing the diffusion of oxygen through the ash layer on the reacting particle is taken to be equal to 0.71 times the intermolecular diffusion coefficient *viz.*, $D'_{eA} = 0.71\, D_A$. The value of X is computed from Eq. (34). The expression given by Avedesian and Davidson[2] for D_B is used to compute the bubble diameter at various values of V. The burn-out time of the carbon particles is computed from Eqs. (56) and (57) for various initial diameters of the particles, $2R_o$; for different gas fluidizing velocities, V; and for different initial charges of carbon to the fluidized bed, m_c. The results are discussed in the following.

The burn-out time of a char particle in a batch charged to the fluidized bed as a function of the carbon in the initial charge is shown in Fig. 2 for three values of the fluidizing gas velocity. The three sets of data points are experimental results corresponding to the three gas velocities. Similarly, the set of three solid lines were calculated with the proposed model, Eq. (56), while the set of three dashed lines are based on Eq. (57) and the theory of Avedesian and Davidson.[2] The two sets of calculated results and the experimental data points are in qualitative accord with each other. The two general trends are:

Table 1. Constants Used in Burn-Out Calculations of Char and Coke Particles

		Char	Coke
A_o,	cm^2	45.6	45.6
C_{AO},	mol/cm^3	2.18×10^{-6}	2.18×10^{-6}
D_A,	cm^2/s	2.08	2.08
H_o,	cm	8.2	8.2
m_c,	g of carbon	0.75, 1.5, 2.2 3.0, 3.6	3.6
R_o,	cm	0.064, 0.077, 0.094 0.112, 0.13	0.094
T_o,	°C	900	900
V,	cm/s	21.4, 30, 38.3	21.4, 30, 38.3
V_{mf},	cm/s	4.6	4.6
Z,	--	0.02	0.192
μ,	g/cm-s	5×10^{-4}	5×10^{-4}
ε_{mf},	--	0.5	0.5
ρ_c,	g/cm^3	0.72	1.39
ρ,	g/cm^3	0.00028	0.00028
ρ_{ash},	g/cm^3	2.36	2.36
ρ_s,	g/cm^3	1.00	1.93

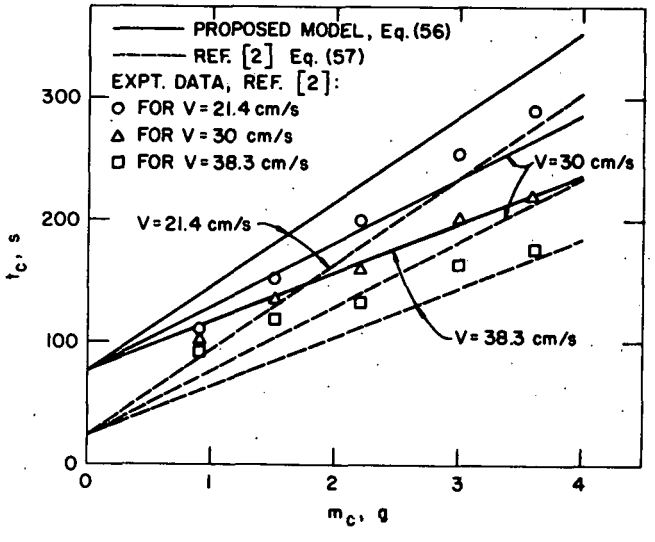

Fig. 2. Burn-Out Time, t_c, of a Char Particle as a Function of the Initial Charge of Carbon, m_c, for Various Values of V for the Two Models. Other parameters are: $R_o = 0.094$ cm, $V_{mf} = 4.6$ cm/s, $\rho_c = 0.72$ g/cm^3, and $Z = 0.02$.

(a) The burn-out time increases as the mass of carbon charged to the fluidized bed is increased at a given fluidizing-gas velocity. This is because the share of available oxygen per unit mass of the carbon charged decreases as the mass of initial charge is increased; therefore, the burn-out time increases to compensate for the reduced rate of available oxygen. (b) For the same value of initial charge, the burn-out time increases with a reduction in fluidizing-gas velocity. This is again simple to explain. With fluidizing-gas velocity reduced, the amount of oxygen available per unit mass of initial charge decreases; therefore, the burn-out time increases.

The quantitative agreement of the theoretical and experimental values is not very satisfactory. In each of the three cases, the burn-out time estimated with the proposed model is about 10-20 percent greater than the experimentally observed values; the predicted burn-out times based on Avedesian and Davidson's[2] model are consistently lower than the experimental results. The systematic difference between the predictions of the two theories from the experiments is puzzling and is reinforced by the dependence of t_c on R_o (discussed below).

In Fig. 3 are presented the results of burn-out time of a fixed amount of initial charge for these

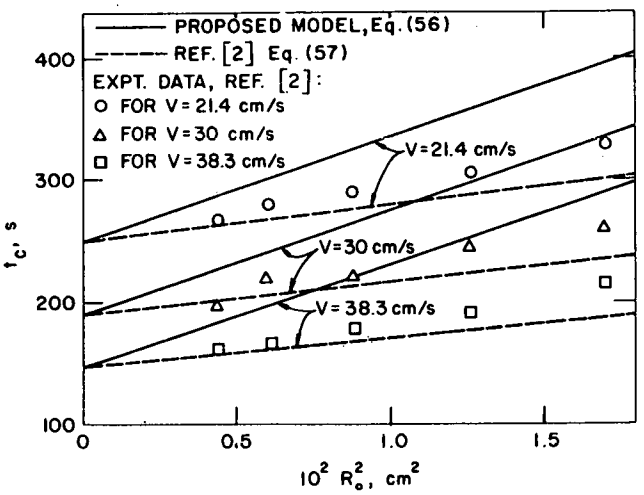

Fig. 3. Burn-Out Time, t_c, of a Char Particle as a Function of Its Initial Radius, R_o, for Various Values of V for the Two Models. Other parameters are: m_c = 3.6 g, V_{mf} = 4.6 cm/s, ρ_c = 0.72 g/cm^3 and Z = 0.02.

fluidizing-gas velocities but with the particle size varied. Here again, the theoretical formulations bear out the qualitative trends of the observed variations. Thus, the burn-out time increases as the size of the particle is increased while the other parameters remain constant. Also, for a particle of given size, the burn-out time increases as the fluidizing-gas velocity is decreased. The former is explained by the fact that as the radius of the particle increases, its surface-to-volume ratio decreases, and the latter trend is explained on the basis that reduction in fluidizing-gas velocity implies a longer time for the particle to receive the amount of oxygen required for complete combustion. However, here again (Fig. 3) as in the previous case (Fig. 2), quantitative agreement is not satisfactory--the two-film model underestimating the experimental results and the direct oxidation model overestimating t_c.

Examination of Eq. (56) suggests that for low-ash char particles, burn-out time will primarily depend on the first and the third terms. The first term, which pertains to the diffusion of oxidant through the gas film, is sensitively dependent upon the value of k_{mA}. The third term, on the other hand, accounts for the transfer of oxygen from the bubble phase to the emulsion phase, and the magnitude of this interphase mass transfer term depends sensitively upon the magnitude of X. The correlation for k_{mA} is based on a large body of experimental information and may be considered rather reliable. The estimation of X, on the other hand, is rather approximate and crude. The validity of accounting for the combustion of char in a free bubbling bed with the two-phase model with equal-size bubbles is questionable. Many other complicated multi-phase models have been considered, such as the one by Chen and Saxena.[10] We have accepted the general applicability of the two-phase model by treating X as a manipulable parameter and hoping that a proper selection of X will compensate for at least some of the shortcomings of this model and of the error it induces in the calculation of interphase mass transfer.

In Fig. 4 are compared the calculated values of the burn-out times from Eq. (56) with X = 1 and X as given by Eq. (34) as a function of m_c and for three values of the fluidizing-gas velocity, along with the corresponding experimental values. The theoretical results corresponding to X = 1 are in much better agreement with the experimental data than are the results for the values of X computed from Eq. (34). In Fig. 5, which is a similar comparison of theory and experiment, the burn-out times are examined as a function of char particle radius and the same three values of fluidizing-gas velocity. The agreement of the theoretical values with the experimental data is much better for X = 1 than for values of X obtained from Eq. (34).

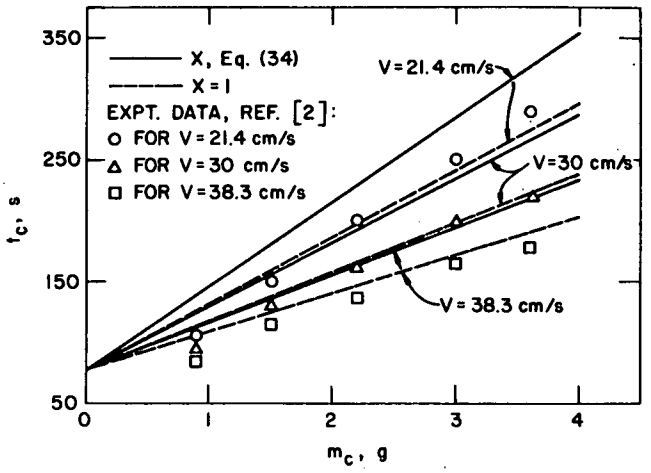

Fig. 4. Burn-Out Time, t_c, of a Char Particle as a Function of the Initial Charge of Carbon, m_c, for Various Values of V and X. Other parameters are: R_o = 0.049 cm, V_{mf} = 4.6 cm/s, ρ_c = 0.72 g/cm^3 and Z = 0.02.

The results of Figs. 4 and 5 clearly point out that the interphase mass transfer between bubbles and emulsion plays a significant role in establishing the values of the burn-out times of char particles in a fluidizing bed. These calculations also suggest that the shortcomings of the two-phase bubbling bed model if constant size of the bubbles is assumed, are compensated to a large extent by choosing an appropriate value of X. The values of X obtained with Eq. (34) appear to be underestimates. The present work supports the view that gas having a volume equal to that of the bubble volume is flushed out of the bubble during its passage through the bed. This does not seem unreasonable because in an unbaffled bed, bubbles may grow by coalescence and more gas be flushed out than average-size bubbles. Also it is well known that the calculation of interphase mass transfer is quite approximate.

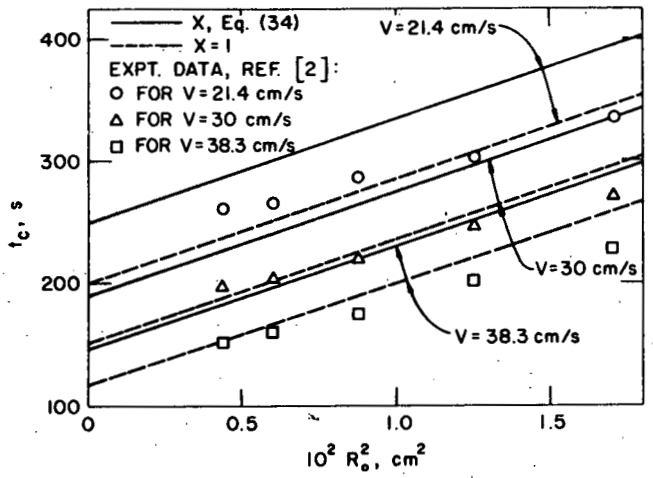

Fig. 5. Burn-Out Time, t_c, of a Char Particle as a Function of Its Initial Radius, R_o, for Various Values of V and X. Other parameters are: m_c = 3.6 g, V_{mf} = 4.6 cm/s, ρ_c = 0.73 g/cm^3 and Z = 0.02.

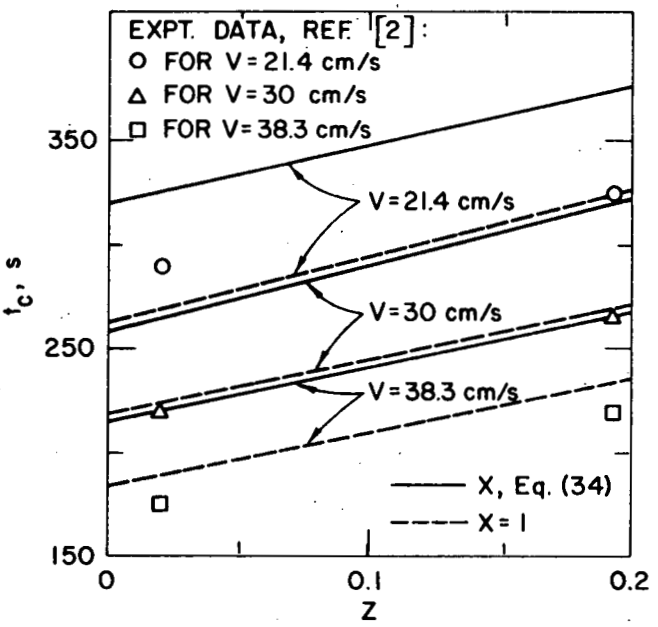

Fig. 6. Burn-Out Time, t_c, of Particles as a Function of Their Growth Factor for Various Values of V and X. Other parameters are: m_c = 3.6 g, R_o = 0.094 cm and V_{mf} = 4.6 cm/s

In Fig. 6 are presented the calculated results and corresponding experimental results for the burn-out times of particles containing different amounts of ash. These are char and coke particles containing 5.2 and 23.6 percent ash, respectively. These calculations are intended to highlight the influence of intraparticle diffusion resistance since the ash layer thicknesses in the two cases are quite different. This contribution for the low-ash-content char towards the burn-out time is only 1 to 2 percent but rises to 7 to 10 percent for the higher ash content. It will be seen that the models as well as the experiments predict a greater value of t_c with greater ash content of the particle when its overall size is constant and the fluidizing-gas velocity is the same. Further, as the fluidizing-gas velocity decreases, the burn-out time increases. Both these qualitative trends can be explained readily. Figure 6 data also encourages the choice of X = 1 on the basis of quantitative agreement of theory and experiment.

Lastly, it may be pointed out that the proposed theory, in contrast to the theory of Avedesian and Davidson[2] accounts for the changing size of gas film around the particle in the calculation of mass transfer. Explicitly, this justifies the presence of Z in the first term on the right side of Eq. (56).

Conclusions

For proper understanding of char combustion in a fluidized bed of inert particles, an adequate theory for particle combustion and a realistic theory for the behavior of fluidized bed are needed. In view of the recent work pointing to the diffusion of oxygen to the reaction surface of a combusting char particle, the direct oxidation model has been developed to mathematically formulate the combustion of char particles. The model is made general by including terms representing the formation of ash layer on the unreacted core of the solid particle as a result of reaction.

The two-phase theory of fluidization with constant size bubbles is employed in computing interphase mass transfer from bubbles to the emulsion phase. Comparison of the results predicted by this proposed model suggests that the two-phase bubbling bed theory underestimates interphase mass transfer by about forty percent. It is therefore proposed that the two-phase fluidized-bed model be refined by assuming that the volume of gas flushed through a bubble during its passage through the bed is equal to the bubble volume. With these modifications, the proposed theory predicts burn-out times which are in good quantitative agreement with experimental values. The theory is found to be adequate for explaining the dependence of burn-out times on the initial carbon charge to the bed, the particle diameter, the ash content of the particle and the fluidizing-air velocity.

Acknowledgments

The authors are grateful to Dr. Irving Johnson for his continued interest and many helpful discussions. They are also thankful to A. A. Jonke, D. S. Webster, and L. Burris for their interest and encouragement. This work is partly supported by the U.S. Department of Energy and the U.S. Environmental Protection Agency.

References

1. Davidson, J. F. and Harrison, D., Fluidized Particles, Cambridge University Pres, 1963.

2. Avedesian, M. M. and Davidson, J. F., Trans Instn. Chem. Engrs. 51: 121 (1973).

3. Andrei, M. A., Sarofim, A. F., and Beér, J. M., Paper No. 57f, presented at the 86th National Meeting of the Am. Inst. Chem. Engrs., Houston, Texas, 1979.

4. Field, M. A., Gill, D. W., Morgan, B. B., and Hawksley, P. G. W., Combustion of Pulverized Coal, The British Coal Utilisation Research Association, Leatherhead (1967).

5. Arthur, J. R., Trans. Faraday Soc. 42: 164 (1951).

6. Basu, P., Broughton, J., and Elliott, D. F., Proc. Inst. Fuel Sym. Series No. 1: Fluidized Combustion Conference, London, September 1975, A3-1 (1975).

7. Rehmat, A. and Saxena, S. C., Ind. Eng. Chem. Process Des. Dev. 16: 502 (1977).

8. Ranz, W. E. and Marshall, W. R., Chem. Eng. Prog. 48: 141 (1952).

9. Rehmat, A. Saxena, S. C., Land, R., and Jonke, A. A., Canadian J. Chem. Eng. 56: 401 (1978).

10. Chen, T. P., and Saxena, S. C., Fuel 56: 401 (1977).

Nomenclature

A_o = cross-sectional area of the fluidized bed, cm^2

C_A = oxygen concentration at distance r within the particle, mol/cm^3

$C_{AB}(H)$ = oxygen concentration in the bubble phase at a distance H above the distributor, mol/cm^3

C_{AC} = oxygen concentration at the core of the char particle, mol/cm^3

C_{AO} = initial concentration of oxygen in the feed gas, air, mol/cm^3

C_{AP} = oxygen concentration in the emulsion phase, mol/cm^3

C_{AS} = oxygen concentration at the surface of the char particle, mol/cm^3

C_{JO} = initial concentration of carbon in the char, mol/cm^3

D_A = molecular gas diffusion coefficient, cm^2/s

D_B = bubble diameter, cm

D_e = dispersion coefficient cm^2/s

D'_{eA} = intraparticle diffusion coefficient through the ash layer, cm^2/s

E_1 = activation energy, cal/mol

g = acceleration due to gravity, cm^2/s

H' = height of the fluidized bed above the distributor, cm

H_o = height of the fluidized bed at incipient fluidization, cm

H = variable space coordinate along the height of the fluidized bed, cm

ΔH = heat of reaction, cal/mol

k = emulsion phase velocity constant, 1/s

k' = dimensionless velocity constant, kH_o/V

k^o = frequency factor, $cm^4/mol \cdot s$

k_1 = reaction rate constant for carbon-oxygen reaction, $cm^4/mol \cdot s$

k_e = effective thermal conductivity of the ash, $cal/s \cdot cm \cdot K$

k_f = thermal conductivity of the fluidizing gas, $cal/s \cdot cm \cdot K$

k_{mA} = mass transfer coefficient of oxygen across the gas film, cm/s

k_r = ratio of the rates of formation of carbon monoxide to carbon dioxide, dimensionless

m = mass of char charged to the fluidized bed, g

m_c = mass of carbon charged to the fluidized bed, $m\rho_c/\rho_s$, g

N = Number of char particles in the fluidized bed, dimensionless

N_{Nu} = Nusselt number, $2Rh/k_f$, dimensionless

N_{Nuo} = modified Nusselt number, hR_o/k_e, dimensionless

N_{Sc} = Schmidt number, $\mu/\rho D_A$, dimensionless

N_{Sh} = Sherwood number, $2Rk_{mA}/D_A$, dimensionless

N_{Sho} = modified Sherwood number, $R_o k_{mA}/D'_{eA}$

N_{Re} = Reynolds number, $2RV_{mf}\rho/\mu$, dimensionless

N_s = number of moles of carbon in a single char particle of size R, dimensionless

n = molar oxygen transfer rate to the char particle, mol/s

Q = total gas exchange flow rate from each bubble, cm^3/s

R = radius of char particle at any instant, cm

R_g = universal gas constant, cal/mol·K

R_o = initial radius of the char particle, cm

r = radial distance within the particle, cm

r_A = rate of carbon consumption or oxygen depletion, $mol/cm^2 \cdot s$

r_c = radius of the core, cm

T = temperature, K

T_c = core temperature, K

T_o = fluidized bed temperature, K

T_s = particle surface temperature, K

t = time, s

t_c = char burn-out time, s

U = reduced temperature, T/T_o, dimensionless

U_B = bubble velocity, cm/s

U_c = reduced core temperature, T_c/T_o, dimensionless

U_s = reduced surface temperature, T_s/T_o, dimensionless

V = velocity of the fluidizing gas, cm/s

V_B = bubble volume, cm^3

V_{mf} = minimum fluidizing velocity, cm/s

X = number of times a bubble is swept out during its passage through the bed, dimensionless

X_A = mole fraction of A, dimensionless

X_{AC} = mole fraction of A at the core, dimensionless

X_{AO} = initial mole fraction of A in the fluidizing gas, dimensionless

X_{AP} = molc fraction of A in the emulsion phase, dimensionless
X_{AS} = mole fraction of A at the surface of the particle, dimensionless
Z = ratio of volume of ash formed to the volume of char burnt, dimensionless

Greek Letters

β = defined by Eq. (33), dimensionless
β_1 = defined by Eq. (63), dimensionless
ω_A = reduced mole fraction of A, X_A/X_{AO}, dimensionless
ω_{AC} = reduced value of X_{AC}, X_{AC}/X_{AO}, dimensionless
ω_{AP} = reduced value of X_{AP}, X_{AP}/X_{AO}, dimensionless
ω_{AS} = reduced value of X_{AS}, X_{AS}/X_{AO}, dimensionless
ϵ_{mf} = bed voidage at minimum fluidization, dimensionless
μ = viscosity of the fluidizing gas, g/cm·s
ξ = reduced distance, r/R_o, dimensionless
ξ_c = reduced value of r_c, r_c/R_o, dimensionless
ξ_s = reduced value of R, R/R_o, dimensionless
ρ = density of the fluidizing gas, g/cm^3
ρ_{ash} = density of ash, g/cm^3
ρ_c = carbon density in the char particle, g/cm^3
ρ_s = density of the char particle, g/cm^3
ϕ_1 = defined by Eq. (13), dimensionless
τ_1 = burn-out time for a single char particle in the absence of diffusion resistances, s

Subscripts

A = oxygen
J = carbon

Question to S. C. Saxena:

Q: (Participant not identified)

These char burning models are very interesting from a theoretical standpoint. But, has some attention been given to photomicrographic analysis of char on a slow time frame? Something has to be done to explain the differences between an anthracite and a high volatile bitumenous coal.

A: As far as this model, it is capable of taking into account particle size charge and subsequent diffusion change.

HEAT TRANSFER, INSTRUMENTATION AND CONTROL

DESIGN RELATIONSHIPS FOR PREDICTING HEAT TRANSFER TO TUBE BUNDLES IN FLUIDIZED BED COMBUSTORS

L. R. Glicksman

N. A. Decker

Department of Mechanical Engineering
Massachusetts Institute of Technology
Cambridge, MA 02139

INTRODUCTION

The design of heat exchange surfaces for fluidized bed coal combustors is of paramount importance to the successful control and optimal performance of these advanced combustion systems, but few of the many models and correlations for heat transfer coefficients in fluidized beds are successful in general application. The absence of a universally accurate correlation stems from the existence of more than a single mechanism of heat transfer and the shift of dominance from one mechanism to another as fluidizing conditions and/or solids properties are altered. Physically based models with clearly defined limits of applicability are required for interpretation of data and for extrapolation to situations yet untested. The principal mechanisms of heat transfer are examined here along with some guidelines for their application.

GENERAL MECHANISMS

Some of the earliest models of fluidized bed heat transfer suggested that the moving solid particles served merely to scrub the gas boundary layer along wall and immersed surfaces. Although it was later shown that in beds of moderately sized particles the solid convective transport greatly exceeded the gas convective transport, this mechanism should play a part in very dilute systems or in beds of extremely large particles. The former may represent conditions in the vicinity of tube banks located well above the dense bed in the freeboard.

Experiments which yielded information about the variation of heat flux with time at immersed surfaces in fluidized beds support the theory that heat transfer from a bed to a surface takes place through rapid transients which cool local "packets" of gas and solids which are swept away and replaced by the bubbling activity of the bed. The large heat capacity of the solids relative to the gas is responsible for the very large ratio of fluidized bed heat transfer coefficients to coefficients of solid-free gas. Quantifying this mechanism produced a mathematical form like

$$h_e = \sqrt{\frac{4\, k_e \rho_s (1-\epsilon_{mf}) c_s}{\pi\, t_r}} \qquad (1)$$

and $h_{avg} = (1-f_o)\, h_e + f_o h_b$ (2)

where f_o is the fraction of solids residence time at the surface, t_r is the mean residence time, and h_b is a heat transfer coefficient during bubble (gas void) contact, normally considered negligible, especially for beds of small particles.

Physically this model is plausible but difficult to apply due to its inherent dependence on two quantities difficult to measure, let alone predict: solids residence fraction f_o and residence time t_r. Furthermore, when experiments with carefully monitored or controlled residence times were attempted, the calculated heat transfer coefficients overestimated the data taken. This was attributed to a "gas gap" between the surface and the solids with a mean thickness estimated between one sixth and one tenth of a particle diameter. It was argued in addition that finite maximum instantaneous heat transfer coefficients were evidence of such a resistance in series with the emulsion.

The application of this model should be restricted to those cases where the residence time is sufficiently long that the thermal disturbance propagates through a zone several particle diameters in thickness. In any shorter time the effective thermal conductivity of the presumed homogeneous emulsion fails to represent the heterogeneous mixture considered.

If residence times are very short, and particle heat capacities sufficiently large, particle temperatures may be changed only slightly during their residence at a surface thereby allowing the heat exchange to be modelled as a quasi-steady process with the full bed-to-wall temperature difference. A particle thermal time constant, derived through a first order model of transient cooling of a single particle, is estimable as

$$\tau = \frac{\rho_s c_s d_p^2}{15\, k_g} \qquad (3)$$

For residence times small with respect to this time constant, the particles may be taken as essentially isothermal. Uniformly sized spheres randomly arranged against a flat surface were analyzed (1) to yield an effective surface heat transfer coefficient with stagnant fluid:

$$h_s^o = \frac{11.2\ k_g}{d_p} \quad (4)$$

From studies done on packed beds (2) it was determined that a gas convective component due to lateral mixing of the gas augments this surface coefficient when particle diameter and superficial velocity are sufficiently large such that

$$h_s = \frac{k_g}{d_p}(11.2 + 0.05\ Re\ Pr) \quad (5)$$

during surface contact. The coefficients involved here are not completely general; they are influenced by overall particle shape and density of packing. The three nonradiant mechanisms of heat transfer are represented schematically in Figure 1.

At the elevated temperatures of fluidized bed combustors, radiant heat transfer will contribute significantly to the overall heat transfer to surfaces.

For transients which propagate well into the emulsion, the radiative effect is present in the improvement of the effective emulsion thermal conductivity. Using the model of Argo and Smith (3)

$$k_{er} = k_e + \frac{4\ \sigma\ \varepsilon_p}{(2-\varepsilon_p)}\ d_p\ T^3 \quad (6)$$

where ε_p is particle emissivity.

At surfaces, the surface conductance is aided directly by radiation even when voids are present at the surface by an effective radiative heat transfer coefficient

$$h_{sr} = \frac{\sigma}{\left(\frac{1}{\varepsilon_w} + \frac{1}{\varepsilon_b} - 1\right)} \frac{T_i^4 - T_w^4}{T_i - T_w} \quad (7)$$

where T_i is the bed temperature during brief residence times. Bed emissivity ε_b should be larger than particle emissivity due to the cavities formed by the spaces between particles in the emulsion

IMMERSED TUBES

Due to their location in the vigorously bubbling region of the bed and due to the large area/volume ratio attainable with immersed tubes, banks of immersed tubes are the primary heat exchange surfaces in fluidized beds of industrial or utility scale. Accurate sizing of exchange surfaces of this type will be necessary for successful design and operation of fluidized bed combustors.

Of the mechanisms discussed above, the emulsion and surface conductances are relevant to most of a horizontal tube. Radiation will be significant over all of a tube surface in a fluidized bed combustor, and particle enhanced gas convection may be the predominant mechanism on the underside of a horizontal tube, although recent studies of tubes in staggered tube arrays (4) suggest that dense phase emulsion makes good thermal contact even on the bottom of the tube.

No complete predictive model exists which can determine local residence times and thus local heat transfer coefficients around an immersed tube or even spatially averaged coefficients. Residence time distributions of solids at immersed tube surfaces cannot be predicted at this time.

Many correlations have been developed to fit specific sets of data, but few have demonstrated enough generality to fit several sets of experimental data. Of these, the Vreedenberg (5) and modified Vreedenberg (6) correlations have been most successful. The modified Vreedenberg correlation

$$h = 900\ \frac{k_g}{d_t}(1-\varepsilon)\left[\frac{Gd_t\rho_s}{\rho_g\mu}\ \frac{\mu^2}{d_p^3\rho_s^2\ g}\right]^{0.326} Pr^{0.3} \quad (8)$$

incorporates a dependence upon bed voidage and has successfully fit data for particle sizes up to 810 μm. Larger particles, and particularly higher pressures produce heat transfer coefficients much larger than those predicted by this correlation. For particles of 800 μm or less viscous forces control the hydrodynamics; the modified Vreedenberg correlation explicitly accounts for these viscous forces. When the particle diameter and the bed pressure are increased inertial effects of the fluid increase and heat transfer by convection in the voids between particles becomes important. Neither of these effects are accounted for in the Vreedenberg correlation.

The isothermal large particle model is based upon a simplification brought on by the use of large particles in fluidized bed combustors with high superficial velocities and consequent short solids residence times. When solids residence time is small with respect to the solids thermal time constant, the residence time itself is unimportant. Solids residence time fraction may be estimated as the emulsion spatial fraction, such that bubble fraction δ may be used to approximate f_o. Observations of single tubes and some tube arrays show a tendency for a steady void to remain along the bottom of horizontal tubes covering approximately one sixth of the cylindrical surface. With these factors incorporated

$$(1-f_o) \sim \frac{5}{6}(1-\delta) \quad (9)$$

for a horizontal tube. Although δ is not predictable from first principles, many correlations for bed expansion have been published, and predictions for bubble fraction δ are thus more abundant, and probably more accurate, than those for f_o. Two of the most promising of these predictors are the correlation due to Babu et al (7)

$$\frac{L}{L_{mf}} = 1 + \frac{10.978(u-u_{mf})^{.738} d_p^{1.006} \rho_s^{.376}}{u_{mf}^{.937} \rho_g^{.126}} \quad (10)$$

which is not dimensionless but is founded upon data of solids typical of those used in fluidized bed combustors, and the drift flux model employed by General Electric (8)

$$\varepsilon = \frac{u}{c_o u + v_{gu}} \tag{11}$$

The velocity V_{gu} is estimated as

$$V_{gu} = \left(\frac{1-\epsilon_{mf}}{\epsilon_{mf}}\right) u_{mf} \tag{12}$$

and the constant c_o varies with particle size and gas pressure but is generally quite close to unity.

In complete form, the large particle model is

$$h = (1-\delta) \frac{k_g}{d_p} (9.3 + 0.042 \text{ Re Pr}) \tag{13}$$

and it has compared favorably with large particle heat transfer data at atmospheric and higher pressures.

Figures 2,3 and 4 illustrate the comparison of this model with data of General Electric (8) and of Catipovic (9)

The modified Vreedenberg correlation is seen to considerably underestimate all of this data with the exception of the small 650 μm General Electric data, figure 2. That data comparison is particularly significant in that it shows improving representation by the isothermal large particle model and deteriorating representation by the modified Vreedenberg correlation as superficial velocity increases. As should be expected at the higher pressures and larger particle diameters of the 2600 μm General Electric data of figure 3, the modified Vreedenberg correlation, based upon low Reynolds number data, departs further from the data. Similarly, the 1.3mm and 2.85mm data of Catipovic figure 4 are underestimated by the modified Vreedenberg correlation. The isothermal large particle model overestimates both the 1.3mm sand data and the 2.85mm dolomite data of Catipovic. This may be due to particle roughness, particularly for the sand with sphericity of 0.82. Zakkay et al (10) found that a modification of the large particle model, reduction of the conductive coefficient to about 5, provided a better fit to their coarse particle data. Physically the roughness can be envisioned as holding the particles farther from the surface, increasing the mean gas conduction length and thereby increasing the resistance to heat transfer. A limited amount of data from a variety of particle sizes, but clustered in a narrow range of superficial velocity is shown in figure 5. This overall heat transfer coefficient data from the Babcock and Wilcox 6'x6' fluidized bed combustor (11) is bounded above and below by the predictions of the MIT FBC system model using the large particle model. The effective radiative heat transfer coefficient is also included in this comparison.

WALL TUBES (WATERWALLS)

Wall heat transfer from fluidized bed coal combustors is significant primarily in smaller systems where wall surface area may be a substantial fraction of the immersed tube surface area.

The dominant particle flow pattern observed near walls in large fluidized beds is the slow downward flow of solids which balances the upward flow of solids in bubble wakes. Solids which come in contact with the wall near the top of the bed tend to translate down the wall with little mixing unless baffles or other flow control devices direct rising bubbles toward the wall.

The emulsion model may be employed to estimate the long transient transfers of heat during solids transit. The surface conductance is used in series such that

$$h_w = \frac{1}{\frac{1}{h_s} + \frac{1}{h_e}} \tag{14}$$

where h_e is estimated using

$$t_r = \frac{L}{u_s} \tag{15}$$

$$\text{with } u_s = \frac{\alpha \delta u_b}{1 - \delta - \alpha\delta} \tag{16}$$

Here α is the wake fraction, normally around 0.1 and u_b is the bubble rise velocity. This relationship is based on a balance of solids upflow in the bubble wake with uniform solids downflow in the emulsion. With insufficient knowledge to predict t_r, a lower bound can at least be found for h_e as that for the case of stationary solids.

$$h_e = \sqrt{\frac{4 k_e \rho_g c_{g\,mf} u_{mf}}{\pi L}} \tag{17}$$

Figure 6 shows the predictions given by this model as incorporated in the MIT fluidized bed combustor system model with L ∿ 1 meter, T_{bed} = 1117°K and T_{wall} = 600°K, as compared with greatly scattered data of Wright et al (12). The comparison provides little more than an order of magnitude agreement between the model and data. The data is scattered due to the large number of immersed tube bundle designs inserted in the bed over the course of the experiments run.

TUBES IN THE FREEBOARD

Freeboard tubes have little effect on dense bed temperature control, but can be used to extract sensible heat from the exhaust stream. Freeboard tubes located close to the dense bed will yield higher heat transfer coefficients than more distant tubes but may quench certain desirable freeboard reactions.

High in the freeboard the principle heat transfer mechanisms are gas convection enhanced slightly by solids interaction and radiation from the dense bed below and refractory walls. For a small number of rows of tubes, radiation is dominant. As the number of tube rows is increased, gas convection plays a stronger role. Augmentation by solids in the gas stream is slight except when large elutriation rates are encountered.

The convective component of heat transfer should be estimated as the solids-free convective heat transfer coefficient to a bank of tubes, as given by McAdams (13)

$$h = .26 \frac{k_g}{d_t} Re_{max}^{0.6} Pr^{0.3} \quad (18)$$

If significant solids carryover is expected, a first order estimate of the augmentation due to solids may be taken from Danziger's work (14) on gas solid suspension heat transfer inside a tube.

$$\frac{h}{h_g} = (1 + \frac{G_s}{G})^{0.45} \quad (19)$$

The flow geometry in a tube bundle differs considerably from the flow within a tube; this application is justified only by expedience.

Radiative transfer to freeboard tubes can be estimated by considering two independent sources, the bed below and the enclosure above, as infinite planes radiating to an infinitely wide bundle of tubes. The tubes have a self-view factor determinable by the Hottel crossed-string method (15) which gets larger with closer tube packing and greater numbers of tube rows.

The MIT system model was used to estimate freeboard heat transfer with this scheme. Results are shown in figure 7, with tube pitch to diameter ratio equal to two. Data taken by Babcock and Wilcox (16) yield a freeboard tube heat transfer coefficient of the order of 5 BTU/hr-ft^2°F, and suggest very little, if any, particle augmentation of the heat transfer rate.

CONCLUSIONS

Plausible physical mechanisms and quantifying expression have been presented to facilitate estimation of heat transfer coefficients for fluidized bed combustors. The nature of each mechanism dictates the conditions under which it will be the dominant mode. These concepts should be helpful in selecting the best model or correlation to be used in any given design.

NOMENCLATURE

c_g	gas specific heat capacity J/kg°C
c_o	distribution constant
c_s	solid specific heat capacity J/kg°C
d_p	particle diameter m
d_t	tube diameter m
f_o	bubble residence time fraction
g	acceleration of gravity m/sec^2
G	gas mass velocity kg/m^{2}sec
G_s	solids mass velocity kg/m^{2}sec
h	heat transfer coefficient W/m^2°C
h_b	bubble heat transfer coefficient W/m^2°C
h_e	emulsion heat transfer coefficient W/m^2°C
h_g	gas only heat transfer coefficient W/m^2°C
h_s	surface heat transfer coefficient W/m^2°C
h_s^o	surface heat transfer coefficient with stagnant gas W/m^2°C
h_{sr}	surface heat transfer coefficient due to radiation W/m^2°C
h_w	wall heat transfer coefficient W/m^2°C
k_e	effective thermal conductivity W/m°C
k_{er}	effective thermal conductivity with radiation W/m°C
k_g	gas thermal conductivity W/m°C
L	expanded bed height m
L_{mf}	bed height at minimum fluidization m
Pr	gas Prandtl number
Re_{mf}	minimum fluidization particle Reynolds number
t_r	solids residence time sec
T_i	interface temperature °K
T_w	wall temperature °K
u	superficial velocity m/sec
u_b	bubble velocity m/sec
u_{mf}	minimum fluidizing velocity m/sec
u_s	solids downflow velocity m/sec
V_{gu}	drift velocity m/sec
α	wake fraction
δ	bubble fraction
ϵ	overall bed void fraction
ϵ_b	emissivity of bed

ε_{mf} minimum fluidization void fraction

ε_w emissivity of surface

μ gas viscosity kg/m sec

ρ_g gas density kg/m^3

ρ_s solids density kg/m^3

σ Stefan Boltzmann constant $W/m^2{}^\circ K^4$

τ particle thermal time constant

REFERENCES

1. Glicksman, L. and Decker, N. in Modelling of Fluidized Bed Comustion of Coal, Quarterly Technical Progress Report No. 6, Massachusetts Institute of Technology for U.S. Dept. of Energy under contract E(49-18)-2295, November 1977.
2. Yagi, S. and Kunii, D., Studies on heat transfer near wall surface in packed beds, AIChE Journal 6, 1960, 97-104.
3. Argo, W.B. and Smith, J.M., Heat transfer in packed beds, Chemical Engineering Progress, 49, 1953, 443-451.
4. Chandran, R., Chen, J.C., and Staub, F.W., Local heat transfer coefficients around horizontal tubes in fluidized beds, Journal of Heat Transfer, 102, 1980, 152-157.
5. Vreedenberg, H.A., Heat transfer between a fluidized bed and a horizontal tube, Chemical Engineering Science, 9, 1958, 52-60.
6. Andeen, B.R. and Glicksman, L.R., Heat transfer to horizontal tubes in shallow fluidized beds, ASME paper 76-HT-67, 1976.
7. Babu, S.P., Shah, B., and Talwalker, A., Fluidization correlations for coal gasification materials-minimum fluidization velocity and fluidized bed expansion ratio, AIChE Symposium Series, 74, No. 176, 1978, 176-186.
8. General Electric, Two-phase flow and heat transfer in fluidized beds, final technical report to Electric Power Research Institute, Contract RP525-1, SRD-78-103, 1978.
9. Catipovic, N.M., Heat transfer to horizontal tubes in fluidized beds: experiment and theory, PhD thesis, Dept. of Chemical Engineering, Oregon State University, 1979.
10. Zakkay, V., Miller, G., Rosen, S., Shah, S., and Kolar, A.K., Bed expansion and heat transfer measurement in a pressurized fluidized bed, Report NYU/DAS 79-02, New York University, April 1979.
11. Babcock and Wilcox, EPRI/B&W fluidized bed combustion development facility: initial test results, Report RDTPA 79-3, 86th National AIChE Meeting, April 1979.
12. Wright, S.J., Hickman, R., and Ketley, H.C., Heat transfer in fluidized beds of wide size spectrum at elevated temperatures, British Chemical Engineering, 15, 1970, 1551-1554.
13. Rohsenow, W.M., and Choi, H., Heat, Mass and Momentum Transfer, Prentice-Hall, Inc., 1961.
14. Danziger, W.J., Heat transfer to fluidized gas-solids mixtures in vertical transport, Industrial and Engineering Chemistry, Process Design and Development, 2, 1963, 269-276.
15. Hottel, H. and Sarofim, A., Radiative Transfer, McGraw-Hill, 1967.
16. Babcock and Wilcox, Fluidized bed combustion development facility and commercial utility AFBC design assessment, LR:79:4775:03, prepared for Electric Power Research Institute under contract RP-718-2, September 1979.

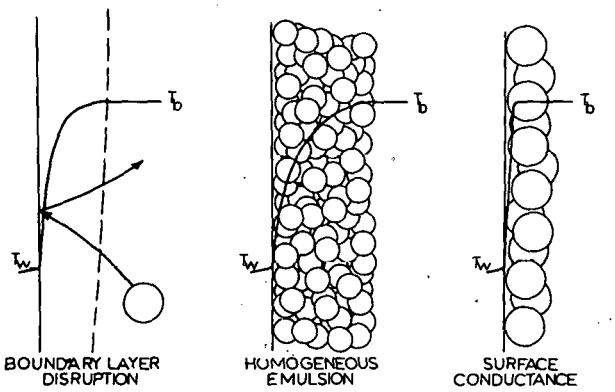

Figure 1. Heat transfer mechanisms

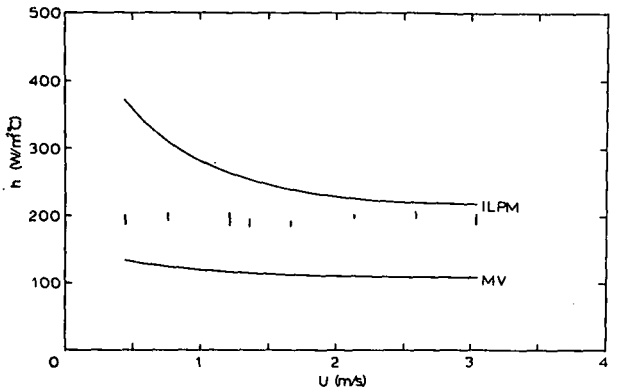

Figure 2. Isothermal large particle model and modified Vreedenberg correlation compared with data of General Electric for 650 μm glass spheres at atmospheric pressure.

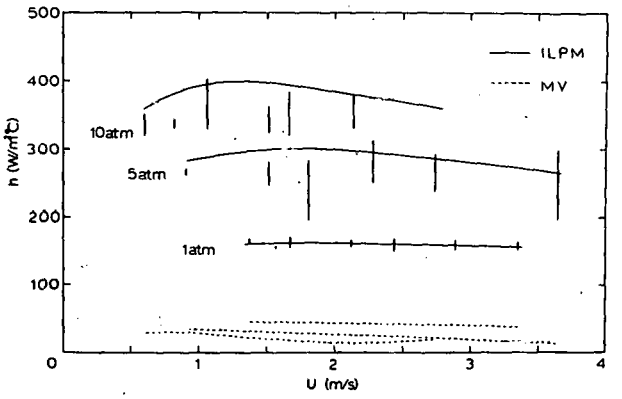

Figure 3. Isothermal large particle model and modified Vreedenberg correlation compared with data of General Electric for 2600 μm glass spheres at 1, 5, and 10 atmospheres.

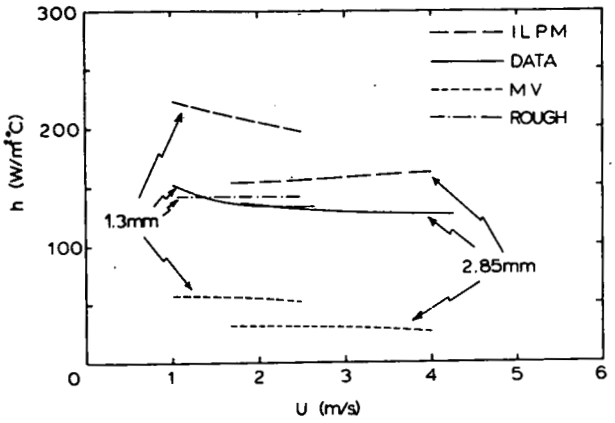

Figure 4. Isothermal large particle model and modified Vreedenberg correlation compared with data of Catipovic for 1.3mm sand and 2.85mm dolomite particles. Shown also is an approximation for rough 1.3mm particles with greater effective gas conduction lengths.

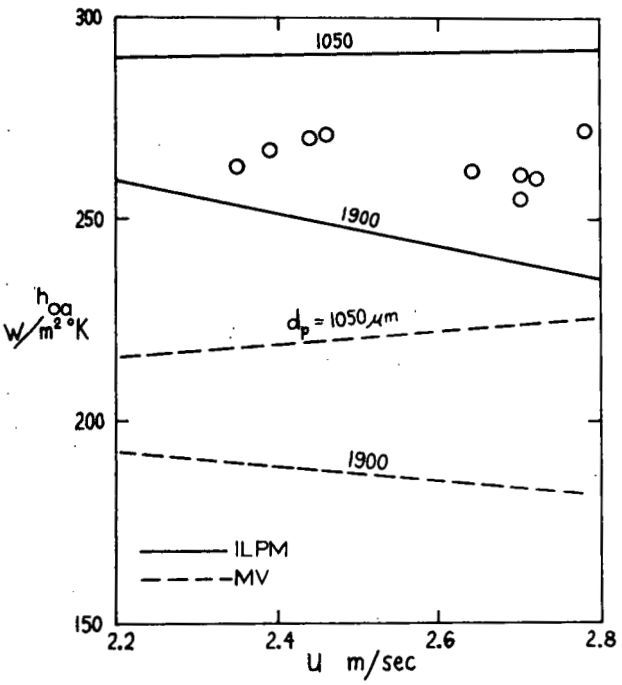

Figure 5. Overall heat transfer coefficient, including radiation: data of Babcock and Wilcox 6'x6' combustor (mean particle diameters between 1050 and 1940 μm) compared with the MIT Fluidized Bed Combustor System Model using the isothermal large particle model and the modified Vreedenberg correlation.

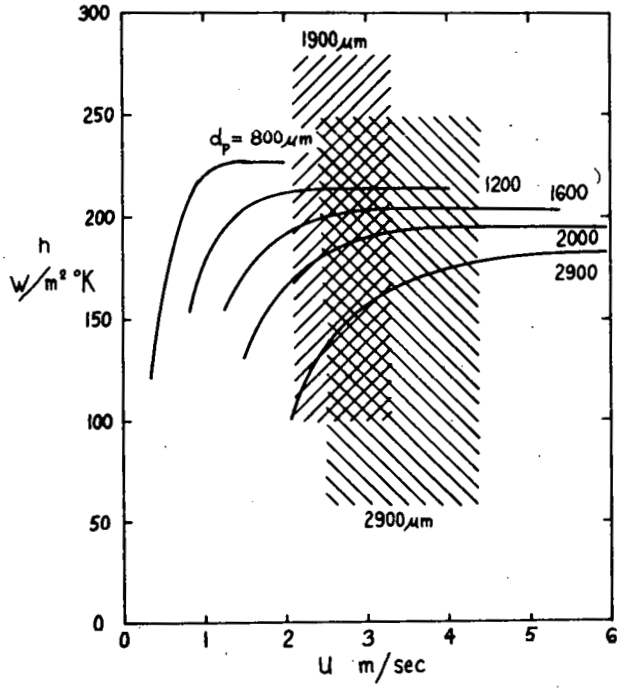

Figure 6. Wall heat transfer coefficient: data of Wright et al compared with the MIT Fluidized Bed Combustor System Model.

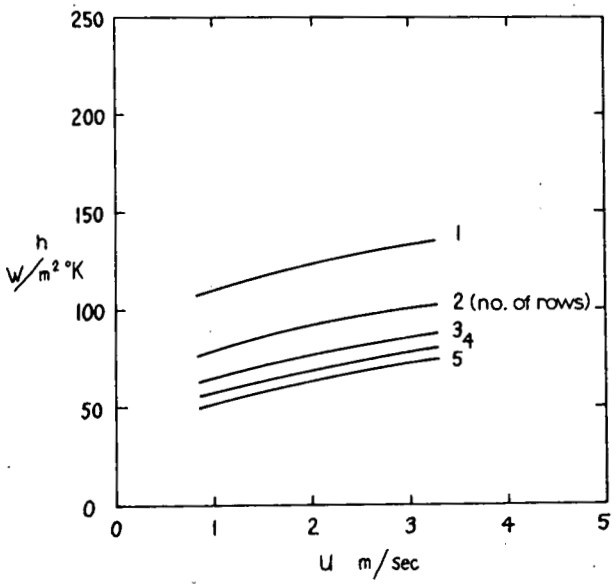

Figure 7. Freeboard tube heat transfer coefficient variation with superficial velocity and number of tube rows: predictions of MIT Fluidized Bed Combustor System Model.

Questions to Norman A. Decker:

Q: Stromberg, Sweden

Did you consider radiative heat transfer between the particle layers, the particles themselves, and the bed and the particles?

A: When I did the estimation of the penetration distance, I used an effective thermal conductivity of the emulsion which included a radiance component.

AN INVESTIGATION OF THE INFLUENCE OF BED PARAMETERS ON THE VARIATION OF THE LOCAL RADIATIVE AND TOTAL HEAT TRANSFER COEFFICIENTS AROUND AN EMBEDDED HORIZONTAL TUBE IN A FLUIDIZED BED COMBUSTOR

R.VADIVEL AND V.N.VEDAMURTHY

Department of Heat Power Engineering
College of Engineering
Perarignar Anna University of Technology, Madras,INDIA

INTRODUCTION

In fluidized bed boilers, steam is generated mostly in horizontal tubes immersed in the bed. The rate of heat transfer to these horizontal tubes depend on the mechanism of bubble and particle movement around the periphery of the tubes. The hydro-dynamic character of the bed adjacent to the tube directly governs the local heat transfer coefficient qualitatively and quantitatively. A thorough knowledge of the components of local heat transfer coefficients will be quite useful for the design optimization of the tubes used in fluidized bed boilers.

A significant number of investigations have been carried out in the past in cold beds with the tube surfaces acting as the heat source. Cherrington et.al [1][ε] conducted experiments to study the heat transfer coefficients around the periphery of a 2 inch diameter tube, with 300μ and 1000μ spherical glass beads with a blend of limestone in an 8 inch circular column at atmospheric temperature and pressure. They observed the highest rate of heat transfer at the 90/270° positions of the tube for low fluidization velocities. At higher velocities the point of maximum heat transfer shifted to the 45/315° position.

Newby and Keairns [2] conducted experiments in a rectangular-vessel of 37cm x 15cm cross section. The bed consisted of magnesia particles of 80μ diameter at a low temperature (< 200°C) fluidized by air. The heater tubes were 3.18 cm in diameter and water tubes were 1.59 cm in diameter located with their axes in the transverse direction. The measured heat transfer coefficients were higher at the top and sides of the tubes.

Berg and Basakakov [3] studied the distribution of the local heat transfer coefficient around the circumference of a horizontal hollow cylinder of low thermal conductivity located in a bed of electrocorundum particles of diameter 60, 100 and 320μ. Air at room temperature was used as the fluidizing medium and the tube was heated electrically. They measured the local temperature around the periphery of the tube and calculated the corresponding heat transfer coefficient. Minimum values were obtained at the lower and upper generatrices of the cylinder. The variation of local heat transfer coefficient was sharply pronounced at lower velocities. Increase in fluidization velocity resulted in an increase of the heat transfer coefficient at the upper generatrix. Further, the variation of the heat transfer coefficient around the circumference was more uniform in a bed of coarse particles.

Selzer and Thomson [4] conducted experiments to obtain simultaneous measurements of the instantaneous heat transfer rates as well as the bubble dynamics at internal heat transfer surfaces in a thin fluidized bed with particles of glass spheres of 230μ and 470μ diameter. A 1.2 cm horizontal tube was located in the bed and the temperatures of the tube surface were measured at four points and was used for calculating the local heat transfer coefficient. They observed lower heat transfer coefficients at the top of the tube for low fluidization velocities. Higher values of heat transfer coefficients were observed for smaller particles.

Gelperin et.al [5] measured the heat transfer profile around a horizontal tube immersed in a bed of particles fluidized at 1.45 times the minimum fluidization velocity and reported nearly equal heat transfer coefficients at the upstream and downstream faces of the tube but found values 75 percent higher at the sides. But studies conducted at CRE [5] on the 3 ft square cold rig showed little significant variation in the bed tube heat transfer coefficient around the tube

---

[ε]Numbers in square brackets denote references at the end of the paper

circumference. In particular, the results showed no consistent tendency for the sides of the tubes to give higher values than the upper and lower surfaces.

The authors have earlier reported [6] the variation of surface temperature and total heat transfer coefficient around a 60 mm outer diameter horizontal steel tube immersed in a 300 mm square fluidized bed combustor. At a bed temperature of 700°C, the local surface temperature was found to vary by 20 to 33 percent, and the local total heat transfer coefficient by 150 percent at low fluidizing velocities. As the velocity was increased, the point of maximum temperature and heat transfer moved to the sides. Further, the deviation of the local heat transfer coefficient from the mean value was found to decrease substantially to about 60 percent.

As the bed temperature in most of these cases were quite low, there was no study of the radiative contribution to the total heat transfer.

The radiative contribution to the total heat transfer coefficient to the wall surface in a fluidized bed combustor was investigated by Vedamurthy and Sastri [7,8]. They observed that the radiative component varies from 20 to 40 percent at bed temperatures of 750 to 1050°C and particle sizes of -6.3 to 3.15 mm.

Prabir Basu [9] studied the effect of radiation on heat transfer to 6.5 mm copper tubes located in a fluidized bed of sand and coal particles. He observed that the radiative contribution was of the order of 5 to 10 percent of the total heat transfer at temperatures of 800 to 900°C.

Thus it can be seen that there is very meagre data available about the contribution of radiation to the total heat transfer coefficient in a fluidized bed coal combustor. Further, the local variation of the radiative and total heat transfer coefficients in a fluidized bed coal combustor have not been adequately studied. Hence, in the present work, an investigation of these variations have been carried out.

EXPERIMENTAL SET-UP

The experimental unit consisted of a 300 mm square water jacketed coal combustor as shown in Fig.1. The air distributor was a perforated plate of 3 mm thick and having an open area of 19 percent. The height of the bed was 310 mm and a free board height of 700 mm. was maintained to minimise elutriation of the particles in the bed. A radiometer and a fluxmeter were fabricated to measure the radiative and the total heat fluxes. These instruments were mounted flush with the outer surface of a 60 mm outer diameter steel tube as shown in Figs.2 and 3.

In the radiometer, a thermistor located in a chamber was used as the sensing element. A quartz glass plate was used to filter the incident conductive and convective heat fluxes. The thermister chamber was cooled by water at 40°C circulated by a thermostat pump.

A steel plug was used as the sensing element in the flux meter. A differential thermocouple was fixed to the ends of the sensing plug. One end of the plug was exposed to the combustor, while the other was cooled by water at 40°C. These meters were calibrated employing a hohlraum as the standard source of heat. The surface temperature of the tube was measured by a copper constantan thermocouple. The circumferential movement of the tube with the meters was caused by an indexing arrangement in steps of 30°.

RESULTS AND DISCUSSION

The experimentally observed circumferential variation of the ratio of the local total heat transfer coefficients to their mean values of fluidizing velocities of 0.87, 1.14, 1.43 and 1.7 m/s and for a particle size of -6mm at the bed temperature of 750°C are shown in Fig.4. It is found that the maximum value of the total heat transfer coefficient occurs at the bottom of the tube for the lowest fluidizing velocity of 0.87 m/s. As the velocity was increased, the point of occurrence of the maximum coefficient was gradually shifted upwards along the sides of the tube. Further, the heat transfer coefficient at the top of the tube continuously increases with the velocity. This may be due to the increased 'particles replacement rate' at the sides and top of the tube at higher velocities.

The variation of the ratio of the local radiative heat transfer coefficient to their mean values with fluidizing velocities for corresponding bed parameters are shown in Fig.5. It is observed that at the lower half of the tube the radiative contribution initially increases as the fluidizing velocity is increased. But, after a certain critical velocity, any further increase in velocity results in a decrease of the radiative coefficient. This phenomenon may be the result of the opposing influences of the fluidizing velocity on the residence time of

the emulsion phase and the volume of the bubble phase.

The variation of the local values of the total and radiative coefficients for fluidizing velocities of 0.87 and 1.7 m/s and particle size of -6 mm at the bed temperature of 750°C are shown in Fig.6. It is found that radiation contributes about 35 percent of the total heat transfer to the tube surface.

The variation of the average values of the total and radiative coefficients with fluidizing velocity are shown in Fig.7. It is seen that while there is a significant variation in the total coefficient with velocity, the variation of the radiative coefficient is only marginal at higher velocities. Further, the radiative coefficient reaches a maximum at a velocity of about 1.1 m/s presumably due to the causes mentioned earlier.

The variation of ratio of the local total heat transfer coefficients to their mean values for particle sizes of -6 mm and -4 mm for a fluidizing velocity of 1.7 m/sec and a bed temperature of 750°C are shown in Fig.8. It is found that there is a marginal increase of the total heat transfer coefficient as the particle size decreases.

The variation of the ratio of the local total heat transfer coefficients to their mean values are shown in Fig.8, for particles sizes of -6 mm and -4 mm at the bed temperature of 750°C. It is seen that there is only a marginal difference in the circumferential variation of the local total heat transfer coefficient for the two particle sizes. But there is a significant effect of the particle size on the local radiative coefficients as seen from Fig.9. It is found that at a particle size of -4 mm, the maximum contribution of radiation is at the bottom of the tube. But as the particle size increases, the maximum contribution shifts to the sides. This may be due to the fact that at smaller particle sizes, the fluidization is better resulting in a better particle mixing and break up of the wake region near the bottom surface.

The circumferential variation of the total and radiative heat transfer coefficients at the bed temperature of 750°C and fluidizing velocity of 1.7 m/s for the particle sizes of -6 mm and -4 mm are shown in Fig.10. It is found that the variation in particle size has opposite effects on the total and radiative heat transfer coefficients. An increase in particle size increases the total coefficient and decreases the radiative coefficient just as in the case of bed wall heat transfer as reported by Vedamurthy and Sastri [8].

CONCLUSIONS

From the experimental investigations reported in the foregoing it is found that radiation contributes about 35 percent of the total heat transfer to a horizontal tube embedded in a fluidized bed combustor. The local values of the radiative and total coefficients vary by 40 to 60 percent and 30 to 90 percent respectively from their mean values. The variation of particle size has opposite effects on the total and radiative coefficients. An increase in particle size increases the radiative contribution but decreases the total coefficient.

ACKNOWLEDGEMENT

The assistance provided by the academic and technical staff of the Central Workshops and Heat Power Engineering Laboratories of the College of Engineering Guindy, Madras, India, is gratefully acknowledged.

REFERENCES

1. Cherrington, D.C., Golan, L.P., and Hermitt, F.G. 'Industrial Application of Fluidized Bed Combustion - Single Tube Heat Transfer Studies, Proc.Fifth International Conference on Fluidized Bed Combustion, Vol.III, pp 184-209, 1977
2. Newby, R.A. and Keairns, D.L. 'Fluidized Bed Heat Transfer between Parallel Horizontal Tube Bundles', Fluidization Cambridge University Press, pp 320-326 1978
3. Berg, B.V. and Baskakov, A.P. 'Investigation of Local Heat Transfer between a fixed horizontal cylinder and a fluidized bed', Int.Chem.Engg. Vol.14, No.3, pp 440-443, July 1974
4. Selzer, V.W. and Thomson, W.J., 'Fluidized Bed Heat Transfer the Packet theory Revisited', A.I.Ch.E.Sym.Series No. 161, Vol.73, pp 29-37, 1979
5. Skinner, D.G. 'The Fluidized Combustion of Coal', National Coal Board, London, pp 74-75, 1970
6. Vadivel, R and Vedamurthy, V.N. 'Experimental Investigation of Surface Temperature and Heat Transfer Coefficient around an Embedded Tube in a Fluidized Bed Combustor', Vol.I, pp 277-282, Proc. Fifth National Heat and Mass Transfer Conf. Hyderabad, India, 1980

7. Vedamurthy, V.N. and Sastri, V.M.K. 'An Analysis of the Conductive and Radiative Heat Transfer to the walls of Fluidized Bed Combustors', Int.J. Heat and Mass Transfer, Vol.17, No.1, pp 1-9, 1974

8. Idem, 'An Experimental Study of the Influence of Bed Parameters on Heat Transfer in a Fluidized Bed Combustor' Future Energy Production Systems, Vol.II, pp 589-597, Academic Press, 1976

9. Prabir Basu, 'Bed-to-wall Heat Transfer in a Fluidized Bed Coal Combustor' A.I.Ch.E.Sym.Series No.176, Vol.74, pp 187-193, 1978

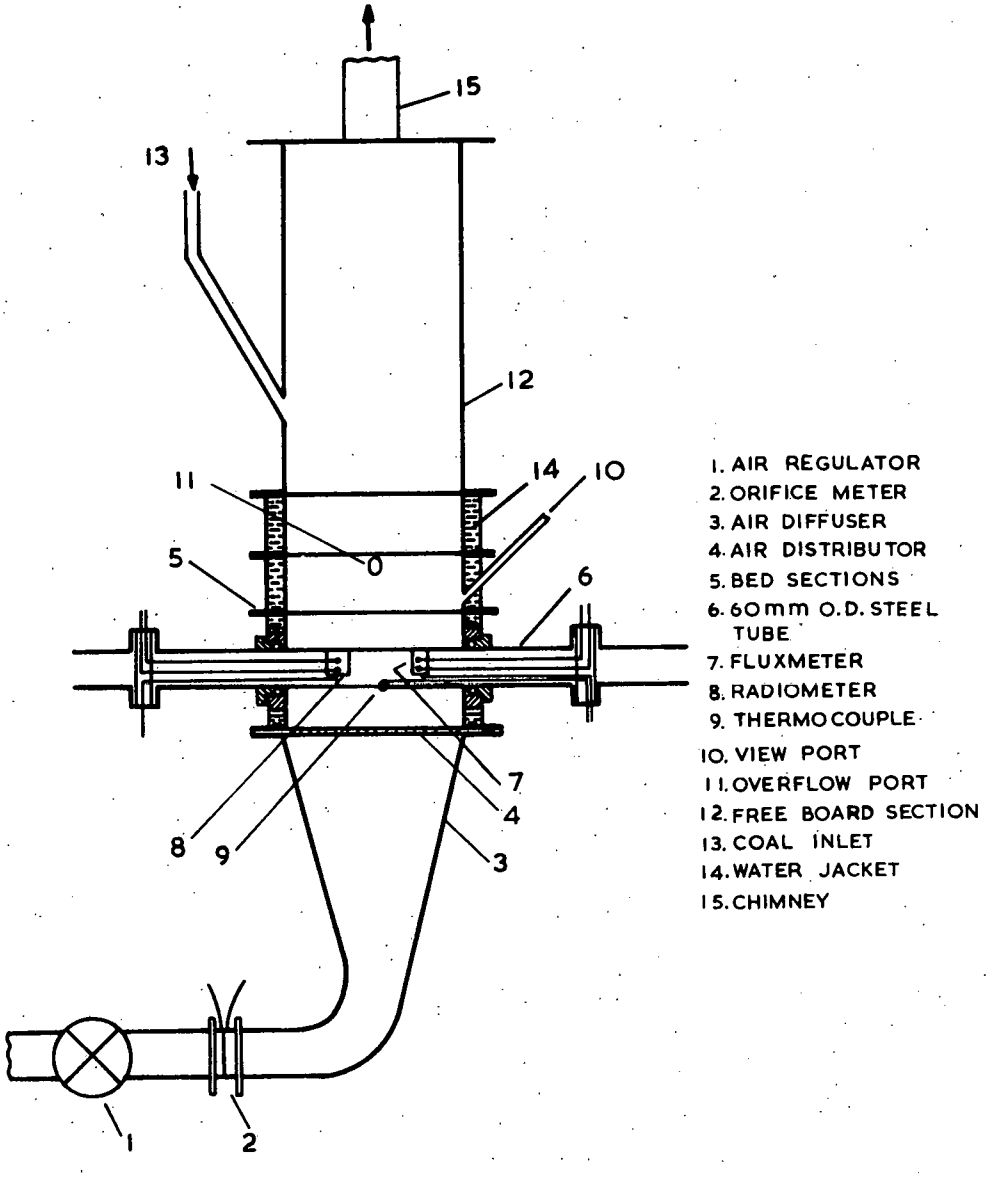

FIG. 1. EXPERIMENTAL SET-UP

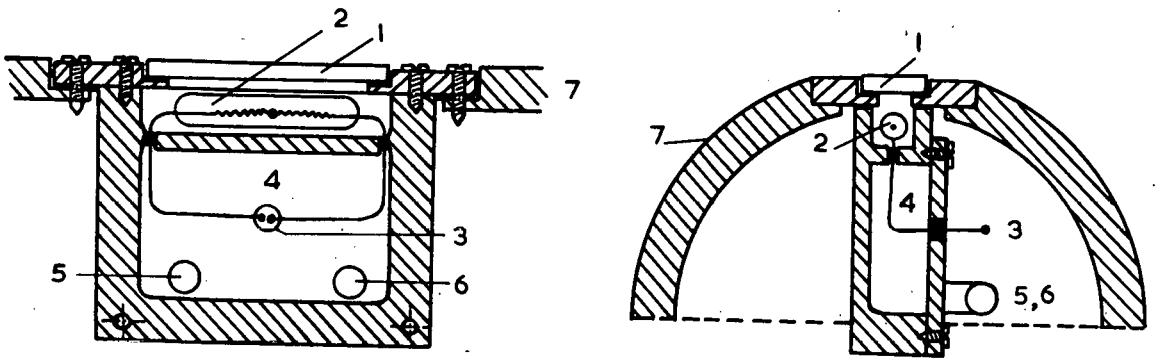

1. QUARTZ PLATE
2. THERMISTOR
3. THERMISTOR LEAD POINTS
4. WATER BATH
5. WATER INLET
6. WATER OUTLET
7. 60mm O.D. STEEL TUBE

FIG. 2. RADIOMETER

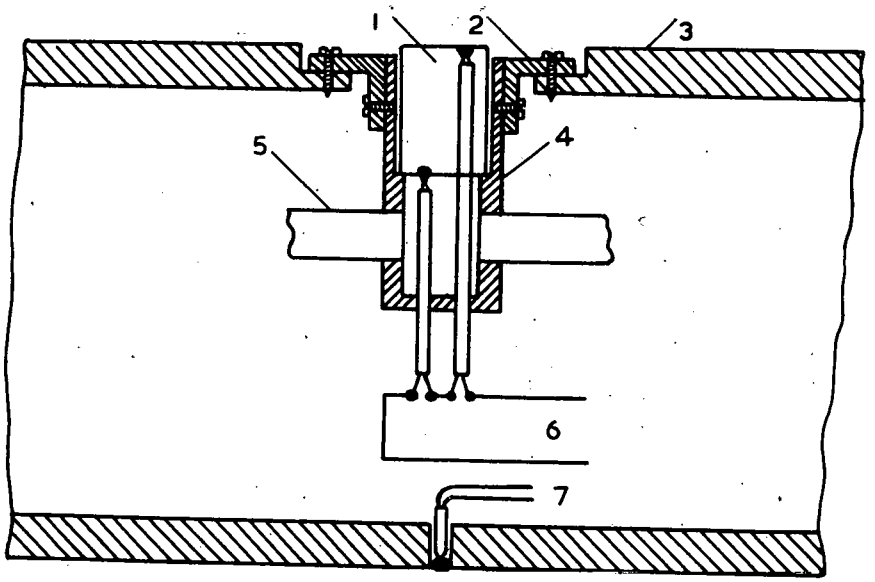

1. STEEL SENSING PLUG
2. COLLAR FOR MOUNTING
3. 60mm O.D. STEEL TUBE
4. BRASS CASING
5. WATER LINE
6. DIFFERENTIAL THERMO COUPLE
7. SURFACE TEMP. THERMO COUPLE

FIG. 3. FLUXMETER

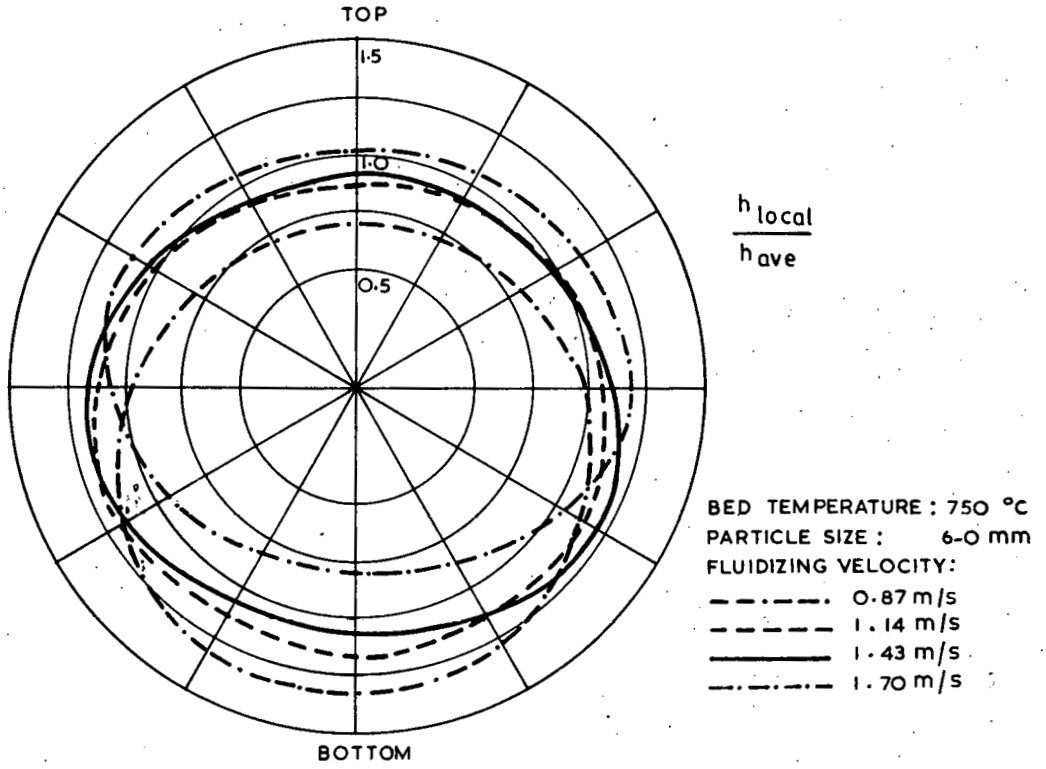

FIG. 4. VARIATION OF LOCAL TOTAL HEAT TRANSFER COEFFICIENT

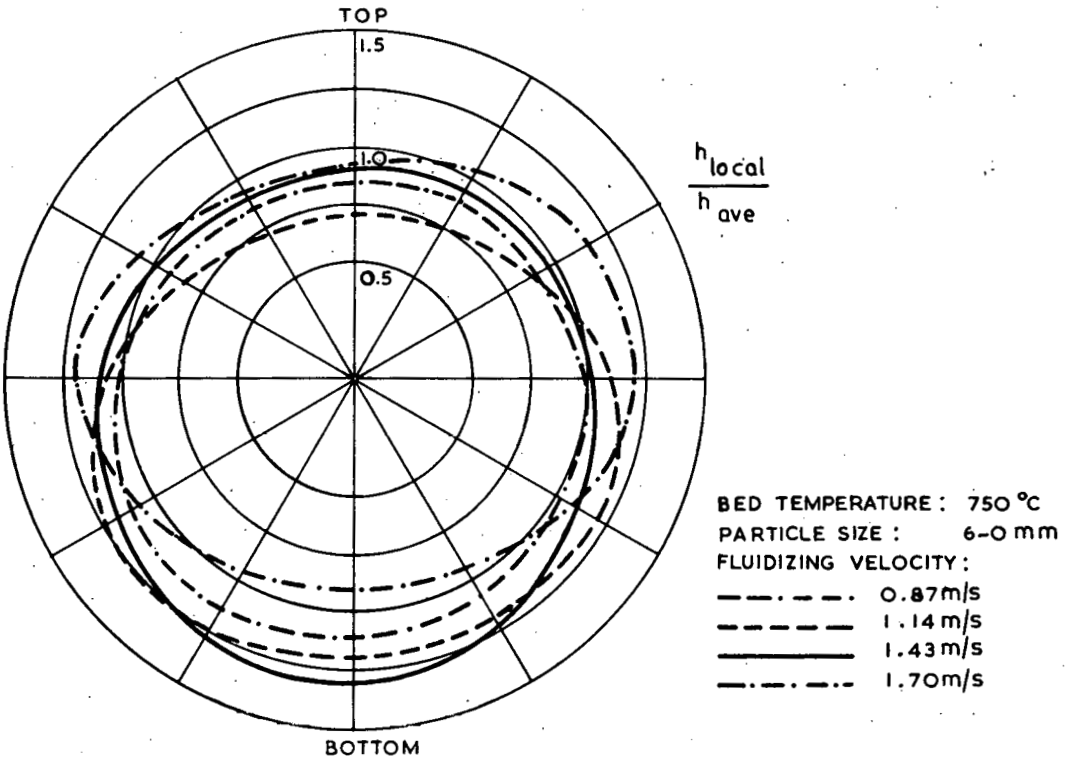

FIG. 5. VARIATION OF LOCAL RADIATIVE HEAT TRANSFER COEFFICIENT

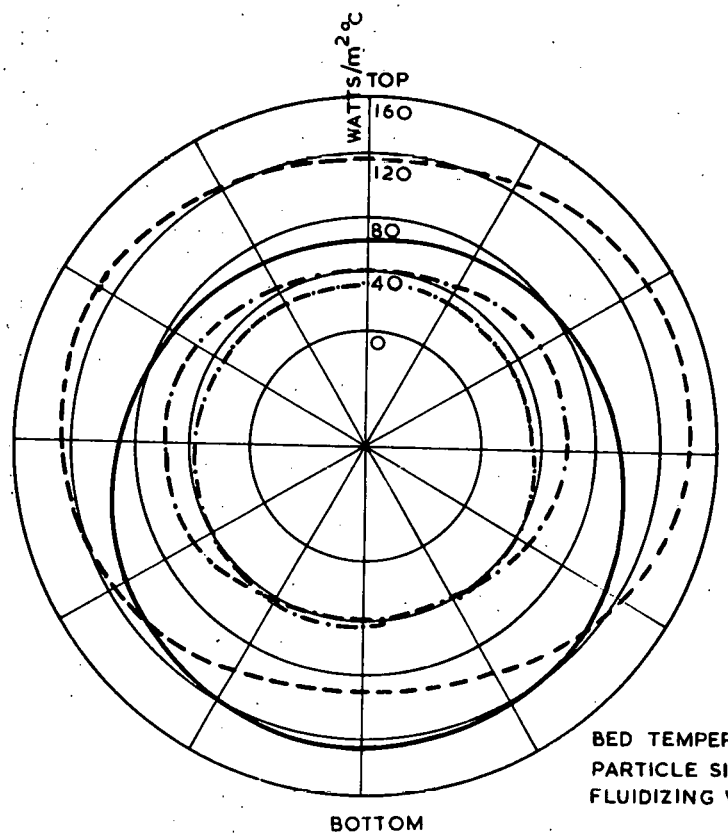

FIG. 6. VARIATION OF TOTAL AND RADIATIVE HEAT TRANSFER COEFFICIENTS

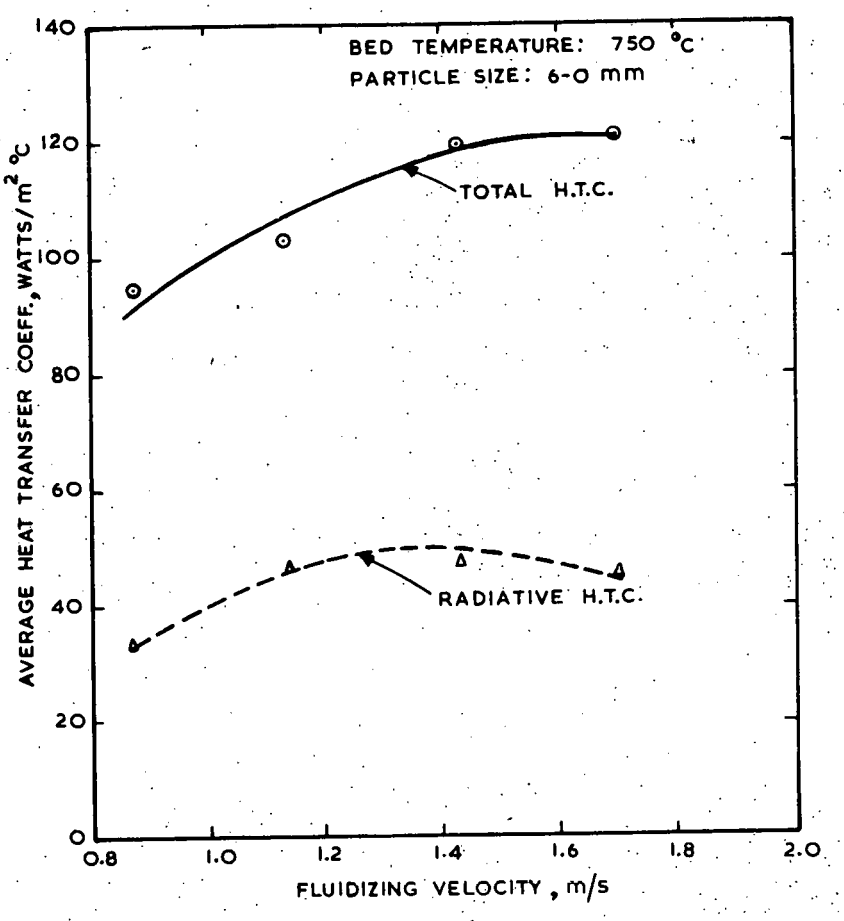

FIG. 7. AVERAGE HEAT TRANSFER COEFFICIENTS WITH FLUIDIZING VELOCITY

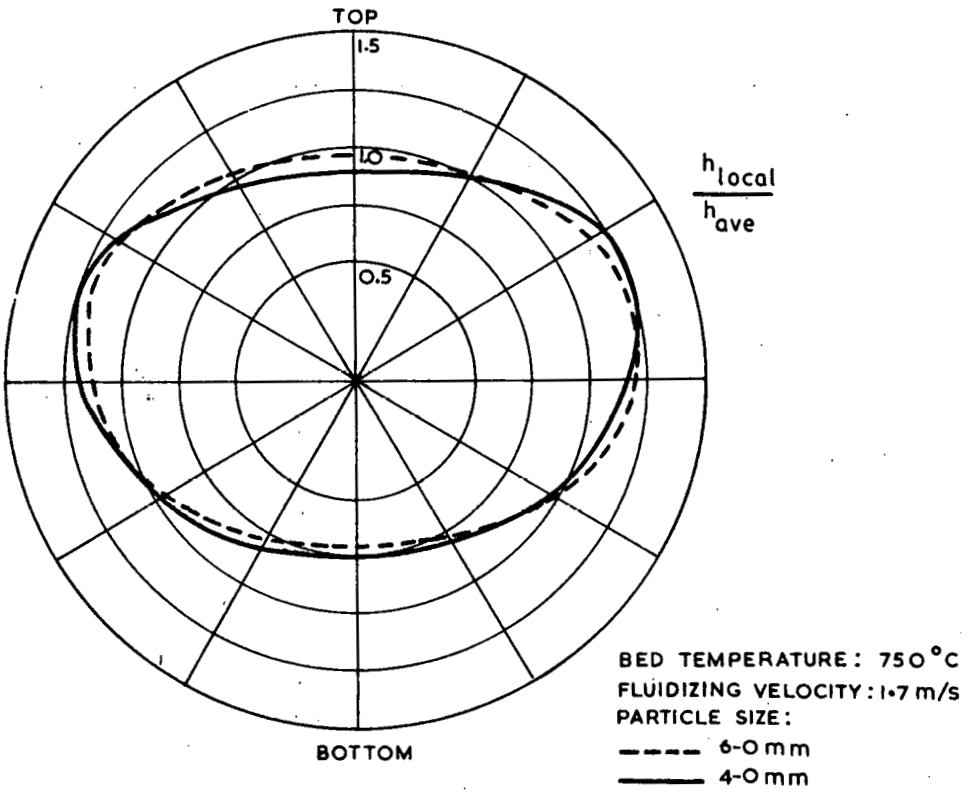

FIG. 8. VARIATION OF LOCAL TOTAL HEAT TRANSFER COEFFICIENT

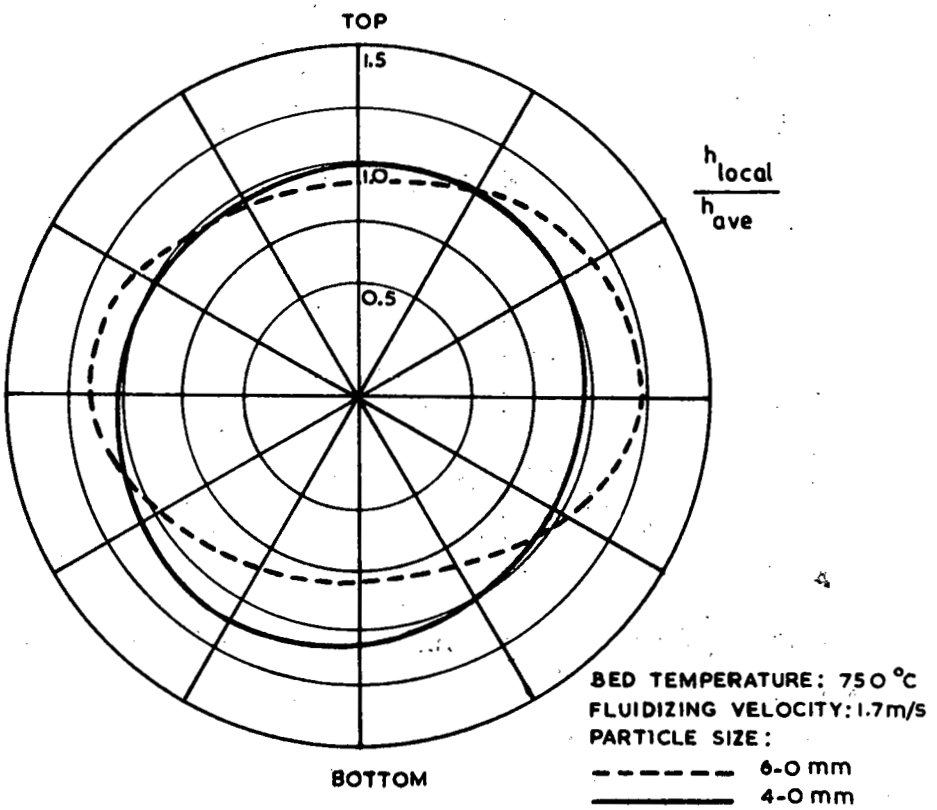

FIG. 9. VARIATION OF LOCAL RADIATIVE HEAT TRANSFER COEFFICIENT

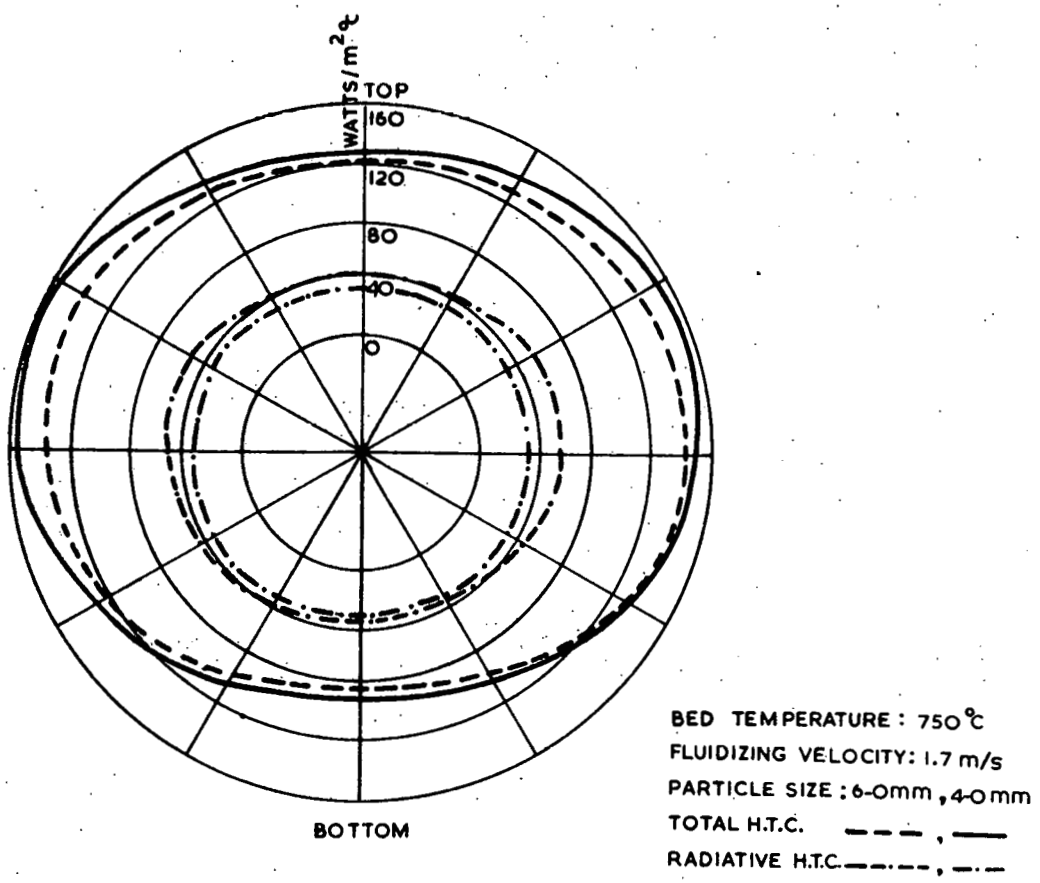

FIG. 10. VARIATION OF TOTAL AND RADIATIVE HEAT TRANSFER COEFFICIENTS

ABSTRACT

Experiments were conducted in a 300mm square, water jacketed coal combustor to determine the influence of fluidizing velocity and particle size on the local radiative and total heat transfer coefficients around an embedded, horizontal, 60 mm outer diameter steel tube at a bed temperature of 750°C. Specially designed instruments located in the mid section of the tube were used for monitoring the radiative and total heat fluxes. The circumferential movement of the tube with the fluxmeter and radiometer assembly was caused by an indexing arrangement in steps of 30°.

The variation of the local total heat transfer coefficient and its radiative component are depicted on polar charts. It is found that the radiation contribution was about 35 percent of the total heat transfer to a horizontal tube embedded in a fluidized bed combustor. The local values of the radiative and total coefficients vary by 40 to 60 percent and 30 to 90 percent respectively from their mean values. The variation in particle size has opposite effects on the total and radiative heat transfer coefficients.

Questions to V. N. Vedamurthy:

Q: (Participant not identified)

Did you take into account that the radiation is reflected at the tube?

A: No. The calibration done on the instuments made them applicable to the whole bed situation.

Q: Leon Glicksman, MIT

Am I correct that the majority of the tube surface was not cooled? Only the portion where you had your flux meter was cooled?

A: Water was circulated to cool the entire tube.

Q: (Participant not identified)

Did you compare your radiation measurements with Steven Bolt's constant with black body radiation?

A: No, they were not compared.

Q: (Participant not identified)

Was the change in transmissivity of the quartz window due to scratching? An alternative to quartz would be sapphire, I think.

A: We did not observe any scratches. There was some pitting.

Q: (Participant not identified)

Have you studied the different gas compositions and their affect on radiation?

A: No.

HIGH TEMPERATURE HEAT TRANSFER STUDIES IN A TUBE FILLED BED

L. P. Golan, G. V. LaLonde, S. C. Weiner

Exxon Research and Engineering Company

Introduction

Several other investigators have conducted experiments where the heat transfer coefficient on a horizontal tube immersed in a fluidized bed was measured. A number of correlations have been proposed as predictive tools, but the results of different correlations give conflicting trends. References (1,2,3,4,5) review these correlations. Many previous studies have limited applicability to industrial applications in that fine or narrow particle range bed material and/or small tube diameters have been used. Industrial heaters require large tubes ranging in size up to six inches in diameter. In addition, the use of large particle bed material with a wide particle size distribution appears likely. This is especially true for fluidized bed combustors where attrition of the limestone will naturally cause a wide particle size distributing to occur.

Large tube heat transfer data is required for these industrial applications. Average and local heat transfer coefficient profiles are required to properly determine the heater tube surface requirements and tube materials. In addition, knowledge of the peak coefficients is needed to determine the effect of the high heat fluxes on process conditions.

This paper presents experimentally determined average and local heat transfer coefficients obtained in a fluidized bed of sulphated dolomite over a series of bed temperatures ($525 \geq T_{bed} \leq 1200^{o}F$) and velocities ($3 \geq V_{bed} \leq 10$). The process tube size was four inches. Data are presented for in-bed as well as freeboard tubes. The tests were conducted without the direct combustion of fuel in the bed so that fuel mixing would not influence the heat transfer measurements. Heat to the fluidized bed was provided through an external combustor where propane was burned and the hot combustion gases were used as the fluidization medium.

Description of the Test Apparatus

A schematic flow sheet showing the principal components of the 12 MBtu/hr combustion system is shown on Figure 1. The heat flux unit was divided into eight identifiable subsystems; these are: 1) air supply and metering system, 2) propane supply system, 3) precombustor and fluidized bed test zone, 4) heat removal system, 5)heat transfer coils, 6) cyclones, 7) flue gas cooler, and 8) dust filter.

The air supply system consisted of a 10,000 scfm centrifugal air blower driven by a 700 hp electric motor. The air was metered in a 10 inch diameter schedule 20 carbon steel orifice meter run. The straight run was 25'0" upstream and 6'0" downstream of the orifice plate. The capacity of the metering system was 3467 cfm when metered at $60^{o}F$ and 14.7 psia.

The propane fuel was stored in five 1000 gallon above-ground tanks. The liquid propane was vaporized in two parallel connected water bath vaporizers. Each vaporizer was capable of supplying vaporized propane equivalent to 9.17 MBtu/hr to the single propane burner located in the precombustor.

The air and vaporized propane were mixed in the burner and combustion occurred in the horizontal precombustor chamber. The burner and precombustor were designed to fire propane at a maximum combustion gas temperature of $2600^{o}F$. The hot flue gases exited the precombustor through a six-inch thick refractory grid with integral metal fibers. The grid holes were 0.25 inches in diameter arranged on a 1.25 inch square pitch. The hot flue gas was used as the fluidization medium. The bed cross section was approximately 2 feet by 4.8 feet yielding a bed cross-sectional area of 9.7 ft^2. After passing through the test zone the hot flue gas and entrained solids passed through two parallel cyclones. The captured solids were recycled to the bed at a point just above the grid via two external diplegs.

The heat transfer coil was the configuration determined in the Two-Dimensional Flow Visualization Studies (6) to be an acceptable bundle for process heater applications. The tube bundle was manufactured from 4 inch diameter tubes which were arranged on a 2 diameter equilateral spacing (Figure 2). The bed width permitted 6 four inch tubes to be positioned per row. The tube bundle was three tube rows high with one additional row located in the free board zone. The tube material was 304 stainless steel. Water was used as the process fluid. Vortex shed meters and manual control valves were located on the inlet side of each pass to provide for flow rate measurement and control. Total water flow rates up to 500 GPM were possible; however, flow rates in the range of 240 to 320 GPM were common during testing.

Only straight pipe lengths were exposed to the fluidized bed. All U-bends were buried in the refractory walls. Coil inlet and outlet water temperature measurements were made as well as individual pass temperature differential measurements of the process water temperature on selected tube passes.

In addition, coils one, two, and three were instrumented with peripheral tube wall thermocouples. These couples were located in the third tube pass of each coil (indicated C on Figure 2). In order to position the thermocouples near the tube center, the pipe was first cut in half, then eight shallow holes (1/16" diameter) were drilled on a common cross section of the inside tube wall at 45° intervals. A thermocouple was placed in each hole and secured by hammering (peening) the tube metal surrounding the hole with a ball-peen hammer. This procedure wedged the thermocouples in place. No other means were used to secure the thermocouples. The thermocouples were type k, 1/16" O.D., six feet long, with grounded junctions. The thermocouple sheaths were type 316ss with MgO insulation.

The bed temperature was determined from six separate measurements. Four temperature measurements were made in a horizontal plane approximately ten inches above the grid. These thermocouples were centrally located one per quadrant of grid area. The final two temperatures were 15 and 23.5 inches above the third horizontal tube row (see Figure 2).

All flows and temperatures were recorded on a combination of trend recorders for visual display, digital temperature indicators for instant access, and on a data logger for permanent record.

Bed Material

A full charge of bed material weighed 1800 pounds. This charge resulted in a bed with a slumped height equal to the distance between the grid and the first tube row centerline. The initial 1800 pound charge consisted of 400 pounds of Crestite limestone and 1400 pounds of sulfated Pfizer dolomite. The particle size distribution for these materials is shown on Figure 3 as is the size distribution for a blend of particles used in the ambient temperature tests (7).

The 400 pound Crestite charge formed a base approximately four inches deep upon which the sulfated dolomite was loaded. The Crestite material was large enough so that it did not bleed through the grid holes and fall into the precombustor. After the Crestite charge was in the test chamber, the bed was fluffed to even out the distribution of material. The sulfated Pfizer dolomite was loaded on top of the static Crestite bed.

The Crestite limestone was a locally quarried material that had been selected for use in the ambient temperature Two-Dimensional Flow Visualization Studies (8). It was selected based on its relative hardness and white color. At elevated temperatures the Crestite material disintegrated very rapidly. Therefore, the Crestite was used only as the base material for initial charging purposes. As a test progressed sulfated Pfizer dolomite was added as makeup for attrition losses. The weight of solids collected in the bag filter drum and the bed pressure drop were the indicators used to determine how much bed material need be added to maintain a constant charge of bed material in the test chamber.

Test Conditions and Background Discussion

The nominal values for bed operating conditions during these tests were:

Nominal Bed Temperature °F	Nominal Superficial Velocity, fps
525	3.0, 4.5, 5.5, 6.5
750	3.5, 4.5, 5.0, 5.5, 6.5
975	5.0, 5.5, 6.5, 8.0, 9.0
1200	8.5, 9.0, 9.5

The fluidized bed temperature was varied by increasing or decreasing precombustor temperature. At each temperature level a combination of the combustion constraints (flame out, maximum precombustor temperature) and the minimum fluidization velocity for the particles controlled the test range. For instance, the lowest velocity at a bed temperature of 525°F was limited by minimum fluidization velocity. For the bed particles used in these tests, u_{mf} was approximately two feet per second; therefore, three feet per second or 1.5 u_{mf} was the lowest flow rate selected to yield adequate fluidization. At 6.5 fps and 525°F in the test zone, the precombustor temperature was 895°F with combustion occurring at 800+.% excess air. This condition was near flame out. At the highest bed temperature (1200°F) the velocity range was limited by the air rate necessary to completely burn the fuel and secondly by the air rate required to limit the precombustor temperature to 2500°F, the maximum safe operating temperature for the refractory grid.

Prior to lighting the burner turbulent water flow was started through the heat removal coil. Reynolds numbers ranged between 55,000 and 120,000. After burner light off the precombustor temperature was gradually increased until the bed temperature reached the first temperature plateau of 525°F. These conditions were held for a period of four to five hours to assure that all refractory had reached equilibrium. If necessary during the warm up period material would be added to maintain bed inventory. Test data were collected only during periods of equilibrium as determined by steady air and water flow rates and a constant bed temperature.

After collecting the first data set the fluidization velocity was increased and the propane rate adjusted to reestablish the 525°F bed temperature. Since the bed temperature was not changed, a one hour hold period was instituted till the next data set was taken. After collecting the

data at all velocity levels of a given temperature plateau, the bed temperature would be increased gradually. The new temperature plateau would be held for approximately three hours prior to data collection. The velocity would be adjusted as necessary to complete the test matrix. This procedure was followed until the data at all velocity and temperature levels was collected.

Generally, the energy gained by the water flow accounted for 75-85% of the energy lost by the flue gas. Energy losses through the refractory accounted for 1-2% of the energy fired while recycle solids accounted for 10-15%. Accounting for these losses generally closed the energy balance to within 10%. Any large discrepancy in these checks negated the value in a test.

The heat transfer test data was collected when the dolomite bed was in full fluidization. This was defined to occur when the pressure drop across the bed remained essentially constant with increases in fluidization velocity. Under these situations the effect of increased velocity was to increase bed voidage and therefore to increase bed height. The bed pressure drop can be expressed as:

$$\Delta P = (1-\epsilon)\ (\rho_s - \rho_g)\ H\ \frac{g}{gc}$$

where ϵ is the bed voidage, H is the bed height, ρ_s is bed particle density, and ρ_g is the fluidization gas density. In situations where ΔP is constant, ϵ and H must increase accordingly.

The bed voidage calculations indicated that during the conditions of full fluidization, the heat transfer tube 3c instrumented for the local heat transfer measurements was fully covered by bed material. The static bed voidage for these sulfated dolomite particles was approximately 0.34 while the minimum fluidization voidage (2) was estimated from the expression

$$\frac{1}{\phi_s\ \epsilon_{mf}^3} = 10$$

ϕ_s = particle sphericity = 0.8

Void fractions at fluidization velocities above minimum fluidization were estimated from the results of the bed expansion experiments performed during the ambient temperature two dimensional flow modelling (8). For the velocity range covered in the heat transfer experiments tube 3c was always immersed in the fluidized bed zone. Heat transfer tube 1c was not located within the dense bed zone during any fluidization conditions; therefore, this tube was characterized as a freeboard tube.

The heat transfer results include:

In-bed tube 3c

+ average outside heat transfer coefficient
+ radiation effect on the heat transfer coefficient
+ maldistribution

Freeboard tube 1c

+ average outside heat transfer coefficient
+ radiation effect

The outside heat transfer coefficients were calculated from measurement of the inside tube wall temperature and bed temperature. It was assumed that all heat transfer occurred in a one dimensional manner across the tube wall. The effect of circumferential conduction in the tube wall was not considered in the calculations. In addition the Dittus Boelter equation was used to predict the water side heat transfer coefficient.

Heat Transfer Results - In-bed tube 3c

The total outside heat transfer coefficient for tube c coil 3 is shown on Figure 4. This heat transfer coefficient was evaluated by numerically averaging the eight local heat transfer coefficients calculated for this tube. The results on Figure 4 are shown plotted against the basic operating variables of bed temperature and superficial velocity. Interestingly, the heat transfer coefficient displayed little dependence on the superficial velocity. This nondependence of the average heat transfer coefficient on velocity for totally immersed tubes was also observed in the ambient temperature heat transfer studies (6) within this velocity range. However, the heat transfer coefficients measured here did display a significant increase in value with increased bed temperatures.

Data at 525°F and 750°F bed temperature were retaken several weeks apart with different charges of the dolomite bed material. These two sets of data are plotted on Figure 4. The conclusion reached from these fifteen tests is that the test results are reproduceable and that bed temperature is important in determining the value of the heat transfer coefficient.

From Figure 4 it can be seen that at identical superficial velocities the heat transfer coefficient increased as the bed temperature increased. The only difference between tests was the flue gas temperature. This in turn resulted in a variation of the thermal properties of the flue gas, hotter dolomite particles, and possibly a different radiation interaction between the bed and tube surface. These effects were briefly

examined. It was assumed that the sum of the convective heat transfer coefficient (h_c) and the radiative heat transfer coefficient (h_r) equalled the measured total heat transfer coefficient. Therefore:

$$h_o = h_c + h_r$$

where

$$h_r = \frac{\delta \sigma \ (T_{bed}^4 - T_{wall}^4)}{T_{bed} - T_{wall}}$$

and σ = stefan Boltzman constant

T_{bed} = fluidized bed bulk temperature

T_{wall} = temperature of the tube surface

δ = emissivity of the 304ss tubes = 0.4

The radiative heat transfer coefficient was evaluated at each peripheral tube wall position and subtracted from the total outside heat transfer coefficient, h_o, to arrive at the convective heat transfer value. The radiative heat transfer coefficients calculated in this manner were approximately h_r = 1.50 Btu/hr ft^2°F at 525°F, 2.3 at 725°F, 4.0 at 975°F and 6.0 at 1200°F.

Calculating the radiative heat transfer coefficient in this manner assumed that the bed particles were in rapid motion and not in contact with the tube surface for "long" periods of time. A "long" residence time at the tube surface would have the effect of cooling the bed particles substantially below the bed temperature and, therefore, reducing the radiant heat transfer effect. Considering the large particles used in these experiments and the visual observations (9) performed as part of the two dimensional flow studies, "long" residence times did not appear to be reasonable. This is especially true for the lower 180° of the tube surface (gas shrouded zone) and the 45° positions (surf line).

The convective heat transfer coefficient evaluated by subtracting h_r from h_o is shown in Figure 5. As can be seen, the difference between the heat transfer coefficients at the various temperature levels has been reduced but the radiation effect did not account for the entire difference. This suggests that the thermal effects of the fluidization media and fluidized solids are also important contributors to the heat transfer coefficient.

Numerous correlations are available for predicting convective heat transfer rates in fluidized beds. Little agreement, however, is seen between these correlations in form or predicted value. The correlations do infer, however, various groupings for the physical variables seen by different investigators as the governing parameters.

A heat transfer correlation proposed by Glicksman (10) is

$$\frac{h_c d_p}{k_g} = (1-\epsilon) \left[9.42 + 0.042 \ Vdp \ (\rho c/k)_g \right]$$

where h_c is the convective heat transfer coefficient, ϵ the void fraction with subscripted g properties referred to the gas phase while p refers to the bed particles. When the bed is composed of a mixture of particles, the representative particle diameter is determined by

$$\frac{1}{dp} = \Sigma \frac{X_i}{d_i}$$

where X_i is the weight fraction of particles with diameter d_i.

The Glicksman equation was developed for a bed of large particles (large is defined as 1 mm or greater). For particles of this size, the time constant for cooling the particles in contact with the heat transfer tube is much greater than the particle replacement time at the tube surface. Therefore, the heat transfer process between bed and tube was considered a steady state process. In addition, it was assumed that little heat transfer occurred on the lower 60° portion of tube surface due to a high void fraction in this zone.

The dominant size of the bed particles used in this series of tests was larger than 1 mm (Figure 3); therefore, the Glicksman equation should be applicable to these tests. The polar heat transfer plots (Figure 7) show that significant heat transfer does occur on the lower 60° portion of tube surface. Therefore, the constants in the proposed equation have been adjusted as suggested by Glicksman to account for this fact. The resulting equation being

$$\frac{h_c d_p}{k_g} = (1-\epsilon) \left[11.2 + 0.05 \ Vdp \ (\rho c/k)_g \right] \quad (A)$$

To compare the trend in heat transfer coefficients predicted by Equation A with those measured in these experiments, two assumptions are necessary. First, it was assumed that the velocity (V) for use in Equation A was the integrated gas velocity within the tube bundle (previously called bundle space velocity, Reference 6). This velocity was shown to be more representative of events occurring within the tube bundle than the superficial velocity. For the tube bundle installed in the test chamber, the bundle space velocity was 1.42 times the superficial velocity. In addition, the void fraction in the vicinity of the tube was not known, therefore a void fraction of zero was assumed. Obviously this is incorrect; however, in this manner a maximum or bounded coefficient could be predicted. With these assumptions, the

heat transfer coefficients calculated using equation A are shown on Figure 6.

Several interesting trends in the predicted heat transfer coefficient are noted in Figure 6. First, the calculated coefficients have a limited dependence on fluidization velocity and secondly, the heat transfer coefficients are definitely bed temperature dependent. Both of these trends were observed in the actual experiment data. Unfortunately, void fraction data were not available at the tube surface so that actual numerical values for the heat transfer coefficient could not be calculated.

If significant numbers of measured heat transfer coefficients were available, the average void fraction could be empirically determined from a ratio of the Equation A and measured heat transfer coefficients. These empirical values could then be correlated with operating parameters such as bed velocity and temperature. In addition, the void fraction within the three zones of particle activity on the tube surface could be calculated and similarly correlated. Insufficient data is now available to pursue this empirical technique.

To advance the predictive ability in fluidized bed heat transfer on a more theoretical level requires a detailed phenomenological understanding of the events occurring at the tube surface. When that understanding is available, it will be possible to develop an accurate equation to predict fluidized bed heat transfer coefficients. For design purposes, however, Figure 5 presents the heat transfer coefficients for large diameter tubes that can be used till this phenomenological understanding is achieved. On Figure 5 the basic design tool of in-bed heat transfer coefficient is expressed as a function of bed temperature and fluidization velocity.

Figure 7 is a polar plot of the local heat transfer coefficients measured on coil 3. One polar plot is shown for each of the four experimental temperature levels. The polar plots show the effect of the three zones of particle activity around the tube surface that were previously observed in the ambient temperature experiments. This includes the gas shrouded region, surf line, and oscillating cap. Polar plots for all tests were generated and these then reduced to a maldistribution plot, Figure 8. The maldistribution was defined as the peak coefficient divided by the tube average coefficient. The peak coefficient used in the evaluation of the maldistribution was the average value between the two peak coefficients. The peak coefficients always occurred at the 45 and 315 degree position (surf line location) and were generally within 10% of each other. The local heat transfer coefficients measured between 90° and 270° (gas shrouded zone) displayed the same symmetry and uniformity observed in the ambient temperature tests. The maldistribution of heat transfer coefficient displayed little dependence on either temperature or fluidization velocity.

Heat Transfer Results - Freeboard Tube 1c

The total average outside heat transfer coefficient for coil one, the freeboard coil, is shown on Figure 9. The calculated convective coefficient ($h_c=h_o-h_r$) for coil one is shown on Figure 10. Throughout the velocity and temperature range of these tests coil one heat transfer coefficients were lower than those measured on coil three. Although the heat transfer profiles were not parallel the freeboard coefficients were approximately 65% of the in-bed coil three coefficients. At all velocities void fractions in excess of 90% occurred near coil one. This reduced particle concentration is believed to contribute to this reduced heat transfer rate.

The high void fractions in the vicinity of the freeboard tube suggests that these coefficients should be similar to those found for tubes located transverse to an air stream. An equation for heat transfer to cylinders positioned in an air stream is (11):

$$\frac{h_c D_o}{k_g} = C\left(\frac{VD_o}{\nu_g}\right)^n$$

where C and n are empirical constants whose numerical value varies with Reynolds number and D_o is the outside diameter of the cylinder. The physical properties of air are all based on the film temperature. This equation was developed for cylinders up to six inches in diameter. In this Reynolds number range between 4,000-40,000, the reported values for C and n are 0.174 and 0.618 respectively.

Figure 10 data have been replotted in Figure 11 as h_cD_o/k_g vs VD_o/ν_g. An "eye ball" curve fit of the data resulted in a correlating line with a slope of 0.59. Because of the closeness of this slope to the non-particle value of 0.618, the non-particle slope of 0.618 was used and the new constant, c, determined. The resultant equation is

$$\frac{h_c D_o}{k_g} = 2.72\left(\frac{VD_o}{\nu_g}\right)^{0.618}$$

The conclusion reached is that the heat transfer coefficient for the freeboard tube shows the same Reynolds number dependence as a tube in an air stream; however, the heat transfer coefficient has been augmented by a factor of 15.

The ambient temperature data for a similar freeboard tube (see Reference 7 for tube 5 particle blend D data) was subsequently plotted on Figure 11. These ambient temperature points are at substantially higher Reynolds numbers than the hot data; however, the correlating line appears to fit rather well. Throughout the Reynolds number range of 3,000-20,000 the freeboard data agree with the correlating line to within $\pm$ 10%.

Concluding Remarks

Continued efforts in developing a phenomenological understanding of the effects occurring on a tube immersed in a fluidized bed will be required before a complete predictive heat transfer equation becomes available. Until that time design tools are required. Figures 4, 8, and 11 provide this needed design tool for heat transfer coefficients on large diameter tubes (4") with a bed of large dolomite particles. These curves are based on the basic design parameters of bed temperature, velocity, particle size, and tube diameter.

Additional data will be collected during the future phase of this program concentrating on the high bed temperature levels and in generating data with coal combustion directly in the bed.

References

1. Zabrodsky, S. S., Hydrodynamics and Heat Transfer in Fluidized Bed, M.I.T. Press, Cambridge, MA. (1966).

2. Botterall, J.S.M., Fluid Bed Heat Transfer, Academic Press, New York, 1975.

3. Saxena, S. C., et al, "Modeling of the Fluidized Bed Combustor with Immersed Tubes", ERDA Quarterly Report No. FE-1787-6, December 1976.

4. Chen, J.C., "Heat Transfer to Tubes in Fluidized Beds", ASME 76-H5-75, National Heat Transfer Conference, St. Louis, MO., (1976).

5. Golan, L.P., et al, "Particle Size Effects on Heat Transfer to Tubes in a Fluidized Bed", Chemical Engineering Progress, Vol. 75, No. 7, pp. 63-72, July 1979.

6. Cherrington, D.C., and Golan, L.P., "Coal Fired Fluidized Bed Process Heater Studies", 43rd Midyear Refining Meeting, American Petroleum Institute, Toronto, Canada, May 1978.

7. Golan, L.P., et al, "Particle Size Effects in Fluidized Bed Combustion", CEP, pp. 63-72, July 1979.

8. Industrial Application Fluidized Bed Combustion Quarterly Report No. 7, DOE Contract EX-76-C-01-2471, Jan-March 1978.

9. Cherrington, D.C., Golan, L.P., et al, "Industrial Application of Fluidized Bed Combustion - Single Tube Heat Transfer Studies", 5th International Conference on Fluidized Bed Combustion, December 1977.

10. Glicksman, L.R., and Decker, N., "Heat Transfer in Fluidized Beds with Large Particles", Department of Mechanical Engineering Report, Massachusetts Institute of Technology, April 1979.

11. Kreith, Frank, "Principles of Heat Transfer 2n ed", International Text Book Company, Scranton, PA. (1966).

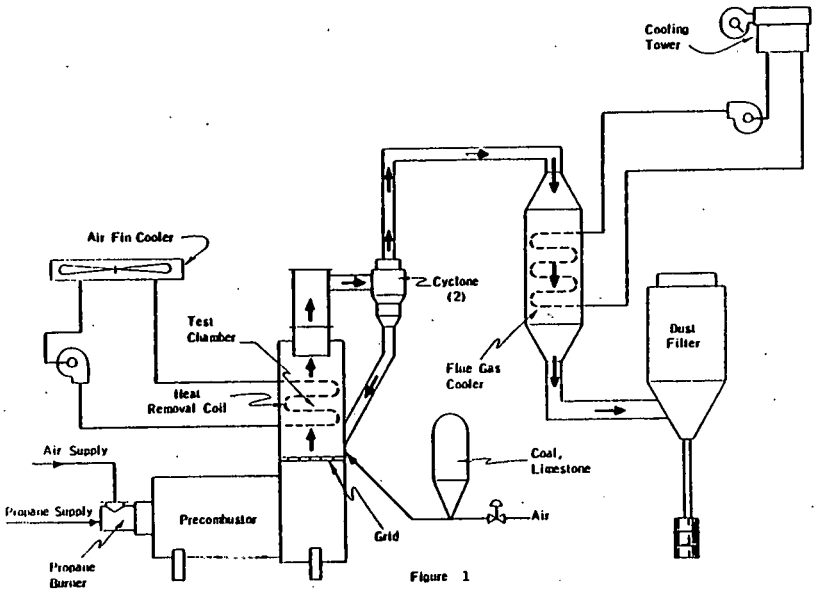

Figure 1

FLOW PLAN
FBC HEAT FLUX UNIT

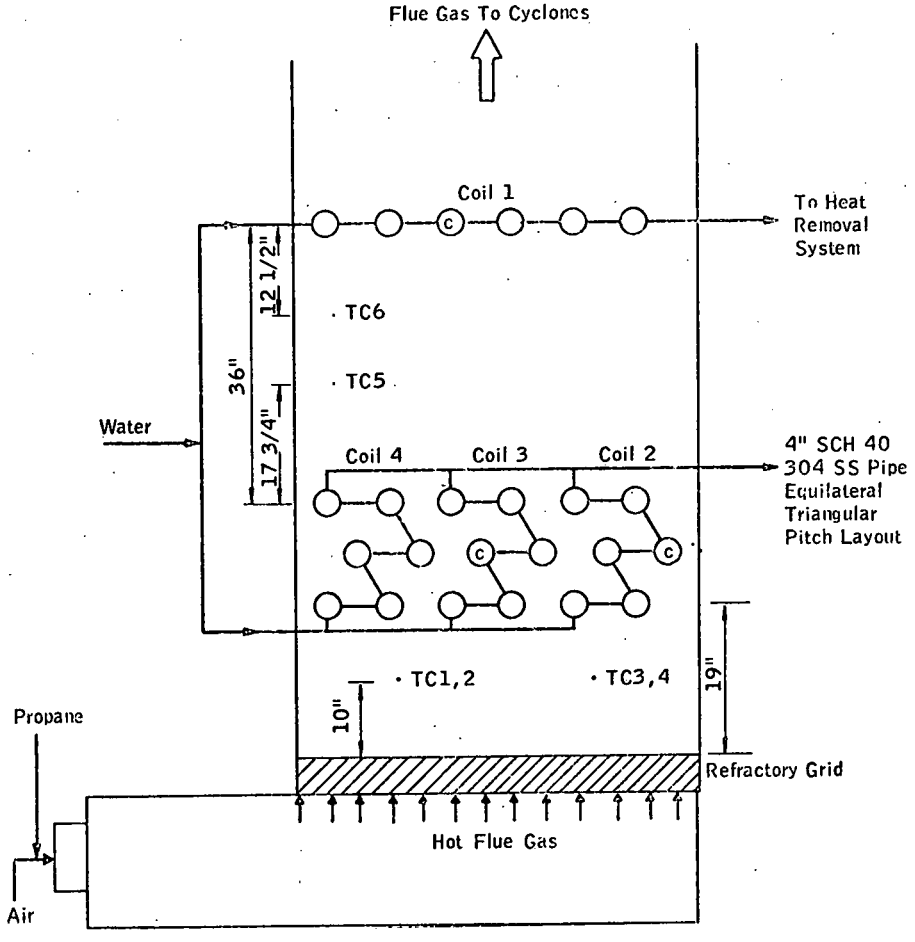

PHYSICAL LAYOUT - HEAT FLUX UNIT TEST CHAMBER

Figure 2

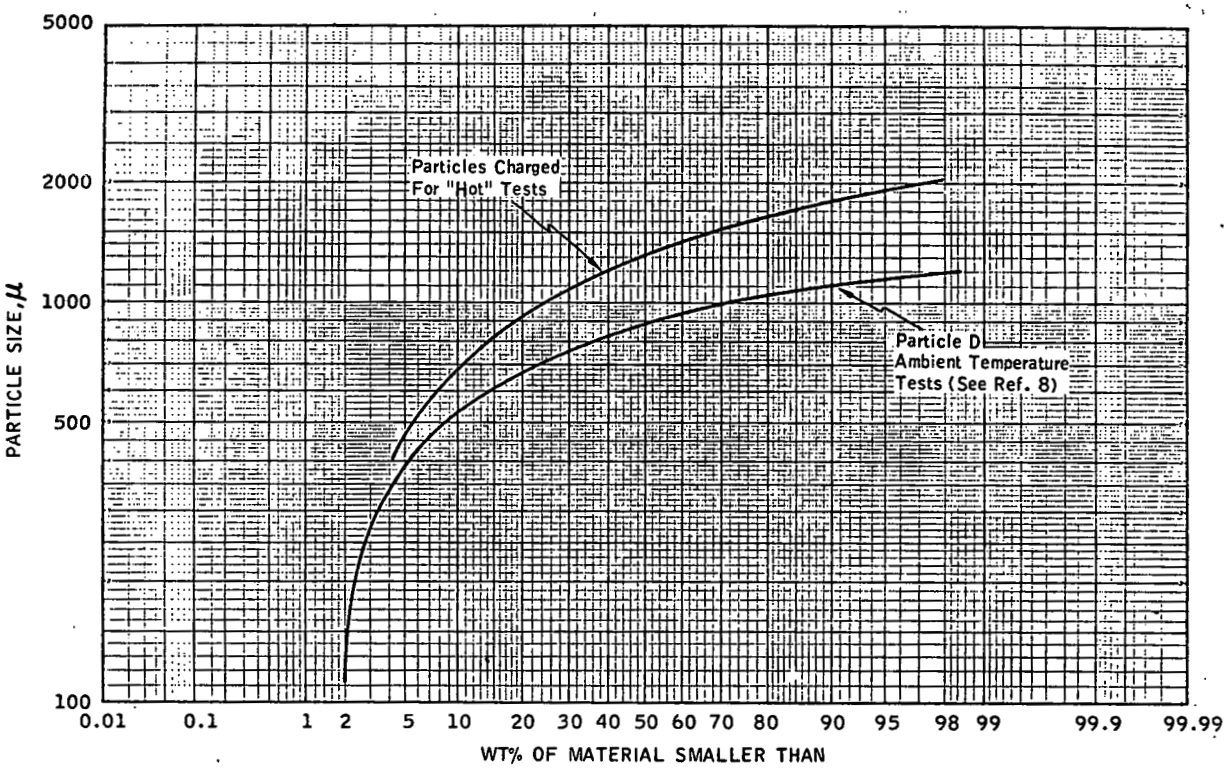

BED MATERIAL PARTICLE SIZE DISTRIBUTION

Figure 3

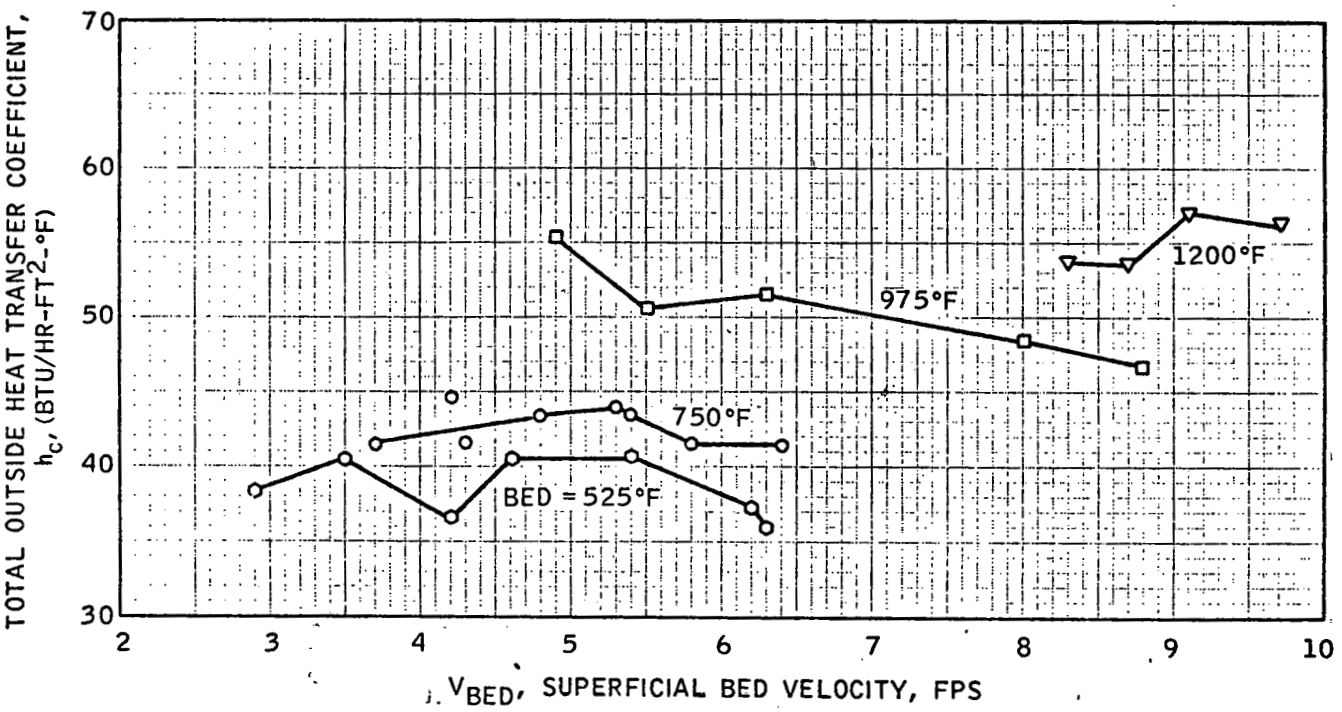

TOTAL OUTSIDE HEAT TRANSFER COEFFICIENT IN-BED TUBE 3C

Figure 4

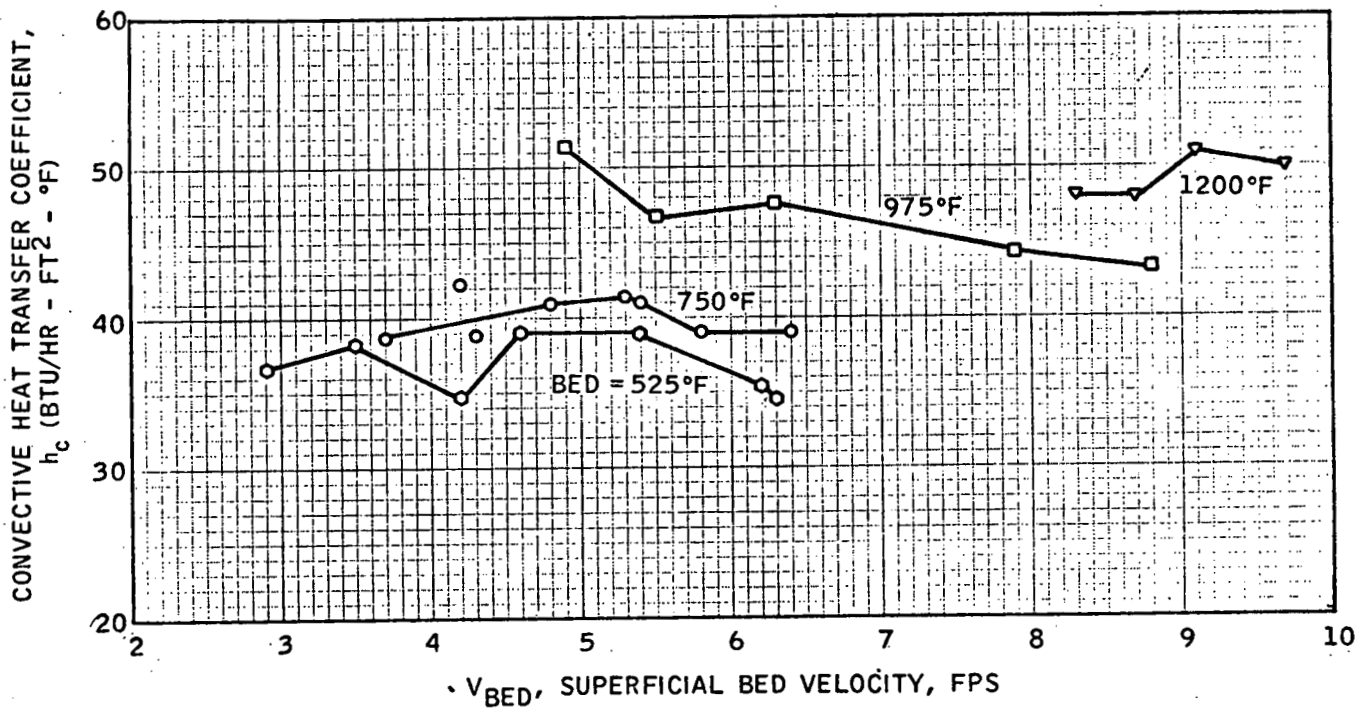

CONVECTIVE HEAT TRANSFER COEFFICIENT IN-BED TUBE 3C

Figure 5

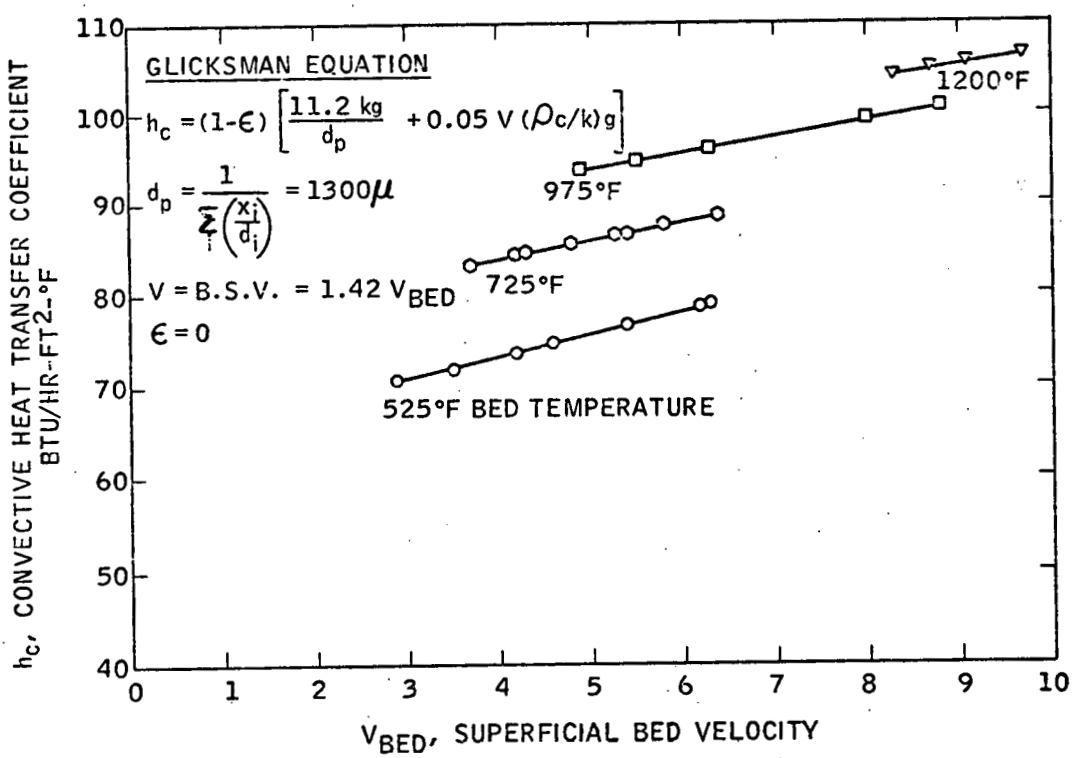

MAXIMUM HEAT TRANSFER COEFFICIENTS
GLICKSMAN EQUATION

Figure 6

Nominal Bed Temperature 525°F

T_{BED} = 522°F

V_{BED} = 6.3 FPS

$h_{o_{Ave.}}$ = 36.0 Btu/Hr-Ft^2-°F

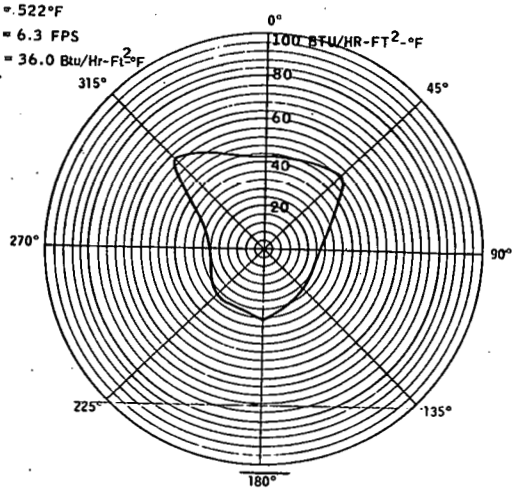

Nominal Bed Temperature 750°F

T_{BED} = 750°F

V_{BED} = 6.4 FPS

$h_{o_{Ave.}}$ = 41.5 Btu/Hr-Ft^2-°F

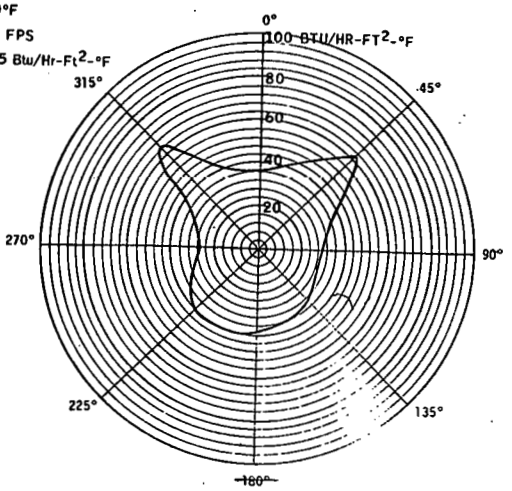

Nominal Bed Temperature 975°F

T_{BED} = 976°F

V_{BED} = 6.3 FPS

$h_{o_{Ave.}}$ = 51.6 Btu/Hr-Ft^2-°F

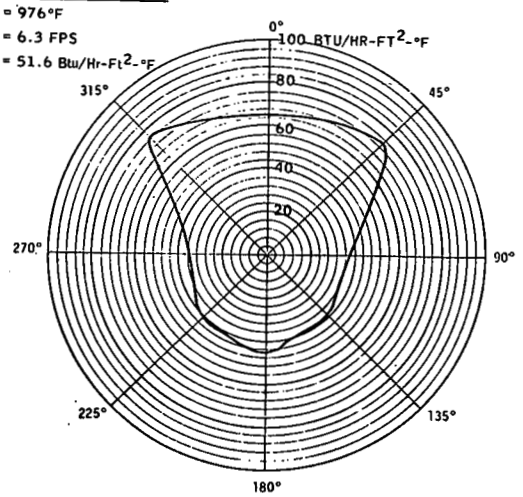

Nominal Bed Temperature 1200°F

T_{BED} = 1231°F

V_{BED} = 9.7 FPS

$h_{o_{Ave.}}$ = 56.1 Btu/Hr-Ft^2-°F

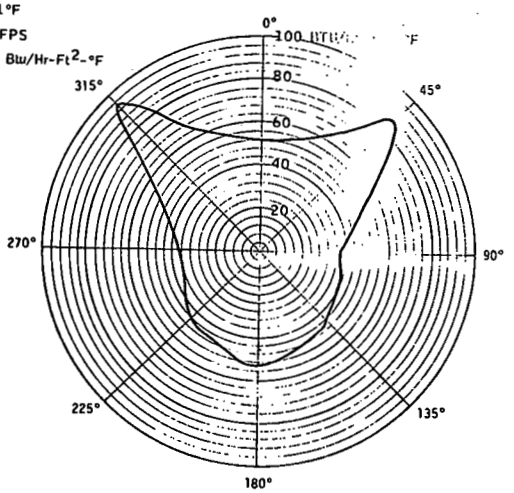

Note: 0° Position Is The Top Of The Tube

180° Position Is The Bottom Of The Tube

POLAR PLOTS IN-BED TUBE 3C TOTAL HEAT TRANSFER COEFFICIENT

Figure 7

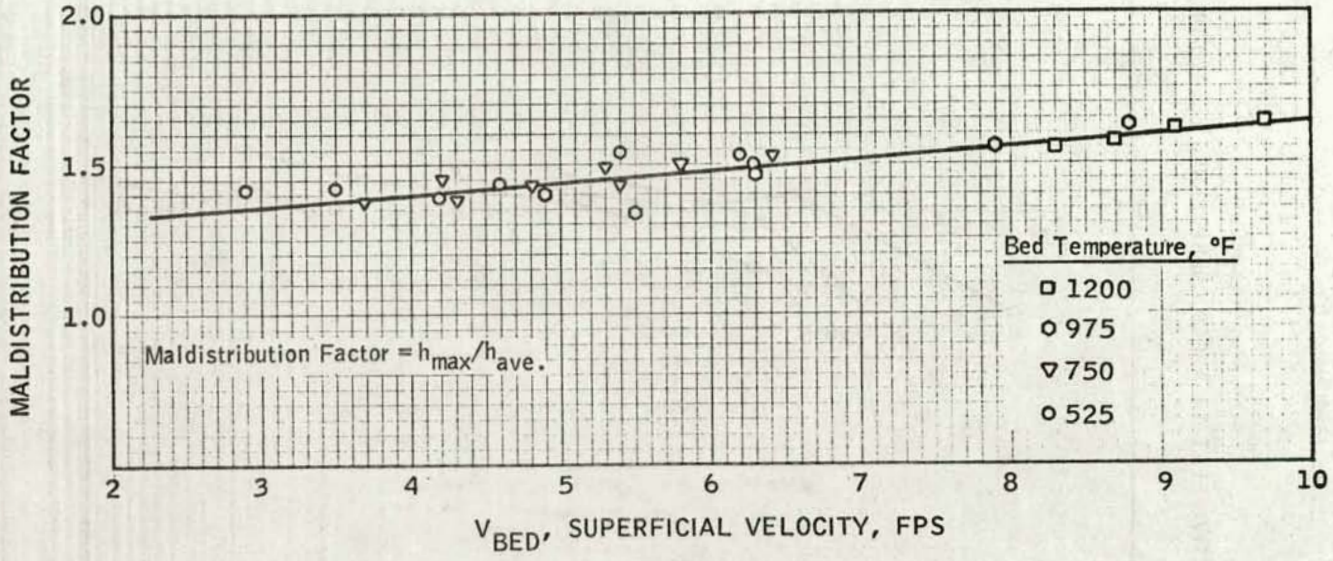

TUBE 3C MALDISTRIBUTION FACTOR

Figure 8

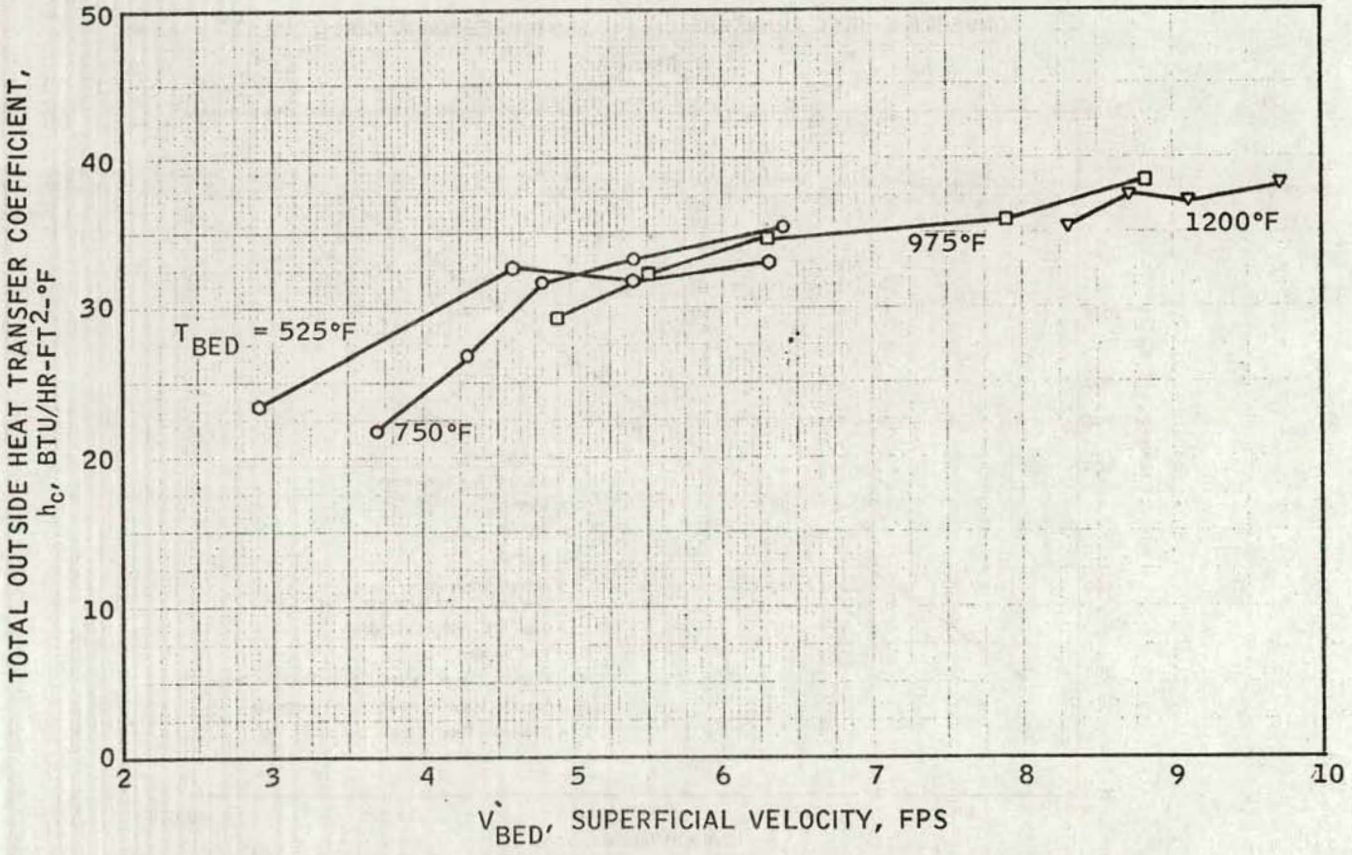

TOTAL OUTSIDE HEAT TRANSFER COEFFICIENT COIL 1 FREE BOARD COIL

Figure 9

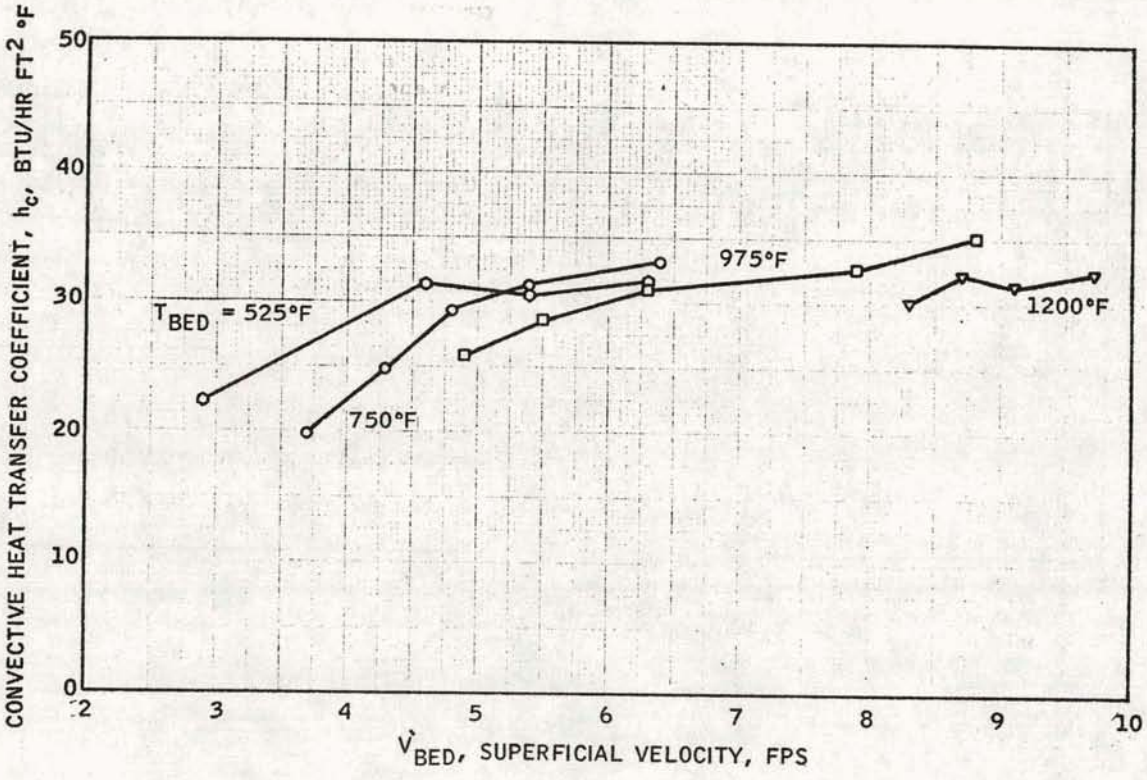

CONVECTIVE HEAT TRANSFER COEFFICIENT FREEBOARD COIL, COIL 1

Figure 10

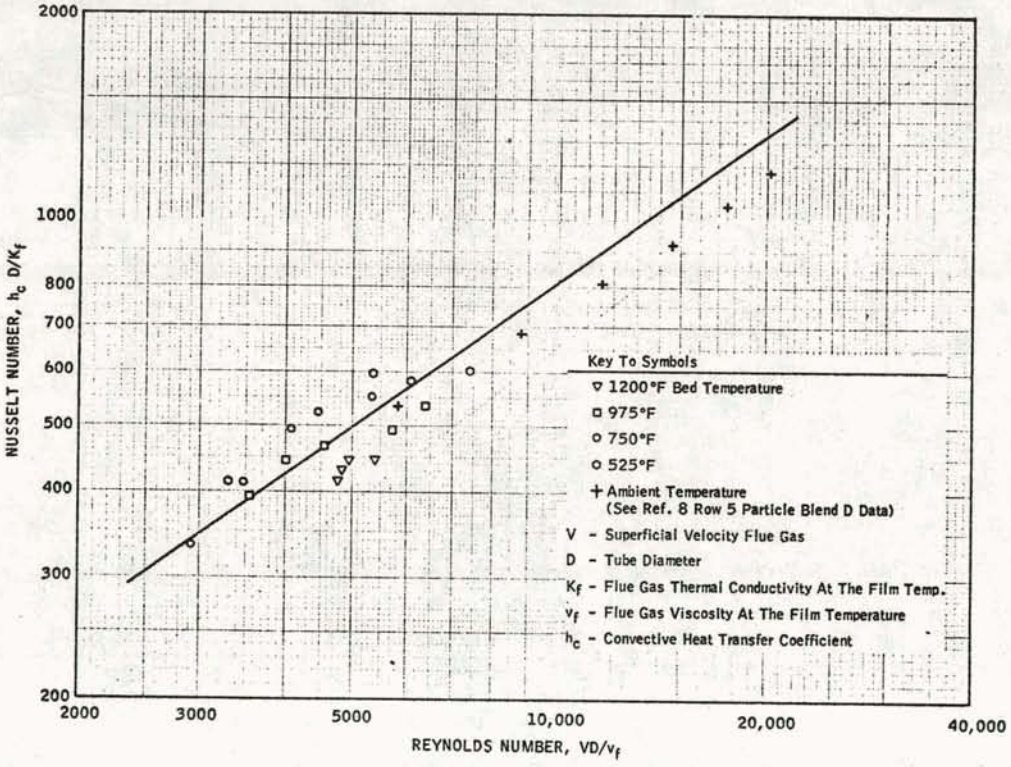

FREEBOARD COIL CORRELATING HEAT TRANSFER RELATIONSHIP

Figure 11

Questions to Larry P. Golan:

Q: (Participant not identified)

How did you arrive at the emissivity of the steel tube?

A: We put the tube in an electric furnace and initially the emissivity was abot .8. As we raised the tube temperature, we got down to about .4.

Q: (Participant not identified)

What was the temperture of your electric furnace?

A: 1500°-1800°F.

Q: (Participant not identified)

Why does your convective componenet show a temperature dependence within the bed, but not in the freeboard?

A: I don't know; but perhaps it is due to the lessened article contact in the freeboard.

Q: (Participant not identified)

Were your freeboard measurements made at one location in the freeboard?

A: Yes, as you move location, particle density would change and the heat transfer coefficient would also change.

Q: Joe Comparato, Cumbustion Engineering

Did you obtain information just for submerged tubes and the freeboard or did you examine the splash region just above the bed?

A: We did not look at a splash region.

AUTOMATIC CONTROL OF THE GEORGETOWN ATMOSPHERIC FLUIDIZED-BED BOILER

Robert J. Divilio

Pope, Evans and Robbins
Alexandria, Virginia

Robert L. Criswell

Foster Wheeler Energy Corporation
Livingston, New Jersey

INTRODUCTION

The 100,000 pound per hour Atmospheric Fluidized Bed Boiler (AFBB), located at Georgetown University, was initially fired in July of 1979. Since that time the AFBB has been operated for over 1700 hours, both in manual and in automatic control. This report describes the automatic control system used on the Georgetown AFBB and also describes the development of the control logic.

The Georgetown AFBB, shown in Figure 1, consists of two beds. Each bed is capable of producing 50,000 lb/hr of steam for a total of 100,000 lb/hr. Each bed can operate independently of the other in a superficial velocity range of 4 to 8 ft/sec giving each bed a 2 to 1 turndown ratio. Therefore, the boiler can operate between 25,000 and 100,000 lb/hr for a total turndown ratio of 4 to 1. Under normal operating conditions bed A is operated in automatic when demand is between 25,000 and 50,000 lb/hr. When demand exceeds 50,000 lb/hr, bed B is started up and both beds operate in parallel much the same way two parallel boilers operate. Thus one bed can be based loaded while the other bed follows load or, in cases of large load swings, both beds can follow the load simultaneously.

LOAD FOLLOWING CONTROL DEVELOPMENT

The control of a fluidized bed boiler differs considerably from that of conventional oil, gas, or even other types of coal fired boilers. The difference is primarily due to the fact that the combustion process takes place at basically the same temperature throughout the load range. This is accomplished by raising or lowering the bed level which in turn increases or decreases the amount of heating surface in contact with the bed. This feature enables the boiler to be operated over a wide range of air flow rates while maintaining the same bed temperature and excess air ratio.

Figure 2 shows the predicted operating conditions for a single bed of the Georgetown AFBB. These conditions were calculated using an in-bed heat balance developed by Pope, Evans and Robbins in Alexandria. Based on observations made so far it appears that this figure gives a reasonable prediction of the actual operating conditions. All of the points on this figure were calculated at a constant excess air ratio of 34% (5% O_2). This figure was used to determine the load following characteristics of the AFBB and to design the controller logic.

In order to increase the steam production the boiler controls will increase the coal feed and the air flow while maintaining a constant flue gas oxygen concentration. Figure 3 shows several ways that this increase can be implemented. In this figure the bed is intially at point A, (4 ft/sec, 1500°F and 18" static bed depth) corresponding to roughly 25,000 lb/hr of steam production. When steam demand is increased to roughly 31,000 lb/hr, the air flow is increased to 5 ft/sec and the coal is increased accordingly so that the O_2 above the bed remains constant at 5%. If the bed depth does not change during this time the bed temperature will increase to point B (1560°F). However, if the static bed level is increased to 20.5 inches (an increase of 2.5 inches) during this time, the bed temperature will remain constant at 1500°F (point C). These results indicate that the boiler's ability to follow load demand is dependent on the speed at which the static bed level can be raised or lowered.

This relationship between load and bed level can be examined further by looking at several ramp changes in load at various bed level change rates. Figure 4 shows a few of these cases for load increases, assuming that the boiler is initially at the conditions of point A (4 ft/sec, 18", 1500°F, and 5% O_2) producing 25,000 pph steam. If the load then increases at a steady rate of 6250 lb/hr per hour and the bed level is increased at a rate of 1" per hour, after 1 hour the boiler will be at the operating conditions shown by point B (following the middle dashed line). After 2 hours at the same rates of increase the conditions will be at point C, 3 hours at these rates will result in conditions at point D and after 4 hours the bed will be at full load at the conditions shown by point D. The upper dashed line on this graph shows what happens if the load is increased at a rate of 12,500 lb/hr per hour at 1" per hour bed building rate. After one half hour the bed will be at B' and in less than 1 hour bed temperatures will exceed 1600°F (C'). The final dashed line on Figure 4 shows what happens when the steam load increases 12,500 lb/hr

per hour at a bed building rate of 4 inches per hour. If the steam load increase was as high as 25,000 lb/hr per hour a bed building rate of 9 inches per hour would be required to maintain nearly constant temperature operation. Similarly rapid turndown of the unit will require rapid bed level changes.

The present limestone feed and bed drain equipment at Georgetown are capable of moving approximately 3 inches of bed per hour when one is on full speed and the other is off. When both items are running, a reasonable bed level change of 1.5 inches per hour can be expected. The load requirements for four typical days, one in each quarter of the year, are shown in Figure 5. The greatest and fastest change took place on the January day shown. It was for a 20,000 pph increase that lasted for one hour. With two beds in service the needed bed level increase is within the capability of the installed equipment.

To obtain the maximum rate of change requires that the bed temperature vary from a low value at low load to a high value at high load. The high and low temperatures must be within the range of efficient sulfur capture by the limestone in the bed. If the temperature is programmed to vary from 1450°F at low load (4 ft/sec) to 1600°F at high load (8 ft/sec), the bed depth need only be changed 2 inches (see Figure 6), instead of almost 9 inches with a constant bed temperature at 1500°F. With this control scheme, the load can be changed as much as 15,000 pph for single bed operation and 30,000 pph when two beds are in service.

CONTROL DIAGRAMS

Figure 7 shows the feed water and drum level control diagram for the Georgetown AFBB. For simplicity only those components that contribute to the control logic are shown. The feed water control scheme is a three element system operating on steam flow, drum level and feed water flow. In this scheme the steam flow and an error signal from the drum level controller (1) are added together in a summing card (2). This signal then becomes the set point for the feed water controller (3). Under normal operation, when drum level is at its set point, the steam flow is the set point for the feed water flow. When the drum level is off its set point, an error signal is added to the steam flow to compensate for the drum level.

Figure 8 shows how the demand signal is generated. Steam flow and an error signal from the drum pressure controller (1) are added in a summing card (2) to generate a total demand signal. This signal is split to the individual bed master demand controllers (3) and (4) which supply a demand signal to each bed. The scaling relay (5) on the B-bed demand signal provides a small amount of bias to compensate for differences between bed performance. A-bed is the only bed with fly ash reinjection and as such usually requires less coal than B-bed to produce steam due to the added heat input from the B-bed fly ash.

The remainder of the control logic is identical for both beds. Thus the diagrams are shown for only one bed. Figure 9 shows the fuel and air control diagram. The control logic used in this figure is that discussed in the control logic development section, namely constant O_2 operation will be maintained throughout the load range and temperature will be allowed to fluctuate between 1450°F at low load and 1600°F at full load.

The demand signal from the bed master demand controller is split into a coal and an air demand signal. The coal demand signal is compared to the corrected air flow signal (a) in a low signal selector (1). This is to prevent overfeeding of coal. Next the coal demand signal passes through a temperature limiter (3). This is designed to prevent operation below 1400°F or above 1700°F. Finally the coal demand signal becomes the set point on the coal feed controller (7).

The air demand signal passes through a 3 way high signal selector (2) that compares air demand to actual coal feed and to bed temperature. The comparison with coal feed prevents over feeding of fuel. The comparison with bed temperature is to prevent temperature runaways. Figure 10 shows the calibration of this temperature signal and its interaction to the air flow. Under normal operation the bed temperature air flow demand relationship will follow the solid line and the demand signal will pass through the selector. If the temperature exceeds the dashed line the selector will select the temperature signal and will begin increasing the air flow to that bed. This will help to moderate the bed temperature until the bed level can increase to the proper height. Returning to Figure 9, the air flow demand signal then passes through a low signal selector (4). This prevents demanding an air flow below minimum fluidization velocity. Finally the air demand signal becomes the set point for the air flow controller (8). The actual air flow signal is combined with a signal from the O_2 controller (5) in a multiplyer card (6). Here the proper fuel to air ratio is determined to maintain constant O_2 operation.

The fuel and air control scheme has two separate operators to limit the bed temperature within a working range. The primary bed temperature control logic, however, is contained in the bed level-bed temperature control diagram shown in Figure 11. The bed demand signal is scaled, according to the solid line of Figure 10, in a scaling relay (1). This signal becomes the bed temperature controller (2) set point. The output from the temperature controller is combined with the scaled demand signal in a summing card (3) to generate a set point for the bed level controller (4). The expanded bed depth is approximated by dividing a total bed differential signal by a partial bed differential signal, in a division card (5), in much the same way that liquid level measurement systems work.

Figure 12 shows the limestone feed-SO_2 control scheme. The actual coal feed rate is divided by a predetermined fuel/limestone ratio in a division card (1). This signal becomes the set point for the limestone controller (2). This allows operation at a fixed Ca/S ratio. The actual limestone feed rate is combined with an error signal from the SO_2 controller (3) in a summing card (4). This allows correction to the Ca/S ratio to compensate for fluctuations in coal sulfur content, or sulfur capture performance.

SUMMARY

Previously, the greatest control limitation to the Georgetown AFBB was the necessity to change bed mass with load. The effect of this limitation has been minimized by allowing a variable temperature operation. This results in reducing the amount of bed that must be added or removed to change load. Nevertheless, the change in boiler steam generation is 1/4 percent per minute for one bed operation and 1/2 percent per minute for two bed operation. These load changes compare favorably with conventional stoker fired units which are typically limited to changes of 1/2 percent per minute. Furthermore, these changes are sufficient to meet the steam demand at Georgetown University.

The control experience on the Georgetown AFBB points out the need to better design in-bed surface for turndown. Ideally a tube bundle design that allows load changes with no bed mass changed would result in a boiler with much faster load response characteristics. Design of such an in-bed tube bundle requires a better knowledge of the effect of bed temperatures, superficial velocity and particle size on parameters such as heat transfer coefficients and bed expansion.

ACKNOWLEDGEMENT

This research is supported by Department of Energy, Fossil Energy Division, Washington, D.C.

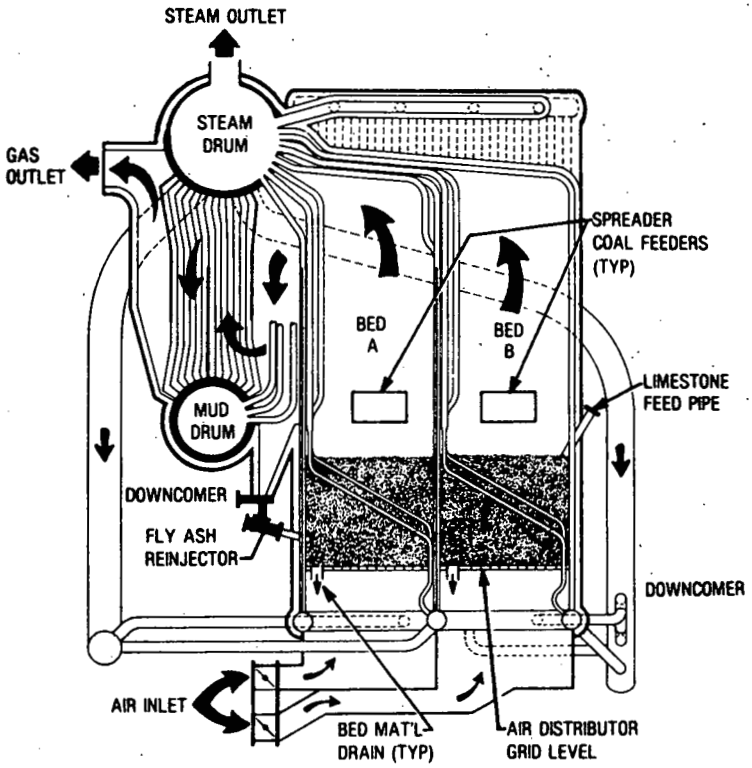

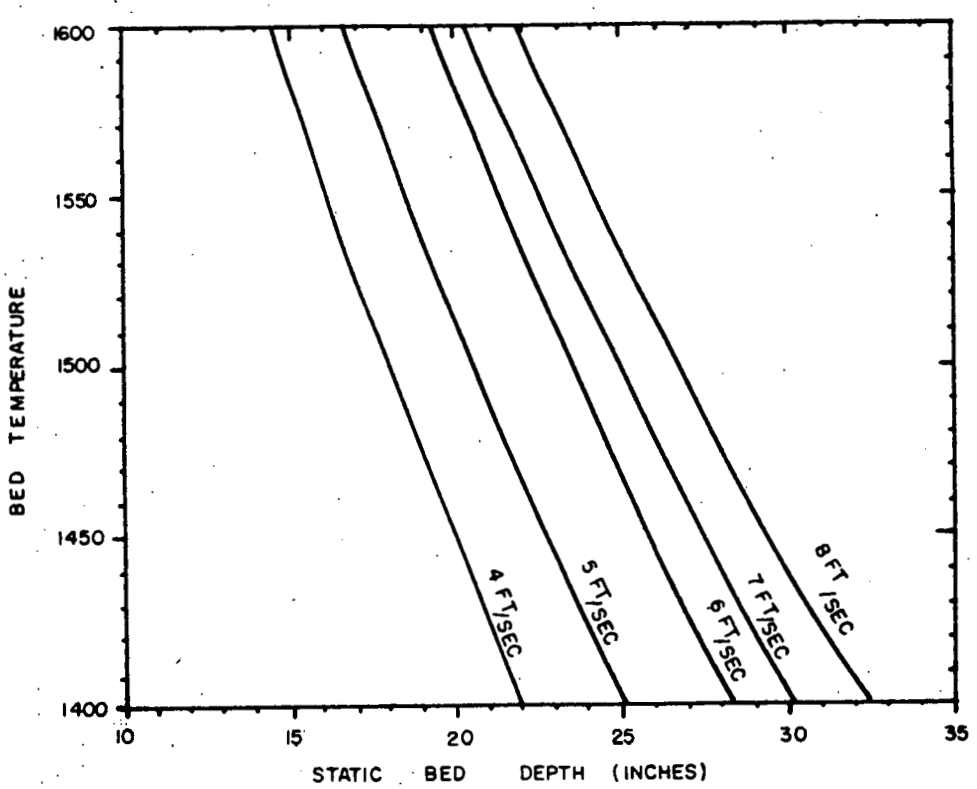

CALCULATED OPERATING CONDITIONS OF THE GEORGETOWN AFBB

FIGURE 2

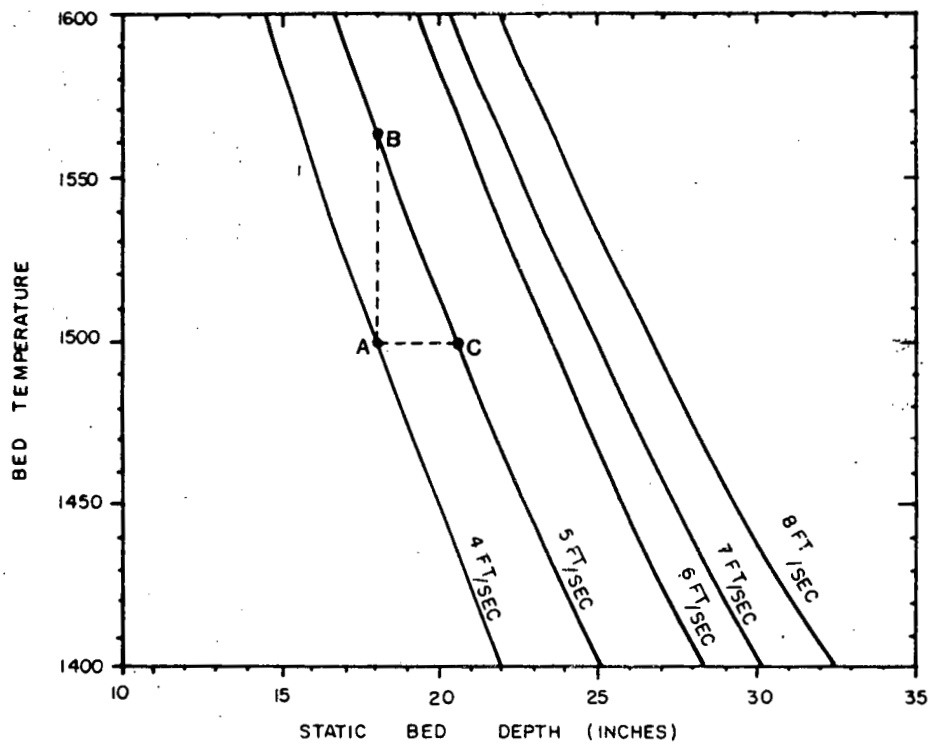

CALCULATED OPERATING CONDITIONS OF THE GEORGETOWN AFBB

FIGURE 3

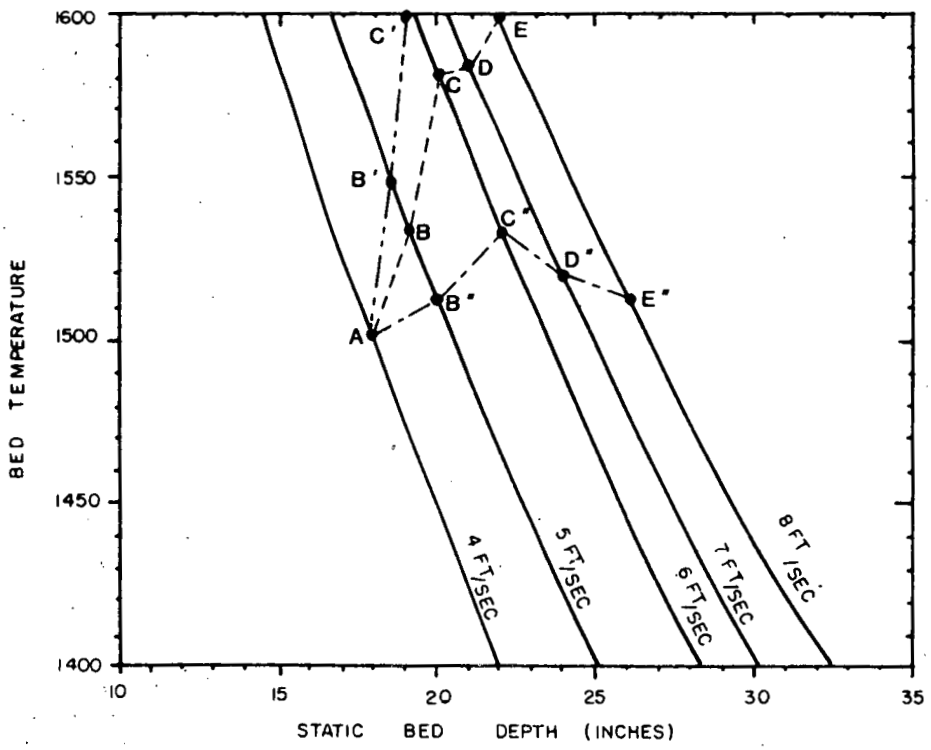

CALCULATED OPERATING CONDITIONS OF THE GEORGETOWN AFBB

FIGURE 4

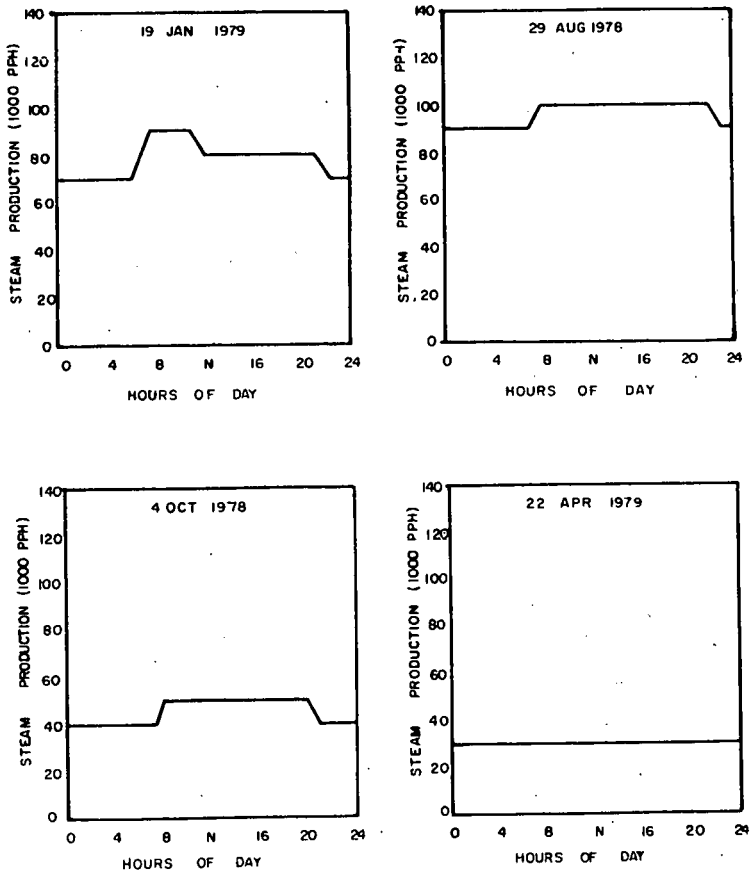

TYPICAL STEAM DEMAND CURVES
FOR THE GEORGTOWN UNIVERSITY CAMPUS

FIGURE 5

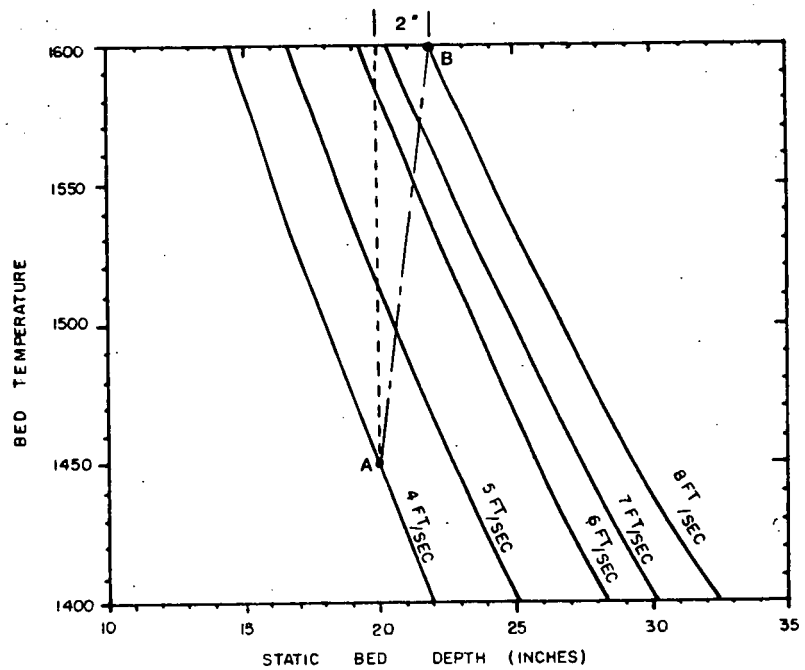

CALCULATED OPERATING CONDITIONS OF THE GEORGETOWN AFBB

FIGURE 6

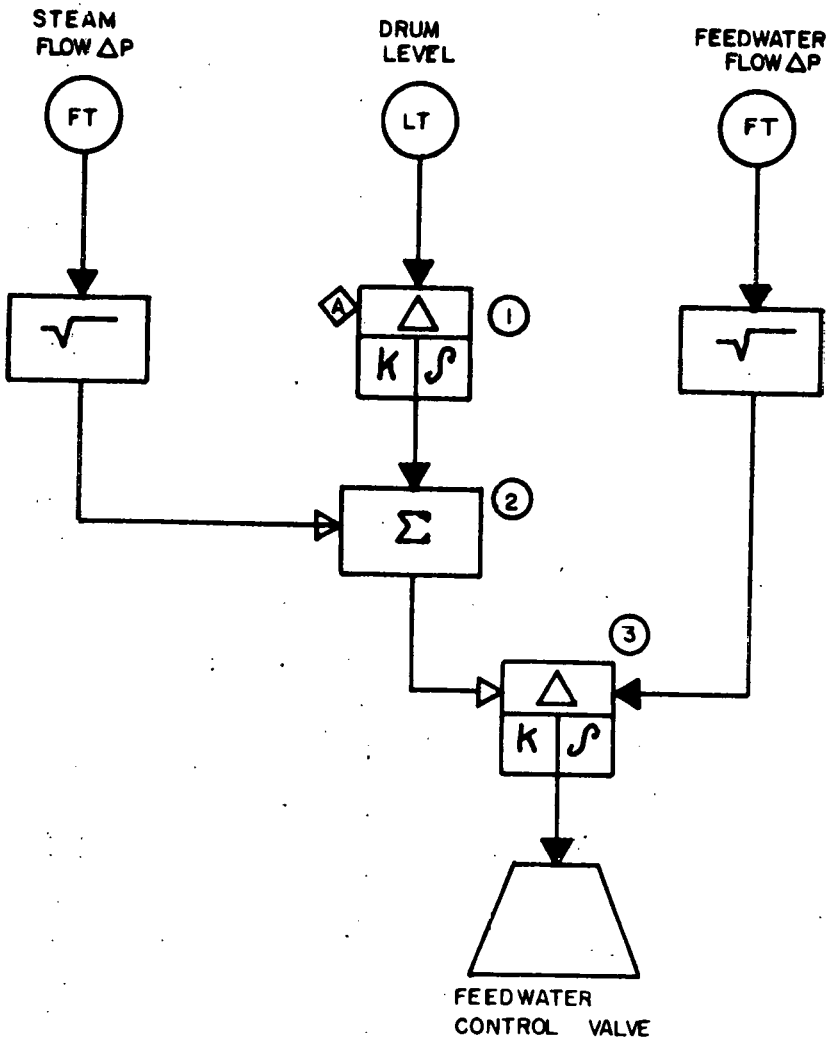

FEEDWATER — DRUM LEVEL CONTROL DIAGRAM

FIGURE 7

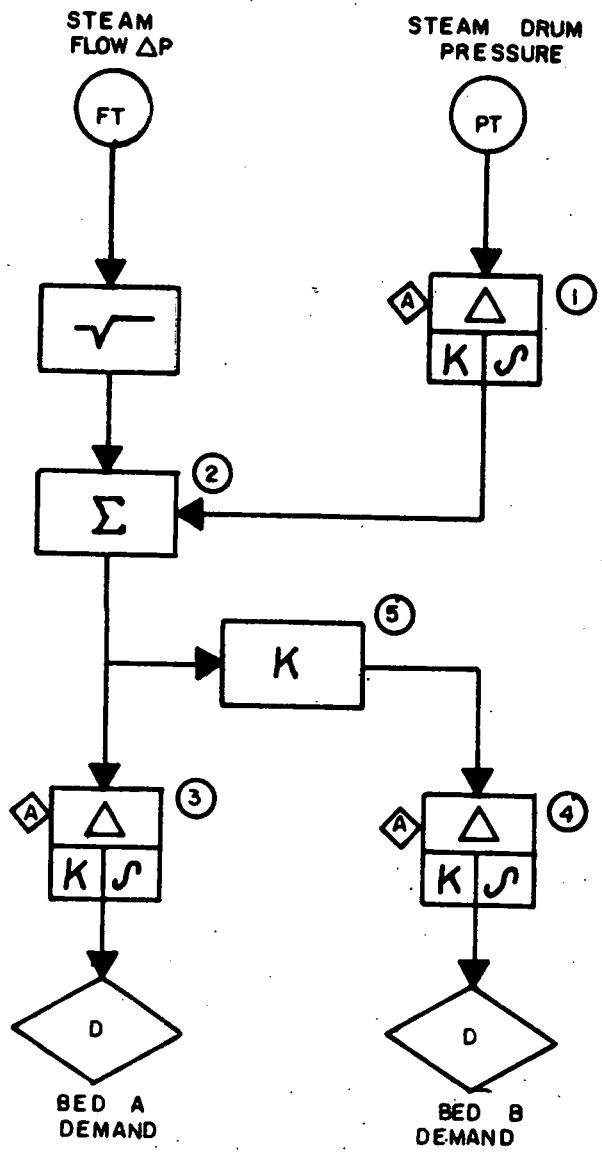

DRUM PRESSURE — STEAMFLOW DEMAND CONTROL DIAGRAM

FIGURE 8

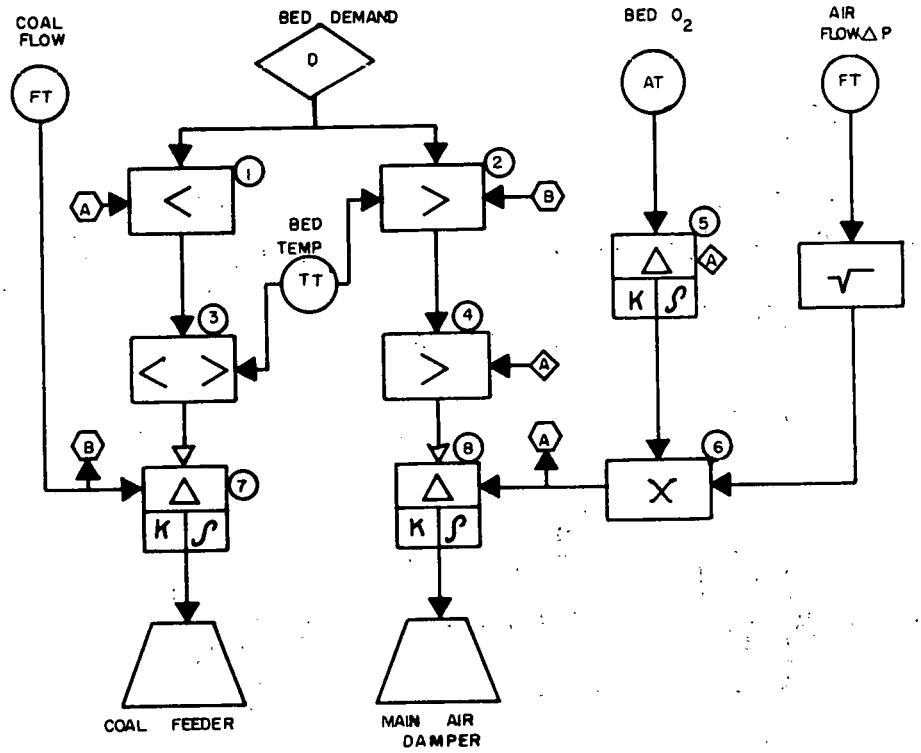

FUEL AND AIR CONTROL DIAGRAM

FIGURE 9

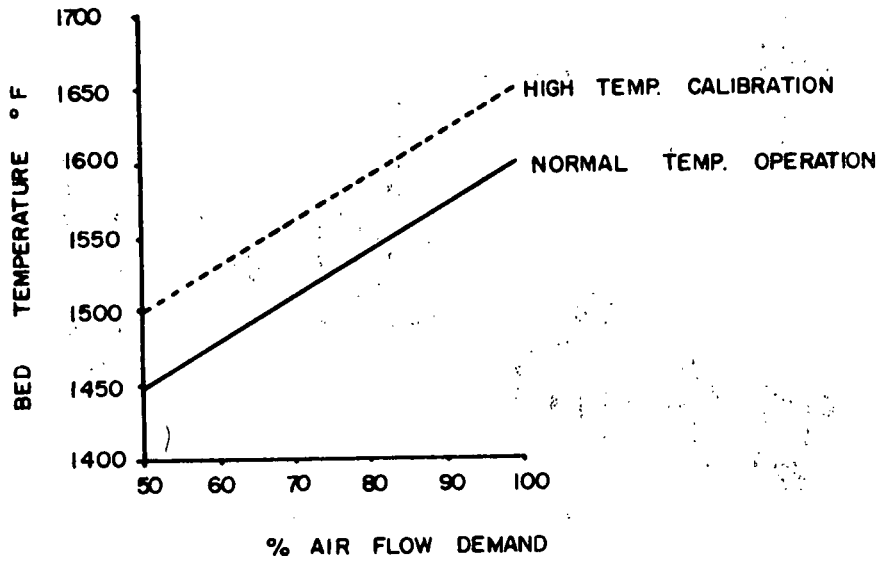

FIGURE 10

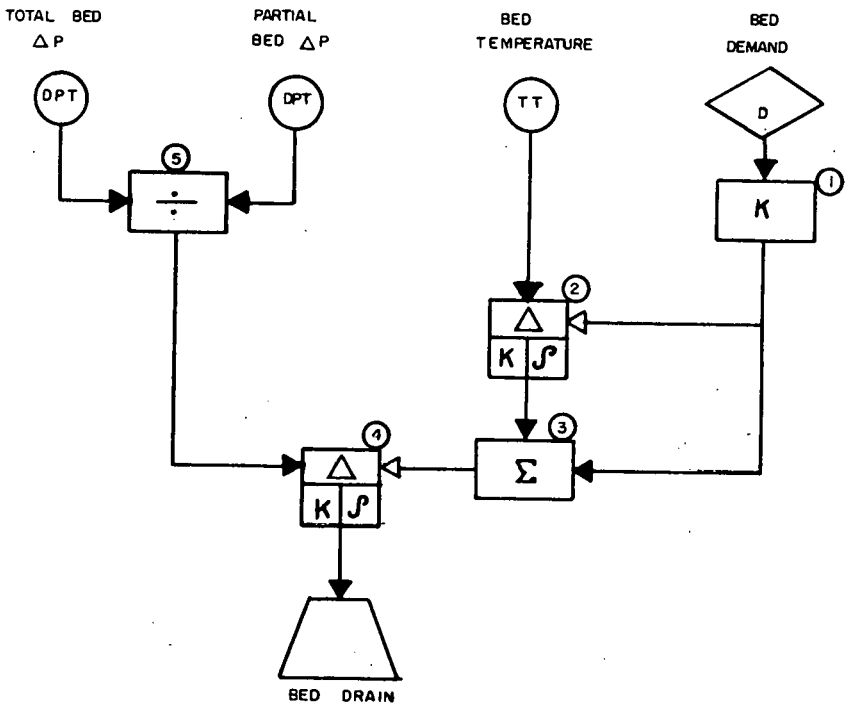

BED LEVEL – BED TEMPERATURE CONTROL DIAGRAM.

FIGURE 11

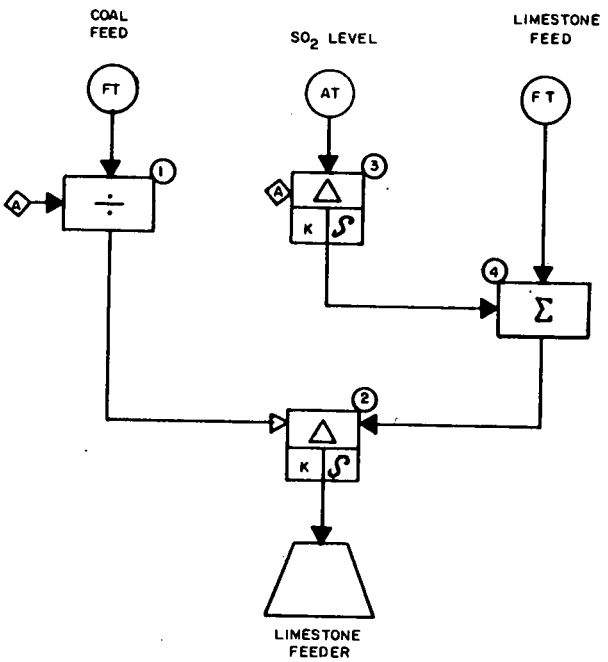

LIMESTONE FEED – SO_2 CONTROL DIAGRAM

FIGURE 12

Questions to Robert Divilio:

Q: Joe Comparato, Cumbustion Engineering

What do you find going down in load?

A: Basically, just the opposite of going up in load, with the same limitations and procedures.

Q: Jerry Farough, TVA

When you go from high load to low load, what affects did you see on unburned carbon, sulfur capture, NO_x control, etc.?

A: We don't have a lot of data on that. Our experience at Alexandria has been that we see only a small difference when load is varied.

Q: (Participant not identified)

How were steam conditions regulated?

A: The purpose of this system was to maintain a constant steam drum pressure.

Q: (Participant not identified)

In the transient condition where you are decreasing load, have you seen any evidence of bed carbon burnout causing a lag in turndown?

A: There probably is some lag, but I think you have to realize that one-half percent per minute is a pretty slow load change. I don't think the lag is really a problem.

A TRANSIENT SULFUR CAPTURE MODEL FOR A FLUIDIZED BED COMBUSTOR

K.J. Daniel* and S.D. Finnigan**

*Corporate Research and Development
**Energy Systems Programs Department
General Electric Company
Schenectady, NY 12345

INTRODUCTION

The study reported here has had two objectives. First, to determine how changes in load and coal sulfur content affect sulfur absorption in fluidized beds. Second, determine cost effective methods to control bed sulfur absorption properties that minimize sorbant usage and minimize effects on load control. The method used to attain these objectives is to mathematically model the fluidized bed power plant with emphasis on the model of the bed. The power plant that is modeled is the baseline GE design of a pressurized fluidized bed (PFB) power plant (1).

MODEL OF FLUIDIZED BED

Modeling of a fluidized bed has been approached in different ways by several investigators (References 2 through 10). These models range from simple to complex, but all assume steady state. In order to meet the objectives of this study, a transient model of the fluidized bed must be formulated that incorporates all the important bed processes, is easily soluble and is not computationally cumbersome.

In formulating a mathematical model it is necessary to understand and properly account for the duration of important processes. Judgments regarding the detail to which they should be included in the model can then be made. If a process is completed in a short time compared to the time scale of the events of interest, the process can be assumed to occur immediately with little loss of accuracy. Advantageously, the problem becomes more easily solvable and generally requires less computation time.

The important processes occurring in a PFB combustor and typical duration periods are given in Table 1. Comparison of the time scales for these processes can be used to justify simplifications of the mathematical model for the PFB.

One of the most important values on this chart is the reasonable response time expected of the sulfur control system. A value of three minutes represents the lower estimate of the time constant of the sulfur monitoring system and the time required to initiate a control action. Many bed processes occur on a time scale much shorter than

Table 1

TIME SCALE OF IMPORTANT PROCESSES

Coal Particle Devolatilization and Combustion of Volatile Products	2 - 10 s
Combustion of Char Particles	35 - 150 s
Time for Particles Injected into the Bed to Become Mixed	15 - 30 s
Residence Time for Absorbant Particles	2 - 8 hours
Gas Residence Time in Bed	2 s
Frequency of Sulfur Emission Variation from Bed Due to Variations in Coal Sulfur Content	seconds - days
Reasonable Response of Sulfur Control System	180 s
Time for Calcination of Fresh Absorbant	2 min - 15 min

the control response time. Mixing time, gas residence time, coal devolatilization, etc., all occur much faster than the probable control response time. Therefore, algebraic equations independent of time may be used to model these processes.

Processes that occur on the same time scale as the control system response time must be included in the model as a differential equation in the time variable, or algebraic expressions that include time as an independent variable. Examples of processes that are included in the model as algebraic expressions in time are calcination, and coal sulfur release. Examples of processes that are included in the model as differential equations in time are the bed inventory and bed temperature.

The differential equation that determines the bed temperature is

$$\dot{Q}_s = (1-\eta_L)\left[\dot{\Delta H}_R - M_b, C_{P,b}\,\frac{(T_{t+\Delta t} - T_t)}{\Delta t}\right] + \sum (h_{in,i}\,\dot{m}_{in,i} - h_{out,i}\,\dot{m}_{out,i}) \qquad (1)$$

i = all species

where η_L is the fraction of energy loss. For each time step this equation is solved iteratively for the new temperature $T_{t+\Delta t}$.

The rate of energy transfer to the steam tubes Q_s has been approximated by

$$Q_s = k_h \, hA\Delta T_{lm} \qquad (2)$$

where ΔT_{lm} is the log mean temperature difference evaluated at the bed temperature and inlet and exit temperatures of the steam generator. The factor k_h accounts for the temperature dependence of the heat transfer coefficient. It is assumed that the inlet and exit enthalpy of the steam generator remains the same for all operating conditions, so that changes in $\dot{Q}_s$ are reflected by changes in the amount of steam produced. It follows from this that changes in steam generation are only limited by changes in bed temperature.

The value of the product hA has been chosen to produce the desired rate of steam generation at the full load design conditions. Over normal operating conditions the change in the fluidizing velocity or particle size distribution will not be sufficient to significantly change the value of this product (11). However, normal changes in bed temperature will be large enough to change the heat transfer coefficient. This change is accounted for by k_h which is a linear fit of experimental data (12).

The flow of gases through the bed has been approximated as plug flow in a single phase. This approximation has two justifications. First, it is expected that the large number of tubes in the bed will enhance the interchange of gas between the bubble and emulsion phases. Second, work by Bar-Cohen (13) has cast doubt on the applicability of using D'Arcy's law to model the exchange of gases between the bubble and emulsion phase for large particle beds where slow bubbles are expected.

The combustor is modeled as a single phase homogeneous bed and the equation governing SO_2 capture becomes a simple differential equation (10):

$$U_e \frac{d[SO_2]}{dx} = -K_1 [SO_2] + G(x) \qquad (3)$$

where K_1 is the overall rate constant for the entire bed, U_e is the average gas velocity through the interstices of the bed and G(x) is the local rate of sulfur generation.

To evaluate this expression, the value of the reaction rate constant as a function of time must be determined. The reaction rate constant is a function of many variables such as temperature, dolomite type, calcination atmosphere, particle size, and particle utilization. There have been many attempts to determine function relations for the reaction rate (References 15 through 20). This study uses the TGA rate data (20) provided by Westinghouse for 1337 dolomite calcined and sulfated under conditions comparable to those expected in a PFB combustor. Rate data was reported as a function of utilization for four specific particle sizes. By determining the bed inventory of dolomite as a function of size and utilization, the Westinghouse data can be interpolated and integrated to determine the instantaneous reaction rate constant for the bed. By expressing the integration in the form of a sum the expression for this rate constant is

$$K_1 = \sum_i \sum_j \frac{k_1(d,U)\, m_{ca,d,U}}{V} \qquad (4)$$

where $k_1(d,U)$ is the rate constant associated with dolomite particles of size d and utilization U, $m_{ca,d,u}$ is the moles of calcium of size d and utilization u, and V is the bed volume minus inerts. The temperature dependence of the rate constant was also determined from Westinghouse TGA rate data.

Determining where sulfur dioxide is generated in the bed is important in determining the amount of sulfur dioxide abosrbed by the bed. This SO_2 generation distribution is difficult to predict due to uncertainties in the rate of sulfur dioxide generation due to devolatilization and combustion. Sulfur dioxide generation in this study will be approximated by an exponential equation of the following form:

$$G(x) = \frac{\dot{m}_{coal}\, f_s\, e^{-\alpha x/L_f}}{M_s\, A_b L_f\, (1-e^{-\alpha})} \qquad (5)$$

where the expanded bed height, L_f, was determined using the expressions developed by Baba (14) and estimates of the bed volume occupied by tubes. The value of α is the only independent variable in the expression. It has been shown (5) that if sulfur dioxide generation is proportional to combustion and combustion in turn is only limited by the partial pressure of oxygen, equation (4) becomes an exact representation if the value of α is chosen as:

$$\alpha = \ln\left[\frac{1 + \text{excess air ratio}}{\text{excess air ratio}}\right] \qquad (6)$$

The excess air ratio is 0.20 for design PFB conditions. This representation is used as the pessimistic limit of the sulfur release distribution. It predicts sulfur release high in the bed and does not account for the large amount of sulfur released in volatile products deep in the bed.

Other distributions deeper in the bed have also been investigated. An optimistic prediction of the sulfur release and capture can be obtained by estimating the location of the devolatilizing coal particles and assuming all the sulfur is released during devolatilization. The location of coal particles can be estimated by assuming that devolatilization occurs uniformly for the 10 seconds after the coal particle is injected into the bed. The distribution of these particles can be approximated by solving the differential equation governing transient diffusion with a constant source term as a boundary condition.

The solution of this equation requires diffusivity of the bed. Many factors affect this value. Horia and Wen (2) have determined the value of this constant for the Exxon miniplant by fitting the temperature profile predicted by their model to test data. For cases of interest here this value ranged from 200 cm^2/s to 500 cm^2/s. The solution of the transient differential equation evaluated at 10 s for both values of D_{SA} is shown in Figure 1. Also shown on this figure is an exponential function that approximates the concentration distribution (α = 6.0) and the exponential sulfur generation distribution corresponding to the pessimistic prediction (α = 1.79). There is a considerable amount of difference between these two exponential distributions.

Combining Equations (3) and (5) an expression for the rate of sulfur leaving the bed can be determined which is

$$R_o = U_{sg} A_b C_2 (e^{-\alpha} - \exp(-K_1 L_f / U_e)) \quad (7)$$

where

$$C_2 = \frac{K_2 L_f}{K_1 L_f - \alpha U_e} \quad (8)$$

and

$$K_2 = \frac{\dot{m}_{coal} f_s}{M_s A_b L_f (1 - e^{-\alpha})} \quad (9)$$

The expression for the instantaneous sulfur retention r' is then

$$r' = \frac{R_{in} - R_o}{R_{in}} \quad (10)$$

where $R_{in} = \dot{m}_{coal} f_s$ which is the rate of sulfur entering the bed.

In this study the time required for a particle of dolomite to become calcined has been estimated by using the following approximations: a) constant dolomite specific heat, b) constant heat transfer coefficient, c) temperature of particle remains constant during half and full calcination processes, and d) calcination is heat transfer (not reaction rate) limited.

By employing these approximations and realizing that the criteria for lumped heat capacity analysis is satisfied for the dolomite particles, a relation can be derived for the time required for calcination. Employing typical thermophysical properties (22) and a value of 2 for the Nusselt number, the time to reach fully calcined conditions is given by

$$t_{cal} = 55800\ r^2 \quad (11)$$

This expression is used to determine the amount of time required before a particle will actively absorb SO_2. During the time that particles are in the half calcined condition, it is estimated that the particles will become only slightly utilized (in the neighborhood of 5%). This effect is ignored and results in little loss of accuracy for beds with an approximate average particle size of 1000 μm.

In order to determine the rate of absorption of SO_2 the size and utilization population distribution of the dolomite within the bed must be known. This population distribution will change with time resulting in a change of the bed reactivity. Consequently, a very important part of this model is the determination of the bed population distribution as a function of time.

The differential equation that governs this distribution is simply derived by noting that the distribution of calcium within the bed, N, is a function of three variables: time, t; size, d; and utilization, U. The governing differential equation then takes the form (24)

$$\frac{dN}{dt} = \frac{\partial N}{\partial t} + \frac{\partial}{\partial d}\left(\frac{N \partial d}{\partial t}\right) + \frac{\partial}{\partial U}\left(\frac{N \partial U}{\partial t}\right) \quad (12)$$

The moles of calcium of a particular size and utilization is defined as

$$M_{d,u} = N_{d,u}\ \Delta d\ \Delta U \quad (13)$$

The first term on the right-hand side of equation (12) is the rate of change of the number of particles of a given size and utilization due to causes other than changes in size or utilization. This term has four components: off-take rate, feed rate, elutriation rate, and rate of increase due to fines generated by attrition of larger particles. The rate of elutriation was determined using the correlation developed by Merrick and Highley (21). All but 3% of the fines produced by attrition were assumed to be elutriated immediately. The remaining 3% were distributed among the sizes within the bed below 700 μm.

The second term on the right-hand side of equation (12) represents the change in bed population due to changes in size by wearing away the surface of particles. The second factor within the parentheses is the rate of size reduction of a single particle of size d by attrition and is given by (21)

$$\frac{\partial d}{\partial t} = \frac{-k_a f_d (U_{sg} - U_{mf})}{3} \quad (14)$$

where the value of k_a was chosen to correspond to data from the large scale pressurized fluidized bed experiments conducted by NCB, CURL in Leatherhead, U.K. (25)

The final term on the right-hand side of equation (12) represents the change in the distribution of a particular size and utilization due to the changes in utilization. The mathematical expression for the second factor within the parentheses is

$$\frac{\partial U}{\partial t} = \frac{k_1 (d,U)(R_i - R_o)}{K_1 V} \quad (15)$$

where $k_1(d,U)$ is the absorption rate constant for particles of size d and utilization U.

MODEL VERIFICATION

In order to determine the effect of uncertainties in the sulfur release distribution, the results of the model were compared using the optimistic and pessimistic approximations of the sulfur release distributions (Figure 2). Although the distributions are quite different, the sulfur capture predicted by the model does not differ significantly except at large sulfur retentions. However, even then the difference is quite small. All results reported in the remainder of this paper employ the pessimistic generation function.

Steady state verification was performed by comparing the model predictions to experimental data of Exxon (5) (Figure 3). The model input parameters were chosen to correspond to runs 43.3, 43.4, and 43.5 of Reference 5. In general the model results are good, but somewhat pessimistic. This trend can possibly be due to the use of the pessimistic sulfur generation function, or errors in the absorption rate data.

In order to verify the transient response predicted by the model, it was compared to experimental transient data obtained from Exxon (23). However, due to large errors in the mass balance for these experimental runs it was impossible to duplicate the experimental value of retention using the reported value of the Ca/S ratio. Consequently, in order to verify the transient response predicted by the model, Ca/S ratios were chosen so that the steady state retention of the experimental data was duplicated by the model (Table 2). In obtaining these ratios, the coal and air feed rates are those used in the experiment. Only the feed rate of dolomite was changed.

Table 2

Ca/S FEED RATES FOR TRANSIENT MODEL VALIDATION

Hours Used	0-6.0 14.0-24.75	6.0-14.0
Ca/S Ratio Set on Feed System	1.25	.32
Calculated Ca/S Ratio (Ca/S = R/U)	.90	.68
Value to Reproduce Retention	1.17	.89
Coal Feed Rate (kg/s)	46.0	50.7
Dolomite Feed Rate (kg/s)	5.90	4.76
Air Feed Rate (kg/s)	680	680

Using these Ca/S feed ratios, the simulation reproduces the experimental results quite well. Figure 4 shows the experimental and model results for several step changes in the Ca/S ratio.

Although agreement is quite good, some of the differences should be commented upon. The sharp change (spike) of the model prediction following a step change is caused by the use of large particles in the experiment and the model input (average size particle approximately 1600 μm). It is predicted that particles of these large sizes require about 20 minutes to become fully calcined, and it is assumed that these particles do not become active absorbers until they are fully calcined. It is clear that this assumption does not faithfully duplicate the experimental data. However, due to the lack of data for the rate of calcination and the rate of sulfation during calcination, no better assumption can be made. Fortunately, the data used for steady state verification and the plant design conditions used in the following parametric study employs particles which are much smaller (approximately 1050 μm average size). Very short calcination times are predicted for these small particles. Consequently, the model does not predict sharp changes following changes in dolomite feed rate.

The sharp change in the model prediction is also due to a much smaller extent on the change in the excess air ratio that occurs at that time. This causes a slight change in the sulfur generation function.

The use of large particles within the bed also resulted in a numerical problem that caused the averaged bed particle size predicted by the model to slowly drift. For the transient verification run in Figure 4, the average bed particle size changed from 1531 μm to 1687 μm. This caused a long-term drift in the retention prediction that resulted in the final retention being different than the initial prediction. This instability was not found for other cases where the bed particle size distribution resulted in a significantly smaller average size.

PFB Power Plant

The fluidized bed model was included in a transient model of the entire GE baseline design of a PFB power plant (1). This overall model included simulations for gas and steam turbine as well as a simplified plant load control. Details are reported elsewhere (26).

Two design parameters which are critical in this study are the expanded bed height, 2.74 m (9 ft), and superficial gas velocity, 1.37 m/s (4.5 ft/s). The dolomite feed rate for the plant is 20.8 kg/s (45.87 lb/s) for a Ca/S ratio of 1.48 using 3.9% sulfur coal. The bed inventory is typically 4.5×10^5 kg (1.0×10^6 lb) of dolomite.

ANALYSIS OF THE TRANSIENT RESPONSE OF THE FLUIDIZED BED COMBUSTOR

All of the following figures are results of exercising the mathematical model for the PFB power plant. The load control system was deactivated for these results in order to evaluate only the transients that result from changes in bed properties.

Step Change in Coal Sulfur Content

Figure 5 shows the changes in retention and the average bed utilization following a step change in the coal sulfur content from 1.95% to 3.9%. The step change represents a change in the Ca/S ratio from 1.48 to 0.74. Note that the utilization and retention curves show considerably different trends. The retention curve shows a distinct inflection point while the utilization curve does not. It simply asymptotically approaches its new steady state value. Both curves are algebraicly related. The retention is a function of the integral of the product of the reaction rate constant and the bed population distribution. The average utilization is simply a molar average, derived from the instantaneous bed population distribution. This highly nonlinear relation causes the time response of each curve to appear different although they are related.

Another important point to note on this figure is the time required to approach the new steady state value. Approximately 20,000 s (5.6 hr) are required. This is an extremely long time period compared to any other transient that will occur in a PFB power plant.

The reader should note that following the step change of coal sulfur, the percentage of sulfur retained in the bed does not abruptly change, although the amount of sulfur released in the bed increases by a factor of two. This is a result of the following properties of the sulfur release and capture process:

1. The sulfation reaction is first order with respect to sulfur dioxide.
2. Rather large changes in the sulfur dioxide generation function do not significantly change the bed retention.

The first property has been commonly accepted. The second is justified by the parametric analysis of the sulfur generation function presented previously. This analysis showed that even large changes in the sulfur generation function did not significantly affect the sulfur retention. The important point that the reader should note is that the percentage of sulfur retained in the bed does not change rapidly irrespective of rapid changes in the amount of sulfur released in the bed. The retention will change only when there is a change in the bed population distribution. This point is used later in the selection of the preferred control system.

Figure 6 shows how the transient in coal sulfur content will affect the power and temperature of the bed. Note that throughout this transient condition, the coal heating value and coal flow rate was maintained at a constant value. In spite of this, the bed temperature and power output rose quickly, then slowly fell to a value slightly above their initial value. The initial rise was caused by the initial increase in the amount of sulfur being absorbed. Since the sulfation reaction is exothermic, more heat is released in the bed, which causes the temperature and power output to increase. Following the initial increase, there is a long-term decrease in the power output and bed temperature. This decrease is caused by the decrease in the rate of sulfur absorption as the retention decreases, i.e., a decrease in the rate of the exothermic sulfation reaction. Note however, the changes are small although the transient represents a radical change in the coal sulfur content.

Step Change in Dolomite Flow Rate

Step changes in dolomite feed rate show similar trends in the change in retention and other parameters. Figure 7 shows the change in retention and average bed utilization following a step decrease by a factor of two in the dolomite flow rate and offtake rate. This results in a step change in the calcium sulfur ratio from 1.48 to 0.74. The transient change in retention and utilization is almost identical to that shown in Figure 5. The similarity is not a coincidence but a result of the fact that changes in coal sulfur and changes in dolomite feed have close to the same effect on the bed population distribution. This similarity in effect on population distribution will be illustrated later in this paper. The differences that do appear are a result of second order effects such as small changes in temperature and excess air.

The power output and bed temperature change for the transient in dolomite flow rate are shown in Figure 8. A similar trend is seen in Figure 6. The temperature rises quickly following the step change then gradually decreases. The increase in temperature is due to a rapid decrease in the endothermic calcination reaction. The gradual decrease is caused by a decrease in the exothermic sulfation reaction as the retention decreases.

Variation of Bed Response

The response of the bed to step changes is nonlinear. Figure 9 shows the normalized response of retention following two step changes in coal sulfur. One is a change from a coal sulfur content of 3.9% to 1.95% (Ca/S 0.74 to 1.48). The other transient is the reverse of the first (Ca/S 1.48 to 0.74). Note the difference in the response of retention. Although both transients have the same end points, the response is significantly different. The initial change in retention is much more rapid for the change that increases Ca/S ratio. However, the transient respone for a decrease in Ca/S ratio initially has a slow response, but reaches equilibrium conditions sooner than the increase in Ca/S ratio. This effect is due to changes in the population distribution of the bed and will be discussed in the next section.

Not only is the retention response of the bed a function of the direction of step, but it is also a function of the size of the step. Figure 10 shows the normalized change in retention following several step changes in dolomite flow rate. Increases in Ca/S ratio produce responses which are initially faster than decreases in Ca/S ratio. This trend is similar to that previously discussed. However, the point to be noted is that the response of the bed is not only a function of the direction of the response but the size of the change.

Bed Inventory Distribution

As previously described, the moles of calcium (and consequently particles) within the bed can be characterized by a distribution over size and utilization. The steady state bed inventory distribution for a Ca/S ratio of 1.48 is shown in Figure 11. The distribution can be thought of as a three-dimensional surface. This surface changes with time in response to changes in the input, offtake, or other bed conditions.

The reader should note that the distribution tends to peak at rather large utilizations. This is due to the rather long residence time of particles within the bed. It also points out the need for knowing the reaction rates of particles to very high utilizations. Although the rate at large utilizations is small, the population is large. Consequently, these particles absorb a significant amount of sulfur. In addition, the reader should note that smaller sizes peak at larger utilizations. This is due to the larger reaction rates of the small particles.

Also note that the population distribution ends at 300 μm. In a PFB with no recycle, particles below this size are quickly elutriated from the bed and do not absorb appreciable amounts of sulfur while they are in the bed (26). Moreover, their steady state population within the bed is extremely small.

The equation that governs the population is equation (12). In word form written for particles of a particular size and utilization, the equation is

Rate of Inventory Change	=	Rate of Feed (1)	-	Rate of Offtake (2)	-	Rate of Elutriation (3)

+	Rate of Production of Fine Particles Due to Attrition (4)	+	Net Rate of Change Due to Sulfation (5)	+	Net Rate of Change Due to Attrition (6)

It is important that the reader understands the terms in this equation, because it will be referred to several times in the next few pages to explain how processes in the bed interact. The physical significance of the first three and the fifth term on the right hand side is obvious. The fourth term is the rate of generation of small particles by attrition. The sixth term is the rate of change due to the shrinking of particles caused by attrition. Not all the terms are finite over the entire population range. For example, the first term, Rate of Feed, is only finite for particles of the lowest utilization.

Particle Size Distribution

Table 3 shows the population size distribution for the dolomite feed material and the bed inventory. The table shows very little difference between these two sets of data. From this it can be concluded that the terms in the population equation that affect the size distribution of the inventory are rather small. For the purpose of obtaining a basic understanding of the processes occurring following a transient, terms 4 and 6 of the inventory equation can be thought of as negligible. Moreover, term 3 can also be neglected because it primarily affects small particles which add little to the net rate of sulfur capture.

Consequently, only terms 1, 2 and 5 are important in understanding the transient response of sulfur capture.

Table 3

COMPARISON OF FEED SIZE DISTRIBUTION AND BED INVENTORY DISTRIBUTION

Size (μm)	% Feed	% Bed
2100	2.00	2.00
1925	2.00	2.00
1750	4.00	4.00
1575	7.00	7.00
1400	10.00	9.99
1225	12.00	11.98
1050	15.00	14.97
875	18.00	17.95
700	18.00	18.02
525	10.00	10.03
350	2.00	2.06

Utilization Distribution

Although the full population distribution was shown in Figure 11, it is valuable to look at the distribution of particles over utilization for a very small size range. Figure 12 shows the steady state utilization distributions for several calcium sulfur ratios for particles of 1050 μm $\pm$ 87 μm. The buildup of particles at high utilizations is more pronounced for low Ca/S ratios than high Ca/S ratios.

An interesting fact to note is that the utilization population distribution is not a strong function of the absolute molar flow rate of calcium and sulfur as long as their ratio remains the same. Table 4 shows the utilization population distribution for a Ca/S ratio of 1.48 for two different feed rates. This fact is used in choosing the preferred control concept.

Table 4

UTILIZATION DISTRIBUTION OF 1050 $\pm$ 87 m PARTICLES FOR TWO SULFUR FEED RATES BUT THE SAME Ca/S RATIO OF 1.48

Utilization (%)	3.9% S Coal (kg moles)	1.95% S Coal (kg moles)
0-10	7.3	7.0
10-20	10.5	10.1
20-30	12.2	11.7
30-40	14.9	14.4
40-50	21.5	21.0
50-60	26.9	26.0
60-70	28.6	37.7
70-80	97.6	98.1
80-90	144.3	151.2
90-100	1.3	0.4

Transient changes in the population distribution show a distinct wave pattern. Figure 13 shows how the population distribution changes when the dolomite feed and offtake rate are decreased. Note that the population of the lower utilization particles are affected first. This effect is somewhat analogous to changes in the birth rate of the U.S. The change is first felt by younger age groups, and then propagates to older age groups.

Surprisingly, changes in the sulfur input to the bed produce the same wave effect. Figure 14 shows how changes in the sulfur feed rate affect the population distribution. The dashed curves represent a change in Ca/S ratio from 1.48 to 0.74 by changing the sulfur feed rate. This change is the same change in Ca/S ratio as that performed for the results shown in the previous figure, but the change was accomplished by changing the coal sulfur content instead of dolomite flow rate. It is easy to see why changing the dolomite feed rate would cause a wave effect in the population, but it is not as obvious for changes in sulfur input. To understand this, the reader must realize that particles are continually moving from low to high utilizations as a result of abosrbing sulfur. When additional sulfur is added to the bed, the rate of sulfur absorption increases. The rate of particles moving to higher utilizations also increases. If the feed rate is not increased in proportion to this increased rate of movement to higher utilizations, the population of particles in the lower utilizations must decrease to a new steady state value.

Also shown on Figure 14 is the reverse transient, i.e., a decrease in sulfur input from a Ca/S ratio of 0.74 to 1.48. Again, a wave effect can be seen traveling from lower to higher utilizations. The reader should note the difference between the transient population distributions for the two cases. Although the end points of the changes are the same, the transient distribution for a change in Ca/S ratio will never be the same as that for the reverse direction. This irreversible effect causes the nonlinear response of retention (Figure 9) as a function of direction of change.

CONTROL OF SULFUR CAPTURE

The previous discussion has given the reader an understanding of how sulfur absorption by a fluidized bed responds to changes in sulfur and absorbent input. In a utility application it is important to maintain the integrated sulfur emission within the emission limits. Natural variations in coal sulfur content and changes in load will affect the sulfur emissions.

While typical load changes are easily evaluated, little data exists in the open literature on natural variations in coal sulfur content. La Mantia et al. (27) has found upward excusrions of up to 46% over 5 months of operation of a 40 MWe plant using high sulfur coal. Meyer (28) has studied the variation in coal sulfur for a low sulfur coal plant and found a standard deviation of 0.17.

This study has evaluated various methods of controlling the sulfur absorption properties of the bed in response to sulfur content variations. There are four methods of control: dolomite feed margin, changing the size distribution of the dolomite feed, feeding dolomite of higher reactivity, and adjusting the dolomite feed rate.

The sulfur capture properties of the fluidized bed may be controlled without any sophisticated control system by simply setting the dolomite feed rate at some level above the minimum Ca/S ratio required to maintain the desired percentage retention. This practice provides a margin so that the integrated retention within the bed complies with emission limits. The margin is required primarily because upward excursions in the coal sulfur content affect the integrated retention more severely than downward excursions.

The amount of margin required is difficult to define. The minimum required margin will be a function of the magnitude and frequency of sulfur excursions because of the nonlinear response of the bed. The designer of this system would like to use as small a margin as is necessary, because margin increases the capital and operating costs of the plant. Additional capacity must be included in the dolomite feed and offtake system. Moreover, additional dolomite will be required per unit output. These additions will cause an increase in the cost of electricity and solid waste disposal.

The remaining three methods of control attempt to control sulfur emissions on an instantaneous basis. However, to maintain constant retention on an instantaneous basis in a fluidized bed power plant, the retention of the bed must be continuously measured. Conventional scrubber plants determine instantaneous sulfur capture by measuring the amount of sulfur in the flue gas before and after the scrubber module. Consequently, control of the absorption system can be performed using only flue gas monitors.

Sulfur leaving a fluidized bed can be measured using normal flue gas techniques, but sulfur entering the bed requires special equipment. From a review (26) it was found that prompt neutron activation analysis (PNAA) of the coal fed into the bed appears to be a fast, accurate, and technically viable method of performing this task.

Changing the size distribution will ultimately change the reactivity of the bed and its rate of absorption. If this were used as a control action, the feed size distribution could be decreased in order to increase the bed reactivity in response to upward excursions in coal sulfur content. Investigation of this control action, using the model, indicated that the response of this control action was too slow to be practical.

Higher reactivity absorbant can be used to control sulfur emissions by feeding some of this material into the bed when there is an upward excursion in coal sulfur content. This control action was rejected because the range of reactivities for

various dolomites was not large enough (29) to insure required changes in bed reactivity. This is particularly true when normal operation of the bed uses an already high reactivity dolomite such as 1337.

Sulfur absorption by the bed can also be controlled by adjusting the dolomite feed rate in proportion to increases and decreases in the rate of sulfur entering the bed. This control maintains a constant Ca/S ratio. The equipment required to perform this function is normal plant equipment, but the equipment must be oversized in order to accommodate excursions in sulfur content. The specific components that will be affected are dolomite feed system, bed particle offtake system and, to a small extent, hot gas clean-up system.

Figure 15 shows the change in retention using this scheme following a step decrease in the amount of sulfur content of the coal. The retention drops, but only by a few tenths of a percent.

In order to understand why this sytem is projected to work well, the processes that occur following the step change will be reviewed. Both the sulfur leaving the bed R_o and the sulfur entering the bed R_i are proportional to coal sulfur content. Consequently, immediately following a step change in the sulfur content of the coal, both R_i and R_o are increased by the same proportion. Retention, r', does not change. The value of r' will change only when the reaction rate constant, K_1, changes or α changes. The value of K_1 will change only when there is a shift in the population distribution. This population distribution was shown previously to remain practically constant as long as the Ca/S ratio was held constant. The reason for this is that the major source and sink terms in the population distribution equations are increased and decreased proportionately.

The value of R_o and r' will also change when α changes. A change in α represents a change in the sulfur generaiton function. From the previous parametric study of the sulfur generation function it was shown that large changes of the sulfur generation function do not significantly affect the retention except at very high levels of retention. However, it is unlikely that the sulfur generation function will change enough to significanlty affect the values of R_o and r'.

An added advantage of this system is the ability for the system to account for variations in the reactivity of dolomite particles. This is done by adjusting the ratio of dolomite feed to sulfur feed in response to long-term trends in retention changes. Moreover, this control system was found to be economically competitive with the dolomite feed margin control system, and will have less solid waste (26). This system was also found to adequately control sulfur emission during load changes.

A possible disadvantage to this control system is that the amount of elutriated fines may increase as the dolomite feed is increased. If one assumes that generation of dolomite fines is proportional to dolomite feed rate, and that the rate of attrition at steady state is similar to the rate found by the NCB in their Leatherhead facility using 1337 dolomite (25), half of the elutriated material will be fly ash. Consequently, the particulate loading of the hot gas will increase by 1% for every 2% increase in dolomite flow. This rate increase represents a maximum rate of increase because it is not certain that the rate of generation of dolomite fines is proportional to dolomite feed. Of the dolomite fines which are found in the flue gas, most are produced by attrition of particles within the bed.

The bed population distribution and bed inventory remain essentially constant during transients as long as the Ca/S ratio is maintained constant. This fact is important because it is known that particles become harder as their utilization increases. Because the population distribution does not change, increasing the dolomite feed rate does not change the number of particles of any given utilization. Consequently, the rate of attrition may not change because the number of weak particles at low utilization does not change.

ACKNOWLEDGMENT

This project has been funded at least in part with Federal funds from the U.S. Environmental Protection Agency under contract number 68-02-3131. The content of this publication does not necessarily reflect the views or policies of the U.S. Environmental Protection Agency, nor does mention of trade names, commercial products, or organizations imply endorsement by the U.S. Government. Mr. D.B. Henchel is gratefully acknowledged as the EPA Project Manager.

LIST OF SYMBOLS

A	= Surface area of tubes within the bed, m^2
A_b	= Cross-sectional area of bed, m^2
$C_{p,b}$	= Specific heat of bed, j/kg^oK
d	= Particle size (diameter), m
d_u	= Particles size of a particular utilization (diameter), m
D_{SA}	= Diffusivity, cm^2/s
f_d	= Fraction of particles below size d (unitless)
f_s	= Weight fraction of sulfur in coal
h	= Heat transfer coefficient, $W/m^{2o}K$
h_{in}	= Enthalpy of species entering the bed, J/kg
h_{out}	= Enthalpy of species leaving the bed, J/kg
ΔH_R	= Rate of energy release by chemical reactions, W
k_a	= Attrition rate constant (unitless)
k_h	= Factor that accounts for changes in the heat transfer coefficient due to changes in bed temperature (unitless)

$k_1(d,U)$ = Specific constant for SO_2 absorption for particle of size d, and utilization U, m^3/s kg mole

K_1 = Overall rate constant for sulfur absorption

K_2 = Constant defined by equation (6), kg moles/m^3

L_f = Height of fluidized bed, m

m_{coal} = Mass feed rate of coal, kg/s

$\dot{m}_{out}$ = Rate of mass leaving the bed, kg/s

$\dot{m}_{in}$ = Rate of mass entering the bed, kg

$\dot{m}_{coal}$ = Rate of coal feed, kg/s

M = Moles of calcium, kg moles

M_b = Moles of calcium in bed, kg moles

$M_{d,u}$ = Moles of particles in the bed of size d and utilization U, kg

M_s = Molecular weight of sulfur, kg/kg mole

N = Molar distribution of bed, kg mole/m

$\dot{Q}_s$ = Rate of energy going to steam, W

r = Particle radius, cm

r' = Retention (unitless)

R_e = Reynolds number (unitless)

R_o = Rate of SO_2 moles leaving the bed, kg moles/s

R_i = Rate of sulfur moles entering the bed, kg moles/s

T = Temperature of bed, ^oK

T_{lm} = Log mean temperature difference between steam and bed, ^oK

t = Time, s

t_{cal} = Calcination time, s

U = Utilization (unitless)

U_e = Gas velocity through interstices of bed, m/s

U_{mf} = Minimum fluidization velocity, m/s

U_{sg} = Superficial gas velocity, m/s

V = Volume of bed, m^3

x = Distance from bottom of reactor, m

Greek Symbols

α = Fitting parameter for sulfur generation (unitless)

η_L = Combustor fraction loss (unitless)

REFERENCES

1. Commercial Plant Design Definition, FE-2357-28 (DOE), General Electric Company, 1979.
2. M. Horio and C.Y. Wen, "Simulation of Fluidized Bed Combustors Part 1. Combustion Efficiency and Temperature Profile," Fluidization: Application to Coal Conversion Processes, AIChE Symposium Series, Vol. 74, 1978, p. 101-111.
3. R. Rajan, R. Krishnan, and C.Y. Wen, "Simulation of Fluidized Bed Combustions, Part II. Coal Devolatilization and Sulfur Oxides Retention," Fluidization: Application to Coal Conversion Processes, AIChE Symposium Series, Vol. 74, 1978, pp. 112-119.
4. S.E. Tung et al., "The Fluidized Bed Combustion Modeling," Proceedings of a Conference on Mathematical Modeling of Coal Conversion Processes, ERDA ONF-761104, 1976, pp. 4-55.
5. R.C. Hoke et al., Miniplant Studies of Pressurized Fluidized Bed Coal Combustion: Third Annual Report, EPA-600/7-78-069, Exxon Research and Engineering Co., 1978.
6. M. Horio and C.Y. Wen, "Analysis of Fluidized Bed Combustion of Coal with Limestone Injection," Fluidization Technology, Hemisphere Publishing Corp., Washington, D.C., 1976.
7. T.P. Chen and S.C. Saxena, "Mathematical Modeling of Coal Combustion in Fluidized Beds with Sulphur Emission Control by Limestone or Dolomite," Fuel, Vol. 56, 1977, pp. 401-413.
8. D.L. Keairns et al., Fluidized Bed Combustion Process Evaluation, Phase II, EPA-650/2-75-027-C, Westinghouse Research Laboratories, NTIS PB246-116, 1975.
9. S.E. Tung, J. Goldman, and J.F. Lewis, "FBC Modeling and Data Base," Proceedings of the Fifth International Conference on Fluidized Bed Combustion Vol. III, Mitre Corporation, McLean, VA, 1978, p. 406.
10. F.V. Bethell, D.W. Gill, and B.B. Morgan, "Mathematical Modeling of the Limestone – Sulfur Dioxide Reaction in Fluidized Bed," Fuel, Vol. 52, 1973, p. 121.
11. F.S. Canada and M.H. McLaughlin, "Large Particle Fluidization and Heat Transfer at High Pressures," Fluidization: Application to Coal Conversion Processes, AIChE Symposium Series, Vol. 74, 1978, pp. 27-44.
12. J.F. Davidson and D. Harrison, Fluidization, Academic Press, London, 1971, p. 514.
13. A. Bar-Cohen, L. Glickman, and R. Hughes, "Fluid Dynamic Modeling of Fluid Bed Combustors," Proceedings of the Fifth International Conference on Fluidized Bed Combustion Vol. III, Mitre Corporation, McLean, VA, 1978, p. 458.
14. S.P. Babu, B. Shah, and A. Talwalkar, "Fluidization Correlations for Coal Gasification Materials – Minimum Fluidization Velocity and Fluidized Bed Expansion Ratio," Fluidization: Application to Coal Conversion Processes, AIChE Symposium Series, Vol. 74, 1978, p. 176.

15. E.P. O'Neill, D.L. Keairns, and W.F. Kittle, "Thermogravimetric Study of the Sulfation of Limestone and Dolomite – The Effect of Calcination Conditions," Thermochimica Acta, Vol. 14, 1976, p. 209.

16. J.W. Chrostowski and C. Georgakins, "Pore Plugging Model for Gas-Solid Reactions," Chemical Reaction Engineering, AES Symposium Series No. 65, 1978, p. 225.

17. M. Hartman M. and R.W. Coughlin, "Reaction of Sulfur Dioxide with Limestone and the Grain Model," AIChE Journal, Vol. 22, No. 3, 1975, p. 290.

18. S. Siegel et al., "Relationship Between the Morphological Properties of Half-Calcined Dolomite and Kinetics of the Sulfation Reaction," Environmental Science and Technology, Vol. 12, No. 13, 1978, p. 1411.

19. R.H. Borgwardt, "Kinetics of the Reaction of SO_2 with Calcined Limestone," Environmental Science and Technology, Vol. 4, No. 1, 1970, p. 59.

20. R.A. Newby et al., Effect of SO_2 Emission Requirements on Fluidized Bed Combustion System, EPA-600/7-78-163, Westinghouse Research Laboratories, NTIS PB-286971, 1978.

21. D. Merrick and J. Highley, "Particle Size Reduction and Elutriation in a Fluidized Bed Process," Recent Advances in Air Pollution Control, AIChE Symposium Series, Vol. 70, 1973, pp. 366-378.

22. L.H. Perry and C.H. Chilton, Chemical Engineers Handbook, McGraw-Hill Book Company, New York, NY, 1976.

23. S. Walter, Letter Report from Exxon to K.R. Murphy of General Electric Co., 1979.

24. H.M. Hulbert and S. Katz, "Some Problems in Particle Technology," Chemical Engineering Science, Vol. 19, 1964, p. 555.

25. A.G. Roberts, P. Roven, and D.M. Wilkins, Pressurized Fluidized Bed Combustions, FE-1511-43 (DOE), National Research Development Corporation, London, England, 1977, p. 146.

26. S.D. Finnigan et al., Automatic Constant Percentage Sulfur Retention in a PFB Power Plant, Final Report EPA Contract 68-02-3131, in publication.

27. C.R. LaMantia et al., Final Report: Dual Alkali Test and Evaluation Program, Vol. III, Prototype Test Program-Plant Scholz, EPA-600/7-77-050C, U.S. Environmental Protection Agency, Research Triangle Park, NC, 1977.

28. J.P. Meyer, "Mathematical Modeling of Changes in the Distribution of Sulfur in Coal as It Undergoes Mining and Transport Operations," Environmental Science and Technology, Vol. 13, No. 9, 1979, p. 1104.

29. J.A. Shearer, I. Johnson, and C.B. Turner, The Effect of $CaCl_2$ Additive on the Reaction of SO_2/O_2 Mixtures with Carbonate Rock, ANL/CEN/FE-79-7, Argonne National Laboratory, Argonne, Ill., 1979, p. 33.

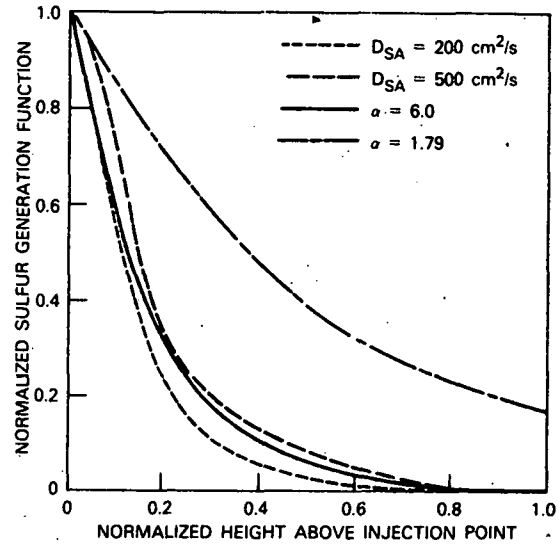

FIGURE 1 NORMALIZED SULFUR GENERATION FUNCTION VERSUS HEIGHT ABOVE INJECTION POINT

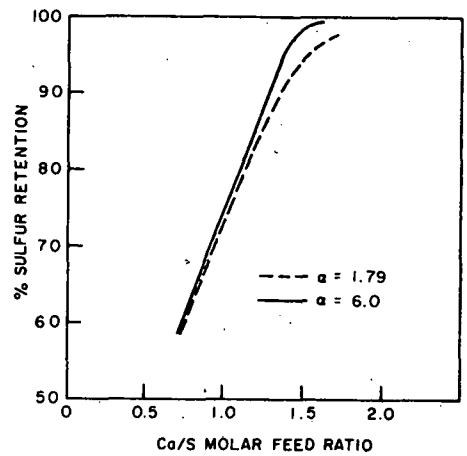

FIGURE 2 PERCENT RETENTION VERSUS Ca/S MOLAR FEED RATIO FOR AN OPTIMISTIC (α = 6.0) AND PESSIMISTIC (α = 1.79) PREDICTION OF SULFUR RELEASE.

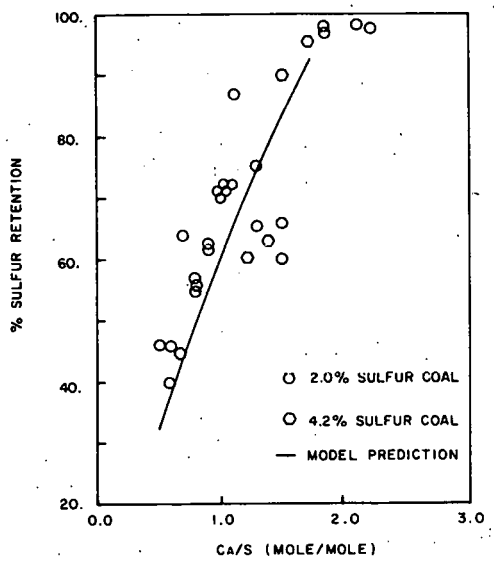

FIGURE 3 COMPARISON OF MODEL PREDICTION AND EXPERIMENTAL RESULTS FOR THE EXXON MIMIPLANT.

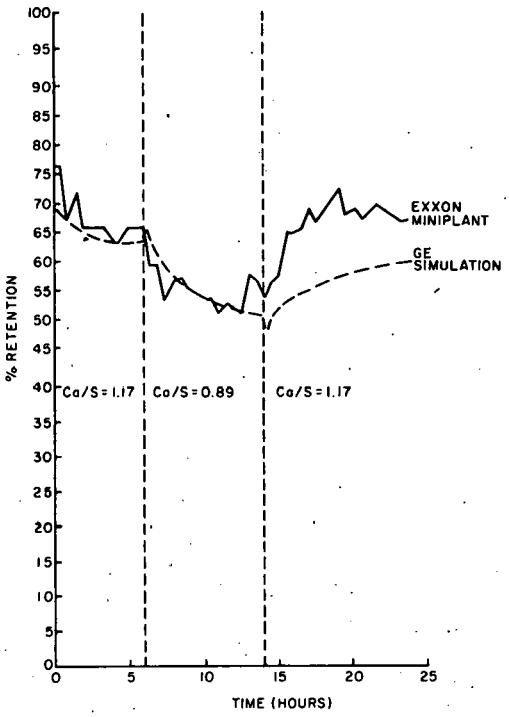

FIGURE 4 SULFUR RETENTION DURING TRANSIENT TEST.

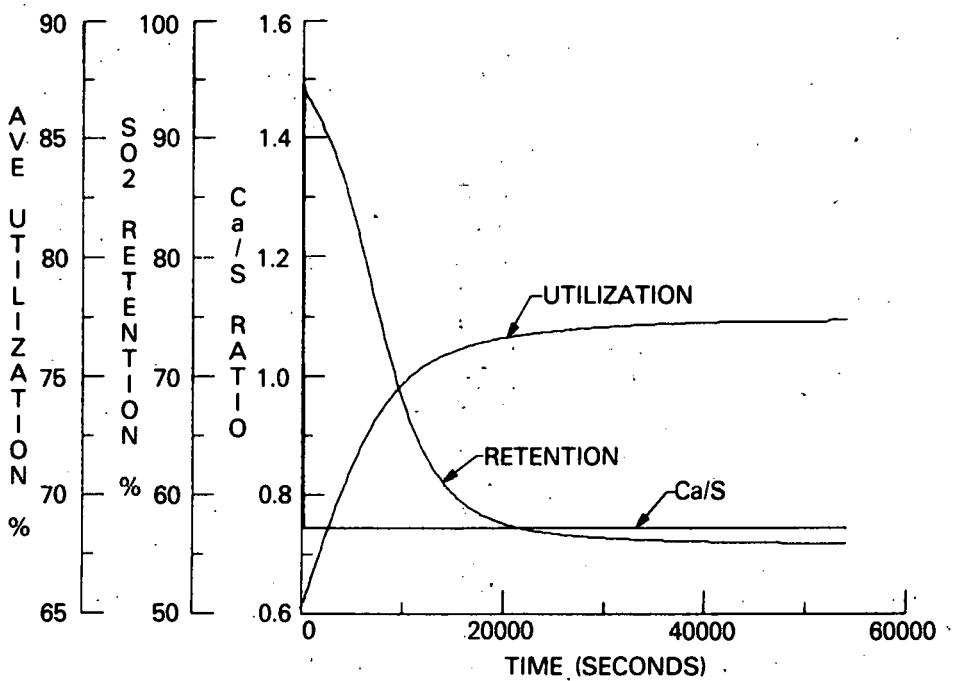

FIGURE 5 RESPONSE OF SULFUR RETENTION AND AVERAGE UTILIZATION FOLLOWING A STEP CHANGE IN COAL SULFUR CONTENT FROM 1.95% TO 3.9% AT 400 s (Ca/S FROM 1.48 TO 0.74)

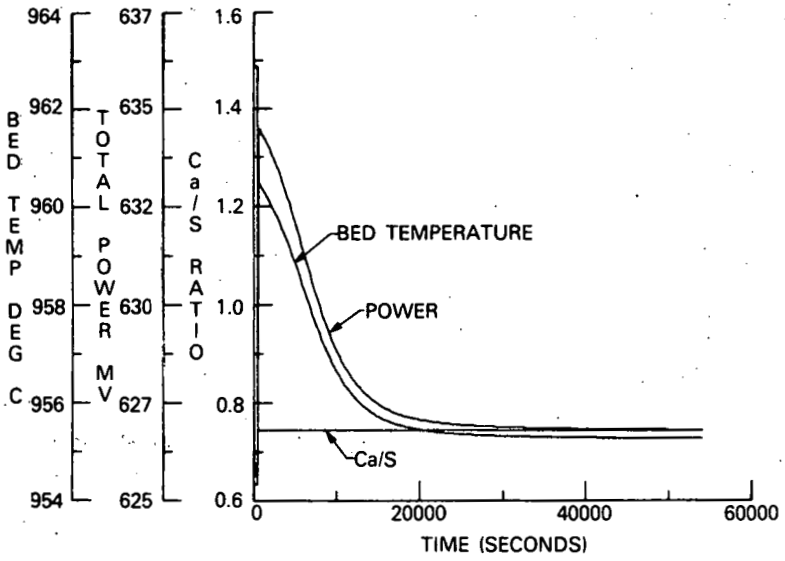

FIGURE 6 TRANSIENT RESPONSE OF BED TEMPERATURE AND POWER FOLLOWING A STEP CHANGE IN COAL SULFUR CONTENT FROM 1.95% TO 3.9% AT 400 s (Ca/S FROM 1.48 TO 0.74)

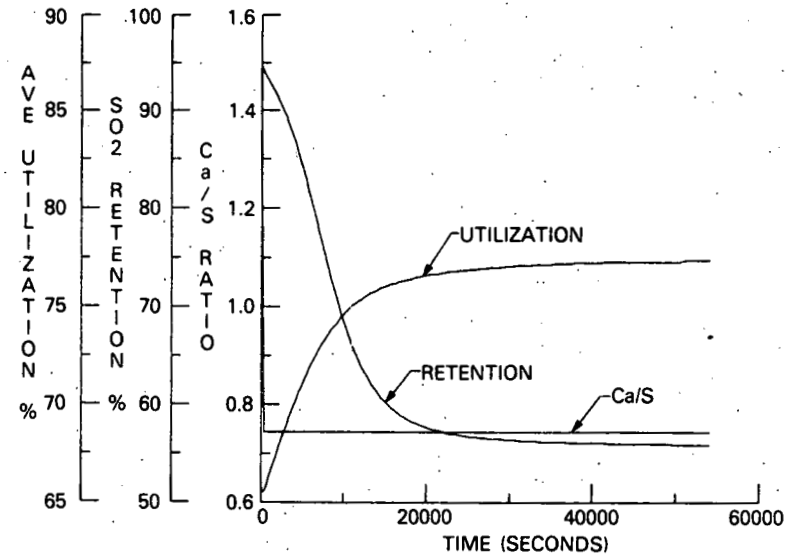

FIGURE 7 TRANSIENT RESPONSE OF SULFUR RETENTION AND AVERAGE UTILIZATION FOLLOWING A STEP CHANGE IN DOLOMITE FLOW RATE AT 180 s (Ca/S FROM 1.48 TO 0.74).

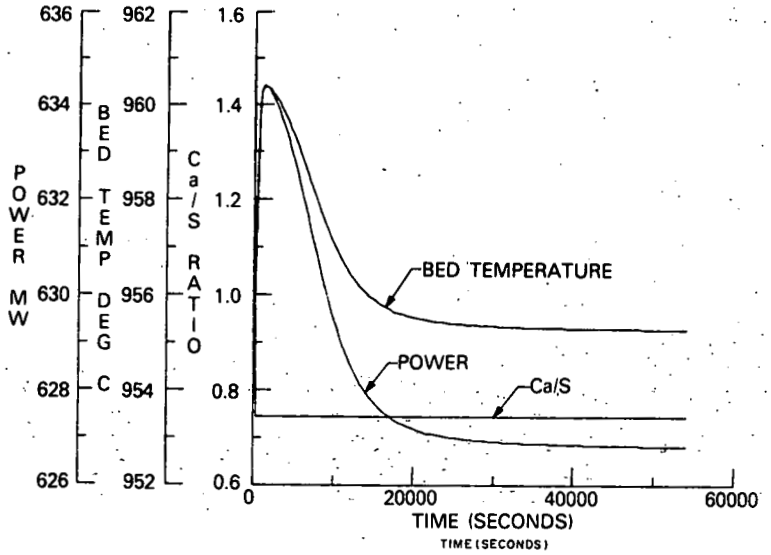

FIGURE 8 TRANSIENT RESPONSE OF BED TEMPERATURE AND POWER FOLLOWING A STEP CHANGE IN DOLOMITE FLOW RATE AT 180 s (Ca/S FROM 1.48 TO 0.74)

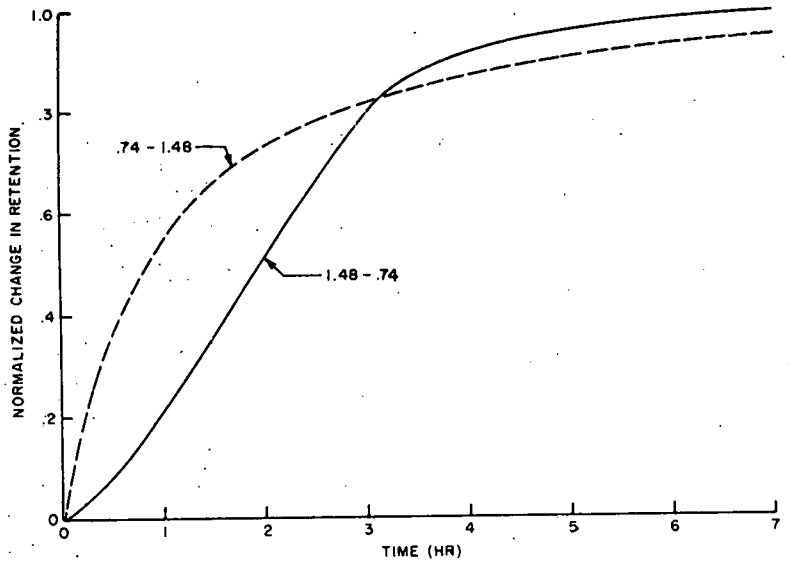

FIGURE 9 NORMALIZED CHANGE IN RETENTION AS A FUNCTION OF TIME FOR A STEP CHANGE IN COAL SULFUR CONTENT (Ca/S, 1.48 - 0.74: Ca/S, 0.74 - 1.48)

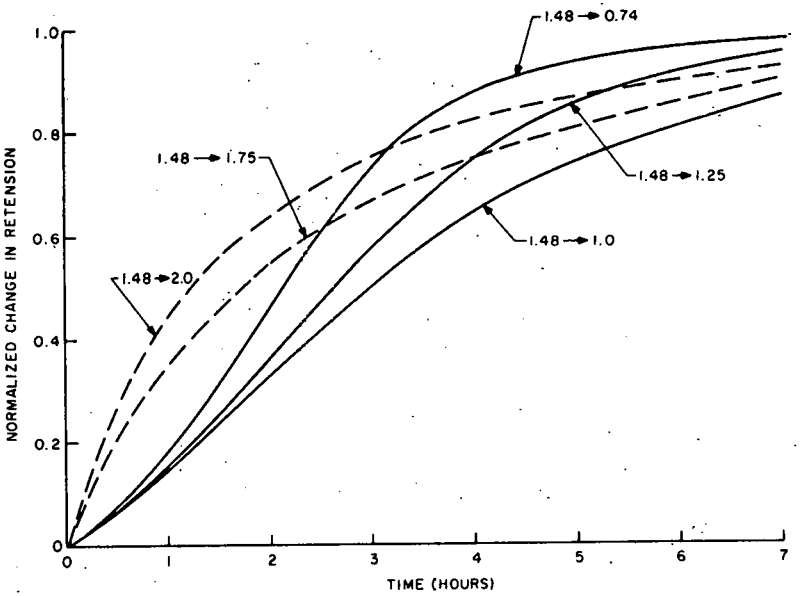

FIGURE 10 NORMALIZED CHANGE IN RETENTION AS A FUNCTION OF TIME FOR VARIOUS STEP CHANGES IN DOLOMITE FEED.

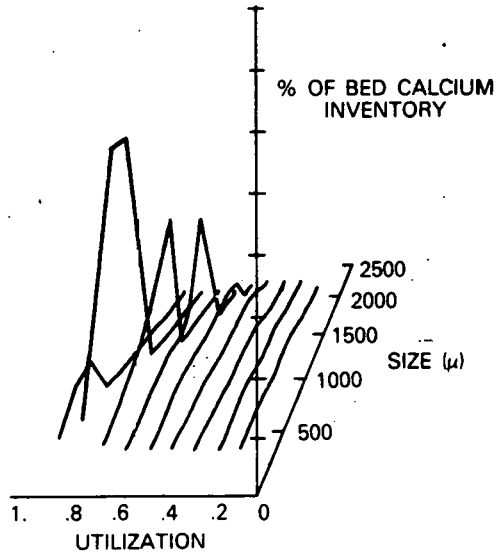

FIGURE 11 STEADY STATE CALCIUM DISTRIBUTION AS A FUNCTION OF SIZE AND UTILIZATION FOR A Ca/S RATIO OF 1.5

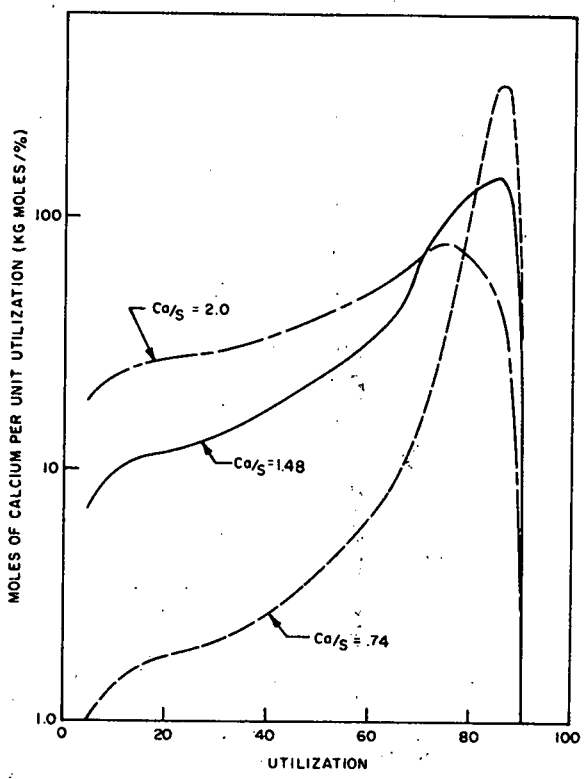

FIGURE 12 UTILIZATION DISTRIBUTIONS OF 1050 ± 87 μm PARTICLES FOR STEADY STATE Ca/S RATIOS OF 2.0, 1.48 AND 0.74

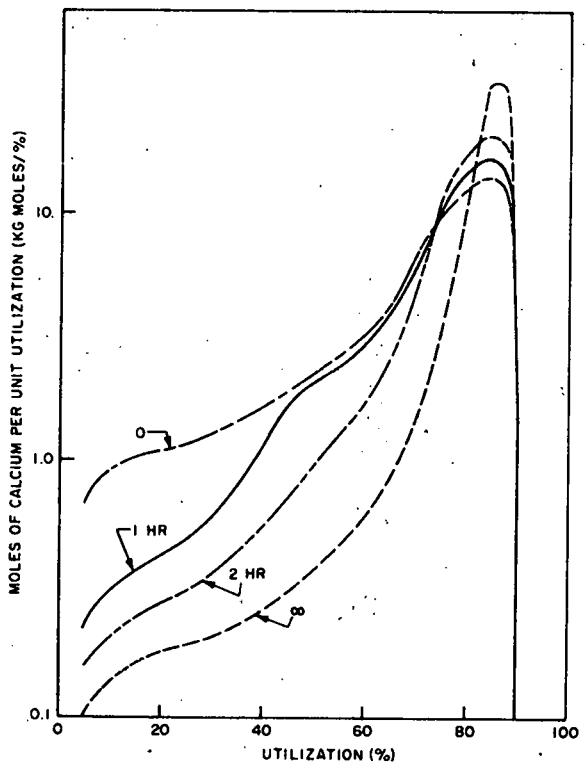

FIGURE 13 TRANSIENT UTILIZATION FOR A STEP CHANGE IN DOLOMITE FROM Ca/S 1.48 TO .74 FOR 1050 = 87 μm PARTICLES.

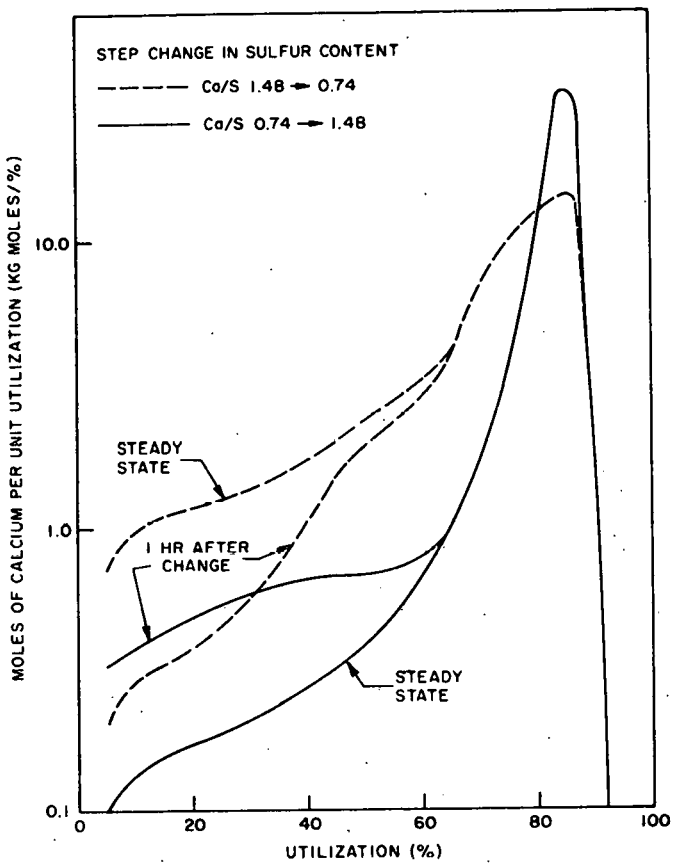

FIGURE 14 UTILIZATION DISTRIBUTIONS OF 1050 ± 87 μm PARTICLES FOR STEADY STATE Ca/S RATIOS OF 1.48 AND 0.74, AND TRANSIENT DISTRIBUTIONS FOR 1 HR AFTER A STEP CHANGE IN COAL SULFUR CONTENT

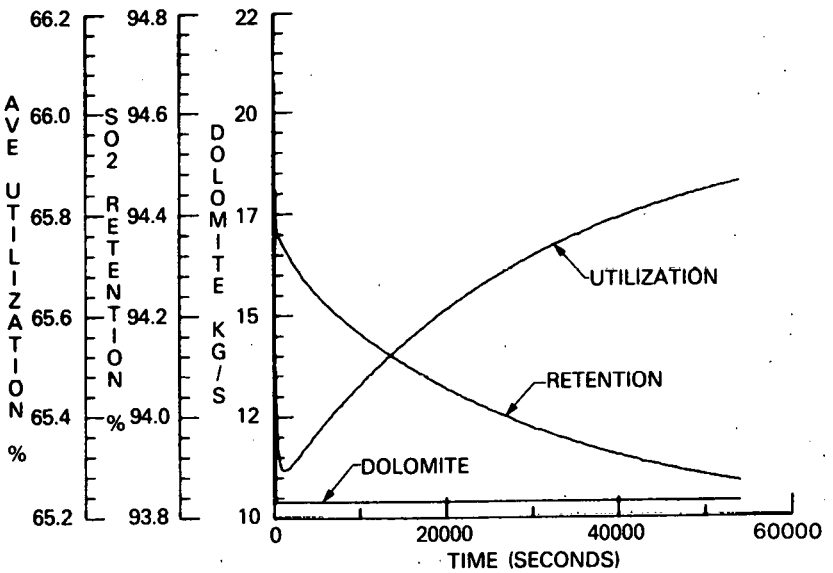

FIGURE 15 RETENTION AND UTILIZATION AS A FUNCTION OF TIME USING CONSTANT Ca/S RATIO CONTROL ACTION FOLLOWING A 50% DECREASE IN COAL SULFUR CONTENT AT 180 s (Ca/S = 1.48)

PROCESS TEMPERATURE CONTROL USING A MIXED PHASE FLUIDIZED BED COMBUSTION SYSTEM

Donald Anson

Battelle-Columbus

Introduction

Fluidized bed combustion of solid fuels is recognized to have a number of potential advantages over suspension burning or burning on grates. These advantages, on the whole, derive from the effectiveness with which chemical reactants in the gaseous fluidizing medium can be brought into contact with the bed solids. Rapid reaction rates approaching those set by chemical kinetics can be achieved, and solids residence times in the reaction zone are limited only by elutriation of fines after size reduction following reaction.

At the same time, heat transfer coefficients between the bed material and internally cooled tubes, etc. within the bed, are high, in the range 100-500 $Wm^{-2}\ K^{-1}$(20-100 $Btu/hr.ft^2F$). Under steady state conditions a fluidized bed combustor can sustain stable and efficient reactions with constant and relatively uniform transfer of heat to an immersed load.

The factors that determine the heat transfer coefficient in a fluidized bed are the particle size, the fluidizing gas velocity, and the tube configuration. In a given apparatus only the gas velocity can be readily varied, and if the apparatus is a combustor a change in gas velocity will also change the combustion rate or the reaction stoichometry. Usually, the gas velocity is determined by the need to control reaction conditions and cannot be used as an independent means of controlling heat transfer coefficient. Since the heat transfer coefficient is relatively invariable, changes in heat transfer rate must be accomplished by changes in the temperature differential between the fluidized bed and the heat absorbing surfaces.

In most industrial heating applications it is desirable, and sometimes essential, to maintain the heat receiver at a nearly constant temperature over a range of heat input rates. In a conventional fluidized bed this is most readily achieved by allowing the bed temperature to drop as the fuel input rate is decreased, until a new equilibrium is reached between the rate of heat generation and the rate of heat absorption by the load. When a major change in heat input to the process is required, the necessary drop in bed temperature can produce a very significant drop in the rates, or even the nature, of the chemical reactions in the bed.

Various methods have been proposed and used to permit control of heat transfer in fluidized bed combustors under conditions of variable fuel input. These include locating heat transfer surface so that it is immersed in the fluidized bed only under conditions of violent fluidization (corresponding to high combustion rate), varying the solids inventory in the bed, and defluidization or slumping of successive increments of the bed. Control may require more than one such method as well as variation in bed temperature.

To put the control problem into perspective, it must be added that coal fired heaters, such as utility boilers, which utilize both radiant and convective heat transfer mechanisms, encounter equally severe difficulties in maintaining simultaneous control of heat transfer, combustion stability, and metal temperatures in the heat exchange elements, during variable load operation.

This paper describes a development of fluidized bed combustion technology which permits independent control of reaction conditions, heat transfer rate, and the temperature of the heat receiving surface. This offers very significant advantages for a number of heating applications.

Description of Multi Phase Fluid Bed System

In this paper we describe the output control features of a fluidized bed system in which several phases of the fluidization process are utilized. The word "phase" is used to define a fluidization phenomenon rather than the physical states of matter in the system; specifically, reference is made to low turbulence fluidization, turbulent fluidization, and entrainment. Low turbulence fluidization occurs in the superficial gas velocity range between the minimum that will produce fluidization and about ten times that velocity. Turbulent fluidization typically requires ten or more times the minimum fluidization velocity, and is typified by relatively violent agitation of the bed with rapid mixing. Entrainment occurs when solids are transported from the fluidized bed by the fluidizing gas moving at velocities exceeding the free fall velocities of the solid particles.

The Battelle Multi Solids Fluidized Bed Combustor (MSFBC) which is illustrated in Figure 1, uses a turbulent fluidized bed of large particles (typically 3-9 mm (1/8 - 3/8") in size) to establish a well mixed reaction zone. Coal fed into this turbulent reactor is rapidly distributed and is

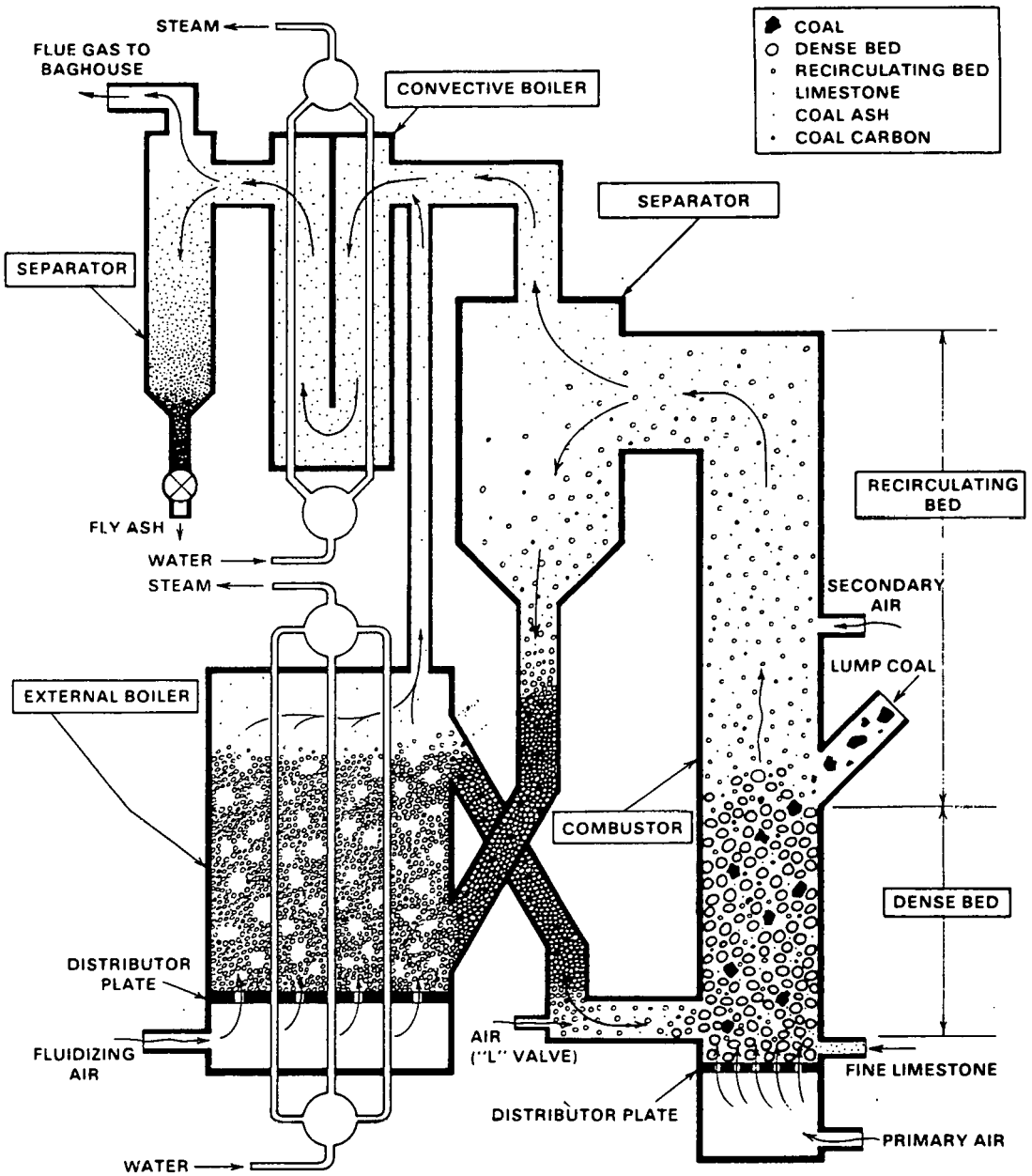

FIGURE 1. BATTELLE MULTI-SOLID FLUIDIZED-BED COMBUSTOR

retained until the particles are burnt to a size at which they are small enough to be elutriated. Fine reactants, in particular limestone for SO_2 removel, are fed into the bottom of the bed, are entrained by the fluidizing gas, and after multiple collisions with the coarse bed solids are eventually elutriated and entrained in the gas leaving the bed.

The heat generated by combustion is removed by feeding a fine granular material (0.5-1 mm (18-25 mesh) in size) into the bottom of the turbulent bed. This material is also elutriated, but in passing through the reaction zone it becomes heated to the bed temperature; thus, leaving the bed are both gas and an entrained stream of fine granules, which includes some fine fuel particles and limestone if sulfur removal is desired. These hot granules are separated from the gas and pass to a second fluidized bed which is maintained in a state of low turbulence. Heat absorbing tubes immersed in this bed reduce the temperature of the granules, which are then returned to the combustor for reheating.

The characteristics of the turbulent fluidized bed reactor are described in a separate paper at this conference*. This paper is concerned only

* Control of Sulfur Dioxide and Nitrogen Oxide Emissions - H. Nack and K. T. Liu.

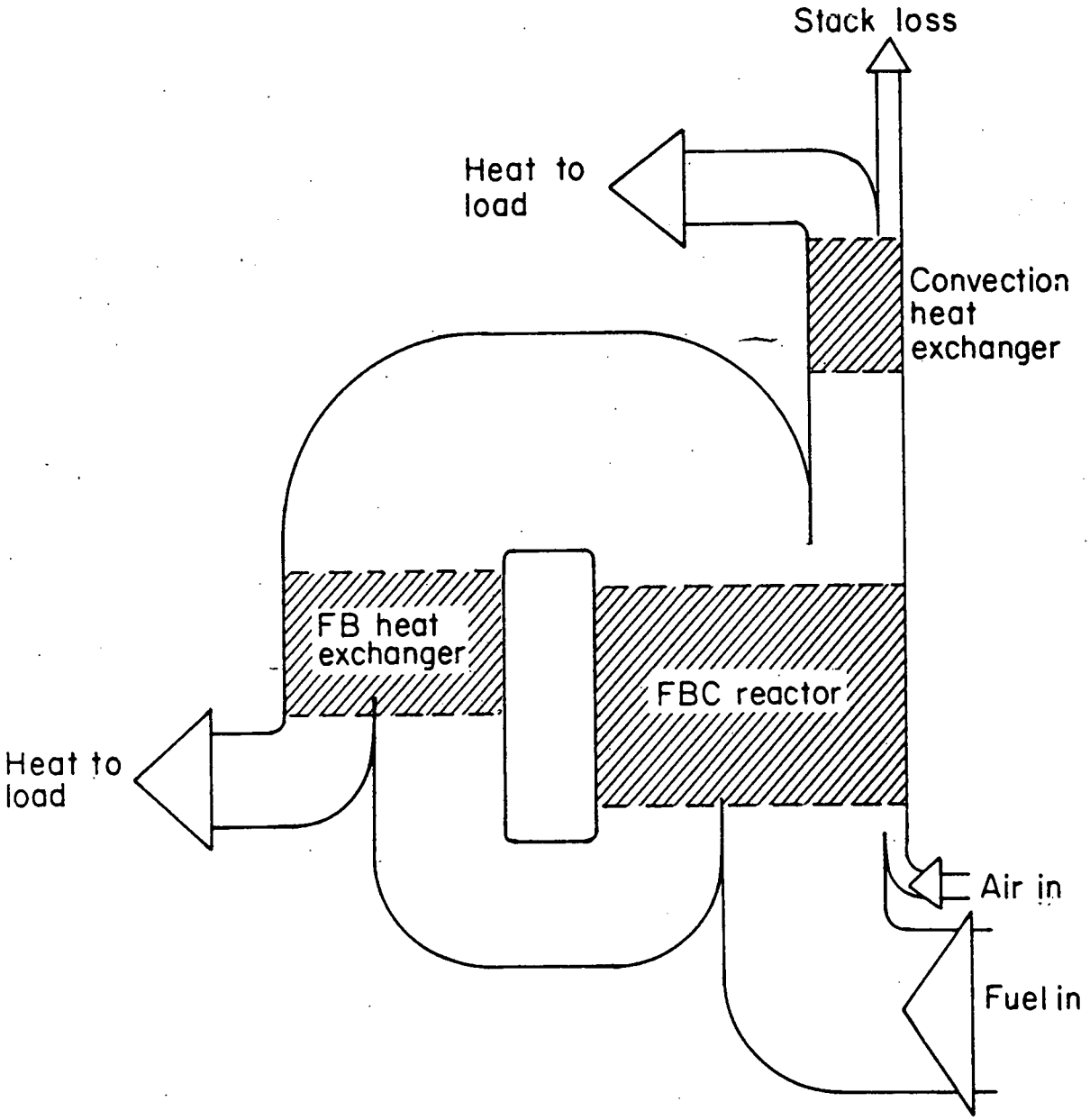

FIGURE 2. HEAT FLOW IN MSFBC SYSTEM

with some of the heat transfer aspects of the system, and with illustrating how they may be applied.

The heat flow in the Battelle MSFBC is illustrated in Figure 2. The rate at which heat is recirculated between the combustor and the fluidized bed heat exchanger may greatly exceed the rate of heat input from the fuel and the rate of heat abstraction from the system. These last two rates must, of course, be in balance, but the recycle rate can be set at any desired level. The heat recycle rate must be carefully distinguished from the mass recycle rate. Thus zero heat recycle rate can occur either when no solids are recycled between the combustor and the heat exchanger, or when the recycled solids are at the reference temperature of the system. In practice, the latter condition is impractical, since the recycled material must be at a higher temperature than the load. Factors limiting the heat transfer capability of the system are discussed in the next section.

System Constraints and Control

The most important constraint on the system as described is the reactor temperature. Generally it is desirable to keep this within fairly close limits which depend on the fuel and other reactants. For coal fired systems in which sulfur emission control is a major objective, the optimum temperature has been found to lie between 850 C and 930 C.

Without emission control, higher temperatures could be tolerated, and combustion reaction rates would be enhanced, but eventually problems would be encountered because of ash softening and agglomeration of the bed material.

As in any other combustion reactor, the temperature in the combustion zone (the turbulent fluidized bed) depends on the relative rates of heat release and heat abstraction from the reactants. In the MSFBC system, heat is abstracted by the cool recycled material from the fluidized bed heat exchanger. The steady state combustor temperature at a given fuel input rate may be controlled only by changing the rate of heat absorption in the fluidized bed heat exchanger, or by changing the air/fuel ratio. This is made clear by reference to Figure 2, which shows that the balance of the heat leaving the combustor is recycled. If the heat absorbing surface in the fluidized bed heat exchanger is to be maintained at constant temperature, then the bed temperature must change or the heat transfer coefficient must be altered. Algebraically, equating the heat lost by the recirculating solids to that gained by the load in the fluidized bed heat exchanger, we get

$$\dot{m}\, C_S\, (T_C - T_r) = (T_r - T_\ell)\, hA$$

Where $\dot{m}$ = solids recycle rate

C_S = specific heat of solids

T_C = combustor temperature

T_r = recycle temperature

T_ℓ = load temperature

h = overall heat transfer coefficient

A = heat transfer area

$$\text{Rearranging, } T_r = \frac{T_C\, m\, C_s + T_\ell\, hA}{hA + \dot{m}\, C_s}$$

If the quantities T_C, T_ℓ and C_S and A are assumed to be constant, then T_r can be controlled by manipulating $\dot{m}$ (the recirculation rate) or L (the fluidized heat exchanger heat transfer coefficient). The value of $\dot{m}$ can be varied over a wide range, and provides the principal means of controlling T_r in practical systems.

Figure 3 shows an example of how the fluidized bed heat exchanger temperature and the heat transfer to the load would vary with the solids recycle rate $\dot{m}\, C_S$. In this case the load is assumed to be kept at the constant (desired) temperature of 550° C, while the fluidized bed combustor is maintained at 900° C. The heat transfer rate can be controlled from zero to 80 kW m^{-2}(25,000 Btu/ft^2 hr.), with only 150° C variation in the temperature of the heat transfer bed. These conditions are typical of those in large steam generators for utility use.

A second way of achieving changes in heat transfer rate to the load is to change the heat transfer coefficient. While the control range by this method is relatively small, generally not more than about ± 15%, the response rate can be high since the output derives directly from heat stored in the bed and is not dependent, in the short term, on changes of other parameters such as firing rate. This method can only be regarded as a way of dealing with transients since the heat capacity of the fluidized bed is normally relatively small. Changes in the heat transfer coefficient can be achieved in beds of fine particles by altering the fluidizing conditions. Figure 4 illustrates this point. The ability to control heat transfer in this way in fluidized bed combustors with immersed tubes is severely restricted by the associated effect on the combustion process.

Because of the good mixing characteristics of fluidized beds the mean temperature in a heat transfer bed is close to the exit temperature of the bed material and not to the inlet temperature. In many applications this is advantageous, since the mean bed temperature can be chosen to place an upper limit on the heat transfer rate and thus protect heat exchanger surfaces from overheating in the event of the coolant flow rate becoming restricted. Where high temperatures are essential, as for instance for indirectly fired gas turbines, the heat transfer bed must be subdivided to provide a succession of small temperature drops. This can be done quite simply by allowing the fluidized solids to cascade under gravity from one subdivision to another. Such systems can be arranged so that an ideal countercurrent system is approached.

In order to maintain the combustor temperature at a constant level the division of heat generated between the gaseous combustion products and the recycled solids must also be kept in a constant proportion. For example, in order to maintain the final reactor temperature at 900° C when burning a bituminous coal with 20% excess air preheated to 300° C, it is necessary to remove 58% of the heat in the recycled solids. The heat in the flue gases would be 42% of that released by combustion, of which perhaps 32% of the total would be recovered in convection heat exchangers and the other 10% lost to the stack. Thus, in a typical coal burning application about two thirds of the heat transfer occurs in the fluidized bed heat exchanger, and one third in the convection surface.

As the fuel and air feed rates are reduced, a point is reached at which the combustor ceases to be adequately fluidized. This represents an absolute lower limit to the operation of the combustor unless the fuel/air ratio is decreased. In practice, the combustor can be operated over about a 3:1 turn down ratio with a constant fuel/air ratio. Operation is possible at lower fuel input rates so long as the air throughout is maintained. Under these conditions the heat carried away in the flue gases must

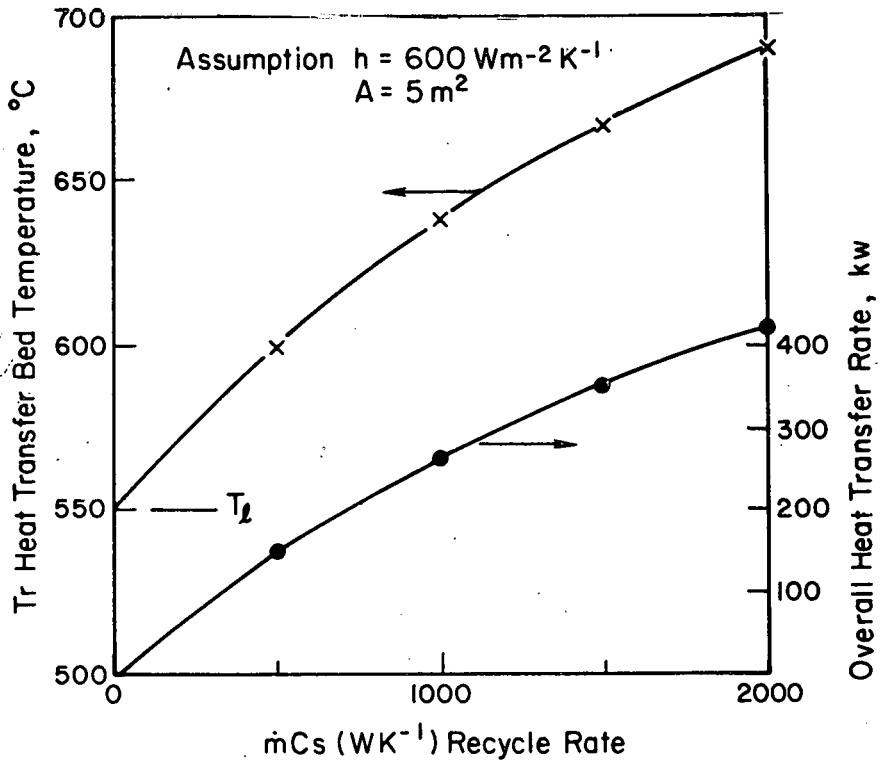

FIGURE 3. HEAT TRANSFER BED TEMPERATURE T_r AND HEAT TRANSFER RATE RELATED TO SOLIDS RECYCLE $\dot{m}C_s$.

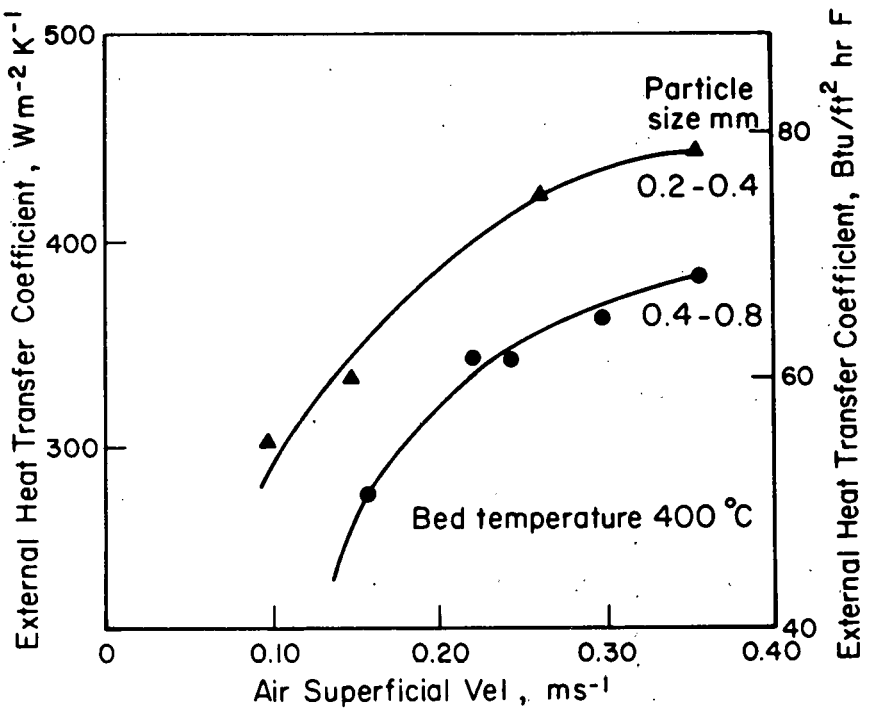

FIGURE 4. EFFECT OF FLUIDIZING GAS VELOCITY ON HEAT TRANSFER

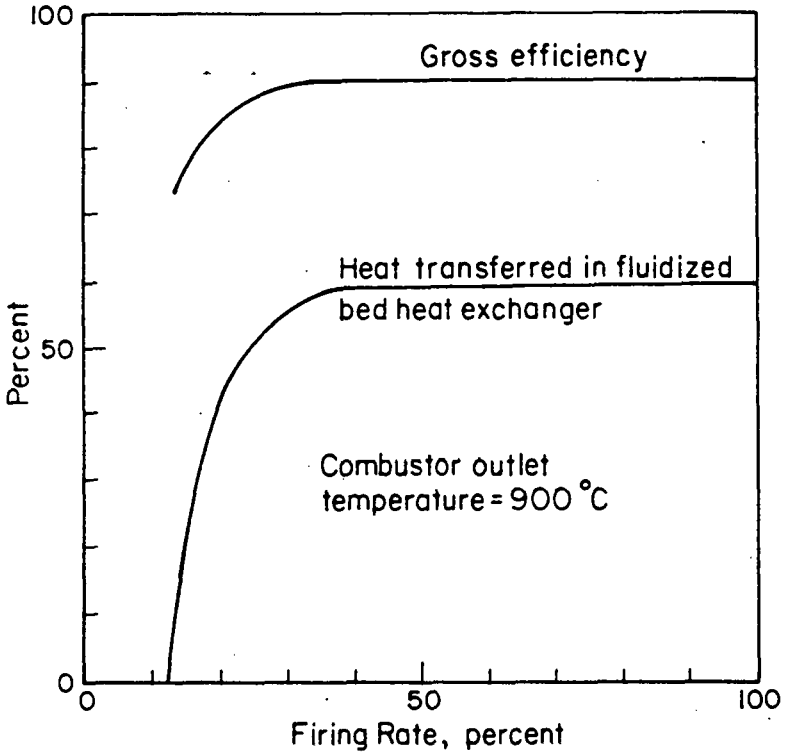

FIGURE 5. EFFECT OF TURN DOWN ON HEATER EFFICIENCY AND HEAT DISTRIBUTION.

increase in relation to that carried out of the combustor by the entrained solids. This is achieved by reducing the thermal recycle rate (Figure 3). Assuming that flue gas temperatures are held constant, the effect on overall heater efficiency is as shown in Figure 5.

Heat Transfer in the Fluidized Bed Heat Exchanger

Figures 4 and 6 summarize the results of a series of heat transfer measurements carried out at Battelle. This work was sponsored by Ohio Department of Energy. Figure 4 illustrates the response of heat transfer coefficient to changes in superficial gas velocity, which has already been discussed as a means of control. Figure 6 shows the variation with bed temperature. Experimental work was in this case limited to bed temperatures around 400 C and lower, but the results correlate closely with values calculated from the empirical equations of Wender and Cooper for vertical tubes, and of Vreedenberg for horizontal tubes. These correlations are quoted and discussed in "Fluidization Engineering" (Kunii and Levenspiel, publisher John Wiley, 1969). To compare them with the experimental data, the serpentine tube bank was treated as being composed of 81 percent vertical and 19 percent horizontal tubes. Extrapolation to higher temperatures, shown by the dashed lines in Figure 6, is based on the combined empirical equations; the experimental data lay very close to the full line at the lower temperatures.

It is worth noting that for more conventional tube arrangements, with predominantly horizontal surface, the same empirical equations predict that the average heat transfer coefficient would be about twice as great.

Applications

Separation of the heat transfer and reaction functions in a fluidized bed system permits the designer to optimize the arrangement so as to obtain control of the heat transfer rate independently of the load temperature, over a wide range. While initial applications are likely to be for steam raising, there is a wide potential for application in processes where a carefully controlled thermal history is required, or where the process temperature is very close to the maximum service temperature of the containment. These are applications which, in the past, have frequently been served by gas-fired heaters. Use of coal or solid wastes as fuel would provide a much more reliable energy source for future industrial use.

Figure 7 shows a possible arrangement for a chemical reactor which provides:

- High overall efficiency
- Rapid heating of reactants
- Prolonged residence time at reaction temperature
- Good control of peak metal and reactant temperature.

With a combustion temperature of 950 C, at which fuel utilization and sulfur retention would be very

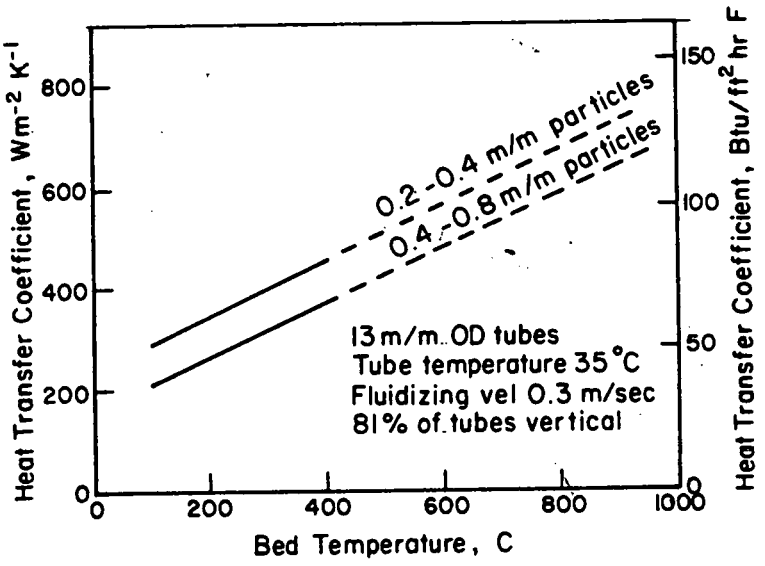

FIGURE 6. NON RADIATIVE EXTERNAL HEAT TRANSFER COEFFICIENTS.

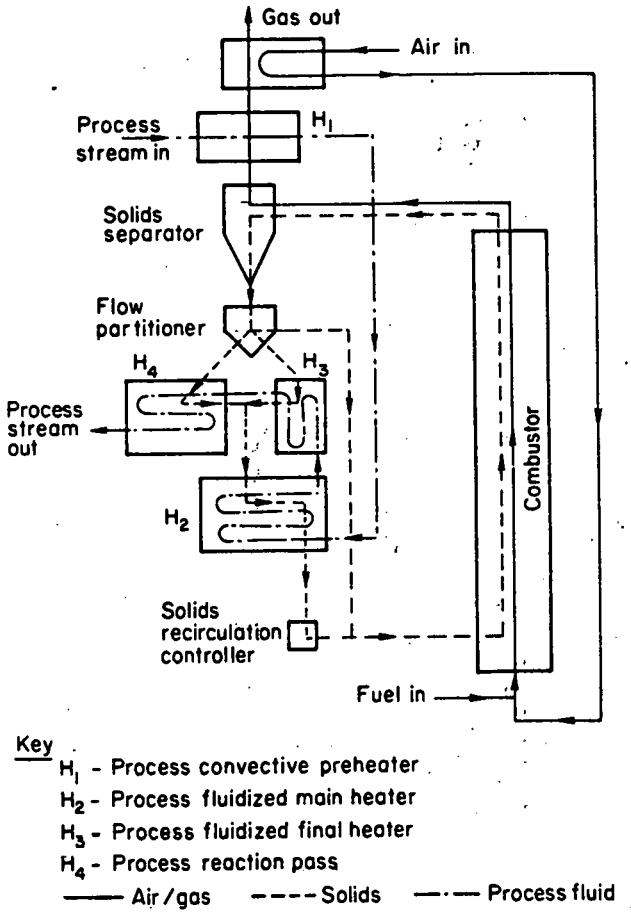

FIGURE 7. SCHEMATIC LAYOUT FOR THERMAL REACTOR CIRCUIT.

efficient, systems such as this are capable of providing controlled process temperatures from as low as 100 C to 750 C or more. The temperatures in the heat transfer fluidized beds can be anywhere between those of the heat absorbing surfaces and that of the combustor, depending on the rate of solids recirculation.

Figure 8 shows a control scheme for the layout shown in Figure 7. This makes it clear that both solids circulation rate and the fuel input rate change in response to process demands, in such a way as to maintain the combustion temperature and the desired process temperatures. The bypass line shown in Figure 7 is not essential, but it provides a means of dropping rapidly the heat fed to the heat exchangers during transient conditions.

Variations of the arrangement discussed above can be used to great advantage in power generating plants. Figure 9 shows the block diagram for a reheat steam power plant, in which the recirculated solids are divided between steam generation, superheating, and reheating heat exchangers arranged in parallel. This allows independent control of the steam temperatures at the turbine inlet and reheat positions over a wide load range. Further, the considerable heat storage capacity of the large particle fluidized bed used in the turbulent combustion zone can be utilized during on/off cycling of the unit. On shut down the bed can be slumped at its full normal operating temperature, 925 C (1700 F). Since there are no heat transfer elements in this zone the bed remains hot for many hours, and combustion can be resumed simply by feeding coal and air to the hot bed. No light-up fuel is required. The heat transfer beds, as illustrated in Figure 3 ,can be shut down at the temperature of the immersed heat transfer surfaces, and kept at that temperature. at a zero heat transfer condition. until operation resumes. This avoids problems due to thermal cycling during shut down and restart, and permits a rapid return to normal working conditions with minimum loss of efficiency during unloading and reloading procedures.

A number of specific applications are currently under consideration. Each will have some unique combination of requirements, but the multi solids fluidized bed system, with its ability to operate each part of the circuit in that phase of the fluidization condition which is best suited to the local process needs, can be tailored to provide a very efficient overall design.

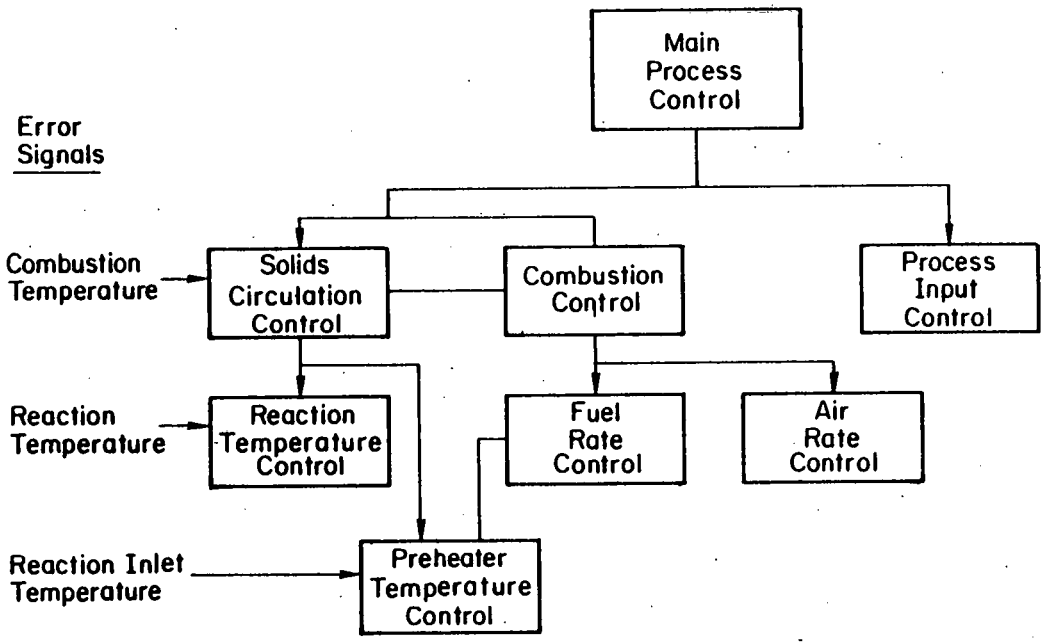

FIGURE 8. CONTROL SCHEME FOR THERMAL REACTOR.

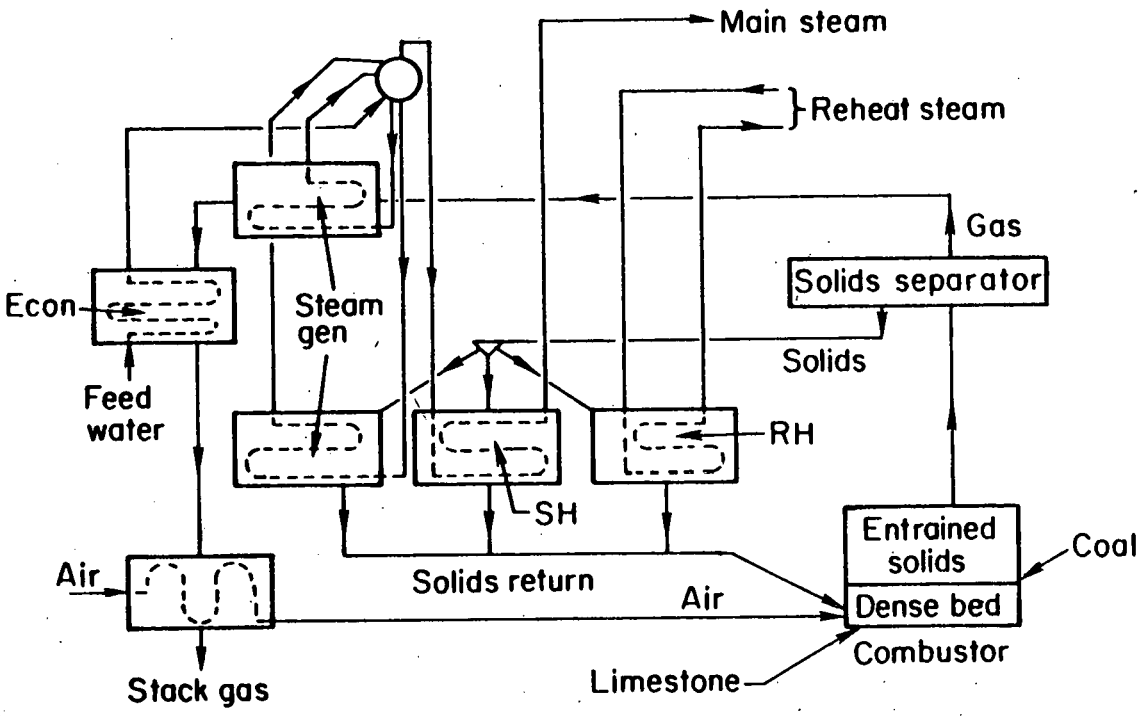

FIGURE 9. BOILER CIRCUIT DIAGRAM.

Questions to Don Anson:

Q: John Rule, Thermal Processes

What do you see as the physical equipment for the splitter and recycling to the combustion bed?

A: These follow standard practices. The L-valve is typically used. The splitter is a flow control device, either fluidic or mechanical. There isn't such a thing to my knowledge yet.

SPECIAL CONTROL & INSTRUMENTATION CONSIDERATIONS FOR PRESSURIZED FLUID BED APPLICATIONS

August H. Zoll - Edward J. Garruto

Curtiss-Wright Corporation Power Systems
Wood-Ridge, New Jersey 07075

INTRODUCTION

The Department of Energy is sponsoring the Curtiss-Wright Corporation in a program to design, construct and operate a coal fired gas turbine pilot plant generating electric power and utilizing a pressurized fluidized bed combustor (PFBC) which can successfully burn high sulphur coal. The design goals for this plant are shown in Figure 1 and includes the following:

- Burn high sulphur coal in a combined cycle
- Satisfy EPA Emission Standards for
  - NO_x
  - SO_2
  - Particulates
- Generate cost competitive power
- Develop suitable control technology

A technology rig has preceded the pilot plant and the Phase I testing has been successfully completed (Reference 1).

Combustion of high sulphur coal in an environmentally acceptable manner has been substantiated in the Curtiss-Wright Pressurized Fluid Bed Technology Rig during more than 3000 hours of testing (2600 hours of coal fired operation). The PFBC process involves the combustion of coal in a fluidized bed of limestone or dolomite which absorbs sulphur with the reaction $CaO + SO_2 + 1/2\ O_2 = CaSO_4$ occurring at temperatures between 1450°F and 1750°F. The control of bed temperature in the PFB combustor is accomplished by controlled extraction of heat from the fluid bed through a vertical tubular heat exchanger using air as the coolant in the tubes. At the design point heat release, one third of the airflow is used for combustion and fluidizing. Two thirds of the total air flow is passed through the heat exchanger tubes to extract heat from the fluid bed and provide bed temperature control. The two streams are combined following hot gas clean-up and, in the technology rig, a portion of this hot air was directed into a small gas turbine to evaluate turbine materials and coatings which would be suitable for the pilot plant being constructed by Curtiss-Wright at their Wood-Ridge, New Jersey Facility.

The technology rig testing was instrumental in evaluating and improving heat exchanger performance, tube materials, gas clean-up devices, particulate sampling techniques, solids injection, solids handling, hot valves, instrumentation requirements, fluid bed response characteristics, sulphur retention capability and hands on experience operating a PFB. It is the purpose of this paper to discuss the special instrument and control concepts related to our experience in operating a PFBC and projecting this knowledge to the pilot plant control concept employing proven hardware and feasible control techniques.

Technology Rig

The Technology Rig is shown in Figure 2. In the view shown here, the 5 foot diameter pressure vessel is supported in the structural steel tower which is approximately 70 feet high. To the left of the major structure is the secondary cleanup system with its inlet coming down the side of the tower from the primary cleanup cyclone located at the top. The coal and dolomite silos are located to the right of the main structure with the coal preparation and coal and dolomite injection equipment located inside the plant structure. The control room is also located in this building and is shown in Figure 3.

Figure 4 shows the analog control panel incorporating the air flow controllers, back pressure controller, various readout indicators, switches and twelve channels of strip chart plotting capability. Most of the channels receive their signals from the process computer and can be switched from one calculated variable to another via operator instruction to the computer.

Figure 5 is a view of the computer peripheral components, including the CRT station, data terminal, disc drive cabinet and data logger. Figure 6 depicts typical graphic displays and operator logs that were found to be very useful both for the operator and the many visitors that toured the facility.

Possibly the most significant achievement associated with instrumentation and control of the technology rig was the successful application of a process control mini-computer. The demonstrated reliability and usefulness of this device provided the confidence for us to expand its use in the pilot plant. The operator's station for this equipment was the focal point of the control system. This system continuously monitored the plant operation

through frequent and direct measurement of the process variables. It aided the process operator in the surveillance and control of the process and provided up-to-date processed data. The system completely automated data collection, processing, evaluating, recording and alarming significant deviations from nominal values.

Real time process data, including calculated data, were displayed on the CRT and permanent logs were recorded by the line printer. Alarm messages were printed out on the data terminal in addition to annunciation on the operator's panel.

The coal and dolomite injection system control panel is shown in Figure 7 and the coal grinding control panel is shown in Figure 8. These systems were conventional relay sequenced panels providing acceptable performance. Some relay faults were encountered. For this reason and because logic modifications and trouble shooting are more difficult to accomplish, solid state programmable controllers are to be incorporated into the pilot plant system.

Some of the significant instrumentation problems and achievements associated with the operation of this rig are reviewed as follows:

Thermocouple Wells -

Fluid bed temperature measurements were obtained using thermocouples in thermal wells mounted in nozzles on the peripherals of the pressure vessel. The wells are slightly more than two feet long and project into the bed material approximately eight inches. Figure 9 shows an overall view of a well and a close-up view of the exposed end. This illustrates the corrosive type attack which was visible on some wells. The material used for these original components was Inconel 600. The deterioration occurred in 1400 hours of operation. For this type application we are now specifying type 310 stainless steel material, a metal which has proven resistant to similar corrosive attacks. The mechanical design of our T/C well assembly provides an external pressure seal so that no hot gas leakage can occur even with a total failure of a well.

The bed thermocouples have provided reliable readings throughout the testing. Acceptable response has been aided by the accelerated heat transfer characteristics in a fluid bed.

Pressure Instrumentation -

Pressure measurement in the fluid bed and hot gas streams is accomplished by using pressure probes (single and dual purge units) mounted in nozzles. Reliable ΔP readings were required for the rig tests for the computation of bed height and for evaluation of the hot gas clean-up cyclones. Other pressure readings were used for space rate determination, a key operating parameter. The mechanical design served well during rig tests and is acceptable for further PFB applications.

Gas Analysis -

The gaseous products of combustion were monitored on a continuous basis for the percent by volume of five gases: SO_2, NO_x, O_2, CO and CO_2. The gas analysis components are shown in Figure 10. The instruments shown here are located in the control room. The sample conditioning cabinet was located outside in close proximity to the downstream sampling probe. Since the dust level in the main gas stream is quite high at the sampling point and the gas temperature is approximately 1600°F degrees, the main problems encountered during testing were related to dust and condensation.

Figure 11 summarizes our problems and the corrective action taken.

It should be noted that this system continues to require a great deal of maintenance to provide reliable data. This data is used to control the ratio of dolomite to coal flow to maintain the required SO_2 level while minimizing the quantities of sorbent used.

Purge Air -

Purge air has many functions in a solids handling system including keeping out dust (plugging), cooling, solids transport, etc. It was demonstrated that by maintaining a positive controlled pressure differential between the metered purge air and the pressure level in the process, reasonably constant actual volume flow could be maintained with a minimum of adjustment. Based on this demonstration, the pilot plant will use compressor discharge air for purge with appropriate booster compressors to provide the pressure differential required at varying power conditions without requiring additional pressure controls.

Solids Flow Measurement -

Testing started with weigh cell readouts manually converted to flow using stop-watches. The method was time consuming, conducive to errors, and necessitated use of additional manpower.

A computer software program change was instituted so that the process control computer received weigh cell signals, converted them to actual flow, and provided CRT readouts and digital displays on the operator's panel for coal and dolomite flows.

Particulates -

Curtiss-Wright designed and built an isokinetic grab sample system in which the hot particulates are captured in a pressurized cylindrical filter. Before and after weighing of the filter provided weight flow (concentration) of particulates in the main stream. This was done at five locations in the process. The collected sample is analyzed for particle size using a Coulter Counter as shown in Figure 12.

Limited testing of a laser technology optical monitor was also conducted. The Leeds & Northrup device is shown in Figure 13. Further development of such a device is needed since continuous monitoring is considered desirable.

The functional features of the counter includes ascertaining the frequency and cumulative distributions of particles according to:

a. Their volume or weight as a percentage of the total sample volume or weight.

b. Their size (diameter) in micrometers.

The Coulter Counter is used to determine the number and size of particulates suspended in an electrolyte by flowing the suspension through a small aperture and monitoring an electrical current which also passes through the aperture. Electrodes are immersed in the conductive fluid on opposite sides of the aperture. As a particle passes through the aperture, a current pulse of short duration having a magnitude proportional to the particle volume is induced. The series of pulses are electronically scaled and counted.

We find the Coulter Counter to be quite suitable for this use and we are able to obtain consistent, reproducible data. It does require experienced operators and a laboratory environment.

The Combined Cycle Pilot Plant

The successful results of the instrumentation and control of the technology rig at C-W provides a significant base upon which to build the control system for the pilot plant. The control system developed for the pilot plant will be directly applicable to commercial plant use with minor modifications to take advantage of scale-up economies.

In order to designate the control and instrumentation requirements, it is essential that the process be defined and its requirements understood. The process is briefly described as follows:

Start-Up -

Start-up of the PFBC System is accomplished in a series of steps which progress in a systematic sequence as follows (Figure 14):

a. Gas Turbine Start-Up

This figure shows the process schematic of the gas turbine starting and running components. The turbine is rotated by a conventional turbine starter. Air flow through the compressor is piped to the external start combustor that is fired with gas or liquid fuel. This heated air is piped to the turbine which drives the compressor, then via valves 8 and 13 to the waste heat boiler. Light-off and acceleration to idle are handled in a conventional manner using an electronic fuel control.

b. Fluid Bed Start-Up

The figure also shows the fluidizing air circuit added to the gas turbine starting components. Although there has been no through air flow during the turbine starting phase, the complete system is pressurized via the hot gas piping. Valve 5 is opened without causing any appreciable change in airflow. Valve 1 is then partially closed forcing air through Valve 5, the auxiliary combustor, and then through the fluid bed and the hot gas clean-up system. The amount of this airflow is preset. The auxiliary combustor is fired and the exit temperature schedule controls the quantity of fuel (liquid or gas) to this combustor. This hot air fluidizes and heats the bed material as well as all the downstream components and piping. When 1200°F bed temperature has been reached, the coal injection system is activated (dolomite feed is also activated, but since it tracks coal flow and SO_2 levels, it will not be considered in this discussion).

Coal flow is controlled by bed temperature and increases the system temperature at a controlled rate. At the set bed temperature, the auxiliary combustor fuel flow is ramped to minimum as additional coal takes over. The combustor is then shutdown from minimum flow and valve 4 is opened to minimize system pressure drop. Valve 1 continues to modulate to maintain the set fluidizing air flow. The start combustor continues to control turbine speed, but with considerably reduced fuel flow.

During this phase, the alternator is synchronized to the electrical grid by opening valve 9 and using valve 8 to modulate speed of the power turbine. When the breaker is closed, valve 8 is closed and a fraction of rated electrical power will be generated.

Once the generator is on line, the control of coal flow is switched from bed temperature to load control. Coal flow is ramped at a controlled rate to reach the megawatt set point. The temperature of the fluid bed continues to increase until 1650°F is attained. The bed temperature control loop, which includes cooling air control valve number 3 (which as been closed up to this point) now opens the valve as required to maintain the bed temperature by allowing compressor air to circulate through the 16 foot vertical heat exchanger tubes submerged in the bed. As valve 3 opens, valve number 1 will close to maintain fluidizing air flow in the bed. The heated air blends with the fluidizing air thus raising the effective turbine inlet temperature and thus the power output of the plant. Maximum power is achieved when all the compressor air flow is utilized for fluidizing and cooling.

As can be seen from the schematic, all air flow streams must be controlled. Therefore their respective flows are measured with elbow taps or flow tubes to provide accuracy with minimum pressure drops.

Pilot Plant Description -

Figure 13 indicates some of the components for the pilot plant. Included in this plant are all the following sub-systems:

- Coal receipt and storage
- Coal grinding and drying
- Dolomite unloading and storage
- Coal injection system
- Dolomite injection system
- Gas turbine system
- Pressurized fluid bed system
- Hot gas clean-up
- Ash removal and cooling
- Power generation
- Waste heat recovery
- Purge and Injection Air System

The entire control scheme is distributed among 5 programmable controllers and 1 process control computer (Figure 15). The PC's do all sequencing for the major sub-systems, including coal grinding and drying, coal injection, dolomite injection, gas turbine/generator sequencing and ash handling. The PC's are installed in local panels permitting automatic or manual operation from the local panels. Fluidized bed control is through the mini-computer. The mini-computer also monitors all the sub-systems, provides data logging for the plant, computes plant performance on a real time basis and provides operator interface with the process via 3 colored CRT's.

A separate control building is provided for the pilot plant. Figure 16 shows the control room floor plan.

A model of the site shows the relationship of the systems mentioned above. See Figure 17.

Instrumentation and control of the plant will follow practices proven in the technology rig, including dedicated programmable controllers, local manual stations, computer monitoring, etc. Due to the complex nature of the start-up sequence, it is planned to use the process computer to accomplish this phase of the operation. The pilot plant is a scaled version of a large utility plant. The control system of the pilot plant is complete and capable of controlling large commercial installations. The philosophy of the control system design follows that usually associated with utility gas turbine systems since, basically, that is what the process is. The PFB is essentially a remote combustor for a dual fuel gas turbine. The full automation of start-up, loading and shutdown, as well as the continuous monitoring of critical parameters with shutdown authority for exceeding critical limits, is normal for this type of equipment. The pilot plant program provides the ideal facility to develop and demonstrate this type of control in advance of commercial application.

This paper has provided some insight into the control and instrumentation requirements for a PFB combined cycle power plant. As evidenced on the process diagram, automation of this plant is an ambitious goal. Handling and metering of solids obviously offer new complexities on the path to automation, but we have seen substantial progress in accomplishing this goal during the operation of the technology rig.

CONCLUSIONS

1. Instrumentation durability was evaluated in the technology rig and improvements were made.
2. The automated control concept utilizing state of the art digital and analog control loops is a viable concept for pressurized fluid bed power generator systems as demonstrated in the C-W technology rig.
3. A control strategy has been developed for the pilot plant utilizing technology rig experience to provide technically sound concepts.
4. The pilot plant control system will be suitable for commercial plant applications virtually without scale up.

REFERENCE

1. Zoll, A.H. Instrumentation and Control of a Pressurized Fluid Bed in a Combined Cycle Power Plant, 1978 Symposium on Instrumentation and Control for Fossil Demonstration Plants, Newport Beach, California.

- BURN HIGH SULPHUR COAL IN A COMBINED CYCLE
- SATISFY EPA EMISSION STANDARDS FOR
  - NO_X
  - SO_2
  - PARTICULATES
- GENERATE COST COMPETITIVE POWER
- DEVELOP SUITABLE CONTROL TECHNOLOGY
- EVALUATE INSTRUMENTATION NEEDS AND RELIABILITY
- PROVIDE OPERATING FLEXIBILITY
- DEMONSTRATE HEAT EXCHANGER PERFORMANCE AND DURABILITY
- DEMONSTRATE TURBINE RELIABILITY

Figure 1. Pilot Plant Design Goals

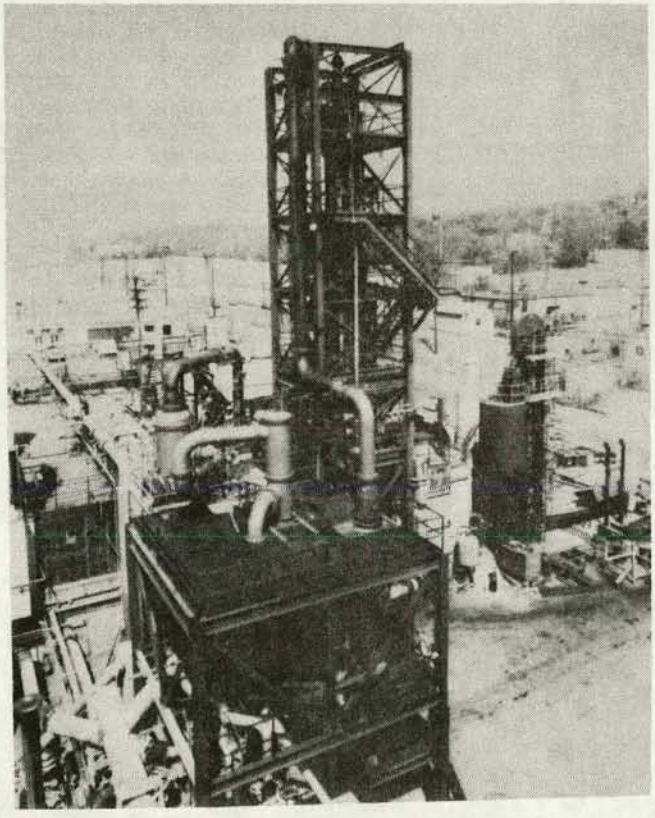

Figure 2. Technology Rig Overview

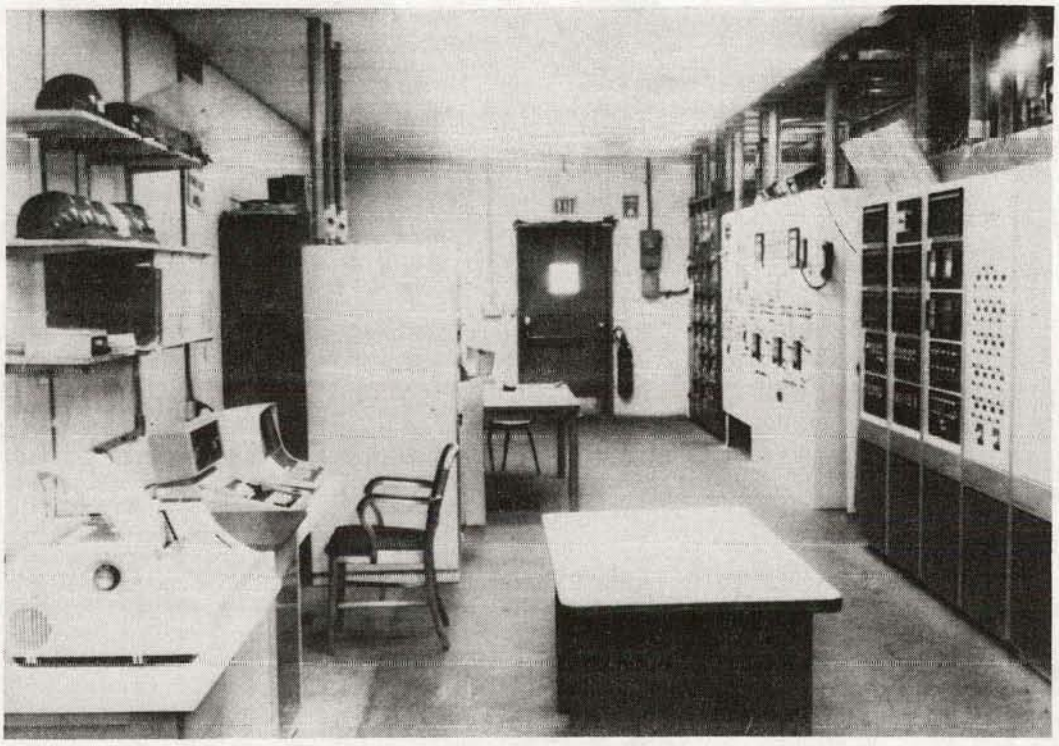

Figure 3. Technology Rig Control Room

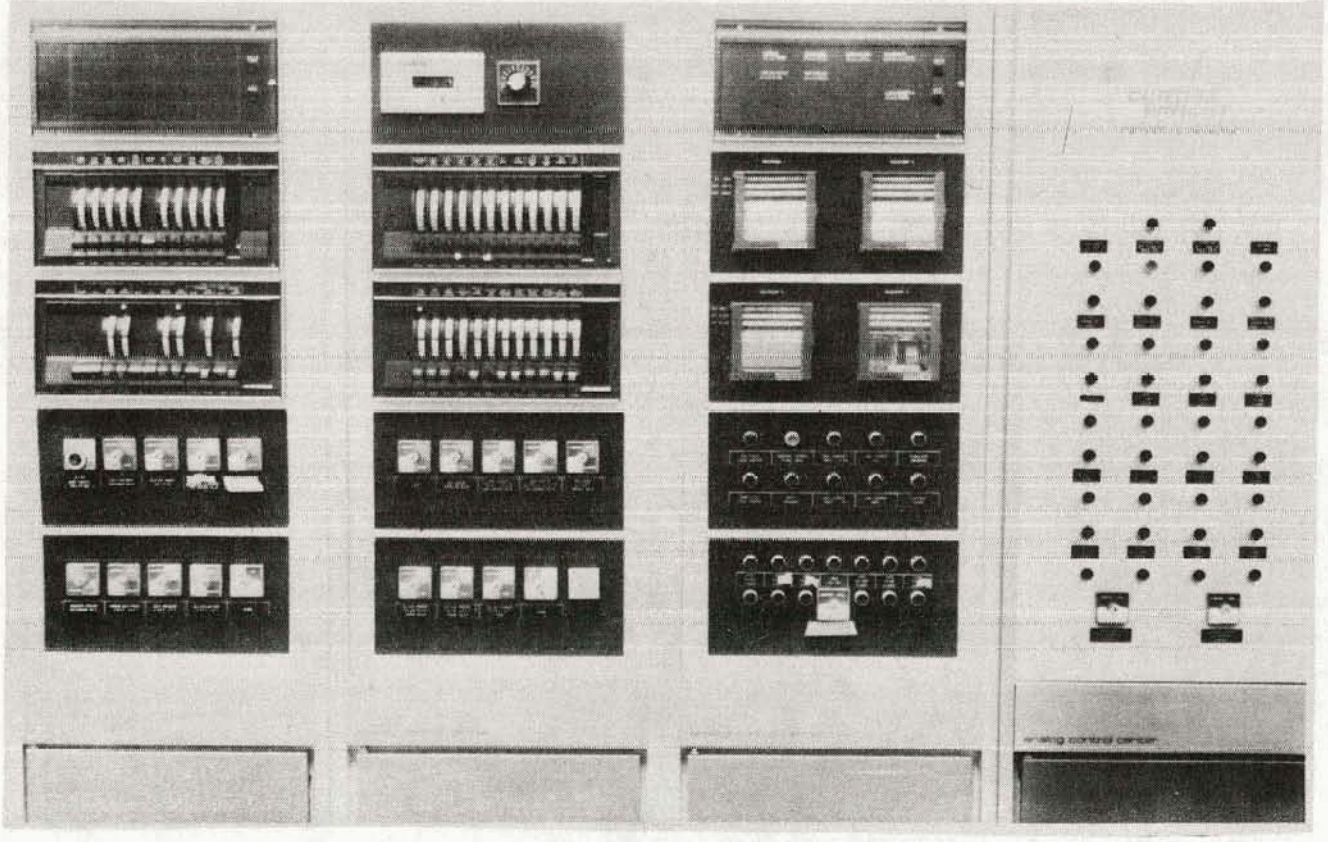

Figure 4. Analog Control Panel

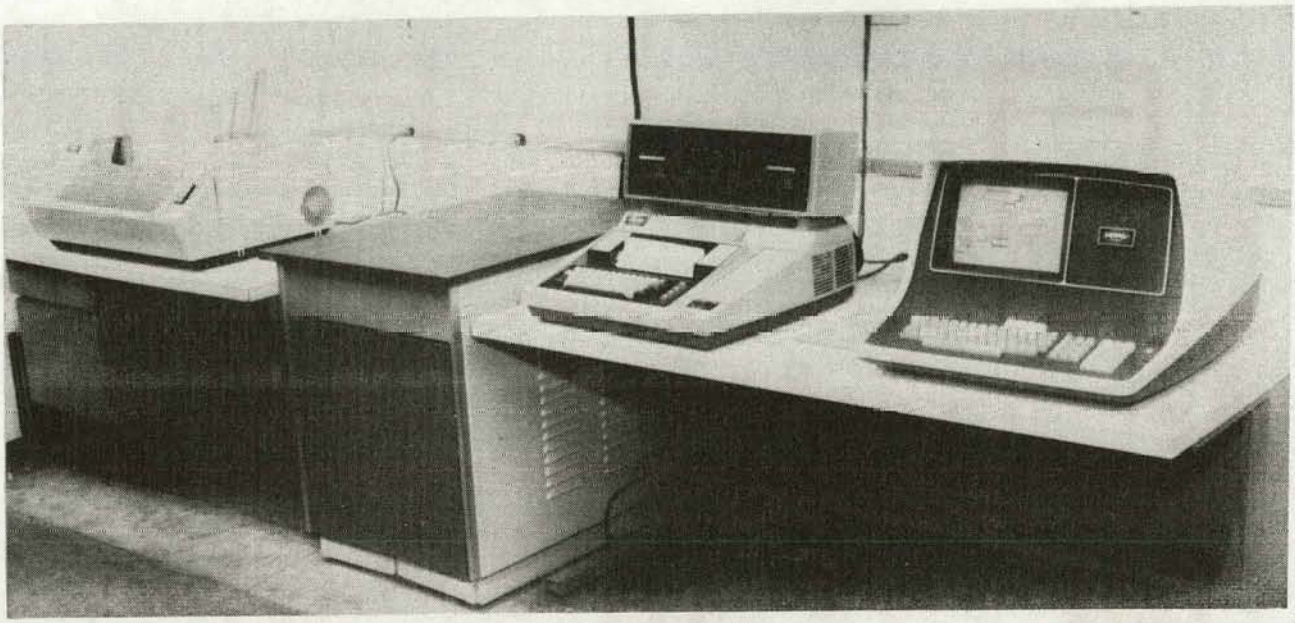

Figure 5. Computer Peripherals

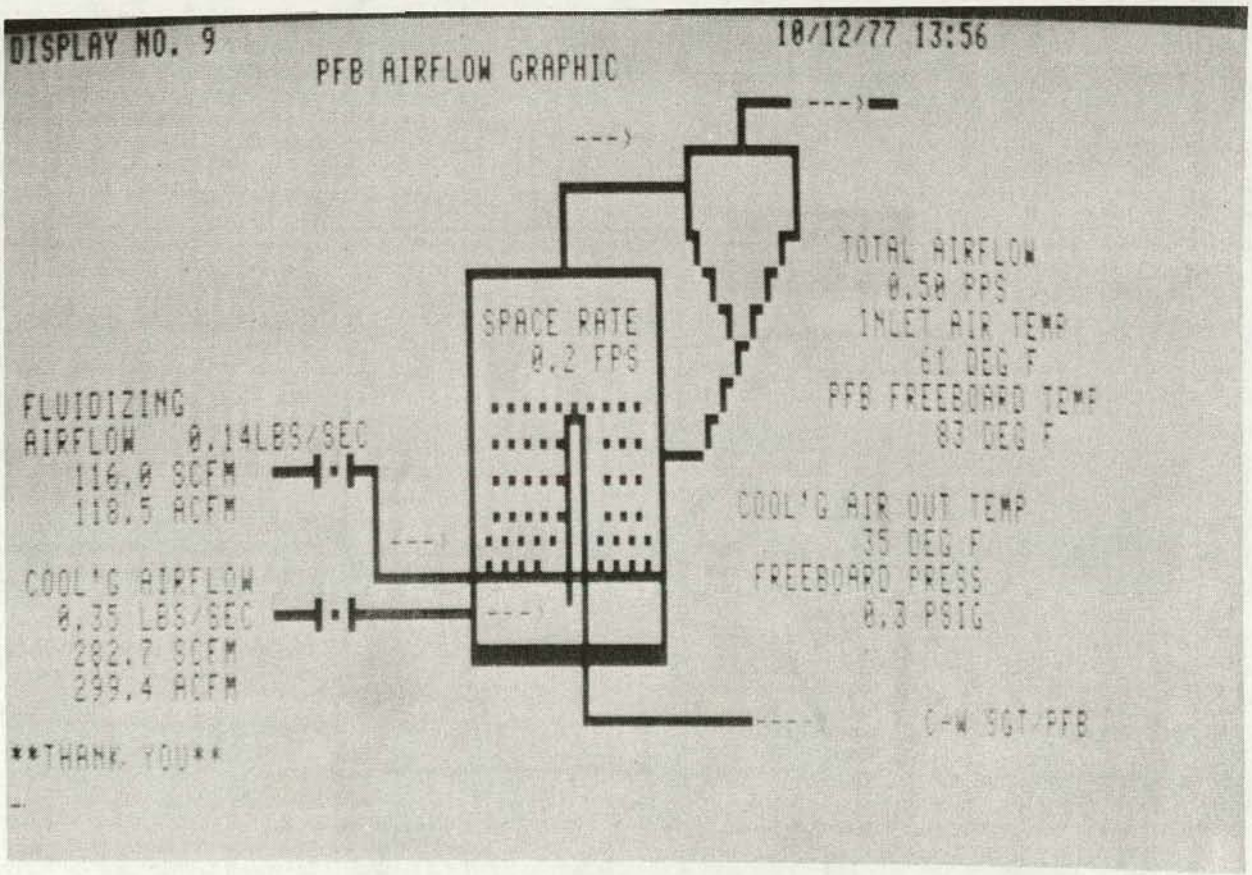

Figure 6. Graphic Display

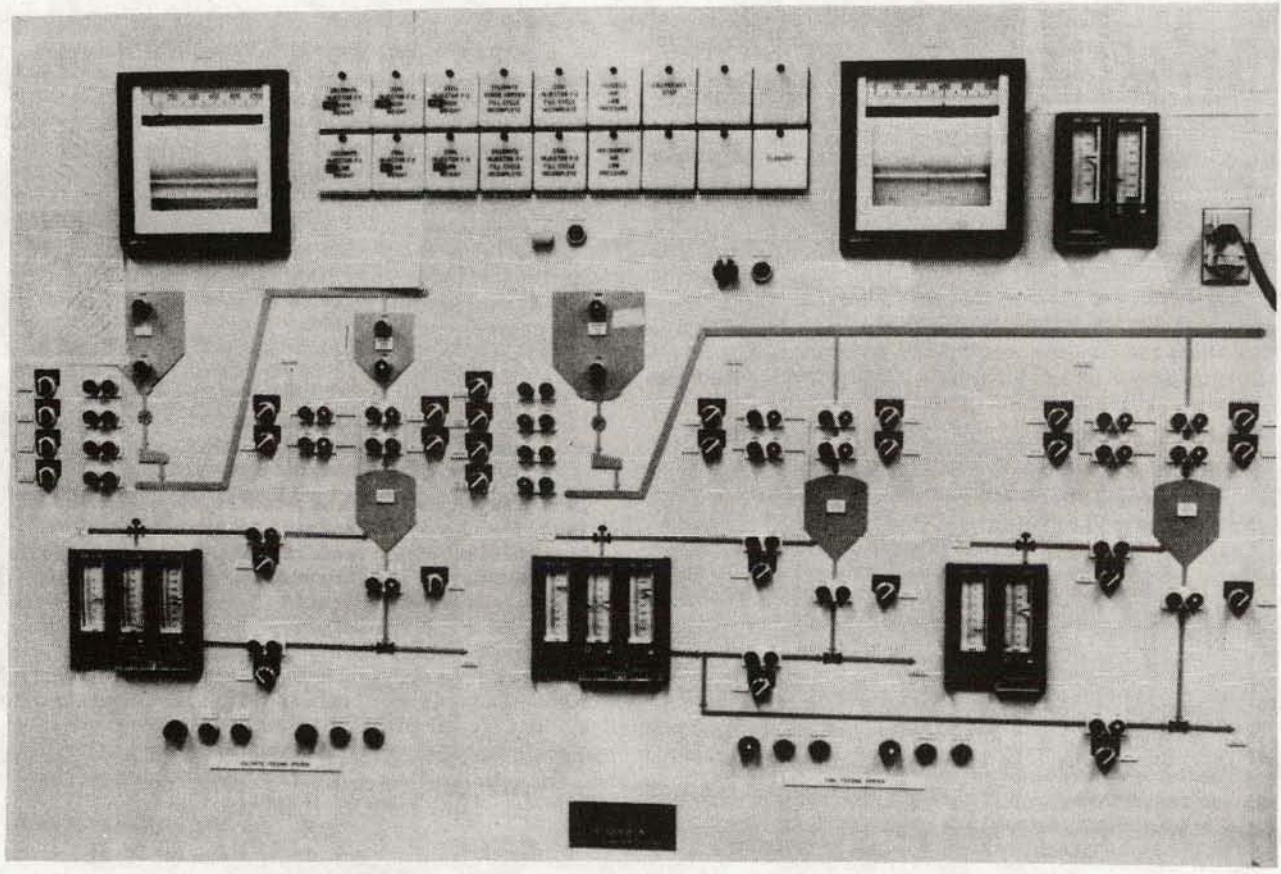

Figure 7. Coal Injection Control Panel

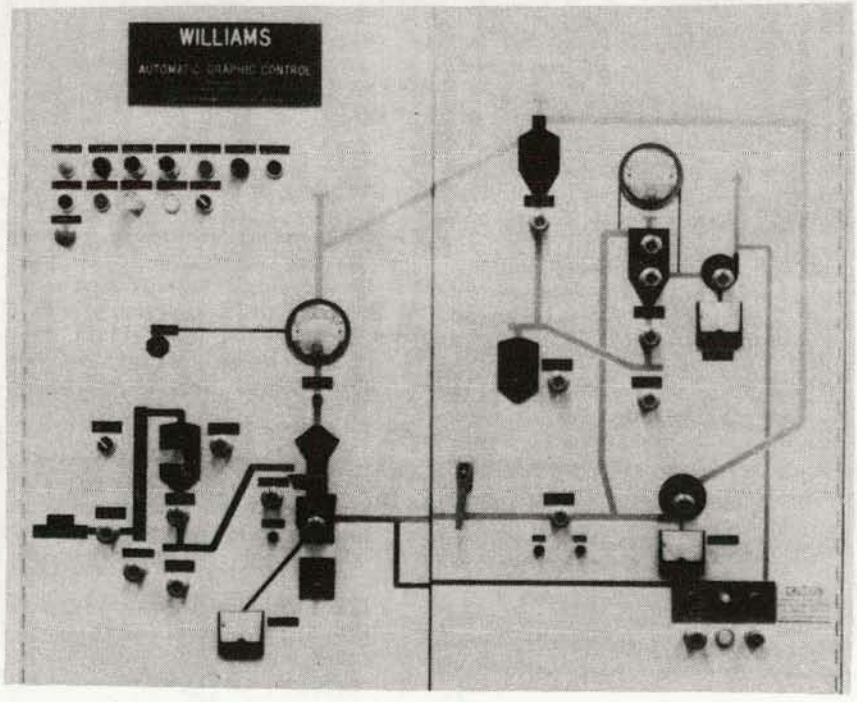

Figure 8. Coal Grinding Control Panel

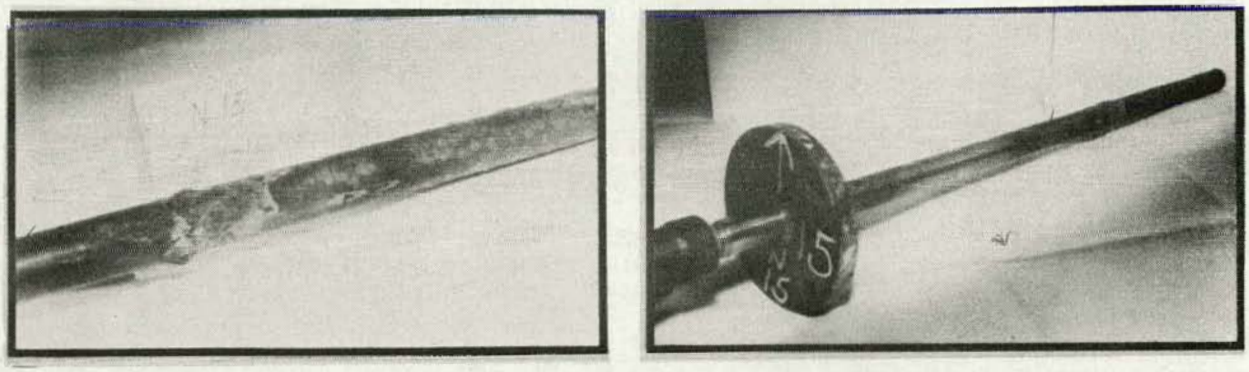

Figure 9. Bed Thermocouple Well

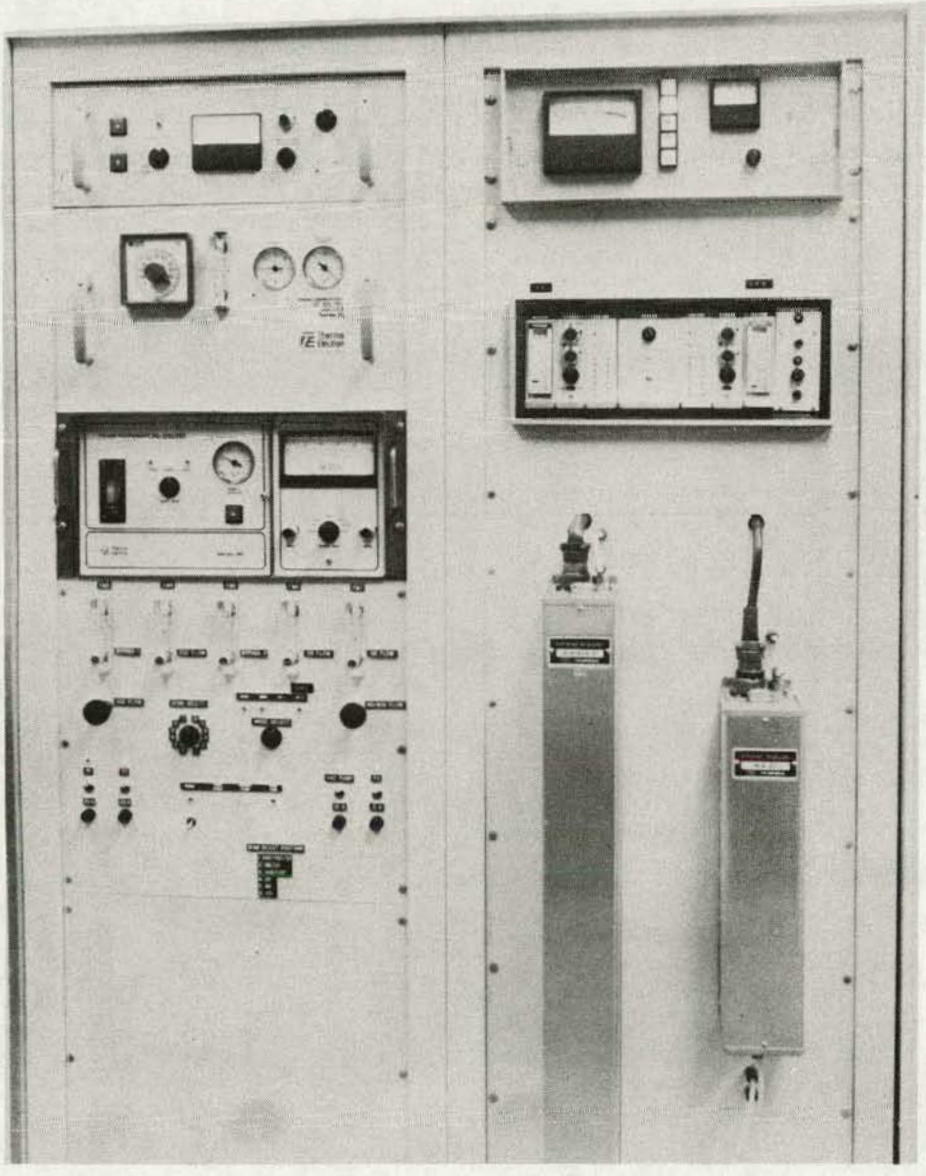

Figure 10. Gas Analysis Control Panel

PROBLEM	CORRECTIVE ACTION
1. CLOGGING OF THE SAMPLING PROBE	• REDESIGNED END OF PROBE-FROM SINTERED METAL TO CLOTH • IMPROVED PURGE AIR SYSTEM-INCREASED FREQUENCY
2. GAS SAMPLE LINE – CONDENSATION CLOGGING OF LINE AND CONDITIONER	• PROVIDE HEAT TRACE LINES FROM SAMPLE PROBE TO CONDITIONER • INCORPORATED ADDITIONAL IN-LINE HOT GAS FILTERS DOWNSTREAM OF THE PROBE
3. OXYGEN SAMPLING CREDIBILITY	. CHANGED SPAN GAS TO 6 OXYGEN-VALUE CLOSE TO OPERATING POINT
4. SAMPLE LINE MATERIAL	• CHANGED FROM STAINLESS STEEL TO TEFLON
5. INCONSISTENT SAMPLE FLOW	• REVISED PUMP CONFIGURATION
6. OUTPUT SIGNAL INCOMPATIBLE WITH PROCESS COMPUTER	• INCORPORATED CONDITIONING UNITS TO MAKE OUTPUT SIGNALS OF ALL MEASURED SIGNALS COMPATIBLE TO THE COMPUTER

Figure 11. Summary of Gas Analysis System

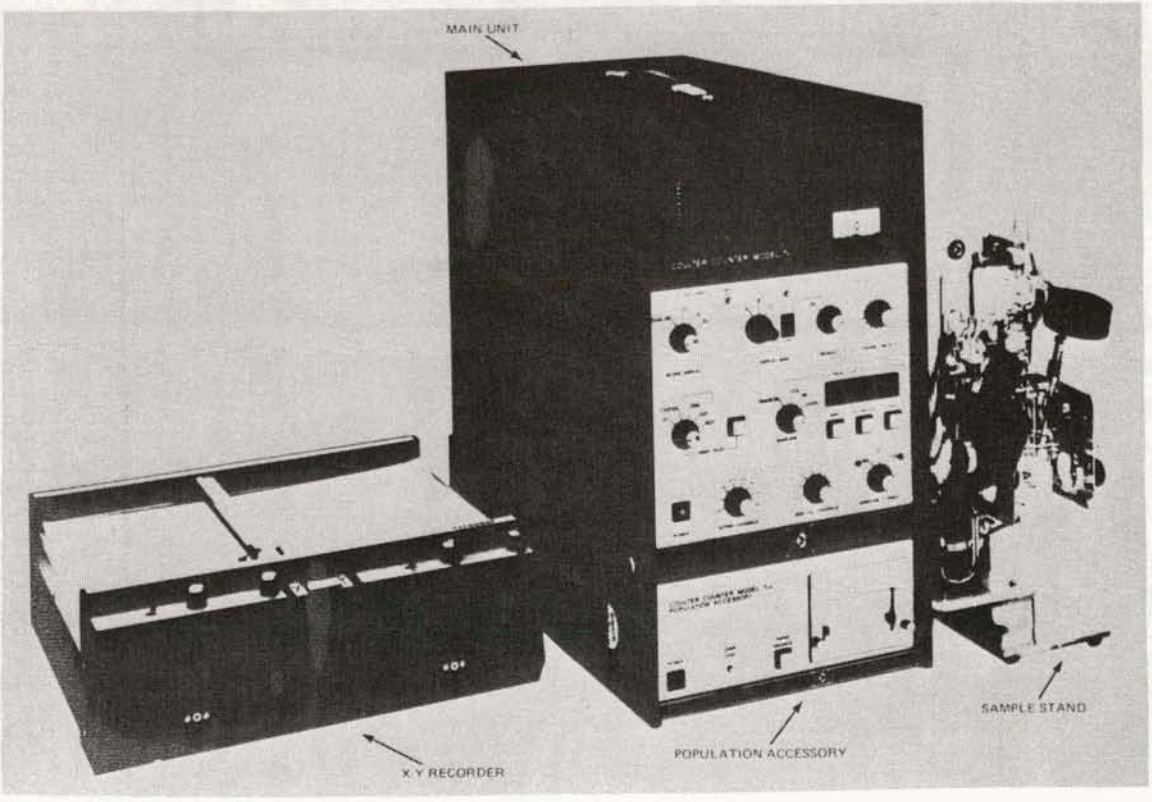

Figure 12. Coulter Counter

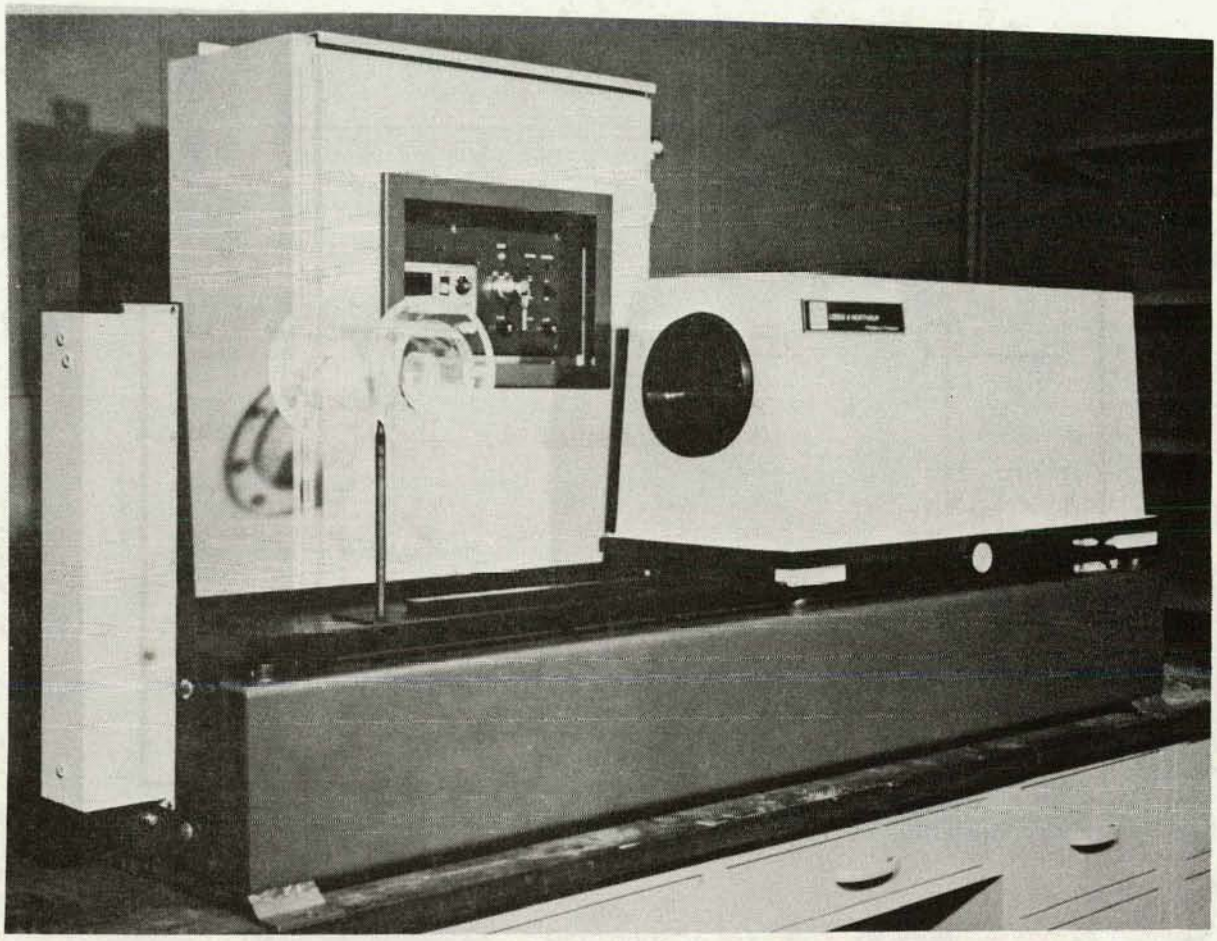

Figure 13. Laser Particulate Monitor

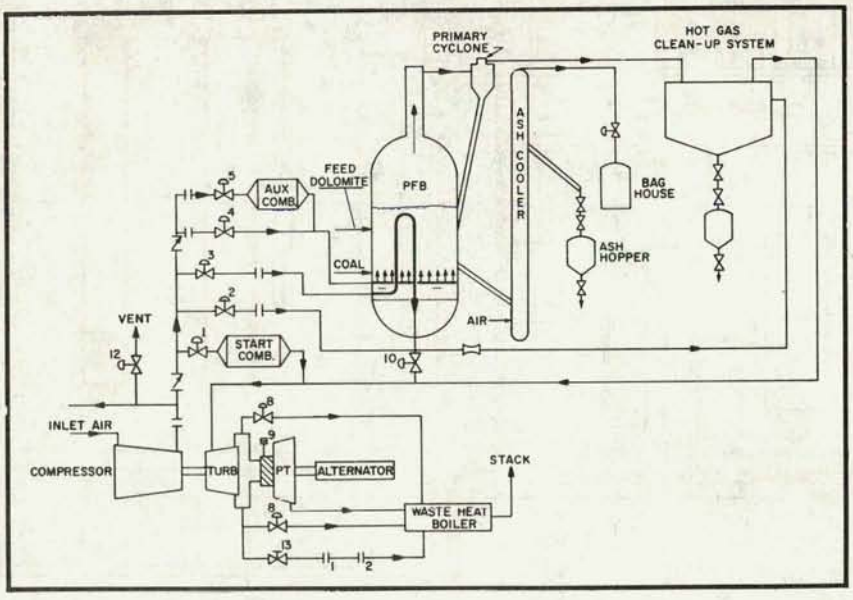

Figure 14. Pilot Plant Process Schematic

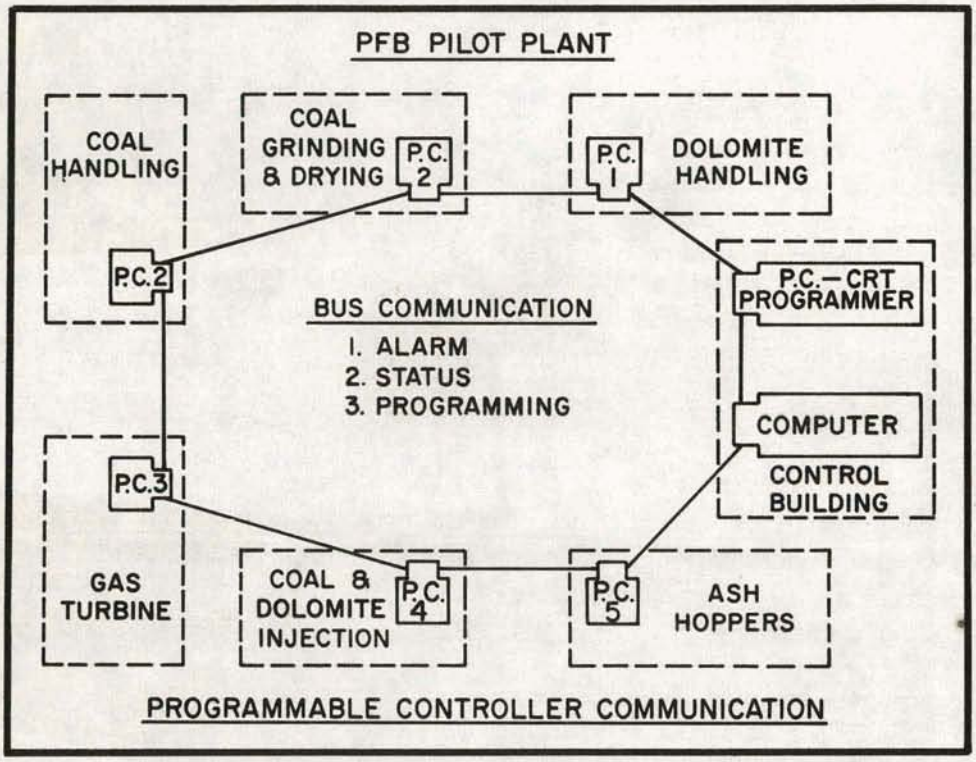

Figure 15. Distributed Control Schematic

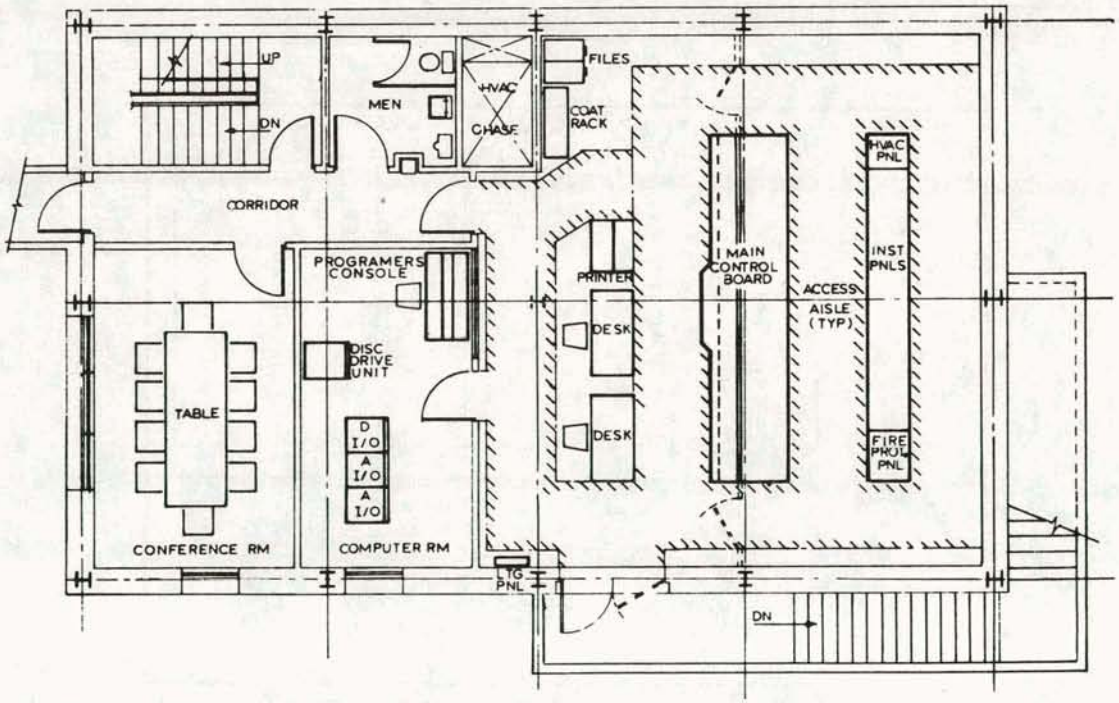

Figure 16. Pilot Plant Control Room Floor Plan

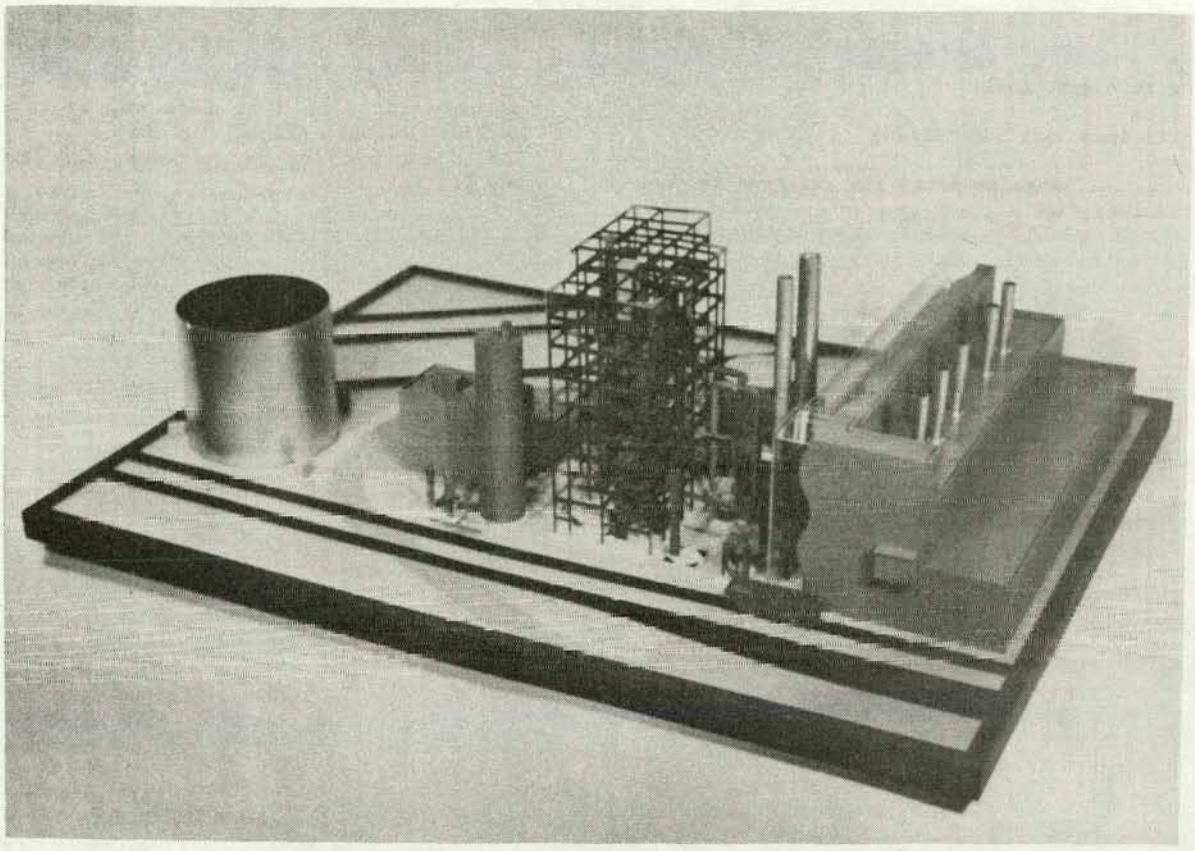

Figure 17. Pilot Plant Model - Overall

Question to August Zoll:

Q: (Participant not identified)

Do you get large pressure fluctuations in your technology rig?

A: These pressures have been very stable and the pilot plant should be more so, because the turbine delivers all of the air to the system. The piping and hot gas cleanup will damp out any fluctuations.

ENVIRONMENTAL EMISSIONS

UPDATE ON EMISSION MEASUREMENTS FROM FLUIDIZED-BED COMBUSTION FACILITIES

P.F. Fennelly, R.R. Hall, C.W. Young, J.M. Robinson, R.J. Kindya, G. Hunt

GCA Corporation, GCA/Technology Division
213 Burlington Road, Bedford, MA 01730

INTRODUCTION

New Data

The most recent data on fluidized-bed combustion emissions can be organized in three categories:

- SO_2/NO_x/Particulates
- Environmental Assessment Data - Organics/Trace Elements
- Bioassay Data

The first category of emission data is of immediate concern because of recent or pending changes in air emission standards. The U.S. Environmental Protection Agency has recently promulgated revised New Source Performance Standards for electric utility boilers. More importantly, the U.S. EPA is currently developing New Source Performance Standards for industrial-sized boilers. It is this latter area which is the market segment wherein fluidized-bed combustion is expected to make its earliest impact; hence, any changes here can have an important influence on the commercialization of FBC.

The second category--environmental assessment data--includes organic compounds and trace elements in both air emissions and solid waste discharges. For the most part, these types of emissions are not now specifically regulated--although they could be regulated in the near future under legislation such as the Resource Conservation and Recovery Act, Toxic Substances Control Act, and Amendments to the Clean Air Act. The environmental assessment data being gathered under EPA's Environmental Assessment Program will help decide whether or not organic and certain trace elements should or should not be regulated--and if so, to what degree.

Bioassay data, the third category, is really a subset of environmental assessment data but it is given special mention here because it is a relatively new approach and it is currently being emphasized within the environmental measurements field.

Environmental Status of Fluidized-Bed Combustion

In the environmental arena, the main battleground for determining FBC success was and continues to be air emissions. This is the area in which FBC offers significant advantages compared with other coal-based combustion technologies. There has been a continuing concern about solid waste disposal, especially in light of the new Resource Conservation and Recovery Act which now governs waste disposal. But the most recent data on solid waste studies and leachate experiments indicate that FBC waste most likely will not be deemed hazardous under the new regulations and hence should not require special or elaborate disposal methods. In fact, the byproduct potential of FBC waste for agricultural or construction materials seems more optimistic than that for coal ash or SO_2 scrubber sludge.

To date, most experimental data on FBC emissions come from pilot plant or laboratory-sized units that do not run under the more stringent operational requirements of commercial applications. Emission data from these development units look very promising with regard to FBC meeting current and anticipated regulations. The acquisition of confirming data from long-running, commercial-sized units is now the highest priority for FBC environmental studies.

SO_2/NO_x/PARTICULATE DATA

The emission targets for fluidized-bed combustion are the New Source Performance Standards which have been recently revised for utility-sized boilers.[1] Another set of New Source Performance Standards is now under consideration by the U.S. Environmental Protection Agency for industrial-sized boilers. Current expectations for these industrial boiler standards along with the existing utility standards are shown in Figure 1.

NO_x Data

Experimental data on NO_x emissions taken over the last 15 years from major FBC experimental facilities are shown in Figure 2. This data analysis was done as part of GCA's participation in a series of EPA-sponsored Technology Assessments related to the development of industrial boiler New Source Performance Standards.[2]

Superimposed on the graph are three levels of emission control--moderate, intermediate, and stringent, which are explained below:

- Moderate - the degree of emission control which can be achieved by normal or routine operation.

LEVELS OF EMISSION CONTROL FOR COAL-FIRED ATMOSPHERIC FBC BOILERS

CATEGORY	SO_2 % REDUCTION	NO_x LB/10^6 BTU	PARTICULATE LB/10^6 BTU
INDUSTRIAL	75-90	0.5-0.7	0.03-0.25
—	CEILING = 1.2 LB/10^6 BTU FLOOR = 0.2 LB/10^6 BTU		99-50 (% CONTROL)
UTILITY	85	0.6	0.03
	WITH CEILING = 1.2 LB/10^6 BTU		

TO GET μg/J, MULTIPLY BY 430.

Figure 1. Emission control levels already in existence for utility size boilers or under consideration for industrial size boilers.

- Intermediate - the degree of emission control which is readily achieved by a well-maintained system operating with some optimization of design conditions.
- Stringent - the degree of emission control which can be achieved with all design parameters optimized so that the system is performing at its technological limit.

These levels are "labels" and were chosen within EPA's industrial boiler study only to encompass all candidate technologies and to form bases for comparison of technologies for control of specific pollutants considering performance, costs, energy, and environmental effects. EPA will perform rigorous examination of several comprehensive regulatory options before any decisions are made regarding the standards for emissions from industrial boilers.

The trend shown in Figure 2 is most encouraging--as the FBC systems increase in size, the range

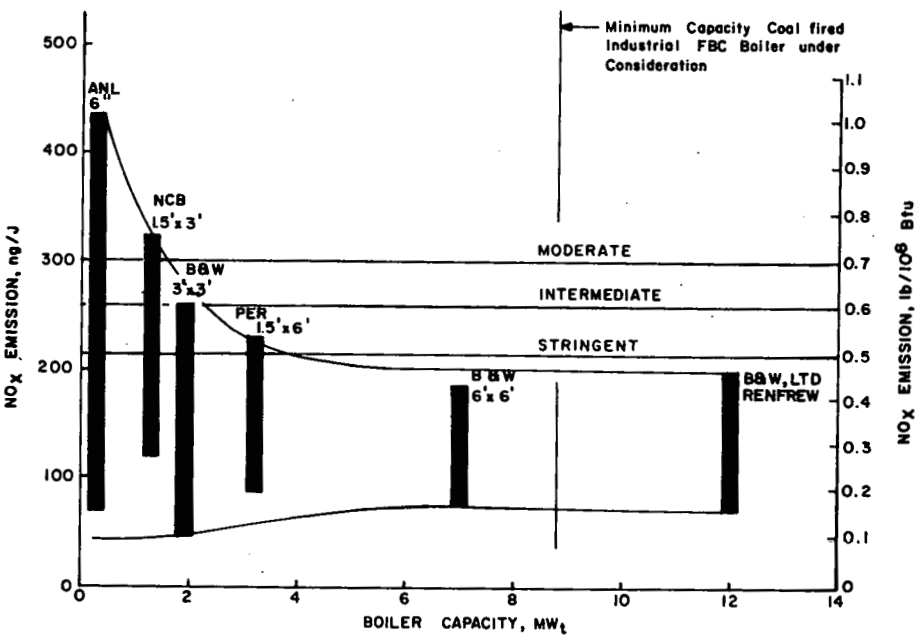

Figure 2. NO_x emissions from FBC facilities as a function of size. Data taken from experiments reported over the last 10-15 years at major FBC development facilities.

of NO_x emissions consistently decreases. When capacities approach those expected for commercial use--i.e., greater than 5-10 MW_t--the range of NO_x emissions falls below even the most stringent levels identified for possible emission standards.* Within the last few years, there seems to have been a preoccupation within the FBC field with SO_2 emission control, and the advantages of low NO_x emissions have tended to be neglected. Our analysis of available data indicates that low NO_x emissions continue to be a featured attraction of FBC technology.

SO_2 Emissions

The facet of fluidized-bed combustion which has attracted the most environmental attention is the capacity for in-situ SO_2 removal. Fluidized-bed combustion is currently viewed as an attractive--but a commercially unproven--option to SO_2 scrubbers. Figure 3 summarizes the SO_2 removal abilities of FBC as a function of Ca/S ratio, which is the predominating operating parameter for SO_2 control. As in Figure 2, three levels of emission control are superimposed--moderate, intermediate, and stringent--all of which were defined previously for NO_x. These data have also been derived from GCA's Technology Assessment for FBC.[2] SO_2 removal is a complex problem which is affected by design and operating parameters such as: Ca/S ratio, gas velocity, bed height, limestone particle size, and temperature. The factor of predominant influence, however, is the Ca/S mole ratio. In Figure 3 a

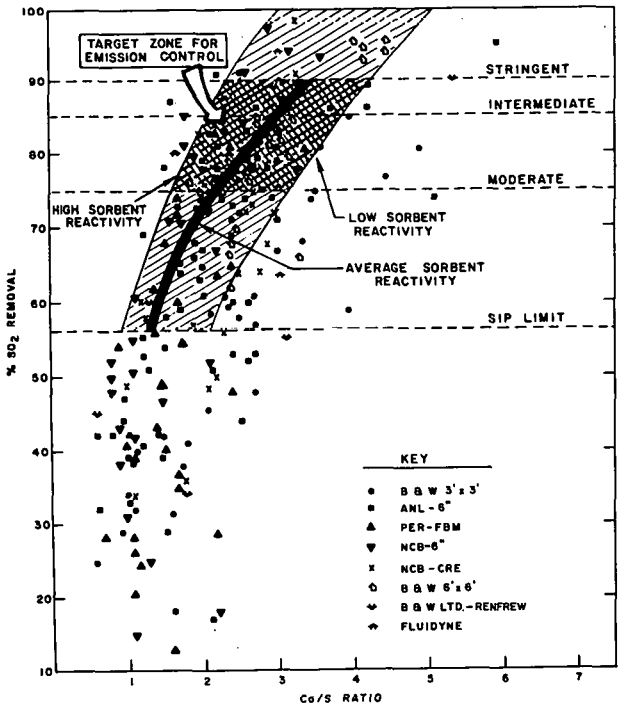

Figure 3. Percent SO_2 removal as a function of Ca/S ratio. Data taken from experiments reported over the last 10-15 years. "Target zone" indicates Ca/S ratio which should insure at least intermediate control levels.

"target zone" is shown, wherein at least intermediate control can be consistently achieved and wherein stringent control levels can be achieved with the optimization of certain design parameters.

These key design parameters optimized for SO_2 control are shown in Figure 4. The relative influence of each of these parameters and the justification of the values shown are discussed in more detail elsewhere.[2]

In assessing fluidized-bed combustion, the central question that always arises in one form or other is, "Can fluidized-bed combustion achieve SO_2 control more reliably and economically than conventional methods--namely, SO_2 scrubbers?" The question of reliability can only be answered as oper-

*Note--These stringent levels are based on an assessment of what FBC can achieve as well as what can be achieved by conventional combustion systems. Developments in conventional combustion technology, such as "low NO_x burners", could cause the NO_x emission targets to drop to lower levels.

DESIGN/OPERATING CONDITIONS RECOMMENDED FOR SO_2 CONTROL

GAS PHASE RESIDENCE TIME ≥ 0.67 seconds

AVERAGE SORBENT PARTICLE SIZE IN BED = 500 μm

BED TEMPERATURE ~ 843°C (1550°F)

PRIMARY RECYCLE

Figure 4. "Best" FBC operating conditions for optimizing SO_2 control. With these conditions, "stringent" control levels should be achievable.

ating data are logged in over the next year or two. As far as cost estimates are concerned, a systems analysis based on best available data indicates that FBC SO_2 control can be achieved with fluidized-bed combustion at a cost competitive with that of conventional combustion.[2] This is shown in Figure 5, where cost data are shown as functions of system capacity. The conventional combustion costs are shown for systems that have no SO_2 control. If SO_2 control is added, costs for conventional units should increase by about 15-20 percent.[3] This is shown in Figure 5 as a dashed line; an error band for this estimate could not be shown with the data available. The most important feature of Figure 5 is the extent of the error bands associated with FBC cost estimates. Currently, these estimates are not better than ± 20-30 percent. Until more operating data become available, the accuracy of such estimates will not improve.

Particulate Emissions

Particulate emissions represent the largest gap in the FBC data base. An FBC system will not be able to operate without some type of particulate control device. The absence of data results mainly from the fact that most of the experimental units have been too small to incorporate conventional or realistic particulate control systems. Available data are summarized in Figure 6; these data are discussed in more detail elsewhere in this

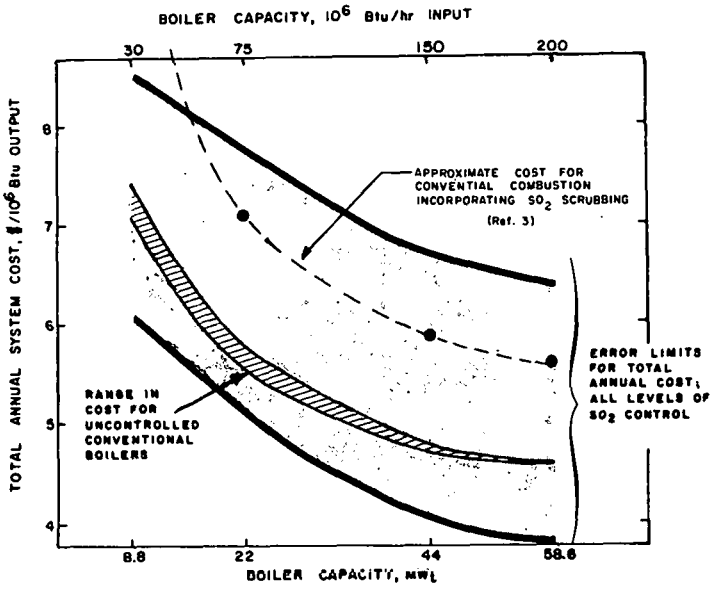

Figure 5. Annual cost of atmospheric fluidized-bed industrial boilers as a function of capacity. Error bands include moderate, intermediate and stringent control levels. Range in cost for conventional combustion uncontrolled for SO_2 and conventional combustion controlled with SO_2 scrubbers (Reference 3) are shown for comparison.

Symposium.[4] Fabric filters should be able to control particulate emissions adequately; detailed particulate emission characterizations of commercial units with baghouses are one of the highest-priority environmental studies for the coming year.

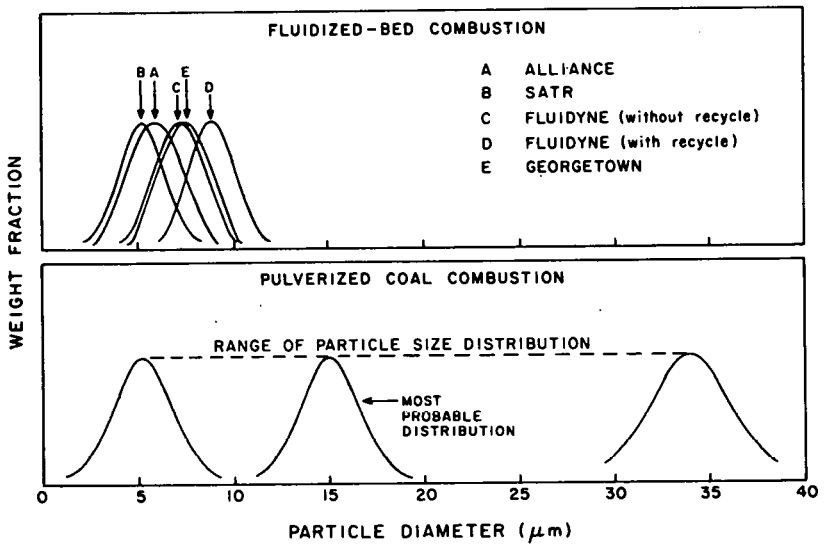

Figure 6. Particulate size data for FBC compared with pulverized coal firing.

Trace Element Emissions

Trace elements, especially metals, have recently been a persistent concern related to coal combustion and questions have been raised as to how fluidized-bed combustion will affect the release of trace elements. Our studies indicate that trace element control is essentially equivalent to particulate control. Most of the elements are concentrated in the particulate matter. The influence of improved particulate control is shown vividly in Figure 7. Emission data are from the Exxon Miniplant and are shown when the unit operated with two cyclones in series and when the unit operated with three cyclones in series.[5,6] A very conservative emission goal based on EPA environmental assessment criteria is shown for comparison.[7] Note that this emission goal is based on total mass--it does not differentiate between solid and vapor phase or between respirable and non-respirable particles. When the three-cyclone system was used (equivalent to about 90 percent removal), the extra degree of particulate control reduced almost all of the trace element emissions below the very conservative emission goal. The use of baghouses, which are capable of 99.9+ percent removal, will provide an even

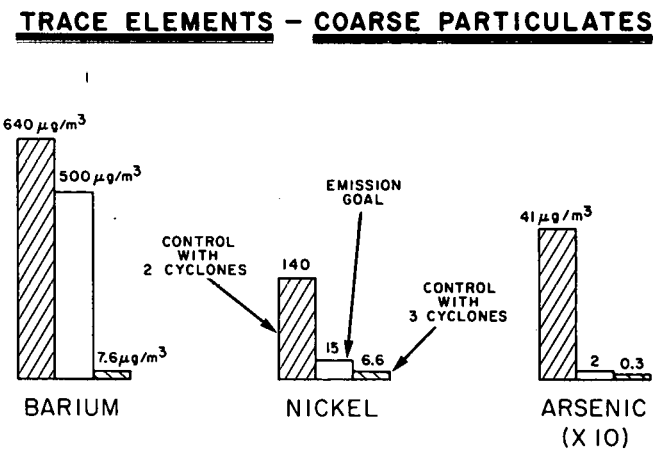

Figure 7. Trace element emissions as a function of particulate control. Control with three cyclones (approximately 90 percent removal) reduces most elements below conservative emission goals based on health effects data.

greater emission control margin. Similar data have been observed from the NCB fluidized-bed unit and samples from the Alliance, Ohio, unit are presently being analyzed.[14]

Our data further indicate that trace elements, notably the trace metals, do not leach from the captured particulates; hence, disposing of the captured material should not pose an environmental problem.

Organic Emissions

Measurements have been made on organic compounds in FBC emissions as part of GCA's environmental assessment studies. Data are reported as TCO--Total Chromatographable Organics--which is a surrogate analytical technique measuring what essentially amounts to volatile organic compounds in the range of C_6-C_{12} hydrocarbons. Data are also reported as GRAV which is a surrogate analytical technique for condensible, relatively non-volatile, organic compounds, such as aromatic hydrocarbons and polynuclear aromatic hydrocarbons. More detail on how TCOs and GRAVs are experimentally determined can be found elsewhere.[8]

FBC data are shown in Figure 8 and compared with similar data from conventional coal-fired systems.[9] Two points can be made from the data in Figure 8: 1) FBC emissions are relatively low in both volatile and condensible organic emissions and 2) FBC emissions are at the lower range of what is found in conventional coal-fired systems.

The TCO and GRAV analyses were supplemented with additional analytical techniques looking for

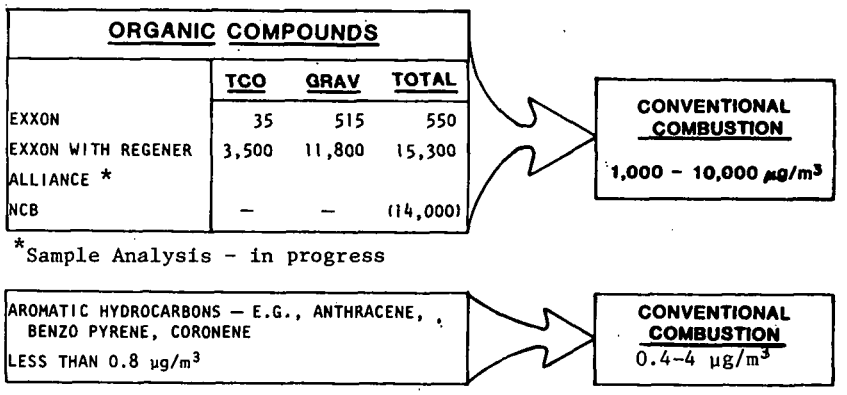

Figure 8. Organic compounds from coal-fired FBC compared with conventional coal combustion.

specific compounds; these results are summarized in Figure 9. Also shown are conservative emission goals based on EPA environmental assessment criteria developed in a manner similar to that men-

Compound	Emission concentration ng/m³	Discharge multimedia environmental goal ng/m³
Napthalene	<68,000	5×10^7
Anthracene	270	5.6×10^7
Fluoranthene[a]	<710	9×10^7
or Pyrene		2.3×10^8
2-Methyl anthracene	750	NA[b]
Benz(a) anthracene		45,000
or Triphenylene	6.2	NA
or Chrysene		2.2×10^6
Benzo(k) fluoranthene	<0.81	1.6×10^6
Benzo(a)pyrene	13	20
or Benzo(e)pyrene		3×10^6
7,12 Dimethyl benz(a)anthracene	<200	260
or Dibenzo(a,c)anthracene		9.9×10^6
Dibenz(a,h) anthracene	<5.8	93
Indeno (1,2,3-cd)pyrene	<250	1.6×10^6
Benzo(ghi)perylene	<9.1	NA
Anthanthrene	<300	NA
Coronene	<1.5	NA

[a]Compounds not separated by HPLC. [b]Data not available.

Figure 9. Results from HPLC screening of selected polynuclear aromatic hydrocarbons in FBC emissions.

tioned previously for trace metals.[7] In general, the FBC emissions of polynuclear aromatic hydrocarbons are well below the limits set by the environmental assessment criteria.

There is scant data available identifying specific polynuclear aromatic hydrocarbons from coal-fired combustion systems. What data that are available indicate that FBC emissions seem equal to or less than what is found in these conventional combustion systems.[10,11,12]

Solid Waste Leachates

Trace metals tend not to leach from FBC particulates or from the spent bed material. Figure 10 summarizes our approach for evaluating leachate data from the various solid waste components of an operating fluidized-bed combustor. The data are taken from the Exxon Miniplant,[6] but similar results have been observed from other systems. The data show that compared with both environmental assessment criteria and with criteria developed by EPA's Office of Solid Waste for judging the degree of hazard of a waste,[13] FBC leachates have a safety factor in the range of 5-15--i.e., the leached concentrations of the metals most often associated with waste disposal problems are 5-15 times below current evaluation criteria. These conclusions are confirmed by other GCA studies and by extensive work done at Westinghouse Research Laboratories.[14,15]

Data available to date indicate that FBC waste should not be deemed hazardous under the criteria of the Resource Conservation and Recovery Act. Disposal may be a problem simply because of the

EXAMPLE:
LEACHATE ANALYSES - μg/ℓ

ELEMENT	COMBUSTOR			REGENERATOR CYCLONE	ENV. GOALS (DMEG)		OFFICE OF SOLID WASTE CRITERIA	SAFETY FACTOR
	BED	2nd CYCLONE	3rd CYCLONE		HEALTH	ECOLOGY		
ARSENIC	28	86	126	66	250	50	500	5-15

SIMILAR RESULTS FOR: BARIUM, CADMIUM, CHROMIUM, LEAD, MERCURY, SILVER, SELENIUM

Figure 10. Leachate analyses from solid waste streams within an FBC system operating with limestone regeneration (Exxon Miniplant).

waste quantities generated or because of problems with high pH, dissolved solids, Ca, or $SO_4^=$. These should not be a serious problem and they should not pose major regulatory problems.

Bioassay Results

Bioassay results have been conducted in parallel with chemical analysis. The purpose of the bioassay studies is to detect the potential for environmental damage that may not be obvious from an analysis of selected elements and compounds. The bioassay tests function as a screening tool; the techniques used in our Program are described elsewhere.[16] They are still at an early stage of development, so the correct way to report and interpret results is currently not well resolved. FBC samples provide mixed bioassay results, as shown in Figure 11. The particulate matter and the collected flue gas tend to produce positive Ames results, but the positive results reflect only a low level of activity. Similar positive results have been observed for samples taken from conventional combustion.[17]

We have taken data for selected compounds that we have measured in FBC flue gas and calculated the dose applied in the Ames Test. As shown in Figure 12, this calculated dose is too low to account for the positive result based on literature data for pure compounds. This is not a rigorous comparison, because one is dealing with complex mixtures and not pure compounds; nevertheless, it does imply that aromatic hydrocarbons are not responsible for the weak mutagenic activity which was experimentally observed.

The results do not seem to warrant special concern for the present time. In future work, emphasis is being placed on testing the reproducibility of the results and on developing additional chemical fractionation schemes for further bioassay testing and bioassay interpretation.

HEALTH EFFECTS TESTS *

EMISSION STREAM	AMES	RAM	CHO
COMBUSTION PRODUCTS — (ORGANIC COMPONENT)	+	N	+
PARTICULATES			
— COARSE	+/-	—	N
— FINE	+/-	+	N
BED MATERIAL	—	+	+
COAL FEED	—	N	N
LIMESTONE FEED	—	N	N
REGENERATOR GAS	+	N	+
REGENERATOR PARTICULATES			

* BASED ON RESULTS FROM: EXXON, ALLIANCE, AND MORGANTOWN

Figure 11. Data from Health Effects Test on FBC emissions.

FUTURE WORK

Emission data from fluidized-bed combustion continue to look very promising in light of current environmental regulations. This includes regulations governing air, water, and solid waste discharges. Where gaps in the data base do exist (for example, more emission data are needed from "commercial-sized" units, especially particulate emissions), plans are already underway to launch the appropriate experiments. Major priorities for future work are listed below.

1. Detailed environmental assessment tests at full-scale facilities - plans are already underway for both Georgetown University and the Great Lakes Naval Training Center.

2. Long-term continuous emission monitoring tests - the proper averaging time for emission limits (e.g. hourly, daily, monthly, etc.) is a topic of concern. Plans are underway to conduct tests for 24 hours per day for 30 consecutive days as part of EPA's NSPS development program.

Compound	Emission concentration ng/m^3	Discharge multimedia environmental goal ng/m^3	Calculated Ames test dose[c] ng	Estimated dose required to produce the observed Ames test response[d] ng	Estimated revertants possibly produced by the applied dose[e]
Napthalene	<68,000	$5 \cdot 10^7$	2,100	>30,000[g]	<1.6
Anthracene	270	5.6×10^7	8	>300,000[g]	<0.0006
Fluoranthene[a]	<710	9×10^7	<22	NA	NA
or Pyrene		2.3×10^8		200,000[g]	<0.02[f]
2-Methyl anthracene	750	NA[b]	<23	NA	NA
Benz(a)anthracene		45,000		480	0.009[f]
or Triphenylene	6.2	NA	0.2	NA	NA
or Chrysene		2.2×10^6		130	0.0015[f]
Benzo(k)fluoranthene	<0.81	1.6×10^6	<0.025	NA	NA
Benzo(a)pyrene	13	20	0.4	46	0.2[f]
or Benzo(e)pyrene		3×10^6		9,000	0.0004[f]
7,12 Dimethyl benz(a)anthracene	<200	260	<6	250	0.024[f]
or Dibenzo(a,c)anthracene		9.9×10^6		35	3.8[f]
Dibenz(a,h) anthracene	<5.8	93	<0.2	550	0.008
Indeno (1,2,3-cd)pyrene	<250	1.6×10^6	<8	NA[c]	NA
Benzo(ghi)perylene	<9.1	NA	<0.3	NA	NA
Anthanthrene	<300	NA	<9	NA	NA
Coronene	<1.5	NA	<0.05	NA	NA

[a] Compounds not separated by HPLC.

[b] Data not available.

[c] Calculated highest dose applied.

[d] Calculated from data in the literature for pure compounds assuming one chemical was responsible for the observed response of 22 to 57 revertants (above background) in TA1537, TA1538, and TA98.

[e] Calculated from dose response data in the literature for pure compounds. Differences in test strains were ignored.

[f] Maximum response based on the assumption that the full fraction consists of the indicated compound.

[g] Mutagenicity results were negative at the highest applied dose.

Figure 12. Comparison of known doses of selected aromatic hydrocarbons with a calculated dosage of pure compound that should produce the observed Ames results.

3. Evaluation of particulate control equipment - the efficiency and reliability of particulate control equipment as used on FBC systems needs to be documented.

4. Further bioassay work - the proper role for these bioassay techniques in judging environmental impact needs further definition. Work is underway to test reproducibility as well as to devise more refined testing techniques.

REFERENCES

1. New Source Performance Standards: Electric Utility Steam Generating Units. Federal Register, Vol. 44, No. 133, pp. 33580-33624. June 11, 1979.

2. C.W. Young, J.M. Robinson, C.B. Thunem, P.F. Fennelly, Technology Assessment Report for Industrial Boiler Applications: Fluidized-Bed Combustion. U.S. EPA Report No. EPA-600/7-79-178e, prepared by GCA Corporation, Technology Division, Bedford, MA, November 1979.

3. J.C. Dickerman, K.L. Johnson, Technology Assessment Report for Industrial Boiler Applications: Flue Gas Desulfurization, U.S. EPA Report No. EPA-600/7-79-178i, prepared by Radian Corporation, Durham, NC, November 1979.

4. D.V. Bubenick, D.C. Lee, R.R. Hall, P.F. Fennelly, Control of Particulate Emissions from Fluidized-Bed Combustion: Fabric Filters or Electrostatic Precipitators, GCA Corporation, Technology Division, Bedford, MA, paper presented at 6th International Meeting on Fluidized-Bed Combustion, Atlanta, GA, April 1980.

5. J.M. Allen, J.E. Howes, S.E. Miller, K.M. Duke, Comprehensive Analysis of Emissions From Exxon Fluidized-Bed Combustion Miniplant, report (Draft) prepared by Battelle Columbus Laboratories for U.S. EPA under EPA Contract 68-02-2138, September 1977.

6. R.R. Hall, R. Kindya, G. Hunt, et al., Source Test Evaluation Report - Exxon Miniplant Fluidized-Bed Combustor with Regeneration, Draft Report prepared for U.S. EPA under Contract 68-02-2693 (in preparation).

7. J.G. Cleland, G.L. Kingsbury, Multimedia Goals for Environmental Assessment (Volumes 1 and 2), prepared by Research Triangle Institute for the U.S. EPA, Report No. EPA-600/7-77-136a and b, November 1977.

8. D.E. Lentzen, D.E. Wagoner, E.D. Estes, W.F. Gutnecht, IERL-RTP Procedures Manual: Level 1 Environmental Assessment (Second Edition), prepared by Research Triangle Institute for the U.S. EPA, Report No. EPA-600/7-78-201, October 1978.

9. C.C. Shih et al., Emissions Assessment of Conventional Stationary Combustion Systems, Volume III, Electricity Generation External Combustion Sources, prepared by TRW Inc., for the U.S. EPA, Draft Report, Contract No. 68-02-2197, October 1979.

also

C.Leavitt, K. Arledge, W. Hamersma, et al., Environmental Assessment of Coal- and Oil-firing in a Controlled Industrial Boiler, Volumes I-III, U.S. EPA Report No. EPA 600/7-78-164b, prepared by TRW Inc., Redondo Beach, CA, for U.S. EPA, August 1978.

10. S.G. Zelenski, N. Pangaro, J.M. Hall-Enos, Inventory of Organic Emissions from Fossil Fuel Combustion for Power Generation, report prepared by GCA Corporation, Technology Division, Bedford, MA, for Electric Power Research Institute, EPRI Project TPS 78-820, January 1980.

11. R.P. Hangebrauk, D.J. vonLehmden, J.E. Meeker, Air Pollutant Emissions from Coal-Fired Power Plants, U.S. Public Health Service, report No. 999-AP-33, 1967.

12. R. Bennett, K.T. Knapp, P.W. Jones, J.E. Wilkinson, P.E. Strup, Measurement of Polynuclear Aromatic Hydrocarbons and Other Hazardous Organic Compounds in Stack Gases, in Proceedings of the Third International Symposium on Polynuclear Aromatic Hydrocarbons. (Ed. P. Liber and P.W. Jones), Ann Arbon Science Publishers, Ann Arbor, MI, in press, 1979.

13. Hazardous Waste Proposed Guidelines and Regulations on Identification and Listing. Federal Register Volume 43, No. 243, pp. 58946-59028, December 18, 1978.

14. R. Kindya, C.W. Young, et al., Source Test and Evaluation Report (Level 1) Alliance Fluidized-Bed Combustion Facility, GCA Corporation, Technology Division, Draft report (in preparation) under U.S. EPA Contract 68-02-2693, June 1980.

15. C.C. Sun, C.H. Peterson, R.A. Newby, W.G. Vaux, D.L. Keairns. Disposal of Solid Residue From Fluidized-Bed Combustion: Engineering and Laboratory Studies, prepared by Westinghouse Research and Development Center, Pittsburgh, PA, for the U.S. EPA, Report No. EPA-600/7-78-049, March 1978.

16. K.M. Duke, M.E. Davis, A.J. Dennis, IERL-RTP Procedures Manual: Level 1 Environmental Assessment Biological Tests for Pilot Studies, report prepared by Battelle Columbus Laboratories for U.S. EPA, Report No. EPA-600/7-77-043, April 1977.

17. C.E. Chrisp, G.L. Fisher, J.E. Lammert, Mutagenicity of Filtrates from Respirable Coal Flyash, Science 199: 73-75, 1978.

CONTROL OF PARTICULATE EMISSIONS FROM FLUIDIZED-BED COMBUSTION: FABRIC FILTERS OR ELECTROSTATIC PRECIPITATORS

David V. Bubenick
David C. Lee
Robert R. Hall
Paul F. Fennelly

GCA/Technology Division
GCA Corporation
Bedford, Massachusetts

Introduction

In June of 1978, the U.S. Environmental Protection Agency awarded a 4-year contract to GCA/Technology Division to perform a comprehensive environmental assessment and systems analysis of fluidized-bed combustion technology. The ultimate objective of this program is to ensure that an adequate research data base is available to EPA Program Offices as they develop or revise pollution standards in conjunction with a national energy policy. As part of the engineering assessment of control technology for atmospheric fluidized-bed combustion (AFBC), GCA is investigating the suitability of fabric filters and electrostatic precipitators (ESPs) as final particulate collectors.

Initial efforts were directed at examining selected, planned, and operating fabric filters and electrostatic precipitators applied to AFBC boilers. This survey led to the conclusion that fabric filters are being installed on virtually all new AFBC units despite the lack of comprehensive test or demonstration data. ESPs, on the other hand, have been applied on a rather limited basis. With this lack of a working data base, a more fundamental approach was elected to assess particulate control device suitability. This consisted of first making basic measurements on selected flyash samples obtained from operating pilot and full-scale AFBCs in the United States. Then, with the aid of analytical mathematical performance models, which are available for fabric filters and ESPs, basic relationships among key design and performance parameters were examined. Both the results of measurements made and relationships examined are presented in this paper along with an assessment of additional data needs, stressing the importance of laboratory and field verification of control device performance.

Fabric Filter Installations

Fabric filters have been installed on numerous fluidized-bed combustors in Europe and the United States. These fabric filters range in size from small 200 acfm systems on experimental FBCs to full-scale 40,000 acfm units on industrial fluidized-bed boilers. Examples of fabric filters being used on FBCs in West Germany include the 35 MW_t Flingern plant in Düsseldorf and the 6 MW_t FBC located at the Köenig Ludwig Colliery in Recklinghausen. Both of these units use woven glass bags with a Teflon/graphite coating. At the Flingern plant, cleaning is accomplished by reverse air and shaking, while only reverse air is used at the Recklinghausen facility. The results of a survey of U.S. fabric filter installations are shown in Table I.

The first full-scale fabric filter to be applied to an FBC in the United States was the Georgetown University unit which began operating in July of 1979. Other industrial-size systems are scheduled to begin operating at the Central Ohio Psychiatric Hospital during May of 1980 and at the Great Lakes Naval Training Center in Illinois in early 1981. Georgetown is the largest of these units with a steam capacity of 100,000 lb/hr compared to 60,000 lb/hr for the Central Ohio FBC and 50,000 lb/hr for the Great Lakes unit. The Georgetown and Great Lakes plants are U.S. Department of Energy (DOE) demonstration units while the Central Ohio Psychiatric Hospital facility is partially funded by the State of Ohio DOE.

There are design similarities among the full-scale FBC units with respect to key parameters. Fluidizing velocities, for example, are all in the range of 7 to 8 ft/sec, Ca/S ratios generally vary from 2 to 4, and bed temperatures range from 1550 to 1600°F. Georgetown University is the only unit using overbed coal feeding. The above parameters and other factors, such as sorbent attrition, coal characteristics, and freeboard height can affect the quantity and characteristics of particulate emissions.

The three full-scale fabric filters discussed above reflect a wide range of vendor designs. The Enviro-Systems design at Georgetown employs a novel "Shock Drag" cleaning system (recently supplemented with pulse jet assist and using a combination fiberglass/nylon fabric) while the American Air Filter design planned for Central Ohio will use off-line pulse jet cleaning with woven glass bags. Filtration velocities range from 1.5 ft/min at Great Lakes, 4.4 ft/min at Georgetown, to 6 ft/min at Central Ohio. The design of the Great Lakes fabric filter appears to be the most conservative in that the combination of low filtration velocities and reverse air cleaning with woven glass bags closely parallels the most successful and accepted designs for fabric filters on conventional boilers.

TABLE I. FABRIC FILTERS PLANNED AND OPERATING ON ATMOSPHERIC FLUIDIZED-BED COMBUSTION UNITS - U.S.

	Georgetown University, Washington, D.C.	Central Ohio Psychiatric Hospital, Ohio	Great Lakes Naval Training Center, Ill.	Pope, Evans, and Robbins Demonstration Unit Alexandria, Va.	Combustion Engineering Demonstration Unit Windsor, Conn.	FluiDyne Engineering Demonstration Unit, Minneapolis, Minn.	EPRI/B&W* Pilot Plant, Alliance, Ohio	SATR† Experimental Unit, EPA, Research Triangle Park, N.C.	Grand Forks Energy Research Center Exper. Unit Grand Forks, N.D.
Manufacturer	Enviro-Systems & Research, Inc.	American Air Filter Co., Inc.	Zurn Industries, Inc., Air Systems Division	Buell Division, Envirotech Corporation	Combustion Engineering, Inc., Air Preheater Division	Eagle Corporation	Fuller Corporation	Young Industries, Inc.	Wheelabrator - Frye, Inc., Air Pollution Control Division
Cleaning method	Shock-Drag with pulse jet assist	Pulse jet (off-line)	Reverse air	Pulse jet and/or reverse air	Reverse air	Pulse jet	Pulse jet	Pulse jet	Pulse jet
Fabric type	Coated woven fiberglass with nylon overlay	Coated woven fiberglass	Coated woven fiberglass	Coated woven fiberglass	Coated woven fiberglass	Felted Nomex	Coated felted fiberglass	Teflon felt	Coated woven fiberglass
Design pressure	Negative, 20 in. W.C.	Negative	Positive	Negative	Negative	Negative	Negative, 40 in. W.C.	Positive	Negative, 5-10 in. W.C.
Rated flue gas flow rate (acfm)	45,000	60,000	23,800	3,000	1,000	3,750	8,000	200	650
Flue gas temperature (°F)	400-525	500	350-500	400-500	350-500	360-380	375-400	350-450	250-350
Air-to-cloth ratio, gross (ft/min)	4.7	6.0	1.5	-	1.5	3.75	2.6	6.0-6.5	2.3
Pressure drop (in. W.C.)	4.0-6.0	8.0	6.0	-	4.0-5.0	1.5-2.0	2.0-2.5	4.0-5.0	<1.0
Number of bags, total	792	760	244	-	48	-	392	7	18
Number of compartments	22	4	3	-	4	1	4	1	1

*Electric Power Research Institute/Babcock & Wilcox

†Sampling and Analytical Test Rig, presently not operating.

Six pilot/experimental units using fabric filters to control particulate emissions are also listed in Table I. The sizes of these FBC units range from EPA's Sampling and Analytical Test Rig (SATR) with a coal-burning capacity of 20 to 110 lb/hr, to the Electric Power Research Institute (EPRI)/ Babcock-Wilcox (B&W) unit at Alliance, Ohio with a capacity of 1950 lb/hr. The fabric filter at this site uses pulse jet cleaning with felted fiberglass fabric, which is a rather recent development. The FluiDyne unit, which uses Nomex felt bags, is the only one of the six FBC fabric filters not using glass bags. Pulse jet cleaning with felt bags, either Nomex, glass or Teflon, generally permits higher filtration velocities compared to reverse air cleaned woven bags, viz., 5 ft/min compared to 2 ft/min. Nomex is not as acid-resistant as Teflon or glass, but it is much less expensive than Teflon and possibly less subject to deterioration with repeated cleaning compared to glass fabrics.

For the small experimental systems, both FBC and fabric filter operating parameters can vary over wide ranges. The emphasis for many of these pilot units appears to be more on optimization of FBC parameters than on the specific design of the particulate collector. In addition, due to recognized scaling factors and the limited number of experimental measurements, pilot fabric filters are not entirely representative of expected full-scale fabric filter operation. The limitations associated with scale-up from pilot to full-scale units is also an important consideration (limitation) with respect to electrostatic precipitators.

Electrostatic Precipitator Installations

The only operating ESP on a fluidized-bed boiler is the hot-side precipitator downstream of a four-cell AFBC at the Monongahela Power Station at Rivesville, West Virginia. Design conditions include an overall mass collection efficiency of 99 percent on a 203,000 acfm gas stream at 730°F, a 0.875 grains/acf inlet grain loading, and an ESP treatment velocity of 3.57 ft/sec. Despite boiler operational instability (viz. inlet loadings and volume flow rates for the three-cell operation were higher and temperatures lower than design) precipitator performance was tested in 1979.[1] A recent 200-hour run has indicated improved ESP performance and further tests are planned to substantiate sizing criteria.[2]

A pilot ESP, designed and built by Denver Research Institute, has been installed on the SATR FBC unit at Research Triangle Park, North Carolina, although the system is not now operating. Another pilot ESP is expected to be installed on a slipstream at the EPRI/B&W Alliance, Ohio FBC facility in order to compare the relative performance of an ESP to a fabric filter with the same flyash and under the same boiler operating conditions.

Approach

Laboratory Measurements

As shown in Table II, five flyash samples were obtained from four FBC sites ranging from pilot to full-scale units and covering a wide range of operating conditions. Sample C was obtained under conditions of no flyash reinjection into the boiler while Sample D represents the typical case with flyash reinjection. In the "Results/Discussion" section, it will be shown that samples C and D contained 12.4 and 10.9 percent combustibles respectively. The relatively high excess air and conservative fluidizing velocities noted in Table II appear to correlate well with the relatively low values for percent combustibles.

Each of the four FBC sites are equipped with fabric filter collectors. Flyash samples were extracted from the hopper at each site, screened to less than 125 μm, and riffled.[3] Aliquot test samples were then prepared for subsequent laboratory analyses which are listed in Table III.

All measurements of particle size distribution and filtration parameters were conducted using the GCA bench scale fabric filter test (panel) system.[4] The flyash samples were redispersed at high pressure into an approach duct that was connected to a fabric panel assembly. After a period of startup, a sample was extracted from a location opposite the midpoint of the panel and sized using an Andersen Mark III (eight-stage) Cascade Impactor. Replicate tests were run at a flow rate of 0.5 acfm for a period of 1 to 2 minutes for sample extraction. The manufacturer's calibration data for stage jet diameters and the inertial impaction parameter were used and stage cut diameters were calculated by an iterative procedure. Cumulative particle size distributions were then plotted and the mass median aerodynamic diameter (aMMD) and the geometric standard deviation (σ_g) were obtained from a straight line fitted to the data.

The specific coefficient of resistance, referred to as K_2, is simply a measure of the filterability of the dust cake on a fabric surface. Each of the FBC flyash samples was filtered through a panel of 10 percent Teflon-B coated fiberglass fabric, which is often specified for use in fabric filter collectors applied to conventional coal-fired utility and industrial boilers. All runs were made at an air-to-cloth ratio of 2.5 ft/min with inlet concentrations ranging from 0.7 to 1.2 grains/acf depending on the sample. Pressure loss across the fabric panel was monitored and the panel was periodically removed from its holder for weighing. Curves of fabric drag versus dust loading were constructed from the data collected and K_2 was determined for each ash by a linear approximation of the slope of the drag versus dust loading curve.

Resistivity measurements for the flyash samples were conducted by Denver Research Institute using a parallel plate resistivity cell apparatus.[5] Electrical resistivity was determined by measuring the current conducted through the sample under an applied voltage of approximately 10,000 volts/in. The resistivity cell is housed in an electrically controlled oven to allow variation in temperature from 250 to 750°F. Humidity was set at 5, 10, and 20 percent H_2O by volume, by passing the air

TABLE II. FBC OPERATING CONDITIONS FOR FLYASH SAMPLES

Parameter	Facility/Sample Designation: EPRI/B&W Pilot Plant Alliance, Ohio — A*	SATR Experimental Unit EPA, Research Triangle Park, North Carolina — B	FluiDyne Engineering Demonstration Unit Minneapolis, Minn. — C*	D	Georgetown University Washington, D.C. — E†
Gas flow rate (acfm)	8,180	100-400	2,100	2,150	45,000
Bed temperature (^{o}F)	1540	1450-1570	1540	1530	1600
Coal feed rate (lb/hr)	1,950	22-110	514	516	9,570
Calcium-to-sulfur ratio, Ca/S (mole/mole)	3.4	3.0	2.8	2.3	3.0‡
Excess air (%)	18	25	33	32	20
Fluidizing velocity (ft/sec)	8.0	3.0-16.0	4.4	4.4	8.0
Air-to-cloth ratio, A/C (ft/min)	2.0	6.5 max.	2.1	2.2	4.4

*Sample taken without flyash reinjection.

†Design conditions.

‡Ca/S during sample extraction was 4 to 5.

TABLE III. SUMMARY OF FBC FLYASH MEASUREMENTS

Parameter/analysis	Instrument/technique
Particle size distribution	Andersen Mark III (eight-stage) cascade impactor
Specific coefficient of resistance	GCA/Technology Division bench scale fabric filter test panel system
Resistivity	Denver Research Institute single and multiple cell resistivity apparatus.
Chemical/spectral analysis	Amray Model 1200 SEM* with EDXRA†
Carbon analysis	Low temperature ashing (LOI)‡ High temperature ashing (CHN)§
Morphology	Amray Model 1200 SEM*

*Scanning Electron Microscope

†Energy Dispersive X-ray Analysis unit

‡Loss on ignition

§Carbon-Hydrogen-Nitrogen test using a Perkin Elmer Model 240B Elemental Analyzer

through one of three temperature-controlled fritted glass water bubblers.

Chemical analysis of the flyash samples was accomplished by using a scanning electron microscope (SEM), also used for particle morphology analysis, integrated with an energy dispersive X-ray analysis unit (EDXRA). This system provides approximate quantitative elemental analyses of individual particles or a field of particles. Although not an absolute indicator of all chemical elements present (it is limited, for example, by the small sample size used which may not be representative of the total sample), elements attributed to the following oxides were measured: Al_2O_3, SiO_2, CaO, Fe_2O_3, K_2O, and TiO_2.

As part of an effort to correlate electrical and chemical properties of the five FBC flyash samples, two techniques were employed to assess the free carbon concentration present in the samples. Initially, a simple loss on ignition (LOI) analysis was performed whereby desiccated weights of each sample were taken before and after being placed in a flow ashing chamber. This procedure was repeated after the samples had been treated with hydrochloric acid to remove any carbonates present. These steps were supplemented with a carbon-hydrogen-nitrogen (CHN) test. This procedure involves the high temperature ashing of a flyash sample in the presence of a reagent to provide excess O_2 for complete combustion. The off-gases are passed through a gas chromatograph column to separate and identify the oxides present.

Fabric Filter Model

Under contract with the U.S. Environmental Protection Agency, GCA/Technology Division has developed a working mathematical model that can be used to predict the field performance of large fabric filter systems applied to coal-fired utility boilers.[4,6,7] The model applies to specific collector types using woven glass fabrics with any of several surface treatments and simulates fabric cleaning by a collapse and reverse flow process and/or shake assist. The model takes into account the physical properties of the boiler effluent, the basic design and operating parameters of the filter collector as well as the filtration parameters associated with the dust and fabric. Both average and instantaneous pressure drop and particle penetration as a function of time can be predicted. Comparison of the model with measured field data on fabric filters applied to conventional boilers at the Sunbury Station of Pennsylvania Power and Light and the Nucla Station of Colorado-Ute Electric Association, has shown excellent agreement with respect to performance.

Several key concepts, based largely on laboratory and pilot testing, form the basis for the model simulation of full-scale fabric filter operation and performance. The model simulates the distribution of gas flow to a number of parallel compartments of the collector. Resistance to flow created by the dust cake is a function of the velocity at which the dust is deposited on the fabric. Removal of dust from a bag is nonuniform in that some portions of the fabric surface retain a complete dust layer after cleaning whereas others shed all of the deposited dust, except for a small residual amount which remains embedded in the fabric. With respect to dust deposition and removal, the model reflects the results of test observations which conclude that no appreciable particle size segregation occurs. Finally, the penetration of dust through the dust/fabric medium is a function of the dust cake thickness as well as the filtration velocity.

With respect to design parameters required as input to the model, the following parameters are noted: number of compartments, cleaning method, cleaning schedule, and reverse flow velocity. Required operating parameters include flue gas temperature, inlet dust concentration, and gross filtration velocity (air-to-cloth ratio). Important inlet dust properties to be considered include the specific resistance of the dust cake, K_2, and the effective residual drag of the fabric, S_E. These two parameters define a straight line on a fabric drag versus loading plot that relates the overall resistance to flow created by the fabric and the dust, to the amount of dust on the fabric. Finally, an estimate of the degree of cleaning that can be expected must be made. This parameter, referred to as a_c, relates the amount of dust removed from a bag to the amount of dust present before it is cleaned.

In this study the effects of K_2 on penetration and pressure drop across the fabric as a function of the filter face velocity and a_c are examined.[8] In order to conceptually examine the relationships among key performance and design parameters, an "average system" is defined with respect to the parameters discussed above.

Electrostatic Precipitator Model

In recent years, increasing attention has been given to the development of theoretical relationships that describe the physical, chemical, and electrostatic mechanisms interacting in the electrostatic precipitation process. Under EPA sponsorship, Southern Research Institute has developed a mathematical computer model that incorporates many of these relationships.[9,10] The model depends on the basic Deutsch-Anderson equation to calculate the particle collection efficiency for each incremental length along the precipitator collecting plate. A key parameter in this relation is the particle migration velocity (or particle drift velocity) which is a function of electrical energization of the precipitator, gas properties, and entering particle size distribution. In the model, migration velocity is calculated using field and diffusion charging theories, and is adjusted using empirical correction factors to account for unmodeled effects. The model also accounts for the nonideal effects of nonuniform gas velocity distribution, gas bypassage of electrified regions, and particle reentrainment due to rapping and other causes. Overall collection efficiency is estimated by summing the incremental collection efficiencies over the entire precipitator length and iteration is exercised until a convergence on the overall

collection efficiency is obtained. Estimation of nonideal collection efficiencies is accomplished by adjusting the ideal efficiencies for nonideal effects after convergence is obtained.

The model can be used as a tool in troubleshooting precipitators that are not meeting the overall mass collection efficiency that is expected or anticipated. To exercise this feature, certain experimental data are required, such as operating voltages and currents, inlet mass loading and particle size distribution, ash resistivity, average gas flow rate and velocity, and average temperature and pressure. Furthermore, with proper care in selection of input data, the model can be used as a rough guide in precipitator sizing.

The SRI/EPA model was used in this study to investigate the relationship between specific collection area (SCA) and overall mass collection efficiency using measured resistivity and particle size distribution data for three FBC flyash samples. Assumptions regarding other factors such as flue gas properties and current-voltage characteristics were made on the basis of past experience in using the model as well as on model validation tests conducted by SRI. The model is also used to demonstrate the effect of particle size distribution on efficiency.

Results/Discussion

Table IV shows the results of resistivity, particle chemical composition, particle size distribution, and filtration measurements conducted on each of the five FBC flyash samples. These results are used in conjunction with other assumptions to examine the relationships among key design and performance parameters for fabric filters and ESPs.

TABLE IV. RESULTS OF FUNDAMENTAL MEASUREMENTS PERFORMED ON FBC FLYASH SAMPLES

	Resistivity (ohm-cm) @ 10% moisture			Chemical/spectral analysis* constituents (% by weight)							Particle size distribution		Specific coefficient of resistance
Sample designation	300°F	500°F	700°F	Al_2O_3	SiO_2	K_2O	CaO	TiO_2	Fe_2O_3	C†	aMMD, $\bar{x}$ (μm)	σ_g	(in. W.C.-min-ft/lb)
A‡ - Alliance	3.3×10^7	1.2×10^7	§	11.1	33.2	1.8	10.1	1.0	4.1	33.7	6.0	2.8	29.0
B - SATR	3.2×10^{11}	5.0×10^{10}	5.0×10^9	21.4	48.5	1.7	10.7	1.6	3.6	7.5	5.3	2.6	31.7
C‡ - FluiDyne	8.0×10^{11}	1.4×10^{11}	5.0×10^9	12.0	39.5	3.0	20.7	1.8	7.8	10.2	7.3	2.6	11.6
D - FluiDyne	1.1×10^{12}	2.6×10^{11}	8.0×10^9	12.3	40.0	3.0	22.6	1.0	7.6	9.5	8.9	3.0	14.6
E - Georgetown	7.1×10^5	3.3×10^5	§	9.9	24.2	1.3	7.0	-	6.4	46.2	7.7	2.7	28.3

*The six oxides were derived from SEM/EDXRA analysis. This method is relatively insensitive to elements of low atomic number. Some elements (attributed to their common oxides, e.g., SO_3) could not be measured, hence the total does not equal 100%.

†Percent carbon was determined using a CHN test. Results closely agree with those from a simple LOI determination. For samples A, B, C, D, and E, the percent combustibles (LOIs) were 25.9, 7.5, 12.4, 10.9, and 43.0, respectively.

‡Without flyash reinjection.

§Both samples A and E sparked over above 500°F, hence, testing could not be continued.

With respect to electrical resistivity, samples B, C and D exhibit values that fall within the moderate to high range generally observed with conventional coal-fired boiler flyash. The characteristic variation of resistivity with temperature is also observed. The fact that samples A and E have such unusually low resistivities is attributed to the rather high carbon contents present, as determined by both simple LOI and CHN analyses. In fact, due to these high carbon contents, samples A and E exhibited spark over at 500°F and, as a result, further measurements could not be made.

As discussed earlier, two methods were used to determine the amount of carbon (combustibles) present in each sample. While the weight loss of a sample associated with simple LOI analysis is usually representative of carbon content, losses from other carbonaceous matter such as carbonates and volatile species, if they are present, will be reflected in the results. In order to determine the carbonate contribution to the LOI results, the LOI analysis was repeated after the sample had been treated with hydrochloric acid to remove any carbonates. These results are, within experimental error, identical to those from the simple LOI test with respect to the carbon content measured. It may be inferred, therefore, that the carbonate content of the samples is relatively small. A CHN analysis yielded results that are in good agreement with the LOI results shown in Table IV. In the absence of carbonates, the CHN data provide an excellent characterization of the free carbon constituent.

The chemical analysis presented in Table IV is not intended to be a comprehensive assessment of all of the oxides present. Indeed, spectral analysis using an SEM in conjunction with EDXRA analysis is limited by the small sample size used in the apparatus (which may not be representative of the whole sample) as well as by the fact that even with computer correction, some elements are more responsive to X-ray analysis than others. Silicon, for example, is more efficiently excited by X-rays whereas sulfur, below 4 percent by weight, is usually not detectable.

With respect to filtration parameters, the specific coefficient of resistance, K_2, is shown to vary from 11.6 to over 30 in. W.C.-min-ft/lb while the particle size distribution remains fairly

constant. Since K_2 is usually related to particle size, with a fine particle size distribution implying a high K_2, it appears that particle size does not account for the K_2 variation. Differences may be attributed to particle shape, surface characteristics or charge effects, although additional investigation is needed to resolve this issue.

Figures 1 and 2 provide a comparison of FBC flyash morphology with conventional coal-fired flyash particle morphology. These photomicrographs illustrate the fact that conventional flyash is generally more spherical in nature whereas FBC flyash represents a broad composition of irregularly-shaped particles. Particle surface characteristics can be important in dust cake buildup and in dust cake porosity for fabric filters. Surface characteristics can also be important in how flyash is naturally conditioned within the gas stream so as to enhance electrostatic precipitation. Clearly more work has to be done to substantiate how flyash morphology affects collection by filtration and electrostatic precipitation.

Fabric Filter Analysis

Filterability of the filter dust cake is an important parameter in predicting filter penetration and pressure drop. As noted in Table IV, the filterability parameter (K_2) varies by a factor of 2.5 over the five FBC flyash samples tested. In order to examine this variation in K_2, the GCA fabric filter mathematical model described earlier was used. For this conceptual analysis, an average system was defined, consisting of 14 compartments, a 35-minute cleaning cycle, and a reverse flow velocity of 2 ft/min. To simulate AFBC boiler effluent, an uncontrolled particulate concentration of 3.5 grains/acf and a gas temperature of 400°F were chosen. The value of K_2 was chosen to be 30 in. W.C.-min-ft/lb in contrast to 12 in. W.C.-min-ft/lb for conventional coal-fired boiler flyash. With respect to the woven glass fabric, a representative value of 0.49 in. W.C.-min/ft was selected for S_E.[4]

Under the assumption that FBC flyash is removed from the fabric surface to the same degree as conventional flyash, Figures 3 and 4 show the effect of K_2 on penetration and pressure drop respectively as a function of filter face velocity. The higher K_2 associated with FBC flyash results in a higher pressure drop and higher local velocities through "relatively clean" fabric areas, which cause increased particle "seep-through" (penetration) compared to the conventional flyash case. At an air-to-cloth ratio of 2 ft/min, the difference in K_2 results in roughly a 30 percent increase in fractional penetration and a 100 percent increase in pressure drop. To achieve a collection efficiency of 99.5 percent, for example, a 3 ft/min filtering velocity would be acceptable with a flyash having the lower K_2, but not with a flyash at the higher K_2 level. Although these are modeled results, they do conceptually describe the effect of a less porous dust cake (high K_2), the resultant higher pressure drop, and that particle seep-through under the driving force of higher local velocities can account for increased filter penetration.

If it is found that FBC flyash does not have dust-fabric release properties similar to conventional flyash, then the "cleanability" of the fabric would be expected to be different. The cleanability parameter, more properly termed the fraction of the filter area cleaned, is simply an indicator of how much dust is removed from a woven glass bag during reverse air or shake cleaning. The degree of cleaning is determined by model calculation based on experience with conventional flyash. For a K_2 of 30 in. W.C.-min-ft/lb and an air-to-cloth ratio of 2 ft/min, the model calculates that approximately 25 percent of the flyash is removed upon cleaning. Figure 5 shows how penetration and pressure drop will vary as a function of the degree of cleaning. If less than 25 percent of the filter cake is removed, pressure drop increases considerably with only a slight decrease in penetration. (This is due to the fact that more of the filter cake is present to filter additional flyash). With a greater degree of cleaning compared to conventional flyash, more of the dust cake is removed, the pressure drop decreases but the penetration increases. As the degree of cleaning varies from 10 to 40 percent, pressure drop is reduced by approximately 70 percent while penetration increases by roughly 12 percent. Clearly, the ease of dust removal from the bag surface as a result of cleaning is an important factor in predicting fabric filter operating pressure drop and performance.

Electrostatic Precipitator Analysis

Particle resistivity is an important consideration in the application of electrostatic precipitators to fluidized-bed combustion. Very low concentrations of SO_3 have been recorded in FBC flue gas, which implies a reduced conditioning effect on the particles, resulting in increased resistivity. In addition, all sorbent materials ($CaCO_3$, CaO, MgO, and $CaSO_4$) have high resistivities. However, carbon content exerts a strong influence in lowering flyash resistivity.

Resistivity measurements for each of the five flyash samples studied are compared with other reported data as shown in Figure 6. The resistivity curves for samples B, C, and D at 10 percent moisture, closely resemble one another and attain their maximum resistivities at 300 to 350°F. The characteristic shape of these curves and the magnitude of the measurements are in agreement with measurements obtained by Pope, Evans and Robbins for flyash samples from their Alexandria FBC facility.[11]

The resistivities of samples A and E are similar to one of the test runs conducted on flyash from the Rivesville hot-side ESP. The carbon content of the Rivesville sample was found to be 47 percent, which compares to the relatively high percent combustibles noted for samples A and E (see Table IV). While the Rivesville FBC has four cells (three main cells and one carbon burnup cell), only one cell was operating when the test was run. Examination of Alliance and Georgetown operating data revealed that sample E was obtained at low load conditions while sample A was obtained without flyash recycle. Based on these observations, the high carbon contents of these samples can be attributed

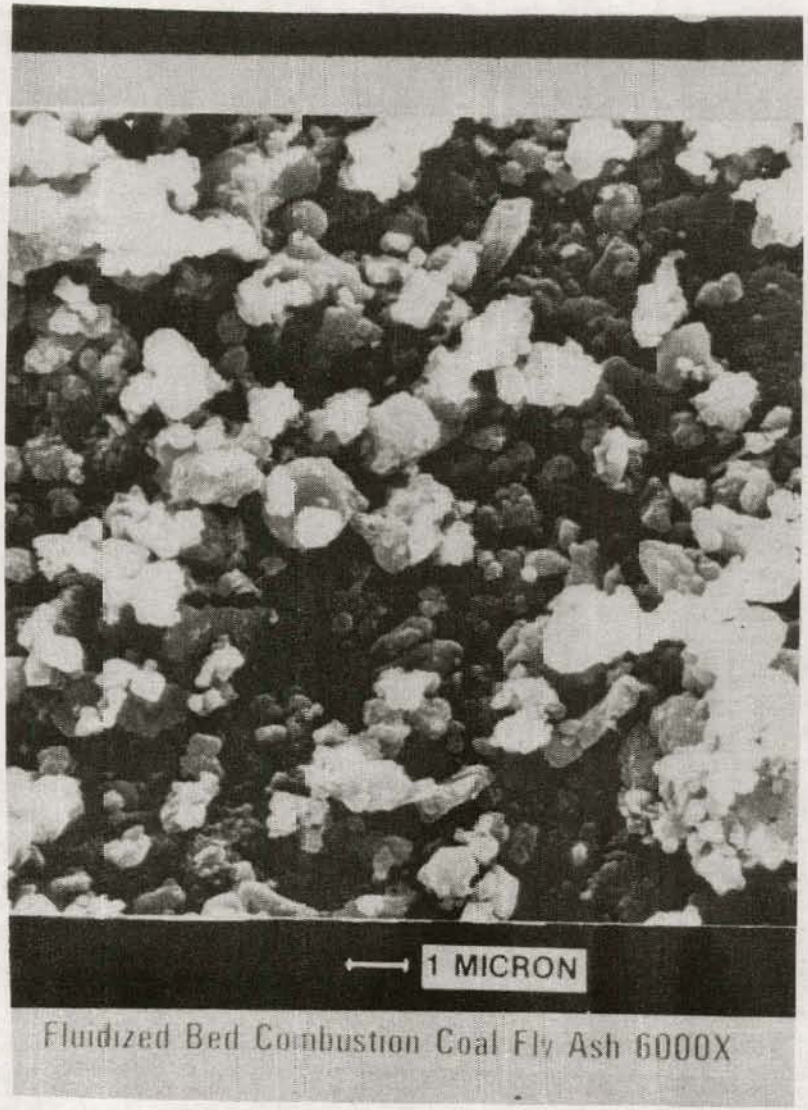

Figure 1. Representative morphology for FBC flyash.

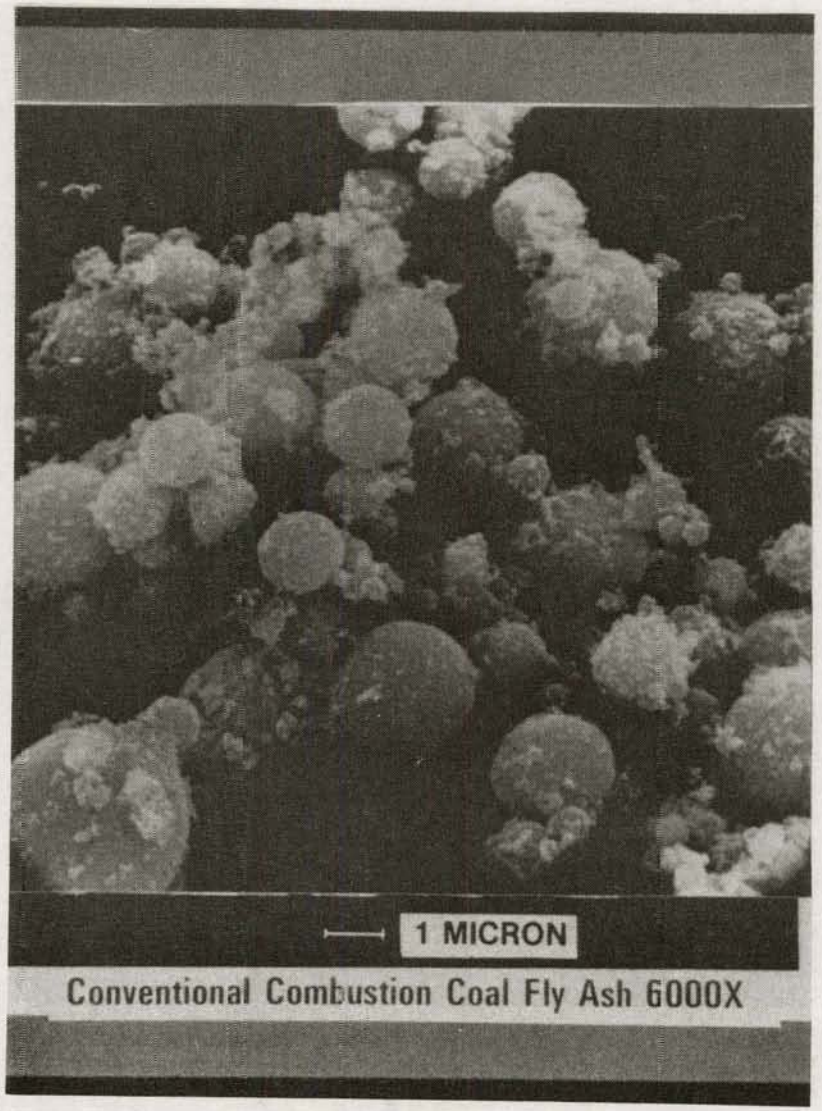

Figure 2. Representative morphology for conventional coal-fired boiler flyash.

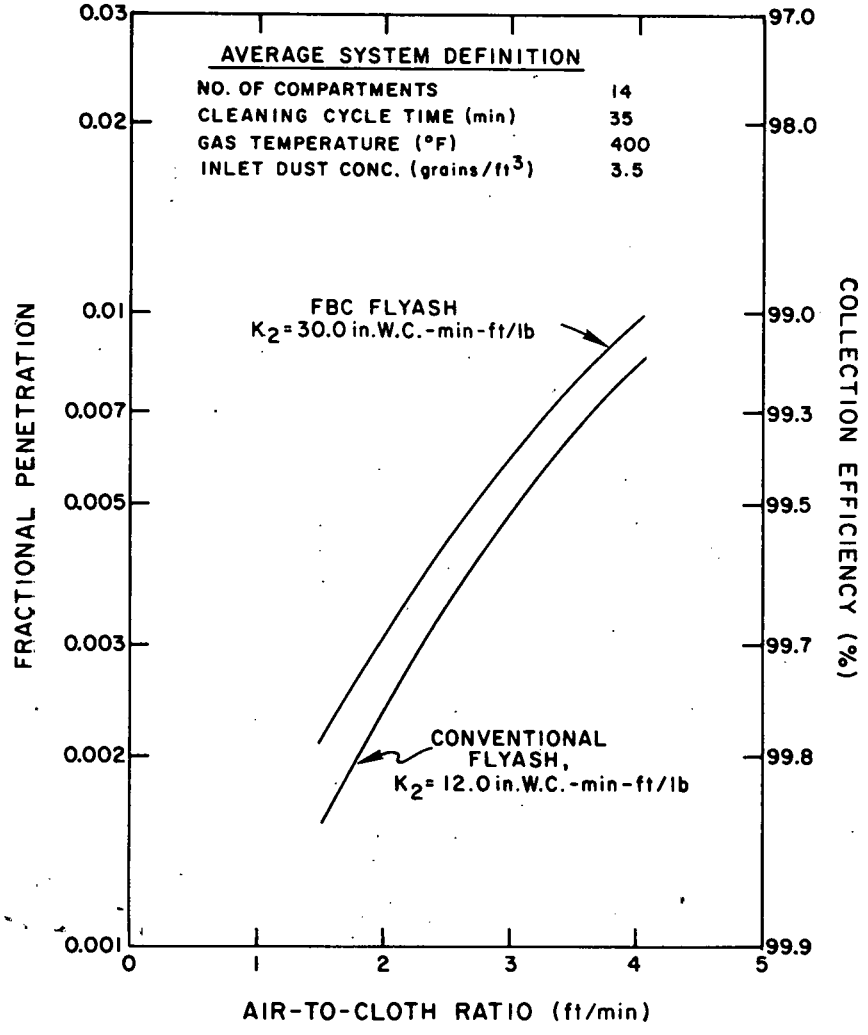

Figure 3. Effect of K_2 on particle penetration as a function of air-to-cloth ratio.

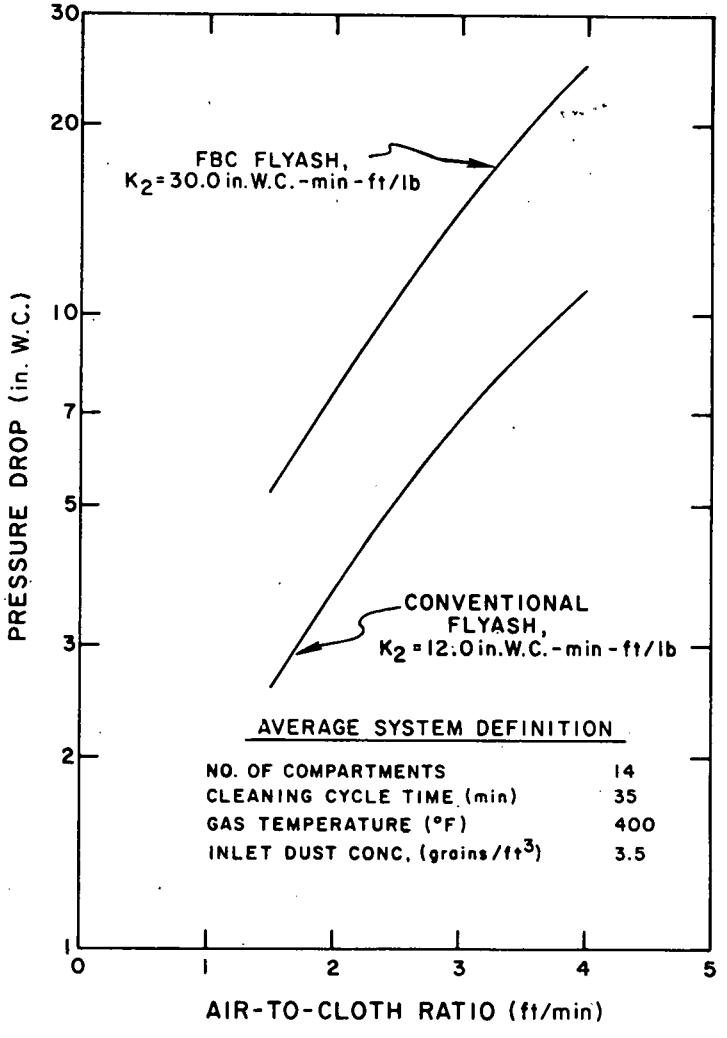

Figure 4. Effect of K_2 on filter pressure drop as a function of air-to-cloth ratio.

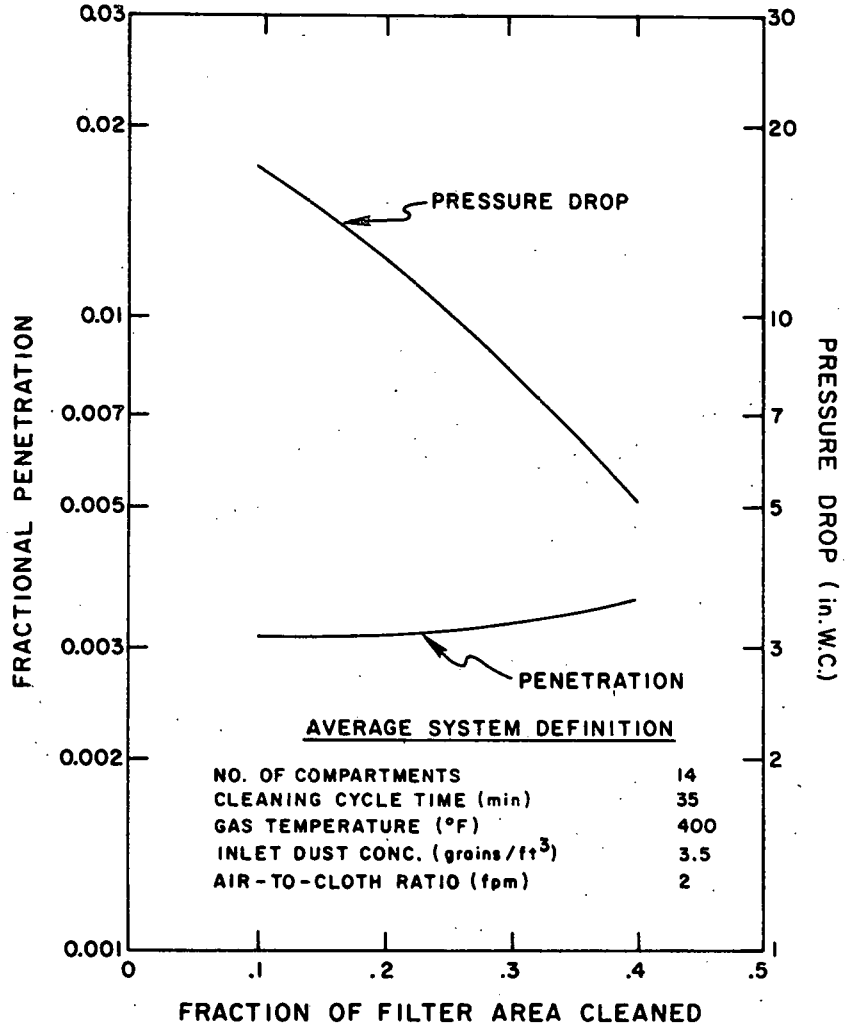

Figure 5. Penetration and filter pressure drop as a function of fraction of filter area cleaned (K_2 = 30 in. W.C.-min-ft/lb).

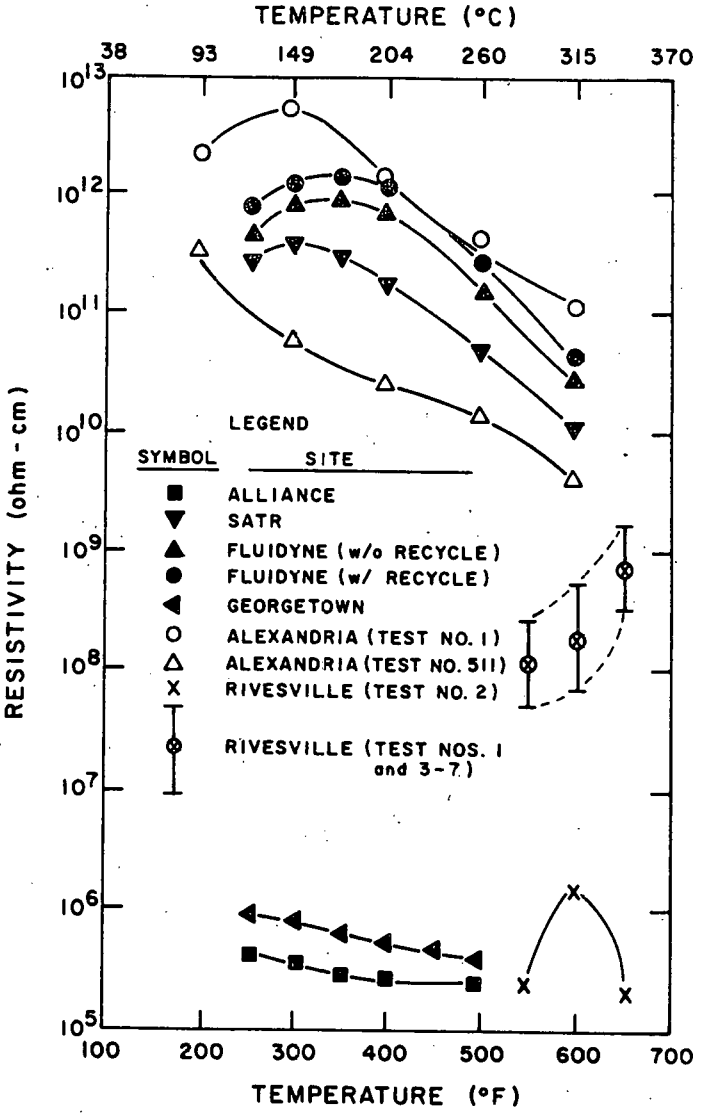

Figure 6. Summary of resistivity data.

to the low collection efficiency of the cyclones under low load conditions and, in one case, the lack of recycle. Also shown in Figure 6 is a band of other resistivity measurements (ranging from 10^8 to 10^9 ohm-cm) for Rivesville flyash. These samples were obtained when the carbon burnup cell was not operating and contained 20 to 25 percent carbon.

For conventionally generated flyash, carbon contents above 8 to 10 percent have been found to be a critical factor in decreasing resistivity.[12] The results shown in Figure 6 suggest that resistivity of FBC flyash is substantially reduced when the carbon content is above 20 percent by weight. High carbon carryover is suspected to be a more significant problem with fluidized-bed combustion compared to conventional combustion. This emphasizes the importance of the primary cyclone in providing reliable, high particulate collection capability so that unburned carbon is returned to the boiler for efficient combustion and the downstream collector is protected from the effects of carbon carryover.

Figure 7 shows the effect of flyash resistivity on cold ESP overall mass collection efficiency as a function of specific collection area. The slope of the reference line reflects the exponential design relationship between SCA and collection efficiency. The two points shown correspond to actual design cases for conventional combustion of a high sodium lignite coal (10^9 ohm-cm resistivity) and a low sulfur western U.S. bituminous coal (10^{13} ohm-cm resistivity). The SRI electrostatic precipitator model was used to predict the collection efficiencies at an SCA of approximately 250 ft^2/1000 acfm for samples B, C, and D using their measured resistivities at 300°F and particle size distributions. These results were extrapolated over a range of SCAs using the slope of the reference line and are shown by the cross-hatched band. It is noted that the predicted SCA requirements for samples B, C, and D with resistivities between 10^{11} and 10^{12} ohm-cm, fall within the range of design experience for cold ESPs applied to the collection of conventional flyash. Under the assumptions used to generate the band for cold ESPs, the hot ESP band would be expected to lie parallel to and above the existing cross-hatched area.

The SRI model was also used to investigate particle size effects on ESP performance. Figure 8 summarizes the particle size distributions obtained for five FBC flyash samples compared to pulverized coal combustion flyash. Since the FBC samples were obtained from a fabric filter preceded by cyclones, their finer size relative to conventional flyash is attributed to the capability of the cyclones to collect coarse particles. With the exception of samples A and C, the finer particle sizes for FBC flyash may also result, in part, from attrition when primary cyclone materials are reinjected into the boiler.

Figure 9 shows the effect of particle size distribution on the performance of ESPs. The lower broken line represents the predicted performance at 300°F for sample B whose mass median diameter and geometric standard deviation are 5.3 μm and 2.6 respectively. The upper broken line corresponds

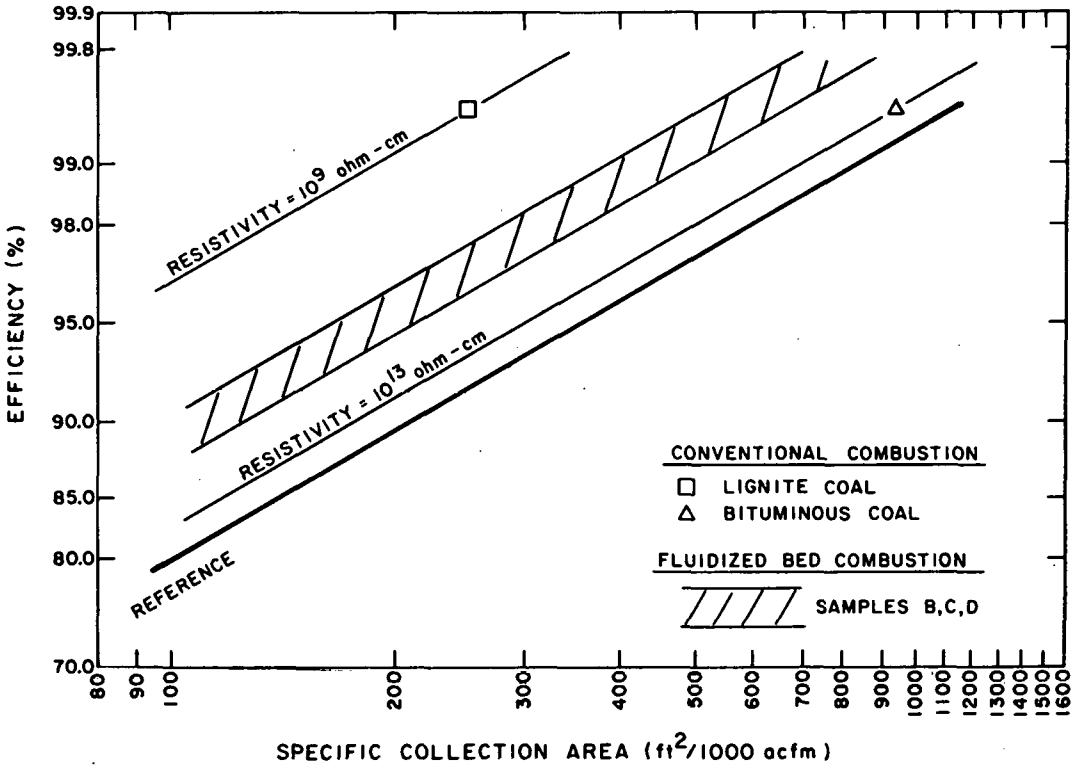

Figure 7. Effect of flyash resistivity on cold ESP overall mass collection efficiency as a function of specific collection area.

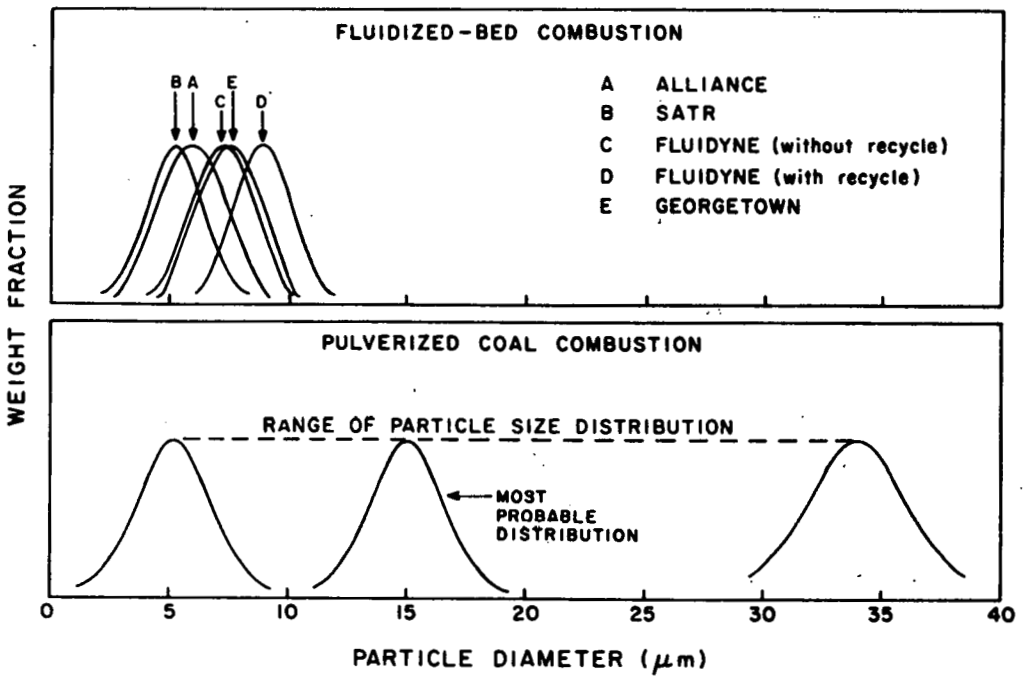

Figure 8. Summary of flyash particle size distributions.

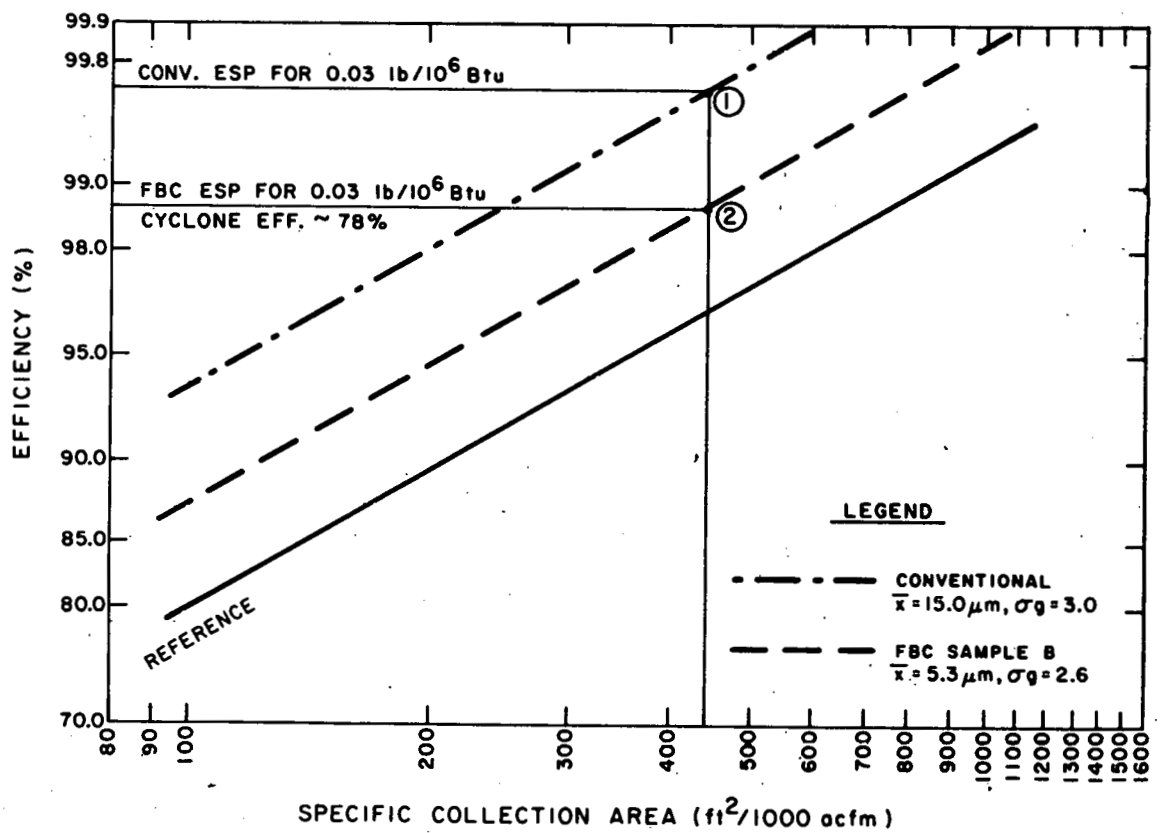

Figure 9. Effect of particle size distribution on cold ESP overall mass collection efficiency as a function of specific collection area.

to a conventional flyash with the same resistivity as sample B. The mass median diameter and geometric standard deviation were assumed to be 15.0 μm and 3.0 respectively. It is evident from these results that smaller particles require a larger precipitator for a given efficiency, provided that all other factors are held constant. In comparing an FBC system to a conventional combustion system generating the same amount of flyash from the boiler, the collection efficiency of the cyclones in the FBC system must be considered. For example, point "1" on Figure 9 represents the ESP efficiency and SCA requirements for a conventional system without cyclones to meet a particulate emissions standard of 0.03 $lb/10^6$ Btu. Point "2" illustrates the fact that if the cyclones in the FBC system have a combined efficiency of 78 percent or more, then a comparable or smaller SCA will be capable of achieving the same emissions standard. Thus, the fact that FBC flyash is generally smaller than conventional flyash (see also Figures 1 and 2) does not necessarily imply a higher SCA requirement. Depending on the collection efficiencies of the cyclones, as well as other important factors such as rapping reentrainment losses, however, a more conservative estimate of SCA may be required.

Field Operating Considerations

Some of the more common problem areas encountered with fabric filter operation include fabric/dust deposit interaction, bag failures, design or maintenance failures relating to bag support and the cleaning mechanism, and structural design problems including isolation dampers and the ash removal system. One of the most important areas for maintenance has to do with interactions between the fabric and the dust.[13] This includes the manner in which the dust deposits on the fabric, the ease with which it is removed, and any damage to the fabric caused by the dust. Choice of the wrong fabric can result in excessive penetration due to the development of pinhole leaks and inadequate bag service life. A dust which is hygroscopic may, in the presence of moisture, cause blinding, impede proper cleaning, cause excessive pressure buildup across the fabric, reduce bag service life, and promote ash removal problems.

With regard to fabric filters applied to FBC boilers, the presence of any appreciable amounts of calcium compounds in the flyash would suggest that increased attention be given to the use of hopper heaters and insulation to prevent moisture accumulation and subsequent bridging. This would also be an important consideration for electrostatic precipitators applied to FBC. In addition, the concern for possible bag plugging would suggest the use of continuous warm air flow during maintenance and shutdown periods to prevent moisture accumulation on the bags.

The carryover of unburned carbon during start-up or during a transient boiler condition may cause fabric blinding and permanent damage. For this reason it may be advisable to consider introducing flyash ahead of the fabric filter to coat the bags and thereby protect them from atypical FBC operating conditions. At one coal-fired conventional utility fabric filter installation, dolomite lime was used to precoat the bags.[14] It was suspected that when the baghouse was shut down and opened for inspection, the residual dolomite coating on the bag absorbed moisture, resulting in higher pressure drop across the bags compared to the case when a flyash precoat was used. Moreover, since atypical FBC operation may sometimes entail the carryover of unreacted limestone (as well as unburned carbon), a flyash precoat would be the optimum choice to protect the bags and keep pressure drop to a minimum.

Potential problem area considerations for precipitators applied to FBC units will include: electrode fouling due to buildup of flyash on the wires; incidence of local burning on the wires due to high carbon carryover (and manifested by heavy sparking); rapping reentrainment losses; and transient conditions associated with boiler startup.[2]

One of the most important factors that will affect both mass and fractional collection efficiency capabilities of an ESP is rapping reentrainment losses. Under a research program sponsored by the Electric Power Research Institute investigating rapping reentrainment emissions from six full-scale ESPs servicing conventional coal-fired boilers, it was found that a significant portion of the total mass emissions was caused by reentrainment of coarse particles. For the hot-side ESPs tested, 60 to 85 percent of the total mass emissions was attributed to rapping, whereas only 30 percent was noted for cold-side units.[15,16,17] The high rapping losses were thought to be attributed to reduced dust cohesivity at high temperatures and/or relatively short rapping intervals (as noted at one of the hot-side installations tested). Since rapping losses constitute a major fraction of the overall penetration, optimization of the ESP cleaning system, whether for FBC or conventional boilers, will be an important factor in reducing emissions.

Summary/Future Work

Fabric filters are being installed on virtually all new AFBC units despite the lack of comprehensive test or demonstration data. This appears to stem in part from their increasing use on industrial and utility conventional boilers to meet more stringent mass collection efficiency and opacity requirements. An analysis of fundamental filtration parameters using redispersed flyash in a filter test panel assembly has shown that filtration of certain FBC flyashes may be more difficult than conventional flyash. In three out of five FBC flyash samples tested, the filterability parameter (or specific coefficient of resistance) was noted to exceed twice that normally observed for conventional flyash. Particle size distribution does not appear to account for the noted differences in filterability. It is suspected that charge effects or particle shape factors may be responsible. Fabric cleanability is also an important consideration since pressure drop across the fabric increases significantly when only a small fraction of the dust is effectively removed from the bag surface.

Electrostatic precipitators have a limited operating history on AFBC units. Early difficulties at the Rivesville hot-side ESP were attributed to unstable boiler operation. A recent 200-hour run has indicated improved collector performance and further tests are planned to substantiate sizing criteria.

Comparison of measured resistivities of the five flyash samples investigated in this study with other reported data shows a strong correlation between percent combustibles and resistivity. Combustibles contents, consisting mainly of free carbon, in excess of 20 percent by weight can reduce resistivities; in some cases to levels below optimum (viz., below 2.0×10^{10} ohm-cm). Other measurements confirm the suspected effect of low SO_3 on the FBC flyash in that resistivities fall within the moderate to high range of design experience with ESPs applied to conventional coal-fired utility and industrial boilers. The observed finer particle size distribution of FBC flyash compared to conventional flyash does not necessarily imply a higher SCA requirement, although depending on the collection efficiency of the cyclone as well as other important factors such as rapping reentrainment losses, a more conservative SCA may be required.

It is clear that the performance of the final particulate collector depends on the FBC operating parameters, and in particular on cyclone efficiency, carbon burnup cell combustion efficiency, optimized freeboard height, bed depth, and fluidizing velocity. Carbon carryover, for example, can cause severe deterioration of electrical conditions in an ESP, with the possibility of ignition and fire. It can also cause blinding in fabric filter bags. Low load conditions can reduce cyclone efficiency and add to the carbon carryover problem. One important conclusion of this paper is that the precollector or cyclone must be considered as an integral part of the total particulate control system. Furthermore, the entire collector system must be flexible enough in both design and operation to handle most of the potential transient conditions in AFBC operation.

With regard to future plans, under EPA sponsorship GCA will be conducting a comprehensive evaluation of the Georgetown University fabric filter during the summer of 1980. The primary objectives will be to determine total mass and fractional particle size collection efficiencies at full and partial loads. To accomplish these goals, a 4-week field program emphasizing simultaneous particulate measurements before and after the fabric filter will be conducted. Total particulate mass concentration for particle sizes in the range of 0.5 to 15 μm will be determined using EPA Method 5 and cascade impactors. This will be supplemented with particle number concentration measurements in the size range of 0.03 to 10 μm using diffusion batteries, condensation nuclei counters, and electro-optical particle counters. EPA may sponsor similar tests at other large-scale facilities using fabric filters or electrostatic precipitators as these units come on-line.

Acknowledgments

The authors express their appreciation to Mr. D. Bruce Henschel, EPA Project Officer, for his technical support and guidance throughout the program.

This project has been sponsored by the U.S. Environmental Protection Agency under Contract No. 68-02-2693. The contents of this publication do not necessarily reflect the views and policies of the U.S. Environmental Protection Agency, nor does mention of trade names, commercial products, or organizations imply endorsement by the United States Government.

Our thanks are also extended to the Health Effects Research Laboratory of EPA at Research Triangle Park, North Carolina for providing the photomicrographs used in Figures 1 and 2.

Finally, the authors wish to acknowledge the work of Mssrs. Hans A. Klemm and John A. Dirgo of GCA/Technology Division who helped in providing fabric filter computer analysis and filtration measurements respectively.

References

1. Buell Emission Control Division, Envirotech Corporation, "Precipitation performance evaluation at Monongahela Power Company, Rivesville Unit #3, Rivesville, West Virginia" prepared for Pope, Evans and Robbins (September 1979).

2. N. Z. Shilling and W. J. Morris, "The response of hot-side electrostatic precipitators and fabric filters to fluidized-bed combustors," presented at The 6th International Conference on Fluidized-Bed Combustion, Atlanta, Georgia (April 9-11, 1980).

3. American Society for Testing and Materials, "Standard method of preparing coal samples for analysis," ANSI/ASTM D 2013-72.

4. R. Dennis et al., "Filtration model for coal flyash with glass fabrics," prepared by GCA/Technology Division for the U.S. Environmental Protection Agency, EPA-600/7-77-084 (August 1977).

5. W. J. Culbertson, "Development of standard laboratory resistivity apparatus," prepared by Denver Research Institute for the Electric Power Research Institute, EPRI FP-805 (August 1978).

6. R. Dennis and H. A. Klemm, "Fabric filter model format change: Volume I. Detailed technical report," prepared by GCA/Technology Division for the U.S. Environmental Protection Agency, EPA-600/7-79-043a (February 1979).

7. R. Dennis and H. A. Klemm, "Fabric filter model format change: Volume II. User's guide," prepared by GCA/Technology Division for the U.S. Environmental Protection Agency, EPA-600/7-79-043b (February 1979).

8. R. Dennis, H. A. Klemm, and W. Battye, "Fabric filter model sensitivity analysis," prepared by GCA/Technology Division for the U.S. Environmental Protection Agency, EPA-600/7-79-043c (April 1979).

9. J. R. McDonald, "A mathematical model of electrostatic precipitation (revision 1): Volume I. Modeling and programming," prepared by Southern Research Institute for the U.S. Environmental Protection Agency, EPA-600/7-78-111a (June 1978).

10. J. R. McDonald, " A mathematical model of electrostatic precipitation (revision 1): Volume II. User manual," prepared by Southern Research Institute for the U.S. Environmental Protection Agency, EPA-600/7-78-111b (June 1978).

11. Pope, Evans and Robbins, Inc., "Multicell fluidized-bed boiler design, construction and test program," Research and Development Report No. 90, Interim Report No. 1 for Period October 1972-June 1974, prepared for the U.S. Department of the Interior, PB 236 254 (August 1974).

12. C. C. Shale, J. H. Holden, and G. E. Fasching, "Electrical resistivity of flyash at temperatures to 1500°F," U.S. Bureau of Mines Report, No. RI 7041.

13. C. E. Billings and J. Wilder, "Handbook of fabric filter technology, Volume I," prepared by GCA/Technology Division for the National Air Pollution Control Administration, Contract No. CPA-22-69-38 (December 1970).

14. E. W. Stenby, L. W. A. Bye, and R. J. Beaton, "The Kramer baghouse," presented at the American Power Conference, Chicago, Illinois (April 23-25, 1979).

15. Electric Power Research Institute (EPRI), test data reported in the "Precip Newsletter," published by the McIlvaine Co., Northbrook, Illinois, Number 18 (July 20, 1977).

16. Electric Power Research Institute (EPRI), test data reported in the "Precip Newsletter," published by the McIlvaine Co., Northbrook, Illinois, Number 21 (October 20, 1977).

17. J. P. Gooch and G. H. Marchant, "Electrostatic precipitator rapping reentrainment and computer model studies," prepared by Southern Research Institute for the Electric Power Research Institute, EPRI FP-792, Volume 3 (August 1978).

THE RESPONSE OF HOT-SIDE ELECTROSTATIC PRECIPITATORS AND FABRIC FILTERS TO FLUIDIZED BED COMBUSTORS

Dr. N. Z. Shilling
W. J. Morris

Buell Emission Control Division
Envirotech Corporation

INTRODUCTION

Atmospheric fluidized bed combustion (AFBC) represents a promising technology for combining combustion and sulfur reduction in a single process. Fluid bed combustion also provides significant reduction of nitrogen oxides relative to conventionally-fired boilers because of reduced combustion temperatures. However, there are operating factors peculiar to fluidized bed combustion which must be incorporated into the design and operation of air pollution control equipment. Buell designed and supplied the hot-side electrostatic precipitator at the 30 MW AFBC at Rivesville, W. Va. and the baghouse which is cleaning the flue gas at the 500 KW AFBC at Alexandria, Va. This paper presents operating data and experience obtained at these installations. The specific intent is to characterize particulate control as it applies to atmospheric fluidized bed combustors and associated particulate control equipment. Due to differences in boiler size, design, operational characteristics and the location of the precipitator and baghouse in the process, direct comparison of performance is limited. Therefore, the paper is divided into two parts - in Part I, the Rivesville precipitator is discussed and Part II treats the Alexandria fabric collector.

PART I - RIVESVILLE, W. VA. AFBC

DESCRIPTION

The flue gas process flow diagram is shown in Figure 1. The precipitator controls flyash emissions from a Foster-Wheeler atmospheric fluidized bed boiler. The boiler has three main cells and a carbon burnup cell. Flyash, along with entrained bed material, exits the boiler and passes through one of two multi-cyclone mechanical collectors. One serves the three main boiler cells while the other is dedicated to the carbon burnoff cell (CBC). The design efficiencies of these collectors is 95%. Output from the mechanicals join with the output from various other dust collection points prior to entry into the precipitator.

The Buell electrostatic precipitator (ESP) has a single chamber with 35 gas passages and plate height of 36 feet. Design efficiency is 99% at a design gas flow of 203,000 ACFM, 730°F, and 3.57 ft./sec. treatment velocity. The ESP has electromagnetic rappers on both the emitting and collecting system and additional side rappers on the collecting system. In lieu of prior experience on fluidized bed combustors, the precipitator was designed by both an analogy technique and basic design theory. Cement and lime kiln data was also used to establish size criteria (Reference 1).

Mass loadings, particulate size and chemistry from the Rivesville AFBC can change drastically during the various modes of boiler startup indicated in Figure 2. For example, fluidization of all four cell beds begins prior to fuel addition and combustion. During fluidization, elutriated bed material consisting of CaO and residual $CaSO_4$, silica and iron oxides will be carried out of the cell (Reference 2). Particulate loading is primarily determined by the superficial velocity in the combustion bed.

As oil combustion starts in the carbon burnoff cell (identified as Cell D in Figure 2), there will be additional fine carbon particulate, reacted bed material and combustion flue gas. Changeover to coal is accomplished while still on one cell. Finally, the primary boiler cells (Cells C, B and A in Figure 2) are successively fired up after the carbon burnoff cell attains operating temperature. The precipitator is not energized until the flue gas temperature attains 250°F which occurs after full coal firing. This precautionary measure is followed to minimize contact of high resistivity bed material with condensed flue gas moisture that has wetted ESP collecting plates and emitting wires. For example, a coherent coating of calcium sulfate with a resistivity approaching 10^{15} ohm-cm need only be a few mils thick to degrade precipitator performance. Although the precipitator is not energized prior to the flue gas attaining 250°F, some capture may still occur. When the combustor attains normal operation, the composition and outlet loading from the bed will depend again in part upon the superficial velocity and the decrepitation rate of limestone or dolomite. The high resistivity of the bed material will be moderated by the flyash and carbon.

During April-May, 1979, performance evaluation tests were conducted to define effluent characteristics and precipitator operating conditions during one and three-boiler cell operation. Two of the three primary combustion

cells in addition to the carbon burnoff cell were operational during this portion of the test. There was no flyash reinjection to the boiler. The measured parameters were:

- o Particle size (ESP inlet and outlet)
- o Particle loading (ESP inlet and outlet)
- o Gas volumes and temperatures
- o Particle resistivity (sample catch, wire and plate analysis)
- o Particle chemistry
- o Coal and coal ash
- o Precipitator electrical performance
- o Internal inspection of ESP

Test data was obtained at the inlet of the ESP and at the outlet of the air heater. Sampling directly at the precipitator outlet was precluded due to lack of a satisfactory sampling point in the shoehorn fit of the precipitator and outlet ducting into an existing facility. A summary of test results is given in Figure 3. Inlet loadings and volume for three-cell operation were higher and temperatures lower than design.

RESULTS

Inlet Conditions

Particle size is important relative to the performance of the final particulate cleanup device. For precipitators, particles in the 0.5 um range are difficult to collect due to a minimum occurring in the sum of diffusion and impact particle charging. Additionally, a high fraction of sub-micron particles also has the potential to cause corona quenching. For baghouse operation, small particle size could result in excessive filter pressure drop and penetration. Figure 4 shows the cumulative particulate mass distribution measured at the inlet of the ESP (Micromeretics Sedigraph Analysis). The average mass median particle diameter was 7.8 microns with 11.8% of the particle mass below 2 microns. Standard deviations were 0.86 um and 1.6%, respectively, based upon six (6) tests. For single cell operation, the mass median diameter increased to 19.5 um with 7% by weight less than 2 microns. These sizes are roughly equivalent to that obtained from normal PC boiler operation, but it should be noted that the boiler's cyclone precollectors were operating at approximately 75% efficiency - far below design efficiency (see below). Had these cyclones been able to produce the design inlet loading, it is estimated that the mass median diameter at three-cell operation would have been reduced to 4.7 microns with approximately 35% by weight less than 3 microns. Particle size is not perceived to be a problem for precipitator operation. First, based upon a correlation provided by the Sumitomo Mining Company, the reduction in ESP secondary current would be approximately 13% and of secondary effect. Additionally, the proportion of fines (particles less than 1 micron in diameter) would increase from approximately 6% to 10%. Proportionally, nearly all of the decrease in inlet loading would also be reflected in the net outlet loading.

Resistivity

There are several opposing factors which will determine the resistivity of the combined products of coal combustion. Factors favoring high resistivity are:

- o Low SO_3 and SO_2 levels - here typically 5ppm
- o High resistivity of bed additives ($CaCO_3$ and siliceous compounds)
- o High resistivity of bed products ($CaSO_4$)

Factors favoring moderate resistivity are:

- o Flyash - typical West Virginia coal flyash, lime (CaO)

Factors favoring low resistivity are:

- o Carbon and devolatilized products of combustion
- o High Fe_2O_3 and Fe_3O_4 content in ash.

The applicability of precipitators to the AFBC will depend upon how these various factors balance in the collected flyash. Laboratory measurements were made to determine the resistivity of various forms of calcium as they may exist in the flyash. The bulk resistivity of CaO (lime), $CaSO_4$ and various combinations of both at two moisture levels are shown in Figure 5. Gypsum can attain nearly 10^{15} ohm-cm and, as discussed earlier, has a high potential for causing difficulties.

The flyash resistivity (average of six tests at three-cell operation) from Rivesville are shown in Figure 6. The resistivity of a hopper sample of flyash is shown for comparison. The resistivity over the temperature range encountered during the Rivesville test is acceptable for hot-side precipitator operation. Due to the non-typical temperature characteristic, performance problems are not expected for operation below approximately 700°F. The decomposition of calcium hydroxide back to lime is likely a contributing factor. It should also be noted that back corona was present for at least one of the seven tests despite these and similar seemingly acceptable resistivities measured on plate and wire flyash samples. This is further addressed below under DISCUSSION.

Chemistry

The chief feature brought out by chemical analysis was the high carbon content with the flyash. Loss on ignition (LOI) averaged 23% during the full load tests. The design carryover limit was 15%. The four major constituents in order of quantity present are SiO_2, Carbon (LOI), Al_2O_3 and Fe_2O_3. Granular bed materials have been reported (Reference 2) as developing outer vitreous crusts of inert material which contain high percentages of alumina, silicon and iron (Fe_2O_3) which form gradually. This is reflected in the present flyash. Fresher material has been seen to have a veneer (2-25 um thickness) of Fe_2O_3 and $CaSO_4$.

Assuming that all of the SO_3 in this balance is present as $CaSO_4$, the $CaSO_4$ and CaO weight fractions would be 5.3% and 4.6%, respectively. Flyash and coal analyses are given in Figure 7 from all performance tests.

Precipitator Internal Inspections

Normally, grey-colored ash is seen in the precipitator due to its high LOI. However, in internal inspections, random sections of light-colored sections of ash were seen on the emitting wires. This was intriguing; particularly since these spots coincided with sections of degraded mechanical properties on the emitting wires. While the wire flyash samples normally turned up high in LOI, these light regions show nearly a complete absence of LOI. Buell performed a kinetics analysis using as-measured ash and flue gas compositions. The result was that temperatures in excess of 1240^{0} can occur due to pyrolisis and combustion of the flyash on the wires. In order to resolve this problem, Buell recommended and supplied stainless steel replacements for the original mild steel emitting wires. Another advantage which accrued from this change is discussed below.

Precipitator Performance - Efficiency

Reference to Figure 3 shows that the average precipitator efficiency for three-cell operation was 92% (6 test average). Correcting to the design volume of 203,000 ACFM, this increases to 93.7%. A fractional efficiency curve derived from inlet Sedigraph analysis and outlet Anderson impactor data is shown in Figure 8. Additionally, utilizing as-measured volumes, particle sizes and resistivities, the Buell precipitator simulation model predicts approximately 99% efficiency at test conditions. Also, the design efficiency was 99% working without any prior experience in this application. There is an approximate 5% discrepancy that must be accounted for in regard to potential future design work.

DISCUSSION

The factors contributing to the depressed efficiency are:

Electrode Fouling

During the test program, secondary currents were depressed to very low levels - typically 30-50 mA on transformer-rectifier sets with saturation limits of 1200mA. It had been recognized that potential for electrode fouling was high based upon comparison with other hot side ESPs operating on Western coal. Since the installation of stainless steel emitting wires, substantial power increases (3x-10x) for the precipitator have been reported. Stainless is recommended as a standard for this application.

Condensible Hydrocarbons

Nuclear magnetic resonance (NMR) analysis of catches of precipitator outlet flyash have indicated the presence of the following organics and boiling points:

Napthalene, B.P. = $424^{o}F$
Anthracene, B.P. = $669^{o}F$
Phenanthrene, B.P. = $644^{o}F$

These compounds were not present in any of the inlet samples and evidence points to these compounds contributing to the discrepancy between measured and design efficiency. These compounds condense out in passage through the air heater and are likely the result of poor combustion (volatilization and outgassing without combustion).

In-situ Combustion

As discussed below, evidence was found which indicates that local burning occurred on the emitting wires. The resultant high temperatures may be causing low sparking levels.

Re-entrainment

Although the treatment velocity (3.57 fps) was lower than normal velocities at which re-entrainment is believed to be a problem, it was not possible to perform normal rapper optimization procedures prior to test. This was prevented by the inability to maintain stable boiler operation for a sufficient period of time and will be resolved.

Boiler Startup

Close clearances and periodic shorting of fields have occurred due to rapid thermal transients during boiler startup. For example, precipitator inlet temperatures have risen at a rate of over $1000^{o}F$/hr. during boiler cell transfer. Operating clearances in the precipitator have been increased and boiler startup procedures have been modified to reduce flue gas heating rates to approximately $50^{o}F$/hour when the flue gas is over $400^{o}F$. These steps have eliminated loss of precipitator fields during startup.

These are the factors that have been or will have to be resolved in order to attain full design potential of the precipitator.

PART II - ALEXANDRIA, VA

DESCRIPTION

The fluid bed boiler at Alexandria is a Pope, Evans and Robbins design built by Cleaver-Brooks to produce 4200-5200 lb./hr. steam from a single 3' by 3' section fluid bed cell. The fluid bed unit has both saturated and superheated steam capabilities. This process development unit (PDU) combines both carbon burnoff and coal combustion in one cell. The process and flue gas

flowpath are shown in Figure 9 along with design values of the various feed rates. Typical values of solid materials and flue gas composition are given in Figure 10. It is noted that the baghouse dust shows a considerably lower ash content (18%) than the larger scale Rivesville unit. Note that the mechanical collectors selectively reduce the carbon carryover fraction to the baghouse.

This fluidized bed combustor is equipped with a Buell Norblo fabric collector. Design details are provided in Figure 11. It is located downstream of an air cooler to simulate conditions typical of cold-side operation. The collector is a unique design which provides for testing of the three commonly used methods of bag clean - (1) reverse air, (2) shake, (3) combined reverse air/shake and (4) pulsejet cleaning. It will provide an excellent opportunity for evaluation of these methods as they relate to control of AFBC emissions. To date, only the shake mode has been rigorously tested and these are the results reported here.

Tests were run to collect data sufficient to evaluate mass collection efficiency, penetration, bag cleaning capability and outlet dust loading. Grove and Lowelville limestone were used as the sorbents. Flyash reinjection varied from zero to approximately 1300 lb/hour. Baghouse inlet loading ranged from approximately 60 lb./hour (normal) to a maximum of 200 lb./hour, which occurred during primary cyclone hopper overflow to the baghouse. The cleaning cycle consisted of 60-65 seconds of shake with a 60 second dwell period to permit the dislodged dust to settle into the weigh hopper. The interval between cleaning cycles was manually set from 30 to 60 minutes, depending upon boiler conditions. Temperatures averaged 275-285^{o} at the baghouse inlet during these tests.

RESULTS

Collection Efficiency

The measured outlet particulate emissions were consistently below the new source performance standards of 0.03 lb. particulate/10^6 BTU Mass collection efficiencies consistently exceeded 99.5% for all boiler conditions and loadings. As a specific example, for Test Number 704-24, a test run at A.C. = 2.0 fps, outlet emissions (lb./10^6 BTU) are shown in Figure 12 as a function of bag pressure drop where dust penetration is seen to decrease slightly as bag pressure drop and cake thickness increase. Specific emission data (lb./10^6 BTU) was found to be fairly independent of air-to-cloth ratio - for example, an air-to-cloth ratio of 2.0, an average rate of 0.0134 lb./10^6 BTU obtained; whereas, at A/C = 3.0, the mean emissions were 0.0122 lb./10^6 BTU. These emissions probably would have been lower had tests been excluded where grain loading increased from a normal 3-6 gr/SCF loading to 10-12 gr/SCR due to overfilling of the primary cyclone hoppers. Since the new bags were installed immediately prior to the tests at A/C - 2.0, the difference is ascribed to aging and cake improvement for the A/C = 3.0 tests. No test exceeded 0.03 lb./10^6 BTU. Fractional penetration was less than 0.003 and measured opacities were consistently below 1%.

Pressure Drop

A typical pressure time trace obtained after the baghouse is returned to line following a cleaning cycle is shown in Figure 13. Three distinct regimes are identified (labeled A, B and C). During Period A, flow is re-established to full volume following opening of the compartment isolation valve. During Portion B, re-establishment of a homogenous filter cake occurs. In Region C, the cake has been reformed and the increase in pressure drop per pound of particulate is constant. Two parameters are reported here -- the first is the clean bag pressure drop. The value that is reported is the hypothetical extrapolation of the curve to zero time and is a measure of the cleaning effectiveness and bag condition (Ref. Figure 13). Typically, at an A/C = 2.0, the clean bag pressure drop was 2.4" W.G. and 5 in. W.G. for an A/C = 3.0.

The second parameter is related to the amount by which a given mass of particulate increases the resistance to flow and is appropriately defined only over Region C. Operationally, we define a filter cake resistance coefficient K by the expression:

$$\Delta P = K(A/C)\alpha(A/C)\Delta T$$

where $\Delta P/\Delta T$ = Slope of pressure-time chart (in.W.G./min.)

α = Inlet grain loading (gr./ACF)

A/C = Air-to-cloth ratio (ACFM/ft^2)

K (equivalent to the K_2 coefficient defined in Reference 3) is a function of several parameters, including the packing and aglomerating tendencies of the particulate, size, distribution, particle shape, hydroscopy and flue gas moisture and electrostatic properties. Higher air-to-cloth ratios tend to increase the bed resistance. For the Alexandria particulate, this constant was $K = 2.811 \times 10^{-3}$ at the A/C = 2.0, with a standard deviation of 0.71×10^{-3}.

DISCUSSION

Particulate loading produced by the Alexandria AFBC was not constant throughout test and varied from approximately 2.25 gr/ACF to 4.22 gr/ACF (excluding 7 gr/ACF which was obtained during operation with filled cyclone hoppers). The primary variables influencing carryover to the baghouse were fuel type (i.e., ash content and of fines) and fuel feed rate. The rate of reinjection from the primary cyclone was seen to have a minor influence on carryover. The bed superficial velocity in the combustor did not vary significantly from approximately 12.5 fps

throughout the testing, so the effect of this parameter could not be quantified.

The factors which were made evident by the testing and could negatively impact the operation of fabric particulate control devices were identified: Calcium oxide is one of the carryover constituents and readily forms its hydroxide through an exothermic reaction. This problem is compounded in two ways - first, the high loss-on-ignition characteristic of fluidized bed boiler flyash creates a potential for spontaneous combustion. At Alexandria, smouldering piles of flyash were found in the collector on two occasions (at Rivesville, clinkers were found in the hopper which may also be indicative of the same phenomenon). With regard to reaction on the bag surface, short time of contact on the bag, as well as heat transfer to the flue gas, was found sufficient to prevent physical damage during normal operation; however, in the case of shutdown, the potential for damage, both to bag and bag finish, must be considered. Thorough clean-down is recommended prior to extended shutdown periods.

The levels of hydrocarbons measured in the flue gas ranged from 30 to 800 ppm. At Rivesville, condensible hydrocarbons were believed to be responsible for chronic air-heater fouling and a contributor to lower computed precipitator efficiency. Although evidence of bag blinding or long-term cleaning problems were not seen, this could represent a potential problem for baghouse application at the Rivesville boiler. It will probably be resolved when combustion problems are eliminated at that installation.

SUMMARY

At the Rivesville AFBC, both boiler and precipitator are completing their shake-down periods. To date, the performance of the precipitator has been intimately tied to the performance of the boiler. Boiler stability problems are being resolved and will allow completion of a rapper optimization program. Boiler efficiency is being improved through changes in the coal distribution system within the bed, and when combined with improvement of the precollection cyclone efficiencies and utilization of flyash reinjection, it is expected that the high LOI and condensible hydrocarbon fraction will be reduced. The importance of proper choice of materials for this application was made clear in the case of the emitting wires. The change to Type 430 stainless emitting wires together with improved boiler performance has resulted in substantial increase in precipitator power levels, and a corresponding increase in precipitator performance. Recent field reports indicate improved performance. Further tests will substantiate sizing criteria for this application.

The test baghouse serving the Alexandria AFBC has consistently exceeded new source performance standards over a wide range of boiler operating conditions. Performance of this unit has been encouraging; however, bag material performance and life under long-term exposure to basic flyash and for reverse air operation (more likely to be specified for utility boiler operation) remains to be demonstrated.

Buell wishes to express its appreciation to the personnel at Pope, Evans and Robbins who have provided assistance and data for both the Rivesville and Alexandria installations.

REFERENCES

1. Brummer, J. H., "Fluidized-Bed Boiler Promises Coal Burning with less Pollution", Electric Utility Generation Plan Book, McGraw-Hill, Inc. 1977.

2. James L. Crowe and Steale, S. K., "Characterization of Solid Residues from Fluidized Bed Combustion Units", Report No. EPA-600/7-78-135, TVA, dated July 1978.

3. Richard Dennis and Klemm, H. A., "Fabric Filter Filler Model Format Change; Volume 1, Detailed Technical Report," Report No. EPA-600/7-79-043a, dated February, 1979.

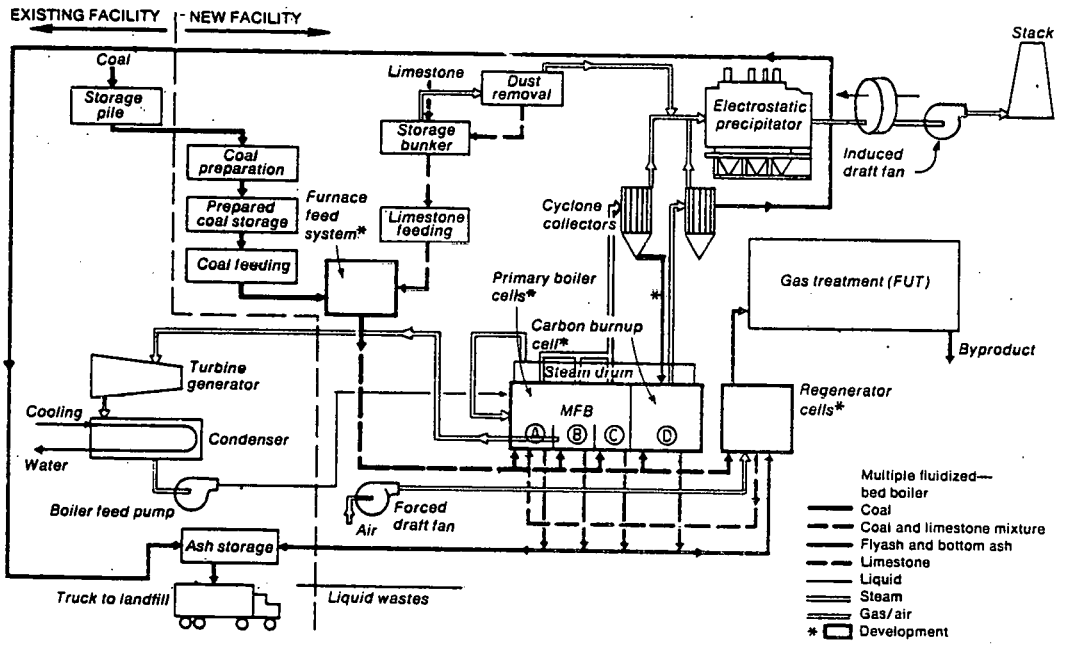

FIGURE 1 - SCHEMATIC - PROCESS FLOW DIAGRAM
RIVESVILLE, W. VA. AFBC

Startup Mode	Cells Fired	Cells Fluidized	Fuel	Precip.
1	none	D, B, C, A	None	off
2	D	B, C, A	Oil	off
3	D	B, C, A	Coal	off (temp<250°F) on (temp>250°F)
4	D, C	B, A	Coal	on
5	D, C, B	A	Coal	on

FIGURE 2 - STARTUP PROCEDURE - RIVESVILLE, W. VA. AFBC

	DESIGN	TEST #1	TEST #2	TEST #3	TEST #4	TEST #5	TEST #6	TEST #7
Date		4-24	4-26	5-1	5-1	5-3	5-3	5-3
No. Cells (Boiler)	4	3	1	3	3	3	3	3
INLET								
Gas Volume, ACFM	203,000	205,250	-	213,940	224,540	234,510	230,820	228,950
Gas Temp., °F	700-730	600	562	586	588	605	607	606
Dust Conc. gr/ACF	.875		.9098	1.3588	1.3425	1.4746	1.4572	1.4583
Dust Conc. gr/SCF		3.5401	1.8520	2.7888	2.7645	3.1127	3.0796	3.0790
Emission Rate (lb/MBTU)		8.25	5.73	6.92	7.99	9.54	9.35	9.35
% H_2O		6.8	3.4	4.0	5.2	7.2	6.2	6.3
% O_2		-	-	10.0	10.0	-	-	-
% CO_2		-	-	8.0	8.0	-	-	-
OUTLET								
Gas Volume, ACFM		146,400	85,600	154,500	157,000	164,200	164,200	166,600
Gas Temp., °F		306	237	309	287	299	312	329
Dust Conc. gr/ACF	.0088	0.3037	0.0491	0.1780	0.1215	0.1434	0.1211	0.1401
Dust Conc. gr/SCF		0.4495	0.0673	0.2638	0.1749	0.2119	0.1821	0.2153
Emission Rate (lb/MBTU)		1.0058	0.2046	0.6548	0.5058	0.6299	0.5443	0.6465
% H_2O		2.9	1.6	4.0	5.2	4.2	4.7	5.2
% O_2		7.4	11.1	8.6	10.2	10.6	10.6	10.6
% CO_2		10.8	8.1	6.8	8.1	8.8	8.8	8.8
Efficiency	99.0	87.81	96.43	90.54	93.67	93.40	94.18	93.09

FIGURE 3 - TEST RESULTS SUMMARY - RIVESVILLE AFBC

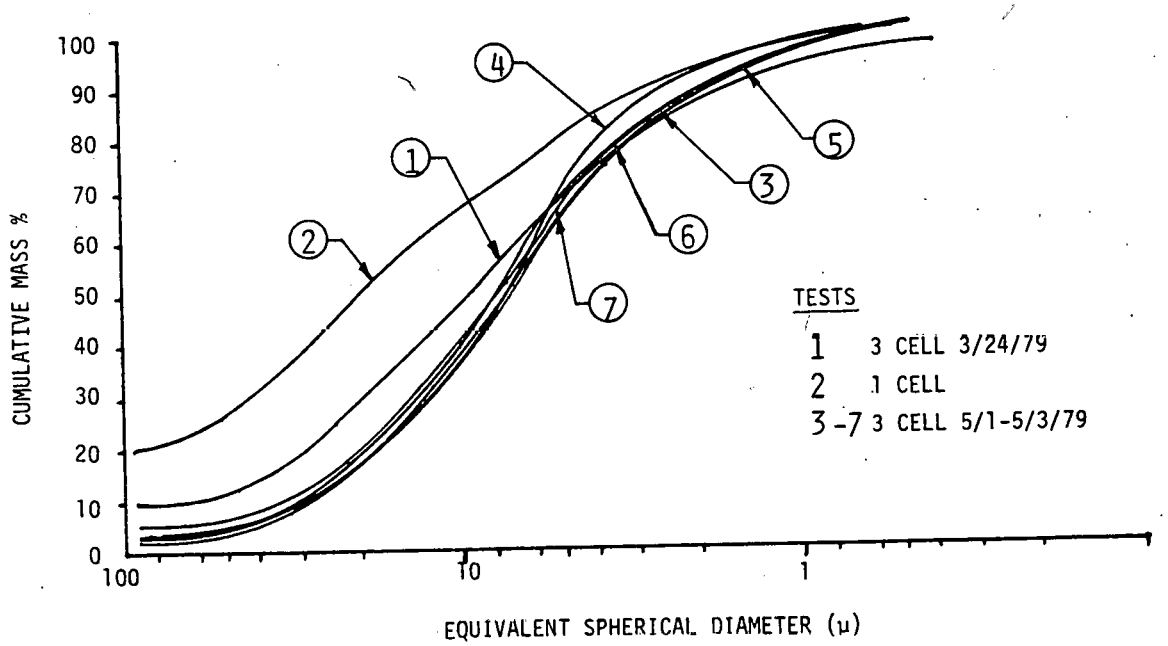

FIGURE 4 - ESP INLET CUMULATIVE PARTICLE SIZE DISTRIBUTIONS

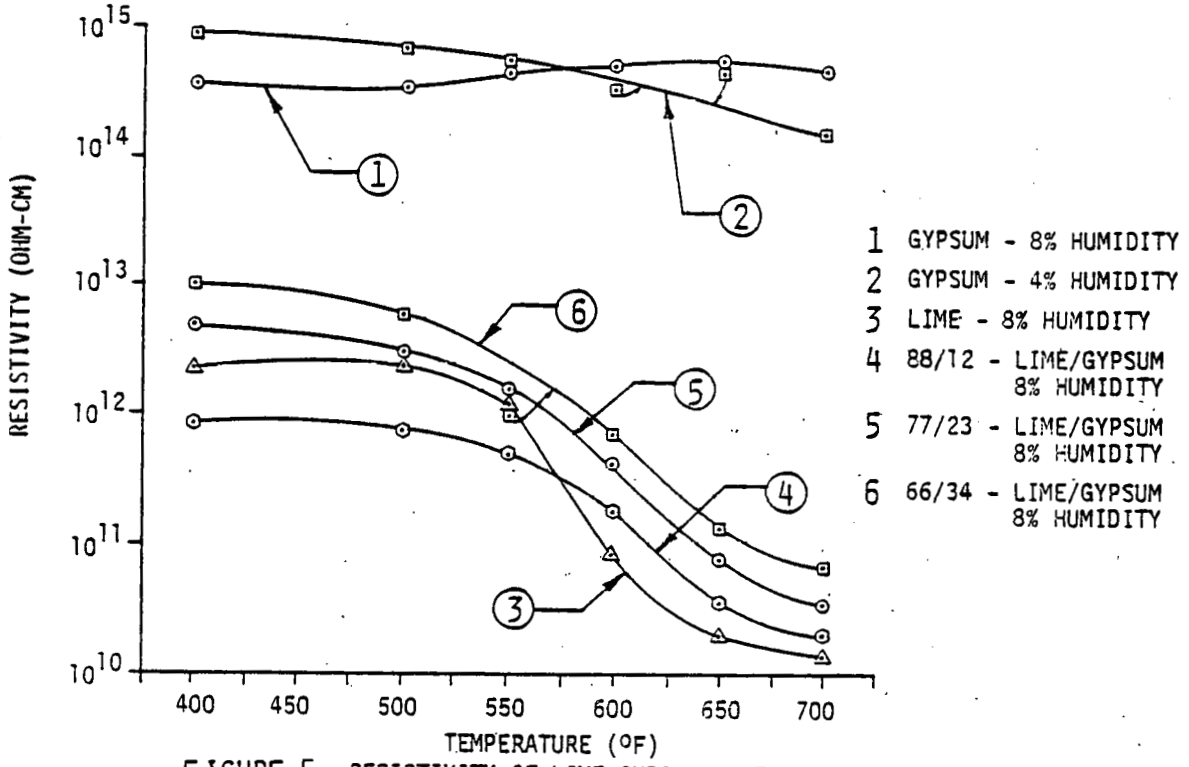

FIGURE 5 - RESISTIVITY OF LIME-GYPSUM MIXTURES

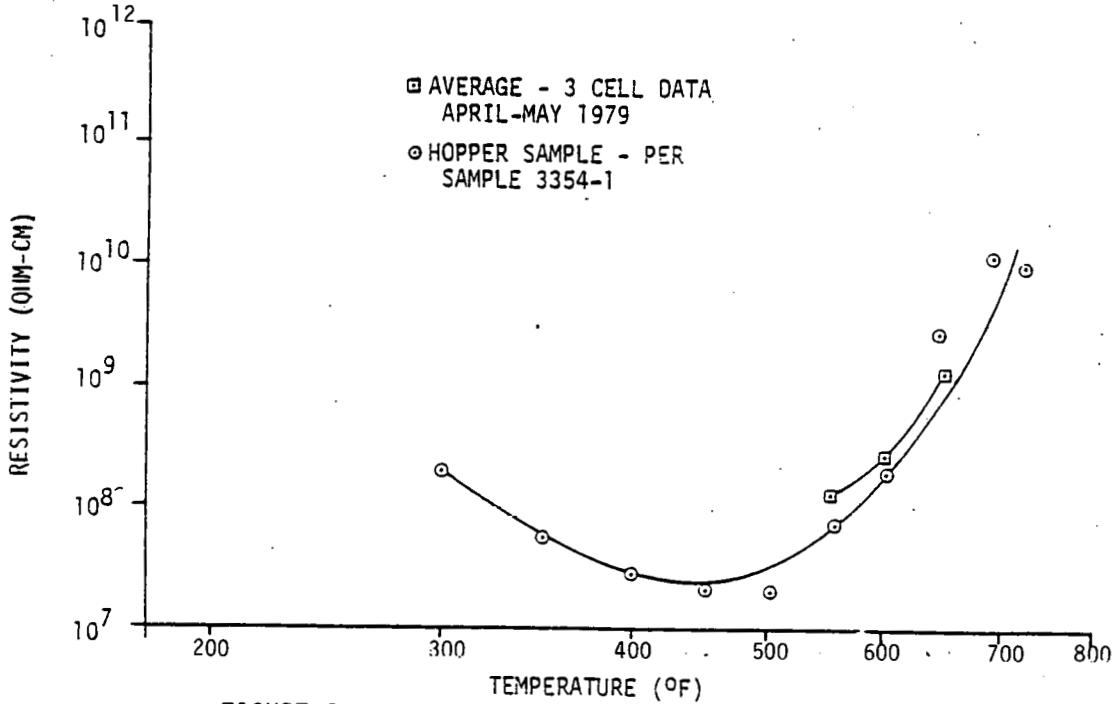

FIGURE 6 - FLYASH RESISTIVITY ISOKINETIC SAMPLE AND HOPPER CATCH - RIVESVILLE, W. VA.

COAL ANALYSIS

TEST	C	H	O	N	S	ASH	MOISTURE	H.H.V.(BTU)
1	71.32	4.96	0.00	1.36	2.94	14.40	1.86	12580
2	71.65	4.99	0.00	1.35	2.50	17.30	0.70	12448
3	71.65	4.99	0.00	1.35	2.50	17.30	0.70	12448
4	71.65	4.99	0.00	1.35	3.13	16.09	0.70	12568
5	71.65	4.99	0.00	1.35	3.13	16.09	0.70	12568
6	71.65	4.99	0.00	1.35	3.13	16.09	0.70	12568
AVG.	71.59	4.98	0.00	1.35	2.89	16.21	0.89	12530

FLYASH ANALYSIS - INLET OF ESP

TEST	LOI	SIO_2	FE_2O_3	AL_2O_3	CAO	MGO	SO_3	TIO_2	K_2O	P_2O_5	NA_2O	LI_2O
1	25.36	34.78	8.44	13.72	13.91	0.71	0.00	0.71	1.27	0.11	0.26	0.02
2	23.17	37.38	9.73	17.57	5.93	0.72	2.24	0.85	1.48	0.16	0.38	0.03
3	20.56	38.01	10.20	17.87	6.25	0.70	2.83	1.03	1.50	0.17	0.63	0.03
4	27.26	33.11	9.91	16.69	5.52	0.64	3.70	0.85	1.43	0.14	0.49	0.03
5	26.52	34.37	10.59	16.98	4.30	0.66	3.34	0.79	1.49	0.15	0.27	0.03
6	27.23	34.97	9.88	15.80	4.71	0.65	3.53	0.79	1.44	0.15	0.29	0.03
AVG	25.02	35.43	9.79	16.44	6.77	0.68	3.13	0.84	1.43	0.15	0.39	0.03

FIGURE 7 - COAL AND FLYASH CHEMICAL ANALYSIS - RIVESVILLE AFBC TESTS OF APRIL-MAY 1979

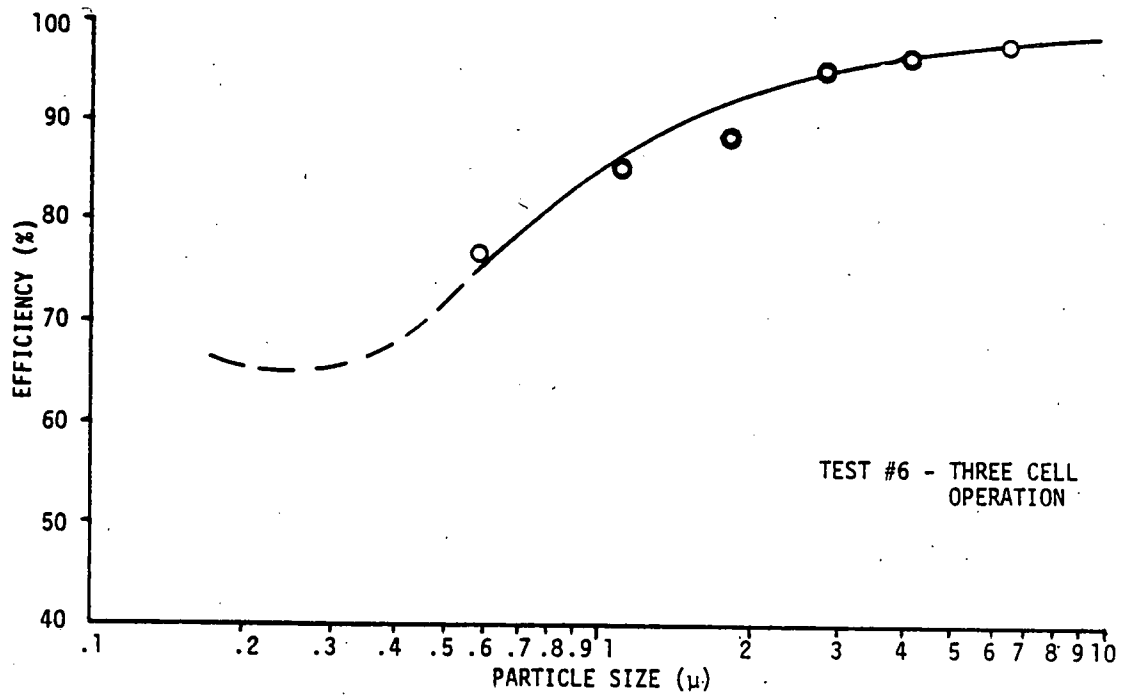

FIGURE 8 PRECIPITATOR FRACTIONAL EFFICIENCY HSEP - RIVESVILLE, W. VA.

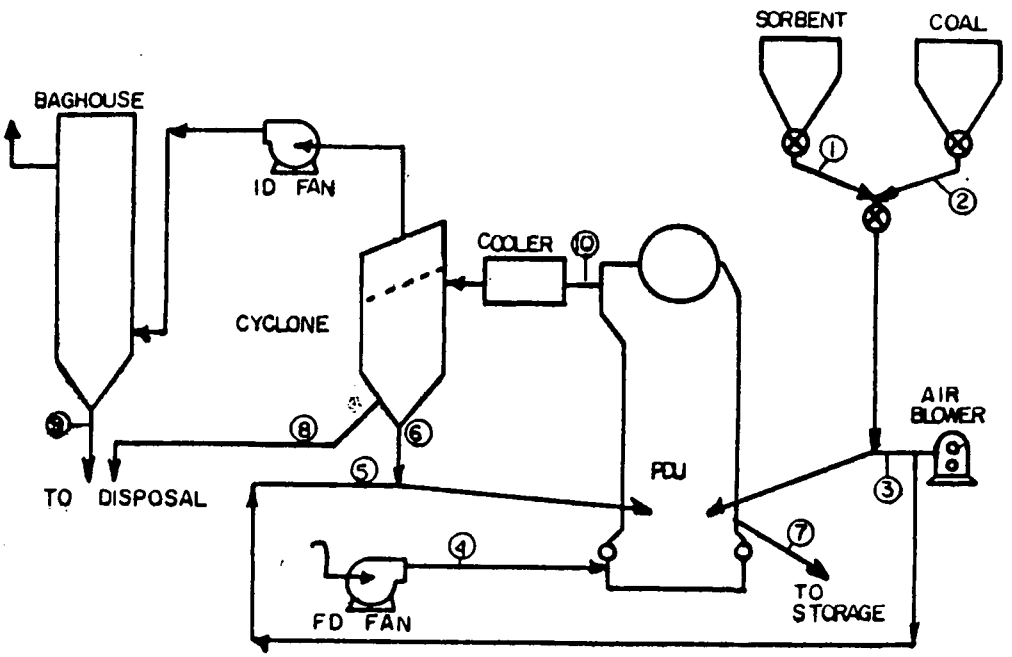

Stream No.		lbs/hr
1	Limestone	300
2	Coal	800
3	Coal Transport Air	350
4	Main Air	7440
5	Fly Ash Transport Air	200
6	Fly Ash Recycle	1200
7	Bed Material Drain	200
8	Fly Ash	130
9	Dust	70
10	Flue Gas	8640

FIGURE 9 - SCHEMATIC - PROCESS AND FLUE GAS FLOWSTREAMS - ALEXANDRIA, VA. AFBC

FIGURE 10

PROCESS DEVELOPMENT UNIT
FLUID BED BOILER
ALEXANDRIA, VIRGINIA
SYSTEM MATERIAL CHEMICAL COMPOSITIONS

% BY WEIGHT

COMPONENT	CARBON	HYDROGEN	SULFUR	CALCIUM	ASH
Coal	70.12	4.38	2.86	0.28	16.91
Limestone	12.10	0.11	0	39.86	57.27
Bed Mat. (Drain)	0.97	0.06	5.46	48.30	99.00
Flyash Recycle (Cyclone)	28.79	0.56	3.18	22.19	69.25
Dust from Bghse (Hopper)	18.32	0.44	2.08	20.75	76.17

NOTE: These are typical values taken from a run to evaluate the baghouse.

FIGURE 11

BAGHOUSE DESIGN DATA - ALEXANDRIA, V.A. AFBC

Manufacturer	Buell Division, Envirotech Corp.
Gas Flow Rate	3,000 ACFM
Temperature	500°F Maximum
Compartments	1
Total Bags	32 (reverse air/shake configuration) 66 (pulsejet configuration)
Bag Supplier	Buell Division, Envirotech Corp.
Diameter	8" shake and RH, 6" pulsejet
Length	23' (reverse air/shake) 10' (pulsejet)
Active Area/Bag	48.2 sq. ft. (shake/RH) 15.7 ft^2 (pulsejet)
Fabric	Glass, 54x30 count, 3x1 twill
Finish	Teflon "B", 7-10% by wt.
Permeability	50-75 CFM @ 1/2 in. H_2O (shake/RH) 25-40 CFM @ 1/2 in. Hd (pulsejet)
Weight	9.5 oz./sq. yd (shake) 14.5 oz/sq. yd (pulsejet)
Air-to-cloth Ratio	1.95 ACFM/ft^2 (shake) 2.90 ACFM/ft^2 (pulsejet)

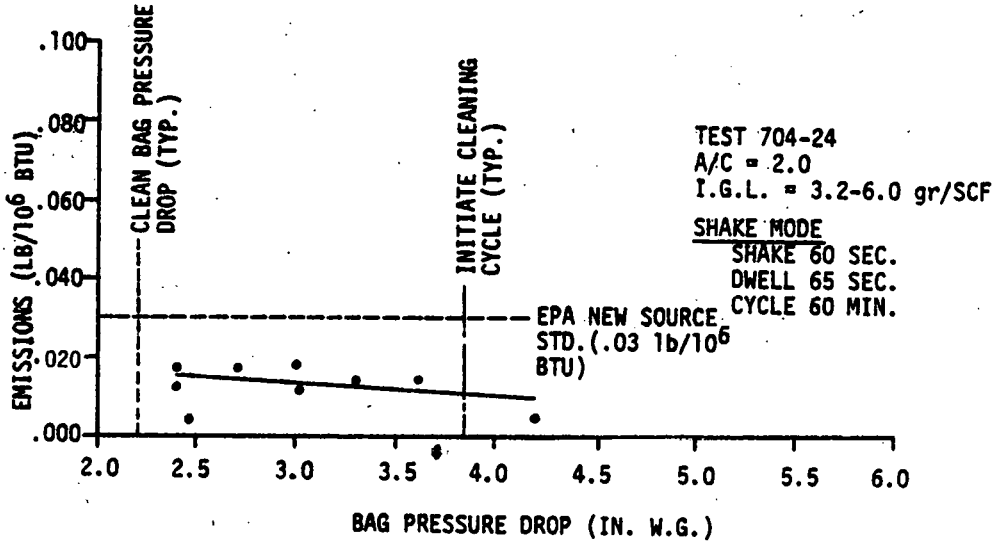

FIGURE 12- OUTLET SPECIFIC LOADING VERSUS PRESSURE DROP, ALEXANDRIA, VA. AFBC

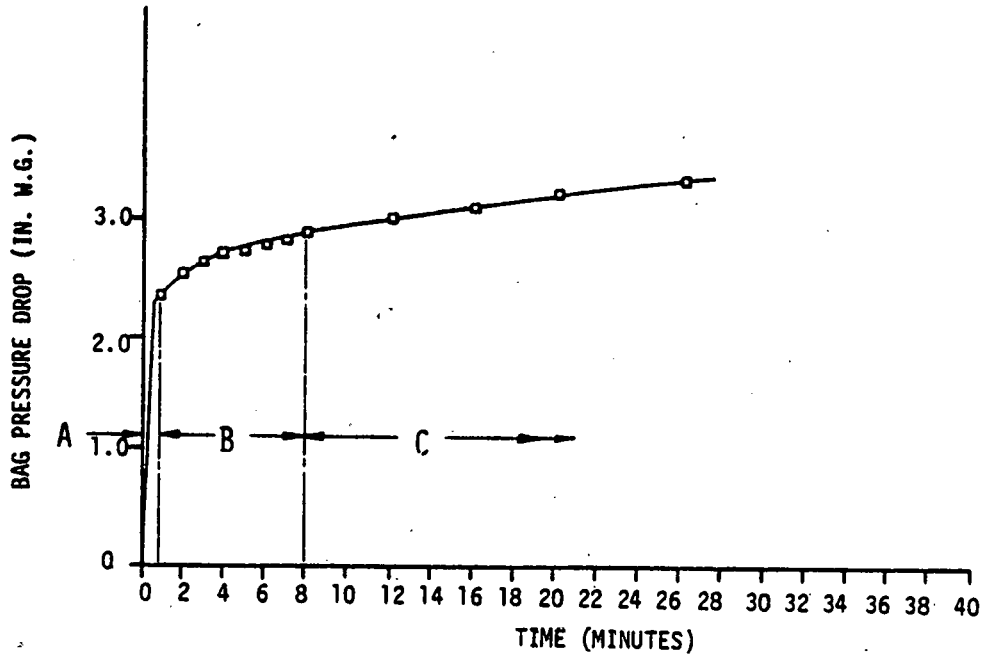

FIGURE 13- TYPICAL BAG PRESSURE DROP - TIME TRACE ALEXANDRIA, VA., AFBC

Questions to Norm Z. Shilling:

Q: (Participant not Identified)

If you were starting out which system would you recommend?

A: For this kind of a situation, you would have to say baghouse. Once we get full operational data from Rivesville, we should review that position.

Q: Ralph Morehouse, Power Authority of New York State

Does the grain loading size have any affect on efficiency for the precipitator?

A: For the loading we saw in these tests, it should not have any influence on efficiency.

Q: Roger Adams, Kimberly-Clark

Due to the many variations of fuels possible, is there any way we could possibly go other than a baghouse?

A: I don't see any alternative at this point.

PHYSICAL, CHEMICAL AND BIOLOGICAL CHARACTERIZATION OF ATMOSPHERIC PRESSURE FLUIDIZED BED COAL COMBUSTION EFFLUENTS

C. H. Hobbs, R. L. Carpenter, G. J. Newton, C. R. Clark, R. F. Henderson, R. L. Hanson, S. H. Weissman, L. C. Griffis, J. O. Hill

Inhalation Toxicology Research Institute,
Lovelace Biomedical and Environmental Research Institute,
P.O. Box 5890, Albuquerque, New Mexico 87115

INTRODUCTION

Since April 1977, the Inhalation Toxicology Research Institute (ITRI) has been actively engaged in a collaborative effort with the Morgantown Energy Technology Center (METC) to determine the potential health risks to man from the atmospheric fluidized bed combustion (AFBC) of coal. The research effort, involves the chemical and physical characterizations of potential effluents from an experimental 18-inch AFBC being operated at METC. Emphasis has been placed on characterizing the potential airborne particulate and hydrocarbon emissions from the AFBC. Characterization is followed by toxicological testing of the potential effluents at ITRI. The approach being used to assess the potential toxicity of the materials collected at METC is the utilization of *in vitro* and *in vivo* screening tests for toxicity and mutagenicity. The screening results are being used to select materials for longer term inhalation studies in experimental animals, including exposures of rodents over their total life span to aerosols of selected FBC effluents to characterize their potential for producing chronic respiratory disease as well as cancers of the respiratory tract and other organs.

The purpose of this report is to summarize the currently available data from the physicochemical characterization and the toxicological testing of samples that have been obtained from the 18-inch AFBC at METC while it was burning several coal types and operating under various conditions. More detailed presentations of the data have been published previously (1-12). A special effort has been made to compare our data with that available in the literature on the conventional combustion of coal. The need for this comparison in evaluating the two technologies is well recognized, but is difficult because of the different techniques used for sampling the two technologies.

It should also be recognized that the AFBC at METC is a relatively small experimental unit and that such things as control technology for fine particles have not been optimized. However, the data from this unit may be used to approximate the emissions of a full scale AFBC and will supply information on needed control technology until sampling of larger units is possible.

MATERIALS AND METHODS

Figure 1 is a schematic of the METC 18-inch atmospheric fluidized bed combustor. Inside the combustor a bed of coal and limestone is supported by a conical plate perforated by 1/8-inch holes through which the fluidizing air passes. Water passing through a heat exchanger bank buried in the bed extracts heat from the bed. A screw conveyor meters pre-sized coal into a pneumatic feed tube which conveys fuel into the combustor near the bottom of the bed. Limestone or other sorbent may be fed into the combustor by a screw conveyor above the fluidized bed. Combustion products pass through two cyclone separators. Partially cleaned combustion gases pass through a baghouse filter system for final particle removal. Solids from the primary cyclone contain enough unburned fuel to justify reinjection into the combustor. A system of valves allows the baghouse to be placed in the cleanup system or to be bypassed.

The AFBC was sampled at four positions (1-4, in Figure 1). Samples obtained at Position 1 (stack breech) were of greatest interest as an approximation of atmospheric releases. Samples from Positions 2, 3 and 4 were representative of source material for potential fugitive emissions to the work place environment. Samples from all four positions provide an engineering assessment of the combustion process and the effectiveness of cleanup devices. Major emphasis has been placed on aerodynamic size-selective sampling because of the critical importance of aerodynamic size in predicting lung deposition of inhaled particles. Similarly, chemical and biological characterization of aerodynamically sized samples is a major goal. A detailed discussion of the sampling system used in these studies has been published (1,2).

Sampling probes in the FBC exhaust system withdrew 15-25 liters per minute (LPM) of AFBC exhaust aerosol which was diluted with 100 LPM of dry ambient air. Immediately after the diluter, a portion of the sample was passed through the Tenax adsorbent to collect vapor phase hydrocarbon samples. The remaining sample was conveyed to a sampling chamber. A battery of aerosol samplers attached to the chamber collected particles (Table 1). These instruments can be changed at will during sampling to supply the mix of samples required for characterization and biological testing.

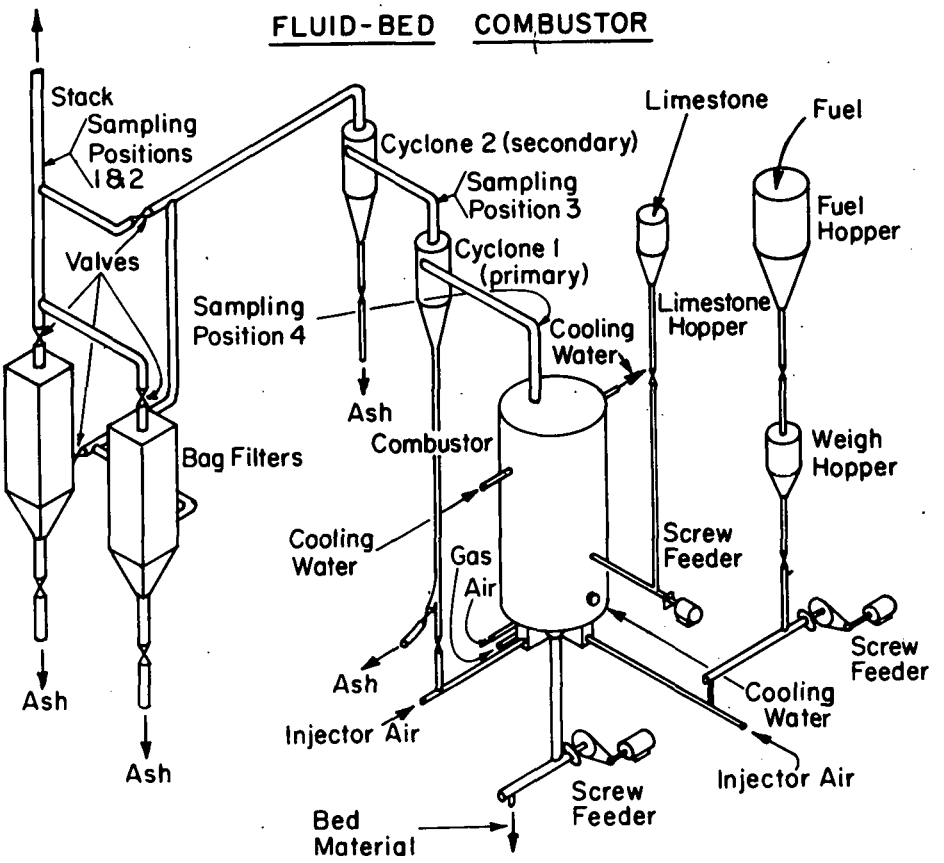

Figure 1. Schematic diagram of METC experimental atmospheric pressure fluidized bed combustor. Samples were obtained at positions noted. Positions 1 and 2 involved sampling from the same port with the baghouse switched in (Position 1) or out (Position 2) of the process stream. Position 1 represented the stack breech with the effluent going through the baghouse. Position 2 represented samples taken when the baghouse is bypassed (baghouse inlet). Position 3 was between the cyclones. Position 4 represented sampling at the top of the combustor freeboard, at the inlet to the primary cyclone.

Table 1

Samplers Used on Effluent Streams from METC-FBC

Sampling Device	Flow Rate (l/min)
Lovelace Multi-Jet Cascade Impactor (LMJ)	25
Sierra Radial Slit Jet Cascade Impactor (SRSJ)	21
Mercer Cascade Impactor (MI)	0.5
Lovelace Aerosol Particle Separator (LAPS)	0.3
Filter (47 and 90 mm diameter)	25
Point-to-plane Electroatatic Precipitator	0.5
Tenax Sampler	2.0
Concentric Electrostatic Precipitator	100-125

Excess sample is passed through a cleanup system and exhausted.

It is emphasized that the system was designed to have an upper size limit of about 10 μm aerodynamic diameter. The sampling system is thus not directly comparable to Environmental Protection Agency's Compliance type sampling devices.

Samples from the above sampling system as well as coal, bed material, cyclone ash, bag filter ash, and bottom ash have been collected when the AFBC was operating under various conditions with several coal types and bed materials (Table 2). Table 3 illustrates a set of typical operating conditions during a sampling period.

Inorganic analysis of the samples from the aerosol sampling system used for the AFBC was done

Table 2

Summary of Coal Feed Stocks, Bed Temperatures and Bed Materials Used in the FBC During the ITRI Field Sampling Trips

Coal	Bed Temperature (°F)	Bed Material
Montana Rosebud I	1450	Limestone
Montana Rosebud II	1650	Limestone
Texas Lignite I (bulk)	1550	Glass sand
Texas Lignite II (refuse)	1600	Glass sand
Texas Lignite III (refuse)	1600	Limestone
Texas Lignite IV (refuse)	1450	Glass sand
Texas Lignite V	1450	Limestone
Texas Lignite VI (washed)	1600	Glass sand
Western Kentucky	∿ 1500	Limestone

Table 3

Typical FBC Operating Conditions During Sampling

Fuel	Montana Rosebud subbituminous
Bed material	Geer limestone
Fluidizing air flow	2600 scfh
Fluidizing air pressure	3 psi
Injector air flow	960 scfh
Total air flow	4980 scfh
Fluidizing velocity	3.0 ft/s

by spark source mass spectrometry (SSMS)* using rhodium and indium as internal standards. The methods for organic analysis of the particle-associated and vapor phase hydrocarbons have been presented elsewhere (5,6). Particles were ultrasonically extracted with methylene chloride while Tenax material was Soxhlet extracted with pentane. Gas chromatography and gas chromatography/mass spectrometry were used to characterize the samples.

Mutagenicity testing of the particle or Tenax (a polymeric absorbant used to trap vapor phase hydrocarbons) extracts was done with strains TA1535, TA100, TA1537, TA1538 and TA98 of *Salmonella typhimurium*** Homogenates for enzyme activation were prepared from the livers of rats treated with Aroclor 1254 (500 mg/kg IP) (14). For mutagenicity testing, samples of particles were extracted ultrasonically with methylene chloride, but Tenax samples were Soxhlet extracted with pentane. The extracts were evaporated to dryness at room temperature and reconstituted in DMSO for the Ames test (14). The cytotoxicity of fly ash from the FBC and coal-gas aerosols was evaluated in alveolar macrophages by a modification of the methods of Waters *et al.* (15).

Fly ash collected from the bag filter of the FBC was resuspended as an aerosol for the inhalation exposure of rats or Syrian hamsters. A fluidized bed aerosol generator recently developed at ITRI was used to generate the aerosol. Thirty days before exposure of one group of rats, fly ash was neutron activated for 40 h with a flux of 9 x 10^{13} neutrons cm^{-2} s^{-1} by methods previously reported (8). The deposition, retention, and distribution of the fly ash following inhalation was determined by whole-body counting and serial sacrifice of the animals followed by liquid scintillation or Ge(Li) detector counting of tissues to obtain the distribution of the material. Syrian hamsters and rats were also exposed in modified Rochester chambers to graded levels of ash that had not been neutron activated or ash combined with NO_2 for 6 h. These animals were also serially sacrificed and the levels of selected enzymes determined for airway fluid and lungs by previously described methods (16,17) as indicators of acute lung damage.

RESULTS AND DISCUSSION

Mass concentrations and size parameters of respirable flue gas aerosols produced by the AFBC have been determined for the fuels shown in Table 2 (2). The respirable aerosol released into the stack breech ranged from 2.2 to 2.8 μm mass median aerodynamic diameter (MMAD) for all fuels and AFBC operating conditions studied. This is well below the 10 μm upper size limit of our sampling system and is probably not affected by the sampling system size cut-off. The "< 10 μm fraction" of the flue aerosol entering the exhaust cleanup system from the AFBC ranged from 3.2 to 6.1 μm MMAD and appeared to vary with fuel type and AFBC operation. Insufficient data are currently available to explain the relationship. The 10 μm sampling system cut-off did not appear to influence the observed MMAD at the AFBC cleanup system inlet. For all fuels considered, the observed aerosol size at the sampling point between cyclones was lower than that observed at the cleanup system inlet, evidence that the first cyclone captures large particles elutriated from the bed. The second cyclone and baghouse filter appear to have little effect on observed size distributions, suggesting that the collection efficiency of both devices for particles below 10 μm is not highly size dependent.

Respirable aerosol concentration at the stack breech remained relatively constant as fuel type and AFBC operating conditions varied, ranging from 7 x 10^{-3} to 7 x 10^{-2} g/m^3. One exception to this observation was noted. During the bulk Texas lignite combustion studies, an abnormally high stack inlet aerosol mass loading concentration was observed. Upon subsequent disassembly, the baghouse filters were found to have holes.

Cleanup system device penetration by respirable aerosol particles is tabulated in Table 4 as

*All SSMS analyses were done by CDM/Accu Labs, Wheatridge, CO.
**Obtained from B. N. Ames.

Table 4

Respirable (< 10 μm) Aerosol Penetration of Exhaust System Cleanup Devices on an Experimental Atmospheric Pressure FBC

Coal Type	Percent Penetration		
	First Cyclone	Second Cyclone	Baghouse
Montana Rosebud I	26	32	18
Montana Rosebud II	17	95	5
Texas Lignite I	--	97	58[a]
Texas Lignite II	--	--	3
Texas Lignite III-VI	--	--	2-6
Western Kentucky	24	56	4

[a]Verified baghouse filter leak

a measure of cleanup efficiency. Penetration is defined as the ratio of device outlet mass loading divided by device inlet mass loading. Fine particle penetration of the exhaust system devices appeared to be a function of fuel type and combustor operation. The baghouse filter was the most efficient device for fine particle removal, although this efficiency dropped as the filter wore and developed holes.

Morphology of AFBC flue gas aerosol particles was examined by scanning electron microscopy (SEM) and transmission electron microscopy (TEM) of particles collected by electrostatic precipitation and with the Lovelace Aerosol Particle Separator. Although particle size varied, effects of operating the AFBC below the ash fusion temperature were readily seen. For all fuels examined, particles escaping the AFBC were irregularly shaped. Very few fused, spherical particles were seen. This is in contrast to fly ash from pulverized coal combusion which consists mainly of fused, spherical particles.

It is recognized that emissions from a power plant may have a number of environmental effects and the size of emitted particles plays a role in most of them. The primary consideration of this analysis is to address the particles in the respirable size range which may be inhaled by man. If assumptions are made concerning fly ash density and power plant efficiency, one may compare data by Ondov, Lynn and Mesich (18-20) with data obtained from the METC AFBC by ITRI. Table 5 summarizes these data. Since inhalation of the released fly ash is the major concern, data are expressed as respirable mass loading which was determined from cumulative size distribution estimates. Examination of these data demonstrates that the METC AFBC, equipped with a baghouse filter, does not emit more respirable particles than conventional pulverized coal combustion power plants (PCC). The AFBC total particulate mass loading was comparable or lower than that of the PCC plants examined. Note that the AFBC mass loading was a function of coal type as is probably true for PCC. The effects of optimizing cleanup devices on an AFBC such as is done for large PCC plants is unknown, athough one could assume some decrease in effluent particulate loading.

Filter, impactor and hopper ash samples were analyzed for elemental composition using spark source mass spectrometry. Particle trace element concentration varied with position sampled in the effluent stream, fuel and operating parameters. A limited number of elements had concentration variations with particle size. A detailed listing of the inorganic composition of the AFBC effluents has been published (9,12).

The elemental composition of the AFBC ash was a function of sampling location, as indicated by differences in enrichment factors and penetrations (12). Enrichment factors account for enrichment of elements in combustor feed material due to loss of carbon during combustion. Penetrations show the extent of removal of the particulate form of an element by a cleanup device. The reasons for this are being investigated. No elements showed significant differences in penetration through the primary cyclone compared to the inorganic marker Zr. Two elements (Li and Se) showed penetration differences through the secondary cyclone and two elements (I and Li) showed differences through the baghouse. Baghouse ash was significantly depleted in Te and Tl and enriched in Ge. However, for stack breech ash there was no significant difference between enrichment factors for Te, Tl and Ge in comparison with Zr. Six other elements (Bi, B, Co, F, Li and Sc) were enriched in stack breech fly ash. Eight elements (Cl, Dy, I, Li, Te, Tl, W and Yb) were significantly depleted in the spent bed material, which is primarily ash and limestone (with chemisorbed SO_2).

Differences in elemental concentration were observed for samples obtained under different combustor operating conditions (12). Concentrations of a majority of the elements studied were significantly affected by operating parameters. The elements affected were Be, Bi, B, Br, Ce, Cl, Cr, Co, Er, Eu, Hf, I, La, Pb, Li, Lu, Nd, Ni, P, Pr, Sm, Sc, Se, Na, Sr, Tb, Tl, Tm, W, U, Yb, Y and Zn. Although one of the major changes in operating parameters was combustion temperature, the concentrations of several volatile elements (Sb, As, Cd, and Mo) were not significantly changed.

The concentrations of minor and trace elements determined in METC AFBC ash were similar to reported values for other AFBCs and pressurized fluid beds (12). More P and less Cu was found in METC AFBC ash than has been reported for other FBCs.

The environmental impact of introducing AFBCs into use for electrical generation depends partly on whether AFBC and PCC ash differ in elemental composition. The data indicates that ash from the two combustion technologies is similar in elemental concentration. The observed concentration ranges overlap in most cases, usually with the extremes of one range extending beyond that of the other. This was true despite major differences in PCC plant design, fuel, operating conditions,

Table 5

Comparison of Conventional Pulverized Coal Power Plants and 18-inch METC AFBC: Respirable and Total Mass Loadings Emitted

Plant Type	Fuel Type	Total Mass Loading g/10^6 Btu	Respirable[a] Mass Loading g/10^6 Btu
180 MW Venturi Scrubber[b]	Western Subbituminous	73.2	73.0
280 MW Cold Side ESP[b]	Western Subbituminous	186.7	56.0
280 MW Hot Side ESP	Eastern Bituminous	0.45	0.45
350 MW Hot Side ESP	Western Subbituminous	2.7	-
330 MW Venturi Scrubber	Western Subbituminous	20.0	-
250 MW Cyclone	Lignite	680.4	-
AFBC Baghouse	Lignite (bulk)	501.0[c]	391.4[c]
AFBC Baghouse	Lignite (refuse)	17.8	13.9
AFBC Baghouse	Lignite (washed)	4.7	4.2
AFBC Baghouse	Western Kentucky	2.5	2.1
AFBC Baghouse	Montana Rosebud	12.0	10.5
AFBC Baghouse	Parahoe Oil Shale	252.5	214.6

[a]Fraction < 5 μm aerodynamic diameter
[b]Plant steam capacity
[c]Verified leaks in baghouse

cleanup devices and sampling methodology. The similarity in ash composition indicates that the two combustion processes will not have radically different environmental impacts.

Several investigators have shown that particles produced by PCC have variations in elemental composition as a function of particle size. We found fewer elements concentrated in small particles with Montana Rosebud combustion effluents than have been reported for PCC. With Montana Rosebud coal (9), only three elements (Be, Ga and Hf) were found enriched in small particles from the AFBC exhaust. Iodine and terbium were found to decrease in concentration with decreasing particle size. The enrichment of I in large particles collected from the stack breech can be attributed to entrainment of limestone particles in the exhaust stream and penetration of the cleanup devices. Our classification of Hf as an element exhibiting small particle enrichment was not expected on the basis of its chemical and physical properties.

The extent of small particle enrichment was also greater for PCC ash compared to AFBC ash (12). The ratio of elemental concentrations in small particles versus large particles for PCC was greater than for AFBC except for Pb. The largest difference in concentration ratios was found for Cr. Less small particle enrichment was also observed from similar calculations done with data published by Murthy *et al.* (21) on pressurized fluidized bed combustors. The reduced small particle enrichment observed for FBC in comparison with PCC is probably due to the lower combustion temperature for FBC (800 to 1000°C) compared to that of conventional PCC (1300 to 1500°C). The lower temperatures result in less vaporization, decreasing the extent of selective condensation or adsorption onto small particles.

Vapor and particulate phase samples were analyzed for organic compounds (5,6,12). Following extraction, gas chromatography and gas chromatography mass spectrometry were used for quantitation and tentative compound identification. Vapor phase organic concentrations in stack effluent (after the baghouse) ranged from 0.084-20 mg/m^3. The highest vapor phase organic concentrations were obtained with Montana Rosebud subbituminous coal combustion effluents where concentrations as high as 20 mg/m^3 were observed. Although there was variation in vapor phase organic concentrations at different sampling positions, no uniform trend was apparent. For all fuels studied the concentration of vapor phase organics was higher than the extractable particle associated organic concentration. For Texas Lignite, 95-98% of the organics present in the exhaust stream at all four sampling locations were in the vapor phase. Similar results were obtained for other coals.

Particle associated hydrocarbon concentrations varied with sampling position. High volume filter samples taken after the bag filter had concentrations of 650-880 μg/g of ash. Samples from ash collected by the cleanup system had considerably lower concentrations, 4.4-51 μg/g. The hydrocarbon concentration in ash increased with distance from combustor as the temperature decreased, suggesting particle adsorption of vapor phase organics with cooling. Samples taken from the stack (after the bag filter) following cooling and diluting had much higher hydrocarbon levels than those taken in front of the bag filter.

There have been relatively few reported measurements of effluents hydrocarbons from coal combustion technologies. The concentrations reported here for vapor and particle phase hydrocarbons are similar to those reported for other atmospheric and pressurized FBC's (21-23) (Table 6). For both

Table 6

Concentrations of Organics Associated with Particles and in the Vapor Phase of Various Fluidized Bed Combustors

	ANL PFBC	Exxon PFBC	BCL AFBC	METC AFBC
Vapor Phase (mg/m^3)	2-30	2.2	11.5	0.084-20
Particle Associated (mg/g)	0.8-4	-	0.66-1.1	0.66 -0.88

vapor and particle phase samples, Argonne National Laboratory (ANL) reported the highest hydrocarbon level.

Fewer data are available for PCC. The results of two early studies are compared to some of the results from this study (Table 7). The AFBC appears to have higher vapor phase organic levels. The total of 11 compounds were measured at a PCC plant in 1965 (24). The methodology used in the 1965 study is considerably different from current procedures and may have resulted in smaller polycyclic organic mater (POM) concentration than would be obtained with current techniques. It has been hypothesized that as the effluent stream cools, the vapor-phase hydrocarbons condense onto particles or are adsorbed by particles. Our AFBC measurements for vapor-phase POM and particle-associated hydrocarbons to date show that even 2 minutes after cooling and diluting, most of the POM remains in the vapor phase. Although condensation or adsorption may occur in power plant plumes, these effects were not observable in the 2 minute time frame after cooling and diluting. Compounds which have been tentatively identified in AFBC samples have been reported (5,6,12).

The *Salmonella* mutagenicity (Ames) bioassay has provided a rapid method for detecting potential mutagens at different locations in the process stream and in the cleanup system of the FBC, and for evaluating changes in mutagenicity associated with different fuel types and operating conditions (7). Samples evaluated to date include: (A) vapor phase hydrocarbons collected on Tenax adsorbent at three different positions in the effluent stream; (B) methylene chloride extracts of material trapped by the primary and secondary cyclones; and (C) methylene chloride or DMSO extracts of fly ash collected in bag filters, on high volume filters placed at the stack breech, and extracts of size separated fly ash collected by cascade impactors placed at the stack breech. Samples collected while the AFBC was burning Montana Rosebud subbituminous, Western Kentucky Bituminous, and Texas Lignite coals have been evaluated.

To date, none of the vapor phase hydrocarbons adsorbed from the process stream on Tenax traps have demonstrated any mutagenicity. As pointed out

Table 7

Estimated Aromatic Hydrocarbon Emissions from Conventional and AFBC Combustors

Plant Type	Aromatic Hydrocarbons $mg/10^6$ Btu
Total of 11 Compounds at PCC Plant	
METC AFBC Montana Rosebud Coal > C_6 Vapor Phase	38-12,000
METC AFBC Montana Rosebud extractable from particles	6.1
METC AFBC Texas Lignite > C6 Vapor Phase	340-13,000
METC AFBC Texas Lignite extractable from particles	22-24
METC AFBC Texas Lignite refuse > C_6 Vapor Phase	93-16,000
METC AFBC Clean Texas Lignite refuse > C_6 Vapor Phase	130-970
METC AFBC Western Kentucky > C_6 Vapor Phase	43-3,700

in the section on organic analysis of the effluent, the great majority (over 90% in most cases) of the hydrocarbons in the gaseous effluents are in the vapor phase and no mutagenicity has been detected in these samples.

No mutagenicity was detected in any of the primary cyclone samples (Table 8) and only 3 of the secondary cyclone samples were positive corresponding to the two sampling periods for which mutagenicity of the bag filter ash was the highest. Compounds responsible for mutagenicity may have been adsorbed or condensed more efficiently by the lower temperatures and the smaller sized particles collected in the bag filter than by the larger particles collected at higher temperatures in the cyclones.

Mutagenicity of extracts of bag filter ash varied over 200-fold (Table 9). Montana Rosebud ash samples collected during seven different sampling periods were tested. Two of the seven samples were not mutagenic when up to 2 g of fly ash were extracted and tested. There was some correlation between combustor bed temperature and mutagenicity of the fly ash extracts; the three most mutagenic samples were burned at higher temperatures than most of the negative samples.

Mutagenicity of ash collected by high volume filters in the stack breech was similar to that of the bag filter ash. Fly ash collected in cascade impactors demonstrated size dependent mutagenicity, i.e., mutagenicity per mg ash increased with decreasing particle size (10). The amount of hydrocarbon per mg ash also increased with decreasing particle size so that the mutagenicity per µg hydrocarbon remained relatively constant. Mutagenicity was detected in size selected samples only when bag filter ash obtained during the same

Table 8

Mutagenic Evaluation of Bag Filter Ash

Coal Type	Bed Temperature (°F)	Revertants/100 mg Cyclone Material[a,b]		Revertants/100 mg of Bag Filter Fly Ash[b]
		Primary	Secondary	
Texas Lignite	1420-1540	0	0	65
Western Kentucky	1520-1580	0	0	0
Montana Rosebud	1425-1460	0	0	0
Montana Rosebud	1420-1540	-	-[c]	1
Montana Rosebud	1440-1460	0	8	397
Montana Rosebud	1650-1655	0	0	5
Montana Rosebud	1650-1670	0	16	987
Montana Rosebud	1635-1655	0	0	146
Montana Rosebud	1540-1575	0	16	208

[a]Calculated from 2000 mg extracted ash/plate concentration
[b]TA-98 without S-9, background subtracted, calculated from linear portion of dose response curve
[c]No sample available

Table 9

Mutagenic Evaluation of Size Selected Ash Collected on High Volume Sierra Impactors (HVSI)
(Montana Rosebud Coal, Bed Temperature = 1650°F)

HVSI Stage Number	Effective Cut-off Diameter[a] (μm)	Revertants[b]/mg Ash Extracted	μg HC[c]/mg Ash	Revertants/μg HC
1	8.3	4.6	0.20	23
2	3.6	5.7	0.13	44
3	2.3	7.4	0.20	37
4	1.2	9.0	0.30	30
5	0.7	11.8	0.56	21
6	< 0.7	15.1	0.60	25

[a]Approximate mass median aerodynamic diameter
[b]TA-98 with S-9
[c]HC = hydrocarbon

burn was mutagenic. Physical characterization of the process stream aerosol further indicated that the size distribution of the aerosol entering the bag filters was similar to that collected in the stack.

Chrisp *et al.* (25) have reported on the mutagenicity of extracts of fly ash collected from a conventional PCC. We also participated in an exchange of fly ash samples and fly ash extracts with the University of California at Davis (Chrisp) and Argonne National Laboratories (Kubitschek) to compare the interlaboratory variation in the results of mutagenicity testing (26). Although it is still difficult to make direct comparisons between the AFBC ash collected by us and the PCC ash collected by Chrisp *et al.*, due to differences in sample collection and handling techniques, none of the AFBC samples tested to date have had mutagenic activity (revertants/mg of ash extracted) as high as that reported by Chrisp *et al.* (12,25,26). The mutagenic activity of the AFBC ash tested by us has been about one-tenth that of the PCC ash tested.

Although direct comparisons are difficult at this time due to differences in combustor size and sampling techniques, the AFBC effluents (ash and vapor phase hydrocarbons) certainly appear to have no greater and probably less mutagenic activity than similar effluents from PCC plants.

Numerous AFBC and comparable PCC fly ash samples have been evaluated for cytotoxicity as compared to the cytotoxicity of a quartz standard. None of the samples tested to date from either AFBC or PCC have shown significant cytotoxicity in this system.

To determine the best method of assessing dose to the lung from the inhalation of AFBC ash. AFBC baghouse ash was neutron activated and administered to Fischer 344 rats via a single nose-only inhalation exposure (8). Six major gamma-emitting radionuclides were present in the fly ash

and it was found that ^{152}Eu, ^{134}Cs, ^{54}Mn and ^{60}Co disappeared from the lung at a faster rate than ^{46}Sc and ^{59}Fe. This indicates that some elements may be preferentially dissolved from the fly ash *in vivo*.

Based on these studies, ^{46}Sc and ^{59}Fe appear to be suitable tracers for determining deposition and retention of inhaled fly ash. Measuring overall radioactivity (^{46}Sc is the major component), the whole-body clearance of ash from the rat can be described by the three-component exponential equation $y = 97e^{-1.4t} + 2e^{-0.03t} + 1e^{-0.0089t}$ (8). The long-term component (1% of initial body burden) cleared with a half-life of 78 days. This can be compared to a similar study done with Syrian hamsters exposed to PCC ash which showed a whole-body clearance described by the equation $y = 64e^{-1.2t} + 28e^{-0.30t} + 8e^{-0.0084t}$. The long-term component of clearance (8% of initial body burden) in this case had a similar biological half-life ($T_{1/2}$ = 83 days) to the AFBC ash.

Syrian hamsters have been exposed by inhalation for 6 hours to 60 mg/m^3 and 120 mg/m^3 of baghouse ash from the AFBC burning of Montana Rosebud coal. Neither the biochemical cytological parameters (16,17) assayed in the airway fluid nor the histopathology of the tissues gave any indication of lung injury. When the same fly ash exposure occurred during the first 6 hours of a 48-hour exposure to NO_2, the lethal concentrations for 50% (LC_{50}) for NO_2 decreased from 36 to 31 ppm. Thus, the ash itself did not appear to be toxic in short-term *in vivo* inhalation exposures, but the ash may aggravate the injury caused by other noxious agents.

The expected mode of human exposure to FBC effluents is repeated or continuous inhalation at low doses for long periods of time ranging up to life span. There are no reports of studies of the inhalation of FBC fly ash, but Alarie and coworkers (27,28,29) have studied the response of Cynomolgus monkeys and guinea pigs to the inhalation of ash from conventional coal combustion. This research indicated that 1 to 1-1/2 year exposures to 0.5 mg/m^3 conventional fly ash did not result in biological effects other than collections of ash in lung cells and lymph nodes, and some nodules of aggregated macrophages. These studies, however, did not employ functional measurements such as forced expiratory flow-volume and volume-time indices which have been recommended for use in detecting lung disease from environmental pollutants and demonstrated to be useful in human epidemiologic studies. Thus, there is a critical need for chronic inhalation studies on both FBC and PCC fly ash. We plan to initiate chronic inhalation studies of this type in the near future.

SUMMARY AND CONCLUSION

Based on our studies of the potential emissions of AFBC and comparing them to data available in the literature from PCC, the following conclusions have been made.

- o AFBC particle emissions are comparable or lower than from conventional power plants
- o AFBC trace element emissions are comparable or lower than conventional power plant emissions
- o AFBC polycyclic organic emissions appear to be higher than estimated for conventional power plants and are primarily vapor phase as measured
- o Mutagenic activity has not been detected in AFBC vapor phase polycyclic organic AFBC samples tested to date
- o Mutagenic activity has been detected in some fly ash samples from the AFBC bag filter and stack
- o The mutagenic activity per mass of fly ash extracted appears to be less in the METC fluidized bed combustor ash than that reported for one conventional power plant
- o Results to date indicate that AFBC emissions pose no unique environmental problems compared to conventional combustion
- o More comparisons are needed between FBC and conventional combustion emissions especially for organic emissions
- o Chronic inhalation studies on both FBC and conventional combustion emissions are needed

ACKNOWLEDGEMENTS

We acknowledge the enthusiastic support of the Morgantown Energy Technology Center's staff, especially John Kovach, Bill Wallace, Ulrich Grimm, Dick Rice, John Wilson, Jack Halow and A. A. Pitrolo. Equally important were the efforts of our sampling crew which included in addition to the authors D. D. Horinek, J. A. Stephens, E. B. Barr, K. L. Yerkes, R. Tamura, R. E. Peele, S. H. Weissman and R. E. Royer. Finally, we note the encouragement of Drs. B. B. Boecker, R. K. Jones and R. O. McClellan.

Research was performed under the U.S. Department of Energy Contract Number DE-AC04-76EV01013 and in facilities fully accredited by the American Association for Accreditation of Laboratory Animal Care.

REFERENCES

1. Newton, G. J., R. L. Carpenter, H. C. Yeh, and E. R. Peele, "Respirable Aerosols from fluidized Bed Coal Combustion. 1. Sampling Methodology for an 18-inch Experimental Fluidized Bed Coal," *Environ. Sci. Technol.* *14*(7):849-853, 1980.

2. Carpenter, R. L., G. J. Newton, S. J. Rothenberg, and P. B. DeNee, "Respirable Aerosols from Fluidized Bed Coal Combustion. 2. Physical Characteristics of Fly Ash," *Environ. Sci. Technol. 14*(7):854-859, 1980.
3. Newton, G. J., R. L. Carpenter, H. C. Yeh, S. H. Weissman, R. L. Hanson, and C. H. Hobbs, "Sampling of Process Streams for Physical and Chemical Characterization of Respirable Aerosols," in *Potential Health and Environmental Effects of Synthetic Fossil Fuel Technologies*, CONF-780903, pp. 78-94, NTIS, Springfield, VA, 1979 (invited paper).
4. Hobbs, C. H., R. O. McClellan, C. R. Clark, L. C. Griffis, R. F. Henderson, J. O. Hill, and R. E. Royer, "Inhalation Toxicology of Primary Effluents from Fossil Fuel Conversion and Use," in *Potential Health and Environmental Effects of Synthetic Fossil Fuel Technologies*, CONF-780903, pp. 163-175, NTIS, Springfield, VA, 1979 (invited paper).
5. Hanson, R. L., R. L. Carpenter, G. J. Newton, and S. J. Rothenberg, "Studies of Organic Material Present in the Exhaust Stream of an Experimental Fluidized Bed Coal Combustor," *J. Environ. Sci. Health A14*(4):223-250, 1979.
6. Hanson, R. L., R. L. Carpenter, and G. J. Newton, "Chemical Characterization of Polynuclear Aromatic Hydrocarbons in Airborne Effluents from an Experimental Fluidized Bed Combustor," (A. Borseth, ed). Proceedings of Fourth International Symposium on Polynuclear Aromatic Hydrocarbons, Battelle Columbus Laboratories (in press).
7. Clark, C. R. and C. H. Hobbs, "Mutagenicity of Effluents from an Experimental Fluidized Bed Coal Combustor," *Environ. Mutag.* (accepted).
8. Griffis, L. C., M. B. Snipes, and A.L. Brooks, "Clearance of Fluidized Bed Coal Combustion Fly Ash Inhaled by the Rat," *J. Toxicol. Environ. Health* (accepted).
9. Carpenter, R. L., S. H. Weissman, G. J. Newton, R. L. Hanson, E. R. Peele, M. H. Mazza, J. J. Kovach, D. A. Green and U. Grimm, "Characterization of Aerosols Produced by an Experimental Fluidized Bed Coal Combustor Operated with Sub-bituminous Coal," LF-57, NTIS, Springfield, VA, 1978.
10. Inhalation Toxicology Research Institute Annual Report, 1977-1978, (R. F. Henderson, J. H. Diel and B. S. Martinez, eds.), LF-60, NTIS, Springfield, VA, 1978.
11. Inhalation Toxicology Research Institute Annual Report, 1978-1979, (R. F. Henderson, J. H. Diel and B. S. Martinez, eds.), LF-69, NTIS, Springfield, VA, 1979.
12. Fluidized Bed Combustion Emissions Toxicology Program. Status Report, October 1979, (R. L. Carpenter, ed.), LF-74. NTIS, Springfield, VA,
13. Zlatkis, A., W. Bertsch, H. A. Lichtenstein, A. Tishbee, F. Shunbo, H. M. Liebich, A. M. Coscia, and N. Fleischer, *Anal. Chem. 45:*763-767, 1973.
14. Ames, B. N., J. McCann, and E. Yamasaki, "Methods for Detecting Carcinogens as Mutagens with the *Salmonella*/Mammalian Microsome Mutagenicity Test," *Mutat. Res. 31*:347-364, 1975.
15. Waters, M. D., D. E. Gardner, C. Aranyi, and D. L. Coffin, "Metal Toxicity for Rabbit Alveolar Macrophages *In Vitro," Environ. Res. 9:*32-47, 1975.
16. Henderson, R. F., A. H. Rebar, J. A. Pickrell, and G. J. Newton, "Early Damage Indicators in the Lung. III. Biochemical and Cytological Response of the Lung to Inhaled Metal Salts," *Toxicol. Appl. Pharmacol. 50:*123-136, 1979.
17. Henderson, R. F., A. H. Rebar and D. B. DeNicola, "Early Damage Indicators in the Lung. IV. Biochemical and Cytological Response of the Lung to Lavage with Metal Salts," *Toxicol. Appl. Pharmacol. 51:*129-135, 1979.
18. Ondov, J. M., R. C. Ragaini and A. H. Biermann, "Elemental Emissions from a Coal-Fired Power Plant. Comparison of Venturi Wet Scrubber System with a Cold-Side Electrostatic Precipitator," *Environ. Sci. Technol. 13:*598-607, 1979.
19. Lyon, W. S., *Trace Element Measurements at the Coal-Fired Steam Plant.* CRC Press, 1977.
20. Mesich, F. G., "Coal-Fired Power Plant Trace Element Study," Radian Corp. Report (EPA Contract 68-01-2663), Region VIII, Vol. 1-4, 1975.
21. Murthy, K. S., J. E. Howes, H. Nack and R. C. Hoke, "Emissions from Pressurized Fluidized-Bed Combustion Processes," *Environ. Sci. Technol. 13:*197-204, 1979.
22. Isaacson, H. R. and D. A. Haugen, "Toxicology of Samples of FBC Process and Effluent Streams," ANL-CENI-7306, p. 39, 1978.
23. Merryman, E. L., A. Levy, G. W. Felton, K. T. Liu, and J. M. Allen, "Method for Analyzing Emissions from Atmospheric Fluidized-Bed Combustor," U.S. Environmental Protection Agency Report EPA-600/7-77/034, 1977.
24. Gerstle, R. W., S. T. Cuffe, A. A. Orning and C. H. Schwartz, "Air Pollutant Emissions from Coal-Fired Power Plants, Report No. 2," *JAPCA 15*:59-67, 1965.
25. Chrisp, C. E., G. L. Fisher and J. E. Lammert, "Mutagenicity of Filtrates from Respirable Coal Fly Ash," *Science 199*:73-76, 1978.
26. Chrisp, C. E., C. R. Clark, C. H. Hobbs and H. E. Kubitschek, "An Interlaboratory Comparison of Mutagenesis Testing of Coal Fly Ash Derived from Different Coal Technologies," in *Proceedings from 19th Annual Hanford Life Sciences Symposium on Pulmonary Toxicology of Respirable Particles*, 1979 (in press).
27. MacFarland, H., C. E. Ulrich, A. Martin, A. Krumm, W. M. Busey, and Y. Alarie, "Chronic Exposure of Cynamolgus Monkeys to Fly Ash," in *Inhaled Particles III, Vol. 1,* (W. H. Walton, ed.) Unwin Bros, Ltd., Surrey, England pp. 313-327, 1970.
28. Alarie, Y., R. J. Kantz, II, C. E. Ulrich, A. A. Krumm, and W. M. Busey, "Long-Term Continuous Exposure to Sulfur Dioxide and Fly Ash Mixtures in Cynomolgus Monkeys," *Arch. Environ. Health 27:*251-253, 1973.
29. Alarie, Y., A. A. Krumm, W. M. Busey, C. E. Ulrich, and R. J. Kantz, II, "Long-Term Exposure to Sulfur Dioxide, Sulfuric Acid Mist, Fly Ash, and Their Mixtures. Results of Studies in Monkeys and Guinea Pigs," *Arch. Environ. Health 30:*254-262, 1975.

Questions to C. H. Hobbs:

Q: (Participant not Identified)

Power companies talk about turning down the combustors at night. Perhaps slumping the beds. Are you planning to look at what affect start-up will have on the organic emissions?

A: One of the things we would like to do is look at that on a relative basis. Our concentration has been when the unit was operating at a steady state.

Q: Paul Rennlly, GCA Corporation

You showed increased mutagenic acticity as a function of small particle size. Do you really think that is so?

A: I don't know; we feel it is a real affect, but it is difficult to get enough samples to accurately measure the trend on a graph.

Q: (Participant not identified)

I noted in your talk that you were cautious about organic emissions. To what extent is that a real problem?

A: Hydrocarbons raise a concern because of their traditional role on carcenogenic lists. We, however, have not found samples to be mutagenic, That is really all I could say at this time.

Comprehensive Characterization of Emissions from a 6' x 6' Atmospheric Fluidized Bed Combustion System

J.E. Howes, Jr. and S.E. Miller
Battelle Columbus Laboratories
Columbus, Ohio

T. Modrak
Babcock and Wilcox
Research Center
Alliance, Ohio

C. Aulisio
Electric Power Research
Institute
Palo Alto, California

PAPER NOT AVAILABLE AT TIME OF PRINTING